U.S. DEPARTMENT OF ENERGY | Energy Efficiency & Renewable Energy

DOE/EE-1023

Vehicle Systems Simulation and Testing

2013

VEHICLE TECHNOLOGIES OFFICE

CONTENTS

LIST OF FIGURES

LIST OF TABLES

I. INTRODUCTION

On behalf of the U.S. Department of Energy's (DOE) Vehicle Technologies Office (VTO), I am pleased to submit the Annual Progress Report for Fiscal Year (FY) 2013 for the Vehicle and Systems Simulation and Testing (VSST) Program activities.

Mission and Objectives

VSST advances Light Duty (LD), Medium Duty (MD), and Heavy Duty (HD) vehicles and systems to support DOE goals of reducing petroleum consumption, and reducing Green House Gas (GHG) emissions in the Transportation Sector of the United States. To help reach those goals, the VTO conducts R&D programs implementing strategies to help maximize the number of Electric Vehicle (EV) miles driven, and increase the energy efficiency of transportation vehicles.

VSST's mission is to accelerate the market introduction and penetration of advanced vehicles and systems with research and development (R&D) that significantly impacts Petroleum Displacement, GHG Reduction, and Vehicle Electrification Goals. Figure I-1 below outlines the outcome objectives that VSST uses to fulfill its mission. Figure I-2 lists the primary processes and examples of tangible R&D project objectives that contribute to one or more VSST outcome objectives.

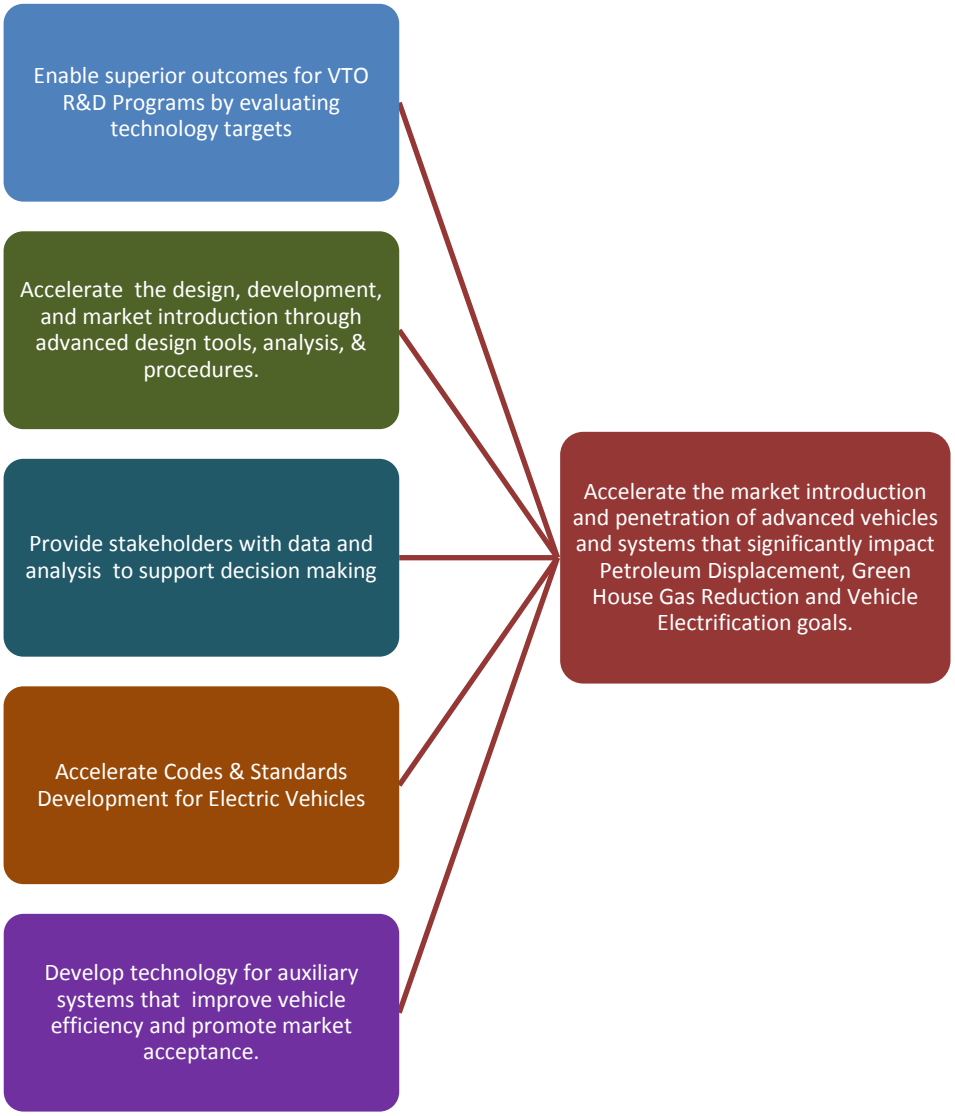

Figure I-1: VSST Outcome Objectives and Mission.

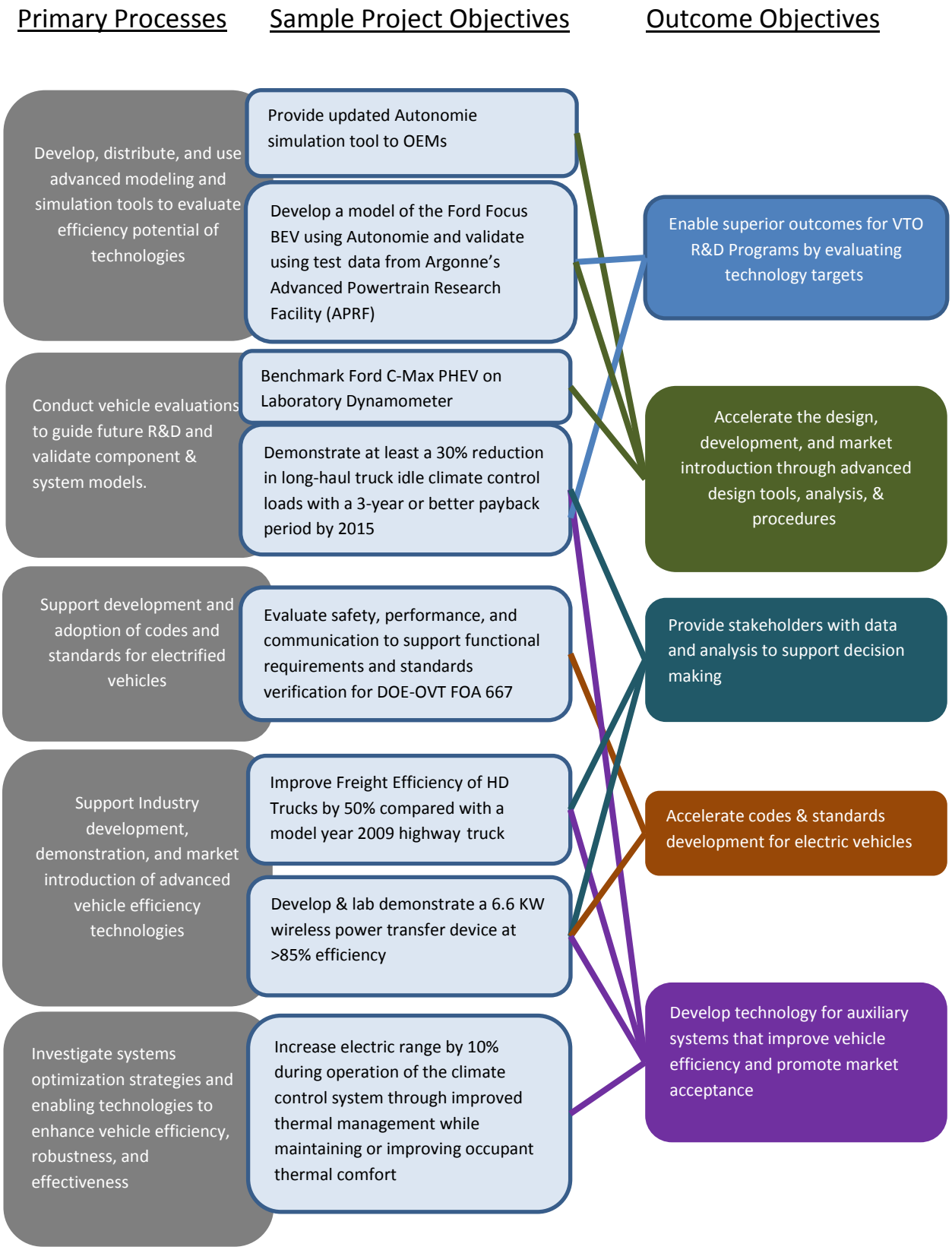

Figure I-2: VSST Primary Processes, Project Objectives, and Outcome Objectives.

Major Accomplishments for FY 2013

The accomplishments listed below are grouped into categories that facilitate mapping the accomplishments to the VSST outcome objectives of Fig I-1. Where appropriate, each highlight contains one or more *links* to a project report that describes the work that contributed to the accomplishment.

- **Developed and applied engineering procedures to address vehicle operations that adversely impact the energy efficiency of Light Duty EVs**
  - Developed and used procedures to evaluate regenerative braking effectiveness that enable original equipment manufacturers (OEMs) to enhance regenerative braking controls; the analysis identified and characterized sources of inefficiency during vehicle decelerations (*Level 1 Benchmark of Advanced Technology Vehicles, Benchmarking of Advanced Technology LD Vehicles: MY 2012 Ford Focus Battery Electric Vehicle)*
  - Characterized auxiliary loads that reduce EV range; the analysis is useful for guiding R&D efforts that investigate technology solutions *(Assessment of Climate Control Settings and Loads on Energy Consumption for HEVs, PHEVs and BEVs in Freezing or Hot Sunny Environments)*
- **Evaluated the contributions of advanced component technologies to vehicle system performance**
  - Evaluated alternative energy storage systems for increasing Hybrid Electric Vehicle (HEV) market penetration; the Cooperative Research and Development Activty (CRADA) with Ford Motor Company created a test platform for evaluating devices provided by system suppliers (*Lower-Energy Energy Storage System (LEESS) Component Evaluation)*
  - Evaluated the impacts of low temperature combustion (LTC) technology on fuel economy and engine-out emissions; researchers completed a simulation study comparing the fuel economy benefits of LTC to those of port fuel injection and spark ignition direct injection (*Evaluation of the Fuel Economy Impact of Low Temperature Combustion (LTC)* Using Simulation and Engine-in-the-Loop)
  - Benchmarked seven advanced-technology production vehicles ranging from conventional to plug-in hybrids (*Level 1 Benchmark of Advanced Technology Vehicles)*
  - Completed field evaluations of HEV Class 7 box trucks, Class 3 & 4 light aerial HEV bucket trucks, and Class 7 delivery trucks; the study defines a set of usage requirements for a micro-turbine series hybrid powertrain system (*Medium and Heavy Duty Field Testing)*
- **Developed technologies and designs that address objectives**
  - Reduce petroleum consumption by HD trucks by reducing aerodynamic drag (Aerodynamics and Underhood Thermal Analysis of Heavy / Medium Vehicles,DOE's Effort to Improve the Fuel Economy of Heavy Trucks through the Use of Aerodynamics).
  - Improve convenience of recharging EVs; the Wireless Power Transfer (WPT) projects developed lab prototypes of high power chargers for LD vehicles (*Wireless Charging for Electric Vehicles (FOA-667), High Efficiency, Low EMI and Positioning Tolerant Wireless Charging of EVs*)
  - Integrate EVs with the Power Grid; the Codes and Standards support projects enabled availability of two Smart-Grid Electric Vehicle Supply Equipment (EVSE) technologies for commercial application; Pacific Northwest National Laboratory (PNNL) technology was integrated into a commercial smart-grid charger and Argonne National Laboratory (ANL) made its Society of Automotive Engineers (SAE) standard compliant communication module available for commercial license(*Grid Connectivity Support, Vehicle to Grid Communications Field Testing)*
  - Extend the range of EVs in warm weather by increasing the efficiency of the Climate Control subsystem; researchers collaborated with a Vehicle OEM to identify zonal cooling configurations that cut energy consumption by up to 16.7% for constant climate control settings, and up to 41.3% with reduced blower settings (*Electric Drive Vehicle Climate Control Load Reduction)*
- **Provided stakeholders with data and analysis**
  - Developed and disseminated analysis and reports based on real-world plug-in electric vehicle (PEV) charging behaviors and PEV usage reported by EV Project assets; PEV charging behavior data was collected from 12,065 Level 2 EVSE and Direct Current Fast Chargers (DCFC) located in seven Transportation Electrification early adopter regions in the United States. During FY 2013; the project disseminated more than 500 reports that characterize the charging and EV usage patterns within the 3.5 million charge events (*EV Project and ChargePoint Data Collection and Dissemination*)
  - Helped the United States (U.S.) Package Delivery Industry to assess alternatives for reducing petroleum consumption
  - Assessed the viability of Electric Delivery Vehicles for Federal Express (FEDEX) (FedEx Collaboration for Improved BEV Delivery Vehicle Using Specific Usage Information)
  - Tested, analyzed, and quantified the benefits of advanced Medium Duty and HD fleet vehicles in real world operations; evaluations with FedEx (Electric Hybrid Cargo Trucks), United Parcel Service (UPS) (Hydraulic Hybrid Delivery Vans)

and Frito Lay (Fully Electric Delivery trucks), will help to optimize designs and deployment of vehicles (*Medium and Heavy Duty Field Testing)*

- **Fostered superior outcomes from VTO component research programs by providing system level requirements**
  - Established a mechanism to infuse system level requirements into a DOE component R&D program; the project supported DOE Advance Power Electronics and Electric Motors (APEEM) group modeling activities that taught electric machine and power electronics designers how to use a vehicle simulation tool (Autonomie) to evaluate electric powertrain technologies at the vehicle system level (*APEEM Components Analysis and Evaluation)*
  - Established requirements for a thermoelectric generator (TEG) to provide cost-effective power for hybrid electric vehicles (HEVs) by analyzing the fuel-saving potential of auxiliary power sources on a midsize vehicle over different drive cycles (*Establishing Thermo-Electric Generator Design Targets for Hybrid Vehicles)*
- **Accelerated the development of numerous codes & standards for EVs such as**
  - SAE J2953/1 PEV-EVSE Interoperability Requirements standard (final), and *SAE J2953/2 PEV-EVSE Interoperability Procedures* standard (draft)
  - Sections of two National Institute of Standards and Testing (NIST) standards that address sub-metering of electricity for EVs
  - SAE J2847/3 Communication between PEVs and the Utility Grid for Reverse Power Flow (Codes and Standards Support for Vehicle Electrification)
  - Supported ANSI Electric Vehicle Standards Panel publication entitled '*Standardization Road Map for Electric Vehicles* (Version 2.0)' that contains a consensus list of gaps and priorities for future EV standards developments (*Codes and Standards and Technical Team Activities*, *Codes and Standards Support for Vehicle Electrification)*
- **Provided tools that accelerate development of advanced vehicles by OEMs and enable assessments on the impact of advanced component technologies on system performance**
  - Enhanced and maintained the Autonomie simulation environment to support the DOE, the user community, and hardware-in-the-loop/rapid control prototyping projects(*Autonomie Maintenance*)
  - Achieved milestone to have all major U.S. vehicle OEMs holding licenses for Autonomie
  - Developed comprehensive thermal models and controllers-for vehicle components such as the engine, battery, and cabin system- that are compatible with Autonomie (*HEV Thermal Model Development and Validation*)
  - Developed CoolCalc modeling tool to help quantify the impact of advanced load reduction technologies for HD trucks (*CoolCalc Rapid HVAC Load Estimation Tool*)
  - Developed an air conditioning (A/C) component model that improves the robustness and accuracy of the fully-detailed A/C system model (*A/C Model Development)*.

I.A.1. Approach and Organization of Activities

VSST groups its projects into Focus Area Activity categories that implement its primary processes (from Figure I-2). In FY 2013 these Focus Areas were Vehicle Modeling and Simulation, Component and Systems Evaluations, Laboratory and Field Evaluations, Codes and Standards, Industry Projects, and Vehicle Systems Optimization.

Projects within each Focus Area typically produce outputs in one or more of the following forms: data, analysis, reports, tools, specifications, and procedures. The outputs from one project s are often used as the inputs for one or more projects in other Focus Areas. The integration of computer modeling and simulation, component and systems evaluations, laboratory and field vehicle evaluations, and development and validation of codes and standards is critical to the success of the VSST Program. Information exchange between focus area activities enhances the effectiveness of each activity (illustrated in Figure I-3).

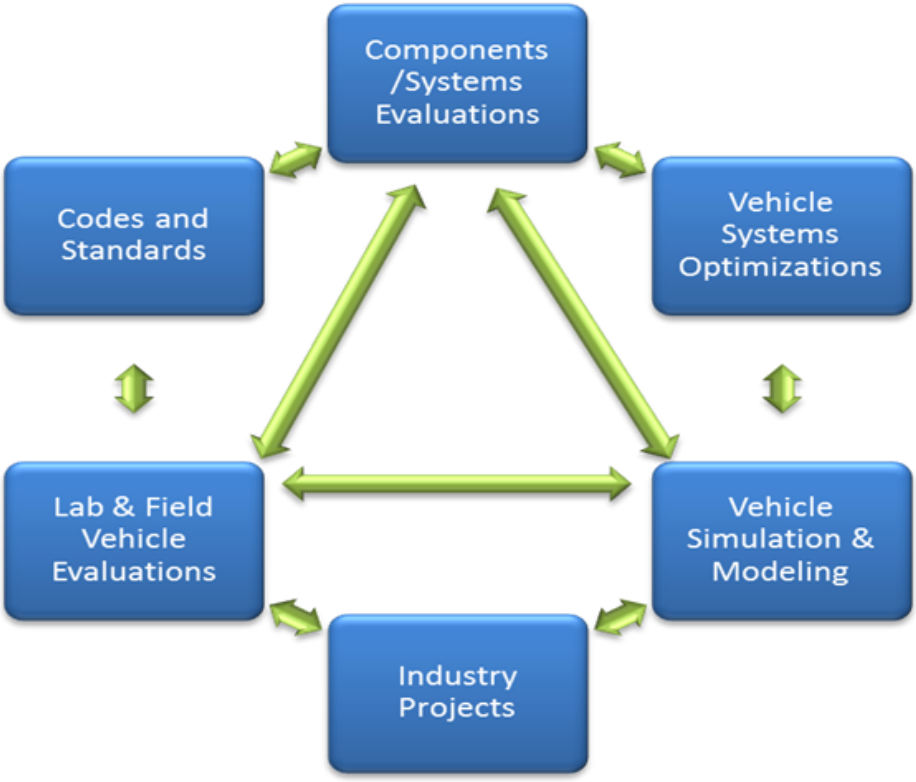

Figure I-3: VSST Activities Integration—Arrows represent information flow between activity focus areas that enhances effectivenets of individual activities.

An example of beneficial data exchange is the increased accuracy of predictive simulation models for advanced technology vehicles made possible by empirical test data that characterizes a vehicle's real world performance (In the example case Lab & Field Vehicle Evaluations activities feed information to the Vehicle Simulation & Modeling Activity). Another example is that the credibility and scope of Lab and Field Technology Evaluation studies benefit from real world performance data that is collected from thousands of advanced technology vehicles from the Vehicle Electrification Demonstration Projects (under Industry Projects Activity).

VSST provides an overarching vehicle systems perspective in support of the technology R&D activities of DOE's VTO and Hydrogen Fuel Cells Technologies Program (HFCTP). VSST uses analytical and empirical tools to model and simulate potential vehicle systems, validate component performance in a systems context, verify and benchmark emerging technologies, and validate computer models. Hardware-in-the-loop testing allows components to be controlled in an emulated vehicle environment. Laboratory testing provides measurement of progress toward VTO technical goals and eventual validation of DOE-sponsored technologies at the Advanced Powertrain Research Facility (APRF), for LD and MD vehicles, and at the ReFUEL Facility, for HD vehicles. For this sub-program to be successful, extensive collaboration with the technology development activities within the VTO and HFCTP is required for both analysis and testing. Analytical results of this sub-program are used to estimate national benefits and/or impacts of DOE-sponsored technology development (illustrated in Figure I-4.).

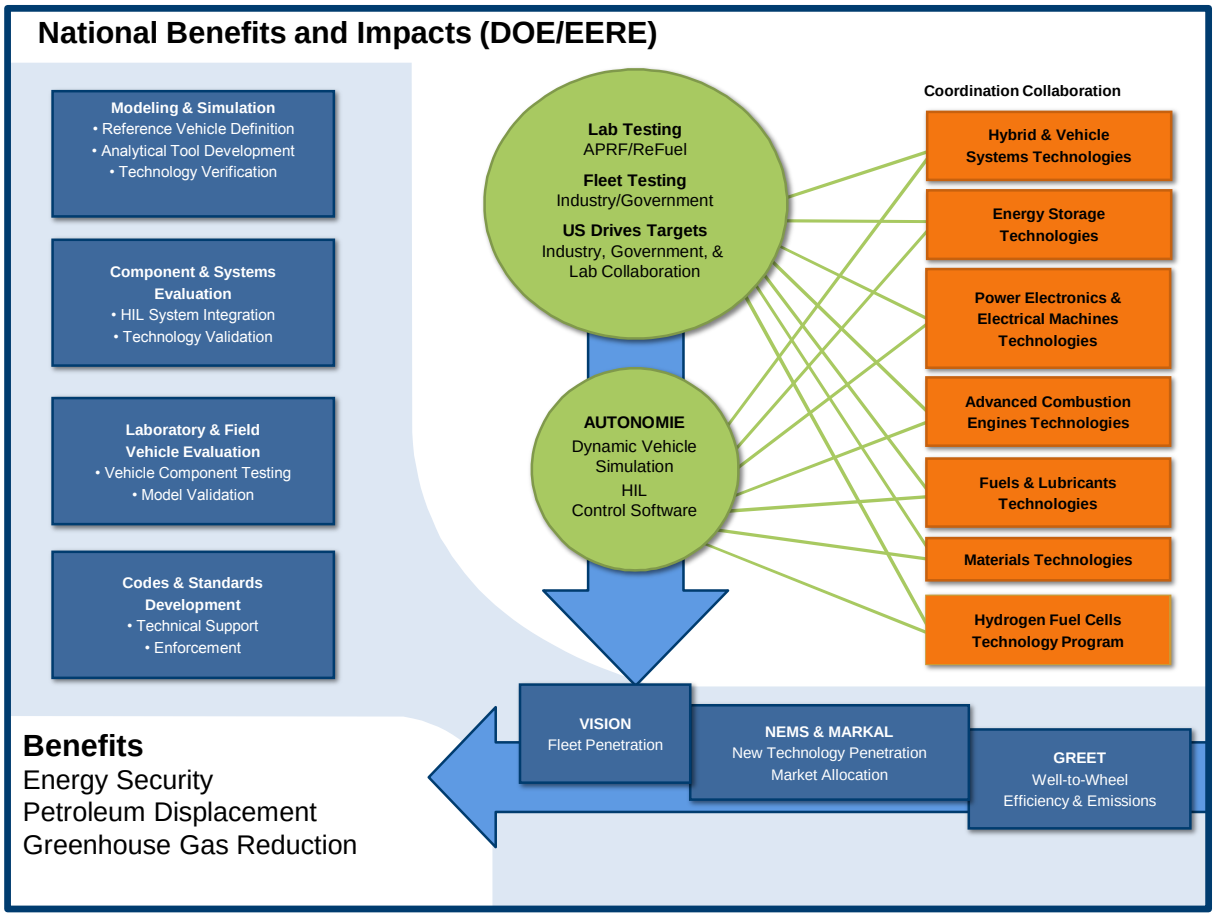

Figure I-4: VSST activities providing estimates of National benefits and impacts of advanced technologies.

During FY 2013, VSST activities were organized into the six focus areas that are described below.

1. Modeling and Simulation

DOE has developed and maintains software tools that support VTO research. VISION, NEMS, MARKAL, and GREET are used to forecast national-level energy, environmental, and economic parameters including oil use, market impacts, and greenhouse gas contributions of new technologies. These forecasts are based on VTO vehicle-level simulations that predict fuel economy and emissions using VSST's Autonomie modeling tool. Autonomie's simulation capabilities allow for accelerated development and introduction of advanced technologies through computer modeling rather than through expensive and time-consuming hardware building. Modeling and laboratory and field testing are closely coordinated to enhance and validate models as well as ensure that laboratory and field test procedures and protocols comprehend the needs of new technologies that may eventually be commercialized.

Autonomie is a MATLAB-based software environment and framework for automotive control system design, simulation and analysis. This platform enables dynamic analysis of vehicle performance and efficiency to support detailed design, hardware development, and validation. Autonomie was developed under a CRADA with General Motors and included substantial input from other OEMs, and replaces its predecessor, the Powertrain Systems Analysis Toolkit (PSAT). One of the primary benefits of Autonomie is its Plug-and-Play foundation which allows integration of models of various degrees of fidelity and abstraction from multiple engineering software environments. This single powerful tool can be used throughout all the phases of Model Based Design of the Vehicle Development Process (VDP).

2. Component and Systems Evaluation

Hardware-in-the-loop (HIL) simulation provides a novel and cost effective approach to isolate and evaluate advanced automotive component and subsystem technologies while maintaining the rest of the system as a control. HIL allows actual hardware components to be tested in the laboratory at a full vehicle level without the extensive cost and lead time of building a complete prototype vehicle. This approach integrates modeling and simulation with hardware in the laboratory to develop and evaluate propulsion subsystems in a full vehicle level context. The propulsion system hardware components: batteries, inverters, electric motors and controllers are further validated in simulated vehicle environments to ensure that they meet the vehicle performance targets established by the government-industry technical teams.

High energy traction battery technology is important to the successful development of plug-in electric vehicles (PEVs). To support the evaluation of advanced prototype energy storage systems, in FY 2013 Idaho National Laboratory (INL), with assistance from Oak Ridge National Laboratory (ORNL) continued to developed and implement the Electric-Drive Advanced Battery (EDAB) test platform. This test-bed allows advanced battery packs to be evaluated in real-world operating conditions in an on-road vehicle that emulates a variety of electric-drive powertrain architectures.

3. Laboratory and Field Vehicle Evaluation

This section describes the activities related to laboratory validation and fleet testing of advanced propulsion subsystem technologies and advanced vehicles. In laboratory benchmarking, the objective is to extensively test production vehicle and component technology to ensure that VTO-developed technologies represent significant advances over technologies that have been developed by industry. Technology validation involves the testing of DOE-developed components or subsystems to evaluate the technology in the proper systems context. Validation helps to guide future VTO research and facilitates the setting of performance targets.

The facilities that perform Lab and Field Testing activities include the Advanced Powertrain Research Facility (APRF), INL Transportation Testing Facilities, the National Renewable Energy Laboratory

(NREL)'s ReFuel, and Thermal Test Facilities, and ORNL's Vehicle Systems Integration Lab (VSI).

The APRF is equipped with-dynamometers (for testing integrated components such as engines, electric motors, and powertrains), and a thermal chamber (for testing BEVs, HEVs and PHEVs in temperatures as low as 20°F, up through 95°F).

INL's transportation testing facilities encompass the Advanced Vehicle Test and Evaluation Activity ((AVTE), for Light Duty Vehicles) Facility, the Heavy Duty Transportation Test Facility, and the Energy Storage Technologies Laboratory. AVTA's capability to securely collect, analyze, and disseminate data from multiple field tests located throughout the U.S. is critical to VSST Lab & Field activities.

NREL's ReFuel facility is equipped with dynamometers (for testing MD vehicles and components). NREL's Thermal Test Facilities include capabilities for LD vehicle cabin thermal studies and outdoor HD vehicle cabin studies. NREL also has facilities for testing subsystems (such as Energy Storage Systems (ESS) and EVSE) and functions as the VSST data collection and evaluation hub for MD and HD vehicle fleet tests.

ORNL's facilities for integrated testing include the Advanced Engine Technologies (E.g., advanced combustion modes, fuels, thermal energy recovery, emissions after-treatment), Advanced Power Electronics and Electric Machines (E.g., motor drives, components, power electronics devices, advanced converter topologies), and Vehicle Testing and Evaluation (E.g., chassis and component dynamometers, integrated powertrain stands, test track evaluations, field operational testing).

The AVTE, working with industry partners, conducts field and fleet testing to accurately measure real-world performance of advanced technology vehicles via a testing regime based on test procedures developed with input from industry and other stakeholders. The performance and capabilities of advanced technologies are benchmarked to support the development of industry and DOE technology targets. The testing results provide data for validating component, subsystem, and vehicle simulation models and hardware-in-the-loop testing. Fleet managers and the public use the test results for advanced technology vehicle acquisition decisions. INL conducts light-duty testing activities. In FY 2013, INL continued its partnership with an industry group led by ECOtality North America. Accelerated reliability testing provides reliable benchmark data of the fuel economy, operations and maintenance requirements, general vehicle performance, engine and component (such as ESS) life, and life-cycle costs. These tests are described below.

Baseline Performance Testing

The objective of baseline performance testing is to provide a highly accurate snapshot of a vehicle's performance in a controlled testing environment. The testing is designed to be highly repeatable. Hence it is conducted on closed tracks and dynamometers, providing comparative testing results that allow "apples-to-apples" comparisons within respective vehicle technology classes. The APRF at ANL is used for the dynamometer testing of the vehicles.

Fleet Testing

Fleet testing provides a real-world balance to highly controlled baseline performance testing. Some fleet managers prefer fleet testing results to the more controlled baseline performance or the accelerated reliability testing.

During fleet testing, a vehicle or group of vehicles is operated in normal fleet (field) applications. Operating parameters such as fuel-use, operations and maintenance, costs/expenses, and all vehicle problems are documented. Fleet testing usually lasts one to three years and, depending on the vehicle and energy storage technology, between 5,000 and 12,000 miles are accumulated on each vehicle.

For some vehicle technologies, fleet testing may be the only viable test method. NEVs are a good example. Their manufacturer-recommended charging practices often require up to 10 hours per charge cycle, while they operate at low speeds (<26 mph). This makes it impractical to perform accelerated reliability testing on such vehicles.

Accelerated Reliability Testing

The objective of accelerated reliability testing is to quickly accumulate several years or an entire vehicle-life's worth of mileage on each test vehicle. The tests are generally conducted on public roads and highways, and testing usually lasts for up to 36 months per vehicle. The miles to be accumulated and time required depend heavily on the vehicle technology being tested. For instance, the accelerated reliability testing goal for PHEVs and BEVs is to accumulate 12,000 miles per vehicle in one year while the testing goal for HEVs is to accumulate 160,000 miles per vehicle within three years. This is several times greater than most HEVs will be driven in three years, but it is required to provide meaningful vehicle-life data within a useful time frame. Generally, two vehicles of each model are tested to ensure accuracy. Ideally, a larger sample size would be tested, but funding tradeoffs necessitate only testing two of each model to ensure accuracy.

Depending on the vehicle technology, a vehicle report is completed for each vehicle model for both fleet and accelerated reliability testing. However, because of the significant volume of data collected for the HEVs, fleet testing fact sheets (including accelerated reliability testing) and maintenance sheets are provided for the HEVs.

4. Codes and Standards Development

A comprehensive and consistent set of codes and standards addressing grid-connected vehicles and infrastructure is essential for the successful market introduction of Electric-Drive Vehicles (EDVs). The VTO is active in driving the development of these standards through committee involvement and technical support by the National Laboratories. The VTO also supports activities of the U.S. DRIVE's Grid Interaction Tech Team (GITT), a government/industry partnership aimed at ensuring a smooth transition for vehicle electrification by closing technology gaps that exist in connecting vehicles to the electric grid. In FY 2013, GITT worked with Pacific Northwest National Laboratory (PNNL) and ANL to participate in SAE and NIST standards development for connectivity and communication for grid-connected vehicles.

Codes and Standards work objectives in 2013 included: (1) Identify gaps in technology and recommend enabling solutions through the creation of proof-of-concept hardware/software and validation of proposed approaches. (2) Provide direct support of SAE standards committees and global cooperation/harmonization for EV initiatives for Interoperability, communications, enabling technologies, and test procedures.

During FY 2013, VSST pursued codes and standards objectives at the strategic and tactical levels. At the strategic level, VSST helped develop a strategy for addressing the needs of a diverse set of stakeholders via development of the Electric Vehicle Roadmap V2.0 by the American National Standards Institute (ANSI). The EV Roadmap V2.0 provides the EV community with a current status of all PEV charging infrastructure/Smart Grid-related standards (and a prioritized list of gaps). At the tactical level, VSST supported National Laboratory staff led and served on SAE committees that developed standards that address communications, interoperability, security, safety, and performance of PEVs and EVSE. Support included J1772 for connector standards, SAE J2836, J2847, J2953, and J2931 for EV-Grid communication standards, and investigations to support development of EV Wireless Charging Standard J2954. PEV powertrain performance support included validation and development of testing procedures for J1634 and J1711. VSST researchers also contributed to SAE J2953 PEV-EVSE Interoperability standards development.

The consumer markets for EVs transcend national boundaries. ANL was employed in international cooperative initiatives to adopt international EDV standards and promote market penetration of grid-connected vehicles (GCVs). Many new technologies require adaptations and more careful attention to specific procedures. ANL supported development of interoperability validation procedures and opened the SmartGrid Joint Interoperability Center as the U.S. base for International cooperative work between the EU and U.S. Energy R&D Laboratories.

Codes and standards were also developed for sanctioned sporting regulations to stimulate rapid vehicle technology development and to educate consumers about the benefits of fuel efficient technologies. The Green Racing Initiative features teams using advanced fuels with significant renewable percentages in ALMS racing to include all but two Grand Touring category cars and two Le Mans Prototype cars. Green Racing worked with the American Le Mans Series (ALMS) to strengthen and improve the visibility of the green racing program through the development and application of scoring protocols. The Green Racing Initiative supports technology advancement through motorsports competition, and promotes market acceptance of advanced vehicle technologies.

5. Vehicle Systems Optimization

This focus area involves research and development on a variety of mechanisms to improve the energy efficiency of light, medium, and heavy duty vehicles. Projects in this focus area involve reducing the aerodynamic drag of vehicles, thermal management approaches to increase the engine thermal efficiency and reduce parasitic energy losses, the development of advanced technologies to improve the fuel efficiency of critical engine and driveline components by characterizing the fundamental friction and wear mechanisms, and fast and wireless charging technology development.

Aerodynamic Drag Reduction

The primary goal of this focus area is improving the freight-efficiency of vehicles. Aerodynamic drag reduction, thermal management, and friction and wear are the main focuses of this area. Reduction of aerodynamic drag in Class 8 tractor-trailers can result in a significant improvement on fuel economy while satisfying regulatory and industry operational constraints. An

important part of this effort is to expand and coordinate industry collaborations with DOE and establish buy-in through CRADAs and to accelerate the introduction of proven aerodynamic drag reduction devices into new vehicle offerings.

The primary approach in drag reduction is through the control of the vehicles flow field. This is can be achieved with geometry modifications, integration, and flow conditioning. During 2013 the goal of the research was to develop and design the next generation of aerodynamically integrated tractor-trailer.

Thermal Management

Thermal management of vehicle engines and support systems is a technology area that addresses reduction in energy usage through improvements in engine thermal efficiency and reductions in parasitic energy uses and losses. Fuel consumption is directly related to the thermal efficiency of engines and support systems. New methods to reduce heat related losses are investigated and developed under this program.

FY 2013 Thermal Management R&D focused on exploring:

- The possibilities of repositioning the class 8 tractor radiator and modifying the frontal area of the tractor to reduce aerodynamic drag.
- The possibilities of using evaporative cooling under extreme conditions of temperature and engine load.
- Assess use of nanofluids for cooling of power electronics.

Friction and Wear

Parasitic engine and driveline energy losses arising from boundary friction and viscous losses consume 10 to 15 percent of fuel used in transportation, and thus engines and driveline components are being redesigned to incorporate low-friction technologies to increase fuel efficiency of passenger and heavy-duty vehicles. Research to improve the fuel efficiency and reliability of critical engine and driveline components included:

- Experimentally investigating fundamental friction and wear mechanisms.
- Modeling and validating the impact of friction on components and overall vehicle efficiency.
- Developing advanced low friction technologies (materials, coatings, engineered surfaces, and advanced lubricants)
- Developing requirements of a high power density driveline system that can be applied across many of the vehicle types regardless of the powertrain or fuel type

Fast and Wireless Charging

Electrification of the transportation sector will be enabled by adoption of vehicle charging technologies that minimize costs in terms of time and money while maximizing energy throughput, battery life, safety, and convenience.

6. Industry Awards

Industry projects for FY 2013 include the categories of PHEV Technology Acceleration Deployment Activities, Transportation Electrification, SuperTruck, Wireless Charging, and Zero Emissions Cargo Transport (ZECT). Two new projects in the category of 'Energy Load Reduction and Energy Management, Advanced HVAC Equipment, & Cabin Pre-Conditioning' were awarded during FY2013. These technology development and demonstration projects were awarded through DOE's competitive solicitation process and involve resource matching by DOE and Industry.

Major projects that were conducted by the National Laboratories and Industry partners in support of these areas in FY 2013 are described in this report. The reports describe the approach, accomplishments and future directions for the projects. For further information, please contact the DOE Project Leader named for each project.

I.A.2. Future Directions for VSST

Near-term solutions for reducing the nation's dependence on imported oil, such as PHEVs, will require the development, integration, and control of vehicle components, subsystems, and support systems. These solutions will require exploration of high capacity energy storage and propulsion system combinations to get the most out of hybrid propulsion. Analysis and testing procedures at the national labs will be enhanced to study these advanced powertrains with simulation tools, component/subsystem integration, and hardware-in-the-loop testing. DOE-sponsored hardware developments will be validated at the vehicle level, using a combination of testing and simulation procedures.

In FY 2014, the VSST will continue activities in the area of vehicle simulation and modeling, and laboratory and field testing including further baseline performance testing of conversion and original equipment manufacturer (OEM) electric-drive vehicles. Field and laboratory testing will continue to be integrated with modeling/simulation activities, including validation of simulation models for advanced vehicles tested in the APRF. Fleet evaluation of plug-in vehicles will continue, with continued emphasis on evaluation fleets of OEM production vehicles.

In addition to the HEV and PHEV activities, a full range of simulation and evaluation activities will be conducted on the BEVs as they are brought to market by OEMs. Because EVs are dependent on a robust charging infrastructure for their operation and ultimate consumer acceptance, VSST will greatly increase efforts to address issues related to codes and standards for EVs, charging infrastructure, and vehicle/grid integration.

VSST will pursue the objective of using less energy for cabin climate control of Light and Heavy Duty Vehicles. This work will contribute to progress on reaching the EV Everywhere Blueprint's 'Efficient Climate Control Technologies Objective' and the VSST 2015 target objective to Increase freight efficiency of heavy duty vehicles by 50%, through system-level innovations'.

VSST will also be deeply involved in the collection and analysis of data from the American Recovery and Reinvestment Act of 2009 (ARRA) Transportation Electrification Demonstration projects. These eight demonstrations will placed several thousand electric drive vehicles and recharging stations in service, and VSST will direct the collection an analysis of data from these units. In addition to performance, reliability, and petroleum displacement results, VSST will use the data to determine the impact of concentrations of electric drive vehicles on the electricity grid, as well as the changes in operators' driving and recharging patterns as they become more comfortable with this new technology.

Vehicle systems optimization work in the areas of aerodynamics, thermal management, and friction and wear will continue. The focus of these activities will revolve around cooperative projects with industry partners with the goal of bringing developed technologies to market quickly. New efforts will be supported to conduct evaluations of methods to improve thermal heat transfer efficiencies and reduce parasitic loads with coordination from industry partners. Additionally, activities to develop solutions for wireless power transfer and fast charging of electric-drive vehicles, while evaluating the market barriers and technology impacts for deploying this infrastructure, will continue to ramp up within the Vehicle Systems Optimization area.

Inquiries regarding the VSST activities may be directed to the undersigned.

Lee Slezak
Technology Manager
Vehicle and Systems Simulation and Testing
Vehicle Technologies Program

II. THE EV EVERYWHERE GRAND CHALLENGE

II.A. Background

In March 2012, President Obama announced the *EV Everywhere* Grand Challenge—to produce plug-in electric vehicles (PEVs) as affordable and convenient for the American family as gasoline-powered vehicles by 2022. Realizing the promise of PEVs is one of the grand challenges of this era. Today, our transportation system is dependent on internal combustion engines and oil. In fact, 93% of our transportation fuel is derived from petroleum and much of this is imported. PEVs can decouple personal mobility from oil, cut pollution and help build a 21st Century American automotive industry that will lead the world.

America is the world's leading market for electric vehicles and is producing some of the most advanced PEVs available today. Consumer excitement and interest in PEVs is growing—in 2012, PEV sales in the U.S. tripled, with more than 50,000 cars sold, and a plug-in electric vehicle (the Chevrolet Volt) beat all other vehicle models in Consumer Reports' owner satisfaction survey for the second time. In 2013, PEV sales are on pace to nearly double prior year sales, with nearly 100,000 annual sales of PEVs projected.

PEVs have won critical acclaim with awards such as 2011 World Car of the Year (Nissan Leaf), 2013 Motor Trend Car of the Year (Tesla Model S) and 2012 Green Car Vision Award Winner (Ford C-MAX Energi). To maintain this leadership, strong growth in the U.S. PEV sector will need to continue.

The Department of Energy (DOE) developed an *EV Everywhere* "Blueprint" document that provides an outline for technical and deployment goals for PEVs over the next five years (*Blueprint*). DOE will pursue these targets in cooperation with a host of public and private partners. The technical targets for the DOE PEV program fall into four areas: battery R&D; electric drive system R&D; vehicle light weighting; and advanced climate control technologies. Some specific goals include:

- Cutting battery costs from their current $500/kWh to $125/kWh
- Reducing the cost of electric drive systems from $30/kW to $8/kW
- Eliminating almost 30% of vehicle weight through light weighting

These numbers represent difficult to reach "stretch goals" established in consultation with stakeholders across the industry—including the *EV Everywhere* workshops held during the summer and fall of 2012. When these goals are met, the levelized cost of an all-electric vehicle with a 280-mile range will be comparable to that of an ICE vehicle of similar size. Even before these ambitious goals are met, the levelized cost of most plug-in hybrid electric vehicles—and of all-electric vehicles with shorter ranges (such as 100 miles)—will be comparable to the levelized cost of ICE vehicles of similar size. Meeting these targets will help to reduce the purchase price for plug-in electric vehicles

The *EV Everywhere* Blueprint document also describes the deployment programs related tocharging infrastructure and consumer education. Efforts to promote home, workplace, and public charging can also help speed PEV deployment.

EV Everywhere Technical Targets

DOE defined *EV Everywhere* technology targets using an analytical framework that evaluated the performance of component technologies as well as vehicle cost and performance. We synthesized data about future vehicle potential by using expert projections of component technology to create virtual vehicles of the future via computer modeling and simulation. The range of vehicle costs and efficiencies made possible a comparison of the degree to which the portfolio of these technologies must progress, in both performance and cost terms, to yield PEVs that are cost-competitive, as measured by the initial vehicle purchase price and the fuel expenditure accrued over a 5-year ownership period. Ultimately, an analysis of this balance yielded technical targets at the technology progress frontier: *EV Everywhere* targets are consistent with what experts see as very aggressive but still possible within the *EV Everywhere* timeframe.

The complete set of *EV Everywhere* technical targets are presented in the Blueprint document.

II.B. 2013 Highlights

VSST achieved sub-objectives for achieving the goals of (a) Extending Vehicle range by reducing and managing auxiliary loads, (b) Integrating EVs into the Electrical Grid, and (c) Accelerating Market Penetration of EVs by supporting Codes and Standards Development. Table II-1 below provides an executive summary of the accomplishments and the R&D project reports that contain the details.

Table II-1: VSST EV Everywhere Achievements for FY 2013.

Goals & Objectives	Accomplishment	Benefit	Where to find the Details of R&D Activities
Extend Range by Reducing and Managing Auxiliary Loads	Developed new Heating Ventilating and Air Conditioning (HVAC) component models compatible with Autonomie.	Reduces Industry costs to evaluate candidate strategies for improving EV range. Validated HVAC component models enable virtual system design experiments to determine impact of candidate technologies.	*A/C Model Development., HEV Thermal Model Development and Validation*.
Extend Range by Reducing and Managing Auxiliary Loads	Quantified the impact of cabin climate control systems on the energy consumption of a HEV, PHEV, and BEV at different temperature settings and in different ambient temperature environments. (E.g., EPA 5 cycle label fuel economy test conditions.)	Test data and analysis provide researchers with the information needed to focus development of technology solutions that minimize the impact of hot and cold temperatures on EV range.	*Assessment of Climate Control Settings and Loads on Energy Consumption for HEVs, PHEVs and BEVs in Freezing or Hot Sunny Environments*
Foster Integration of EVs into Electrical Grid	Publish Real-World EVSE Data Collection Products Usage informing decision makers on consumer demand patterns. During FY 2013, VSST researchers generated more than 527 reports, fact sheets, special analysis, white papers, and technical papers.	Increases market efficiency for adoption of EVSE technologies. The empirical information fills the knowledge gaps that hinder accurate prediction of demand for EVSE equipment & public infrastructure. Accurate predictions are critical for infrastructure planning and business model assessments.	*EV Project and ChargePoint Data Collection and Dissemination*
Foster Integration of EVs into Electrical Grid	Fast DC Charging Communications Module Technology made available for incorporation into commercial product. Invention is a Spin-off from Codes & Standards R&D.	Accelerates market penetration of Fast Charging by providing validated communication solution for OEMs and EVSE suppliers. Building block for communication with the Smart Grid.	*Codes and Standards Support for Vehicle Electrification*
Foster Integration of EVs into Electrical Grid	Advanced Technology R&D incorporated into commercial product. Aerovironment has introduced a commercial Smart Grid Charger.	Accelerates market penetration of EVSE with Smart Grid capability. Device minimizes impact of EV charging on Electric Grid Resources.	*SAE Standards Development Support.*
Eliminate Barriers to EV Market Penetration by supporting Codes & Standards Development	ANSI published the EV Codes & Standards Roadmap Version 2.0. This effort was supported by DOE funding. The Roadmap is the collaborative product from a series of workshops that engaged stakeholders from multiple domains. The document provides a consensus perspective of codes and standards gaps for EVs and priorities for addressing the gaps.	(1) Facilitates development of standards and codes by several organizations. (E.g., IEC, NEMA, NIST, NFPA, SAE, and UL.) (2) Facilitates market access and cross-border trade. (3) Facilitates achievement of regulatory objectives. (E.g., NHTSA Quiet Car rule making.) (4) Fosters understanding of issues related to EVs and EVSE technology and proposes solutions. (5) Provides stakeholders with a resource that anticipates future deployment of new and related technologies.	*Codes and Standards and Technical Team Activities, Codes and Standards Support for Vehicle Electrification*

II.C. Planned Activities

Using less energy to achieve comfortable climate control in PEVs will allow for a smaller, less expensive battery, and thus contribute to lowering the cost of PEVs (assuming travel distance is held constant). Currently, these climate control loads on a PEV can double vehicle energy consumption, effectively halving vehicle range. *EV Everywhere* will focus on the following specific research areas:

- ENERGY LOAD REDUCTION AND ENERGY MANAGEMENT strategies can minimize energy consumption by reducing the thermal loads that the systems must address. Advanced windows and glazing, surface paints, advanced insulation, thermal mass reduction, and ventilation and seating technologies can better control heat transfer between the passenger cabin and the environment, minimizing the thermal loads that the Heating, Ventilation and Air-Conditioning (HVAC) systems must address to ensure passenger comfort.
- ADVANCED HVAC EQUIPMENT, such as advanced heat pumps or novel heating/cooling subsystems, can reduce the auxiliary loads. Innovative heating and cooling concepts to achieve passenger comfort, such as infrared and thermoelectric devices and phase change materials, can also reduce energy requirements.
- CABIN PRE-CONDITIONING while the vehicle is connected to the grid can reduce the amount of energy needed from the battery upon initial vehicle operation to either pull-down (hot conditions) or raise (cold conditions) the temperature in the cabin. Another approach to cabin pre-conditioning is to utilize waste heat generated within the battery and/or charging circuit during charging.

In support of the *EV Everywhere* Grand Challenge, DOE released a Funding Opportunity Announcement (FOA) in March 2013, soliciting proposals in the areas of energy storage, electric drive systems, lightweight materials, and auxiliary load reductions.

DOE announced the selection of 38 awards from the FOA in September 2013. These projects were initiated in September 2013 and will be described in more detail in next year's annual report.

In the area of advanced climate control to reduce auxiliary load energy consumption, two projects representing a DOE investment of $4 million were awarded. Reducing the impact of heating and cooling on plug-in electric vehicles can significantly increase all-electric driving range. The Halla Visteon project will develop, integrate, and demonstrate an efficient heating and cooling system as well as other novel solutions to achieve and maintain passenger comfort using less battery power. The Delphi Automotive project will develop and integrate a new heating system for vehicles and demonstrate a significant reduction in the energy used for passenger cabin heating in electric vehicles. These two projects are focused on developing innovative heating and cooling technologies that reduce battery demands and improve range by 20 to 30 percent.

III. INDUSTRY

PHEV TECHNOLOGY ACCELERATION AND DEPLOYMENT ACTIVITY

III.A. Chrysler Town & Country Mini-Van Plug-In Hybrid Electric Vehicle

Abdullah A. Bazzi, Principal Investigator
Chrysler Group LLC
800 Chrysler Drive
Auburn Hills, MI USA 48326-2757
Phone: (248) 944-3093
E-mail: aab5@Chrysler.com

Lee Slezak, DOE Technology Development Manager
Phone: (202) 586-2335;
E-mail: Lee.Slezak@ee.doe.gov

John Jason Conley, NETL Project Manager
Phone: (304) 285-2023
E-mail: John.Conley@netl.doe.gov

DOE Award Number: DE-EE0004529
Submitted to: U.S. Department of Energy–National Energy Technology Laboratory

III.A.1. Abstract

Phase I Project Objective

- Demonstrate 25 minivans (RT) in diverse geographies and climates, spanning from Michigan, California, and Texas and across a range of drive cycles and consumer usage patterns applicable to the entire NAFTA region
- Run the vehicles for 2 years with relevant data collected to prove the product viability under real-world conditions
- Quantify the benefits to customers and to the nation
- Develop & demonstrate charging capability
- Develop and demonstrate Flex Fuel (E85) capability with PHEV technology.
- Support the creation of "Green" Technology jobs and advance the state of PHEV technology for future production integration
- Develop an understanding of Customer Acceptance & Usage patterns for PHEV technology
- Integration of PHEV technology with Renewable energy generation

Phase II Project Objective

- Demonstrate the viability of the high voltage energy storage system with a new cell technology for a new production application
- Test advanced Li-Ion Battery technologies, charging systems, and Electrified Powertrain Control Systems

Major Accomplishments

Vehicle Build & Test

- Utilized the standard Chrysler Group LLC Vehicle Development Process for a production intent program
  - Designed and built all development and test vehicles
  - Augmented development process with modified testing procedures to address specific plug in Hybrid Technologies
- Successful completion of the demonstration fleet vehicles. Deployed 23 Chrysler Town & Country Minivan PHEVs
- Deployed Chrysler Town & County Minivan PHEVs were returned to Chrysler Group LLC. The returned vehicles completed an inspection and preparation work for the high voltage battery upgrade was initiated
- Corrective actions for three PHEV issues observed in the field were identified
- Development activities for the upgraded battery pack remain on-track. Cell design was completed and they are being shipped for module development and battery pack characterization
  - Completed Internal Chrysler Group LLC technology assessment of battery pack upgrade and vehicle retrofit plan
  - Completed directional setting of battery pack design

Deployment Fleet

- The close out of Phase I included returning the deployed Chrysler Town & Country Minivan PHEVs to Chrysler Group LLC and then decommissioning the vehicles. Vehicles built during Phase I of the project are being decommissioned using one of the following five strategies:
  - Retrofitted for development vehicle and deployment fleet
  - Pulled for Service Parts
  - Saved for Full Vehicle Replacement
  - Scrapped Completely
  - Used for Development
- Chrysler Group LLC is implementing a new battery cell technology

Future Activities

- Execute validation testing of 4 retrofitted vehicles with upgraded high voltage batteries
- Initiate deployment of retrofitted vehicle to Chrysler Group LLC development team and begin data collection.

✧ ✧ ✧ ✧ ✧

III.A.2. Technical Discussion

Introduction

The Chrysler Product Creation Process (CPCP) defines the strategy and method used to execute the development of world class vehicles from concept to market. The Chrysler Town & Country PHEV is following the CPCP process. Fundamental principles include:

- Voice of the Customer–Dictates product decisions
- Timeline Compression–Enables speed to market
- Flexibility–Allows for unique vehicle program characteristics
- Consistency of Execution–Facilitates continuous improvement
- Clear Performance Indicators–Drives accountability
- Interdependencies Identified–Aligns activities across functional areas

Vehicle Decommissioning Strategy for Minivan PHEV

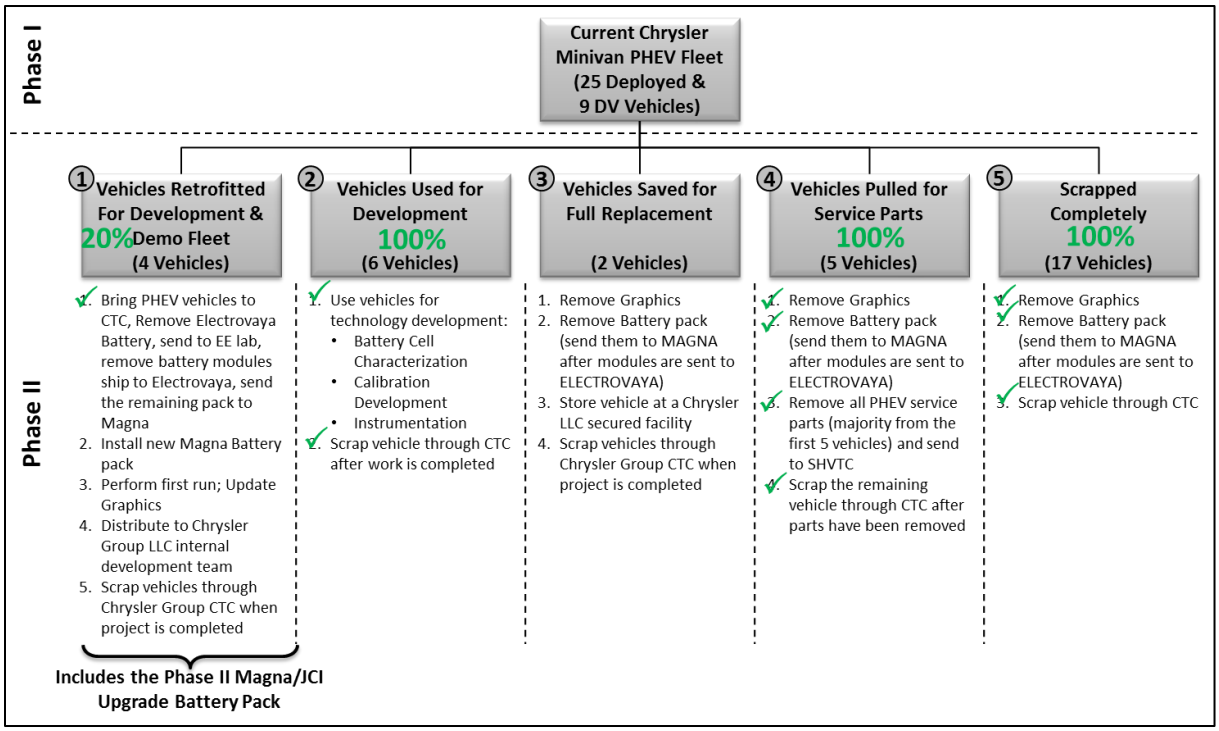

Figure III-1: Minivan PHEV Decommissioning Categories with Major Steps.

Results

Federal Test Procedure Results

Table III-1: Minivan PHEV Federal Test Procedure Results.

Objective	Target	Status	Procedure	R/G/Y
RANGE	EAER 10	EAER 14 (Based on simulations)	California Exhaust Emission Standards and Test Procedures, as amended December 2, 2009	GREEN

Conclusions

Chrysler LLC has completed initial builds of the upgraded high voltage battery to be used in the Chrysler Town & Country Minivan. Critical design reviews for the high voltage battery pack system was conducted successfully. Testing of upgraded battery pack is currently in process. Four vehicles will be retrofitted with the upgraded battery pack and decommissioning of vehicles will continue to follow the five step plan.

III.A.3. Products

Publications

- A High Efficiency Low Cost Direct Battery Balancing Circuit Using A Multi-Winding Transformer with Reduced Switch Count. IEEE APEC 2012, Orlando, FL, Feb. 5–9, 2012

Public Presentations

- Annual Merit Review. Washington, DC.

Patents

- None to Report

Tools & Data

1. Vector Cantech–Canalyzer equipment utilized for data collection and software development (communication between vehicle controllers)
2. ETAS–Equipment utilized for software development and drivability / emissions calibration
3. Security Inspection utilized for upgraded infrastructure environment (increased bandwidth requirements and storage requirements) for implementing Microstrategy vehicle logging and data analysis
4. Bright Star Engineering–Data Recorder Modules (DRM) for each vehicle and monthly cellular access.

III.B. Development of Production-Intent Plug-In Hybrid Vehicle, using Advanced Lithium-Ion Battery Packs with Deployment to a Demonstration Fleet (DE-FC26-08NT04386)

Mr. Greg Cesiel, Principal Investigator
General Motors
30001 Van Dyke Avenue
Warren, MI 48090
M/C: (480) 210-240
Phone: (586) 575-3670
E-mail: greg.cesiel@gm.com

Lee Slezak, DOE Technology Development Manager
Phone: (202) 586-2335
E-mail: lee-slezak@ee.doe.gov

Jason Conley, Principal Investigator:
Phone: (304) 904-7590
E-mail: john.conley@netl.doe.gov

III.B.1. Abstract

Objective

Overall Objectives

- The primary goal of the project is to develop the first commercially available, OEM-produced plug-in hybrid electric vehicle (PHEV). The performance of the PHEV is expected to double the fuel economy of the conventional hybrid version of the same vehicle. This vehicle program, which incorporates advanced lithium-ion battery packs and features an E85-capable FlexFuel engine, seeks to develop, fully integrate, and validate the plug-in specific systems and controls by using GM's Global Vehicle Development Process (GVDP) for production vehicles. The Engineering Development related activities include two physical builds that produced 29 mule vehicles and 29 integration vehicles for internal deployment at GM. Continued work includes engineering tasks for the development of a new thermal management design for a second generation battery module.

FY2013 Objectives

- Phase III of the proposed project captures the first half or Alpha phase of the Engineering tasks for the development of a new thermal management design for a second generation battery module. This new design will incorporate reduced complexity, thus allowing for a more cost efficient design. Thermal management of batteries is essential to propulsion system performance. Effective thermal management ensures the maintenance of proper operating temperatures thus increasing range, reliability and durability.

Major Accomplishments

- Battery module selected design part procurement complete to allow module assembly for testing
- Module testing initiated, enhanced and completed with satisfactory results
- Additional development from test results reviewed and module design refinement accomplished
- Final technical review with DOE Technology Development Manager and NETL Program Manager completed in Washington, DC with GM Engineering Team

Future Achievements

On September 30, 2013, all project work for this PHEV Technology Acceleration project was completed. The remainder of the work to complete for this project is the final Program Management reports. This work will be complete by December, 2013.

✧ ✧ ✧ ✧ ✧

III.B.2. Technical Discussion

Introduction

Engineering Development of Year 1 Mule Vehicles

The first phase of the project captures the first half of the Engineering tasks for the development of key plug-in technologies. This involves the development of components and subsystems required for a PHEV and fully integrate them in a production vehicle.

Approach

Engineering Development of Year 1 Mule Vehicles

This development includes Charge Depletion Development, Lithium-Ion Battery Development, Battery System Integration, Charger Development, Powertrain Systems Integration, and Vehicle Integration.

Results

Engineering Development of Year 1 Mule Vehicles

The PHEV vehicle development team coordinated the above mentioned development testing working towards final designs. At the end of the Mule Vehicle phase, the vehicle packaging and component designs were nearly production intent.

Conclusions

Vehicle and Powertrain Development

All development was completed to the extent required to meet all required Vehicle Technical Specifications (VTS) requirements. This type of development testing will ensure that the vehicle will meet all Federal Motor Vehicle Safety Standards (MVSS).

Introduction

Engineering Development of Year 2 Integration Vehicles

The second phase of the project captures the second half of the Engineering tasks for the development of key plug-in technologies. This involves the development of components and subsystems required for a PHEV and fully integrate them in a production vehicle.

Approach

Engineering Development of Year 2 Integration Vehicles

This development includes Charge Depletion Development, Lithium-Ion Battery Development, Battery System Integration, Charger Development, Powertrain Systems Integration, and Vehicle Integration.

Results

Engineering Development of Year 2 Integration Vehicles

The PHEV vehicle development team coordinated the above mentioned development testing working towards final designs. At the end of the Integration Vehicle phase, the vehicle packaging and component designs are intended to be production intent.

Conclusions

Vehicle and Powertrain Development

All development was completed to the extent required to meet all required Vehicle Technical Specifications (VTS) requirements. This type of development testing will ensure that the vehicle will meet all Federal Motor Vehicle Safety Standards (MVSS).

Introduction

Battery Thermal Development of Alpha Module

Phase III of the proposed project captures the first half or Alpha phase of the Engineering tasks for the development of a new thermal management design for a second generation battery module.

Approach

Battery Thermal Development of Alpha Module

The engineering team developed a battery module design based on multiple design concepts. Through detailed design and engineering analysis, a module concept was selected. The module performance will be demonstrated through the following testing parameters: thermal, vibration, aging and sealing.

Results

Battery Thermal Development of Alpha Module

The selected battery module prototype parts were procured and testing was started. The concept design was deemed manufacturable, cost effective and performance requirements were met. Design elements are being considered for future applications subject to vehicle packaging constraints and vehicle performance requirements.

III.B.3. Products

Publications

1. Plug-In Charging Symposium (San Jose, CA)—July 22nd, 2008
2. California Air Resources Board (CARB) vehicle demonstration (Milford, MI)—Sept 9, 2008
3. EPA vehicle demonstration (Milford, MI)—Oct 30, 2008
4. Hollywood Goes Green Event—Dec 8, 2008
5. North American International Auto Show (NAIAS)—Jan, 2009

Patents

To date, there have been 25 subject invention disclosures and six patents issued. As the contents of these patent applications are not yet subject to public disclosure, GM respectfully refrains from further disclosure regarding these inventions. GM looks forward to sharing the contents of the patent applications once they are publicly available.

Tools & Data

N/A

TRANSPORTATION ELECTRIFICATION

III.C. Interstate Electrification Improvement Project

Jon Gustafson, Principal Investigator
Cascade Sierra Solutions
4750 Village Plaza Loop
Eugene, OR 97405
Phone: (541) 852-4343
E-mail: jgustafson@cascadesierrasolutions.org

Lee Slezak, DOE Program Manager
Phone: (202) 586-2476
E-mail: lee.slezak@ee.doe.gov

III.C.1. Abstract

This Department of Energy (DOE) demonstration project will accelerate the reduction of petroleum consumption and associated emissions and greenhouse gases by (1) implementing transportation electrification at fifty sites along major interstate corridors and (2) by providing a rebate incentive (up to 20%) for battery operated and/or shore power enabled idle equipment on medium and heavy-duty trucks. Both Truck Stop Electrification (TSE) connections and grid appropriate equipment rebate promotions will be implemented at the travel centers. The project adopted the market title "Shorepower Truck Electrification Project" or STEP project, in March, 2011.

Objectives

- Overall Objectives
  - Identify, finalize selection and secure contracts to build 50 TSE sites.
  - Design and produce build plans for each TSE site.
  - Develop the marketing plan for rebates and introduce the rebate program to the trucking industry.
  - Complete site development by July, 2013.
  - Conduct grand openings at all locations.
  - Distribute all rebates by July, 2013.
  - Monitor utilization.
  - Report on all program component requirements.
  - Manage DOE funding to accomplish program goals.

- FY 2013 Objectives
  - Recruit remaining number of trucks/fleets into the project and complete rebate operations.
  - Identify the remaining sites for development to complete the fifty (50) truck stop power goal.
  - Launch marketing systems to promote utilization with the rebated truck fleets.
  - Form a data collection and analysis alliance with National Renewable Energy Laboratory (NREL).

Major Accomplishments

- Completed rebate incentive awards for 4,482 vehicles.
- Processed 177 adaptor kit applications with 113 kits installations completed and confirmed.
- Administrative procedures and policies were formulated for operating and managing all 50 sites. Local contractor relationships were established to repair and maintain each site.
- Completed inspections at 50 sites and identified a punch list of items for completion and/or correction prior to final contractor payment.
- Completed all infrastructure development
  - Designed and completed system construction at 50 locations on July 30, 2013.
  - Installed system software to operate pedestal power and support data collection on August 30, 2013.
  - Powered all sites by September 23, 2013
  - Commenced data tracking on January, 2013
  - Completed grand opening events at all 50 truck stops.
- Collected 31,100 hours of data on site utilization from Janurary 1, 2013 to September 30, 2013.

Future Achievements

- Stabilize network software and increase system-wide uptime to 95%.
- Support truck stop promotions and retail staff training.
- Finalize data metrics and stabilize data collection to support the final TSE project study.
- Fully support the analysis activities of NREL.
- Promote maximum utilization.
  - Increase power utilization up to a steady 10,000 hours per week system wide.
  - Update software to achieve 95% system reliability targets.
  - Expand participation of independent owner/operators and fleets.

✧ ✧ ✧ ✧ ✧

III.C.2. Technical Discussion

Background

The Department of Energy awarded Cascade Sierra Solutions (CSS) the charge to lead an initiative to develop a large-scale truck stop electrification infrastructure within the United States. The geographic scale of the project was nationwide with a focus on nine trucking corridors that span different regions of the country. Across all corridors, CSS was tasked with facilitating the installation of electrification infrastructure at 50 truck stops to be distributed evenly across the corridors.

The initiative sought to incentivize up to 5,000 truck drivers to purchase and install the equipment necessary to retrofit their trucks to accept electrification connections. The objective of the electrification initiative was to jointly provide truck drivers and truck stops with the necessary infrastructure to power truck cabin amenities with affordable electricity and to reduce or eliminate idling as a truck battery power source.

At present, the adoption of truck stop electrification is hampered by the lack of evidence of profitability for the truck stops; they are reluctant to invest in infrastructure that most truck drivers are not asking for. Truck drivers have different issues: they are unaccustomed to using electric power; or there is not a STEP site along their regular route; or fleet drivers must pay for power out of pocket—diesel is reimbursed but not power. Owner operators express a strong desire to use grid power because their profit margins are so narrow. Their biggest complaint is that there aren't enough sites with grid power.

Proliferation of a robust truck stop electrification infrastructure would provide considerable environmental, economic and even national security benefits for the United States as it reduces the country's dependence on oil and provides a clean power source. These benefits make this project a national priority for the DOE.

Introduction

Three Basic Components

Three program components are necessary to study how and when long distance trucks use electric power during mandated rest periods: rebates, infrastructure construction, and data collection/analysis:

Rebate Program Component

The rebate program produces a study fleet willing and able to use electric power rather than idle the main engine using diesel fuel for cabin power. It incentivizes truck owners to install idle reduction equipment modified for grid power on trucks by offsetting a portion of equipment cost. Truckers apply to CSS for a rebate of 20% of the cost of qualified idle reduction equipment and agree to participate in the program over an 18 month period stopping whenever possible at the 50 truck stops equipped with power pedestals. The program equipment includes diesel Auxiliary Power Units (APU's), battery HVAC systems, cargo cold plate systems, and Truck Refrigeration Units (TRUs).

CSS processes the trucker's rebate application for approval and when approved notifies the truck owner to proceed with the installation. When the unit is installed, the installer submits certified completion documents to CSS which then approves and submits the invoices for DOE rebate funding.

Adaptor Kits are offered to truckers who agree to participate in the program. Installation of an adaptor kit makes the truck grid power capable. Owner operators with older vehicles are enthusiastic about the kits and self install them. Preliminary results alo indicate they are also more likely to use them.

Construction/Infrastructure Component

The construction component creates a source of electricity specifically designed for truck application at a location where trucks typically idle engines for power. Installation of electric power pedestals is intended to give truckers easy access to grid power during mandatory rest periods, especially at outside temperatures above 80 degrees or below 40 degrees.

Shorepower Technologies (SPT) is a manufacturer of Truck Stop Electrification (TSE) equipment in the form of pedestals with multiple electrical outlets, TRU electrical outlet modules and payment kiosks to collect payment and turn the pedestal outlets on and off. SPT was contracted to produce and install the electrification equipment at 50 truck stop sites throughout the U.S. SPT subcontracted with EC Contractors of Portland (EC) for the construction component of the installation.

Data Collection and Analysis Component

The collection and analysis of actual utilization data received from the rebate fleet and other users is the basis of the utilization analysis at the end of the project. This analysis provides insight into the desirability and feasibility of electric power as a substitute for diesel idling power at rest stops.

SPT and CSS collaborate on an internet-based data collection system tied into the STEP pedestals. CSS has an agreement with NREL for NREL to analyze the data and report their analysis each month. This portion of the project began when the first pedestal came on line and began sending data to SPT and CSS in January, 2013.

Data collection is tied to the rebate program where individual owner/operators or fleet drivers provide information about their trucks, their company and their routes driven. Each profiled truck is assigned a unique identification (STEP ID) number. When ordering power at the STEP pedestal, the driver signs in with his/her STEP ID creating a pedestal connection report tied to a specific truck. Over a study period of 18 months, connection reports will be collected in a variety of sample groups and analyzed.

Approach

The three components of the project were divided between CSS and SPT according to background capabilities.

CSS is lead in grant administration, project management and promotion of incentives to trucking companies that choose to save fuel by using grid power.

SPT is the lead in recruiting travel centers to receive power pedestals, manage construction and operate the network to sell power to truckers. SPT also collects connection reports for the database.

CSS qualifies and enrolls trucks into the rebate program, supplying up to 20% of the cost of the equipment acceptable for the project. Once installed, CSS profiles the trucks as to: routes driven; idling history; engine make and model; miles driven; and fuel mileage experienced, and inputs this data into the project database according to the assigned STEP ID number,

Additionally, CSS manages agreements with a group of equipment manufacturers/installers whose equipment on board trucks makes use of electric power. Each of these manufacturers (or their dealer) entered into agreements to take the incentive payment along with the trucker's payment for the purchase and installation of the equipment, thereby reducing the price paid by the trucker to acquire the equipment.

For actual site construction SPT selected an electrical contractor with the capacity to operate across the U.S., finding local subcontractors to do the actual work. EC Contractors of Portland, OR provided detailed construction design engineering services and permitting on all the sites. EC competitively bid work locally and insured that federal rules were followed by all sub-contractors. When work was completed, EC commissioned the sites and performed operational tests prior to site acceptance by SPT and CSS.

SPT located fifty (50) sites having a history of 100 long haul trucks parked there overnight. After five year lease agreements were completed at each of the 50 sites, a construction plan and local sub-contractors were assembled to complete site development. Each site was inspected, and its completion celebrated with a grand opening.

With 50 sites developed and 4,482 trucks ready for grid power, utilization is ready to be measured and analyzed. The metrics kept for each truck connection include: hours plugged in, kilowatts of power drawn, date and location of use, purchase cost, and outside temperature and weather conditions. The data analysis will characterize the study fleet by average use of grid power, by truck type, site location, time of year, outside weather conditions, and duty cycle.

Results

Construction and Infrastructure

Status

All major site construction was completed in this quarter. There are three priorities now being addressed:

(1) Correcting deficiencies in pedestal protection (bollards, barriers) to prevent damage to power pedestals and power panels from trucks backing into parking spots;

(2) Constructing railings and removing trip hazards to increase user safety;

(3) Managing and addressing a punch list of items to be corrected that were discovered during site inspections.

Accomplishments in 2013

All 50 STEP sites were inspected. In Q4, site acceptance inspections were completed at five site locations in Maryland, two in Virginia, three in New York and two in Texas.

With 765 total items on the current punch list, 73% have been resolved. For eleven sites, all punch list items were completed and/or resolved.

Plans for resolution

Construction documentation comprises the largest portion of the punch list at this time. CSS will continue to collaborate with SPT to support, manage and monitor repairs. CSS will continue efforts to verify SPT's efforts independently through contacts with host site personnel.

Operations and Management

Status

Administrative procedures and policies are now in place for operating and managing all 50 sites; local contractor relationships are being established for the repair and maintenance of the sites. Contractors are also being trained to troubleshoot and repair the IT network. SPT is communicating with host sites with chronically low power utilization and network problems. SPT is taking corrective actions remotely or via local contractors.

Accomplishments in 2013

The New York Energy and Research Development Authority (NYSERDA) funded a $200,000 construction match for three sites in New York.

Challenges

Based on inspections, multiple sites have limited protection for pedestals and power panels and pedestal access needs to be improved. Power pedestals and power panels need to be protected from impacts due to trucks backing into parking spaces and hitting them. Trip hazards, standing water, and pedestals located on terrain that slopes away steeply need correction.

Plans for resolution

CSS has made a commitment to correct pedestal protection and user safety regardless of cost or code requirements even in instances where damage has never occurred before. CSS identified and detailed a list of requirements supported by cost estimates and photographs. SPT is now in negotiations with EC Construction to correct items for which EC is contractually responsible.

CSS is managing all of the construction-related documents and determining how to limit liability and designate responsible parties for future construction problems/issues. CSS is currently obtaining the appropriate documents or signatures, etc., for final construction close out.

Power Network and Information System

Current Status

The SPT network operating system is maturing but each geographical location presents unique challenges. Data that is recorded and tracked are: kiosk uptime, connection point uptime, KWH, customer profile and system stability. Customers currently purchase power online or through a payment kiosk at most locations or call an answering service to activate a connection point remotely. There are four different payment options: COMDATA (fleet card), SPT gift card, authorize.net, and SPT promotional opportunities.

Accomplishments in 2013

The software and the hardware have been overhauled to make improvements based on driver feedback which is now taken into consideration and factored into the next engineering phase.

For system stability, a virtual server was set up in the cloud to facilitate all incoming transactions from kiosks and to host web sites for public access.

Challenges

At multiple sites, there have been kiosk-to-connection point and kiosk-to-server communication problems. Each of these is increasingly difficult to monitor, identify and diagnose from a remote location without local SPT staff on-site.

Plans for resolution

The following steps toward resolution are underway and beginning to show positive results:

(1) A full-time technician remotely monitors each site and each connection point and also travels to sites for service calls when needed. When possible, suitable contractors near site locations are being identified and trained on technical aspects of the system and dispatched for service calls as needed.

(2) Stability data trends are being analyzed to find software bugs and/or hardware faults. SPT uses identical equipment/software that is tested in SPT's own shop to duplicate and correct problems. Rigorous testing is being conducted on each of the pedestal stations to ensure they are operational and indices are in bounds.

Data Collection and Analysis

Rebate Distribution

CSS completed the awarding of 4482 STEP rebates in April, 2013. An additional 28 approved rebates are awaiting final submission and acceptance of documentation.

Status

The breakdown of all rebates by equipment technology (inclusive of currently approved projects) is listed in Table III-2 and shown in Figure III-2:

Table III-2 Rebates by Equipment Technology.

Technology	# of Rebates
Battery HVAC	1,776
APU Units	1,472
TRU Units	258
Cold Plate Units	202
Evap Coolers	60
eHybrid TRU	571
Adaptor kits	143

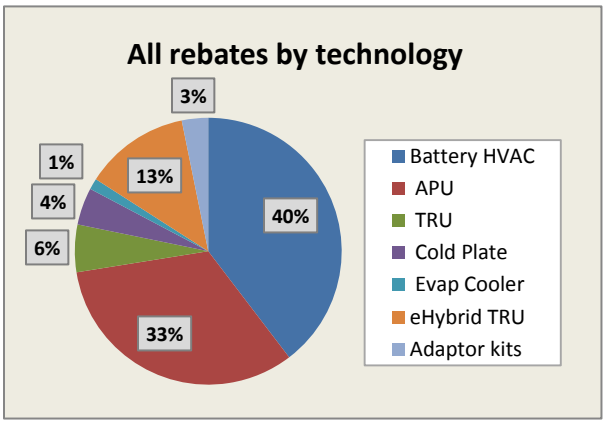

Figure III-2: All Rebates by Technology.

STEP IDs were assigned to an additional 382 vehicles that did not receive rebated equipment this quarter. These were for a large fleet that is collaborating with CSS on a separate case study for the final report. STEP IDs were also assigned to 177 vehicles that received adaptor kits, which were also profiled in the STEP database. Of these, 113 kits are confirmed installed and/or used.

As of this report, utilization data has been reported from 62 SPT sites. This includes all 50 STEP project sites and SPT non-STEP locations. On a weekly basis the number of STEP sites with utilization was 20-25 on average with a low value of 16 sites and a high value of 30 sites.

STEP ID Use:

- 82 power transactions at all SPT sites with STEP IDs during Q4
- 67 were at STEP truck stop locations (Q3 had 43, with 38 at STEP sites)
- 38 unique named users, 3 anonymous users
- 19 repeat users
- 10 repeat users with 3 or more sessions
- total connect time–1,185 hrs
- total KWH used–707.94
- session length: (avg KWH use)—average session length—14.45 hrs

less than 10 hrs:	28	(3.67 KWH)
10-20 hrs:	40	(7.02 KWH)
21- 48 hrs:	11	(23.7 KWH)
longer than 48 hrs:	3	(insufficient data)

Challenges

The use of a free power offer at the STEP sites to incentivize utilization was discontinued during the quarter, expiring at the end of August. However, the impact of the free power offer on utilization levels was not discernible in the previous utilization data or in other feedback from rebated companies and drivers.

Distribution of STEP IDs to drivers in some fleets has been fragmented, incomplete or not done. Follow-up with rebate recipients after STEP ID packets are mailed has revealed the mail recipient is often not the contact for distributing STEP IDs. Confirming that STEP IDs are received

and distributed and drivers are encouraged to use them is an ongoing process subject to delays and confusion

For drivers who have received STEP IDs, software glitches and connectivity issues when ordering power has been inconvenient, time-consuming or sometimes not even possible. This discourages drivers from using the system.

The AnswerNet service that connects power by phone has been inconsistent. Issues include failure to solicit STEP IDs in the sign-up and difficulty capturing a user profile and starting a power session. These difficulties have negatively influenced drivers' willingness to use pedestal power.

Plans for Resolution

CSS is examining customer records to find those with STEP IDs who are not using power and CSS is supplying their contact information to Alan Bates of SPT. He uses this data in his outreach to users to encourage continued STEP ID use.

Graphic Analysis

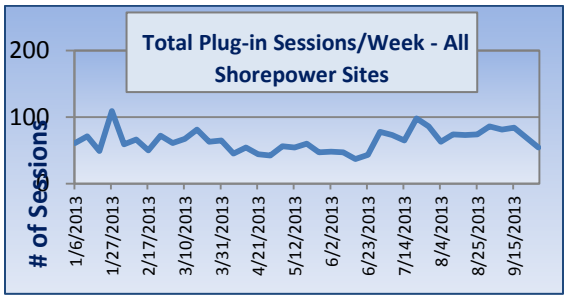

Figure III-3: Total Plug-in Sessions per Week.

Income from power sessions at the pedestals rose by almost 50% in Q4 (Figure III-4). The expiration of any free power offers for STEP ID users would seem to be a major factor. But the use of STEP IDs when free power was available did not occur so a causal relationship cannot be assumed. It is more likely the increased use is a response to the heat of summer and this is responsible for the increase in income.

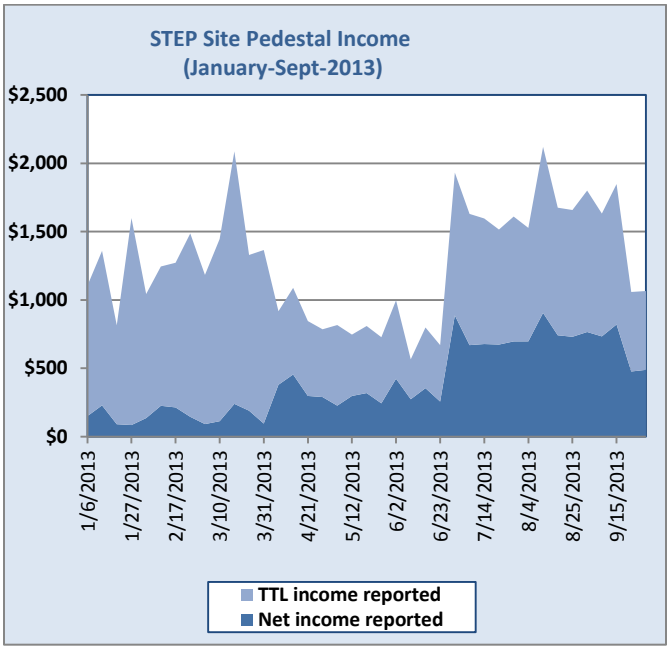

Figure III-4: STEP Site Pedestal Income.

Utilization records come from all sites (totals given as Figure III-3), 50 STEP sites and 12 additional non-STEP sites. Utilization at the STEP sites continues to account for about 80% of the total. Even though only about half of the 50 STEP sites have utilization records on a weekly basis, the 80%-20% split remains consistent. About 80% of all sites are STEP sites, suggesting the overall visitation pattern across the network is relatively constant.

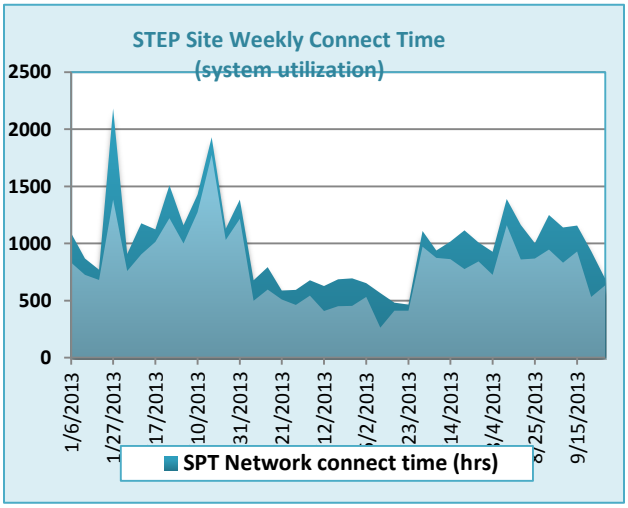

Figure III-5: STEP Site Weekly Connect Time.

Average plug-in sessions lengths that were increasing at the end of Q3 (late June) continued to rise slightly through July and August, reflecting the higher use of a/c equipment during hot summer weather. Figure III-6 shows that Power use and session length both peaked during Q3 in mid-August exhibiting a strong connection to the highest ambient temperatures of the calendar year before trending lower with the onset of more moderate conditions in September.

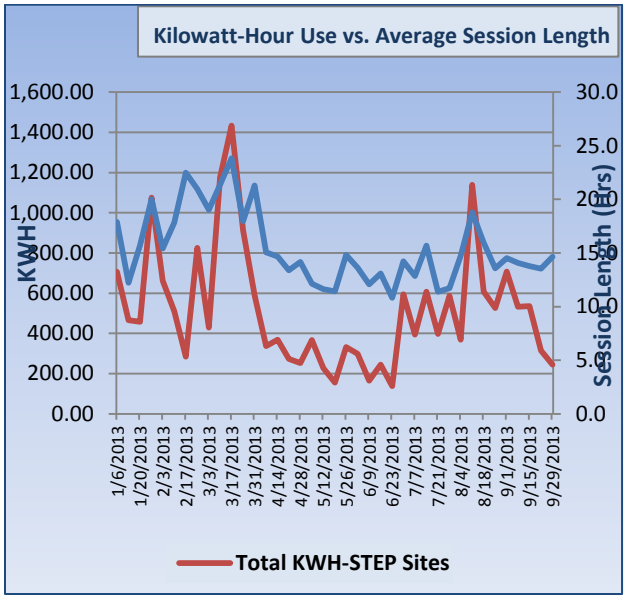

Figure III-6 Power Use and Average Plug-In Session Length.

Power Use and Cost of Power

Based on the utilization records, over 25,000 KWH of power has been reported to date. Challenges mentioned above impact power use but KWH has increased over 40% during the fourth quarter. Average Power Costs for Shorepower and STEP sites is provided in Table III-3 Power Costs and Power Use.

Table III-3 Power Costs and Power Use.

4/1/2013–6/30/2013	Connect time (hrs)	KWH used	Total cost	Cost per hour	KWH per hr
All Shorepower sites	8,636	4,878	$6,818.00	$0.79	0.56
STEP sites	6,562	3,790	$1,482.72	$0.23	0.58

CSS will identify 2-5 fleets from each of the major equipment technology categories for a more targeted analysis of how STEP rebated equipment is used. These fleet case studies will reveal more about how the equipment reduces fuel consumption. One fleet has already been identified for a study: Mesilla Valley Transportation of Las Cruses, New Mexico.

GOAL: Increase the response rate to 25% to collect more data on the size and composition of the rebated vehicle fleets; contact all fleets receiving 20 or more rebates.

Conclusions

At the end of the third year of the four year project, all sites have been developed and commissioned. A fleet of 4,482 trucks have been recruited and equipped with electrically powered devices, and 177 drivers have received adaptor kits, which will demonstrate use of grid power to displace diesel. In the last year of the project, researchers are prepared to document actual use of grid power to displace petroleum as an energy source for trucking.

III.C.3. Products

Publications

Project publications to date are limited to promotional literature and operational guides.

Patents

No patents have been filed with this project.

Tools and Data

Not used.

III.D. RAM 1500 Plug-In Hybrid Electric Vehicle

Abdullah A. Bazzi, Principal Investigator
Chrysler Group LLC
800 Chrysler Drive
Auburn Hills, MI USA 48326-2757
Phone: (248) 944-3093
E-mail: aab5@Chrysler.com

Lee Zlezak, DOE Technology Development Manager
Phone (202) 586-2335
E-mail: Lee.Slezak@ee.doe.gov

John Jason Conley, NETL Project Manager
Phone: (304) 285-2023
E-mail: John.Conley@netl.doe.gov

DOE Award Number: DE-EE0002720
Submitted to: U.S. Department of Energy–National Energy Technology Laboratory

III.D.1. Abstract

Phase I Project Objective

- Demonstrate 140 pickup trucks in diverse geographies and climates, spanning across the United States, and a range of drive cycles and consumer usage patterns applicable to the entire NAFTA region
- Verify plug-in charging mode performance based on charger and battery model
- Verify AC power generation mode
- Prove product viability in "real-world" conditions
- Develop bi-directional (communication and power) charger interface
- Support the creation of "Green" Technology jobs and advance the state of PHEV technology for future production integration
- Develop an understanding of Customer Acceptance & Usage patterns for PHEV technology
- Quantify the benefits to customers and to the nation

Phase II Project Objective

- Advanced Li-Ion batteries demonstrated an unexpected degradation rate which required a directional change using a new cell design built into new packs
- Demonstrate the viability of the high voltage energy storage system with a new cell technology for a new production application
- Test advanced Li-Ion Battery technologies, charging systems, Reverse Power Flow (RPF), and Electrified Powertrain Control Systems
- Demonstrate 24 pickup trucks in diverse geographies and climates

Major Accomplishments

Vehicle Build & Test

- Deployed Ram 1500 PHEVs were returned to Chrysler Group LLC.
  - The returned vehicles completed an inspection and work to integrate the upgraded high voltage battery into the vehicles continued
- Completed design freeze for long lead items on February 4, 2013
- Completed the critical design review for the high pack systems on March 4, 2013
- Continued to work on two issues observed in the field, transmission main shafts and internal communication faults
- Development activities for the upgraded battery pack remain on-track. Cell design was completed and the cells are being shipped for module development and battery pack characterization
- Completed Validation Trip from Las Vegas to Denver September 23rd through October 1st of 2013
  - Performed real world validation of test cell work (hot, cold, altitude, grades, towing)
  - Verified consistent SOC reporting of Magna battery pack performance
- Completed five technology and supplier assessment, directional setting, and testing & integration of Phase II Battery Upgrade
- Successfully demonstrated Reverse Power Flow and A.C Power Generation at the launch of the Smart Grid Interoperability Center at Argonne National Laboratory in July 17, 2013
- Achieved DOE Annual Merit Review Results greater than the average across all of the scored categories; approximately by one standard deviation

Deployment Fleet Activities

- Set up available test time in October at CTC and CPG to conduct a fuel economy test on the Ram 1500 PHEV to establish EAER-10, as it relates to the California Exhaust Emission Standards and Test Procedures
- Completed Reverse Power Flow (RPF) rollout prior to the deployment vehicles being returned to Chrysler Group LLC.
- Reverse Power Flow will be activated during Phase II and re-validated with the Phase II packs
- Smart Charging will be activated during Phase II and MPRs will be installed
- Development and feature optimization to continue at Chrysler Group LLC

Future Activities

- Capture vehicle fleet data to support calibration and controls development to increase fuel economy
- Updated RPF feature to be included in 10 of the vehicles that are redeployed

III.D.2. Technical Discussion

Introduction

The Chrysler Product Creation Process (CPCP) defines the strategy and method used to execute the development of world class vehicles from concept to market. The RAM 1500 PHEV is following the CPCP process. Fundamental principles include:

- Voice of the Customer–Dictates product decisions
- Timeline Compression–Enables speed to market
- Flexibility–Allows for unique vehicle program characteristics
- Consistency of Execution–Facilitates continuous improvement
- Clear Performance Indicators–Drives accountability
- Interdependencies Identified–Aligns activities across functional areas

Vehicle Decommissioning Strategy for RAM 1500 PHEV

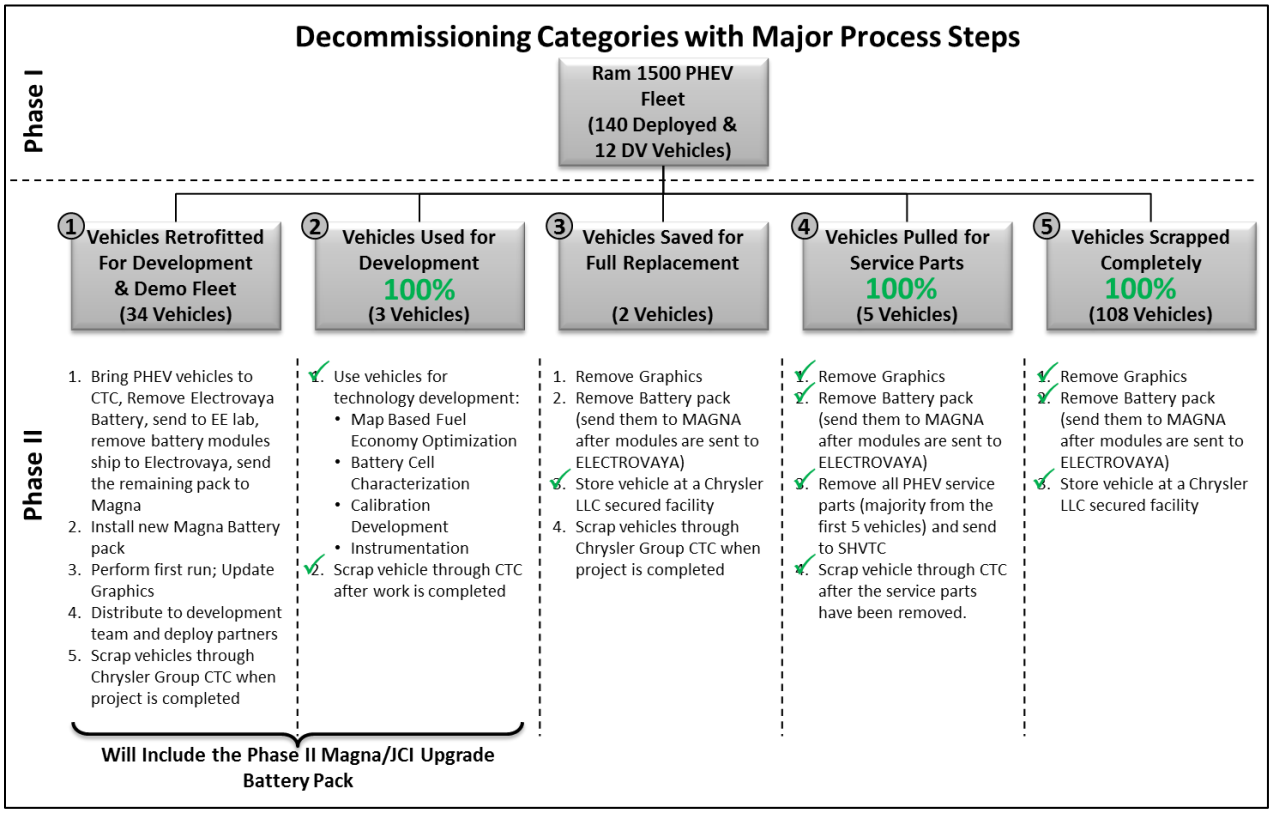

Figure III-7: RAM 1500 PHEV Decommissioning Categories with Major Steps.

Results

Federal Test Procedure Results

Table III-4: RAM 1500 PHEV Federal Test Procedure Results.

Objective	Target	Status	Procedure	R/G/Y
RANGE	EAER 10	EAER 14 (Based on simulations)	California Exhaust Emission Standards And Test Procedures, as amended December 2, 2009	GREEN

Ram 1500 PHEV Fleet Redeployment

PartnerIn	# of Vehicles	Contract Status	Features Included			Phase II Equipment			Feature Set Status
			Smart Charging	Reverse Power Flow	Map Based Fuel	EVSE MPR	ALG	Gateway	
SMUD	5	Approved	Yes		Yes	7	3	0	Map Based Fuel Economy: • Phase II will use Phase I's implementation. Hardware installation required during vehicle preparation Reverse Power Flow: • Will be activated during Phase II. Phase I implementation will be used during Phase II. Will have to be re-validated with the Phase II pack. See Appendix for details Smart Charging: • Will be activated during Phase II. MPRs will be installed during vehicle preparation. Status of feature to follow • 24 PHEVs with Smart Charging feature • 12 PHEVs with Map-Based Fuel Economy feature • 10 PHEVs with Reverse Power Flow feature
			Yes						
			Yes						
			Yes	Yes					
			Yes	Yes					
Detroit Edison	5	Approved	Yes		Yes	5	0	3	
			Yes	Yes					
			Yes		Yes				
			Yes		Yes				
			Yes	Yes					
Duke Energy	5	Approved	Yes		Yes	2	0	0	
			Yes		Yes				
			Yes		Yes				
			Yes	Yes					
			Yes	Yes					
Tri-State	3	Approved	Yes	Yes		3	0	2	
			Yes		Yes				
			Yes		Yes				
National Grid	2		Yes		Yes	3	3	0	
			Yes		Yes				
CenterPoint Energy	2		Yes	Yes		2	1	0	
		Approved	Yes		Yes				
EPRI	1	In Process	Yes	Yes		1	1	1	
EPRI / ANL	1	In Process	Yes	Yes					
Chrysler	10	N/A		Yes	Yes	12	12	9	
Totals	**24**		**24**	**11**	**13**	**35**	**20**	**15**	

Figure III-8: RAM 1500 PHEV Deployment Partners slated for Phase II.

Conclusions

Decommissioning process for removal of PHEV service parts and vehicle scrapping has been completed for all vehicles. Retrofit of Magna batteries in Partner Vehicles and CTC DV Vehicles are on schedule towards completion. RAM 1500 PHEV replacement fleet replacement contracts and vehicles shipments to partners have been completed.

- Sacramento Municipal Utility District (SMUD) in California—5 vehicles
- Detroit Edison—5 Vehicles
- Duke Energy in Charlotte North Carolina—5 Vehicles
- Tri-State—3 Vehicles
- National Grid placed vehicles in New York—2 vehicles
- Centerpoint Energy, Houston, Texas—2 vehicles
- EPRI (North Carolina and California)—2 vehicles
- Chrysler Group LLC—10 vehicles

III.D.3. Products

Publications

1. A High Efficiency Low Cost Direct Battery Balancing Circuit Using A Multi-Winding Transformer with Reduced Switch Count. IEEE APEC 2012, Orlando, FL, Feb. 5–9, 2012
2. Hybrid / Plug-in-Hybrid Technology Overview—Torque Feed forward Control for IPM Motors

Public Presentations

Annual Merit Review. Washington, D.C.

Patents

None to Report.

Tools & Data

1. Vector Cantech—Canalyzer equipment utilized for data collection and software development (communication between vehicle controllers)
2. ETAS—Equipment utilized for software development and drivability / emissions calibration
3. Security Inspection utilized for upgraded infrastructure environment (increased bandwidth requirements and storage requirements) for implementing Microstrategy vehicle logging and data analysis
4. Bright Star Engineering—Data Recorder Modules (DRM) for each vehicle and monthly cellular access

III.E. ChargePoint America

Richard Lowenthal, Principal Investigator
ChargePoint, Inc.
1692 Dell Avenue
Campbell, CA 95008
Phone: (408) 841-4501
E-mail: Richard.Lowenthal@chargepoint.com

Lee Slezak, DOE Technology Development Manager
Voice: (202) 586-8055
E-mail: Lee.Slezak@ee.doe.gov

John Jason Conley, NETL Project Manager
Phone: (304) 285-2023
Email: John.Conley@netl.doe.gov

III.E.1. Abstract

Objective

- CHARGEPOINT® AMERICA will demonstrate the viability, economic and environmental benefits of an electric vehicle charging infrastructure. With the arrival of electric vehicles (EVs) and plug in electric vehicles (PHEVs) late 2010, there is a substantial lack of infrastructure to support these vehicles. CHARGEPOINT AMERICA will deploy charging infrastructure in ten (10) metropolitan regions in coordination with vehicle deliveries targeting those same regions by our OEM program partners: Chevrolet, BMW, THINK, Nissan, CODA, Fisker, Tesla, Ford and smart USA. The metropolitan regions include Austin/San Antonio (TX), Bellevue/Richmond (WA), Boston (MA), Southern Michigan, Los Angeles (CA), New York (NY), Orlando/Tampa (FL), Sacramento (CA), San Francisco/San Jose (CA) and Washington (DC). CHARGEPOINT AMERICA will install more than 4000 Level 2 (220V) SAE J1772™ compliant, UL Listed networked charging ports in home, public and commercial locations to support more than 2000 program vehicles. ChargePoint will collect data to analyze how individuals, businesses and local governments are using their vehicles. Understanding driver charging behavior patterns will provide the DOE with critical information as EV adoption increases in the United States. Deployment of the charging station infrastructure has begun in July 2010.
- The project will provide public and private Level 2 charging ports from which data will be collected and forwarded to INL for compilation and analysis. The project will leverage other company efforts and infrastructure. The project is also working with the local press to expand awareness and receptivity. The first phase of the program, which began in June 2010, involved the deployment of the charging stations. Phase 2 will have a two-year duration, during which time data will be collected concerning the times of highest charging, charging rates, and load on the grid.

Major Accomplishments

- We are extremely pleased with the progress of the program and met the 2000 program vehicles milestone and installed more than 4600 charging ports. We are fully allocated our supply of charging ports and are no longer accepting applications for free residential and public charging ports.
- ChargePoint America program deployed over 4600 charging ports.
  - Installed public and residential charging ports over 4600
  - Met 2000 program vehicles milestone
- 100% of Public charging ports are deployed.
- 100% of Residential & MDU ports are deployed.
- In June 2013, ChargePoint, Inc. announced the completion of its ChargePoint America Program with more than 4600 shipments and installations of its home, public and commercial charging ports for electric vehicles (EVs).

Future Achievements

ChargePoint is planning to wrap up the program and will continue with data collection and reporting until the end of the program.

- Data collection and reporting will continue and data will be uploaded to INL on a regular basis.
- INL will continue to provide CPA reports.

✧ ✧ ✧ ✧ ✧

III.E.2. Technical Discussion

- All charging stations data is regularly forwarded to Idaho National Labs for analysis and summary. INL released first report on ChargePoint America program in November 2011. The vehicle charging infrastructure summary report provides information on:
  - Charging unit by state
  - Charging units installed to date
  - Number of charging events performed
  - Charging unit usage by type (residential, commercial and public stations)
  - Electricity consumed (AC MWh)
  - Percent of time with a vehicle connected

  - Percent of time with a vehicle drawing power
  - Charging availability
  - Charging demand
- Commercial and Residential EVSE report:
  - Number of charging events
  - Charging energy consumed
  - Percent of time with a vehicle connected to EVSE
  - Percent of time with a vehicle drawing power from EVSE
  - Average number of charging events started per EVSE per day
  - Charging availability
  - Charging demand
  - Average length of time with a vehicle connected per charging event
  - Average length of time with a vehicle drawing power per charging event
  - Average energy consumed per charging event

Detailed ChargePoint product information can be found at ChargePoint Products.

Sample ChargePoint customer list can be found at: ChargePoint Ecosystem.

III.E.3. Products

Patents

We did not file any patents using DOE funds

Figure III-9 Map of all the publicly available charging spots.

III.F. Recovery Act—Strategy to Accelerate U.S. Transition to Electric Vehicles (DE-EE0002628)

Mr. Greg Cesiel, Principal Investigator
General Motors
30001 Van Dyke Avenue
Warren, MI 48090
M/C: 480-210-420
Phone: (586) 575-3670
E-mail: greg.cesiel@gm.com

Lee Slezak, DOE Technology Development Manager
Phone: (202) 586-2335
E-mail: lee.slezak@ee.doe.gov

Jason Conley, NETL Project Manager
Phone: (304) 904-7590
E-mail: John.Conley@netl.doe.gov

III.F.1. Abstract

Objective

Overall Objectives

- The objective of this project is to develop Extended Range Electric Vehicles (EREV) advanced propulsion technology and demonstrate a fleet of EREVs to gather data on vehicle performance and infrastructure to understand the impacts on commercialization while also creating or retaining a significant number of jobs in the United States. This objective will be achieved by developing and demonstrating EREVs in real world conditions with customers in several diverse locations across the United States and installing, testing and demonstrating charging infrastructure.

FY2013 Objectives

- In 2013, we continued the project demonstration leveraging the unique OnStar telematics platform, standard on all Chevrolet Volts, to capture the operating experience that will lead to better understand of customer usage. The project utility partners completed the installation of charging infrastructure that allows the demonstration and testing of charging infrastructure located in home, workplace and public locations. Thus providing a better understanding of installation issues, customer usage and interaction with the electric grid. In 2013, we continued to work with the Volt owners at the electric utility company participants and continued to gather data for the demonstration portion of this project.

Major Accomplishments

- Customer usage of demonstration fleet maintained
- Regular data delivery to Idaho National lab continues
- Quarterly reports continue to be published by Idaho National Lab
- All utility and residential charging stations installed by January 2013
- OnStar smart charging demonstrations continue
- Battery to Grid demonstration completed
- Fast Charging demonstration with Home Plug Green PHY
- DIN communication standard published and an errata was released in January 2013

Future Activities

- Continue smart Charging OnStar demonstrations to exhibit capabilities with various utilities
- Continue to demonstrate Application to show vehicle and home energy consumption at PecanStreet.org subdivision
- Continue to collect data from demonstration vehicles across the United States
- Utilize first generation vehicle information to refine the technology and enhance adoption of the second generation technology into the marketplace

✧ ✧ ✧ ✧ ✧

III.F.2. Technical Discussion

Introduction

Smart Charging

The capability to identify and manage electric vehicle charging loads through OnStar and Power Line Communications (PLC) will be developed and demonstrated. This technology will support managing interaction with the electric grid using the current grid infrastructure.

Approach

Smart Charging

OnStar's task is to design, develop and implement smart charging to interface with utility systems.

The PLC portion will design, develop and implement the interface that enables communication between a smart meter and the vehicle.

Results

Smart Charging

OnStar has been actively participating in SAE, OpenADR, IEEE and IEC standards for developing Telematics based smart charging standard and leading SAE PEV Hybrid taskforce group J2836/5 dealing with customer facing smart charging solutions. GM/ OnStar have worked with other Automakers to create an OEM server concept. The idea is that most Automakers agree on the best approach to interface our respective Electric Vehicles with the Utility industry.

2013 work completed surrounded the assembly of our second and third demonstration benches. The second bench incorporates Smart Energy Profile (SEP) 1.0 messages using a variety of input methods. A Utility can communicate directly to the Itron meter or the Zigbee module (if they use their own meter) and connect to the homeplug PLC module. The messages are then translated to the communication protocol (CAN) used in the electric vehicle simulator. This bench provides direct communication from the Utility and also includes a Utility simulator if necessary. The third bench utilizes the Utility configuration from the second bench, a communications path has been established with an Itron meter and work is ongoing to have this as an additional communications path, providing a SEP 1 message that will be converted via a modified Dreamplug module to SEP2 and transferred through the MPRs. Modification of the Vehicle software has commenced to support the new hardware configuration combining the two screens of information to a single laptop computer that is located in the vehicle.

Introduction

Fast Charging

Charging an EV battery in less than 30 minutes provides additional opportunities for the customer to fuel with electricity and increase petroleum displacement. Fast charging shall support development of standard electrical and communication interfaces between the EV and the charger and increase the understanding of the vehicle and grid impacts of fast charging.

Approach

Fast Charging

This approach starts with the development of a standard DC connection interface and communication standard for fast charging; this includes integration of this into a vehicle. From here, the demonstration period will be utilized to collect and analyze data to study grid impacts, vehicle impact, thermal management, charging profiles, user ergonomics and efficiency.

Results

Fast Charging

The fast charge development team completed tasks for internal development as well continuing to provide feedback to the standards community.

GM continues to work with suppliers developing the SAE combo standard and have confirmed interoperability with six EVSE suppliers. Vehicles continue to be fast charged on a daily basis exercising both the hardware and communications.

Two separate test events were held using the DC fast charging “Combo” standard to ensure customer satisfaction. The first event was held in the U.S. with GM and BMW as the participating OEM’s. Charge station suppliers Eaton, Aker Wade, IES Synergy and ABB provided charge stations for the event. In June, a follow up event was held in Europe with BMW, VW and GM. Charge station suppliers IES Synergy, ABB, EVtec and Efacec participated in this event. Following both events GM is confident that there are DC Fast Charge Stations from several suppliers that will allow an electric vehicle to charge 80% in 20 minutes.

The fast charge development team completed several significant milestones in the 3rd quarter of 2013. The first was submission of the final DIN communication standard to be published. This was done after several months of collaborative work including two joint testing sessions with BMW and VW. The second milestone was the installation and grand opening of the first public SAE Combo DC fast charging station in San Diego, California. The station is installed in a high traffic mall parking lot and had a public demonstration of SAE charging on September 30th.

Introduction

Battery to Grid

The increased demand for stationary energy storage on the electric grid to enable renewable energy sources and reduce infrastructure stress through load management is an opportunity to extend the usage of automotive batteries. This task will study the technical challenges of automotive battery reuse for grid storage and demonstrate this application.

Approach

Battery to Grid

This task studies the stationary energy storage requirements and compares them to battery capabilities following vehicle use. In order to demonstrate battery to grid functionality, a grid-tied bidirectional power converter with a battery pack will be utilized. Communication requirements for grid to storage systems shall be developed to provide dispatched power capability. A demonstration period will collect and analyze data to study the grid and battery impacts of bidirectional power flow.

Results

Battery to Grid

This task was complete on December 31, 2012. The BMC (Bi-Matrix Converter) demonstrated both charging and inverter mode. Battery operating voltages inputs up to 430V were demonstrated. The concept successfully demonstrated functionality for battery to grid using a single converter. Commercialization of the technology though will greatly be affected by the development of reverse blocking semiconductor switches, e.g., RBIGBT's.

Introduction

Second Generation Volt

The RESS development shall focus on key battery systems and components. The development shall be completed to established levels of enhanced performance consistent with conventional production RESS requirements, including but not limited to, operating environment, duty cycle, and durability. To effectively demonstrate an improved implementation to the marketplace, measurable targets will be utilized.

Approach

Second Generation Volt

To effectively demonstrate an improved implementation to the marketplace, measurable targets are being utilized. The established targets are:

- 20% reduction in cost
- 10% increase in volumetric density
- 10% increase in gravimetric energy density

Results

Second Generation Volt

Our second generation battery results demonstrate an improved implementation by a reduction in cost, an increase in volumetric density and an increase in gravimetric energy density. The engineering team continues to work towards these targets.

III.F.3. Products

Publications

Idaho National Laboratory website; listed under “General Motors Chevrolet Volt Vehicle Demonstration”—aggregated data report http://avt.inel.gov/evproject.shtml.

Patents

To date, this demonstration program has not generated any subject inventions or made any related patent filings.

Tools & Data

Driving and charging data is being transferred from the vehicles via the OnStar telematics to the OnStar lab. OnStar personnel receive the data and process it appropriately for transfer to Idaho National Labs. The following data is a list of what is collected by OnStar and transferred to Idaho National Lab:

All trips combined:

- Overall fuel economy
- Total number of trips
- Total distance traveled
- Average ambient temperature
- Vehicle maintenance records

Trips in charge depletion mode:

- Fuel economy
- Number of trips
- Percent of trips city/highway
- Distance traveled
- Average trip aggressiveness (scale of 0-10)
- Percent of total distance traveled

Trips in both charge depletion and charge sustaining mode:

- Fuel economy
- Number of trips
- Percent of trips city/highway
- Distance traveled
- Average trip aggressiveness (scale of 0-10)
- Percent of total distance traveled

III.G. Smith Electric Vehicles Medium Duty Electric Vehicle Demonstration Project (EE0002614)

Robin J.D. Mackie, Principal Investigator, President & Chief Technology Officer
Smith Electric Vehicles U.S. Corp.
12200 N.W. Ambassador Drive, Suite 326
Kansas City, MO 64163
Phone: (816) 243-1611
E-mail: robin.mackie@smithelectric.com

Lee Slezak, DOE Technology Development Manager
Nicholas D'Amico, NETL Project Manager
Phone: (412) 386-7301
E-mail: nicholas.damico@netl.doe.gov

III.G.1. Abstract

Objective

- The objective of the SEV-U.S. Demonstration Project is to obtain performance information from an All Electric Vehicle (AEV) fleet to accelerate production, reduce costs, enhance the technology, and procure early acceptance of AEV's in the U.S. commercial vehicle marketplace.
- Smith will demonstrate 500+ electric vehicles based on the Newton medium duty platform. The vehicles will be placed in locations including California, Missouri, Ohio, Michigan, Washington, DC, New York, and Texas. A Generation II Newton platform will be developed during the project utilizing the performance data collected. The development of this platform will enable the Company to reduce cost, expand the vehicle range from class 4 through 7, and make additional improvements in powertrain and battery technology. It is intended that the base vehicle platform be applied to both shuttle bus and step-through van applications.

FY2013 Objectives-

- Deploy to customers the remainder of the 500+ vehicle fleet.
- Continue to expand and upgrade Smith Link providing data to:
  1) NREL
  2) Smith service
  3) Smith engineering
  4) Selected Smith customers.
- Sales & Marketing:
  1) Expand the market boundaries to support the overall fulfillment of the DOE objectives.
  2) Continue to establish the Smith brand as the pre-eminent supplier of Zero Emission Electric Commercial Vehicles.
  3) Continue to develop our route analysis capabilities to provide more comprehensive duty cycle studies enabling customers to better manage the battery capacity to the required customer applications.
  4) Continue development of Smith's service capabilities including infrastructure definition, pre delivery training, vehicle handover and post-deployment driver training and optimization to ensure the customers gain the maximum benefit from their vehicles.
- Operationally:
  1) Continued recruitment and cross-discipline training of assembly staff,
  2) Continued expansion of the service team and resources to meet customer deployment plans,
  3) Continuous improvement of Gen 2 Newton and Stripped Chassis platforms.
- Supply Chain:
  - Continue the development of the supply chain to support engineering activities, production requirements for Gen 2 systems, cost down activity, and to meet the "Buy America" criteria.
- Engineering:
  1) Addition of a long wheelbase version of the step van to accommodate the laundry and uniform markets,
  2) Expansion of Smith Power to augment our 80 kwh battery configuration with 60, 100 and 120 kwh alternatives allowing Smith to match battery capacity to customer requirements, and to develop, test, validate and produce a prismatic cell system that enables Smith to utilize additional battery chemistries and vendors.
  3) Continued development of the school and shuttle bus platforms.
- Quality:
  - Maintain and strengthen ISO standards implementation and documentation.
- Finance and Administration:
  1) Continued development and maturation of internal administrative processes, including strengthening the enterprise software, and further developing written internal accounting and operating policies.
  2) Comply with all project reporting requirements for the DOE and ARRA.

- Corporate:
  1) Fund raising to support ongoing development and company growth.
  2) Develop different and appropriate business relationships to support entry into multiple countries within the global market where there is identified latent demand for AEVs.

Major Accomplishments

- Deployed to customers 439 of the 500+ vehicles under the Participation Program through September 30, 2013
- Continued to reliably deliver data to NREL and received back NREL's initial feedback reports of operating data.
- In collaboration with key customers continued to develop the Smith Link portal, improving reliability and providing enhanced data internally to both engineering and service teams.
- Delivered 5 vehicles to TARDEC retrofitted with full bi-directional charging/discharging capabilities.
- Sales & Marketing:
  1) Continued to expand the customer base and received significant re-orders from initial launch partners.
  2) Continued to participate in local, national and international conferences to support awareness creation for commercial AEV's.
- Operations:
  1) In Q4 completed the introduction and successful testing of the bi-directional (V2G) systems in the 5 vehicles sold to TARDEC at Ft. Carson, CO. in conjunction with the SPIDERS program.
  2) Delivered 84 vehicles into the 500+ vehicle project fleet.
- Supply Chain:
  1) Further reduced purchasing and manufacturing costs by additional 5%, and remained on schedule to meet our cost down goals by the end of calendar 2014.
  2) Began prototype testing of the Smith Drive of our volume production supplier, with initial production deliveries to begin in Q2 of 2014.
- Engineering:
  1) Developed and successfully tested the bi-directional charging/discharging capability of the Newton platform vehicles.
  2) Developed the prismatic cell into the Smith Power structure.
  3) Introduced the option of hydraulic brakes for the all electric stripped chassis.
  4) Continued to improve reliability and efficiency of vehicle sub-systems, including HVAC and air brake systems.
  5) Maintained regulatory compliance and extended the scope on a global basis to include European whole vehicle approval, and specific requirements for markets including Russia, the Middle East and the Far East.
- Quality:
  - Expanded and strengthened the ISO documentation and verification processes.
- Finance and Administration:
  - Continued development and maturation of internal administrative processes, including strengthening the enterprise software, building a public company consolidated external financial reporting platform, developing and further written internal accounting and operating policies.
  - Complied with all project reporting requirements for the DOE and ARRA with the exception of timely delivery of the 2012 financial audit report.
- Corporate:
  1) Maintained fund raising activities in line with corporate goals.
  2) Developed the concept of licensing Smith technologies into other geographic markets in partnership with local OEMs.

Future Activities

- Deliver vehicles to committed customer orders for the remaining 64 vehicles of the demonstration fleet by April 30, 2014.
- Continuously develop Smith Power, Smith Drive and Smith Link, enhancing reliability, efficiency and reducing cost.
- Maintain supplier development and cost down activities to reduce overall vehicle cost by a targeted incremental 23%, improving market competitiveness with traditional ICE commercial vehicles.
- Expand Smith Link to support the requirements of the demonstration fleet for the full duration of the project, ensuring the timely delivery of data to NREL.
- Development activities:
- Investigation of the application of a hydrogen fuel cell based range extender;
- Integration of wireless/inductive charging;
- Develop application of multi-speed transmission to Smith Drive;

Support the DOE funded project to develop and apply a non-rare earth electric drive to commercial vehicles. Technical Discussion

✧ ✧ ✧ ✧ ✧

III.G.2. Technical Discussion

Introduction

Smith's overall technical objectives are to leverage the 80 years of knowledge and experience of its UK subsidiary within

the electric vehicle market in Europe, and apply it to the North American marketplace. This activity can be broken down into two main phases:

Phase1: The homologation of the European Newton Gen 1 platform to U.S. Department of Transportation standards to support immediate production during 2010-2011.

Phase 2: The development of Smith proprietary driveline, battery and telemetry systems under the technical sub-brands of Smith Power, Smith Drive and Smith Link.

The Gen 1 driveline and battery systems were developed in conjunction with vendor system providers with the final vehicle integration being carried out by Smith. By using this approach Smith limited its ability to influence both cost and development, suffering from early quality issues.

It was decided that the experience gained through the use of these system providers that Smith should develop its own powertrain, battery and telemetry systems, thus enabling greater control over the specification, test and validation of the new system to improve quality and reduce warranty issues.

This approach also enables the Company to buy at the component level and reduce overall systems costs in line with its goals.

Smith Drive-System objectives over Gen1-

- More efficient drive motor- 150kw permanent magnet.
- Drive motor and controller to be compatible with electric gearbox development.
- Higher speeds- 65 mph.
- Improved grade ability.
- Fully integrated drive controller including auxiliary inverters for power assisted steering and brakes.
- Drive motor and controller compatible with cooling system.

Smith Power-System objectives over Gen1-

In-house development of the Smith battery management system (BMS) with the following capabilities-

- Management of different cell chemistries,
- Support a modular approach to battery pack sizing,
- Active thermal management.

Modular approach to the mechanical and electrical integration of cells allowing battery pack sizes from 40 kwh to 120 kwh.

On-vehicle modular charging strategy to support differing battery pack configurations.

Smith Link-System objectives-

- Development of the telemetry unit for vehicular use, interfacing with Smith Drive and Smith Power systems,
- Real time collection of over 1200 data points per second per vehicle,
- Secure transmission of the data to in-house server arrays for post-processing,
- The development of portals to create appropriate access to vehicular data for use by the following internal and external customers-
  1) Smith service
  2) Smith engineering
  3) Department of Energy agent NREL
  4) Customers.

III.G.3. Products

Existing products-

Cargo Van

Utility Truck with Lift

Refrigerated Van (Cold Plate)

Military Transport Vehicle

Step Van

Stake Bed Truck

School bus

Cargo Van

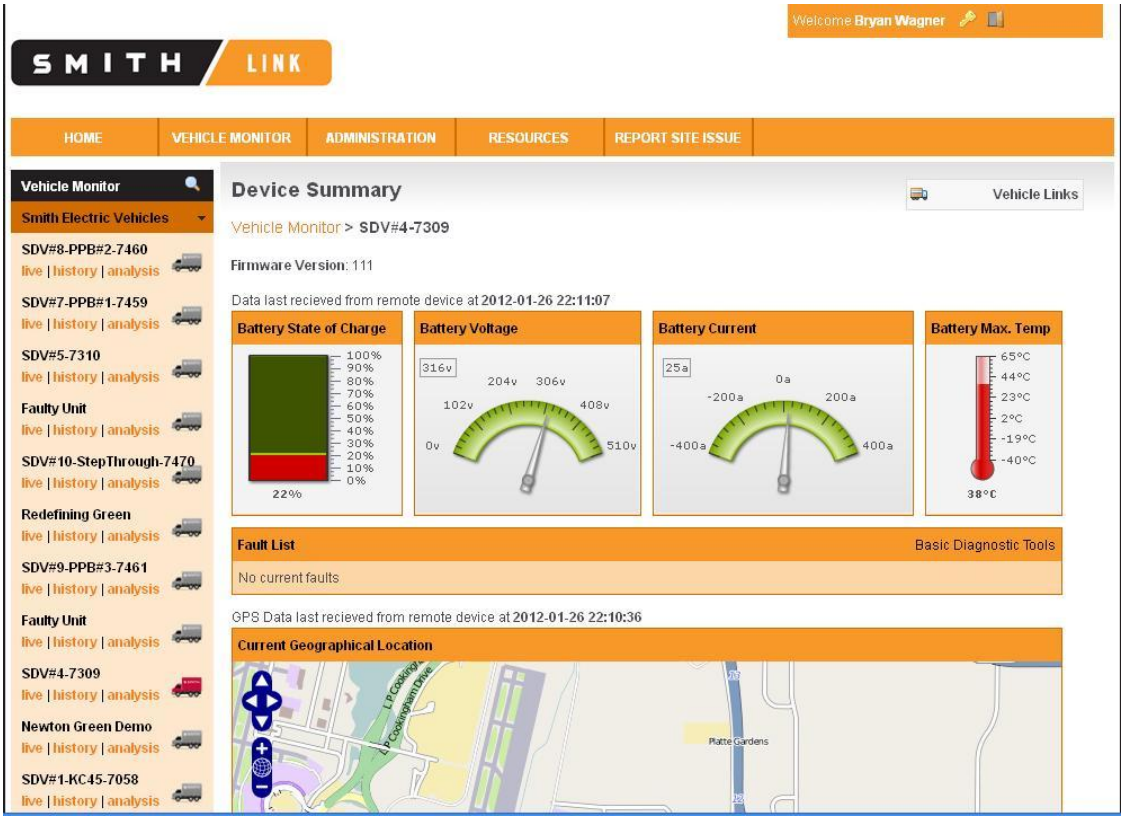

Smith Link

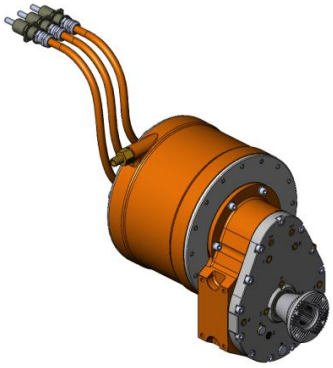

Smith Drive Motor

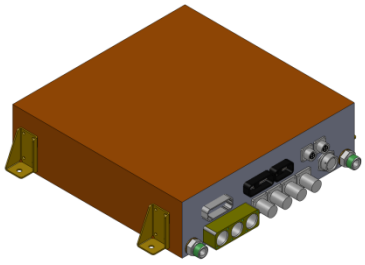

Smith Drive Motor Controller

Left- Smith Gen 2 cab.chassis

Publications

None.

Patents

None.

Tools & Data

None.

III.H. Plug-In Hybrid Electric Commercial Fleet Demonstration and Evaluation (DE-EE0002549)

Dr. Matt Miyasato, Principal Investigator
South Coast Air Quality Management District
21865 Copley Drive
Diamond Bar, CA 91765
Phone: (909) 396-3249
E-mail: mmiyasato@aqmd.gov

Jason Conley, NETL Program Manager
Phone: (304) 285-2023
E-mail: john.conley@netl.doe.gov

III.H.1. Abstract

Objectives

This program will develop and deploy a fleet of medium-duty plug-in hybrid vehicles that will provide improved fuel economy and reduced emissions by grid connecting a portion of the vehicle's use-profile. These vehicles will be fully-integrated with production plug-in hybrid systems for Class 2 pick-ups and vans as well as Class 6–8 work truck applications. A demonstration fleet of approximately 280 vehicles will be deployed for nationwide testing in daily fleet use. This deployment will also include the development and installation of 'smart' charging infrastructure.

These program objectives will be met through the following activities:

- Develop two discreet production-ready plug-in hybrid electric vehicle systems.
- Develop production-ready 'smart charging' capability for vehicle and the supporting charging infrastructure for these vehicles.
- Evaluate technical feasibility and build substantial customer familiarity and interest in a nationwide fleet test and demonstration program.
- Launch system into commercial production in 2014.
- Use project results for system development to optimize performance and reduce costs.

Major Accomplishments

The majority of the work efforts were focused on restructuring the program due to the departure of one of the key hybrid system developers. The restructured program still meets the intent of the original solicitation, and will result in approximately 120 Class 6–8 work trucks being developed by Odyne Systems and 160 Class 2 PHEV pick-ups and vans by VIA Motors

Future Achievements

The major milestones left to complete the program include:

- Complete validation testing of the VIA Motors PHEV drive system and finish PPAP'ing their supply chain.
- Finalize the calibration of the Odyne Class 6–8 PHEV drive system and complete PPAP.
- Build and deploy a nationwide fleet of approximately 280 PHEV's built on the VIA and Odyne drive systems.
- Install the requisite charging infrastructure to support the vehicle fleet.
- Conduct a one year evaluation of the nationwide test fleet.

✧ ✧ ✧ ✧ ✧

III.H.2. Technical Discussion

Background

The South Coast Air Quality Management District (AQMD) received an award from the DOE (DE-EE0002549), effective November 30, 2009, to develop plug-in hybrid electric vehicle technology for commercial trucks, establish production capability and conduct a demonstration of the vehicles and a supporting infrastructure with smart charging capability. At the beginning of the year, there were three plug-in hybrid products that were going to be deployed on a nationwide basis. This deployment would have included a combined total of 250 vehicles produced between Azure Dynamics, Inc. and Odyne Systems, LLC.

On March 26, 2012, Azure Dynamics, Inc. announced that it had filed for bankruptcy protection under Canadian and United States law. Azure Dynamics was the supplier for an E450 and the F550 PHEV vehicle with approximately 10 miles of all electric range. As a result of its bankruptcy filing, Azure Dynamics was no longer able to provide vehicles to the program or assure a pathway to future commercialization.

As a result of the filing, the program was restructured so that it would continue to meet the objectives of the original solicitation. The program would continue to utilize Odyne Systems, LLC to provide coverage for the Class 6-8 work truck applications, but substituted VIA Motors in place of Azure Dynamics. VIA Motors will deploy Class 2 PHEV pick-ups and vans with approximated 35 miles of all electric range. The program would also marginally increase the total number of vehicles deployed from 250 to approximately 280.

Approach

The Odyne PHEV system is a PTO-driven architecture with the stock powertrain being augmented by a 60 kW continuous output electric motor. The electric machine interfaces with the vehicle's drive system through the PTO. This enables the electric machine to wholly operate the PTO at the worksite, as well as supplement or displace the use of the primary drive engine for traction operation. A schematic of the system architecture is shown in Figure III-10.

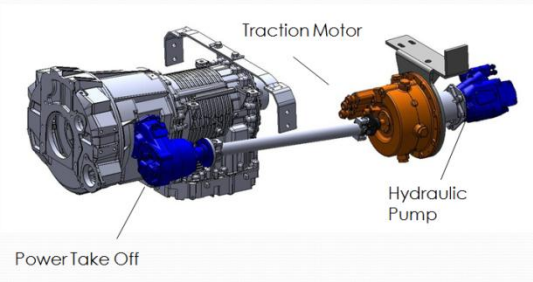

Figure III-10: Odyne PHEV Drive System Architecture.

The VIA hybrid configuration is a series architecture that does not modify the stock engine. VIA removes the transmission and directly couples a generator to the crankshaft of the engine. A 150 kW traction drive motor will be coupled to the rear differential through a shortened prop shaft. The Front End Accessory Drive (FEAD) will be modified to run the water pump only. The following accessories are added: a 42V power steering system, a high voltage electric HVAC compressor, and a 12V electric vacuum boost for the brakes. A large energy battery pack is used to provide fuel displacement during traction events that will afford an all electric driving range of approximately 35 miles. Additionally, the vehicles will be equipped with an export power panel that will be capable of providing a duplexed 120V outlet as well as a 240V outlet for worksite operation. A schematic of the hybrid system architecture is provided in Figure III-11.

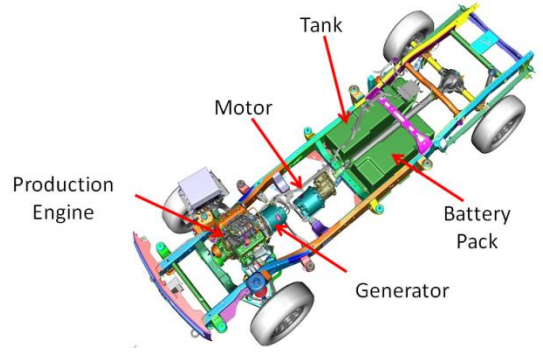

Figure III-11: VIA Motors PHEV Drive System Architecture.

The program has partnered with large fleet partners that are predominantly involved in the electric utility industry and geographic locations that are diversely located throughout the nation. These vehicles will be deployed with the fleet partners throughout the 2014 calendar year and will be extensively data logged at acquisition rates up to 1Hz. This data will also be coupled with periodic user surveys to capture the end-users subjective feedback so that the entire PHEV experience is gauged. Additionally, the vehicles will be equipped with a multi-protocol router that was a development effort between Pathways Technologies and the Electric Power Research Institute to enable the vehicle to communicate with the grid. This communication will allow for smart charging demonstrations to occur at select utility partners.

Results

The program was able to continue the product validation efforts on both the VIA Motors and Odyne Systems PHEV products. These validation efforts have included both design validation through product durability testing as well as supply chain readiness activities through their production parts approval process. These activities are expected to yield a robust product and minimize early failure modes associated with the launch of both of these products.

Additionally, the majority of the fleet participants have executed their agreements and are anxiously awaiting delivery of their vehicles. So, homes for the test fleet have been identified, and their support infrastructure is being readied.

Conclusions

The program will commercialize two discreet plug-in hybrid vehicle products, which will provide coverage across for the Class 2 and Class 6–8 work truck markets. VIA Motors will target the lighter weight class vehicles by developing plug-in hybrid systems for Class 2 pick-ups and van platforms and Odyne would cover the heavier Class 6–8 vehicles for nearly any vehicle equipped with an Allison transmission. Targeting these vehicle segments will provide the opportunity to meaningfully impact fossil fuel consumption through the deployment of a relatively small fleet deployment, due to the higher per capita fuel usage. Each of these vehicle technologies will provide reductions in fossil fuel consumption and emission of air pollutants through the electrification of a portion of each vehicle's daily drive cycle, with the work truck applications additionally benefiting from the electrification of their jobsite operation.

SUPERTRUCK

III.I. Systems Level Technology Development and Integration for Efficient Class 8 Trucks

Derek Rotz, Principal Investigator
Daimler Trucks North America
4747 N. Channel Avenue
Portland, OR 97217
Phone: (503) 745-6303
E-mail: Derek.Rotz@Daimler.com

Roland Gravel, DOE Program Manager
Phone: (301) 938-3347
E-mail: Roland.Gravel@ee.doe.gov

III.I.1. Abstract

Objectives

- Overall Objectives
  - Demonstration of a 50% total increase in vehicle freight efficiency measured in ton-miles per gallon (at least 20% improvement through the development of a heavy-duty diesel engine)
  - Development of a heavy-duty diesel engine capable of achieving 50% brake thermal efficiency on a dynamometer under a load representative of road load
  - Identify key pathways through modeling and analysis to achieving a 55% brake thermal efficient heavy-duty diesel engine
- FY2013 Objectives
  - Experimental demonstration of technology building blocks that achieve 50% vehicle freight efficiency improvement on a systems level.
  - Experimental demonstration of technology building blocks that achieve 50% engine brake thermal efficiency.

Major Accomplishments

- 50% vehicle freight efficiency improvement achieved based on system level tests.
  - Engine + Waste Heat Recovery bench test
  - External Aerodynamics optimization using scale models and CFD
  - Powertrain/Drivetrain improvements measured via SAE fuel economy tests
  - Hybrid electric powertrain measurements via SAE fuel economy test
- Build up of 'A-Sample' SuperTruck for vehicle level integration of multiple systems.
  - Engine, Waste Heat, eHVAC, Accusteer, Cooling
  - Prove out high-voltage & thermal interfaces\
  - Conduct vehicle level performance and functional tests

Future Achievements

- Final Demonstrator Build
  - Complete design and initiate buildup of single vehicle with all technologies integrated.
  - Conduct SAE fuel economy test on designated SuperTruck routes to measure 50% freight efficiency improvement.

✧ ✧ ✧ ✧ ✧

III.I.2. Technical Discussion

Background

SuperTruck is a 5 year research and development program with a focus on improving diesel engine and vehicle efficiencies. The objective is to develop and demonstrate a class 8, long haul tractor-trailer which achieves a 50% vehicle freight efficiency improvement (measured in ton-miles per gallon) over a best-in-class 2009 baseline vehicle. The engine for the SuperTruck program will deliver 50% brake thermal efficiency.

Introduction

Daimler's SuperTruck program is currently on track to meet the project deliverables by the scheduled Q1 2015 target date. In FY 2013, phase 3 targets of reaching 50% vehicle freight efficiency on a systems level were achieved. In parallel the buildup of an 'A-Sample' SuperTruck was initiated with the goal for completing and testing vehicle level integration of multiple complex systems onto a single truck.

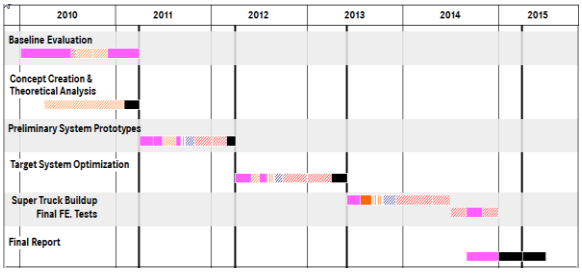

Figure III-12: SuperTruck Project Schedule.

Approach

Systems Level Testing

Phase 2 activities during the previous reporting period encompassed the detailed design, installation and testing of technologies on a system level by conducting on-highway fuel economy tests. In this phase the program target of experimentally demonstrating 25% vehicle freight efficiency was successfully reached. In parallel the engine target of 46% brake thermal efficiency was reached by means of dynamometer tests.

Several SAE Fuel Economy tests were conducted on numerous systems, spanning powertrain drivetrain, auxiliary components, idle reduction, and control systems. Furthermore aerodynamics testing was accomplished via scale model wind tunnel testing and Computational Fluid Dynamics. Lastly prototype lightweight chassis component were built and tested for strength and stiffness.

During Phase 3, the program target of experimentally demonstrating 50% vehicle freight efficiency was successfully reached through continued development and improvement of external aerodynamics, powertrain components and hybrid testing, which are discussed below.

Aerodynamics

Research on aerodynamics in phase 3 encompasses additional improvements in both tractor and trailer systems. The methods employed in quantifying these improvements entail a combination of scale model wind tunnel testing and computational fluid dynamics.

To date, a total drag reduction of 48% has been measured and correlated, through refinement of the basic shape concepts. On the tractor 23% drag reduction was achieved through refinements of aero systems such as side extenders, bumper and chassis fairing/wheel cover enhancements. On the trailer side, 25% drag reduction was reached through refinements of side skirt, boat tail and tractor trailer gap minimization approaches. Combined, this overall drag reduction represents a 16% overall improvement in vehicle freight efficiency.

In addition an aerodynamic trailer was built and an on-highway SAE fuel economy test was conducted. The trailer aero system consisted of a mixture commercially available systems and customized SuperTruck designs, including a 3 sided boat tail, full length trailer skirts with modified geomertry and a custom trailer nose cone. A 2013 Cascadia evolution tractor was used. The fuel economy improvement of the aero trailer vs. the baseline correlated well with analytical predictions both on the scale model testing as well as computational fluid dynamics software, which further reinforces confidence in the results generated by analyitical means.

Powertrain

Powertrain improvements in phase 3 centered on the further development of axle, tire and hybrid technologies, which combined achieve a 16.5% total improvement in vehicle freight efficiency.

Incremental efficiency gains in axle technology improvements were achieved through testing and measurement of gear ratios and lubrication to identify an optimum. On-highway testing of rear axle ratios was conducted to evaluate engine operating points and shifting. In parallel, axle dynamometer testing was completed, which evaluated the impact of gear oil formulations, levels and temperatures on efficiencies.

Low rolling resistance tires were evaluated, with an emphasis on non-driven, wide based singles on the trailer, in collaboration with our tire partner Michelin. Additional freight efficiency gains were achieved through decreasing resistance forces and through weight reduction on the tire, wheel and hub design.

Hybrid

Lastly, a fuel economy test of the A-sample parallel electric hybrid powertrain was conducted in 2013, which demonstrated positive fuel savings. The hybrid system consists of a Daimler proprietary eMotor and inverter in a parallel configuration and an A123 Li-Ion battery pack. The test data confirmed the base regeneration functionality traveling across hilly terrain as designed. However the control interfaces between the hybrid controller, engine controller and ABS controller were not optimized, causing an unexpected limit on available regeneration torque. Improved calibration is needed to optimize the system to maximize the amount of recouperated energy.

This test provided input for further optimization of the hardware components and software for the final SuperTruck hybrid system.

A-Sample Build

In addition to reaching the freight efficiency milestones, another development milestone was reached through the buildup of the A-Sample SuperTruck. The purpose is to integrate multiple technologies onto a single chassis in order to design and test thermal and high voltage interface and to complete a series of functional and performance tests of multiple systems on one vehicle.

Given the complexities of each system individually in addition to vehicle integration complexities which were not well understood, the buildup was deemed necessary. The scope of the A-sample build includes the target supertruck engine and aftertreatment system, waste heat recovery, an updated hybrid electric system and an automated manual transmission with updated controls. A 6x2 axle with custom rear axle ratio, electric HVAC system, a custom cooling package with variable speed fan drive were also incorporated. Lastly a custom hood, bumper and grille were fabricated and installed. The buildup and commissioning occurred in four phases, each culimating with a key-on event as follows:

- Engine Key-On (04/13)
- Hybrid Key-On (06/13)
- Waste Heat Thermal Key-On (08/13)
- Waste Heat Electrical Key-On (11/13 *planned*)

A series tests were conducted to prove out functionality across numerous use cases, to test the performance of cooling systems under a variety of load cases as well as to

study underhood airflow at highway speeds in the full scale wind tunnel. Inferfaces were designed and documented. Troubleshooting lists were created and addressed. As of the end of FY 2013, the first three key-on events were successfully completed, with the remaining scheduled for November 2013.

Results

The figure below illustrates the aggregate results to date. As can be seen the 50% vehicle freight efficiency target was exceeded with an aggregate total of 56.5% improvement measured on a systems level.

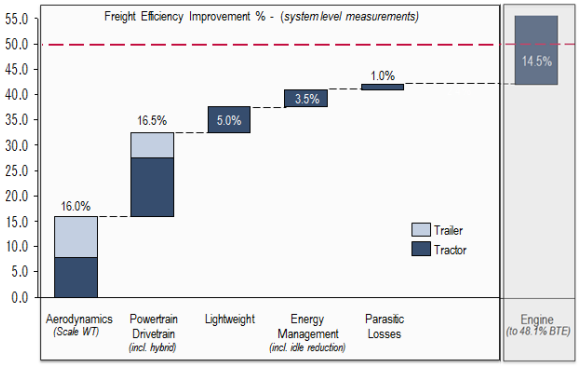

Figure III-13: Experimental Freight Efficiency Results to Date.

Conclusions

The analysis in phase 1 provided a technology path that when implemented and tested will demonstrate the overall 50% freight efficiency target and 50% engine brake thermal efficiency. Phase 2 built upon these results through the design, implementation and on-vehicle testing of systems which met the interim program target.

In phase 3 the 50% vehicle freight efficiency targets were met on a systems level and an A-sample vehicle was built to provide out vehicle interfaces and perform vehicle level test of multiple integrated system.

The next phase entails packaging all technologies in a final demonstrator vehicle and demonstrating 50% Vehicle freight efficiency on the defined SuperTruck routes.

III.I.3. Products

Publications

1. Sisken, Kevin: "Super Truck Program: Engine Project Review Recovery Act—Class 8 Truck Freight Efficiency Improvement Project", Project ID:ACE058, DoE Annual Merit Review, May 16, 2013
2. Rotz, Derek: "Super Truck Program: Vehicle Project Review Recovery Act—Class 8 Truck Freight Efficiency Improvement Project", Project ID ARRAVT080, DoE Annual Merit Review, May 16, 2013

Patents

None

Tools and Data

None

III.J. Volvo Energy Efficient Vehicle—SuperTruck

Pascal Amar, Principal Investigator
Volvo Technology of America
7825 National Service Road
Greensboro, NC 27409
Phone: (336) 291-5842
E-mail: pascal.amar@volvo.com

Roland Gravel, DOE Program Manager
E-mail: Roland.Gravel@ee.doe.gov

III.J.1. Abstract

Objectives

- Increase freight efficiency by 50% [ton-mi/Gal] compared with a *'best in class'* MY 2009 highway truck
- Demonstrate 50% brake thermal efficiency (BTE)
- FY2013 Objectives
  - Validate and deploy complete vehicle simulation tools
  - Demonstrate 47% BTE in engine dynamometer
  - Define technology content for 50% BTE powertrain
    Install all technologies selected for evaluation on concept vehicle in preparation for complete vehicle testing on-road and on chassis dynamometer

Major Accomplishments

- All simulation tools, including models and duty cycles, are fully validated with on-road measurements
- The virtual aerodynamic optimization of VEV-1 is complete and predicts a total drag reduction of 28.5% compared with the MY2009 baseline.
- Advanced powertrain system demonstrated 48% brake thermal efficiency (BTE) on a dynamometer 1 year ahead of schedule
- Concept evaluation chassis VEV-1 is upgraded with all candidate technologies below, commissioned and ready for testing
  - trailer aerodynamic devices optimized through CFD to deliver up to 15% fuel savings
  - advanced powertrain system, including Waste Heat Recovery (WHR), Turbo Compound, new combustion system, low friction components, etc.
  - dual clutch transmission
  - parasitic loss reduction technologies (new lubes, axles, tires and lighting systems)
- The base engine for the final demonstrator was installed in the engine dynamometer and is on-going performance testing ahead of schedule. Technology content to achieve 50% BTE with this powertrain is fully defined
- The solid model for the final demonstrator is complete and the design direction is finalized.

Future Achievements

- Validate aerodynamic drag reduction of optimized trailer
- Initiate fleet testing of trailer aerodynamic add-on devices
- Validate on-road fuel savings of complete vehicle concept VEV-1, which includes
  - Optimized aerodynamic trailer
  - Enhanced tractor wheel fairings
  - LED interior & exterior lighting
  - Advanced powertrain with WHR
  - Advanced transmission
  - Efficient 6x2 axle & low rolling resistance tires
  - Lightweight wheels and suspension

✧ ✧ ✧ ✧ ✧

III.J.2. Technical Discussion

Background

Volvo's SuperTruck project is divided into two main phases: the first phase delivers a concept evaluation vehicle (VEV-1) which is used to validate candidate technologies during 2013; the second phase delivers a final SuperTruck demonstrator (VEV-2) comprising the technologies selected in the previous phase to demonstrate the efficiency improvements compared with the 2009 baseline.

Introduction

Aerodynamic drag force accounts for the major part of the tractive load of a vehicle-trailer moving at highway speeds, and must be reduced in order to improve complete vehicle efficiency. The project team is investigating ways to increase the aerodynamic performance of standard trailers, and optimize tractor design with regard to shape and contour to reduce aerodynamic drag and provide a smooth interface to the trailer.

Reducing the weight of the vehicle directly benefits the freight efficiency of a long-haul truck. New designs and materials are therefore evaluated to provide maximum weight reduction without sacrificing structural integrity, safety, durability or ergonomics.

Another key contributor to freight efficiency is the efficiency of the powertrain. We are therefore exploring various solutions to improve the combustion process, recover energy which would otherwise be rejected in the form of heat, and reduce friction losses in the complete driveline in order to maximize the amount of energy which actually contributes to moving freight.

Such changes to the driveline will impact packaging and heat rejection. Therefore the installation, cooling and venting concepts need to be modified to provide optimum vehicle efficiency.

Earlier studies have shown that auxiliary devices account for 5–7% of the total fuel consumption. The Volvo SuperTruck team is designing a complete energy-balancing system to optimize the trade-off between mission performance and energy consumption. A new high-efficiency lighting system will help reduce electrical consumption of the complete truck. The reduced power requirements will also enable redesign of some components for lighter weight and/or lower air resistance.

Field data shows that some long haul fleets idle as much as 40% of vehicle operating time. In order to address the efficiency of long-haul trucks under their complete operating cycle it is crucial for long-haul applications to address energy use during idling time.

Approach

Complete Vehicle Aerodynamics

The team uses complete vehicle CFD simulations to help design and optimize aerodynamic parts or add-on devices for the tractor and the trailer, for lowest overall aerodynamic drag of the complete vehicle. Freight Wing's latest designs for trailer aerodynamic devices were used as a starting point in the complete vehicle aerodynamic simulations. Another key output from this method is the predicted overall vehicle coefficient of drag, which is a critical input to the complete vehicle simulations described above.

In parallel with the aerodynamic optimization activities, Freight Wing explored opportunities to make the trailer add-on devices more practical from an operational perspective. In particular, new methods for enabling the tail fairing geometry to fold and provide convenient access to cargo are investigated. Different materials including reinforced composite panels were also evaluated for opportunities to improve product durability. The intent is to make the aerodynamic geometry that has proven to be effective in prior work as practical as possible for real word utilization and production.

Advanced Materials and Structures

A study was completed for a lightweight Cab/Sleeper concept, which combines a High-Strength Steel frame and aluminum skin. Several assemblies were built at our Cab plant in Virginia, with varying methods of attaching the skin to frame to evaluate their performance with regards to coating and thermal expansion.

A supplier for an aluminum driveshaft was selected, and a prototype was delivered and installed in VEV-1. This allows replacing the baseline 2-piece configuration with a 1-piece unit replaces and provides a 25% reduction in weight. Along with the conversion to the new and lighter 6x2 axle configuration, VEV-1 was upgraded with a prototype proprietary lighter weight suspension, prototype lightweight aluminum wheels and wide base tires.

A new roof concept is being developed, which reduces weight through use of high-strength material as well as structural simplification. This will yield a lighter component as well as reduce the parts count and eliminate assembly steps. The materials investigated for this concept must be cost effective for the highway truck operating environment.

A study of a new chassis structure concept was started in partnership with a frame rail supplier with the goal to reduce the weight of the frame rails and mounting brackets in the baseline vehicle by 40%. This development explores use of alternative materials, integration of components, as well as new frame geometries and architectures. A prototype lightweight frame is planned to be used in the VEV-2 demonstrator vehicle

Powertrain Integration

In-house engine dynamometer testing of the advanced powertrain equipped with the Rankine Waste Heat Recovery (WHR) system was completed, and it was installed into our concept evaluation vehicle VEV-1 to validate the complete vehicle improvements. The information gained in the first chassis testing is being fed into the second generation requirements to fully optimize the system for the targeted application.

The exhaust aftertreatment system was modeled for implementation in the complete vehicle simulation platform. In order to verify the SCR model, data is compared against two experimental test configurations. Experimental data was collected through the use of a small-scale rig to determine the chemical kinetics needed for initial model calibrations where each reaction for the catalyst NOx reduction is isolated and measured. Subsequent large-scale muffler based testing was also performed, considering both steady state and transient cycles, for system-level validation.

The virtual model of the advanced powertrain system was digitally installed in the chassis in preparation for the retrofit which began early in 2013.

During 2013 the vehicle engineering focus gradually shifted to the packaging of the 11-liter engine which is being developed for the final demonstrator vehicle VEV-2. This packaging study led to a development agreement with a frame manufacturer to create a whole new chassis concept for the final demonstrator VEV-2, the integration of the driveline, engine and cooling package is heavily connected to the design of new chassis structure and lightweight components.

As a result of the studies performed during 2012, we were able to improve the cooling performance of the system while improving aerodynamics.

Parasitic Losses

The team has deployed efficient LED lights for both interior and exterior lighting to further reduce the energy consumption of the vehicle. The trailers' exterior lighting uses Grote's LightForm technology to replace incandescent bulbs and fixtures, and a new set of LED headlamps was designed, built and installed in the concept evaluation vehicle.

The Volvo SuperTruck concept vehicle uses state-of-the art low friction tires which the team will select from existing suppliers and industry partners. The team is further reducing

the rolling resistance of the complete vehicle by optimizing synthetic lubes for axles and transmission, as well as using improved bearings for axles and wheel ends.

In order to reduce driver impact on the efficiency of the complete vehicle, the Volvo team plans on implementing advanced driver assistance solutions for powertrain, and controls optimized for best fuel economy and safety based on preview information. Telematics will also be investigated as a mean to improve transport efficiency.

Complete Vehicle Simulations

The SuperTruck project aims at developing multiple technologies to achieve the goals of freight efficiency increase and thermal efficiency increase. These new technologies and concepts can interact with each other.

The Volvo team uses its complete vehicle simulation capabilities to support the SuperTruck concept development. It consists of a virtual concept truck made of models for the vehicle, driver and the road and environment. Each of these models is further built from component sub-models in a modular form. This platform provides a quantitative insight into potential interactions between vehicle systems, allowing the development of a completely integrated vehicle.

Idle Reduction

In order to maximize overall system efficiency, the team is working to increase the insulation of the cab and improve the efficiency of the heating and cooling systems, which will allow for downsized climate unit components and Auxiliary Power Unit system. The energy management system is designed to always select the most efficient energy source / storage system to power typical Hotel Mode loads.

Results

Complete Vehicle Aerodynamics

Prototype parts corresponding to the designs simulated through CFD were fabricated, installed and tested on the concept evaluation vehicle VEV-1 under real-world conditions during the fuel economy tests. The initial tests demonstrated 11.5% fuel efficiency improvements for the complete vehicle compared with the MY 2009 baseline, which correlated very well with the simulated aero drag reduction for the corresponding geometry and confirmed the accuracy of the method.

A full wheel cover concept is being evaluated to improve the robustness of the overall aerodynamic performance. A prototype was designed for on-road testing on VEV-1 (see Figure III-14) and a functional prototype was installed on the vehicle at the end of the reporting period.

Figure III-14: Prototype Tractor Wheel Skirting Installed on VEV-1.

The devices were then optimized through a series of smaller incremental changes, and the resulting configuration was installed on the test vehicle for verification through on-road fuel economy testing during Q3 2013, as shown in Figure III-15. The combined real-life fuel savings are expected to be up to 15% at highway speeds.

Figure III-15: Concept Evaluation Vehicle Ready for Testing.

Freight Wing completed the redesign of the second generation aerodynamic trailer components for VEV-1 to incorporate the benefits of composite technology and enhanced manufacturing capability as a result of the merger with Ridge Corp. The resulting designs are expected to significantly enhance durability, longevity and operational effectiveness. The tail device that is mounted on the rear side of the trailer is the most challenging from an operational standpoint. The final design is constructed of durable and lightweight thermoplastic composite panels hinged to enable the device to collapse into a stored mode to enable convenient door access. A prototype was impact tested to evaluate durability, with positive results.

Plans were solidified to initiate operational testing of the devices next reporting period with a leading fleet. This test is intended to evaluate the durability, operational effectiveness, and ease of use of the equipment in a demanding real word

environment. Recent work therefore concentrated on finalizing the design of the devices for this test.

In summary the achievements reported this fiscal year through the work done on the concept evaluation vehicle VEV-1 was the result of several investigations initiated earlier in the project. The first step was the investigation into cab architecture, which led to the starting point for the future demonstrator VEV-2. By using the existing cab structure, development of the final demonstrator is progressing at a faster pace than originally planned. The current design includes a modified cab, new roof, new hood and side fairings. The parallel activities on aluminum sleeper side panels, lightweight roof, bumper and side fairing ground clearance work are all aligned with the development of the VEV-2 concept since they allow for modifying the shape of the cab.

As VEV-1 was completed from an aerodynamics perspective, the focus shifted to the design of VEV-2 during 2013. Modeling work is on-going on the chassis fairing combined with the cab position, hood and bumper work to define the best design direction for aerodynamic performance. A clay model was completed and scanned into a model for further analysis to ensure the aerodynamic targets will be met.

Advanced Materials and Structures

A complete Body-In-White (BIW) side assembly was built with the aluminum outer panel at our Cab plant in Virginia following the manufacturing process. The panels performed well in the E-coat process with good results related to thermal expansion of dissimilar materials. Thanks to the success of the build we were able to begin the design for the final demonstrator VEV-2 over 6 months ahead of the original plan.

The aluminum driveshaft installed in VEV-1 was tested for over 3,000 miles of road tests and performed well regarding driveline vibration and drivability. A complete vibration analysis was performed with very positive results. The combined weight savings resulting from the aluminum driveshaft, the proprietary suspension, the new 6x2 axle, new lightweight wheels and wide base tires is approximately 900lbs.

The first prototype roof was built with RTM material and evaluated at Volvo's vehicle engineering division in Greensboro, NC. It was successfully painted and fitted to a current BIW. The paintability and the fit were very good. The next step is to develop the B side surface to accept interior trim components and improve manufacturability. The knowledge gained from this first investigation will be carried into the new VEV-2 roof, possibly incorporating carbon fiber into the design. The hope is to find a ratio of carbon fiber and RTM that will significantly reduce the weight while maintaining acceptable levels of cost.

In order to select a design path for the lightweight frame study, four concepts were evaluated against the current design in a Pugh matrix based on 4 criteria: vertical bending, weight reduction, innovation, and manufacturability. This analysis narrowed the focus on two of the four design concepts, which were benchmarked in more details including stiffness analysis and FEA analysis with 6 different load cases for each. After completing the analysis, a design direction was chosen in a design freeze in June 2013. The key features for the concept selected include a new architecture, possible use of traditional processes e.g., stamping, roll-forming, casting, extrusion, the ability to incorporate Aluminum, and result in a 45% weight reduction (over 800 lb.). Tooling requirements has been determined and parts will be ordered shortly. The final frame structure will be subjected to a full FEA along with a simulated track test before the prototype assembly begins. Delivery of the prototype concept frame is scheduled for Q1 2014.

Powertrain Integration

The WHR system exceeded previous improvements in steady state optimization despite the addition of a more efficient combustion chamber and turbocompounding, which both reduced the heat available to the system. Recovery was possible during nearly all positive power operation, with interrupts during coasting or engine brake operation. The advanced powertrain system installed in the VEV-1 chassis has successfully completed multiple on-road tests with varying route profiles and vehicle loads. The vehicle performs as expected, and the WHR system generates power during normal operation. The second generation WHR system components are defined and being procured for test starting next fiscal year.

A chemical model of the EATS system was developed for the unit delivered as part of VEV-1, allowing for transient evaluation of the EATS in the SuperTruck environment.

The design of the piping, routing and mounting of chassis components was completed in time to support the physical installation of advanced powertrain and transmission in Q2 2013. The new cooling package was designed and the detailed integration into the chassis is nearing completion.

Parasitic Losses

The prototype LED tractor headlamps and trailer lights installed on the concept evaluation vehicle were tested to ensure that they meet all performance requirements, as well as for power consumption compared to their incandescent baseline. Assuming that a highway truck is operated 240 days per year, and with reasonable assumptions regarding usage of each lamp function, the power savings measured should result in approximately 420kW-hr and 560kW-hr lower electrical energy consumption for tractor and the trailer respectively, compared with standard incandescent systems. Using typical efficiency and usage figures for a baseline MY2009 truck, this adds up to over 120 Gal of diesel fuel saved per vehicle per year.

Complete Vehicle Simulations

During this reporting period the virtual duty cycles representing reference road sections used by the team for on-road fuel economy and performance testing were improved using barometric altitude measurements. This allowed for a much closer correlation of the simulation results to road test results so far as parameters like mean torque, fuel consumption etc. are concerned. This tool is now a very strong complement to chassis dynamometer and on-road test capabilities available to support the project.

In order to investigate the potential for various idle reduction concepts, it was necessary to understand the detailed energy usage and balance over a 24-hour period. Several shorter road cycles were therefore combined with a

number of stops and engine off events to form 24 hour cycles. The proportion of the different types of roads (flat, hilly etc.) was verified to remain representative of typical North American long-haul operation.

In order to help size and ultimately optimize the hotel load systems, a 24-hour electrical load consumption profile was also developed using representative electrical configurations, historical weather conditions, etc. With such a load profile, it was possible to establish rough requirements for energy storage capacity, potential fuel savings, etc.

Idle Reduction

The requirements established for the APU include 10,000 BTUs of cooling, 10,000 BTUs of heating, flexibility to operate during driving, parked in hotel mode and able to operate from a battery pack or connected to an external power supply (Shore Power). A supplier was selected and the design direction is decided in early 2013. The first prototype system will be bench tested late this year, and the first chassis installation will take place early next year to identify any final changes necessary to the design prior to the final assembly.

Conclusions

During this fiscal year the Volvo SuperTruck team has focused on validating the various concepts identified at the beginning of the project, and building a complete vehicle concept for further evaluation of the integrated system. A few new activities were started during the reporting period as a result of ideas emerging from the on-going research, such as the lightweight frame concept. All components tested so far met or exceeded their predicted performance described above.

Simultaneously, the simulation tools and methods developed previously were thoroughly validated and correlated with measured data from chassis dynamometer and on-road tests.

The next fiscal year will see the thorough evaluation of the vehicle concept VEV-1 to quantify and validate the improvements at a complete vehicle level. The team will continue to develop and refine the most promising technologies and start to build the final demonstrator VEV-2.

III.J.3. Products

Publications

1. Bolander, A., Brooks, T., and Thompson, P., "LED Headlamp for DOE Super Truck," SAE Technical Paper 2013-01-0753, 2013, doi:10.4271/2013-01-0753

Patents

To date, the project team has generated eight subject inventions and five patent applications have been filed. We look forward to sharing the details of these applications once they become publicly available.

Tools and Data

N/A

WIRELESS CHARGING

III.K. Wireless Charging for Electric Vehicles (FOA-667)

John M. Miller, Principal Investigator
Oak Ridge National Laboratory
National Transportation Research Center
2360 Cherahala Boulevard
Knoxville, TN 37932
Phone: (865) 946-1469; Fax: (865) 946-1262
E-mail: millerjm@ornl.gov

Lee Slezak, DOE Program Manager
Phone: (202) 586-2335
Lee.Slezak@ee.doe.gov

III.K.1. Abstract

Wireless power transfer (WPT) is a paradigm shift in electric-vehicle (EV) charging that offers the consumer an autonomous, safe, and convenient option to conductive charging and its attendant need for cables. WPT can be fully autonomous, and is non-contacting, so issues with leakage currents, ground faults, and touch potentials do not exist. Furthermore, the high-frequency magnetic fields employed in power transfer across a large air gap are focused and shielded, so that fringe fields (i.e., magnetic leakage fields) attenuate rapidly over a transition region to levels well below limits set by international standards for the public zone (which starts at the perimeter of the vehicle and includes the passenger cabin). The convenience of WPT cannot be overstated. The ORNL approach to WPT charging places strong emphasis on radio communications in the power regulation feedback channel, augmented with software control algorithms. The over-arching goal for WPT is minimization of vehicle on-board complexity by keeping the secondary side content confined to coil tuning, rectification, filtering, and interfacing to the regenerative energy-storage system (RESS). This report summarizes program work performed during year one at the National Transportation Research Center.

Objectives

- Coordinate multi-party team, develop 10 kW capable wireless power transfer (WPT) apparatus, and demonstrate on bench at full power. The program team consists of ORNL as overall lead, plus:
  - Evatran as commercialization partner
  - Clemson University ICAR for radio communications
  - General Motors and Toyota Motor companies will provide demonstration vehicles
  - Duke Energy and International Rectifier are links into utility and power semiconductor industries
- Overall program goal is to integrate ORNL developed WPT technology into demonstration vehicles and validate at an independent testing laboratory.

Major Accomplishments

- Achieved >10kW power transfer at >85% utility input to WPT dc output (battery input) using laboratory bench demonstration hardware and software.
  - Using new coupler design based on rectangular ferrite plate flux guides and minimal turns of Litz cable
  - Obtained very low loss tuning capacitors from High Energy Corporation needed for high voltage in resonant configuration.
  - Using full wave rectification on load side with fast recovery silicon diodes. Opportunity to replace with wide bandgap (WBG) Schottky Barrier Diodes (SBD).
- Demonstrated active front end (AFE) to ORNL's WPT base station that uses commercial wide bandgap silicon carbide (SiC) MOSFET transistors.
  - Completed thorough evaluation and down select of most promising power factor corrector (PFC) architectures and fabricated and validated the interleaved, boost configuration in a two-switch design. Provides variable voltage output of 340V_{dc} to 800V_{dc} to high frequency (HF) power inverter.
- Developed and demonstrated HF power transformer for isolation of WPTB station electronics from HF feed cable and primary pad.
  - Documented technology evolution from Metglas core to MnZn ferrite ring core to coaxial winding transformer (CWT).
- Accessed CAN network in Prius Hymotion plug-in hybrid test vehicle to demonstrate that battery management system (BMS) messages needed for power flow regulation are available.
  - Used information for in-cabin display and to alert vehicle operator on state-of-charge (SOC) level of the charge sustaining (CS) battery, a nickel metal hydride (NiMH) and the charge depleting (CD) battery, Hymotion L5 Lithium-ion pack.
- Developed and delivered all WPT schematics and bill of materials (BOM) to commercialization partner.
  - Including WPTB station electronics, HF transformer, HF couplers, and vehicle electronics.
  - Used teleconf and webinar for weekly updates to program partners.

- Held bi-weekly WPT team meetings at ORNL to review progress against schedule and action items by individual.

Future Achievements

- Apply lessons learned from previous electromagnetic coupler designs to FOA program specific requirements.
  - Continue evaluation of soft ferrites as flux guides, means to improve robustness, and materials that increase flux density.
  - Work with Aegis Technology Inc. on iron-cobalt (FeCo) magnetics for use in CWT, couplers, and very importantly on PFC stage line input inductors.
- Enhance the present SiC two-switch PFC to fully interleaved four-switch SiC PFC.
- Implement DOT compliant dedicated short range communications (DSRC) radio.
- Validate fringe field emissions and compliance with international standards.
- Demonstrate up to 20 kW power levels.

✧ ✧ ✧ ✧ ✧

III.K.2. Technical Discussion

Background

During FY 12 the WPT team launched into a deep dive of wireless charging that included development of a robust high frequency power inverter, electromagnetics design of coupling coils (i.e., couplers), and experimental characterization of laboratory scale hardware. By the conclusion of FY 12 the team had demonstrated 6.6 kW charging of a test vehicle, a GM Equinox that was modified by a University of Tennessee ChallengeX team. This vehicle contained a Cobasys 300V nickel metal hydride (NiMH) battery pack for energy storage.

Power Inverter Development

The ORNL experimental inverter shown in Figure III-16 employs dual Powerex Intellimod IGBTs in an H-bridge arrangement with each phase leg connected to one terminal of the primary coil and tuning capacitor network. The control system of the inverter is implemented within a TMS320F28335PGFA DSP module from Texas Instruments. The DSP generates the switching signals, dead band control, shoot-through prevention, and incorporates condition monitoring based protection and termination systems. For demonstration purposes, the inverter can also be controlled and monitored via RS232 by a host computer. The control system involves instantaneously variation of the switching frequency and the duty ratio to adapt to the changing conditions such as battery SOC and the coupling coefficient while taking the efficiency and power transfer level into account. The Intellimod IGBT modules rated 600V, 600A, insure that the HF inverter is scalable to high power levels without needing modifications. High quality film capacitors are employed at the dc link (AVX 800V polymer film) and module snubber capacitors (Kemet 1000V polymer film).

Figure III-16: Wireless power transfer HF inverter (air cooled).

Electromagnetic Design of Couplers

Electromagnetic design of WPT coupling coils provides the most fundamental investigation into their performance. At ORNL the WPT team developed couplers based on the magnetic vector potential at a field point due to current flowing in an ideal primary coil conductor. The potential at this field point is defined to lie at the location of the secondary coil. For a coil pair of radius **a**, assuming infinitesimal conductor radius, and having a coil to coil spacing, z, then the radius vector from the primary coil origin to the field point becomes $r=\sqrt{(a^2+z^2)}$. The corresponding vector potential, $\mathbf{A_\phi}$, for the case of N_1 primary turns and I_1 Amps yield a primary excitation of N_1I_1 amp-turns. This primary excitation is depicted as **Idl** in Figure III-17 where $a_1=a_2=a$ for convenience.

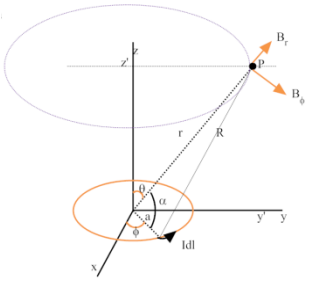

Figure III-17: Analytical construct for coupler design.

At the field point, P, the magnetic vector potential is strongly dependent on primary coil radius, total current, the co-elevation angle, θ, and inverse with separation distance, **r**, squared. However, it is the flux density, **B(r,θ)**, and total flux, ϕ, at the secondary coil that is most relevant to WPT performance and is given as (1).

$$B(r,\theta) = \hat{r}\frac{\mu_0 N_1 I_1 a_1^2}{2r^3}\cos\theta + \hat{\theta}\frac{\mu_0 N_1 I_1 a_1^2}{4r^3}\sin\theta \qquad (1)$$

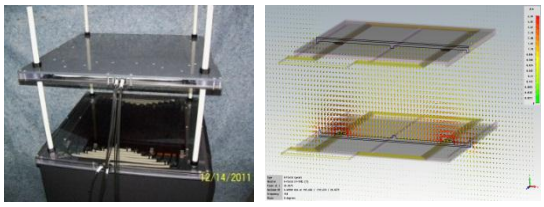

Figure III-18: Coupling coil (coupler) and electromagnetic model.

Good agreement was found between analytical and electromagnetic modeling of coupler designs, including assessment of coupling coefficient, k, as shown in Figure III-18. Coupling coefficient is the most important parameter in WPT work and defines that fraction of primary coil developed flux that links the secondary coil mounted to a vehicle.

WPT Coupler Fabrication Sequence

Coil designs ranged from rectangular to circular and square during the course of early development. Based on performance the shallow rectangular, nearly square, design was adopted and will carry forward in future WPT work.

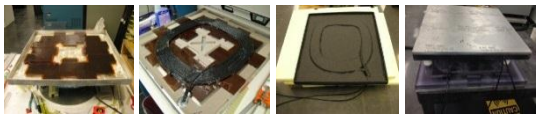

Figure III-19: Coupler assembly sequence.

During the assembly sequence shown in Figure III-19 an aluminum pan forms the structure for the coil and provides magnetic shielding. A pattern of ferrite plates then define flux guide regions and have a layer of Kapton for electrical insulation. The Litz cable is then put on, conformal coated and sealed.

Introduction

Wireless charging of electric vehicles has the potential to eclipse conductive chargers because of its autonomy and convenience to the customer. Use of private and secure radio communications, especially vehicle to infrastructure (V2I), and standardization means that any vehicle can charge at any location. The complete charging process can in effect be totally transparent to the customer. A visionary would even say that combined with GPS a battery electric vehicle could be completely autonomous. It could essentially then drive itself to the nearest wireless charger and then be available for personal use.

In this project the goal is to develop a deep understanding of WPT, to find through analytical and experimental work, what the challenges and issues are so that technology gaps can be addressed. The following sections on technical approach and results will do that and conclude with a summary of state-of-the-art for WPT and research needed for its advancement.

Approach

The FOA program is organized to develop WPT charging technology (hardware and software) suitable for bench top demonstration that achieves continuous throughput power of 10 kW into 370V nominal load (e.g., Volt pack under charge 370 +/- 25V) and dc-to-dc efficiency >90% and 240Vac grid input power to dc load power efficiency >85%.

Given this overall power and efficiency requirement the WPT team has also set specific performance targets for grid connection power factor and total harmonic distortion. Internal requirements for set at PF>95%, THD<5%, and WPT output current filtered to the load having I_{pp}<15A. Internal criteria for coupling coils are set for leakage magnetic field B<6.25 μT and electric field E< 87 V/m at 0.8 m laterally from center of the primary coil midway in gap.

Control strategy that adjusts primary excitation frequency according to coil spacing, k(z), and load power variation (e.g., due for example to battery state-of-charge (SOC)). The ORNL WPT base station (WPTB) uses a single digital signal processor (DSP) controller to manage both the PFC and HF inverter stages. A Spectrum Digital board houses the DSP and communicates with the DSRC radio via a controller area network (CAN) and to a local laptop via a USB port. The DSP used is a Texas Instruments (TI) TMS-320F28335PGFA floating point device programmed with algorithms that match PFC output voltage (U_{do}*) to load power demand and HF inverter frequency to the setpoint (ω*). The role these control variables in WPT power flow control can be seen through examination of (2) and noting that prior work determined that duty ratio, d, control is not as viable in WPT as variation of dc link voltage, U_{do}*.

$$U_s(t) = \frac{4U_{do}^*}{\pi} \sin\left(d^* \frac{\pi}{2}\right) \cos(\omega^* t) \qquad (2)$$

Radio communication is needed to close outer power regulation loop based on measured load power so it can be sent to the grid converter for adjustment of dc rail voltage U_{do}* according to demand. Figure III-20 illustrates the overall concept in which the active front end (AFE) contains the PFC and harmonic filtering at the grid connection, the high frequency (HF) bridge (transistors T_1-T_4), the coupler, vehicle side rectifier and filter, and radio communications in the feedback loop.

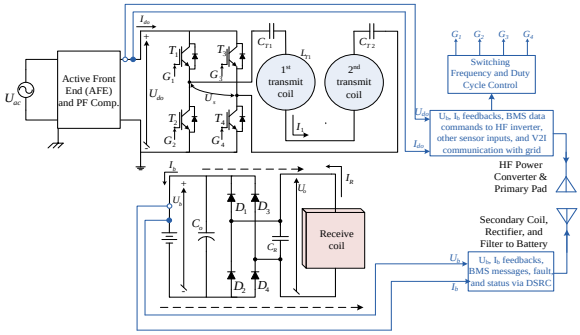

Figure III-20: Wireless power transfer having grid-side regulation and radio in the feedback loop.

WPT Field Pattern Assessment

The operation of WPT can be better appreciated at this point through examination of what (1) and (2) reveal for electromagnetic and electrical performance. First, electromagnetic behavior from (1) that identifies a radial, **r**, and "across" field, **θ**, that viewed from above has the appearance of a fountain. The implications of these became very clear when a pair of primary coils were tuned and connected in-phase. In-phase connection enhances the **r**-field component so that when a secondary coil passes above the pair it intercepts a strong field, then partial cancellation during overlap, and finally a strong field again above the 2nd coil in the pair. Next, when the tuned pair were connected anti-phase the q-field component (1) was enhanced producing a strongly donut shaped field that crossed between the coil pair in close proximity, hence the term "flat" field. It was found that when a secondary coil passes over the same pair of coils connected in anti-phase the power transfer encounted extremely sharp transistions from maximum to zero, a significant region at zero power, then sharply back to maximum power when aligned with the 2nd coil in the pair.

WPT Electrical Assessment

Secondly, electrical performance based on (2) identifies three control variables: U_{do}*, d*, and ω*. Controllable dc link voltage to regulate power transfer level, and HF inverter frequency variation to maintain it against gap changes have been discussed above. At this point it is important to document the influence of duty ratio variation, d*. Testing was performed under constant power loading (using a Chroma 14 kW active load as battery emulator) to examine the control authority of d* on power. Table III-5 summarizes this test and shows that when d* is decreased from a nominal 0.8 to a 0.4 that two things happen, first, input voltage, U_{do}, must increase to maintain source voltage, U_s, in (2), and second that input reactive power increases dramatically, nearly quadrupling. For this reason the WPT team elected to fix d*=0.8 in all future testing and vehicle integration programs.

Table III-5: HF power inverter U_{do} and duty (d) inter-relationship.

f	*Udo*	*d*	*VSI*	*Po*	Q_1
(kHz)	(Vdc)	(#)	(mWb)	(W)	(VA)
22.5	41.87	0.8	0.743	2055	-2249
22.5	55.26	0.6	0.736	2017	-3112
22.5	117.66	0.4	1.18	2011	-7005

WPT Fringe Field Assessment

At this time a new development occurred related to leakage field and maximum permissible exposure (MPE) levels for humans. The U.S. Federal Communications Commission issued a notice of proposed rule making regarding radio frequency electromagnetic fields below 100 kHz that would set MPE thresholds. The crux of the matter is that existing guidelines such as the Australian ICNIRP1998 specify magnetic field thresholds for frequencies below 100 kHz as due primarily to electrostimulation of nerve and muscle tissue. For frequencies above 100 kHz the thresholds are derived from tissue heating and given in terms of SAR—specific absorption ratio. ORNL has teamed with Momentum Dynamics in a reply to the FCC that it omit WPT operating below 100 kHz from this ruling, but if it does include WPT and publishes MPE thresholds that these be derived from ICES IEEE C95.1 and C95.6 standards. Using the IEEE standards would limit magnetic fields to 1.13 mT (3.35 kHz to 100 kHz) for the general public rather than the ICNIRP threshold of 0.027 mT for this frequency range. Note that the ICNIPR 2010 level of 0.027mT is forty times lower than IEEE C95.

ORNL maintains that health and safety are paramount in all WPT work due to the presence of high voltages and high frequency magnetic and electric fields. Figure III-21 and Figure III-22 illustrate the measurement procedure for recording exposure levels and the arrangement of coupler and Narda measurement instrument. ORNL uses an industry standard L3 Communications, Narda EHP-50D E&H-Field Analyzer calibrated for use in the 5Hz to 100 kHz range with accuracy from 0.3 nT to 10 mT.

Appropriate recording of MPE for persons near a WPT charger are best taken at four measurement points and averaged.

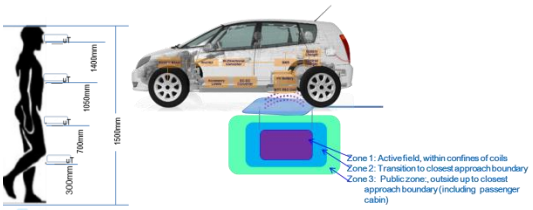

Figure III-21: Assessment of leakage fields.

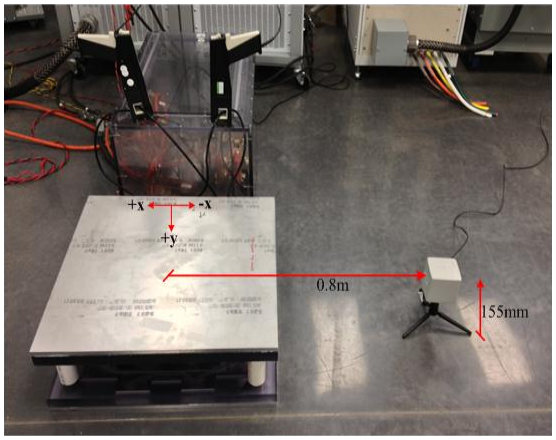

Figure III-22: WPT coupler and Narda placement for testing.

For the Narda placement shown in Figure III-22 the coupler fringe field would correspond to a persons feet and ankles when standing alongside a light duty (LD) passenger vehicle under WPT charge. Table III-6 summarizes the readings taken at two power levels. Note that when these tests were performed the MPE levels specified in ICNIRP1998 were followed, specifically that B-field at the measurement point not exceed 6.25 μT rather than the IEEE allowable 27 μT.

Table III-6: Measured leakage field for WPT coupler.

Power	Coupler Gap	Field Point Distance	B-field	E-field
(kW)	(mm)	(m)	(μT)	(V/m)
5	155	0.8	5.36	52.1
7	155	0.9	4.38	52.6

ORNL will maintain testing to the lower MPE levels until the Society of Automotive Engineers (SAE) adopts the ICES IEEE standard levels, or FCC issues its rule making on part 18 dealing with radio frequency electromagnetic fields below 100 kHz.

WPT Efficiency Assessment

Bench evaluations of WPT efficiency are completed in two stages: first, a dc to dc measurement using a laboratory power supply and electronic battery emulator. The second, is ac input power from the grid to dc output power at the battery emulator. In the first case the laboratory power supply replaces the AFE PFC stage so that efficiency loss is circumvented. The second case is more realistic and for a fully functional WPT it includes a cascade of five power stages: 1-PFC, 2-HF Inverter, 3-isolation transformer, 4-coupler, and 5-rectifier and filter.

Figure III-23 shows these five stages in their functional arrangement with supporting control and communications

logic. This functional representation makes is clear why the goal of 85% efficiency from grid to vehicle battery pack is so challenging. With all the power electronic synthesizing and filtering underway one might be inclined to assign an efficiency loss of 3% to each of the five stages. This in fact is realistic, and taking five such efficiency losses brings the grid to battery overall efficiency right into the 85% range.

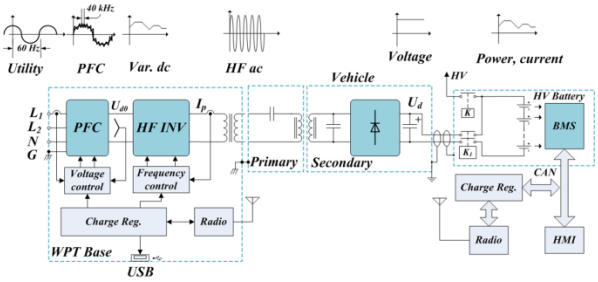

Figure III-23: WPT functional diagram and waveforms.

The results section of this report goes into detail on how the ORNL WPT team took up the challenge of optimizing the efficiency of each of the five major functional stages. What must be kept in mind is that the ORNL system shown as Figure III-23 inlcudes functionality not necessarily found in commercial offerings. Two stages in particular would not in general appear in a commercial system: 1-the front end PFC, and 2-the HF isolation transformer. It may take UL certification procedures before one or both of these become part of the National Electrical Code (NEC) for WPT installation into residential or commercial buildings. Until that happens, ORNL has undertaken the most general case and developed WPT as if these requirements were in place.

Results

FY 13 progress and results will be summarized over a series of subsections that focus on the major functional stages of the WPT cascade shown above in Figure III-23. This will help keep the different areas concise and focused.

Conductive Versus Wireless Charging

Vehicle charging, regardless of mode, relies on availability of standardized connectors and power transfer so that infrastructure and vehicles are compatible. Figure III-24 illustrates a typical conductive charger plug and on-vehicle receptacle. It should be noted that different plug and pin assignments are used for different power level EVSE—electric vehicle supply equipment. This means that mating connectors on the vehicle must be both standardized, and if not RPO's—required production options, then purchased.

Figure III-24: Conductive charger plug and vehicle receptacle.

Standardized power levels for conductive chargers are given in SAE J1772 standard and repeated here for convenience as Table III-7.

Table III-7: SAE power levels for conductive charging (J1772).

EVSE Type	EVSE Input	EVSE Output	EVSE Vehicle Control Method	Charger Current	Charger Location	Power Max.
AC Level 1	120 V AC	120 V AC	SAE J1772™ Pilot	12 A	Vehicle	1.4 kW
AC Level 2	208-240 V AC	208-240 V AC	SAE J1772™ Pilot	<80 A	Vehicle	19.2 kW
AC Level 3	208-240 V AC	208-240 V AC	SAE J1772™ Pilot	<80 A	Vehicle	96 kW
DC Charging	208-600 V	0-600 V DC	SAE J1772™ and SAE J2293	<400 A	EVSE	240 kW

Note: SAE J1772 includes 3.3 kW, 6.6 kW, and 11.2 kW chargers

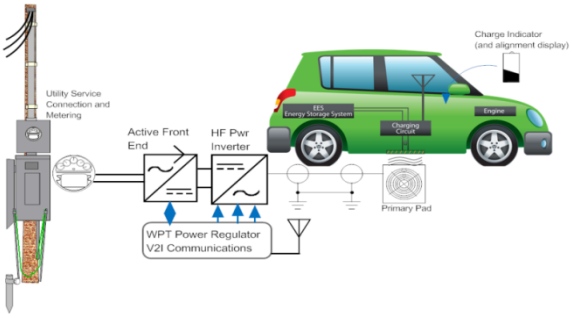

Figure III-25: Wireless charging: utility pole to vehicle battery.

With WPT all infrastructure is compatible with conductive charging since the WPTB station in essense performs the functional duties of a conductive on-board-charger (OBC), but without need to use cable and plug. WPToff-board infrastructure and on-board components are illustrated in Figure III-25.

Table III-8: SAE power levels for wireless charging (J2954).

Classification		SAE TIR J2954 WPT Power Class Guideline			
		WPT1	WPT2 Private/Public Parking	WPT3 L.D. Fast Charge	WPT4 H.D.
Ground: Primary Coil	Maximum EVSE Power Source (Pin From Mains)	3.7 kW	7.7kW	22 kW	200 kW

Rather than listing the charge power delivered to the battery as SAE J1772 does, the wireless charging guideline, SAE J2954 specifies the power demand at the utility interface.

Active Front End Electronics and Control

In order to determine a suitable PFC architecture the team evaluated several (5) candidates and down selected the highest efficiency design. The candidate architectures are: A-Buck Rectifier; B-Interleaved Boost; C-Interleaved Boost/Buck; D1-Bridgeless Interleaved Boost/Buck; D2-Bridgeless Interleaved Boost Converter. Table III-9 summarizes the results of the Pareto comparison and selection (C) based on cost.

Table III-9: SAE power levels.

	Circuit A	Circuit B	Circuit C	Circuit D1	Circuit D2
Number of switches X rating	4 X 70A	2 X 70A	2 X 35A 1 X 28A(Buck)	4 X 35A 1 X 28A(Buck)	8 X 35A
Number of inductors	1 X 70A 1 X 28 A	2 X 70 A	2 X 35 A 1 X 28A(Buck)	4 X 35 A 1 X 28A(Buck)	8 X 35A
One or two stage	One	One	Two	Two	One
Efficiency of boost	Lowest	Low	Fair	Good	Fair
Input voltage	240 V AC	2X 120 V AC	240 V AC	240 V AC	2 X 120 V AC
Total efficiency of AFE	Low	>A	>B	>C	> B, but < D1(to be verified).

Figure III-26 offers a schematic of the selected PFC stage that has been built using SiC power devices and is dual-loop controlled: 1-inner current loop to regulate line current, and 2-slower voltage loop to regulate dc output voltage (i.e., dc-link voltage U_{do}. The controller functional diagram is shown.

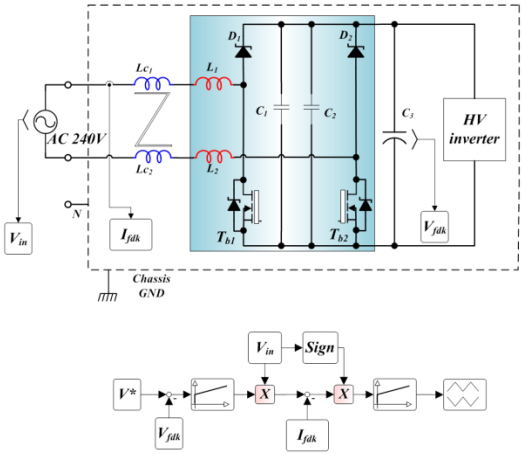

Figure III-26: Interleaved boost converter PFC stage.

The ORNL implementation of the PFC uses ROHM 100A and 1200V SiC power MOSFET and SBD's. In each half-bridge module (D_1, T_{b1}) only the SBD of the upper switch, D1, is used and its complementary MOSFET biased OFF.

Test results are shown in Figure III-27 for 220Vac line voltage (top), line current (center sinewave), dc output voltage, and dc output current (bottom trace). In this test the output power was 4.65 kW and U_{do}=590V_{dc}.

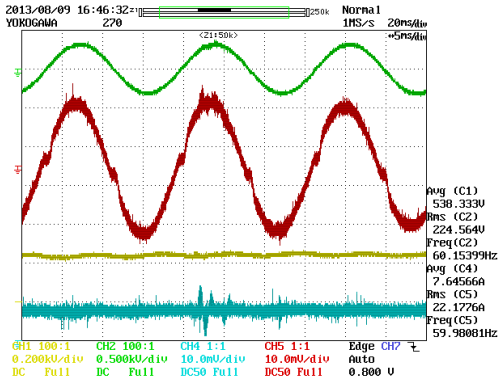

Figure III-27: Interleaved boost PFC: PF~97%, THD<5%, eff~97%.

HF Power Inverter

The team found that using an interleaved boost PFC stage meant that SiC devices were necessary since 40 kHz capable silicon MOSFET's would have taken up substantially move package space. However, this election meant that dc-link voltages would be significantly higher so that the earlier program work using PowerEx Intellimod 600V modules had to be replaced with Intellimod 1200V, 450A modules. Fortunately the replacements were accommodated on the existing heat sink. Figure III-28 shows the boxed power inverter that uses a standard NEMA enclosure that is weather sealed for installation outdoors.

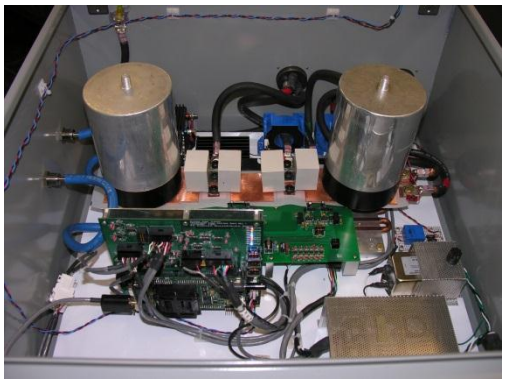

Figure III-28: WPT base station power inverter rated >10 kW.

The major components in the WPTB station inverter are visible in Figure III-28, including the large 2,000 mF, 800V, film capacitors that provide a stiff dc-link to HF ripple currents of both the WPT primary power (low power factor) and the PFC stage ripple current. These therefore do double duty in a power electronics sense.

In the foreground of Figure III-28 is the Spectrum Digital DSP card with its interface connectors and mating to ORNL developed signal conditioning and gate driver board. The power modules are mounted to a heat sink directly below the large film capacitors. The smaller film capacitors are module snubbers, Kemet 1,000V film type.

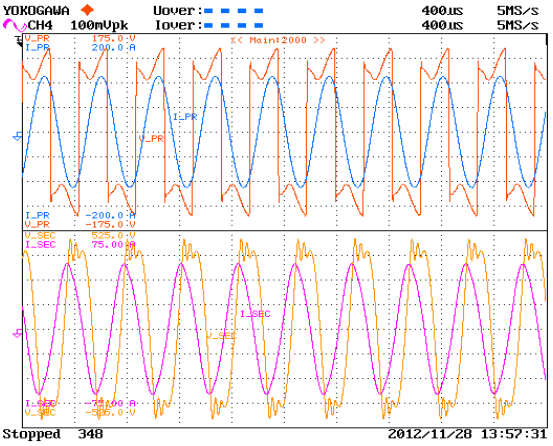

Figure III-29: WPT power inverter output voltage and current.

Figure III-29 is a screen shot from the Yokagawa PZ4000 power analyzer used to monitor WPT signals. In this case both primary and secondary voltage and currents are visible for a power transfer of 5 kW at 23 kHz over a gap z=150mm.

Top waveforms in Figure III-29 the HF bridge quasi-square wave voltage (d=0.8) forced into square wave by reactive current and the very sinusoidal primary current at lagging PF.

Bottom waveforms in Figure III-29 are the secondary side voltage at the rectifier input and the secondary coil current, also a clean sine wave. The sinusoidal primary and secondary currents are the result of series resonance on the primary and parallel resonance at the secondary.

HF Isolation Transformer

Although not essential to WPT operation the WPT team elected to incorporate a HF isolation transformer for two reasons: 1-as matching element between the now high voltage power inverter stage, and 2-for voltage isolation. Figure III-30 shows the construction of the soft ferrite HF transformer as a stack of ferrite rings that act as a low reluctance flux path to couple primary and secondary Litz windings.

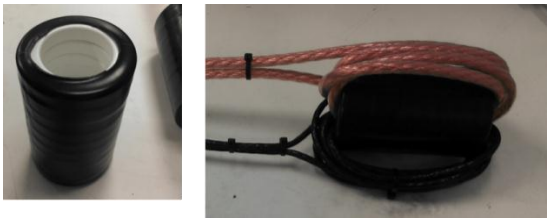

Figure III-30: HF isolation transformer core and windings.

Table III-10 presents the HF transformer design details and parameter characterization test results. The transformer shown is a single stack, but this has also been realized as a CWT with the same turns ratio but half the ferrite rings (Ferroxcube 3C94 low loss MnZn ferrite) in two separate stacks for a more compact structure.

Table III-10: HF ferrite transformer design details.

Core Parameter	Unit	Value
Outside diameter, OD	(mm)	88
Inside diameter, ID	(mm)	64
Stack, L	(mm)	140
Core mass (3C90)	(kg)	2.343
Core loss factor, Pv@25 kHz	(W/lit)	100
Core saturation flux density, Bs	(T)	0.38
Primary turns, Np	(#)	10
Secondary turns, Ns	(#)	4

Table III-11: HF ferrite transformer characterization data.

Transformer Parameters	Unit	Value
Pri Leakage Inductance	(μH)	14.5
Sec Leakage Inductance	(μH)	3.52
Mutual Inductance	(mH)	2.68
Coupling coefficient	(#)	0.9946
Primary Res @ 22 kHz	(Ohm)	0.2397
Secondary Res @ 22 kHz	(Ohm)	1.384

Another aspect of high power transfer at high frequencies is the fact that the ac resistance of conductors increases exponentially with frequency over their dc values (3).

Moreover, even at very low frequencies such as line frequency, the ac currents distribute themselves according to proximity to adjacent conductors and this adds to the resistive losses.

$$R_{ac}(f) = R_{dc}[1 + bf^{\alpha}] + R_{prox} \quad (3)$$

Where the proximity contribution can be derived from the additional power loss due to currents in adjacent wires that develop a magnetic field strength, H, at the field point conductor. In (4) the field point conductor has length, L, conductivity, σ, and coefficient of proximity effect, D_s.

$$P_{prox} = \frac{L}{\sigma} H^2 D_s \quad (4)$$

Some effort was applied to quantify the proximity coefficient in (4), including measuring R_{ac} of the WPT Litz conductor coils at several frequencies, down to 100 Hz, without repeatable results. Figure III-31 illustrates the normalized Rac for a WPT primary coil compared to a exponential (3). At dc current the function shown in Figure III-31 should cross at 1.0, but it won't due to proximity effect.

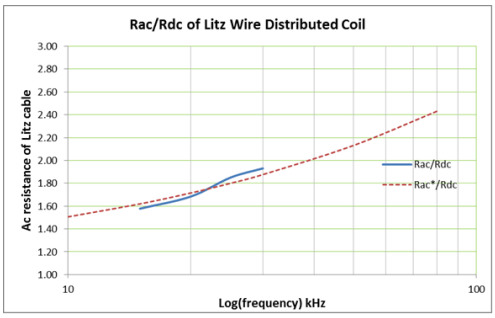

Figure III-31: Normalized R_{ac}/R_{dc} of Litz wound WPT coil.

WPT Coupler

Coupling coil assembly sequence was shown in Figure III-19 and results of that construction are provided here for reference. A coupler designed for 7 kW power transfer has the design values listed in Table III-12.

Table III-12: WPT 7 kW coupling coil parameters.

Parameter	Unit	Value	Description
Side, a	(mm)	533	Width
Side, b	(mm)	558	Length
Radius, r_{eq}	(mm)	300	Equiv. radius
Face area, S	(m2)	0.297	Net area
Turns, Nc	(#)	11	Coil turns
R_{dc}	(mΩ)	22	Dc resistance
R_{ac}	(mΩ)	64	Ac resistance
L_{11}	(μH)	122	Self inductance

The coil itself, and shown as coupler with gap, z, and coefficient of coupling k(z) is shown in Figure III-32. The aluminum tray shown surrounding the coil provides additional shielding of the fringe field.

Figure III-32: Wireless coupler, environmentally sealed.

There are two very important characterization tests for all WPT couplers, in addition to understanding R_{ac}/R_{dc}, and that is quantification of coupling coefficient vs gap and how this coefficient varies with misalignment. ORNL elected to characterize all couplers by three independent methods referred to as open circuit, k_{oc}, inductance aiding, k_{aid}, and compensated in which the effects of both voltage and current are included, k_{comp}. Figure III-33 shows the results of these characterization tests for the coupler of Table III-12. For clarity (5) documents the characterization process.

$$k_{oc}(z) = \frac{U_2}{U_1}\Big|_{\substack{U_2=U_{OC} \\ I_1=10\,A_{rms} \\ gap=z}} \qquad k_{aid}(z) = \frac{L_{aid}-(L_1+L_2)}{2\sqrt{L_1L_2}}\Big|_z \qquad k_{comp}(z) = \sqrt{\frac{U_{2oc}\times I_{sc}}{U_{1oc}\times 10}}$$

$$I_1 = 10\,A_{rms} \qquad (5)$$

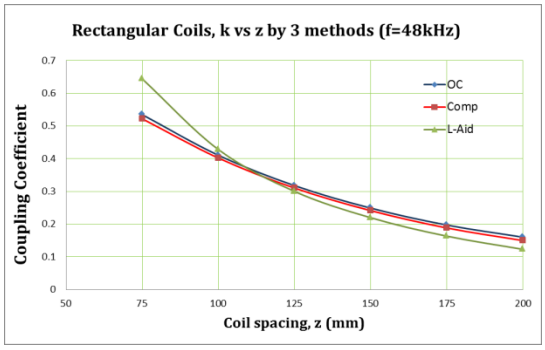

Figure III-33: Coupling Coefficient by 3 methods of (5).

Misalignment has the same effect on coupling coefficient as increasing the gap. This is shown from test result in Figure III-34 in which circular coils were misaligned by given percentages. This test was intentionally done for the general case and the coils in question had slightly different radii, which means the misalignment effect is not apparent until the somewhat smaller secondary coil "touches" the larger primary coil perimeter.

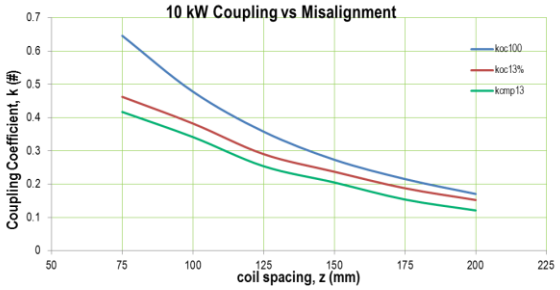

Figure III-34: Coupling Coefficient for misalignment.

Derivation of the misalignment for the general case of non-equal circular coils has been documented elsewhere and is beyond the scope of this report. What is interesting to note by comparing the open circuit with compensated coupling coefficient data in Figure III-33 with that of Figure III-34 is that with misalignment k_{oc} and k_{comp} have separated significantly. It is know that k_{comp} according to (5) is the square root of the product of a voltage based and current based coupling coefficient. It may be that when compensated the value of k_{comp} during misalignment is more accurate. This is the subject of on-going research.

Secondary Electronics

The objective of ORNL's primary side regulation is that all vehicle mounted components be minimized. This means minimal complexity, mass, volume, and cost. Implementing this objective was achieved by reducing the size of the secondary coil, using a compact rectifier, filter, and disconnect and protection electronics. The CAN connection gateway and associated radio modem are minimal as possible.

Figure III-35 shows that the secondary electronics are indeed minimal. However, at a higher systems level, that includes interfacing to various vehicle subsystems, human-machine-interface (HMI), and radio communications the requirements on WPT interfacing increase dramatically as Figure III-36 shows.

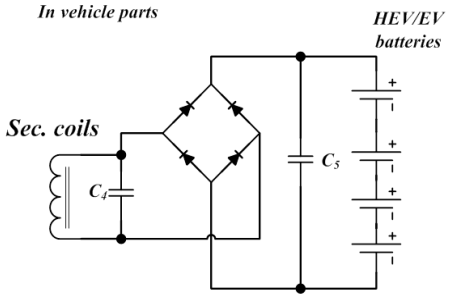

Figure III-35: Secondary coil, rectifier, and filter capacitor.

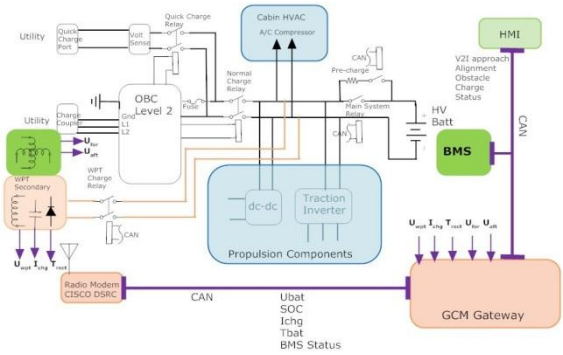

Figure III-36: Secondary electronics considering vehicle interfaces.

It will be the role of the program commercialization partner during year 2 to implement vehicle interfaces similar to those illustrated in Figure III-36 for a fully operational WPT charger.

Communications

Figure III-36 in secondary electronics has partially introduced the role of communications as it includes both on vehicle CAN messaging and the wireless modem for power flow regulation, status, and fault reporting. What is important to note is that dealing with an existing OBC is problematic. Not only may the CAN messaging be proprietary, but interfacing to the OBC, and this will be necessary in order for conductive

and wireless charging to be mutually exclusive, means that since it tracks the vehicle high voltage battery pack SOC that this same function must be performed seamlessly during wireless charging.

In addition to accessing CAN, the WPT gateway, and HMI (shown in Figure III-37), the secondary communications system must also coordinate new and existing contactors so that all vehicle functions remain intact.

Figure III-37: HMI display of battery pack data in Prius Hymotion.

At the conclusion of year 1 activities a DSRC radio modem, shown in Figure III-38, is being validated. Early work on WPT charging relied on the Zlinx 2.8 GHz radio. Communications hardware and software plays a large role in year 2 effort.

Figure III-38: DSRC radio modem for WPT communications.

The radio is a CISCO 819 router (figure 23) designed to operate from 5Vdc, 8 to 60W of power draw, the case is IP54 rated and its capable of operating in 20ºC to +60ºC ambient.

Control

Control algorithms continue to evolve and are being executed using the hardware and software listed in the Tools and Data section of this report. For this project the controller monitors voltage and current delivered to the vehicle regenerative energy storage sstem (RESS), performs calculations based on RESS SOC and other criteria and develops appropriate control levels for PFC voltage U_{do}* and HF power inverter frequency command (selected band center frequency ω_0 +/- $\delta\omega$, an offset increment).

It has been determined through analytical and experimental work that control action is required to not only manage power transmission magnitude, for which the variable U_{do}* is very effective, but also the need to provide incremental adjustment as noted above. For example, if the coupler gap changes for any reason at a give power command then a frequency adjustment is necessary (6). According to (6) an increase in gap will result in k_z decreasing (see Figure III-33) so that frequency must decrease, since the resonance point of the secondary shifts to lower frequencies.

$$\omega_0 = \frac{1}{\sqrt{L_S(1-k_Z)C_S}} \quad (6)$$

$$U_0(SOC) \approx \frac{U_s}{Z_p} \approx \frac{\omega U_S I_p}{\left[\left(\frac{\omega}{\omega_0}\right)^2 - 1\right]} \quad (7)$$

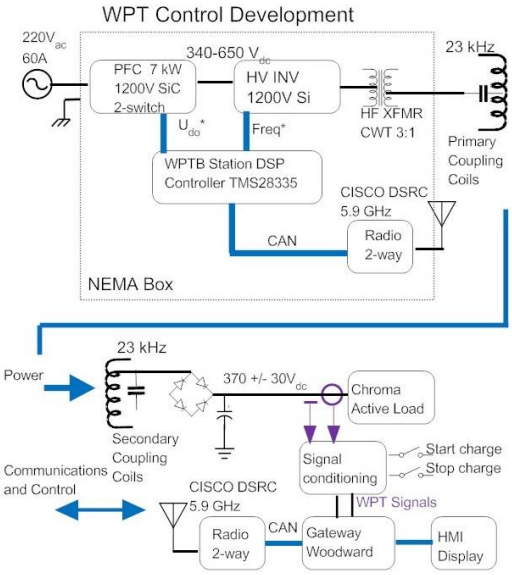

Figure III-39: Control high level functional diagram.

The control algorithm must also accommodate changes in vehcle battery pack SOC, which according to (7) presents as a change in output voltage, U_0. For example, increasing SOC results in an increase in U_0 and from this a demand for frequency to decrease. This is so because the denominator in (7) responds much faster to frequency than its numerator. Because of this phenomenon the ORNL team selected series-parallel (S-P) tuning of the WPT system where the primary is series tuned, and the secondary parallel tuned as shown in Figure III-39. With S-P tuning, unlike S-S or P-S, the power transfer function versus frequency has more gently sloping skirts that useful to monitor and take corrective action for power regulation as shown in Figure III-40. S-S tuning in contrast has a power transfer function with virtually vertical skirts.

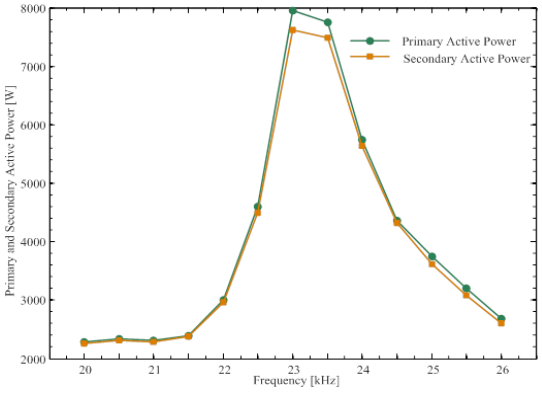

Figure III-40: Power transfer vs frequency for S-P tuning.

Another aspect of control is that it must manage all the handshaking, vehicle immobilization, status, even utility time of use and utility power curtailment due to network loading. Most of these requirements are part of a fully developed product. For this program functions that duplicate these needs are shown as vehicle side command inputs such as start charge and stop charge. To duplicate RESS pack SOC variation the battery emulator voltage is varied.

Efficiency Test Results

A full function WPT system will consist of five power processing stages, each of which will be challenged to deliver >97% efficiency, therefore putting a lower bound on grid to battery power transfer efficiency of 85%. It has been reported earlier in this report that transitioning from silicon to wide bandgap power semiconductors facilitates higher efficiency because these devices have much lower switching loss and can tolerate higher operating temperatures. The ORNL team has taken the first steps in this direction by fabricating the PFC stage with SiC. At the time of this writing the ORNL team has also fabricated SiC power inverter that is being used to make comparisons of efficiency and leakage fields in the four center frequency bands currently promoted for WPT operation. Figure III-41 shows the equipment set-up and results of efficiency testing in the 4-center frequency bands in Table III-13.

Table III-13: WPT Center Frequency Bands.

HD: Heavy Duty Vehicles		LD: Light Duty Vehicles	
(21.05–38.1) kHz	(42.0–56.9) kHz	(81.38–90.0) kHz	(140.91–148.5) kHz

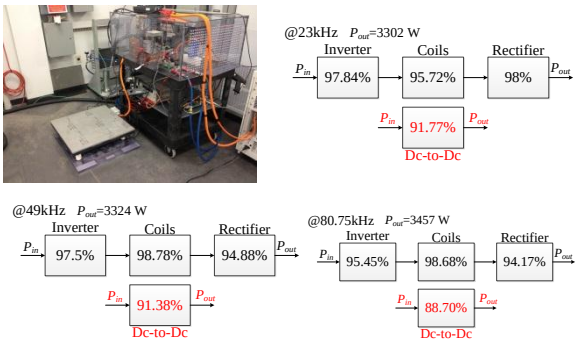

Figure III-41: Efficiency comparison at different frequencies.

Details of ORNL's center frequency band comparisons using a SiC H-bridge power inverter, the coupler defined in Figure III-32, and secondary rectifier discussed in Figure III-35 have been shared with the SAE J2954 wireless charging task force.

Figure III-42 provides a breakdown of losses that serves to highlight the areas needing more research and development. For example, the major loss components are due to the HF power inverter (silicon in this case) and the coupler primary coil ac resistance (see eq's.3 and 4).

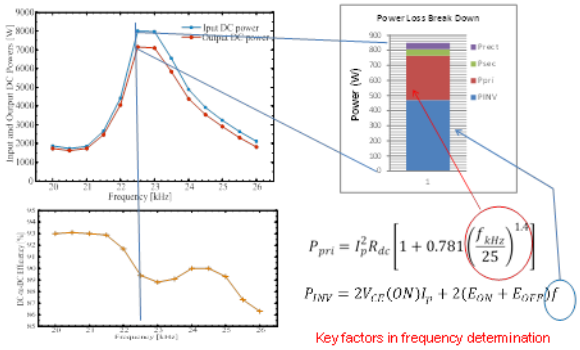

Figure III-42: WPT inverter and coupler efficiency breakdown.

The ORNL team also investigated coupler misalignment and tilt of the secondary coil. Tilt may occur for example due to uneven vehicle loading, defective suspension components, or for ground embedded primary, heaving due to frost.

Coupler Misalignment and Tilt

Misalignment calculations for square and rectangular coils are straight forward and given as the percent total secondary coil area not over-lapping the primary coil area. ORNL tested misalignment up to +/-10% in both x-axis (longitudinal) and y-axis (lateral). The hardware configuration and test results for an output power, Po=5 kW are given in Figure III-43 for misalignment and Figure III-44 for tilt tests.

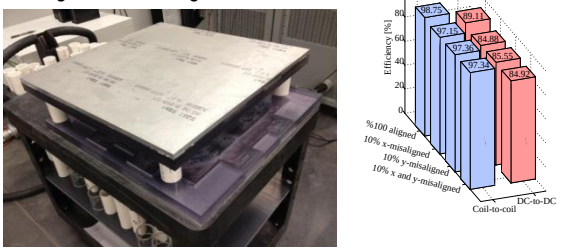

Figure III-43: WPT coupler efficiency vs. misalignment.

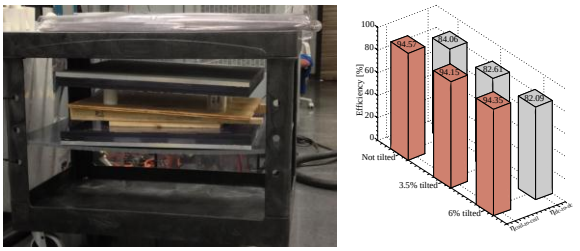

Figure III-44: WPT coupler efficiency vs. secondary tilt.

In these tests the WPT operating conditions are: Gap: z=150mm (magnetic airgap, measured from center to center at all cases including not tilted and ~3.5% and ~6% tilted conditions), Load voltage: V_{batt}=420V, Duty cycle: d=70%, C_{series}=0.39μF, switching frequency: f_s=23.5kHz.

Objects in Coupler Active Zone

Any conductive object placed in the WPT active zone (see Figure III-21 for definitions) will experience induced electrical currents (e.g., Faraday's law) that in turn give rise to Joule heating in direct proportion to the materials electrical conductivity. Metallic objects will heat very rapidly, especially if they present a large surface area to the WPT primary coils, and materials such as foil backed paper will result in paper

charring and even combustion. Figure III-45 illustrates the case for copper and aluminum foils in the WPT active zone when operating at P_0=5 kW and f_0=23 kHz.

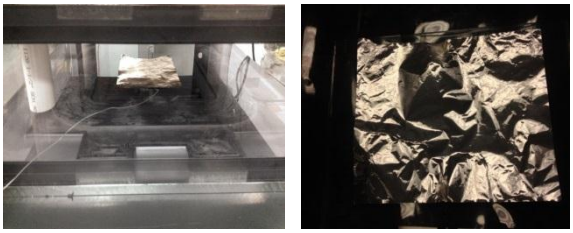

2-mil copper foil in working gap Aluminum foil in gap

Figure III-45: Metallic foils in coupler active zone.

Objects such as coiled extension cords placed on the primary coil during charging will have induced voltages present. In one test 20 V_{ac} was measured across the pins of an extension cord. If the cord ends were plugged together this induced voltage would give rise to currents in all three of the cord's conductors at a magnitude limited only by its resistance (mΩ). For small objects such as a Coke can, keys, jewelry and the like will have much lower response and may heat by only two or so degrees Celsius.

Variations in the Coupler Gap

The control section of this report provided insights into what the expected results will be if the magnetic gap is varied during power transfer (e.g., see eq's. 6 and 7). The effect is detuning of the resonant operating condition. Corrective action requires that the controller increment the operating frequency down (increasing gap) or up (decreasing gap).

Under the similar conditions as in Figure III-43 and Figure III-44, namely the battery emulator load set to U_{batt}=420V, DC link voltage: U_{do}=135V, Duty cycle: d=70%, C_{series}=0.44 μF, and f_0=21.7 kHz for P0= 5 kW throughput, then the frequency increment, shown as Figure III-46, is on the order of 28 Hz/mm.

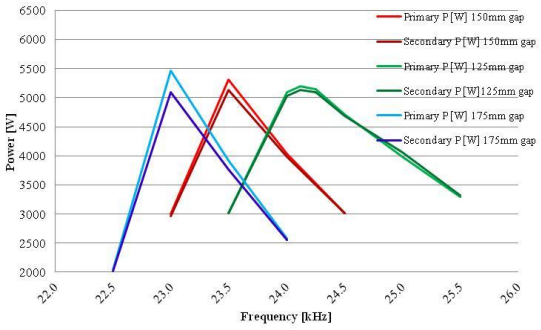

Figure III-46: WPT frequency detuning due to gap variation.

In terms of the center frequency f0 = 23.5 kHz a variation of +/- 25mm results in only +/-3% frequency increment by the HF power inverter. Consider a scenario where charging is taking place at gap, z=150mm, and the vehicle then lowers by 25mm. In Figure III-46 this means that without frequency compensation the throughput power drops from 5 kW to approximately 3.5 kW. As noted earlier, the gradual sloping skirts of the S-P tuning facilitate much easier power recovery. In this case the power inverter frequency would be incremented by +3%. As with misalignment, WPT efficiency due to gap variations also suffers. This is summarized in Figure III-47 that shows not only lower overall efficiency as gap increases, but that it will tend to roll-off much faster with frequency.

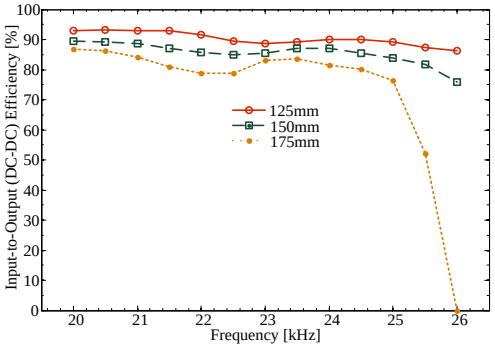

Figure III-47: WPT efficiency vs gap vs frequency.

Conclusions

This report summarizes significant progress, deep insights, and promotion of international standards for wireless charging technology at ORNL and advocated by the U.S. Department of Energy. These findings include assessment of WPT versus the four center frequency bands available showing that operation in the 20 kHz band is preferable for efficiency and misalignment tolerance. It was also found that a full function WPT installation will consist of a cascade of five major functional subsystems in order to meet grid power quality, electrical isolation, and low harmonic frequency generation.

Technology innovations also occurred during execution of year one of this program. Specifically, the incorporation of wide bandgap semiconductor devices operating at high frequency in the WPT PFC stage, and low loss soft ferrites in magnetic components. One innovative material yet to be evaluated is nanocomposite ferrite developed by Ageis Technologies that shows promise of dramatic bulk and mass reduction of magnetic components. Areas of application for nanocomposite ferrites include the PFC stage input inductors, the HF isolation transformer, and the coupler flux guides. The flux guides in particular tend to be thin and long making them susceptible to fracturing under flexure. ORNL's material scientists devised a coating process and material that significantly increases their flexure strength.

ORNL has also worked closely with our program partners, especially for commercialization and shared with them specifics of the WPT system design, schematics, BOM, and test data.

III.K.3. Products

Publications

1. Omer C. Onar, John M. Miller, Madhu S. Chinthavali, Lixin Tang, Steven Campbell, "*SiC MOSFET based Single Phase Active Boost Rectifier with Power Factor Correction for Wireless Power Transfer Applications*,"

IEEE Applied Power Electronics Conference, APEC2014, Fort Worth Convention Center, 16-20 March 2014.

2. Madhu Chinthavali, John M. Miller, Omer C. Onar, "*A Comprehensive Analytical and Circuit Level Model Development for Wireless Power Transfer Systems*," IEEE Applied Power Electronics Conference, APEC2014, Fort Worth Convention Center, 16-20 March 2014.
3. Madhu Sudhan Chinthavali, Omer C. Onar, John M. Miller, Lixin Tang, "*Single-Phase Active Boost Rectifier with Power Factor Correction for Wireless Power Transfer Applications*," IEEE 5th Energy Conversion Congress & Exposition ECCE2013, Denver Convention Center, Denver, CO, 16-20 September 2013.
4. Puqi Ning, John M. Miller, Omer C. Onar, Clifford P. White, "*A Compact Wireless Charging System for Electric Vehicles*," IEEE 5th Energy Conversion Congress & Exposition ECCE2013, Denver Convention Center, Denver, CO, 16-20 September 2013.
5. John M. Miller, Omer C. Onar. P.T. Jones, "*ORNL Developments in Stationary and Dynamic Wireless Charging*," Special Session: Advances in Wireless Power for Electric Vehicles, IEEE 5th Energy Conversion Congress & Exposition ECCE2013, Denver Convention Center, Denver, CO, 16-20 September 2013.
6. O.C. Onar, J.M. Miller, S.L. Campbell, C. Coomer, C.P. White, L.E. Seiber, "*A Novel Wireless Power Transfer for In-Motion EV/PHEV Charging*," IEEE Applied Power Electronics Conference, APEC2013, Long Beach Convention Center, Long Beach, CA, 17-21 March 2013.
7. P. Ning, J. M. Miller, O. C. Onar, C.P. White, "*A Compact Wireless Charging System Development*," IEEE Applied Power Electronics Conference, APEC2013, Long Beach Convention Center, Long Beach, CA, 17-21 March 2013.
8. M. Chinthavali, O.C. Onar, J.M. Miller, "*A Wireless Power Transfer System with Active Rectification on the Receiver Side*," presented at the Conference on Electric Roads and Vehicles, CERV2013, Newpark Hotel, Park City, UT, 4-5 February 2013.
9. J.M. Miller, "Wireless Charging for Electric Vehicles," presented to DOE VT Vehicle Systems Subprogram and NETL, ORNL-NTRC-2, DOE FOA-DE-000670 Award Kick-off, 9 November 2012.
10. J.M. Miller, "*Wireless Charging for Electric Vehicles*," presented to VSATT Meeting and Project Deep-dive, ORNL-NTRC-2, 7-8 November 2012.
11. *J.M. Miller, "ORNL's in-motion wireless power charging,"* invited talk to U.S. Department of Transportation (DOT) Research and Innovative Technology Administration (RITA) workshop on inductive mobile vehicle charging at Turner-Fairbanks Highway Research Center, McLean, 28 Nov 2012.

Patents

1. J.M. Miller, O. C. Onar, P.T. Jones, *Dynamic Power Tracking of Wireless Charging Apparatus*, in work as of August 2013.
2. O. Onar and J.M. Miller, Buffering Energy Storage Systems for Reduced Grid and Vehicle Battery Stress for Wireless In-motion Wireless Power Transfer Systems (ID-2956) by was filed 11 October 2012.

Tools and Data

- Texas Instruments Code Composer Studio v3.3
- Microsoft Windows Software Development Kit 7.1.NET Framework 4.0 (alternative is to use Microsoft Visual C++ 2010 Professional Service Pack 1)
  - MathWorks family of products for rapid prototyping and fast code development:
    - MATLAB & Simulink
    - Real Time Windows Target
    - Embedded Coder
    - Simulink Coder
    - MATLAB Coder
    - Real Time Workshop

III.L. High Efficiency, Low EMI and Positioning Tolerant Wireless Charging of EVs

Allan Lewis, Principal Investigator
Hyundai America Technical Center Inc
6800 Geddes Road
Superior Township, MI, 48198
Phone: (734)-337-3170
E-mail: alewis@hatci.com

John Jason Conley, NETL Program Manager
Phone: (304) 285-2023
E-mail: John.Conley@netl.doe.gov

III.L.1. Abstract

Objectives

- The objective of this project is to develop, implement, and demonstrate a wireless power transfer system that is capable of the following metrics:
- Total system efficiencies of more that 85%.
- Power transfer at over 6.6kW.
- Maximum lateral positioning tolerance that can be achieved while meeting regulatory emission guidelines.

Major Accomplishments

- Defined end-to-end block diagram and control interfaces.
- Created accurate electrical simulations of power chain from AC input to DC supply to EV battery.
- Calculated power efficiency estimates of the system based on simulations and projections from Mojo Mobility low power wireless charging systems.
- Created complete electromagnetic models of receiver and transmitter coils and magnetics.
- Simulated the electromagnetic system in effort to optimize the wireless power transfer.
- Defined system block diagram
- Developed custom Charger system: AC / DC converter; voltage boost and resonant converter + comms. & control system
- Developed custom Vehicle system: Rectification, comms. and control, DC power transfer to HV battery
- Developed custom Electromagnetic coil sub-system

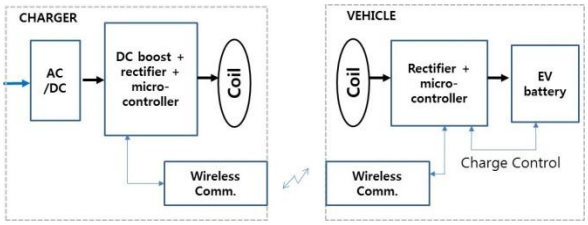

Figure III-48: Wireless charging system block diagram.

Future Achievements

- The target misalignment tolerance is ±0.5 m along the width of the vehicle and ±1 m along the length of the vehicle at greater than 20 cm coil to coil gap with the capability for real-world operation.
- The work in Phase I will also include a cost analysis to show initial production costs for the system.
- In Phase II, the system will be further developed and integrated into a vehicle while meeting safety standards. A commercial viability analysis of the system and cost benefits for components both on-board and off-board the vehicle will be performed.
- In Phase III, the real-world test results of operation of the system on a fleet of five light-duty electric vehicles will be demonstrated and all required safety and electromagnetic field (EMF) emission test results and real world performance results obtained and provided.

✧ ✧ ✧ ✧ ✧

III.L.2. Technical Discussion

Background

Timeline

- Start date–Oct. 2012
- End date–Sept. 2015

Partner

- Mojo Mobility

Technical Barriers

- Conductive charging stations introduce limitations regarding access, range, and usability.
  - ADA access
  - Cord length and inconsistent vehicle port placement
  - Overall usability
- Wireless charging systems are prone to EMI, position intolerance, and low efficiency.

Introduction

The purpose of this project is to address the following technical barriers

- Reduce the dependence on conductive charging stations which will allow more convenience to the user, increased access and usability in support of ADA, and provide a charge with potentially no action required by the driver.
- Develop a wireless charging system that meets industry guidelines, while operating with position tolerance, large vertical distance, and efficiency of more than 85%.

Approach

The project team has formed a team to review and monitor regulatory requirements and standards. The team has joined, and interfaces regularly with the following Society of Automotive Engineers (SAE) task forces.

- SAE J2954 Wireless Charging Task Force and the following subgroups:
  - Alignment & Communication.
  - Safety, Performance, Robustness Testing & Validation.
  - Magnetic Field Interoperability.
  - Verification Testing.
  - Bus Charging.
  - Frequency Determination & EMC/EMF Definition.
- SAE J2836/6 Wireless Charging Specific Use Cases.
- SAE J2847/6 Wireless Charging Specific Messages.
- SAE J2931/6 Wireless Charging Specific Protocols.

The project team has completed the electrical and magnetic system modeling tasks required to develop component level specifications

- Electrical system from AC outlet to DC into high voltage battery.
- Electromagnetic models of receiver and transmitter coils and magnetics.
- Combining the coil and magnetics modeling with the electrical model
- Optimize total system

The prototyping strategy for our high power wireless charging system is to develop discrete functional sub-systems with the following functions that will become further integrated into a packaged system:

- AC/DC Front End
  - High efficiency (93-94%)
  - 240VAC single phase input
  - 500V DC output
- High Frequency resonant converter sub-system (charger system)
  - Custom electrical circuit PC board with microprocessor control
  - Closed loop power control loop
  - Rectification, filtering and resonating circuitry
  - Current and voltage measurement
  - Wireless communication control loop
- Electro-magnetic power transfer sub-system
  - Custom designed charger system coil and magnetics
  - Custom designed vehicle system coil and magnetics
- High frequency rectifier sub-system(vehicle system)
  - Custom electrical circuit PC board with microprocessor control
  - Rectification of resonant power from coils
  - Filtering
  - Current and voltage measurements
  - Wireless communication control loop

The hardware and software systems are being designed to account for real world conditions that will allow for the complete usage life cycle.

- Power level flexibility.
- Interface with vehicle onboard battery and charge system.
- Charger and receiver coil alignment systems.
- Receiver Identification, Error or Fault handling, End of Charge, etc.

The design team has made efficiency considerations in every area of the system. These considerations include:

- Material, geometry, component selection.
- Feedback control

Based on the project schedule demands, there is little allowance for trial and error in the hardware design process, therefore a specific concentration has been made in the area of electromagnetic interference mitigation.

- Charger and receiver coil and magnetics design.
- Board layout.
- Secondary system placement and packaging.

The project team has identified the surrogate Grid Connected Electric Drive Vehicle's (GCEDV) make and model thus allowing for more informed mechanical considerations.

- Thermal issues, size, weight, integration into vehicle.

Based on our goal of wireless charging system tolerance enhancement, a considerable amount of time and effort has been spent defining and developing the coil and magnetics design and geometry that will allow our significant improvement over existing industry metrics.

As with any comprehensive engineering development project, our design efforts are evaluated against predefined verification tests that measure the system capabilities in the following disciplines:

- Power transfer rates.
- Efficiency.
- Position tolerance.
- Electromagnetic emission.

In summary, our approach is a systematic design and development of a grid connected electric drive vehicle wireless charging system that meets the expectations of low EMI, high position tolerance, and operates with high efficiency.

The goal upon completion of Phase III of our development project is the introduction of system that meets the needs of electric vehicle drivers that allows for series manufacturing

and commercialization of the technology with the following considerations.

- Cost of materials throughout the design process.
- Emphasis on simplicity and user convenience.

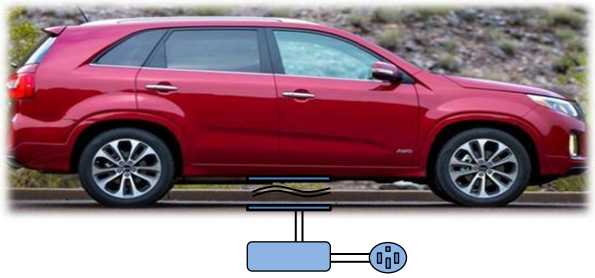

Figure III-49: GCEDV wireless coil placement.

Based on the objectives of the project our system will provide inherent position tolerance to the driver however a guidance system may be available to assist if needed. This system will wake up based on proximity to vehicle and provide alignment aids to driver in cases of gross misalignment. This area of EV charging is quickly emerging and therefore our team is assuring that all alignment and communication strategies are in-line with the SAE J2954 works-in-progress.

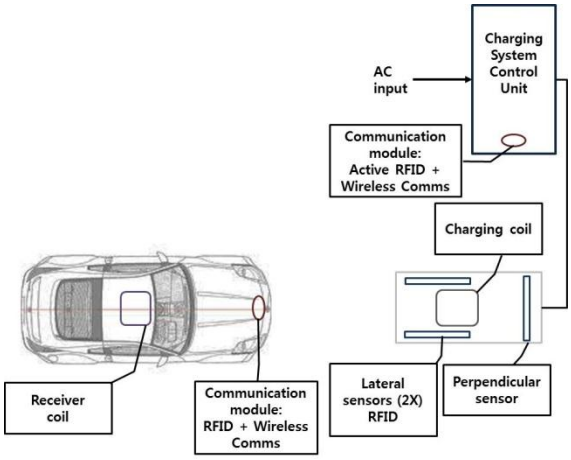

Figure III-50: Wireless system alignment diagram.

Results

Development efforts have provided efficiency estimates for Phase 1–Part 1–in regards to the systems' DC to DC conversion illustrated in Figure III-51.

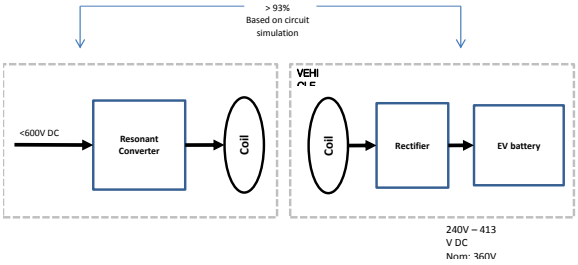

Figure III-51: Wireless power transfer subsystem efficiency.

Our current circuit simulation model of the power transfer efficiencies from the DC charger input to the DC receiver output to the EV battery show the following promising outcomes.

- Efficiencies exceeding 93%.
- EV battery voltage ranges (240-413V) can be achieved.

Modeling in each specific system domain is revealing insights into the design parameters that provide a rapid acceleration in confidence in initial system and subsystem specification. An example of such model design aiding work is presented below in Figure III-52, which shows a weak dependence on charger inductance when evaluating the charger efficiency versus traction battery pack voltage.

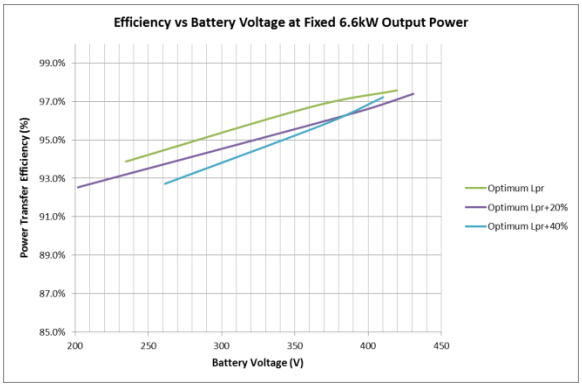

Figure III-52: System efficiency calculation for various charger inductances over battery voltage.

In Figure III-53, the DC-DC efficiency and output voltage are plotted as a function of output power showing a steady efficiency curve over the full range.

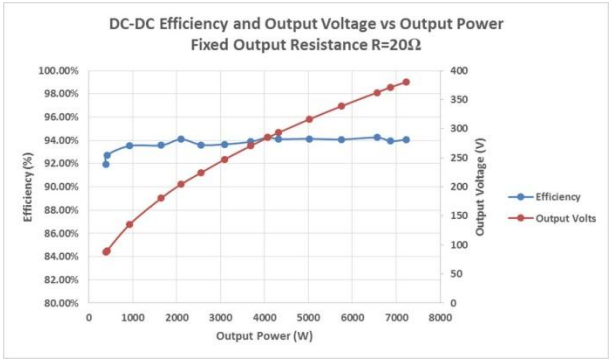

Figure III-53: DC-DC efficiency and output voltage versus output power for a fixed output resistance.

Figure III-54 shows actual measurements taken on a prototype system and are compared to simulation results under the same conditions. This shows a very accurate correlation between simulation and actual results, which help the development team prove early predictions and can extrapolate for future results.

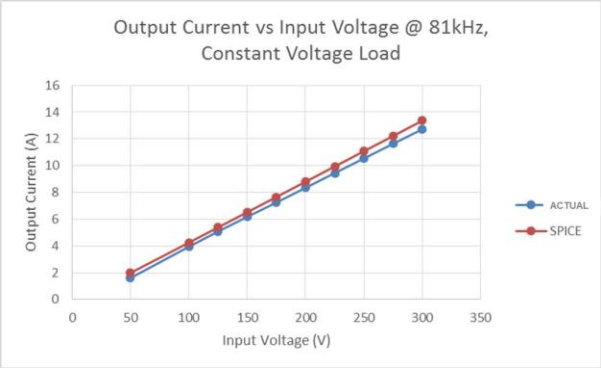

Figure III-54: Actual output current measurements versus simulation results at a fixed frequency and load.

Conclusions

The benefits provided by wirelessly charging Grid Connected Electric Drive Vehicles (GCEDV) are motivating innovation in the area to address technical challenges. The early design work by HATCI and Mojo Mobility is leading towards the ability to present new state of the art performance capabilities in the areas of:

- Low spurious unwanted emissions into the environment.
- High power transfer efficiencies.
- Large coil to coil misalignment allowance and large vertical gap separation.

The cooperation of HATCI and Mojo Mobility provides an opportunity to develop a next generation GCEDV wireless charging system that can be quickly integrated into production ready vehicles for vehicle level testing that will provide proof of concept systems for evaluation for commercial potential.

Commercial Viability Study performed in FY14 will provide and understanding of the following considerations:

- Commercial viability and cost benefits.
- Comparison with SAE 1772 compliant conductive charging system.
- Expected market penetration.
- Potential petroleum reduction.

III.L.3. Products

Publications

None

Patents

None

Tools and Data

1. NH Research Model 4760-12 Programmable DC electronic load, Up to 24kW
2. Magna Power model TSA800-30 High power AC/DC programmable power supply (up to 24kW) with over current and over voltage protection
3. High current measurement probes
4. High voltage measurement probes
5. Yokogawa Model WT3000 Precision Power Analyzer
6. Rohde & Schwarz—ZNB Vector Network Analyzer
7. Agilent Model CXA signal Analyzer
8. Tektronics Digital oscilloscope model MSO2024
9. Rigol DG1022U Arbitrary Waveform Generator
10. 10.FLIR Thermal Imaging Camera
11. Electromagnetic simulation software
12. Firmware integrated development environment development software
13. Laboratory Laptops and multimeters

ZERO EMISSIONS CARGO TRANSPORT

III.M. Zero Emission Heavy-Duty Drayage Truck Demonstration—Los Angeles

Matt Miyasato, Principal Investigator
South Coast Air Quality Management District
21865 Copley Drive
Diamond Bar, CA 91765
Phone: (909) 396-3249
E-mail: mmiyasato@aqmd.gov

Brian Choe, Project Manager
Phone: (909) 396-2617
E-mail: bchoe@aqmd.gov

Lee Slezak, DOE Program Manager
Phone: (202) 586-2335
E-mail: lee.slezak@ee.doe.gov

Bruce Mixer, NETL Project Manager
Phone: (304) 285-4161
E-mail: bruce.mixer@netl.doe.gov

III.M.1. Abstract

Objectives

- The objective of this program is to evaluate and demonstrate technical feasibility and market viability of various zero emission truck technologies in drayage service to promote and accelerate deployment of zero emission cargo transport technologies in the South Coast Air Basin.
- This program will fund development of 13 zero emission drayage trucks based on four different technology platforms, consisting of three battery electric drivetrains and one fuel cell hybrid electric drive system for a two-year demonstration in real world drayage service between Ports of Los Angeles and Long Beach and nearby rail yards and warehouses.

Major Accomplishments

- Completed a contract modification with the DOE to allocate necessary funding for National Renewable Energy Lab (NREL) to conduct data analysis in this program
- Completed contracts with the four EV manufacturers: Balqon, TransPower, U.S. Hybrid and Vision Industries

Future Achievements

- Finalize systems and components design of demonstration vehicles
- Complete integration of 13 demonstration vehicles
- Complete validation of demonstration vehicles including chassis dynamometer testing
- Deploy vehicles in drayage service with partnering fleets for field demonstration
- Analyze the field test data to evaluate the performance and O&M costs of demonstration vehicles.

✧ ✧ ✧ ✧ ✧

III.M.2. Technical Discussion

Introduction

On-road heavy-duty diesel trucks are one of the largest sources of diesel particulate matter and NOx emissions in the South Coast Air Basin (SCAB). The impact on air quality and public health is more pronounced in the surrounding communities along the goods movement corridors near the Ports of Los Angeles and Long Beach, and next to major freeways in Southern California. As a measure to reduce the impact and to meet future Federal ambient air quality standards, South Coast Air Quality Management District has been working with other regional stakeholders, including the Ports of Los Angeles and Long Beach, to promote and support the development and deployment of advanced zero emission cargo transport technologies. The purpose of this program is to evaluate and demonstrate technical feasibility of various zero emission heavy-duty drayage truck technologies in real world drayage service to accelerate deployment of zero emission cargo transport technologies in the SCAB.

Approach

The program will develop 13 zero emission heavy-duty drayage trucks for demonstration based on four different technology platforms, consisting of three types of battery electric drivetrains from Balqon, TransPower, and U.S. Hybrid, and a fuel cell hybrid electric drive system by Vision Industries. The trucks will be deployed in real world drayage service for a two-year demonstration with partnering fleets to evaluate technical feasibility and market viability of these technologies in cargo transport operations.

Balqon will build three Class 8 battery electric drayage trucks incorporating design improvements and lessons learned from testing and operation of their prototype, MX-30 which is shown in Figure III-55. Each truck will be powered by a 240 kW induction motor with an automatic transmission and the battery pack will use lithium iron phosphate cells with 380 kWh in total capacity. Balqon will also provide an energy storage system utilizing a 500 kWh battery pack for storage with a DC to DC charger that can fast charge vehicles in approximately one hour. This system will offer fleets an option to charge the vehicles during mid day for an extended operation. It will also offer potential to reduce excess utility costs from high power demand charges by charging the storage system during off peak hours.

Figure III-55: Balqon Prototype MX-30.

Figure III-56 shows an illustration of Balqon's demonstration vehicle with major components including:

- 240 kW induction motor coupled to an Allison six speed automatic transmission
- Liquid cooled traction controller with 450–700 VDC input and 460 VAC 3-phase output
- Lithium iron phosphate battery modules with 380 kWh in total capacity, air cooled
- Approximately 100 miles of range in normal drayage operations
- Recharge in 3-4 hours with a 160 kW charger; 1 hour with a DC to DC fast charger

TransPower will develop four Class 8 battery electric drayage trucks building on their prototype ElecTruck, which is shown in Figure III-57. The drive system will be powered by an innovative dual motor system with two 150 kW Fiskar motors, leveraging mass produced components for cost savings and proven reliability. TransPower will use an automated manual transmission with proprietary software to control transmission shift, enabling operation in multiple gears to maximize vehicle efficiency without losses from the torque converters used in conventional automatic transmissions. Each vehicle will be equipped with two Inverter-Charger Units (ICUs) that combine the functions of the vehicle inverter and battery charger to reduce capital costs and simplify charging logistics. The battery pack will use lithium iron phosphate chemistry with 269 kWh in total capacity.

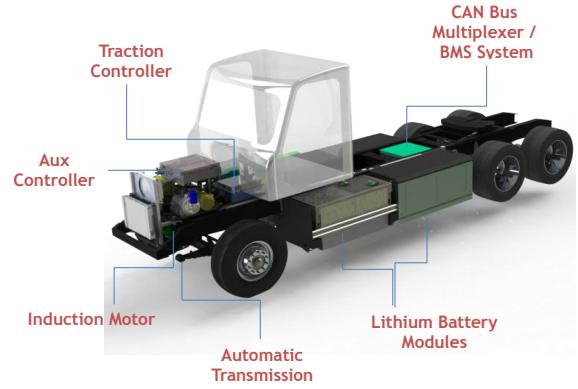

Figure III-56: Balqon Demonstration Vehicle.

Figure III-57: TransPower Prototype ElecTruck.

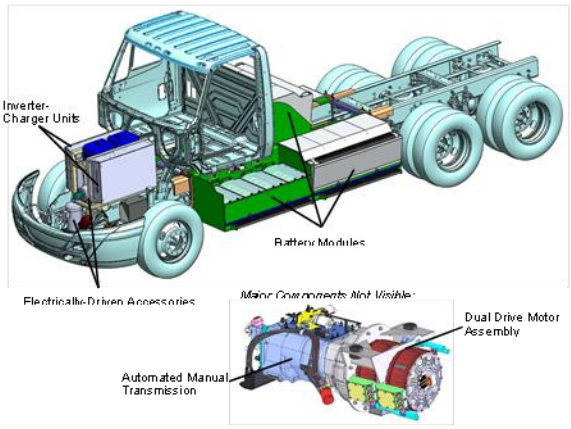

Figure III-58: TransPower Demonstration Vehicle.

Figure III-58hows an illustration of TransPower's demonstration vehicle with major components including:

- 300 kW dual motor assembly with two 150 kW Fiskar motors coupled to a 10-speed Eaton automated manual transmission
- Power control and conversion system with two ICUs, each rated at 150 kW for motor control and 70 kW for charging
- Lithium iron phosphate battery modules with 269 kWh in total capacity

- 70 to 100 miles of range in normal drayage operations
- Recharge in 4 hours with a 70 kW ICU

U.S. Hybrid will develop two Class 8 battery electric trucks in this program. Each truck will be powered by a 320 kW drive system with an induction motor and an automatic transmission, controlled by a 320 kW motor control unit. U.S. Hybrid will use lithium ion battery cells with 300 kWh in total capacity.

Figure III-59shows an illustration of U.S. Hybrid demonstration vehicle with major components including:

- Driveline with a 320 kW induction motor and an Allison automatic transmission
- 320 kW MCU with 6.6 kW on-board charger
- Lithium ion battery modules with 300 kWh in total capacity, air cooled
- Approximately 100 miles of range in normal drayage operations
- Recharge time of 3 hours with a 120 kW charger

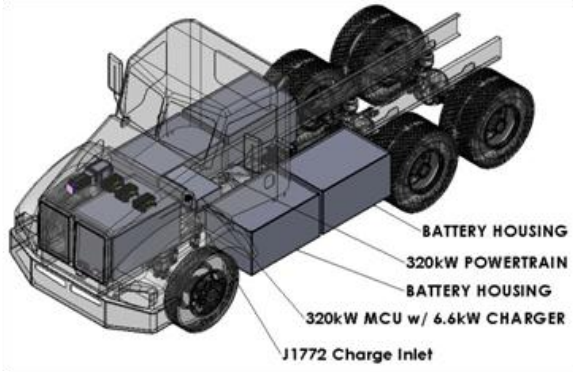

Figure III-59: U.S. Hybrid Demonstration Vehicle.

Vision Industries will use a fuel cell hybrid electric drive system to build four demonstration vehicles integrating design improvements and refinements from the operation of their prototype truck, Tyrano which is shown in Figure III-60. The vehicles will use a Siemens 320 kW ELFA drivetrain powered by lithium iron phosphate battery cells with 130 kWh in total capacity. In order to extend the vehicle's range, two Hydrogenics 16.5 kW PEM fuel cells (33 kW combined) will be added providing an estimated range of 200 miles under normal operating conditions.

Figure III-61 shows an illustration of Vision Industries demonstration vehicle with major components including:

- Siemens 320 kW ELFA drivetrain with two 165 kW inverters
- Lithium iron phosphate battery modules with 130 kWh in total capacity, air cooled
- Two Hydrogenics 16.5 kW PEM fuel cells
- On-board hydrogen storage tanks with 21 kg in total capacity
- 200 miles of range in normal drayage operations
- Recharge/Refuel Time—8 hrs with Level 2 charger/10-15 minutes for hydrogen refueling

Figure III-60: Vision Industries Prototype Tyrano.

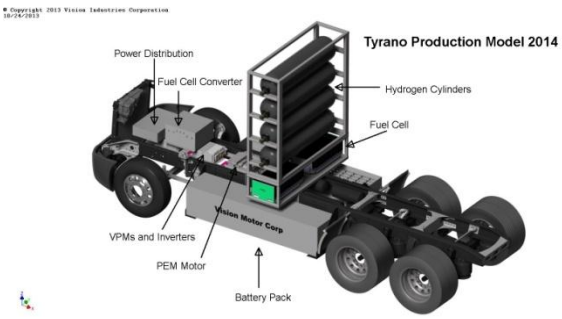

Figure III-61: Vision Industries Demonstration Vehicle.

In order to provide consistent and objective evaluation, NREL will conduct data analysis for all of the 13 vehicles during the two-year demonstration in drayage service. NREL will analyze raw data collected by on-board data collection devices for vehicle performance and efficiency. NREL will also analyze operations and maintenance data to assess the vehicle and infrastructure operating costs in this program.

III.M.3. Products

Publications

None

Patents

None

Tools and Data

None

III.N. Hydrogen Fuel-Cell Electric Hybrid Truck Demonstration—Houston

Allison Carr, Principal Investigator
Houston-Galveston Area Council
3555 Timmons Lane, Suite 120
Houston, TX 77027
Phone: (832) 681-2583
E-mail: Allison.Carr@h-gac.com

Lee Slezak, DOE Program Manager
Phone: (202) 586-2335
E-mail: Lee.Slezak@ee.doe.gov

Charles Alsup, NETL Program Manager
Phone: (304) 285-5432
E-mail: Charles.Alsup@netl.doe.gov

III.N.1. Abstract

Objectives

- Accelerate the introduction and penetration of electric transportation technologies (ETT) into the cargo transport sector.
- Demonstration of twenty (20) Class 8 hydrogen fuel-cell electric hybrid port drayage truck
  - Vehicles included in the project will be the Vision Industries Corporation TYRANO truck
  - Vehicles will meet or exceed all applicable federal and state emission requirements and safety standards
- Operate vehicles under real world conditions at or near the Port of Houston to measure and demonstrate operational cost-effectiveness and commercial viability.

Major Accomplishments

- Engagement with Vision and TTSI to fleet partners to establish performance agreements for vehicle deployment

Future Achievements

- Full deployment and demonstration of 20 Class 8 hydrogen fuel-cell electric hybrid port drayage trucks.
- Reduce emissions of harmful air pollutants
  - Reduce more than 1, 500 metric tons of CO2 per year
  - Reduce more than 0.8 tons of PM per year
  - Reduce more than 38 tons of NOx per year
- Reduce diesel use by more than 143,500 gallons/yr
- Release of technical report on cost-effectiveness of Class 8 hydrogen fuel-cell electric hybrid trucks in regional fleet(s)

✧ ✧ ✧ ✧ ✧

III.N.2. Technical Discussion

Background

The Houston-Galveston Area Council (H-GAC), Total Transportation Services, Inc. (TTSI), Vision Industries, and Environmental Defense Fund have partnered to establish the Hydrogen Fuel-Cell Electric Hybrid Truck Demonstration Project. The primary objective of the project is to acceleration the introduction and penetration of electric transportation technologies into the cargo transportation sector. The project will deploy vehicles, establish required fueling infrastructure, and demonstrate that vehicles will meet or exceed all emissions requirements.

To meet this objective, the grant will support development and demonstration of 20 class 8 hydrogen fuel-cell electric hybrid trucks in the Houston-Galveston-Brazoria NAAQS 8-hour ozone nonattainment area. These vehicles will be demonstrated by TTSI vehicle operators in the Houston-Galveston region. Many of the trucks will serve as goods transport for Wal-Mart, one of the world's largest retailers. The project will demonstrate vehicle operations, collect data, and report on project results for a period of two years after deployment.

Long term benefits of the program may include improved air quality in highly traveled areas in the Houston region and particularly near the active Port facilities. Additionally fleets may realize savings on fuel expenditures and can work towards meeting sustainability and corporate social responsibility goals.

Introduction

This project supports ongoing efforts to reduce criteria pollutant emissions, greenhouse gas emissions, and fossil fuel use among drayage truck vehicles within the Houston region. As the project team works to create the largest demonstration of hydrogen fuel cell electric hybrid drayage trucks within the United States, the vehicles will be monitored and fleet operators will be surveyed in order to measure and demonstrate operational cost-effectiveness and commercial viability of the trucks.

Approach

The vehicles proposed for this project are the Vision Industries Corporation (Vision) TYRANO™. Tthe TYRANO™ is a heavy duty vehicle with a gross vehicle weight rating

(GVWR) of 80,000 lbs. that runs on a hydrogen fuel cell plus plug-in hybrid electric batteries (Figure III-62). The hydrogen fuel cell-powered truck has an electric motor powered by Lithium-ion batteries. The batteries are constantly charged by a fuel cell that converts hydrogen gas into electricity. The batteries can also benefit from the use of regenerative braking to incrementally add charge.

TTSI and H-GAC expect the trucks to transition from demonstration during the project to service upon completion of the project at the PHA for the remaining life of the trucks.

System Description

The Vision TYRANO™ was designed for short-distance (<50 mile) containerized cargo movement with trade corridor communities in mind. It is extremely quiet, thus allowing fleet operators to pass through residential areas, move at night or in the pre-dawn hours of the morning. The Vision TYRANO™ is a zero-emission vehicle utilizing an alternative fuel source that is abundantly available within the United States.

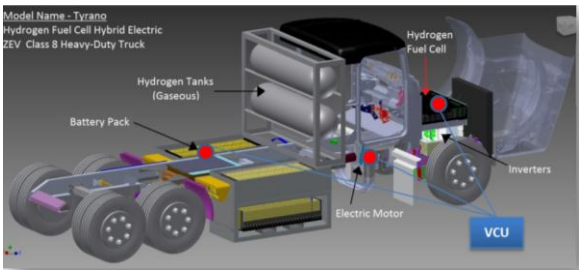

Figure III-62: Diagram of the Vision TYRANO™ Class 8 Heavy-Duty HFCV.

The vehicle consists of three main subsystems, which are the traction subsystem, battery energy subsystem and the fuel cell power subsystem. The traction subsystem aims to provide the mechanical moving power for the vehicle, the battery energy subsystem aims to store energy and to support the traction subsystem, and the fuel cell power subsystem aims to generate electrical energy and store them into the battery energy subsystem.

Fuel Cell Power Subsystem

In the fuel cell power subsystem, the up to 6,250 psi hydrogen is filled into the hydrogen tank and converted into electricity by the fuel cell. Since the fuel cell output voltage is much lower than the battery pack, a boost converter is inserted in between to match their ratings. After the power conversion by the boost converter, the fuel cell power subsystem can charge the battery pack up to 50A, due to the efficiency factor.

Battery Energy Subsystem

The battery pack connected to three components, the inverter (in the traction subsystem), the boost converter (in the fuel cell power subsystem) and the onboard charger. The battery pack has 200 lithium-ion batteries connected in serial and each of them has a 200 Ahr capacity. The total energy capacity can reach 128 kWh and the usable value is 80% of the total capacity (102.4 kWh). The on-board charger converts the AC input to DC current and then charges the battery pack with up to 24A. Theoretically, it takes around 6 hours to charge the whole pack from 20% to 100%.

Testing

Qualitative evaluations and quantitative documentation for the tested parameters will be collected during the program using a combination of an on-board data collection system and input obtained by surveying drivers and maintenance personnel**.** These findings will be included in the monthly, quarterly and final reports.

Testing Variables

The scope of this project includes collection of a substantial dataset that examines and documents a variety of parameters and observations. Variables included in testing are:

- Vehicle speed
- Vehicle horsepower and torque
- Performance over different road grades
- Vehicle acceleration
- Recharging time
- Refueling time Vehicle weight
- Vehicle range
- Ambient temperatures
- Motor temperatures
- Battery temperatures
- Noise
- Fuel consumption
- Energy consumption and pathways
- Maintenance costs
- Operational costs

Unloaded and loaded conditions will be tested during round trip operations.

Data Collection Strategy

This demonstration includes multiple tasks designed to test parameters important to the commercial deployment of this technology. It also includes making ongoing observations designed to track more qualitative variables, such as driver experiences, over the course of the project. Data collection and documentation can be categorized into three types: remote performance monitoring, physical performance monitoring, and physical maintenance monitoring.

All remote performance monitoring will be conducted by Vision. During vehicle operation data will be automatically uploaded to Vision's web portal; this upload will occur every 15 minutes over the Global System for Mobile Communications (GSM) network. The test vehicle comes equipped with a controller that has a built-in GSM device that connects to a GSM network. The advantage of remote monitoring is that it is cost effective because on site personnel are not needed.

TTSI will be responsible for administering all onsite and physical performance monitoring on a daily and weekly basis. Drivers will be given a survey to qualitatively determine the durability and performance characteristics of the TYRANO™. The survey also asks that the drivers to note any safety incidents, unusual experiences, any issues with refueling and other feedback for the TYRANO™.

Any maintenance performed and cost associated with maintenance events will be documented in the vehicle maintenance logs. Vision and TTSI will both maintain a thorough record of all services performed, and document downtime per service. An assessment of vehicle availability (as defined by the percentage of time the vehicle is not undergoing maintenance and is available for use) will be made from analyzing data in fueling logs and service and maintenance records.

Demonstration Period

The project will include a two-year demonstration of hydrogen fuel cell—electric hybrid vehicles under real world conditions.

Infrastructure Requirements

For this proposal, hydrogen will be delivered as liquid hydrogen and then stored in the vehicle's on-board tanks in a gaseous form. The maximum hydrogen demand of this project is 560 kg per day. Recharging infrastructure needed for the plug-in component of this project will be co-located with the hydrogen fueling system Vision engineers are working with hydrogen providers to ensure that the necessary adjustments are made to allow the proper charging of the trucks utilizing the facility.

Commercialization

To date, Vision has demonstrated a prototype of the TYRANO vehicle in the Port of Long Beach. Building upon these early successes to conduct a larger demonstration is a natural and necessary next step towards commercialization. The experience and data collected from this project will help validate hydrogen and electric as a feasible alternative fuel option. Confirming durability and driver acceptance are also key results expected from this demonstration that would advance commercialization of the TYRANO vehicle.

The location of this demonstration is ideal for establishing the foundation for future deployment of this technology. In the Houston, Texas area, there are currently five gaseous hydrogen-producing plants next to the Houston Shipping Channel.

Results

The project team is currently in the process of preparing for the manufacture and delivery of vehicles. To date, no performance data has been collected.

Expected results:

H-GAC, Vision Industries, and TTSI anticipate the following actions to occur as a result of this project:

1) increased adoption of technology for the TTSI fleet
2) increased adoption of technology for Port of Houston Authority operators as a result of outreach and exposure to the project
3) increased adoption of technology through other outreach and education efforts to ports in other areas, through DOE meetings, participation in DOE Clean Cities/Clean Fleets partnership programs

Conclusions

This project will produce on-road experience and gather data which will serve to accelerate the introduction and penetration of electric transportation technologies. Specifically, 20 hydrogen fuel cell electric hybrid trucks will be deployed into the drayage cargo transportation sector. Current delays in project initiation will require an aggressive timeline for manufacture of advanced vehicle technologies and the establishment of adequate hydrogen fueling infrastructure in early 2014.

III.N.3. Products

Publications

None to date.

Patents

None to date.

Tools and Data

None to date.

III.O. Zero Emission Delivery Vehicle Deployment—Houston

Allison Carr, Principal Investigator
Houston-Galveston Area Council
3555 Timmons Lane, Suite 120
Houston, TX 77027
Phone: (832) 681-2583
E-mail: allison.carr@h-gac.com

Lee Slezak, DOE Program Manager
Phone: (202) 586-2335
E-mail: Lee.Slezak@ee.doe.gov

Charles Alsup, NETL Program Manager
Phone: (304) 285-5432
E-mail: Charles.Alsup@netl.doe.gov

III.O.1. Abstract

Objectives

- Accelerate the introduction and penetration of electric transportation technologies (ETT) into the cargo transport sector.
- Deployment of thirty (30) all-electric trucks
  - Vehicles included in the project will be the *Smith Newton* truck produced by Smith Electric Vehicles
  - Vehicles will be operated by selected fleet operators including large national fleets and progressive regional fleets with delivery operations
- Testing and data collection for vehicles in real-world conditions to measure and demonstrate operational cost-effectiveness and commercial viability.

Major Accomplishments

- Route evaluation of potential fleet to determine whether *Smith Newton* trucks can effectively serve duty cycles and selected routes for fleet operators
- Engagement with fleet partners to establish performance agreements for vehicle deployment

Future Achievements

- Full deployment of 30 zero-emission all electric delivery vehicles.
- Reduce emission of 4,180 tons of criteria pollutants over the two year project deployment phase.
- Reduce emissions of greenhouse gases by 75 MMTCE over the two year project deployment phase.
- Reduce over 250,000 gallons of diesel fuel over the year project deployment phase.
- Release of technical report on cost-effectiveness and emission reductions related to vehicle deployment

✧ ✧ ✧ ✧ ✧

III.O.2. Technical Discussion

Background

The Houston-Galveston Area Council (H-GAC), Center for Transportation & the Environment (CTE), and Smith Electric Vehicles Corporation (Smith Electric) have partnered to establish the Houston Zero Emission Delivery Vehicle Demonstration Project. The primary objective of the project is to demonstrate the effectiveness of all-electric delivery vehicles to perform at the same level of operation as similarly sized diesel delivery vehicles, while reducing vehicle emissions and petroleum consumption.

To meet this objective, this project will support the deployment of 30 all-electric delivery trucks in the Houston-Galveston-Brazoria NAAQS 8-hour ozone nonattainment area.

Assembled in the United States by Smith Electric and using batteries supplied by A123 Batteries and electric chargers supplied by Clipper Creek, these vehicles will be demonstrated by selected national, regional, and/or local fleets. All vehicle deployment and operation of the vehicles will occur with the Houston-Galveston region. In addition to the deployment of delivery vehicles and charging infrastructure, the project will demonstrate vehicle operations, collect data, and report on project results for a period of two years after deployment.

Introduction

The primary objective of this project is to deploy thirty zero-emission all electric trucks and demonstrate the effectiveness of the all-electric delivery vehicles to at the same level of operation as similarly sized diesel delivery vehicles while reducing vehicle emission and petroleum consumption.

The vehicles deployed, to be produced by Smith, are the world's largest battery-electric powered truck. The *Smith Newton* all-electric medium/heavy-duty truck offers predictable routes up to 100 miles per day with a top speed of 55 mph. It has a range of 50-120 miles on a single charge and a payload of more than 16,000 pounds. The vehicles will be deployed through five fleets operating delivery routes in the Houston-Galveston area.

The *Smith Newton* operates at peak effectiveness in urban applications that demand heavy stop and go driving. A single charge provides more than enough range for most urban delivery routes. However, the AC load and unique geography of the Houston area will test the range and feasibility of the vehicles in a city that covers a large geographic area and typically includes increased mileage on highway travel. Many large national fleets and progressive regional fleets that operate diesel and gasoline delivery

vehicles in the region and will be the initial targets for fleet deployment and testing. Integration of all-electric vehicles into their fleets will result in both emission and noise reductions over diesel and gasoline counterparts. The fleets will also reduce their reliance on petroleum-based fuels and realize significant cost savings.

Approach

The medium-duty Newton step van has a GVW of approximately 14,000 to 22,000 pounds and a payload capacity of approximately 2,700 to 10,000 pounds. Smith Electric expects the vehicles will be used primarily for delivery of parcels, uniforms, and baked goods. Smith Electric is also developing a heavy-duty Newton that will have a GVW of approximately 33,000 pounds to meet the needs of delivery and transit customers, which the company expects to be available in the second half of 2012.

The initial cost of a Newton ranges from $156,000 to $175,000, depending on the battery configuration and upfit of the cargo bay at initial purchase. Smith Electric will work with the selected operators chosen vendor to upfit the vehicles with a minimum 20ft. cargo compartment to meet the specific needs of the operator.

CTE will work with Smith Electric and each of the operators to plan, select, and model routes on which the vehicles will be deployed. The project team will also install and test the charging stations in preparation for vehicle deployment. Once the vehicles are delivered, the project team will conduct a series of test to validate vehicle performance against the model. Once deployed in delivery service, the team will collect operational data and submit reports for two years.

System Description

In November 2011, Smith Electric developed a prototype for a second-generation Newton, which incorporates the Smith Drive, Smith Power, and Smith Link technologies. During the first quarter of 2012, Smith introduced a Newton model that is configured as a step van in the United States. Smith Electric is also developing a heavy-duty Newton that will have a GVW of approximately 33,000 pounds to meet the needs of delivery and transit customers, which the company expects to be available in the second half of 2012.

Testing

Vehicle routes will be evaluated and selected prior to deployment through route reviews with Smith Electric and the selected operators. CTE will collect route data, including time, speed, distance, elevation, etc., which will be used to model vehicle performance using the Powertrain Systems Analysis Toolkit (PSAT) or Autonomie. The objective for route and vehicle modeling is to determine the energy requirements of the vehicle on a given route to establish an operational profile. This profile will provide an estimated state of charge of the battery pack throughout the day to assess charging and operator training requirements.

Prior to full service operations, the vehicles will undergo route validation. CTE will coordinate with the operators to drive the vehicles along the planned route under reasonable worst-case conditions (temperature, AC load, cargo load, traffic patterns). This will confirm that the vehicles will perform as expected, in accordance with the model developed earlier in the project.

Selected operators will use the project vehicles in the ordinary course of their delivery services throughout the Houston-Galveston-Brazoria NAAQS 8-hour ozone nonattainment area. Once the vehicles are deployed, Smith Electric will collect data from the fleets and provide it to the CTE for analysis and reporting. Smith Electric will collect two types of data concerning the vehicles participating in the project. The first is telemetric data. This data will not be personally identifying data and will be collected automatically and wirelessly. This data will provide quantitative, raw data on the vehicles' performance, state of charge, charging cycles, actual duty cycle, daily mileage, etc. In addition, the charging stations will be metered to capture electricity consumed to charge the vehicles.

The second type of data collected will be qualitative data. Smith Electric will interview and/or submit questionnaires on a quarterly basis to operators and service providers inquiring as to their more subjective experience with the electric vehicle. This data will include vehicle performance and effectiveness on the job. Fuel savings and emissions benefits will be estimated from the quantitative data sets and compared with the baseline data.

Demonstration Period

The project will include a two-year demonstration of each all electric truck under real world conditions.

Data Collection Strategy

Each vehicle deployed in the program will undergo several layers of testing. Components are tested prior to assembly to ensure compliance with specifications. Once the vehicle is tested, it will undergo a series of tests to ensure operational specification. Battery packs are charged and discharged through complete cycles. The vehicles are fully inspected prior to delivery to the selected operators. Once delivered, the selected operators will perform their own inspection and acceptance test.

After the vehicles are placed in service, data is automatically recorded every five seconds through an on-board telemetric data logger. Data is wirelessly transmitted to Smith Electric after the vehicle returns to the depot. This data will provide quantitative, raw data on the vehicles' performance, state of charge, charging cycles, actual duty cycle, speed, mileage, etc. In addition, the charging stations will be metered to capture electricity consumed to charge the vehicles.

Infrastructure Requirements

Each Smith Newton will be delivered with a Level 2 charger delivering up to 18 kW of electricity for overnight charging of the battery pack. Fully recharging the vehicle will take approximately 6 to 10 hours per night, depending on the battery pack and the state of charge when the vehicle returns to the fleet depot.

Each selected fleet operator will designate parking sites that will be outfitted with a charging station.

Chargers must be provided with 208 or 240 VAC, 60 Hz, 75 amp electric service. Qualified electricians will be engaged to install the chargers, which may require a permit. Installation of a separate meter may require services of the local utility. Installation of each unit generally requires a couple of hours, however, depending on the location of the power source. The cost for each charging unit plus installation is expected to average $8,000 per unit.

Fleet Engagement

CTE and Smith Electric will work with selected fleet operators to identify appropriate vehicles and routes for Smith Electric zero-emission truck deployment. To determine battery pack requirements, it is necessary to understand the route, duty-cycle, and cargo weight.

Vehicle routes will be evaluated and selected prior to deployment through route reviews with Smith Electric and the selected operators. CTE will collect route data, including time, speed, distance, and elevation. This profile will provide an estimated state of charge of the battery pack throughout the day to assess charging and operator training requirements.

Figure III-63: Smith Electric Vehicles Box Truck & Step Van.

Commercialization

Each of the selected fleet operators for the project vehicles believes that the Smith Electric 2nd Generation Newton will result in a positive business case on a total cost of ownership basis. This is due to the lower cost of electricity and lower maintenance costs as compared to fuel and maintenance of diesel medium- and heavy-duty vehicles.

Results

The project team is currently in the process of selecting fleet participants and preparing for the manufacture and delivery of vehicles. To date, no performance data has been collected.

Expected results:

H-GAC, CTE, and Smith Electric Vehicles anticipate the following actions to occur as a result of this project.

1) Reduction of petroleum use in the demonstration period during and after the project activities
2) Reduction of greenhouse gases, criteria pollutants, and toxic emissions
3) Demonstration and evaluation of market viability
4) Opportunity to increase adoption of the demonstration technologies
5) Expansion of U.S. manufacture and production of electric vehicles and U.S. suppliers of batteries and equipment for electric vehicles

Conclusions

This project will produce on-road experience and gather data which will serve to accelerate the introduction and penetration of electric transportation technologies. Specifically, 30 zero emission all-electric trucks will be deployed across the Houston region. The project has experienced delays due to challenges in identifying appropriate routes in the Houston area as a result of typically longer travel routes. Continued outreach and education have identified routes and vehicles for deployment of vehicles in early 2014.

III.O.3. Products

Publications

None to date.

Patents

None to date.

Tools and Data

None to date.

IV. LAB & FIELD VEHICLE EVALUATIONS

LIGHT DUTY

IV.A. Advanced Vehicle Testing Activities

James Francfort, Principal Investigator
Idaho National Laboratory
P.O. Box 1625, Idaho Falls, ID 83415-2209
Phone: (208) 526-6787
E-mail: James.francfort@inl.gov

Lee Slezak, DOE Program Manager
Phone: (208) 586-2335
Email: Lee.slezak@ee.doe.gov

IV.A.1. Abstract

Objectives

- Benchmark battery performance and life in hybrid electric vehicles (HEVs) and battery electric vehicles (BEVs) because the batteries are continuously the subject of research, funding, and life questions
- Provide support to New York City's (NYC's) evaluation of electric taxis
- Benchmark smart grid electric vehicle supply equipment (EVSE) for the U.S. Department of Energy (DOE)
- Support the DOE/Department of Defense (DOD) memorandum of understanding (MOU) and other Federal fleets' petroleum reduction activities
- Complete the Ultra Battery Honda Civic HEV benchmarking
- Introduce new alternative fuel and high-efficiency petroleum fueling transportation technologies to Advanced Vehicle Testing Activity (AVTA) benchmark testing.

Major Accomplishments

- Completed 54 testing reports and fact sheets benchmarking HEV, BEVs, and stop/start HEV performance, maintenance requirements, life-cycle costs, and battery performance
- Signed non-disclosure agreements with the data providers for the NYC Taxi Commission pilot of electric taxi cabs and produced the first report to NYC
- Completed the first of five cyber security tests of smart grid EVSE and signed non-disclosure agreements with the remaining four companies
- Continued the micro climate study at one DOD joint base, initiated two additional DOD base studies, and instrumented the first 130 Federal fleet vehicles in eighteen different Federal fleets within seven different Federal agencies to identify suitable missions for substituting electric drive vehicles
- Completed the 100,000-mile onroad testing of the Ultra Battery Honda Civic HEV
- Added eight CNG and TDI vehicles into AVTA testing.

Future Achievements

- Continue high-mileage HEV and BEV vehicle and battery testing, reporting, and presentations
- Complete reporting for the six NYC electric taxis
- Complete the five initial EVSE cyber security tests during FY 2014
- Complete bench testing of the Ultra Battery's deliverables and report the results to the U.S. Drive Energy Storage tech team.

✧ ✧ ✧ ✧ ✧

IV.A.2. Technical Discussion

Background

DOE's AVTA is part of DOE's Vehicle Technologies Office, which is within DOE's Office of Energy Efficiency and Renewable Energy (EERE). AVTA is the only DOE activity tasked by DOE to conduct field evaluations of vehicle technologies that use advanced technology systems and subsystems in light-duty vehicles to reduce petroleum consumption. A secondary benefit is the reduction in exhaust emissions.

Most of the advanced technology vehicles and components that AVTA tests include the use of electric drive propulsion systems and advanced energy storage systems. However, other vehicle technologies that employ advanced designs, control systems, or other technologies with production potential and significant petroleum reduction potential are also considered viable candidates for testing by ATVA.

The AVTA light-duty activities are conducted by the Idaho National Laboratory (INL) for DOE. INL has responsibility for AVTA's execution, direction, management, and reporting, as well as data collection, analysis, and test reporting. INL is supported in this role by various subcontracts for specific tasks when greater value can be achieved for DOE. The AVTA sections of the FY 2012 Annual Program Report jointly cover the testing work performed by INL and any subcontractor-conducted work that INL manages. When

appropriate, AVTA partners with other governmental, public, and private sector organizations to provide maximum testing and economic value to DOE and the United States' taxpayers via various cost-sharing agreements.

Introduction

DOE's AVTA is evaluating grid-connected plug-in electric drive vehicle (PEV) technology in order to understand the capability of electric grid-recharged electric propulsion technology to significantly reduce petroleum consumption when vehicles are used for transportation. In addition, many companies and groups are proposing, planning, and have started to introduce PEVs into their fleets.

It should be noted that grid-connected PEVs include several vehicle/energy storage schemes that include BEVs (or simply EVs) such as the Nissan Leaf and Mitsubishi i-MiEV, plug-in hybrid electric vehicles (PHEVs) such as the Toyota Prius and Chrysler Ram PHEVs, and extended range electric vehicles (EREVs) such as the General Motors Chevy Volt.

Today's original equipment manufacturer PEVs mostly have 4 to 15 kWh of onboard battery storage in PHEVs and EREVs and more than 20 kWh of onboard storage for BEVs. AVTA makes extensive use of in-vehicle and in-charging infrastructure data loggers to collect a variety of vehicle and infrastructure-generated performance parameters. Experience has shown that automated data collection in fleet environments is the only way to ensure accurate data are collected.

The concept of advanced onboard energy storage and grid-connected charging raises questions that include the life and performance of these larger batteries; the charging infrastructure required; how often the vehicles will actually be charged (i.e., driver and smart grid behavior and controls); and the actual amount of petroleum displaced over various missions, drive cycles, and drive distances; all of this is achieved with automated data loggers.

Other activities conducted under the umbrella of AVTA include DOD-related work that supports the DOE MOU with DOD, support for DOE's Federal Energy Management Program (FEMP), and general Federal fleet support.

Approach

Three basic types of test methods are used to test vehicles and they are discussed as follows.

Baseline performance testing during which a vehicle is track and dynamometer tested. Track testing includes acceleration, range, braking, and fuel use (both electricity and gasoline or whatever fuels are being used) at different battery states-of-charge. The vehicles are also coast-down tested to determine dynamometer coefficients, which are used during the various urban and highway dynamometer test cycles. Note that the AVTA dynamometer testing is conducted by Argonne or Oak Ridge National Laboratories for AVTA. This sharing of vehicles and testing expertise also reduces costs to DOE.

Accelerated testing uses dedicated drivers to complete a series of drives and charges (for PEVs) on city and highway streets. This testing often is used to ensure PEVs can accomplish several charge and drive cycles in 1 day. For some vehicles, this can include more than 5,000 miles of operation per month. More commonly, AVTA partners with various fleets that utilize light-duty vehicles in high-mileage missions (e.g., bank curriers or taxis).

Fleet testing is normally conducted by placing vehicles into fleets with no highly controlled structure to ensure repeatable drive missions. AVTA partners with government, private, and public fleets for fleet testing because these fleets are often overwhelmingly the earliest adaptors of advanced technology vehicles. Note that the AVTA fleet testing normally does not include operations by the general public.

PHEVs and EREVs can operate on gasoline even when the vehicles' battery packs are not charged. Therefore, with some exceptions, fuel-use reporting is normally broken down into the following three operating modes for these vehicle technologies:

Charge-depleting mode: During each entire trip, there is electric energy in the traction battery pack to provide either all-electric propulsion or electric assist propulsion throughout the entire trip.

Charge-sustaining mode: During a trip, there is no electrical energy available in the PHEV or EREV traction battery pack to provide any electric propulsion support beyond normal HEV operations.

Combined (or mixed) charge-depleting and charge-sustaining mode: There is electric energy in the traction battery pack available at the beginning of a trip. However, during the trip, the PEV battery is fully depleted.

Results

General Motors Chevrolet Volt EREV

During FY 2011, a non-disclosure agreement was signed with OnStar that detailed data collection, analysis, and reporting by AVTA for vehicle performance, fuel use, and charging patterns for approximately 150 General Motors Chevrolet Volt EREVs. This work is still being performed to support an ARRA grant General Motors received from DOE.

Using server-to-server data transmission, INL receives the raw data generated by OnStar from onboard data loggers installed on the Volts. With these data, which are generated for every key on and off event, INL generates a series of periodic reports that can be accessed at: http://avt.inl.gov/gmvehicledemo.shtml.

Quarterly reports are being generated for this project. For the project-to-date report, May 2011 to June 2013 (the third quarter 2013 report was not yet published when this report was prepared), the 150 Volts where averaging 70.1 mpg and 169 AC Wh per mile (Wh/mi) overall after 2.8 million test miles. When operating in electric vehicle mode operation (or EV mode), the vehicles were averaging 353 AC Wh/mi. In extended range mode operations, the Volts were averaging 36.5 mpg. During the May 2011 to June 2013 period, the 150 vehicles have been driven 2.8 million miles and have used 477,000 AC kWh.

During EV mode, only electricity is being used to propel the Volt; the gasoline engine does not operate. In extended range mode, the vehicle operates like a traditional HEV, with the traction battery accepting regenerative braking energy. However, the Volt does have to be recharged from the grid for EV mode operations to resume.

As Figure IV-1 shows and as would be expected, more EV mode trips occurred during shorter distance trips. Figure IV-2 documents the near-full battery state of charge at the end of each charge event prior to driving events and Figure IV-3 documents the low state of charge at the end of the drive prior to charging.

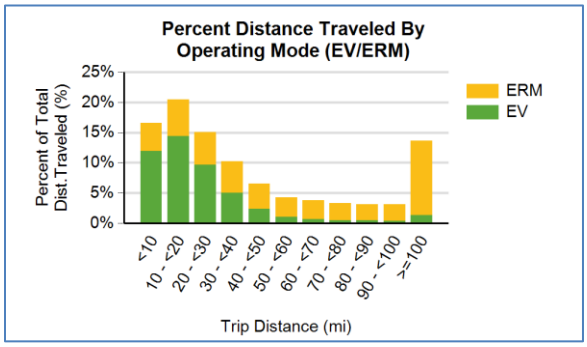

Figure IV-1: Operating mode for 150 Chevy Volts in the DOE program.

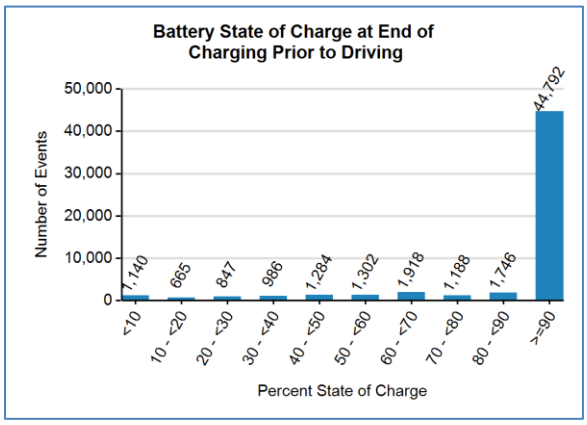

Figure IV-2: State of charge at the end of the charging events for 150 Chevy Volts in the DOE program.

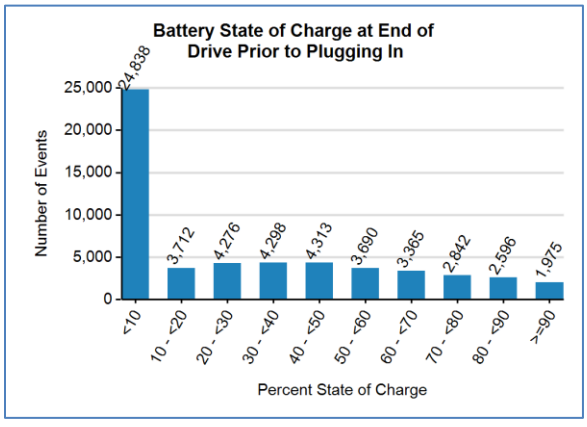

Figure IV-3: State of Charge at beginning of the charging events for 150 Chevy Volts in the DOE program.

Table IV-1 documents the charging and operating results for the 150 Chevy Volt fleet. Note that only 146 vehicles operated during the most recent reported quarter of April to June 2013. Table IV-1 also includes some of the results for the Volts operating in the EV Project, which is more of an infrastructure-focused project. DOE's 150 Chevy Volt fleet is more focused on testing the vehicle rather than the infrastructure, which is the focus of the EV Project. The intent of including EV Project data is to show the potential of the Volt to reduce petroleum use when it is charged more often. The 150 Volt fleet is mostly commercial operators, who are predominately in electric utility fleets, meaning the drivers do not purchase the gasoline, which reduces the economic incentive to charge more often and drive more electric. The EV Project drivers are predominately private citizens that purchase their own fuel.

The biggest differences in the results are the 1.5 charging events per day for citizens and 1.1 charging events for commercial drivers. Therefore, private citizens are averaging 142 mpg, while commercial fleet drivers are only averaging 68 mpg. The private citizens are also driving in EV mode 60% more often than the commercial drivers (i.e., 74.6% to 46.5%).

Table IV-1: Charging and operational results for 150 Chevy Volts commercially driven in the DOE program and the 1,895 Chevy Volts being driven by private citizens in the EV Project.

	150 DOE	EV Project
Number Vehicles	146	1,895
Miles	407,000	5.8 million
Reporting period	April through June 2013	
Overall mpg	68.2	142
Overall AC Wh/mi	157	231
Number of Trips	19	676,000
Average number of charging event per vehicle day	1.1	1.5
Average miles between charging events	50	27.6
Average number of trips between charging events	4.1	3.3
Percent of total distance traveled in EV mode	46.5%	74.6%

New York City Electric Taxi Fleet Pilot

INL is supporting demonstration of an electric vehicle taxi fleet that is comprised of six Nissan Leafs (Figure IV-4). The demonstration brings electric taxis back to NYC. They first made their debut in NYC during 1897, totaling 2,000 electric taxis in 1899, and were gone by the 1950s. The pilot project is a cooperative effort between the NYC Taxi and Limousine Commission and Nissan North America. Other partners include Related Management, Seward Park Cooperative, Con Edison, New York Power Authority, DOE, New York State Energy Research and Development Authority, NYC Mayor's Office of Long-term Planning and Sustainability, and NYC Department of Transportation.

INL's role is data collection from the vehicles via Nissan's telematics system and the analysis, quality control, and reporting both vehicle performance and the drivers' operations

of the electric taxis back to the team partners. The first report was prepared and shared with the NYC partners when FY 2013 ended. That report was still under review by the partners as this report was written; therefore, the initial results cannot be provided.

Figure IV-4: Nissan Leaf in NYC taxi fleet pilot. Source: http://www.nyc.gov/html/tlc/html/news/initiative_ev_pilot_program.shtml.

Smart EVSE Testing for DOE Office of Electricity and Energy Reliability

The DOE Office of Electricity and Energy Reliability has funded, via a competitive competition, four companies (i.e., General Electric, Delta Electronics, Siemens, and Eaton) to produce low-cost, smart grid EVSE. The four companies were preparing to ship their new EVSEs to INL when FY 2013 ended. INL will be conducting both efficiency and reliability testing of the EVSE, as well as conducting cyber security testing of the four units. During FY 2103, INL previously conducted successful cyber security testing of a fifth manufacturer's smart grid EVSE.

DOD/DOE MOU Support

During July 2010, DOE and DOD signed the MOU "Concerning Cooperation in a Strategic Partnership to Enhance Energy Security," which covers several energy efficiency areas, including transportation, fueling, and grid issues. At a high level, the MOU required DOE, when possible, to assist DOD with their petroleum reduction activities. In support of the MOU, during FY 2013, AVTA had nearly completed the micro climate study at Joint Base Lewis McCord in Tacoma, Washington and additional studies were kicked off at the combined Naval Air Station Jacksonville and Naval Seaport Mayport and Marine Corps Base Camp Lejeune.

Micro climate studies take into account traffic patterns, attractions, transportation hubs, and existing and potential electric infrastructure and charging locations. A subset of a base's vehicle fleet also has been instrumented to document mission profiles. This work supports the future deployment of charging infrastructure and electric drive vehicles on DOD bases. It should be noted that the micro climate studies are jointly funded by EERE and FEMP.

AVTA has also supplied eighteen Blink Level 2 EVSE to Andrews Air Force Base (outside of Washington D.C.) for installation by base personnel. As FY 2013 was ending, preparations were near completion for commissioning of the eighteen EVSE.

Other Federal Fleet Support

In addition to the above DOD support, AVTA has been able to benchmark the first 130 of 800 Federal fleet vehicles as FY 2013 ended. This exercise will support identification of vehicles and missions that will be suitable for replacing current internal combustion engine vehicles with various electric drive vehicle technologies, with the main emphasis on introducing PEVs. This is a joint EERE and FEMP-funded project. The Federal agencies and the number of fleets per agency with vehicles that have been instrumented to date include the following:

- U.S. Forest Service—2
- National Aeronautics and Space Administration—4
- U.S. Department of Health and Human Services, ASPR—4
- U.S. Coast Guard—1
- U.S. Department of Veterans Affairs—2
- U.S. National Park Service—4
- National Institute of Health—1.

eGallons Methodology Development

In another miscellaneous support activity, INL was tasked by DOE with developing the methodology for DOE's new eGallon calculator. The eGallon website (http://energy.gov/articles/egallon-how-much-cheaper-it-drive-electricity) allows for a calculation of the much lower cost of driving PEVs compared to internal combustion engine gasoline vehicles. Both national and by-state calculators are provided, using actual monthly gasoline and electricity prices.

International Testing Support

INL is supporting the outreach and cooperation by DOE with the European Union, China, and Canada. For European Union activities, AVTA is setting up a cooperative data activity with the Electric Supply Board of Ireland to collect data from fifteen Mitsubishi i-MiEV electric cars and five Nissan Leafs operating in Ireland.

AVTA is also conducting a U.S./China sister cities-type of data sharing activity, with both INL and various research centers in China sharing PEV results for Shanghai and China. This work has included visits by two different groups of Shanghai dignitaries. During one three-day visit, INL put on a "how-to" seminar on PEV and charging infrastructure data collection and reporting.

Hybrid Electric Vehicle Testing

Today's light-duty HEVs use a gasoline internal combustion engine, electric traction motors, or electric stop-start technology, along with less than 2,000 watt-hours (Wh) of onboard energy storage to increase petroleum efficiency as measured by higher mpg results compared to non-HEV models. HEVs are never connected to the grid for charging the battery. The HEV batteries are charged by an onboard internal combustion engine-powered generator, as well as by regenerative braking systems.

At the end of FY 2013, AVTA performed, or is performing, testing on 68 HEVs, which is comprised of 26 HEV models. The HEV models and number of each model tested are listed as follows:

- Generation (Gen) I Toyota Prius—6
- Gen II Toyota Prius—2
- Gen I Honda Insight—6
- Honda Accord—2
- Chevrolet Silverado—2
- Gen I Honda Civic—4
- Gen II Honda Civic—2
- Ford Escape—2
- Lexus RX400h—3
- Toyota Highlander—2
- Toyota Camry—2
- Saturn Vue—2
- Nissan Altima—2
- Chevrolet Tahoe—2
- Gen II Honda Insight—2
- Gen III Toyota Prius—2
- Ford Fusion—2
- Mercedes S400—2
- Honda CRZ—2
- Smart Fortwo Pure Coupe (MHV)—3
- MAZDA 3 Hatchback (MHV)—2
- Volkswagen Golf TDI (MHV)—2
- Hyundai Sonata—2
- Honda Civic with advanced lead acid battery—1
- Honda Civic—3
- Chevrolet Malibu—4.

AVTA continues to collect data that allows it to publish several fact sheets for each HEV (see: http://avt.inel.gov/hev.shtml), including the following:

- Maintenance fact sheets, including mileage, date, maintenance event, cost for repair, or if repair was under warranty.
- Fleet testing summary fact sheets, including operating costs based on the purchase and sale delta and the maintenance and operating costs (e.g., insurance, fuel, and registration). The monthly and cumulative mpg and monthly mileage accumulation are also provided.
- Battery fact sheets and testing reports for when the vehicles are new and at 255,000 miles, which is up from the previous end-of-testing at 160,000 miles.
- Fleet testing results to-date fact sheets.

Much discussion could occur here about the significance of the battery testing being conducted by AVTA on HEVs. However, only one figure will be used as an example of the type of battery testing that occurs when the HEVs are new and at the perceived end of life. Figure IV-5 is a plot of the battery's useable energy as a function of discharge power for a 2013 Chevy Malibu ECO Hybrid, Vin 6791. The battery was tested with a break-in mileage of 5,715 miles, which is considered the beginning of testing for the battery in this vehicle.

The x-axis indicates a desired discharge power level and the y-axis indicates the useable energy at that power. The dashed horizontal line shows the DOE energy performance goal of 300 Wh. The dashed vertical line shows the DOE HEV power performance goal of 25 kW. A portion of the battery's useable energy curve falls above the DOE useable energy goal. However, the entire curve falls to the left of the DOE power performance goal. The maximum power that can be delivered while meeting the DOE energy performance goal is 6.2 kW at 300 Wh. The battery from Malibu 6791 does not meet the DOE power performance goal for any energy value. These results indicate that at the time of beginning of testing, the battery from Malibu 6791 was below the DOE HEV battery performance goals.

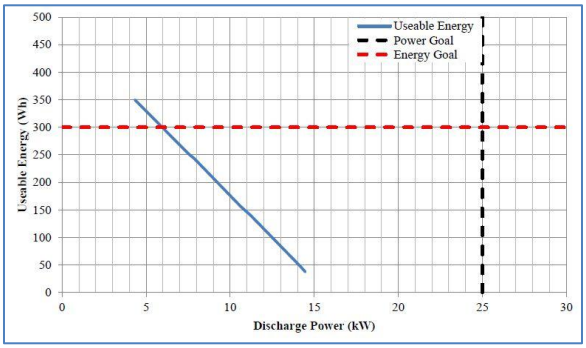

Figure IV-5: Chevy Malibu ECO Hybrid beginning of testing battery useable energy versus discharge power curve.

The fact that the Hitachi cylindrical lithium-ion battery does not meet the DOE goals should not be taken to suggest there is anything substandard with the battery or the vehicle. It simply suggests that where the battery was selected and how it is controlled was of consideration for use in the Malibu, but not for meeting a DOE goal. AVTA has four Malibu HEVs in fleet operations and they are averaging almost two mpg higher than the combined EPA rating of 29 mpg. In fact, steady speed track testing has benchmarked over 46 mpg at constant speeds of 30 and 60 mph, and more than 50 mpg at a constant speed of 50 mpg; therefore, it appears the battery is meeting the design requirements for this model.

Battery Electric Vehicle Testing

Similar to the HEV testing, full-size BEVs are also in testing, including the 2011 Nissan Leaf, 2013 Nissan Leaf, and 2013 Mitsubishi i-MiEV. The three models are in various stages of testing and fact sheets benchmarking maintenance histories, track and dyno testing, battery testing, and fleet testing are available for some models (see http://avt.inel.gov/fsev.shtml).

BEV testing results can be confusing to non-engineering readers because the results can vary significantly. However, this is reflective of the technology and how much more sensitive BEVs are to environmental influences and driver demands (such as aggressive or high-speed driving). Viewing the Nissan Leaf baseline testing results (http://avt.inel.gov/pdf/fsev/fact2011nissanleaf.pdf) shows ranges of 54.2 miles for the US06 testing to 90.2 miles for the UDDS testing. Similarly, constant speed testing can have significant delta in the results. At a constant speed of 45 mph, the 2011 Nissan Leaf had an AC Wh per mile consumption rate of 254. At 70 mph, the result was 403 AC Wh per mile; almost 60% higher. While INL will continue to publish engineering testing results, ways to also publish less complex explanations of testing results are being explored.

Ultra Battery HEV Project

Two special HEV vehicle projects, The Ultra Battery Retrofit Project and Carbon-Enriched Project C3, aim to demonstrate the suitability of advanced lead battery technology in HEVs. The projects have been partially funded by DOE and by the Advanced Lead Acid Battery Consortium through ETEC Labs for AVTA.

An important objective of the projects has been to benchmark the performance of the ultra batteries from both Furukawa Battery Co., Ltd., Japan (Furakawa) and East Penn Manufacturing Co., Inc. (East Penn). Accordingly, Ultra Battery packs from both Furakawa and East Penn have been characterized under a range of conditions. Resistance measurements and capacity tests at various rates show that both battery types are very similar in performance. Both technologies, as well as a standard lead-acid module (included for baseline data), were evaluated under a simple HEV screening test. Both Furakawa and East Penn Ultra Battery packs operated for over 32,000 HEV cycles with minimal loss in performance, whereas the standard lead-acid unit experienced significant degradation after only 6,273 cycles. The high-carbon, Advanced Lead Acid Battery Consortium battery manufactured in Project C3 also was tested under the advanced HEV schedule. Its performance was significantly better than the standard lead-acid unit, but was still inferior compared with the Ultra Battery. The batteries supplied by Exide as part of the C3 Project performed well under the HEV screening test, especially at high temperatures. The results suggest that higher operating temperatures may improve the performance of lead-acid-based technologies operated under HEV conditions; it is recommended that life studies be conducted on these technologies under such conditions.

The Project DP1.8 consists of a retrofit of the original NiMH battery with a pack of 14 Ultra Battery modules, manufactured by East Penn, in a new 2010 Honda Civic HEV. In October 2011, the converted HEV was put into the AVTA fleet of test vehicles in Phoenix, Arizona, and the onroad vehicle-based portion of the testing has completed and results are discussed as follows. The laboratory-based battery cycling is continuing and the results will be available during FY 2014.

Results from the laboratory beginning-of-test and end-of-test static capacity tests are provided in Table IV-2. The battery did measure a 4.2% decrease in capacity after 100,000 miles, but the fuel economy seemed relatively unimpacted (Figure IV-6) and the ending fuel economy was 38.2 mpg.

Table IV-2: Static capacity test results for the Ultra Battery Civic HEV (BOT = beginning of test and EOT = end of test).

	Test Date	Odometer (miles)	Rate Capacity (Ah)	Measured Capacity (Ah)	Measured Energy (Wh)
BOT	9/2/11	0	7.5	7.55	1.260
EOT	4/16/13	100,099	7.5	7.23	1.198
Differ -ence		100,099	—	0.32 (4.2%)	0.62 (4.9%)

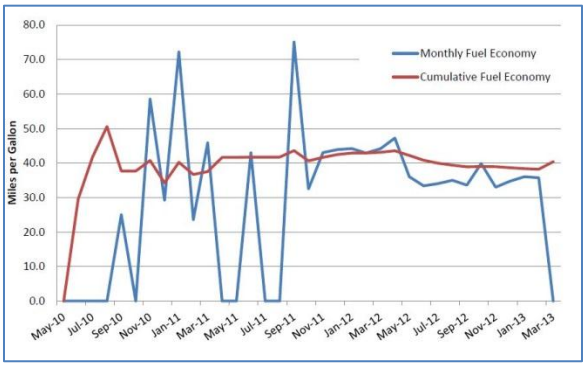

Figure IV-6: Ultra Battery combined monthly and cumulative fuel economy. Note: wide monthly results can come from fueling either the last day or first day of a month, while the mileage may have been accumulated another month.

Conclusions

AVTA will continue to provide the real-world testing needed to benchmark DOE technology investments, including the critical tasks of determining suitability for deployment, lifetime performance, and the life-cycle costs of new technology components and vehicle systems. This testing includes understanding the infrastructure requirements of PEVs and other alternative fuels and HEVs, as well as the proper placement of that infrastructure. New, non-gasoline internal combustion engine vehicles that started testing during FY 2013 included four Honda Civic CNG vehicles and four Volkswagen Jetta Turbocharged Direct-Injection vehicles.

The quality of the vehicles and the batteries and, thus, the expected operational life, has improved significantly and fleets have been found that can significantly accumulate high per-vehicle mileage. Therefore, hybrid and internal combustion engine vehicle fleet testing distances have been increased to 255,000 miles per vehicle. This also includes CNG and TDI vehicles to 255,000 miles. The PHEVs entering testing will accumulate 195,000 miles per vehicle and the BEVs will operate for 60,000 miles per vehicle.

IV.A.3. Products

Publications

1. Gray, T., M. Shirk, and J. Wishart, 2013, *2010 Honda Civic Hybrid Ultra Battery Conversion 5577—Hybrid Electric Vehicle Battery Test Results*, INL/EXT-13-29677, Idaho National Laboratory, Idaho Falls, ID, July 2013.
2. *2013 Chevrolet Malibu ECO, Advanced Vehicle Testing-Baseline Testing Results,* Idaho National Laboratory, Idaho Falls, ID, January 2013.
3. *2013 Honda Civic Hybrid, Advanced Vehicle Testing-Baseline Testing Results,* Idaho National Laboratory, Idaho Falls, ID, May 2013.
4. Gray, T., M. Shirk, and J. Wishart, 2013, *2011 Hyundai Sonata 4932—Hybrid Electric Vehicle Battery Test Results*, INL/EXT-13-29678, Idaho National Laboratory, Idaho Falls, ID, July 2013.

5. The remaining 53 fact sheets that documented maintenance, fuel economy, and life-cycle reports are generally a one-page, fact-sheet type of reporting method. They can be found on the AVTA website at: http://avt.inel.gov/hev.shtml for HEVs, http://avt.inel.gov/microHEV.shtml for the start/stop HEVs, and http://avt.inel.gov/fsev.shtml for BEVs.

Patents

This is a test program that is not designed to develop patents. The intent is to provide independent testing and feedback to DOE and industry on DOE and other funded technologies and technology improvements.

Tools and Data

The data generated by this testing are used to populate publications in the form of testing fact sheets, reports, and industry-referred papers.INL/MIS-13-30556

IV.B. Nissan Leaf Battery DC Fast Charging Study and Advanced Battery (EnerDel) Testbed Testing

James Francfort, Principal Investigator
Idaho National Laboratory
P.O. Box 1625
Idaho Falls, ID 83415-2209
Phone: (208) 526-6787
E-mail: James.francfort@inl.gov

Lee Slezak, DOE Program Manager
Phone: (208) 586-2335
E-mail: Lee.slezak@ee.doe.gov

IV.B.1. Abstract

Objectives

- Provide the U.S. Department of Energy (DOE) with independent and unbiased benchmarked testing results that evaluate battery technologies that DOE and industry have invested in.
- Benchmark the impacts (if any) that DC fast charging (DCFC) has on battery life in Nissan Leaf battery electric vehicles compared to Level 2 charging of the same vehicle model.
- Test a variety of advanced energy storage systems (ESSs) that are at or near commercialization in onroad, real-world operation; quantify the ESS capabilities and limitations; and performance fade over the life of the ESS. The current ESS being tested is an EnerDel lithium-ion battery that is being tested in a purpose-modified test platform that is named the Electric Drive and Advanced Battery Components Testbed (EDAB). However, the EDAB has been nicknamed the "battery mule" and this term will be used throughout this report.
- Continue to provide testing results to other DOE programs and national laboratories, as well as several U.S. Drive technical teams that Idaho National Laboratory (INL) staff are members of.

Major Accomplishments

- Accumulated 30,000 test miles on each of four Nissan Leafs. Two are being recharged only with DCFC technology and the other two are being recharged only with Level 2 technology.
- When new (i.e., baseline) and at 10,000-mile, 20,000-mile and 30,000-mile intervals, each of the four Leaf lithium-ion batteries have been capacity and peak power tested. This equates to 16 battery tests to date.
- The EnerDel lithium-ion battery in the battery mule has been operated for 23,450 miles, with 39,500 Amp hours of throughput.
- Including the initial baseline test, 10 capacity and resistance tests have benchmarked the battery performance and a 17% capacity loss in the EnerDel battery.

Future Achievements

- The four Nissan Leafs will continue operations and 10,000-mile battery testing to at least 50,000 miles. It is possible testing may continue beyond that limit, but this will be based on testing results that are starting to demonstrate greater capacity loss during DCFC operations and Level 2 operations.
- An additional two Nissan Leaf batteries will be tested in the INL ESS test facility starting FY 2014. One will be DCFC charged and the other Level 2 charged.
- The EnerDel battery will continue operations and testing until it reaches the DOE and industry set end-of-battery life level, which is considered to be 77% state of charge (SOC).
  A new Toshiba battery pack is being fabricated as the next test ESS in the battery mule.

✧ ✧ ✧ ✧ ✧

IV.B.2. Technical Discussion

Background

DOE's Advanced Vehicle Testing (AVTA) is part of DOE's Vehicle Technologies Office, which is within DOE's Office of Energy Efficiency and Renewable Energy. AVTA is the only DOE activity tasked by DOE to conduct field evaluations of vehicle technologies and fueling infrastructure that use advanced technology systems and subsystems in light-duty vehicles to reduce petroleum consumption. A secondary benefit is reduction in exhaust emissions.

Most of these advanced technologies include the use of electric drive propulsion systems and advanced ESSs. However, other vehicle technologies that employ advanced designs, control systems, or other technologies with production potential and significant petroleum reduction potential are also considered viable candidates for testing by ATVA.

The ESS is generally considered the Achilles heel of electric drive vehicles for several reasons, including cost and life uncertainties, how environmental and charging may impact life, and the large mass and volume of today's battery technologies. This is especially true for battery electric vehicles and plug-in hybrid vehicles. Hybrid electric vehicles, with their much narrower SOC limits and their mostly nickel metal hydride chemistries, have proven to generally have

excellent cycle and calendar life. Therefore, the core interest for both DCFC testing and battery mule-type testing is developing and using testing methods that best predict cycle and calendar life uncertainties.

The AVTA light-duty activities are conducted by INL for DOE. INL has responsibility for AVTA's technical execution, direction, management, and reporting, as well as data collection, analysis, and test reporting.

The current AVTA staff has 20+ years of experience testing grid-connected, plug-in electric vehicles, as well as plug-in hybrid vehicle charging infrastructure. This experience includes significant use of DCFCs with various battery chemistries since the middle 1990s and those that have important legacy of experience still available today. AVTA is currently collecting performance and use data from more than 16,000 Level 2 EVSE and DCFC, as well as from approximately 8,000 plug-in hybrid vehicles.

Introduction

The INL and ETEC Labs have collaborated to purchase, operate, and conduct battery tests at 10,000-mile intervals to determine battery capacity fading for the two DCFC and Level 2 charging methods.

INL and ETEC Labs have collaborated with the Oak Ridge National Laboratory to develop an onroad testbed for testing advanced ESSs for the EDAB Project. The project objective is to be able to test a variety of advanced ESSs that are at or near commercialization in onroad, real-world operation and to quantify the ESS capabilities, limitations, and performance fade over the life of the ESS.

Approach

DCFC Study

INL purchased four new 2012 Nissan Leaf battery electric vehicles that were instrumented with data loggers and operated over a fixed onroad test cycle. Each vehicle is operated over the test route and charged twice daily. Two vehicles are charged exclusively by AC Level 2 EVSE, while two are exclusively DCFC with a Hasetec 50-kW charger. The vehicles were performance tested on a closed test track when new and at the conclusion of the study. The traction battery packs were removed and laboratory tested when the vehicles were new and at 10,000-mile intervals. Battery tests include constant-current discharge capacity, electric vehicle power characterization, and low peak power tests. The onroad operations and 10,000-mile battery testing is currently scheduled at 50,000 miles. At the conclusion of onroad cycling, the final battery tests will be performed. All of the raw test data and raw data collected from the onboard data loggers are sent to INL for analysis and reporting. It should be noted that a small set of dedicated drivers are being used; they rotate driving duties in a method designed to give equal miles to all operating vehicles.

Two additional 2012 Nissan Leaf vehicles were purchased, with their battery packs being removed and shipped to INL for laboratory testing in environmental test chambers. This testing will demonstrate whether laboratory-based DOE battery testing procedures can predict DCFC impacts that occur in onroad environments.

Figure IV-7: Four Nissan Leafs Level 2 and DCFC charging in Phoenix.

Battery Mule EnerDel ESS Testing

Performance of the ESSs being tested in the battery mule is measured by the following metrics:

- Discharge rate
- Capacity
- Charge rate
- Durability
- Reliability
- Lifetime
- Temperature resilience.

The performance is measured under both controlled and real-world conditions and the project results will inform the research community and automotive original equipment manufacturers about the state-of–the-art of ESSs for plug-in hybrid electric vehicles and battery electric vehicles. The data and findings from this project have also been made available to support U.S. DOE modeling and energy storage development efforts.

The first ESS selected for testing is the EnerDel Type I Electric Vehicle lithium-ion chemistry with a mixed-oxide cathode and amorphous hard carbon anode. The pack has 384 cells (96 in series, four strings in parallel) and each cell has a maximum voltage (at 100% SOC) of 4.1 V and a rated capacity of 17.5 Ah (at a C/3 rate). The pack has a maximum voltage of 393.6 V, a nominal voltage of 345 V, and a rated capacity and energy of 70 Ah and 23 kWh, respectively. The ESS is a sealed unit, meaning there is no thermal management system and cooling can be done only by passive radiation or forced air on the enclosure. The ESS uses controller area network communications. This EnerDel ESS is designed for a small electric vehicle.

The base test platform is a Colorado pickup truck; it was converted into a series hybrid electric vehicle by mating a UQM 145-kW motor/generator to the stock 5.3-L, V8 engine to form an auxiliary power unit; removing the stock driveshaft; introducing a second UQM 145-kW motor/generator as the drive motor; and inserting a custom-built driveshaft assembly. The power electronics, including the motor controllers, DC/DC converters, onboard charger, and ESS cooling fans were located in the bed of the truck, along with the ESS. The motor/generator configuration is shown in Figure IV-8. The components in the figure, from left to right, are the motor

controllers of the drive motor and generator, the drive motor, and the generator on the right.

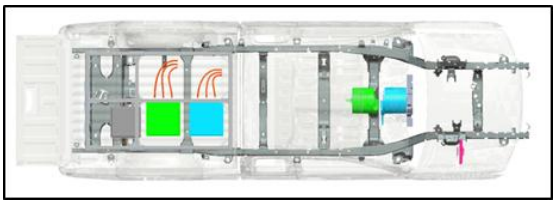

Figure IV-8: Locations of the drive motor, generator, and motor controller units. The front of the truck is to the right.

The hybrid controller is overlaid on top of the base vehicle controls, and it manages the driver requests and translates these into control of the various vehicle subsystems and components. Acceleration and braking requests are also sent via controller area network to the high-level system controller. The high-level system controller contains the physical characteristic algorithms that determine the demand on the ESS, based on the algorithms and on the information provided by the battery management system on the battery SOC, temperature, maximum available charge, and discharge current. Once the ESS demand is determined, the value is sent back to the hybrid controller and the amount of drive power or mechanical braking that must be made up by the auxiliary power unit and friction brakes, respectively, is determined.

Battery testing is normally conducted in a laboratory with maintained environments and repeatable test cycles. While repeatability is excellent for comparing battery to battery results, there are shortcomings to this method, including the usual practice of only testing modules, not packs. This type of testing does not allow for the variability that onroad testing introduces, including the following:

- Onroad pack size testing introduces a larger number of cells, allowing for the greater probability of failures
- Onroad pack size testing also introduces greater variability in internal pack heat and possible negative impacts
- Onroad testing introduces vibration that can impact pack integrity
- Onroad testing may introduce irregular charge/discharge cycles, which are present in real-world operations.

For the above reasons and other reasons, the battery mule has been used to test the EnerDel battery.

Results

DCFC Study

As mentioned previously, two Nissan Leafs are only recharged using the DCFC charging and the other two are only recharged using Level 2 EVSE.

Using the data in Table IV-3 and using an average for each of the two KWh capacities for each test, comparisons can be made. To explain this better, the average capacity for the two Level 2-charged vehicles is 23.45 kWh [(23.31 + 23.59) / 2] at baseline testing. The two DCFC vehicles have an average capacity at baseline testing of 23.31 kWh [(23.38 + 23.24) / 2] of capacity at baseline testing.

Table IV-3: Testing results for the four Nissan Leafs being DCFC and Level 2 charged. The numbers represent the kWh capacities remaining at various 10,000-mile intervals. L2 = Level 2 charging. The four digit numbers are the last four numbers of each VIN.

C_3 Energy Capacity (KWh)				
	1011 L2	4582 L2	2183 DCFC	2078 DCFC
Baseline	23.31	23.59	23.38	23.24
10k Miles	21.75	22.30	21.97	21.93
20k Miles	21.53	21.51	21.64	21.07
30k Miles	19.99	20.20	19.42	19.33

At baseline testing, the DCFC vehicles had an average lower capacity of 0.6% compared to the Level 2 vehicles. At 10,000 miles, the DCFC vehicles capacity was 0.36% lower; at 20,000 miles, it was 0.74% lower; and at 30,000 miles, it was 3.58% lower. The 30,000-mile results are the first significant indication that there may be greater capacity loss from DCFC charging than Level 2 charging. However, one set of test results does not indicate a trend. There may be summer heat impacts and the results from testing during the fall may accelerate or reverse the 30,000-mile test results.

The graph in Figure IV-9 does suggest a possible acceleration in capacity loss when comparing kWh test results. When comparing the 30,000-mile and baseline results, the Level 2 charged Leafs had an average 14.29% decrease and the two DCFC Leafs had an average 16.86% decrease. While the actual numbers of KWh difference is relatively small, the baseline to 30,000-mile results do indicate that the DCFC Leafs have experienced a 17.98% greater decrease in capacity than the Level 2 charged Leafs at the same 30,000-mile test intervals.

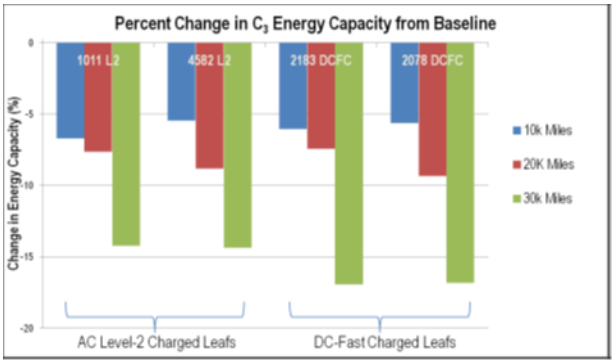

Figure IV-9: Change in energy capacity from baseline testing.

Battery Mule EnerDel ESS Testing

The EnerDel battery has been in testing since March 2012. As of the most recent test (i.e., September 2013), a total of 23,415 miles have been driven. The breakdown in operations has been 55% of the miles are city driving and 45% highway driving. The total amp hours throughput has been 39,500. The vehicle is controlled to operate using both the EnerDel traction battery and the original gasoline engine as required for safety and drivability purposes. Controlling the electric power allows for battery testing in any cycle or mode

desired. For the EnerDel battery, the average energy consumption has been 234 DC Wh per mile.

In addition to the initial baseline battery test, there have been nine additional battery tests, each at a distance of approximately 2,600 miles. The original measured capacity was 63.2 amp hours. At the most recent test at 23,451 miles, the capacity has been reduced to 52.3 amp hours (Figure IV-10), which is 83% of the original measured capacity and 75% of the rated capacity of 70 amp hours.

Figure IV-11 documents the high SOC present with the start of each trip, as well as the SOC at the end of each trip. Figure IV-12 and Figure IV-13 identify the lifetime amp hour throughput during onroad operations by battery pack current and temperature.

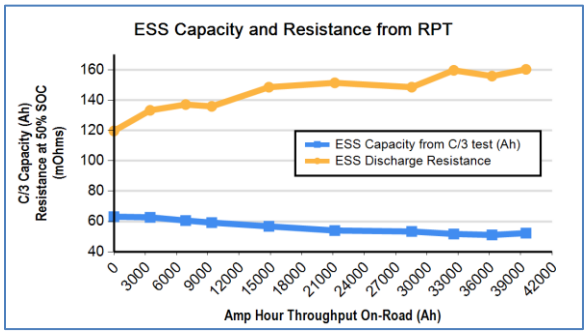

Figure IV-10: Capacity and resistance test results.

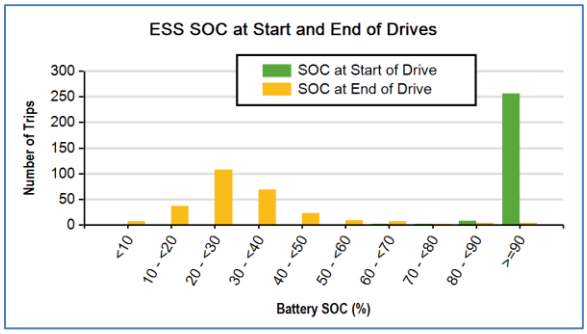

Figure IV-11: Start and end of drive state of charge levels.

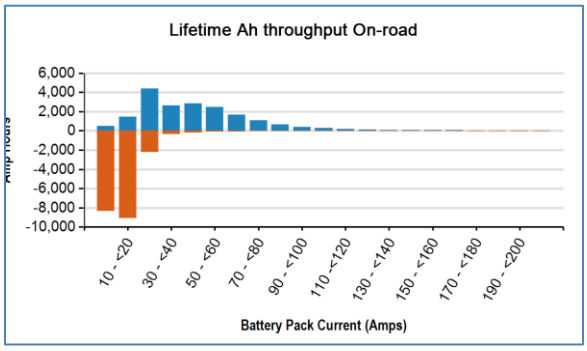

Figure IV-12: Lifetime amp hour throughput binned by battery pack current (amps).

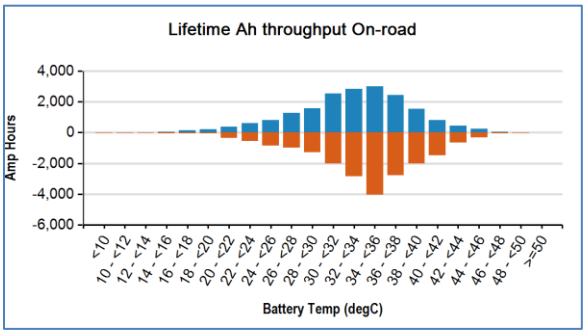

Figure IV-13: Lifetime amp hour throughput binned by battery operating temperature.

Conclusions

The DCFC study with the four Nissan Leafs is demonstrating greater battery capacity loss in the two vehicles being DCFC when compared to the capacity losses demonstrated by the two Nissan Leafs being charged at Level 2. The four vehicles are being operated in the Phoenix, Arizona area; therefore, there may be some high ambient temperatures that are impacting the DCFC vehicles. Additional testing at 40,000 and 50,000 miles during the cooler fall months will be closely studied and additional operations and testing beyond 50,000 miles will be considered.

The capacity reduction results for the EnerDel lithium-ion battery being tested in the battery mule have been well documented, with the result that only 83% of baseline capacity remains at 23,451 miles when compared to the beginning of testing benchmark. Testing will likely end at 78% of capacity. It should be noted that at the initial baseline test, the battery was only able to produce 90% of the rated capacity.

IV.B.3. Products

Publications

1. *DC Fast Charge Effects on Battery Life and Performance Study—30,000 Mile Update,* 2013, INL/MIS-13-29877, Idaho National Laboratory, August 2013.
2. *Electric Drive and Advanced Battery and Components Testbed (EDAB) March 5, 2012–December 5, 2012,* 2013, INL/MIS-12-25146, Idaho National Laboratory, January 2013.
3. *Electric Drive and Advanced Battery and Components Testbed (EDAB) March 5, 2012–February 25, 2013,* 2013, INL/MIS-12-25146, Idaho National Laboratory, March 2013.
4. *Electric Drive and Advanced Battery and Components Testbed (EDAB) March 5, 2012–February 25, 2013,* 2013, INL/MIS-12-25146, Idaho National Laboratory, March 2013.
5. *Electric Drive and Advanced Battery and Components Testbed (EDAB) March 5, 2012–April 29, 2013,* 2013, INL/MIS-12-25146, Idaho National Laboratory, May 2013.

6. *Electric Drive and Advanced Battery and Components Testbed (EDAB) March 5, 2012–June 6, 2013*, 2013, INL/MIS-12-25146, Idaho National Laboratory, July 2013.
7. *Electric Drive and Advanced Battery and Components Testbed (EDAB) March 5, 2012–July 25, 2013*, 2013, INL/MIS-12-25146, Idaho National Laboratory, August 2013.
8. *Electric Drive and Advanced Battery and Components Testbed (EDAB) March 5, 2012–September 9, 2013*, 2013, INL/MIS-12-25146, Idaho National Laboratory, October 2013.

Patents

This is a test program that is not designed to develop patents. The intent is to provide independent testing and feedback to DOE and industry on DOE and other funded technologies and technology improvements.

Tools and Data

The data generated by this testing are used to populate publications in the form of testing fact sheets, reports, and industry-referred papers.

INL/MIS-13-30556

IV.C. EV Project and ChargePoint Data Collection and Dissemination

James Francfort, Principal Investigator
Idaho National Laboratory
P.O. Box 1625
Idaho Falls, ID 83415-2209
Phone: (208) 526-6787
E-mail: James.francfort@inl.gov

Lee Slezak, DOE Program Manager
Phone: (208) 586-2335
E-mail: Lee.slezak@ee.doe.gov

IV.C.1. Abstract

Objectives

- Provide plug-in electric vehicle (PEV) and charging infrastructure costs and deployment testing results to fleet managers, EV Everywhere decision makers, and the general public to support their PEV and charging infrastructure acquisition and deployment decisions
- Continue to provide testing results to other DOE programs and national laboratories, as well as the several U.S. Drive technical teams that Idaho National Laboratory (INL) staff are members of
- Reduce the uncertainties about drivers' recharging practices and PEV acceptance
- Blend EV Project data streams from OnStar, Nissan, ECOtality, and Daimler into usable analysis that supports future infrastructure deployment decisions at residencies, public access, and work locations
- Use ChargePoint data to identify charging infrastructure use rates
- Identify driver preferences for Level 1, Level 2, and DC Fast Charger (DCFC) technologies.

Major Accomplishments

- PEV charging behavior data collected from 12,065 Level 2 (electric vehicle supply equipment (EVSEs) and DCFC from ECOtality North America as part of the EV Project. As Fiscal Year (FY) 2013 ended, 3.5 million charge events occurred and 29,085 MWh of electricity were used.
- PEV use data collected from 8,113 Nissan Leafs, Chevy Volts, and Smart EVs in the EV Project. As FY 2013 ended, 103 million test miles of PEV use were documented.
- Continued data collection from 4,249 ChargePoint EVSE. At the end of June 2013 (most recent published and approved results), data had been collected from 1.3 million charge events that used 9,020 MWh of electricity.
- For these data collection activities, much information has been disseminated by INL, including charging profiles in 15-minute increments, days of the week, charging infrastructure types, and impacts that time of use electricity pricing can have on driver behavior.
- Workplace charging behavior has been analyzed using EV Project data and presentations generated for DOE that support the EV EveryWhere activities, which are encouraging greater workplace charging options.

Future Achievements

- Continue to report on performance and use of the vehicles and charging infrastructure in the EV Project. Data collection for this project will conclude at the end of Calendar Year (CY) 2013 and, at that point, significant analysis will commence because there will be nearly one complete year of data for all EVSE and DCFC deployed.
- Additional EV Project analysis will include travel corridor use of charging infrastructure. Focusing on I-5 travel corridor data, analysis will be provided to U.S. Department of Transportation and the departments of transportation for Washington State and Oregon.
- Separate analysis of public access and private non-residential EVSE.
- Analysis of the ratios of EVSE placements to workplace ownership of PEVs.
- There will be a major transition from concentrating on data collection and data quality to analysis of the EV Project data.
- For the ChargePoint data collection, this activity will also conclude at the end of CY 2013. There will not be as much follow-up analysis as the EV Project because vehicle data collection was not part of this project's scope. However, greater analysis will be undertaken to understand workplace charger use.

✧ ✧ ✧ ✧ ✧

IV.C.2. Technical Discussion

Background

DOE's Advanced Vehicle Testing Activity (AVTA) is part of DOE's Vehicle Technologies Office, which is within DOE's Office of Energy Efficiency and Renewable Energy. AVTA is the only DOE activity tasked by DOE to conduct field evaluations of vehicle technologies and fueling infrastructure that use advanced technology systems and subsystems in light-duty vehicles to reduce petroleum consumption.

INL activities conducting AVTA have resulted in INL developing data collection systems from vehicles and charging infrastructure that use wireless data collection and

transmission methodologies. INL has accumulated this experience over 20 years of PEV, hybrid electric vehicle, and internal combustion engine vehicle testing, including laboratory, track, and field testing. Approximately 18 million miles of vehicle testing data had been accumulated by the late 2000s when DOE decided on a series of deployment and study projects that included the EV Project and the ChargePoint Projects. Given the anticipated large amount of data to be generated from vehicles and charging infrastructure, DOE tasked INL with collecting, managing, analysis, and dissemination of the data generated by the light-duty PEVs and charging infrastructure discussed as follows and elsewhere in this report.

Introduction

For the EV Project, data collection agreements and non-disclosure agreements were signed with Nissan (Leafs), ECOtality (infrastructure), OnStar (for Chevy Volt data), and Daimler (Smart EVs). The importance of successfully negotiating the non-disclosure agreements cannot be understated. In the case of OnStar, this was their first ever partnership where they shared raw vehicle data with an outside party. Similarly with Nissan, ECOtality, and Daimler, a project of this type was revolutionary in that raw data from very competitive entities would allow a third party (INL) to have all the raw data and the ability to produce reports that accurately benchmarked how over 11,000 general public partners were operating their vehicles and the charging infrastructure. The EV Project also necessitated signing agreements with the 11,000 individual owners of the vehicles and the public charging infrastructure.

For the ChargePoint Project, a single non-disclosure agreement was negotiated with ChargePoint that would enable INL to receive raw data that documented charging infrastructure use. Given the lack of vehicle data, there were not as many concerns with personal identification issues.

Approach

EV Project

INL has highly automated the data collection, processing, and reporting system used to collect most data from vehicles and charging infrastructure. The history of automated data collection at INL goes back to the use of databases for tracking electric vehicle performance and use in the mid 1990s. These systems have been refined as technology options (such as cellular communications and much lower cost data loggers) have progressed. Today, a multi-step process (Figure IV-14) is used to transmit vehicle and charger data from the vehicle, through the INL firewalls, and into the INL protected enclave. From there, additional processing steps are used within INL (Figure IV-15) to develop summary reports and various partner-requested custom reports.

INL reviews the public reports with its main testing partners before posting them on the EV Project website, as well as mailing various other reports to program partners.

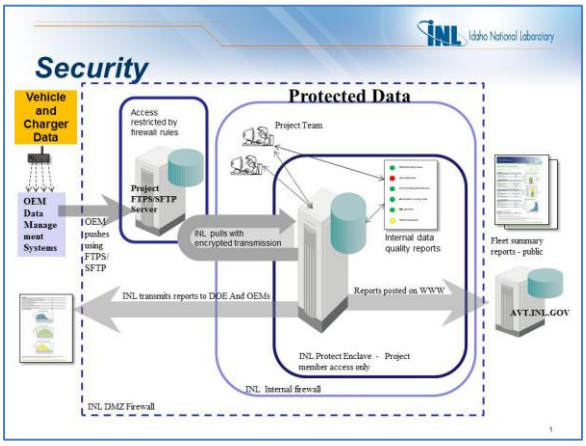

Figure IV-14: Overview of INL data collection input system for the EV Project and ChargePoint Project, as well as all data collection activities.

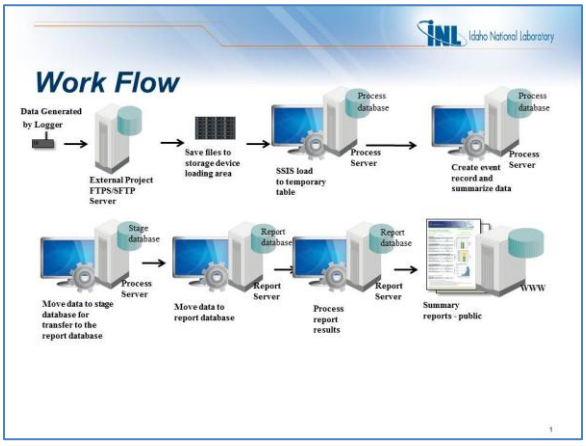

Figure IV-15: Internal main eight steps for handling wireless vehicle and charging infrastructure data.

The objective of the EV Project is to create a real-world laboratory to understand how a large mass of vehicle operators will both operate their PEVs and use the charging infrastructure that they have access to. For the EV Project, this mass included more than 22,000 vehicles and charging infrastructure units and the results of this deployment and analysis are presented in the next section.

ChargePoint

The ChargePoint Project involved deployment of infrastructure only and data collection and reporting of the infrastructure use by unknown drivers. The same methods of data collection from EVSE in the EV Project were used for the ChargePoint Project.

Results

EV Project

The EV Project is a DOE-funded ARRA Project for deploying and testing PEV recharging infrastructure. Lead by ECOtality North America, it has been the largest deployment and testing of EVSE and DCFC ever attempted. Approximately 22,000 Level 2 EVSE and DCFC Nissan Leafs,

Chevrolet Volts, and Smart EVs are being deployed in the major population areas of the following:

- Phoenix and Tucson, Arizona areas
- San Diego, San Francisco, and Los Angeles, California areas
- Atlanta, Georgia area
- Chicago, Illinois area
- Southern New Jersey
- Portland, Eugene, Salem, and Corvallis, Oregon areas
- Philadelphia, Pennsylvania area
- Chattanooga, Nashville, Knoxville, and Memphis, Tennessee areas
- Dallas, Fort Worth, and Houston, Texas areas
- Washington, D.C. area
- Washington State.

The project's intent has been to deploy Level 2 EVSE at the private residences of each Leaf or Volt purchaser and Level 2 EVSE and DCFC in public locations in order to characterize charging infrastructure and vehicle use in diverse topographic and climatic environments, evaluate the effectiveness of public versus private charge infrastructure, and conduct trials of various revenue systems for public charge infrastructures. The Smart EVs are all rental cars; therefore, no residential EVSE are associated with these vehicles. These vehicles utilize public Level 2 EVSE when a charge event is required.

As FY 2013 ended and this report was being compiled, the total reported project mileage was 103 million test miles on the 8,113 Leafs, Volts, and Smart EVs (Figure IV-16) reporting results. The more than 12,000 public and residential Level 2 EVSE and DCFC (Figure IV-17) have reported 3.5 million charging events.

A more in-depth discussion will have to be limited to the most recent published and approved reports that cover the second quarter of calendar year 2013 (April through June 2013). As of the end of the second quarter of 2013, data had been published from 5,729 Nissan Leaf battery electric vehicles, 2,012 Chevrolet Volt extended range electric vehicles, and 363 Smart EVs, and 11,933 ECOtality EVSE and DCFC were providing data from eleven states and the District of Columbia. A total of 93.1 million test miles and 2.93 million charging events have been documented on the Project Overview Report for the EV Project (http://avt.inel.gov/pdf/EVProj/EVProjOverviewQ22013.pdf) as of June 2013.

The EV Project's Nissan Leaf summary report for April to June 2012 (http://avt.inel.gov/pdf/EVProj/EVProjNissanLeafQ22012.pdf) provides national and regional Leaf usage statistics and these data include the national vehicle usage data seen in Table IV-4. Additional data for each region can be found in the same above PDF.

Figure IV-18 and Figure IV-19 document the Nissan Leaf battery state of charge (SOC) before and after charging events. It will be interesting to see if SOC before-charging changes as operators become more familiar with the vehicles and if SOC at end-of-charging changes as drivers use public charging, including DCFCs for shorter periods of time.

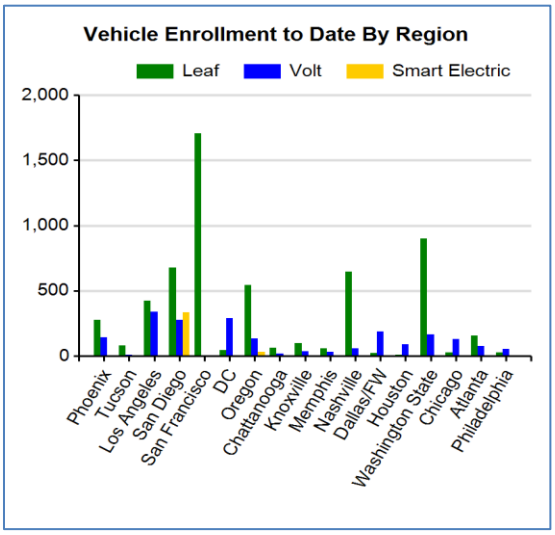

Figure IV-16: Number of EV Project vehicles providing data by major cities as of the end June 2013.

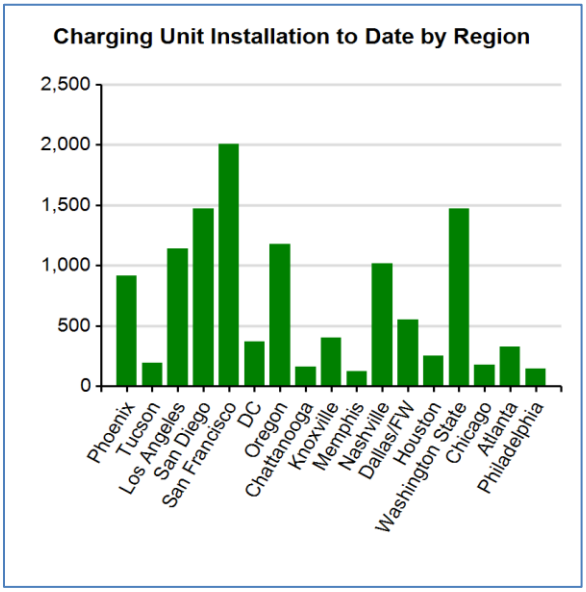

Figure IV-17: Charging unit installations by EV Project area.

Table IV-4: EV Project Nissan Leaf usage data for the April to June 2013 quarter.

Number vehicles	4,261
Total miles	8.04 million
Average miles per trip	7.1
Average miles driven per day when driven	29.5
Average number of trips between charge events	3.8
Average miles driven between charge events	28.1
Average number of charges per day when driven	1.1
Number of at-home charging events	222,008
Number of away–from-home charging events	61,639
Unknown charging event locations	17,614

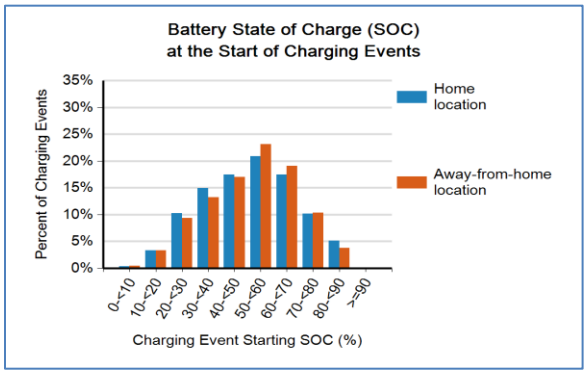

Figure IV-18: EV Project Nissan Leaf battery SOC at start of charging events.

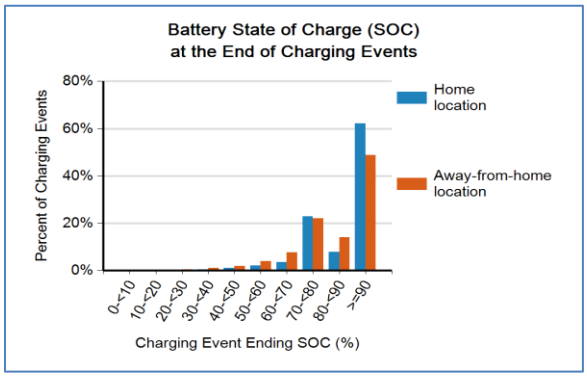

Figure IV-19: EV Project Nissan Leaf battery SOC at end of charging events.

The EV Project's Chevrolet Volt Leaf summary report for April to June 2013 (http://avt.inel.gov/pdf/EVProj/EVProjChevroletVoltQ22013.pdf) provides national and regional Volt usage statistics and these data include the national vehicle usage data seen in Table IV-5. Additional data for each region can be found in the same above PDF.

Figure IV-20 and Figure IV-21 document the Volt battery SOC before and after charging events.

Table IV-5: EV Project Chevy Volt usage data for the April to June 2013 quarter.

Number vehicles	1,895
Total miles	5.8 million
Overall mpg	142
Overall electricity consumption (AC Wh/mi)	231
Average miles per trip	8.3
Average miles driven per day when driven	41.0
Average number trips between charge events	3.3
Average miles driven between charge events	27.6
Average number of charges per day when driven	1.5
Number of at-home charging events	161,750
Number away-from-home charging events	27,872
Unknown charging event locations	13,584

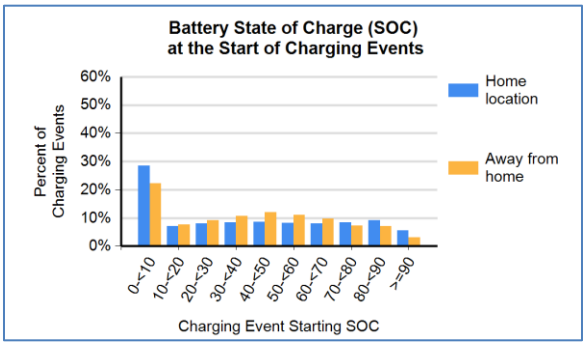

Figure IV-20: EV Project Chevy Volt battery SOC at start of charging events.

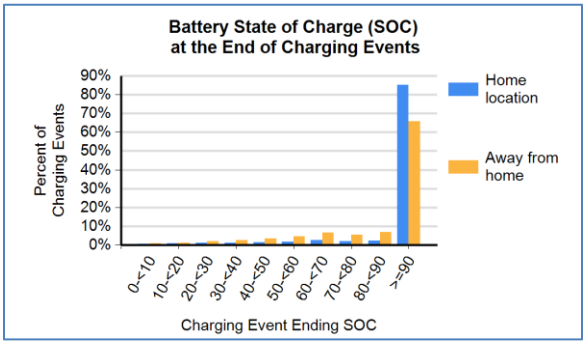

Figure IV-21: EV Project Chevy Volt battery SOC at end of charging events.

The April to June 2013 quarterly infrastructure summary report documents infrastructure utilization nationally and regionally for residential Level 2 EVSE, publicly available Level 2 EVSE, and DCFC (http://avt.inel.gov/pdf/EVProj/EVProjectInfrastructureQ22013.pdf).

Figure IV-22 highlights the percent of all national Level 2 EVSE charging units in 15-minute increments with an EV Project vehicle connected during week days. Figure IV-23 gives the same information for weekend days.

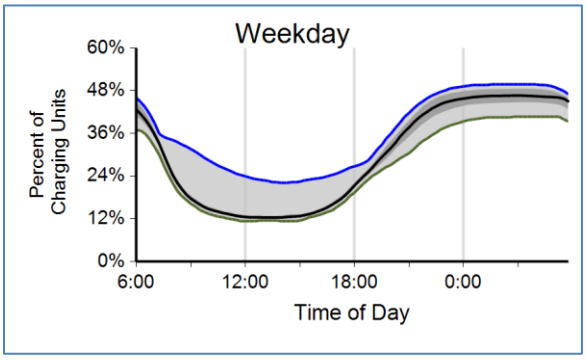

Figure IV-22: EV Project percent of all national Level 2 EVSE with a vehicle connected during weekdays. Data are in 15-minute increments.

Note that in both figures, the blue line is the peak for the reporting period, the green line is the minimum, the black line is the mean, and the darker gray areas above and below the black line are the 25 to 50% and 50 to 75% quartiles. This is true for all figures in this section that report percent of

charging units with a vehicle connected and the electricity demand in AC MW.

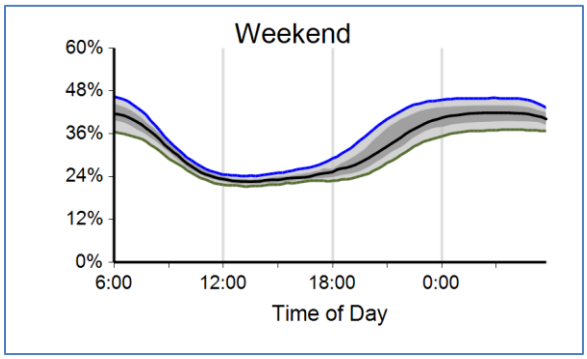

Figure IV-23: EV Project percent of all national Level 2 EVSE with a vehicle connected during weekends. Data are in 15-minute increments.

Figure IV-24 is the charging profile in AC MWh for all Level 2 EVSE in the EV Project for weekdays and Figure IV-25 is for weekends. Note the heavy use of post-midnight charging.

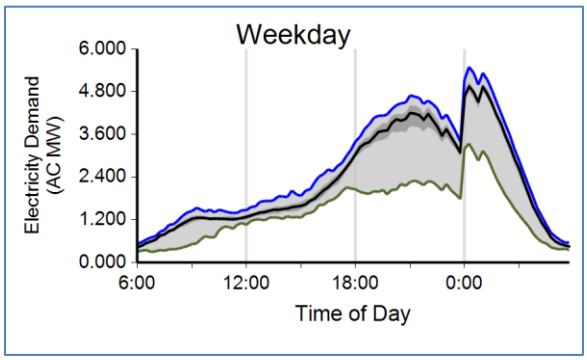

Figure IV-24: EV Project charging profile based on national energy demand for weekdays. Data are in 15-minute increments for any time in the reporting quarter.

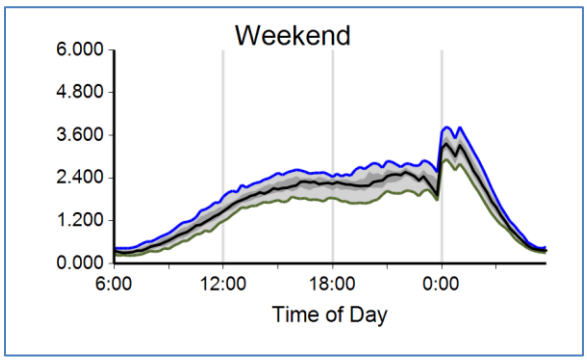

Figure IV-25: EV Project charging profile based on national energy demand for weekends. Data are in 15-minute increments for any time in the reporting quarter.

Figure IV-26 documents the length of time vehicles are connected to residential EVSE. The two sets of peaks suggest short-opportunity charging for less than 1 or 2 hours and overnight charging for 10 to 14 hours. Figure IV-27 shows the same set of vehicles drawing power for much shorter periods of time than when they were connected as shown in Figure IV-26. The general shape of Figure IV-28 matches Figure IV-27 as would be expected as the distribution of energy consumed would have a similar profile to the length of time the vehicles draw power.

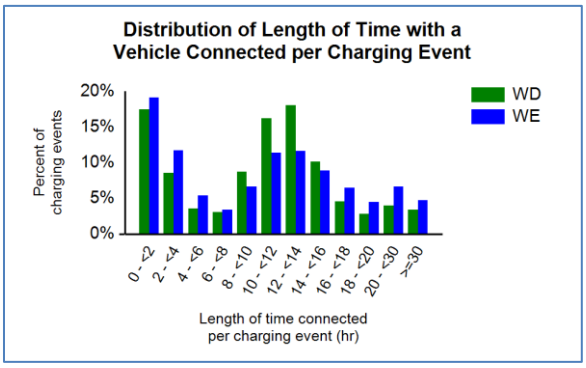

Figure IV-26: EV Project distribution of length of time with a vehicle connected per charging unit for residential Level 2 EVSE.

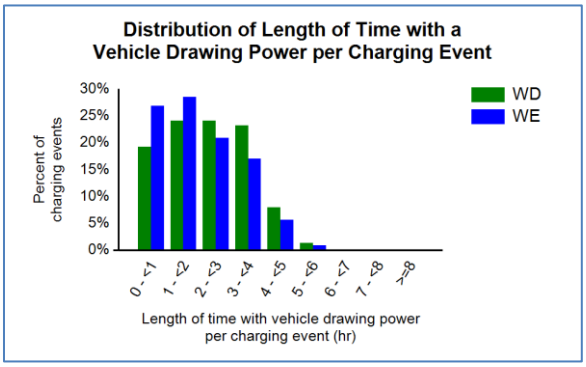

Figure IV-27: EV Project distribution of length with a vehicle drawing power per charging event for residential Level 2 EVSE.

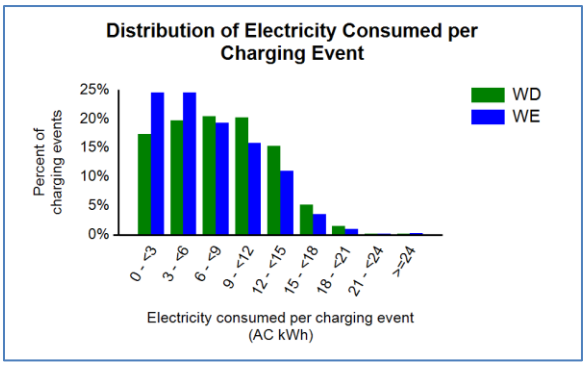

Figure IV-28: EV Project distribution of electricity consumed per charging event for residential Level 2 EVSE.

Figure IV-29 is the charging profile for public access Level 2 EVSE as measured by the number of vehicles connected as a percent for weekdays and Figure IV-30 is the weekend data. It is assumed that at-work or near-work public access charging is creating the higher peak in weekday public charging.

Figure IV-31 documents a similar public access day profile when vehicles are connected to public EVSE and start drawing power about 9 a.m. on weekdays. Figure IV-32 documents the less significant peak in public charging on weekends.

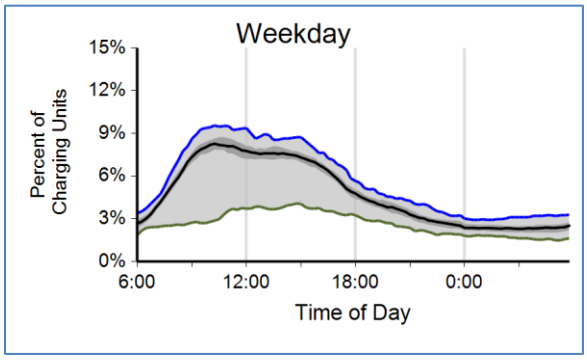

Figure IV-29: EV Project percent of all publicly available Level 2 EVSE with a vehicle connected during weekdays. Data are in 15-minute increments for any time in the reporting quarter.

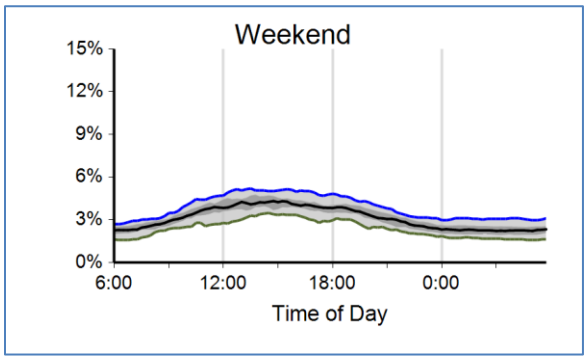

Figure IV-30: EV Project percent of all publicly available Level 2 EVSE with a vehicle connected during weekends. Data are in 15-minute increments for any time in the reporting quarter.

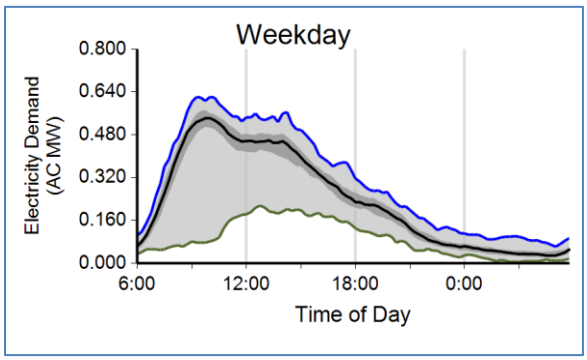

Figure IV-31: EV Project publicly available Level 2 EVSE charging profile based on energy demand for weekdays. Data are in 15-minute increments for any time in the reporting quarter.

Time of use (TOU) electric utility billing rates for residential charging warrants an expanded discussion. While Figure IV-24 and Figure IV-25 clearly show national peak demand at night as measured in AC MW, regional residential profiles significantly highlight TOU rate impacts. Figure IV-33 shows San Diego weekday peak demand that is influenced by the TOU rates that start at midnight. Figure IV-34 shows similar impacts that also occur on weekends.

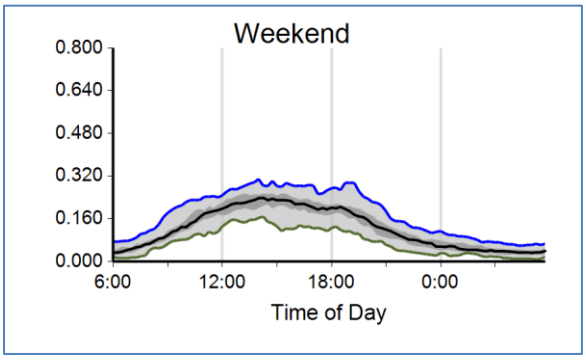

Figure IV-32: EV Project publicly available Level 2 EVSE charging profile based on energy demand for weekends. Data are in 15-minute increments for any time in the reporting quarter.

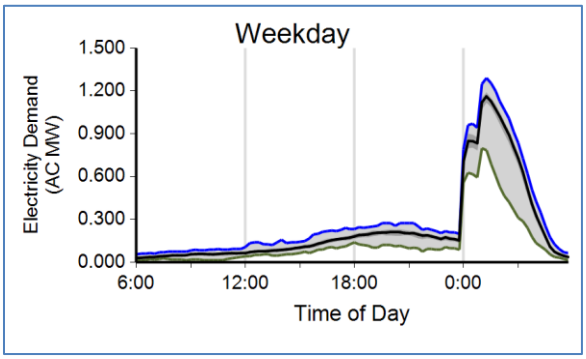

Figure IV-33: San Diego residential EVSE electric demand for weekdays.

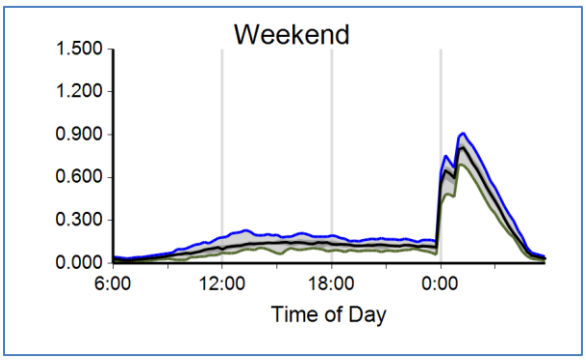

Figure IV-34: San Diego residential EVSE electric demand for weekends.

A contrast to the San Diego profiles is the weekday and weekend (Figure IV-35 and Figure IV-36) demand curves for Washington State. Washington has relatively low electricity rates due to its extensive hydropower generation system. San Diego has more expensive rates; therefore, incentives to shift demand to midnight can be successful with TOU charging and TOU whole house rates. In Washington State, there simply is not the ability to offer much lower rates when general electricity rates are low to start with.

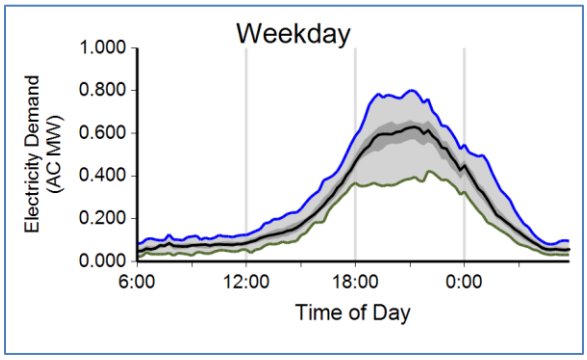

Figure IV-35: Washington State residential EVSE electric demand for weekdays.

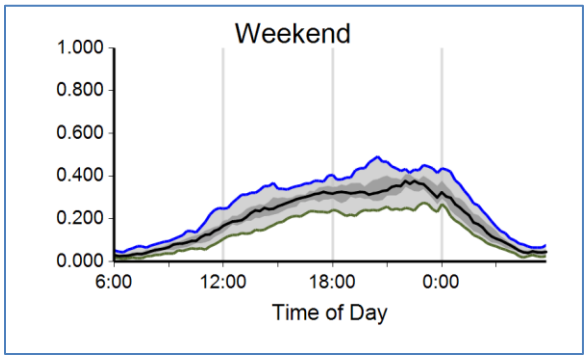

Figure IV-36: Washington State residential EVSE electric demand for weekends.

DCFC results are significantly different than either public or residential Level 2 EVSE. DCFC, by the nature of their design, are intended to recharge approximately 50% of a vehicle's battery pack in 30 minutes or less. The time required to replace 50% of a pack's energy can vary with extremely large or small battery packs, as well as by DCFC peak power design. In the EV Project, a 50-kW DCFC model is used and it should be noted that the Nissan Leaf controls the current during DCFC. During charge events, power transfer rates of 50 kW have been documented, which suggests that the 50% in 30-minutes rule is true.

In the EV Project, approximately two-thirds of the charge events are from 15 to 25 minutes (Figure IV-37). Energy transfer rates are between 6 and 10 kWh approximately 70% of the time (Figure IV-38).

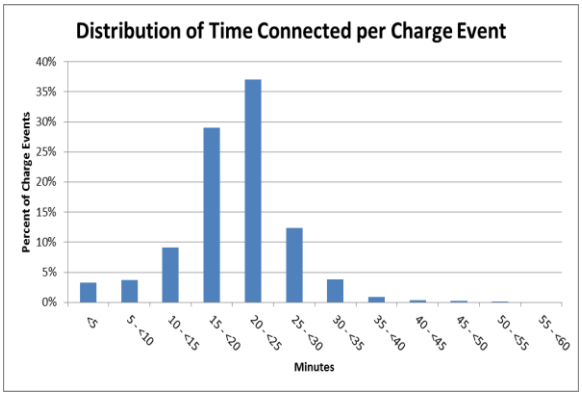

Figure IV-37: DCFC vehicle connect time profile.

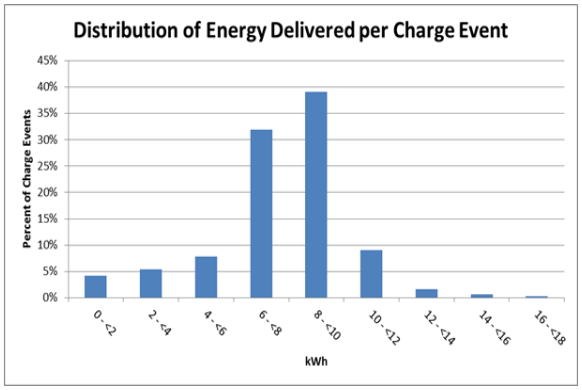

Figure IV-38: DCFC energy transfer profile for the EV Project.

Using the most used ranges of 15 to 25 minutes for average charge times and 6 to 10 kWh as average total energy transferred in Figure IV-37 and Figure IV-38, an estimated average charge power of 24 kW can be calculated. Using all of the time connected and energy transferred bins, the average estimated charge power is 23 kW. Using the binned percent DCFC power levels (Figure IV-39) suggests an average charge level of 26.5 kW. The result of all of this is that the average DCFC power level is probably about 25 kW for fast charging a Nissan Leaf. Therefore, even though the DCFC can provide the Leafs with 50-kW peak power, the vehicle controls the power level it will accept. This can be driven by the SOC of the battery at beginning-of-charge and end-of-charge or the batteries ability to accept additional charge due to pack temperatures.

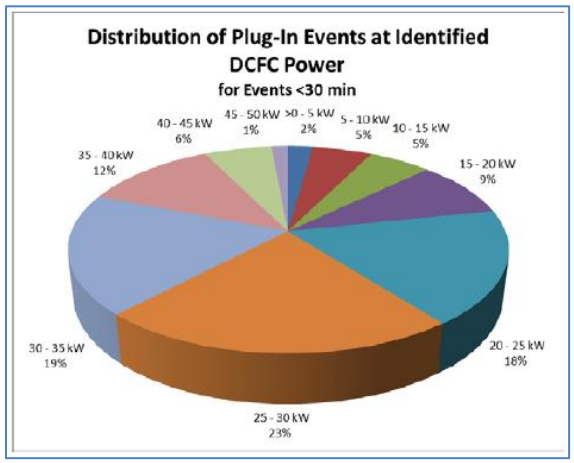

Figure IV-39: Binned percent DCFC power.

In addition, peak fast charge level is not an instantaneous process. When looking at a fast charge profile, there are ramp up and down periods (Figure IV-40). During the Hasetec DCFC test, 47.1 DC kW was the peak charge to the Leaf, while a total of 13.3 DC kWh was delivered over 31 minutes and 40 seconds. The average power during this test is 25.2 kW.

This has important implications for mitigating demand charges of as high at $1,500 per fast charge. Distributed energy at each DCFC would likely be required to only have to provide an additional 5 kW of power above the usual 20-kW threshold for incurring demand charges. In other words, if research showed that if the total peak of 47.1 could be

avoided, and the average of 25 kW charged nearly the entire charge cycle, demand charges can be avoided via smarter charging and distributed energy storage, which would mean a smart grid.

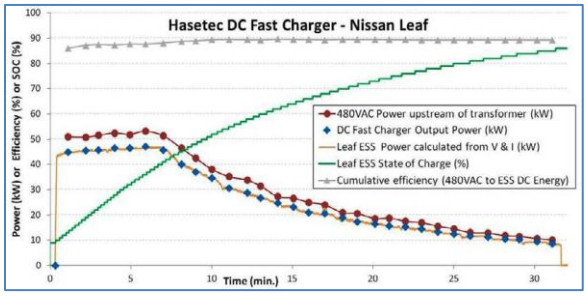

Figure IV-40: Profile of a Nissan Leaf being fast charged by a DCFC from Hasetec.

It should be noted that early DCFC usage rates data, on a per unit basis, have been shown to be 17 times higher than publicly sited Level 2 EVSE (Figure IV-41).

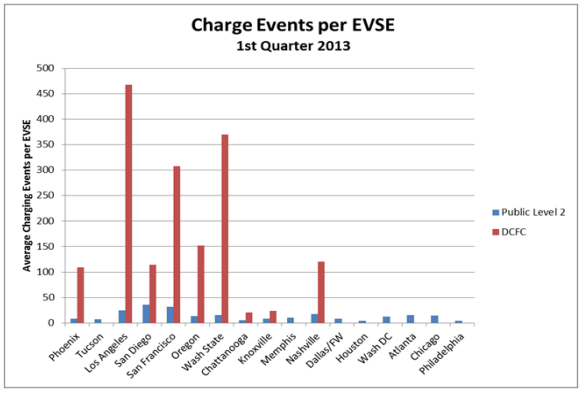

Figure IV-41: Per unit charging frequencies for public access Level 2 EVSE and DCFCs.

While DCFC appears popular for public recharging for vehicles that are DCFC capable, it should be noted that the installation costs of DCFC units can be significant. The average (mean) cost to install the first 99 DCFC is $20,848 (Figure IV-42). It should be noted that the installation costs can have significant ranges. For the EV Project DCFC, the costs have ranged from $8,440 in Arizona to $47,708 in California.

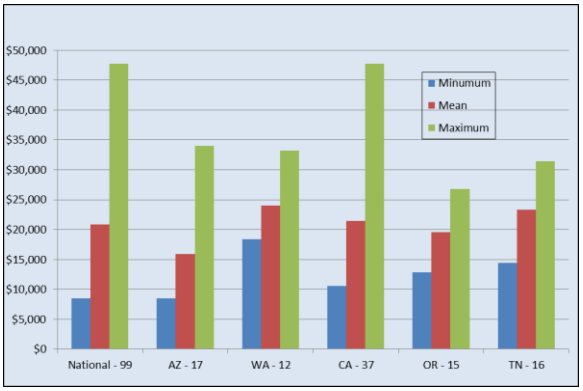

Figure IV-42: National and five regional DCFC installation costs by national and five regions in the EV Project with the most DCFC.

ChargePoint

The ChargePoint data in draft form for the third quarter of the 2013 report has project to-date totals of more than 1.5 million charging events at 4,253 residential, public, and fleet locations, with 11,000 MWh of energy used to-date. Approximately 43% of the EVSE are at residences and the remaining 57% installation sites are public (51%) or fleet EVSE with no public access (6%). The majority (53%) of the charge events occur at residential locations (Figure IV-43), even though they are not the majority of the installation locations. Slightly less than half (49%) of the energy consumed is also used at residential locations (Figure IV-44). Similar to the EV Project, the residential EVSE have the highest percentage of times, both with a vehicle connected and power being drawn (Figure IV-45).

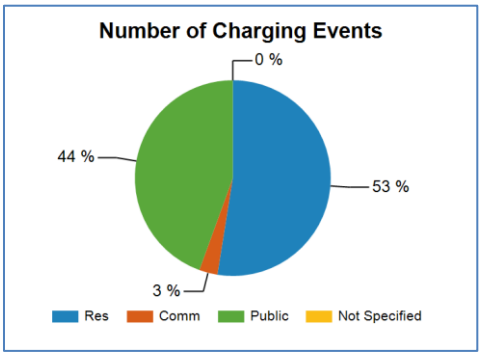

Figure IV-43: ChargePoint charging event locations.

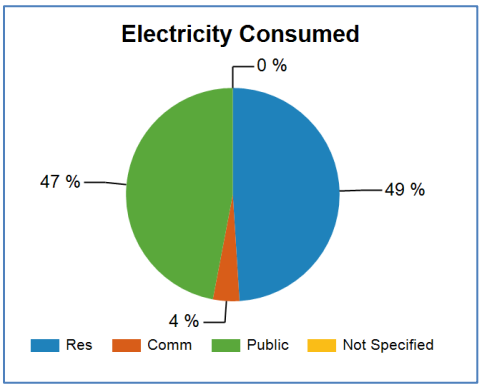

Figure IV-44: ChargePoint AC energy use by EVSE location.

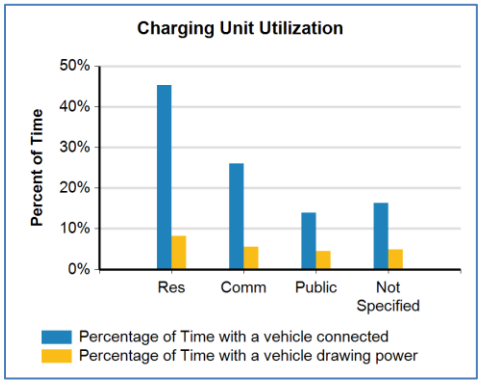

Figure IV-45: ChargePoint percent of time an EVSE has a vehicle connected and a vehicle drawing power.

It should be noted that a super majority of the ChargePoint EVSE are Level 2. There is a very small minority of Level 1 EVSE. All Level 1 and 2 EVSE are grouped together for reporting.

When looking at the ChargePoint weekday charging profiles for residential locations (Figure IV-46), the peak is similar to the similar EV Project EVSE (Figure IV-24). Similarly to the EV Project results (Figure IV-31), the ChargePoint public access EVSE has peak demand between 6 a.m. and noon (Figure IV-47), when drivers are believed to be charging at work or work-related public parking.

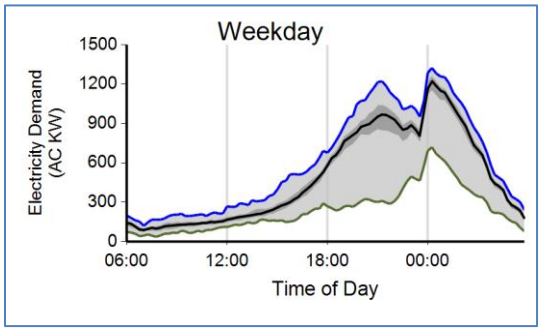

Figure IV-46: ChargePoint residential EVSE charging profile for weekday charging.

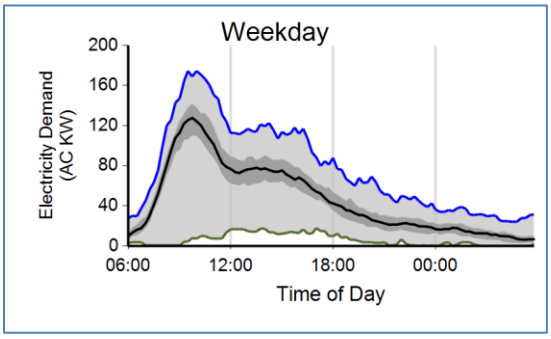

Figure IV-47: ChargePoint public EVSE charging profile for weekday charging.

Conclusions

As FY 2013 ended, the EV Project was extremely close to completion, with only a single quarter of data remaining to be collected. Non-EV Project events that have ranged from a tsunami to a less-than-optimal economy and subsequent delays in vehicle uptakes have impacted schedules. In spite of challenges, data collection and use agreements were signed and, in some cases extended for 11,000 private drivers and the owners of non-residential EVSE and DCFC charging locations. The result is the largest accumulation of PEV driver miles and charging behaviors ever accumulated. The final stages of the EV Project are seeing a transition from a focus on deployments and data collection to the more important phase of non-routine data analysis and reporting. Previous reporting has focused on statuses and custom reporting for electric utility and funding partners. Most recently, analysis is being used to support decisions such as EV EveryWhere Workplace charging initiatives, original equipment manufacturers' negotiations with California-based regulators, and modeling efforts by DOE laboratories and non-governmental organizations, as well as university researchers.

Taking multiple data streams from competitive vehicle and charger providers that had never before shared raw data and blending those data streams into useable research products has been a significant accomplishment. There continue to be legal and personally identifiable information constraints on handling the raw data, but a wealth of information for DOE and other cooperative research purposes now exists.

Going forward, the EV Project's primary data collection task will conclude at the end of CY 2013 and many final quarterly and standard end-of-project reports will be generated. Beyond that, research partnerships will allow greater use of the over 100 million miles of vehicle operations and charging profiles that DOE envisioned at project inception.

The ChargePoint Project was funded at a lower level than the EV Project and the lack of vehicle data limits some research opportunities. However, with a higher percentage of public and potentially work place EVSE, there are also significant opportunities for new analysis to occur.

IV.C.3. Products

Publications

1. *Overview Report Project to date through September 2012*, 2012, INL/MIS-12-21898, Idaho National Laboratory, Idaho Falls, ID, October 2012.
2. *Nissan Leaf Vehicle Summary Report. July–September 2012*, 2012, INL/MIS-11-21904, Idaho National Laboratory, Idaho Falls, ID, October 2012.
3. *Chevrolet Volt Vehicle Summary Report. July–September 2012*, 2012, INL/MIS-11-24041, Idaho National Laboratory, Idaho Falls, ID, October 2012.
4. *Electric Vehicle Charging Infrastructure Summary Report: July–September 2012*, 2012, INL/MIS-10-19479, Idaho National Laboratory, Idaho Falls, ID, October 2012.
5. *Overview Report Project to date through December 2012*, 2013, INL/MIS-12-21898, Idaho National Laboratory, Idaho Falls, ID, February 2013.
6. *Nissan Leaf Vehicle Summary Report. October–December 2012*, 2013, INL/MIS-11-21904, Idaho National Laboratory, Idaho Falls, ID, February 2013.
7. *Chevrolet Volt Vehicle Summary Report. October–December 2012*, 2013, INL/MIS-11-24041, Idaho National Laboratory, Idaho Falls, ID, February 2013.
8. *Electric Vehicle Charging Infrastructure Summary Report: October–December 2012*, 2013, INL/MIS-10-19479, Idaho National Laboratory, Idaho Falls, ID, February 2013.
9. *Overview Report Project to date through March 2013*, 2013, INL/MIS-12-21898, Idaho National Laboratory, Idaho Falls, ID, April 2013.

10. *Nissan Leaf Vehicle Summary Report. January–March 2013*, 2013, INL/MIS-11-21904, Idaho National Laboratory, Idaho Falls, ID, April 2013.
11. *Chevrolet Volt Vehicle Summary Report. January–March 2013*, 2013, INL/MIS-11-24041, Idaho National Laboratory, Idaho Falls, ID, April 2013.
12. *Electric Vehicle Charging Infrastructure Summary Report: January–March 2013*, 2013, INL/MIS-10-19479, Idaho National Laboratory, Idaho Falls, ID, April 2013.
13. *Overview Report Project to date through June 2013. 2013*, 2013, INL/MIS-12-21898, Idaho National Laboratory, Idaho Falls, ID, July 2013.
14. *Nissan Leaf Vehicle Summary Report. April–June 2013*, 2013, INL/MIS-11-21904, Idaho National Laboratory, Idaho Falls, ID, July 2013.
15. *Chevrolet Volt Vehicle Summary Report. April–June 2013*, 2013, INL/MIS-11-24041, Idaho National Laboratory, Idaho Falls, ID, July 2013.
16. *Electric Vehicle Charging Infrastructure Summary Report: April–June 2013*, 2013, INL/MIS-10-19479, Idaho National Laboratory, Idaho Falls, ID, July 2013.
17. Shirk, M., *Electrifying the Vehicle Market in the Southeast: In-Use Performance of Electric Drive Vehicles and Infrastructure: EV Project Results to Date (SLIDES),* INL/CON-13-29016, Knoxville, TN, May 2013
18. *ChargePoint America Vehicle Charging Infrastructure Summary Report through September 2012*, 2012, INL/MIS-11-24311, Idaho National Laboratory, Idaho Falls, ID, December 2012.
19. *ChargePoint America Vehicle Charging Infrastructure Summary Report through December 2012*, 2013, INL/MIS-11-24311, Idaho National Laboratory, Idaho Falls, ID, February 2013.
20. *ChargePoint America Vehicle Charging Infrastructure Summary Report through March 2013*, 2013, INL/MIS-11-24311, Idaho National Laboratory, Idaho Falls, ID, April 2013.
21. *ChargePoint America Vehicle Charging Infrastructure Summary Report through June 2013*, 2013, INL/MIS-11-24311, Idaho National Laboratory, Idaho Falls, ID, August 2013.

Patents

This is a test program that is not designed to develop patents. The intent is to provide independent testing and feedback to DOE and industry on DOE and other funded technologies and technology improvements.

Tools and Data

The data generated by this testing are used to populate publications in the form of testing fact sheets, reports, and industry-referred papers.

INL/MIS-13-30556

IV.D. Level 1 Benchmark of Advanced Technology Vehicles

Kevin Stutenberg, Principal Investigator
Argonne National Laboratory
9700 South Cass Avenue
Argonne, IL, 60439
Phone: (630) 252-6788
E-mail: kstutenberg@anl.gov

Lee Slezak, DOE Program Manager
Phone: (202) 586-2335
E-mail: Lee.Slezak@ee.doe.gov

IV.D.1. Abstract

Objectives

- Provide independent evaluation of advanced automotive technology by benchmarking of hybrids, plug-in hybrids, battery electric vehicles, and alternative fuel vehicles as part of the U.S. Department of Energy's (DOE's) mission of laboratory and field evaluations.
- Establish the state-of-the-art automotive technology baseline for powertrain systems and components through development of test data and the corresponding analysis.
- Disseminate vehicle and component testing data to partners of the DOE, such as other national laboratories, the U.S. Council for Automotive Research (USCAR), OEMs, suppliers and universities.
- Provide data to support codes and standards development, as well as supporting powertrain simulation model development and validation.

Major Accomplishments

- Extensively benchmarked seven advanced-technology vehicles ranging from conventional vehicles to plug-in hybrids. The vehicles are part of DOE's Advanced Vehicle Testing Activity (AVTA):
  - 2013 Chevrolet Malibu Eco
  - 2013 Volkswagen Jetta TDI
  - 2012 Honda Civic GX
  - 2013 Chevrolet Volt
  - 2013 Honda Civic HEV
  - 2013 Toyota Prius PHV
  - 2013 Volkswagen Jetta HEV
- Distributed the test results and analysis through several formats such as reports, presentations, and sharing of raw data.
- The testing activity directly contributed in the development of some codes and standards, and supported powertrain simulation model development and validation.

Future Achievements

- Provide testing and vehicle systems analysis to further contribute to DOE's missions.

✧ ✧ ✧ ✧ ✧

IV.D.2. Technical Discussion

Background

Since its inception, the Advanced Powertrain Research Facility (APRF) at Argonne National Laboratory has been testing advanced-technology vehicles to benchmark the latest automotive technologies and components for the U.S. Department of Energy (DOE). The staff has tested a large number of vehicles of different types, such as hybrid electric vehicles (HEVs), plug-in hybrid electric vehicles (PHEVs), battery electric vehicles, and conventional vehicles, which include those operating on alternative fuels.

Introduction

Over the last decade, the staff has developed a fundamental expertise in the testing of the next wave of energy-efficient vehicles. During this time, the instrumentation of the powertrains has evolved and the test procedures have been refined. Two levels of testing exist today; the first level (Level-1) involves comprehensive but non-invasive instrumentation of a vehicle, leaving the vehicle unmarked after the testing. The second level (Level-2) involves in-depth and comprehensive invasive instrumentation of a vehicle and powertrain components, which leaves the vehicle with irreversible alterations.

This report summarizes the Level-1 benchmark activities of FY 2013. The first section describes the test approach for the DOE's Advanced Vehicle Testing Activity (AVTA), and is followed by a second section where the vehicle tests results and a brief analysis are presented.

Approach

General Test Instrumentation and Approach

The testing presented in this report is focused on the comprehensive non-invasive Level-1 type of testing. Typically, Argonne receives these vehicles on loan from partners; therefore, the vehicles need to leave the test facility in the "as-received" condition. This requirement limits the instrumentation to sensors that can be easily removed without leaving any damage.

Despite this limitation, Argonne strives to achieve a maximum level of instrumentation. If the vehicle has an

internal combustion engine, instrumentation is applied to monitor the engine speed, fuel flow (at least from modal emissions or a fuel flow meter if possible) and engine oil temperature (achieved through dipstick instrumentation). For electrified vehicles, a power analyzer is used to record, at a minimum, the voltage and main current from the stored-energy system. If the vehicle requires charging, the electric power from the charging source is recorded. Furthermore, any sensors that can be implemented without permanent damage, such as temperature sensors, are typically included in locations of interest (a battery pack vent, for example). These additional sensors vary from vehicle to vehicle. A final part of the level-1 benchmark is the recording of messages from the vehicle's information buses, the content of which varies widely from vehicle to vehicle.

In addition to the minimum instrumentation described above, further sensors may be added, depending on the vehicle powertrain and special interests, so long as they are non-invasive.

Purpose of Benchmarking

A major goal of the benchmarking activity is to enable petroleum displacement through data dissemination and technology assessment. The data generated from the vehicle testing and analyses are shared through several mechanisms, such as raw data, processed data, presentations and reports.

A fundamental gateway to the data is Argonne's **Downloadable Dynamometer Database (D³)**, which is a public website at http://www.transportation.anl.gov/D3. The D³ website provides access to data and reports from vehicles tested on the standard test cycles. The data directly serve the development of codes and standards as well as the development and validation of simulation models. These activities then in turn impact the modification of test plans and instrumentation. Further partners in the testing are U.S. manufactures and suppliers, through the U.S. Council for Automotive Research. Many of the research activities of the DOE rely on the benchmark laboratory and fleet testing results to make progress towards their own goals. Figure IV-48 details some of these DOE research activities and partners.

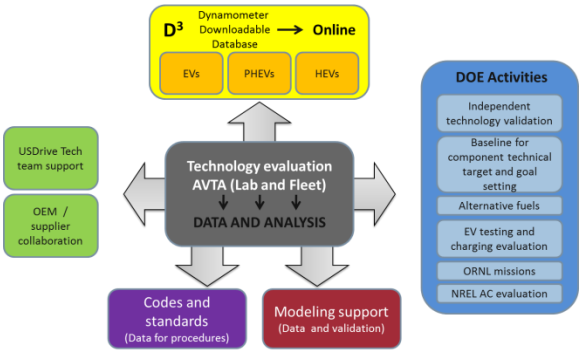

Figure IV-48: Data dissemination and project partners.

This benchmark program leverages the DOE's AVTA activities. Through this program, Idaho National Laboratory procures new advanced-technology vehicles to evaluate through accelerated fleet testing. As part of the evaluation, these vehicles are benchmarked in the APRF. Figure IV-49 illustrates the process.

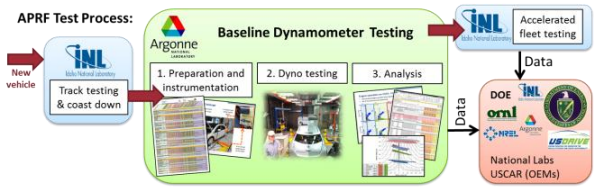

Figure IV-49: Advanced Vehicle Testing Activity process.

Further information on the AVTA is available at http://avt.inel.gov/.

Advanced Powertrain Research Facility

In order to evaluate a variety of vehicle conditions, the 4WD chassis dynamometer of the APRF is EPA 5-cycle capable. The test cell includes a thermal chamber and an air-handling unit with a large refrigeration system that enables vehicle testing at the EPA "Cold CO Test" ambient temperature of 20°F (-7°C). The other standard test temperatures are 72°F (25°C) and 95°F (35°C). In addition, a set of solar emulation lamps can provide 850 W/m² of radiant sun energy. The test cell is shown in Figure IV-50.

Figure IV-50: Illustration of testing at 95°F with sun emulation (left) and at 20°F cold ambient temperature (right).

Downloadable Dynamometer Database (D³)

D³ is a public repository of independent vehicle test data that provides a high level of detail useful in the research community. This web-based portal to Argonne vehicle test data is designed to provide access to dynamometer data that are normally too expensive for most research institutions to generate. The data are intended to enhance the understanding of vehicle system-level interactions of advanced vehicle technologies for researchers, students, and professionals engaged in energy-efficient vehicle research, development, and education. Figure IV-51 shows the structure and content of the database for each vehicle.

Figure IV-51: Map of Downloadable Dynamometer Database content.

The data and analysis from each vehicle tested under this program are posted to D³. A significant effort was spent this year on automating the standard analysis process, streamlining the data processing, and reducing the time frame between vehicle testing and data availability. The reader is encourage to visit the D³ website to get significantly more information and analysis for each vehicle presented in this report.

This document will provide a quick summary of powertrain operation and one or two points of interest for each vehicle that was baseline tested on the dynamometer for the AVTA. Each year the AVTA partners select a set of vehicles that best represents the new fuel-saving technologies available in the market. This year, the vehicles were as follows:

- 2013 Chevrolet Malibu Eco
- 2013 Volkswagen Jetta TDI
- 2012 Honda Civic GX
- 2013 Chevrolet Volt
- 2013 Honda Civic HEV
- 2013 Toyota Prius PHV
- 2013 Volkswagen Jetta HEV

Results

2013 Chevrolet Malibu Eco

Vehicle description

The 2013 Chevrolet Malibu Eco is a mild hybrid version of the Chevrolet Malibu allowing for start-stop vehicle operation as well as mild electric assist and regenerative braking. The vehicle combines a 2.4-L four-cylinder engine with a 15-kW electric motor mounted as a **Belt-Alternator-Starter** (**BAS**) system providing torque to the engine crankshaft. Table IV-6 gives additional technical specifications for the vehicle.

Table IV-6: 2013 Chevrolet Malibu Eco powertrain specifications.

Architecture	Belt alternator starter (BAS) hybrid vehicle
Engine*	ECOTEC 2.4-L DOHC I4, DI* 182 HP, 171 Nm
Transmission	6-speed automatic transmission
Motor *	Permanent magnet^ 15 kW max power*
Battery *	Lithium-ion* 115 V nominal * 0.5 kWh capacity^
EPA Label Fuel Economy (mpg)	25 city / 37 hwy / 29 combined*

* Manufacturer's data
^ Edmunds.com

Vehicle operation

The operation of the mild hybrid system in the Malibu Eco on hills 3-5 of a hot start UDDS drive cycle is shown in Figure IV-52. The BAS is used for engine starting as well as momentary traction power during acceleration events. Following engine start, tractive force is mainly provided by the engine, with the electric drive used to assist in gear changes and providing a reverse torque for engine deceleration. During braking events, the engine remains spinning while unfueled, as the electric drive captures energy from regenerative braking.

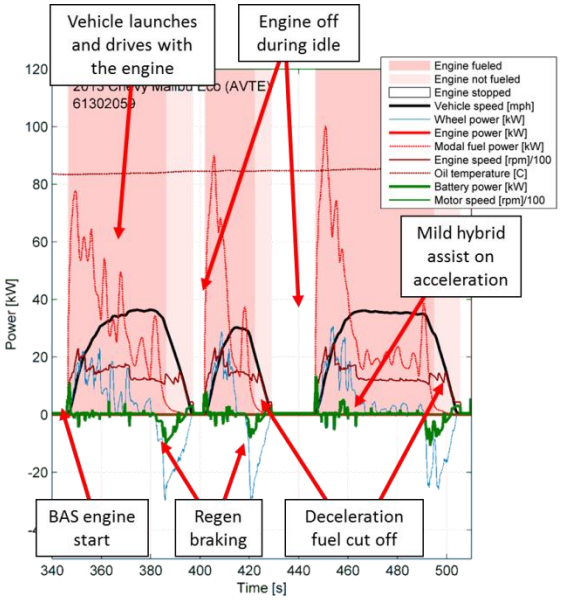

Figure IV-52: 2013 Chevrolet Malibu Eco operation on a hot start UDDS cycle.

The mild hybrid system provides a regenerative braking power level of 15 kW throughout the aggressive US06 cycle, though a peak of 12 kW regenerative power is the highest seen during the UDDS cycle. This energy is used for electric launch and light assist, and at higher temperatures the high-

voltage system also provides power to the air conditioning compressor, allowing for idle stop operation while still cooling the passenger compartment.

Point of interest

Battery use by the Malibu Eco

Figure IV-53 and Figure IV-54 display the effect of ambient temperature on the battery during evaluation at the temperatures of 20°F, 72°F, and 95°F with solar emulation during a progression of UDDS, HWY, and US06 tests. As seen in these cycles, the resistance of the lithium-ion battery drops to 0.197 ohm at 20°F, while the pack resistance remains between 0.06 ohm and 0.09 ohm at 72°F and 95°F. This variation in resistance is most effective at 20°F, with slight resistance changes seen between the test temperatures of 72°F and 95°F.

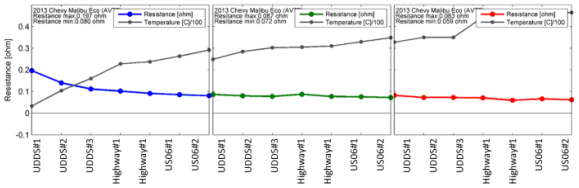

Figure IV-53: Variations in battery resistance at varying test temperatures of 20, 72, and 95°F with solar emulation.

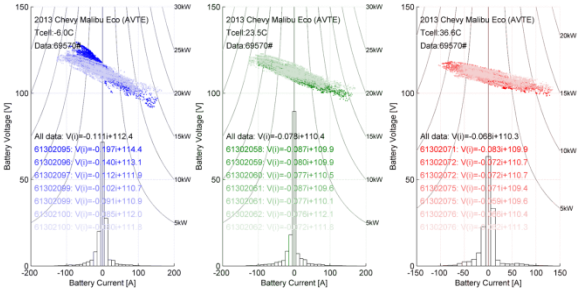

Figure IV-54: Voltage vs. current at varying temperatures for the 2013 Chevrolet Malibu Eco.

2013 Volkswagen Jetta TDI

Vehicle description

The Jetta TDI is equipped with a 2.0-L four-cylinder diesel engine with common rail direct injection, providing power through a six-speed dual clutch transmission (DCT). Table IV-7 gives additional technical specifications for the vehicle.

As would be expected with a conventional vehicle without an idle stop system, the engine remains operating throughout the cycle. The vehicle does operate with a high frequency of deceleration fuel cutoff, a fuel-saving measure that occurs when the vehicle is decelerating and engine torque is not requested.

The DCT of the Jetta TDI directly links the engine crankshaft with the transmission's output shaft, and thus the wheels, so the engine is kept spinning by the vehicle momentum. This allows for the engine to be defueled, improving efficiency, while still rotating at the desired speed for a quick restart if the driver immediately demands torque. Deceleration fuel cutoff is commonly used to improve the efficiency of current-generation conventional vehicles, and the Jetta TDI often utilizes this strategy.

Table IV-7: 2013 VW Jetta TDI powertrain specifications.

Architecture	Conventional vehicle (diesel fuel)
Engine*	2.0-L DOHC I4, TDI 140 HP, 320 Nm* 16.5:1 compression ratio*
Transmission	Dual clutch 6-speed automated manual
Motor *	N/A
Battery *	N/A
EPA Label Fuel Economy (mpg)	30 city / 42 hwy / 34 combined*
* Manufacturer's data ^ Edmunds.com	

Vehicle operation

Figure IV-55 shows the engine operation of the Jetta TDI on hills 3-5 of the UDDS cycle.

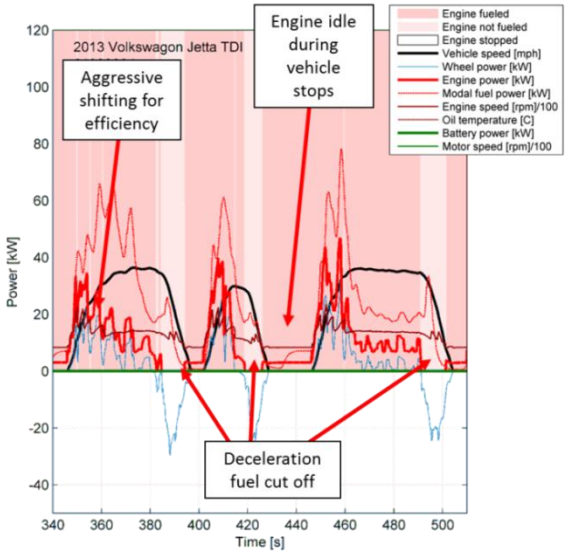

Figure IV-55: 2013 VW Jetta TDI operation on a hot start UDDS cycle.

Point of interest

Conventional-vehicle fuel economy competitive with hybrids

Figure IV-56 displays the EPA listed fuel economy of the Jetta TDI in comparison with several hybrid vehicles. By combining the efficient operation of a turbocharged diesel engine with an efficient DCT, the Jetta TDI is able to produce highway fuel economy results comparable to or higher than that of many hybrids. This benefit is much diminished when urban driving is considered, owing to the lack of a hybrid system allowing for optimization of engine operation, regenerative braking, and engine idle stop.

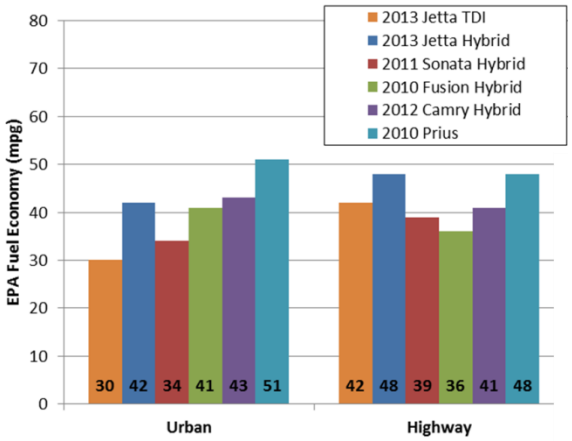

Figure IV-56: Fuel economy of the 2013 Jetta TDI compared to hybrid vehicles.

2013 Honda Civic GX

Vehicle description

The Honda Civic GX was acquired as part of the APRF automotive technology benchmarking endeavor. As it is the only vehicle tested this year fueled by compressed natural gas (CNG), its performance and efficiency are of particular interest. The vehicle is equipped with a 1.8-L spark-ignited engine fueled with CNG and a 5-speed automatic transmission equipped with a torque converter. Table IV-8 shows the vehicle's relevant technical specifications.

Table IV-8: 2012 Honda Civic GX powertrain specifications.

Architecture	Alternative-fuel (natural gas) conventional vehicle
Engine*	1.8-L SOHC I-4 w/ i-VTEC VVT 110 hp@ 6500 rpm 106 lbf-ft @ 4300 rpm
Transmission	5-speed torque converter automatic
Motor *	N/A
Battery *	N/A
EPA Label Fuel Economy (mpge)	27 city / 38 hwy / 31 combined*

* Manufacturer's data
^ Edmunds.com

Vehicle operation

Like the VW Jetta TDI, the Civic GX is of conventional vehicle architecture and uses an internal combustion engine as the only motive power source. The engine speed is governed by the desired vehicle speed and the selected transmission gear ratio. Engine torque is managed by the engine control unit, which provides torque as requested by the driver. The transmission typically defaults to the highest gear possible during cruising conditions to maximize fuel economy. The engine is fueled at all times except during aggressive deceleration events above approximately 12 mph. Figure IV-57 shows the operation of this vehicle during a hot start UDDS cycle.

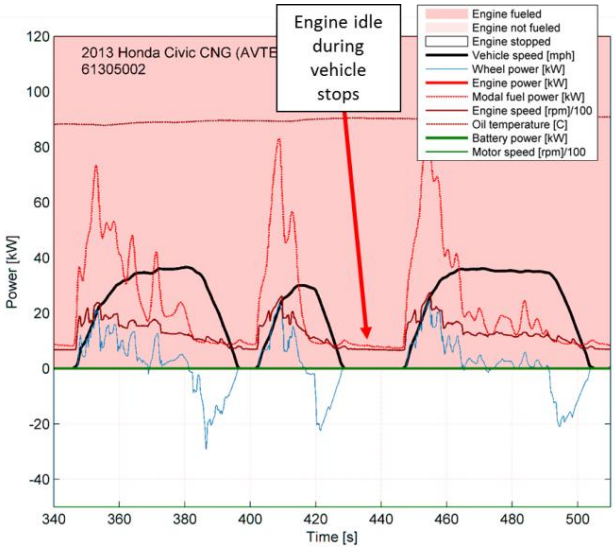

Figure IV-57: Honda Civic GX operation on a hot start UDDS cycle.

Point of interest

Comparison of CNG and gasoline Civic engine operation

The Civic GX is based heavily on the conventional Honda Civic 1.8-L engine, which operates on gasoline. The vehicles are nearly identical in terms of size and weight, and the driveline configurations and transmissions are shared. The differences between the two are limited to the engines and fuel systems; the CNG engine has a higher compression ratio, largely owing to modifications in piston geometry, and its fuel system is converted to store and supply CNG rather than gasoline. Results from testing of a MY 2012 Honda Civic Gasoline vehicle are provided for comparison within this section, and the fuel economy results for both vehicles, using miles per gasoline gallon equivalent for CNG, are shown in Figure IV-58.

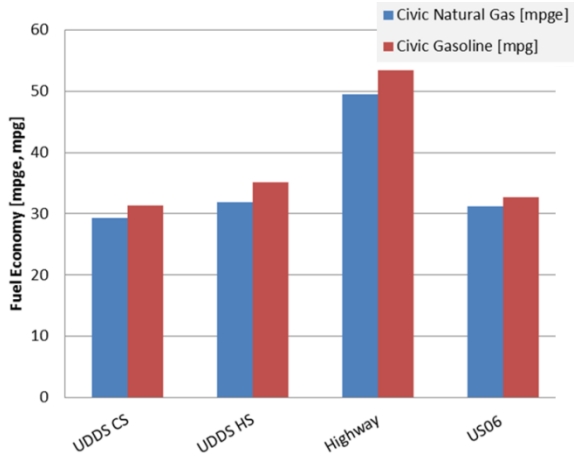

Figure IV-58: 2012 Honda Civic GX and Civic Gasoline fuel economy.

It was found that the Civic GX returned slightly lower fuel economy on the UDDS, HWY, and US06 drive cycles. Its EPA ratings are lower by 1 mpg in the city, highway, and combined categories, suggesting that the Civic GX is slightly less efficient than its gasoline-fueled counterpart. To further

explore this finding, the vehicles were subjected to quasi-steady-state testing while instrumented with an in-cylinder pressure-indicating system. Indicated-efficiency maps were generated for both vehicles, and are shown in Figure IV-59 and Figure IV-60.

The Civic Gasoline exhibits a peak indicated thermal efficiency of 40%. This value is found at moderate engine speed and moderate load, peaking at around 3400 rpm and 9 bar indicated mean effective pressure (IMEP). As load is increased from this point, efficiency drops considerably. This finding is most likely due to knock prevention considerations, which result in less optimal ignition timing to lower cylinder temperatures and decrease the likelihood of knock events.

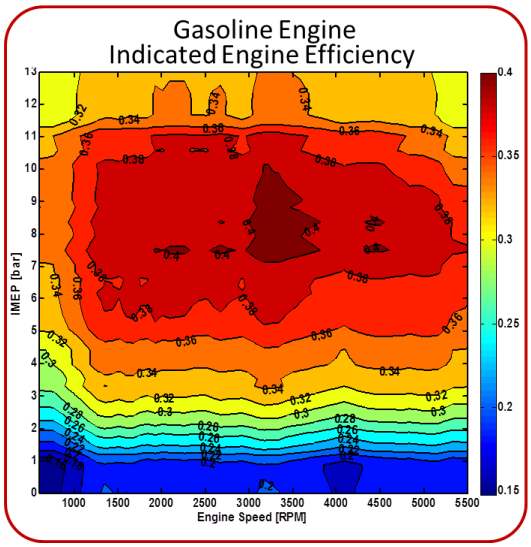

Figure IV-59: Honda Civic Gasoline indicated efficiency map.

The Civic GX returned a maximum of 39% indicated thermal efficiency. Like the Civic Gasoline, peak efficiency is found at moderate engine load. However, in the case of the Civic GX, peak efficiency is found near maximum engine load; efficiency is maximized at around 3400 rpm and 10.25 bar IMEP. It can be seen that as load increases, efficiency does not suffer an appreciable reduction in the case of the Civic GX.

The difference in indicated efficiencies of the two engines is likely affected by several factors relating to the change in compression ratios as well as the characteristics of the fuels. CNG exhibits a slower flame speed and longer combustion duration than gasoline. The longer combustion duration changes the distribution of cylinder pressure over the engine cycle, reducing efficiency.

Because of the reduced energy density of CNG as compared to gasoline, the Civic GX produces 30 fewer brake horsepower than the Civic Gasoline. Figure IV-61 illustrates the wide-open throttle (WOT) performance of the two vehicles. It can be seen that the shared transmission provides identical shift points, while the Civic GX produces approximately 20% less maximum tractive effort for a given vehicle speed.

The Chevrolet Volt is a PHEV, which operates as a pure electric vehicle (EV) at standard temperatures until its traction battery is depleted. Once depleted, the Volt operates as a charge-sustaining HEV, using a 1.4-L internal combustion engine for power generation as well as direct vehicle propulsion. Table IV-9 shows the vehicle's relevant technical specifications.

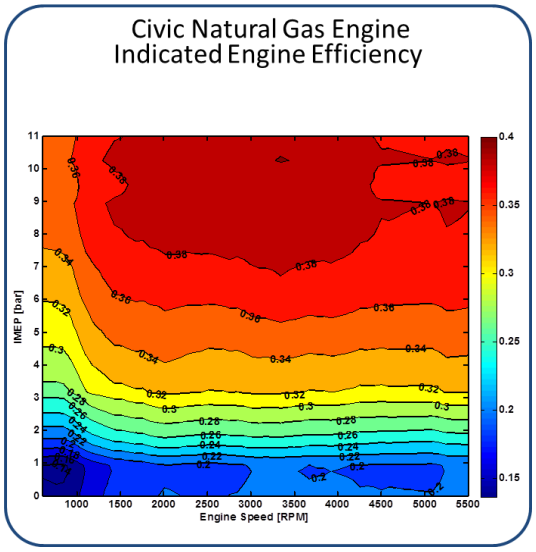

Figure IV-60: Honda Civic GX indicated efficiency map.

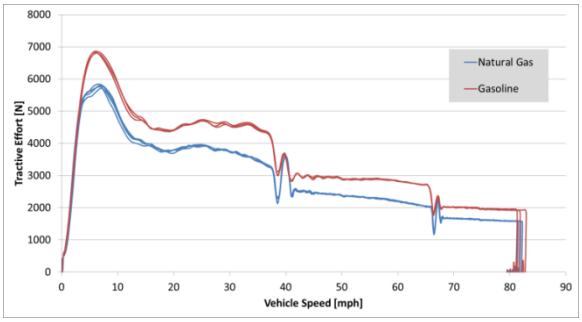

Figure IV-61: Honda Civic GX and Civic Gasoline WOT performance.

2013 Chevrolet Volt

Vehicle description

Table IV-9: 2013 Chevrolet Volt powertrain specifications.

Architecture	Power split extended-range electric vehicle
Engine*	1.4-L DOHC I4 VVT* 84 hp (63 kW)^
Transmission	1-speed direct drive*
Motor *	Main traction motor AC induction:111 kW peak power^ Generator Permanent magnet: 55 kW peak power^
Battery *	LG Chem^ Lithium-ion* 355 V nominal voltage^ 16.5 kWh total capacity* 111 kW^
EPA Label Fuel Economy (mpg)	35 city / 40 hwy / 37 combined+ 98 mpge combined+ 38 miles EV (electric-only) range+

* Manufacturer data
^ www.energy.gov
+ Edmunds.com

Vehicle operation

The Volt offers considerable electric-only driving range, listed at 38 miles by the manufacturer. During the non-aggressive UDDS driving cycle at a temperature of 72°F, the 2013 Volt evaluated performed the first engine start following 50 miles of electric-only driving range. The fuel economy (FE) and energy consumption rate (ECR) for a full charge test of the UDDS cycle are shown in Table IV-10.

Table IV-10: Fuel economy and energy consumption rate during a UDDS full charge test.

UDDS				
Cycle #	Cumulative Distance (mi)	Cumulative FE (MPG)	Cumulative ECR (DC Wh/mi)	Cumulative ECR (AC Wh/mi)
61303053	10	Inf	232.1	268.2
61303054	20	Inf	223.9	258.8
61303057	40	Inf	219.8	254.1
61303060	60	253.4	181.9	210.2
End of 9th UDDS	67.19	174.3	162.0	187.2
				AC Charge Effeciency
	Engine Start @	50.73 miles		86.5%

Point of interest

Variation in electric-only range of 2011 vs. 2013 Chevrolet Volt

For MY 2013, the Chevrolet Volt remained largely unchanged, with the exception of an increase in battery capacity to 16.5 kWh from 16 kWh as stated by the manufacturer. This change resulted in a manufacturer-listed electric-only range increase from 35 to 38 miles.

This effect can be seen in Figure IV-62, which displays a series of full charge tests of UDDS cycles on both the 2011 and 2013 Chevrolet Volt.

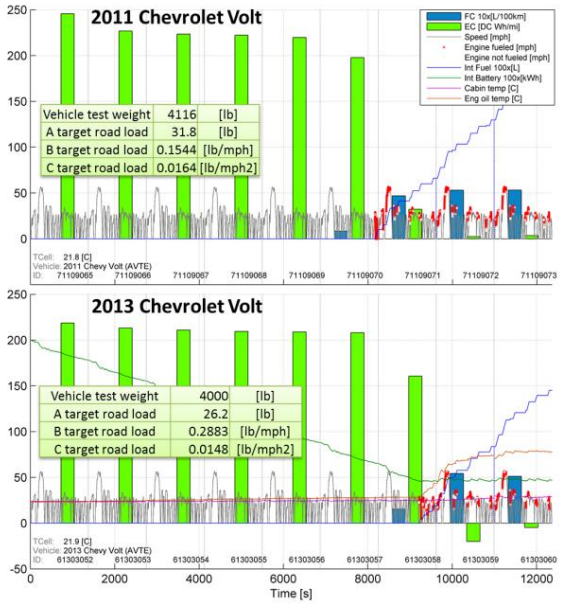

Figure IV-62: 2011 vs. 2013 Volt operation during a UDDS full charge test.

Changes to the battery capacity as a result of improved battery chemistry were claimed by the manufacturer. Figure IV-63 displays a scatter plot of the voltage and current during a UDDS full charge test. The zero crossing voltage corresponds to the y-intercept value of the curve for each test, while the slope of the curve corresponds to the battery system resistance.

The data show a lower charge-sustaining voltage for the 2013 Volt. In addition, the changes resulted in a lower zero crossing voltage for the 2013 model (339 V vs. 349 V) during charge-sustaining operation, demonstrating increased use of the overall capacity of the battery pack.

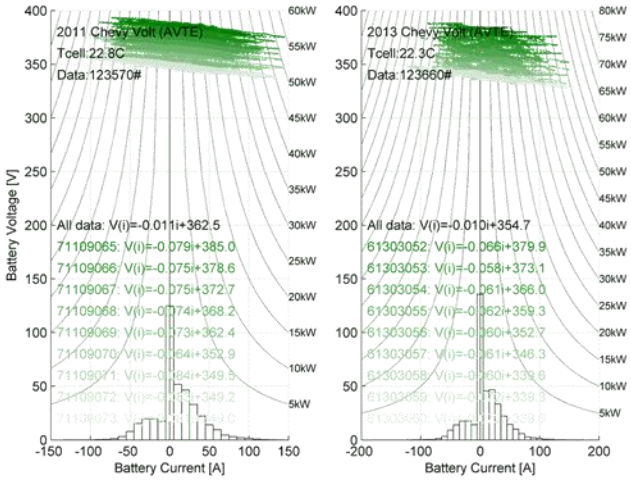

Figure IV-63: Voltage vs current for the 2011 and the 2013 Chevrolet Volt.

2013 Toyota Prius PHV

Vehicle description

The 2013 Toyota Prius PHV (plug-in hybrid vehicle) is based on the third-generation Toyota Prius. Most powertrain components remain the same, while the NiMH in the standard Prius is replaced by a 4.4-kWh lithium-ion system. Like the standard third-generation Prius, the Prius PHV uses an Atkinson-cycle 1.8-L engine and two electric machines. A power split device is used to control the proportion of power transfer between the mechanical and the electrical systems. Table IV-11 shows the vehicle's relevant technical specifications.

Table IV-11: 2013 Toyota Prius PHV powertrain specifications.

Architecture	Power-split plug-in hybrid electric vehicle
Engine*	1.8-L Atkinson engine 98 HP (73 kW)
Transmission	Compound planetary Ratios 3.172–0.529, FD 3.94
Motor *	60 kW, 207 Nm, 650 V
Battery *	Lithium-ion 202 V nominal (from testing) 4.4 kWh* 2.3–2.5 kWh (measured usable) 39 kW (from testing)
EPA Label Fuel Economy (mpg)	CS mode: 51 city / 49 hwy / 50 combined^ CD mode: 95 MPGe (0.2 gal/100 mi + 29 kWh/100 mi)^
* Manufacturer's data ^ www.fueleconomy.gov	

Vehicle operation

As with all PHEVs, the Toyota Prius PHV operates in charge-depleting mode until the high-voltage battery is fully depleted, at which time the vehicle blends into charge sustaining operation.

The battery of the PHV is sized such that it offers full electric operation on the UDDS and HWY certification cycles, but at higher power demands the internal combustion engine is required to provide the needed torque. This was found to occur both during high-power acceleration and at vehicle speeds above 63 mph, owing to high component rotational speeds linked to the power split architecture. The effect of the blended operation can be seen in Table IV-12 and Figure IV-64.

Table IV-12: Toyota Prius PHV fuel and electric energy consumption for UDDS full charge test.

UDDS Full Charge Test				
Cycle #	Distance (mi)	Cumulative Fuel Economy (MPG)	Cumulative ECR DC (Wh/mi)	Cumulative ECR AC (Wh/mi)
61306055	5	Inf	187.4	233.1
61306056	10	337.3	150.7	187.5
61303057	15	578.7	157.6	196.1
61303057	20	176.7	119.5	148.6
61303058	25	134.3	102.7	127.7
61303058	29.83	125.7	82.7	102.9
				AC Charge Effeciency
Engine Start @		8.30 miles		80.4%

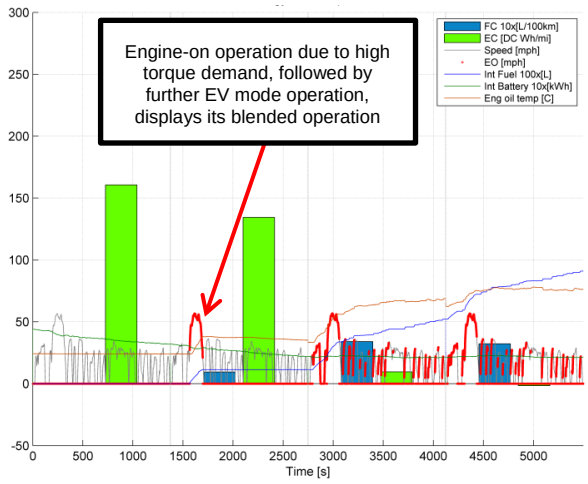

Figure IV-64: Toyota Prius PHV operation during the UDDS full charge test.

Points of interest

Charge-sustaining and charge-depleting operation

Figure IV-65 displays the variations in the charge-depleting and charge-sustaining electric-only operation. As charge-depleting operation continues, EV operation is reduced from the area seen in green to the area seen in red.

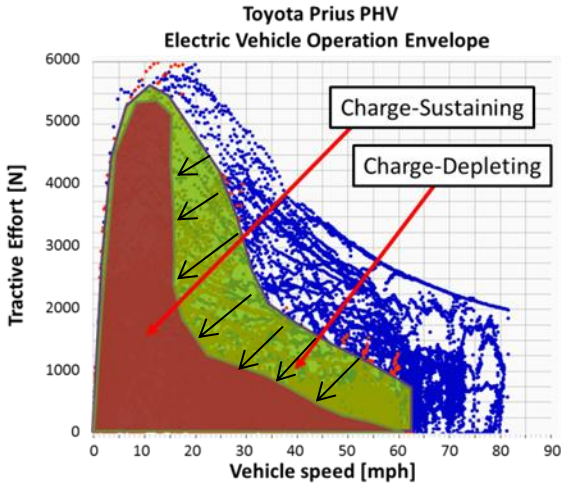

Figure IV-65: 2013 Toyota Prius PHV electric-only operation in charge-sustaining and charge-depleting modes.

Increased battery usage compared to standard Prius

Variations in vehicle operation for the Prius PHV compared to the standard Prius Hybrid HEV are seen in charge-sustaining mode as well. At higher vehicle speeds, the amount of energy available for regeneration is limited by the maximum battery power of a vehicle. Owing to the higher power limits of the lithium-ion battery in the Prius PHV, a higher amount of energy can be regenerated. Figure IV-66 demonstrates the limits of battery power for the 2010 Prius HEV (~19 kW) and the 2013 Prius PHV (~29 kW). The added energy captured during the deceleration that occurs between 470 and 480 seconds can be seen as additional positive energy in the subsequent accelerations.

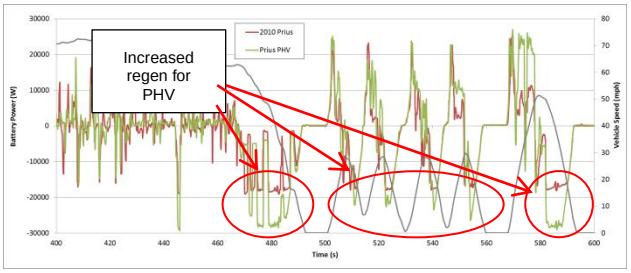

Figure IV-66: Battery power on the US06 cycle for the 2010 Prius HEV and 2013 Prius PHV in charge-sustaining operation.

2013 Honda Civic HEV

Vehicle description

The Honda Civic Hybrid is a variant of the conventional Honda Civic equipped with a mild hybrid system. The powertrain consists of a downsized 1.4-L four-cylinder engine, with a 23-kW permanent-magnet electric motor, mounted to the engine's flywheel, driving a continuously variable transmission (CVT). For 2013, the Civic Hybrid also includes a lithium-ion battery pack. Table IV-13 shows the vehicle's relevant technical specifications.

Table IV-13: 2013 Honda Civic Hybrid powertrain specifications.

Architecture	Pre-transmission flywheel motor
Engine*	1.4-L I4.8 V SOHC i-VTEC* 110 HP, 172 Nm*
Transmission	CVT* Ratios 3.172–0.529, FD 3.94
Motor *	Permanent magnet* 23 kW, 106 Nm*
Battery *	Lithium-ion* 144 V nominal* 20 kW*
EPA Label Fuel Economy (mpg)	44 city / 44 hwy / 44 combined+

* Manufacturer's data
\+ www.fueleconomy.gov

Vehicle operation

Operation of the Honda Civic Hybrid through the period of hills 3-5 of a hot start UDDS cycle can be seen in Figure IV-67.

The operational features that enable fuel savings in the Honda Civic Hybrid include engine idle stop, enhanced unfueled operation, regenerative braking and electric assist, and a CVT allowing for optimization of engine loading.

As seen in Figure IV-67, upon release of the brake pedal, the hybrid system starts the engine, which is then used to provide the majority of the power for the acceleration with mild assist from the motor. While cruising at speed, the engine is often spun while unfueled, at which time the motor provides the tractive power required. As the engine is still spinning, it is easily restarted when additional power is requested. This amount of engine-off operation continues as the vehicle decelerates and comes to rest. It is worth noting that with the addition of an electric drive on the shaft of the air conditioning compressor, engine-off operation continues at hot temperatures while the climate control supplies cooled air to the passenger compartment.

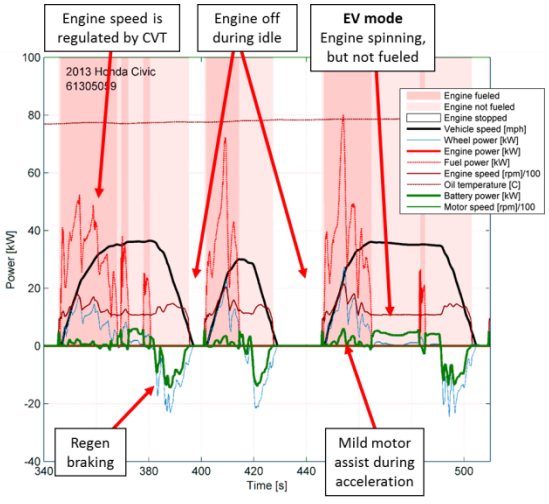

Figure IV-67: 2013 Honda Civic Hybrid operation during a hot start UDDS cycle.

Point of interest

CVT optimizes engine operation for higher efficiency

Another unique feature of the vehicle is the use of a CVT. By the nature of its design, a CVT allows for a continuous change of gear ratios across the transmission within the CVT's operating range. This differs from a standard automatic transmission, which commonly allows for between 4 and, in recent years, up to 9 fixed gear ratios.

This flexibility allows for higher engine loading at lower engine speeds, reducing throttling losses and improving overall engine efficiency. The CVT can quickly vary the ratio and engine speed to provide desired torque on demand. Gearing of the CVT in the Honda Civic Hybrid is such that the engine can consistently be loaded at speeds between 1000 rpm and 1500 rpm at vehicle speeds lower than 40 mph. Figure IV-68 and Figure IV-69 demonstrate the engine operation of the Honda Civic Hybrid compared to a standard 2012 Honda Civic with a 6-speed automatic transmission, tested at the APRF in 2012.

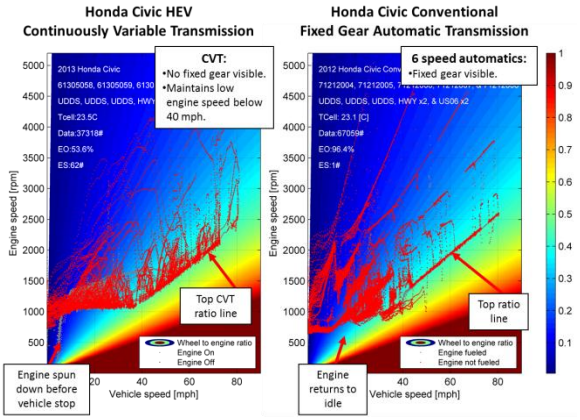

Figure IV-68: Operation of 2013 Honda Civic Hybrid and 2012 Civic with conventional engine.

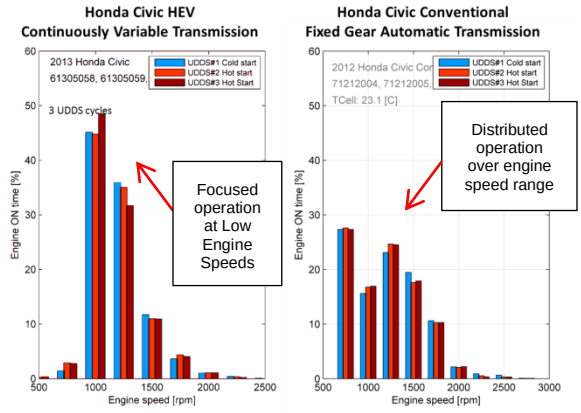

Figure IV-69: Operation of 2013 Honda Civic Hybrid and 2012 Civic with conventional engine on a UDDS cycle.

2013 Volkswagen Jetta HEV

Vehicle description

The Volkswagen Jetta Hybrid is the first turbocharged hybrid vehicle available in the U.S. market. It couples a downsized 1.4-L turbocharged gasoline engine with a 7-speed DCT. In addition, a clutch is installed between the engine and

the electric drive, allowing for electric-only operation at high speeds without pumping losses created by driving unfueled engine rotation. The vehicle architecture is of high interest, as it provides a high level of performance (0–60mph in 8.6 s) while still achieving a high level of efficiency. Table IV-14 shows the vehicle's relevant technical specifications.

Table IV-14: 2013 VW Jetta Hybrid powertrain specifications.

Architecture	Pre-transmission with engine disconnect clutch (P2)
Engine*	1.4-L I4 turbocharged TSI* 150 HP, 250 Nm*
Transmission	7-speed DCT*
Motor *	Permanent magnet* 28 kW as generator, 20 kW as motor 150 Nm* max. torque
Battery *	Lithium-ion* 222 V nominal voltage* 1.1 kWh total capacity*
EPA Label Fuel Economy (mpg)	42 city / 48 hwy / 45 combined+

* Manufacturer's data
^ Edmunds.com

Vehicle operation

The architecture of the Jetta hybrid allows for some unique operations compared with other hybrid technologies. The engine-to-electric-motor clutch is heavily utilized with a high amount of electric-only driving. In addition, in order to properly match engine speed to the desired speed of the DCT during a shift, the electric motor is called upon to reduce or increase engine speed matching.

This loading and unloading of the engine can be seen in the multiple spikes during accelerations and decelerations shown in Figure IV-70. During general engine operation, the electric drive is used to load the engine to more efficient operating points, meanwhile generating energy for later EV operation.

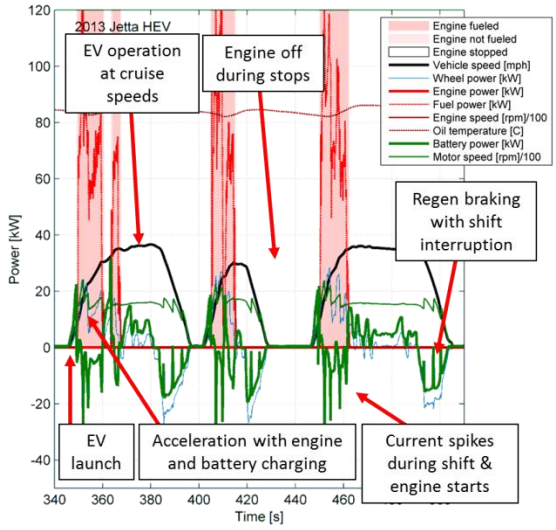

Figure IV-70: 2013 VW Jetta Hybrid operation on a hot start UDDS cycle.

Points of interest

P2 architecture enables high amount of engine-off operation

The P2 architecture used in the Jetta Hybrid is similar to that of the Hyundai Sonata Hybrid, with the exception of a flywheel-mounted electric drive rated at 20 kW instead of the BAS 30-kW motor used in the Sonata Hybrid. The P2 architecture utilizes a high amount of EV operation, as evidenced by the engine use in the UDDS drive cycle, shown in Figure IV-71.

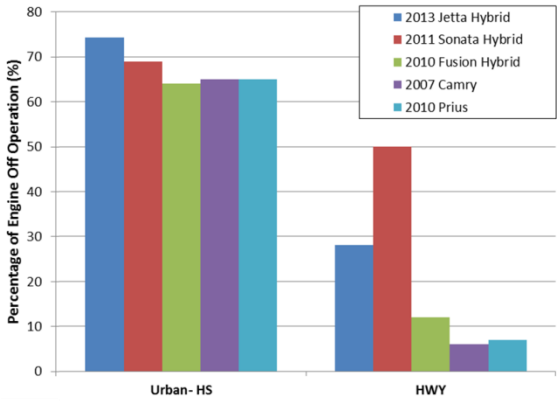

Figure IV-71: Engine Off operation of Jetta Hybrid compared to other hybrids.

As vehicle speeds increase in the HWY cycle, the EV operation of all HEVs is reduced because of the additional power requirement. At speeds exceeding 55 mph, the EV operation is limited to times of low torque demand, such as in cruising or decelerations. It should be noted that although the Jetta Hybrid demonstrates decreased EV operation at higher speeds, a higher amount of EV operation is still seen than with a power split architecture, owing to the lack of component speed limitations encountered with those components common to power split architectures.

EV envelope extends to high speed

The electric operation of the Jetta Hybrid can be seen in Figure IV-72. As vehicle speed increases above 55 mph, EV operation becomes limited, owing to the high tractive effort required to overcome road load forces.

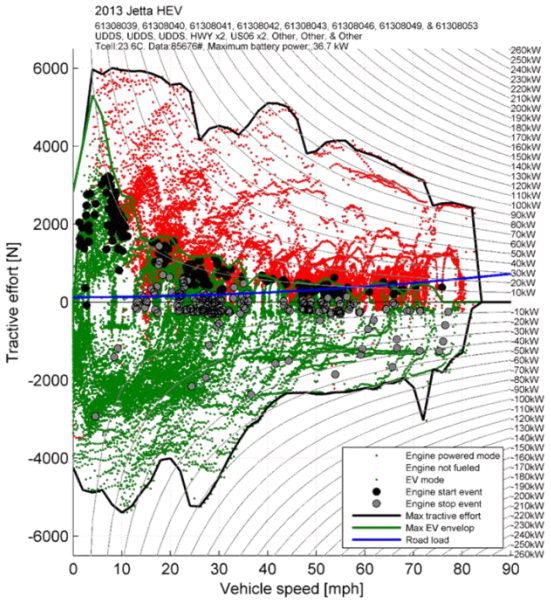

Figure IV-72: EV operation of the 2013 Jetta Hybrid.

Conclusions

Beginning in February of 2013, the APRF benchmarked multiple advanced-technology vehicles. The data and the analysis generated from this testing were used in multiple reports and presentations, and distributed as raw data through the APRF online website and directly to DOE collaborators. In addition, the work performed within this project was used to support codes and standards development and support model development with test data for validation.

This report provides a high-level overview of Argonne National Laboratory's basic vehicle benchmark activity, with a quick summary of the multiple vehicles studied in FY 2013. For a more detailed analysis, the reader is encouraged to view the vehicle testing reports and utilize the raw data on the APRF website (www.transportation.anl.gov/D3).

IV.D.3. Products

Publications

1. "Ambient Temperature (20°F, 72°F and 95°F) Impact on Fuel and Energy Consumption for Several Conventional Vehicles, Hybrid and Plug-In Hybrid Electric Vehicles and Battery Electric Vehicle", Lohse-Busch, H., Duoba, M., Rask, E., Stutenberg, K. et al, 2013-01-1462

Tools and Data

1. The basic vehicle test data are uploaded to APRF's Downloadable Dynamometer Database and are available for public download at www.transportation.anl.gov/D3.
2. A more thorough listing of test data and vehicle signals is available for DOE and partnering organizations upon request.
3. Additionally, some of the dynamometer test results are integrated into the AVTA website maintained by Idaho National Laboratory at http://avt.inel.gov.

IV.E. Electric Drive Vehicle Climate Control Load Reduction

John P. Rugh, Principal Investigator
National Renewable Energy Laboratory
Transportation and Hydrogen Systems Center
15013 Denver West Parkway, MS 1633
Golden, CO 80401
Phone: (303) 275-4413
Email: john.rugh@nrel.gov

Lee Slezak and David Anderson,
DOE Program Manager
Phone: (202) 586-2335
E-mail: Lee.Slezak@ee.doe.gov
Phone: (202) 287-5688
E-mail: David.Anderson@ee.doe.gov

IV.E.1. Abstract

Objectives

- Minimize the impact of climate control on electric-drive vehicle (EDV) range
- Reduce size of the battery by minimizing
  - Energy consumption of vehicle climate control
  - Time the battery exceeds the desired temperature range
- Develop new strategies for thermal comfort evaluation
- Increase electric range by 10% during operation of the climate control system through improved thermal management while maintaining or improving occupant thermal comfort

Major Accomplishments

- Completed baseline characterization of test vehicles in warm weather
- Evaluated three zonal cooling configurations with a new thermal manikin
  - Up to 16.7% reduction in energy consumption after 20 minutes for the same climate control settings
  - Up to 41.3% energy savings and improved cooling with reduced blower setting
- Evaluated thermal load reduction strategies
  - Interior air temperature reduction of 5.3°C achieved with solar-reflective film in thermal soak test
  - 30-minute pre-ventilation with HVAC blower reduced interior air temperature by 8.0°C, consumed 0.14 kWh
- Improvement in range over baseline air conditioning (A/C) using zonal A/C varies from 7% to 15%
- A computational fluid dynamics (CFD)/RadTherm/human model was built, validated, and used to assess a zonal climate concept

Future Achievements

- Conduct baseline cold weather tests
- Evaluate zonal climate control heating configurations
- Evaluate cold weather thermal load reduction strategies
- Continue warm weather testing, Summer FY 2014
  - More aggressive vehicle configurations
  - Combined strategies
  - Evaluate potential unintended consequences of cold weather solutions in warm weather

✧ ✧ ✧ ✧ ✧

IV.E.2. Technical Discussion

Background

As in conventional vehicles, passenger compartment climate control is required in EDVs for comfort and safety (e.g., demisting and defrosting). A challenge with EDVs is that electrical energy consumed for climate control can significantly reduce the vehicle range. Air conditioning and heating have been shown to reduce the range of a Mitsubishi iMiEV by 46% and 68%, respectively [1]. In addition, a Nissan Leaf tested at Argonne National Laboratory's Advanced Powertrain Research Facility showed a reduction in range of 48% due to heating and 18% due to A/C over the Urban Dynamometer Driving Schedule (UDDS) drive cycle [2]. Range anxiety will impact customer acceptance of EDVs and the penetration of these vehicles into the national fleet.

Last year, NREL researchers installed numerous thermocouples, incorporated vehicle controller area network data acquisition, and performed transient tests (after a thermal soak) to characterize the power requirements of the Ford Focus Electric's on-board A/C and heater systems. Hot-weather and cold-weather baseline tests characterized the inherent differences between the vehicles and enabled accurate measurement of the impact of load reduction technologies in FY 2013.

Introduction

Currently, conventional vehicles heat cabins with engine waste heat, but because EDVs do not have an engine, automobile manufacturers are presented with new climate control challenges. Using the battery for cabin electrical resistance heating takes valuable energy away from propulsion. Therefore, it is critical to minimize climate control loads in EDVs to maximize vehicle range.

The climate control system and interior cabin temperatures impact the traction battery in two ways. First, the impact of climate control on range affects battery size. If a range target is identified with the climate control operating, a

larger battery will be required compared to operation without climate control. Second, depending on the battery location and cooling strategy, the cabin climate control system can impact battery temperature. Higher lithium-ion battery temperatures can lead to degradation and reduced life of the battery. Designing batteries to account for high-temperature degradation leads to larger and higher-cost batteries.

The objective of this task is to increase in-use EDV range by minimizing climate control energy requirements. The initial goal is to increase range by 10% with improved thermal management during operation of the climate control system. The target range improvement is expected to increase customer acceptance of EDVs through the reduction of range anxiety. In addition, improving thermal comfort upon entry into a hot-soaked or cold-soaked vehicle may lead to additional motivation for drivers to adopt EDVs and improved safety through reduced driver distraction due to thermal stress.

Approach

Our approach is to collaborate with the automotive industry to research and develop techniques that will reduce cooling and heating loads on EDVs to improve range. The following areas will be considered:

- Thermal load reduction technologies
- Occupant thermal comfort optimization
- Intelligent HVAC control to minimize energy use
- Thermal preconditioning.

Testing and analytical techniques will be used to develop and evaluate the effectiveness of strategies to reduce climate control loads.

Vehicle Thermal Testing

Under a cooperative research and development agreement (CRADA), Ford has provided two Focus Electric vehicles (Figure IV-73). These vehicles were used in outdoor thermal tests at NREL's Vehicle Testing and Integration Facility. During the summer of 2013, thermal soak and cool down tests were conducted to evaluate zonal climate control configurations and thermal load reduction strategies.

Figure IV-73: Ford Focus battery electric vehicles.

A/C Cool-down Test Procedure

For FY 2013 summer testing, all cool-down tests were initiated at noon Mountain Standard Time (MST) after the test vehicles had remained undisturbed in a "steady-state thermal soak" condition overnight and throughout the morning. This test procedure allows the impacts of a test configuration to be captured for both "steady-state" solar soak and transient cool-down scenarios. Around noon MST, solar irradiance reaches peak intensity and the ambient temperature approaches the daily maximum.

Outdoor vehicle testing is highly weather dependent. Weather conditions between summer test days may be very similar, but are never exactly repeatable. Large weather variations between test days potentially distort test results such that comparison becomes difficult. Thus, temperature and power data from the test vehicle were adjusted according to control vehicle metrics to normalize the results across the summer test period and evaluate potential weather-related bias. For test days deemed to be valid, it was determined that day-to-day variations in environmental conditions were minor enough to have no significant impact on the vehicle temperatures or the cumulative energy consumption results obtained.

Zonal Climate Control

The primary focus of FY 2013 vehicle testing was evaluation of zonal climate control strategies. A thermal manikin from Measurement Technologies Northwest was used to assess performance. The "HVAC Manikin," shown in Figure IV-74, represents a 50th percentile western male body type. It is instrumented with sensors to measure near-surface air temperature and velocity (60 locations), solar and thermal radiative heat flux (31 locations), and relative humidity (5 locations). The manikin records these local environmental conditions that strongly impact occupant thermal comfort to identify an occupant's thermal boundary conditions under various climate control scenarios. After testing, the boundary conditions are supplied as input to a RadTherm simulation. The RadTherm software was developed by ThermoAnalytics, Inc. (TAI) and contains a human physiology model that takes the supplied environmental conditions and predicts occupant thermal sensation and comfort values for the tested climate control scenarios. Modifications were made to the RadTherm human model to improve accuracy for a vehicle climate control application, including realistic seat temperature profiles and thermal initialization of the model.

Three zonal climate control configurations were tested in FY 2013. For the first configuration, titled "Driver Vents," the passenger vents were closed to direct conditioned air to the driver solely through the driver-side panel vents. For the second configuration, titled "Overhead Vent" (shown in Figure IV-74), one of the passenger panel vents was extended from the instrument panel to the driver headliner area to deliver conditioned air directly to the driver's face and upper torso, which is known to have a strong impact on thermal sensation. This vent was used along with the existing panel vents on the driver's side. The third configuration, "Lap Vent," was similar to the second, with the extended outlet vent positioned near the center console over the driver's lap rather than near the headliner.

Figure IV-74: Zonal vent configuration with HVAC Manikin.

Thermal Load Reduction

The second focus of FY 2013 testing efforts was the evaluation of strategies to reduce thermal loads on a parked vehicle. This approach aims to reduce the impact of solar loading on the vehicle and attempts to lower the vehicle soak temperature to as close to ambient as possible, thereby reducing the required A/C loads during cool down and steady state conditioning. Two different films were applied to all windows of the test vehicle to reduce transmitted solar energy. The first was a semi opaque white film that approximates an idealized exterior shade. Figure IV-75 shows this film applied to the test vehicle glazing. The second film, a solar reflective film from Eastman Chemical, represents a more realistic application of solar reflective glazing because an original equipment manufacturer installed laminate glazing can meet vehicle visible light transmission standards.

Figure IV-75: Solar load reduction, white film on all glazing.

Parked car ventilation tests were conducted to determine the impact of "pre-ventilation" on interior temperatures and A/C power consumption. The windows remained closed during the pre-ventilation tests, and only the blower of the onboard HVAC system was used for ventilation. The recirculation damper was closed to keep the vehicle in outside air mode. For "continuous" operation mode, the blower was turned on full speed at a predetermined time before cool-down. This test was conducted with 15-minute and 30-minute ventilation periods. For "pulsed" blower operation, two temperature set points were defined, with a deadband between them, such that the blower automatically turned on when the interior temperature reached the upper threshold, and automatically turned off when the lower threshold was reached. In this way, the vehicle was kept within a defined range of the ambient temperature and was prevented from reaching full soak temperatures. Upper threshold temperatures of 10°C and 15°C above ambient were tested; for both cases, the deadband was 5°C.

Thermal Analysis

Thermal analysis tools (including CFD, RadTherm, and human thermal comfort) were used to evaluate the effectiveness of potential strategies to reduce the climate control loads. Under a CRADA, Ford provided the CAD geometry of a Focus Electric. Using this geometry, RadTherm and CFD meshes were developed. These meshes are fundamentally different as CFD uses a volume mesh, and RadTherm uses a surface mesh. Thermal soak simulations were performed to calibrate and validate the model. After calibration, the model was used for transient cool-down and human comfort simulations.

RadTherm Thermal Comfort Analysis Methodology

A virtual manikin based on NREL's ADAM thermal manikin was added to both the RadTherm and Fluent models. The virtual manikin is a key element for enabling the human thermal comfort analysis. The virtual manikin seated in the Ford Focus is shown in Figure IV-76.

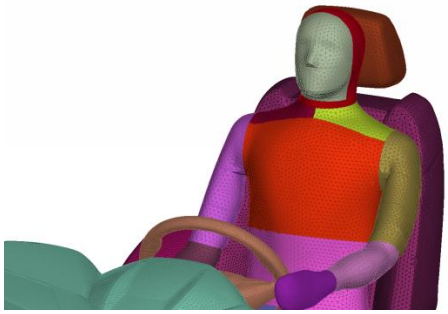

Figure IV-76: Virtual manikin in Ford Focus seat.

Thermal comfort analysis is performed with RadTherm and TAI's human comfort plugin. The plugin uses a human physiology model and calculates heat loss or gain to the environment to predict the thermal sensation and thermal comfort of a human. Inputs to the model include clothing ensemble and metabolic rate. Thermal boundary conditions include the local air velocity and temperatures from around the virtual manikin calculated in Fluent. Several thermal comfort and sensation metrics are output by the thermal comfort analysis, including Berkeley sensation and comfort, Predicted Mean Vote (PMV), Predicted Percentage Dissatisfied (PPD), and Dynamic Thermal Sensation (DTS).

Fluent/RadTherm Transient Analysis Methodology

Fluent and RadTherm must be run consecutively (not in parallel) and use bidirectional communication. For a steady-state analysis run, this can be done manually, but for a transient analysis run, the process must be automated to maintain time synchronization. A script was developed to execute the Fluent/RadTherm analysis on NREL's Linux supercomputer Peregrine. Using this script, a complete 20-

minute cool-down transient analysis can be completed in three days using 128 processors. This was a significantly faster turn-around time compared to running locally.

Results

Vehicle Thermal Testing

Zonal Climate Control

The HVAC Manikin provided a direct evaluation of occupant thermal sensation and comfort impact of zonal climate control approaches. Because the zonal configurations did not impact the thermal soak of the vehicles, the primary metrics used for evaluation were thermal sensation, average air temperature surrounding the manikin, and energy consumption. Thermal sensation was calculated by the HVAC Manikin RadTherm human model.

The two baseline cool-down tests showed very similar results, indicating good repeatability. Therefore, the average cool-down test was used for comparison to zonal test configurations. For all cool-down tests, the vehicle HVAC systems were configured with A/C on, panel vents active, 59°F interior temperature set point, and maximum air recirculation. Combined, these settings represent the maximum A/C cool-down configuration. The HVAC blower was set to maximum flow rate (control level 7) for both baseline tests and each of the zonal configurations. The blower air flow rate was reduced from 7 to level 5 for additional tests with "Driver Vents" and "Overhead Vent" configurations to evaluate energy savings while maintaining thermal comfort.

Figure IV-77 shows the average air temperature recorded by the HVAC Manikin 20 minutes after the start of cool down for each test as well as the cumulative climate control energy savings as a percent reduction over the 20 minute time interval. At 20 minutes, all three zonal configurations achieve equivalent or better cooling than the baseline for the same level 7 blower setting. The "Driver Vents-7" configuration produced the same average temperature, while "Overhead Vent-7" and "Lap Vent-7" were cooler than the baseline by approximately 5°C and 4°C, respectively. Cooler temperatures are a result of the third vent directing cool air onto the driver in these cases. "Driver Vents-7" reduced the climate control energy by more than 16.7%, and the "Overhead Vent-7" configuration resulted in 7.4% energy savings. Because the lap vent configuration used the same air ducting and air flow as the overhead vent configuration, it is assumed that the energy consumption from these two cases is equal. For the same blower setting, these modified vent configurations created additional flow resistance and reduced the overall air flow rate through the evaporator. This reduced the capacity of the A/C system and produced these energy savings, but also enhanced cooling of the driver.

When the blower was changed to control setting 5 to decrease the supply air flow, energy savings of 50% and 41.3% were achieved with the "Driver Vents-5" and "Overhead Vent-5" configurations, respectively. "Driver Vents-5" had an average air temperature 2°C above the baseline case, while the "Overhead Vent-5" average air temperature was 1.4°C cooler than the baseline.

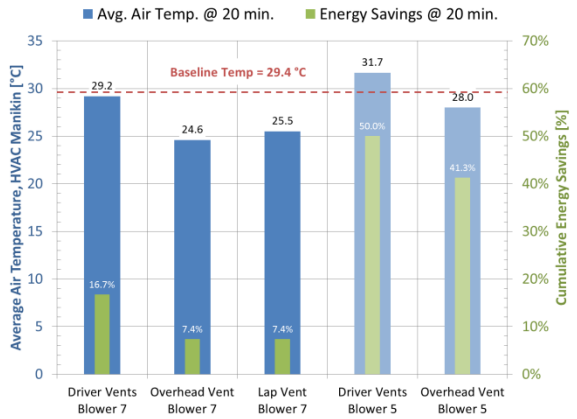

Figure IV-77: Average air temperature surrounding the HVAC Manikin and percent reduction in cumulative battery energy for zonal climate control configurations, 20 minutes after start of cool-down.

Preliminary RadTherm simulations were conducted using recorded HVAC Manikin test data to evaluate thermal sensation and comfort for the zonal configurations. Figure IV-78 shows predicted thermal sensation and comfort votes for a baseline test. Processing and interpretation of the thermal sensation/comfort results are in progress.

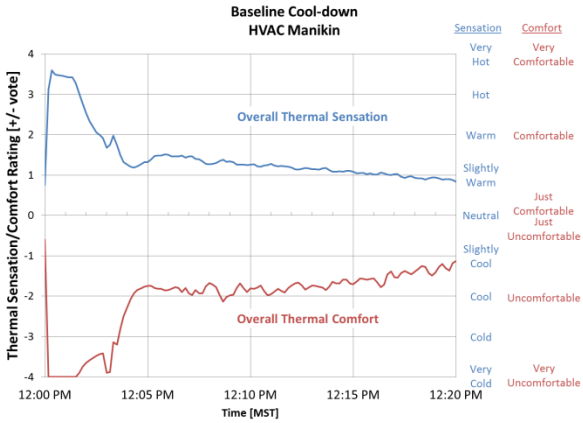

Figure IV-78: Predicted thermal sensation and comfort, baseline cool-down test, 7/3/2013.

Thermal Load Reduction

Thermal load reduction configurations focused on reducing the vehicle temperature prior to cool-down. Therefore, the primary metrics used for evaluation of these configurations were vehicle surface temperatures, average interior air temperature, interior rise above ambient temperature during thermal soak, and energy consumed for ventilation.

For the passive window film technologies evaluated, the solar-reflective film reduced the average interior air temperature by 5.3°C during thermal soak, while the white film achieved a 9.0°C reduction.

Using the onboard HVAC blower, pre-ventilating the vehicle 15 minutes prior to cool down reduced the interior air temperature by 7.0°C; increasing the ventilation time to 30 minutes before cool down improved the temperature reduction to 8.0°C, revealing diminishing returns. The two pre-ventilation

configurations required 0.08 kWh and 0.14 kWh from the high voltage battery, respectively. Using pulsed ventilation with an upper threshold of 10°C required 1.0 kWh and reduced the interior temperature by 9.5°C. For a threshold of 15°C, 0.4 kWh were consumed to achieve a 6.7°C temperature reduction. Temperature reduction and energy consumption for the configurations are shown in Figure IV-79. While continuous pre ventilation is more efficient, pulsed pre ventilation would be beneficial if a person does not know their departure time and their vehicle is connected to the grid.

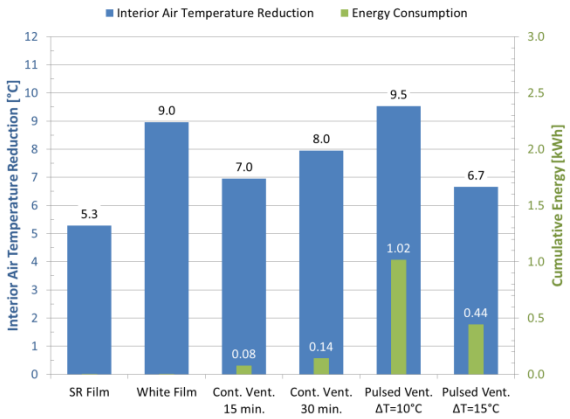

Figure IV-79: Temperature reduction and average power consumption for thermal load reduction configurations after thermal soak.

Thermal Analysis

A steady-state soak simulation was performed using weather data from the baseline cool-down day of July 3, 2013. The analysis was performed both to check the accuracy of the model and to obtain an initial state for the cool-down simulation.

The simulation steady state soak temperatures at 12:00 pm MST were compared to soak test data from July 3, 2013, averaged over 20 minutes from 11:40 AM to 12:00 PM MST. Minor adjustments were made to model parameters to improve correlation. The baseline soak analysis temperatures shown in Figure IV-80 compared favorably to the test data. The most important locations (air, dash, windshield, and driver's seat) matched within 5°C. The steering wheel temperature showed the largest difference, where the model under-predicted the temperature. Because the steering wheel is directly in the sun, the data may have been affected by solar radiation. The close match of the simulation results to soak data validated the inputs to the steady state model.

The next step was to perform a transient cool-down analysis and comparison to data. Experimental data from the same day were used, and the simulation was compared to data for the first 20 minutes of the cool-down beginning at 12:00 PM MST. The simulation used the same conditions as the cool-down test: maximum A/C with the blower on high and 100% recirculation. The model used the panel vent inlet velocities obtained from Ford. The panel vent velocities were validated by measurement. The transient temperatures at the A/C vents were obtained from test data.

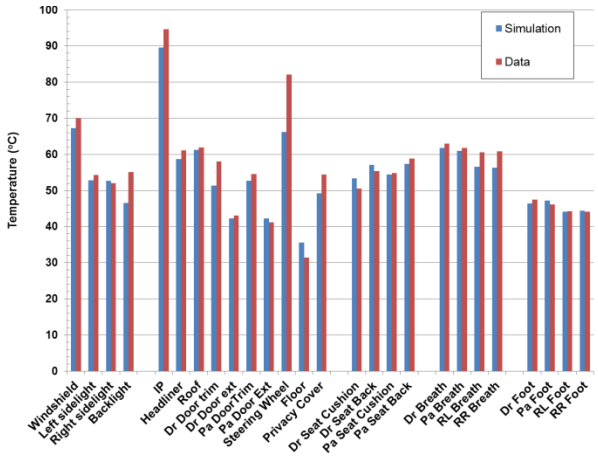

Figure IV-80: Baseline comparison of analysis temperature results to test data for 7/3/13.

Figure IV-81 and Figure IV-82 show comparisons of temperatures predicted by the simulation to temperature measurements of a cool down test performed on July 3, 2013.

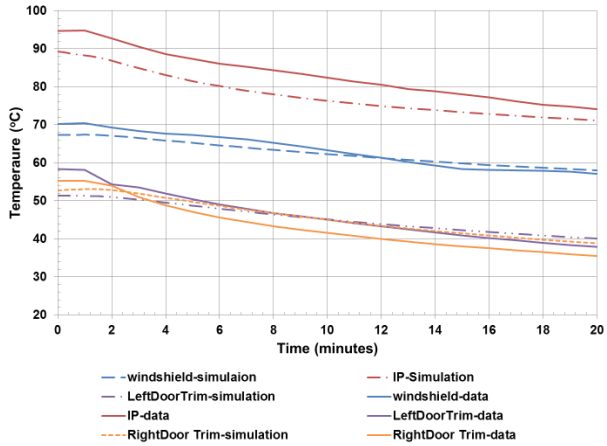

Figure IV-81: Comparison of selected interior temperature results to cool down test data for 7/3/13.

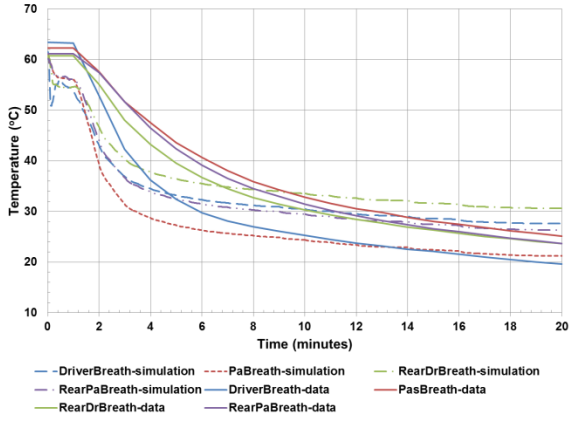

Figure IV-82: Comparison of breath-level air temperatures to cool down test data for 7/3/13.

The results of the simulation compare well to test data. The rear breath temperatures were lower than the test data for the first portion of the test, but were within 4°C for the second half of the cool down. The results show that the model can

closely predict the thermal conditions during a soak and cool-down test. The model will be used to predict the thermal results of additional tests, and can be used to predict vehicle thermal behavior under conditions that are difficult to test.

Figure IV-83 shows the results of a human thermal comfort analysis performed using the results of the transient cool down analysis. The thermal sensation predicted by the Berkeley correlations is consistent with the PMV model, showing that the driver would be cold.

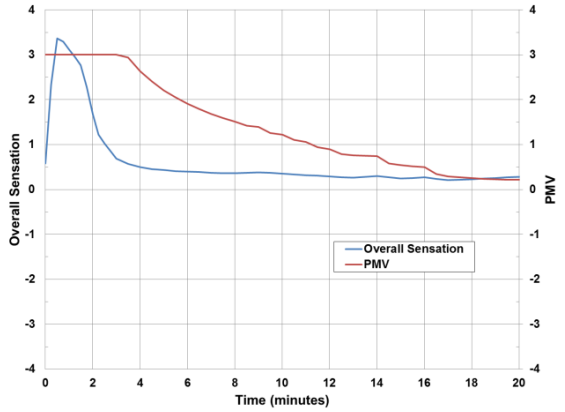

Figure IV-83: Sensation and PMV during cool down for 7/3/13.

Vehicle Simulation Analysis

Argonne National Laboratory's vehicle simulation tool Autonomie was used to assess the impact of climate control on range. Argonne provided NREL with an Autonomie model of the Focus Electric. The model was modified to enable input of measured A/C compressor power from the vehicle test. Three conditions were compared: no A/C, baseline A/C, and overhead vent zonal A/C (blower level 5). The ambient temperature during the A/C tests was approximately 27°C with a solar load of 925 W/m^2. The Focus Electric uses a 23-kWh capacity lithium-ion battery pack. The usable pack energy was assumed to be 70%, corresponding with a state-of-charge range of 95% to 25%; therefore, we calculated 16.1 kWh of usable energy in the battery pack.

Calculating the vehicle efficiency over a single 10-minute SCO3 drive cycle and applying it to calculate the overall range would overestimate the impact of A/C because the A/C loads decrease when the passenger compartment temperatures attain steady state. Because the average vehicle trip duration in the United States is approximately 20 minutes, the average vehicle efficiency was calculated over several drive cycles that lasted approximately 20 minutes. The drive cycles used were: UDDS (22.8 minutes), back-to-back SC03 cycles (19.8 minutes), and back-to-back HWYFET cycles (25.5 minutes). The compressor power applied to the vehicle was a composite profile (Figure IV-84) that included measured compressor power at maximum A/C setting for the first 10 minutes (simulating a pull down), and then the measured compressor power for auto 72 setting for the remainder of the drive cycle (simulating steady state).

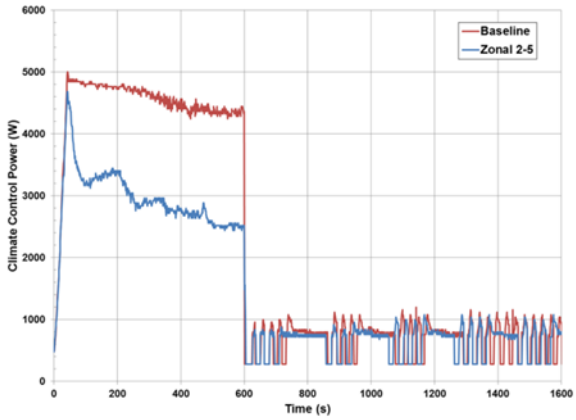

Figure IV-84: Climate Control Power vs. Time.

Table IV-15 shows the predicted range of the Focus Electric. For the SCO3 drive cycle, the baseline A/C reduces the range by 37%, from 90.3 to 56.6 miles. The reduction in range using baseline A/C varies from 21% to 38%. The overhead vent zonal blower 5 configuration increased the range 7.5% to 15% compared to operation with the baseline A/C system.

Table IV-15: Predicted Focus Electric Range (miles).

Drive Cycle	No A/C	Baseline A/C	Zonal 2-5 A/C	% Increase*
SC03	90.3	56.6	65.1	15%
UDDS	92.2	57	65.5	15%
HWFET	80.4	63.7	68.5	7%
* % increase of Zonal 2-5 over baseline A/C				

Vehicle efficiency was calculated over a single 10-minute SCO3 drive cycle. Because the A/C power is higher during the first 10 minutes of a cool-down, the impact of A/C will be higher than on a longer drive cycle. The assumption of maximum A/C also amplifies the impact of A/C because drivers typically turn down the A/C as they attain thermal comfort. Additional analyses are underway to calculate the impact of A/C on range under typical driving conditions.

Conclusions

As part of a 4-year CRADA project with Ford, NREL researchers completed summer testing on two Ford Focus Electric vehicles. Three zonal climate control configurations and six thermal load reduction configurations were assessed. For the same flow rate as the baseline, zonal vent configurations had more than a 16.7% reduction in climate control energy. Reducing the total air flow rate increased the savings up to 50%. Zonal vent configurations also improved cooling of the driver airspace up to 5°C while reducing climate control energy by 7%. These results show that a zonal approach to climate control can achieve equivalent or better driver cooling while decreasing energy consumption. Vehicle simulations over the SCO3, UDDS, and HWFET drive cycles show a zonal A/C system has the potential to increase vehicle range 7% to 15% during operation of the A/C.

Solar-reflective film on all vehicle glazings reduced the interior air soak temperature by over 5.3°C. In addition, the use of grid power to "pre-ventilate" a parked vehicle reduced the interior air soak temperature by up to 9.5°C. Continuous ventilation, starting just before cool-down, was determined to be a more energy-effective strategy than automatic pulsed ventilation.

A thermal analysis process using CFD, RadTherm, and human thermal comfort models was developed to evaluate the effectiveness of potential strategies to reduce the climate control loads. The baseline steady-state and transient results matched test data well.

References

1. Kohei Umezu and Hideto Noyama, Mitsubishi, presented at the 2010 SAE Automotive Refrigerant and System Efficiency Symposium.
2. Argonne National Laboratory Advanced Powertrain Research Facility data, EV Everywhere Workshop presentation, Lee Slezak, September 13, 2012.

Acknowledgements

- Co-authors: Lawrence Chaney, Matthew Jeffers, NREL
- Jeff Tomerlin, Cory Kreutzer, NREL
- Paul Hoke, Clay Maranville, Ken Jackson, Ford
- Rick Burke, Measurement Technologies Northwest
- Mark Hepokoski, Tony Schwenn, Craig Makens, ThermoAnalytics

IV.E.3. Products

Publications

1. Rugh, J.; Chaney, L.; Ramroth, L.; Venson, T.; and Rose, M. "Impact of Solar Control PVB Glass on Vehicle Interior Temperatures, Air-Conditioning Capacity, Fuel Consumption, and Vehicle Range." Proceedings of 2013 SAE Congress, Paper # 2013-01-0553, Society of Automotive Engineers, Detroit, MI.

IV.F. Integrated Vehicle Thermal Management—Combining Fluid Loops on Electric Drive Vehicles

John P. Rugh, Principal Investigator
National Renewable Energy Laboratory
Transportation and Hydrogen Systems Center
15013 Denver West Parkway, MS 1633
Golden, CO 80401
Phone: (303) 275-4413
Email: john.rugh@nrel.gov

Lee Slezak and David Anderson,
DOE Program Manager
Phone: (202) 586-2335
Email: Lee.Slezak@ee.doe.gov
Phone: (202) 287-5688
E-mail: David.Anderson@ee.doe.gov

IV.F.1. Abstract

Objectives

- Improve vehicle range and reduce cost from combining thermal management systems
- Collaborate with industry partners to research the synergistic benefits of combining thermal management systems in vehicles with electric powertrains

Major Accomplishments

- An experimental combined fluid loop (CFL) system was constructed
  - Prototype heat exchangers provided by partner Delphi
  - A prototype automotive electric compressor was provided by partner Halla Visteon Climate Control
- A test apparatus was constructed to simulate load, control, and measure the performance of the CFL system
  - The experiment can be operated in a variety of different test configurations over a range of vehicle operating conditions from very cold to very hot

Future Achievements

- CFL cooling mode and heating mode bench testing
  - Measured energy consumption will be used to estimate the improvement in vehicle range during transient drive cycle operation
  - The CFL system advantages will be experimentally evaluated, including power electronics and electric motors (PEEM) and energy storage system (ESS) waste heat recovery, ambient cooling of the PEEM and ESS, active cooling of the ESS, and heat pump operation
- Investigate strategies to reduce overall vehicle thermal management system energy consumption
- Work with industry partners to design a vehicle-level test to demonstrate CFL energy savings

✧ ✧ ✧ ✧ ✧

IV.F.2. Technical Discussion

Introduction

Plug-in hybrid electric vehicles and battery electric vehicles (BEVs) have increased vehicle thermal management complexity (e.g., PEEM, ESS, and vehicle cabin). Multiple cooling loops may lead to reduced effectiveness of fuel-saving control strategies. The additional cooling loops increase weight, volume, aerodynamic drag, and fan/pump power, thus reducing electric range. This reduces customer acceptance of BEVs by increasing range anxiety and presents a barrier for the penetration of BEVs into the national vehicle fleet. Our goal is to improve vehicle performance (fuel use or BEV range) and reduce cost by capturing the synergistic benefits of combining thermal management systems. The overall goal is to solve vehicle-level heat transfer problems, which will enable acceptance of vehicles with electric powertrains.

The objective of this project is to research the synergistic benefits of combining thermal management systems in vehicles with electric powertrains. Currently, electric drive vehicles (EDVs) typically have a separate cooling loop for the PEEM components. It would be beneficial to have a PEEM coolant loop with temperatures less than 105°C without requiring a dedicated system. Range would be increased in the winter by minimizing electrical resistance heating through a combined thermal management system that maximizes the usage of waste heat from the PEEM and ESS components and enables heat pump operation. With increased focus on aerodynamics, minimizing the area and number of heat exchangers in the front end of the vehicle has the potential to reduce drag. An additional benefit of combining cooling loops is that the ESS, passenger compartment, and thermal management fluid loops can be preconditioned.

Background

In the first year of the project (FY 2011), Halla Visteon Climate Control, a Tier 1 automotive heating, ventilation and air conditioning (HVAC) component supplier, supplied detailed thermal component and system information. This included drawings, thermal and flow component data, and system performance data. The National Renewable Energy Laboratory (NREL) researchers built component models in KULI [1] using the geometry, heat transfer, and pressure drop information. The individual component models were verified to function as expected. Cabin thermal, air conditioner (A/C), and PEEM cooling loop models were then developed by combining the

individual component models into systems, which were then compared to test data.

In the second year of the project (FY 2012), the individual thermal models of the cabin A/C, cabin heater, PEEM, and ESS fluid loops were improved based on the results from comparisons to test data. A baseline electric vehicle thermal system model was created from these sub-system models, and its performance was evaluated. The A/C system and ESS cooling loop controls were updated with more sophisticated models, and several CFL strategies were investigated. The CFL system modeling demonstrated that the design properly conditioned the ESS during heating and cooling, maintained cabin air comfort temperatures, lowered PEEM temperatures to enable higher power, and reduced heating energy through heat recovery [2].

Approach

The overall approach of the project is to demonstrate the feasibility and energy savings benefits of an integrated vehicle thermal management (IVTM) system through modeling with KULI software and experimental validation using a bench testing apparatus. Previously conducted KULI modeling work demonstrated that the IVTM system decreased energy consumption while reducing the number of system components and satisfying the thermal management requirements of the ESS, PEEM, and cabin. An experimental test system was designed and constructed to validate the KULI modeling results previously obtained, as well as further investigate both heating and cooling performance.

To perform the experimental study, a test apparatus capable of evaluating the steady-state and transient performance of an electric vehicle thermal system was constructed. The ultimate goal of the test apparatus is to measure the impact of the IVTM technology on EDV range. In order to demonstrate the effect on vehicle range, a variety of drive cycles will be simulated on the IVTM experimental hardware over a range of ambient air temperatures from -30°C to 43°C.

In addition to measuring the energy efficiency enhancement, the experiment will also investigate control strategies and system configurations. This information will then provide feedback and insight for manufacturers when selecting system designs for vehicle implementation. The expectation is that the results will lead to a future project in which a prototype system is installed into a test vehicle with a design based on the KULI modeling and experimental test bench findings.

Combined Fluid Loop Concept

The CFL concept is an experimental system design that is one possible configuration for an IVTM system. The goal of the CFL design is to provide a platform through which a variety of IVTM operation modes can be tested. Choosing the best IVTM system configuration for a given vehicle will involve making tradeoffs between cost and capability or, in other words, complexity and energy savings. The CFL concept is designed to investigate a number of the possible system configurations in order to quantify their performance. As such, the experimental CFL design is more complex than would be expected for most vehicle applications.

The CFL concept that was developed for bench testing is intended to allow operation of the system with a variety of control strategies under a wide range of operating conditions. The system loads will be representative of a typical passenger BEV. In addition to cooling the cabin in A/C mode, it also enables waste heat recovery from the PEEM and ESS when beneficial, ambient cooling of the PEEM and ESS when possible, active cooling of the ESS as required, and heat pump operation.

In this CFL design, a “secondary loop” configuration is used, in which the vapor compression cycle transfers heat between the R134a refrigerant and the 50%/50% by mass water/ethylene glycol (WEG) liquid coolant mixture. This is accomplished through the use of aluminum brazed plate-type heat exchangers as the condenser and evaporator/chiller. One of the biggest advantages of this design is that it is more compact than the typical automotive design, which uses refrigerant-to-air heat exchangers at the front of the vehicle and within the vehicle console HVAC unit. This also eliminates the necessity for long lengths of permeable hose, reducing refrigerant leakage.

A basic component-level schematic of the CFL system is shown in Figure IV-85. The five three-way valves with “S” controllers represent solenoid valves capable of switching the flow between two ports. The two two-way valves with “S” controllers represent simple on/off solenoid valves. The three three-way valves with “Var.” controllers represent variable proportioning valves that can modulate the degree of heat exchanger flow bypass. The “PTC Heater” represents a supplementary positive temperature coefficient (PTC) electrical resistance heater.

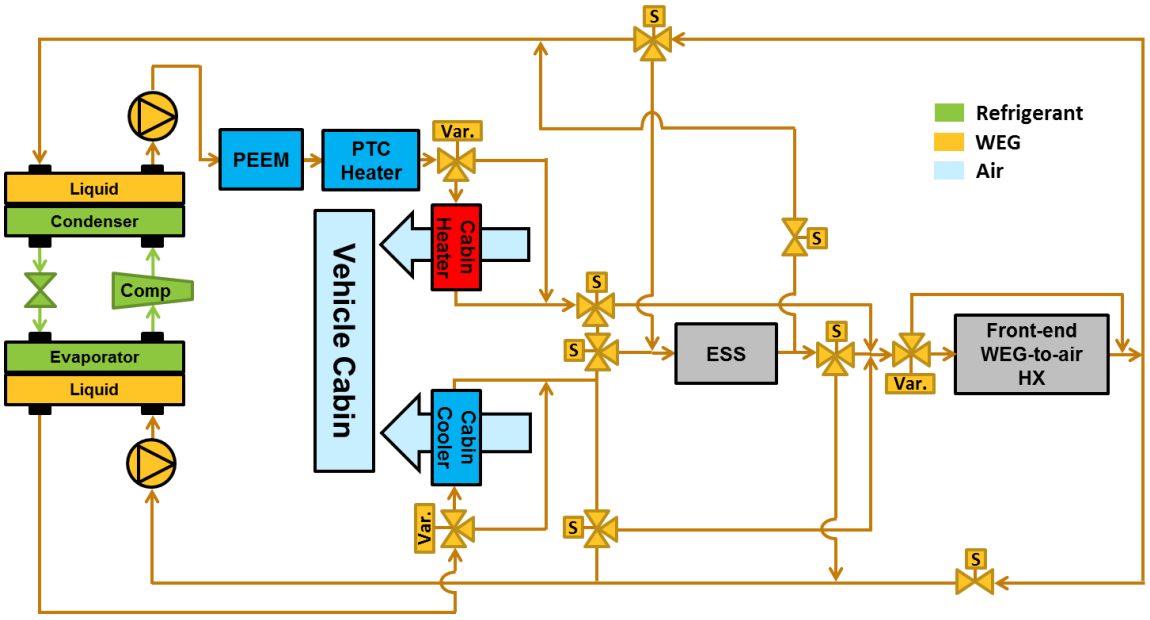

Figure IV-85: Combined fluid loop concept schematic.

For the experimental system being tested, Delphi has provided prototype heat exchangers from its "Unitary HPAC" system, as shown in Figure IV-86. In addition to the condenser and chiller heat exchangers shown, they have also supplied WEG-to-air heat exchangers for the low-temperature front-end heat exchanger (FEHX), cabin heater core, and cabin cooler core, as represented in Figure IV-85. These heat exchangers are designed to deliver the heating and cooling capacities necessary for a small to mid-size BEV.

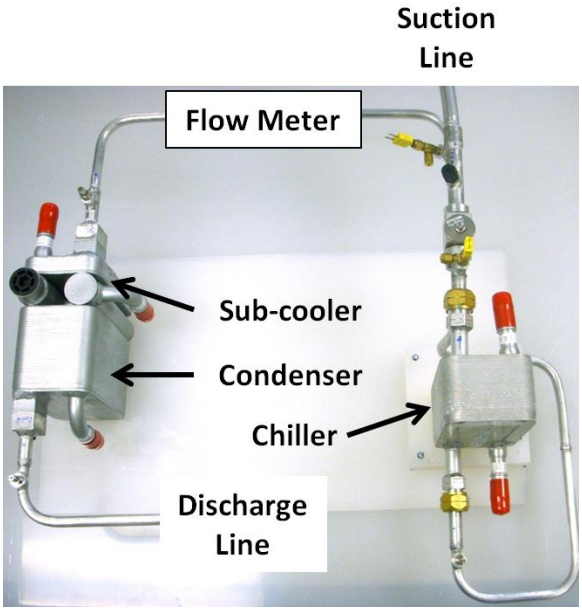

Figure IV-86: Prototype Delphi "Unitary HPAC" system.

To complete the vapor compression cycle system, a compressor is needed. To most accurately reflect the performance in a passenger BEV, an automotive electric compressor is used instead of the more traditional automotive belt-driven compressor. The compressor was provided by Halla Visteon Climate Control and is shown in Figure IV-87. The compressor is a prototype unit that is designed to operate over a wider range of conditions than a typical automotive A/C compressor. The ability to handle extended conditions is necessary for the lower suction pressures and higher pressure ratios inherent to heat pump operation.

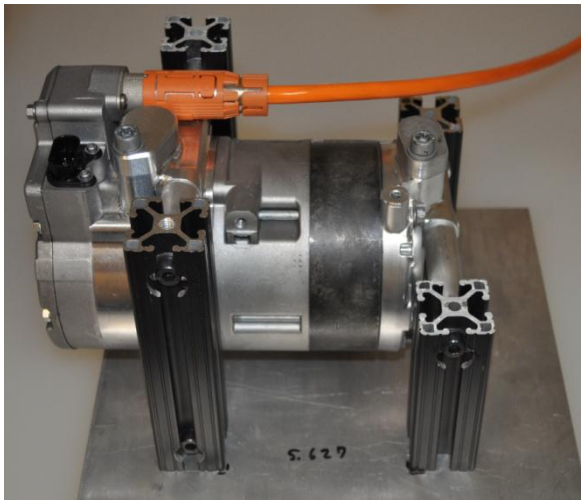

Figure IV-87: Halla Visteon Climate Control "E-comp" electric compressor.

Test Apparatus

A test apparatus was constructed in order to subject the experimental CFL system to realistic loads and measure the resulting performance. The test apparatus consists of two air loops that are designed to condition and measure the air temperatures and flow rates to the air-side heat exchangers of the experimental CFL system. A basic schematic of the test apparatus is shown in Figure IV-88, and a picture of the completed assembly is shown in Figure IV-89.

.

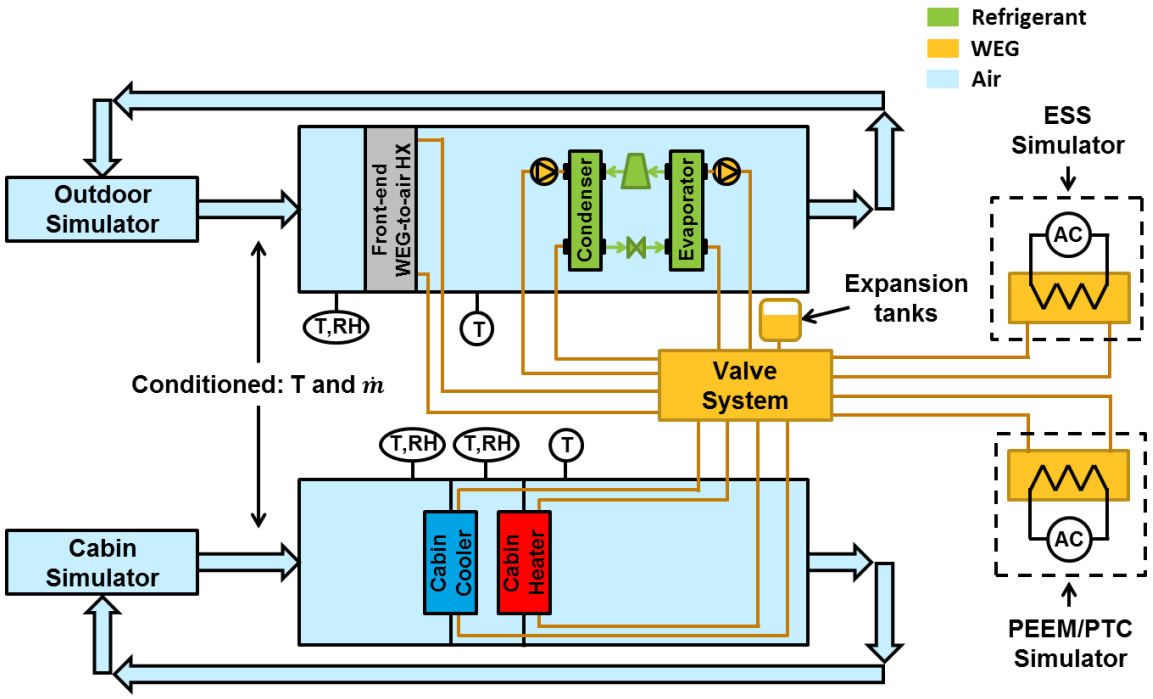

Figure IV-88: Basic overview of bench test apparatus design.

The larger air duct delivers a constant air temperature and variable air flow rate to the FEHX to simulate the outdoor ambient air passing over the front of the vehicle. The smaller air duct delivers a variable air temperature and air flow rate to the cooler core and heater core heat exchangers to simulate the cabin recirculation temperature. The test apparatus also employs two electrical resistance heaters to simulate the PEEM/PTC and ESS heat loads on the experimental CFL WEG system.

Figure IV-89: Constructed bench test apparatus.

All of the controlled parameters of the test apparatus are designed to simulate steady-state and transient vehicle operation. Without an environmental chamber housing the test apparatus, it is capable of operating at test conditions from the ambient room temperature, up to a 43°C outdoor temperature and a 63°C cabin soak temperature. The test apparatus is built on wheels so that it can be moved into an environmental control chamber for low temperature testing. When housed in a low-temperature environmental chamber, the range is extended down to -30°C for both the outdoor and cabin soak temperatures. The intention is that the experimental testing will simulate conditions of operating a vehicle in ambient outdoor conditions from -30°C to 43°C for both city and highway driving.

The instrumented measurement equipment of the test apparatus and CFL system include relative humidity sensors, air flow venturis, barometric air pressure sensors, air-side thermocouples, WEG flow rate Coriolis meters, WEG thermocouples, refrigerant turbine flow meter, refrigerant thermocouples, and refrigerant pressure transducers. The accuracies of the selected sensors were chosen to maintain propagated uncertainties for the key experimental parameters under 5%. This includes measurements such as flow rates, cooling and heating capacities, and coefficient of performance (COP). The thermocouples were calibrated to obtain accuracies better than 0.3°C.

To put realistic loads on the CFL system, LabVIEW [3] data acquisition and control code was written to simulate the loads and thermal responses of a BEV. Controls integrated into the LabVIEW code will modify the test apparatus hardware outputs as necessary to maintain the operational conditions specified by the software models. The mathematical models from NREL's Future Automotive Systems Technology Simulator (FASTSim) [4] vehicle simulation software were written into the LabVIEW code to calculate the simulated vehicle's propulsion loads based on the selected drive cycle profile. The FASTSim models provide the waste heat outputs from the PEEM and ESS.

To calculate the expected thermal response of the PEEM and ESS components and their interaction with the CFL WEG system, the heat transfer models created for the KULI

model [2] were written into the LabVIEW software. These models interact with the measured performance of the experimental CFL WEG system, i.e., inlet WEG temperatures, such that the temperatures of the simulated components can be calculated. Additionally, a heat transfer model was created for the vehicle cabin to predict the air and interior mass temperatures, including the temperature of the recirculation air of the HVAC unit. The cabin model is a transient, physics-based model developed by Gado [5]. The temperatures calculated by the ESS, PEEM, and cabin thermal models are particularly important as performance metrics because the CFL system must be able to maintain the ESS and PEEM temperatures within specific ranges to maximize performance and reliability, and the cabin temperatures can be used to predict passenger comfort.

Results

Initial testing of the CFL concept in the test apparatus is in progress.

Conclusions

An experimental CFL system was constructed using prototype heat exchangers from Delphi and a prototype automotive electric compressor from Halla Visteon Climate Control. The system is designed to be operated in a variety of different test configurations over a range of operating conditions from very cold to very hot. The CFL system enables cabin A/C, PEEM and ESS waste heat recovery, ambient cooling of the PEEM and ESS, active cooling of the ESS, and heat pump operation.

A mobile test apparatus was constructed to load, control, and measure the performance of the CFL system for a BEV. Mathematical models were integrated into the data acquisition and control system to simulate ESS, PEEM, and cabin loads due to propulsion and ambient conditions, as well as their thermal responses. The test apparatus imposes these transient loads on the CFL system via hardware in order to measure the energy consumption of the IVTM system. The measured energy consumption will then be used to estimate the improvement in vehicle range.

References

1. "KULI: Overview." [Online]. Available at http://kuli.ecs.steyr.com/. Accessed: 18-Sep-2013.
2. Rugh, J. P., and Bennion, K., Electric Vehicle Thermal Modeling to Assess Combined Cooling Loop Concepts. SAE 2012 Thermal Management Systems Symposium, October 2012.
3. "LabVIEW: System Design Software." Available at http://www.ni.com/labview/. Accessed: 18-Sep-2013.
4. "NREL: Vehicle Systems Analysis—Future Automotive Systems Technology Simulator." Available at http://www.nrel.gov/vehiclesandfuels/vsa/fastsim.html. Accessed: 18-Sep-2013.
5. Gado, A., Development of a Dynamic Test Facility for Environmental Control Systems. University of Maryland Ph.D. Dissertation, 2006.

Acknowledgements

- Co-author: Daniel Leighton, NREL
- Lee Slezak, David Anderson, DOE Vehicle Technologies Office
- Susan Rogers, Steven Boyd, DOE Vehicle Technologies Office
- Carrie Kowsky, Tim Craig, Delphi
- John Meyer, Tim VanBritson, Halla Visteon Climate Control
- Jeff Tomerlin, Cory Kreutzer, NREL

IV.F.3. Products

Publications

1. Rugh, J. P., and Bennion, K., (2012) "Electric Vehicle Thermal Modeling to Assess Combined Cooling Loop Concepts," Proceedings of the SAE Thermal Management Systems Symposium, October 31–November 1, 2012, Scottsdale, AZ.

IV.G. Assessment of Climate Control Settings and Loads on Energy Consumption for HEVs, PHEVs and BEVs in Freezing or Hot Sunny Environments

Henning Lohse-Busch, Ph.D., Principal Investigator
Argonne National Laboratory
9700 South Cass Avenue
Argonne, IL, 60439
Phone: (630) 252-9615
E-mail: hlb@anl.gov

Lee Slezak, DOE Sponsor
Phone: (202) 586-2335
E-mail: Lee.Slezak@ee.doe.gov

IV.G.1. Abstract

Objectives

- Quantify the impact of cabin climate control systems on the energy consumption of a hybrid electric vehicle at different temperature settings and in different ambient temperature environments.
- Establish the trend of climate control settings on the range of a battery electric vehicle.
- Investigate the impact of climate control on a plug-in hybrid vehicle.
- The ambient temperature conditions included in the study are the EPA 5 cycle label fuel economy test conditions of 72F, 20F and 95F with 850 W/m^2 of radiant solar emulation.
- Disseminate vehicle and component testing data to partners of the DOE such as; other national laboratories, the U.S. Council for Automotive Research (USCAR), OEMs, suppliers and universities. Support powertrain simulation model development and simulation.

Major Accomplishments

- Tested several Hybrid Electric Vehicles (HEVs), Plug-in Hybrid Electric Vehicles (PHEVs) and a Battery Electric Vehicles (BEVs) at different temperatures with both the climate controls set to a target cabin temperature of 72F or inactive/off.
- The impact of climate controls on the fuel consumption of a 2010 Toyota Prius HEV was studied:
  - At 20F, the cold start UDDS energy consumption increased by almost 90% with the cabin heated and 40% when the cabin is not heated. The cold weather fuel penalty (compared to 72F ambient temperature) shrinks as the powertrain reaches higher operating temperatures.
  - At 95F, the hot weather fuel consumption penalty (compared to the 72F testing) is a constant 60% on the UDDS which is caused by the continuous power required to run the air conditioning compressor.
- The impact of climate control settings on the range and energy consumption of a 2012 Nissan Leaf BEV was studied:
  - The largest impact of climate control settings on EV range occurs in middle city type driving as the low average propulsion power is easily rivaled by the climate control system power requirements.
  - In 20F cold weather conditions, driver behavior can impact the range significantly. A range reduction of 12% was observed with the heater off, versus a greater 48%range reduction observed with the heater set to a comfortable 72F cabin temperature.
  - Similarly, in95F hot weather conditions with simulated solar loading, the climate control settings can diminish EV range. With the air conditioning set to a cabin target temperature of 72F, an 18% reduction in range was observed, while a range reduction of up to 42% (versus 72F nominal ambient conditions) was observed when setting the climate control system to a 'worst-case' continuous AC Max cooling.
- Tested the impact on energy and fuel consumption of a 2013 Focus C Max Energi PHEV for several discrete cabin target temperature settings at different ambient temperatures.
  - At 20F, in charge depleting mode, utilization of cabin heating causes the internal combustion engine to run as well as supplemental electric heater to be used. This has a significant impact on the energy and fuel consumption in cold weather. Without cabin heating, the vehicle will operate as an EV (in charge depleting engine off mode) in a 20F ambient environment.
  - At 95F in city driving, by selecting the AC max setting an increase the electric energy consumption (in charge depleting EV mode) of 17% was measured. Alternatively, by targeting a cabin temperature of 78F instead of 72F in the same hot weather conditions, a 9% energy savings was realized (vs. 72F setpoint).
  - In hot weather (95F) the air conditioning system uses between 0.4 kW to 2.8 kW of electric power depending on the target cabin temperature, which can have a significant impact on electric energy consumption and resulting range.

Future Achievements

- Investigations of climate control effects at different temperatures will continue, using Argonne's heavily

instrumented Ford Focus (Level 2) with specific thermal instrumentation.

- Some of the climate control setting testing will be introduced into the standard test plan for AVTA vehicles.

✧ ✧ ✧ ✧ ✧

IV.G.2. Technical Discussion

Background

The powertrain efficiency of Advanced Technology Vehicles (ATVs) is significantly affected by the use of climate control such as cooling down the passenger cabin on a hot sunny day or heating the passenger cabin on a freezing winter day. The more efficient the powertrain, the larger the relative impact of the climate control system on energy consumption can be. This impact on energy consumption is dictated by the target cabin temperature set by the driver. The Advanced Powertrain Research Facility (APRF) has quantified the impact of various ambient outside temperatures and their commonly associated climate control systems on the energy consumption of different vehicle architectures using our chassis dynamometer in a thermal chamber.

Introduction

In FY2012, the Advanced Powertrain Research Facility quantified this impact of ambient temperatures and climate control on the energy consumption and range of a Nissan Leaf. A major finding was that the energy consumption for a small battery electric vehicle in cold weather (at 20°F ambient temperature) is twice that observed at 72°F during city-type driving. The 20°F ambient temperature is a challenging condition for an electric vehicle, since, unlike a vehicle with an internal combustion engine, it cannot rely on waste heat from its powertrain for cabin heating.

In another comprehensive study which focused on the impact of ambient temperature on energy consumption for a range of powertrain types (SAE 2013-01-1462), it was concluded that the more efficient the powertrain, the larger the relative impact of the climate control system (heating or cooling) on the energy consumption. The impact of temperature on energy consumption is greater for HEVs than for conventional vehicles, and is highly dependent on the air-conditioning system type (mechanical or high voltage), the powertrain architecture and powertrain capabilities. The PHEV and BEV are the most affected by extreme ambient temperatures, and the large relative impact of climate on energy consumption is due to their very efficient powertrain operation at 72°F.

In all prior studies, the climate control systems were set to a consistent target cabin temperature of 72F per regulation requirements. This investigation attempts extend the prior studies by quantifying the impact of the target cabin temperature setting on the climate control system and the resulting energy consumption.

Approach

Advanced Powertrain Research Facility

The 4WD chassis dynamometer of the APRF is EPA 5-cycle capable which enables the testing of vehicles in a variety of ambient temperature and environmental conditions. The test cell includes a thermal chamber and an air-handling unit with a large refrigeration system that facilitates vehicle testing at the EPA "Cold CO Test" ambient temperature of 20°F (-7°C). The other standard test temperatures are 72°F (25°C) and 95°F (35°C). In addition, a set of solar emulation lamps can provide 850 W/m² of radiant sun energy. The test cell is shown in Figure IV-90.

Figure IV-90: Illustration of testing at 95°F with sun emulation (left) and at 20°F cold ambient temperature (right).

Advanced Technology Vehicles in this study include:

1. A 2010 Toyota Prius (third generation Prius) which features a very refined hybrid electric eCVT powertrain.
2. A 2013 Ford C Max Energi which is a plug-in hybrid with sufficient electric-only range that it is capable of completing the UDDS cycle in electric mode only (without using the engine).
3. A 2012 Nissan Leaf which is a pure battery electric vehicle.

The report is broken into three sections: The first section quantifies the fuel consumption changes between several ambient temperatures conditions and climate control usages on a hybrid electric vehicle using the 2010 Toyota Prius test data. In the second part, the impact of several extreme climate control settings on the range of an electric vehicle is investigated using the 2012 Nissan Leaf test data. In the third and final part, the 2013 Ford C Max Energi is tested to quantify the impact of the heater usage in a 20F ambient temperature environment on the charge depleting range, as well as to study the impact of target cabin temperature settings on energy consumption in a 95F 'sunny' environment.

Results

Fuel consumption changes of extreme climate control settings at different ambient temperatures for a Hybrid Electric Vehicle

A 2010 Toyota Prius was tested in the thermal chamber at the three EPA 5 cycle test conditions. The 2010 Toyota Prius uses a high voltage air conditioning compressor for cabin climate control. The battery pack thermal management then draws from cabin air to heat or cool the pack with an active fan.

Test setup

The intent of testing is to dissociate the impact of heating or cooling the cabin air from other climate imposed energy-consumption penalties. Such penalties include cold start penalties for warming the powertrain and batteries, or running the air conditioning system at high output to initially cool down the interior after heat-soak.

In each case, the car completes a full test sequence, starting with a cold-start UDDS, followed by two additional UDDS cycles, a pair of HWFET, and a pair of US06 cycles. Note that the cold start UDDS cycle requires particular preparation procedure: First, to prepare the battery pack's State of Charge (SOC) in order to ensure a charge sustaining cold start test, a UDDS prep cycle is performed at the target climate condition the night before. Then, the vehicle undergoes thermal soak at the target test cell temperature for at least 12 hours prior to the test. Subsequent (aka 'Hot Start') test cycles are separated by an approximate rest/soak period of 10 minutes.

A 20F ambient temperature test day was performed once with the climate control setting targeting a cabin temperature of 72F, and a second time with the climate control system turned off. Similarly, the 95F ambient temperature with 850 W/m^2 radiant solar energy emulation test day was repeated twice, wherein the climate control setting targeted a cabin temperature of 72F the first time, and with the climate control system turned off for the second test. For each case, results are compared to baseline control tests conducted at an ambient temperature of 72F.

Results and analysis

The fuel consumption results for the sequence of three UDDS cycles at the different test conditions are shown in Figure IV-91. The 72F test sequence shows that the first UDDS (also referred to as the cold start cycle) has higher fuel consumption then the following hot start UDDS cycles. This represents the aforementioned 'cold start penalty' which is caused by additional frictional losses the powertrain and the internal combustion engine have to overcome, as well as added battery losses due to higher internal battery resistance. This losses will diminish with increasing temperature until a steady powertrain operating temperature is reached.

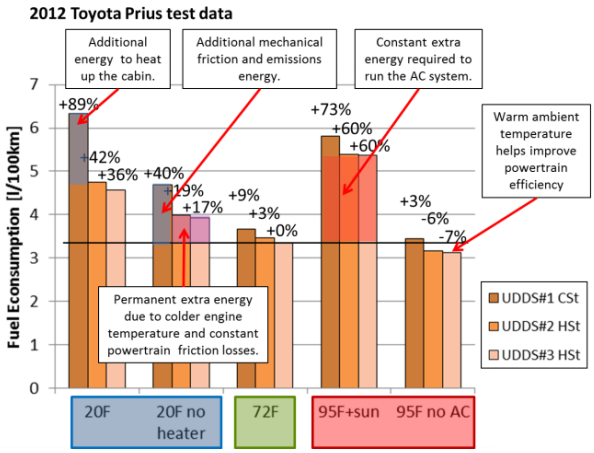

Figure IV-91: 2013 Toyota Prius Fuel consumption at different ambient temperatures with climate control set to 72F and climate control off.

On a cold start UDDS at 20F, the fuel consumption increases by almost 90% when the cabin is heated, or by 40% when the cabin is not heated, as compared to a 'hot start' UDDS cycle at 72F baseline. The 40% increase when the climate control system is turned off over the baseline 72F therefore represents the predicted cold-start penalty—the additional energy required by the powertrain to overcome additional mechanical and battery losses. These cold-start losses diminish as the powertrain temperature approaches thermal equilibrium, and thus the fuel consumption penalty is reduced on the hot start tests in the 20F environment.

It is interesting to note that the fuel consumption increase is doubled when the cabin is heated (set to 72F) on the cold start at 20F. On the Prius, the cabin heat is provided by waste energy from the internal combustion engine via a traditional coolant/heater core. In order to generate enough heat quickly, the powertrain runs the engine more often (83.4% of time compared to 43.4%) at lower loads (20.9 kW of average fuel compared to 29.3 kW) when the cabin heat is requested. This operation is a significantly less efficient use of the engine compared the no heat tests at 20F. Table IV-16 shows some of the relevant component operations for the different cold start tests.

Table IV-16: Cold start UDDS vehicle operation characteristics for the different test conditions.

	20F with heater	20F no heater	72F baseline	95F with AC	95F no AC
Engine ON time [%]	83.4	43.4	33.7	48.3	33.4
Average fuel power when Engine ON [kW]	20.9	29.3	29.2	32.6	27.6
Average positive battery power [kW[	2.3	2.5	2.6	3.5	2.5
Average negative battery power [kW[	3.7	-4.1	-4.4	-4.1	-4.7

Figure IV-91 also shows how the fuel consumption increase at 20F (compared to the 72F baseline tests) is reduced over time as powertrain reaches equilibrium operating temperature—but is never fully eliminated. In tests where the cabin is heated, the vehicle suffered a larger permanent fuel consumption penalty compared to no-heat UDDS tests. This can be explained in part by a significantly lower engine operating temperature (50-55C engine oil temperature at end of third UDDS) as compared to no heat test case (65-70F engine oil temperature at end of third UDDS) resulting from heat being diverted to the heater core.

In the 95F with 850W/m^2 radiant sun emulation test environment, the air conditioning system imposed a constant significant additional load on the powertrain, caused by the engine operating more frequently as shown in Table IV-16. Because of this a constant and significant fuel consumption increase at 95F compared to 72F ambient temperature occurs when the cabin is cooled to 72F. It is noteworthy that the fuel consumption in the 95F environment is actually lower then at 72F baseline when the air conditioning system in turned off.

Range Impact of different Climate Control settings at different ambient temperatures for a Hybrid Electric Vehicle

Test setup

In this study, the 2012 Nissan Leaf was also tested at the EPA five cycle fuel economy label conditions of 20F, 72F and 95 with 850W/m^2 radiant sun emulation. The tests were repeated for climate control settings of cabin target temperature of 72F in all ambient temperature conditions. At 20F a test sequence with the climate control system turned off (no heat) was performed. At 95F a test sequence with the climate control system set to 'AC Max' was performed to check the worst case scenario in the hot test environment. The test sequences are based on the new SAE J1634 Shortcut Multi Cycle Test (MCT) test method which enables the extrapolation of the test data to accurate energy consumption and range estimates for each cycle.

Results and analysis

The ranges of the different test conditions are shown in Figure IV-92. The longest range occurs in city type driving as represented by the UDDS cycle. The largest range reduction occurs in the 20F ambient environment while heating the cabin to the 72F on the UDDS. The 48% reduction in range is explained by the 3 to 4 kW of electric going to the heater to warm up the vehicle. If the driver turns of the heater off, the range will only suffer a 12% reduction, which is caused by higher frictional losses and higher battery system resistance. The corollary is that the driver can trade range for comfort.

Similarly, the range is reduced by 18% on the UDDS at 95F with the air-conditioning system set to a target cabin temperature of 72F. The range reduction will jump to a 42% decrease if the driver selects the coldest air conditioning setting. So even in a hot environment the driver can trade some significant range for comfort.

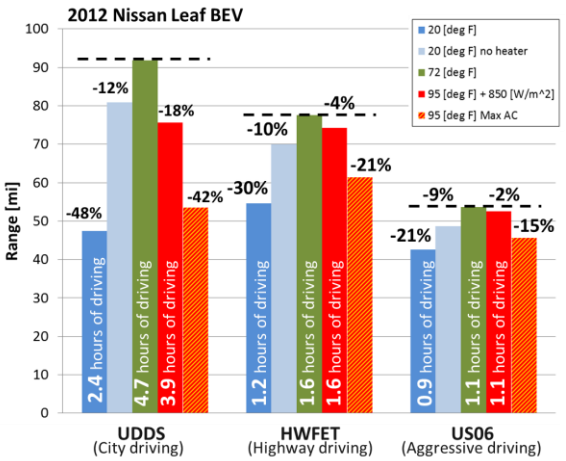

Figure IV-92: 2012 Nissan Leaf ranges for different climate control settings at different ambient temperatures.

The relative impact of the climate control on range, in both a 20F and a 95F test environment, is more limited as the drive cycles increase in intensity. The average power to complete a UDDS, a HWFET and a US06 are 3.8 kW, 10.8 kW and 16 kW of battery power respectively. The 3-4 kW heater power or 1 to 2 kW air conditioning power are proportionally less significant on the higher power cycles.

Energy consumption extremes and range impact at different Climate Control settings and different ambient temperatures for a Plug-In Hybrid Electric Vehicle

A 2013 Ford C-Max Plug-In Hybrid was tested in the thermal chamber at the three EPA 5 cycle test conditions. The 2013 Ford C-Max has significant EV-only range, and uses a high voltage air conditioning compressor for cabin cooling. Heat is supplied by traditional coolant heater-core, supplemented with an electric auxiliary coolant heater.

Test setup

A 2013 Ford C Max Energy was tested in the APRF. Two particular test sequences addressed the impact on energy consumption on the climate control setting as part of a larger and comprehensive benchmark test plan. The first test set is composed of UDDS full-charge EV depletion tests at the different EPA 5 cycle test conditions with the climate control setting targeting a cabin temperature of 72F or turned off. The second test sequence focused on the 95F test environment and a range of discrete target cabin temperatures.

Results and analysis

The energy consumption and fuel consumption of the full charge depletion tests at the different ambient temperature conditions are shown in Figure IV-93. The 72F test results are considered the baseline tests. In 95F ambient temperature tests with the air conditioning set to 72F, the electric energy consumption is increased by about 15%. For hybrid (engine-on) operation at 95F, charge sustaining fuel consumption increased by 11 to 12%.

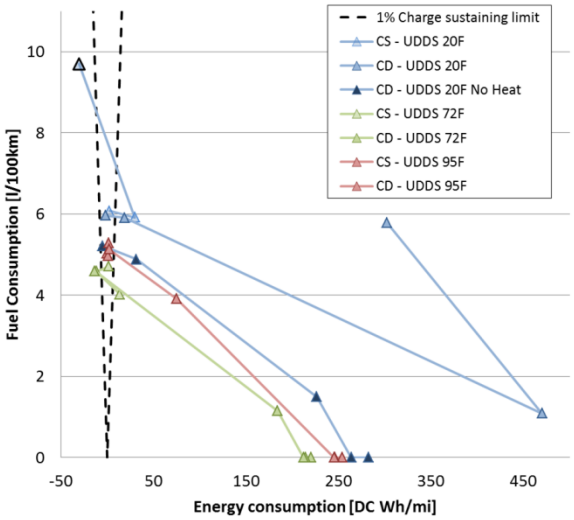

Figure IV-93: 2013 Ford C Max Energi fuel and energy consumption results at different ambient temperatures for the UDDS cycle.

Impact for climate control in 20F ambient temperatures

Figure IV-94 shows more detail on both 20F full-charge EV operation tests which include the test sequence with cabin heating set to 72F target temperature, and the test sequence where the climate control system was turned off. The third test sequence displayed is the 72F reference full charge test.

On the 'no heater' test sequence, the vehicle operated similarly to the 72F full depletion test. In charge depletion mode, the UDDS cycle was covered in electric-only mode and the internal combustion engine did not turn on until the end of the third UDDS. The electric energy consumption in charge depleting EV mode at 20F with no heat is 23 to 28% higher on the UDDS compared to the 72F baseline, which reduces the all-electric range by about 4 miles.

If the driver requests a cabin temperature of 72F in a 20F test environment, the powertrain engages the internal combustion engine on the first cycle to provide the energy to heat the cabin. The large fuel consumption is caused by the 20F engine cold start penalty, with the supplemental electric heater causing the electric energy consumption to be slightly larger than the 20F no heat cold start UDDS. The second UDDS uses the engine less but the electric consumption is increased by the usage of the electric heater. The third UDDS cycle is an already a charge sustaining cycle.

At 20F the driver's choice to heat the cabin has a very significant impact on the fuel and electric consumption of the vehicle.

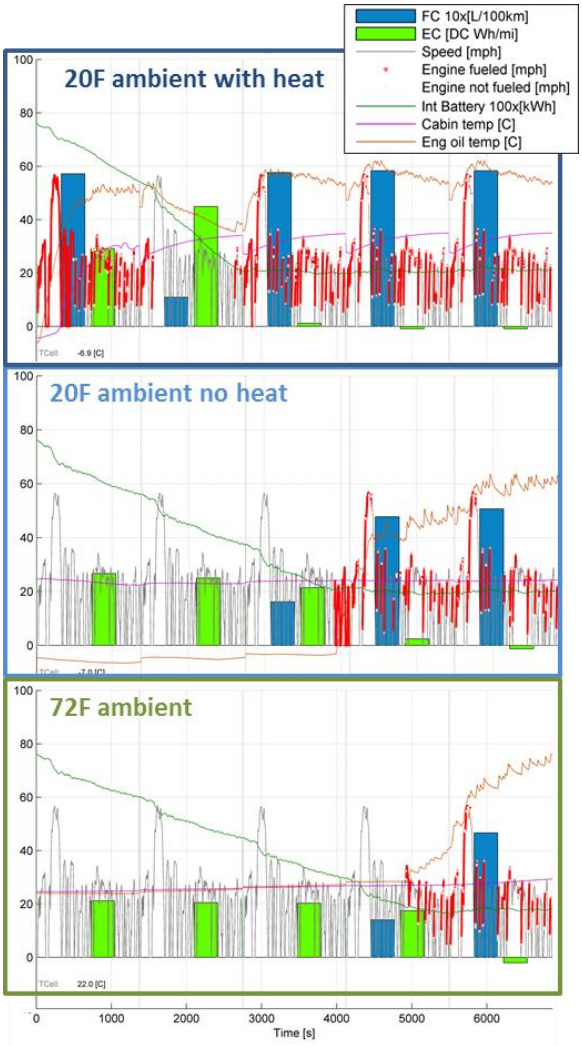

Figure IV-94: 2013 Ford C Max Energi system behaviors in charge depleting at 20F with cabin heating request and without.

Impact discrete climate control target temperatures on energy consumption in 95F ambient temperatures with 850 W/m² radiant energy emulation

Test setup

The cooling of a cabin with an air conditioning system can be divided into two phases. The first phase is a 'pull down' phase where the air and the component inside the cabin need to be actively cooled which can be rather energy intensive. The second phase the 'maintain' phase, where the air conditioning system only needs to cool enough to maintain the temperatures.

The goals of this testing were to capture both the pull down effect and the maintain energy consumption. Measurements of the impact of the air conditioning system on energy consumption for a transient cycle as well as steady state speeds was desired. These goals had to be achieved with a reasonable test effort. Figure IV-95 shows to final test sequence design. The vehicle was fully charged and a sequence of three cycles was repeated. The first cycle in the sequence served only to thermally condition the cabin and the

powertrain temperatures—the results of this first cycle were disregarded. The next two cycles were completed with a specific target cabin temperature for each cycle. To ensure identical thermal starting conditions, a strict 10 minute soak/rest period was implemented between tests while the test cell was maintained at 95F with the 850W/m^2 of radiation solar emulation. The vehicle was recharged after each test sequence of three cycles. The sequences were repeated until all the desired cabin target temperatures were tested. This process ensures that the vehicle was always operating in electric mode (charge depleting).

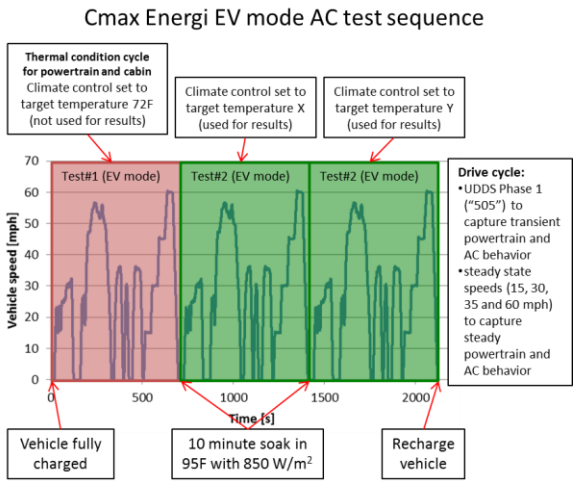

Figure IV-95: Air condition test setup to capture energy consumption variation on transient drive cycles and steady state speeds.

The actual drive cycle was a composite of the first phase of the UDDS (also called '505' as it is the first 505 seconds of the UDDS) and four steady state speeds (15, 30. 45 and 60 mph). The pull down phase was completed during the 505 and the air conditioning system only had to maintain the temperature during the steady state speed test as shown in Figure IV-96. The cabin target temperature selected on the climate control interface were varied at the following settings: 60F (AC max), 68F, 72F, 75F, 78F and 95F (AC off). All the testing was completed in the ambient temperature of 95F with 850 W/m^2 of radiant solar emulation.

Drive cycle results

The energy consumption results on the '505' drive cycle are shown in Figure IV-97. The regulation testing requires setting the air conditioning system to a cabin target temperature of 72F. If the driver would set the climate control to the AC max setting, the energy consumption in city type driving would increase by 17%. Conversely if the driver were to turn off the air conditioning system, he could reduce the energy consumption by 18%. But more realistically if the driver were to scale back the target cabin temperature to 78F he could reduce the energy consumption by 9% on a hot sunny day in city type driving.

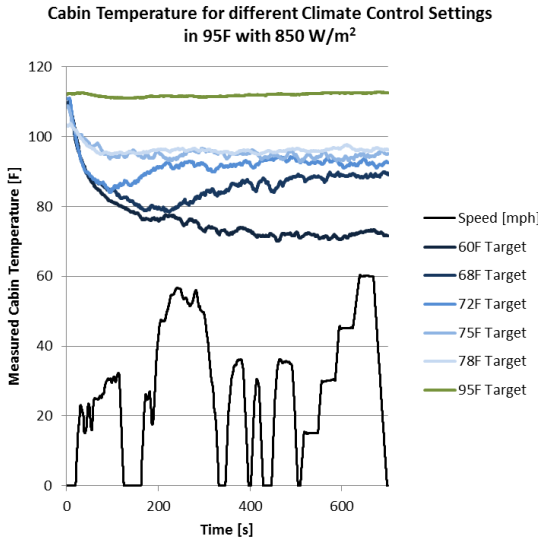

Figure IV-96: Cabin temperatures achieved during the different air conditioning tests.

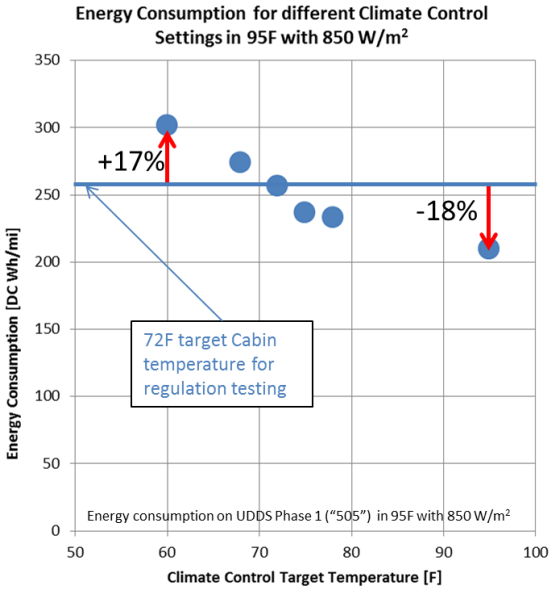

Figure IV-97: Electric energy consumption on '505' in 95F ambient temperature for different climate control target temperatures.

Steady state speed results

The energy consumption results for the steady state speed testing with different discrete target cabin temperature settings are shown in Figure IV-98. The colder the target temperature the higher the energy consumption at all speeds. When the air conditioning is turned off the energy consumption shows that the powertrain is a less efficient at lower speeds (energy consumption to road load curve which is the power at the wheels). At 15 mph about 1.8 kW of battery power are required to propel the vehicle forward as shown in Figure IV-99. The air conditioning power will vary from 3.3 kW in the AC max setting to 0.4 kW of the cabin target temperature of 78F as shown in Table IV-17. The 2.8 kW power requirements in the AC max setting out weight power

required to move the vehicle forward and explain the dramatic looking energy consumption increase.

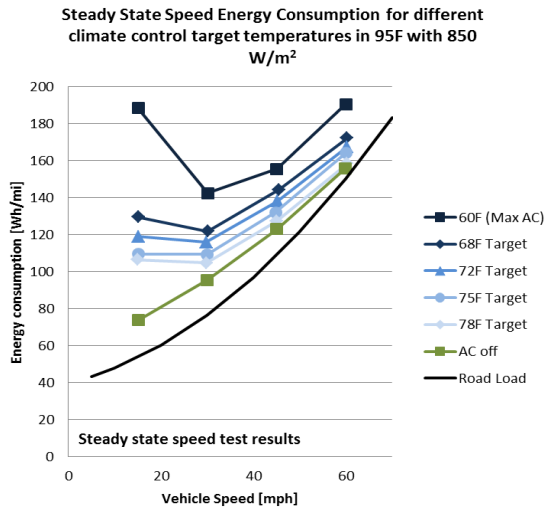

Figure IV-98: Electric energy consumption at steady state speeds in 95F ambient temperatures for different climate control target temperatures.

Table IV-17: Air conditioning power for different cabin target temperatures.

Target Cabin temperature	Max AC power [kW]	Min AC power [kW]	Average AC power [kW]
60 F	3.3	2.3	2.7
68 F	1.6	1.3	1.4
72 F	1.1	1.0	1.1
75 F	0.9	0.6	0.7
78 F	0.8	0.2	0.4
95 F	0.0	0.0	0.0

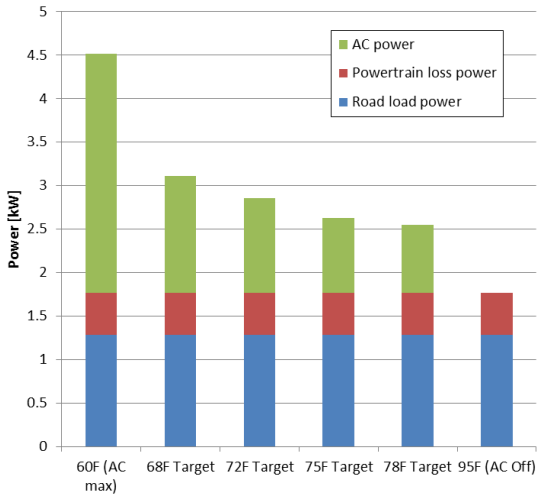

Figure IV-99: Power distribution at different cabin target temperature settings for 15 mph.

IV.G.3. Products

Publications

1. Lohse-Busch, H., Duoba, M., Rask, E., Stutenberg, K. et al, "Ambient Temperature (20°F, 72°F and 95°F) Impact on Fuel and Energy Consumption for Several Conventional Vehicles, Hybrid and Plug-In Hybrid Electric Vehicles and Battery Electric Vehicle", 2013 SAE World Congress, Detroit MI, SAE 2013-01-1462
2. Lohse-Busch, H., Duoba, M., "Advanced Powertrain Research Facility: Vehicle testing and results focused on Thermal Management", IEA (International Energy Agency), Task 17 Workshop, Thermal Management Concepts for Hybrid & Electric Vehicles, Vienna Austria
3. Lohse-Busch, H., Duoba, M., "Impacts of Hot and Cold Temperatures on Plug-in Vehicle Efficiency and Range", A3PS Conference Eco-Mobility 2013, Vienna, Austria

Tools and Data

1. Some raw 10 Hz vehicle test data in this report is available at the APRF's Downloadable Dynamometer Database for public download at www.transportation.anl.gov/D3.

MEDIUM AND HEAVY DUTY

IV.H. FedEx Collaboration for Improved BEV Delivery Vehicle Using Specific Usage Information

Forrest Jehlik, Principal Investigator
Argonne National Laboratory
9700 S. Cass Avenue
Argonne, IL 60439-4815
Phone: (630) 252-6403
E-mail: fjehlik@anl.gov

Lee Slezak, DOE Sponsor
Phone: (202) 586-2335
E-mail: lee.slezak@ee.doe.gov

IV.H.1. Abstract

Objectives

- Deliver an unbiased assessment of the performance of two all-electric-powered vehicles (EVs), with emphasis on economy of operation and suitability for FedEx Corporation's delivery operations, and taking into account the impact of seasonal climate changes.

Major Accomplishments

- Consultation and recommendations on in-vehicle data acquisition completed.
- Testing and data analyses of the benchmark Isuzu Reach diesel completed.
- Testing and data analyses of the Navistar eStar EV completed.
  - Vehicle tested under hot/cold conditions.
- Testing and data analyses of the Smith Newton EV completed.
  - Vehicle hot/cold conditions simulated for comparison.
- Comparative analysis of energy consumption over pertinent drive cycles completed.
- Cost-per-mile analysis completed, on the basis of energy input costs only (no maintenance or capital costs included).
- Final report and presentation completed.

✧ ✧ ✧ ✧ ✧

IV.H.2. Technical Discussion

Background

The role of the U.S. Department of Energy's (DOE's) Advanced Vehicle Testing Activity (AVTA) is to help bridge the gap between R&D and the commercial availability of advanced vehicle technologies that reduce petroleum use and meet air quality standards. AVTA supports DOE's Vehicle Technologies Program by examining market factors and customer requirements, and evaluating the performance and durability of alternative-fuel and advanced-technology vehicles in fleet applications. The Advanced Powertrain Research Facility (APRF) group at Argonne National Laboratory conducts evaluations of advanced-technology vehicles with support from AVTA. The group's main objective is to conduct comprehensive, unbiased evaluations in order to obtain valuable data about the state of the technology. This information is provided to DOE so that future resources and research can be directed appropriately.

In this project, testing and analysis was conducted for three FedEx fleet vehicles: an Isuzu Reach turbodiesel-powered benchmark, a Navistar eStar (Navistar) EV, and a Smith Newton (Smith) EV. Each vehicle was instrumented and tested over a series of specific drive cycles, in which some tests were conducted under a range of ambient temperatures, and some assessments were made of the energy consumption variations due to ambient temperature. The work was performed to determine the potential economic and environmental benefit of utilizing EVs in the FedEx truck fleet.

Introduction

The work discussed in this report represents one of the earliest studies of real-world electric truck operations in which seasonal climate impacts are being determined. The EV trucks discussed here are owned and maintained by FedEx and were loaned to Argonne for the study. Argonne researchers provided technical advice to FedEx personnel on procuring data acquisition (DAQ) instrumentation. The EV trucks were tested under controlled laboratory conditions in Argonne's dynamometer test facilities, and their performance parameters were collected, measured, and analyzed. The results were compared with data from a conventional diesel-powered delivery van provided by FedEx that served as the baseline case. Argonne provided a final report summarizing the measured economies of operation and observed suitability of the EV trucks for FedEx-defined delivery operations.

Approach

Prior to testing, each vehicle was instrumented with a combination of analogue sensors, in conjunction with the controller area network (CAN) signals, to determine energy utilization over the drive cycles of interest. Response Surface Methodology (RSM) models of the Isuzu, Navistar EV, and Smith EV were developed to predict consumption over the drive cycles of interest. Depending upon the vehicle, tests were conducted at 20°F, 70°F, and/or 95°F conditions. Additionally, three vehicle weights were tested for each of the EVs: 8,940 lb. (baseline weight), 10,440 lb. (baseline weight + 1,500 lb.), and 11,940 lb. (baseline weight + 3,000 lb.).

For the Isuzu, fueling rate calculations were based on exhaust emissions carbon counting techniques. Energy consumption for the EVs was determined using a Hioki Power meter, which provided both current and voltage data for the high-voltage battery pack.

In order to complete this work, the project was broken down into three separate tasks, as described below.

Task 1: Selection and installation of instrumentation and DAQ system

- Offer technical advice to FedEx to guide its purchase of the DAQ instrumentation for the test vehicles.
- Provide technical support to FedEx for installing the selected instrumentation and DAQ system.
- Troubleshoot the test vehicle instrumentation to ensure its proper operation as the vehicle is placed in service.

Task 2: Vehicle testing

- Compare data collected on operational parameters for the EV trucks with data for the conventional truck.
- Measure the conventional truck's performance and electrical energy consumption under 70°F standard conditions, under the specified payload conditions of 8,940 lb. (baseline weight), 10,440 lb. (baseline weight + 1500 lb.), and 11,940 lb. (baseline weight + 3000 lb.).
- Test EVs, if capable, for one payload weight in Argonne's environmental chamber at the test cell temperature extremes of 95°F and 20°F to determine the impact on EV range when the in-cabin heater and air conditioning (A/C) are in use.
- Report the energy used, on a watt-hour per mile basis, and the overall electrical energy efficiency.
- Use standardized drive cycles (UDDS and HWFET) and a FedEx-provided in-service duty cycle to enable a detailed comparison of the EV trucks' energy consumption and evaluation of their suitability for FedEx urban delivery/pickup operations.
- Determine and report the effect of ambient temperature on battery system performance.
- Measure and report the in-cabin heater and A/C temperatures to determine the heating/cooling impacts on auxiliary accessory energy loads and electric range.

Task 3: Data analysis and vehicle comparisons

- Analyze the vehicle dynamometer test data and prepare a data analysis summary for each vehicle tested.
- Structure the summary results to provide a means for simple vehicle-to-vehicle comparisons that can be done for all of the EV trucks tested under DOE-directed funding.
- Report electrical energy consumption on a per-mile basis from the various test cycles and payload conditions, with provisions for comparisons to the conventional vehicle tested.
- Determine the overall energy conversion efficiency.
- Compare the impacts of the ambient temperature and accessory usage on energy consumption and electric range.

Figure IV-100–Figure IV-102 show the three test vehicles in the APRF dynamometers.

Figure IV-100: Navistar eStar EV in Argonne's APRF 4WD testing facility.

Figure IV-101: Smith Newton EV in Argonne's APRF 4WD testing facility.

Figure IV-102: Isuzu Reach diesel benchmark in Argonne's APRF 2WD testing facility.

Test Plan and Drive Cycle Development

Energy consumption for two EV delivery trucks was determined and compared with that of a diesel-powered benchmark. The vehicles tested were the Navistar eStar (EV), Smith Newton (EV), and Isuzu Reach (diesel benchmark). Three weights were investigated for each vehicle: baseline, baseline + 1500 lb., and baseline + 3000 lb. Energy consumption was determined from data collected by FedEx during three days of New York City (NYC) driving, which were collected on December 22, 23, and 24. Since the top speed of the Navistar EV was limited to 50 mi/hr, the drive-cycle data were all scaled to a maximum speed of 48 mi/hr. Since the cycles were over 3 hours in duration, 1800 seconds of the December 22 cycle were used as reference and the models developed from the data were used to determine energy consumption measured against the truncated cycle. Details of the drive cycle are protected under a nondisclosure agreement and are not shown.

Results

The findings from each of the vehicles are given below, followed by a comparison summary.

I. Isuzu Reach (diesel benchmark)

NYC cycle consumption

RSM models were used to determine the Isuzu Reach fuel consumption over the three days of NYC driving for which data were supplied. In addition, an analysis was done to compare the amount of fuel consumed if the engine remained running during vehicle stops (no idle stop) with the amount consumed under idle start/stop conditions (idle stop). The results are presented in Figure IV-103.

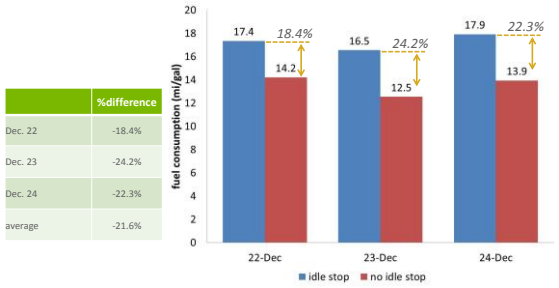

Figure IV-103: 44Isuzu Reach fuel consumption based on three-day-averaged NYC drive-cycle data. (Results show the effects of idle start/stop on fuel consumption.)

Figure IV-104 shows that consumption on each of the three days of driving is relatively similar. The data for December 23 show an increase in positive acceleration, indicating more aggressive driving resulting in reduced fuel economy.

On average, if aggressive idle start/stop is used, a reduction of 21.6% in fuel consumption is realized. Note that the impacts on the particulate filter loading (and thus regeneration) are not included in this analysis; they are discussed after the vehicle weight analysis.

Effects of GVW on consumption: Isuzu Reach

The integrated fuel consumption data as a function of weight on December 22 is plotted along with the NYC drive-cycle data for that date in Figure IV-104. This figure highlights the generalized effect of increased GVW on consumption. Results using the RSM model predicting consumption over the three-day NYC cycle are shown in Figure IV-104. Note that the data shown in is averaged over the three days. The total difference in consumption between the baseline weight and the maximum loading of +3000 lb. is approximately 22%.

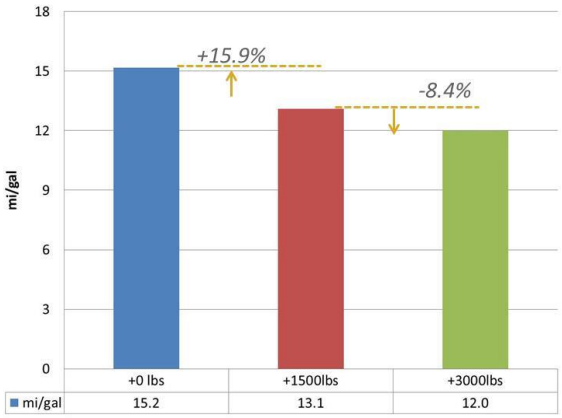

Figure IV-104: 55Effects of increased GVW on fuel consumption, based on three-day-averaged NYC drive-cycle data.(Results average the modeled consumption over the period of December 22–24.)

Finally, scaled back-to-back UDDS/HWY/UDDS tests at 48 mi/hr (maximum) for the three weights are compared in Figure IV-105. In these tests, a 70°F cold start UDDS cycle began the series, followed by a HWY cycle, then finally a warm UDDS cycle. This sequence captures the relative effect of efficiency gains as the system warms, as well as the effect

of frequent stops (UDDS cycle) versus higher average speed cycles (HWY) without frequent stops.

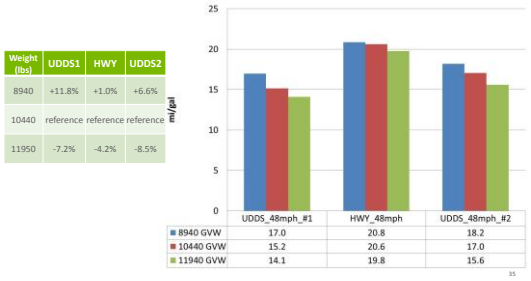

Figure IV-105: Back-to-back UDDS/HWY/UDDS tests at three weights.

These results indicate that there is a significant decrease in fuel consumption for all weights for the second UDDS cycle when compared to the first one. This decrease is due to reductions in the powertrain's friction as the fluid warms. Finally, note that at higher speeds in which there are not many starts and stops (HWY cycle), the sensitivity of fuel consumption to weight is minimal (i.e., a total spread of 5% for a 3000-lb change in GVW) relative to the UDDS cycle (~17% spread, on average, between the first and second UDDS cycle). This finding is consistent with the physics of acceleration, according to which a UDDS cycle requires greater amounts of energy than a HWY cycle conducted at relatively low speeds (48-mi/hr maximum).

Diesel Particulate Filter (DPF) regeneration effects on fuel consumption

As previously noted, analysis of the effects of the DPF on energy consumption was completed. A review of the DPF control system shows that there are four modes of regeneration.

- Passive catalyst regeneration: Smaller quantities at lower temperatures catalyze passively.
- Throttle regeneration: The intake throttles, the exhaust stream is enriched, and soot is catalyzed.
- Throttle plus injection retardation: The intake throttles, injection is retarded, and hot/rich exhaust enters the catalyst, assisting oxidation.
- Post-injection: A late injection during the blowdown process enters the exhaust stream, resulting in oxidation at the catalyst.

The fourth mode of regeneration negatively affects fuel consumption the most because extra fuel is used, causing oxidation at the DPF. Steady-state regeneration tests of the fourth mode were completed to determine the excess fuel required for regeneration to occur (Results Figure IV-106).

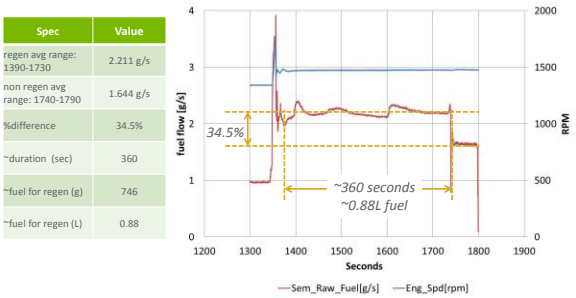

Figure IV-106: DPF regeneration fueling rate (regeneration mode 4).

From the test data it was determined that a full DPF regeneration event requires about 6 minutes of regeneration time, and that about 0.9 L of fuel is required. A literature review on the DPF revealed that regeneration occurs at approximately every 150 miles of normal driving. On the basis of this normal frequency of regeneration and the assumption that the RSM fueling models constructed contain the first three regenerative-mode effects, the estimated impact of DPF regeneration was calculated and is shown in Figure IV-107.

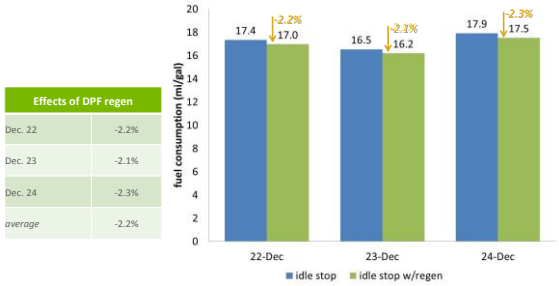

Figure IV-107: Effects of DPF regeneration on fuel consumption. (Results are calculated on the basis of a month of driving and assumes a 150-mi span between full DPF regeneration events.)

Assuming one month of driving on the three-day NYC cycle, it was determined that the DPF regeneration increases consumption by approximately 2%. Note that this analysis assumes regular regeneration effects and does not take into account (1) DPF loading variations due to frequent-start/stop driving patterns or (2) constant high-speed driving (HWY cycles). The former driving pattern should result in more frequent regeneration (and therefore more fuel consumption), and the latter pattern should result in lower rates of regeneration (and less fuel consumption).

Effect of deceleration fuel cutoff on consumption

In Figure IV-108, the actual fuel measured (shown in red) is compared with a more aggressive fuel cutoff calibration. In this case, the deceleration fuel shutoff shown is for negative accelerations that are less than 10% of the maximum deceleration rate. For this analysis, the UDDS cycle was considered. Similar results would be anticipated from other city driving cycles (e.g., the NYC cycle). Results show that a decrease of approximately 9% in fuel consumption could be available with more aggressive deceleration fuel shutoff strategies. This result does not take into account noise, vibration, and harshness calibrations for the vehicle, which could negatively affect aggressive fuel shutoff strategies.

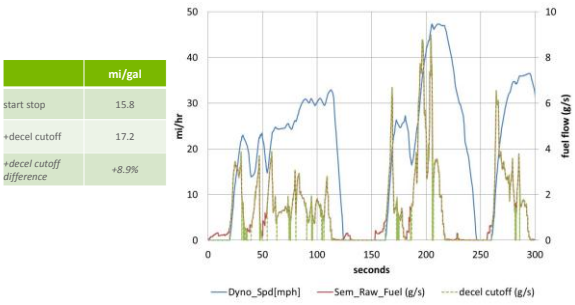

Figure IV-108: Deceleration fuel cutoff analysis. (Deceleration fuel cutoff, in green, represents additional potential fuel cutoff to improve travel efficiency.)

II. Navistar eStar EV

NYC cycle consumption plus GVW effect

The RSM models generated were used to predict the consumption during the NYC three-day cycles at the three different weights: 9,280, 10,780, and 12,280 lb. (baseline, +1500 lb., and +3000 lb.). In all tests, the three days were considered with the assumption that the vehicle started with a full charge before being driven (i.e., it was charged overnight prior to route delivery). This assumption resulted in the inclusion of brake regeneration limits in the modeling, which would initially reduce the energy recovered during regeneration. Effects of GVW on energy consumption for the Navistar EV are shown in Figure IV-109.

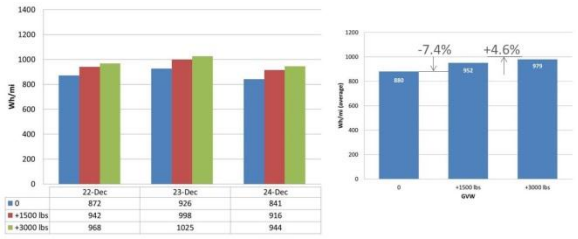

Figure IV-109: RSM-modeled electrical consumption for the Navistar EV based on three-day-averaged NYC drive-cycle data. (GVWs of 9,280, 10,780, and 12,280 lb. were considered.)

Figure IV-109 shows that more energy was consumed on December 23 than on either of the other two days. Analysis shows that the positive acceleration rates were 8% greater on that day (thus resulting in greater fuel consumption). It could also be observed that increasing the weight by 1500 lb. from the baseline GVW results in an increase in fuel consumption of 7.4%. The next increment of 1500 lb. of weight (3000 lb. payload) increases consumption an additional 4.6%. No heating, ventilation, and A/C (HVAC) systems were included in this analysis; these factors are analyzed in the following section.

Finally, analysis was conducted to determine the percentage of energy that was recovered from brake regeneration. The models that were used to predict overall consumption were used to calculate the energy returned to the battery pack and averaged over the three days of driving for the three vehicle weights. It was determined that, on average, about 15% of the drive-cycle energy from the regenerative braking system was recovered and used. These results were calculated from the RSM model for all three vehicle weights (Figure IV-110).

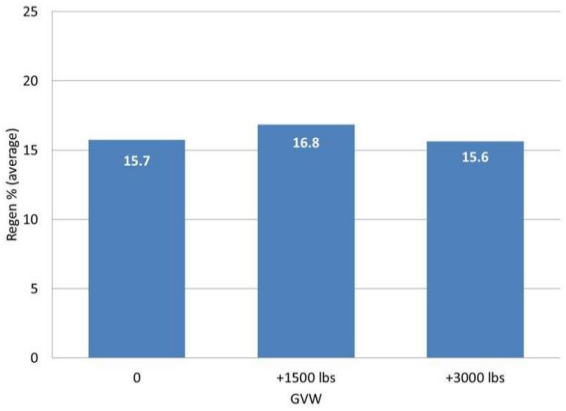

Figure IV-110: Percent of regenerative braking energy returned to the battery pack for the Navistar EV. (Values are defined as energy into pack divided by energy out.)

HVAC and thermal effects on consumption

Back-to-back UDDS/HWY/UDDS cycles were conducted at three ambient temperatures: 20°F, 70°F, and 95°F. The middle weight of 10,780 lbs (+1500 lbs.) was selected as the reference weight for all tests involving temperature. The effect of temperature on energy consumption at the higher and lower weights would be similar in magnitude to that observed at the 10,780-lb reference weight. Effects on ambient-temperature fuel consumption over these cycles, without additional air/heat usage, are shown in Figure IV-111.

Temp (°F)	UDDS1	HWY	UDDS2
20F*	+53.6	+30.8%	+49.7%
70F	reference	reference	reference
95F**	-2.9%	-3.6%	-2.0%

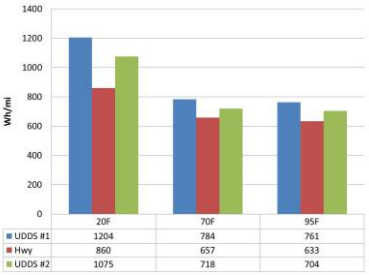

Figure IV-111: Effect of ambient temperature on energy consumption during back-to-back UDDS/HWY/UDDS cycles. (First UDDS cycle is full charge, cold start.)

Figure IV-111 shows that there was a significant impact on energy consumption during the 20°F cold test. An average increase of 44.7% in energy consumption was observed between the 70°F reference temperature and the cold temperature. This increase was due to powertrain inefficiencies in the cold and even more to the on-board electrical heater. In addition, for all tests, less consumption was observed during the second UDDS cycle in comparison to the first. At the start of the first cycle, the battery was fully charged, limiting brake regeneration. This factor increased the overall cycle consumption. Also, as the powertrain warmed, it became more efficient (lubricity and heat transfer effects decreased). The combination of these effects reduced overall consumption.

Figure IV-112 shows the measured energy consumption for the HVAC system. During cold (20°F) operation, the battery consumed from 2 to 5 more kW of energy to generate heat. For the 95°F tests, the on-board A/C unit supplied cool air, requiring only about 0.6 kW of energy, far less energy than

required for heating (and coming from a secondary energy source) and thereby having a much smaller impact on overall energy consumption.

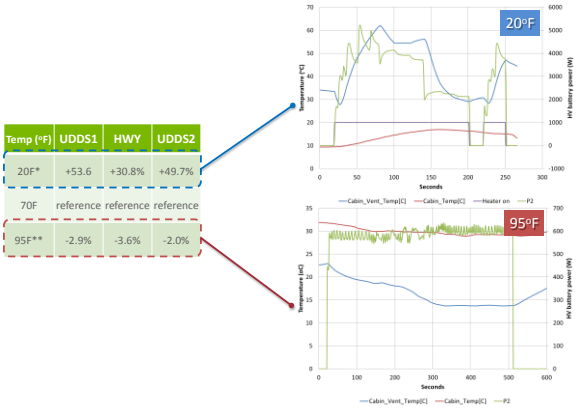

Figure IV-112: Heater and HVAC system power consumption, measured during 20°F (cold) and 95°F (hot) operation.

Brake regeneration effects on consumption

Tests were conducted to determine if ambient temperature had a significant impact on regenerative braking energy recovery. Potential limitations in the battery management system as well as variability in friction between the tire and the road could limit the amount of energy recovered. UDDS cycle test results were analyzed at 20°F, 70°F, and 95°F to determine if the energy recovered was limited or not. As shown in Figure IV-113, limitations in energy recovery did occur at 20°F; however, recovery was nearly identical for the two warmer temperatures.

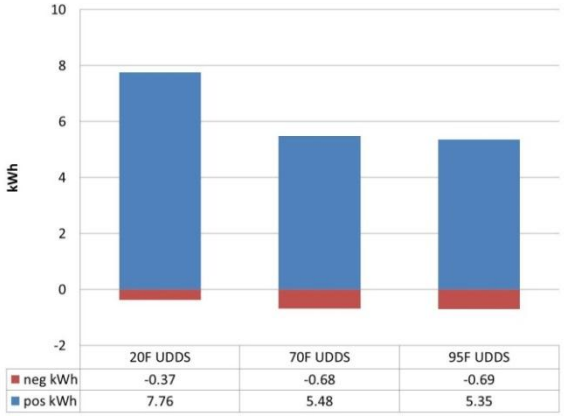

Figure IV-113: Temperature effects on regenerative brake utilization during UDDS cycle.

III. Smith Newton EV

Effect of GVW on consumption during NYC cycle

The RSM models generated were used to predict the consumption during NYC three-day cycles at the three different weights: 11,440, 12,900, and 14,440 lb. (baseline weight, +1500 lb., and +3000 lb.). In all tests, the assumption was that the vehicle started with a full charge prior to driving the cycle (i.e., it was charged overnight prior to route delivery). This assumption resulted in the inclusion of brake regeneration limits in the modeling, which would initially reduce the energy recovered during regeneration. Effects of GVW on energy consumption for the Smith EV are shown in Figure IV-114.

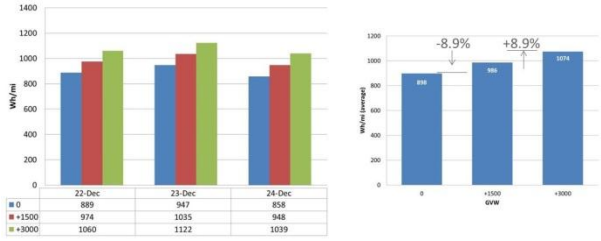

Figure IV-114: RSM-modeled electrical consumption for the Smith EV, based on three-day-averaged NYC drive-cycle data, with GVWs of 11,400, 12,900, and 14,400 lb.

Increasing the weight by 1500 lb. from the baseline GVW increased fuel consumption by 8.9%, and adding 1500 lb. more increased consumption by an additional 8.9%. In this analysis, it was assumed that no HVAC systems were being used.

A final analysis was conducted to determine the percentage of energy that was recovered from using brake regeneration over the three days of driving. The models that were used to predict overall consumption were used to calculate the energy returned to the battery pack. It was determined that, on average, about 21% of the drive-cycle energy from the regenerative braking system is recovered and used. These results were calculated from the RSM model for all three vehicle weights, as shown in Figure IV-115.

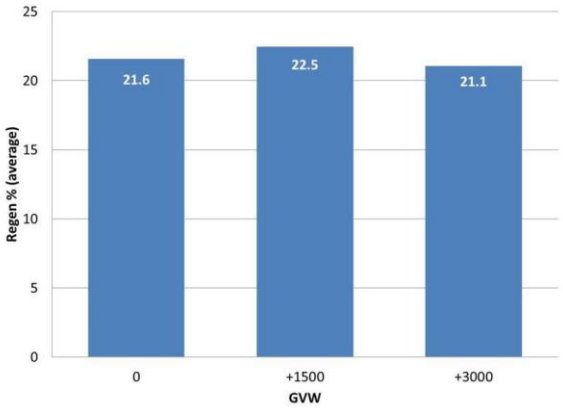

Figure IV-115: Percentage of Smith EV regenerative braking energy returned to pack. (Values are defined as energy into pack divided by energy out.)

In comparing Figure IV-115 with Figure IV-110, one finds that the Smith EV recovers a higher percentage of energy into the pack than the Navistar EV. However, even though the Smith EV has the regenerative braking advantage, it still consumes more energy during the NYC cycle at each of the weights investigated.

HVAC and thermal effects on consumption

HVAC investigations for the Smith EV involved simulating and estimating the losses for hot and cold operation. There were issues with fitting the vehicle into the 4WD test facility because of the vehicle's height. As a result, all tests were conducted at 70°F while running either the heater or the air conditioner. Additionally, powertrain losses due to thermal

effects were estimated from the Navistar EV data and integrated into the total energy usage.

The baseline +1500 lb. weight was selected as the reference weight for all tests involving temperature. The effect of temperature on energy consumption at the higher and lower weights would be similar in magnitude to that observed at this reference weight. Effects of ambient temperature on energy consumption during NYC cycles are shown in Figure IV-116.

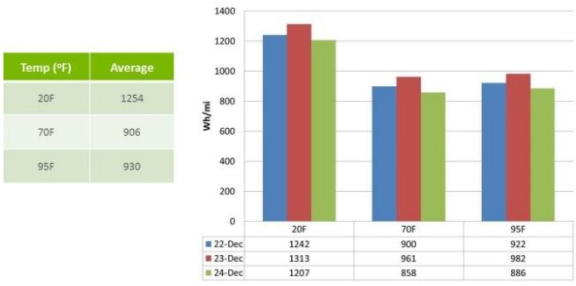

Figure IV-116: Effect of ambient temperature on energy consumption for the Smith EV during back-to-back UDDS/HWY/UDDS cycles (first UDDS cycle is full charge, cold start.) Note: results are estimated, as tests were run at 70°F while operating either the heater or the A/C unit. Additional losses due to powertrain inefficiency at alternative temperatures were estimated and added.

Pull-down tests were conducted to determine the HVAC system's energy consumption independent of the vehicle's energy consumption. The vehicle was keyed on and both the heater and AC were operated with various fan settings to determine the consumption. The results are shown in Figure IV-117.

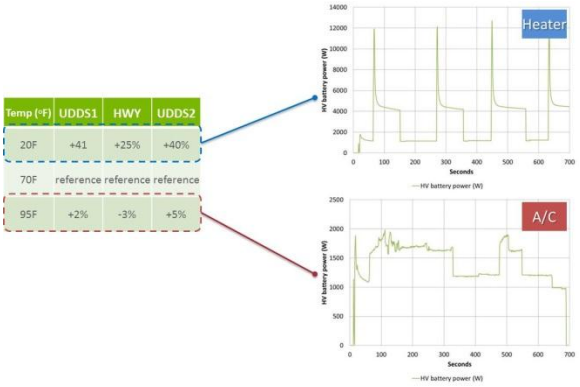

Figure IV-117: Power consumption by heater and A/C system, measured during simulated 20°F (cold) and 95°F (hot) operation.

For the simulated 20°F operation (heater on), the battery consumed approximately 4 kW for heat generation. From a peak of 12 kW, the consumption tapered down to a 4-kW steady-state rate. For the simulated 95°F tests (A/C on), far less energy was required. Maximum consumption was recorded at approximately 1.6 kW, with the levels dependent upon the fan settings (falling to a minimum of 1 kW). The unit required only about 0.6 kW of energy and thereby had a much smaller impact on overall energy consumption.

Comparisons of Fuel or Electricity Costs per Mile

The three-day-averaged consumption results for all three vehicles over the NYC cycles were analyzed and Wh/mi costs were calculated across a range of energy costs. For the conventional vehicle, energy cost is the cost of diesel per gallon; for the EVs, it is the cost per kilowatt-hour (kWh) of electricity supplied. In these comparisons, no additional costs are embedded in the calculation; i.e., maintenance, initial capital costs, recovered capital costs, electrical vehicle supply equipment, and all other additive variables are excluded. Values shown below are for energy costs on a per-mile basis only (cost of fuel/mile or cost of Wh/mile averaged over three days of NYC drive cycle data). However, costs are calculated across the three payloads (baseline weight, +1500 lb., and +3000 lb.) as well as across the three temperatures (20°F, 70°F, and 95°F). Total economic analysis would require the above-mentioned additive costs to be considered.

In conclusion, the climate control analysis in conjunction with the GVW analysis, demonstrates that the Navistar EV has an advantage in energy consumption with regard to vehicle payload; however, neither vehicle has a clear advantage relative to climate-control energy consumption. The overall cost per mile for the EVs with a given payload is approximately three times lower than that of the Isuzu diesel benchmark, on a per-mile basis. These findings are summarized in Figure IV-118.

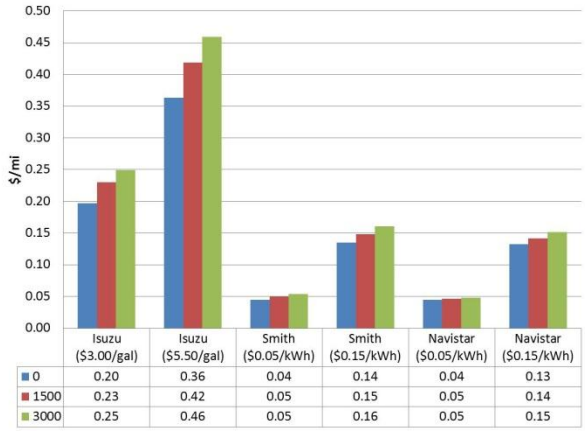

Figure IV-118: Cost-per-mile summary for Isuzu, Smith, and Navistar vehicles. Low and high energy costs are calculated for baseline weight, +1500 lb., and +3000 lb.

Estimations of the impact on energy consumption of utilizing the heater under 20°F conditions suggest a 38% increase in consumption. This is on the order of the increase observed for the Navistar EV. Utilizing the A/C unit (95°F simulated operation) increased energy consumption by 2.6%. Use of the high-voltage pack heater, as in the Navistar case, resulted in a significant increase in energy consumption. However, because the powertrain exhibits slightly higher efficiencies at the 95°F temperature (as estimated from the Navistar findings), the losses attributable to use of the A/C unit are not nearly as severe.

In Figure IV-119, the Isuzu Reach fuel cost per mile over three vehicle weights is averaged over the three-day-averaged NYC cycle data. Results for the Isuzu were calculated at 70°F only (no cold or hot tests were completed). Costs are shown in dollars per mile for fuel costs ranging from $3 to $5.50 per gallon. It may be seen that with the baseline payload, costs range from $0.20 to $0.36 per mile, depending upon the cost

of fuel. At full payload (+3000 lb.), costs range from $0.25 to $0.46 per mile.

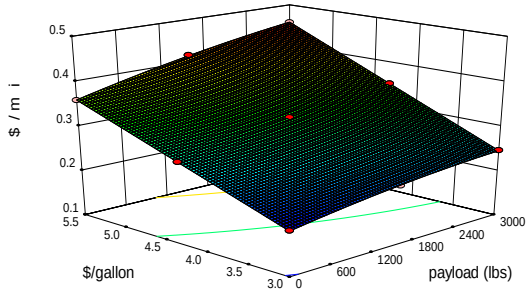

Figure IV-119: Isuzu cost per mile vs. vehicle payload, based on three-day-averaged NYC drive-cycle data. Results are shown for 70°F tests only. Fuel costs range from $3 to $5.50/gallon.

For comparison, Figure IV-120 and Figure IV-121 display the cost of the Smith and Navistar EVs with the identical payload weight and with energy costs ranging from $0.05 to $0.15 per kilowatt-hour. Figure IV-120 shows that with the baseline payload, costs for the Smith EV range from $0.045 to $0.135 per mile, depending upon the cost of energy. At full payload (+3000 lb.), costs range from $0.054 to $0.161 per mile. Figure IV-120 shows that with the baseline payload, costs for the Navistar EV range from $0.045 to $0.132 per mile, depending upon the cost of energy. At full payload (+3000 lb.), costs range from $0.048 to $0.152 per mile.

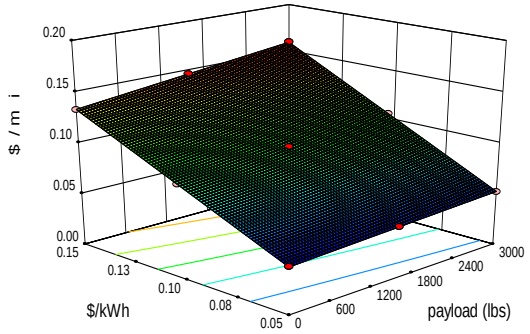

Figure IV-120: Smith EV cost per mile vs. vehicle payload, based on three-day-averaged NYC drive-cycle data. Results are shown for 70°F tests only. Energy costs range from $0.05 to $0.15/kWh.

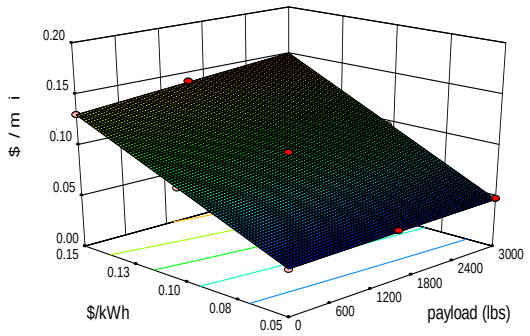

Figure IV-121: Navistar EV cost per mile vs. vehicle payload, based on three-day-averaged NYC drive-cycle data. Results are shown for 70°F tests only. Energy costs range from $0.05 to $0.15/kWh.

Figure IV-122 shows the cost-per-mile ratio of the Smith EV over the Navistar EV. This ratio is calculated to demonstrate the cost-per-mile advantage of the Navistar EV over the Smith EV, accounting for the energy cost per mile alone. Figure IV-122 shows that the Navistar EV exhibits a 2–12% reduction in cost per mile, depending upon the vehicle loading and cost of energy. The Navistar EV exhibits greater reductions in cost as the payload increases.

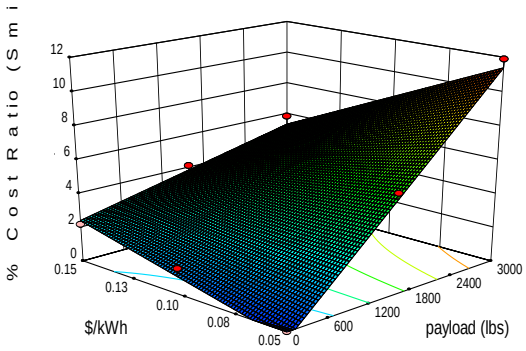

Figure IV-122: Smith/Navistar EV cost-per-mile ratio (cost in $/kWh) vs. vehicle payload, based on three-day-averaged NYC drive-cycle data. Results are shown for 70°F only. Plot is the ratio of cost-per-mile data from Figure IV-120 to those from Figure IV-121.

Comparisons of Energy Cost versus Ambient Temperature

An analysis of the temperature effects is shown in Figure IV-123. For all calculations involving temperature, the medium payload of +1500 lb. was selected for analysis. Additionally, the surface plots here assume smooth transitions in cost per mile relative to temperature and climate control settings. Although the actual behavior may involve some step changes, this assumption was applied consistently between the vehicles, so the comparison remains accurate.

Figure IV-123 shows that cost for the Smith EV range from $0.049 to $0.187 per mile, depending upon the cost of energy and the ambient temperature.

Figure IV-124 shows that cost for the Navistar EV range from $0.049 to $0.192 per mile.

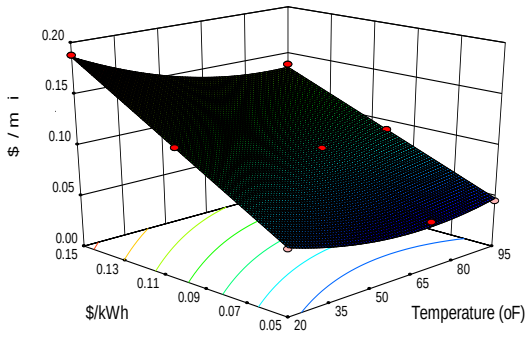

Figure IV-123: Smith EV cost per mile vs. temperature, based on three-day-averaged NYC drive-cycle data. Results are shown for +1500-lb payload only. Energy costs range from $0.05 to $0.15/kWh.

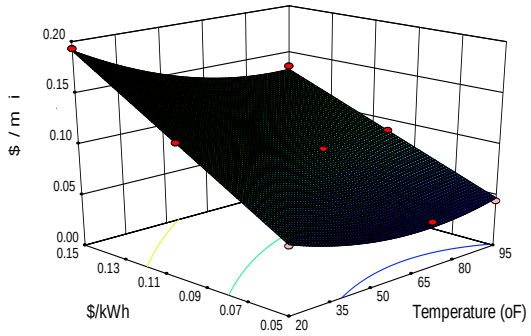

Figure IV-124: Navistar EV cost per mile vs. temperature, based on three-day-averaged NYC drive-cycle data. Results are shown for +1500-lb payload only. Energy costs range from $0.05 to $0.15/kWh.

The ratio of cost per mile for the Smith EV vs. the Navistar EV, shown in Figure IV-125, was calculated to demonstrate the cost-per-mile advantage of either EV relative to the energy cost per mile alone. From Figure IV-125, it may be seen that there is no particular advantage: the two vehicles' costs are within ~2% of each other, depending upon ambient temperature conditions.

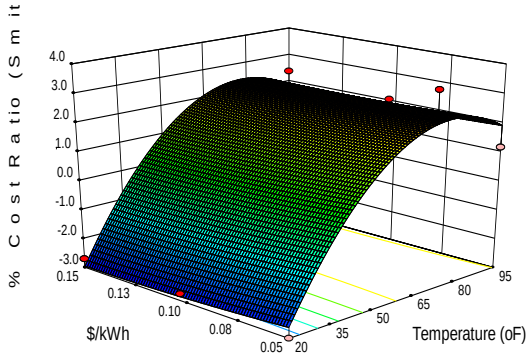

Figure IV-125: Smith/Navistar EV cost-per-mile ratio (cost in $/kWh) vs. ambient temperature, based on three-day-averaged NYC drive-cycle data. Results are shown for +1500-lb payload only.

Conclusions

Three FedEx delivery vehicles were benchmarked and tested against one another to determine the relative energy usage and cost on the basis of NYC drive-cycle data supplied by FedEx. The three vehicles tested were an Isuzu Reach diesel, a Navistar eStar EV, and a Smith Newton EV.

Comparison of EV Delivery Truck Energy Consumption

In Figure IV-126, the average energy consumption of the Navistar and Smith EVs during the three-day NYC cycle is shown across three vehicle payloads: baseline, +1500 lb., and +3000 lb. GVW. Based on these comparisons it can be determined that the Smith EV, on average, consumes 5% more energy per mile than the Navistar EV. These results are calculated at a 70°F ambient temperature.

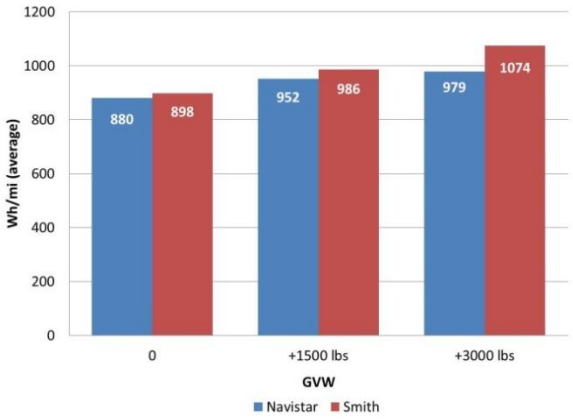

Figure IV-126: NYC 3-day average energy consumption for Navistar EV vs. Smith EV. (Results are shown at 70°F only.)

Figure IV-127 shows the amount of braking regeneration across the vehicle payloads [Note: brake regeneration % here is defined as the ratio of energy into the battery pack, or energy from braking, divided by the energy out, or positive tractive effort]. Although the Smith EV consumes 17% more energy averaged over the three days of NYC cycle data, brake regeneration for the Smith EV is on the order of 20% for all payloads, whereas the Navistar EV only regenerates 15%. This increase in braking regeneration efficiency exhibited by the Smith EV offsets some of its overall energy consumption.

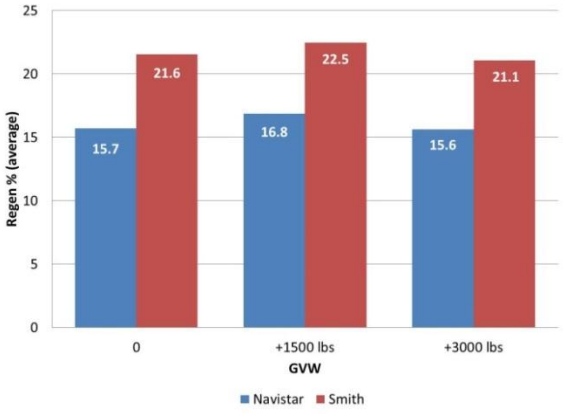

Figure IV-127: Energy regeneration during braking averaged over three days of NYC drive-cycle data, for three vehicle payloads.

Comparison of Ambient Temperature Impact on Energy Consumption

To determine energy consumption at various ambient temperatures, modeling of the vehicles averaged over the three days of NYC cycle data at 20°F, 70°F, and 95°F using the heater and A/C units was conducted. For the Navistar EV, the energy required to charge and run the A/C unit was added to the calculation, as the unit derives its energy from a separate battery from the propulsion system. The Smith EV's A/C energy came directly from the high-voltage battery pack. The energy consumption of the two EVs as a function of ambient temperature is shown in Figure IV-128. Data are shown for the +1500-lb weight only. Variation in energy consumption at different ambient temperatures at the three payload weights is expected to be similar in magnitude to the data shown.

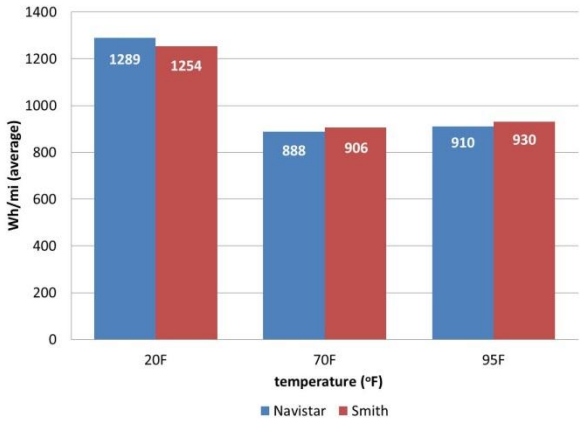

Figure IV-128: Average energy consumption over NYC three-day drive cycle as a function of ambient temperature.

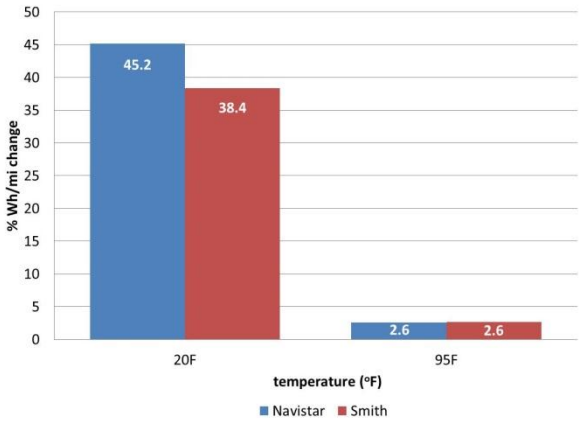

Figure IV-129: Three-day-averaged NYC drive-cycle data on energy consumption at 20°F and 95°F compared to 70°F data.

Figure IV-129 summarizes the 20°F and 95°F energy consumption data as a percentage increase relative to the 70°F data. On average, the Navistar EV's energy consumption increased by 45% during use of the heater at cold temperatures (full heater setting), whereas the Smith EV's energy use increased by 38%. Both vehicles increased energy consumption by nearly 3% when using the air conditioning.

Data used for Figure IV-128 and Figure IV-129 show that the Smith EV consumes 2.7% less energy than the Navistar EV at the 20°F ambient temperature; however, the Smith EV consumes more energy at 70°F and 95°F ambient temperatures than the Navistar EV (2.0% and 2.2%, respectively).

IV.H.3. Products

Publications

1. Forrest Jehlik, Glenn Keller, Kevin Stutenberg, and Craig Pavlich (2013), *Vehicle Testing of Electric-Powered Delivery Trucks for FedEx*, report delivered to FedEx.

IV.I. Medium and Heavy Duty Field Testing

Kevin Walkowicz, Principal Investigator
National Renewable Energy Laboratory
15301 Denver West Parkway
Golden, CO 80401
Phone: (303) 275-4492
E-mail: Kevin.Walkowicz@nrel.gov

Lee Slezak, DOE Program Manager
Phone: (202) 586-2335
E-mail: Lee.Slezak@ee.doe.gov

IV.I.1. Abstract

Objectives

- The main goal of this project is to test and/or validate advanced propulsion technologies in medium- and heavy-duty (MD & HD) applications and to provide data from this activity to help facilitate transitioning these vehicles from the research and development (R&D)/prototype stage into the marketplace. This will be accomplished by means of the following:
  - Testing and analyzing near-term advanced technologies in vehicles and comparing them with conventional technologies in vehicles in similar service.
  - Providing data and feedback to the R&D community (including other offices and programs within the U.S. Department of Energy [DOE]) to guide technology development that will lead to fuel-saving commercial products.
  - Providing potential vehicle customers and original equipment manufacturers (OEMs) with the unbiased, accurate data and analysis they need to make informed decisions on advanced-technology vehicle purchases and fleet implementation.

Major Accomplishments

- Completed a 6-month field evaluation in Ontario, California, and a Renewable Fuels and Lubricants (ReFUEL) research laboratory test to evaluate HEV Class 7 box trucks. Results to date are included in this report. An SAE paper was published at SAE's Commercial Vehicle Engineering Congress (COMVEC) in October 2013.
- Completed an effort to collect field data in New York and California on Class 3 and 4 light aerial hybrid electric vehicle (HEV) bucket trucks. The effort was focused on drive-cycle and aerial device duty cycle analysis as well as assessing deployment options for HEV drivetrains.
- Completed an effort to collect field data in California on class 7 delivery trucks to help Paccar define the usage requirements for a microturbine series hybrid powertrain system for this application.
- Initiated effort to study hydraulic hybrids in service with United Parcel Service (UPS) in Baltimore, Maryland. Field data collection is underway, and ReFUEL laboratory testing is scheduled for October 2013.
- Initiated effort to study Smith electric vehicles in service with Frito-Lay in Federal Way, Washington. This evaluation will utilize data obtained from Smith Electric Vehicle Company and compare the operation of new deployed EVs to that of their diesel counterparts in Federal Way, Washington. Operational data from the diesel trucks as well as facility and charging infrastructure will be collected and analyzed. A detailed battery degradation testing and analysis effort to quantify expected battery life versus usage and environment is also being completed as part of this project.

✧ ✧ ✧ ✧ ✧

IV.I.2. Technical Discussion

Background

The DOE funds many projects to develop components and subsystems for advanced vehicles. Testing, validating, and providing data on the real-world service performance of these technologies, as well as others not funded by DOE, are necessary to help transition the technology into widespread use in the marketplace. To accomplish this, DOE and industry need a process to document testing, validation, and benchmarking of the advanced technologies to provide this data from an unbiased party. The information provided by this project is vital to OEMs to identify areas of improvement and to fleets to aid them in making purchase decisions that will be appropriate for the vehicle application. DOE can also utilize this information to help identify future R&D opportunities.

Approach—General

This project will cooperate with fleet and/or OEM partners to select, test, and validate advanced technologies in commercial vehicle applications. Specific technologies will be selected based on (1) their potential for reducing fuel consumption, (2) their potential for widespread commercialization, and (3) interest at DOE (including the 21st Century Truck Partnership and other DOE programs). Once a technology area has been identified, NREL will collect vehicle data on system performance, maintenance (if applicable), and/or operational costs relative to the new technology. The data will be analyzed and sent back to DOE and the project teams, and its potential for improvement in real-world service will be compared to baseline data, if a comparable conventional technology vehicle is available.

The approach for the FY 2013 medium- and heavy-duty field evaluation projects includes:

- Working cooperatively with commercial fleets to collect operational, performance, and cost data for advanced technologies
- Characterizing vehicle drive/duty cycles
- Analyzing performance and cost data over a period of 6 months to 1 year or more
- Testing and analyzing in-use performance of advanced technologies in a laboratory setting to duplicate observed real-world conditions
- Producing fact sheets and reports on advanced heavy-duty vehicles in service
- Providing updates on new, advanced technologies to DOE and other interested organizations as needed.

HEV Straight Truck—Ontario, California, 6-Month Fleet Study

Background

FedEx Express recently deployed new hybrid electric vehicles (HEVs) and conventional diesel powertrain Class 7 straight trucks into their fleets in California. The National Renewable Energy Laboratory (NREL) worked in conjunction with FedEx Express to perform an in-use field and dynamometer evaluation of many of these vehicles. The field evaluation took place in Ontario, California, and the dynamometer testing was performed at NREL's ReFUEL research laboratory in Denver, Colorado. The study compared fuel economy and emissions of modern heavy-duty diesel HEVs (hybrid system manufactured by Eaton Corporation) and equivalent conventional diesel vehicles. A technical paper was also submitted to SAE for this study, SAE 2013-01-2468.

Introduction

In-Use Field Evaluation

The Ontario, California, FedEx Express fleet included 2010 Freightliner M2-106 Class 7 straight trucks that met the criteria of the targeted testing in this program which included having a 2010 certification level engine. 2010 certified diesel engine vehicles have exhaust aftertreatment technology including diesel oxidation catalysts (DOCs), diesel particulate filters (DPFs), and selective catalytic reduction (SCR) systems on the exhaust. The Ontario fleet also initially included one diesel-powered 2010 certified HEV of the same make and model-type as the conventional trucks, see Figure IV-130. Ontario was selected as an ideal location for this evaluation as the fleet there operates over duty cycles that were thought to be targeted for HEV use.

Figure IV-130: HEV Freightliner straight truck (Source: Jonathan Burton, NREL).

Approach

Isaac Instruments DRU900/908 data loggers were deployed on 12 of the original Ontario vehicles in the fleet, including the 1 HEV and 11 conventionals, for 3 weeks initially. The recorders logged a total of 52 channels of data as the FedEx Express drivers drove their usual daily routes. Some of the recorded data parameters were global positioning system (GPS) data and J1939 controller area network (CAN) bus communication data including parameters such as accelerator position, engine speed, engine load, vehicle speed, diesel aftertreatment conditions, transmission gear and shaft speeds, and vehicle temperatures and pressures. This initial field data collection set primarily focused on establishing baseline vehicle operation, route assessment and vehicle fuel consumption of the conventional vehicles.

After the initial 3-week evaluation was performed on the conventional vehicles, five Freightliner M2-106s HEVs were transferred to Ontario from another FedEx Express California location, for a total of six HEVs in the Ontario, CA fleet. These six HEVs, in addition to six equivalent conventional diesel vehicles of the same make and model, were included in a 6-month performance evaluation. The drivers of these 12 vehicles were asked to complete fuel logs so that fuel economy comparisons could be made for the entire 6 months. Other maintenance records for vehicles included in the study were kept as well. Also, during the 6-month study period, one conventional vehicle and one HEV recorded J1939 data with the data loggers. The results of the in-use field evaluation are presented later in this report.

Laboratory Fuel Economy and Emissions Testing

Two of the FedEx Express straight truck vehicles were tested on the heavy-duty chassis dynamometer at NREL's ReFUEL research laboratory. One of the vehicles had a conventional diesel powertrain while the other had a diesel HEV powertrain. Both test vehicles were loaded with 6,500 lbs. payload, which is approximately half the maximum capacity payload. This payload would be very typical for loads seen by these trucks on a daily basis.

Test Cycle Selection

NREL's Drive-cycle Rapid Investigation, Visualization, and Evaluation (DRIVE™) analysis tool was used to filter and analyze the initial 3 weeks of field data collected as part of the study. Examining drive cycle metrics including average driving speed, stops per mile, kinetic intensity and others, a highly representative set of chassis dynamometer test cycles was chosen to highlight shortcomings and advantages of the HEV under varying in-use duty cycles. The cycles selected were the New York Composite (NYComp), which represents the "most urban" or low speed cycle; the Hybrid Truck Users Forum Class 6 (HTUF 6), which represents the most "mean" cycle observed in operation; and the California Air Resources Board (CARB) Heavy Heavy-Duty Diesel Truck (HHDDT), which represents the highest speed cycle observed in operation.

Results: On-Road & In-Lab Fuel Economy

Laboratory Fuel Economy Results

Fuel economy results from the dynamometer tests are shown in Figure IV-131. The fuel economy of the HEV increased by 45% over the conventional when tested on the NYComp drive cycle and increased by 33% when tested on the HTUF 6 drive cycle. Both of those cycles have sections that generally are beneficial for regenerative systems. However, when operating on the HHDDT drive cycle, the HEV consumed 4% more fuel than the conventional vehicle. This data was published in the SAE technical paper SAE referred to earlier. It should be noted that the fuel economy percent differences used in the SAE paper were calculated with the HEV as the baseline for the comparison. This report uses the conventional vehicle as the baseline for that same calculation, which is the standard procedure. As a consequence, the resulting values for changed percent are different between these two reports; however actual test result values shown are the same.

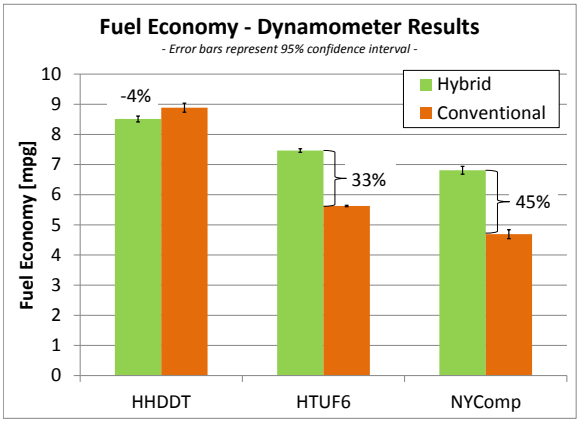

Figure IV-131: Fuel economy for chassis dynamometer testing of both the HEV and conventional vehicles.

Laboratory NO_x Emission Results

The HEV showed increased NO_x emissions for two out of the three drive cycles, as seen in Figure IV-132. The HTUF 6 cycle showed no measureable difference in NO_x emissions, whereas the HEV had higher NO_x emissions for both other cycles: 77% higher on the NYComp cycle and 46% higher on the HHDDT. Both vehicles had a NO_x FEL of 0.33 g/bhphr. The HEV's diesel engine was originally marked as a Cummins ISL200 manufactured in 2009 with a NO_x FEL of 0.40 g/bhphr; however, the engine calibrations of the HEVs were changed after delivery to FedEx Express to a rating of 250 HP and a 0.33 g/bhphr FEL rating.

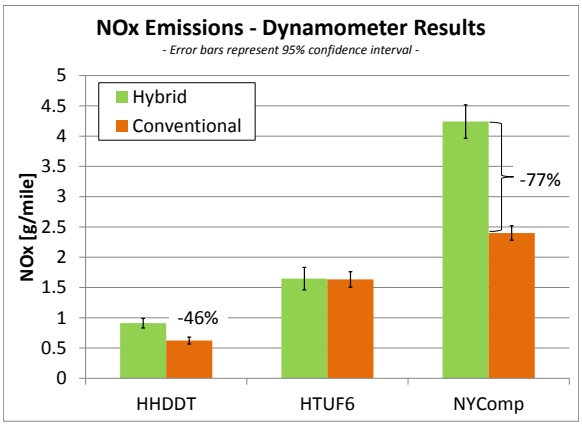

Figure IV-132: NO_x emission for chassis dynamometer testing of both the HEV and conventional vehicles.

Maximum Acceleration

Both vehicles were tested for maximum acceleration rates with a simulated 6,500-lb. payload (≈50% maximum payload) on the chassis dynamometer. Figure IV-133 shows that the HEV was slower than the conventional vehicle to accelerate up to highway speeds. The conventional vehicle accelerates to 50 mph approximately 12 seconds (20%) faster on average than the HEV. The HEV uses an automatic shifting manual transmission, whereas the conventional vehicle has a fully automatic transmission. The calibrations of the HEV transmissions were changed to a "performance" shifting mode by the manufacturer to improve overall acceleration after FedEx Express took delivery of the vehicles.

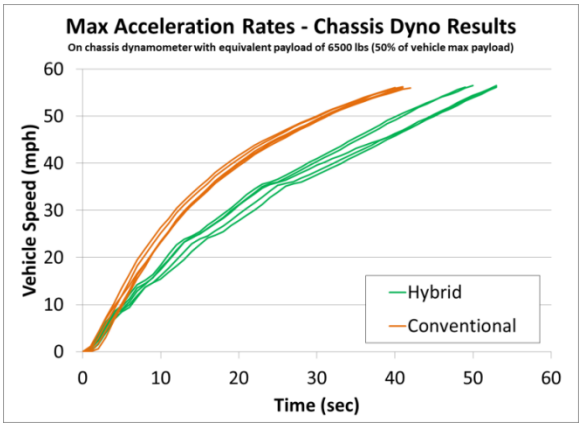

Figure IV-133: Maximum acceleration rates for both the HEV and the conventional vehicle on the chassis dynamometer. Both vehicles' payloads were simulated to 6,500 lbs., which is 50% of the maximum payload.

On-Road Data Collection and Comparison to Laboratory Results

The evaluation of the in-use field study contained data from the initial 3-week assessment on 12 vehicles, with only 1 HEV, for drive-cycle analysis. The 6-month data recording period following that included 6 HEVs and 6 conventional diesel vehicles logging fueling records and 1 HEV and 1 conventional vehicle continuing to log data.

Figure IV-134 shows the fuel economy results for all the data from this entire study, including the chassis dynamometer results, plotted against KI. The HEVs tend to have better fuel economy advantages at higher KIs because a higher KI is more representative of a stop-and-go type drive cycle, which allows more electric regenerative braking to occur on the HEVs. This is quite evident in Figure IV-134, where both of the higher KI drive cycles from the chassis testing show fuel economy improvements from the HEV. The driver recorded fuel logs showed an average HEV fuel economy advantage of 12% while the data from the data loggers indicated the HEVs had a 17% fuel economy improvement over the conventional vehicles.

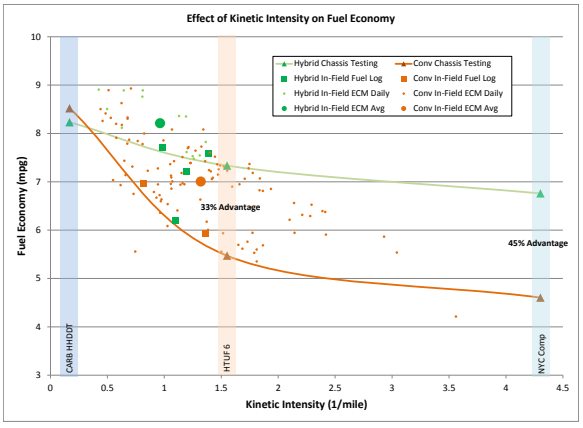

Figure IV-134: Effect of KI on vehicle fuel economy for both in-use field evaluation and chassis dynamometer results.

Conclusions

A 6-month in-use HEV field evaluation was carried out to compare the potential performance improvements of a heavy-duty HEV vs. a conventional diesel truck. The results were:

- Field data indicate that the HEVs had 12% to 17% better fuel economy than the conventional vehicles when driven over a variety of routes
- Data from the vehicles driven on three drive cycles on a heavy-duty chassis dynamometer found:
  - The HEV had 31% better fuel economy on the NYComp drive cycle, 45% better fuel economy on the HTUF 6 drive cycle and 4% worse fuel economy on the HHDDT cycle when compared to the conventional vehicle. This data shows that improvements in fuel economy are possible if vehicles are placed on more ideal routes than the routes observed for the 6 month evaluation
  - The HEV emitted more NOx than the conventional vehicle over two drive cycles which were representative of some of the driving observed in the field. Emissions were 77% higher on the NYComp cycle and 45% higher on the HHDDT. There was no difference in NOx emissions on the HTUF 6 cycle which was representative of the most typical driving observed in the field.
  - The conventional vehicle reached highway speeds approximately 10 seconds (20%) faster than the HEV when tested for maximum acceleration rates.

Additional data on this study can be found at: http://www.nrel.gov/vehiclesandfuels/fleettest/.

Telecom Fleet Data Collection and Evaluation

Background

This study was conducted to help understand possible applications for HEV drivetrains and electrified bucket operations in a telecom fleet. Two types of vehicles will be studied including Class 3-4 'light aerials' as well as class 2b service vans. Operational drive cycle data was collected as well as bucket duty cycle information. The results are shown here and will help telecom companies understand possible applications of advanced technology in this type of fleet.

Introduction & Approach

A total of 36 telecom van and light aerial vehicles in the Long Island (Bohemia), New York, and Los Angeles (Irwindale), California, areas were equipped with data loggers for 2 to 3 weeks each to collect GPS duty cycle data, resulting in data collection from 351 operational days and over 9,600 miles of driving. Vans were '07-'11 Chevrolet G2500's while light aerials were '06-'12 Ford F350's and '05 Chevrolet C4500's. Light aerial vehicles were also equipped with sensors to detect and record "genset on" condition and "boom out of rest" (B.O.O.R.) condition.

Results

Vehicle Usage (Drive Cycle)

Fifty non-operational days were recorded but removed from the analysis because the vehicles were used (engine started) but never reached a speed of 15 mph and therefore had very low miles driven. Even with this purge, 38 operational days (11% of the data) were vehicles that drove fewer than 10 miles, and on 29 of those 38 days (8% of total data) the vehicles drove fewer than 5 miles. Because the vehicles did achieve road speeds on these 38 days and their calculated operational hours were also more than an incidental yard operation, they have been included in the analysis as representing real operational days. Furthermore, on 201 operational days (57% of total), the vehicle drove fewer than 30 miles indicating that low daily miles is normal for these vehicles. The duration of time spent working at a job site dominates the operational day, not driving to and from those sites.

Figure IV-135 compares kinetic intensity and driving distance for all operational days recorded at both locations. Note that at almost all points with a kinetic intensity greater than 3, the vehicle drove fewer than 5 miles. In general, in order to provide a beneficial payback period to the operator (to pay for the added cost of a hybrid system), a vehicle should both have a kinetically intense driving cycle (to utilize the regenerative braking of a typical hybrid system) and drive enough miles for potential fuel savings to pay off. Figure IV-135 shows most vehicle days do not have the combination of high KI and high miles per day for payback of the incremental cost of a hybrid system. Also note that vans and bucket trucks at both locations drive similar daily miles and KI range indicating they are not used in significantly different ways and can be considered together regarding drive cycle analysis.

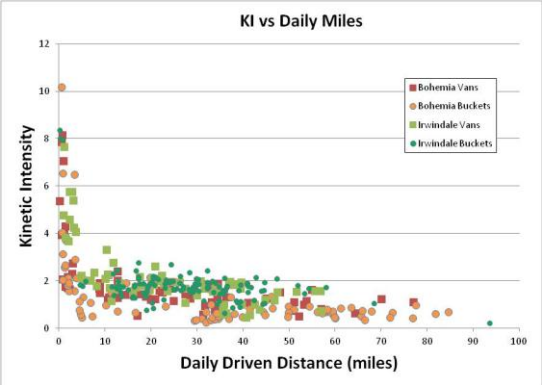

Figure IV-135: Kinetic intensity vs. daily driving distance.

Figure IV-136 shows the daily distance driven of the vehicles at both locations. On 49% of operational days, the vehicles drove 25 or fewer miles, which is not ideal for hybrid electric vehicle or electric vehicle payback because the vehicles are not consuming enough fuel to offset the incremental cost of the technologies.

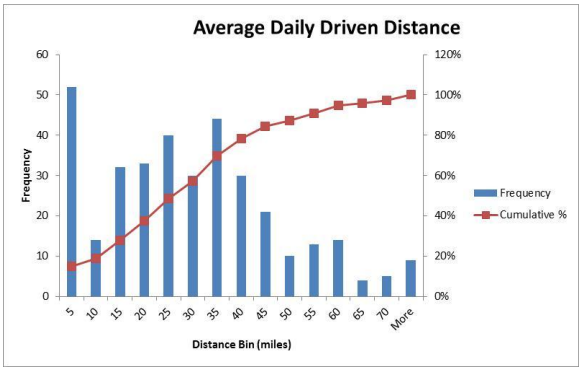

Figure IV-136: Average daily driven distance.

Boom Operation (Aerial Device)

Figure IV-137 shows the hours per day that the light aerials had their boom out of rest (B.O.O.R.) or in use. The light aerials used their buckets on 55% of the observed operational days, but for a very short overall time—usage time was less than an hour 73% of the time. As such, the generator sets that are used to power the aerial devices are used substantially less than an hour a day as well, reducing the opportunity for savings from electrifying the generator system as part of a hybrid system.

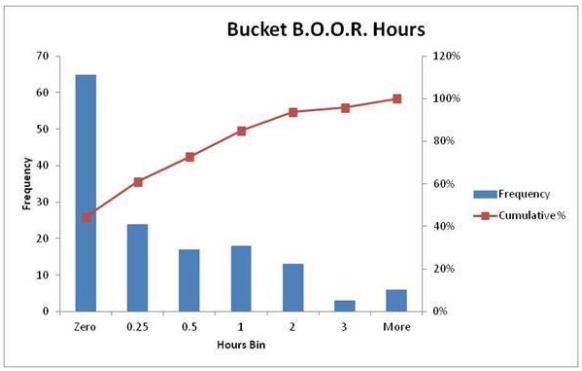

Figure IV-137: B.O.O.R. hours per day.

Conclusions

These vehicles do not appear to be suited for adoption of hybrid electric vehicle drivetrain technology or plug in vehicle technology. Both types of vehicles have demonstrated low kinetic intensity, and they operate too few miles per day to provide a payback of the additional technology cost within a reasonable amount of time. Furthermore, the aerial devices on the class 3-4 vehicles are used too little time per day (73% are used 1 hr or less) to benefit from electrification of that subsystem.

Paccar Fleet Evaluation

Background

This study was conducted in partnership with Paccar Incorporated to help understand possible applications for microturbine drivetrains in a class 7 'box truck'. Operational drive cycle data was collected as well as fuel use information. Drive cycle estimations and fuel use for study trucks were completed. The results are shown here and will help delivery and cargo freight companies understand possible applications of advanced technology in this type of fleet.

Introduction

A total of 10 Class 7, single-axle straight delivery trucks serving a major consumer goods retailer in the Los Angeles, California, area were equipped with data loggers for 2.5 weeks, resulting in data collection from 99 operational days and over 9,300 miles of driving. Paccar, Inc., is currently engineering a microturbine series hybrid powertrain for this application, and NREL's drive cycle expertise was utilized to collect data and help define the usage requirements for the system. Data from these Class 7 trucks were also added into the Fleet DNA database.

Approach

Drive Cycle Breakdown

Figure IV-138 is a histogram of miles travelled per day, which shows that about 31% of the days were in the 50–100 mile-per-day range and 41% of days had over 100 miles driven. Because of this wide spread, the vehicles were split into two groups based on miles driven per day. One duty cycle would not adequately cover this range of usage.

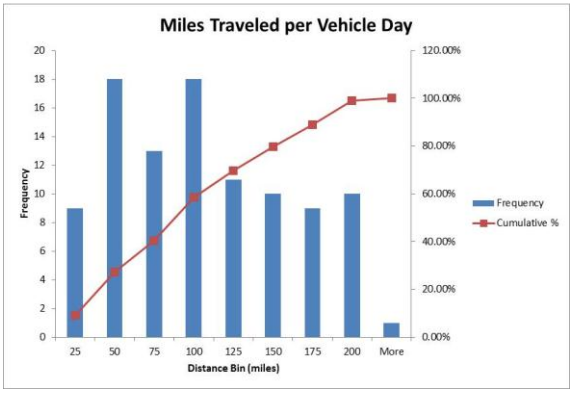

Figure IV-138: Daily miles traveled.

Figure IV-139 shows the mph bins where those miles are driven, most of which are at highway speeds; however there is a significant hump in the 25–40 mph zone indicating some of the vehicles spend significant time driving on surface streets.

Figure IV-139: Miles traveled by speed.

Figure IV-140 and Figure IV-141 demonstrate why the vehicle days were split into two groups (divided at a value of 60 miles per day). First, each individual vehicle travels a relatively consistent number of miles per day, which means it is running a particular assigned route. Four vehicles are shown as ID 3, 4, 13 and 20 and show relatively stable miles per day in Figure IV-140 (below 60 mph). Five vehicles are shown as ID 1, 6, 18, 21 and 22 and show reasonably stable miles per day in Figure IV-141 (above 60 mph).

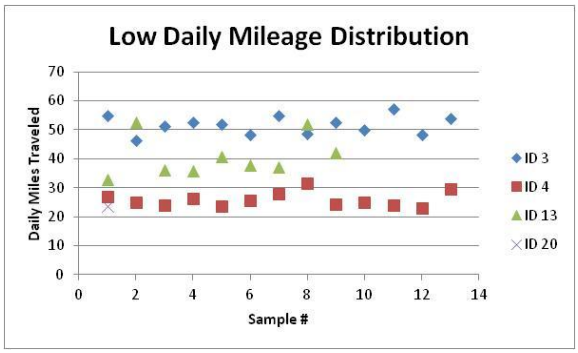

Figure IV-140: Low-mileage (< 60 miles) distribution group.

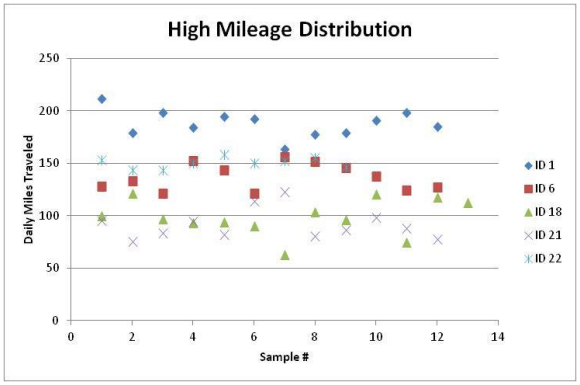

Figure IV-141: High-mileage (>60 miles per day) distribution group.

Figure IV-142, Figure IV-143, and Figure IV-144 show three representative cycles generated using NREL's DRIVE™ tool from the collected duty-cycle data. Figure IV-142 is an average of all days collected; it has a 92% performance match to the complete collected data set. Figure IV-143 is an average of all days with fewer than 60 miles per vehicle day collected; it has a 90% performance match to those days. Figure IV-144 is an average of all days with more than 60 miles per vehicle day collected; it has a 93% performance match to those days. These cycles will be used for vehicle testing on a chassis dynamometer or to design and test models of a conventional vehicle and a microturbine-powered vehicle to examine performance differences and system requirements.

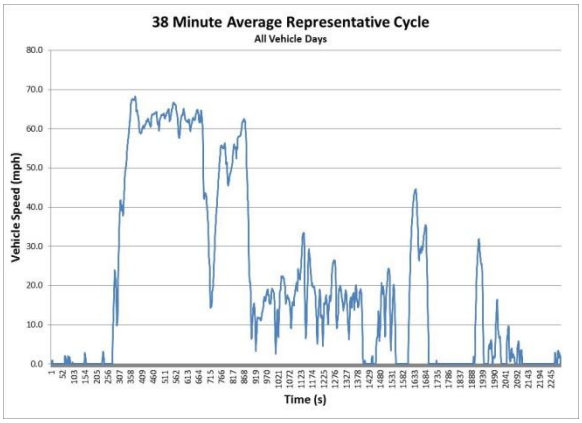

Figure IV-142: Representative cycle.

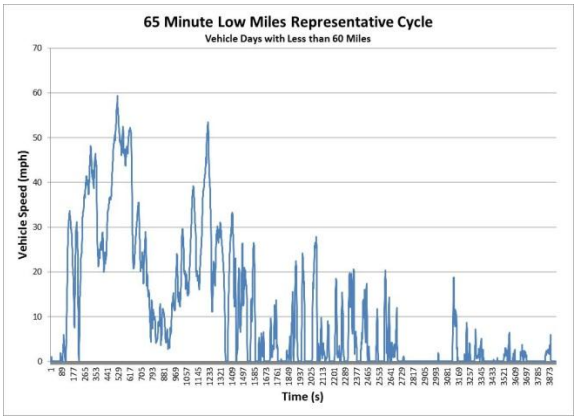

Figure IV-143: Low daily miles representative cycle.

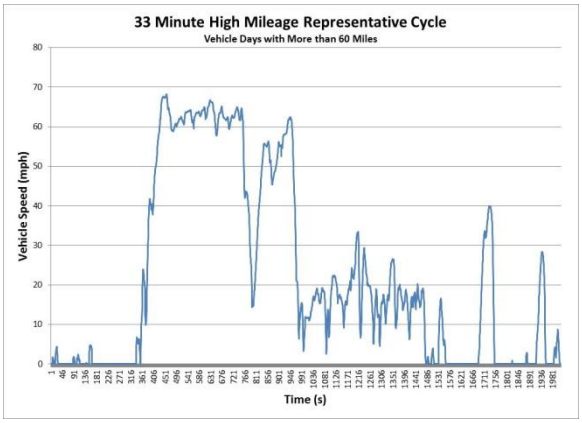

Figure IV-144: High daily miles representative cycle.

Fuel Economy Data

Figure IV-145 shows daily mpg as calculated from J1939-recorded fuel rates. Data from one vehicle was omitted from the 10 truck set in this analysis due to improperly reported fuel rate. The grouping of higher mpg days (near 10 mpg) correlates to the very high mileage days.

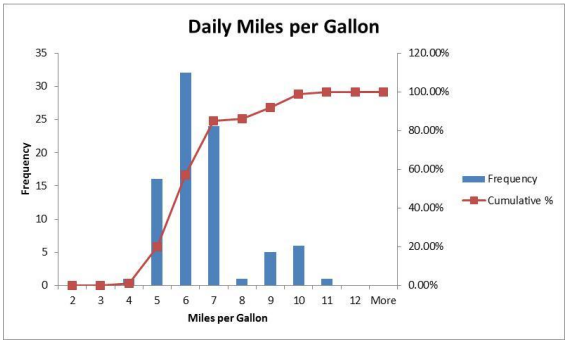

Figure IV-145: Daily mpg.

Results & Conclusions

The detailed data and corresponding analysis are currently being used by Paccar and its microturbine supplier to model and design its microturbine series hybrid for this application. Continued communication with Paccar on the subject verifies the value this data collection and duty cycle analysis has to them.

UPS Hydraulic Hybrid Case Study

Background

This project discusses an in-use evaluation of 20 MY 2012 Freightliner P10HH hybrid step delivery vans that were placed in service at UPS's facilities in Burtonsville and Baltimore, Maryland, at the end of 2012. The new hydraulic hybrid vans (HHVs) with hydraulic drive systems manufactured by Parker Hannifin, feature an infinite variable transmission and an integrated "engine off at idle" feature. Conventional diesel vans of a similar emissions equipment age are not available for comparison because UPS started using gasoline engines for all non-hybrid delivery vans starting in 2010. This in-use evaluation as well the laboratory testing will be compared to gasoline-powered P100 vans.

Introduction

Host Site Profile—UPS, Burtonsville and Baltimore, Maryland

The host site consists of two large distribution facilities serving the Baltimore area. Twenty HHVs are included in this evaluation, 10 at each facility as well as a set of comparative gasoline powered P100's. UPS assigned the hybrid vans to routes with a mix of highway driving and urban delivery, similar to routes which had also had gasoline vans serving them. Dispatch and maintenance practices were the same for both facilities.

Approach

Laboratory Fuel Economy and Emissions Testing Plan

Two delivery vans were tested on the chassis dynamometer at NREL's ReFUEL research laboratory during October 2013. One was an HHV provided by Parker that is identical to those in service in Baltimore; and one is to be a 2012 UPS gasoline-powered delivery van, which is the actual baseline vehicle UPS is currently buying for use in applications similar to those at Baltimore and Burtonsville. Testing protocol will use SAE J2711 as a general guide but modify as needed to accommodate the specifics of the hydraulic hybrid system.

Testing of each of the vehicles (when received on September 30) will include the following elements:

1. Cargo / Vehicle mass ballasting based on information from UPS regarding average daily load on these vehicles.
2. Coast Down Testing—in order to determine correct dynamometer settings each vehicle will undergo a minimum of 5 instrumented coast down test runs in opposing directions of the same track and produce A, B, and C dynamometer coefficients from the analysis of those runs. Testing and post processing protocol is based off of J2263 and J1263.

3. Test Cycle Selection –drive cycle metrics were examined including average driving speed, stops per mile, kinetic intensity and others, a highly representative set of chassis dynamometer test cycles was chosen to highlight shortcomings and advantages of the HHV under varying in-use duty cycles.
4. Emissions measurements—Emissions results for carbon dioxide (CO_2), total hydrocarbons (THC), carbon monoxide (CO), Oxides of Nitrogen (NOx) and particulate matter (PM) will be measured on at least 4 hot runs following at least 1 warm up run. At the NREL ReFUEL laboratory regulated emissions measurements are performed using procedures consistent with SAE J2711.
5. Fuel economy comparison—fuel consumption will be measured using a gravimetric measurement method on at least 4 hot runs following at least 1 warm up run.
6. Zero to sixty acceleration tests will be performed in both directions on the coast down testing track and on the dynamometer to measure the performance differences between the test vehicles.

Results

Initial Evaluation Results

Van Duty Cycle

Parker installed an on-board datalogging / telemetry system on the HHV vans and shared one month of global positioning system (GPS) and fueling data with NREL. In total, 367 days of hybrid operation in the Baltimore area were evaluated. This data was then compared to vans from a previous UPS HEV study NREL conducted in 2011 in Minneapolis, Minnesota in order to understand usage.

Figure IV-146 shows that the Baltimore HHVs drove similar miles to the Minneapolis HEV and conventional groups for speeds lower than 20 mph but the HHVs drove more miles in the mid-range speed bins (35–50 mph) than both Minneapolis groups (HEV and conventional) so a direct comparison between the UPS HEV vans in Baltimore and Minneapolis would not be accurate due to this duty cycle difference.

Figure IV-147 shows the daily average gallons consumed at different vehicle speeds for the Baltimore HHVs. Sixty-four percent of the fuel was consumed below 30 mph, which is where Parker indicates the hybrid system is most active and would likely result in maximized fuel economy benefits for the vehicles.

UPS delivery vans each have significant “cruise” drives (i.e. the drive from the depot to delivery area), Figure IV-148 shows the HHV duty cycle split into cruise and delivery zones and compared to the Minneapolis HEV and conventional groups. Figure IV-148 shows KI vs. average driving speed. While the cruise behavior of the HHVs is similar to the Minneapolis study groups, the delivery sections of the HHVs have notably lower KI than the Minneapolis groups.

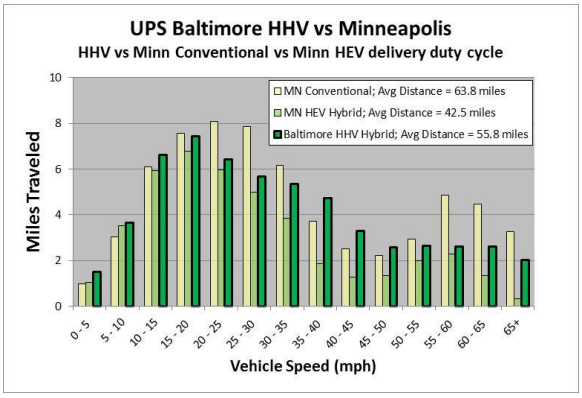

Figure IV-146: Baltimore hydraulic hybrid and Minneapolis HEV and conventional duty cycle breakdown by miles travelled.

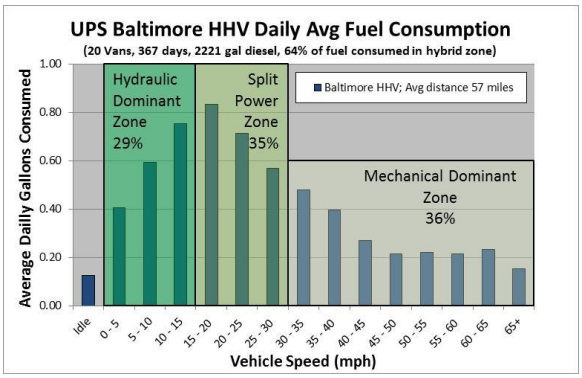

Figure IV-147: Baltimore hydraulic hybrid fuel consumed breakdown.

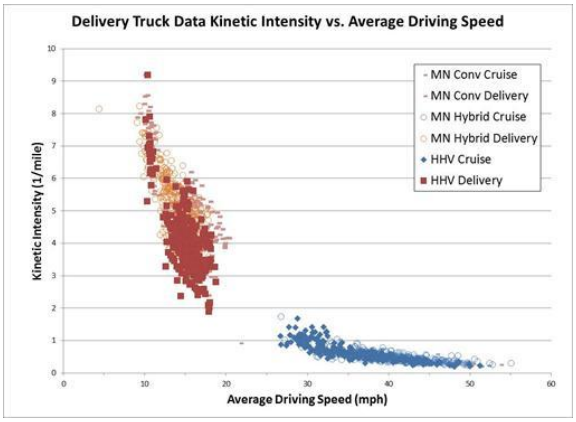

Figure IV-148: Baltimore HHVs and Minneapolis HEVs and conventional cruise and delivery analysis by KI.

Test Cycle Selection—Results

Figure IV-149 illustrates the selected test cycles for dynamometer testing. These results used the data from the 367 days of operation to characterize the present usage of the Parker HHVs. Note how the HHDDT, City Suburban Heavy Vehicle Cycle (CSHVC), and NYC Comp cycles bracket the range of observed daily in-use field data well on both the X and Y axes.

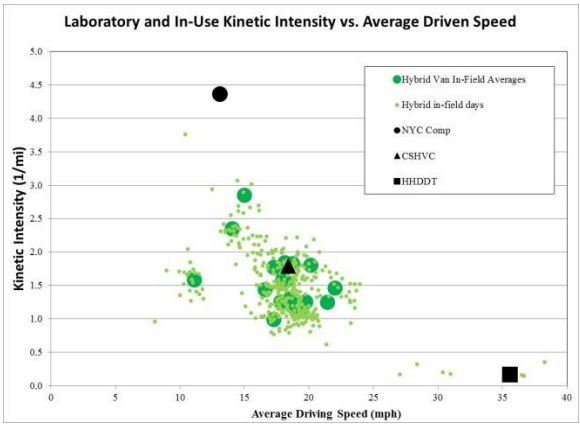

Figure IV-149: Average driving speed and KI comparison.

Conclusions

Still in process at the time of this report was the testing to compare the conventional vs the HHV vans. This testing will compare fuel economy, emissions and performance between the two types of vehicles. Drive cycle analysis has shown that the 'best' representative drive cycles were the NYCC, CSHVC and the HHDDT. These cycles 'bracket' the data observed in the field. The data collected also shows the 'stem' and 'delivery' modes of the data similar to other delivery van drive cycle characteristics observed in other studies.

Frito-Lay North America Plug-in Electric Delivery Truck Case Study

Background

Previous testing and analysis conducted by NREL has illustrated the influence of drive cycle and vehicle usage on both energy consumption (from liquid fuels and high-voltage hybrid battery packs) and exhaust (or well-to-wheels) emissions. Drive cycle has also been shown to influence the all-electric range of battery electric vehicles, the charge depleting range of plug-in hybrid electric vehicles, and the potential fuel economy benefit of hybrid electric vehicles. Accordingly, fleet customers can benefit from a further understanding of advanced vehicle technology deployment in order to minimize fuel consumption and emissions. It has also been shown that large scale deployments of EVs in a localized area can lead to power quality and power cost issues.

Introduction

NREL is currently funded by the DOE to collect operational data on Smith Electric Vehicles (Smith) being deployed as part of the American Recovery and Reinvestment Act. Data collected from these vehicles (up to 500, some of which are located at Frito Lay North America [FLNA] facilities) will be used to understand the overall usage and effectiveness of electric vehicles (EVs) in medium-duty commercial fleet facilities and operations and also compare to operations of conventional counterparts in the same location. Through this collaboration with FLNA, NREL hopes to provide a more focused investigation to understand the implementation and performance of medium-duty EVs in a large-scale commercial facility.

Approach

Overall objectives for FY 2013 for this project were to:

- Initiate collaboration among partners, including Smith, FLNA, and Servidyne (FLNA's energy management contractor)
- Adequately scope out all planned testing and data collection activities, then seek approval from each partner
- Collect available data and facilitate acquisition of new data.

Results

Progress to Date

Task 1: Initial Fleet Identification and Selection

During FY 2013, NREL engaged with FLNA and Smith to establish a program to evaluate the performance of plug-in electric delivery vans in direct comparison to comparable conventional vehicles.

Based on the availability of comparable vehicles, NREL and FLNA decided that the FLNA Federal Way, Washington, fleet depot would be the ideal target site for research. NREL has chosen 10 vehicles from the Federal Way Facility as a baseline for data collection and analysis and which will serve as a comparison for the operational performance of the EV trucks. NREL will select the baseline vehicles based on operational usage metrics to be measured using NREL datalogging equipment in late 2013.

Task 2: Initial Route and In-Vehicle Data Collection

To better characterize EV charging and its impact to facility load profiles, NREL conducted several teleconferences with Servidyne, who designed and commissioned charging station energy management systems for FLNA. Servidyne provided details regarding the data acquisition and control capabilities afforded by its products. The system, currently being installed at Federal Way depot, utilizes open building automation protocols and enables near real-time measurement and control. It is the hope of this project to utilize this data at the Federal Way depot and project an optimized charge strategy for FLNA to reduce bills and improve electrical infrastructure reliability. This data will be

combined with Smith telemetry data and conventional vehicle data collection to analyze costs and investigate alternative charging scenarios. NREL will use the vehicle2campus model—originally developed for vehicle-grid integration research of PEVs at Fort Carson—to assess the potential for utility bill reduction and energy management in conjunction with facility energy consumption at the Federal Way depot.

Task 3: 12-Month Fleet Data Collection

The 12-month fleet data collection will utilize FLNA fueling records, FLNA maintenance reports, Servidyne charging records, and the Smith EV database to characterize long-term vehicle performance. This evaluation is planned to start in late 2013. In addition, NREL will test a Smith EV on it ReFUEL dynamometer to characterize energy efficiency during driving cycles observed at the Federal Way facility and also test one of the baseline diesel vehicles to quantify 'typical' diesel fuel consumption and emission characteristics. These data sources will provide NREL with information to accurately predict fuel consumption and emissions benefits of observed usage, predicted optimal situations for placement of EV's, optimal charging strategies and potential battery life based on usage.

Task 4: Battery Life Degradation Study

NREL has worked with Smith to develop a test plan that will facilitate battery degradation analysis. Using these methods will allow NREL to quantify battery pack health and track battery performance changes over life as well as validate battery life assumptions to help develop a fleet business case.

Using NREL-developed battery performance test equipment, NREL has measured battery resistance and capacity at the beginning of the test period and will continue to do so periodically to acquire data and information necessary to evaluate battery life and degradation rate.

Trips to FLNA's Casa Grande, Arizona, and Federal Way, Washington, facilities were completed in September 2013 to collect baseline data on the battery state of health of four Smith delivery trucks (two at each location).

The load bank was shipped to the Arizona and Washington facilities, where it was attached to each vehicle's battery pack, and distinct discharge profiles were run that capture open-circuit and loaded voltages. Data collected from the tests will be fed into lithium-ion battery models to evaluate the cycle-life degradation of the packs. The controlled discharge test was designed to be minimally intrusive to fleet operations. Each test takes less than one day per truck and is conducted without removing the battery pack from the truck. A successful outcome of the project is targeted to be the dissemination of credible multi-year battery performance data to support increased adoption of EVs in commercial fleets.

Figure IV-150 shows the life testing and Figure IV-151 contains an image of the Servidyne EVSE energy management system in the middle of installation—this box contains meters and relays to log data from the EVSE and control the EVSE power limits in near real-time.

Figure IV-150: 4 FLNA delivery trucks at the Federal Way depot.

Figure IV-151: Installation of the EVSE energy management system near the Frito Lay EV parking/charging lot at Federal Way.

Task 5: Chassis Dynamometer Study

As of this report, NREL had not yet contacted a fleet to acquire a Smith EV or inquired with FLNA to acquire a conventional vehicle to be tested at the ReFUEL laboratory. Once task 2 is completed and test profiles are created based upon vehicle field usage then NREL will acquire these vehicles for full testing and analysis to characterize fuel and emissions reductions.

IV.I.3. Products

Publications

1. Burton, Jonathan, et al, '*In-Use and Vehicle Dynamometer Evaluation and Comparison of Class 7 Hybrid Electric and Conventional Diesel Delivery Trucks*', SAE 2013 Commercial Vehicle Engineering Congress. September 2013.

IV.J. Fleet DNA Vocational Database Project

Kevin Walkowicz, NREL Principal Investigator
National Renewable Energy Laboratory
Transportation & Hydrogen Systems Center
15013 Denver West Parkway
Golden, CO 80401
Phone: (303) 275-4492
E-mail: Kevin.Walkowicz@nrel.gov

Oscar Franzese, Ph.D, ORNL Principal Investigator
Oak Ridge National Laboratory
2360 Cherahala Boulevard
Knoxville, TN 37932
Phone: (865) 946-1304
E-mail: franzeseo@ornl.gov

Lee Slezak, DOE Program Manager
Phone: (202) 586-2335
E-mail: Lee.Slezak@ee.doe.gov

IV.J.1. Abstract

NREL Objectives

The primary focus of the Fleet DNA project in FY13 was to expand existing capabilities through improving current processes, adding additional features and data channels to the data collection and storage process, and deploying a full-scale, publicly accessible web interface for the project. In addition to addressing ongoing technical challenges associated with improvements and deployment, it was also the focus of the project during FY13 to extend project visibility and recruit additional partners/data providers who would provide additional support for database development. Primary objectives included:

- Continuing web integration and deployment of database and results
- Collecting additional vehicle data for inclusion into database
- Recruiting additional research partners to enrich the Fleet DNA database with additional datasets (UMTRI, WVU, CALSTART, etc.)
- Continuing the development of road grade and elevation algorithms
- Integrating available DOE computation tools
  - Exploring integration of tools like FASTSim and Autonomie for vehicle modeling
  - Automating custom drive-cycle generation to provide on demand generation from selected datasets using real world data.
- Expanding standard GPS signal collection to include additional information sources such as J1939 CAN bus signals
- Optimizing processing routines and data organization to improve calculation speed and reduce computational overhead.

ORNL Objectives

- Merging the existing ORNL Heavy Truck Duty Cycle (HTDC) and Medium Truck Duty Cycle (MTDC) databases into the Fleet DNA data repository hosted by NREL by:
  - Identifying and standardizing in conjunction with NREL, high priority 1Hz drive cycle data channels (such as speed, elevation, and other necessary data) recognizing DOE and other partner preferences;
  - Filtering and correcting, where feasible and without degradation of the information, the data collected by ORNL for inclusion into the database;
  - Transferring the extracted information into the format required by the Fleet DNA project.
- Providing summary statistics of each the five vocations included in the HTDC and MTDC databases to NREL.
- Providing additional indexing and cataloguing of the information contained in the HTDC and MTDC databases for quick searching and retrieval of specific duty cycles.

NREL Major Accomplishments

- An SAE technical paper “A Statistical Characterization of School Bus Drive Cycles Collected via Onboard Logging Systems,” was developed based on analysis and characterization of data for the school bus vocation. It is to be published at the close of FY13 at the SAE Commercial Vehicles Congress, and will be included in the SAE International Journal of Commercial Vehicles.
- Two records of invention (ROI) were filed at the National Renewable Energy Laboratory (NREL). The first ROI relates to novel analysis methods and database structures that comprise Fleet DNA, and the second concerns the novel road grade filtration and integration methods derived up to FY13 to allow for road grade information to be added into the database.
- Novel 34-page vocation/vehicle-type reports were developed and posted for public consumption via the Fleet DNA website for each of the 8 vehicle vocations within Fleet DNA.
- The Fleet DNA project website was developed and released to the public (www.nrel.gov/fleetdna). The initial Fleet DNA project website houses reports, technical reports, and conference papers for Fleet DNA-related projects, providing additional visibility to DOE projects and their corresponding findings.

- Road grade information from the United States Geologic Survey was integrated into the database, and new road grade analysis capabilities were added to reporting.
- Road type data from the Navteq roads data layer was integrated into Fleet DNA, providing researchers the capability to analyze drive cycle data geospatially and understand vocational road usage.
- Through ongoing data collection efforts and continued work with our existing data partners, researchers were able to significantly increase the overall size of database (currently 7+TB of data, ~400 vehicles, ~5,000 days, +111 million data points) and expand data reporting to the current 8 vocations/vehicle types.

ORNL Major Accomplishments

- Development of a methodology and procedures to correct short segments of the data collected in the HTDC and MTDC projects that contain errors due to short losses of GPS signals, sensor issues, databus issues, and data-collection equipment issues.
- Development of visualization software to quickly display DC characteristics of the files that ORNL included in the Fleet DNA database. This tool was used to visually inspecting the files and assisted in identifying errors that were not corrected by ORNL data-correction methodology prior to transmission.
- Submission to NREL of the ORNL Fleet DNA files. A total of 3,241 files (1,562 HTDC files, 930 MTDC 1 files, and 749 MTDC 2 files) were uploaded and distributed to NREL.

Technical Challenges

At the conclusion of FY13, a number of challenges and hurdles remain for the Fleet DNA project.

- Integration and development of cross-vocation databases, which consist of mixed vehicle sizes and applications. This will require adapting the data visualization routines to work with mixed data sets and adjusting the data filtration and analysis routines for the variations between medium- and heavy-duty vehicles.
- Technical challenges remain in the area of Web deployment, particularly as it relates to user data upload and download. Providing Fleet DNA users with the ability to automatically upload and download data requires the development of common data structures and formats, and will necessitate additional web design.
- An effort will be required to create an interactive Web environment for dynamic statistical visualization and exploration. The Fleet DNA project team is already working toward developing interactive graphs and reports and should be able to address this hurdle in FY14.
- Significant effort will be required in FY14 to continue to collect large amounts of data in the Fleet DNA database and recruit additional partners to the project.

NREL Future Achievements

Future Data Plans

In FY14, the Fleet DNA project team plans to continue reaching out to existing data partners and recruiting additional partners in order to complete the initial eight vocations of interest reported on the Fleet DNA website. In order to meet the minimum data requirements for data posting (three data partners), the Fleet DNA project will have to collect additional transit bus, refuse truck, line haul, and service van data. Additionally, given the unique vocational applications of the medium-duty data received from ORNL in FY13, NREL will explore collecting additional data from varied geographic locations in order to craft additional subvocation and special use reports on an expanded static Fleet DNA reporting website.

In addition to ongoing data collection from existing project partners, EV delivery vehicle data collected as part of the American Recovery and Reinvestment Act projects administered by NREL will be included in existing data reports as additional data supplying projects, and will also be published in new EV specific vocation/vehicle type reports. It is anticipated that this additional data will add over 500 vehicles, and 1 million miles to the delivery truck, delivery van, and bucket truck data sets.

Future Fleet DNA Phase 2 Reporting Plans

In FY14, the Fleet DNA project team plans to spend extensive time developing a second phase reporting system. This system will include custom user query driven data reporting, graphics, and data requests for composite data products from the Fleet DNA database. In addition, the interactive datasets are planned to be posted on both the Fleet DNA website developed in FY13 as well as integrated into the Alternative Fuels Data Center (AFDC) website for additional visibility and user exposure. It is the goal of Fleet DNA to provide the data and tools necessary for users to explore medium- and heavy-duty vehicle operational data and examine in depth avenues for fuel consumption reduction.

ORNL Future Achievements

Expanded Data Storage and Reporting

In FY14, ORNL researchers plan to work with NREL staff members to incorporate additional data channels into the Fleet DNA database. ORNL and NREL plan to expand the type of data stored in the Fleet DNA database due to increased interest from researchers and industry in vehicle powertrain, fuel, and emissions data coupled with drive cycle information. This will enable expanded reporting capabilities and provided opportunities for more advanced analyses within the existing datasets.

Improved Data Search Tools

ORNL is working towards improved characterization of the files contained in the Fleet DNA database via cataloging and indexing to enable quick searches of the database for specific drive cycles of interest. The indexing and cataloging of the extensive Fleet DNA database will allow industry users and researchers to better identify real world duty cycles with certain characteristics of interest that could serve as the basis

for testing new engine and vehicle technologies. The associated statistics provided will also allow identifying within a given vocation the most predominant duty cycle length and "shape."

✧ ✧ ✧ ✧ ✧

IV.J.2. Technical Discussion

Background

Fleet DNA was initially funded in FY12 through NREL by the Vehicle Systems Simulation and Testing (VSST) project within DOE's Vehicle Technologies Office. The Fleet DNA project was designed to provide a common location for storage and basic analysis of medium and heavy-duty drive cycles. Work performed within NREL, ORNL, other labs and DOE as well as other state and federal agencies has generated data but a common portal and processing routine does not currently exist to store, access, and apply all of this data. As VSST's primary medium and heavy duty data collection laboratories, NREL and ORNL have agreed to collaborate and bring together data analysis techniques and previously collected data, while coordinating future data collection activities. This and future efforts will provide industry (OEM's and fleets), other DOE programs and other federal agencies with valuable drive cycle information to be used to intelligently deploy and design advanced technology vehicles.

Introduction

Designed by NREL in partnership with ORNL, the Fleet DNA project is a vocationally grouped repository of medium- and heavy-duty commercial fleet transportation data designed to enhance user understanding of the operational characteristics of medium- and heavy-duty vehicles, with the goal of accelerating the evolution of advanced vehicle development while supporting the strategic deployment of market-ready technologies that reduce costs, fuel consumption, and emissions. Directed initially at vehicle manufacturers and fleet managers, the Fleet DNA database helps achieve the goals of reduced cost, fuel consumption, and emissions through increased awareness and understanding of the broad operational range for many of today's commercial vehicle vocations. Offering access to easy-to-interpret data summaries and graphical data outputs based on real-world operational information, Fleet DNA provides insights into user vehicle/fleet operation and allows for comparison among multiple fleets and geographic locations. By taking advantage of these capabilities, Fleet DNA users are provided a potential benchmarking tool with which to compare and contrast operational behavior between vehicles and fleets employed in similar capacities or located in similar geographic areas as well as characterize their own fleet behavior.

Approach

Technical Developments

Fleet DNA Overview

Fleet DNA is organized within a broad system configuration to support both internal and external (public) data access operations (Figure IV-152). It maintains multiple levels of security to ensure protection of sensitive data while facilitating data access for both internal and public users. While at first glance these dual mandates may appear conflicting, they are accomplished by providing internal users full access to underlying data through a series of secure virtual desktops. Using the same virtual desktops in place for internal users, public access is restricted to a "cleansed" data area, supporting public distribution.

The cleansed data area provides users access to information on existing datasets as described above and allows users to query and create information from the dataset. Raw data, individual vehicle data, and source data are not disclosed, which provides anonymity to existing data. Internal users (i.e., NREL and ORNL) have access to raw data and individual users have access to their own data, once uploaded, and can compare to information from other sets as needed.

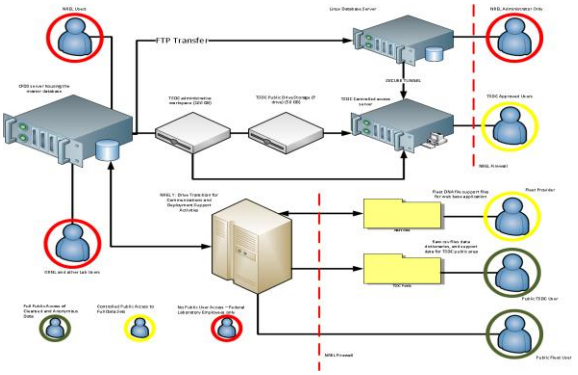

Figure IV-152: Server configuration and security layout for Fleet DNA network.

When examining current Fleet DNA data security measures, it is important to understand the unique challenges associated with data from a fleet provider's perspective. When analyzing data via Fleet DNA, a fleet provider is interested in characterizing their fleet/vehicles operation and comparing their operation to other fleets in similar applications. However, at the same time it is in the same fleet provider's interest not to share operational information that may be considered proprietary with either the public or competitors. To ensure unwanted data release does not occur, extensive security is in place to protect partner data while allowing for comparison. Fleet DNA protects data provider information through a combination of a unique user ID and password that are used to query the database and return only data and results specific to a single user.

Fleet DNA can be thought of as a combination of three major components. The primary component that drives Fleet DNA is the data supplied by users and partners (the yellow box in Figure IV-153), which are uploaded to the database via

data loading modules (green box), and then stored in the greater Fleet DNA analysis server (red box).

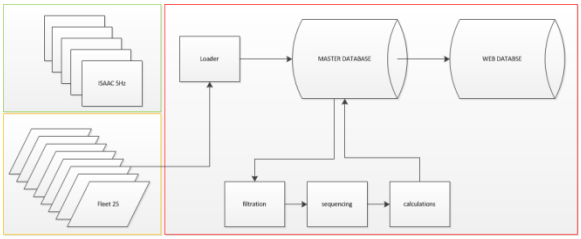

Figure IV-153: Simplified Fleet DNA structure.

Data loaders are designed for each unique data format supplied by participants in the Fleet DNA project and are used to ensure uniform data storage and analysis within the Fleet DNA database.

Once Fleet DNA data have been uploaded using the data loaders, they can be combined with additional data layers found in the database to perform extended analyses such as exploring road utilization and grade effects on drive cycle power requirements (Figure IV-154 and Figure IV-155).

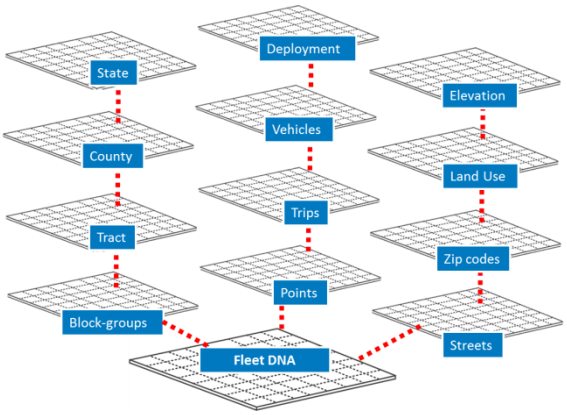

Figure IV-154: Example of Fleet DNA data layers.

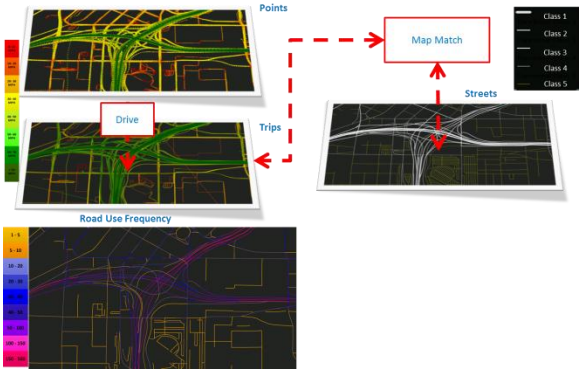

Figure IV-155: Example of analyses via interconnected data layers.

NREL Updated Analysis Capabilities and Routines

As of the completion of FY13, the Fleet DNA processing routine for analyzing data developed by NREL has expanded from initial speed filtration and calculation to a multistage analysis routine that examines both drive cycle data and geospatial information collected by global positioning system (GPS) telemetric systems. The Fleet DNA processing routine developed in FY13 has been expanded into a six-step process resulting in 350+ variables indicating the type of roads used, drive cycle characteristics that incorporate filtered speed and elevation, and trip-type classifications when available (home, work, school). These steps allow the GPS vehicle data from each of the data sources to be compared against one another.

The six steps through which vehicle GPS drive cycle data are fed as are follows:

1. Speed filtration
2. Location filtration
3. Vehicle sequencing (day/trip/micro-trip identification)
4. Map match
5. Elevation/grade
6. Calculations.

Speed Filtration

The first stage of analysis in Fleet DNA data processing is the filtration of speed-time data uploaded to the database. Raw GPS speed traces uploaded to the database are filtered by removing outlying speed/acceleration values, backfilling missing idle time, and performing a global smoothing process on the speed profile. The goal of the filtration process is to remove unrealistic speed data from the drive cycles as they enter the database. An automated filtration method was chosen due to its ability to apply a consistent, repeatable, independent data filtration approach to incoming data, ensuring data quality for downstream applications such as drive cycle analysis and modeling.

Location Filtration

After completing initial filtration of speed-time drive cycle data, it is necessary to ensure the quality of incoming GPS latitude/longitude data associated with uploaded drive cycles. In an effort to ensure high quality spatial data are stored in Fleet DNA and used for statistical analysis, multiple location-based filters are applied to uploaded latitude (lat) and longitude (long) data to remove outlying points and jumps in location caused by sources of error in telemetric signals (water, urban cavern, etc.). The first step in the location filtration process is to locate the mean center of all lat/long pairs recorded for the vehicle. Mean center is found by calculating the mean latitude and mean longitude independently and generating a lat/long pair from the results. The distance from all of the vehicle's lat/long pairs is calculated relative to this mean center.

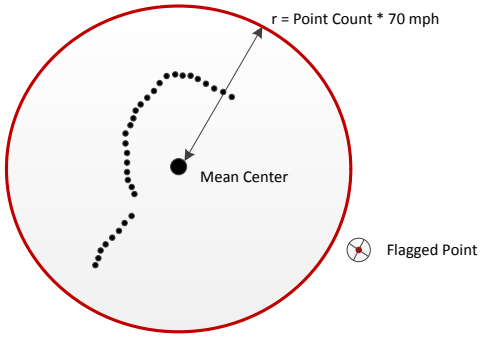

Figure IV-156: Mean Center Filter.

Lat/long pairs where the distance from the mean center is greater than the maximum distance the vehicle can travel over the recorded time interval are flagged as to not be used in spatial analysis (Figure IV-156). For Fleet DNA, it is assumed the vehicle is unable to travel more than 70 mph in a straight line in any direction (1 pair = 1 second, pair count/3600* 70 mph = buffer distance).

Upon completion of the preliminary mean-center distance filter, a second flag is applied to identify consecutive spatial location points where calculated driving speed is in excess of 100 mph. For this filter, speed is approximated using the time and distance between consecutive location points. If a point falls outside the 100-mph constraint, the current point is flagged, as are the points following, until both the last "good" point and the current point fall below the 100 mph constraint. Any points flagged as extreme outliers are removed from future filtration steps. Upon the completion of the mean-center and driving-speed location filters, non-flagged lat/long pairs ("good data") are ordered based on time. As a final step, a geospatial line feature representing the path of travel corresponding to the ordered lat/long points is generated in preparation for the next analysis step.

Sequencing

After completing the second stage in analysis, linked spatial and speed-time drive cycles are passed through a sequencing script to identify vehicle operating days, trips, and micro-trips. Sequences identified by the sorting process are represented by a sequence identifier and a start and end timestamp. A vehicle day is a 24-hour period in which travel occurred and comprises multiple trips. Trips are groupings of micro-trips separated by 3-minute vehicle key-off periods, and micro-trips are defined as zero speed to driving to zero speed events that include all zero speed data collected after the driving event and prior to the start of another micro-trip (Figure IV-157). Combining the micro-trip, trip, and day sequences identified by the sequencing script with the line generated during the location filtration stage, lines representing each of the sequence levels are generated and stored in the Fleet DNA database. Each of the resulting lines is appended to the results at the end of processing, allowing for GIS visualization and spatial analysis for each of the sequences. Additionally, the geospatial reference lines generated during this analysis stage are used to link the drive-cycle data to underlying street information.

Map Match

To match linked drive cycle and geospatial information to street data, the sequence lines generated in the sequencing stage are used to query available street options from the Navteq streets data layer housed in Fleet DNA (Figure IV-158). The geospatial location line, along with the data for the drive cycle (long, lat, time, speed) are fed to a map-match process that returns two tables:

1. Point Street Link—A second-by-second trace of the street identifier, the streets' functional classification, and the streets' speed category
2. Street Sequence—A traveled table that indicates the street, the entry and exit time, and the road classifications.

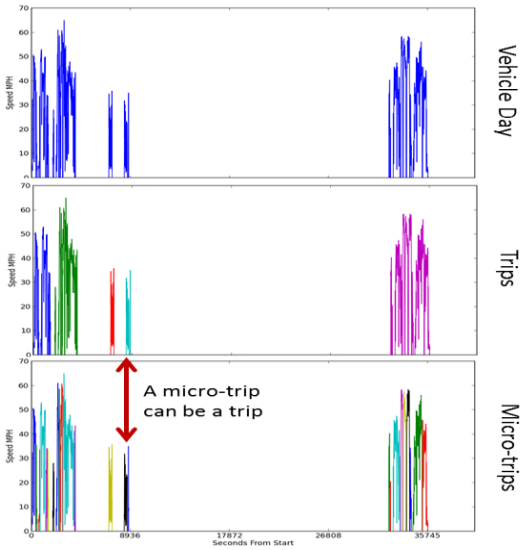

Figure IV-157: Example drive cycle sequencing hierarchy.

Figure IV-158: Lat/long street overlay.

The query applies a buffer of approximately 500 feet to the line representing the path of travel for a vehicle day, and returns street options that intersect with the buffer (Figure IV-159). The streets database is topologically enabled, meaning that all connections between roads are implied through location (start to end/end to start connections) or are identifiable using attributes associated with each street's line feature.

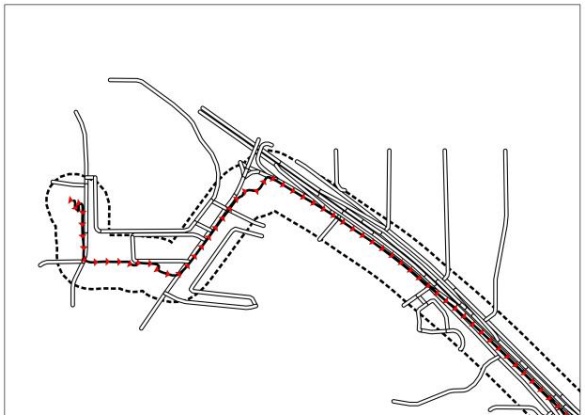

Figure IV-159: Buffer selection.

Before the location trace is assessed against the options returned, the streets are converted into two tables: nodes and connections. The first table is a unique node table where each unique start/end point for the street options is found and given a node identifier. The second table is generated by looking at each road returned, identifying the entry and exit nodes for each link, and choosing the direction/bearing of travel between the two nodes over the road segment (Figure IV-160). This table takes restrictions into account using a direction-of-travel attribute within the streets layer. The direction of travel is indicated by a T, F, or B. T indicates the road can only be traveled using the actual start to end points for the street segment, F indicates the road can only be entered through the end point and exited through the start point, and B means the entry and exit nodes can be either the start or end point (traversable roads). All of this is summarized as a unique connection where the in node, out node, street link identification (ID), bearing, and additional road attributes are stored as the connections table.

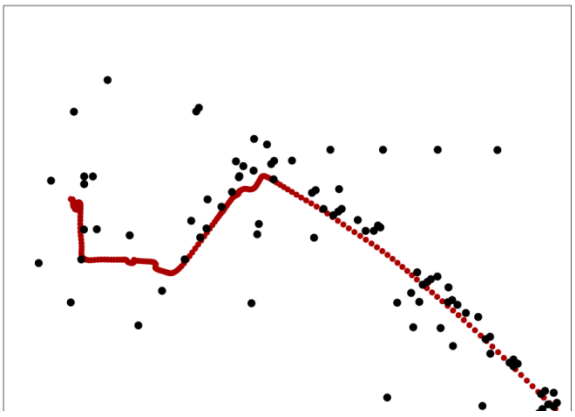

Figure IV-160: Unique node selection.

Generating these two tables provides the means to determine the route traveled along a street.

Following the solution, the streets results are appended to the point trace and the streets table is returned. Each day of data is merged backed to the full vehicle data to go through to the final steps of identifying grade and elevation and running calculations on the data generated.

Elevation Lookup

Once the map matching process is complete, the linked geospatial drive-cycle data (Figure IV-161) are sorted using their latitude and longitude and ready for grade and elevation to be appended. Once the data has been prepared for elevation/grade, Fleet DNA works with the high-resolution United States Geologic Survey National Elevation Data (NED) set stored in the database to back calculate road information from location. The NED 1/3 arc dataset provides accurate elevation information for the entirety of the United States at a grid spacing of ~10 square meters, providing sufficient resolution to determine approximate road grade for tractive power calculations. The files that store NED elevation are organized into folders named according to the degrees of latitude and longitude (grid_lat_lon). Using an iterative process which is repeated thousands of times for each drive trace; the stored NED data is recalled from the Fleet DNA database and appended to the drive cycle data to create a complete geospatially referenced drive cycle. Efficiency is possible because the data are housed locally on NREL servers, taking up approximately a terabyte of data storage.

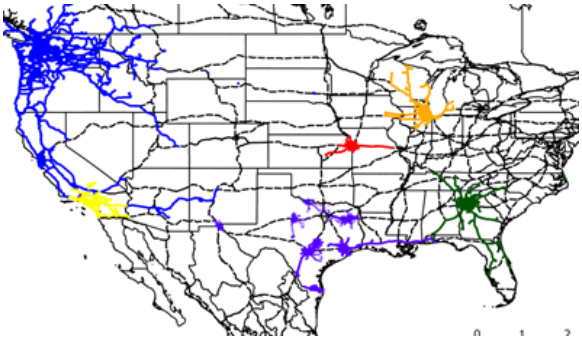

Figure IV-161: Example of geospatial linked drive-cycle map.

To assist with the elevation lookup and speed up the processing, drive cycle data points are linked to a timestamp, allowing the points to run the elevation query one file at a time (the reason for the lat long sort). Grouping the points by file speeds up processing exponentially because the process only has to interpret the elevation file a single time; opening the file is the most computationally intensive step in the processing. The process returns the elevation as a list still linked to a corresponding timestamp that is used to reorder the elevation list to pass to grade and elevation filtration.

Grade Processing

Upon completion of the elevation lookup within the Fleet DNA database, it is necessary to calculate road grade based on vehicle velocity and elevation. As the elevation is based on raw experimental data drawn from the United States Geological Survey Digital Elevation Map (DEM), the raw data requires filtration and smoothing of any outlying elevation values prior to calculating road grade and before performing any vehicle tractive power calculations (Figure IV-162).

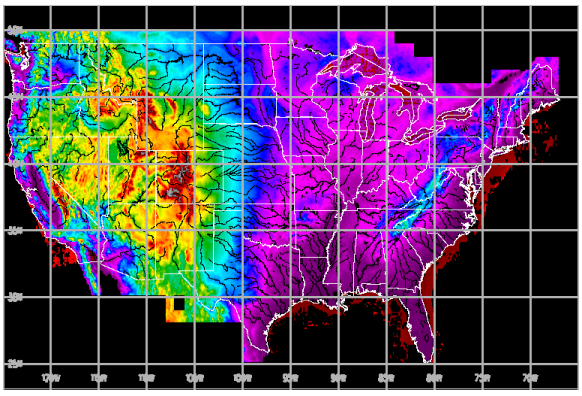

Figure IV-162: Sample DEMS overlay.

In order to successfully complete the elevation filtration process, the algorithms developed at NREL first down-sample the linked drive cycle data to create a vector of elevation values uniformly spaced along the distance the vehicle has traveled. The uniform data are then fed through a low-pass filter that removes any noise found within the elevation data, and then refits any remaining values using a piecewise best-fit spline and interpolation techniques. The filtration method generates an elevation profile with reasonable point-to-point

elevation changes from which road grade can be calculated (Figure IV-163).

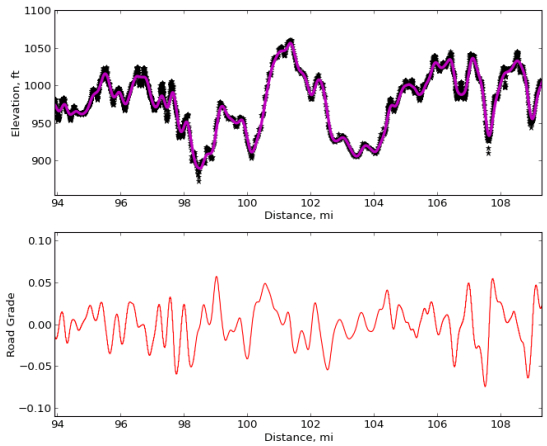

Figure IV-163: Smoothed elevation and road grade profiles.

Calculations

In addition to the standard 270+ metrics calculated as part of the initial drive cycle analysis developed in FY12, Fleet DNA statistics were expanded in FY13 to include an additional ~80 metrics related to the addition of road grade and road type information into the database. Some examples of new metrics added in FY13 include net elevation gained over a drive cycle, cumulative elevation change over cycle, amount of time spent on various road types, as well as average speed by road type. These new metrics provide additional geospatial information that can assist in the overall understanding of vocation-specific drive cycles and aid in their ongoing development. The addition of road grade to tractive power calculations has shown to be a significant contributor to overall fuel consumption.

ORNL Data Sharing and Internal Database Visualization

Discussions among ORNL and NREL researchers (one face-to-face meeting at ORNL and several teleconferences and e-mail communications) identified the data channels that would be extracted from the ORNL HTDC and MTDC databases and included in the Fleet DNA database. It was determined that the data would include a time channel; three vehicle information channels: vehicle speed, vehicle engine speed, and fuel rate; three spatial location channels: latitude, longitude, and altitude; and where available, three channels with the vehicle mass information: steer-axle weight, driver-axle weight, and trailer axle weight. It was also decided that the ORNL HTDC and MTDC 5Hz data would be re-sampled to 1Hz for inclusion in the Fleet DNA database.

To accomplish these tasks, ORNL developed several novel methodologies and associated software. The first component developed as part of this exercise extracted the data channels requested for the Fleet DNA database from the more extensive (more than 70 channels in some cases) ORNL databases. ORNL developed a methodology to eliminate errors found in the HTDC and MTDC data prior to data transfer to the Fleet DNA database. Procedures to rectify anomalies in the data collected in the HTDC and MTDC projects were developed and applied as a first step in the transfer of data from ORNL to NREL. Two main problems were addressed by these procedures: GPS data glitches and sensor information issues. For the former, the main focus was on identifying and eliminating errors in some short segments of the data that were introduced by to short-term loss of GPS signal (five or six seconds in most cases) during the data collection effort. The procedure basically interpolated between known points in the dataset.

During the HTDC and MTDC data collection efforts, ORNL used a very sophisticated data acquisition system (DAS) that could be programmed to indicate when a sensor (deployed by ORNL or already present on board) malfunctioned or did not post information. Those cases were indicated in the corresponding field in the database with values that were pre-defined and therefore easily to identify in a post-processing analysis of the data. After correcting the problems with the GPS information, ORNL proceeded to correct problems in the database that were due to sensor errors. Only those cases in which the identified problems occurred during very short periods of time (one second or less) were corrected by interpolation between known data points and using pre and post tendencies. If the segments were longer than 2 seconds, they were marked and the duty cycle that contained the problem eliminated from the database. Since close to a million mile were logged by the vehicles participating in the HTDC and MTDC, it was possible and advisable to keep only information of the highest quality (i.e., information that was collected by the on-board sensors and was not manipulated by any post processing procedures that affected large data segments of information).

After examining and removing any erroneous data points within the HTDC and MTDC datasets, the 5 HZ datasets were resampled from 5Hz to 1 HZ as specified by NREL for inclusion into Fleet DNA. After resampling, ORNL developed software to quickly display drive cycle characteristics of the data in the database prior to sharing with NREL. The tool allowed ORNL researchers to visually inspect files and helped identify any errors that were not fixed by the ORNL data-correction methodology. The tool allowed the researcher to select any of the channels included in the Fleet DNA database developed by ORNL for a particular vehicle (18 vehicles are included in the database) and specify a frequency for the data to be displayed (see Figure IV-164 below)

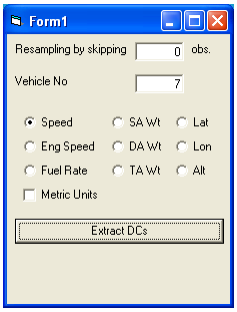

Figure IV-164: Fleet DNA Visualization Tool—Parameters.

After pressing the "Extract DCs" button (see Figure IV-164), the utility presented the researcher with 12 duty cycles at the time until all the files contained in the database for that particular vehicle were exhausted. The Fleet DNA Visualization tool allowed the researcher to display not only

Speed but also all the other channels contained in the database as a function of time. The utility also allowed ORNL researchers to zoom in on data within the graphs to better view information.

Results

NREL Updated Data Collection

One of the primary objectives in FY13 for Fleet DNA was to continue the expansion of data stored within the database. In an effort to achieve this objective, NREL researchers recruited data partners such as CALSTART, California Air Resources Board (CARB), South Coast Air Quality Management District, Minnesota Transit, UPS, and others, in addition to working with Oak Ridge National Lab (ORNL) to house the medium- and heavy-duty data collected through their past efforts.

As a result of efforts in FY13, Fleet DNA data collection currently encompasses more than 397 unique vehicles, accounting for 4,941 operating days, 166,428 vehicle miles traveled, and over 111 million data points collected. Additionally, Fleet DNA data has been collected in over 15 unique geographic areas, and encompassed more than 10 unique vehicle vocations and 8 vehicle types (Figure IV-165).

Figure IV-165: Fleet DNA Data Collection locations through FY13.

The major vehicle types with data collected through FY13 include:

- Transit Bus
- Refuse Truck
- Bucket Truck
- Delivery Van
- Delivery Truck
- Line Haul
- Service Van
- School Bus

NREL Fleet DNA Website and Reporting

In addition to the successful large scale data collection efforts completed in FY 13 as part of the Fleet DNA project, NREL and ORNL are proud to announce the successful development and deployment of 34 page vocational reports which are housed on the newly developed Fleet DNA website located at www.nrel.gov (Figure IV-166). The Fleet DNA website serves as a user portal providing public access to data summaries of the data stored in the Fleet DNA repository.

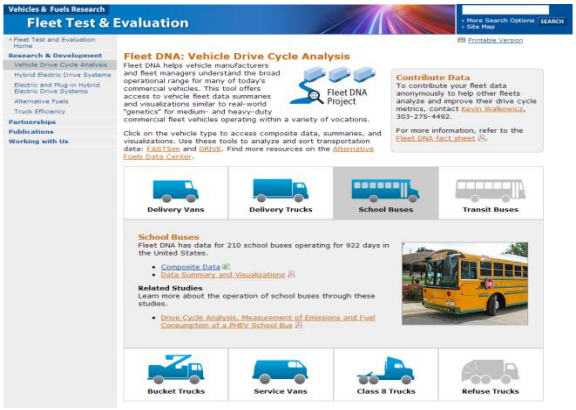

Figure IV-166: Fleet DNA website main page.

ORNL Fleet DNA Data Visualization tool

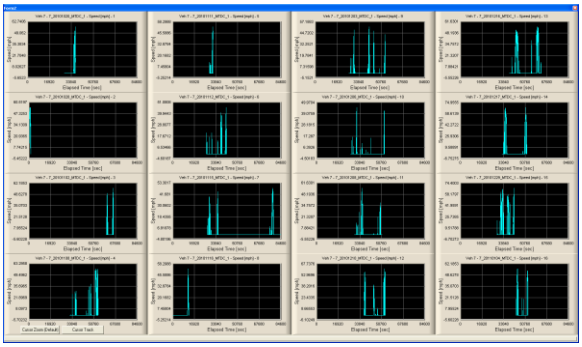

Figure IV-167: Fleet DNA Visualization Tool—Speed vs. Time for vehicle 7.

As part of ORNL's contribution to the Fleet DNA projection via contribution of HTDC and MTDC datasets, ORNL researchers developed the Fleet DNA Visualization Tool to assist with the visual inspection of database data (Figure IV-167). The addition of the Fleet DNA Visualization Tool saved time and effort when performing the "big data" analyses required for the Fleet DNA project, by allowing researchers to visually inspect cycles of interest and remove erroneous data files prior to analysis. The Fleet DNA data visualization tool was used with the set of 3,241 files that were extracted from the ORNL HTDC and MTDC databases (1,562 HTDC files, 930 MTDC 1 files, and 749 MTDC 2 files) and were resampled and formatted to according to NREL specifications for the Fleet DNA database. Table IV-18 below presents a detailed account of all the files examined using the Fleet DNA Visualization tool which were delivered by ORNL to NREL for the Fleet DNA database.

Table IV-18: Fleet DNA Files by Vocation and Vehicle No.

Vocation	Vehicle Number					
	1	2	3	4	5	6
Long-Haul Delivery	244	264	265	287	283	216
Regional Delivery	131	51	138	n/a	n/a	n/a
Transit Bus	271	134	205	n/a	n/a	n/a
Electrical Utility Vehicle	82	68	60	n/a	n/a	n/a
Tow and Recovery	200	156	183	n/a	n/a	n/a

Conclusions

As of the end of FY13, the Fleet DNA project has continued to progress and build on the initial framework developed in FY12. An initial static reporting website has been developed that houses eight unique vocation reports, and additional data layers such as road grade and road type have been incorporated into the database, providing opportunity for additional analyses. As a result of the additional data layers, more than 80 new metrics have been developed and incorporated into the reporting process, providing researchers and industry members with additional insight into the effects of road grade on drive cycles.

Moving forward, the Fleet DNA project plans to continue to grow and develop additional capabilities and reports in FY14. In FY14 Fleet DNA will continue to recruit additional data partners and complete vocational sets, which can then be reported to the public. We would also like to expand our vocational sets in FY14 and add new vocations/vehicle types to our report lists.

In addition to expanding Fleet DNA data and capabilities, in FY14 the project will focus on expanding outward-facing components of Fleet DNA such as the website. Building upon the static reporting website developed in FY13, next year the Fleet DNA project plans to develop and deploy an interactive data portal that will provide users the ability to generate custom reports and visuals based on user driven data queries of the database. Improving visibility and increasing interaction with users will also serve as a source for ongoing feedback, which will be used to drive future project developments.

Finally, Fleet DNA development in FY14 and beyond will be driven toward building bridges for integration with existing/planned analyses tools and interfaces, such as the Alternative Fuels Data Center, DRIVE, Autonomie, and FASTSim, to provide even greater value-added opportunity and offer users the ability to select, model, and generate custom representations of data drawn from the database.

Acknowledgments

The authors wish to thank Lee Slezak, U.S. Department of Energy Vehicle Technologies Office, for his support in conducting this project. The authors would also like to thank the staff of both NREL and ORNL for their support and cooperation in helping to define and develop Fleet DNA, as well as for their cooperation in ongoing data sharing activities. Specifically, the support of NREL staff members Adam Duran, Evan Burton, and Eric Wood were invaluable to the completion of this work. Finally, the authors wish to acknowledge the support of our project partners and participating fleets. Fleet DNA would not be possible without their continued participation and feedback.

IV.J.3. Products

Publications

1. NREL—Duran, A. and Walkowicz, K., "A Statistical Characterization of School Bus Drive Cycles Collected via Onboard Logging Systems," *SAE Int. J. Commer. Veh.* 6(2):2013, doi:10.4271/2013-01-2400.
2. NREL—Fleet DNA Website: www.nrel.gov/fleetdna

Patents

1. NREL ROI—Integrated Geo-Spatial Transportation Analysis Database
2. NREL ROI—GIS tool for appending accurate road grade data to vehicle GPS traces

Tools and Data

1. ORNL—A set of tools to extract, cleanse, resample, and format the information stored in the HTDC and MTDC databases to the Fleet DNA database.
2. ORNL—A Fleet DNA Visualization Tool to quickly and visually examine the information and identify any errors that escaped the numerical cleansing procedures applied to the raw data.
3. ORNL—3,241 data files capturing operating information for 5 unique vehicle vocations was supplied to the Fleet DNA database.
4. NREL—Fleet DNA Database. Created to input, filter, and analyze large amounts of vocational vehicle-use data.
5. NREL—Fleet Drive-Cycle, Rapid Investigation, Visualization and Evaluation Tool (DRIVE), Copyrighted 2011. Tool created to analyze large sets of drive-cycle data.
6. NREL—A total of 4,941 days of data collected from 397 unique vehicles operating in 8 vocations successfully uploaded and stored in the Fleet DNA database.

IV.K. Medium-Duty Electric Vehicle Data Collection and Performance Assessment

Kevin Walkowicz, Principal Investigator
National Renewable Energy Laboratory
15301 Denver West Parkway
Golden, CO 80401
Phone: (303) 275-4492
E-mail: Kevin.Walkowicz@nrel.gov

Lee Slezak, DOE Program Manager
Phone: (202) 586-2335
E-mail: Lee.Slezak@ee.doe.gov

IV.K.1. Abstract

Objectives

- Obtain over 25 parameters each second from each vehicle, to be logged and stored at the National Renewable Energy Laboratory (NREL)
- Obtain truckstop electrification usage records that detail each time a plug-in site is used
- Securely collect, store, and analyze vehicle data transmitted from medium-duty plug-in electric vehicles (EVs) and equipment being deployed/developed as a part of U.S. Department of Energy (DOE)-funded activities (under the American Recovery and Reinvestment Act [ARRA] Transportation Electrification Awards)
- Report data and progress of the data collection efforts as well as analyzed vehicle/equipment performance data to the DOE and the general public
- Provide for the secure storage of data with routine backups
- Refine and optimize processing routines to handle an increasing volume of data as more vehicles come online
- Processed results to obscure proprietary and private information and post on an NREL website quarterly for public review.

Major Accomplishments

Data collection and reporting activities for medium-duty vehicles for 2013 included the following ARRA deployment projects:

- **Smith Electric Vehicles:** Transmission, analysis, and reporting of performance from the Smith Newton EVs to NREL continue. FY 2013 included three additional quarterly reports and a fourth, which will be posted in October 2013. Additionally, a cumulative report covering data collected from November 2011–June 2013 was posted. Data from a total of 258 vehicles were deemed "valid" through the filtering process and recorded through June 2013. This represented 46,102 vehicle days of operation.
- **Navistar:** Although the production of the Navistar eStar has stopped, there are still over 100 vehicles transmitting data back to NREL that remain in operation. FY 2013 included three additional quarterly reports, and a fourth will be posted in October 2013. Additionally, a cumulative report covering August 2012–June 2013 was posted. A total of 101 vehicles were recorded through June of 2013, which represented 7,974 vehicle days of operation.
- **Cascade Sierra Solutions (CSS):** FY 2013 included the first transmission of usage records from CSS to NREL. A cumulative report covering January 2013 through June 2013 has been posted and includes monthly usage statistics over this period. As of June 2013, 48 sites were reporting usage and recorded 1,063 plug-in events.

Future Achievements

- Analysis will continue on all the projects described above. Efforts for FY 2014 will focus on improved integration with datasets from other projects and expanding the number of metrics that are being considered.
- In-use data collected on delivery trucks in similar vehicle classes as the Smith Newton and Navistar eStar will be used to evaluate the petroleum displacement and operating cost reductions realized by these medium-duty EV deployments.
  Additional data will be received in early 2014 on plug-in hybrid electric "bucket" trucks. Similar data collection, screening, and analysis efforts will be completed in FY 2014 for this data set, and reports will be posted for public consumption.

✧ ✧ ✧ ✧ ✧

IV.K.2. Technical Discussion

Background

American Recovery and Reinvestment Act (ARRA) deployment and demonstration projects are helping to commercialize technologies for hybrid electric vehicles (EVs), plug-in hybrid EVs, all-electric vehicles, and electric charging infrastructure.

This effort, which is funded by the DOE's Vehicle Technologies Office within the Vehicle & Systems Simulation and Testing Activities, will utilize data collected from some of these ARRA demonstration projects. Data from EVs from Smith Electric Vehicles (Smith) and Navistar will be collected, compiled, and analyzed. Data from ARRA-funded Cascade Sierra Solutions (CSS) truckstop electrification sites have also been included.

Introduction

NREL will compile the data received from each original equipment manufacturer (OEM) through the NREL Commercial Fleet Data Center (CFDC). This includes more than 25 parameters, which are recorded each second from each vehicle and transmitted to NREL on a regular basis. Compiled data products will be used to better understand the behavior and operating characteristics of electric-drive vehicles being operated in the field. This is in direct support of the Vehicle Technology Office's goals of developing and deploying plug-in EVs.

Information gathered on vehicle drive cycle characteristics along with data collected on specific components, such as electric motors, power electronics, auxiliary loads, and battery performance, can be used to support other DOE-sponsored research and development activities.

NREL will prepare and deliver detailed non-proprietary reports of vehicle performance to the DOE. This information, which will be processed to obscure any proprietary or private information, will also be made available on the NREL website for public review.

Approach

Technical Discussion

Overall Approach

On-board diagnostic data are collected, typically from the control area network along with global positioning system and any additional sensors. The data are transmitted wirelessly back over the cellular network and eventually on to the OEM. The data are then uploaded by the OEM to the NREL secure FTP site, usually as a text file. Once the data have arrived at NREL, a number of automated processes handle downloading, filtering, sorting, and processing the data. The raw and processed data are stored in the CFDC PostgreSQL central database, and summary reports are generated for the DOE and general public. This process is outlined in the schematic shown in Figure IV-168.

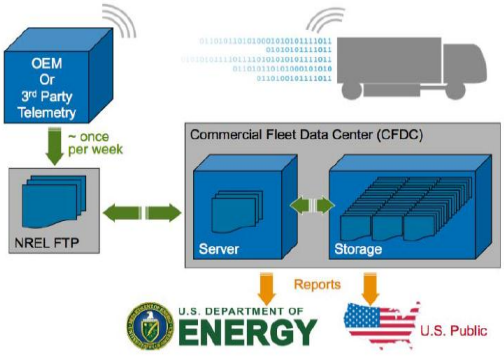

Figure IV-168: Data flow from vehicle to final reporting.

The procedure for taking a more detailed look at the data processing, which happens at the CFDC, can be broken down into a number of steps. The two primary software packages used for calculations and analysis are MATLAB and Python. Raw data can be loaded directly from individual files or read from the CFDC PostgreSQL central database. All data received by the secure FTP site are stored; however, if data are found to be erroneous or corrupt during the filtering process, they are flagged and are not included in the subsequent processing steps. Time and date are adjusted for geographic location, and then binned into "driving days" that capture one full day of driving and any subsequent charging, even if the charge cycle goes past midnight. Specific analysis is then carried out on individual aspects including drive cycle, powertrain, power electronics, batteries, and any individual components of interest. These routines include code and calculations specifically designed for these projects, as well as incorporating more universal calculations from NREL's Fleet Analysis Toolkit, which allows the performance of these vehicles and vehicle components to be compared across a large number of current and past projects within the secure data center. This information can be combined with demographic data to better understand localized trends and markets. Final data products are then published for public comment. This process is outlined in the schematic shown in Figure IV-169.

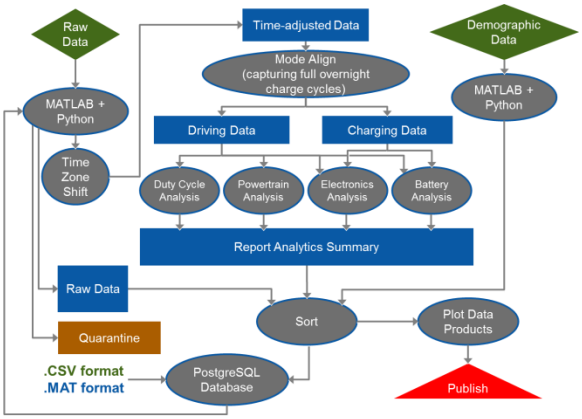

Figure IV-169: Data processing and analysis.

Results: Smith Electric Vehicles Data Collection, Analysis, and Reporting

The main focus for the Smith Newton deployment project in FY 2013 was on refining and increasing speed of calculations as vehicle usage and raw data volume increased. This was crucial because the time required to process the data using the old methodology was approaching the rate at which we were receiving new data. The largest gains were realized when converting some legacy routines over to Python code, which could more easily be run in parallel, allowing calculations to be run on multiple vehicles simultaneously. This reduced the processing time on the full raw data set from weeks to days.

The main data storage structure was also migrated over to a PostgreSQL database. This is not only neater and cleaner from an organizational standpoint, but also adds new functionality in which the database allows multiple users to interact with the data while simultaneously processing results. The database also integrates seamlessly with the new Python scripting and calculations, allowing raw data to be extracted from the database, calculations made, and results saved back

to the database all in one step. A Smith Newton delivery vehicle is shown in Figure IV-170.

Figure IV-170: Smith Newton delivery vehicle (PIX# 22851).

Currently, all the Smith Newton electric-drive vehicles participating in this demonstration project from which we are receiving data are first generation vehicles with 80-kWh battery packs. However, the vehicle is advertised as having a number of battery pack size options ranging from 40 to 120 kWh. A preliminary dataset from a Gen 2 vehicle was received in late September, and the full set of data from an additional 90 vehicles is expected in early FY 2014. Some vehicle specifications are listed in Table IV-19.

Table IV-19: Gen 1 Smith Newton Vehicle Specifications.

GVW	22–27K lbs.
Drag Coefficient	~0.5
Charging Standards	J1772 or 3-phase
Onboard Charger Power	5–6 kW
Battery Capacity	80 kWh
Inverter Efficiency	94%
Motor	
Peak Motor Power	134 kW
Efficiency	90%

NREL has been receiving data from Smith as part of this demonstration project since November 2011. The latest cumulative report posted to the web captures all data that have passed through the filtering and analysis steps described above through the end of June 2013. Table IV-20 shows some summary statistics from this cumulative report.

Table IV-20: Summary Statistics for Smith Newton EVs.

Number of vehicles reporting	258
Vehicle days driven	46,102
Total number of miles driven	1,202,881
Total miles, city | highway	65% | 35%
Average distance per day	26.1 miles per day
Stops per day | mile	49.8 | 2.4
Average max acceleration	0.31 g
Average daily max speed	50.5 mph
Overall energy consumption (idle and driving loads)	1.52 kWh/mile
Driving energy consumption (idle removed)	1.41 kWh/mile
Overall mpg energy equivalent	24.8 mpge
Average charges per day	1.8
Average energy per charge	23.8 kWh
Average charge duration	6.5 hours
Distance between charges	14.7 miles

Figure IV-171 show the home location of Smith EVs currently reporting data back to NREL on a regular basis. Figure IV-172 gives a breakdown of the total data received by state.

Figure IV-171: Home locations of Smith vehicles.

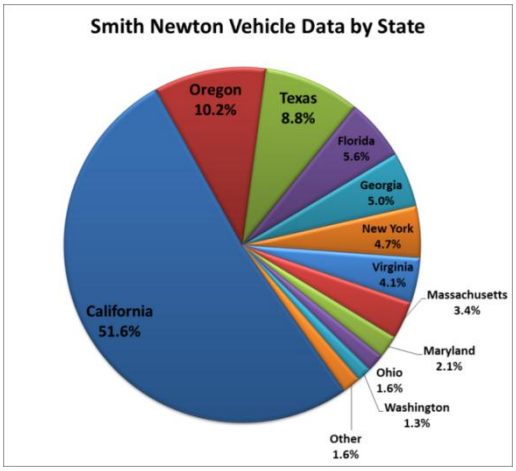

Figure IV-172: Distribution of Smith data by state.

Figure IV-173 shows that the Smith electric vehicles follow a typical pattern for daily commercial use with the vehicles starting operation in the early morning and returning in the evening. Most vehicles are connecting the charger in the late afternoon to early evening with the largest spike around 4–5 p.m. Figure IV-174 shows charging continues well into the night with some vehicles still charging as activity starts the next morning. Figure IV-175 shows the distribution of daily driving distance and an estimated range based on pack size and average energy usage of the vehicles.

Figure IV-176 shows the distribution of daily energy consumption per mile, which varies significantly depending on how the vehicle is being operated. This is also highlighted in Figure IV-177, which aims to quantify the impact of driving aggressiveness on energy consumption. Annual average fuel consumption is shown in Figure IV-178 along with annual cumulative totals in Figure IV-176.

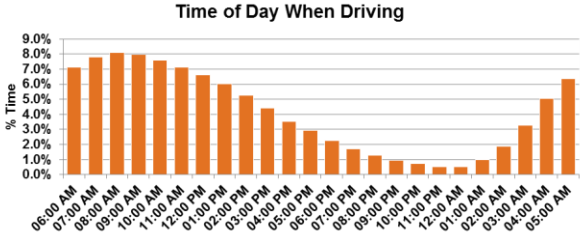

Figure IV-173: Time of day when Smith vehicles are driving.

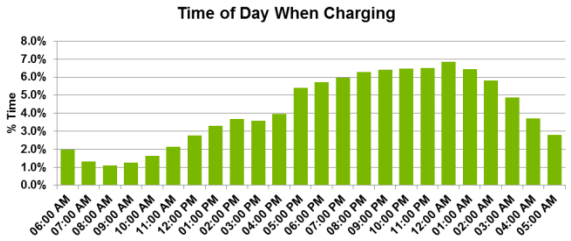

Figure IV-174: Time of day when plugging in (charging begins).

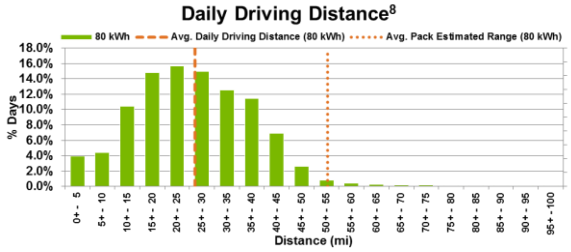

Figure IV-175: Distribution of daily driving distance and estimated range.

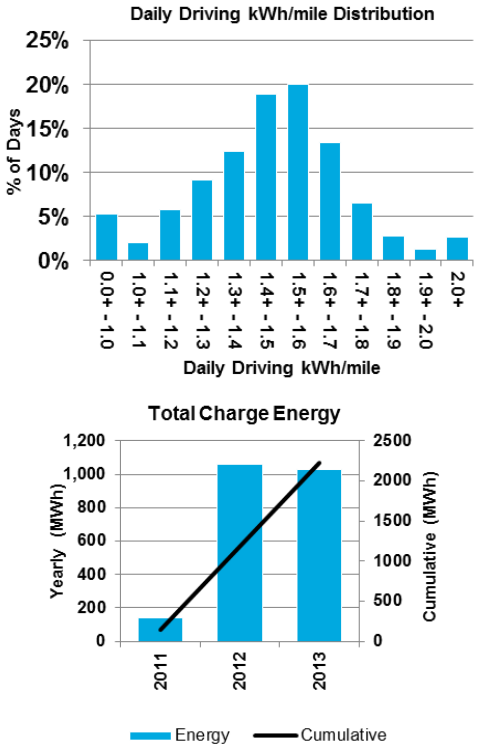

Figure IV-176: Smith EV energy consumption per mile (top) and per year and cumulative (bottom).

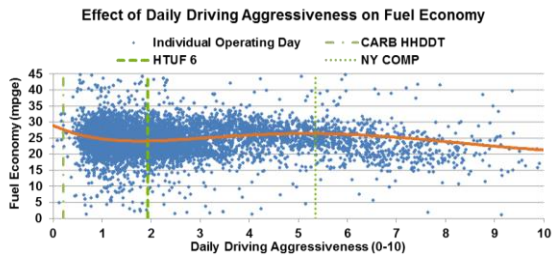

Figure IV-177: Effect of driving aggressiveness on mpge.

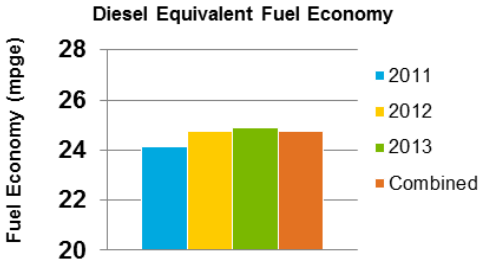

Figure IV-178: Smith diesel equivalent fuel economy by year.

Figure IV-179 shows daily driving kinetic intensity and average driving speed compared with some standard chassis dynamometer test cycles for the Smith Newton vehicles.

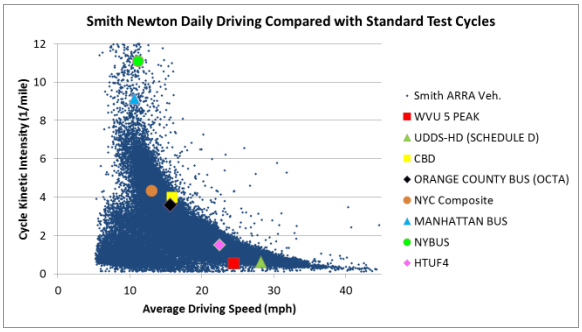

Figure IV-179: Smith Newton kinetic intensity vs. average driving speed.

The latest reports and more detailed results including data through June 2013 can be found at: http://www.nrel.gov/vehiclesandfuels/fleettest/research_electric.html

NREL received a backlog of data from the additional 90 "Gen II" vehicles in September 2013. The data will be processed and will leverage the automated processing routines described above. Once the data have been merged with the current dataset, the quarterly and cumulative reports will be rerun and updated to include this new dataset. Gen I and Gen II vehicle sets will be distinguishable in the reports.

Results: Navistar Data Collection, Analysis, and Reporting

The main focus for the Navistar eStar vehicles reporting back to NREL during FY 2013 was improving data and file transmission consistency by working together with the OEM, Navistar, and the third-party telemetry provider. Calculations were also migrated from legacy MATLAB code to code (as described above for the Smith data) that could run calculations on multiple vehicles in parallel, greatly decreasing the data processing time. All of the Navistar eStar vehicles reporting data back to NREL are first-generation vehicles with 80-kWh battery packs. We do not expect any more vehicles to come online. However, vehicles that have already been deployed are expected to continue transmitting data. The Navistar eStar is shown in Figure IV-180, and some vehicle specifications are presented in Table IV-21.

Figure IV-180: Navistar eStar, battery electric delivery vehicle (PIX# 18624).

Table IV-21: Navistar eStar Vehicle Specifications.

GVW	12,122 lbs.
Payload (Max)	5,100 lbs.
Curb Weight	7,022 lbs.
Charging Standard	J1772
Battery Capacity	80 kWh
Motor Power	70 kW
Top Speed	50 mph
Advertised Range	Up to 100 miles

The ARRA-funded Navistar eStar vehicles have been deployed to a number of different fleets across the United States. The map in Figure IV-181 shows the home charging location of each vehicle and the corresponding number of hours of data transmitted from each vehicle.

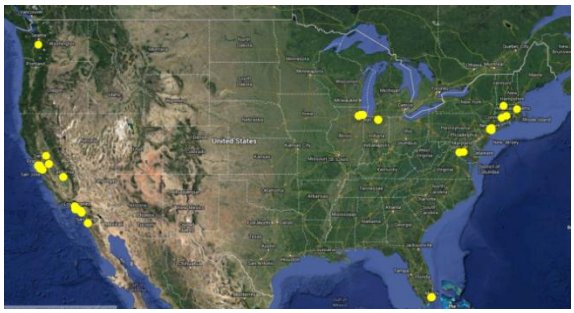

Figure IV-181: Home locations of Navistar vehicles.

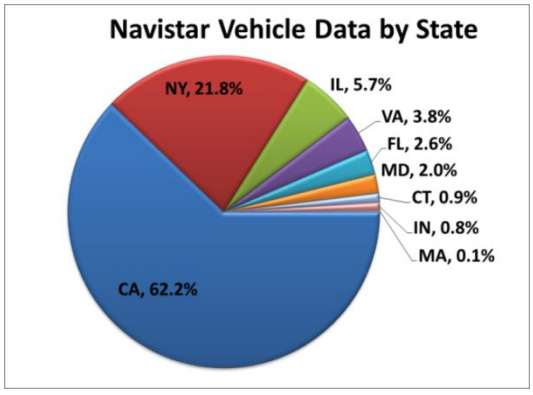

Figure IV-182: Distribution of data by state.

The latest cumulative report posted to the web captures all data that have passed through the filtering and analysis steps in the timeframe above, up through the end of June 2013. Table IV-22 shows some summary statistics from this report.

Table IV-22: Navistar Summary Statistics through June 2013.

Number of vehicles reporting	101
Number of vehicle days driven	7,974
Total number of miles driven	135,527
Overall energy consumption	0.892 kWh/mi
Driving energy consumption	0.751 kWh/mi
Total charge energy	121.1 MWh
Average energy per charge	17.1 kWh
Average charge duration	3.3 hours
Average distance per day	17.0 miles
Average Speed	13.8 mph

Figure IV-183 shows what time of day the vehicles are being driven and shows a typical "daytime" operation pattern with the vehicle being operated roughly between 6 a.m. and 7 p.m. Figure IV-184 shows the distribution of daily driving distance. The average pack estimated range shown in Figure IV-184 estimates the range of the vehicle based on the 80-kWh pack and the 0.892-kWh/mile average energy consumption.

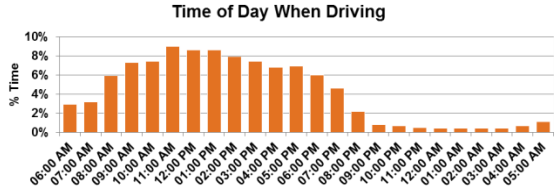

Figure IV-183: Time of day when driving.

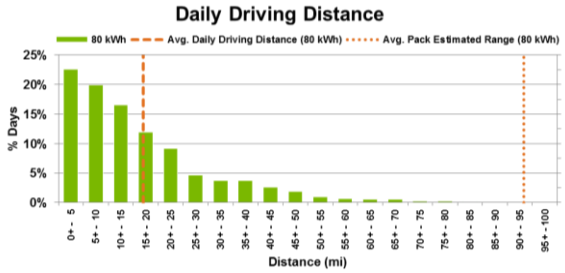

Figure IV-184: Daily driving distance.

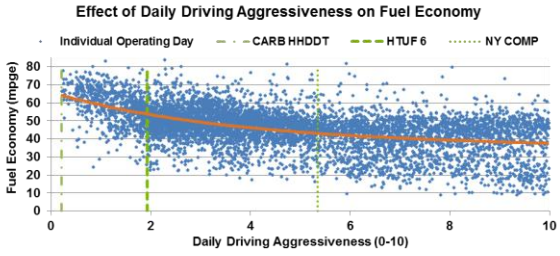

Figure IV-185: Effect of driving aggressiveness on fuel economy.

Figure IV-185 shows the effect driving aggressiveness has on energy consumption. It shows that as driving aggressiveness increases the energy consumed per mile

increases and the calculated mile per gallon equivalent (mpge) decreases. The value for mpge is calculated assuming standard diesel energy content of 37.6 kWh/gallon, which comes from the Alternative Fuels Data Center: http://www.afdc.energy.gov/fuels/fuel_comparison_chart.pdf.

In Figure IV-186, each Navistar eStar point represents one vehicle day of driving. Kinetic intensity and average driving speed for each day can be compared with standard chassis dynamometer tests. To provide a reference for driving style, typical medium-duty drive cycles are plotted along with the daily data points. The Central Business District (CBD), Orange County Bus, and NY City Composite Cycles, appear to be good matches for a typical day of driving for this vehicle on average across all applications. The NY Bus and West Virginia University 5 Peak cycles bound either end with >96% of the drive cycle kinetic intensities falling between these points.

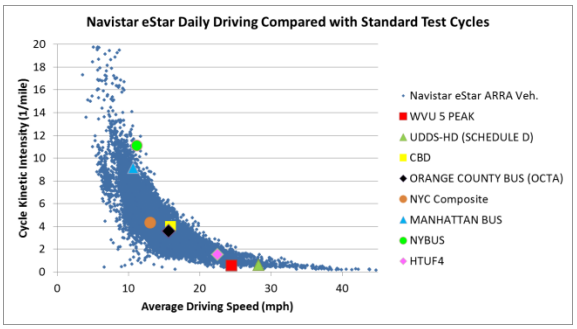

Figure IV-186: Daily driving compared with standard cycles.

Looking at regional and temperature effects, Figure IV-187 shows monthly results for DC energy consumption in the top three states based on data volume transmitted/received. Also shown are monthly average minimum ambient temperatures for these same regions.

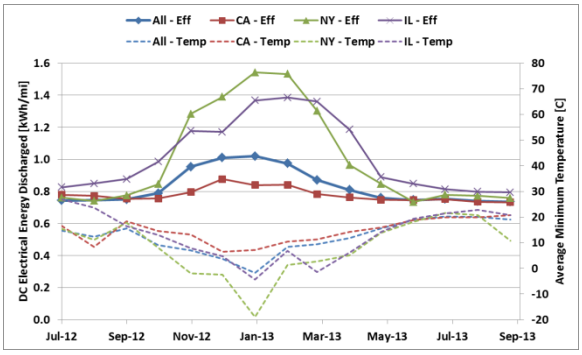

Figure IV-187: Monthly energy consumption and average minimum ambient temperatures by state.

The large increase in energy consumption per mile during the winter months is due to the used of the electric heater which pulls power from the same battery back as the traction motor. This will not only increase the energy usage but also decrease the range and is therefore an important consideration in colder climates. Table IV-23 shows the percentage difference between summer and winter for each state.

Table IV-23: DC Energy Consumption by State.

DC Energy (kWh/mi)	July	January	Difference
Overall	0.74	1.02	31.3%
California	0.78	0.84	7.5%
New York	0.76	1.54	67.7%
Illinois	0.83	1.37	49.3%

The latest reports and more detailed results can be found at:http://www.nrel.gov/vehiclesandfuels/fleettest/research_electric.html

The next scheduled quarterly report will run as soon as all data have been received for September and should be posted to the web along with an updated cumulative report in October.

Comparison of Smith and Navistar Usage and Energy

Both sets of vehicles are being used for various "package delivery" routes. Differences in gross vehicle weight, payload, driving style, and route types will affect the overall energy usage of the vehicles. Table IV-24 captures the differences between the Smith and Navistar data sets to help explain the differences in energy used per mile reported for each vehicle. Table IV-25 summarizes the drive cycle differences observed between the two vehicle sets. It can be seen that the Smith vehicles are operating in a lower "kinetically intense" drive cycle than the Navistar vehicle.

It is estimated that the Smith vehicles are higher mass vehicles (and carrying more cargo); the effects of mass and drive cycle differences are captured in Table IV-26. The calculated "ton-mile/gal" value is shown for each vehicle type. Because mass values are not delivered as part of the data set, an assumed maximum gross vehicle weight value is used to show the operational cargo efficiency possible for each vehicle. While the Smith vehicles probably do not operate at maximum gross vehicle weight, it is shown what the possible effect of mass will have on the overall energy efficiency and cargo freight efficiency.

Table IV-24: Comparison of Operation and Vehicle Specifications between Smith and Navistar Vehicles.

	Smith Newton (Class 6)	Navistar eStar (Class 3)
GVWR (lbs.)	22 - 26k	12,100
Payload (lbs.)	12 - 16k	5,100
Reporting Period	11/1/2011	7/1/2012
	6/30/2013	6/30/2013
Vehicles	258	101
Cities	80	31
Vehicle Days Driven	46,102	7,974
Total Distance Traveled (miles)	1,202,881	135,527
Average Distance / Day (miles)	26.1	17.0

Table IV-25: Comparison of drive cycles for each vehicle type.

	Smith Newton (Class 6)	Navistar eStar (Class 3)
Average Driving Speed (mph)	21.2	13.8
Average Daily Max Speed (mph)	50.5	49.6
City (<35 mph) | Hwy	65% | 35%	76% | 24%
Average Stops per Day	49.8	111.5
Average Stpps per Mile	2.4	6.6
Average Daily Max Accel (g)	0.32	0.37
Average Brake Regens (1/mile)	8.9	16.4
Median Aggressivenenss [KI(1/km) x2]	1.7	4.8

Table IV-26: Energy Consumption and Charging Characteristics for Each Vehicle Type.

	Smith Newton (Class 6)	Navistar eStar (Class 3)
Average Driving Speed (mph)	21.2	13.8
Average Daily Max Speed (mph)	50.5	49.6
City (<35 mph) | Hwy	65% | 35%	76% | 24%
Average Stops per Day	49.8	111.5
Average Stpps per Mile	2.4	6.6
Average Daily Max Accel (g)	0.32	0.37
Average Brake Regens (1/mile)	8.9	16.4
Median Aggressivenenss [KI(1/km) x2]	1.7	4.8

Results: Cascade Sierra Solutions Data Collection, Analysis, and Reporting

In mid- FY 2013, CSS began sending truckstop electrification usage statistics to NREL. Each funded site has multiple pedestals, and each pedestal has four connection points where vehicles equipped with electrified equipment can be plugged in. The dataset from CSS includes a summary of each transaction, which contains location, date, person/business contact information, hours booked/connected, total energy used, and a reference ID that can be linked to truck equipment if available. This reference ID is the only link between energy consumption and the equipment on the truck. The latest cumulative report shows usage statistics through the end of June 2013.Table IV-27 shows some summary statistics from the CSS report:

Table IV-27: CSS Usage Statistics.

Number of sites	48
Total number of plug-in events	1,063
Total hours booked/connected	17,674
Total kWh used	11,914
Average kWh/event	11.2
Average power per event (kW)	0.674

The map in Figure IV-188 shows the total energy consumption by location and by Petroleum Administration for Defense District (PADD) over the current reporting period.

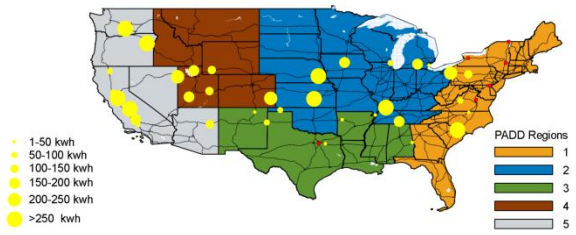

Figure IV-188: Map showing energy consumption by site and PADD regions.

The latest reports and more detailed results can be found at http://www.nrel.gov/vehiclesandfuels/fleettest/

Conclusions

Summary of Vehicle Data

- NREL is currently receiving "usable" data from 258 Smith EVs (vehicles with data that is able to make it through the data filters to meet minimum usage requirements) with an additional backlog of data from 90 vehicles that were received in late September. NREL is also receiving data from 101 Navistar eStar vehicles. These are all battery electric delivery vehicles. The data received include over 25 parameters of 1-Hz data.
- The Smith Newton EVs have driven a total of 46,102 days, covering 1,202,881 miles, for an average of 26.1 miles per day.
- The Navistar eStar vehicles have driven a total of 7,974 days, covering a combined 135,527 miles, for an average of 17 miles per day.
- The CSS—Shorepower Truck Electrification Project (STEP) had 48 of the 50 funded sites active with >90% uptime as of June 2013. The remaining two sites have recently come online and will be included in the next report.
- CSS has reported a total of 17,674 hours booked and 11,914 kWh used. (1APR_Standard paragraph with Indent)

Reporting

- Recent quarterly and cumulative reports up through June 2013 have been posted to the web for the Smith and Navistar projects. Example reports are shown below; these (and all reports) can be found at: http://www.nrel.gov/vehiclesandfuels/fleettest/

- Additional quarterly reports will continue to be added to the website beginning in October 2013 once all the September data are in, continuing the quarterly and cumulative report series.

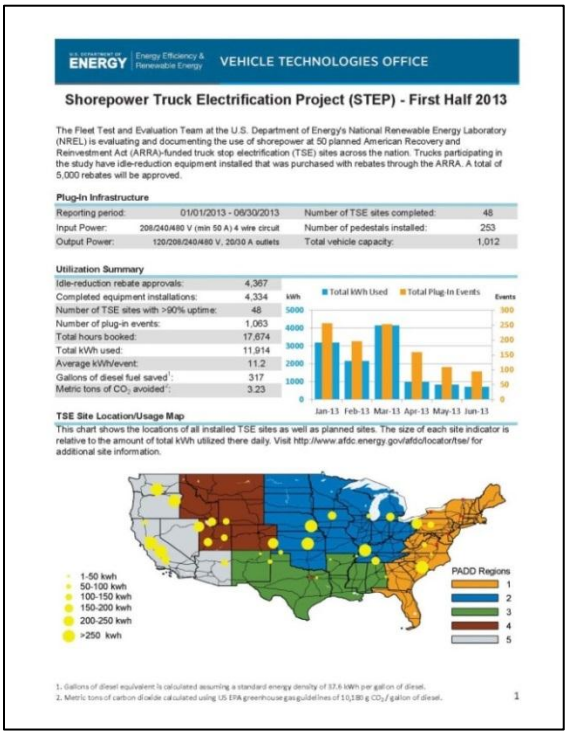

ENERGY | Energy Efficiency & Renewable Energy VEHICLE TECHNOLOGIES OFFICE

Shorepower Truck Electrification Project (STEP) - First Half 2013

The Fleet Test and Evaluation Team at the U.S. Department of Energy's National Renewable Energy Laboratory (NREL) is evaluating and documenting the use of shorepower at 50 planned American Recovery and Reinvestment Act (ARRA)-funded truck stop electrification (TSE) sites across the nation. Trucks participating in the study have idle-reduction equipment installed that was purchased with rebates through the ARRA. A total of 5,000 rebates will be approved.

Plug-In Infrastructure

Reporting period:	01/01/2013 - 06/30/2013	Number of TSE sites completed:	48
Input Power:	208/240/480 V (min 50 A) 4 wire circuit	Number of pedestals installed:	253
Output Power:	120/208/240/480 V, 20/30 A outlets	Total vehicle capacity:	1,012

Utilization Summary

Idle-reduction rebate approvals:	4,367
Completed equipment installations:	4,334
Number of TSE sites with >90% uptime:	48
Number of plug-in events:	1,063
Total hours booked:	17,674
Total kWh used:	11,914
Average kWh/event:	11.2
Gallons of diesel fuel saved[1]:	317
Metric tons of CO_2 avoided[2]:	3.23

TSE Site Location/Usage Map

This chart shows the locations of all installed TSE sites as well as planned sites. The size of each site indicator is relative to the amount of total kWh utilized there daily. Visit http://www.afdc.energy.gov/afdc/locator/tse/ for additional site information.

1. Gallons of diesel equivalent is calculated assuming a standard energy density of 37.6 kWh per gallon of diesel.
2. Metric tons of carbon dioxide calculated using US EPA greenhouse gas guidelines of 10,180 g CO_2 / gallon of diesel.

1

IV.K.3. Products

Publications

1. Navistar eStar Vehicle Performance Evaluation (Brochure). NREL (National Renewable Energy Laboratory). (2013). 4 pp.; DOE/GO-102012-4035 (4th Quarter 2012, 1st Quarter 2013, 2nd Quarter 2013, 3rd Quarter 2013, and Cumulative).
2. Smith Newton Vehicle Performance Evaluation (Brochure). NREL (National Renewable Energy Laboratory). (2013). 4 pp.; DOE/GO-102013-4282 (4th Quarter 2012, 1st Quarter 2013, 2nd Quarter 2013, 3rd Quarter 2013, and Cumulative).
3. Shorepower Truck Electrification Project STEP (fact sheet). NREL (National Renewable Energy Laboratory). (2013). 2 pp.; DOE/GO-102013-4228.

IV.L. Vehicle Systems Integration (VSI) Laboratory

David E. Smith, Principal Investigator
Oak Ridge National Laboratory
National Transportation Research Center
2370 Cherahala Boulevard
Knoxville, TN 37932-6472
Phone: (865) 946-1324
E-mail: smithde@ornl.gov

Lee Slezak, DOE Program Manager
Phone: (202) 586-2335
E-mail: lee.slezak@ee.doe.gov

IV.L.1. Abstract

Objectives

- Integration of advanced technologies for maximum efficiency and lowest possible emissions.
  - Development and evaluation of supervisory control and advanced propulsion strategies.
  - Exposure of full prototype system to transient and thermal conditions consistent with real world drive cycles.
  - Better understanding of component-to-component interactions.
  - Direct emissions measurements of full system necessary due to low-confidence level in predictive emissions modeling.
- Enhancement of existing analytical models and the development of new advanced technology sub-models.
  - New insight into transient and thermal behavior of advanced technologies.
  - Evaluation of component interfacial issues.
  - Source of transient data for component and full system validation.
- Component development, characterization, and commercialization.
  - Pathway to rapid development and commercialization of high efficiency vehicle technologies.
  - Characterization of advanced components after fleet evaluation to ascertain operational deterioration and effectiveness.
- Support of recent EPA-NHTSA rule with coupled experiments and simulation to assess fuel consumption of heavy duty vehicles, as well as SAE J2711 update (engine and “power-pack” testing).

Major Accomplishments

- The AVL Powertrain Dynamometer Test System has been procured and installed. Full functionality of the test system has been demonstrated utilizing a conventional Class 8 heavy duty powertrain comprised of a Cummins ISX
- The AVL eStorage System (battery emuslator) has been procured and installed in the VSI Powertrain Test Cell
- The hardware-in-the-loop (HIL) system has been procured, installed, and commissioned for both engine-in-the-loop and powertrain-in-the-loop configurations. Both conventional and hybrid powertrain architectures have been successfully demonstrated.
- Two (2) complete sets of emissions analyzers have been procured, installed, and commissioned to measure raw, engine out emissions and post-aftertreatment (tail-pipe) emissions.
- An AVL 250 kW high-speed (12,000 RPM) dynamometer has been ordered for the VSI Component Test Cell. The dynamometer features a through shaft to support two (2) separate experimental set-ups in the laboratory.
- A modular, cross hatch deigned bed plate has been ordered for the VSI Component Test Cell to provide adequate space to support two (2) experimental set-ups simultaneously.

Future Achievements

- Final commissioning of the AVL eStorage System (battery emulator) will be completed early in FY14. The commissioning will utilize a Meritor Class 8 heavy duty hybrid powertrain to sink and source up to 400 kW to complete the overall VSI Powertrain Test Cell commissioning.
- The VSI Component Test Cell will be commissioned mid FY2014 utilizing the small, high-speed dynamometer and bedplate.

✧ ✧ ✧ ✧ ✧

IV.L.2. Technical Discussion

Background

Growing transportation costs and future regulations have increased the focus on vehicle fuel efficiency and emissions control, highlighting a need for more aggressive research addressing the complex interactions of advanced powertrain technologies. Developing these technologies to meet the requirements of the transportation industry can be taxing on limited budgets and stretched engineering resources. ORNL’s Vehicle Systems Integration (VSI) Laboratory is changing the pace of powertrain development in the transportation industry by performing prototype research and characterization of advanced systems. VSI Lab capabilities range from advanced light-duty vehicles to hybridized Class 8 powertrains with the goals of improving overall system efficiency and reducing emissions.

Using co-located core research areas, the VSI Lab is equipped to handle a broad range of analysis requests related to hybrid powertrains including advanced combustion engines, fuels and emissions, and power electronics and electric machinery research. The lab's unique evaluation and simulation capabilities can accommodate engines, electric motors, and transmissions in conventional or hybrid powertrain configurations for vehicles regardless of size, duty, or class. The VSI Lab features the ability to handle highly transient test conditions and to perform "X"-in-the-loop hardware evaluations—testing powertrain components and/or subsystems in virtual vehicle environments as they are subjected to real-world driving conditions.

Introduction

ORNL's Vehicle Systems Integration (VSI) Laboratory was created to accelerate the pace of powertrain development by performing prototype research and characterization of advanced systems and hardware components. In doing so, the VSI Lab contributes to the larger mission—established by ORNL's Center for Transportation Analysis (CTA)—of supplying the foundational data needed to define future vehicle architectures. The VSI Lab is capable of accommodating a range of platforms from advanced light-duty vehicles to hybridized Class 8 powertrains with the goals of improving overall system efficiency and reducing emissions. Coupling this data-rich asset with CTA's complementary capabilities in analysis, modeling, simulation, and visualization represents a powerful resource for users.

The VSI Lab is co-located with two other transportation-centric research centers at ORNL to satisfy virtually any research request or project requirement. The Fuels, Engines and Emissions Research Center (FEERC) at ORNL offers advanced analytical chemistry expertise and unique emissions measurement capabilities, as well as extensive expertise in high efficiency combustion, alternative fuels, and advanced lubricants. Engine evaluations can be conducted with or without the emissions aftertreatment system, and sampling of both the engine-out and aftertreatment-out emissions are possible. The VSI Lab is equipped with a transient emissions measurement system capable of measuring CO_2, NO_X, CO, and HC emissions, and extensive particulate matter characterizations can be performed.

For in-depth power electronics and electric machine componentry analysis and evaluation, the VSI Lab can tap into the Power Electronics and Electric Machinery Research Center (PEEMRC). PEEMRC is home to the Power Electronics and Electric Machines (PEEM) Laboratory, which is recognized as the U.S. Department of Energy's (DOE) lead lab for power electronics and electric motor development. PEEM offers a broad spectrum of state-of-the-art measurement equipment along with a rapid prototyping mechanical fabrication shop. Characterization of high power traction drive systems is critical to understanding overall vehicle system efficiency. The VSI Lab features power analysis tools to fully characterize the high-voltage power electronics and electric machine drive system.

Proper evaluation of advanced technology powertrains requires understanding of real-world operating conditions, such as duty cycle. The VSI Lab draws upon ORNL's Center for Transportation Analysis that provides access and use of ORNL's Medium Truck Duty Cycle (MTDC) and Heavy Truck Duty Cycle (HTDC) databases for developing real-world drive cycles, including grade.

ORNL has extensive transportation-related laboratories in support of the DOE. Many of these facilities directly or indirectly support the Vehicle Systems subprogram. As mentioned previously, ORNL currently and historically supports the DOE on multi-cylinder and vehicle applications of diesel combustion, lean burn gasoline combustion, and low temperature combustion processes, and performs principal research for the DOE on emission controls, thermal energy recovery, alternative fuels, transportation materials, and advanced power electronics and electric machinery. The existence and availability of these resources and corresponding expertise in one location offers a unique opportunity for addressing not only component-level but also vehicle-level system integration challenges. Expertise in close proximity is of critical importance to operate specialized instrumentation, diagnose complicated prototype equipment, and perform non-standard experiments. The proposed VSI laboratory will make use of the collocation of diverse expertise, personnel, instrumentation, and hardware resources to perform unprecedented technology characterizations that will more efficiently expedite promising technologies toward the marketplace.

The modeling/analysis and experimental expertise forms the basis of the VSI laboratory. The vision is a flexible engine-system transient dynamometer laboratory for the rapid characterization of transportation technologies from subcomponent and systems perspective under conditions consistent with realistic on-road operation. The VSI laboratory is necessary to expose the powertrain system to operational conditions consistent with transient drive cycles allowing for the identification of issues related to technology performance, drivability, and noise-vibration-harshness (NVH). This laboratory will be modular by design allowing for minimal downtime to reconfigure the powertrain and supporting components such as aftertreatment and thermal energy recovery systems. Open powertrain control architecture will provide full flexibility for developing vehicle management strategies to balance advanced transportation technologies for optimal efficiency and lowest emissions.

The VSI laboratory is instrumented to provide emissions and performance data for use in the development and evaluation of engine, exhaust emissions aftertreatment, and thermal energy recovery models under steady-state and transient duty cycle conditions. The ability to exercise transient operation in a well-instrumented and controlled environment is essential to the development of more accurate analytical tools and identifying potential issues which typically are not evident in steady-state technology evaluations.

The VSI laboratory will also be well suited for characterizing and developing high power electric traction drive technologies such as those necessary for plug-in hybrid-electric and fuel cell powertrain applications. This laboratory will allow for transient evaluations of advanced power

electronics and electric machinery subcomponents, providing extremely valuable information on subcomponent performance and unprecedented assessment of not only subcomponents but also the entire system to better understand possible synergies or operational issues. Subsystem interactions and potential issues are difficult to identify through modeling or quasi-static evaluations and often require the development and implementation of the full powertrain system for a vehicle chassis dynamometer evaluation.

An integrated approach is critical to the expeditious development and implementation of advanced transportation technologies. Significant improvements in vehicle efficiency AND emissions will require an in depth understanding of the interaction of advanced transportation technologies in situ under real-world conditions.

Approach

A facility capable of powertrain integration research is essential for proper development, evaluation, and validation of emerging high risk, long term transportation technologies. The overall objectives of the ORNL Vehicle Systems Integration (VSI) research laboratory are:

- Enable system-level research that integrates the best of advanced combustion, electric drive, controls, and fuels within applicable emissions constraints. ORNL has made numerous contributions within all these individual technology areas.
- Establish a dedicated propulsion dynamometer laboratory to support prototype component and subsystems integration R&D.

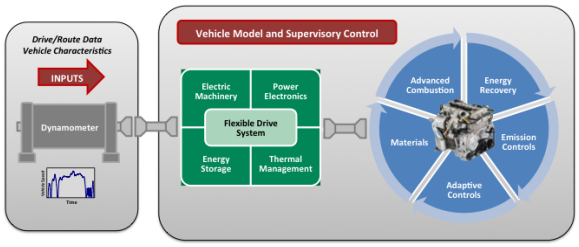

Figure IV-189: VSI Lab Concept for Prototyping and Testing Integrated Components and Subsystems.

The ORNL VSI Laboratory is designed to be a dedicated systems integration facility to fully support the mission of the U.S. DOE Vehicle Technologies Office as it:

- Fosters DOE VTP cross-cutting activities in core areas such as Vehicle Systems, Advanced Combustion and Emissions, Fuels Technologies, and Advanced Power Electronics and Electric Machinery.
- Leverages DOE R&D investments from light-duty vehicles to medium- and heavy-duty vehicles.
- Focuses on systems interactions subjected to "real-world" conditions with focus on emissions, thermal transients, and drivability.

Highlights of the ORNL VSI Laboratory include the following unique capabilities/features:

- Exploits existing co-location of core competencies at ORNL to allow for thorough technology characterizations and for deeper understanding of technology merits.
- Data collection activities fully support DOE VTP modeling/simulation efforts with detailed model development/verification.
- Full heavy-duty capability to support research in emerging medium and heavy duty advanced powertrain systems.
- Modular design with propulsion dynamometer and HIL component emulation minimizes downtime to reconfigure drive systems and supporting technologies.
- Allows better understanding of synergies and/or operational issues for optimal efficiency AND lowest emissions.

As depicted in Figure I-3: VSST Activities Integration—Arrows represent information flow between activity focus areas that enhances effectivenets of individual activitiesFigure IV-190, The VSI Lab features an "X"-in-the-loop (XIL) platform in order to analyze a powertrain component or subsystem in a virtual vehicle environment. The "X" in the loop could be a single component, such as an engine or electric motor. In addition, the "X" could be a complete subsystem, such as an engine plus transmission or even full hybrid powertrain.

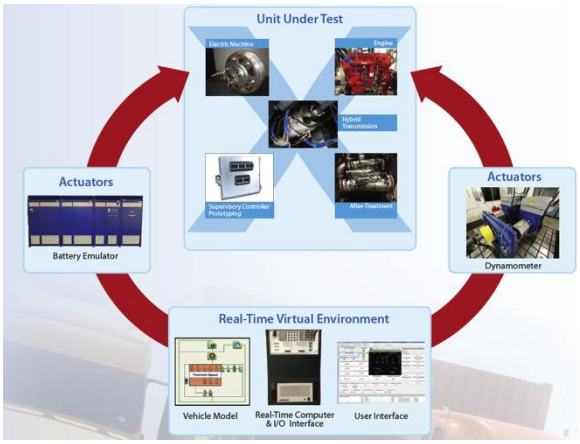

Figure IV-190: VSI Lab X in the Loop.

Results

The ORNL VSI Laboratory has been constructed based upon delivering maximum flexibility for powertrain integration research and evaluation. Two (2) physical test cells represent the VSI laboratory: the Powertrain Test Cell and the Component Test Cell. An overview of each test cell, as well as key specifications, is shown in Table IV-28.

Table IV-28: ORNL VSI Test Cell Highlights.

VSI Powertrain Test Cell	VSI Component Test Cell
• Powertrain "X"-in-the-loop environment capable of testing light-duty to full heavy-duty Class 8 powertrain at a vehicle level • Heavy-duty focus to evaluate engines, transmissions, and integrated powertrains, as well as inherent full light-duty powertrain capability	• Component "X"-in-the-loop environment capable of testing engines, electric machines, and energy storage systems at a vehicle level • Light-duty focus with medium-duty powertrain component capability
Specifications: • Twin AVL 500 kW AC transient dynamometers, each capable of up to 3,750 N·m of torque • Acceleration/deceleration rates of up to 3,500 rpm/sec • Up to 20,000 N·m of torque when dynamometers are linked through summing gearbox for powertrain applications	Specifications: • An AVL 250 kW, low-inertia dynamometer capable of up to 650 N·m of torque • 12,000 rpm high-speed capability • Double-ended to accommodate two independent experiments simultaneously
Shared Features: • An AVL 400 kW (up to 800 V and 600 A) energy storage emulator with stand-alone flexibility to simulate and evaluate different energy storage systems • A dSPACE HIL real-time platform for vehicle and subsystem emulation • Duel transient emissions measurement system for criteria emissions and particulate matter	

A twin dynamometer approach was adopted as this was found to be the most cost effective solution to address the low speed, high torque operating characteristics typical of Class 8, fully loaded trucks. In addition, the twin dynamometer solution offers a wide range of flexibility for evaluating various powertrain components, as well as powertrain architectures. Figure IV-191 represents a single component-in-the-loop (engine or electric machine) test configuration. In this instance, the gearbox is set aside and the engine with or without aftertreatment becomes the unit under test. The rest of the vehicle and powertrain is emulated in the virtual environment. The dynamometers feature low inertia and high response rates such in order to simulate transmission gearshifts.

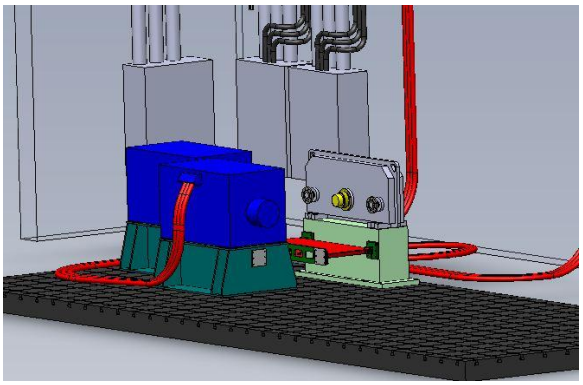

Figure IV-191: ORNL VSI Powertrain Test Cell single engine test configuration.

Figure IV-192 illustrates utilization of the dynamometers for two (2) distinct purposes. The first focuses on characterization of transmissions. One dynamometer is used as a source (such as emulating an engine), and the other is used as a sink. In this configuration, spin losses and limited loading of the transmission can be performed. The second use of this configuration is to test a complete light duty, front wheel drive powertrain.

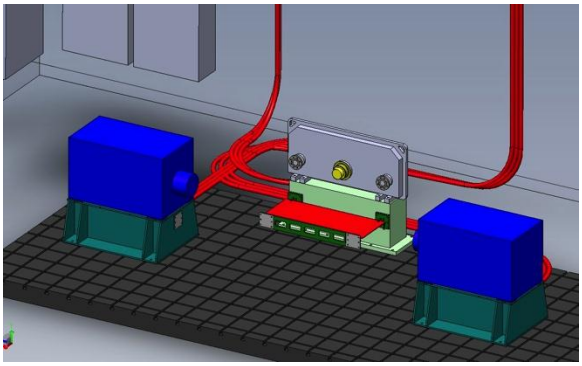

Figure IV-192: ORNL VSI transmissions and front wheel drive powertrain test configuration.

The ability to test a complete "power pack", consisting of an engine plus a transmission, for a fully loaded Class 8 truck is the focus of the VSI laboratory. Figure IV-193 represents an actual installation of a conventional "power pack" comprised of a 15-liter Cummins ISX engine coupled to an Eaton Ultrashift automated manual transmission. The test cell is capable of both conventional and hybrid powertrains for a variety of architectures. The battery emulation system provides a flexible environment for subjecting the powertrain under test to a variety of possible energy storage solutions.

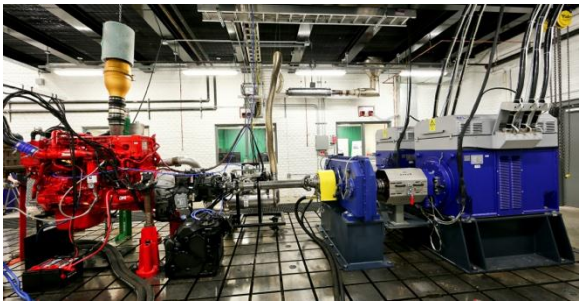

Figure IV-193: ORNL VSI Powertrain Test Cell "power pack" test configuration for heavy duty applications.

To exercise the system and demonstrate performance, the dual dyno configuration was used to characterize the maximum torque curve for the conventional powertrain shown in Figure IV-193. Figure IV-194 shows the results of this testing for all ten (10) speeds of the Eaton transmission for a controlled speed ramp rate of 8 RPM/s, as well as emulated vehicles with masses of 30,000 kg and 60,000 kg. The maximum torque generated by this powertrain was found to be just over 18,000 N*m, demonstrating the full range capability of the VSI Powertrain Test Cell.

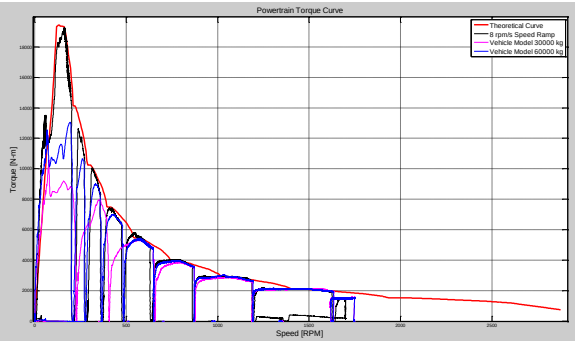

Figure IV-194: Maximum powertrain torque curve for Cummins ISX450 15-L engine and Eaton Ultrashift 10-speed transmission.

More tests were conducted on the conventional powertrain coupled to the twin dynamometer configuration in order to evaluate the hardware-in-the-loop and virtual vehicle capabilities. The GEM model from EPA was incorporated into the system as a further demonstration of the flexibility to integrate a wide variety of vehicle models. Figure IV-195 represents a snapshot of the results of one of these tests that shows the emulated vehicle speed, as well as actual powertrain data. Powertrain torque, gear, and engine speed are just a few of the parameters shown in the Figure IV-195. The ORNL VSI Powertrain Test Cell is monitors and records a wide variety of data, and has the latitude to add further sensors as future tests dictate.

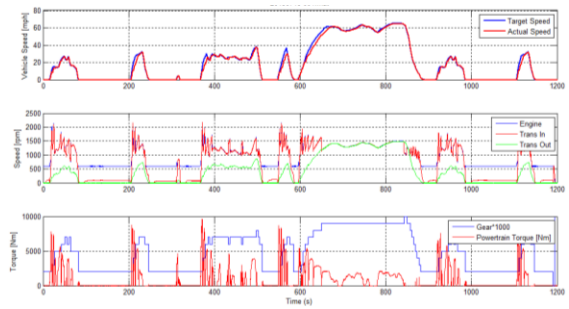

Figure IV-195: Vehicle test cycle (vFTP) combining EPA's GEM model and ORNL's powertrain-in-the-loop environment.

Conclusions

The ORNL Vehicle Systems Integration Laboratory has been established to enhance research and development of advanced powertrain technologies and evaluate them from a vehicle perspective. The goal of the facility is to test candidate technologies in a controlled laboratory environment, while exposing them to "real world" conditions as if they were mounted in actual vehicles. Figure IV-196 represents this concept graphically.

Figure IV-196: ORNL VSI Laboratory Powertrain Test Cell: powertrain testing in a virtual vehicle environment.

V. MODELING AND SIMULATION

LIGHT DUTY

V.A. Autonomie Maintenance

Shane Halbach, Principal Investigator
Argonne National Laboratory
9700 South Cass Avenue
Argonne, IL 60439-4815
Phone: (630) 252-2853
E-mail: shalbach@anl.gov

David Anderson, DOE Program Manager
Phone: (202) 287-5688
E-mail: David.Anderson@ee.doe.gov

V.A.1. Abstract

Objectives

Enhance and maintain Autonomie as needed to support the U.S. Department of Energy (DOE), the user community, and hardware-in-the-loop/rapid control prototyping (HIL/RCP) projects.

Major Accomplishments

- Modeling Enhancements
  - Updated default vehicles to avoid engine speed oscillations
  - Updated look-ahead driver model for performance tests
  - Provided support for Matlab .slx files
  - Provided support for ToWorkspace outputs from models
- User Interface Enhancements
  - New Simulink configuration options
  - Improved model and initialization files import process
  - Improved support for creating new configurations
  - Integrated, Microsoft-style help
  - Integration with CosiMate
  - "Conserve Memory" simulation option

Future Achievements

Continue to enhance Autonomie to support DOE and technical transfer.

✧ ✧ ✧ ✧ ✧

V.A.2. Technical Discussion

Background

Autonomie is a plug-and-play powertrain and vehicle model architecture and development environment that supports the rapid evaluation of new powertrain/propulsion technologies for improving fuel economy through virtual design and analysis in a math-based simulation environment. Autonomie has an open architecture to support the rapid integration and analysis of powertrain/propulsion systems and technologies. This allows rapid technology sorting and evaluation of fuel economy under dynamic/transient testing conditions.

Introduction

To better support DOE and its users community, several new features have been implemented in Autonomie. Some of the most significant accomplishments are described below.

Approach

There are always more ideas for new Autonomie features and enhancements than time to actually implement them. Feedback on which items to prioritize and include is collected in several ways.

First, users of Autonomie register suggestions for improving the software or models through our online issue-tracking system at www.autonomie.net. Second, direct interaction with partners and sponsors while working on shared projects also contributes to collecting new requirements. Finally, DOE studies often drive the improvement of existing capabilities and /or the development of new ones.

Results

Modeling Enhancements

Updated Default Vehicles to Avoid Engine Speed Oscillations

Engine speed oscillations were detected for some of the default vehicles in Autonomie containing automatic transmissions (Figure V-1). Analysis was performed, and the issue was traced to a non-optimal input parameter on the

torque converter. Analysis was performed, and the value was updated to provide more stable and accurate results.

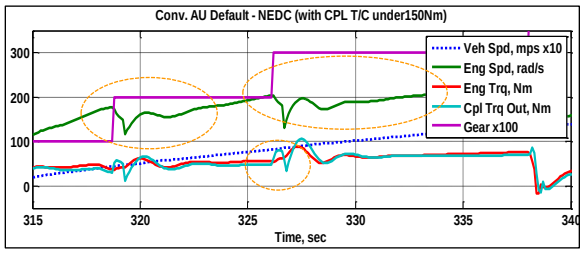

Figure V-1: Engine Speed Oscillation Detected.

Updated Look-ahead Driver Model for Performance Tests

An issue was detected with the look-ahead driver in relationship to performance tests. The look-ahead driver model "peeks" at the upcoming cycle, allowing it to more closely follow the drive trace. However, in the case of a performance test, the look-ahead driver was able to "jump the gun" and get a head start compared to the proportional-integral (PI) driver (Figure V-2).

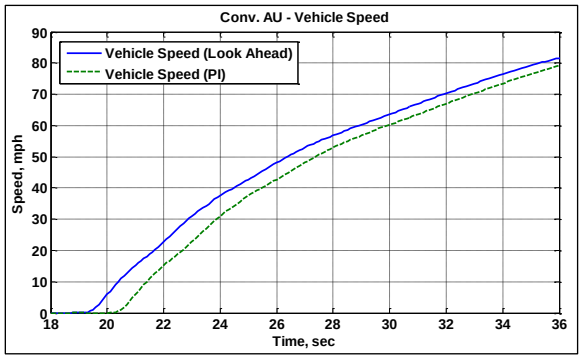

Figure V-2: Before Driver Adjustment.

A new parameter was added to the driver called time_anticipate_start, which was tuned so that the look-ahead driver no longer has a head start on the performance test, resulting in more accurate results (Figure V-3).

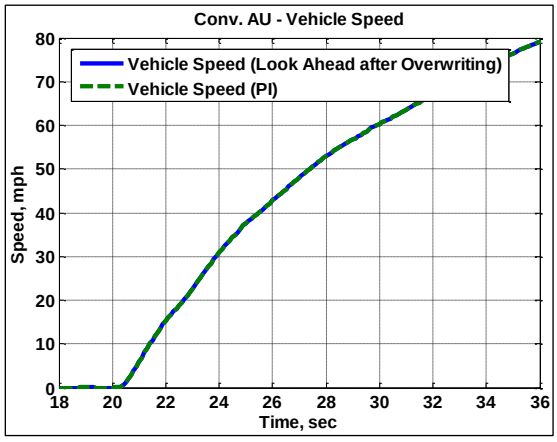

Figure V-3: After Driver Adjustment.

Support for Matlab slx Files

Autonomie is dependent on the Matlab software package, which has two software releases a year. Every attempt is made to support to widest possible range of Matlab releases; however, this can sometimes be difficult to achieve. Matlab changes, intentional or otherwise, are introduced with each new version, and some versions are not backwards compatible.

In particular, starting with Matlab version 2012a, Matlab introduced sweeping new changes that affected all aspects of Autonomie. In particular, they replaced the long-standing mdl file extension for models with a new standard of slx (similar to the way Microsoft Word switched from doc to docx).

Nearly all of the code in Autonomie had to be re-tested and modified to work with these radically different file types, and in some instances special-case code had to be developed in order to be backwards compatible with previous versions of Matlab.

These changes allow users to seamlessly upgrade to the current versions of Matlab, taking full advantage of the new Matlab features without losing any functionality in Autonomie.

Support for ToWorkspace Outputs from Models

Previously, Autonomie could automatically send the information contained in signals to the Matlab workspace for data analysis when the simulation was complete. However, this functionality extended only to information traveling on Autonomie buses; if a user manually added Matlab ToWorkspace blocks to their models, Autonomie did not know about them and could not make them available for data analysis in the user interface.

Now, when a model is imported, Autonomie will catalog those ToWorkspace blocks and store the information for later. In this manner, user-logged ToWorkspace information is now available for data analysis in the regular Autonomie data analysis window. This provides users with the greatest flexibility in designing the data output of their models.

User Interface Enhancements

Improved Model and Initialization Files Import Process

One of the first things new users to Autonomie do is import their own models. Therefore, it is very important that this functionality be robust and easy to use. At the request of numerous users, several improvements have been made to the import processes to help users import their files to Autonomie and to get up and running as fast as possible.

One of the main changes has to do with related files. This section of the import wizard was redesigned to streamline the process and facilitate the selection of the necessary related files (Figure V-4). Selecting the correct related files is an important step, and errors during this part of the import might have consequences when the simulations are run. Often, when the problems do occur later in the process, the user does not know what is causing them or how to fix them. The redesign of the process will minimize these recurring issues.

The other important change is that a new configuration file is provided that can set up defaults for certain parts of the import process. If a user has organizational selections that must be made over and over again, they can be codified into a configuration file. This will minimize errors, because the user will not need to remember to make the selections each time.

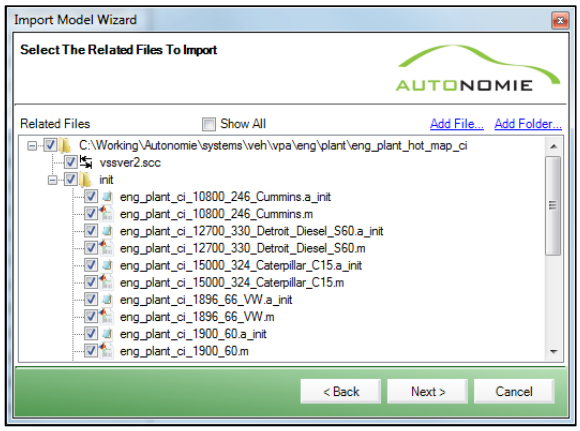

Figure V-4: New Related Files Screen.

Improved Support for Creating New Configurations

Another functionality new users of Autonomie frequently use is the ability to create configurations. Previously, this required a few manual steps, especially if the user wished to start from an existing configuration.

Now, users will have the choice of two wizards, import configuration from model or import configuration from an existing configuration that will walk the user through the process of creating a new configuration (Figure V-5).

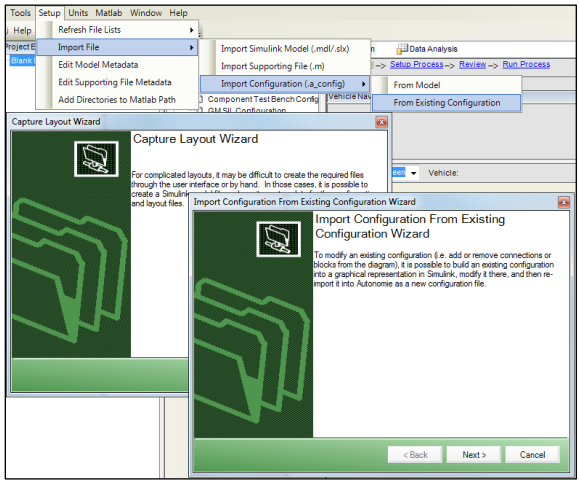

Figure V-5: Import Configuration Wizards.

Integrated, Microsoft-style Help

Previously, help was integrated as a series of task-based pdf files included in the release directory. The help has now been completely redone and revamped as a Microsoft Help Explorer and integrated into the user interface.

The main advantage of the new help is the ability to search the help, as well as browse through all of the help in one location (Figure V-6).

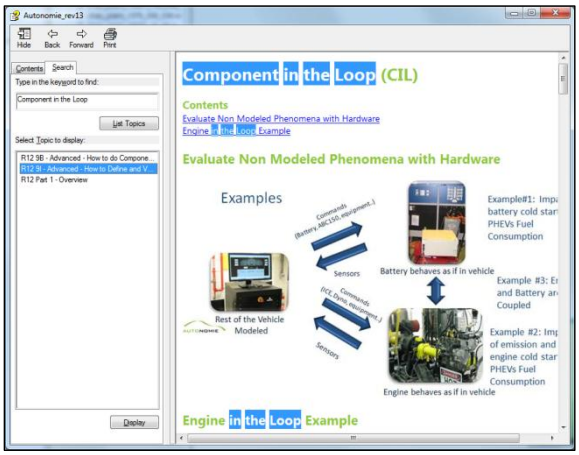

Figure V-6: Search the Autonomie Help.

The help has also been implemented into the user interface, so that context-sensitive help is now possible (i.e., clicking on certain items can open the help to the relevant topic; Figure V-7).

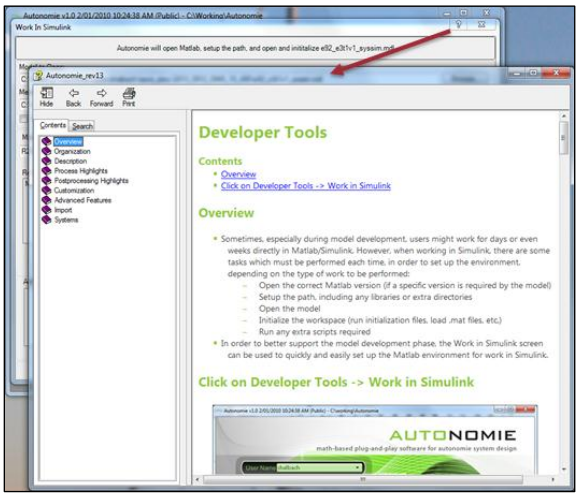

Figure V-7: Context-Sensitive Help for Work in Simulink.

The user interface can also launch context-sensitive help for model files (Figure V-8).

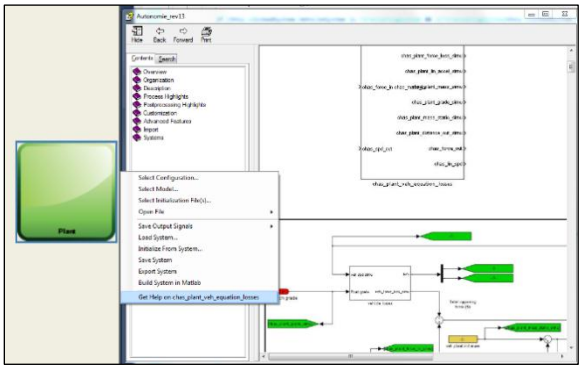

Figure V-8: Launching the Model Help.

Integration with CosiMate

Autonomie is a system integration tool. As such, its usefulness is tied directly to the number and variety of tools that can be used with the software. Autonomie now features a linkage with the CosiMate co-simulation software from ChiasTek. This software allows models from different expert tools to be run in their native environments simultaneously. This means that the Simulink parts of the vehicle can be run in Simulink, while a detailed part of the model, such as a transmission modeled in AMESim, is run in the native AMESim environment.

This provides several advantages. First, the simulation runs faster, because the model can be distributed across several cores or computers. Second, the native environment may provide better data analysis capability for models developed in that tool. Third, CosiMate connects to a wide variety of tools, extending the types of models that can be used in Autonomie. For example, using CosiMate, Autonomie is able to integrate physical models developed in the Saber modeling platform from Synopsys (Figure V-9).

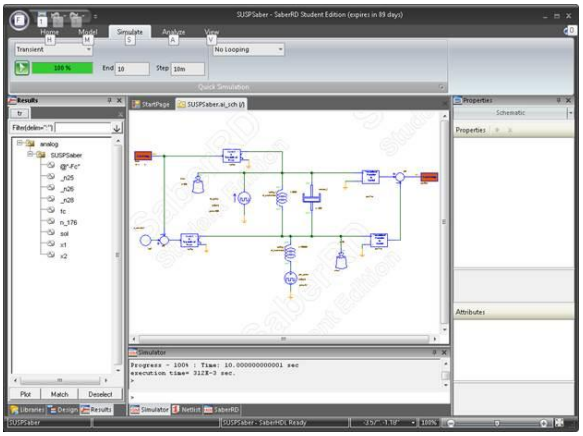

Figure V-9: Saber Model That Has Been Integrated into Autonomie.

New Simulink Configuration Options

Previously, Simulink was configured via a custom-developed solution, which allowed users to set up advanced simulation options via a dialog. Ultimately, this solution was limited because Autonomie dialog did not match the native Simulink dialog, which led to difficulties in trying to find the correct parameters and errors trying to apply them, and was difficult to update and maintain from version to version. Users were therefore prevented from configuring Simulink in ways necessary to run their models.

Now, Autonomie calls the underlying Simulink implementation so that the user experience through Autonomie is identical to that through Simulink (Figure V-10).

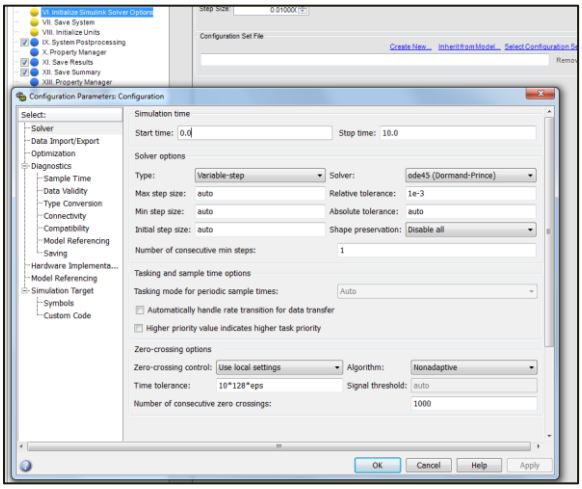

Figure V-10: Simulink Configuration Options.

"Conserve Memory" Simulation Option

Studies are requiring an ever increasing number of simulations, in some cases resulting in terabytes of data. In order to conserve disk space, users can choose to prevent some of the unnecessary signals from saving to the simulation output files. This can be a time-consuming processes, especially since it is not always obvious which signals are necessary and which are not.

Users can now elect to recursively set any unused signals not to save to the output files with a single click (Figure V-11). This avoids the potential of a user accidentally removing a necessary signal. Of course, if desired, individual signals can be once again set to write to the output files on a case-by-case basis.

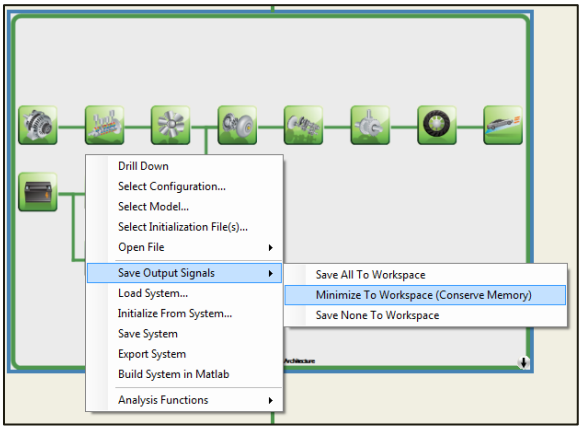

Figure V-11: "Conserve Memory" from a Single Click.

Conclusions

The latest version of Autonomie includes numerous new features that were developed on the basis of feedback from DOE and the user community.

V.A.3. Products

Publications

1. L. Michaels, S. Halbach, N. Shidore, A. Rousseau, "Applications of Model-based Systems Engineering Methods to Vehicle and Subsystem Design and Optimization," 5th Annual Ground Vehicle Systems Engineering and Technology Symposium, Troy, Aug. 20–22, 2013.
2. L. Michaels, A. Rousseau, "Tutorial—Model Based System Engineering (MBSE): The Rise of the Machines?" 2013 ITEC (IEEE Transportation Electrification Conference), Detroit, June 19, 2013.
3. L. Michaels, "MBSE with Autonomie," MBSE Tech-Fast, SAE Detroit Section, March 26, 2013.

Patents

1. "Flexible Evaluator for Vehicle Propulsion Systems" United States Patent No. 8,510,088.

Tools and Data

1. Autonomie Rev13, October 2013.

V.B. Simulation Runs to Support GPRA

Ayman Moawad, Principal Investigator
Organization: Argonne National Laboratory
Address: 9700 South Cass Avenue
Argonne, IL 60439-4815
Phone: (630) 252-2849
E-mail: amoawad@anl.gov

David Anderson, DOE Program Manager
Phone: (202) 287-5688
E-mail: david.anderson@ee.doc.gov

V.B.1. Abstract

Objectives

- Simulate multiple vehicle platforms, configurations, and timeframes to provide fuel economy data for analysis in support of the Government Performance and Results Act (GPRA). This will involve the following:
  - Validate component and vehicle assumptions with the U.S. Department of Energy (DOE) national laboratories and U.S. Drive Tech Teams.
  - Use automatic component sizing to run the study.

Major Accomplishments

- Simulated and sized more than 2,000 vehicles for light duty applications.
- Simulated new vehicles when assumptions or platforms were revised or when additional configurations or timeframes were requested.
- Generated new output format for market penetration models.

Future Achievements

- Continue to provide analytical data to support GPRA in 2014.

✧ ✧ ✧ ✧ ✧

V.B.2. Technical Discussion

Background

Through the Office of Planning, Budget, and Analysis, DOE's Office of Energy Efficiency and Renewable Energy (EERE) provides estimates of program benefits in its annual Congressional Budget Request. The Government Performance and Results Act (GPRA) of 1993 provided the basis for assessing the performance of federally funded programs. Often referred to as "GPRA Benefits Estimates," these estimates represent one piece of EERE's GPRA implementation efforts—documenting some of the economic, environmental, and security benefits (or outcomes) that result from achieving program goals.

Introduction

The simulation tool *Autonomie* was used to evaluate the fuel economy of numerous vehicle configurations (including conventional, hybrid electric vehicles [HEVs], plug-in HEVs [PHEVs], and all-electric vehicles), component technologies (gasoline, diesel, and compressed natural gas [CNG], as well as fuel cells), and timeframes (2013, 2015, 2020, 2030, and 2045). The uncertainty of each technology is taken into account by assigning probability values for each assumption.

Approach

To evaluate the fuel efficiency benefits of advanced vehicles, the vehicles are designed on the basis of component assumptions. The fuel efficiency is then simulated on the Urban Dynamometer Driving Schedule (UDDS) and Highway Fuel Economy Test (HWFET). The vehicle costs are calculated from the component sizing. Both cost and fuel efficiency are then used to define the market penetration of each technology to finally estimate the amount of fuel saved. The process is highlighted in Figure V-12. This report focuses on the first phase of the project: fuel efficiency and cost.

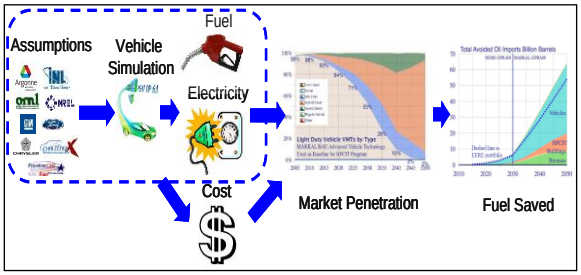

Figure V-12: Process to Evaluate Fuel Efficiency of Advanced Technology Vehicles.

To properly assess the benefits of future technologies, the following options were considered, as shown in Figure V-13:

- Different vehicle classes: compact car, midsize car, small sport utility vehicle (SUV), medium SUV, and pickup truck.
- Five timeframes: 2013, 2015, 2020, 2030, and 2045.
- Five powertrain configurations: conventional, HEV, PHEV, fuel cell HEV, and electric vehicle.
- Four fuels: gasoline, diesel, CNG, and ethanol.

Overall, more than 2,000 vehicles were defined and simulated in Autonomie. The current study includes micro hybrids as they are introduced as a substitute for conventional vehicles starting from 2030 (medium uncertainty case). This study does not focus on emissions.

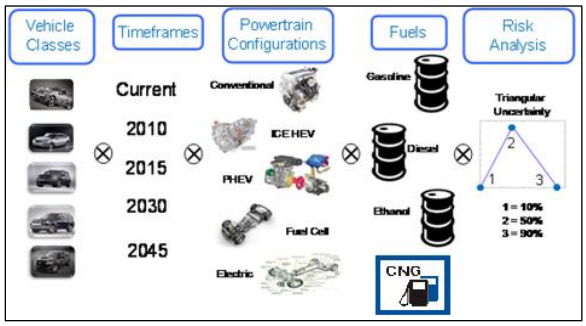

Figure V-13: Vehicle Classes, Timeframes, Configurations, and Fuels Considered.

To address uncertainties, a triangular distribution approach (low, medium, and high) was employed, as shown in Figure V-14. For each component, assumptions regarding efficiency, power density, etc., were made, and three separate values were defined to represent the (1) 90th percentile, (2) 50th percentile, and (3) 10th percentile. A 90% probability means that the technology has a 90% chance of being available at the time considered. For each vehicle considered, the cost assumptions also follow the triangular uncertainty. Each set of assumptions is, however, used for each vehicle, and the most efficient components are not automatically the least-expensive ones. As a result, for each vehicle considered, we simulated three options for fuel efficiency. Each of these three options also has three values representing the cost uncertainties.

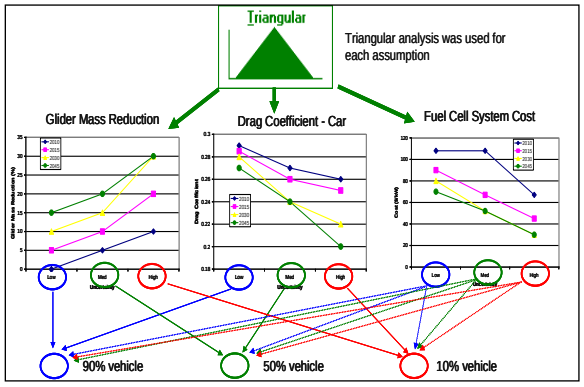

Figure V-14: Uncertainty Process.

Vehicle Technology Projections

The assumptions described below have been defined on the basis of inputs from experts and the U.S. Drive Team targets (when available).

Engines

Several state-of-the-art internal combustion engines (ICEs) were selected as the baseline for the fuels considered: gasoline (spark ignition or SI), diesel (compression ignition or CI), ethanol (E85), and compressed natural gas (CNG). The engines used for reference conventional vehicles were provided by automotive car manufacturers. The proprietary engine data used for HEVs and PHEVs are based on Atkinson cycles. Table V-1 shows the engines selected as a baseline for the study.

Table V-1: Engines Selected.

Fuel	Source	Displacement (L)	Peak Power (kW)
SI (Conv)	Car Manufacturer	1.8	99
CI	Car Manufacturer	1.9	110
CNG	Car	1.5	112
E85 (Conv)	Car Manufacturer	2.2	106

Fuel Cell Systems

Figure V-15 shows the evolution of the fuel-cell system peak efficiencies. The peak fuel-cell efficiency is assumed to be at 60% currently, and will increase to 69% by 2045.

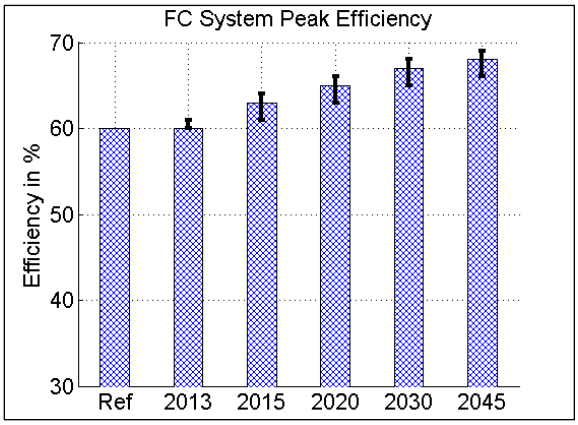

Figure V-15: Fuel-Cell System Efficiency.

CNG Storage Systems

As in the case of the fuel-cell systems, all the assumptions used for natural gas (NG) storage were based on values provided by DOE. Overall, the volumetric capacity dramatically increases (double) between the reference case and 2045, going from 0.24 kg NG/kg to 0.538 kg NG/kg. Also, the percentage NG used in the tank increases over time: it was 83% value for the reference case through 2020, then rose to a constant value of 90% for the next years.

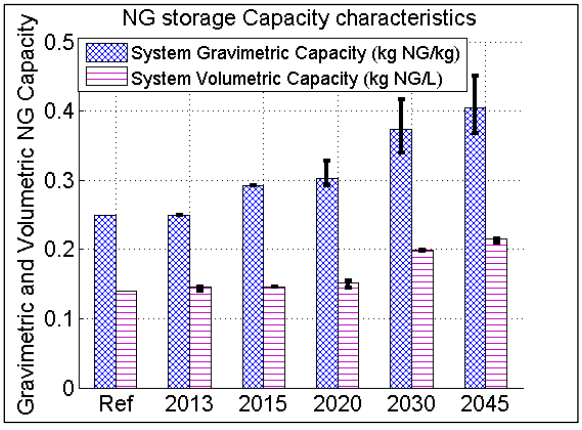

Figure V-16: Hydrogen Storage Capacity in Terms of Hydrogen Quantity.

Electric Machines

Two types of electric machine will be used as references in the study:

- The power-split vehicles are powered by a permanent magnet electric machine (similar to Toyota Camry), which has a peak power of 105 kW and a peak efficiency of 95%.
- The series configuration (fuel cell) and electric vehicles use an induction electric machine with a peak power of 72 kW and a peak efficiency of 95%.

Energy Storage System

The HEV reference case includes a Ni/metal hydride battery. It is assumed that this technology is the most likely to be used until 2015 for the low uncertainty case. This technology is similar to that found in the Toyota Prius. Both the medium and high uncertainty cases use a lithium-ion battery. For PHEV applications, all the vehicles are run with a Li-ion battery from Argonne.

After a long period of operation, batteries lose some of their power and energy capacity. To be able to maintain the same performance at the end of life (EOL) compared to the beginning of life (BOL), an oversize factor is applied while sizing the batteries for both power and energy. These factors are supposed to represent the percentage of power and energy that will not be provided by the battery at the EOL compared to the initial power and energy given by the manufacturer. The oversize factor decreases over time to reflect an improvement in the ability of batteries to uniformly deliver the same performance throughout their life cycles.

Vehicle

As previously discussed, five vehicle classes were considered, listed in Table V-2.

Table V-2: Vehicle Characteristics for Different Light Duty Vehicle Classes.

Vehicle Class	Glider Mass (Ref) (kg)	Frontal Area (Ref) (m^2)	Tire	Wheel Radius (m)
Compact Car	820	2.331	P195/65/R15	0.317
Midsize car	1000	2.2	P195/65/R15	0.317
Small SUV	1150	2.52	P225/75/R15	0.35925
Midsize SUV	1260	2.88	P235/70/R16	0.367
Pickup	1500	3.21	P255/65/R17	0.38165

Because of the improvements in material, the glider mass is expected to significantly decrease over time. Although frontal area is expected to differ from one vehicle configuration to another (i.e., the electrical components will require more cooling capabilities), the reduction values were considered constant across the technologies.

Vehicle Powertrain Assumptions

All the vehicles have been sized to meet the same requirements:

- 0–60 mph in 9 s ± 0.1 s
- Maximum grade of 6% at 65 mph at gross vehicle weight
- Maximum vehicle speed of >160 km/h

For all cases, the engine or fuel cell powers are sized to complete the grade requirement without any assistance from the battery. For HEVs, the battery was sized to recuperate the entire braking energy during the UDDS. For the PHEV case, the battery power is defined as its ability to follow the UDDS in the electric mode for the 10- and 20-mile cases and the US06 drive cycle for the 30- and 40-mile cases, while its energy is calculated to follow the UDDS for a specific distance regardless of distance.

Input modes for the power-split configurations, similar to those used in the Toyota Camry, were selected for all HEV applications and PHEVs with low battery energies. Extended Range Electric Vehicle (EREV) configurations were used for PHEVs with high battery energies (e.g., range of 30 miles and up in EVs on the UDDS). The series fuel cell configurations use a two-gear transmission to allow them to achieve the maximum vehicle speed requirement.

Results

The vehicles were simulated on both the UDDS and HWFET drive cycles. The fuel consumption values and ratios presented below are based on unadjusted values.

Evolution of HEV vs. Conventional

The comparisons between power-split HEVs and midsize conventional gasoline vehicles (same year) in Figure V-17 show that the fuel consumption ratios increase slightly for all fuel cases with time. The advances in component technology will not significantly benefit HEVs. Conventional vehicles tend to improve quickly and catch up to HEVs as the ratio gets closer to 1 by 2045.

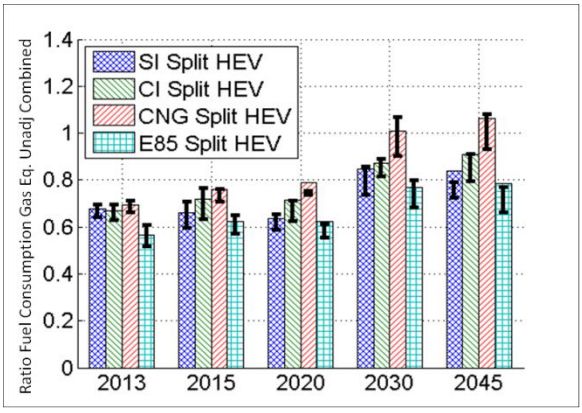

Figure V-17: Ratio of Fuel Consumption Gasoline Equivalent (unadjusted) for HEV to That of Conventional Gasoline Vehicle of Same Year and Size.

Figure V-18 shows the vehicle cost ratio between HEV and conventional vehicles. As expected, HEVs remain more expensive than conventional vehicles, but the difference significantly decreases because costs associated with the battery and electric machine fall faster than those for conventional engines.

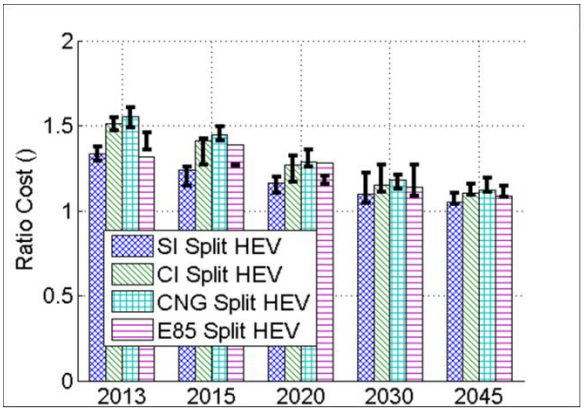

Figure V-18: Vehicle Cost Ratio for HEVs Compared to Gasoline Conventional Vehicle of the Same Year and Size.

Evolution of HEV vs. Fuel Cell

Figure V-19 shows the fuel consumption comparison between HEVs and fuel cell (FC) HEVs for the midsize-car case. Note that the fuel cell vehicles continue to provide better fuel efficiency than the HEVs, with ratios above 1. However, the ratios vary over time, depending upon the fuel considered.

Because of the larger improvements considered for the gasoline engine, the gasoline power split shows the best improvement in fuel consumption in comparison to the fuel cell technology. Both diesel and ethanol HEVs follow the same trend as the gasoline HEV.

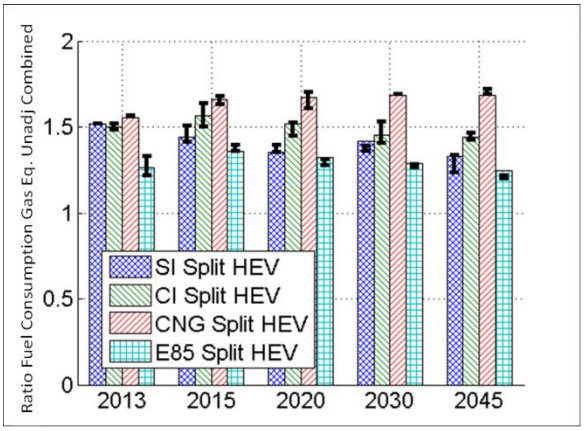

Figure V-19: Ratio of Fuel Consumption Gasoline Equivalent (unadjusted) for HEV to That of Fuel Cell HEV of Same Year and Size.

Figure V-20 shows the vehicle cost comparison between HEVs and FC HEVs. Note that the cost difference between both technologies is expected to decrease over time.

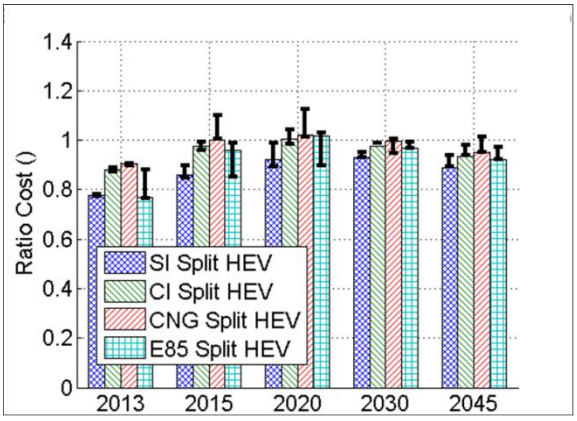

Figure V-20: Cost Ratio of HEV Compared to FC HEV Vehicle of the Same Year and Size.

Evolution of PHEVs

Figure V-21 indicates that the fuel-consumption evolution for power-split PHEVs is similar to that for power-split HEVs with a gasoline engine.

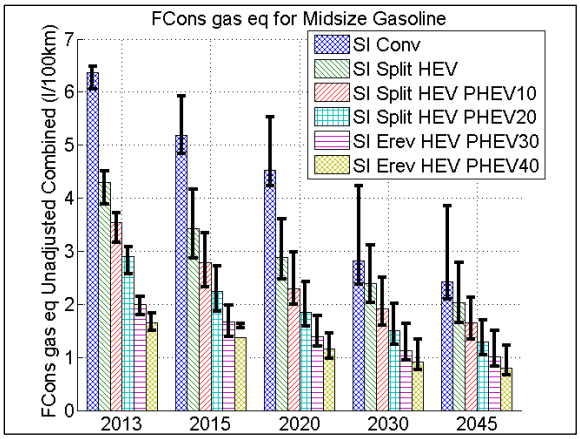

Figure V-21: Fuel consumption evolution for HEV, PHEVs, Gasoline Engine Vehicle (midsize car).

Table V-3 shows that improvement ranges from 28% to 67% for PHEVs with various driving ranges and 40% to 64% for the HEV powertrain.

Table V-3: Fuel Consumption in L/100km of HEV, PHEVs, and Conventional Gasoline Engine Vehicle (midsize car).

				Percentage	
	Ref.	Low	High	Low	High
Conv.	6.4	3.8	2.1	40.6	67.2
HEV	4.5	2.7	1.6	40.0	64.4
PHEV10	3.7	2.1	1.3	43.2	64.9
PHEV20	3.1	1.7	1	45.2	67.7
PHEV30	2.1	1.5	0.8	28.6	61.9
PHEV40	1.8	1.2	0.6	33.3	66.7

Electric consumption trends to decrease over time for all PHEV ranges (Figure V-22); however, EREV electric consumption is almost twice as much as power-split PHEVs. This increase is due to the configuration itself, in addition to the fact that they are being sized on US06 drive cycles.

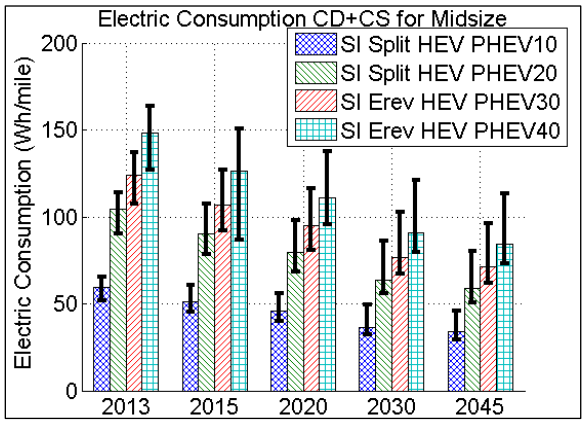

Figure V-22: Electric Consumption for PHEVs with Gasoline Engine (midsize car).

Figure V-23 shows a linear relationship between vehicle mass and electric consumption: the bigger the vehicle, the higher the electrical consumption. For every 200 kg decrease in mass, there is a 50 Wh/mile decrease in electric consumption.

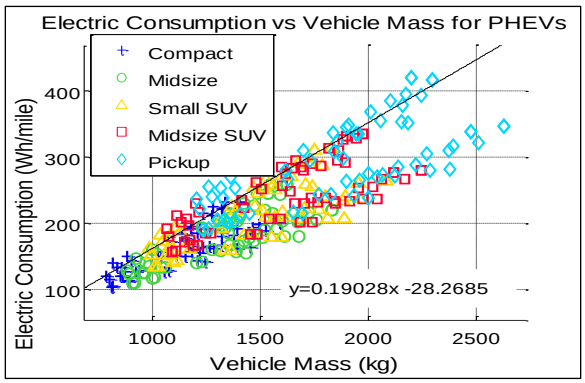

Figure V-23: Electric Consumption in CD+CS Mode for Power-Split PHEVs with Gasoline Engine.

Trade-off between Fuel Efficiency and Cost

Figure V-24 shows the trade-off between fuel efficiency and cost for HEVs with different fuel as a function of time. The overall trend is lower fuel consumption and lower cost. Gasoline and ethanol HEVs offer the best trade-offs over time.

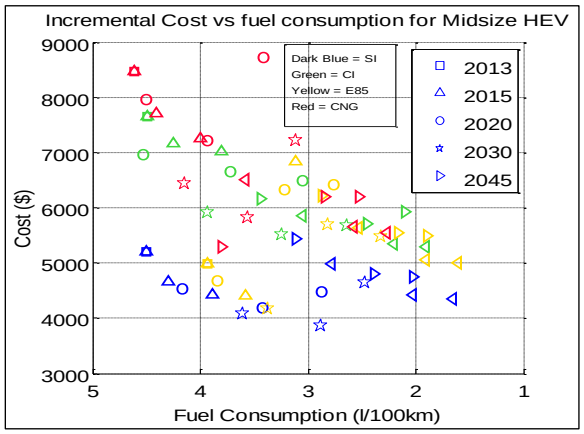

Figure V-24: Incremental Cost vs. Fuel Consumption for Midsize HEVs.

Figure V-25 shows a comparison of all the powertrains, but for gasoline fuel only. The main conclusion is that conventional vehicles are more likely to improve in fuel efficiency than in cost, whereas the higher the electrification level, the more the improvement focuses on cost. For example, the incremental cost for the PHEV40 decreases from $10,800 to $5,200 between 2010 and 2045, whereas the incremental cost for the conventional gasoline vehicle increases from $0 to $3900 over the same period.

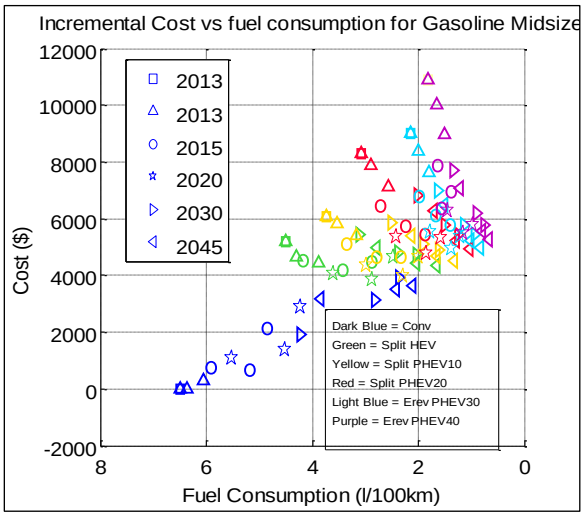

Figure V-25: Incremental Cost (in comparison to the reference conventional gasoline vehicle manufacturing cost) as a Function of Fuel Consumption for Gasoline Vehicles.

Figure V-26 shows the trade-offs between fuel consumption and increased costs for all powertrains and fuels compared to the conventional gasoline vehicle. Overall, the vehicles on the bottom right would provide the best fuel consumption for the least additional cost. All years, all types of vehicle, and all fuels are represented.

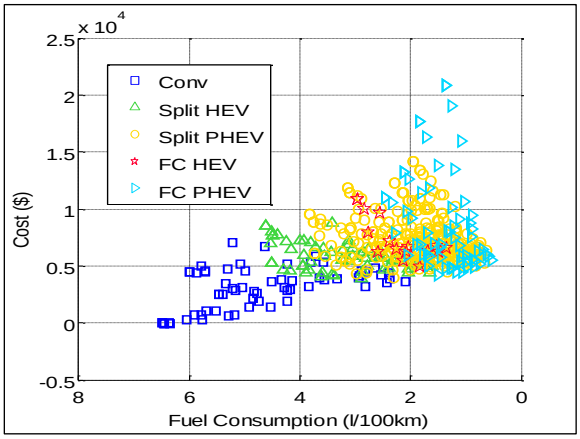

Figure V-26: Incremental Cost (in comparison to the gasoline conventional vehicle) as a Function of Fuel Consumption for All Powertrains.

Conclusions

More than 2000 vehicles were simulated for different time frames (up to 2045), powertrain configurations, and component technologies. Both their fuel economy and cost were assessed to estimate the potential of each technology. Each vehicle was associated with a triangular uncertainty (Figure V-14). The simulations highlighted several points:

- From a fuel-efficiency perspective, HEVs maintain a relative constant ratio compared to their conventional vehicle counterparts. The advances in component technology will not significantly benefit HEVs. Conventional vehicles tend to improve quickly, but the cost of electrification is expected to be reduced in the future, favoring the technology's market penetration.
- Ethanol vehicles will offer the best cost-to-fuel consumption ratio among the conventional powertrains in the near future, which is driving the interest in bio-fuels development. Gasoline vehicle improvements are significant as well.
- Fuel cell HEVs have potential to reduce fuel consumption.

V.B.3. Products

References

1. Autonomie web site, accessed at www.autonomie.net.
2. Office of Energy Efficiency and Renewable Energy web site, accessed at http://www1.eere.energy.gov/ba/pba/program_benefits.html.
3. Henrion, M., *Guide to Estimating Unbiased Probability Distributions for Energy R&D Results*, DOE Risk Analysis Group, 2008.
4. Bohn, T.A., *Implementation of a Non-intrusive In-vehicle Engine Torque Sensor for Benchmarking the Toyota Prius HEV*, SAE paper 2005-01-1046, presented at the SAE World Congress & Exhibition, Detroit, MI, April 2005.
5. Wallner, T., and Lohse-Busch, H., *Performance, Efficiency, and Emissions Evaluation of a Supercharged, Hydrogen-Powered, 4-Cylinder Engine*, SAE paper 2007-01-0016, presented at the SAE Fuels and Emissions Conference, Capetown, South Africa, January 2007 (http://papers.sae.org/2007-01-0016).
6. Olszewski, M., *Evaluation of the 2007 Toyota Camry Hybrid Synergy Drive System*, Department of Energy report, January 2008.
7. Sharer, P., Rousseau, A., Nelson, P., and Pagerit, S., *Vehicle Simulation Results for PHEV Battery Requirements*, Presented at 22th International Electric Vehicle Symposium (EVS22),Yokohama, October 2006.
8. Pagerit, S., Sharer, P., and Rousseau, A., *Fuel Economy Sensitivity to Vehicle Mass for Advanced Vehicle Powertrains*, SAE paper 2006-01-0665, presented at the SAE World Congress & Exhibition, Detroit, MI, April 2006.
9. Freyermuth, V., Fallas, E., and Rousseau, A., *Comparison of Powertrain Configuration for Plug-in HEVs from a Fuel Economy Perspective*, SAE paper 2008-01-0461, SAE World Congress, Detroit, April 2008.
10. Rousseau, A., Sharer, P., Pagerit, S., and Duoba, M., *Integrating Data, Performing Quality Assurance, and Validating the Vehicle Model for the 2004 Prius Using PSAT*, SAE paper 2006-01-0667, SAE World Congress, Detroit, April 2006.
11. Pagerit, S., Rousseau, A., and Sharer, P., *Global Optimization to Real Time Control of HEV Power Flow: Example of a Fuel Cell Hybrid Vehicle*, 20th International Electric Vehicle Symposium (EVS20), Monaco, April 2005.
12. Sharer, P., Rousseau, A., Karbowski, D., and Pagerit, S., *Plug-in Hybrid Electric Vehicle Control Strategy: Comparison between EV and Charge-Depleting Options*, SAE paper 2008-01-0460, SAE World Congress, Detroit, April 2008.
13. Cao, Q., Pagerit, S., Carlson, R., and Rousseau, A., *PHEV Hymotion Prius Model Validation and Control Improvements*, 23rd International Electric Vehicle Symposium (EVS23), Anaheim, CA, December 2007.
14. Karbowski, D., Rousseau, A., Pagerit, S., and Sharer, P., *Plug-in Vehicle Control Strategy: From Global Optimization to Real Time Application*, 22th International Electric Vehicle Symposium (EVS22), Yokohama, October 2006.

Tools and Data

1. Autonomie: www.autonomie.net

V.C. Route-Based Control Benefit for Blended PHEVs

Dominik Karbowski, Principal Investigator
Argonne National Laboratory
9700 South Cass Avenue, Building 362
Lemont, IL 60439
Phone: (630) 252-5362
E-mail: dkarbowski@anl.govmailto:nkim@anl.gov

David Anderson, DOE Program Manager
Phone: (202) 287-5688
E-mail: David.Anderson@ee.doe.gov

V.C.1. Abstract

Objectives

- Demonstrate practical implementations of route-based control.
- Identify use cases in which route-based control is beneficial and the cases in which it is not.
- Assess the average benefits of route-based control.

Major Accomplishments

- Created a vehicle model in Autonomie.
- Improved the existing baseline "EV+CS" control strategy.
- Implemented an optimal control theory into the control strategy for Autonomie.
- Developed a tuning algorithm (co-state prediction).
- Performed preliminary simulations.

Future Achievements

- Investigate techniques for co-state prediction.
- Develop and analyze the benefits of periodical co-state updates.
- Conduct research on the sensitivity to differences between the speed profile used for optimization and the actual observed speed on the same itinerary.
- Investigate alternative trip-prediction techniques.
- Implement online trip prediction for control optimization.
- Analyze the benefits of route-based control for stochastic speed profiles (refer to project 1000294.00).

✧ ✧ ✧ ✧ ✧

V.C.2. Technical Discussion

Background

Plug-in hybrid electric vehicles (PHEVs) often need to use the engine for propulsion, since the battery does not have enough energy for the entire trip. This situation tends to occur when PHEVs are driven on trips longer than their all-electric range (AER). Conventional energy management strategies rely on using battery energy first. Once the battery is depleted, the engine changes to a charge-sustaining (CS) mode. However, this option is not optimal in certain situations.

Various optimization techniques have demonstrated that when PHEVs are driven past their AER, the optimal control is a charge-depleting (CD) mode. Previous dynamic programmatic studies have verified this finding. However, these techniques often are impractical, if not impossible, to implement in real-world controllers. The primary reason for this dilemma is the lack of information available in theoretical studies in the real world.

This study is part of a multi-year endeavor. The objective of this study is to demonstrate trip-based control feasibility and to quantify its fuel savings under different driving conditions. This research involves trip prediction, optimal control, and use of trip prediction for controller tuning, as well as a statistically representative evaluation of the benefits of the technology. The project, "Refine & Validate Cycle Generation from ADAS" (project 1000294.00), addresses vehicle speed prediction. In this project, the goal is to develop an optimal controller in Autonomie, alongside a solid baseline controller, in which we can use the trip prediction to achieve reduced fuel consumption.

Introduction

Past research projects at Argonne National Laboratory highlighted the significant fuel savings that can be achieved for PHEVs by using trip information. The results of those projects often were achieved in theoretical and "best case" scenarios. In this study, we focus on designing an energy management strategy that is implementable in a vehicle controller, meaning that it uses the same type of inputs, is bound to same type of constraints, and is controlling the same type of dynamic systems as a real-world controller. We also plan to model the difference between vehicle speed prediction and actual vehicle speed.

To that end, we modeled a PHEV in Autonomie, which is the forward-looking modeling environment developed at Argonne. We modeled a vehicle similar to the 2012 Toyota Prius PHEV. The existing power-split controller in Autonomie was overhauled to accommodate easy changes of high-level energy management, as well as to ensure consistency when comparing different types of control strategies. As a result, the baseline controller that uses an "EV+CS" strategy includes numerous efficiency-improving features, which ensures that our comparison is not skewed toward benefiting the proposed "optimal" controller. We then created an energy management strategy that uses Pontryagin's Minimization Principle (PMP). Preliminary simulations show positive improvements.

Approach

Baseline Vehicle Definition

A PHEV with a medium AER is probably the best candidate to demonstrate route-based control. It is more likely to drive past its AER, and therefore more likely to require engine use. Among the existing or planned vehicles, the Toyota Prius PHEV corresponds to such a profile. Furthermore, we can leverage the existing vehicle and component models developed at Argonne.

We modeled the vehicle in Autonomie. It is important to note that it is a forward-looking model and replicates the causality of the real world. In particular, the vehicle controller in the model uses the same type of inputs as those available from sensors in a vehicle.

The vehicle powertrain model follows the known specifications of the actual 2012 Prius PHEV. It has a 200 V, 21 Ah Li-ion battery with 168 cells. The top speed in all-electric mode is 100 km/h. The AER of the vehicle is 26 km on the JC08, according to Toyota (23 km for our model). Since many key specifications were not available, we made assumptions, which explain the difference in the AER.

Optimal Operating Lines

The Prius powertrain is a one-mode power-split architecture (Figure V-27). Thanks to two electric machines and a planetary gearset, the engine speed can be decoupled from the vehicle speed, thus introducing a precious degree of freedom. For a given engine speed and vehicle speed, the speeds of the electric machines are defined. Likewise, steady-state electric machines torques also are defined if the gearbox output torque and engine torque are known. However, this may lead to energy recirculation, by which one electric machine generates current to be used totally or partially by the other, with the balance being taken to or from the battery. If we further constrain the battery power, there is only one degree of freedom left, and we can use that property to define the most optimal operating point.

An algorithm was developed to generate the optimal efficiency point for a given trio of gearbox output speed, gearbox output torque, and battery power. The two resulting 3-inputs look-up tables (one outputting engine speed, the other engine torque) can then be used in the online controller. Figure V-28 illustrates a subset of the optimal speed look-up table.

Baseline Controller

In order to provide a fair comparison between an optimal case and a reference case, we must ensure that the reference case is not disadvantaged by the implementation. Therefore, we developed a baseline controller in which the high-level energy management part is clearly separated from other functions of the controller. In particular, engine speed control (or target tracking) is an important part in this particular hybrid powertrain configuration. Figure V-29 shows the top-level view of the controller in Simulink. Such organization facilitates changes in the type of high-level energy management strategy. It also contributes to fairer comparisons between different control strategies, since they share many non-energy-related functions. Using the nomenclature of Figure V-29, Block 3 is related to high-level energy management. As such, it is the only block that changes between the reference and baseline controller.

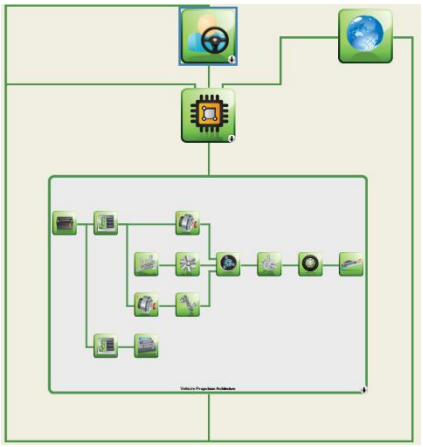

Figure V-27: One-Mode Power Split PHEV Used for the Study.

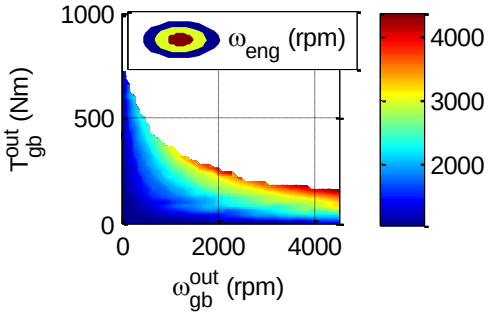

Figure V-28: Optimal Engine Speed for a Battery Power of –10 kW.

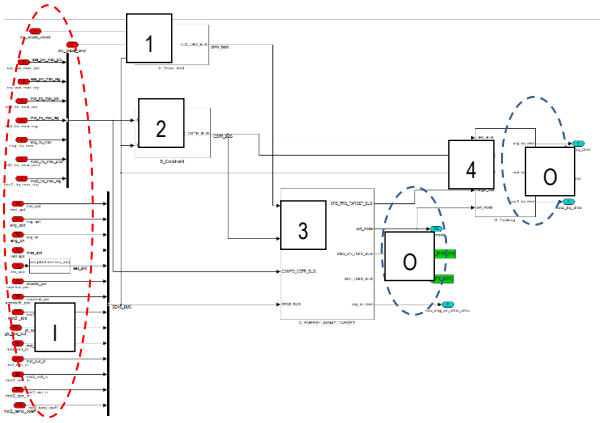

Figure V-29: View of the Vehicle-Level Controller with: Inputs (I), Outputs (O), Driver Interpretation (1), Combined Constraints Computation (2), High-Level Energy Management/Target Generation (3), and Target Tracking (4).

In CS mode, the high-level energy management strategy follows commonly used rules. The engine is turned on when the driver power demand exceeds a state-of-charge (SOC)-dependent threshold (and vice-versa for engine shut down). When the engine is on, a battery power demand is computed from an SOC-dependent look-up table. The optimal operating point maps described previously are then used to generate the speed and torque targets. The strategy is presented in Figure V-30. In CD mode, the engine is kept off until the SOC reaches the discharged level, unless the vehicle speed is too high (above 100 km/h) or the power demand exceeds what the components can provide.

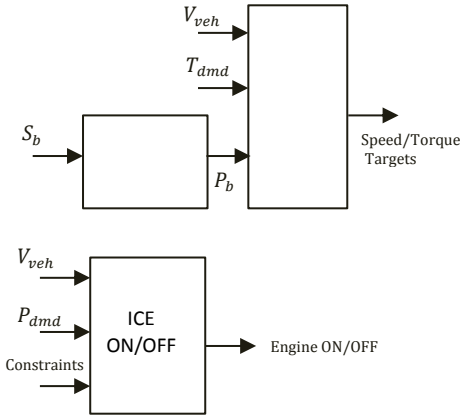

Figure V-30: Schematic View of the Baseline High-Level Energy Management.

Optimization Problem and PMP Theory

The goal of this project is to optimize a PHEV so that it uses less fuel energy than the baseline version. The vehicle must meet the driver demands, so we assume that vehicle speed and gearbox output torque are constraints. The battery state of charge S_b is the state of the vehicle. Since fixing the battery power P_b is enough to compute an optimal operating point, we consider P_b as the command variable. By using the look-up tables described previously, we can link the fuel power to the battery power: $P_f = g(P_b, S_b)$. The battery SOC is linked to the battery power by the following dynamic equation:

$$\dot{S_b} = -\frac{P_b}{QV_n} \frac{2\frac{V_n}{V_{oc}}}{1+\sqrt{1+\frac{4P_bR}{V_{oc}^2}}}$$

$$\Leftrightarrow \quad \dot{S_b} = \lambda_0 \delta(P_b, S_b) P_b$$

where λ_0 is a negative constant, δ is a scalar function close to 1 in the operating range of the system, Q is the battery capacity, V_n is the battery nominal voltage, V_{oc} is the open-circuit voltage, and R is its internal resistance.

Therefore, the optimization problem consists of finding successive optimal battery power demands that will minimize the fuel energy while reaching the target SOC S_{tgt} at the end of the trip:

$$P_b^* = \min_{\substack{P_b \\ S_{b(T)}=S_{tgt}}} \left(\int_0^T P_f(P_b) dt \right)$$

The Hamiltonian H of the system is therefore $H = P_f + p(t)\dot{S_b}$, where p is the co-state. By applying the PMP to the system, we conclude that the optimal solution minimizes the Hamiltonian with a constant co-state p_0:

$$P_b^*(p_0) = \underset{P_b}{\operatorname{argmin}}(P_f + p_0 \dot{S_b})$$

We can re-write this equation using the battery power:

$$P_b^*(r_0) = \underset{P_b}{\operatorname{argmin}}(P_f + r_0 \delta P_b)$$

We call r_0 the equivalence factor because it allows the sum of two powers from energy sources of a different nature. The challenge is that $P_b^*(r_0)$ is the optimal solution for the final SOC, being the one resulting from $P_b^*(r_0)$. Thus, there is another problem to solve, which is to find r_0 such that $S_b(\mathrm{T}) = S_{tgt}$.

PMP Implementation

The PMP optimal controller is derived from the baseline controller. Only the high-level energy management is different. The other three blocks are the same.

Figure V-31 shows a simplified view of the high-level management block. It deals with deciding whether to turn the engine on or leave it off and determining which operating point to pick. The on/off decision is based on the relative difference of the respective Hamiltonians in the electric vehicle (EV) or hybrid electric vehicle (HEV) mode. Next, in the internal combustion engine (ICE) ON/OFF logic, we select the mode with the lowest Hamiltonian. Some filters were implemented to prevent an excessive number of state changes. The computation of the Hamiltonian in the HEV mode first relies on computing it for a vector of battery power demands and the resulting fuel powers. The power demand that minimizes the Hamiltonian is then selected.

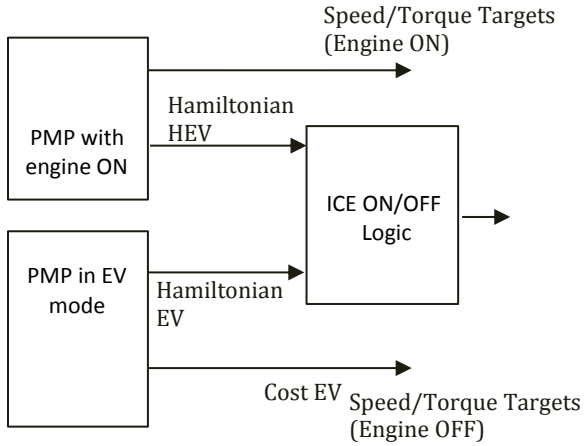

Figure V-31: Schematic of the High-Level Energy Management in the PMP Controller.

Route-Based Parameter Tuning

The equivalence factor is a constant, and it is computed before the simulation. Ideally, it is computed by using a fast and resource-light algorithm. One possibility is to use an ultra-fast backward model and a shooting method in which a wide range of equivalence factors is considered, and the one that results in a final SOC closest to the target SOC is selected. Although the initial results showed some promising outcomes, further investigation is required.

Results

To highlight the potential benefits of our optimal PHEV controller, we designed the following user case:

- Urban driving for the first 3 km, on the way to the highway;
- Highway driving for 25 km, at moderate speeds (under 100 km/h);
- Highway driving with some stop-and-go traffic for another 7 km; and
- Urban driving for the last 7 km.

This user case could be an example of a commuting trip. It was synthesized from bits of standard drive cycles. The speed profile is depicted in Figure V-32.

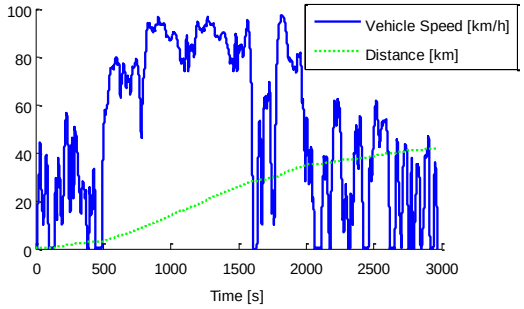

Figure V-32: Vehicle Speed Profile Used for Testing the PMP Controller.

The PMP controller was compared against the baseline controller: EV mode until the "discharged" SOC, followed by a CS mode. The PMP controller clearly behaves as intended and results in a CD mode in which the battery is gradually depleted throughout the trip and the engine is regularly started. Toward the end of the trip, the SOC converges to the target SOC (30%), while the mass of fuel in the baseline case becomes higher than the one in the PMP case.

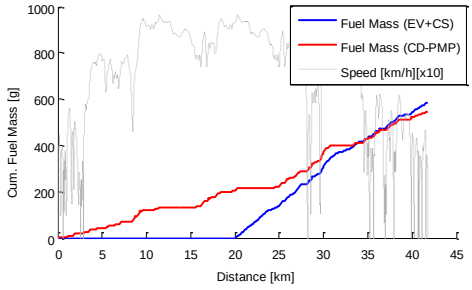

Figure V-33: Cumulative Fuel Mass.

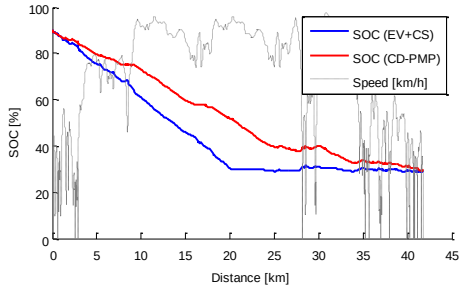

Figure V-34: Battery SOC.

Conclusions

- A powertrain model similar to the 2012 Toyota Prius PHEV was developed in Autonomie.
- The baseline controller was improved and reorganized to:
  - Allow rapid changes in high-level energy management;
  - Keep the differences in implementations of particular energy management strategies to a minimum;
  - Ensure that the baseline control has been improved through best effort; and
  - Establish a fair comparison between the optimal and reference cases.
- An optimal controller was created to:
  - Share non-energy management functions with the baseline controller;
  - Include optimal energy management based on the PMP; and
  - Balance theoretical principles with practical constraints, either dynamic or driveability related.
- A fast co-state prediction algorithm was developed by using a shooting method on a backward-looking model.
- Preliminary simulations demonstrated proper operation of the optimal control, as well as fuel saving potential.

V.C.3. Products

Publications

1. Karbowski, D., V. Smis-Michel, and V. Vermeulen, "Optimal Vehicle Energy Management Using Trip Prediction," SAE 2013 Energy Management Symposium, Dearborn, MI, October 21–22, 2013.
2. Karbowski, D., V. Smis-Michel, and V. Vermeulen, "Using Trip Information for PHEV Fuel Consumption Minimization," International Electric Vehicle Symposium and Exhibition, EVS 27, Barcelona, Spain, November 17–20, 2013.

Tools and Data

1. Baseline controller for one-mode PHEV in Autonomie
2. Optimal, PMP-based controller for one-mode PHEV in Autonomie

References

1. Autonomie, 2012, available at: www.autonomie.net/.
2. Karbowski, D. and A. Rousseau, et al., "Plug-in Vehicle Control Strategy: From Global Optimization to Real Time Application," 22th International Electric Vehicle Symposium (EVS22), Yokohama, Japan, October 23–26, 2006.

3. Katsargyri, G.-E. and I.V. Kolmanovsky, et al., "Optimally Controlling Hybrid Electric Vehicles Using Path Forecasting," 4613–4617, American Control Conference, St. Louis, MO, June 10–12, 2009.
4. Paganelli, G. and S. Delprat, et al., "Equivalent Consumption Minimization Strategy for Parallel Hybrid Powertrains," 55th IEEE Vehicular Technology Conference, 2076–2081, Birmingham, AL, May 6–9, 2002.
5. Kim, N., S. Cha, and H. Peng, "Optimal Control of Hybrid Electric Vehicles Based on Pontryagin's Minimum Principle," IEEE Transactions on Control Systems Technology, 1279–1287, 2011.
6. Sharer, P. and A. Rousseau, et al., "Plug-in Hybrid Electric Vehicle Control Strategy: Comparison between EV and Charge-Depleting Options," SAE technical paper 2008-01-0460, SAE World Congress, Detroit, MI, April 14–17, 2008.
7. Deguchi, Y. and K. Kuroda, et al., "HEV Charge/Discharge Control System Based on Navigation Information," SAE technical paper 2004-21-0028, SAE World Conference, Detroit, MI, March 8–11, 2004.
8. Rousseau, A. and P. Sharer, et al., M., "Integrating Data, Performing Quality Assurance, and Validating the Vehicle Model for the 2004 Prius Using PSAT," SAE technical paper 2006-01-0667, SAE World Congress, Detroit, MI, April 3–6, 2006.

V.D. Connectivity Enhanced Energy Management and Control for EREVs—CRADA with GM

Jeffrey Gonder, Principal Investigator
National Renewable Energy Laboratory
15013 Denver West Parkway, MS 1634
Golden, CO 80401
Phone: (303) 275-4462
E-mail: jeff.gonder@nrel.gov

David Anderson, DOE Program Manager
Phone: (202) 287-5688
E-mail: david.anderson@ee.doe.gov

V.D.1. Abstract

Objectives

- Leverage intelligent transportation system (ITS) information available from advanced vehicle telematics systems, such as OnStar, to further increase energy efficiency in the Chevrolet Volt "extended range electric vehicle" (EREV). Specifically pursue the following energy savings enhancements:
  - Green routing—advise the driver on the least energy consuming route to travel between a given origin and destination (O/D) pair.
  - Adaptive control—intelligently schedule charge depleting (CD) vs. charge sustaining (CS) mode during the course of a predicted route in order to maximize energy efficiency over the route.

Major Accomplishments

- Developed novel approaches on several subtopics while successfully executing the project, including:
  - Predicting drive cycle metrics over potential travel routes.
  - Predicting vehicle-specific energy use from representative drive cycle metrics.
  - Route-connected optimal control mode scheduling for plug-in hybrid or extended range electric vehicles.
- Collaborated with GM on model development and application, as well as on laboratory testing of a modified Chevrolet Volt to validate/complement the modeling approach.
- Demonstrated several percent fuel savings improvements each from green routing and adaptive control enhancements—a significant finding given that realizing these savings simply requires software adjustments.
  - Aggregate savings up to roughly 5% possible for green routing.
  - Average savings in excess of 3% for adaptive control mode scheduling.

Future Achievements

- Add route-based optimization for lower-level controls on top of adaptive CD vs. CS control mode scheduling.
- Formally incorporate a data input layer with real-time traffic/congestion information to further improve cycle metric predictions.
- Evaluate sensitivity of results to various conditions and erroneous predictions.
- Implement, refine and more robustly test both green routing and adaptive control approaches in a development vehicle.
- Apply approaches to other vehicle platforms—e.g., green routing for a conventional and/or non-plug-in hybrid electric vehicle.

✧ ✧ ✧ ✧ ✧

V.D.2. Technical Discussion

Background

Energy security, fuel cost, and air quality concerns have led to increased powertrain electrification in new vehicles. At the same time, ubiquitous availability of advanced vehicle telematics systems, such as OnStar, has made real-time information on driving routes, traffic, and road topology readily accessible. Together, these trends offer the potential for increased powertrain efficiency, particularly in vehicles with both a traction battery and a combustion engine. Such vehicles can leverage route-specific information to anticipate road loads and schedule power flows in the most efficient manner possible.

Introduction

In collaboration with the U.S. Department of Energy (DOE), the National Renewable Energy Laboratory (NREL) and General Motors (GM) evaluated connectivity-enhanced route selection and adaptive control techniques to even further increase energy efficiency in the Chevrolet Volt platform. The project included both simulation and chassis dynamometer testing to develop energy prediction algorithms applied to the Volt over multiple real-world driving profiles. The algorithms were used to implement and evaluate green routing and adaptive intelligent control mode scheduling for the Volt over predicted travel routes.

Approach

Figure V-35 illustrates the overall methodology for developing the energy predictions that serve as the basis for the green routing and adaptive control energy efficiency enhancements. The process begins by identifying candidate routes for traveling between a given (or predicted) origin and destination (O/D) pair. Each route is broken apart into sections characterized by road type information, and which may also take real-time traffic and driver aggression predictions as inputs. A drive cycle model (developed as part of this project) then makes predictions of drive cycle characteristics expected over each driving segment. Based on these cycle metrics, as well as road grade and the current vehicle/battery state, a look-up table model (also developed for this project specific to the Volt powertrain) estimates the vehicle's segment-by-segment fuel and electricity consumption.

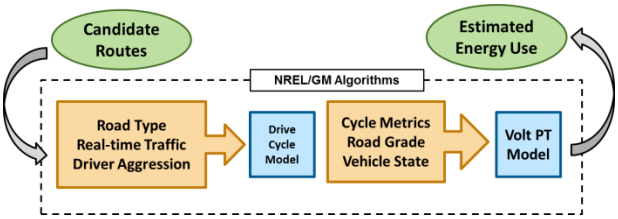

Figure V-35: Overall energy use estimation methodology—providing the basis for green routing and adaptive control efficiency enhancements.

This methodology, and particularly the drive cycle and Volt powertrain (PT) models illustrated in Figure V-35, were very computationally heavy to develop—involving processing, analyzing and simulating hundreds of thousands of drive cycles. However, the resultant look-up table models become quite computationally light to implement in a vehicle by eliminating the need for predicting a second-by-second speed trace or for real-time simulation using a computationally-intensive vehicle model.

Results

Cycle Metric Prediction

After establishing one or more potential driving routes to travel between a given O/D pair (including map matching each segment of the route to an underlying road layer from a provider such as NAVTEQ/Nokia/HERE), the project team drew on information such as road segment type (functional class, speed category, etc.) from the underlying road layer to predict representative cycle metrics (such as average speed, acceleration, road grade and stops per mile) over each segment of the driving route. A data-driven correlation between road type and drive cycle characteristics was established by analyzing thousands of second-by-second real-world driving profiles collected with global positioning system (GPS) devices and archived in NREL's Transportation Secure Data Center (TSDC)—see www.nrel.gov/tsdc. After map-matching the TSDC driving profiles to the underlying road layer (as described above), the driving profiles were sub-divided into smaller increments, such as the 0.1 mile "nanotrips" illustrated in Figure V-36.

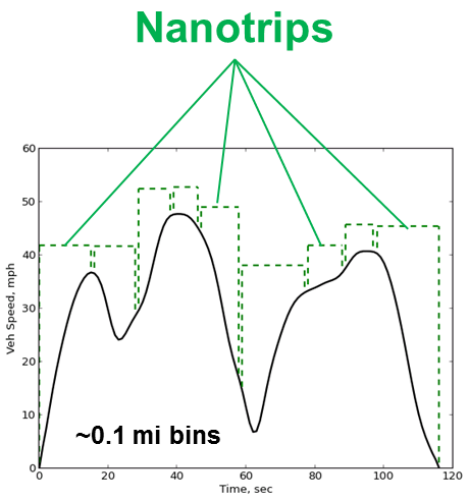

Figure V-36: Illustrative division of real-world driving data into smaller "nanotrip" distance intervals.

The speed and acceleration characteristics for these nanotrips were then correlated to the road functional class (FC) being traversed (FC=1 corresponds to high-throughput interstate travel and FC=5 corresponds to low-throughput neighborhood streets). As illustrated in Figure V-37, this resulted in reasonable predictions of average speed and acceleration characteristics simply given information on the functional class of the current and the previous 0.1 mile segment of the given driving route. Further precision would be obtained by factoring in additional inputs, such as real-time traffic speeds over the given driving segment.

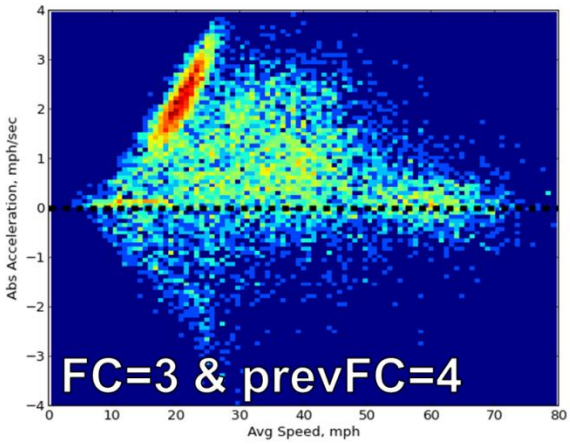

Figure V-37: Significant concentration of nanotrip data around hard accelerations when transitioning from an FC4 to an FC3 road segment (i.e., to a higher speed/capacity roadway).

Energy Use Prediction

The next component of the project involved converting estimated cycle metrics (such as average speed, acceleration, road grade, etc.) into vehicle energy use predictions over a given route. The method developed to accomplish this involved generating detailed energy use maps for the vehicle using detailed simulations (complemented by physical vehicle data collection) over tens of thousands of drive cycles. As mentioned in the above Approach section of this report, these

energy use maps are therefore computationally heavy to develop, but once they are built are computationally light to implement for a green routing or dynamic control application.

For the Chevrolet Volt powertrain used in this study, the energy use maps included both electricity and fuel consumption relationships, and considered charge depleting (CD) operation, charge sustaining (CS) operation and the need to track vehicle state-of-charge (SOC) via the electricity consumption relationships in order to determine the correct operating mode. The effort relied primarily upon simulations using an internal GM powertrain model and secondarily on test data collected from a Chevrolet Volt that had been modified to allow on-the-fly initiation of CS operation even at a high vehicle battery SOC. Note that the results shown here omit proprietary data values specific to the Volt powertrain, but nonetheless convey the relative trends and overall steps employed in the analysis.

The simulation and test results were post-processed into nanotrips using methods described in Figure V-35. In addition to the previously-mentioned cycle characteristic categorization (average speed, acceleration, etc.), the simulation and testing permitted associating each nanotrip with values for electricity and fuel consumption (each value referenced as well to the battery SOC at the start of the nanotrip). Figure V-38 illustrates a discretized look-up map of engine-off electric rate in the average speed and acceleration space. This map was derived from all the engine-off nanotrip simulation results, which showed consistent electric consumption rates for nanotrips with similar cycle characteristics.

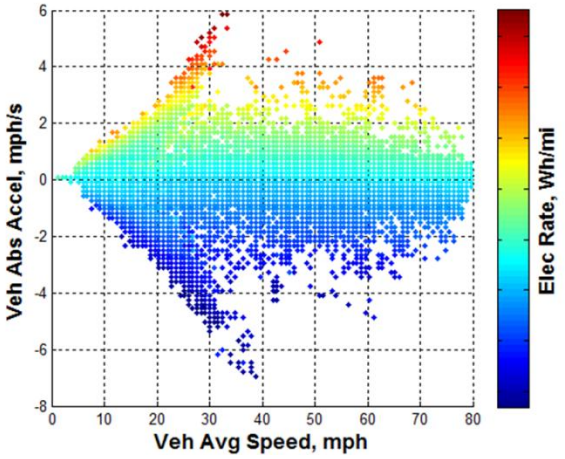

Figure V-38: Discretized correlation between cycle characteristics and electric consumption rate—generated from detailed simulation results when the Volt engine was off.

Figure V-39 provides a similar visualization of the electric consumption rate while the vehicle engine is on—this time organized in a space defined by the SOC of the nanotrip (where the CS hold mode was engaged at a target SOC around the middle of the figure) and the product of the average speed and acceleration characteristics of the microtrip. Consistent results within this space for nanotrips with similar characteristics again enable discretization of the data into a lookup map as illustrated by Figure V-39. The engine-on fuel rate relationship was found to correlate well with the difference between the engine on and engine off electric rate estimates (as provided by the cycle-characteristic-based lookup maps in Figure V-38 and Figure V-39). Figure V-40 illustrates the resulting correlation established as compared to the actual results from the detailed simulation.

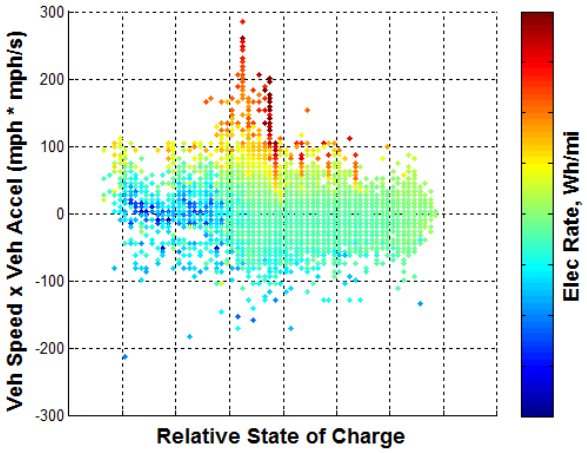

Figure V-39: Discretized correlation between cycle characteristics, SOC and electric consumption rate—generated from detailed simulation results when the Volt engine was on.

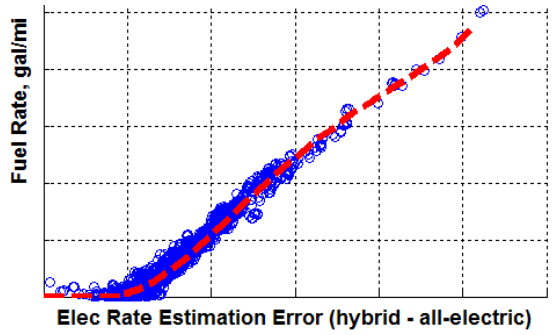

Figure V-40: Engine-on fuel rate estimates correlate with the difference or "error" between the hybrid (engine-on) electric rate and the all-electric (engine-off) electric rate estimates.

The described look-up maps/correlations define everything needed to predict energy use (fuel and electricity consumption) from speed and acceleration cycle characteristics. The predictions can be further refined by establishing similar correlations for additional cycle segment characteristics such as road grade. Figure V-41 illustrates the translation model (trained by the detailed simulation and test data over cycles run at different grades) in order to estimate electric rate impact as a function of road grade for similarly characterized nanotrips. As shown in Figure V-42, the grade-based translation model shows very good ability to predict the grade-adjusted electric consumption rates based only on the zero-grade electric rate as an input.

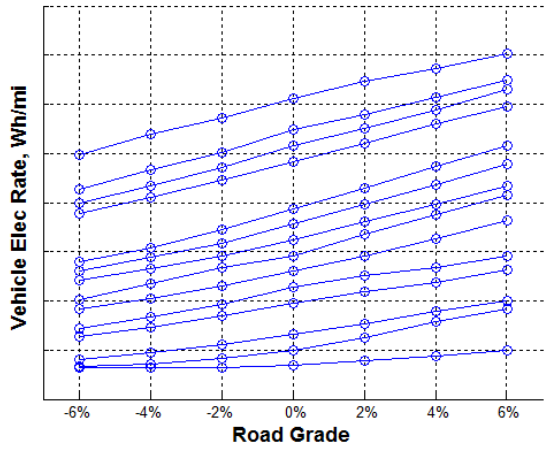

Figure V-41: Grade-based electric rate translation model—created to adjust the zero-grade lookup maps described in Figure V-38—Figure V-40 to account for driving segment grade.

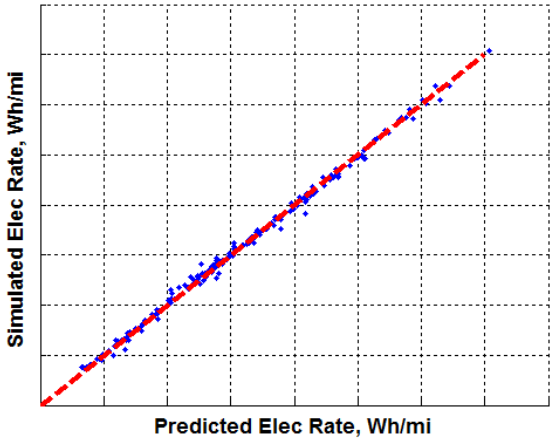

Figure V-42: The grade translation model agrees well with individual electric rate adjustments observed from simulation and test data over similarly characterized nanotrips at different road grades.

Green Routing

Evaluation of the connectivity-enabled green routing and route-based control enhancements again involved leveraging the TSDC—specifically the large set of real origin and destination (O/D) locations contained in the database. NREL leveraged Google Maps' application programming interface to generate route options between each O/D pair, and applied the cycle metric and fuel/electricity prediction approach outlined above to evaluate each route. Figure V-43 categorizes the results for the nearly 43,000 O/D pairs and highlights that for many O/D pairs Google's routing software either recommends only one route, or the fastest recommended route also turns out to be the most energy efficient route. However, 37% of the time the fastest route does not correspond with the greenest route, so that fraction of driving trips is taken to be the potential opportunity where green routing could result in energy saving benefits (relative to the fastest route being the assumed default).

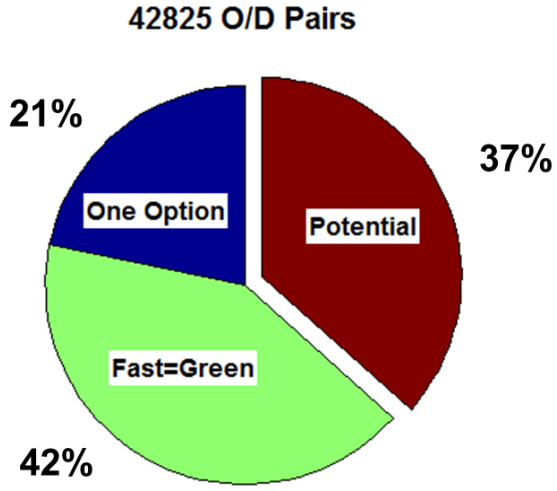

Figure V-43: 37% of the nearly 43,000 O/D pairs show green routing energy savings potential relative to the fastest route option.

Under this set of assumptions, any green routing energy savings will come at a cost of increased travel time. Figure V-44 explores this trade off by arranging the results as a function of the vehicle operator's hypothetical monetary value of time spent in the vehicle. The top line in the plot corresponds to percent increased travel time, and the bottom line corresponds to percent energy and cost reductions provided by the "greenest" route.

To facilitate interpretation, consider two example vertical slices on this plot. The points intersected by the y-axis represent the extreme scenario with no value of time penalty counted against increased time requirements by the green route. The aggregate results represented by this scenario could realize a 12.3% reduction in energy use and cost, but a 14.4% increase in travel time. As a second example, consider the vertical slice at a time value of $35/hr. For this scenario energy use and cost could be decreased by 1.0% with a negligible increase in travel time.

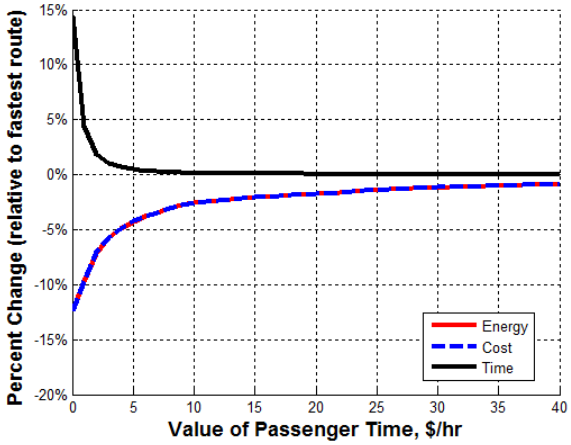

Figure V-44: Trade-off between energy/cost savings and travel time increases as a function of passenger/driver value of time (for the 37% of O/D pairs where the least energy consuming route prediction was not the fastest route).

Control Mode Scheduling

The intelligent CD vs. CS mode scheduling evaluation involved similar large-scale analysis—specifically of over 100,000 potential routes identified from the TSDC O/D database. The evaluation required first adding an extra analysis layer to compare the default mode schedule (CD followed by CS) as compared to the optimal (least fuel consuming) mode schedule. As a simplified overview, the methodology included in the added layer begins by assuming that all driving could be accomplished in CD mode (initially ignoring energy limits of the vehicle battery). It then incrementally substitutes driving segments from CD to CS operation, until the final trip SOC equals that from the default CD followed by CS operation. Trip segments are prioritized for substituting from CD to CS control based on minimizing the cost/benefit ratio of doing so, where the cost is defined as the increase fuel use incurred by the substitution and the benefit is defined as the decreased electric depletion rate.

The top plot in Figure V-45 shows an example nominal vs. optimal battery SOC depletion profile generated from the above-described methodology. Note for evaluating this project's high-level CD vs. CS mode scheduling opportunity that each considered trip was assumed to begin at an initial SOC such that 50% or more of the trip was completed in CS mode. The bottom plot in Figure V-45 shows the corresponding fuel consumption profile for the nominal vs. optimal control mode scheduling over the example profile. In this example, fuel consumption was reduced 25% by scheduling CS operation during highway driving segments in the first half of the route, and saving CD operation for the city driving anticipated at the end of the route.

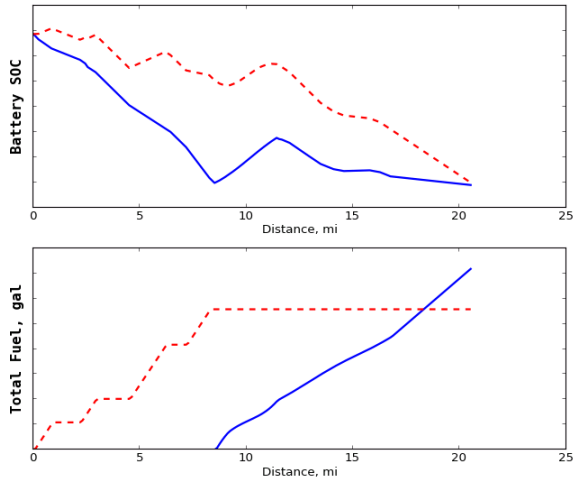

Figure V-45: Nominal (solid line) vs. optimal (dashed line) battery SOC and fuel use profiles for one example route.

Figure V-46 shows the scatter of fuel savings opportunity from optimal mode scheduling applied to over 100,000 trips. These results indicated that very large fuel savings results predominantly occur at short driving distances, which may be an artifact of the reduced starting SOC approach applied for these shorter trips. However, a number of trips (even longer than 30-40 miles in length) realize fuel savings on the order of 10%, and the average fuel savings across all trips exceeds 3%.

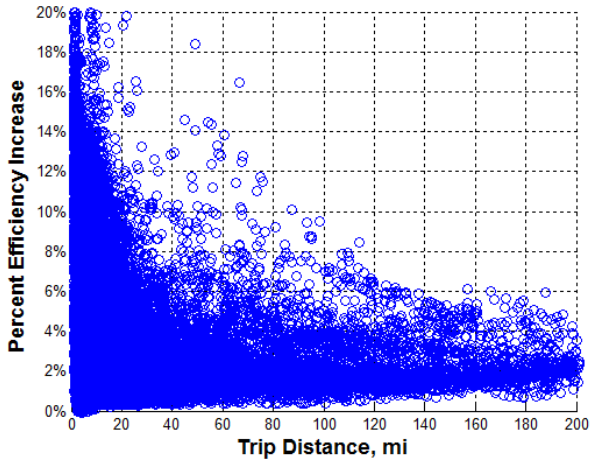

Figure V-46: Efficiency improvements from control mode scheduling optimization evaluated across over 100,000 representative driving routes.

Conclusions

Under this project NREL collaborated with GM to evaluate connectivity-enabled efficiency enhancements for the Chevrolet Volt. Project accomplishments included developing and demonstrating the ability to estimate drive cycle characteristics over anticipated driving routes. The project team further developed a high-level model to predict vehicle fuel and electricity consumption based on driving characteristic and vehicle state inputs. The team combined and leveraged these techniques in pursuit of energy efficiency optimization via green routing and intelligent control mode scheduling.

The green routing and intelligent control mode scheduling enhancements were evaluated using prospective driving routes between tens of thousands of real-world O/D pairs. Considering the maximum aggregate green routing benefit multiplied by the fraction of O/D pairs where the default (fastest) route consumed more fuel, the overall green routing fuel savings opportunity could approach 5%. The average efficiency benefit from intelligent high-level scheduling of CS vs. CD control showed a similar magnitude—a little over 3% potential fuel savings. These represent substantial opportunities considering that they only require software adjustments to implement.

Future work efforts could include adding route-based optimization to lower-level controls (in addition to the high-level CD vs. CS control mode scheduling), formally incorporating real-time traffic/congestion information to further improve cycle metric predictions, and evaluating result sensitivity to various conditions and erroneous predictions. Additional options could include implementing, refining and more robustly testing both green routing and adaptive control approaches in a development vehicle, and/or considering additional vehicle platforms/powertrains.

V.D.3. Products

Publications

1. Wood, E., Gonder, J., and Rajagopalan, S. "Connectivity-Enhanced Route Selection and Adaptive Control for the Chevrolet Volt." Invited project overview presentation at the October 2013 VSATT Deep Dive Meeting.
2. Wood, E., Gonder, J., and Rajagopalan, S. "Connectivity-Enhanced Route Selection and Adaptive Control for the Chevrolet Volt." Proceedings of the October 2013 SAE Energy Management Symposium, Dearborn, MI.

Patents

1. Wood, E., Gonder, J., Burton, E., and Rajagopalan, S. "Connectivity-Enhanced Route Selection and Adaptive Control Methods." NREL Provisional Patent 13-69, October 4, 2013.
2. Wood, E., Burton, E., and Gonder, J. "Predicting Drive Cycle Metrics over Potential Travel Routes." NREL Record of Invention ROI-13-69, September 24, 2013.
3. Wood, E., Gonder, J., and Rajagopalan, S. "Predicting Vehicle-Specific Energy Use from Representative Drive Cycle Metrics." NREL Record of Invention ROI-13-70, September 24, 2013.
4. Wood, E., Gonder, J., and Rajagopalan, S. "Route-Connected Optimal Control Mode Scheduling for Plug-In Hybrid or Extended Range Electric Vehicles." NREL Record of Invention ROI-13-71, September 24, 2013.

Tools and Data

1. Multiple datasets leveraged from the Transportation Secure Data Center (TSDC). See www.nrel.gov/tsdc.

V.E. VSATT, TSDC and RWDC Support

Jeffrey Gonder, Principal Investigator
National Renewable Energy Laboratory (NREL)
15013 Denver West Parkway, MS 1634
Golden, CO 80401
Phone: (303) 275-4462
E-mail: jeff.gonder@nrel.gov

David Anderson, DOE Program Manager
Phone: (202) 287-5688
E-mail: david.anderson@ee.doe.gov

V.E.1. Abstract

Objectives

- Support three crosscutting activities:
  - NREL's participation in the U.S. DRIVE Vehicle Systems Analysis Technical Team (VSATT).
  - Partnership with the U.S. Department of Transportation (DOT) on operating the Transportation Secure Data Center (TSDC).
  - Collaboration with DOT and PTC Software on the Real-World Design Challenge (RWDC) Surface Challenge.

Major Accomplishments

- Delivered presentations (described below) to VSATT automaker and national lab partners on studies of pre-competitive interest to advance commercialization of vehicle efficiency technologies.
  - Received and incorporated partner feedback to improve NREL's research projects, and provided input to help similarly improve partners' studies.
- Supported analyses for hundreds of TSDC users that would not otherwise be possible without access to the real-world travel data.
  - Users include DOE national laboratories, universities, and automakers; the U.S. Council for Automotive Research (USCAR) specifically issued a letter of support in appreciation for the value provided by the TSDC data.
  - Thanks to DOE's and NREL's involvement, the analyses often focus on real-world implications for electrified and other advanced vehicle technologies—multiplying DOE's impact to advance research in this space.
- Added second-by-second TSDC datasets from California, Georgia and Illinois covering nearly one million miles of travel.
  - Completed quality control processing and value addition steps on the data, such as linking each point to the underlying road infrastructure and appending grade information.
- Helped formulate the RWDC Surface Challenge problem statement, and provided a customized version of FASTSim for use by the student teams.
  - The students successfully used the tool for exploring vehicle efficiency improvement opportunities, and improved their skills in STEM subject areas—hopefully influencing many of them toward future career paths in science and engineering.

Future Achievements

- Continue supporting VSATT and refinement of the more formal project review and feedback process into FY14.
- Add further TSDC datasets to improve geographic representation and capture more longitudinal data (i.e., travel behavior over time periods longer than one or two days).
- Respond to user questions, and enhance data processing routines to even better support advanced vehicle studies by users both inside and outside the national lab system.

✧ ✧ ✧ ✧ ✧

V.E.2. Technical Discussion

Background

This report summarizes NREL's FY 2013 efforts supporting three different activities: (1) participation in the Vehicle Systems Analysis Technical Team (VSATT), (2) operation of the Transportation Secure Data Center (TSDC), and (3) assistance with the Real-World Design Challenge (RWDC) Surface Challenge.

Introduction

VSATT is one of several technical teams participating in the U.S. Driving Research and Innovation for Vehicle Efficiency and Energy Sustainability (U.S. DRIVE) program. NREL provides on-going support for VSATT as requested by the co-chair with U.S. Department of Energy (DOE) approval. NREL's role focuses on the application of analysis tools (e.g., via simulation, trade-off analysis, and optimization), and support for component model development, calibration, and validation.

For the TSDC project, the U.S. Department of Transportation (DOT) Federal Highway Administration has provided the primary funding to maintain the data center and perform data processing that supports travel activity and spatial and other transportation-focused analyses. The DOE contribution via this task enables further data processing focused on supporting vehicle fuel use and energy analyses.

DOT, along with PTC Software (PTC), also serves as a key sponsor of the RWDC—a high school competition intended to strengthen the science, technology, engineering, and mathematics (STEM) workforce. DOE requested NREL's participation to support use of the Future Automotive Systems Technology Simulator (FASTSim) in the Surface Challenge portion of the competition.

Approach

The approach for VSATT includes regular participation in team meetings, presentation of research plans and results, and responding to any analysis requests.

The overall approach for the TSDC project includes operating the data center in a manner that first and foremost protects survey participant privacy, but secondarily maximizes usability within the privacy protection constraints. To help accomplish these balanced priorities, NREL maintains three distinct data areas for the TSDC: (1) an enclave for raw data processing and archiving with no external access, (2) a public website where cleansed data are available for download (with detailed location and other potentially identifying information removed), and (3) a secure portal for detailed spatial data that permits controlled access to users who complete an application and approval process.

The approach for the RWDC included meeting regularly via conference call with DOT and PTC organizers, helping them understand the capabilities of NREL's Future Automotive Systems Technology Simulator (FASTSim), and working with them to formulate the challenge statement and customize FASTSim for use in the Surface Challenge.

Results

FY 2013 VSATT results included delivery of project overview presentations during the first quarter of the fiscal year at a meeting hosted by Oak Ridge National Laboratory. NREL received and incorporated feedback into execution of the project plans that were presented. Other presentations made during the year at regular VSATT meetings included an explanation of the results for NREL's Air Conditioning Model Development and Validation project, for which NREL also prepared a U.S. DRIVE accomplishment highlight. Activities at the end of the fiscal year included preparing to host the next VSATT "deep dive" planning meeting at NREL during the first quarter of FY 2014.

FY 2013 accomplishments for the TSDC activity included supporting the over 200 users of the cleansed public download area and roughly a half dozen applicants to the secure portal environment. The users represent several DOE national laboratories, major automotive manufacturers, universities, and other research organizations. The data application examples section of the website (www.nrel.gov/tsdc) highlights numerous electrified and advanced vehicle research papers by these users that have relied on data from the TSDC. A paper by Chrysler published at the May 2013 Conference on Innovative Automotive Transmissions, Hybrid and Electric Drives provides one specific recent example. As a further show of support for the value provided by the TSDC data, the U.S. Council for Automotive Research issued a letter of support for the on-going operation of the TSDC, and NREL responded to member queries from Chrysler, Ford, and General Motors through the course of the fiscal year.

Datasets added to the TSDC in FY 2013 included both vehicle- and person-based global positioning system (GPS)-instrumented studies from Atlanta, Chicago, and the state of California. The California survey was the largest single regional household travel survey ever conducted in the United States. It included on-board diagnostic sensor data for most of the vehicle-mounted GPS sample, as well as origin and destination data for the roughly 42,500 households that participated in the full (including non-GPS) sample. Table V-4 provides further information about these and other datasets included in the TSDC.

Table V-4: Sample TSDC Data Sets.

Data Source	Date(s)	Vehicles	Vehicle Days	Study Length
California Household Travel Survey a	2010-2012	2,910	14,367	7 days
Atlanta Regional Commission Travel Survey a	2011	1,653	8,589	7 days
Chicago Regional Household Travel Inventory a	2007	408	1,773	7 days
Puget Sound Regional Council Traffic Choices Study	2004-2006	484	145,273	18 months
Texas DOT Travel Surveys from Austin, Houston, San Antonio and many other cities	2002-2011	3,404	5,258	1 day
Southern California Association of Governments Regional Travel Survey	2001-2002	624	1,208	1-10 days

[a] Also includes a wearable GPS component to capture other travel modes.

Further TSDC results included implementation of several data processing enhancements, such as:

- A robust map-matching algorithm that links vehicle operation to a specific road segment, allowing information on road functional class and speed category to be added to the data.
- A refined procedure drawing from U.S. Geological Survey elevation data and an NREL-developed filtering routine to append road grade to all of the GPS data points.
- Linking travel data origin and destination information to census geographies and land use data.

NREL produced a webinar demonstrating the various data features and analysis tools available to TSDC users, and met multiple times with the TSDC advisory group to receive their guidance and endorsement for the operating procedures adopted in conjunction with the various developed enhancements. NREL has been invited to present on the TSDC and related Fleet DNA project activities at the

November 2013 Federal Committee on Statistical Methodology Research Conference and will include even more details on the project progress at that event.

For the RWDC Surface Challenge, NREL helped formulate the problem statement inviting students to vary four Class 8 truck vehicle design parameters with different cost vs. benefit tradeoffs to achieve an optimal design that satisfied minimum fuel efficiency criteria. Prior to the competition, NREL performed an initial sweep of the design space to demonstrate potential solutions that the student teams might identify, and created a simplified interface for the FASTSim tool specifically for the students to use in the competition (see Figure V-47). NREL's efforts were recognized on several occasions in appreciative comments from individuals at U.S. DOT, PTC, and DOE. The competition concluded at the end of the school year, with Rancho High School from Las Vegas, Nevada, winning the Surface Challenge.

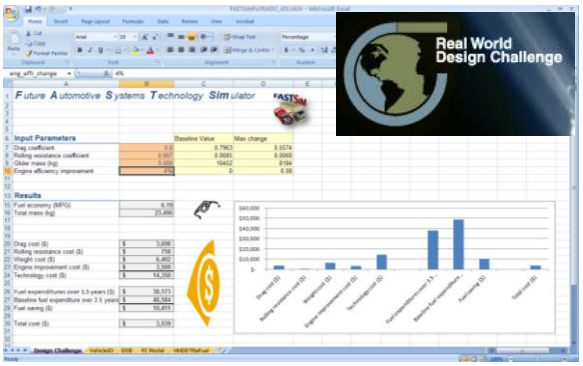

Figure V-47: Screen shot of the customized version of FASTSim that NREL developed for the RWDC Surface Challenge.

Conclusions

NREL's on-going involvement in VSATT provides an important avenue through which to receive feedback on analysis priorities and input assumptions from partners at U.S. automobile companies and other national laboratories. Constructive comments received through interactions and presentation of research findings also helps to strengthen NREL's analyses and increase confidence in the generated results.

NREL's efforts through the TSDC project provide a further avenue for interaction with other researchers and technical experts. The data and processing enhancements also provide invaluable inputs to analyses conducted by NREL as well as externally. These include a variety of travel demand and transportation planning research topics, and much of the time (thanks to NREL's and DOE's involvement) focus on the implications of the real-world driving insights on electrified and other advanced vehicle technologies. This has served to greatly multiply the impact of DOE's support for the project by enabling a considerable amount of additional vehicle efficiency research projects that rely on the data made available by the TSDC.

With the RWDC activity, NREL leveraged the user-friendly and rapid-calculating FASTSim tool to expose high school students to a real-world surface vehicle design challenge. The students successfully used the tool for exploring vehicle efficiency improvement opportunities, and improved their skills in STEM subject areas—hopefully influencing many of them toward future career paths in science and engineering.

V.E.3. Products

Publications

VSATT related:

1. Rugh, J., Lustbader, J., Gonder, J., Markel, A., and Walkowicz, K., "Current NREL Vehicle Systems Simulation and Testing (VSST) Activities." Invited presentation at the November 2012 VSATT Deep Dive Meeting, Oak Ridge, TN.
2. Lustbader, J., "Air Conditioning Model Development and Validation." Invited presentation at the June 2013 VSATT Meeting, Southfield, MI.

TSDC related (including example 2013 publications using the data for advanced vehicle analyses):

1. Neubauer, J., and Wood, E., "Accounting for the Variation of Driver Aggression in the Simulation of Conventional and Advanced Vehicles." SAE International 2013 World Congress, 2013-01-1453.
2. Attibele, P., Makam, S., and Lee, Y., "A Comparison of Real World and Accelerated Powertrain Endurance Cycles for Light-Duty Vehicles." Innovative Automotive Transmissions, Hybrid and Electric Drives, May 2013.
3. Burton, E., Gonder, J., Duran, A. and Wood, E., "Map Matching and Real World Integrated Sensor Data Warehousing." Abstract accepted for presentation at the Federal Committee on Statistical Methodology Research Conference, November 2013.

Patents

1. Burton, E., Duran, A., Gonder, J. and Walkowicz, K., "Integrated Geo-Spatial Transportation Analysis Database." NREL Software Record SWR-13-27, August 2013.
2. Wood, E., Burton, E., Duran, A., Gonder, J., and Walkowicz, K., "GIS Tool for Appending Accurate Road Grade Data to Vehicle GPS Traces." NREL Software Record SWR-13-32, August, 2013.

Tools and Data

1. Multiple datasets available at the TSDC website: www.nrel.gov/tsdc.
2. Customized version of FASTSim provided to the RWDC Surface Challenge teams through the RWDC team portal. Note that the full version of FASTSim remains available from www.nrel.gov/fastsim.

V.F. A/C Model Development

Jason A. Lustbader
National Renewable Energy Laboratory
15013 Denver West Parkway
Golden, CO 80401
Phone: (303) 275-4443
E-mail: Jason.Lustbader@nrel.gov

David Anderson and Lee Slezak
Phone: (202) 287-5688 (David Anderson)
E-mail: David.Anderson@ee.doe.gov
Phone: (202) 586-2335 (Lee Slezak)
E-mail: Lee.Slezak@ee.doe.gov

V.F.1. Abstract

Objectives

- Improve the robustness and accuracy of the Fully-Detailed A/C system model
- Develop new, faster model versions that are better suited for vehicle drive cycle based air conditioning (A/C) system simulation while minimizing losses to accuracy. Validate new models to data and to the Fully-Detailed model
- Update integration of Fully-Detailed model into Autonomie.

Major Accomplishments

- Improved the Fully-Detailed finite volume formulation model increasing robustness and user-friendliness.
  - Added detail to the air-side louvered fin heat exchange rate calculations, improved refrigerant material property lookup functions, and improved the modeling of heat exchange rate on the boundaries between different refrigerant phase regions.
  - Created combined mechanical and electric drive compressor model from the previously separate model versions. In this new model, the compressor curves and system controls can be easily switched between the two options.
  - Verified updated model with a data set provided by Halla-Visteon. The average errors in refrigerant mass flow rate, condenser heat transfer rate, evaporator heat transfer rate, and evaporator-out air temperature were 2.65%, 1.03%, 2.12%, and 1.24°C, respectively.
- Developed the new Quasi-Transient model that runs 10 times faster than the Fully-Detailed model while preserving good accuracy
  - Uses a marching-in-space finite volume formulation, and trades some transient process accuracy for increased model solution speed.
  - The average errors compared to data for the refrigerant mass flow rate, condenser heat transfer rate, evaporator heat transfer rate, and evaporator-out air temperature were 4.08%, 1.21%, 2.08% and 1.21°C, respectively
  - Over an SC03 drive cycle, the Quasi-Transient model average heat exchange rates and compressor power were within 3% of the Fully-Detailed model.
- Created the Mapped-Component model, which runs 100 times faster than the Fully-Detailed model. This model trades more accuracy for even higher model execution speed.
  - This model replaces the condenser and evaporator sub-models of the Quasi-Transient model with lookup tables generated by the Quasi-Transient model.
  - The average errors compared to data for the refrigerant mass flow rate, condenser heat transfer rate, evaporator heat transfer rate and evaporator-out air temperature were 4.89%, 2.17%, 3.68%, and 1.50°C, respectively.
  - Over an SC03 drive cycle, the Mapped-Component model average heat exchange rates were within 3% and compressor power was within 15% of the Fully-Detailed model.
- Conversion between the three A/C system model approaches is relatively simple, which is advantageous. For example, a new control method could first be developed in one of the faster model versions, and the algorithm then can be refined using one of the slower, but more detailed model versions.
- Made a number of changes to the A/C model structure so that it would integrate into the new version of Autonomie released in April 2013 (Autonomie_Rev12). The initial updated integration of the mechanical A/C model was completed. Example simulation results using a default vehicle over an SC03 drive cycle showed the A/C system caused a reduction in fuel economy of 18%, and a 21.9% increase in fuel consumption with an A/C coefficient of performance of approximately 2.

Future Achievements

- This project is completed; however, the tools developed in this project will provide a strong foundation for a new project in which vehicle thermal system and system components working on single-phase liquid heat transfer will be modeled

✧ ✧ ✧ ✧ ✧

V.F.2. Technical Discussion

Background

When operated, the A/C system is the largest auxiliary load on a vehicle. A/C loads account for more than 5% of the fuel used annually for light-duty vehicles in the United States [1]. A/C loads can have a significant impact on the performance of hybrid electric vehicles, plug-in hybrid electric vehicles, and electric vehicles. Hybrid electric vehicles have 22% lower fuel economy with the A/C on [2]. Mitsubishi reports that the range of the i-MiEV can be reduced by as much as 50% on the Japan 10–15 cycle when the A/C is operating [3]. The Advanced Powertrain Research Facility at Argonne National Laboratory has reported a nearly 20% reduction in the range of the Nissan Leaf operating on the Urban Dynamometer Driving Schedule (UDDS) cycle [4]. Increased cooling demands from the battery thermal management system in an electric vehicle may also add additional loads on the A/C system. Air conditioning in heavy-duty vehicles also uses significant fuel for both down-the-road and idle conditions. A flexible open-source analysis tool is needed to assess the A/C system's impact on advanced vehicles. Industry has expressed a need for both a standalone A/C system model as well as an A/C model that can co-simulate with a vehicle simulator such as Autonomie [5]. This model expands the capability of Autonomie to address industry needs.

Introduction

The A/C system contains complex flow, thermodynamics, and heat transfer. On the refrigerant-side, the flow is transient and both compressible and two phase. Calculating refrigerant properties near the phase transitions can also be computationally difficult.

Air flow through the condenser can vary widely depending on vehicle speed and condenser fan speed. Heat is transferred from the refrigerant to the metal heat exchanger surface, then from the heat exchanger surface to the air.

Simulation of air flow through the evaporator must account for the condensation of water vapor from the humid air stream. The result is that the mass flow of air through the evaporator is constantly changing. The latent heat of water vapor condensation can account for a significant portion of the evaporator heat load. Heat is transferred from the air through the layer of condensed water on the heat exchanger surface to the metal of the heat exchanger, then to the refrigerant.

A cabin model is also needed to provide a realistic load on the evaporator. The cabin model must consider all the major pathways of heat transfer into the cabin, including solar and convective loads from the environment, heat from the engine compartment, and sensible and latent heat loads in the air stream.

MATLAB/Simulink was chosen as the platform to develop the model. Using this platform has several advantages. Autonomie is also built on Simulink, which facilitates integration of the model into Autonomie. MATLAB/Simulink is widely used in industry, so the standalone, freely available version of the A/C model can be widely distributed.

In FY 2011, the A/C model was evaluated for functionality. In FY 2012, the model was extensively validated against data sets provided by Visteon, and the first integration with Autonomie was carried out. In FY 2013, the original Detailed-Model was improved and two new models, Quasi-Transient and Mapped-Component, were developed to increase simulation speed while minimizing accuracy loss, Figure V-48. The goal of these new model versions is to provide faster simulation tools for less detailed, vehicle-focused drive cycle based evaluation of A/C systems.

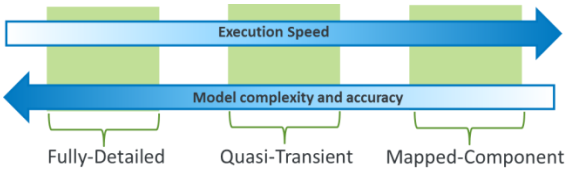

Figure V-48: Three model versions to match need with accuracy and speed.

Approach

The Detailed-Model was improved to include the addition of fin efficiency calculations [6] and Chang and Wang's more complex heat transfer model [7] that uses detailed fin geometry to improve accuracy. The solution robustness of the code was improved by replacing property tables generated with REFPROP with quality-averaged refrigerant properties in the saturated mix region. The previous tables for this region had "spikes" in them that did not appear real, and they caused the solutions to be noisy. The code robustness was improved further by smoothing the transition between the heat transfer correlations at the boundaries of their usable range. There were a number of other changes, mainly to address improving user friendliness, including a combined model that can be switched between mechanical and electric compressor drive and their associated control algorithms. A flag in the file setup input parameters switches between the models. The improved model was documented in an SAE journal article [8].

Autonomie Integration

The Detailed-Model was then modified to work with the new version of Autonomie, Autonomie_Rev12, which was released in April 2013 (Figure V-49). Many changes were made to the A/C model structure so that it would integrate into Autonomie. The compressor was split out of the cooling circuit block, and the cabin model was placed into the chassis block. The integration of the NREL A/C model into Autonomie is illustrated in Figure V-49 through Figure V-53. Figure V-50 shows the mechanical accessory block that contains the mechanically driven A/C system. The upper-level Simulink block diagram of the A/C model is shown in Figure V-51, and the Simulink diagram of the cooling circuit model is shown in Figure V-52. The red ovals indicate data into the model from the Autonomie data bus, and the cyan ovals indicate data out of the model to the data bus. Figure V-53 shows the component level of the A/C Simulink model. Figure V-53 shows the Simulink diagram of the cabin model in the chassis block. The red ovals indicate data into the model from the

Autonomie data bus, and the light blue ovals indicate data out of the model to the data bus.

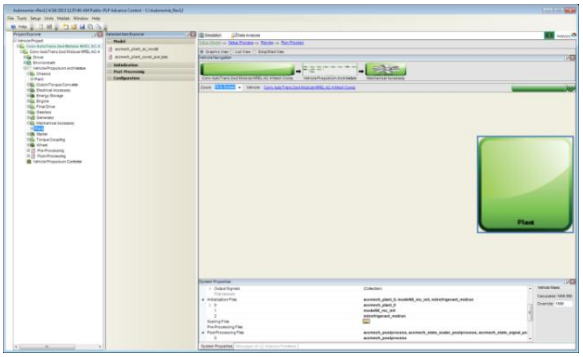

Figure V-49: Autonomie mechanical accessory block.

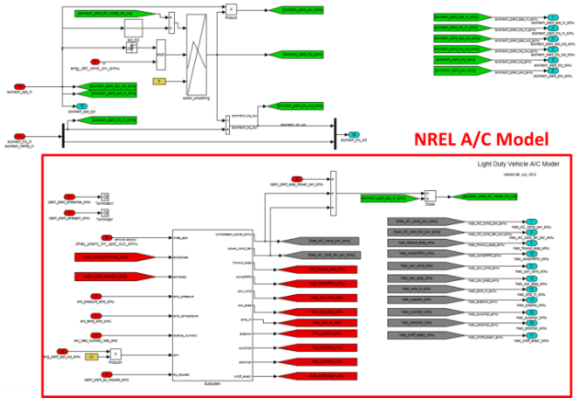

Figure V-50: Top level of the Simulink A/C model.

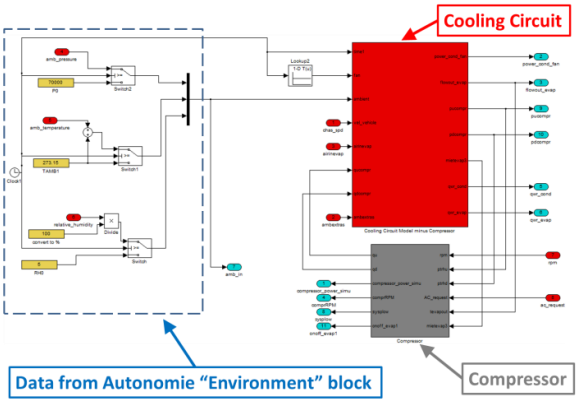

Figure V-51: Cooling system and compressor model.

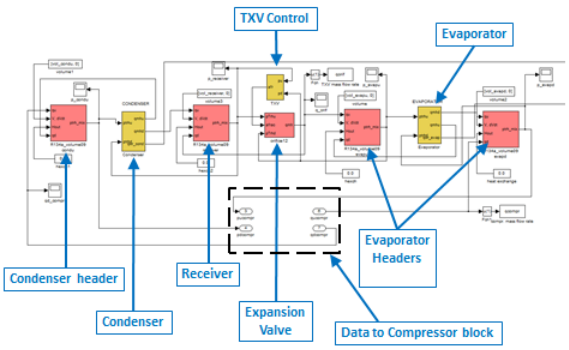

Figure V-52: Component level A/C system block diagram.

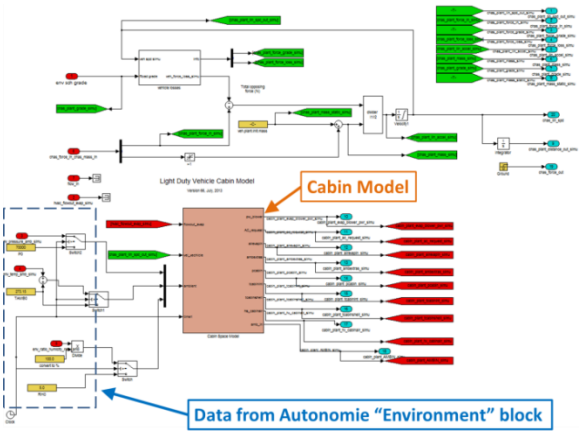

Figure V-53: Cabin model within chassis block.

The simulation speed was limiting the usefulness of the Detailed-Model for less detailed, vehicle-focused drive cycle-based compressor power evaluation; therefore, in FY 2013, model versions were created that are significantly faster while minimizing degradation of accuracy.

New Faster Models

To meet the various A/C modeling needs, two additional complementary models were developed, the Quasi-Transient and the Mapped-Component model. The user can switch between these models to match the model detail with the current needs of a project. The Quasi-Transient model runs 10 times faster and theoretically matches the steady-state conditions of the Fully-Detailed model, but will lose some accuracy during transients. The Mapped-Component model is 100 times faster, but instead of detailed calculations of flow and heat transfer in the heat exchangers, these variables are obtained from multi-dimensional lookup tables. The lookup tables used in the Mapped-Component models are created with the evaporator and condenser sub-models of the Quasi-Transient model.

The Quasi-Transient Model

The Quasi-Transient model was created to provide an option for much faster model simulation speed that better facilitates drive cycle-based A/C system studies. It is also useful for debugging the Fully-Detailed system model when a new control algorithm or modified components are installed. This model comes at a cost of some accuracy, mainly for transient process predictions. The Simulink S-functions that constitute the heart of the simulation model and the Simulink "masks" that improve user communication were created such that any Fully-Detailed model can very quickly be converted into the Quasi-Transient model. A model can be converted by swapping out the Fully-Detailed model's 1-D line and 0-D volume Simulink S-functions with their Quasi-Transient equivalents. Some straightforward adjustments to the initialization files also have to be made.

For the Quasi-Transient model, some non-conservation error is allowed in order to increase the simulation speed. The approach works by pulling the solution towards the steady-state solution that belongs to the boundary conditions prevailing at that time step. Using a strong "pull" will make the Quasi-Transient solution approximate the solution that would

be obtained with a hypothetical quasi-steady model that in every time step calculates the steady-state conditions. Making the model "pull" too large will result in oscillations and model instability. The Fully-Detailed model uses a finite volume formulation in the refrigerant lines marching in time only, whereas the Quasi-Transient model uses a finite volume method marching in both space and time. It is worth noting that these different formulations of the same physics equations will inherently provide slightly different numerical solutions. When all the time derivatives of the flow and other variables are zero, the equations incorporated in the Quasi-Transient model will closely match those incorporated in the Fully-Detailed model.

The line model used in the Quasi-Transient model has a refrigerant mass flow rate that is constant along the line and is also a simulation state variable. In each time step, the refrigerant pressure drop across the line is compared to the pressure drop obtained from the two attached 0-D volumes. A numerical method is applied to continuously adjust the refrigerant mass flow rate in the lines to match the pressure drop in the line to the pressure drop between the attached 0-D volumes better. The refrigerant mass flow rate responds with some delay. This results in the Quasi-Transient model solution "pull."

In each of the 0-D refrigerant volumes, the refrigerant is represented by one single bulk modulus valid for all conditions. With this simplification, the pressure is a function of density only. By setting the right bulk modulus in each volume, it can be ensured that the volumes in the system model all have similar "stiffnesses" and high stiffness in the volumes with liquid is avoided. This allows for a larger solution time step resulting in much faster model execution. The cost of this approach is that the total refrigerant mass in the system is slightly fluctuating, and the energy balance is slightly off, especially for shorter simulated time periods. For steady-state conditions, however, the conservation of mass and energy for each component (1-D lines and 0-D volumes) and for the system as a whole is valid.

There are significant approximations involved in the Quasi-Transient model; however, it provides a good balance between accuracy and speed. Ultimately, the utility of this model is determined by how well it approximates the results of the Fully-Detailed model, which is demonstrated later in this report.

The Mapped-Component Model

The Mapped-Component model represents another step towards increased model execution speed at an additional cost of reduced accuracy. The Mapped-Component model is created from the Quasi-Transient model by replacing the condenser and the evaporator with simplified sub-models that use lookup tables. For the condenser, the refrigerant mass flow rate and the air-to-refrigerant heat exchange rate are each obtained from a separate five-dimensional lookup table based on upstream refrigerant pressure, upstream refrigerant enthalpy, refrigerant pressure drop, air mass flow rate, and air inlet temperature. For the evaporator, the lookup tables also have to incorporate the relative humidity of the incoming air for acceptable accuracy. Therefore, if the evaporator had been treated similarly to the condenser, the lookup tables would be six-dimensional. Adding a sixth dimension to the lookup tables greatly increases the time needed to generate them. The hysteresis due to the evaporator wall mass is also important when the compressor starts cycling for evaporator freeze prevention. To solve these issues, the lookup tables for the evaporator were split into refrigerant and air-side tables coupled through the wall temperature. For the four-dimensional refrigerant-side tables, the refrigerant mass flow rate and the wall-to-refrigerant heat transfer rates are looked up from the upstream refrigerant pressure, upstream refrigerant enthalpy, the refrigerant pressure drop, and the wall temperature. For the air-side, the air-to-wall heat transfer rate is looked up from the air mass flow rate, air-in temperature, air-in relative humidity, and the wall temperature. Creating these three four-dimensional maps is much more time efficient than creating two maps each with six-dimensions. This approach reduced the time needed to create the evaporator maps from 86 to 4 hours.

The lookup tables are used in the following way: refrigerant-out enthalpy is the sum of the refrigerant-in enthalpy flow rate and the heat transfer rate to refrigerant, for both the condenser and the evaporator. Air-out temperature on the evaporator is calculated the same way as in the fully-detailed model, accounting for condensation of water on the metal surfaces, if present.

The lookup tables were generated with stand-alone Quasi-Transient models of the condenser and the evaporator. For each point in the lookup tables, the condenser and evaporator models were run until steady-state conditions were reached. The heat transfer rates and refrigerant mass flow rates were recorded and placed into a large array that the Simulink lookup table block of the Mapped-Component model could read. This entire process was automated. The necessary maps can be created with the automated process on an Intel(R) i7-3520 M 2.9GHz CPU 64 bit personal computer with 4 GB of RAM in a matter of 10–12 hours.

Results

Detailed-Model Improvements

One application that demonstrates the capabilities of this improved Detailed-Model is a refrigerant charge effect study. The model nearly perfectly preserves the refrigerant mass and therefore is capable of such a study.

The refrigerant charge effect results (Figure V-54) show trends consistent with expected behavior. As the refrigerant charge increases, there is a limit above which the system high pressure suddenly increases. This results in a rapid compressor power increase. At the same time, this overcharged system provides little improvement in evaporator performance.

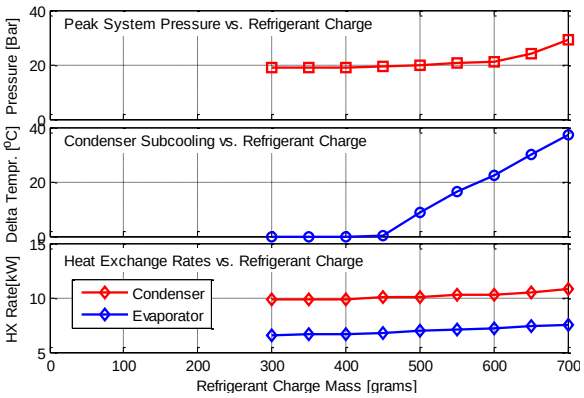

Figure V-54: Refrigerant charge effect study.

Autonomie Integration

The A/C model was co-simulated in Autonomie using a default midsized automobile on the SC03 drive cycle. Figure V-55 shows engine and compressor speed in RPM. The compressor follows the engine speed. The compressor power and condenser and evaporator heat transfer dynamics all follow the rapidly changing compressor speed. Note that the compressor begins to cycle at approximately 120 seconds (as indicated by the first vertical dashed line) because the evaporator has reached the freeze protection set point. The second vertical dashed line, at approximately 280 seconds, indicates where the cabin temperature has reached its set point and clutch cycling for the cabin temperature control begins.

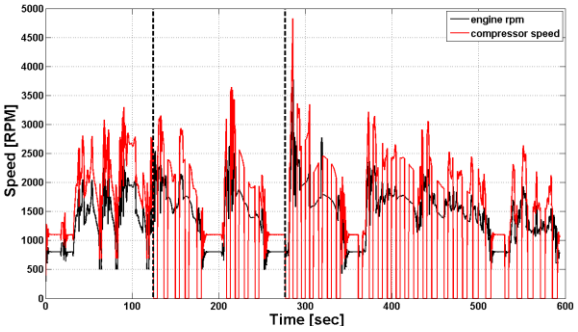

Figure V-55: Engine and compressor speed [RPM].

Figure V-56 shows the compressor power requirement and the condenser and evaporator heat transfer. This model uses a mechanically driven compressor, so the compressor power and heat transfer are affected by the rapidly changing engine speed as well as the cycling of the compressor.

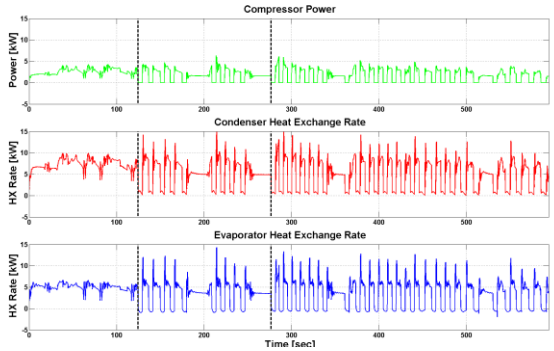

Figure V-56: Heat transfer and compressor power.

Figure V-57 shows the cabin air temperature and the dead band control signal. When the cabin temperature falls below the lower deadband temperature limit, it switches the compressor off; when the temperature rises above the upper deadband temperature limit, it turns the compressor back on. The model cycles the compressor, capturing the behavior that takes place in an actual automotive A/C system.

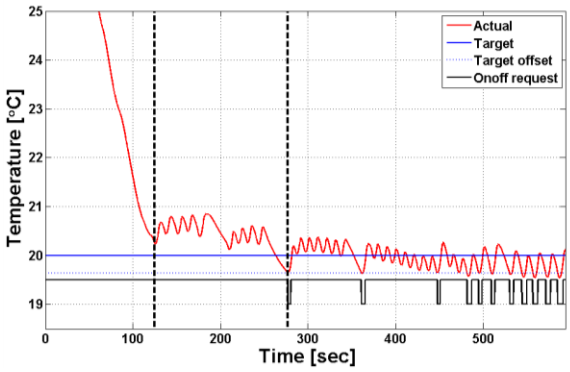

Figure V-57: Cabin air temperature, control signal, and control upper and lower limits.

Figure V-58 shows the summary table from two Autonomie simulations, one with A/C on and one without A/C.

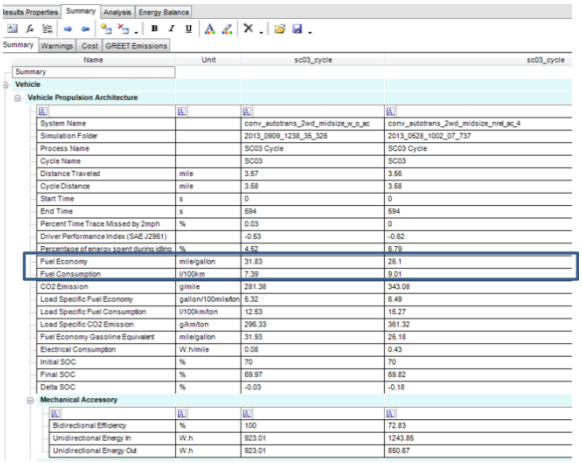

Figure V-58: Autonomie summary table.

The simulation results show that the use of A/C causes a reduction in fuel economy of 18%, and a 21.9% increase in fuel consumption over an SC03 drive cycle with an A/C coefficient of performance of approximately 2.

Validation and Comparison of the Models

Previous successful validation of the Fully-Detailed model was refined further this year by model improvements. The Quasi-Transient model was evaluated against the same set of steady-state measured data provided by Halla Visteon, using the same calibration coefficients for the heat transfer models as the Fully-Detailed model in the calibration process. The results are shown in Figure V-59, where the simulated and measured compressor mass flow rate, evaporator heat exchange rate, condenser heat exchange rate, and the evaporator-out air temperature are compared. The average errors in these performance parameters over the 22 operating

points are 4.08%, 1.21%, 2.08%, and 1.21°C, respectively. For reference, these errors for the current Fully-Detailed model are 2.65%, 1.03%, 2.12% and 1.24°C, respectively. It can be concluded that for steady-state prediction, the Quasi-Transient model is equally as accurate as the Fully-Detailed model.

Comparisons between the predictions by the Fully-Detailed and the Quasi-Transient models for the first 300 seconds of the SC03 cycle are shown in Figure V-60.

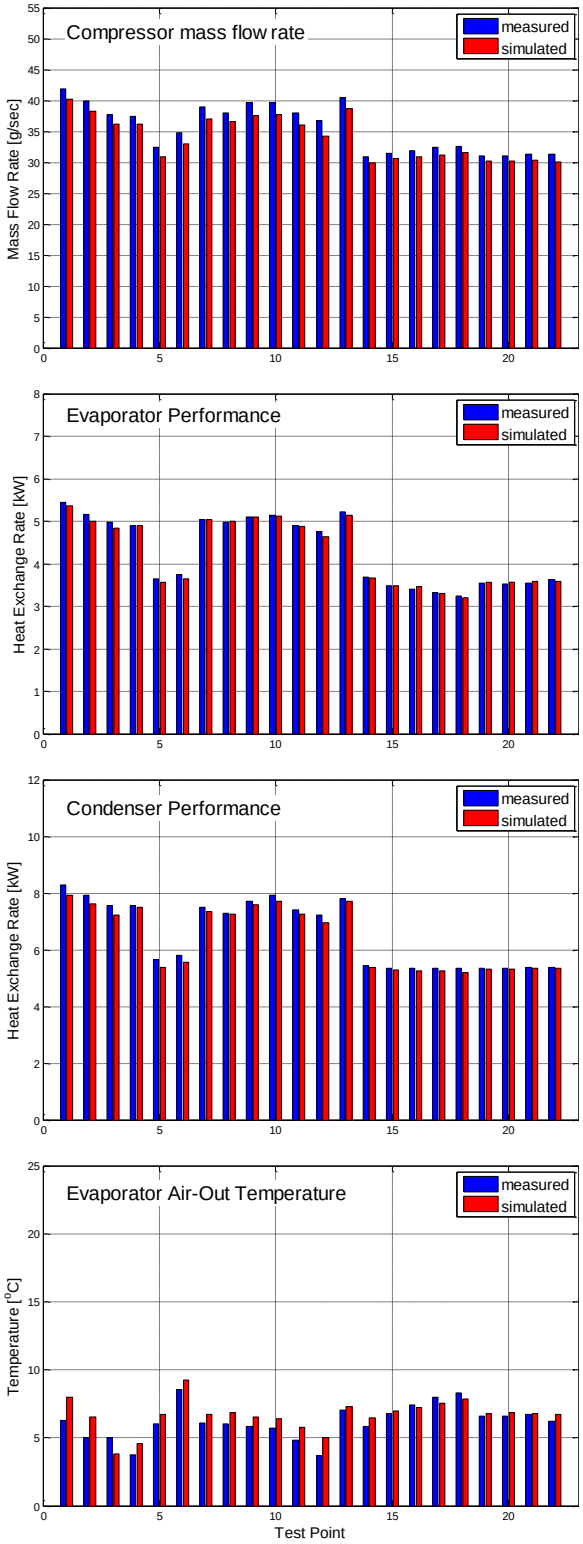

Figure V-59: Simulation vs. measurement for the Quasi-Transient model.

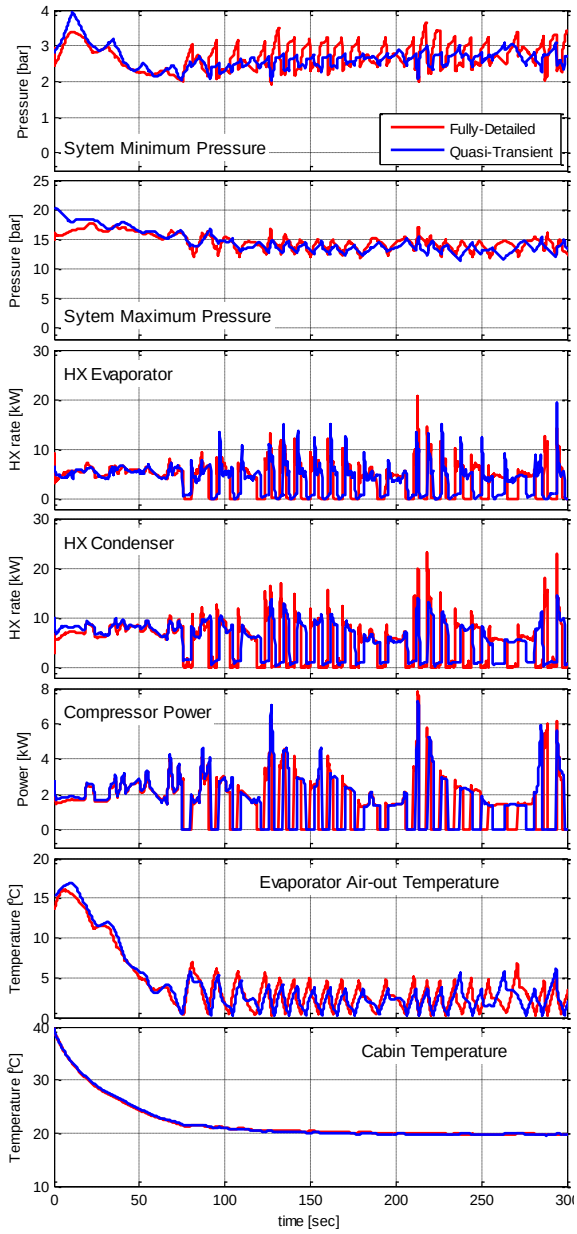

Figure V-60: Fully-Detailed vs. Quasi-Transient models for first 300 seconds of the SC03 cycle.

Similar plots comparing the results of the Mapped-Component model to the results of the Fully-Detailed model for the first 300 seconds of the SC03 cycle are shown in Figure V-61. The less accurate, but faster model results match the results of the Fully-Detailed model well. It is notable that the cycling due to evaporator freezing prevention starts at around the same time for all three models. Then, due to slight differences in predictions, the start and end points of the cycling periods drift apart. After some time, the cycling periods may be far off, yet such discrepancy does not mean there is a large difference in the accuracy of the predictions in general.

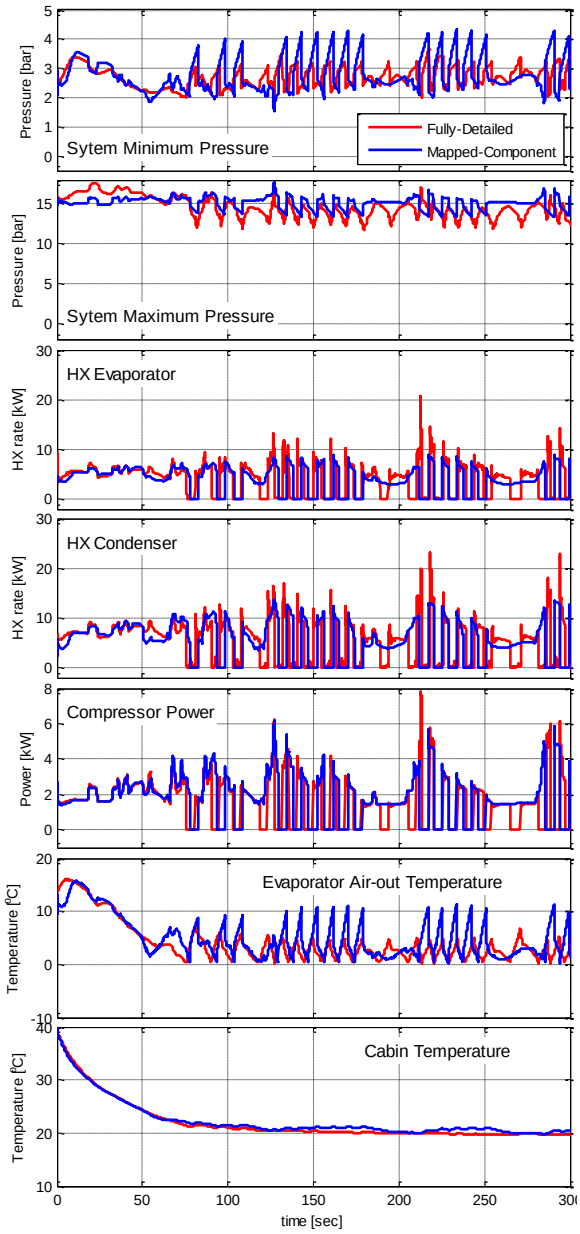

Figure V-61: Fully-Detailed vs. Mapped-Component models for the first 300 seconds of the SC03 cycle.

For vehicle-focused analysis, the agreement of the models over a drive cycle is important. Of particular interest are the average compressor power and the average heat transfer rates on the heat exchangers. These data are shown in Figure V-62. Over the SC03 drive cycle, both models were within 3% of the Fully-Detailed model for evaporator and condenser heat transfer and compressor power, except for the Mapped-Component compressor power, which was 15% high.

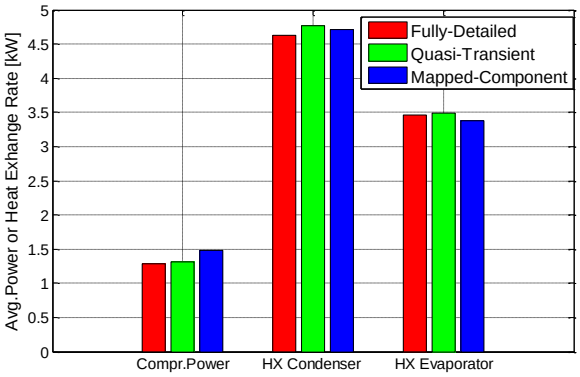

Figure V-62: Average power/heat exchange rates predicted by model versions for SC03 cycle.

These small losses of accuracy come at a large benefit to simulation execution speed. In Figure V-63, the simulation execution speed is compared for the three model versions. The speeds were evaluated with the mechanical compressor and from the same runs of the SC03 cycle shown in Figure V-60 and Figure V-61. The simulation execution speed for the Fully-Detailed, Quasi-Transient, and Mapped-Component models were 0.10, 0.98, and 9.96 times faster than real time, respectively. For reference, "10 times faster than real time" speed means that one second of simulated time takes 0.1 second to simulate.

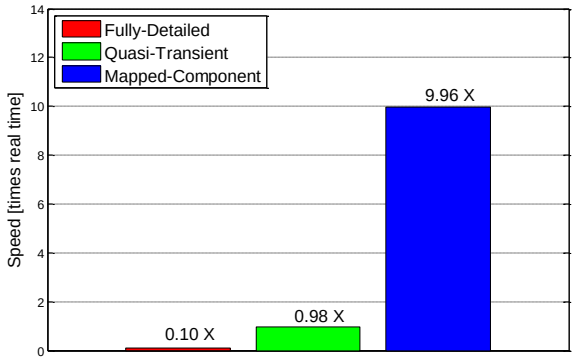

Figure V-63: Comparison of simulation speed for the different model versions.

Conclusions

A MATLAB/Simulink model of a light-duty vehicle HVAC system developed in FY 2012 was further improved. The main improvements include the addition of fin efficiency calculations and a more complex air-side heat transfer model that uses detailed fin geometry to improve accuracy. Changing to quality-averaged refrigerant properties improved the robustness of the model. There were a number of other changes to improve user friendliness, including a combined model that can be switched between mechanical and electric compressor drives and their associated control algorithms.

New model versions were created with the goal of greatly increasing the simulation speed while minimizing loss of accuracy. These include the Quasi-Transient model and the Mapped-Component model. The Quasi-Transient model provides essentially the same accuracy for steady state condition prediction as the Fully-Detailed model. The Mapped-Component model does lose some accuracy in steady-state conditions. For the SC03 cycle, the averaged results of power and heat exchange rates obtained with the Quasi-Transient model are within 3% of the results of the Fully-Detailed model. The Mapped-Component model results are within 15% of the results of the Fully-Detailed model. Short transients, such as those occurring during compressor cycling, produce the most deviation from the Fully-Detailed model for both simplified models. The speed at which the simplified models run is 0.98 and 9.96 times real time speed, respectively, versus the speed of the Fully-Detailed model, which is 0.10 times real time speed. Conversion from one A/C system model approach to another of the three models (Fully-Transient, Quasi-Transient, and Mapped-Component) is relatively simple. This allows a new model to be developed in a faster version before the results are refined using a slower, more detailed solution method as needed.

In the trade-off of speed and accuracy, the three models occupy very different parts of the scale, and it is believed that the simplified models are significant additions to the tools available, especially for vehicle focused cycle-based evaluation of A/C systems.

Finally, a number of changes were made to the A/C model structure so that it would integrate into the new version of Autonomie released in April 2013 (Autonomie_Rev12). The integration was completed, and simulation results show that the use of A/C causes a reduction in fuel economy of 18% and a 21.9% increase in fuel consumption with an A/C coefficient of performance of approximately 2.

References

1. John Rugh, Valerie Hovland, Stephen Andersen, "Significant Fuel Savings and Emission Reductions by Improving Vehicle Air Conditioning", Presented at the 15th Annual Earth Technologies Forum and Mobile Air Conditioning Summit, April 15, 2004.
2. NREL, Vehicle Technologies Program 2007 Annual Report, p. 45.
3. Hideto Noyama, Kohei Umezu, "Air-Conditioning System for Electric Vehicle (i-MiEV)", Presented at the SAE Automotive Refrigerant & System Efficiency Symposium, 2010.
4. Argonne National Laboratory Advanced Powertrain Research Facility data, EV Everywhere Workshop presentation, Lee Slezak, September 13, 2012.
5. Computer Software "Autonomie," www.autonomie.org
6. Incropera, F.P., DeWitt, D.P., "Fundamentals of Heat and Mass Transfer," 2nd edition, 1985, John Wiley and Sons, Inc.
7. Chang, Y.J., Wang, C.C., "A Generalized Heat Transfer Correlation for Louver Fin Geometry," Int. J. Heat Mass Transfer, Vol. 40, No. 3, pp. 533–544, 1997.

8. Kiss, T., Chaney, L., Meyer, J., "A New Automotive Air Conditioning System Simulation Tool Developed in MATLAB/Simulink," SAE Int. J. Passeng. Cars—Mech. Syst. 6(2):2013, doi:10.4271/2013-01-0850.

V.F.3. Products

Publications

1. Kiss, T., Chaney, L.J., Meyer J.J., (2013) "A New Automotive Air Conditioning System Simulation Tool Developed in MATLAB/Simulink," SAE World Congress, April 15-18, SAE 2013-01-0850.
2. Kiss, T., Chaney, L., Meyer, J., "A New Automotive Air Conditioning System Simulation Tool Developed in MATLAB/Simulink," *SAE Int. J. Passeng. Cars—Mech. Syst.* 6(2):2013, doi:10.4271/2013-01-0850.

Tools and Data

1. CoolSim v66, A/C modeling Tool for MATLAB/Simulink Environment

Acknowledgements

- Co-authors: Tibor Kiss and Larry Chaney (NREL)
- Additional thanks to: John Rugh and Lisa Fedorka (NREL)
- Special thanks to our partners: Halla-Visteon, Daimler Trucks, and Argonne National Laboratory.

V.G. Autonomous Intelligent Electric Vehicles

Andreas Malikopoulos, Principal Investigator
Oak Ridge National Laboratory
National Transportation Research Center (NTRC-2)
2370 Cherahala Boulevard
Knoxville, TN 37932-6472
Phone: (865) 946-1529
E-mail: andreas@ornl.gov

David Anderson, DOE Program Manager
Phone: (202) 586-8055
E-mail: david.anderson@ee.doe.gov

V.G.1. Abstract

Objectives

- Develop the control algorithms for making a hybrid propulsion system into an autonomous intelligent system capable of realizing its optimal operation in real time while the driver is driving the vehicle.

Major Accomplishments

- Completed an extensive literature review of more than 160 archival publications covering key state-of-the-art power management control algorithms and reported the review in a survey paper submitted in the IEEE Transactions on Intelligent Transportation Systems.
- Developed the control algorithms that allow a hybrid propulsion system to operate at the instantaneous equilibrium operating point. Implemented the control algorithms into Autonomie software platform.
- Evaluated the efficiency of the algorithms in the Meritor heavy duty Dual Mode Hybrid Powertrain (DMHP), Cooperative Research and Development Agreement (CRADA), demonstrating up to 5% fuel economy improvement.
- Evaluated the efficiency of the algorithms in a series hybrid propulsion system demonstrating up to 7% fuel economy improvement and reported the results in a paper published in the 2013 American Control Conference.
- Evaluated the efficiency of the algorithms in a parallel hybrid propulsion system and reported the results in a paper submitted in the IEEE Transactions on Intelligent Transportation Systems.

Future Achievements

- The projected was completed.

✧ ✧ ✧ ✧ ✧

V.G.2. Technical Discussion

Background

The necessity for environmentally conscious vehicle designs, in conjunction with increasing concerns regarding U.S. dependency on foreign oil and climate change, has led to significant investment in enhancing the propulsion portfolio with new technologies. Among the promising technologies are hybrid electric vehicles (HEVs), which have shown the potential to achieve greater fuel economy than vehicles powered only by internal combustion (IC) engines. The main advantage of HEVs is the existence of two individual subsystems, thermal (IC engine) and electrical (motor, generator, and battery), that can power the vehicle either separately or in combination. Recently, PEVs—the U.S. Department of Energy (DOE) defines both plug-in hybrid electric vehicles (PHEVs) and all-electric vehicles (EVs) as PEVs—have attracted considerable attention due to their potential to increase fuel economy and reduce emissions. PEVs are hybrid vehicles with rechargeable batteries that can be restored to full charge by connecting a plug to an external electric wall socket, and thus they share some of the characteristics of both HEVs and EVs. They are especially appealing in situations where daily commuting is over short distances (about 60% of U.S. passenger vehicles travel less than 30 miles each day). Under the average mix of electricity sources in the United States, PEVs can be driven with lower operating costs and fewer greenhouse gas (GHG) emissions per mile when powered by electricity rather than by gasoline.

These hybrid propulsion systems have the potential to reduce petroleum consumption and GHG emissions by means of sophisticated supervisory power management control algorithms. The latter is of great importance in both HEVs and PEVs as it determines how to split the power demanded by the driver between the thermal and electrical subsystems to improve fuel economy and reduce emissions. The overarching goal of this project is to develop an intelligent supervisory controller combining and stochastic control algorithms that will optimize fuel economy and emissions in advanced hybrid propulsion systems.

Introduction

Widespread use of hybrid powertrains is inevitable, and many opportunities for substantial progress remain. HEVs and PEVs have attracted considerable attention due to their potential to reduce petroleum consumption and greenhouse gas emissions in the transportation sector. This capability is mainly attributed to (a) the potential for downsizing the engine, (b) the potential for recovering energy during braking and thus recharging the energy storage unit, and (c) the ability to minimize the operation of the engine in inefficient brake specific fuel consumption (BSFC) regimes.

A typical HEV consists of the fuel converter (internal combustion engine), the inverter, the battery, and the electric machines (motor and generator). Depending on their architecture, HEVs fall into one of several categories: (1) parallel, (2) series, or (3) power spit. In parallel HEVs, both the engine and the motor are connected to the transmission, and thus they can power the vehicle either separately or in combination. The series HEV, in which the electric motor is the only means of providing the power demanded by the driver, is the simplest HEV configuration. Finally, the power split HEV can operate either as a parallel or a series HEV, combining the advantages of both. HEVs may also be classified based on the degree of hybridization as either (1) micro HEVs, (2) mild HEVs, or (3) full HEVs. In micro HEVs, or start/stop vehicles, the engine is turned off during braking or at stop to avoid idling operation and the starter-motor is used to start the engine when the driver presses the accelerator pedal. A mild HEV is essentially a conventional vehicle with oversized starter, also allowing the engine to be turned off whenever the car is coasting, braking, or stopped, and restart quickly whenever the driver presses the accelerator pedal. The motor is often mounted between the engine and transmission, substituting for the torque converter, and it can be used to supply additional power when accelerating. Micro and mild HEVs include only some of the features of HEVs, and therefore usually achieve only limited fuel savings. In contrast, full HEVs, also called strong HEVs, have a larger electric machine and battery. The electric machine (in motor mode) can power the vehicle separately if necessary, and also regenerate energy (in generator mode) from braking and store it in the battery. The supervisory power management control algorithm is of great importance in both HEVs and PEVs as it determines how to split the power demanded by the driver between the engine, motor/generator and battery to improve fuel economy and reduce emissions.

A significant amount of research has been focused on power management control algorithms that employ deterministic and stochastic dynamic programming (DP) to derive offline the optimal control policy with respect to a given driving cycle or family of driving cycles. Although DP can provide the optimal solution in both the deterministic and stochastic formulation of the power management control problem, the computational burden associated with deriving the optimal control policy prohibits online implementation in vehicles, and it can grow intractable as the size of the problem increases. To address these issues, research efforts have been concentrated on developing online power management algorithms yielding suboptimal solutions. The main aspects of these algorithms are concerned with the self-sustainability of the electrical path, which must be guaranteed for the entire driving cycle, and the fact that either no or limited a priori knowledge of the future driving conditions is available. Such algorithms consist of an instantaneous optimization problem that accounts for storage system SOC variation through the equivalent fuel consumption (EFC). The latter is evaluated by considering average energy paths leading from the fuel to the energy storage of the electrical path. Another more simplified approach is to develop a set of fuzzy logic control rules based on the driver's commands, the SOC of the battery, and the motor/generator speed to effectively split the power between the thermal and electrical paths. The underlying scheme of the fuzzy rules is to optimize the operational efficiency of all components, considered as one system. Once again, though, these algorithms can be efficient in minimizing fuel consumption and emissions only for the given driving cycles for which they have been designed due to the inherent assumption of average efficiencies of the subsystems restricting the efficiency of these algorithms. These recent developments and future trends in the modeling, design, control, and optimization of energy storage systems for hybrid propulsion systems have been presented in the literature with a detailed review and classification of current control strategies. Other recent research has focused on optimal operation of the motor, generator, and battery in HEVs and PEVs, another issue critical to deeper market penetration of EVs.

Although the aforementioned power management algorithms can be efficient in minimizing fuel consumption and emissions for a given driving cycle, state-of-the-art power management control algorithms cannot guarantee continuous optimum operation of the powertrain system on any different driving cycle. However, to fully exploit the potential benefit in fuel economy and emissions in hybrid propulsion systems, it is important to guarantee continuously efficient cooperation of all subsystems and components for any different driver. The research objective in this project is to develop the control learning algorithms that can make the hybrid propulsion systems into intelligent systems with the aim of realizing continuously their optimal operating point, defined as an instantaneous equilibrium operating point, for all subsystems, e.g., engine, motor, generator, battery, etc, with respect to any different driver.

This project had two main objectives: (1) to develop the framework that can yield an optimal solution online for any given driving style and (2) to develop the algorithms that can provide the optimal control policy. The contributions of this project are (1) the analytical formulation for modeling HEV operation as a controlled Markov chain, (2) the development of the analytical offline solution of the stochastic optimal control problem using the average cost criterion, (3) the development of a multiobjective optimization framework that can be used online to derive the optimal control policy, and 4) the development of the Pareto control policy that minimizes the average cost criterion.

Approach

We have addressed the problem of optimizing online the supervisory control in a parallel HEVs by achieving the HEV instantaneous equilibrium operating point. In this context, we developed a new approach by treating the control problem as a multi objective optimization problem, and we showed that the control policy yielding the Pareto optimal solution for the one-stage cost is an optimal control policy equivalent to the one derived by DP offline. We considered the problem of deriving an optimal power management control algorithm for a parallel HEV illustrated in Figure V-64 with a diesel engine and manual transmission. The electric machine (motor/generator) is coupled to the output shaft of the engine through a clutch and gear ratio before the transmission (pre-transmission configuration).

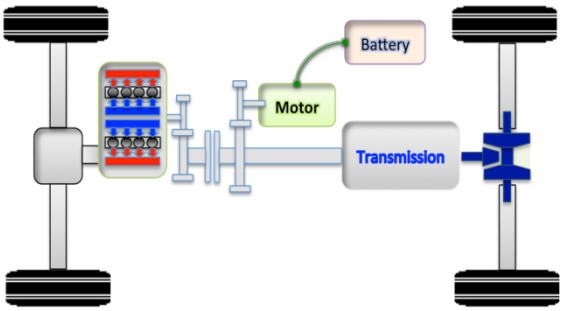

Figure V-64: Parallel hybrid electric vehicle configuration.

In this configuration, both the IC engine and electric motor can provide the power demanded by the driver either separately or in combination. Since the engine and motor speed depends on the vehicle speed, the available controllable variables are the engine and motor torque. The power management control problem of the HEV is addressed in a centralized fashion. The objective of the centralized controller is to guarantee the self-sustainability of the electrical path and distribute the power demanded by the driver optimally between the engine and the motor to minimize fuel consumption. The controller observes the state-of-charge (SOC) of the battery as well as the engine and motor speed, and then computes the optimal engine and motor torque, and based on the power demanded by the driver.

In previous research reported in the literature adopting the stochastic optimization framework described here, the SOC of the battery has been used as a component of the state. However, this may lead to a significant large state space with implications to increasing the computational burden associated with solving the problem. In our approach, the SOC is treated as an additional uncertainty by having it correlated to an additional power demand by means of a one-on-one mapping illustrated in Figure V-65. Namely, depending on the SOC value there is a corresponding amount of power P_{SOC} that needs to be provided to the battery in order to stay at the target SOC. This additional amount is added to the driver's power demanded as shown in Figure V-66. The one-on-one mapping aims to provide an increasing power request, P_{SOC}, as the SOC drops up to a certain maximum value. If the SOC is above the target value, then P_{SOC} is zero.

We seek the theoretical framework and control algorithm that will aim to yield the optimal control policy on-line while the driver drives the vehicle. In our proposed approach, HEVs are considered as cooperative multi agent systems in which the subsystems, i.e., engine, motor, and battery, are treated as autonomous agents. While the agents interact with each other, a centralized controller attempts to establish an equilibrium among the agents that maximizes the overall HEV efficiency. The problem is formulated as a sequential decision-making problem under uncertainty where the centralized controller is faced with the task to select control actions (engine and motor torque) in several time steps (decision epochs) to achieve long-term goals efficiently (fuel economy). In the HEV configuration adopted here, the engine and the motor are coupled together and their speed is a function of the vehicle speed depending on the gear ratio of the transmission. At each instant of time t, the controller needs to split optimally the torque demanded by the driver, between the engine and motor, to optimize fuel economy. Employing a myopic approach, namely, selecting the engine to provide portion of the driver's requested torque so as to operate the engine at a minimum break specific fuel consumption (BSFC), may result in operating the motor at a lower efficiency. As such, the motor would give away energy from the battery to losses. Wasting the battery's energy affects fuel economy since this energy will be provided back to the battery from the engine to maintain the SOC close to target value.

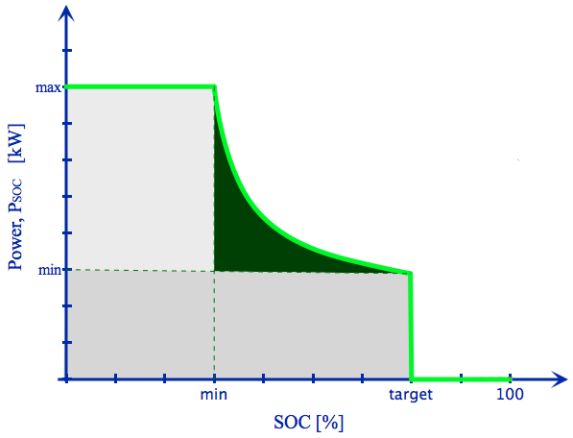

Figure V-65: Power required from the battery with respect to its state of charge.

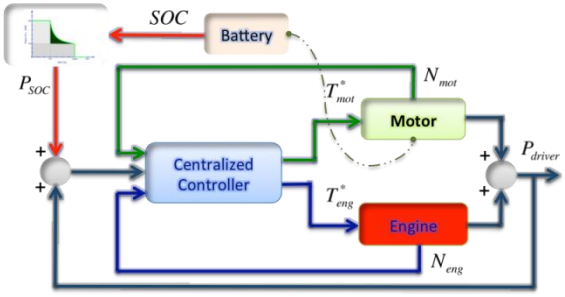

Figure V-66: The centralized control scheme.

Consequently, we need to identify an equilibrium, defined as HEV equilibrium operating point, among the agents, i.e., engine, motor, and battery that will assure maximization of the overall efficiency. To simplify the problem, the focus is on establishing the equilibrium between the engine and the motor only. However, future research should also consider the battery as an agent and investigate the implications associated with this. To compute the HEV equilibrium operating point we formulate a multiobjective decision making problem consisting of the engine's BSFC, and the motor's efficiency. The objective is to find the optimal torque for the engine and the motor that minimizes HEV fuel consumption for a given speed and torque request. To avoid dominance of one objective over the other both objectives are normalized with respect to their maximum value. In the parallel HEV configuration considered here, the Pareto efficiency set between the engine and the motor at a given speed is illustrated qualitatively in Figure V-67. At each instant of time t and based on the current vehicle speed, the Pareto efficiency can yield the HEV equilibrium operating point that minimizes the multi objective function.

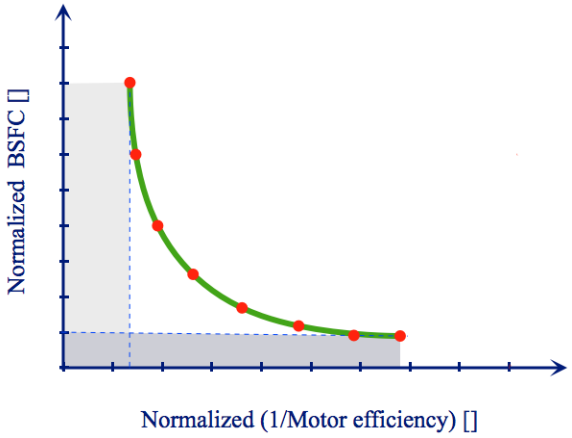

Figure V-67: Pareto efficiency for the engine's normalized brake specific fuel consumption (BSFC) and the motor's normalized inverse of efficiency in a parallel hybrid electric vehicle.

Results

To validate the effectiveness of the power management controller using the Pareto control policy, we used Autonomie. Autonomie is a Matlab/Simulink simulation package for powertrain and vehicle model development developed by Argonne National Laboratory. Autonomie provides a variety of existing forward-looking powertrain and vehicle models that can support the evaluation of new control functions in a math-based simulation environment. A vehicle model representing a heavy duty parallel HEV specified by the sponsor was developed in Autonomie and used in this study. The vehicle carries a diesel engine with maximum power of 374 kW, an electric machine with a continuous power of 200 kW and peak power of 360 kW, and a 12 V battery with 40 Ah energy capacity. The gear ratio between the engine and the output shaft is 3, whereas the gear ratio between the motor and the output shaft is 6.

The HEV model was simulated over standard dynamometer driving schedules (DDSs) (or simply driving cycles), which are vehicle speed profiles established by the U.S. Environmental Protection Agency (EPA) for testing and measuring fuel economy and emissions. These driving cycles are representative of typical urban and highway commutes. They essentially represent situations in which the driver requests a particular vehicle speed profile deemed characteristic of his/her driving style. The following driving cycles were used in this study: (1) the city-suburban heavy vehicle route (CSHVR), (2) the elementary urban driving cycle, (3) the extra urban driving cycle (EUDC), (4) the federal test procedure (FTP), (5) the Japanese 10 mode cycle, (6) the Japanese 15 mode cycle, (7) the New York city cycle (NYCC), and (8) the urban dynamometer driving schedule (UDDS). Although some of these driving cycles might be a bit aggressive for heavy-duty vehicles, the intention here is to validate the effectiveness of the Pareto control policy under any driving scenario. For each different vehicle speed and torque demand, the Pareto efficient was computed and stored.

To validate that the Pareto efficiency exists in our study we compute the normalized BSFC with respect to the engine torque for different engine speeds as illustrated in Figure V-68. Similarly, we compute the normalized inverse of the motor efficiency with respect to the motor torque for different motor speed shown in Figure V-69.

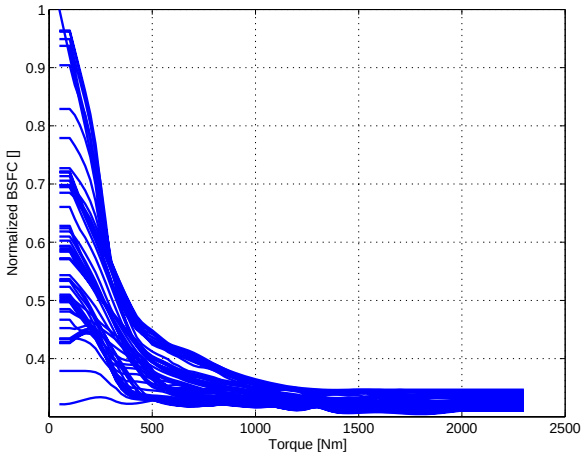

Figure V-68: Normalized brake specific fuel consumption (BSFC) for different engine speeds with respect to engine torque.

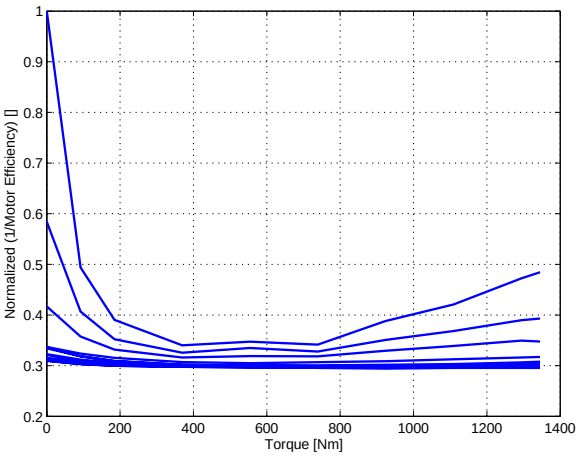

Figure V-69: Normalized inverse of the motor efficiency for different motor speeds with respect to motor torque.

It can be seen that for a given vehicle speed, and thus engine and motor speed, a different combination of engine and motor torque can yield different values of the normalized BSFC and inverse motor efficiencies. Figure V-70 shows the Pareto efficiency at 21 km/h when the torque demand is 6,975 Nm and the transmission gear ration is 1.5. Figure V-71 illustrates the set of all Pareto optimal solutions, i.e., the optimal engine and motor torque.

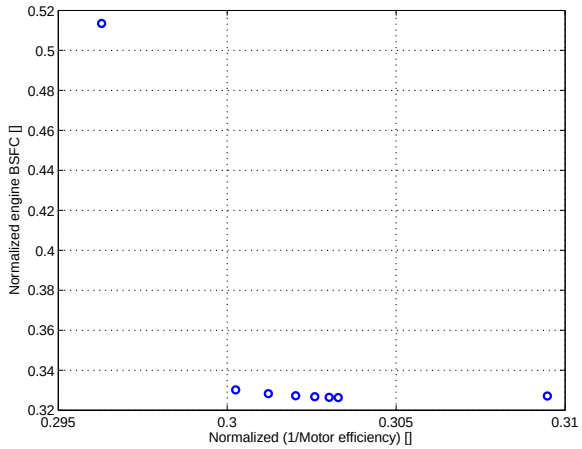

Figure V-70: Pareto efficiency at 21 km/h vehicle speed.

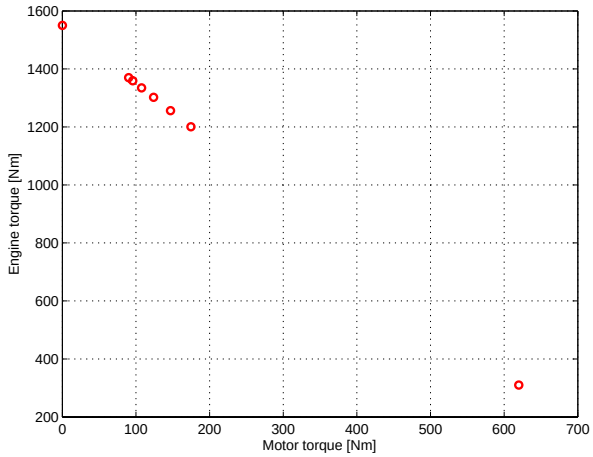

Figure V-71: Optimal engine and motor torque at 21 km/h vehicle speed.

The Pareto control policy was evaluated over the eight driving cycles and the effectiveness of its efficiency was compared to the DP control policy. The DP control policy was derived by iteratively simulating the HEV over the driving cycle. Figure V-72 shows SOC of the HEV battery using the DP and the Pareto control policies over the CSHVR driving cycle. The one-on-one correlation, shown in Figure V-65, between SOC and the power added to the driver's power request aimed at maintaining SOC at the target value, i.e., 70% in this case. Both control policies achieved the same cumulative fuel consumption (Figure V-73), which illustrates that the control policy yielding the Pareto optimal solution is an optimal control policy that can be implemented online.

The simulation results corresponding to the other driving cycles are summarized in Table V-5.

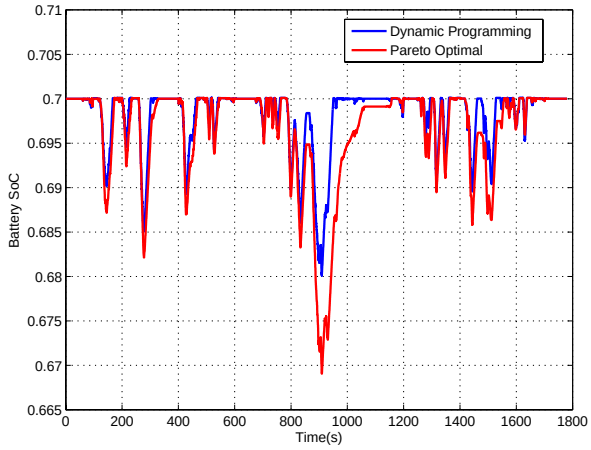

Figure V-72: State of charge of the battery for hybrid electric vehicles with dynamic programming and the Pareto control policy.

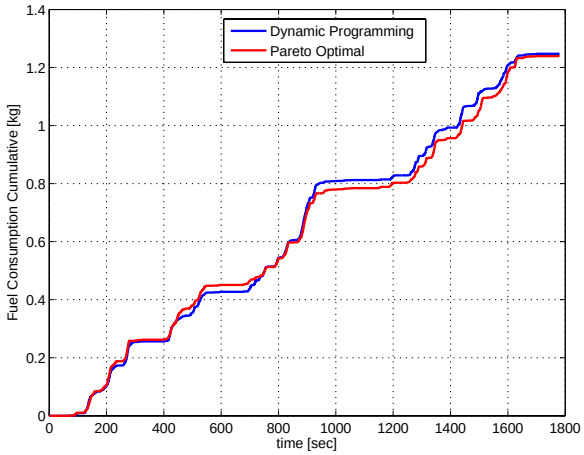

Figure V-73: Cumulative fuel consumption for hybrid electric vehicles with dynamic programming and the Pareto control policy.

Table V-5: Different Driving Cycles.

!	INITIANL SOC [%]	FINAL SOC [%]	FUEL CONSUMPTION [KG]
CSHVR[1]	70	70	1.24
ECE[2]	70	70	0.08
EUDC[3]	70	66	0.44
FTP[4]	70	66	1.99
JAPAN10[5]	70	70	0.06
JAPAN15[6]	70	70	0.25
NYCC[7]	70	69	0.35
UDDS[8]	70	70	1.34

[1] The city-suburban heavy vehicle route, CSHVR.
[2] The elementary urban driving cycle, ECE.
[3] The extra urban driving cycle, EUDC.
[4] The federal test procedure, FTP.
[5] The Japanese 10 mode cycle, JAPAN10.
[6] The Japanese 15 mode cycle, JAPAN15.
[7] The New York city cycle, NYCC.
[8] The urban dynamometer driving schedule, UDDS.

Conclusions

In the research reported here, we developed an analytical formulation for modeling HEV operation as a controlled Markov chain and presented an analytical, offline solution of the stochastic optimal control problem using the average cost criterion. Then we formulated a multiobjective optimization framework that can be used online to derive the optimal control policy and developed the Pareto control policy that minimizes the average cost criterion. The Pareto control policy can be implemented online without requiring a priori knowledge of the vehicle speed profile (driving cycle).

The effectiveness of the efficiency of the proposed power management control algorithm was validated through simulation of an HEV model for different driving cycles, and it was compared to the DP control policy. Both policies achieved the same cumulative fuel consumption, demonstrating that the Pareto control policy is an optimal control policy that minimizes the average cost criterion. Future research should enhance the proposed multiobjective optimization framework by considering the battery in the problem formulation in addition to the engine's BSFC and motor's efficiency.

V.G.3. Products

Publications

1. Malikopoulos, A.A., "Supervisory Power Management Control for Hybrid Electric Vehicles: A Survey," *IEEE Transactions on Intelligent Transportation Systems. (in review)*
2. Malikopoulos, A.A., "A Multiobjective Optimization Framework for Online Optimal Control in Parallel Hybrid Electric Vehicles," *IEEE Transactions on Intelligent Transportation Systems. (in review)*
3. Malikopoulos, A.A., "Pareto Efficient Power Management Control in Parallel Hybrid Electric Vehicles" *Proceedings of the 21st World Congress on Intelligent Transportation Systems. (in review).*
4. Malikopoulos, A.A. "Impact of Component Sizing in Plug-In Hybrid Electric Vehicles for Energy Resource and Greenhouse Emissions Reduction," *J. Energy Resour. Technol,* **135**, No. 4, 2013, pp. 041201-041209.
5. A Multiobjective Optimization Framework for Stochastic Optimal Control of Advanced Propulsion Systems, *2013 IEEE Workshop on Open Problems and Challenges in Automotive Control*, Washington, D.C., June 20, 2013.
6. Malikopoulos, A.A., "Stochastic Optimal Control for Series Hybrid Electric Vehicles," *Proceedings of 2013 American Control Conference*, Washington DC, June 17-19, 2013.
7. Autonomous Intelligent Hybrid Propulsion Systems, AMR, Washington, D.C., May 15, 2013.
8. Self-Learning Hybrid Propulsion Systems, VSATT Meeting, Knoxville, TN, Nov. 17, 2012.
9. Malikopoulos, A.A., "Self-Learning Hybrid Propulsion Systems," *ORNL final report*.
10. Malikopoulos, A.A. and Smith, D.E., "An Optimization Model for Plug-in Hybrid Electric Vehicles," *Proceedings of the 2011 Technical Conference of the ASME Internal Combustion Engine Division*, Morgantown, West Virginia, Oct 2-5, ICEF2011-60028.
11. Malikopoulos, A.A., Stochastic Optimal Control for Advanced Propulsion Systems, 2012 DOE Crosscut Workshop on Lean Emissions Reduction Simulation, University of Michigan, Dearborn, MI, April 30- May 2, 2012.
12. Malikopoulos, A.A., Autonomous Intelligent Plug-In Hybrid Electric Vehicles, DOE Hydrogen and Vehicle Technologies Program Annual Merit Review and Peer Evaluation, Washington D.C., May 14, 2012.
13. Malikopoulos, A.A., The Meritor Dual Mode Hybrid Powertrain (DMHP): Opportunities and Potential for Systems Optimization (CRADA), DOE Hydrogen and Vehicle Technologies Program Annual Merit Review and Peer Evaluation, Washington D.C., May 15, 2012.
14. Malikopoulos, A.A., Self-Learning Control for Advanced Propulsion Systems, Cummins Inc., Columbus, IN, May 23, 2012.
15. Malikopoulos, A.A., "The Meritor Dual Mode Hybrid Powertrain (DMHP): Optimal Control Algorithms," Annual presentation, September 2012.

Patents

1. Malikopoulos, A.A., Power Requirement for Self-Sustainability of the Electrical Path in HEVs, DOE S-Number: S-124,623, ORNL Invention Disclosure Serial No. 201303042.
2. Malikopoulos, A.A., Online Optimal Power Management Control for Hybrid Propulsion Systems, DOE S-Number: S-124,622, ORNL Invention Disclosure Serial No. 201303041.
3. Malikopoulos, A.A., Optimal Supervisory Control for Series Hybrid Electric Vehicles, DOE S-Number: S-124,621, ORNL Invention Disclosure Serial No. 201303040.

V.H. Autonomie Documentation

Principal Investigator, Lawrence Michaels
Argonne National Laboratory
9700 South Cass Avenue
Argonne, IL 60439-4815
Phone: (248) 935-7222
E-mail: lmichaels@anl.gov

DOE Program Manager, David Anderson
Phone: (202) 287-5688
E-mail: David.Anderson@ee.doe.gov

V.H.1. Abstract

Objectives

- Create detailed Help documentation for the Autonomie user community.

Major Accomplishments

- Converted PowerPoint presentation files to Microsoft Word.
  - Existing documentation was in the form of 57 PowerPoint presentation files.
  - The PowerPoint files were converted to Word documents to facilitate production of the Help documentation.
  - Textual descriptions were added to the Word documents to add details to the Help documentation.
- Created Help Documentation from Word documents.
  - A tool exists (RoboHelp) that automatically converts Word documents to Help documentation modules.
  - The conversion to Help documentation modules has begun.
  - The Help documentation has been integrated into the Autonomie Graphical User Interface (GUI).

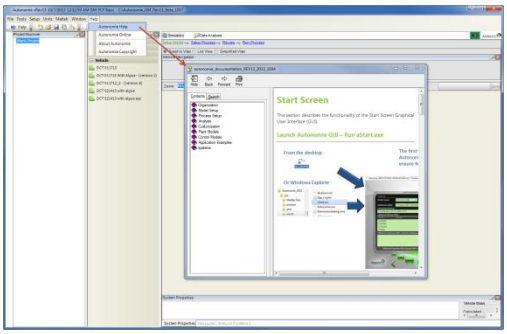

Example of Invoking Help from the GUI.

Future Achievements

- Continue the conversion to Help documentation modules.
- Review the Help documentation for correctness and completeness.

✧ ✧ ✧ ✧ ✧

V.H.2. Technical Discussion

Background

Autonomie is a plug-and-play powertrain and vehicle model architecture and development environment that supports the rapid evaluation of new powertrain/propulsion technologies for improving fuel economy through virtual design and analysis in a mathematical-based simulation environment. Autonomie is an open architecture that supports the rapid integration and analysis of powertrain/propulsion systems and technologies. This allows rapid technology sorting and evaluation of fuel economy under dynamic/transient testing conditions.

Introduction

To better support the U.S. Department of Energy (DOE) and its users, detailed Help documentation has been developed to assist users in taking advantage of the many features that Autonomie provides.

Approach

An extensive set of PowerPoint presentations existed to describe and present the features and capabilities of Autonomie. It was decided to use those presentations as a starting point for the Help documentation.

Several steps were taken to convert the information in the PowerPoint files to Help documentation.

- The PowerPoint files were converted to Microsoft Word documents.
- The Word documents were enhanced with descriptive text to elaborate on the functionality and operational details of the software.
- The elaborated documents were converted to Help documentation (.chm files) via the utility program RoboHelp.

Results

Help Documentation

Conversion of PowerPoint Files to Microsoft Word

Fifty-seven PowerPoint files were successfully converted to Microsoft Word.

Addition of Descriptive Text

All of the Microsoft Word files that had been converted from PowerPoint were modified with detailed descriptive text to provide the user with sufficient information to utilize the many features that Autonomie provides.

Conversion to Help Documentation

Most of the Word documents have been converted to the Microsoft Help format (.chm files) via RoboHelp. Those files are being reviewed for adequacy and comprehension prior to conversion of the remaining files.

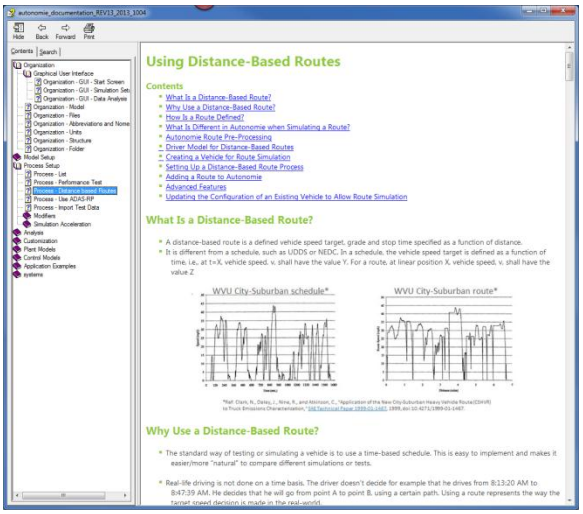

Example of Help Screen.

Help Documentation Structure

When all the Word documents have been converted to Help files, the structure of the documentation will be as follows:

- Overview
- Organization
  - Software
  - Abbreviations and Naming Nomenclature
  - GUI
  - Model
- Getting Started
  - How To Simulate an Existing Vehicle in the GUI
  - Description of Saved Files from Simulation
  - How To Analyze Results
  - How To Simulate a Single System
- List
  - Configurations
  - Plant Models
  - Vehicle Controls Models
  - Low-Level Control Models
  - Preprocessing Files
  - Postprocessing Files
  - Generic Vehicles
  - Processes
- Description
  - Plant Models
  - Engine Plant Models Improvements
  - New Driver Models
  - Vehicle Control Logic
  - Low-Level Control Logic
  - Shifting Algorithm
- Process Highlights
  - How To Run an Acceleration Test
  - How To Run a Sensitivity Analysis
  - Distance-based Routes
- Post-processing Highlights
  - Advanced Plots
  - Results Comparison
  - Energy Balance
- Customization
  - How To Modify an Existing Vehicle Model, Files and Parameters
  - How To Lock and Unlock Items
  - How To Save a System
  - How To Create a Vehicle from Saved Systems
- Advanced
  - Developer Tools
  - How To Interface with AMESim
  - How To Interface with CarSim
  - How To Interface with GT Power
  - How To Interface with Other Tools
- Import
  - How To Import a User's Model File and Initialization File
  - How To Create a Drive Cycle
  - How To Add a New Configuration through XML
  - How To Add a New Configuration through Simulink
  - How To Implement Your Own Process
  - How To Implement Your Own Analysis Function
  - How To Transfer Files from a Previous Version
- New Features
  - New Features by Package

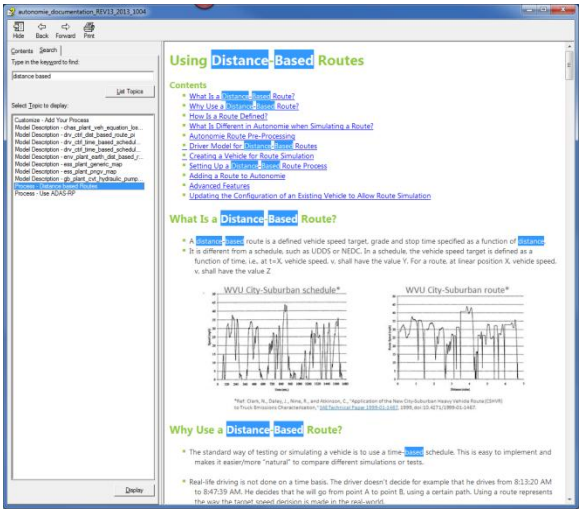

Example of Search Capability.

Conclusions

The latest version of Autonomie includes detailed Help documentation to assist the user in taking advantage of the multiple features provided by this release.

V.H.3. Products

Publications

1. L. Michaels, S. Halbach, N. Shidore, and A. Rousseau, "Applications of Model-based Systems Engineering Methods to Vehicle and Subsystem Design and Optimization," 5th Annual Ground Vehicle Systems Engineering and Technology Symposium, Troy, Michigan, Aug. 20–22, 2013.
2. L. Michaels, and A. Rousseau, "Tutorial—Model Based System Engineering (MBSE): The Rise of the Machines?", 2013 ITEC (IEEE Transportation Electrification Conference), Detroit, Michigan, June 19, 2013.
3. L. Michaels, "MBSE with Autonomie," MBSE Tech-Fast, SAE Detroit Section, March 26, 2013.

Patents

1. "Flexible Evaluator for Vehicle Propulsion Systems," United States Patent No. 8,510,088.

Tools and Data

1. Autonomie Rev. 13, October 2013.

V.I. Legacy Process Integration

Phillip Sharer, Principal Investigators
Argonne National Laboratory
9700 South Cass Avenue, Building 362
Lemont, IL 60439
Phone: (630) 252-7261
E-mail: arousseau@anl.gov

David Anderson, DOE Program Manager
Phone: (202) 287-5688
E-mail: david.anderson@doe.ee.gov

V.I.1. Abstract

Objectives

- The Systems Modeling and Control Group at Argonne National Laboratory develops and utilizes a substantial number of custom internal tools and algorithms. The objective is to integrate these tools into Autonomie to facilitate their internal use and/or to make them available for distribution with Autonomie to support model-based systems engineering (MBSE).

✧ ✧ ✧ ✧ ✧

V.I.2. Technical Discussion

Background

The Systems Modeling and Control Group at Argonne has supported DOE vehicle research initiatives for over 14 years. During this time, the group has conducted numerous studies and published more than 60 papers. Some of these studies involved running thousands of vehicles with tens of thousands of individual simulation runs. These studies often included sizing powertrain components and optimizing powertrain controls, as well as postprocessing gigabytes of data. While the majority of the studies were performed within Autonomie, additional tools to run and analyze such studies have been developed over the years. However, these tools are command-line tools without uniform interface.

Introduction

As system studies are conducted at Argonne, specialty tools and code bases are developed outside of the Autonomie framework. Some of these tools are study-specific with a limited ability for reuse, while others have the potential for reuse across many studies. The goal of this project is to format these tools in such a way that they fit into the Autonomie framework as either processes or analysis files. Much of this work involves refactoring an existing code base and performing significant integration testing to ensure that these tools work with other existing entities in the Autonomie framework.

Approach

An in-depth, exhaustive survey was performed to ascertain the existence and state of internal tools within the group. Once a complete list of internal tools was developed, the items were categorized and prioritized based on the following criteria: (1) the possibility of reuse in other studies, (2) the potential for enhanced efficiency and speed to complete a study, (3) the likelihood of reuse as part of the Autonomie release, and (4) the amount of effort required to refactor the code base. The categorization and analysis were in large part qualitative and relied on the experience of the team as a whole. The tools that were found to be acceptable are described in the next section.

Results

Process Modifiers

The following algorithms were integrated under this task as process modifiers. Process modifiers are added to a process to change the execution of the process. Adding a parametric study to a cycle is an example of a process modifier.

DIRECT

DIRECT (Divided RECTangles) is a derivative-free optimization algorithm that recursively divides the domain of the objective function into smaller and smaller partitions and converges to an optimal solution. Figure V-74 illustrates this operation. DIRECT has long been an algorithm used by Argonne to support several advanced control studies. However, it was designed for use in the legacy tool Powertrain Systems Analysis Toolkit (PSAT), and it was launched outside of the user interface at the command line.

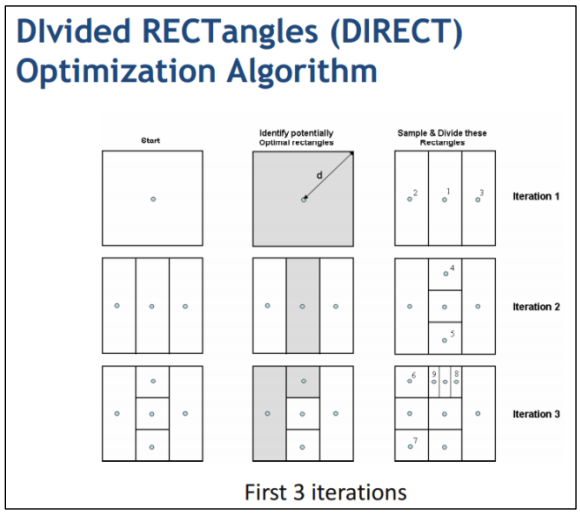

Figure V-74: DIRECT Optimization Algorithm in Action.

As part of the legacy process integration effort, an Autonomie plug-in was developed. In addition, the back-end DIRECT Matlab code was formatted to facilitate calling DIRECT as an Autonomie process.

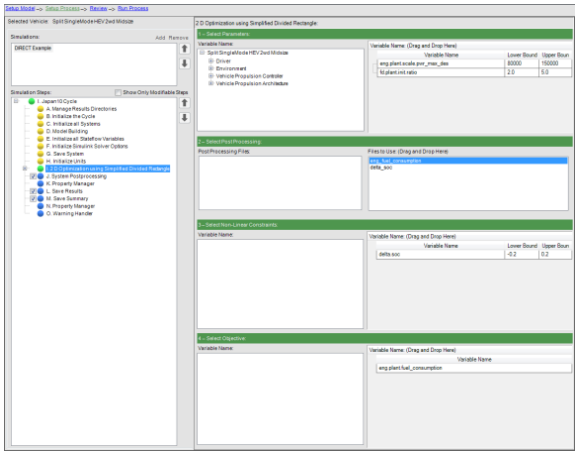

Figure V-75: User Interface for DIRECT.

The user interface for DIRECT is generic and could be used for any optimization algorithm (Figure V-75). It provides selection for an objective function, as well as selection for both linear and nonlinear constraints on both the domain and range of the objective function. DIRECT has been integrated so that it is easy to drag and drop this process modifier onto another process, such as a cycle or standard procedure and run. The benefit to users of Autonomie is significant.

POUNDER

POUNDER (Practical Optimization Using No DERivatives) is another more advanced derivative-free optimization algorithm developed by Argonne's Mathematics and Computer Science Division. It also divides the objective functions domain into smaller and smaller partitions recursively. However, it uses selected points from previous iterations to fit a performance surface to the partitions. By using the performance surface, a better estimate for a local minimum in each partition can be obtained. Since the partitions are better categorized, the algorithm can make better decisions about which partitions would have an optimal value on the next iteration of the algorithm. Because a user interface had already been developed for DIRECT, only the back-end code required to interface with Autonomie needed to be developed.

Since the generic optimization interface developed for DIRECT can be reused with any optimization algorithm, it was used for POUNDER (Figure V-76). However, the POUNDER code base had to be modified so that it could be called as a process from Autonomie.

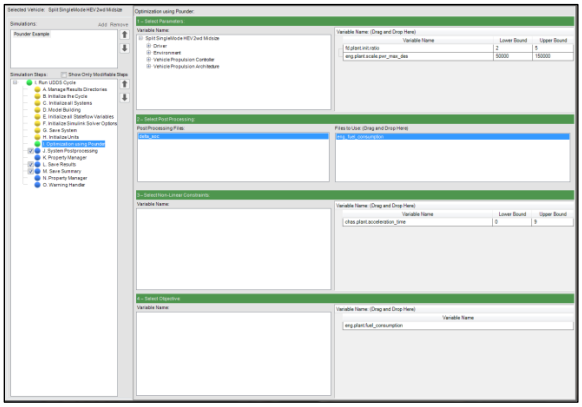

Figure V-76: Reusable Optimization Interface Used for POUNDER.

Monte Carlo

A Monte Carlo simulation accounts for uncertainty in vehicle analysis. It is similar to a parametric study, except that probability distributions are chosen for each parameter instead of single values. Combinations of values for input parameters are then chosen by the algorithm by using the probability distributions that are assigned to each parameter. Values that are more likely are simulated more often. Usually hundreds of simulations are run to obtain the output distributions for a vehicle.

The Monte Carlo algorithm was integrated as a process plug-in. The user interface for the Monte Carlo algorithm is shown in Figure V-77.

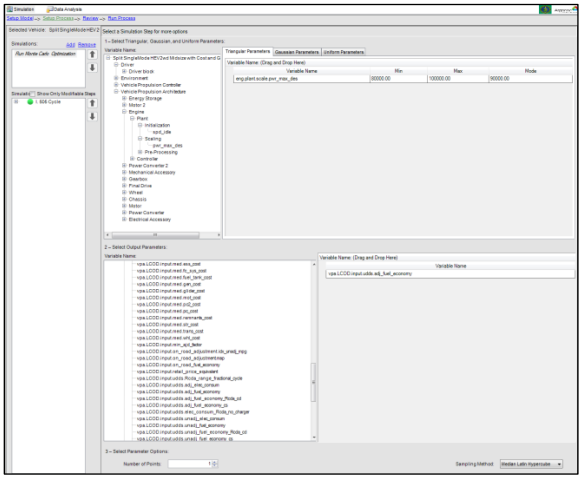

Figure V-77: Monte Carlo Interface in Autonomie.

Process Architecture

This task actually added features to the process architecture of Autonomie.

Autonomie Message Passing Interface

The System Modeling and Control Group at Argonne developed a Matlab Message Passing Interface (MPI) to allow parallel execution of simulation runs on multiple machine cores. This code was developed to facilitate other studies run outside of Autonomie that required integration into Autonomie.

The Autonomie MPI was integrated into heavy-duty and battery-electric vehicle standard test procedures, which benefited from running multiple cycles simultaneously.

Postprocessing and Analysis

An extensive body of postprocessing code was developed and called outside of the user interface. This task integrated the most beneficial parts.

Cost and Greenhouse Gas Estimates

Cost and greenhouse gas (GHG) emissions have long been estimated for many of our DOE studies. However, this code has been called by study-specific code, and it needed to be better integrated with vehicles in Autonomie. The GHG emissions are generated from tables produced by pathway runs in the Greenhouse Gases, Regulated Emissions, and Energy Use in Transportation (GREET) model. The most frequently examined pathways were generated by GREET and incorporated into an xml database for use with calculations in Autonomie.

Figure V-78 shows the cost and GHG calculations integrated into Autonomie default vehicles.

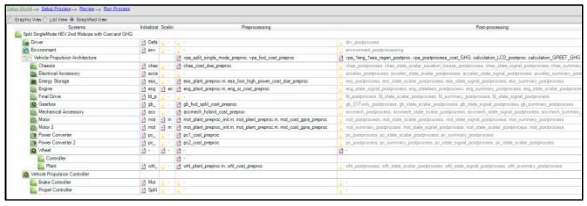

Figure V-78: Cost and GHG Calculations Integrated with an Autonomie Default Vehicle.

Levelized Cost of Driving Graphical User Interface

The levelized cost of driving (LCOD) has been estimated in place of simple cost for advanced vehicles to understand and compare the total cost of ownership.

The LCOD graphical user interface (GUI) is a Matlab guide-based user interface that was integrated into Autonomie as an a_analysis plot. Since the plot is dynamic and has controls capable of changing assumptions and updating the graphs, changes had to be made to accommodate this plot over the more traditional static analysis plots. User inputs are vehicle cost, fuel price, electricity price, vehicle lifetime, and discount rate (Figure V-79).

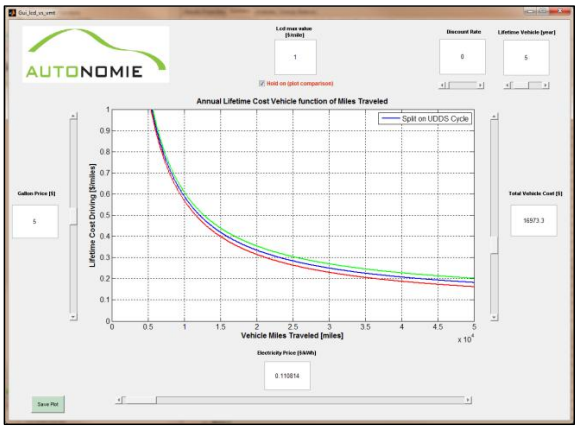

Figure V-79: Levelized Cost of Driving GUI.

Net Present Value Fuel Calculations

Net present value (NPV) calculations are analogous to LCOD in that they are another way to capture the cost of a vehicle. In this case, only the NPV of the fuel cost is calculated as a way of comparing operating costs among different vehicles in Autonomie. This calculation was integrated as an a_postprocess file into Autonomie.

The top of Figure V-80 displays the NPV calculations chosen on a vehicle propulsion architecture (VPA) configuration in the GUI. The bottom of Figure V-80 shows the results of the NPV calculations as they appear in the Autonomie results tab.

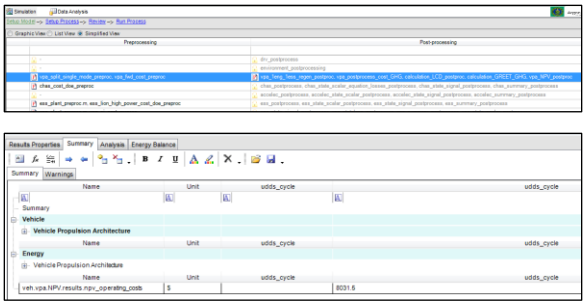

Figure V-80: Net Present Value Calculations.

Autonomie Matlab Quick Plotter

Autonomie provides extensive native data analysis capabilities. However, this does not preclude users from developing their own custom data analysis tools, which can be called from Autonomie. As part of his analysis of vehicle validation of large test data sets at Argonne, Namwook Kim developed the Autonomie Matlab Quick Plotter (AMQP).

Figure V-81 shows the AMQP. This tool facilities the rapid loading and comparing of data sets. It was integrated into Autonomie as an a_analysis plot, which demonstrates the flexibility of Autonomie when integrating a user's code base for reuse in Autonomie.

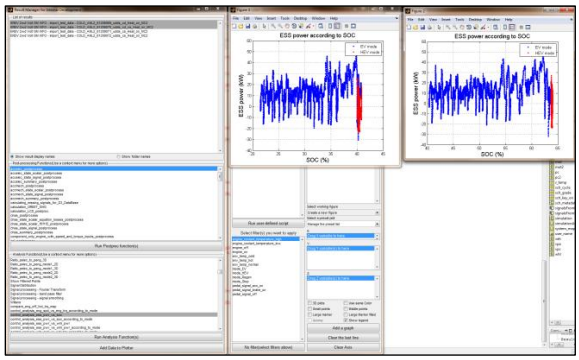

Figure V-81: Autonomie Matlab Quick Plotter.

Conclusions and Future Directions

An extensive code base has been developed by the Systems Modeling and Control Group at Argonne to support further studies. Some of this code lies outside of the Autonomie interface, thereby limiting its reusability and increasing the difficulty of its reuse in other studies. Several of these tools have been examined as part of this effort, and they have been successfully integrated into Autonomie. However, more code exists that could be integrated into Autonomie proper, such as the distributed computing code base and the vehicle sizing algorithms. Since this effort has been successful, future efforts will focus on integrating these additional code bases. These added features benefit the program in terms of enhanced efficiency and speed to execute a study.

References

1. Halbach, S., Sharer, P., Pagerit, P., Folkerts, C., and Rousseau, A., "Model Architecture, Methods, and Interfaces for Efficient Math-Based Design and Simulation of Automotive Control Systems," SAE 2010-01-0241, SAE World Congress, Detroit, MI, April 2010 (pdf).

V.J. Battery Electric Vehicle Validation

Daeheung Lee, Principal Investigator
Argonne National Laboratory
9700 South Cass Avenue
Building 362
Lemont, IL 60439
Phone: (630) 252-5386
E-mail: daeheung@anl.gov

David Anderson, Lee Slezak,
DOE Program Managers
Phone: (202) 287-5688
E-mail: David.Anderson@ee.doe.gov

V.J.1. Abstract

Objectives

- Develop a model of the Ford Focus battery electric vehicle (BEV) using Autonomie simulation tool and validate it using test data from Argonne's Advanced Powertrain Research Facility (APRF). This will involve the following:
  - Import the vehicle test data into Autonomie
  - Analyze preliminary test data to obtain key parameters to develop the component and vehicle model.
  - Estimate effort and flow of each component (i.e., torque, current, voltage…).
  - Validate the Ford Focus BEV model using APRF test data for ambient conditions.
  - Assess the electric energy consumption for several driving speed profiles.

Major Accomplishments

- Analyzed preliminary Ford Focus BEV test data for multiple driving cycles:
  - Developed electric machine performance data
  - Developed battery pack performance data including open circuit voltage and internal resistance
  - Quantified auxiliary power
  - Analyzed rolling resistance
  - Analyzed mechanical braking
- Conducted effort-flow analysis of each component (energy balance) and verified calculations of additional signals:
  - Compared measured data and calculated values for the electric machine showed good correlation.
- Developed a complete vehicle model and validated its energy consumption with test data:
  - For 10 preliminary sets of driving cycle test data, the estimated electric consumption results were within 2~3% except for one US06 test.
  - The normalized cross-correlation power (NCCP) indicated a high correlation between test and a simulation signals for the energy storage system (ESS).

Future Achievements

- The current BEV model will be refined based on new sets of vehicle test data from APRF.
- A complete thermal model of the Ford Focus BEV will be developed and validated.
- The vehicle model will be used to investigate the impact of numerous factors on electrical consumption, including:
  - Thermal effect on each component
  - Additional sub-system power loss (due to air conditioning, heating, electric power steering, etc.)
  - Battery system operating status with respect to its temperature
  - Test environment

✧ ✧ ✧ ✧ ✧

V.J.2. Technical Discussion

Background

Battery Electric Vehicles

The issues of the exhaustion of energy resources and climate change have increased the need for improved energy efficiency from all sectors of industry, especially the transportation sector. Therefore, improving the efficiency of the fleet of tens of millions of vehicles not only has economical and societal impacts but also is strategically important. As a near- and long-term solution, the electrification of conventional vehicles will lead to lower energy consumption and emissions. All-electric vehicles use only the electricity as a power source, namely, a high-capacity battery that is directly charged from an external power station. Their drivetrain involves one or two electric motors for propulsion. Due to the advantages of zero emission vehicles, many transportation-related companies have started mass production of battery electric vehicles (BEVs).

Due to the rapid evolution of the technology, it is important to study and understand the strengths and weaknesses of today's state-of-the-art BEVs by analyzing their performance under different conditions. Due to cost and time constraints, a large number of conditions will be evaluated using a validated vehicle model that has been developed and validated using a significant but smaller set of test conditions.

Model Development

Since the late 1990s, Argonne has modeled and validated numerous vehicle models for a wide range of advanced technologies. Model validation is critical to ensure that state-of-the-art technologies are properly represented. This on-going activity provides confidence when Autonomie is used to evaluate the benefits of future component, powertrains and control. Over the past several years, based on on-road and dynamometer test results, component thermal behavior has been integrated to the validation process.

In this study, we developed a reliable battery electric vehicle model based on the Autonomie simulation tool and validated the simulated results using vehicle test data from Argonne's Advanced Powertrain Research Facility (APRF).

Approach

Vehicle Specifications

The main vehicle specifications of the Ford Focus BEV are summarized in Table V-6.

Table V-6: Ford Focus BEV Model Specifications and Assumptions.

Parameters	*Value*
Tire radius	0.321 m
Final drive gear ratio	7.82
Final drive gear efficiency	97.5%
Torque coupler ratio	1:1
Torque coupler efficiency	98%
Vehicle mass	1700 kg
Frontal area	2.42 m^2
Drag coefficient	0.26
Driving motor power/torque	107 kW/250 N-m
Battery pack capacity	23 kWh

Electric Machine Performance Data

The Ford Focus BEV uses a single electric machine connected mechanically to the final drive gear. The electric machine can be operated in the "motoring mode" to drive the mechanical connection or in the "generating mode" to produce electrical power (or electrical braking). The liquid-cooled synchronous motor is rated at 107 kW and develops 250 N-m of torque. The electric machine maximum speed was assumed to be 10,000 rpm based on the maximum vehicle speed.

The efficiency map was developed based on the measured effort and flow upstream and downstream of the component. Figure V-82 depicts the assumed efficiency contour lines of the electric motor used in Autonomie, which are expressed for four operating regions.

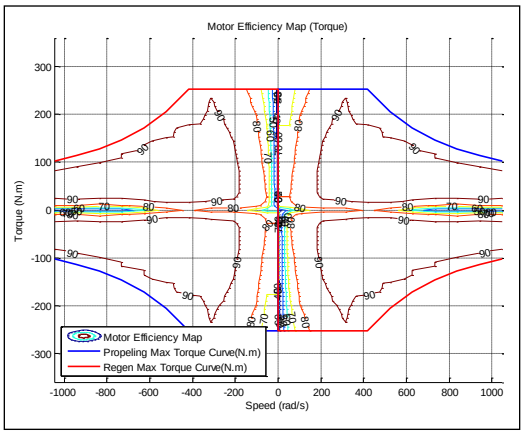

Figure V-82: Motor Efficiency Map Showing Torque versus Motor Speed.

Battery Pack Performance Data

The high-voltage battery assembly consists of 3.8-volt Li-ion battery cells connected in series-parallel circuit to produce approximately 350 V. The battery main characteristics are shown in Table V-7.

Table V-7: Specifications for the High-Voltage Battery Model.

Parameters	*Value*
Total cell #	430
Cell # per module	86
Cell voltage (max)	3.8 V (4.2 V)
Cell capacity	13 Ah
Module #	5
Module series #	1
Module parallel #	5
Module voltage (max)	326 V (361 V)
Module capacity	13 Ah
Pack voltage	361 V
Pack capacity	65 Ah
Pack power	23.4 kWh
Max current	305 A
Max power	110350 W

Figure V-83 illustrates the battery output current and voltage over the different driving modes, where UDDS is the Urban Dynamometer Driving Schedule, HWY is the Highway Fuel Economy Driving Schedule, US06 is a high acceleration aggressive driving schedule, and SSS is steady state driving. From the preliminary test results, the maximum operating voltage is close to 350 V, which occurs when the battery state of charge (SOC) is near 95%. When the SOC approaches less than 10%, the operating voltage falls to around 280 V. From these operating characteristics, we can estimate the OCV value with respect to SOC level when the current is close to zero (the minimum battery output power due to the auxiliary base load). In Figure V-83, when the test vehicle stopped, the output current from the battery is almost 1.5 A for the auxiliary system. The OCVs with regard to SOC level were estimated from 10 driving cycle tests under the assumption that 1.5 A is relatively small compared with the output current for driving operation. This method provides a reasonable estimate.

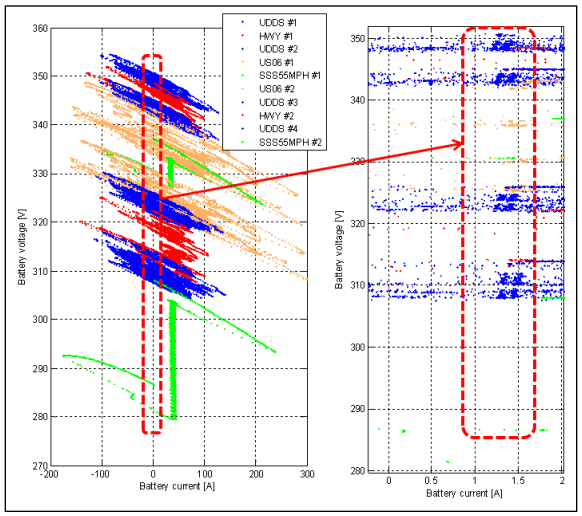

Figure V-83: Operating Characteristics of the High-Voltage Battery for Multiple Driving Modes.

With regard to the internal resistance (IR) used in the simulation, it is difficult to directly quantify the charge and discharge IR from the vehicle operating test. Therefore, we adjusted the value according to SOC level to the test results of the Ford Focus BEV based on information for the Nissan Leaf's battery. The final operating characteristics used in the Autonomie battery model are shown in Figure V-84. The OCV of the Ford Focus BEV is lower than that of the Nissan Leaf over the entire SOC range, and the estimated IR of the pack system is similar to that of the Leaf.

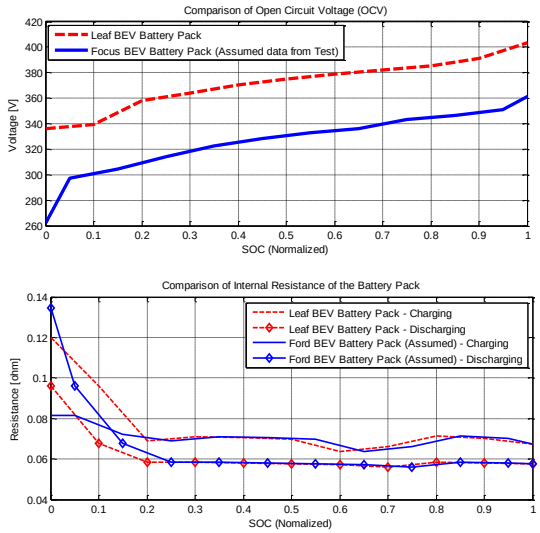

Figure V-84: Assumed OCV and Internal Resistance with Respect to the SOC Level.

Effort-Flow for Each Component and Validation of Non-Measured Signals

To estimate how each component is operated in a vehicle, one needs a large number of parameters including effort (i.e., torque, voltage…), flow (i.e., rotational speed, current…)… Due to the complexity of measuring all the signals, a smaller number of signals is usually recorded during vehicle testing. As a result, several parameters need to be estimated as part of the validation process based on measured signals.

For example, the dynamometer force signal and output current/voltage signals of the battery system from test data, were used to calculate the in/out wheel torque, the final in/out drive gear torque, and the motor torque output. When each component parameters were available, either from measurement or calculations, the estimated signals were validated. Figure V-85 presents a flowchart showing each vehicle component in the validation process to verify the input current and voltage to the electric motor.

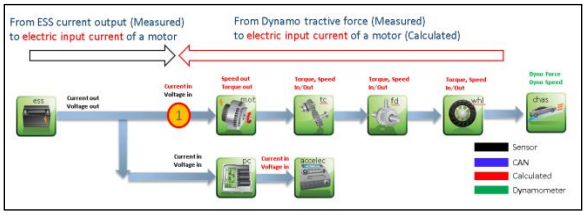

Figure V-85: Flowchart for BEV Components Used in Validation Process.

The validation results between the test and the calculated values are shown in Figure V-86 for three driving modes: UDDS, HWY, and US06. Since the measured and estimated signals are very close over different driving cycles, we concluded that the input and output results were appropriately calculated.

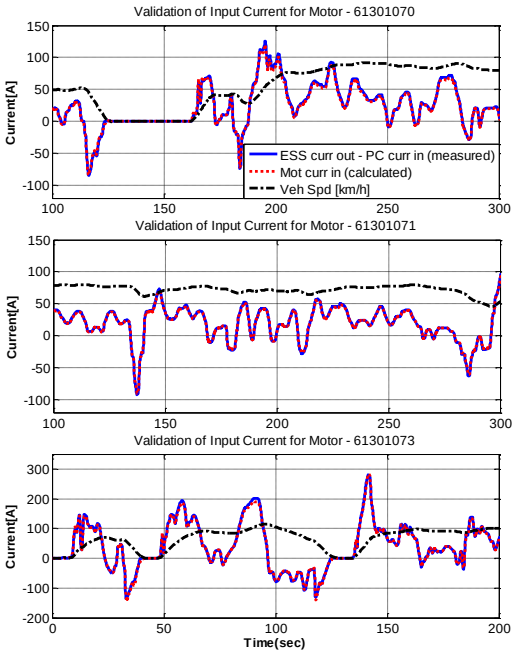

Figure V-86: Validation of Input Current for the Motor in Three Driving Modes: UDDS (top), HWY (middle),and US06 (bottom).

Energy Balance of Test Data

One of the first phase of the validation process is to understand the vehicle operating conditions. As all the effort and flow of each components are now available, analyzing the energy balance for each component over different conditions is very useful. A generic process in Autonomie is used to display the energy balance. The input and output energies of

each component were analyzed. Figure V-87 illustrates one example of the energy balance for US06 test data.

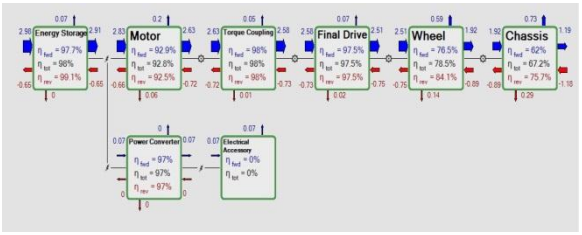

Figure V-87: Example of the Energy Balance for Test # 61301073 (US06, Initial SOC: 75.28%).

Ford Focus BEV Model in Autonomie

The complete vehicle model was them developed based on the component performance data previously defined. The regenerative braking control algorithm and wheel loss torque were estimated by analyzing test data and applying the results to the final Ford Focus BEV model. The operating states of the battery system in the BEV model were demonstrated under tested driving cycles, as shown in Figure V-88.

The overall trends of the output voltage from the battery on all driving cycles are very similar to the vehicle test results. This agreement indicates that the open circuit voltage and internal resistance with respect to the SOC were properly estimated.

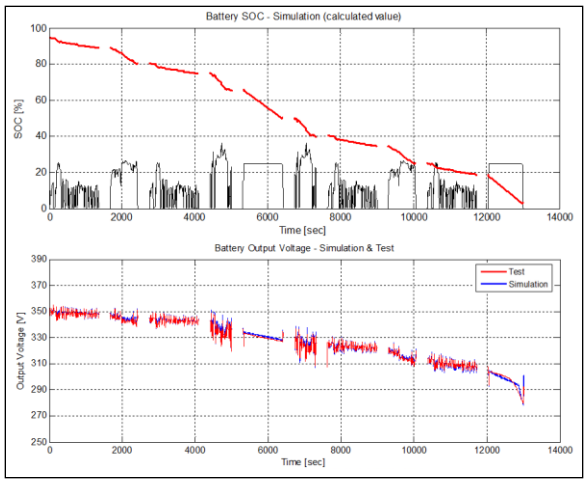

Figure V-88: Simulation and Test Results on SAE J1634 Shortcut MCT.

Normalized Cross-Correlation Power in Autonomie

Selecting an appropriate set of metrics is important for quantitively determining the level of correlation between a simulation result and a set of tests. To establish a single metric indicating the level of correlation between any two signal traces, we used the normalized cross-correlation power (NCCP) metric. The NCCP function was also added to the post-simulation processing in Autonomie. When applied to a test signal and a simulation signal of the same quantity, a value of NCCP equal to or greater than 0.9 indicates a high level of correlation.

Results

Comparison of Battery Operating States for Validation

Fundamentally, it is critical for a BEV to validate the performance of the high voltage battery over the tested driving cycles. In this section, we compare the output signals of the battery in the developed BEV model with those of the test vehicle. The NCCP metrics for compared signals are also presented on each plot.

Figure V-89 and Figure V-90 plot the SOC level, output voltage, output current, and electric output power of test and simulation with respect to driving time on the HWY and UDDS cycles, respectively. Each output signal of the BEV model is very close to the test results. As stated in the previous section, the output voltage of the model is calculated from the estimated OCV and internal resistance, and the output current of the model is determined through the assumed efficiency map of an electric motor. The NCCP values clearly show a high correlation between test and simulation results.

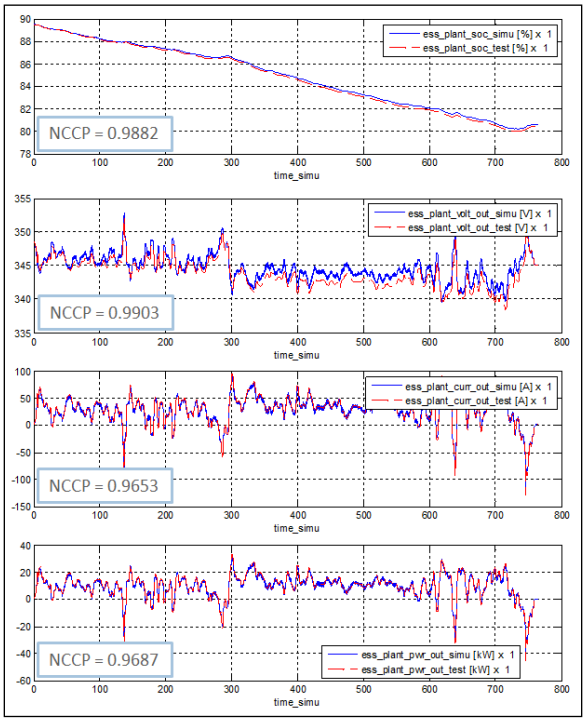

Figure V-89: Comparison between Simulation and Test Signals of the High Voltage Battery on HWY Driving Cycle.

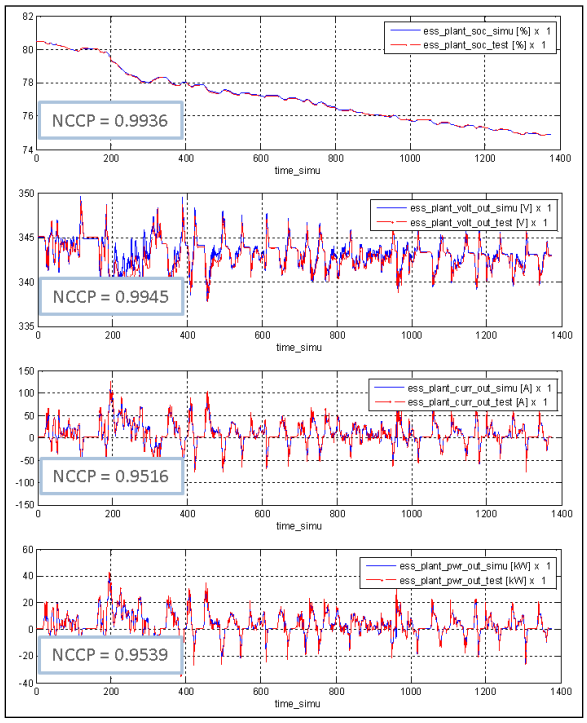

Figure V-90: Comparison between Simulation and Test Signals of the High Voltage Battery on UDDS.

Energy Comparison Results and NCCP Level

Table V-8 summarizes the discrepancy between vehicle model and the test results. The electric consumption level is in units of watt-hour (DC) per mile at the output terminal of the battery system. The discrepancies between the test results and simulations are within 0.5% to 3.7%, except for the US06 #1 test.

Table V-8: Summary of the Electric Consumption Comparison between a Simulation and a Test.

Test Results			*Autonomie Simulation*		
Driving Cycle	Test #	Electric Consumption [DC Wh/mile]	Electric Consumption [DC Wh/mile]	Discrepancy to Test Results	Initial SOC (Estimated)
WOT X 4	57	353	344	-2.3%	95.1%
UDDS #1	70	178	172	-3.4%	94.8%
UDDS #2	72	168	172	+2.1%	80.7%
UDDS #3	77	166	172	+3.5%	40.8%
UDDS #4	79	166	172	+3.7%	25.2%
HWY #1	71	200	199	-0.5%	89.6%
HWY #2	78	196	199	+1.8%	34.9%
US06 #1	73	282	270	-4.2%	75.3%
US06 #2	76	278	270	-2.8%	50.3%
SSS #1	75	209	213	+2.1%	66.6%
SSS #2	80	210	213	+1.8%	19.1%

All NCCP values of key signals on the multiple driving cycle tests are shown in Figure V-91. The NCCP levels are more than 0.935, indicating a high correlation between test results and simulations.

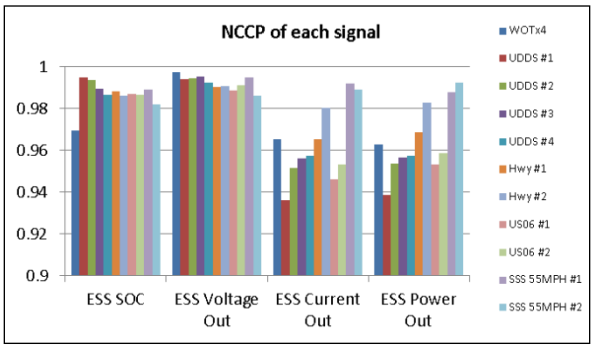

Figure V-91: NCCP Values for SOC, Voltage, Current, and Power.

Conclusions

The Ford Focus BEV was instrumented and tested at the Argonne APRF. Preliminary vehicle test data were used to develop performance parameters for specific components (i.e., the electric motor efficiency and the high voltage battery specifications) as well as understand control logic (i.e., use of mechanical braking).

Through this process, a reliable vehicle model for the Ford Focus BEV was developed and validated under ambient temperature for different drive cycles (UDDS, HWY, US06, WOT, and Steady State). The model was validated within 2%~4% for electrical consumption. An NCCP calculation function was also developed to quantify the correlation between the simulation and test data, and it has been integrated into the Autonomie post-processing. Most of the key signals show good comparison between simulation and test data.

Using the developed BEV model, it is possible to quickly and accurately predict or evaluate the energy consumption and dynamic performance.

Since the study has been completed, the Ford Focus BEV vehicle has been heavily instrumented and will be tested under a wider range of thermal conditions and driving cycles. Using the new set of test data, the current model will be refined to minimize the remaining discrepancies under ambient temperature. A complete thermal model of the Ford Focus BEV will also be developed and validated using both cold and hot ambient temperature test data.

V.J.3. Products

Publications

1. D. Lee, A. Rousseau, and E. Rask, “Development and Validation of a Battery Electric Vehicle Using Autonomie,” SAE 2014 World Congress, USA, April 8-10, 2014.

Tools and Data

1. Autonomie
2. Matlab/Simulink

References

1. "Autonomie," accessed at www.autonomie.net.
2. Meng, Y., Jennings, M., et al., "Test Correlation Framework for Hybrid electric Vehicle System Model," Technical Paper SAE 2011-01-0881, 2011.
3. Khanipour, A., Ebrahimi, K. M., and Seale, W. J., "Conventional Design and Simulation of an Urban Hybrid Bus," Proceedings of World Academy of Science, Engineering and Technology, Vol. 22, pp. 26-32, 2007.
4. Ehsani, M., Gao, Y., Gay, S., and Emadi, A., *Modern Electric, Hybrid Electric and Fuel Cell Vehicles*, CRC Press, Boca Raton, LA, 2004.
5. Lee, D., Kim, N., et al., "The Component Sizing and Engine Optimal Operation Line Analysis for a Plug-in Hybrid Electric Transit Bus," *International Journal of Automotive Technology*, Vol. 14, No. 3, pp. 459-469, 2013.

V.K. HEV Thermal Model Development and Validation

Namwook Kim, Principal Investigator
Argonne National Laboratory
9700 South Cass Avenue, Building 362
Argonne, IL 60439.
Phone: (630) 252-2841
E-mail: nakim@anl.gov

David Anderson, DOE Program Manager
Phone: (202) 287-5688
E-mail: David.Anderson@ee.doe.gov

V.K.1. Abstract

Objectives

- Develop and validate thermal model for hybrid electric vehicle (HEV) and its components such as the engine, battery, motor, transmission, and cabin based on analysis results obtained from bench dynamometer test data.
  - Analyze test data for the 2010 Toyota Prius obtained from the Argonne Powertrain Research Facility (APRF) to understand thermal impacts on vehicle performance.
  - Improve existing thermal models developed for the GM Volt.
  - Develop a supervisory controller that manages the thermal components.
  - Validate the 2010 Toyota Prius vehicle thermal model under different ambient temperatures.

Major Accomplishments

- Analyzed vehicle test data for the 2010 Toyota Prius obtained under different thermal conditions.
- Developed comprehensive thermal models for vehicle components such as the engine, battery, and cabin system.
- Developed a vehicle level controller to manage the thermal components in the HEV.
- Built a vehicle model for the 2010 Toyota Prius by integrating the developed component thermal models and vehicle level controller.
- Achieved simulation results comparable with test results (simulated fuel economies within 4% of the test results).

Future Achievements

- Develop and validate a blended plug-in hybrid vehicle (PHEV) system to analyze vehicle performance under different thermal conditions.
- Build a generic, or easy-to-use, procedure to analyze vehicle control behaviors based on test data.
- Develop parameter estimation techniques for engines and batteries with bench dynamometer tests.
- Optimize the thermal management control algorithm to improve fuel economy under severe weather conditions.

✧ ✧ ✧ ✧ ✧

V.K.2. Technical Discussion

Background

Hybrid systems provide outstanding fuel economy. One of the main reason is the ability to turn engine off and operate in the electric drive mode. However, when it is turned off for a long time, the engine temperature can become too cold to achieve high efficiency, especially when the weather is very cold. Further, other component performance and losses are also affected under extreme ambient temperatures. In hot weather, the vehicle also requires more energy to manage the cabin temperature by operating the air-conditioning (AC) system.

Until recently, the vehicle performance degradation in cold or hot weather conditions had not been thoroughly examined. The U.S. Environmental Protection Agency (EPA) standard test procedures now include tests under severe weather conditions. As a result, performance degradation under different thermal conditions has become a more significant issue. By using reliable simulation models validated with test data, one can analyze the performance degradation due to temperature, and evaluate solutions to improve the fuel economy under severe weather conditions. All the vehicle test data used in the study were measured at Argonne APRF.

Introduction

The fuel consumption test data shown in Figure V-92 were obtained from the Urban Dynamometer Driving Schedule (UDDS); however, the figure shows very different fuel consumption results. As expected, one notices that the amount of fuel consumed increase with lower ambient temperature. Under hot ambient conditions, additional energy is also required to operate a climate control system, such as an AC system.

To understand the thermal impact on fuel economies, the operating behaviors of each component in the vehicle system need to be analyzed. To do so, all the results obtained from vehicle testing were imported into Autonomie. The main objective in this analysis was to determine the principal concepts of the vehicle level control under a wide range of thermal conditions. As a result, each component behavior should be properly modeled for the different temperatures considered. While some thermal component models including engine, electric machine and battery were developed for a

previous study related to the GM Volt, some new plant models were developed based on thermodynamic equations.

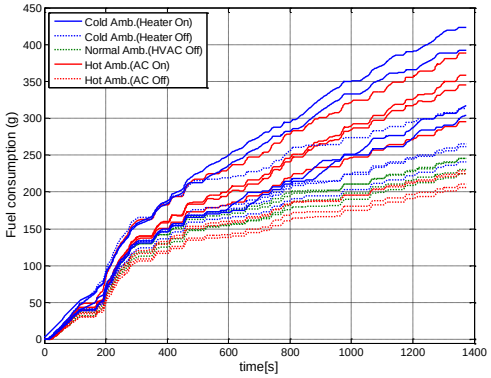

Figure V-92: Cumulative fuel consumption test data according to thermal conditions under an Urban Dynamometer Driving Schedule (UDDS)—APRF Test Data.

The information for the models and the controller was obtained or estimated by analyzing the vehicle test data.

Approach

Last year, a generic process was developed to import vehicle test data from different data formats into the Autonomie environment. During that step, one could change the signal names, units… of the measured signal to match with Autonomie nomenclature. By following the same conventions, the existing post-processing routines from Autonomie can also be used to analyze the imported test data. The process also facilitates the comparison between simulated and test signals for the validation.

For the thermal model development, equations for heat transfer or heat inertia were considered to calculate each component temperature. The component models were assumed to have uniform temperatures, and transient behaviors like the fluid dynamics of coolant or geometrical heat distribution were not examined.

Results

Bench Dynamometer Test

Test data were imported into Autonomie through the import test data process, and all necessary signals needed to analyze the data were calculated if the signals were not obtained from the test data (Figure V-93).

Fifty-three separate tests were conducted at the APRF, across a wide range of thermal conditions, including:

- Cold ambient test: −7°C
- Normal ambient test: 21°C
- Hot ambient test: 35°C

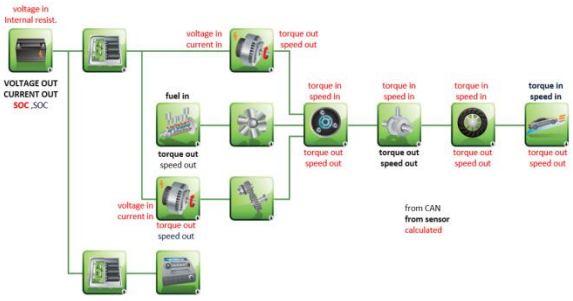

Figure V-93: Schematic of the vehicle configuration. Additional signals (in red) were calculated based on measured ones.

Test Data Analysis

In this section, the vehicle control behaviors are interpreted based on the analyzed results, in order to understand the overall control behaviors of the vehicle when operated in hot or cold ambient conditions.

Mode Control—Engine Turn ON Points

Since the 2010 Toyota Prius can provide the required wheel power through its electric machine under most driving conditions; the engine can be frequently turned. Figure V-94 shows the wheel speed and wheel demand torque when the engine is turned on. As one notices, the engine is turned on when the demand power is greater than 9 kW. Further, the figure in the upper right side shows that the threshold power increases when the battery State of Charge (SOC) is increased. This means that the engine is turned on early if the SOC is low, so that the SOC can be managed in an appropriate range.

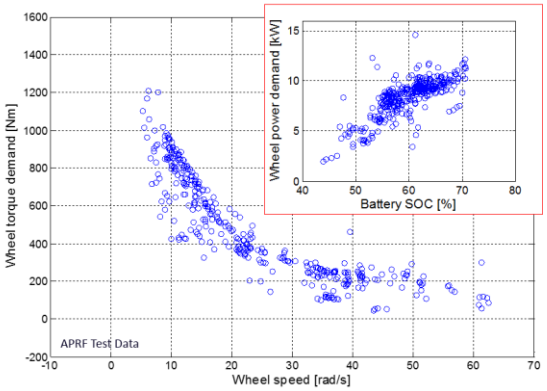

Figure V-94: Operating points when the engine is turned on. The engine is mostly turned on if demand power is increased over a predefined power threshold—APRF Test Data.

While the engine is hot, the vehicle coolant is circulated to sustain the engine temperature within an appropriate range, just as in conventional vehicles. On the other hand, Figure V-95 and Figure V-96 show a specific control behavior related to the engine thermal control when the engine is too cold. In Figure V-95, the controller forces the engine to turn on if the engine coolant temperature is too low. In Figure V-96, the controller does not allow the engine to be turned off if the coolant temperature is too low.

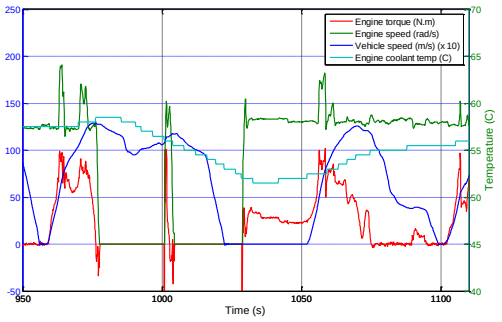

Figure V-95: Engine is turned on even when there is no power demand from a driver if the engine coolant temperature is too low—APRF Test Data.

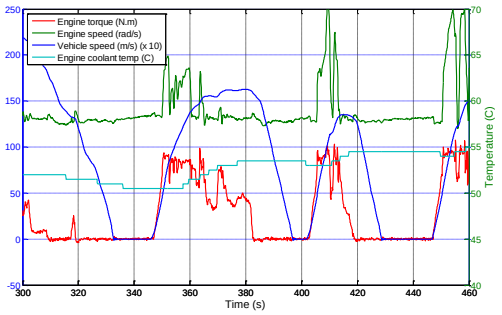

Figure V-96: Engine is not turned off if the engine coolant temperature is too low—APRF Test Data.

These control concepts sustain the engine temperature at more than 55°C. Thus the operating mode, like the pure electric mode or hybrid driving mode, is determined by the engine on/off control.

Energy Management Strategy—SOC Balancing

One other important control concept in the vehicle level is how to manage the battery SOC within the appropriate range. This control concept is highly related to vehicle performance because the engine cannot be operated within the high-efficiency region or the vehicle cannot recuperate braking energy if the SOC is not sustained within an appropriate range.

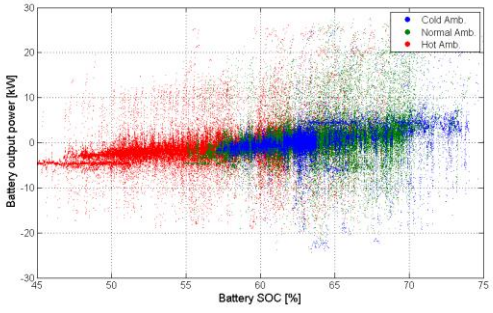

Figure V-97: Battery power is determined according to current SOC level—APRF Test Data.

Figure V-97 shows the battery output power when the engine is turned on. It shows that the controller starts to charge the battery if the SOC is lower than 60%, and the charging power is proportionally increased according to the decreased SOC. There is no essential difference in SOC management, even for hot or cold ambient conditions; however, the SOC is maintained at lower range under hot conditions because the A/C system. With the engine on/off condition, this proportional demand power for the battery sustains the SOC level at an appropriate range near 60%.

Impact on Component Control by Thermal Effects

The engine operating points are selected to make the powertrain system operate within the high-efficiency region. The test data showed that the engine is forced to operate within a different region when the engine coolant temperature is low.

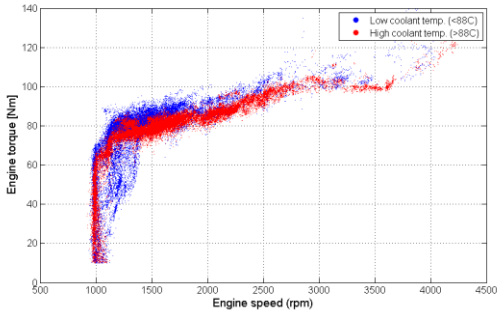

Figure V-98: Engine operating target is different when the coolant temperature is low—APRF Test Data.

Figure V-98 shows that the engine torque is controlled to be a higher if the coolant temperature is lower than 88°C. On the other hand, the maximum battery power is limited when the battery is too hot, as shown in Figure V-99.

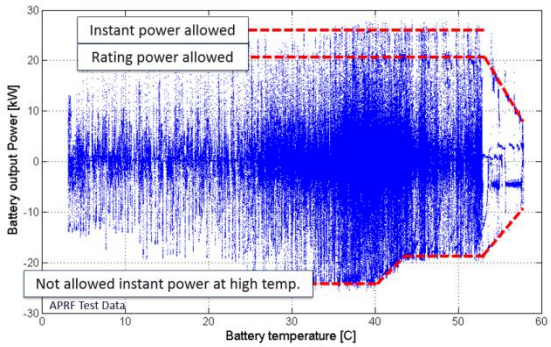

Figure V-99: The battery charging and discharging power is limited by the battery temperature—APRF Test Data.

Figure V-99 shows that the battery charging and discharging power limits are influenced by the component temperature.

Impact on Performance Degradation by Thermal Effects

We have shown the analysis results for the control behaviors according to different thermal conditions of each component. System performance can be affected by the change of the control or by the change of the performance of each component itself. For example, Figure V-100 shows that the impact of temperature on engine fuel rate.

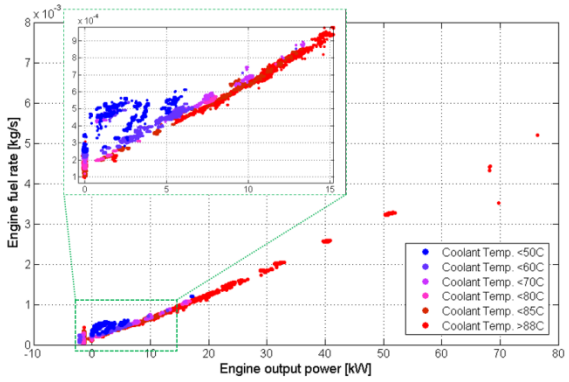

Figure V-100: Fuel consumption rate according to engine coolant temperature—APRF Test Data.

Similarly to the engine, the battery performance is also affected by the temperature.

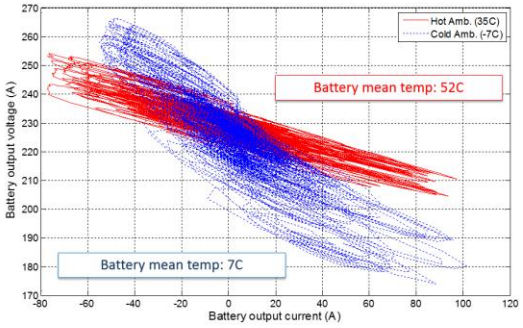

Figure V-101: Polarization curves of the battery under two different thermal conditions—APRF Test Data.

In Figure V-101, the slope of the curve indicates the battery internal resistance. Figure V-102 shows the correlation between the battery temperature and the estimated internal resistance.

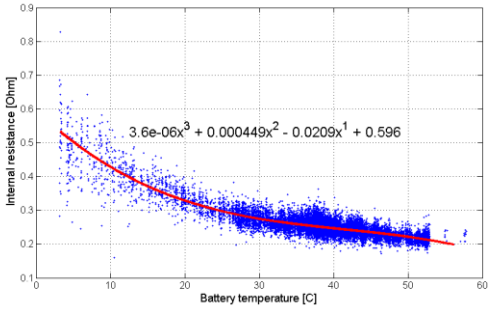

Figure V-102: Estimated internal resistance decreases according to an increase in battery temperature—APRF Test Data.

Another significant impact on performance is related to tire losses, which is shown in Figure V-103. In Figure V-103, the wheel input energy from the powertrain under cold ambient conditions (blue) is much higher than the input energy under hot ambient conditions (red). As the powertrain must provide the required energy to the wheel; these differences should be carefully considered to develop the thermal model of the wheels.

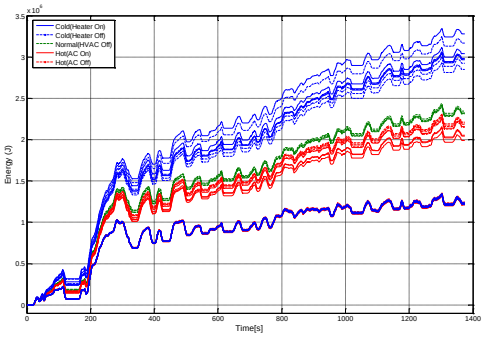

Figure V-103: Input energy of wheels significantly increases if the ambient temperature is low—APRF Test Data.

Finally, we have determined that the AC system consumes power from 2 to 2.5 kW, according to the cabin temperature, and the accessory base load is about 200 W.

All these results were used to develop both the component and vehicle system model.

Component Models Development and Validation

Figure V-104 shows the thermal model for engines.

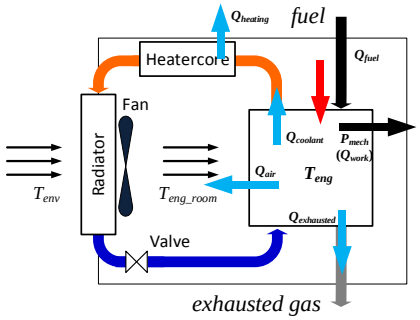

Figure V-104: A schematic for the engine thermal model.

Based on the analyzed results, heat source models and heat transfer models were developed to represent the real thermal behavior, which is explained in [1].

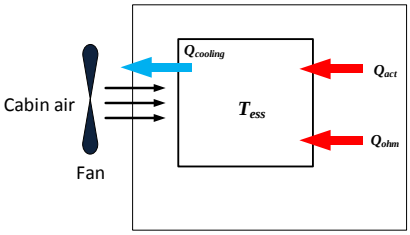

Figure V-105: Battery thermal model.

For the battery thermal system, a heat exchanger model between the input air and the battery body was developed, and the heat source was calculated from the battery loss. The battery loss was modeled by two factors—activation loss and ohmic loss (See Figure V-105).

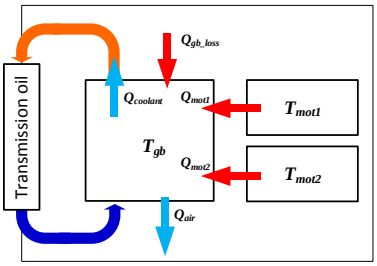

Figure V-106: Transmission thermal model.

As shown in Figure V-106, heat generated from the two electric machines and heat generated from the loss of the gearbox are considered as a heat source. Because the vehicle does not have any active cooling system for the transmission system, a passive model based on heat transfer by the transmission oil was developed for the thermal model. In addition to these models, a climate control system, a wheel loss model, and a cabin model were developed and integrated into the vehicle system. Detailed information is included in [1].

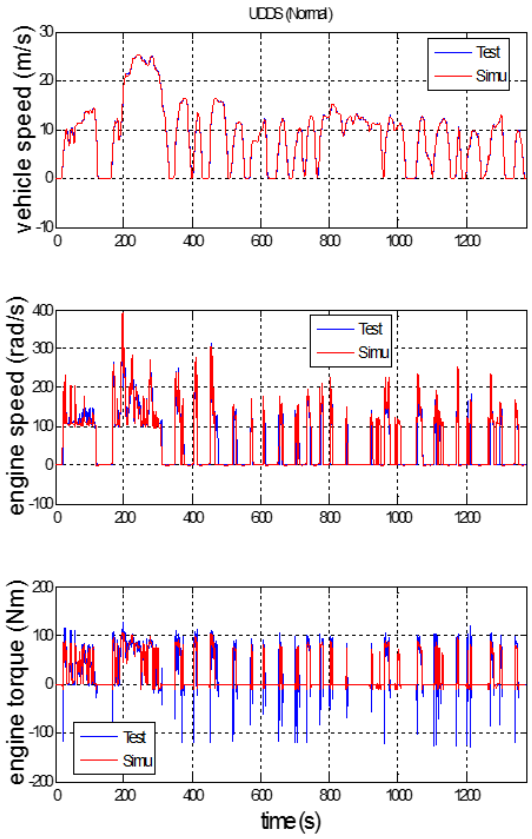

Figure V-107: An example of comparative results. Engine operating behavior obtained from a simulation is very close to the test data.

System Validation

All the developed thermal components were integrated into the 2010 Toyota Prius system, and the vehicle model was validated under different thermal conditions in Autonomie.

An example of a comparison between the simulation results and the test data for engine operating points is shown in Figure V-107; more results obtained from various thermal conditions are shown in Table V-9.

Table V-9: Comparative results for fuel consumption and final SOC between test data and simulation results.

	Fuel Mass Consumed (kg)			Final SOC		
	test	simu	Difference (%)	test	simu	ΔSOC
UDDS(Normal)	0.300	0.303	1.2	56.9	55.8	-1.1
UDDS(Cold)	0.523	0.543	3.8	65.7	68.4	2.7
UDDS(Hot)	0.478	0.462	-3.3	50.8	48.2	-2.6
HWFET(Normal)	0.914	0.915	0.1	65.8	66.6	0.8
HWFET(Cold)	1.035	1.012	-2.2	65.8	66.2	0.4
HWFET(Hot)	1.089	1.104	1.4	64.6	64.3	-0.3

The comparative results in Table V-9 show that the fuel consumed can be estimated within 4% under different ambient conditions and driving cycles.

Conclusions

The 2010 Toyota Prius vehicle test data were analyzed for different thermal conditions. The component thermal behavior as well as the impact of temperature on vehicle level control were analyzed, including

- Engine
  - Engine operating target depends on coolant temperature.
  - Engine on/off condition is constrained by the coolant temperature (performance degradation).
- Battery
  - Because of AC power, SOC in the hot test is usually lower than under other conditions.
  - Battery performance is degraded in cold conditions.
  - Battery maximum power is constrained by the battery temperature.
- Gearbox
  - Based on the current analysis, there is no significant performance impact by thermal conditions.
- Wheel
  - Wheel torque loss is affected by tire temperature.

A complete vehicle thermal model was developed and validated within 4% for fuel consumed under different ambient conditions and driving cycles.

The model, along with the previous one for the GM Volt, will be used to evaluate the impact of temperature on vehicle energy consumption.

V.K.3. Products

Publications

1. Namwook Kim, Daeheung Lee, Henning Lohse-Bush, Aymeric Rousseau, "Thermal Component Modeling and Validation for 2010 Toyota Prius," 2014 SAE World Congress.
2. Namwook Kim, Henning Losh-Bush, Aymeric Rousseau, "Test Analysis under Different Thermal Conditions for 2010 Toyota Prius," IMechE: Part D, Automotive Engineering.

Tools and Data

1. Autonomie.

References

1. www.autonomie.net
2. Sungjin Park, "A Comprehensive Thermal Management System Model for Hybrid Electric Vehicles," dissertation, University of Michigan, 2011.
3. M. Konz, "A Generic Simulation of Energy Consumption of Automobile Air Conditioning Systems," dissertation, M Tech Eng, 2007.
4. Tessa J. Morgan, "The Modelling of Internal Combustion Engine Thermal Systems and Behavior," dissertation, University of Nottingham, 2003.
5. Stefano Barsali and Massimo Ceraolo, "Dynamical Models of Lead-Acid Batteries: Implementation Issues," IEEE Transactions on Energy Conversion, vol 17, no 1, March 2002.

V.L. Stochastic Trip Modeling Using Geographical Information

Dominik Karbowski, Principal Investigator
Argonne National Laboratory
9700 South Cass Avenue, Building 362
Lemont, IL 60439
Phone: (630) 252-5362
E-mail: dkarbowski@anl.govmailto:nkim@anl.gov

David Anderson, DOE Program Manager
Phone: (202) 287-5688
E-mail: David.Anderson@ee.doe.gov

V.L.1. Abstract

Objectives

- Develop and validate realistic trip prediction based on starting and end points, using a geographical information system such as NAVTEQ's ADAS-RP.
- Supplement all the real-world drive cycles previously collected by DOE with accurate grade information.
- Develop prediction algorithms that can be used for control optimization purposes (project 1000151.00).

Major Accomplishments

- Developed a process to generate stochastic vehicle speed profiles under constraints.
- Processed a real-world speed profile database for stochastic profile generation.
- Developed a process to generate stochastic vehicle speed profiles for a given itinerary defined in ADAS-RP, using micro-trips.
- Evaluated the validity of the algorithms.

Future Achievements

- Further improvement and validation of the algorithms.
- Integration of the processes into Autonomie.

✧ ✧ ✧ ✧ ✧

V.L.2. Technical Discussion

Background

Route prediction is a promising research topic, as the knowledge of future driving conditions, if used effectively, can contribute to improving the efficiency of advanced vehicles such as hybrid electric vehicles (HEVs) and plug-in HEVs. For example, several studies showed that the fuel consumption reduction afforded by HEVs can be higher on roads with slopes if future road information is made available to the vehicle controller.

Route prediction is also an essential input for optimal HEV controllers. Dynamic programming and the Pontryagin minimization principle are the two main control theory techniques used for advanced powertrains. Both require full knowledge of the trip profile ahead to compute the optimal control law. Some heuristically optimized controls also rely on trip prediction.

Furthermore, a process to generate grade and vehicle speed profiles would be useful for benchmarking vehicle technologies in a wider array of situations than specific standard drive cycles.

In FY 2012, we initiated work on vehicle speed prediction by developing a process to create simple speed profiles for a given itinerary. This process relies on ADAS-RP, a geographical information system (GIS) developed by NAVTEQ, for the trip definition. A plug-in created by Argonne allows the user to export the itinerary information to Autonomie, which can then be used for vehicle simulation. The resulting speed profile was, however, made of simple segments: constant acceleration, constant speed, or constant deceleration. It is suitable for simulation, but lacks the randomness observed in the real world. The object of this study is to use a stochastic method for vehicle speed generation.

Introduction

A GIS, such as ADAS-RP, can provide extensive information about the different segments of an itinerary: grade, speed limit, historical traffic speed, etc. This information is, however, not sufficient to be used "as-is" in a high-fidelity fuel consumption vehicle simulation tool such as Autonomie. The reason is that it provides a succession of constant speeds without stops, which is not representative of real-world driving.

On the other hand, existing research highlights how Markov chains can be used to model and generate vehicle speed profiles. They include the stochastic aspect of driving. However, the result is so stochastic that it is hardly related to the actual speed achieved on a given itinerary.

The goal of this project is to link these two approaches so that a vehicle speed profile with a stochastic aspect can be generated for a given itinerary.

Our work consisted of first processing a large database of real-world trips to generate the probability tables composing a Markov chain. We then developed a process to generate stochastic cycles under constraints, which can naturally be taken from a GIS. Finally, we developed a complete process that takes an itinerary from ADAS-RP and outputs a stochastic vehicle speed profile.

Approach

Database processing

It is necessary to rely on real-world trips to define the transition probability matrix (TPM) used in the stochastic speed profile generating process. The real-world trips used in this project come from the Chicago Regional Household Travel Inventory. In this survey, sponsored by the Chicago Metropolitan Agency for Planning (CMAP) and the Illinois Department of Transportation, GIS data-logging devices were deployed in 300 vehicles, and close to 10,000 trips were logged.

The raw data included in the database include false data, probably arising from GIS loggers' limitations. To use these data for vehicle simulation, we applied several filters to circumvent the different issues encountered:

- *Short and slow trips* (maybe a person walking with the GIS recorder?): These trips are removed.
- *Trips beginning/finishing at non-zero speeds*: Only the sections between stops are kept.
- *Outlier speeds:* These are removed/replaced using a smoothing function.
- *Excessive accelerations:* These are removed using non-causal filtering.

Approximately 10% of the data points were removed during the filtering process. The distance distribution of the filtered data is shown in Figure V-108.

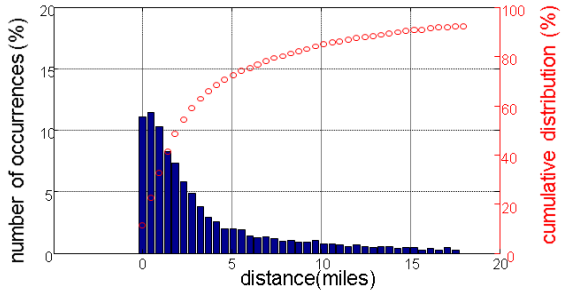

Figure V-108: Trip distance distribution of the filtered CMAP database.

Micro-trips and clustering

Once the trip database was filtered, we divided every trip into micro-trips; a micro-trip is a portion of a trip between two stops. Working on micro-trips allows us to better group data points corresponding to similar driving conditions. A trip may indeed be a combination of different types of driving conditions—e.g., urban driving followed by highway and then secondary-road driving. On the other hand, micro-trips are very likely to correspond to only one type of driving.

The next objective was to group micro-trips with similar features. Each micro-trip was assigned meta-data called explanatory variables: average speed, distance, etc. The proper choice of explanatory variables will capture the different types of driving conditions. In this project, we eventually intend to associate each segment of the trip, as defined by the GIS, with a particular cluster, relying on the available GIS information for that segment. We therefore chose to use explanatory variables that could be directly obtained from the GIS: duration, distance, average speed, and maximum speed. We then applied a clustering technique called principal component analysis (PCA). Figure V-109 shows the clustering obtained through that technique.

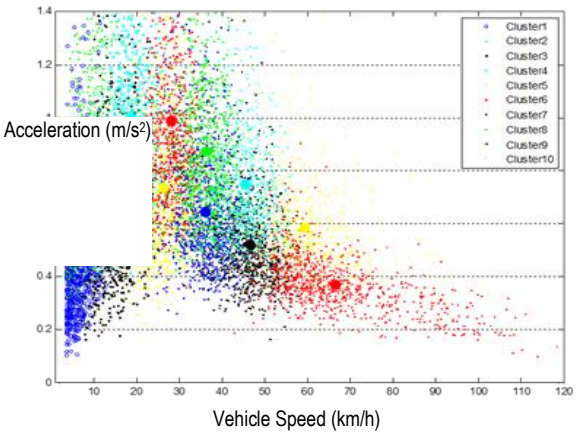

Figure V-109: Distribution of micro-trips by vehicle speed and acceleration, grouped in clusters using PCA.

Generation of stochastic speed profiles under constraints

A Markov chain is a random process characterized as memoryless: the next state only depends on the current state and not on the sequence of past events. This is the type of mathematical model we chose to represent vehicle speed. On the basis of existing research, we chose speed and acceleration as the states of the process.

The transition from one state to the other is governed by a TPM, which can be built by processing all the datapoints from the real-world trip database. We can create one TPM for the entire dataset, or one TPM per cluster as identified above.

One fundamental aspect of the Markov chain is that the outcome is stochastic, and the only control over its result is the time at which we stop the Markov chain. Our eventual goal is, however, to generate a speed profile that will be representative of driving on a given itinerary. For example, each segment/micro-trip must be of a certain distance. To that end, we created an algorithm which consists of generating speed profiles until a result with desired characteristics emerges. This process is illustrated in Figure V-110.

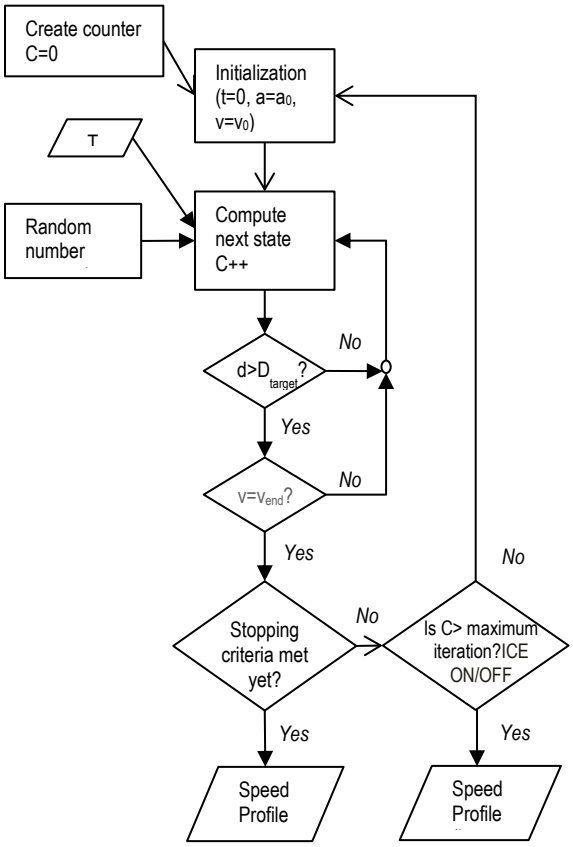

Figure V-110: Stochastic vehicle speed generation under constraints.

The stopping criterion considers average speed, number of stops, excessive speed, and distance. It is given by the Performance Value (PV):

$$PV = \alpha \frac{|V_{avg} - V_{target}|}{V_{target}} + \beta \frac{N_{stop}}{d_{seg}} + \gamma \sum_{t=T_1 \ldots T_2} \max((V(t) - V_{lim}), 0)^2 + \delta \frac{|d_{seg} - d_{target}|}{d_{target}} \quad ,$$

where

- $(\alpha, \beta, \gamma, \delta)$ are constants;
- V_{avg}, N_{stop}, d and V are explanatory variables for the generated speed profile: V_{avg} is the average speed, N_{stop} is the number of stops, d is the distance, and $V(t)$ is the speed at time *t*; and
- V_{target}, V_{lim}, d_{target} are the constraints: V_{target} is the target average speed, V_{lim} is the speed limit, and d_{target} is the desired distance of the section.

This PV evaluates the capability of the generated section to fit to some constraints: the speed average must be close to the traffic speed, the car should avoid stopping for no reason (although we still allow unplanned stops), speed shouldn't be higher than the speed limit, and the distance of the micro-trip must be very close to the distance of the segment.

Finally, the speed profile is filtered to remove the quantization—in the Markov chain generation, speed only takes discrete values (from 0 to 38 meter/sed every 1 meter/sec. This rule will ensure that we end up with a realistic speed profile, suitable for fuel-consumption simulation.

Speed profile generation using a GIS

In FY 2012, we developed a linkage between ADAS-RP, a GIS developed by NAVTEQ, and Autonomie. The user can select a particular itinerary on a map, and a specific plug-in developed for Autonomie exports relevant data for further processing in Autonomie. One of the results of this processing is the segmentation of the itinerary into sections for which distance, average speed, and speed limit are given. We can use this information as a constraint for the speed profile generation described above.

For each section of the trip, we need to find the cluster in the micro-trips database that is the most representative of the section. Since the clustering previously described is done with explanatory variables that are directly given by ADAS-RP, the choice of the cluster is straightforward.

This process is repeated for all segments, and is described in Figure V-111.

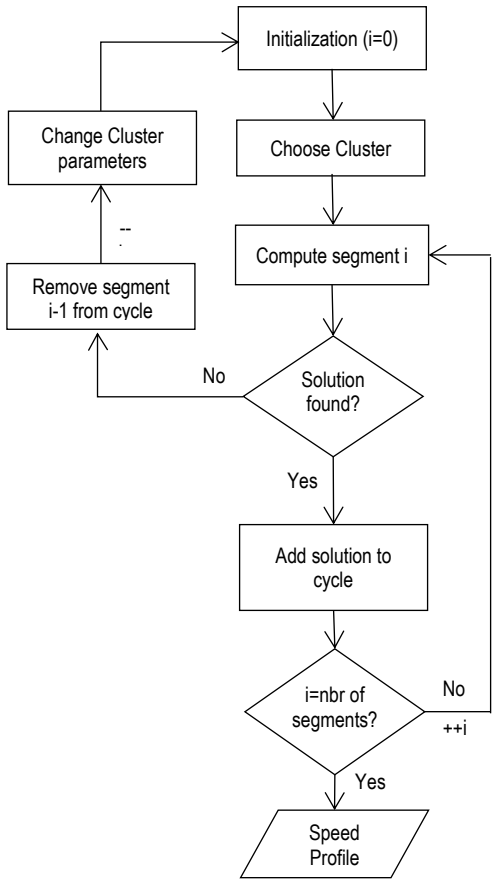

Figure V-111: Process for generating a speed profile using GIS.

Results

Validation

To test our methods and the clustering, we generated cycles close to the unified cycle LA92 and compared our cycles to the original. This approach allowed us to try our algorithm on the generation of a generic cycle, see the effect of clustering on convergence, and check our validation criteria.

The method used to recreate LA92 was to first divide it into micro-trips which have their own characteristics (speed average, length…); the duration of stops was taken directly from the LA92 cycle. To test the efficiency of clustering and the division of trips into micro-trips, we created four different types of cycle:

- *Cycle 1* uses clustering and the separation of LA92 into micro-trips.
- *Cycle 2* uses separation into micro-trips but no clustering, which means that the TPM is created using the whole database.
- *Cycle 3* uses clustering but no separation of the LA92 into micro-trips: the cycle generated will only try to fit the average speed of LA92 and its distance.
- *Cycle 4* uses neither clustering nor separation.

Figure V-112 shows the original LA92 cycle and how we segmented it, and Figure V-113 shows cycle 1, synthesized from the LA92 cycle.

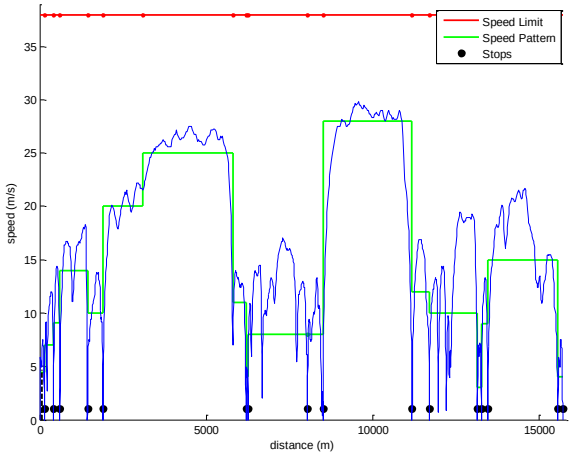

Figure V-112: Division of the LA92 cycle into micro-trips.

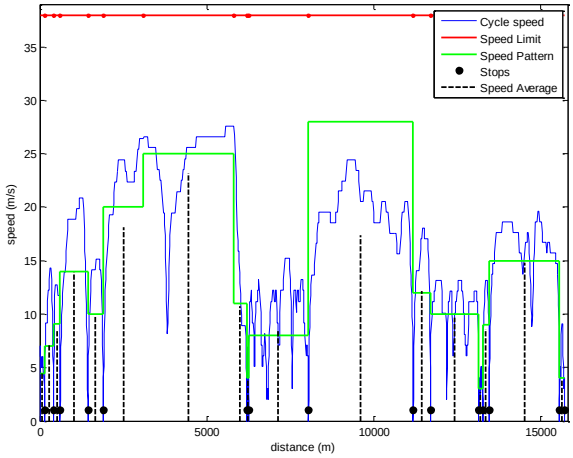

Figure V-113: Cycle 1, synthesized from LA92.

We then compared the impacts of our methods on fuel economy. To do so, we simulated two default vehicles in Autonomie—a conventional manual-transmission vehicle and a one-mode split HEV—on each of the synthesized cycles. The results are compiled in Table V-10. Fuel economy achieved on each of the synthesized drive cycles is comparable to that achieved on the LA92 cycle. Segmentation is definitely an important factor, while the impact of clustering is less clear.

Table V-10: Fuel economy of a manual-transmission vehicle and an HEV on the LA92 cycle and the various synthesized versions.

Cycle	Speed of Convergence (s)	Fuel Economy of Manual (mpg)	Fuel Economy of HEV (mpg)
LA92		31.92	40.58
Type 1 (clustering + segmentation)	4.01	31.95 (+0.1%)	42.2 (+4.0%)
Type 2 (segmentation only)	8.13	31.16 (-2.4%)	41.3 (+1.7%)
Type 3 (clustering only)	3.5	35.2 (+10.1%)	44.9 (+10.1%)
Type 4 (neither)	3.6	35.8 (+11.5%)	45.2 (+12.1%)

Example of trip generated from an itinerary

The previous example did not use the GIS. To demonstrate the entire process, we generated a speed profile (Figure V-114) for an itinerary defined in ADAS-RP (Figure V-115). The trip is in Chicago, from the Bucktown neighborhood to the Loop, which is the central business district of the city.

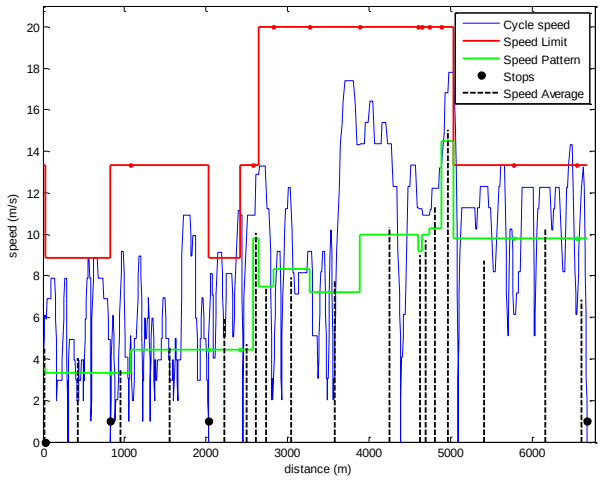

Figure V-114: Synthesized speed profile for Chicago itinerary.

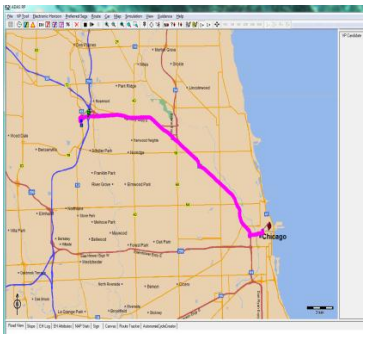

Figure V-115: Itinerary in ADAS-RP.

Conclusions

In this project, we developed a novel process to generate a stochastic vehicle speed profile along with a deterministic grade for a given itinerary defined in ADAS-RP, a GIS with extensive road network data.

Preliminary validation trials showed that the output can be used towards predicting fuel consumption. We will continue to validate the algorithm to provide more statistically representative results. We will also use the results from this project to evaluate the benefits of route-based control.

Finally, we will integrate the process into Autonomie so that this work can be reused, especially for design and analysis of route-based controllers.

V.L.3. Products

Publications

1. Dominik Karbowski, Vivien Smis-Michel, and Valentin Vermeulen (2013), *Optimal Vehicle Energy Management Using Trip Prediction*, presented at the 2013 SAE Energy Management Symposium.
2. Dominik Karbowski, Vivien Smis-Michel, and Valentin Vermeulen, *Using Trip Information for PHEV Fuel Consumption Minimization,* EVS 27 Conference

Tools and Data

1. Method to process a large database of real-world vehicle speed recordings.
2. Process to generate a stochastic vehicle speed profile under constraint.
3. Process to generate a stochastic vehicle speed profile for an itinerary defined in ADAS-RP.
4. Processed trip and micro-trip database from original CMAP data.

References

1. www.autonomie.net/
2. Fincher, S., Palacios, C., Kishan, S., Preusse, D., and Perez, H. (2010). “Final Report for: Modifying Link-Level Emissions Modeling Procedures for Applications within the MOVES Framework.” 4.(0-14)
3. Stochastic Modeling for Studies of Real-World PHEV Usage: Driving Schedule and Daily Temporal Distributions.
4. André, M. (2004). “Real-world driving cycles for measuring cars pollutant emissions—Part A: The ARTEMIS European driving cycles.” LTE, Laboratoire Transports et Environnement, Report No. 34-40.
5. Dai, Z., Niemeier, D., and Eisinger, D. (2008). “Driving cycles: A new cycle-building method that better represents real-world emissions.” 7-12
6. Lee, T., and Filipi, Z. “Synthesis and Validation of Representative Real-World Driving Cycles for Plug-In Hybrid Vehicles.”
7. Press, W., Teukolsky, S., Vetterling, W., and Flannery, B. (2007). “Numerical Recipes: The Art of Scientific Computing.” 14.8
8. Karbowski, D., Pagerit, S., and Calkins, A. (2012). “Energy Consumption Prediction of a Vehicle Along a User-Specified Real-World Trip.”
9. Lin, J., and Neimeier, D. (2002). “An exploratory analysis comparing driving cycle to California’s regulatory cycle.”

V.M. Advanced Transmission Impact on Fuel Displacement

Namdoo Kim, Principal Investigator
Argonne National Laboratory
9700 South Cass Avenue, Building 362
Lemont, IL 60439
Phone: (630) 252-2843
E-mail: nkim@anl.gov

David Anderson, DOE Program Manager
Phone: (202) 287-5688
E-mail: David.Anderson@ee.doe.gov

V.M.1. Abstract

Objectives

- The objectives are to update the current transmission model and shifting algorithm and to develop new models and algorithms to evaluate the latest technologies.
  - Argonne National Laboratory has developed and validated shifting algorithms for 4-speed and 5-speed automatic transmissions, but no work has been done on 6+ speeds or advanced transmissions such as dual-clutch (DCTs).
  - Transmissions have evolved significantly over the past 5 years, and they have a significant impact on fuel consumption. However, little work has been done within the Vehicle Technologies Office (VTO).
  - A validated model will be used to provide an evaluation of VTO benefits and to guide future research and development with more accuracy.

Major Accomplishments

- Integrated more than a dozen sets of vehicle test data into Autonomie.
- Created two new algorithms to calculate some of the critical signals not recorded during testing, such as gear ratio and torque converter lockup.
- Developed a new shifting initializer to create a new set of calibration (i.e., the entire shift map) and validated it with the Argonne Advanced Powertrain Research Facility (APRF) test data for three automatic transmission vehicles.
- Produced a model of a DCT in Simulink based on the original system schematic.
- Developed and integrated the local controller to define the operating mode based on the principle of DCT operation.

Future Achievements

- Automate the calibration process from test data.
- Build vehicles with DCT and validate the model based on APRF data (2012 Ford Focus I4 6DCT and 2013 WV Jetta TDI 6DCT).
- Develop additional advanced transmission models (i.e., continuously variable transmission).
- Formulate and validate an algorithm to select optimum gear ratios for future transmissions.

✧ ✧ ✧ ✧ ✧

V.M.2. Technical Discussion

Background

As a result of more stringent regulations and customer expectations, auto manufacturers have considered numerous technology options to improve vehicle fuel economy. One such technology is transmission technology, since transmissions are one of the most cost-effective options. Over the past couple of years, transmissions have evolved significantly and have impacted both performance and fuel efficiency. This study validates the shifting control of advanced automatic transmission technologies in a vehicle systems context by using Autonomie, a model-based system simulation tool.

Introduction

Different midsize vehicles, including several with automatic transmissions (6-speed, 7-speed, and 8-speed), were tested at Argonne APRF. For the vehicles, a novel process was used to import test data. In addition to importing the measured test signals into the Autonomie environment, the process also calculates some of the critical signals not recorded during vehicle testing, such as gear ratio and torque converter lockup. Numerous analysis functions have been developed to quickly analyze the shifting map by using the integrated test data in Autonomie to generate model parameters. In addition, a set of calibrations for the generic shifting algorithm has been developed to match the test data. We intend to demonstrate the validation of Autonomie transmission component models and control strategy by using APRF vehicle test data over different driving cycles.

Approach

The project workflow is shown in Figure V-116. The Argonne APRF has already tested many vehicles on the dynamometer and measured their major performances (i.e., fuel economy or 0 to 60 mph based on several signals.) With the results obtained from various driving schedules with several types of transmissions, we analyzed the advanced

powertrain system. We also validated the transmission model and shifting algorithm in Autonomie.

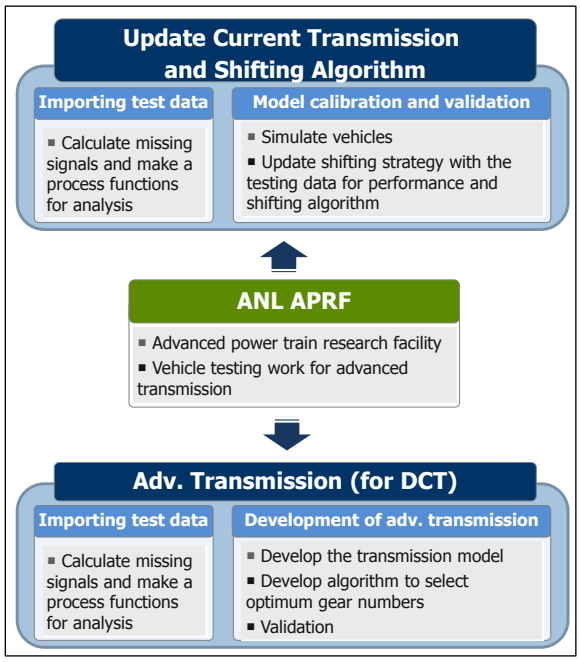

Figure V-116: Study Process for Updating Current Transmission Models and Shifting Algorithm.

Results

Importing Test Data

More than a dozen sets of vehicle test data have been integrated into Autonomie, including the latest Jetta TDI and Mazda 3 from the Advanced Vehicle Testing Activity Program.

Additional Signals Calculation

For all the vehicles, the new import test data process was used to not only import the measured signals into Autonomie, but also to calculate some of critical signals that were not measured during testing, such as gear ratio (Figure V-117) and torque converter lockup (Figure V-118). To do so, two new algorithms were created and validated by using vehicles that had these measured signals available.

Gear Ratio Calculation Algorithm:

1. Signals are aligned based on vehicle speed.
2. SR = speed in (measured from turbine speed)/speed out (calculated from vehicle speed).
3. SR = 1st gear ratio when the vehicle speed = 0 and the engine speed is < idle speed.
4. The elements of SR are rounded to the nearest known value of gear ratio.
5. SR is filtered out to keep the current gear ratio for 0.8 second (minimum).

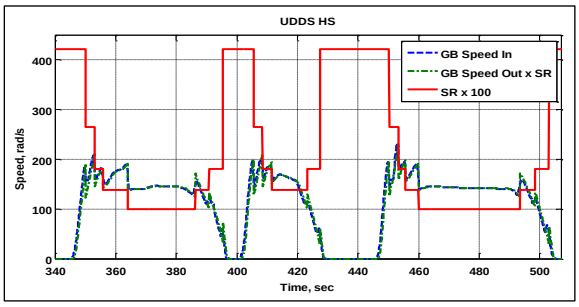

Figure V-117: Gear Ratio Calculation for UDDS.

Status of Torque Converter Lockup:

1. Signals are aligned based on vehicle speed.
2. cpl_cmd = 1 (locked) when the gap between speed in and out is < 10 rad/s.
3. cpl_cmd = 0 (unlocked) for 1st gear ratio or 2nd gear ratio.
4. cpl_cmd = 0 (unlocked) when the accel of speed_in > 1 rad/s^2.
5. cpl_cmd is filtered out to keep the current status for 1 second (minimum).

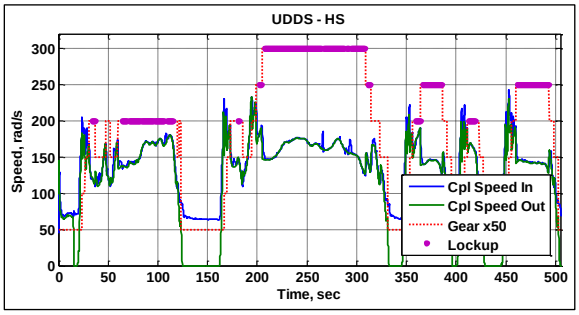

Figure V-118: Calculation of the Torque Converter Lockup Status for UDDS.

Test Data Analysis for the Automatic Transmission

Numerous analysis functions have been developed to quickly analyze the shifting map by using the integrated test data in Autonomie.

Figure V-119 shows the impact of a higher gear number on automatic transmissions. The higher gear ratios are consistently used for the 8-speed transmission compared with the 6-speed transmission. By lowering the engine rotational speed, the engine operating torque is expected to increase, thereby leading to lower fuel consumption. Table V-11 also shows the comparison results for time spent in each gear number for the Urban Dynamometer Driving Schedule (UDDS).

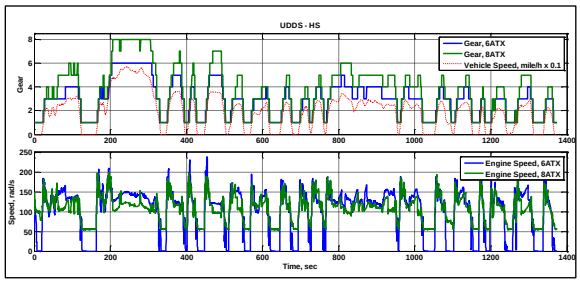

Figure V-119: Impact of a Higher Gear Number.

Table V-11: Time Spent in Each Gear Number.

Percent. (UDDS)	Gear 1	Gear 2	Gear 3	Gear 4	Gear 5	Gear 6	Gear 7	Gear 8
6 ATX	28.5	5.9	34.6	18.2	5.2	7.6	-	-
8 ATX	29.4	4.5	16.0	15.8	19.0	5.9	2.8	6.7

Figure V-120 shows the comparison results between the Sonata conventional (Conv.) and the Sonata hybrid electric vehicle (HEV) for the shifting map and engine operation points. The Sonata HEV has a higher final reduction gear ratio than the Sonata Conv., since there is no torque convertor to multiply the torque. An additional reason is that the HEV is heavier than the Conv. Therefore, to meet the same grade-ability requirement, this reduction gear ratio might be sized higher than the Conv. The operation range of each gear ratio is also narrower than the Conv.

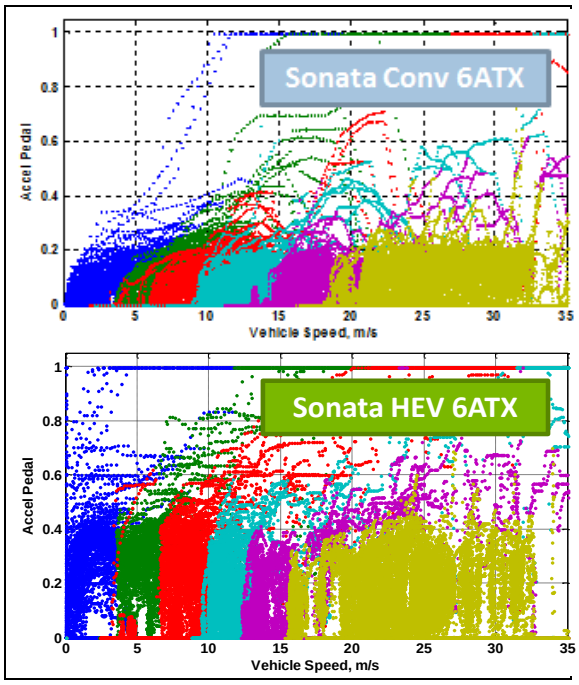

Figure V-120: Impact of Powertrain Technology.

The analysis functions were developed to dedicate and generate shifting curves by using the integrated test data in Autonomie. With these functions, the sets of information shown in Figure V-121 could be generated to implement the shifting curves (upshifting and downshifting).

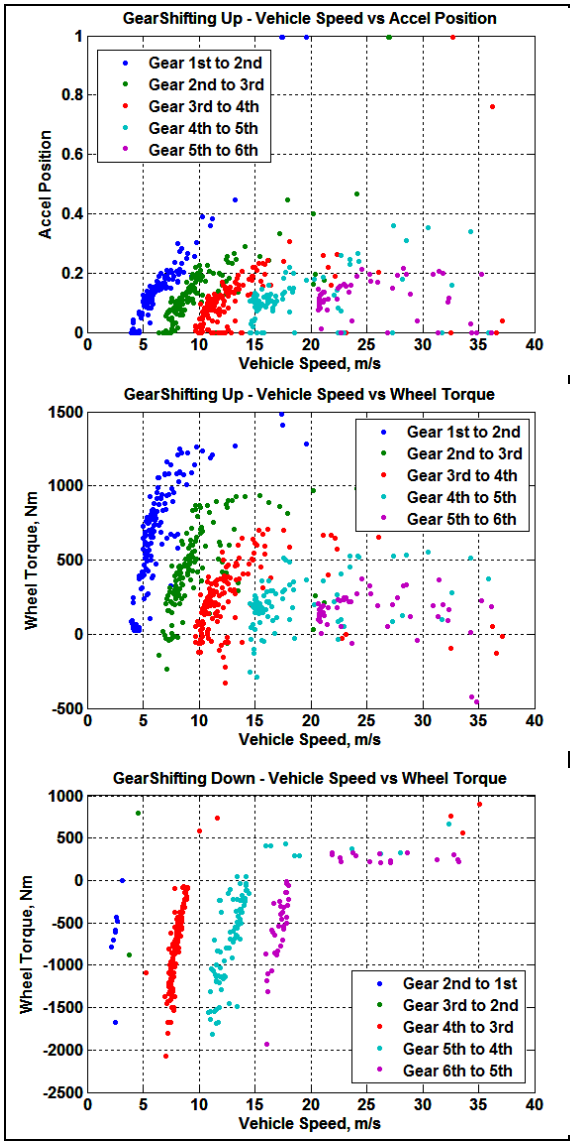

Figure V-121: Implementing Shifting Curves Generation Functions.

Development of a New Shifting Initializer

The shifting initializer defines the shifting maps (i.e., values of the parameters of the shifting controller) specific to a selected set of component assumptions. A new shifting initializer was developed to create a new set of calibration (i.e., the entire shift map) from test data. In this case, the exact map was used in simulation instead of our generic algorithm.

Current Shifting Algorithm Overview

For each shifting curve, there are two key points: the "economical" shifting speed (at very low pedal position) and the "performance" shifting speed (at high pedal position). The objective of the control engineer is to combine both goals of the shifting control to fulfill the driver expectations—minimization of fuel consumption on the one hand and maximization of vehicle performance on the other. Figure V-122 shows the engine speed range in the economical driving and economical shift.

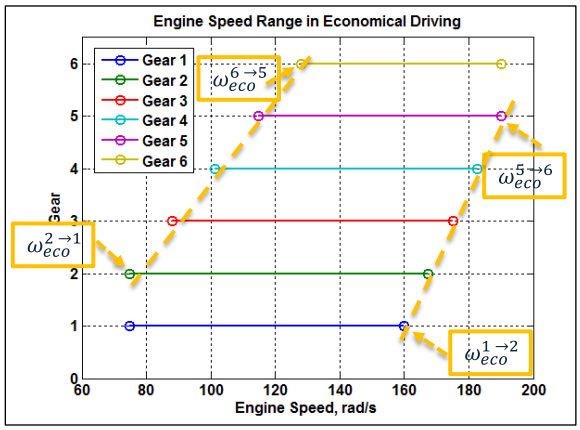

Figure V-122: Economical Shifting Speeds (at very low pedal positions).

During performance, the gears are automatically selected to maximize the torque at the wheel. Figure V-123 shows that gear selection, which consists of finding the point where the engine peak torque curve at the gear falls under the one at the next gear.

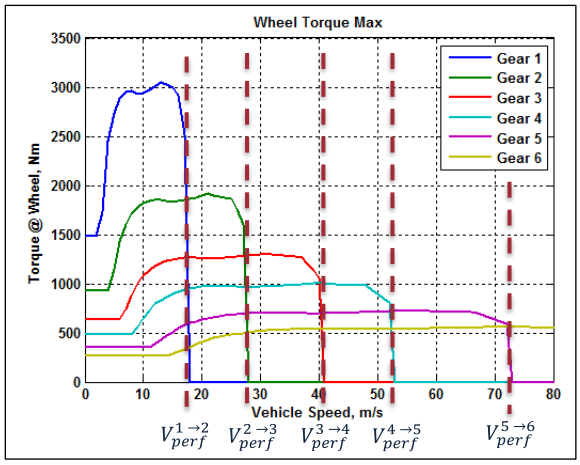

Figure V-123: Performance Shifting Speeds (at high pedal positions).

Refined Shifting Algorithm/Calibration

A new shifting initializer was developed to create a new set of calibration from test data. The new values of the parameters of the shifting controller are added in the shifting initializer to define the shifting maps created from test data. The parameters can be calibrated by the users through Autonomie Graphical User Interface (GUI). However, during performance, the gears also are automatically selected to maximize the torque at the wheel. Figure V-124 shows an example of the new shifting initializer in Autonomie.

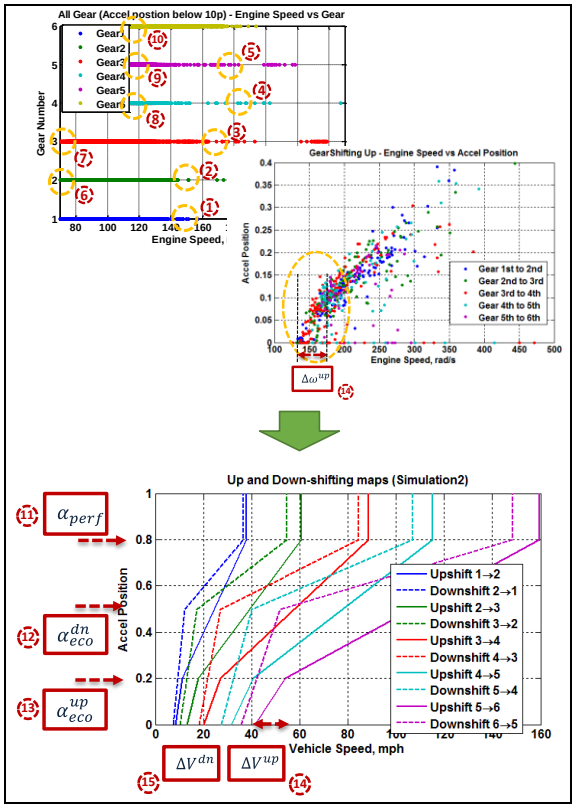

Figure V-124: Refined Shifting Algorithm.

Simulation Results Comparison

Three automatic transmission vehicles (Hyundai Sonata, Ford Fusion and Chrysler 300) were simulated and validated with test data. The lockup/release algorithms were identical. The shifting algorithm for the vehicles was calculated by using two approaches:

- Calibration of the initial algorithm (simulation 1), and
- Refined algorithm and calibration (simulation 2).

The simulations were performed on the standard driving cycles, and the simulation results were compared with the test data. Figure V-125 depicts the vehicle speed and the gear number on the UDDS compared with the test data. Both simulations show closed correlation with the test data.

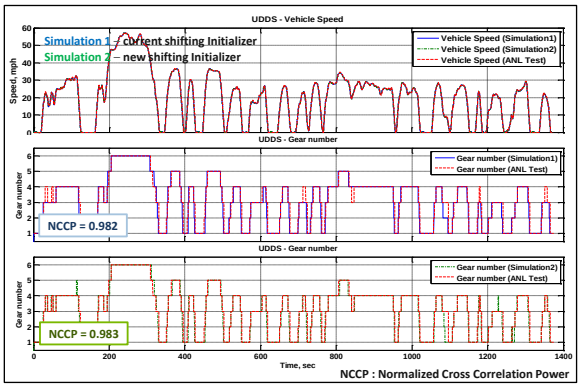

Figure V-125: Simulation and Testing Results on UDDS.

Table V-12: Shifting Algorithm Model Validation.

- 2013 Hyundai Sonata Conv. 6ATX

	UDDS	HWFET	NEDC	LA92
Simulation 1 – current shifting Initializer	0.982	0.990	0.980	0.986
Simulation 2 – new shifting Initializer	0.983 (0.10%)	0.996 (0.61%)	0.982 (0.20%)	0.991 (0.51%)

- 2012 Ford Fusion (6 ATX)

	UDDS	HWFET	NEDC	LA92
Simulation 1 – current shifting Initializer	0.968	0.998	0.951	0.994
Simulation 2 – new shifting Initializer	0.995 (2.79%)	0.998 (0%)	0.981 (3.15%)	0.988 (-0.6%)

- 2013 Chrysler 300 (8 ATX)

	UDDS	HWFET	NEDC	LA92
Simulation 1 – current shifting Initializer	0.956	0.984	0.970	0.938
Simulation 2 – new shifting Initializer	0.962 (0.63%)	0.993 (0.91%)	0.973 (0.31%)	0.957 (2.03%)

Table V-12 shows the results of normalized cross correlation power (NCCP) for both simulations. When applied to a test signal and a simulation signal of the same quantity, a value of NCCP equal to or greater than 0.9 indicates a high level of correlation. Both simulations show closed correlation with the test data (NCCP > 0.9).

Development of a DCT Clutch Transmission Model

A model of a DCT was developed in Simulink based on the original schematic of the system and bibliographic search. The operating logic was defined based on the principle of DCT operation, and the local controller was also developed.

DCT Plant Model Development

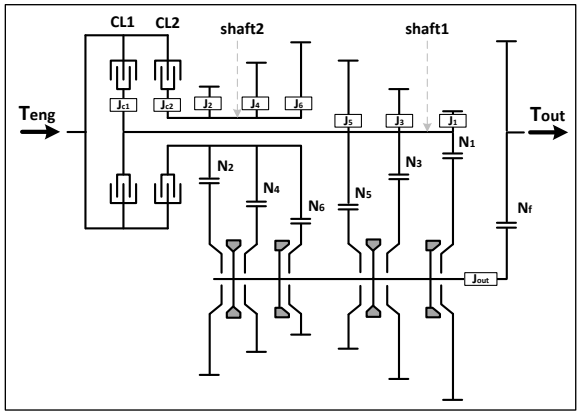

Figure V-126: Schematic of DCT Powertrain.

Figure V-126 shows the schematic diagram of DCT model. A dynamic model of the DCT was developed including individual clutch and drivetrain models. The following assumptions are made for the model:

- The consistency of the current models and the local controller in Autonomie should be ensured.
- Synchronizer dynamics are neglected.
- All shafts are assumed to be rigid.
- The inertia of the shaft1 is lumped with clutch1.
- The inertia of the shaft2 also is lumped with clutch2 inertia.

Development of a DCT Controller

A local controller of a DCT also was developed. A gearbox transient block coordinates all components during the transient phases, as illustrated in Figure V-127.

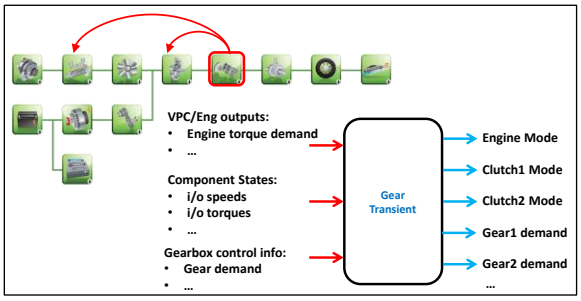

Figure V-127: DCT Controller Development.

Simulation Results during Shifting

To validate the behavior of the plant model and its control, a conventional vehicle with a DCT model was built. The simulations were compared with a Conv. manual transmission vehicle demonstrating proper behavior. The vehicle speed, gear number, and wheel torque during acceleration performance processes are compared with test data in Figure V-128. The DCT model is able to transmit power during shifting, demonstrating a smooth acceleration with uninterrupted traction.

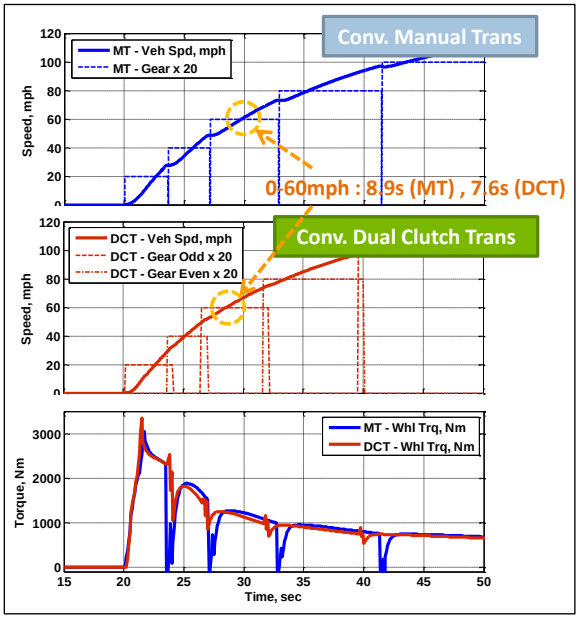

Figure V-128: Simulation Results Comparison.

Conclusions

The highlights of this project are summarized below.

- Test data was imported for numerous vehicles and driving cycles:
  - Input name and unit conversion data were defined to import test data into Autonomie; and

    - Missing signals were calculated and a new process for analysis was developed (gear ratio, input and output effort, and flow for each component).
- Dedicated analysis functions were generated for shifting logic.
- The shifting algorithm for several vehicles was calculated by using two approaches:
    - Calibration of the initial algorithm, and
    - Refined algorithm and calibration.
- Closed correlation with the test data (NCCP > 0.9) was shown in the simulation.
- Plant and controller models for the DCT were developed.

V.M.3. Products

Publications

1. Kim, N., A. Rousseau, and H. Loshe-Bush, "Advanced Automatic Transmission Model Validation Using Dynamometer Test Data," SAE World Congress 2014, submitted.
2. Kim, N. A. Rousseau, and H. Loshe-Bush, "Developing a Model of Dual-Clutch Transmission in Autonomie and Validation with Dynamometer Test Data," *International Journal of Automotive and Mechanical Engineering*, 2014, submitted.

Tools and Data

1. Autonomie (a model-based vehicle simulation tool).

References

1. www.autonomie.net.
2. LeGuen, D., T. Weck, A. Balihe, and B. Verbeke, "Definition of Gearshift Pattern: Innovative Optimization Procedure Using System Simulation," *SAE Int. J. Engines,* 4(1):412-431, 2011.
3. Viet, N., H. Hofman, M. Steinbuch, and A. Serrarens, "Optimal Shifting Strategy for a Parallel Hybrid Electric Vehicle," *EVS-25* World Battery, *Hybrid,* and Fuel Cell *Electric Vehicle* Symposium, Shenzhen, China, Nov. 5–9, 2010.
4. Matthes, B., "Dual-Clutch Transmission—Lessons Learned and Future Potential," SAE Technical Paper 2005-01-1021, 2005.
5. Joshi, A., N. Shah, and C. Mi, "Modeling and Simulation of a Dual-Clutch Hybrid Vehicle Powertrain," in proceedings of the IEEE Vehicle Power and Propulsion Conference 2009, VPPC '09, Dearborn, MI, Sept. 7–10, 2009.

V.N. Establishing Thermo-Electric Generator Design Targets for Hybrid Vehicles

Ram Vijayagopal, Principal Investigator
Argonne National Laboratory
9700 South Cass Avenue
Lemont, IL 60439
Phone: (630) 252-6960
E-mail: ram@anl.gov

Gurpreet Singh, David Anderson,
DOE Program Managers
Phone: (202) 586-2333; (202) 287-568
E-mail: gurpreet.singh@ee.doe.gov,
david.anderson@doe.ee.gov

V.N.1. Abstract

Objectives

Establish requirements for a thermoelectric generator (TEG) to provide cost-effective power for hybrid electric vehicles (HEVs):

- Quantify fuel economy benefits that can be obtained by using auxiliary electric power sources in a HEV
- Develop a TEG model based on published information
- Assess the fuel-saving potential of TEG
- Estimate the net present value (NPV) of the fuel savings
- Establish the performance and cost targets for TEGs to be economically feasible

Major Accomplishments

- Analyzed the fuel-saving potential of auxiliary power sources on a midsize vehicle over different drive cycles
- Developed a TEG model and validated it against test data from General Motors (GM)
- Considered two types of hybrid for TEG evaluation:
  - Mild HEV using belt-integrated starter generator (BISG)
  - Full HEV using split powertrain
- Evaluated the potential of current prototypes
- Determined that on a US06 cycle, the NPV of fuel savings resulting from the use of a TEG with 40 modules in a midsize HEV could vary from $110 (split) to $146 (BISG)

Future Achievements

- TEG model can be improved if more module test data are made available from the original equipment manufacturers (OEMs).
  - More advanced models that can factor in detailed material and cost data can be used for optimization studies involving cost

✧ ✧ ✧ ✧ ✧

V.N.2. Technical Discussion

Background

Thermoelectric Generators

Thermoelectric generators (TEGs) can be used for a variety of applications in automobiles. Waste heat recovery and more efficient heating, ventilation, and air conditioning (HVAC) are two areas where there is a lot of work going on. This work is related to recovering the waste heat from the engine exhaust.

Introduction

Argonne National Laboratory (Argonne) conducted a study on the potential of using TEGs in conventional vehicles in FY11. The study pointed out the limitations in a conventional vehicle's ability to utilize the electric power generated by the TEG. That study also revealed the need to improve the overall conversion efficiency of TEGs in order to make them economically feasible. The evaluation of TEGs in HEVs was a natural follow-up to that study. The TEG system design must take into account many factors, including where the TEG will be placed and how the temperature difference across the TEG will be accomplished. This study assumes that the system is shown as in Figure V-129.

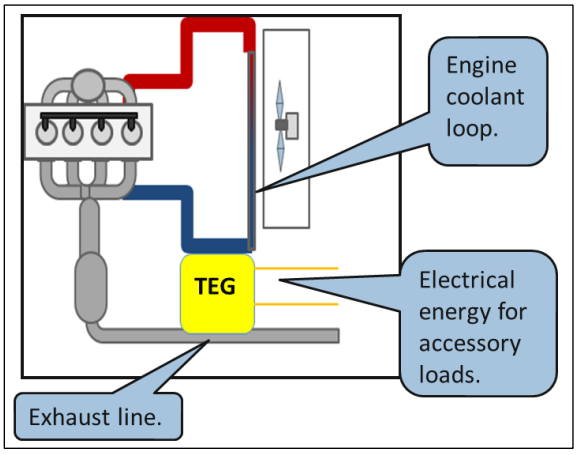

Figure V-129: Position of TEG System in the Vehicle.

In this project, the TEG module is sized on the basis of a Generation II prototype from General Motors (GM). It uses Skutterudite materials, which have been shown to possess better material properties than the earlier Pb-Te modules. This study considers only the thermoelectric properties of the modules and ignores the mechanical properties that are necessary for operating under extreme ambient temperatures and rapid thermal cycling.

Approach

Evaluating the Potential Benefits of Auxiliary Power Source in a Vehicle

The first step in evaluating the benefits of TEG is to establish the fuel-saving potential of an auxiliary electric power source in a vehicle. This source might be TEG or some other device. If the fuel-saving potential or money-saving potential can be estimated for every unit of power, that will provide a high-level target for sizing such components.

The default midsize belt-integrated starter generator (BISG) vehicle in Autonomie [1] was used as the baseline vehicle for this analysis. A vehicle schematic is shown in Figure V-130, and the detailed specifications are provided in Table V-13.

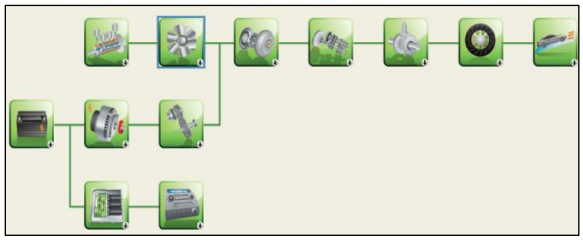

Figure V-130: Overview of the Baseline Vehicle from Autonomie.

Table V-13: Vehicle Specifications.

Technology	BISG
Engine	115 kW
Motor	10 kW
Battery	1.4 kWh
Aux. Power Source	Variable up to 1 kW

The fuel-saving potentials of auxiliary power sources were estimated through simulations and are shown in Figure V-131. This estimation is done with a few assumptions. A steady power supply is assumed over the entire drive cycle. This may not be true in all cases, but previous studies have shown that such an approximation can give a good estimate of the fuel-saving potential [2]. It is also assumed that the motor can assist the engine at all speeds, thus ensuring that the energy generated by the TEG is consumed. Autonomie ensures that the simulations are charge sustaining, thereby precluding the effect of the stored energy at the battery.

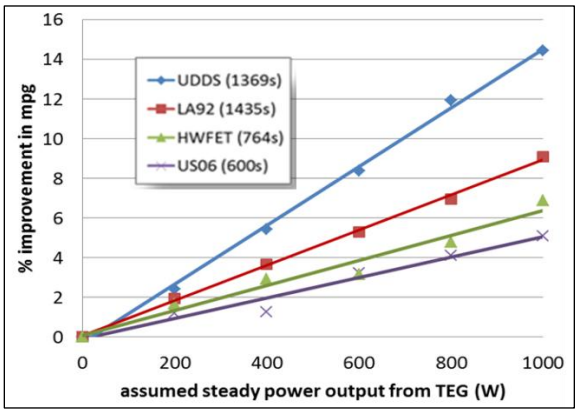

Figure V-131: Estimation of Fuel-Saving Potential for Devices like TEGs.

The benefits of devices like TEGs increase with increases in the power output from the device, and the sensitivity varies with drive cycle, too. For any given auxiliary power, the Urban Dynamometer Driving Schedule (UDDS) cycle will show a more pronounced effect than US06 because the average propulsion power required in US06 is higher than that in UDDS.

Longer and less-aggressive cycles can be expected to show more benefits from devices like TEGs. The monetary benefits from the fuel economy improvements are quantified and represented in Figure V-132.

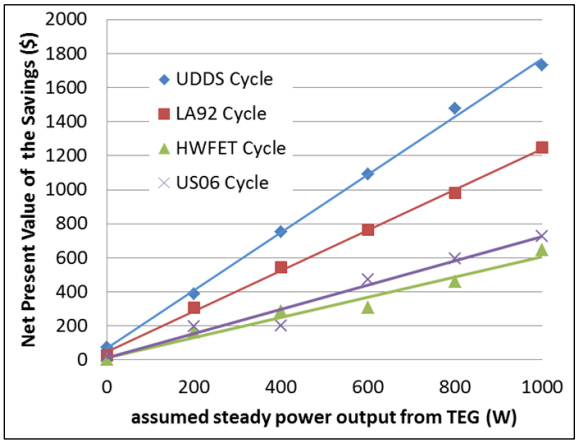

Figure V-132: Estimation of NPV for Savings from TEG-like Devices.

What Is Needed to Improve Fuel Economy by 5%?

The U.S. Department of Energy (DOE) has challenged OEMs and TEG manufacturers to improve vehicle fuel economy by 5% (in the US06 cycle). In the case of a midsize mild hybrid vehicle, this will be possible if 1 kW of power is provided from the auxiliary power source. To produce this much electrical power, a TEG will require about 8% overall conversion efficiency.

Initial estimates of the NPV of gasoline savings indicate that a TEG capable of producing a steady 1-kW power output will save a little over $600 for an average consumer. The NPV estimation assumptions are carried over from an earlier work [3].

TEG Model –Based on Data from GM

For the phase 1 studies, a model was used based on module test data done from GM. For the phase 2 studies, this model was improved by adding sublevels for the hot and cold heat exchange (Figure V-133), as well as a TEG model based on material properties.

The detailed module test data published by GM [4–6] was used to develop the model parameters.

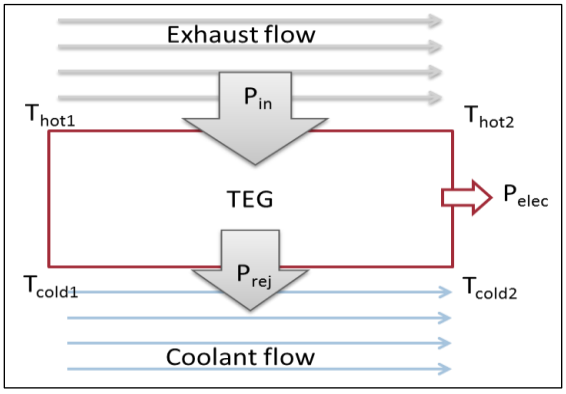

Figure V-133: Schematic for TEG Model.

This model does not factor in the layout of the TEG system. It assumes that the exhaust gas and cooling fluids are distributed between all the available modules evenly, and every TEG module is subjected to similar temperature differences. In practice, this layout design itself is a challenging problem. Apart from that limitation, the model can handle the different material properties or scale the number of modules. The output from the validated model is shown in Figure V-134.

The model can predict the power produced when the TEG is subjected to certain operating conditions. It is assumed that load matching to internal resistance can be accomplished to maximize the power output. The presence of a battery should make it possible to accomplish this without much difficulty.

The model relies on an Autonomie engine model for computing the exhaust gas flow rate. The engine model provides the TEG with a fuel consumption rate, and the flow rate of exhaust gas can be computed from that information. The gas temperature is assumed to be constant; however, the hot side heat exchanger will have a delay in warming up, as observed in TEG test cases. Similarly, the coolant will start with a predetermined ambient temperature and will warm up as the TEG and engine start to work.

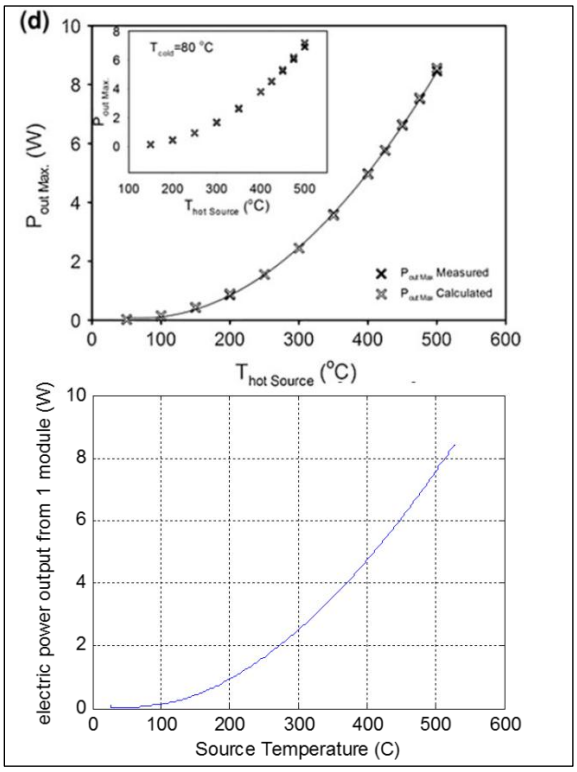

Figure V-134: Validation of the Model versus Published Test Data.

Results

Estimating the Potential Benefits of TEG

A parametric study is conducted by changing the number of modules in the TEG in order to estimate benefits. Both belt integrated starter generator (BISG) and power split vehicles were used in this study. The baseline for each case was the vehicle without any TEG system. The average power produced by the TEG, the improvements in fuel economy, and the NPV of gasoline savings thus obtained are monitored.

Figure V-135 shows the benefits obtained by using TEG in a midsize BISG mild hybrid vehicle and a split hybrid vehicle.

As shown in Figure V-135, the incremental benefits start to decrease when the number of modules increases. This is expected because the energy input to the system is fixed, and as more modules are added, the average operating temperature difference will also decrease, resulting in less power production from each individual module.

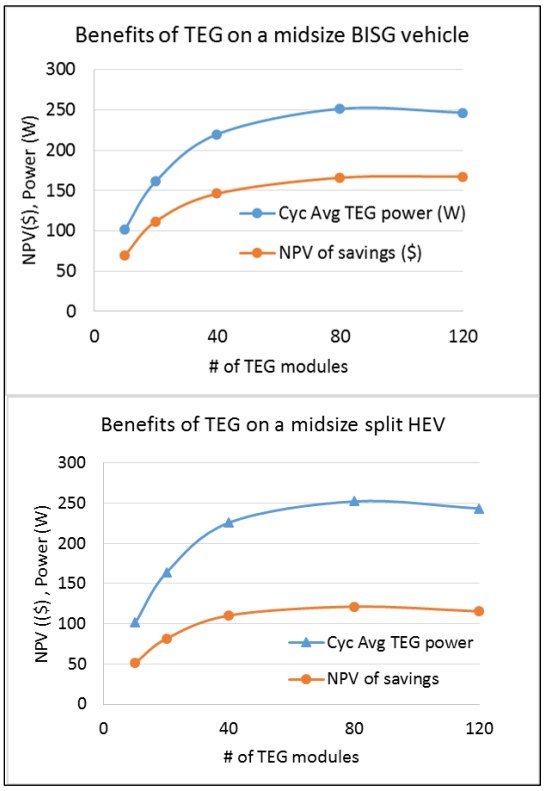

Figure V-135: Effect of TEG on Midsize Hybrid Vehicles with US06.

Both the midsize BISG mild hybrid vehicle and the split hybrid vehicle can shut down their engines while idling, so they produce significantly less exhaust energy when compared to conventional vehicles. The aggressive US06 also plays a significant role in the observed benefits. The cycle is quite aggressive and even forces the stronger split hybrid to use the engine almost as long as the BISG vehicle. This all contributes to the similarities in the benefits observed in this study. The TEG benefits are summarized in Table V-14.

Table V-14: Summary of the Benefits of Using a TEG in Hybrid Vehicles over the US06 Cycle.

TEG with 40 modules	BISG	Split
Cycle average power (US06 drive cycle)	225 W	225 W
Improvement in fuel consumption	0.89%	0.96%
NPV of lifetime gasoline cost savings	$ 146	$ 110

Conclusions

TEG model was developed on the basis of data from GM, and the capability of the prototype was evaluated. Figure V-136 shows how the prototypes have improved over the past few years, and it also shows how far it has to go in order to meet the targets.

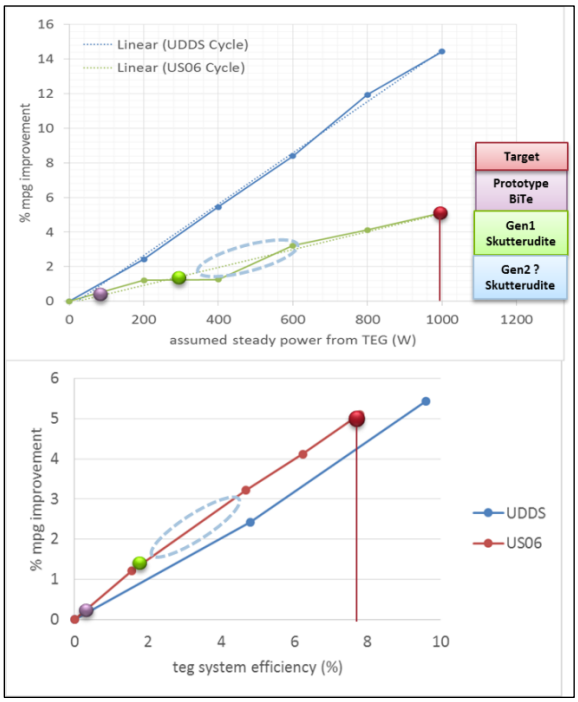

Figure V-136: Status of Prototype TEG Systems Evaluated in This Study.

The NPV provides estimated benefits for consumers. The benefits could vary with drive cycle, from $1.75/W in a UDDS cycle to $0.7/W for a US06 cycle. If the cost to the consumer is less than these targets, this would be compelling economic justification for TEG. This study can also help manufacturers decide on the size of the TEG needed in a vehicle, and quantify the potential fuel economy benefits.

Improvements in the overall conversion efficiency of TEGs can bring significant benefits for HEVs. New ways to achieve these efficiency improvements should be explored. Argonne now has the ability to perform simulation analysis of these systems and can aid the DOE by generating system design options or evaluating proposals from other agencies.

V.N.3. Products

Publications

1. R.Vijayagopal, N.Shidore, et al., “Estimating the Fuel Displacement Potential of a Thermoelectric Generator in a Conventional Vehicle, using Simulation and Engine in the Loop Studies,” EVS27, 2013.
2. N.Shidore, R.Vijayagopal, et al., “Thermoelectric Generator (TEG) Fuel Displacement Potential using Engine-in-the-Loop and Simulation,” U.S. DoE Thermoelectric Applications Workshop III, 2012.

Tools and Data

1. Autonomie

References

1. www.autonomie.net
2. N. Shidore, R. Vijayagopal, et al. “Thermoelectric Generator (TEG) Fuel Displacement Potential using Engine-in-the-Loop and Simulation,” U.S. DoE Thermoelectric Applications Workshop III, 2012.
3. R. Vijayagopal, J. Kwon, A. Rousseau, P. Maloney, “Maximizing Net Present Value of a Series PHEV by Optimizing Battery Size and Vehicle Control Parameters,” SAE, 2010.
4. J. Salvador, et al. “Thermal to Electrical Energy Conversion of Skutterudite-Based Thermoelectric Modules,” *Journal of Electronic Materials*. DOI: 10.1007/s11664-012-2261-9.
5. J. Salvador, et al., “Materials, Modules, and Systems: An Atoms to Autos Approach to Automotive Thermoelectric Systems Development,” DEER, 2012.
6. M. Reynolds, “Development of Thermoelectric Technology for Automotive Waste Heat Recovery,” presentation to the U.S. Department of Energy, December 3, 2008, Washington D.C.

V.O. Behavioral Driver Model and Analysis

Jan-Mou Li, Principal Investigator
Oak Ridge National Laboratory
2370 Cherahala Boulevard
Knoxville, TN 37932
Phone: (865) 946-1461
E-mail: lij3@ornl.gov

Lee Slezak, DOE Program Manager
Phone: (202) 586-2335
E-mail: lee.slezak@ee.doe.gov

V.O.1. Abstract

Objectives

- Bring actual driving behavior into vehicle simulation
  - Investigate the effects of the behavioral component ("driver behavior") on different powertrain configurations and especially while traversing a host of various routes
  - Establish a behavioral model suitable for use in Autonomie

Major Accomplishments

- An extensive literature review of behavioral component in vehicle simulation has been performed;
- Actual driving data, collected by the HTDC project in a challenging interstate section, have been identified for the development;
- A new truck driving model has been developed for using in Autonomie
  - It is able to perform driving tasks from start to stop;
  - It captures behaviors including uphill preparation, curve negotiation, and cooperation with long steep downhill section;
  - It can describe individual driver behavior with a driver-dependent parameter set;
  - It is based on the Gipps' behavioural car-following model.

Future Achievements

- This effort is postponded in FY14 but the following future achievements can be made after it resumes:
  - To bring actual driving behavior with different powertrain architectures into vehicle simulation;
  - To gain a better insight into power demand for facilitating designs to maximize the potential for fuel efficiency improvement;

✧ ✧ ✧ ✧ ✧

V.O.2. Technical Discussion

Background

Driver is a key component in vehicle simulation. An ideal driver model should be able to mimic human driving patterns along a given route. There are simulation packages having the capability to simulate driver behavior. However, it is rare documented how they work with road profiles. As a result, driver-independent or even questionable fuel consumption estimation may be offered.

Observing from the HTDC data, individual driver could make different fuel efficiency while they travelling through a same route. To make a clear case, this project first challenged an issue about how truckers would drive through a curry hill interstate section with a long steep downhill segment. A new truck driver model therefore has been developed based on the Gipps' car-following model. With a calibrated driver-dependent parameter set, the proposed model can describe how the driver may work with road features including a combination of grade and curvature. The preliminary results not only show a reliable estimation of speed profile but also point out the needs for considering driver in a vehicle simulation.

Introduction

Driver in vehicle simulation

The capability to incorporate real driving behavior into vehicle simulation for verification and validation of contemporary vehicle system design is important in evaluating how a system may perform under human drivers' control. It was already stated in the 1960s that automobile and driver form a closely coupled man-machine system and must consequently be treated as a whole [1]. However, the major concern and focus of vehicle simulation, with a large number of technical publications in mind, remained on the vehicle. The need for capable driver models can be noted in literature, e.g., [2-5], but the products are still insufficient. One of the unsolved issues is to mimic truck driving along a curvy, hilly route with a long, steep downhill section.

Due to distinctive demands on the models in accordance with different kinds of applications, a variety of driver models is available. Plöchl and Edelmann [2] provided a comprehensive overview of driver model with respect to their application and different modeling approaches. They grouped the applications into four categories after defining driving task and environmental situation. In applications with focus on the vehicle, a driver model is mainly required to resolve given driving tasks, i.e., for closed-loop tests and simulations. Most of these models have been developed to control lateral vehicle dynamics which is often simply kept to follow a given speed profile rather independent from the steering task of the driver. On the other hand, interest and concern of applications with

focus on the driver are related to typical driver tasks for a better understanding of individual driver behavior. Path and speed planning as an internal driver task may be a priori incorporated in these applications. Applications with focus on combination of vehicle and driver consider reactions of the systems to driver behavior, e.g., vehicle handling dynamics with respect to driver, or design criteria from the driver point of view including accident avoidance, active safety, and driver support systems. Applications with focus on the environment and traffic, like car-following, consider the environment of the vehicle and driver combination in particular the interaction with one or more other vehicles. Car-following forms one of the main processes in all microscopic simulation models as well as in modern traffic flow theory, which attempts to understand the interplay between phenomena at the individual driver level and global behavior on a more macroscopic scale [6]. Since influence of environment is taken into consideration, models from the car-following family may bring a more realistic driving behavior, on a kinematic basis, into vehicle simulation.

As a matter of fact, to negotiate road features is so important that it has drawn attention in different fields. Modern road features are usually designed based on selected design speeds. Studies (e.g., [7], [8]) discussed the relation between road design and speed behavior because driving speed does not always agree with the design speed. Ottesen and Krammes [9] proposed a speed-profile model for estimating the speed reduction from an approach tangent to a horizontal curve with the regression equations for 85th percentile speeds on curves. They found that the degree of curvature, the length of curvature, and the deflection angle had a statistically significant effect of curve speeds. With experiments on a test track and a driving simulator, Reymond et al., [10] modeled lateral acceleration in curve driving to describe the maximum speed choice behavior in curves as an adjustment of their perceived lateral acceleration according to a dynamic safety margin. Their model predicted a quadratic decrease of maximum vehicle lateral acceleration with driving speed. Adamatsu et al., [11] reported that driving behavior changes in reverse curves were caused by the road structure. In their experiments with a driving simulator, the combination of reverse curve and dip might affect the driver's behavior and analysis of timing of the accelerator decrease showed that the changes occurred when the vehicle approached the reverse point of the curve. These observations indicate that real drivers may prepare to negotiate road features. However, the behavior of preparedness is rare addressed in driving models.

In addition to road design and safety point of view, the behavior to negotiate road features has also been considered in studies looking for a better fuel economy, especially for heavy duty trucks. Road grade can be identified as a major factor for this type of analysis. According to American Association of State Highway and Transportation Officials (AASHTO) [12], trucks generally increase speed by up to about 5% on downgrades and decrease speed by 7% or more on upgrades as compared to their operation on level. A 3D road geometry based optimal control system was designed by Huang et al. [13] to minimize class 8 trucks' fuel consumption and travel time. 1.09% to 2.6% savings in fuel consumption with about 0.5% longer travel time were reported according to their simulation results. Hellström et al., [14] developed a fuel-optimal control algorithm for heavy diesel trucks which utilizes information about the road topography ahead when a route is given. According to the test results on a 120-km segment of a Swedish highway, the look-ahead controller, focusing on road topography ahead, facilitated a decrease of 3.5% (in average) in fuel consumption without increasing the trip time and the number of gear shifts decreased 42% in traveling back and forth, compared to the standard cruise controller.

Speed choice with road features

Factors affecting speed decision can be varied. A fundamental relation for vehicle operation on a horizontal curve developed from the laws of mechanics may look like what Schurr et al., [15] mentioned in Equation 1.

$$R_{min} = \frac{v^2}{127(0.01e+f)} \quad (1)$$

where

R_{min}: minimum radius (m),

e: superelevation (%)

f: side friction factor (dimensionless), and

v: design speed (km/h)

Equation 1 represents a minimum radius by which a motorist can comfortably traverse a horizontal curve at the design speed, for a given maximum superelevation rate and allowable side friction factor. It implies a straightforward but important fact, that is, a vehicle in real world may run out of road if the road features was not taken into consideration. Therefore, road features should be considered when a real driving behavior is simulated.

A traditional method to determine the relation for all the operating speed parameter equations was a stepwise multiple linear regression using the backward variable selection process. With the regression approach, Schurr et al., [15] developed equations for speed estimation at curve approach and midpoint locations, like

$$V_{85,approach} = 70.2 + 0.434V_p - 0.001307T_{ADT} \quad (2)$$

$$V_{85,midpoint} = 103.3 - 0.1253\Delta + 0.0238L - 1.039G \quad (3)$$

where

$V_{85,approach}$: the 85th percentile speed (km/h) of free-flow passenger cars at the approach location

V_p: posted speed (km/h)

T_{ADT}: number of vehicle per day

$V_{85,midpoint}$: the 85th percentile speed (km/h) of free-flow passenger cars at the curve midpoint

Δ: deflection angle (decimal degrees)

L: length of curve (m)

G: road grade (%)

Although the mathematical forms can be very different, regression equations like Eq. (2) and Eq. (3) (e.g., [16]-[19]) provide snapshots of speed distribution at associate studying sites with a consideration of variety variables. Relation between speed and road features at curve can be described by these empirical models. However, these models have to be calibrated with data collected from a study site for localized

results. In addition, data like posted speed and average daily traffic could change over time. It can prevent the models from generating realistic results. A major challenge to adapt these models in vehicle simulation is their nature of stepwise. For example, Eq. (2) can be used for estimation of operating speeds on the tangent segment in advance of the curve where it is expected that drivers are traveling at speeds they wanted. The challenge is when the simulation should switch from Eq. (2) to Eq. (3). It can be an art because how to define the length of tangent segment is unclear, not to mention a real driver can barely identify a start of curve.

More comprehensive driver models considered the reciprocal relationship between lateral acceleration and vehicle speed in general curve driving situations. It was observed in [10] and [20]-[22] about that the lateral acceleration decreases monotonically as the vehicle speed increases in steady turns with various degrees of road curvature. Reymond et al. [10] suggested that the phenomenon might represent drivers' risk taking behavior because the influence of errors in the estimated road curvature is intensified as the vehicle speed increases and it decreases the available safety margin. Allen et al. [23] discussed concepts of steering and speed behavior control and reported a driver model implemented in a nonlinear vehicle dynamics simulation referred to as VDANL (Vehicle Dynamics Analysis NonLinear). However, it had an issue of brake overheating and fade while simulating a heavy truck operation in downgrades. With the driver model, brake overheating causes brake fade while the heavy vehicle traveling along a 4-mile, 5% downgrade section which overwhelms speed control and results in increasing speed then leads to rollover. Using a similar approach, Yu and Ozguner [24] reported development of a two-loop steering control structure with look-ahead yaw rate feedback perception control, proportional-integral (PI) stabilizing compensation, and proportional-integral-derivative (PID) speed control to achieve a trajectory matching task for heavy truck simulation in VDANL. A good matching result was reported in graph but neither error measurement nor road feature information is provided in their paper.

Approach

Since interaction with driving environment is a major objective to the development, car-following models, as discussed in the Introduction section, may offer a proper solution. In microscopic traffic simulation, car-following models (e.g., [25]-[27]), defined by ordinary differential equations, describe the complete dynamics of the vehicles' positions and velocities. As summarized by Brackstone and McDonald [6], a typical linear car-following model is

$$a_f(t) = K_v \Delta v + K_d \Delta d \quad (4)$$

where

a_f: the vehicle acceleration,

Δv: relative speed,

Δd: distance error,

K_v and K_d are driver control gains, determined by the individual driver, road conditions and traffic flow.

Rooted in the typical form as Eq. (4), studies like [28] and [29] show values of car-following models in fuel economy and driver behavior analysis, for heavy duty trucks. After investigating several candidate models, including the optimum velocity model [26] and the intelligent driver model [27], with a consideration of free-flow driving behavior, the Gipps model [25] is selected as the baseline driving model for this study. Assuming the drivers will travel as close to their desired speed as possible and considering the dynamics limitations, the speed of vehicle n at time t+T in the Gipps model can be expressed as,

$$u_n(t+T) = min\left\{u_n(t) + 3.6\left[2.5a_{max}T\left(1 - \frac{u_n(t)}{U_n}\right)\sqrt{0.0025 + \frac{u_n(t)}{U_n}}\right], 3.6\left[-bT + \sqrt{b^2T^2 + b\left\{2[s_n(t) - L_{n-1}] - \frac{u_n(t)}{3.6}T + \frac{u_{n-1}(t)^2}{3.6^2 \times b'}T\right\}}\right]\right\} \quad (5)$$

where

$u_n(t)$: speed of vehicle n at time t (km/h),

a_{max}: maximum desired acceleration rate of vehicle n (m/s^2),

T: driver's reaction time (s),

U_n: desired speed of vehicle n,

b and b': deceleration parameters of vehicle n (m/s^2),

L_{n-1}: the effective length of vehicles n-1 (m),

$s_n(t)$: the spacing between vehicle n and n-1 at time t (m),

$u_{n-1}(t)$: speed of the preceding vehicle n at time t (km/h).

It is worthwhile to note that the desired speed for a driver in Eq. (5) is a constant. To take road features into the consideration, it is assumed that the desired speed will be adjusted according to road features. This assumption reflects what a human driver may do in actual roads and is supported by literature as discussed previously.

Instead of degree of curvature, a concept of "critical portion" mentioned in [30] is adapted to incorporate curve speed decision with the Gipps model. The critical portion of a curve is defined as the section that has a radius and superelevation rate that combine to yield the largest side friction demand. Unless a curve is truly circular for its entire length, the associated critical portion will not have the same radius estimate as those made in other portions of the curve. The deflection angle associated with a "critical portion" is referred to the "partial deflection angle" which is defined as difference between consecutive compass headings. To adjust the desired speed accordingly, the "partial deflection angle" is used along with a given route. In considering road grade and curvature simultaneously, an empirical adjustment factor for the desired speed is introduced as,

$$f_{road} = \left(1 - p_g \sin\varphi\right)\cos\omega \quad (6)$$

where

p_g: driver-dependent parameter for the effect of road grade,

φ: road grade (rad),

ω: partial deflection angle (rad).

With the adjustment factor, the enhanced Gipps model has the term of desired speed as,

$$U_{en} = U_n \times f_{road} \quad (7)$$

With Eq. (7), the enhanced Gipps model considering the desired speed adjustment is able to explain speed transitions while negotiating road features. However, the enhancement is still not able to explain the speed decision on a long steep downhill section during a trip. In reality, derivers usually slow down while travelling through such a section, especially when driving heavy-duty trucks. As discussed in [31]-[32], heavy-duty trucks have to reduce their speeds significantly to avoid brake overheating and fade while travelling on long downgrades. To mimic truck driving on a long steep downhill section during a trip, a look-ahead decision-making algorithm for further reducing the adjustment factor is developed. The look-ahead steps are assumed depending on the length of the long steep downhill section. A pseudocode of the algorithm is provided as,

$$f_{road} = f_{road} \times p_{lsd}, when\ u_n(t) < \gamma U_n\ and\ \sum f_{ri} \geq \sum i \quad (8)$$

where

p_{lsd}: driver-dependent parameter for the effect of long steep downgrades,

γ: driver-dependent parameter for the speed reduction at long steep downgrades,

i: the i step of look-ahead,

f_{ri}: the adjustment factor at the i step of look-ahead.

Parameter Estimation

Truck driving data, collected in an 89 kilometers section of I-40 near Ashville, NC area from a Heavy Truck Duty Cycle (HTDC) project [33], were used to estimate parameters for the proposed model. Figure V-137 shows the road section where the data were collected and the associated elevations. Major curves and grades along the route can be observed in the figure. The red down arrow on the map indicates the highest point along the road section as well as the start of a long steep downhill section. Length of the long downhill section is slightly over 7 kilometers.

Results

With the look-ahead decision-making algorithm as described in Eq. (8), Figure V-138 shows speed profile estimated by the proposed model using a set of calibrated parameters for the trucker #3. The red line represents the simulated speed profile, the blue for observed speeds, and the green for elevations (referring to the right vertical axle). As shown in Figure V-138, the proposed model captures most of speed transitions for the entire trip. The coefficient of determination is 0.93 for the model along the 88.87 km route. The discrepancy in total distance travelled is 132.75 meters which is about 0.15% more than the observed data. Therefore, not only the impact of a combination of road grade and curvature but also the effect of a long steep downhill section for truck driving are described reasonably by the proposed model.

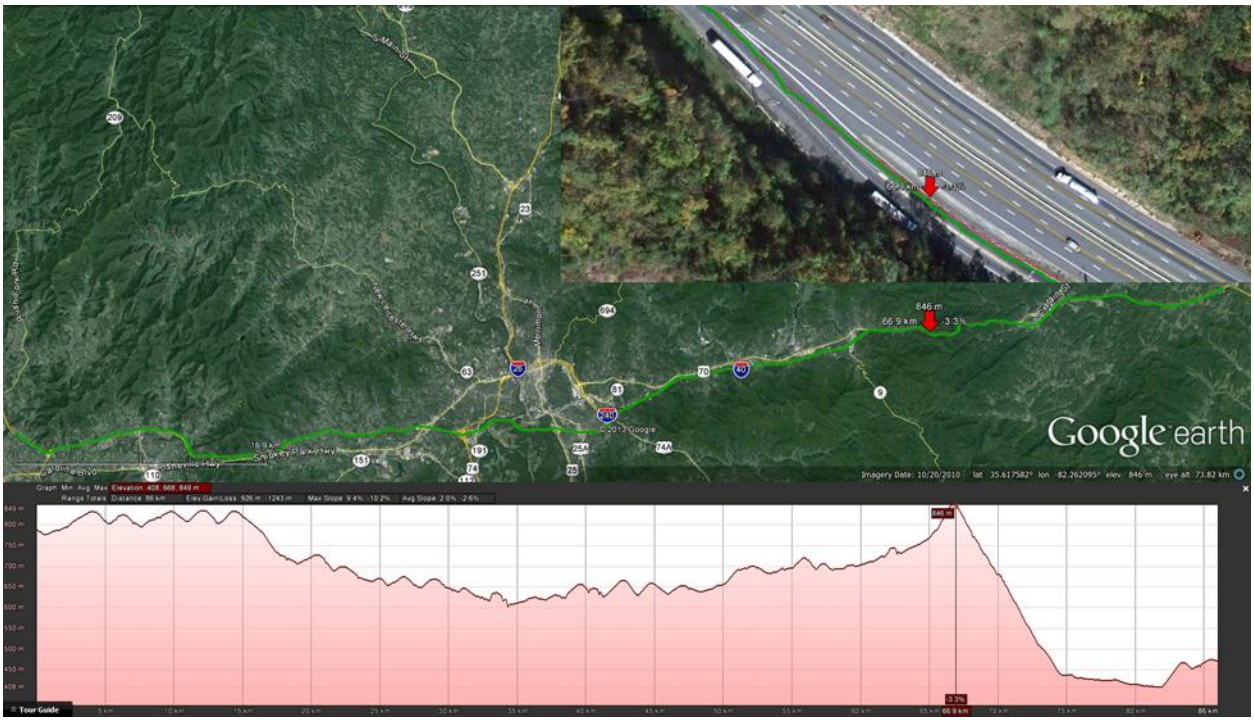

Figure V-137: The section studied, an 89-km section of I-40 near Ashville, NC area.

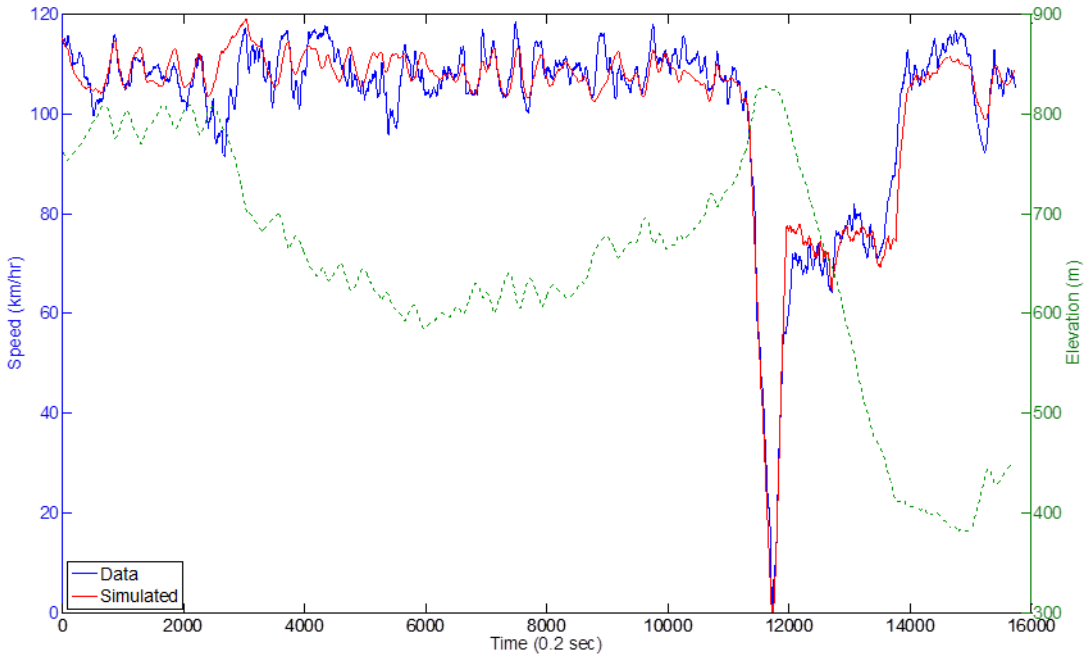

Figure V-138: Speed profile simulated by the proposed model (in Red) vs. observed data (in blue).

A performance comparison of the three models is summarized in Table V-15. As shown previously, the proposed model has the highest coefficient of determination which indicates the least error variance in the estimation. The row of root mean square error (RMSE) is added to Table V-15 as another measure of the differences between speeds estimated by the models and the observed ones. According to values of RMSE, the proposed model has the best fit in the speed estimation. It is worthwhile to note that only the column of the proposed has estimations for the entire 88.87-km trip in Table V-15. Because the other two models have significantly unrealistic estimations after the planned stop, it is meaningless to make a comparison under the circumstance.

Table V-15: Comparing the models' prediction to the data.

Performance of Models	Original Gipps*	Enhanced Gipps*	The Proposed
R^2	0.86	0.86	0.93
RMSE (km/hr)	11.99	14.94	4.76
Discrepancy of total distance travelled (m)	-138.49	275.51	132.75
Discrepancy of total distance travelled (%)	-0.20%	0.40%	0.15%

* Not comparing the entire trip but only the portion before preparation of stop

Conclusions

A truck driving model incorporating the impact of road grade and curvature is proposed for mimicking a more realistic driving behavior in vehicle simulation. The newly proposed model can perform starting from rest, slowing down to a stop, cruising, negotiating road grade and curvature as well as their combination, and travelling through long steep downhill sections in a reasonable manner. These competencies are critical to make the proposed model being a better agent of trucker for vehicle simulation. An implement of the proposed model, calibrated with field data collected from an 89-km hilly interstate section, has been demonstrated. Measures, including the coefficient of determination, root-mean-square error of speed, and discrepancy in total distance travelled, of the simulation show that most speed transitions in the example can be explained by the proposed model based on changes of road features along the freeway segment. These indices support that the proposed model has good capability in explaining the proportion of the variance in observed speed data which is critical to vehicle simulation.

References

1. Rashevsky, N. “Neglected Factors in Highway Safety,” University of Michigan Mental Health Research Institute, Grant GM-12032-01, 1966.
2. Plöchl, M. and Edelmann, J. “Driver Models In Automobile Dynamics Application,” Vehicle System Dynamics, 45(7-8), pp. 699-741, 2007.
3. MacAdam, C.C. “Understanding and Modeling the Human Driver,” Vehicle System Dynamics, 40(1–3), pp. 101–134, 2003.
4. Ranney, T. A. “Models of Driving Behavior: A Review of Their Evolution,” Accident Analysis & Prevention, 26(6), pp. 733–750, 1994.
5. Reid, L. D. “A Survey of Recent Driver Steering Behavior Models Suited to Accident Studies,” Accident Analysis and Prevention, 15(1), pp.23–40, 1983.

6. Brackstone, M. and McDonald, M. “Car-following: a historical review,” Transportation Research Part F: Traffic Psychology and Behaviour, 2(4), pp.181–196, 1999.
7. Martens, M. H., Comte, S., & Kaptein, N. A. The Effects of Road Design on Speed Behavior: A Literature Review (TNO report TM-97-B021). Soesterberg, the Netherlands: TNO Human Factors Research Institute, 1997.
8. Abdelwahab, W. and Morral, J. “Determining Need for and Location of Truck Escape RAMPS,” J. Transp. Eng., 123(5), pp.350–356, 1997.
9. Ottesen, J. L. and Krammes,R. A. "Speed-Profile Model for a Design-Consistency Evaluation Procedure in the United States," Transportation Research Record, 1701, pp.76-85, 2000.
10. Reymond, G., Kemeny, A., Droulez, J. and Berthoz, A. "Role of Lateral Acceleration in Curve Driving: Driver Model and Experiments on a Real Vehicle and a Driving Simulator," Human Factors, 43(3), pp. 483-495, 2001.
11. Akamatsu, M., Imachou, N., Sasaki, Y., Ushiro-Oka, H., Hamanaka, T., and Onuki, M. “Simulator Study on Driver’s Behavior While Driving through a Tunnel in a Rolling Area,” Proceedings of Driving Simulation Conference, Michigan, USA, 2003.
12. American Association of State Highway and Transportation Officials (AASHTO), A policy on geometric design of highways and streets, 6th edition, 2011.
13. Huang, W., Bevly, D. M., Schnick, S. and Li, X. "Using 3D Road Geometry to Optimize Heavy Truck Fuel Efficiency," In 11th International IEEE Conference on Intelligent Transportation Systems, pp. 334-339, 2008.
14. Hellström, E., Åslund, J., and Nielsen, L. "Design of An Efficient Algorithm for Fuel-Optimal Look-Ahead Control," Control Engineering Practice, 18(11), pp.1318–1327, 2010.
15. Schurr, K. S., McCoy, P. T., Pesti, G., and Huff, R. "Relationship of Design, Operating, and Posted Speeds on Horizontal Curves of Rural Two-Lane Highways in Nebraska," Journal Transportation Research Record, 1796, pp.60-71, 2002.
16. Hong, S. and Oguchi, T. "Evaluation of Highway Geometric Design and Analysis of Actual Operating Speed," Journal of the Eastern Asia Society for Transportation Studies, 6, pp.1048-1061, 2005.
17. Bonneson, J., Pratt, M., Miles, J. and Carlson, P. "Development of Guidelines for Establishing Effective Curve Advisory Speeds," Report FHWA/TX-07/0-5439-1, Texas Transportation Institute, College Station, Texas, 2007.
18. Chen, X., Lu, M., Zhang, D., Chi, R., and Wang, J. “Integrated Safety Speed Model for Curved Roads,” FISITA 2010 World Automotive Congress, FISITA2010/FISITA2010-SC-O-25, 2010.
19. Esposito, T., Mauro, R., Russo, F., and Dell’Acqua, G. “Operating Speed Prediction Models for Sustainable Road Safety Management,” International Conference on Sustainable Design and Construction (ICSDC), Kansas City, Missouri, March 23-25, 2011, pp.712-721.
20. Felipe, E., and Navin, F. "Automobiles on Horizontal Curves: Experiments and Observations," Transportation Research Record, 1628, pp.50-56, 1998.
21. Levison, W. H., Bittner Jr., A. C., Campbell, J. L., and Schreiner, C. "Modification and Partial Validation of the Driver/Vehicle Module," Transportation Research Record, 1803, pp.52-58, 2002.
22. Odhams, A. M. C., and Cole, D. J. "Models of Driver Speed Choice in Curves," Proceedings of the 7th International Symposium on Advanced Vehicle Control (AVEC), pp. 439-444, 2004.
23. Allen, R., Chrstos, J., Aponso, B., and Lee, D., "Driver/Vehicle Modeling and Simulation," SAE Technical Paper 2002-01-1568, 2002.
24. Yu, Hai, and Umit Ozguner. "Heavy Truck Trajectory Matching and Simulation with VDANL." Proceedings of the American Control Conference, Denver, Colorado, June 4-6, 2003. vol. 6, pp. 4693-4698, 2003.
25. Gipps, P.G. "A behavioural car-following model for computer simulation," Transportation Research Part B: Methodological, 15(2), pp.105–111, 1981.
26. Bando M., Hasebe K., Nakayama A., Shibata A. and Sugiyama Y. “Dynamical Model of Traffic Congestion and Numerical Simulation”, Phys. Rev. E, 51(2), pp. 1035-1042, 1995.
27. Treiber, M., Hennecke, A., and Helbing, D. “Congested Traffic States In Empirical Observations And Microscopic Simulations,” Phys. Rev. E, 62(2), pp.1805–1824, 2000.
28. Zhang, J. and Ioannou, P. “Control of Heavy-Duty Trucks: Environmental and Fuel Economy Considerations,” California PATH Program, Inst. Transp. Studies, Univ. California, Berkeley, California PATH Research Rep. UCB-ITS-PRR-2004-15, 2004.
29. Li, S., Wang, J., Li, K., Lian, X., Ukawa, H., Bai, D. "Modeling and Verification Of Heavy-Duty Truck Drivers’ Car-Following Characteristics," International Journal of Automotive Technology, 11(1), pp.81-87, 2010.
30. Bonneson, J., Pratt, M., Miles, J. and Carlson, P. ”Horizontal Curve Signing Handbook,” Report No. FHWA/TX-07/0-5439-P1., October 2007.
31. Myers, T. T., Ashkenas, I. L., Johnson, W. A. "Feasibility of a grade severity rating system: Final Report," FHWA-RD-79-116, August 1980.
32. Fancher, P., Winkler C, and Campbell, M. "The Influence of Braking Strategy on Brake Temperatures in Mountain Descents," Report No. UMTRI-92-11, The Univ. of Michigan Transp. Res. Inst., Ann Arbor, Mich., 1992.
33. Capps, G., Franzese, O., Knee, B., Lascurain, M. B., Otaduy, P., Class-8 Heavy Truck Duty Cycle Project Final Report, ORNL/TM-2008/122, Oak Ridge National Laboratory, 2008.

V.O.3. Products

Publications

1. Li, J-.M. and Smith, D. “Modeling the Impact of Road Grade and Curvature on Truck Driving for Vehicle Simulation.” Paper abstract accepted for publication at the 2014 SAE World Congress and Exhibition, Paper number #14M-0227.

Patents

None to report

Tools and Data

1. The proposed truck driving model.

V.P. Benchmarking of Advanced Technology LD Vehicles: MY 2012 Ford Focus Battery Electric Vehicle

Eric Rask, Principal Investigator
Argonne National Laboratory
9700 S. Cass Avenue
Argonne, Il, 60349
Phone: (630) 252-3110
E-mail: erask@anl.gov

Lee Slezak, DOE Program Manager
Phone: (202) 586-2335
E-mail: Lee.Slezak@ee.doe.gov

V.P.1. Abstract

Objectives

To perform thorough vehicle instrumentation, testing, and analysis on the MY2012 Ford Focus Battery Electric Vehicle. Data collected will be used for a wide range of tasks including technology benchmarking and evaluation, simulation validation, advanced vehicle component evaluation, and vehicle testing procedure development and validation.

Major Accomplishments

- Leveraged previous high-level data collection and insight from other PHEV and BEV testing.
- Performed significant instrumentation development and installation
  - Particular focus on HVAC and accessory loads
- Recorded Controller Area Network (CAN) signals through testing as a means of measuring parameters that would otherwise be too difficult, too expensive, or impossible to obtain
- Ran a broad range of tests for drive-cycle based W-hr/mi, general energy consumption, and performance for vehicle assessment, component evaluation, and technology benchmarking across a range of ambient temperatures and HVAC conditions.
- Analyzed efficiency and vehicle behavior during charge events.

Future Achievements

- Continued data collection leveraging installed vehicle instrumentation. Areas of particular interest include improved component efficiency testing/mapping and vehicle temperature sensitivity testing when exposed to more extreme ambient conditions.

✧ ✧ ✧ ✧ ✧

V.P.2. Technical Discussion

Background

This work revolves around in-depth instrumentation, testing, and analysis of new and emerging vehicle technologies. Vehicles are selected for evaluation on the basis of technical merit for technology assessment and data collection. Vehicles are tested primarily on a chassis dynamometer using state-of-the-art instrumentation and data analysis equipment. Testing and instrumentation plans are specifically developed for each vehicle and reflect specific technical merits and unique features.

Introduction

The vehicle selected for this year's in-depth testing and analysis is the MY 2012 Ford Focus BEV. The vehicle represents one of the most recent fully battery electric vehicle to arrive on the market. The Focus utilizes a single speed gearbox connected to a permanent magnet traction motor to provide all vehicle motive power. Battery power is provided by a li-ion battery capable of supplying 105 kW. As with other electrified vehicles, cabin air-conditioning and heating is done using an electric a/c compressor and electric cabin heater. Additionally, battery thermal management, including both heating and cooling, is done utilizing liquid coolant that can be heated or cooled separately from the cabin. This vehicle also uses a 6.6kW Level-2 charger, which is an increase in power from the roughly 3.3kW chargers seen in several recent vehicles. This increased off-board charging capability is also of interest. Figure V-139 shows the Focus mounted in Argonne National Laboratory's Advanced Powertrain Research Facility in preparation for testing.

Figure V-139: MY 2012 Ford Focus Battery Electric Vehicle.

Table V-16 below summarizes some of the main parameters for the Focus BEV. Namely, the peak power rating of roughly 105 kW for both the traction battery and electric machine. Reported total battery capacity is 23 kW-hr, of which 19.8 kW-hr is usable, which equates to roughly 86% usable battery capacity during a full depletion cycle.

Table V-16: Ford Focus BEV Basic Powertrain Specifications.

MY 2012 Ford Focus BEV	
Vehicle architecture	Single speed BEV (7.82:1 FD reduction ratio)
Test weight	3,750 lbs
Power plant	Main traction motor Permanent magnet 107 kW max reported power 250 Nm max reported torque
Battery	Lithium-ion 23 KWh Total capacity (19.8 Usable) 105 kW Peak observed power 6.6 kW Charger
EPA Label "Fuel" Economy	MPGe: 110 City / 99 Hwy / 105 Cmb.
Performance	Reported 0-60 Time: 9.5 s Top Speed: 84 mph claimed

As more BEVs enter the marketplace, it becomes important to understand these vehicles in detail. In contrast to a Hybrid Electric Vehicle (HEV) or Blended Plug-in Hybrid Electric Vehicle (PHEV), a BEV is more similar to a conventional vehicle in many aspects relating to energy consumption. More specifically, since a BEV uses only electric energy for propulsion, some basic operating characteristics are easier to calculate due to the single-fuel nature of the vehicle. Despite this simplification, many other aspects of BEVs merit in-depth testing and analysis. For example, accessory loads across a range of operating conditions are of particular interest since any power allocated to these loads is taken directly from power that could be used to move the vehicle. Similarly, electrical loads and vehicle behavior related to HVAC and component temperature regulation (especially battery temperature), are also of great importance for a BEV. Lastly, much of this data will be used for in-depth thermal modeling, thus all thermal nodes of importance have been instrumented to provide inlet and outlet temperatures and coolant flow when relevant. With these issues in mind, a great deal of invasive instrumentation was installed in this vehicle in order to assess overall power flows, electrical loads, component operation, and related items. Figure V-141 through Figure V-140 illustrates some of the specific sensors installed in this vehicle. In order to better understand the cabin conditions, an interior humidity/barometric pressure/temperature sensor was installed to better assess the effectiveness and power draw of the vehicle's air conditions across a range of ambient temperatures.

Figure V-140: In-vehicle relative humidity, temperature and pressure sensor.

The majority of component cooling for the Focus is provided by glycol based coolant, in order to assess the operating temperatures of the coolant and understand the losses associated with the various components, in-line coolant temperature sensors were installed across most important thermal nodes of the vehicle. Figure V-141 shows an example sensor, which is mounted directly in the coolant hose to assess the actual operating temperature of the fluid.

Figure V-141: Example coolant temperature sensor installation.

In addition to the temperature sensors, coolant flow was also measured for various sections of the vehicle's overall thermal system. As with temperature, in-line sensors were installed to appropriately assess all coolant flows within the system. Figure V-142 shows an example of this type of sensor installation.

Figure V-142: Example in-line coolant flow sensor.

As mentioned previously, accessory loads are of great interest to a BEV. Figure V-143 illustrates one of the inductive type sensors used to assess various fan and pump currents throughout the vehicle.

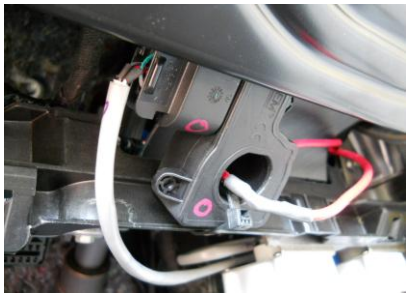

Figure V-143: Example accessory current sensor.

Although only a few highlighted examples are shown in the preceding discussion, the Ford Focus BEV evaluation vehicle was fitted with numerous sensors to better understand both overall vehicle operation as well as component usage and efficiency.

Approach

As discussed in the Background section, vehicles were outfitted with a significant number of sensors to provide a range of information from temperatures to mechanical and electrical power flows. A specific test plan was developed to evaluate the particularly interesting facets of this Battery Electric Vehicle. Testing was done using a vehicle chassis dynamometer and sophisticated instrumentation under laboratory conditions to aid in repeatability, accuracy, and sensitivity.

Results

The following paragraphs discuss some of the noteworthy findings related to the testing of this vehicle. These discussion items represent a small fraction of the information and insight gained during testing and analysis of this vehicle.

Figure V-144 shows the battery energy consumption of the Focus for the UDDS, HWFET, and US06 drive cycles. Moreover, the repeated runs of the UDDS starting from a "cold" start are shown in addition to two "hot" repeats of the HWFET and US06 cycles. While the repeated HWFET and US06 cycles are very repeatable (within 2%), the first UDDS shows roughly 5% higher energy consumption. As with other vehicles, this increased initial consumption is related to the initial conditions of a "cold" soaked vehicle, but the specific allocation of the penalty and causes are somewhat specific to a BEV. Specifically, the additional energy consumption is related to decreased regenerative braking in the first cycle due to an initially fully charged battery as well as general vehicle warm-up related to both vehicle as well as tire warm-up. It is worth noting that these results are similar to the penalty associated with other BEVs tested at Argonne.

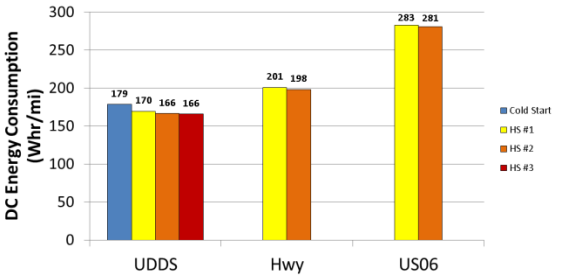

Figure V-144: UDDS, HWFET, and US06 energy consumption.

Figure V-145 shows negative measured battery power for both a "cold" and "hot" run. As mentioned earlier, the initial cycle shows reduced regenerative braking power as indicated by the visible orange spikes which represent increased battery power during braking for operation following the initial "cold" cycle.

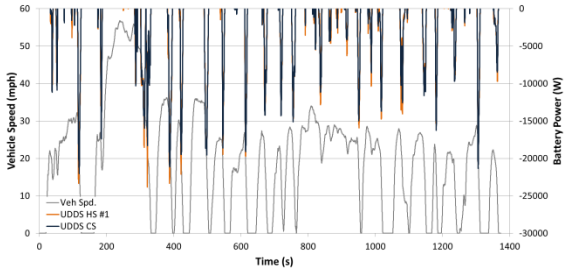

Figure V-145: UDDS Cold-start versus UDDS Hot-Start regenerative braking power.

In addition to the reduced regenerative braking energy recovery, vehicle warm-up and especially tire losses play an important role in the overall vehicle "cold start" penalty. Namely, the colder tire temperatures as shown in Figure V-146 are associated with higher losses and thus contribute to the overall penalty of roughly 5%.

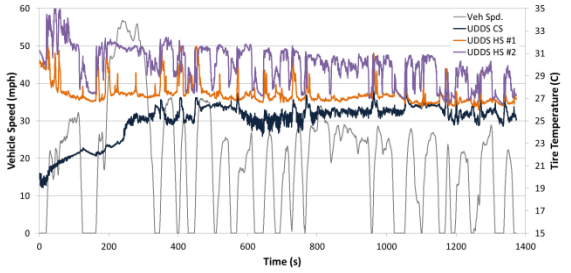

Figure V-146: Tire temperature over repeated UDDS runs.

Another important aspect of overall BEV performance and energy consumption is the operational limits of the vehicle's regenerative braking system. Previous Argonne research identified several key parameters with which to compare different braking envelopes across vehicles. To illustrate these parameters within a typical operating space, Figure V-147 shows the observed axle torque overlaid with the vehicle tractive force at the road. For positive tractive events, axle and tractive loads are roughly proportional since they are roughly scaled by the final drive and tire size, but in the negative quadrant, the regenerative braking envelope can easily be observed at the area in which the tractive force (blue) and axle torque (red) are not roughly proportional and thus not

overlapping. Below roughly 5 mph, no regenerative braking takes place as evidenced by no axle torque and thus no motor power to provide regenerative braking energy. Between 5 and 9 mph, the braking force is ramped in as indicated by increasing, but not overlapping axle versus tractive force points. Finally, beyond 9 mph a maximum regenerative braking force can be observed by the roughly flat axle torque points versus vehicle speed. Beyond roughly 45 mph, regen. power becomes the limitation since the higher speed points show a lower maximum axle torque value.

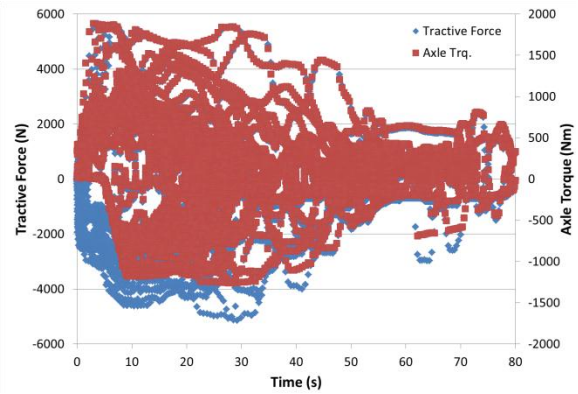

Figure V-147: Ford Focus BEV axle torque and tractive force versus vehicle speed for the UDDS, HWFET, and US06 cycles.

These results are fairly consistent with other BEV and PHEV observation, but the relative *g* level of the maximum regenerative braking force as well as the ramp-in parameters are interesting to observe across several vehicles. These parameters are shown in Table V-17 which provides values for both the Ford Focus as well as several other electrified vehicles.

Table V-17: Regenerative braking envelope parameters for a variety of vehicles.

	Estimated Regen Ramp-In Speed (mph)	Estimated Speed @ Max Regen Force (mph)	Max. Estimated Regen Axle Force (g)
MY 2010 Prius	4	8.5	-0.19
MY 2011 Hyundai Sonata	5	12	-0.25
MY 2012 Chevrolet Volt	2	6.5	-0.20
MY 2012 Ford Focus BEV	**5**	**9**	**-0.22**

Another interesting research aspect of this vehicle is the difference between the dynamometer estimated energy consumption as compared to the estimates provided by the vehicle's fuel/energy economy window sticker. Several adjustments are made to increase the observed energy consumption of a particular vehicle in an attempt to better capture the real-world overall energy usage of this vehicle. These adjustment steps are shown in Figure V-148. The first adjustment increases the tested energy economy by 30% to estimate real-world-to-test variation in energy economy due to driving style. It is worth noting that the actual in-service adjustment is a topic of much research and debate. As second adjustment of 9.5% is also applied to account for losses that cannot typically be simulated on a chassis dynamometer. Lastly, the DC battery energy consumption is increased by the specific charging efficiency, resulting in the overall AC kW-hr per distance estimate. As seen in the figure below, the APRF testing shows very similar results to the EPA labeling, especially for the UDDS which is within rounding to the EPA estimate. The HWFET cycle results are slightly higher, but still very much in line with the EPA estimates. Factors such as actual vehicle losses, 12V using operation, and several other factor likely account for the differences and are still being evaluated.

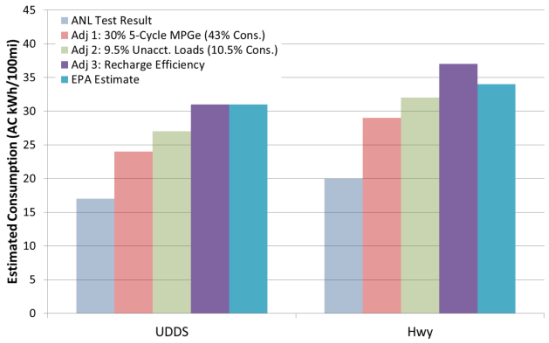

Figure V-148: Walkup of battery energy consumption to EPA adjusted label energy consumption.

In the previous section, a 30% energy economy penalty was applied to account for real-world vehicle driving, but the accuracy of this adjustment factor is still a heavily researched topic. Figure V-149 seeks to expand on this topic by comparing the standard UDDS and HWFET cycles to their more aggressive US06 subsection counterparts for three vehicle technologies. Interestingly, the penalty associated with more aggressive UDDS driving is similar between HEVs and BEVs despite differing behaviors in response to more aggressive driving. The HWFET impacts of more aggressive driving for a BEV are quite a bit less as compared to those of the HEV Prius results. With these two issues in mind, it suggests that a true BEV adjustment might need to differ between the UDDS and HWFET cycles, give the different penalty behaviors. While just a quick example, this highlights one of the most interesting facets of BEV research, namely, what is a true real world adjustment for the in-use electrical consumption of these vehicles.

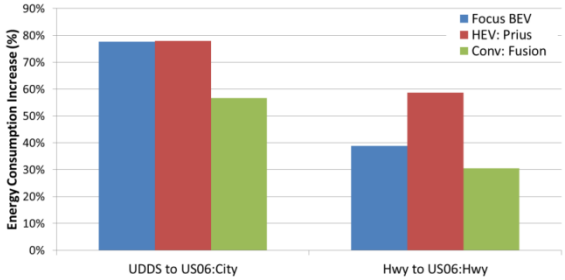

Figure V-149: Penalties associated with more aggressive driving for a range of vehicle technoligies.

Figure V-150 shows some very basic data from a UDDS run at 95F with the climate control set to 72F. The compressor power, plotted in orange, shows a large preliminary spike that corresponds with the increased HVAC power draw to bring the initial cabin tempter down to the set point. Following this increased loading, the A/C system draws roughly 500 watts of power to maintain cabin temperature.

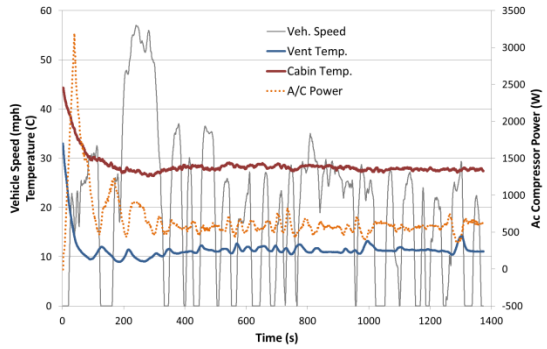

Figure V-150: Cabin temperature, vent temperature and A/C compressor power during A/C pull-down at 95F ambient.

As mentioned previously, this data and analysis is only a brief snapshot of the work that has gone into the testing and analysis of the Ford Focus BEV. Moreover, it is expected that this data will be used in more upcoming analysis by Argonne as well as many other interested parties.

Conclusions

As with previous years, a significant amount of time and effort was spent on the instrumentation, testing, and analysis of the MY 2012 Ford Focus BEV. Specific instrumentation was developed to evaluate the most noteworthy aspects of the vehicle. Additionally, testing was tailored to BEV testing issues in order to efficiently and effectively benchmark and evaluate this type of vehicle. The results and analysis contained in this report represent a small but important subset of the entire project. Research regarding these as well as additional hybrid vehicles should continue, given the ever-charging dynamics of the advanced vehicle marketplace. For more in-depth work regarding this and many additional advanced vehicles, the reader is pointed toward the *Argonne Downloadable Dynamometer Database:* (http://www.transportation.anl.gov/D3/)

V.P.3. Products

Publications

1. Rask, E., Santini, D., and Lohse-Busch, H., "Analysis of Input Power, Energy Availability, and Efficiency during Deceleration for X-EV Vehicles," *SAE Int. J. Alt. Power.* 2(2):350-361, 2013, doi:10.4271/2013-01-1473.
2. Lohse-Busch, H., Duoba, M., Rask, E., Stutenberg, K. et al., "Ambient Temperature (20°F, 72°F and 95°F) Impact on Fuel and Energy Consumption for Several Conventional Vehicles, Hybrid and Plug-In Hybrid Electric Vehicles and Battery Electric Vehicle," SAE Technical Paper 2013-01-1462, 2013, doi:10.4271/2013-01-1462.
3. Kim, N., Duoba, M., Kim, N., and Rousseau, A., "Validating Volt PHEV Model with Dynamometer Test Data Using Autonomie," *SAE Int. J. Passeng. Cars—Mech. Syst.* 6(2):985-992, 2013, doi:10.4271/2013-01-1458.

MEDIUM and HEAVY DUTY

V.Q. Long-Haul Truck Thermal Load and Idle Reduction

Jason A. Lustbader
National Renewable Energy Laboratory
15013 Denver West Parkway
Golden, CO 80401
Phone: (303) 275-4443
E-mail: Jason.Lustbader@nrel.gov

David Anderson and Lee Slezak
Phone: (202) 287-5688 (David Anderson)
E-mail: David.Anderson@ee.doe.gov
Phone: (202) 586-2335 (Lee Slezak)
E-mail: Lee.Slezak@ee.doe.gov

V.Q.1. Abstract

Objectives

- Demonstrate at least a 30% reduction in long-haul truck idle climate control loads with a 3-year or better payback period by 2015
- Collaborate with industry partners in the development and application of commercially viable climate control solutions that minimize long-haul truck rest period idling
- Develop technologies that can help reduce the 838 million gallons of fuel used annually for rest period idling to increase national energy security and sustainability.

Major Accomplishments

- Demonstrated a 7.3% reduction in daily air conditioning (A/C) system energy consumption when switching from blue to a color-matched solar-reflective blue paint
- Measured a 12.7% reduction in daily A/C system energy consumption using an idealized cab/sleeper thermal separation barrier in place of the standard sleeper curtain
  - Identified improved sleeper curtain design opportunity
- Demonstrated a 13.3% reduction in daily A/C system energy consumption using an idealized film to reduce the transmission of solar energy through the glazings
  - Identified significant opportunity for advanced glazings and improved privacy curtain design
- Developed HVAC emulator experimental apparatus for the direct quantification of heating and A/C thermal loads for climate control in vehicles.

Future Achievements

- Using a combination of solar load reduction, conductive pathway improvement, interior design, and controls, develop full cab thermal design concepts and quantify the impacts on thermal and idle loads
- Develop test methods to improve quantification of cab climate conditioning energy demands
- Use experimental and analysis methods to quantify fuel use and payback period of climate control solutions.

✧ ✧ ✧ ✧ ✧

V.Q.2. Technical Discussion

Background

Cab climate conditioning is one of the primary reasons for operating the main engine in a long-haul truck during driver rest periods. In the United States, long-haul trucks (trucks that travel more than 500 miles per day) use approximately 838 million gallons of fuel annually for rest period idling [1]. Including workday idling, over two billion gallons of fuel are used annually for truck idling [2]. Idling represents a zero freight efficiency operating condition for the truck. As awareness of idle fuel use has increased, federal regulations and incentives have been created. An example is the idle reduction technology credit in the Heavy-Duty Greenhouse Gas Emissions Standards, which are set to begin in 2014 [3]. Increased awareness has also spurred implementation of many stringent state and city anti-idling regulations [4].

By reducing thermal loads and improving the efficiency of climate control systems, there is a great opportunity to reduce fuel use and emissions associated with idling. Enhancing the thermal performance of cab/sleepers will enable smaller, lighter, and more cost-effective idle reduction solutions. In addition, if the fuel savings from new technologies provide a one- to three-year payback period, fleet owners will be economically motivated to incorporate the new technologies. Therefore, financial incentive provides a pathway to rapid adoption of effective thermal load and idle reduction solutions.

Introduction

The U.S. Department of Energy's National Renewable Energy Laboratory's (NREL's) CoolCab project is researching efficient thermal management systems to maintain cab occupant comfort without the need for engine idling. The CoolCab project uses a system-level approach that addresses thermal loads, designs for occupant thermal comfort, and maximizes equipment efficiency. In order to advance the goals of the CoolCab project and the broader goals of increased national energy security and sustainability, the CoolCab team works closely with industry partners to develop and apply

commercially viable solutions to reduce national fuel use and industry costs.

Approach

NREL is closely collaborating with original equipment manufacturers (OEMs) and suppliers to develop and implement a strategic approach capable of producing commercially viable results to enable idle reduction systems. This three-phased approach was developed to evaluate commercially available and advanced vehicle thermal management and idle reduction technologies. The three phases, illustrated in Figure V-151, are: Baseline Testing and Model Development, Thermal Load Reduction, and Idle Reduction. Each phase features applications of NREL's suite of thermal testing and analysis tools.

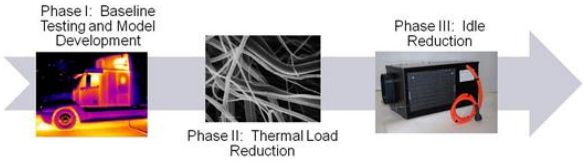

Figure V-151: NREL's three-phase approach.

In Phase I, Baseline Testing and Model Development, thermal data are collected on a test vehicle and on a control vehicle simultaneously. Several days of data are collected for each test procedure under varying weather conditions. The data are used to calibrate the control vehicle to represent an unmodified baseline test vehicle. Once the control vehicle is calibrated to predict the performance of the test vehicle, validation tests are conducted. Validation data are collected with the control and test vehicles under unmodified baseline conditions. Calibration coefficients are applied to the control vehicle validation data, and the results are used to confirm the accuracy of the calibration. After calibration verification, the test vehicle is modified with technologies for Phase II evaluation. Baseline performance data of the test vehicles are also used for development and validation of CoolCalc [5] models.

In Phase II, Thermal Load Reduction, CoolCalc parametric studies are used as a screening tool for potential thermal load reduction technologies. Reductions in cab/sleeper thermal loads are quantified through experimental investigation of selected commercial and advanced technologies identified from CoolCalc modeling.

In Phase III, Idle Reduction, the most promising of the evaluated technologies are researched further by closely collaborating with industry partners and their suppliers to design and evaluate cab thermal packages that improve thermal performance, reduce climate control loads, and enable market penetration of idle reduction systems. In this phase, vehicles are equipped with commercial and advanced cab thermal management packages coupled with an idle reduction system. NREL experimentally characterizes the impact of these technologies on idle loads. CoolCalc analysis and vehicle simulations are also used to characterize the reduction in idle loads and fuel consumption over a wide range of use and environmental conditions.

In order to experimentally characterize the impacts of the technologies being studied, thermal test procedures are conducted in each phase of the project. For technology evaluation in FY 2013, thermal soak and daytime rest period air conditioning testing were utilized.

The test program was conducted at NREL's Vehicle Testing and Integration Facility, shown in Figure V-152, during the months of May through September. The facility is located in Golden, Colorado, at an elevation of 5,997 feet at latitude 39.7 N and longitude 105.1 W. The experimental setup included an NREL-owned test truck and two cab test "bucks." Both bucks were the cab section from a representative truck in current production provided by Volvo Trucks North America. One buck was utilized as the control buck while the other was experimentally modified.

For the experimental setup, the modified truck, test buck, and control buck were oriented facing south and separated by a distance of 25 feet to maximize solar loading and minimize shadowing effects. To keep the buck firewalls from receiving direct solar loads, a firewall shade cloth was implemented on both the control and test bucks. In each vehicle, five curtains were available for use depending on the test being conducted. The curtains available were the privacy, cab skylight, sleeper, and two bunk window curtains.

Figure V-152: NREL's Vehicle Testing and Integration Facility.

A National Instruments SCXI data acquisition system was used to record measurements at a sampling frequency of 1.0 Hz, which was averaged over one-minute intervals. Among the three vehicles, over 140 calibrated type K thermocouples were used. An isothermal bath and reference probe were used for thermocouple calibration, achieving a U95 uncertainty of ±0.32°C in accordance with ASME standards [6]. Air temperature sensors were equipped with a double concentric cylindrical radiation shield to prevent errors due to direct solar radiation.

Weather data were collected from both NREL's Solar Radiation Research Laboratory and NREL's Vehicle Testing and Integration Facility [7] weather station, which together feature more than 160 instruments dedicated to high-quality

measurements of solar radiation and other meteorological parameters.

Thermal soak tests were conducted to evaluate the impact of technologies in an engine-off solar loading condition. This test procedure was used to characterize technology impacts on interior air temperatures in a test truck or buck ($\overline{T}_{modified}$) compared to interior air temperatures in the baseline buck ($\overline{T}_{baseline}$). During summer operation with passive vehicle thermal load reduction technologies, the best possible steady-state performance is to reduce the interior temperature to ambient temperature. The percent of maximum possible temperature reduction (β) was developed to describe this maximum possible reduction in interior air temperature rise above ambient ($\overline{T}_{ambient}$), as described in **Equation 1**. A β value of 0% indicates that the technology under evaluation did not change the rise over ambient temperature, while a β value of 100% indicates the technology reduced the interior air temperature in the modified vehicle to equal the temperature of ambient air in the environment.

$$\beta = \frac{\overline{T}_{baseline} - \overline{T}_{modified}}{\overline{T}_{baseline} - \overline{T}_{ambient}} \cdot 100\% \quad (1)$$

For the evaluation of β, the interior air temperature was determined as a volume weighted average of the combined sleeper and cab air temperatures. The average interior cab air temperature was calculated by averaging six thermocouples with four located in accordance with the American Trucking Association Technology Maintenance Council's recommended practice RP422A [8] as shown in Figure V-153A. Similarly, average sleeper air temperature was calculated by averaging eight thermocouples with six located in accordance with RP422A, illustrated in Figure V-153B. The addition of two thermocouples located in both the cab and sleeper air spaces improved the accuracy of the average air temperature by more accurately capturing the air temperature distribution. During testing, it was determined that the cab footwell air temperature measurements were exposed to occasional direct solar radiation. Due to the increased variability that would occur in the calculation of average interior air temperature, these two measurements were omitted from the calculation.

For the thermal soak testing, data were collected for a time interval from 5:00 AM to 3:00 PM MST. During baseline thermal soak measurements, all privacy curtains were removed. The thermal soak performance of the bucks in their baseline conditions was used to characterize and calibrate the inherent differences between the two bucks and between the control buck and the test truck. Calibration was accomplished by collecting four days of baseline data and generating a time-of-day dependent correction factor between the control buck and test buck and between the control buck and test truck. Solar load intensity peaked at approximately 12:00 PM daily during thermal soak testing. In addition, peak differential temperatures were found to occur within the 11:00 AM to 1:00 PM MST time interval corresponding to this peak solar load. Therefore, interior air and ambient temperatures from 11:00 AM to 1:00 PM MST were used for the calculation of β.

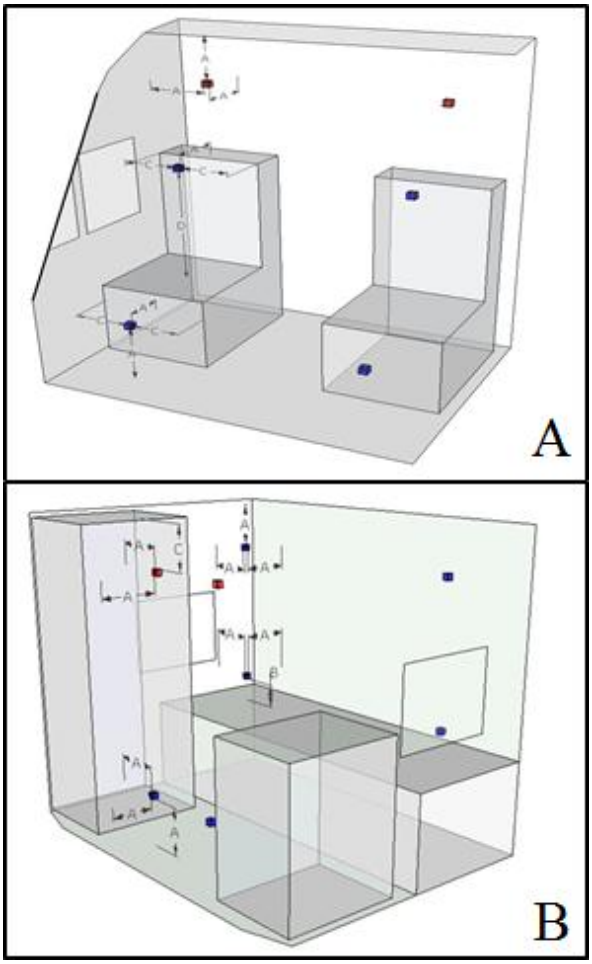

Figure V-153: Cab (A) and sleeper (B) thermocouple locations, blue—TMC standard [8], red—NREL added, dimensions A = 12", B = 6", C = 18".

For quantifying idle load reduction of advanced paints, NREL collaborated with Volvo Trucks North America, PPG Industries, and Dometic Environmental Corporation. Daytime rest period A/C tests were conducted to characterize thermal management technology impacts on an electric no-idle A/C system. A 2,050 W (7,000 Btu/hr) Dometic electric A/C system [0] was installed in the sleeper compartment of each vehicle. For air conditioning experimentation, all five curtains were utilized on the control buck, test buck, and test truck. All curtains were employed to match the expected standard configuration during a rest period operation. The test period was defined as A/C system first-on to last-off to quantify the daily A/C energy consumption. A standard battery-powered A/C system containing four 1,500 W•h lead acid batteries and weighing a total of 132 kg (291 lb) was used for the calculation of system improvements in the results section. A/C electrical power consumption was measured using a Load Controls Incorporated model UPC adjustable capacity power sensor. The power sensor was calibrated to ±15 W. Air conditioning systems were controlled to a target sleeper air temperature of 22.2°C (72°F). Calibration of the modified buck A/C system was performed by collecting multiple days of baseline data. A clear solar day with insignificant cloud cover was required for data to qualify as a baseline test day.

For FY 2013, emphasis was placed on long-haul truck solar envelope and conditioned air volume management. Solar envelope management focuses on the identification of technologies that minimize the penetration of solar energy into the vehicle. Conditioned air volume management seeks to minimize and effectively deliver the conditioned air. For solar envelope management, the impacts of paints and glazings on thermal and idle loads were measured. For conditioned air volume management, an idealized sleeper curtain was evaluated.

Solar Envelope Management

For paint evaluation, experimental testing built off of FY 2012 results, which showed a 20.8% reduction in daily A/C electrical energy load by changing from black to white paint [9]. Since paint color can affect aesthetics and brand identification, advanced paint that has improved thermal performance is of interest. An advanced solar-reflective paint that was color matched to a reference baseline blue color but had an increased solar reflectivity in the infrared spectrum was evaluated.

In addition to the evaluation of paint, the potential impact of improved glazings on idle loads was explored. A white plastic film was applied to all glazing exterior surfaces of the test truck. The applied film allowed for the quantification of the maximum possible idle load reduction that could be obtained from reduced solar transmittance glazing technologies.

Conditioned Air Volume Management

For the idealized sleeper curtain study, a CoolCalc model of a Volvo truck cab was updated to incorporate a heating, ventilating, and air conditioning (HVAC) system. Shading control mechanisms were also added to more effectively model the truck's sleeper and privacy curtains. The improved cab model was used to evaluate the sensitivity of model parameters to the thermal loads on an auxiliary sleeper HVAC system. The model showed that the thermal properties of the sleeper curtain had a strong effect on the thermal load of the HVAC system. Specifically, the thermal and solar reflectivity of the curtain along with the air exchange rate between the cab and sleeper zones were identified as having a strong impact on the magnitude of thermal load required to condition the sleeper air space. The insight gained through model evaluation supported quantification of an effective sleeper curtain for zonal isolation of the sleeper from the front cab. Rest period A/C experimental tests were completed to quantify the maximum possible impact of an improved sleeper curtain design on idle load reduction.

Results

Baseline Testing

To measure the impact of color-matched solar reflective blue paint, thermal soak and A/C baseline data from FY 2012 were utilized [9]. Validation of the test buck thermal soak calibration was within ±0.4°C between the peak solar loading time of 11:00 AM and 1:00 PM MST. The calibration data for A/C paint testing is shown in Figure V-154 and is labeled "2012 Data." After completion of the paint testing, both control and test bucks were repainted a standard white color, and daily electrical A/C baseline data were collected. A comparison of previous (FY 2012) and repainted (FY 2013) baseline data, shown in Figure V-154, indicates the two datasets are not statistically different at the 95% confidence interval. For this reason, the combined baseline results were used for the remainder of FY 2013.

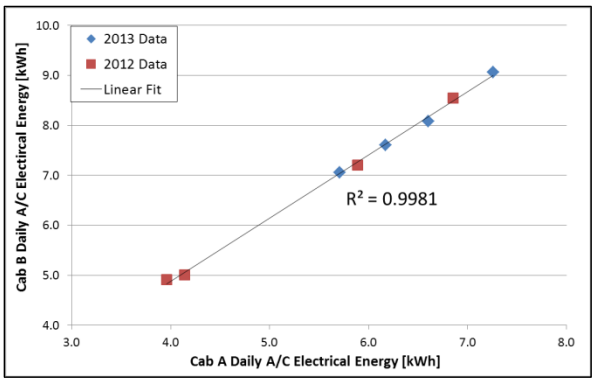

Figure V-154: Daily A/C energy calibration data for test and control bucks before and after paint testing.

Solar Envelope Management

To study the impact of advanced paint on cab air temperatures in thermal soak conditions, blue and color-matched solar-reflective blue paints were provided through partnership with PPG Industries. Radiative properties of black, white, blue, and solar-reflective blue paints were quantified. Figure V-155 shows the reflectance spectra in the ultraviolet, visible, and infrared (IR) regions as well as solar-weighted reflectivity and absorptivity. The reflectance spectrum of blue and solar-reflective blue show identical behavior throughout the visible spectrum (380–750 nm) followed by a sharp increase in reflectance for solar-reflective blue in the IR region.

Paint Color	Black	Blue	SR Blue	White
Total Hemispherical Emittance @ 20°C	0.951	0.950	0.948	0.953
Solar Weighted Reflectivity	0.047	0.120	0.258	0.628
Solar Weighted Absorptivity	0.953	0.880	0.742	0.372

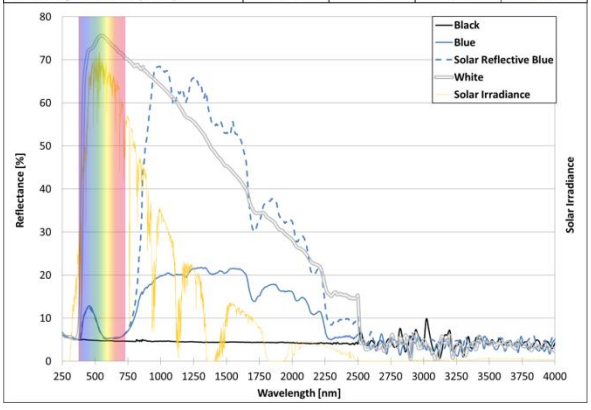

Figure V-155: Select weighted radiative properties and reflectance spectrum for paint colors used in testing.

Thermal soak testing of blue and solar-reflective blue exterior surfaces showed a percent of maximum possible temperature reduction of β = 6.0% during peak solar loading from 11:00 AM–1:00 PM MST. The average interior air temperature for blue and solar-reflective blue during thermal soak conditions are shown in Figure V-156A. In addition to

experimental testing, CoolCalc modeling was performed using the test day's weather as input. Model predicted average interior air temperatures are provided in Figure V-156B. The model predicted a maximum possible temperature reduction of β = 6.2%, which closely matched experimental results.

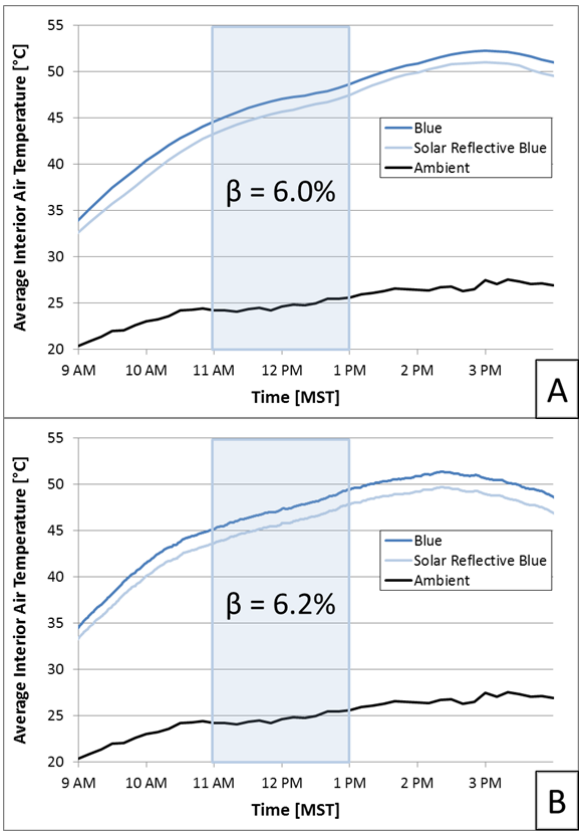

Figure V-156: Thermal soak results with blue and solar-reflective blue opaque surfaces. A—Experimental results, B—CoolCalc model results.

Idle load reduction testing showed the average daily A/C electrical load was reduced by 563 W•h, representing a 7.3% savings going from blue to solar-reflective blue paint. A 563 W•h reduction in daily electrical energy equates to a 9.4% reduction in battery capacity and 12.4 kg (27.3 lb) reduction in battery weight.

To quantify the potential impact of improved glazings on idle loads, a white plastic film was applied to all glazing exterior surfaces of the test truck. For the baseline configuration, all curtains were used. For the film configuration, all privacy curtains were open and the sleeper curtain was closed. A plot of hourly average A/C electrical power with and without the glazing film is shown in Figure V-157. The average daily A/C electrical load was reduced by 13.3% with plastic film covering the truck's glazing surfaces.

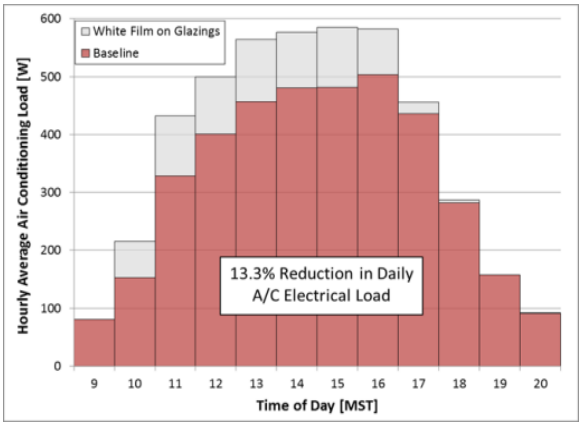

Figure V-157: Hourly average A/C electrical power with and without film over glazing exterior surfaces.

Conditioned Air Volume Management

Minimizing the conditioned air volume is a potential strategy for idle load reduction. Curtains are typically employed to separate the sleeper compartment from the front cab, but design criteria are typically focused on privacy and light mitigation. In order to quantify the maximum possible impact of a sleeper curtain designed for rest-period idle load reduction, a thermal barrier was placed between the sleeper and front cab in place of the standard sleeper curtain. The thermal barrier consisted of 1-inch-thick rigid polyisocyanurate foam insulation with thermal conductivity of 0.024 W/m-K and included a foil radiant barrier on both sides of the panel.

Hourly average A/C electrical loads for the test cab with the ideal sleeper curtain and baseline condition (stock curtain) are shown in Figure V-158. The ideal sleeper curtain reduces rest-period idle loads significantly during the daytime under peak solar loading conditions, resulting in a 12.7% reduction in daily A/C electrical load. The 12.7% reduction corresponds to a 1,153 W•h reduction in electrical energy, 19.2% reduction in standard battery pack size, and 25.4 kg (55.9 lb) reduction in mass.

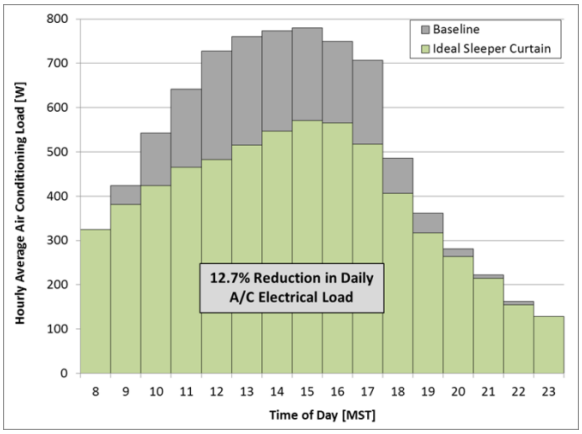

Figure V-158: Hourly average test cab air conditioning power consumption using stock (baseline) and ideal sleeper curtains.

Experimental Capabilities Development

Direct quantification of heating and air conditioning thermal loads for climate control in vehicles is challenging when using OEM and third-party climate control systems. These systems have fixed control strategies that differ by manufacturer and product range. In addition, the systems have variable efficiency that is dependent on thermal load. Quantifying thermal load directly requires invasive measurements and detailed system mapping and could potentially disrupt the normal system operation. For these reasons, direct measurement of thermal load is best accomplished using custom equipment designed specifically for the task. During FY 2013, NREL developed an HVAC emulator testing apparatus for the purpose of direct thermal load measurement and control strategy evaluation (Figure V-159). As shown in Figure V-160, filtered air enters the emulator blower after which it passes through a chiller that consists of a temperature-controlled liquid-to-air heat exchanger. After passing through the chiller, the airstream passes through an electrical resistance heater. The mass flow rate of the air is then quantified with a venturi flow meter coupled with process humidity, temperature, and pressure measurements. The conditioned air enters the vehicle, and select measurements are made at the vehicle entrance and exit to quantify the thermal load. The developed HVAC emulators will be used extensively in future testing for direct thermal load measurement during technology evaluation.

Figure V-159: HVAC emulator.

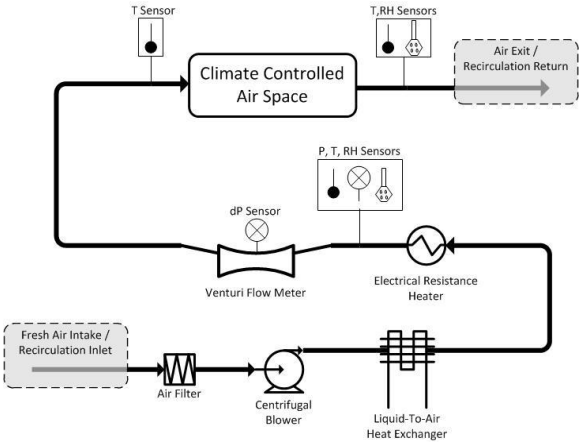

Figure V-160: Emulator Process Flow Diagram.

Conclusions

By using an advanced solar-reflective blue paint, long-haul truck daytime rest period A/C electrical energy consumption was reduced by 7.3% for Colorado summer environmental conditions. The reduction in energy consumption equates to a 563 W·h reduction in electrical energy, 9.4% reduction in standard battery pack capacity, and 12.4 kg (27.3 lb) reduction in battery pack weight. In addition, a percent of maximum possible temperature reduction, β, of 6.0% under thermal soak conditions was obtained for advanced solar-reflective blue paint. The reductions in idle and thermal loads were achieved without a visible change in paint color, potentially giving long-haul trucking companies the ability to adopt the technology without a change in brand recognition or aesthetics. Future work is planned to model the impact of paint color and advanced paints over a wide range of use and operating conditions in order to estimate payback period and fuel use reduction potential at the national level.

In addition to the impact of paint, opaque glazing covering showed a 13.3% reduction in daily average A/C system electrical load in Colorado summer conditions. This reduction identifies both advanced glazings and improved privacy curtain design as future areas of detailed focus for idle load reduction opportunities.

With the implementation of an idealized sleeper curtain to reduce the climate controlled air volume, a 12.7% reduction in daytime rest-period A/C electrical load was obtained compared to the standard sleeper curtain. This reduction equates to a 1,153 W·h reduction in electrical energy, 19.2% reduction in standard battery pack capacity, and 25.4 kg (55.9 lb) reduction in battery pack weight. While the design tested is not practical for implementation, the results indicate that a sleeper curtain designed for thermal management of the sleeper compartment would provide significant improvements in idle energy consumption for climate control.

By working closely with industry partners, further developing both experimental and modeling capabilities, and applying these capabilities, NREL has identified significant reduction opportunities in long-haul truck rest-period climate control loads. Implementation of these technologies can improve the payback period of idle reduction systems by reducing their required capacity and therefore cost, volume, and weight. Identification and quantification of payback periods of promising technologies reduces the risk of adoption for OEMs and fleet owners and operators, and provides economic motivation for technology adoption. Improving current idle reduction technologies and providing new technologies will help to reduce the 838 million gallons of fuel used annually for long-haul truck rest period idling in the United States.

References

1. Stodolsky, F., Gaines, L., Vyas, A., *Analysis of Technology Options to Reduce the Fuel Consumption of Idling Trucks*. Argonne National Laboratory, ANL/ESD-43, June 2000.
2. Gaines, L., Vyas, A., Anderson, J., "Estimation of Fuel Use by Idling Commercial Trucks." 85th Annual Meeting of the Transportation Research Board, Washington, D.C., January 22–26, 2006, Paper No. 06-2567.
3. "Greenhouse Gas Emissions Standards and Fuel Efficiency Standards for Medium- and Heavy-Duty Engines and Vehicles, Final Rule." Federal Register 76 (15 September, 2011): 57106–57513.
4. "Idling Regulations Compendium, American Transportation Research Institute." http://atri-online.org/2013/02/20/idling-regulations-compendium/ Accessed on 9/16/2013.
5. Lustbader, J., Rugh, J., Rister, B., Venson, T., "CoolCalc: A Long-Haul Tuck Thermal Load Estimation Tool," SAE World Congress, Detroit, MI, April 12–14, 2011, Paper Number 2011-01-0656.
6. Dieck, R.H., Steele, W.G., Osolsobe, G., *Test Uncertainty.* ASME PTC 19.1-2005. New York, NY. American Society of Mechanical Engineers. 2005.
7. http://www.nrel.gov/midc/vtif_rsr/.
8. "Cab Insulation Testing Methodology." RP422A-1-9, in *Technology and Maintenance Council's Recommended Maintenance Practices Manual,* 2010–2011 edition, Arlington, VA: American Trucking Association, p. RP422A-1.

   http://www.dometic.com/enus/Americas/USA/Truck/ Accessed on 10/18/2013.
9. "Vehicle and Systems Simulation and Testing 2012 Annual Progress Report." DOE/EE-0834, Section IV.N. CoolCab Truck Thermal Load & Idle Reduction, pg. 284-291.

Publications

1. Lustbader, J., Venson, T., Jeffers, M., Adelman S., Dehart, C., Yeakel, S., Sanchez, M. "Long-Haul Truck Sleeper Cab Thermal Management Technologies to Reduce Idle Climate Control Loads," SAE Thermal Management Systems Symposium, 12TMSS-0058, October 3–4, 2012.
2. Lustbader, J., Kreutzer, C., Jeffers, M., Cosgrove, J., Tomerlin, J., Langewisch, R., Kincade, K., "CoolCab Test and Evaluation & CoolCalc HVAC Tool Development," DOE Annual Merit Review, VSS075, May 15, 2012.

Tools and Data

1. CoolCalc rapid HVAC load estimation tool version 2.3. Only available to industry and laboratory partners at this time. See CoolCalc section in this report for more information.
2. CoolSim V66 A/C modeling software for the MATLAB/Simulink software environment. See CoolSim section in this report for more information.

Acknowledgments

- Co-author: Cory Kreutzer (NREL).
- Additional thanks to: Matt Jeffers, Jeff Tomerlin, Jon Cosgrove, John Rugh, Lisa Fedorka, and Matthew Gray (NREL).
- Special thanks to: Our industry partners Volvo Trucks, PPG Industries, and Dometic Corporation's Environmental Division.

V.R. CoolCalc Rapid HVAC Load Estimation Tool

Jason A. Lustbader
National Renewable Energy Laboratory
15013 Denver West Parkway
Golden, CO 80401
Phone: (303) 275-4443
E-mail: Jason.Lustbader@nrel.gov

David Anderson and Lee Slezak
Phone: (202) 287-5688 (David Anderson)
E-mail: David.Anderson@ee.doe.gov
Phone: (202) 586-2335 (Lee Slezak)
E-mail: Lee.Slezak@ee.doe.gov

V.R.1. Abstract

Objectives

- Develop modeling tools to help quantify the impact of advanced load reduction technologies and show progress toward at least a 30% reduction in long-haul truck idle climate control loads with a three-year or better payback period by 2015.
- Reduce the risk of advanced technology adoption by improving quantification of thermal load reduction technology impacts for both design points and in-use estimation.
- Investigate opportunities to reduce truck cab thermal loads through modeling and simulation to reduce the 838 million gallons of fuel used for truck rest period idling.

Major Accomplishments

- Improved CoolCalc's robustness and added features including: weather viewer tool, schedule creator, custom convection coefficient model, parallel run capability, and large-scale analysis tools. Released version 2.3 to industry partners.
- Applied CoolCalc to guide CoolCab outdoor testing, identifying thermal load reduction opportunities for the sleeper divider curtain and solar-reflective paint.
- The CoolCalc-predicted maximum possible percent reduction in rise over ambient temperature (β) for black-to-white and blue-to-solar reflective blue paint at peak solar load was within 4.5%.
- Predicted a significant national-level reduction in rest-period cooling thermal loads by switching from black to white paint.
- Identified a strong sensitivity for cooling loads and an insensitivity for heating loads to paint color and regional climate conditions.

Future Achievements

- Improve and apply CoolCalc's rapid parametric analysis tools to help industry estimate design impacts on fuel use and payback period across a broad range of weather and operating conditions.
- Continue validation of CoolCalc models, including heavy-duty vehicle heating and cooling systems.
- Begin development, validation, and application of medium- and light-duty vehicle models.
- Improve integration of CoolCalc with NREL's air conditioning model (CoolSim) and with Autonomie.

✧ ✧ ✧ ✧ ✧

V.R.2. Technical Discussion

Background

Heating and air conditioning are two of the primary reasons for long haul truck main engine operation when the vehicle is parked. In the United States, trucks that travel more than 500 miles per day use 838 million gallons of fuel annually for rest period idling [1]. Including workday idling, over 2 billion gallons of fuel are used annually for truck idling [2]. By reducing thermal loads and improving efficiency, there is a great opportunity to reduce the fuel used and emissions created by idling. Enhancing the thermal performance of cab/sleepers will enable cost effective idle reduction solutions. If the fuel savings from new technologies can provide a one to three year payback period, fleet owners will be economically motivated to incorporate them. This provides a pathway to rapid adoption of effective thermal and idle load reduction solutions.

The U.S. Department of Energy's (DOE's) National Renewable Energy Laboratory's (NREL's) CoolCab project is researching efficient thermal management strategies that keep the vehicle's occupants comfortable without the need for engine idling. To achieve this goal, NREL is developing tools and test methods to assess idle-reduction technologies. The heavy-duty truck industry needs a high-level analysis tool to predict thermal loads, evaluate load-reduction technologies, and calculate their impact on climate control fuel use.

To meet this need, NREL has developed CoolCalc, a software tool, to assist industry in reducing climate control loads for heavy-duty vehicles. CoolCalc is a heating, ventilating, and air conditioning (HVAC) load estimation tool that enables rapid exploration of idle reduction design options for a range of climates.

Introduction

CoolCalc is an easy to use, simplified, physics based HVAC load estimation tool that does not require meshing, has flexible geometry, excludes unnecessary detail, and is less time intensive than more detailed computer aided engineering (CAE) modeling approaches. For these reasons, it is ideally suited for performing rapid trade off studies, estimating technology impacts, and sizing preliminary HVAC designs. CoolCalc complements more detailed and expensive CAE tools by first exploring the design space to identify promising technologies and specific parameters that require deeper investigation.

CoolCalc, described in more detail in [3], was built on NREL's original OpenStudio platform as a plug in extension for Trimble's SketchUp three dimensional design software and has been adapted to better suit the transportation industry. DOE's EnergyPlus software (developed for building energy modeling) is used as the heat transfer solver for CoolCalc.

CoolCalc fills an important role in the CoolCab project's suite of experimental and analytical tools, as well as equipping industry partners with a valuable and cost effective research and design tool.

Approach

The goals of the CoolCab research project are to reduce thermal loads, improve occupant thermal comfort, and maximize equipment efficiency to eliminate the need for rest period engine idling. To accomplish these goals, NREL is closely collaborating with original equipment manufacturers and suppliers to develop and implement commercially viable thermal management solutions.

The CoolCab project employs a strategic, three-phased approach to evaluating commercially available and advanced vehicle thermal management and idle-reduction technologies. The three phases are (i) Baseline Testing and Model Development, (ii) Thermal Load Reduction, and (iii) Idle Reduction. Each phase features applications of NREL's suite of thermal testing and analysis tools. CoolCalc is applied throughout the entire research process to complement the evaluation of idle-reduction strategies through outdoor testing and more detailed CAE modeling.

In Phase I, CoolCalc models of the test vehicles are built, starting from computer-aided design (CAD) models and other information provided by original equipment manufacturers and suppliers. The models are validated against actual test data collected at NREL's Vehicle Testing and Integration Facility (VTIF). Local weather data logged at the VTIF weather station are input into the CoolCalc simulation to ensure that the model behaves similarly to the test vehicle under the same weather conditions.

CoolCalc is leveraged in Phase II to identify opportunities to reduce thermal loads via rapid simulation of technologies and thermal management strategies. Top candidates from the parametric simulations are selected for further investigation through outdoor testing.

Testing results from Phase II serve as a launching point for CoolCalc simulations to analyze performance and estimate fuel use savings across a wide variety of weather and time-use distributions. For each set of conditions, CoolCalc will supply thermal loads to CoolCab's air-conditioning model, which calculates required compressor power. The model will then couple with Autonomie to predict fuel use for the weather and operating conditions. The analysis provides industry with the necessary information to adopt solutions that reduce or prevent engine idling and save fuel.

Results

CoolCalc Improvements and New Features

Many enhancements were made to the CoolCalc HVAC load estimation tool to improve functionality and usability:

1. CoolCalc source code was updated for compatibility with new versions of SketchUp (2013) and EnergyPlus (v8.0).
2. A new tool was created within CoolCalc for viewing any standard EnergyPlus format weather data file. The Weather Viewer tool, shown in Figure V-161, allows users to quickly and easily identify weather conditions of interest for a location that meet simulation needs. This saves the user considerable simulation setup time but can also be used independent of a specific CoolCalc project.
3. A custom graphical user interface (GUI) was developed within the Object Browser to facilitate adding and managing all schedule objects. Schedules are used to control HVAC system operation, vehicle occupancy, convection coefficients, and a wide variety of other model components. This GUI greatly simplifies schedule creation for the user, which can be cumbersome to define otherwise.
4. Two new features were added to the Output tab of the Run Simulation GUI. The first feature gives the user the option to provide simulation output file names prior to file generation. This feature prevents inadvertent deletion of previously generated simulation results in the output folder. The second feature, labeled "Populate Variables" in the Run Simulation dialog, allows the user to generate a list of all available output variables and select those of interest. The population of available output variables is dependent on model settings and therefore aids the user in the identification and selection of desired output data.
5. The vehicle modeling process was improved to include vehicle specific convection correlations that were developed from computational fluid dynamics. A new convection GUI (Figure V-162) was developed to facilitate implementation of custom interior convection correlations to surfaces in a vehicle model. Light and heavy duty vehicle convection models developed for CoolCalc will be supplied as defaults. The interface allows the user to edit existing correlations or create additional correlations and provides the ability to save correlations for future use. The convection modeling process and default correlations will continue to be refined, validated, and extended to a variety of different vehicles and air distribution configurations.

6. The vehicle modeling process was improved through the addition of privacy curtains to a vehicle interior. Existing EnergyPlus components were used to apply a curtain model to the inside of window surfaces. The curtain model uses detailed input parameters such as thermal and optical properties of a curtain material and window-to-curtain distances to capture the complex thermal behavior of the curtains. The user can also supply scheduling information to control when the curtains are open or closed. The addition of curtains in a model improves CoolCalc's heavy-duty vehicle thermal modeling capabilities.
7. Additional changes have been made to a number of primary CoolCalc components to improve the overall stability and functionality of the software.

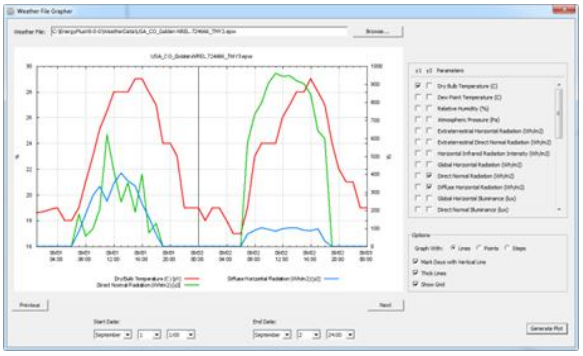

Figure V-161: CoolCalc weather file viewing tool.

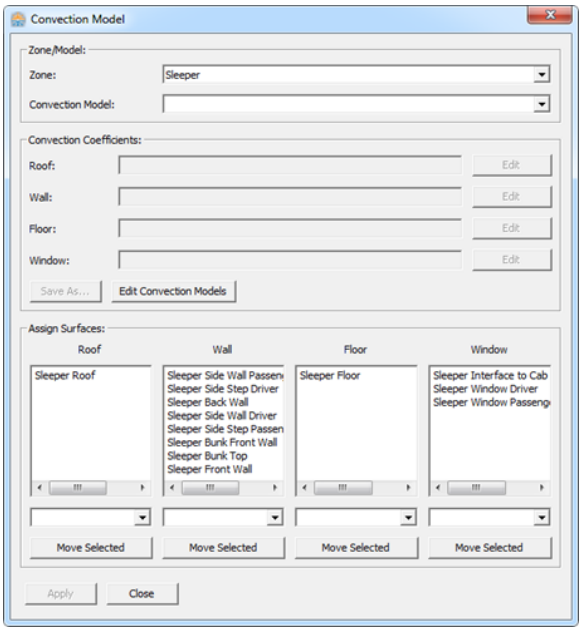

Figure V-162: Interior convection model GUI.

The CoolCalc user guide has been updated to reflect the new features and improvements. This documentation is continually improved to better assist CoolCalc users. Future versions will be expanded to include sections about troubleshooting common errors, drawing custom geometry, modeling HVAC systems, and modeling suggestions for advanced users. The latest version of CoolCalc was released to industry partners at the end of FY 2013.

Volvo CoolCalc Modeling Improvements

The CoolCalc model of a Volvo truck (shown in Figure V-163) that was previously developed and validated to experimental data was updated with additional capability to enable the next phase of thermal modeling. CoolCalc's HVAC System GUI was utilized for the implementation of a HVAC system in the truck model sleeper compartment. This system allows thermal loads for heating and cooling to be estimated for more realistic rest period climate control scenarios.

In addition to the HVAC system, a heavy duty vehicle convection model was applied to the sleeper compartment. This convection correlation model provides a functional dependency of the interior surface convection coefficients on the HVAC air exchange rate to more accurately model the forced convection that occurs with an active HVAC system. The last major improvement to the model was the addition of privacy curtains to the inside of all the vehicle glazings.

The improved CoolCalc model was used to identify opportunities to reduce long haul truck thermal loads and help guide testing efforts. Preliminary CoolCalc simulations showed that the sleeper divider curtain properties had a significant impact on sleeper compartment heating and cooling loads. This sensitivity identified the sleeper curtain as an area of focus for FY 2013 outdoor vehicle testing with the Volvo test bucks (Figure V-164). Strategies for improvements to the sleeper curtain were tested to evaluate the potential reduction in climate control loads.

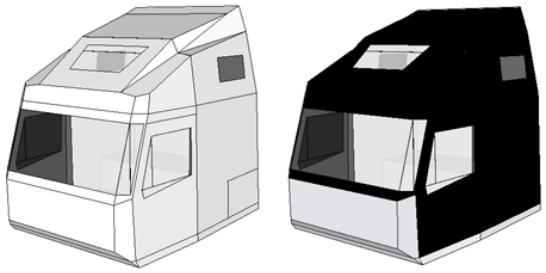

Figure V-163: CoolCalc model of Volvo test bucks.

Figure V-164: Volvo test bucks at NREL's VTIF.

CoolCalc modeling of paint color's effect on thermal load reduction was completed prior to experimental investigation. However, after experimental tests were completed, the weather data corresponding to experimental test days were used to simulate the experiment within CoolCalc. Figure V-165

contains experimental (A) and CoolCalc model (B) test buck average interior air temperatures throughout daytime thermal soak conditions for both white and black paint. In addition, the figure shows both experimental and model results for the percent of maximum possible reduction in interior air temperature rise above ambient, β, between 11:00 AM and 1:00 PM MST. The CoolCalc model accurately captures air temperature with time for both black and white painted cabs and also shows close agreement with experimental results obtained for the percent of maximum possible reduction in interior air temperature rise above ambient, with β = 31.1% for experiment and β = 32.5% for the CoolCalc model. The CoolCab section of this report shows a similar comparison of blue to solar reflective blue.

CoolCalc will continue to be used in conjunction with outdoor testing to estimate the impact of thermal load reduction technologies and advanced climate control strategies.

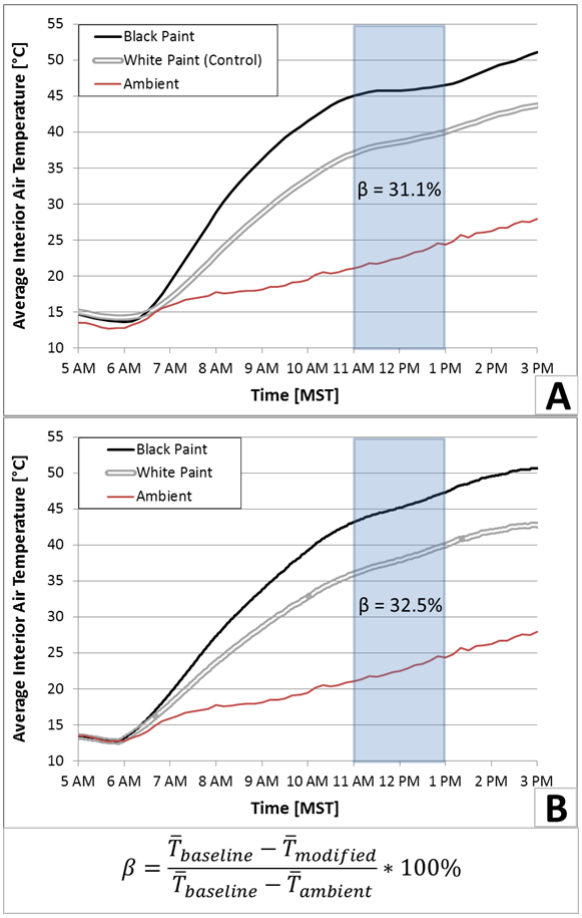

Figure V-165: Average interior air temperature of Volvo test buck during thermal soak conditions for both experimental testing (A) and CoolCalc model (B).

Large-scale Parallel Simulation Capability

A powerful feature of CoolCalc is the ability to evaluate a model under any environmental conditions using the weather input file. This feature allows analysis of models at any geographic location in the world provided weather data exists for that location. Capturing the regional- and national-level impact of a potential thermal load or idle load-reduction technology is important for both exploring the design space and understanding how technologies will perform beyond design conditions across a number of in-use conditions. Evaluating a model across a range of U.S. locations coupled with a parametric technology evaluation can require hundreds to thousands of independent simulations in the CoolCalc software. In FY 2013, a suite of components were added to the CoolCalc framework to evaluate large numbers of simulations both in series on a local machine and in parallel on an in-house, high-performance computing cluster for rapid simulation.

To implement the parallel simulation capabilities of CoolCalc, a CoolCalc Job Manager was created to interface with a high-performance computing cluster. In addition, the CoolCalc Run Simulation dialog was updated to allow for a *Parallel Simulation* selection. The CoolCalc Job Manager was created so that parallel simulation using different high-performance computing systems could be accomplished through modification of the Job Manager code. Emphasis was placed on ensuring that large-scale serial simulation capabilities remain functional for users without access to parallel simulation resources.

A high level process diagram for implementation of the parallel run simulation capability in CoolCalc is shown in Figure V-166. The model of interest is created and manipulated in the existing user interfaces. Parametric variables are configured as necessary and the Use Parametric Simulation checkbox is selected in the Run Simulation dialog box (Figure V-167). Parametric variables and simulation options are selected and parallel input file structure creation is initiated with the Run Parallel Simulation button. Thereafter, the CoolCalc Job Manager is executed for task submission to the high performance computing system. The Job Manager monitors the progress of tasks and resubmits failed tasks as needed. Finally, the Job Manager collects completed tasks and relocates them to an organized file structure for future data analysis. For FY 2013, the CoolCalc Job Manager was written to interface with NREL's Windows based WinHPC system.

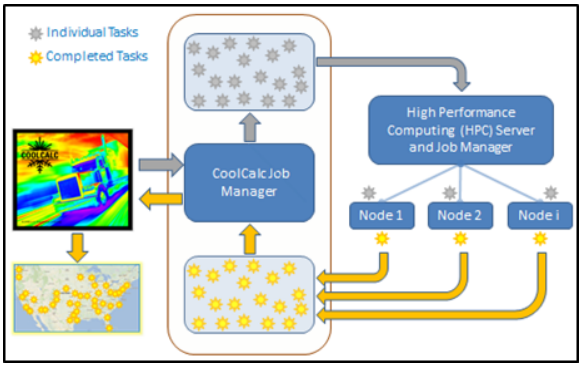

Figure V-166: Process diagram for parallel run simulation using CoolCalc and a high performance computing system.

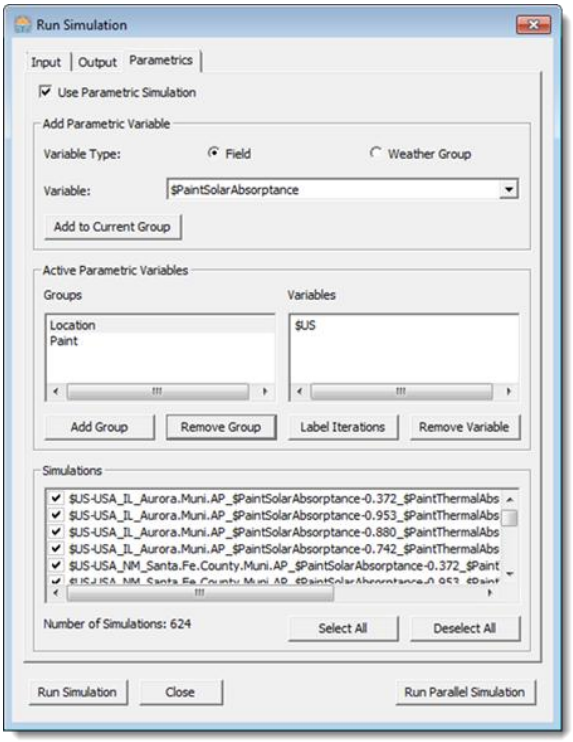

Figure V-167: Run Simulation dialog box configuration.

A national-level full-factorial analysis with three different paint colors, three cab insulation thicknesses, three glazing packages, and 160 weather locations requires 4,320 simulations and produces more than 500 GB of data. To handle the large datasets, post-processing tools were developed in the MATLAB software environment. Design of the post-processing tools was focused on the following functions:

- Import the dataset into a well-defined MATLAB data structure
- Create user-defined selection of subsets of a larger dataset
- Perform statistical and other mathematical analysis on selected subsets of data
- Generate graphical output.

After development of the parallel run simulation post-processing tools, the new tools were used to evaluate the impact of cab paint color at the national level.

National Paint Impact Study

To investigate the impact of exterior paint color on long haul truck HVAC thermal loads, a large parallel run simulation was performed with the CoolCalc modeling software. For the simulation, typical meteorological year (TMY) weather data [4] were collected for the three most populous cities in each state of the United States. TMY weather data consist of actual hourly weather information representative of typical local climatic conditions on a monthly basis concatenated into an entire year. For the evaluation, paint color was defined as a parametric variable, and the colors used for the model matched those used for experimental outdoor testing. The paint colors were black, blue, white, and an advanced paint color matched to blue but having a higher solar reflectivity. The paint spectral properties are provided in the CoolCab section of this report. For the simulation, the sleeper compartment was heated when the interior air temperature dropped to 18.3°C (65°F) and cooled when the indoor air temperature increased to 23.9°C (75°F), leaving a 5.6°C (10°F) deadband between the two temperatures. The model was configured with all curtains closed and the front of the cab facing directly south.

Figure V-168 shows national maps of normalized cooling and heating thermal loads for the four paint colors in the study. The data represent the 95th percentile for heating and cooling loads, meaning that 95% of the weather days evaluated have a lower thermal load. For the figure, cooling and heating loads were independently normalized to cooling maximum and heating maximum loads; therefore, their scales do not indicate the same magnitude. As shown in the figure, changing from black to white paint significantly reduces the cooling thermal loads and has a minimal increase in heating loads. In addition, cooling loads with black paint show a strong sensitivity to regional climate while white paint shows a much smaller sensitivity. Similarly, changing from blue to solar reflective blue paint has a measurable reduction in thermal load with no significant change in heating loads.

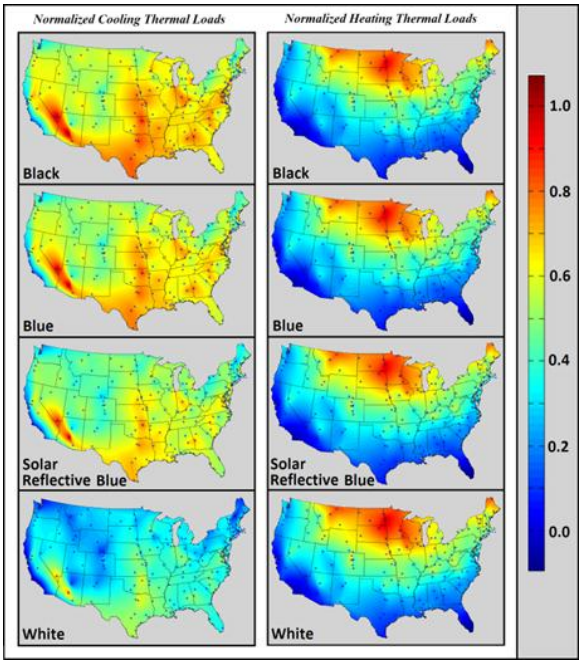

Figure V-168: National daily cooling (left) and heating (right) sleeper HVAC thermal loads for the four cab paint colors of interest. Data represent 95th percentile thermal loads and are normalized based on peak load.

The results of the national paint impact study confirm that paints with higher solar reflectivity reduce thermal loads significantly in cooling conditions and have little to no detrimental impact on heating loads. When the choice of paint color is critical for brand recognition and aesthetic purposes, load reductions are obtainable through the use of advanced color-matched solar reflective paints. CoolCalc's parallel run simulation and analysis capabilities will be used in the future to identify viable idle load-reduction technologies, generate statistically significant national level data to assist industry,

and ultimately to determine technology payback period and estimate fuel use.

Conclusions

CoolCalc was enhanced with the addition of the Weather Viewer tool, multiple GUIs, parallel run capability, and large-scale analysis tools. In addition, the CoolCalc model predicted a significant national-level reduction in daily rest-period cooling thermal loads by going from black to white paint. Model results also show an improvement in cooling thermal loads when switching from a blue to color-matched solar reflective blue paint. The model indicates cooling thermal loads are highly sensitive to regional climate conditions for black paint and a significantly reduced sensitivity for white paint. Thermal load trends agree with experimental results obtained under local weather conditions and provide load estimations for a typical year of weather across the entire United States.

CoolCalc's recent improvements have added significant modeling capability and made the modeling environment much easier to use. Reducing the user learning curve allows for much quicker adoption and implementation of the tool by industry partners.

CoolCalc continues to be used effectively to guide testing efforts through preliminary technology performance evaluation. The development of tools to aid in the application of CoolCalc across a wide variety of weather conditions contributes to the overall goal of quantification of fuel savings and payback periods for potential thermal and idle load-reduction technologies. Providing industry with the proper tools and information necessary to clearly identify idle load-reduction solutions dramatically reduces their risk, which creates a pathway for rapid adoption of technologies. CoolCalc was used to assist partners including Volvo Trucks, Daimler SuperTruck project, Oshkosh, Aearo E-A-R, PPG, and The Aerospace Corporation on DOE- and industry-funded projects.

References

1. Stodolsky, F., Gaines, L., Vyas, A., Analysis of Technology Options to Reduce the Fuel Consumption of Idling Trucks. Argonne National Laboratory, ANL/ESD-43, June 2000.
2. Gaines, L., Vyas, A., Anderson, J., "Estimation of Fuel Use by Idling Commercial Trucks," 85th Annual Meeting of the Transportation Research Board, Washington, D.C., January 22–26, 2006, Paper No. 06-2567.
3. Lustbader, J., Rugh, J., Rister, B., Venson, T., "CoolCalc: A Long-Haul Tuck Thermal Load Estimation Tool." SAE World Congress, Detroit, MI, April 12-14, 2011, Paper Number 2011-01-0656.
4. http://rredc.nrel.gov/solar/old_data/nsrdb/1991-2005/tmy3/. Accessed 9/1/2013.

V.R.3. Products

Publications

1. Lustbader, J., Kreutzer, C., Jeffers, M., Cosgrove, J., Tomerlin, J., Langewisch, R., Kincade, K., "CoolCab Test and Evaluation & CoolCalc HVAC Tool Development," DOE Annual Merit Review, VSS075, May 15, 2012.

Tools and Data

1. CoolCalc rapid HVAC load estimation tool version 2.3. Only available to industry and laboratory partners at this time.

Acknowledgements

1. Co-authors: Cory Kreutzer and Matthew Jeffers (NREL).
2. Additional thanks to: Ryan Langewisch, Kameron Kincade, Henry Horsey, John Rugh, Matthew Gray, Brent Griffith and Lisa Fedorka (NREL).
3. Special thanks to our industry partners: Volvo Trucks, Daimler Trucks, Kenworth Trucks, Oshkosh, EAR Thermal Acoustic Systems, and PPG Industries.

V.S. Advanced Heavy Duty Engine Systems and Emissions Control Modeling and Analysis

Zhiming Gao, Stuart Daw
Principal Investigators
Oak Ridge National Laboratory
National Transportation Research Center
2360 Cherahala Boulevard
Knoxville, TN 37932-6472
Phone: (865) 946-1339, (865) 946-1341
E-mail: gaoz@ornl.gov, dawcs@ornl.gov

Lee Slezak, David Anderson
DOE Program Managers
Phone: (202) 586-2335
E-mail: lee.slezak@ee.doe.gov
Phone: (202) 287-5688
E-mail: david.anderson@ee.doe.gov

V.S.1. Abstract

Objectives

- Develop powertrain component models that can be used to accurately simulate and optimize the overall fuel efficiency and emissions control of advanced medium (MD) and heavy-duty (HD) hybrid powertrain systems powered by current and leading-edge combustion engines with exhaust aftertreatment over transient driving conditions.
- Reduce U.S. dependence on imported fuels by collaborating with an industry Cooperative Research and Development (CRADA) partner to identify and overcome major technical barriers to commercial implementation of hybrid MD and HD powertrains.

Major Accomplishments

- Constructed a 2010-certified 15-L HD engine map that accounts for fuel consumption, exhaust temperature, and engine-out emissions under steady-state operating conditions.
- Implemented the above map in Autonomie with estimated adjustments for transient effects to simulate comparative drive cycle fuel consumption and engine-out emissions with a previously characterized 2007-certified engine.
- Simulated a parallel hybrid Class 8 HD long-haul truck powered by the 2010 compliant 15-L engine above with a fully integrated aftertreatment train over freeway-dominated driving cycles.
- Developed three representative MD drive cycles for delivery trucks, utility vehicles, and transit city buses, respectively, by utilizing one-year of real transportation data available at the ORNL MD truck database.
- Simulated the fuel economy and tailpipe emissions for a hypothetical parallel hybrid transit bus equipped with a 5.9L diesel engine and full aftertreatment train over six city driving cycles.
- Published simulated fuel economy and emissions performance of a HD hybrid truck during city and interstate driving.

Future Achievements

- Utilize measurements from a Class 8 emulated vehicle in the ORNL Vehicle Systems Integration (VSI) Lab with the 15-L CUMMINS 2010 ISX engine to refine and validate the engine and aftertreatment models for simulating class 8 hybrid truck powertrains.
- Continue refining and updating diesel exhaust aftertreatment models utilizing the most recent laboratory and dynamometer measurements for emerging commercial catalysts and emission control devices.
- Support investigation of alternative management strategies for engines, aftertreatment devices, batteries, and exhaust heat recovery and compare the integrated performance in MD and HD hybrid powertrains.
- Refine experimental data and component models of mechanical and electrical accessory loads in MD/HD trucks in support of intelligent management of vehicle accessory power.
- Evaluate the potential impact of natural gas, dimethyl ether (DME), biodiesel, and other alternative fuels on fuel efficiency and tailpipe emissions in conventional and hybrid MD and HD trucks.

✧ ✧ ✧ ✧ ✧

V.S.2. Technical Discussion

Background

The U.S. transportation sector consumes nearly 13.5 million barrels of petroleum per day, more than 22% of which goes to MD and HD vehicles. Thus, MD and HD vehicle hybridization could play a vital role in reducing the overall greenhouse gas generation and imported oil consumption in the U.S. Typically lean-burn diesel engines offer a significant fuel efficiency advantage over stoichiometrically fueled engines. This is one of the reasons why current MD and HD vehicles are overwhelmingly powered by diesel engines. However, emissions control challenges are higher for diesels because aftertreatment of lean engine exhaust requires utilization of special catalysts and aftertreatment devices to remove nitrogen oxides (NOx), particulate matter (PM), unburned hydrocarbons (HCs), and carbon monoxide (CO).

Unlike the tree-way catalyst technology used to control stoichiometric gasoline engine exhaust, the technology for diesel emissions control is still under intense development. As advanced diesel engines become even more efficient, their exhaust temperatures are becoming even cooler, and this is challenging the limits of current diesel catalyst technology. Thus it is important that simulations of advanced MD and HD diesel hybrid vehicles accurately account for the current and expected trends in both diesel engine and aftertreatment technology.

In this project we are specifically concerned with developing engine and aftertreatment component models that allow comparative simulations of different vehicle configurations, operating strategies, and component hardware. Our overall goal is to support DOE's vehicle systems analysis and simulation efforts by providing computational models, validations of those models, and model predictions that assist in evaluating candidate MD and HD hybrid technology options. To build our models, we rely heavily on extensive experimental measurements from both engines and emissions control devices made in multiple facilities at Oak Ridge National Laboratory (ORNL). We transform these measurement data into physically consistent computational models that can be implemented directly in simulation platforms such as Autonomie. This provides DOE with the capability to analyze the impact of advanced vehicle systems from multiple perspectives, including energy efficiency, energy security, global climate change, and environmental impact.

Introduction

In FY2013, we concentrated our model building efforts in the following specific areas:

- Construction of steady-state fuel consumption and engine-out emissions and temperature maps for a 2010-certified 15-L HD engine.
- Development of three representative MD drive cycles for delivery trucks, utility vehicles, and city transit buses, respectively.
- Updating ORNL's catalyzed DPF component model through improvement of the kinetics for oxidation of CO and unburned hydrocarbons (HCs).
- Assessment of the fuel economy and emissions of a Class 8 parallel hybrid HD long-haul truck powered by a 2010 emissions compliant 15-L diesel engine with fully integrated aftertreatment train.
- Comparisons of simulated fuel economy and emissions for conventional versus hybrid city buses over various representative city bus drive cycles.
- Assessment of the impact of motor and battery size on the fuel economy and emissions of a parallel hybrid city bus over multiple representative drive cycles.

Many results from the above have been reported in multiple journal and conference publications and presentations at meetings of the Society of Automotive Engineers (SAE), the Joint U.S. National Combustion Meeting, the Transportation Research Board Annual Meeting, and Directions in Engine Efficiency and Emissions (DEER) Conference. Additional manuscripts documenting the major findings city bus studies are still under preparation.

Approach

Because of the inherent complexity of internal combustion engines and their performance under transient conditions, our approach for transient engine modeling relies on a coarse representation of internal engine heat transfer and highly simplified assumptions about how engine-out species change as the engine heats up. The result is expressed in the form of an experimentally parameterized transient correction term that is applied to steady-state or pseudo-steady-state engine-dynamometer data. While this approach is admittedly crude, we have confirmed that it is able to rapidly and efficiently estimate important trends in the fuel consumption and engine-out exhaust characteristics for both conventional and advanced combustion modes under drive cycle conditions. We are continually working to improve the accuracy of these estimates as additional transient and advanced combustion engine data become available. The planned implementation of highly controlled transient measurements in the ORNL Vehicle Systems Integration (VSI) Lab will be a major step in this direction.

We also continuing to develop and improve low-order, physics and chemistry-based computational models for diesel emissions control devices including diesel oxidation catalysts (DOCs), lean NOx traps (LNTs), diesel particulate filters (DPFs), selective catalytic reduction (SCR), and passive hydrocarbon traps. These device models typically incorporate 1-D differential transient mass and energy balances with available global reaction kinetics and heat and mass transport information to simulate the performance of each aftertreatment component based on its past history and the input streams it is exposed to at its specific location in the aftertreatment train. This makes it possible to compute the instantaneous properties of the output stream from each component at each point in the drive cycle, which maintaining reasonable execution speeds.

After the above models are integrated into Autonomie, we use them to explore possible control strategies and configuration options in different HD hybrid vehicles. Generally, we do not seek to develop fully optimized control of design strategies (so our simulated strategies and designs tend to be highly simplified and/or non-proprietary and come from the open literature). Instead, we utilize such simulations to identify major trends and possible R&D opportunity areas that deserve more emphasis in the DOE portfolio or that can lead to specific partnerships with industry.

Results

Engine mapping

This year we utilized stationary dynamometer measurements to construct a steady-state emissions and fuel consumption map for a Cummins 2010-certified, 15-L heavy-duty diesel engine used in Class 8 HD trucks. These maps account for fuel consumption, exhaust temperature, and engine-out emissions, and have been implemented in

Automonie. Since the available dynamometer data only covered engine speeds between 900 and 1800rpm, we used linear extrapolation to extend the engine maps down to 625rpm and up to 2100rpm. Figure V-169 depicts example color-coded plots of the maps for engine-out temperature and NOx. Once additional experimental data become available from the ORNL VSI Lab, we will continue to refine and update the maps.

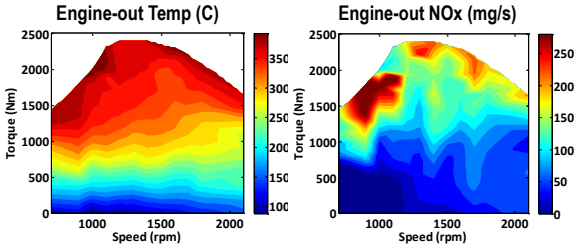

Figure V-169: Example steady-state maps of the 2010 certificated Cummins 15-L diesel engine as a function of engine torque and speed.

As in other cases of hybridization that we have studied, we have begun our analysis of HD long-haul trucks by simulating conventional trucks operating over drive cycles of interest to establish points of reference. Utilizing transient corrections of maps such as the above for both the 2010 engine and previously developed maps for a 2007 certified engine, we compared the simulated performance of conventional Class 8 long-haul tractors powered by each engine, respectively, with a 16,000-kg load over an interstate driving cycle from Knoxville to Nashville. The simulated fuel economy of the 2010 engine was 10% higher, and the CO/HC/PM engine-out emissions were considerably less. However, the estimated 2010 engine-out NOx was significantly higher. These differences seem to be consistent with recently reported trends in engine design and operation that achieve higher fuel efficiency by favoring more efficient combustion conditions while relying on improved aftertreatment for NOx control.

The higher efficiency of the 2010 engine also results in a lower engine-out exhaust temperature, which is one of the most significant current emissions control challenges being faced by industry. Because NOx reduction and oxidation of CO, HCs, and PM are controlled by chemical kinetics at low temperatures, improvements have to be made to the catalysts so that they continue to maintain sufficient activity.

Component model updates

Adequate oxidation of accumulated PM in the DPF is necessary in order to prevent buildup of back pressure, which penalizes engine output power. In some cases, it is necessary to inject added fuel to the engine or engine exhaust in order to heat up the DPF sufficiently to ignite the soot. This is referred to as active DPF regeneration. In other cases, the temperature of the exhaust may be sufficiently high that the rate of soot oxidation is high enough to remove the accumulated PM without taking any additional action (passive regeneration). The former situation directly contributes directly to increased fuel consumption, so accurate simulation of the accumulated DPF soot levels and the relative oxidation rates is important for determining fuel economy. Our catalyzed DPF model assumes a simplified 3-zone approximation of the different internal areas, which include an inlet channel zone, an outlet channel zone, and the filter wall. The deposited PM is assumed to include a deep layer in close proximity to the catalyst overlain by an outer cake layer. Oxidation of the cake layer occurs without any catalytic acceleration, while oxidation of the deep layer is accelerated by the proximity of the catalyst. In addition, the DPF catalyst can oxidize CO and HCs in the exhaust entering the DPF.

This year we updated the catalyzed part of the DPF component model to add reactions for CO and HC oxidation. The resulting CO and HC conversions predicted by this model appear to be more in line with recent experimental DPF observations at ORNL. In addition, we also included NO oxidation into NO_2. These gas species oxidation reactions are considered only in the deep layer where there is exposure to the catalyst. The kinetic parameters for oxidation of CO and HCs in the DPF are currently assumed to be the same as those in the DOC, except that they are adjusted for differences in catalyst loading. Using these modifications, we see significant reductions in the estimated CO and HCs in the DPF exit. Figure V-170 illustrates how the DOC and DPF both reduce CO and HCs in a simulation of a conventional city bus over the first 1000s after a cold-start.

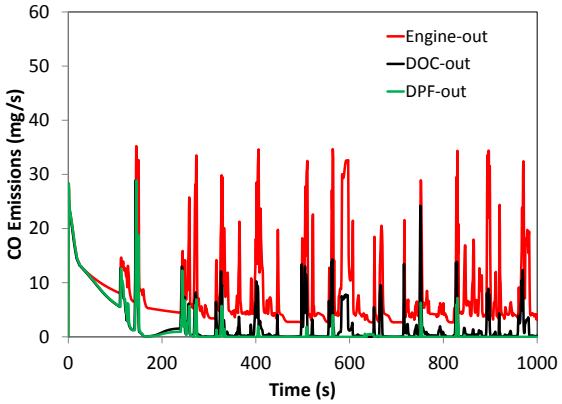

Figure V-170: Comparison of simulated CO emissions in a conventional city bus over the first 1000s of a cold-start city bus cycle constructed from the ORNL MD truck database. The DOC is assumed to be upstream of the DPF.

Representative MD Drive Cycles

Three proposed MD drive cycles were constructed for delivery trucks, utility vehicles, and school buses, respectively, based on one year of experimental measurements documented in the ORNL MD truck database. This database includes measurements from multiple sources including: delivery trucks of the H.T. Hackney Company; utility vehicles from the Knoxville Utilities Board; and transit buses of the Knoxville Area Transit (KAT) system.

Figure V-171 depicts the proposed KAT city bus drive cycle developed from the KAT data for three Class-7 buses. All these buses were 2005 Optimal LF-34 buses powered by Cummins ISB-02 5.9-L diesel engines with 5-speed automatic transmissions. Although identical in construction, the buses were operated over different routes. The statistical speed and acceleration distributions in the proposed cycle exhibits similar

speed and acceleration patterns shown by all three buses, and also captures characteristically long periods of idle operation (typically more than 50% of the time) as revealed by the measurements.

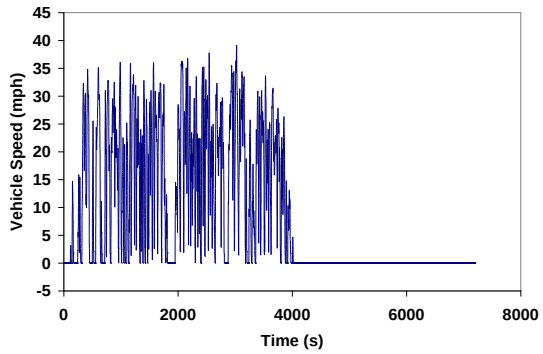

Figure V-171: The speed profile for the proposed MD transit bus drive cycle derived from the KAT bus data.

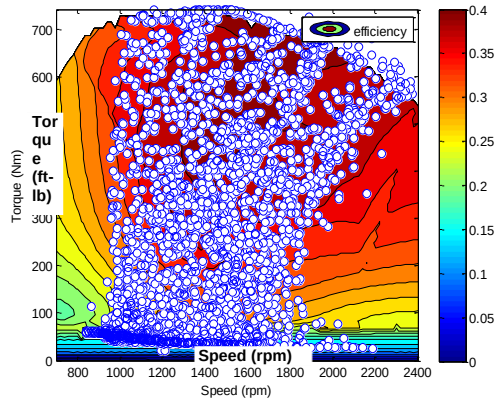

Figure V-172: Simulated trajectory of a conventional 5.9-L bus diesel engine operating over the KAT city drive cycle superimposed on the engine efficiency map. Circles indicate engine speed and load every 1s. Red areas are where the engine efficiency is highest; blue where it is lowest.

To create reference points for evaluating the impact of bus hybridization, we simulated a conventional city bus operating over the proposed KAT cycle and other representative city bus cycles, including the Central Business District (CBD) cycle, Orange County Transit Agency (OCTA) cycle, Manhattan bus cycle, Washington Metropolitan Area Transit Authority (WMATA) cycle, New York Bus Cycle (NYBC). With each of these cycles it is possible to observe how the drive cycle requirements match up with the intrinsic engine characteristics by plotting the speed and load points traversed in the cycle (at 1 s intervals) on the steady-state engine maps as depicted in Figure V-172. Here we observe directly how the cycle demands relate to the engine efficiency, which typically maximizes at higher speed and loads. Due to the extended idle periods in the KAT cycle, the engine spends a lot of time operating at sub-optimal conditions, where fuel efficiency is low.

Hybrid Truck and Bus Simulations

We simulated parallel hybrid HD trucks with the Cummins 2010-certified, 15-L engine operating over the interstate driving cycle from Knoxville to Nashville described above. For these simulations, we included a full aftertreatment train consisting of a 5.8-L DOC, a 19-L catalyzed DPF, and a 24-L urea-SCR catalyst. To account for the effects of different loads, three different fully loaded weights were included: 16,400 kg (light), 25,400 (medium), 35,400 (heavy). All three of these include the weight of the electric motor, the battery, and accessory components.

The predicted cumulative fuel consumption and emissions from these simulations are summarized in Table V-18. Since NOx control was simulated with a urea-SCR catalyst, there is no associated direct fuel consumption, but the urea consumed adds to the operating cost. To account for this, we converted the value of the urea consumed into an equivalent 2.3-2.5% added fuel consumption based on their relative costs ($2.74/gal for urea and $3.82/gal for diesel) and added this to the inducated fuel consumption in Table V-18. Urea-SCR NOx control also produces a small NH_3 slip at the tailpipe. In our simulations the average NH_3 tailpipe level is about 20ppm, but there are significantly higher peaks during transients. This implies that means that it could be important to add a downstream NH_3 oxidation catalyst to the aftertreatment train in future simulations.

Table V-18: Simulated fuel economy, engine efficiency, and tailpipe emissions from a parallel hybrid class 8 long-haul tractors powered by a 2010 certificated HD diesel engine over an interstate driving cycle from Knoxville to Nashville.

Vehicle Weight	FE	Eff	CO	HC	NOx	PM	NH_3
ton	mpg	%	g/mi	g/mi	g/mi	mg/mi	g/mi
16.4	6.79	40.5	0.141	0.013	1.254	0.3	0.006
25.4	5.76	40.4	0.175	0.020	1.336	0.8	0.017
35.4	4.92	40.6	0.188	0.024	1.426	1.3	0.032

Figure V-173 and Figure V-174 show the relatively high exhaust temperatures and resulting passive oxidation of engine-out PM for this particular drive cycle, indicating that there should be no need to have active regeneration of the DPF. Thus, under these conditions there would be no fuel penalty required for DPF regeneration and the only remaining fuel penalty associated with PM control would be due to the slightly increased engine back pressure created by the DPF.

We also simulated a hypothetical parallel hybrid transit bus equipped with a 5.9-L diesel engine and full aftertreatment-train, which included a 2.3-L DOC, a 9.7-L catalyzed DPF, and a 7.7-L urea-SCR catalyst. Four motor/battery size combinations were also considered by initially assuming a baseline motor (max power 120kw/continuous power 60kw) and baseline battery (28Ah

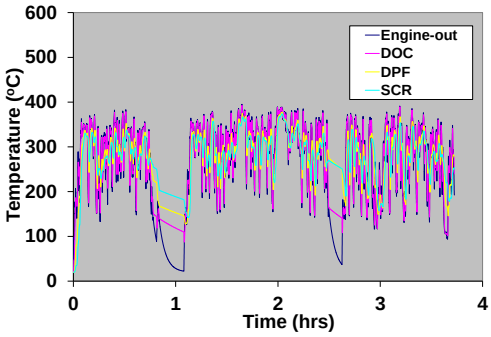

Figure V-173: Simulated temperatures at different aftertreatment locations for the class 8 HD diesel hybrid truck with a 25,400kg weight load.

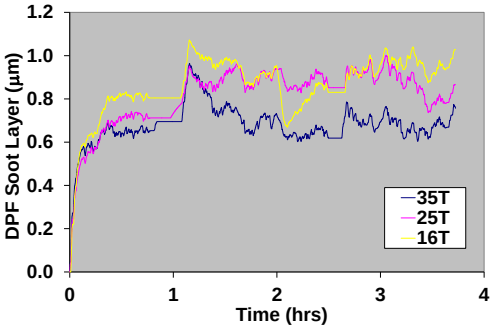

Figure V-174: Transient catalytic DPF soot layer thickness for the three different simulated loads in the class 8 HD diesel hybrid truck.

capacity & max charge rate 120kw/max discharge rate 140kw), and then repeating cases with the motor and battery both downsized to 75%, 50%, and 25% of their baseline values. These cases are referred to, respectively, as mode A, B, C, and D. Each of these combinations was then used to simulate the six city bus drive cycles mentioned above.

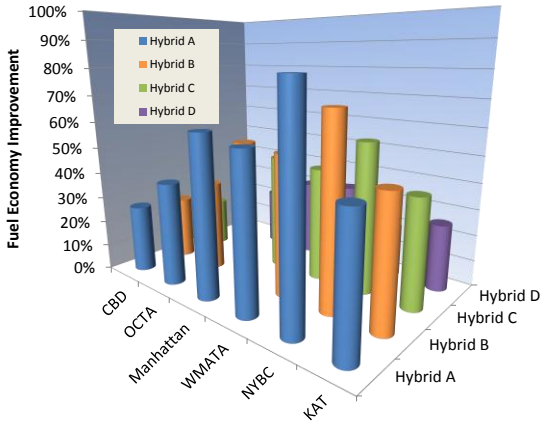

Figure V-175: Simulated fuel economy improvement for various motor/battery sizes of hybrid powertrain over different drive cycles.

Figure V-175 illustrates the fuel economy results for each of the four cases. As one might expect, the larger motor and battery combinations tend to achieve better fuel economy. Also the results reveal that the fuel economy benefits of hybridization appear higher for drive cycles with extended idle times. The idle time rates of CBD, OCTA, Manhattan, WMATA, NYBC, and KAT are 20%, 27%, 39%, 44%, 54%, and 69%, respectively.

Trends in cumulative CO, HC, and NOx tailpipe emissions are depicted in Figure V-176, with the horizontal axis representing the corresponding fuel economy improvement for each of the four motor/battery combinations. The 0% point on this axis represents a conventional bus with no hybridization. For CO and HC emissions, hybridization lowered the simulated tailpipe emissions for cases with higher idling times, reaching a minimum at motor/battery combinations that yielded between 20 and 50% improvement in fuel economy. One major factor here is that the oxidation catalyst tends to cool below the effective lightoff point for extended idling, thereby reducing the effectiveness of engine exhaust aftertreatment. The six drive cycles studied appeared to group into three distinct zones, where idling time comprised 20%-27%, 39%-44%, or 54%-69% of the cycle time. However, for NOx emissions, the clustering was different, and the 20%-27% idle cases appeared to cluster with the 39%-44% cases. One major cause of this difference is likely to be the distinctive temperature response characteristics of the NOx reduction catalyst compared to the oxidation catalyst.

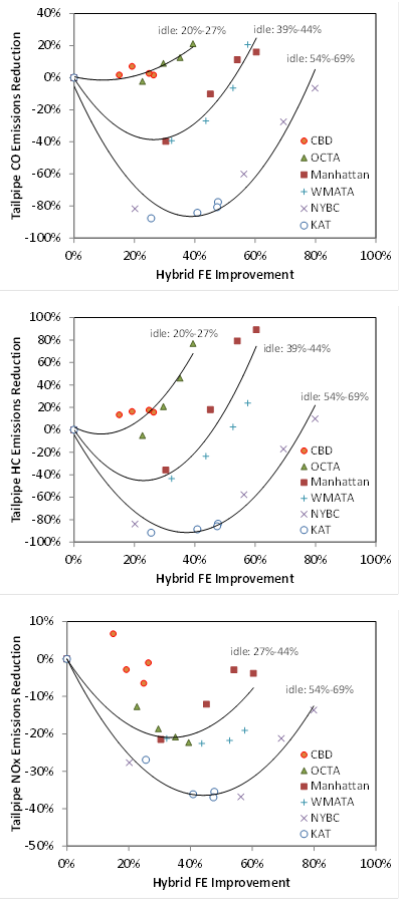

Figure V-176: Simulated tailpipe emissions versus hybrid fuel economy improvement (emissions units are mg/mile).

Unlike tailpipe emissions, cumulative engine-out emissions are significantly reduced by hybridization. As expected, increasing hybridization tends to monotonically reduce fuel economy and engine-out emissions, but this

doesn't match the trends in tailpipe emissions depicted in Figure V-176. Thus there are clearly different trends between fuel economy and tailpipe emissions, and accurate modeling of the aftertreatment train is important for resolving the competing effects.

Conclusions

- Maps for a 2010-certified 15-L HD engine accounting for steady-state fuel consumption, exhaust temperature, and engine-out emissions have been constructed from experimental measurements and implemented in Autonomie to support simulations of different configurations of HD hybrid trucks.
- The 2010 engine achieves better fuel efficiency and lower PM emissions than a previously studied 2007-certified engine, but the 2010 engine-out NOx is significantly higher and requires more efficient aftertreatment for NOx control.
- We have assessed the comparative fuel economy and emissions of a parallel hybrid long-haul truck powered by a 2010 emissions HD diesel engine with fully integrated aftertreatment train versus a comparable conventional HD truck operating over a freeway dominant cycle.
- Under highway driving conditions, it appears that current HD long-haul engine exhaust temperatures are still high enough to enable passive regeneration of the DPFs in both hybrid and conventional trucks, thereby avoiding any direct fuel penalty for DPF regeneration.
- ORNL's catalyzed DPF component model has been updated by adding kinetics for oxidation of unburned HCs and CO in the deep filter layer.
- Three MD drive cycles designated for delivery trucks, utility vehicles, and school buses, respectively, were developed from extensive on-board measurements available from the ORNL MD truck database.
- We have established baseline fuel economy and emissions for a conventional MD bus operating over six different city transit cycles.
- We have simulationed the fuel economy and emissions for a hypothetical transit, parallel hybrid city bus equipped with a 5.9L diesel engine and full aftertreatment-train over six representative city bus drive cycles and with four different motor and battery sizes.
- The benefits of bus hybridization are strongly dependent on the drive cycles characteristics, especially the fraction of time spent idling.

V.S.3. Products

Publications

1. Z. Gao, S. Curran, C.S. Daw, R.M. Wagner, Light-duty drive cycle simulations of diesel engine-out exhaust properties for an RCCI-enabled vehicle, the 8th U.S. National Combustion Meeting, May, 2013.
2. Z. Gao, C.S. Daw, D.E. Smith, Comparative urban drive cycle simulations of light-duty hybrid vehicles with gasoline or diesel engines and emissions controls, SAE paper 2013-01-1585, 2013.
3. C.S. Daw, Z. Gao, D.E. Smith, T.J. LaClair, J.A. Pihl, K.D. Edwards, Simulated fuel economy and emissions performance during city and interstate driving for a heavy-duty hybrid truck, SAE Int. J. Commer. Veh. 6(1):2013.
4. Z. Gao, C.S. Daw, R.M. Wagner, K.D. Edwards, D.E. Smith, Simulating the impact of premixed charge compression ignition on light-duty diesel fuel economy and emissions of particulates and NOx, Journal of Automobile Engineering, 227(1), January, 2013 (Invited).
5. Z. Gao, T.J. LaClair, C.S. Daw, D.E. Smith, Fuel consumption and cost saving of natural gas as alternative fuel in class 8 heavy-duty trucks, TRB-13-2945, the 92nd Transportation Research Board Annual Meeting, January, 2013.
6. C.S. Daw, Z. Gao, Advanced HD Engine Systems and Emissions Control Modeling and Analysis, 2012 Annual Report, October, 2012.
7. V.Y. Prikhodko, Z. Gao, S. Curran, C.S. Daw, R.M. Wagner, J.E. Parks II, Modeling emissions controls for RCCI engines, 2013 Engine Research Consortium, Madison, Wisconsin, June, 2013 (Invited).
8. Z. Gao, C.S. Daw, Advanced Heavy-Duty Engine Systems and Emissions Control Modeling and Analysis, U.S. DOE Hydrogen Program and Vehicle Technologies Program, Annual Merit Review and Peer Evaluation Meeting, Washington DC, May 15, 2013.
9. Z. Gao, C.S. Daw, M.-Y. Kim, J.-S. Choi, J.E. Parks II, D.E. Smith, Cold-start emissions control in hybrid vehicles equipped with a passive adsorber for hydrocarbons and NOx, DOE-DEER Conference, October 16-19, 2012.
10. Z. Gao, D.E. Smith, C.S. Daw, T.J. LaClair, J.A. Pihl, Fuel economy and emissions reduction of HD hybrid truck over transient driving cycle and interstate road, DOE-DEER Conference, October 16-19, 2012.

Patents

None

Tools and Data

1. All the data and aftertreatment component models described above are summarized in the cited publications [1-10].

V.T. Medium- and Heavy-Duty Vehicle Validation

Daeheung Lee, Principal Investigator
Argonne National Laboratory
9700 South Cass Avenue
Building 362
Lemont, IL 60439
Phone: (630) 252-5386
E-mail: daeheung@anl.gov

David Anderson, DOE Program Manager
Phone: (202) 287-5688
E-mail: David.Anderson@ee.doe.gov

V.T.1. Abstract

Objectives

- Compare Autonomie with the different vehicle system regulatory tools for the United States, European Union, Japan, and China.
- Analyze the reasons for the main differences.

Major Accomplishments

- The medium-duty (MD) and heavy-duty (HD) vehicle simulation tools used for regulations by the United States, Japan, European Union, and China were installed and analyzed to evaluate their principle features.
- The key equations and algorithms of the Greenhouse Gas Emissions Model (GEM) for the U.S. government and the Japan Fuel Consumption Model (JFCM) were analyzed.
  - The comparison result of GEM with Autonomie shows good similarity in the fuel economy (FE) value under the same conditions. The internal structure of the component models in GEM is analogous with the model structure of Autonomie.
  - The results of JFCM are being compared with the results of Autonomie under similar conditions.
- Simplified simulations were performed for VECTO for the European Union and for China's simulation tool, because VECTO and China's tool are compiled programs.
- The details of the process are summarized below:
  - Understand the fundamental functions and major features of each simulation tool,
  - Analyze the input data set and output result of each tool,
  - Select the target HD vehicle applicable to each country's regulation category,
  - Convert the required data set in order to archive the comparability of each data set,
  - Develop a comparison post-processing tools,
  - Examine the comparison results for signals of key components, and
  - Determine the FE level and compare its deviation.

Future Achievements

- Analyze VECTO software for more detail to obtain additional information and to evaluate the new feature.
- Examine individual models to determine if they could be integrated in Autonomie.

✧ ✧ ✧ ✧ ✧

V.T.2. Technical Discussion

Background

Regulation for MD and HD Vehicles

Several countries with large vehicle markets have developed or are in the process of developing regulatory programs to reduce the fuel consumption and greenhouse gas (GHG) emissions of MD and HD vehicles. At the same time, manufacturers increasingly are developing global product platforms for the HD market, offering an opportunity to accelerate the development and adoption of fuel efficiency technologies. Regulators can facilitate this outcome by coordinating the design of fuel efficiency technologies and GHG emissions reduction programs across regions. In February, 2013, Canada adopted an HD vehicle GHG emissions program very similar to the U.S. program. Mexico is considering a similar step, which would result in a very high degree of program alignment across North America. Aside from these examples, however, regulatory programs across the United States, European Union, and Asia are widely divergent in regulation start timing, standard units, and weighting factors for the test cycles and the target fuel efficiency. The objective of the project is to compare the different simulations tools that are currently being used or might be used in the near future with Autonomie.

Introduction

Fuel Economy Evaluation Using a Simulation Program

The United States, Japan, and Canada have adopted standards to reduce GHG emissions and raise the fuel efficiency of HD vehicles. Other countries are planning to do the same.

Multiple technical approaches are used to evaluate vehicle fuel consumption. These approaches generally require the physical testing of vehicles and/or vehicle components and systems, together with calculation or modeling to translate the test results into the desired measure of performance. In China, the regulation program under development is based on chassis testing, but would require testing for only a representative set of vehicles. Results for similar vehicles

would be generated through simulation. Due to the very large number of HD vehicle configurations sold and the varying conditions in which they are driven, chassis testing of every vehicle configuration would be prohibitively expensive. Under these various restrictions, the simulation method is widely accepted as the proper way to evaluate the FE or GHG emissions for regulations. The European Union researchers' investigation of the merits of the various test procedures led to the conclusion that a simulation-based approach was clearly preferable to other options.

However, the quality of the simulation remains a significant challenge. Vehicle system simulation can deliver a very rough or very accurate estimate of vehicle performance, depending on the detail of the component information provided and the model sophistication.

MD and HD Validation in Autonomie

Autonomie was developed by researchers at Argonne National Laboratory in cooperation with General Motors. It is a Plug-and-Play Powertrain and Vehicle Model Architecture and Development Environment designed to support the rapid evaluation of new powertrain/propulsion technologies for improving FE through virtual design and analysis in a math-based simulation environment. Although specific processes would have to be developed to support the rules, processes already exist to develop parameter files from component test data for specific formats. In addition, a proof-of-concept version of Autonomie to support MD and HD rules has already been developed in collaboration with the European Automobile Manufacturers Association.

Currently, several regulatory tools have been developed. These tools include GEM in the United States, JFCM in Japan, VECTO in Europe and a software developed in China. The purpose of this research is to compare the key features and fuel efficiency levels of different HD vehicle analysis tools with those of Autonomie.

Approach

United States: Greenhouse Gas Emissions Model

The U.S. program uses the EPA Greenhouse Gas Emissions Model (GEM). While in theory GEM accepts a large number of vehicle-specific inputs, including an engine fuel consumption map, mechanical attributes, control algorithms, and driver inputs, the majority of the inputs to GEM for purposes of vehicle certification in the current program are default values provided by the regulating agencies. The manufacturer or user should provide information about the vehicle type and model year, coefficients of drag and rolling resistance, existence or non-existence of specific weight-reducing components, idle reduction system, and vehicle speed-limiting system, as shown in Figure V-177.

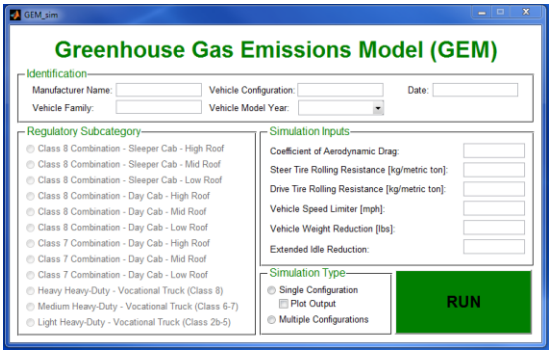

Figure V-177: Main Window of GEM Version 2.

The GEM Version 1 was released to the public in October 2010 as a part of the proposed rules. The most noticeable improvements to the GEM Version 2 are the new driver model, and many other refinements, including the graphical user interface.

Whereas GEM Version 2 is a closed source format, GEM Version 1 is a fully open source code that can be obtained from the EPA website. Thus, we can analyze the program in detail (i.e., engine map, driver model, gear efficiency, shifting control, model configuration, and so forth). However, Matlab codes and the model file of GEM Version 2 are encrypted as an 'exe' file format. The program has been converted to a standalone version of Matlab, which can be operated without Matlab/Simulink. Therefore, we can see only the converted carbon dioxide (CO_2) and FE level as results. This analysis for the GEM concentrated on GEM Version 1 due to this limitation, although GEM Version 2 is intended for the final regulation.

Fuel consumption and emissions of all Class 8 tractor trucks are simulated by using the fuel map of a fixed 15-liter, 455-horsepower engine. The simulation also uses predefined transmission features, rather than those of the vehicle's actual transmission, and a standard trailer, though the assumed trailer type depends on the cab roof height.

The equations for calculating the FE and CO_2 level are summarized as follows:

- Combined FE[mpg] = ARB wt X FE_ARB
  + 55SS wt X FE_55SS
  + 65SS wt X FE_65SS
- CO_2 level [g CO_2/ton-mile] = a / (Combined FE[mpg] X b)

The weighting factors and coefficients ('a' and 'b' in CO_2-level calculation) for each cycle and vehicle category are determined as shown in Table V-19 and Table V-20.

Table V-19: Weighting Factors for the Fuel Economy Calculation with Respect to the Vehicle Categories.

DRIVING CYCLES & WEIGHTINGS	SLEEPER CAB	DAY CAB	VOCATIONAL VEHICLE
ARB Transient	5%	19%	42%
55 mph Cruise	9%	17%	21%
65 mph Cruise	86%	64%	37%

Table V-20: Converting Coefficients to Calculate the CO_2 Level.

Constant	Class 8	Class 7	HHD Vocational	MHD Vocational	LHD Vocational
a [g CO_2/gal]	10180				
b [ton]	19	12.5	7.5	5.6	2.85

In order to compare the Autonomie model with the GEM model, the specifications and component parameters of a standard HD vehicle in the GEM software were analyzed. The corresponding information for the target vehicle was applied to the new HD model in Autonomie. That is, to validate the FE level between the two simulators, we intended to use the same values for the data set, such as the fuel consumption map, information of transmission, vehicle exterior, auxiliary power loss, and so forth. The detailed specifications of the target vehicle are summarized in Table V-21.

Table V-21: Specifications for the Class 8 Sleeper Cab—High Loop in Autonomie and GEM Version 1.

			Autonomie		GEM Ver. 1
			Default	GEM Case version	Default
Simulation	Vehicle name		Conv_10_Spd_MT_Class8_LineHaul		Class 8 - SC - HR
	Driving cycle		ARB Transient, 55MPHSS, 65MPHSS		
	Simulation mass	kg	30000	31978	31978
Engine	Engine max power	W	321000	339.43	339.43
	Engine displacement	cc	15000	15000	15000
	Engine BSFC map	g/s	eng_plant_ci_15000_324_Caterpillar_C15	eng_plant_ci_15000_339_GEM_Class8	Default Setting Engine Map
	Engine Max torque	Nm	2000	2100	2100
	Engine brake torque	Nm	-500	-500	-5*-10
	Engine idle speed	rad/s	68	65.45	65.45
	Engine rated speed	rad/s	120	125.66	125.66
	Engine max speed	rad/s	230	251.33	251.33
	Engine inertia	kg*m^2	0.45	4.17	4.17
Gear box	gb.gear ratio	1	14.78	14.8	14.8
		2	11	10.95	10.95
		3	8.17	8.09	8.09
		4	6	5.97	5.97
		5	4.46	4.46	4.46
		6	3.31	3.32	3.32
		7	2.46	2.45	2.45
		8	1.83	1.81	1.81
		9	1.34	1.35	1.35
		10	1	1	1
	gb.gear efficiency	%	97	0.96(1-4)/0.98(5-10)	0.96(1-4)/0.98(5-10)
	gb.inertia	kg*m^2	0.004+0.003(cpl+tr)	0.2+0.5(transfer case)	5
Chassis	chas.body_mass	kg	15000	15000	14742
	chas.cargo_mass	kg	10000	10000	17236.8
	chas.drag_coeff	-	0.6	0.6	0.6
	chas.frontal_area	m^2	10	10.4	10.4
Wheel	# of Axle	-	5	5	5
	Axle inertia	kg*m^2	1 (per whl)	20(per whl)	360
	whl.radius	m^2	0.48925	0.489	0.489
	whl.coeff_roll1		0.006	0.006	
	whl.coeff_roll2	1/(m/s)	0.00012	0	(6*0.425+6*0.425+6*0.15)/1000
	whl.coeff_roll3	1/(m/s)^2	0	0	
	whl.coeff_roll4	1/(m/s)^3	0	0	
Final drive	fd.ratio	-	2.64	2.64	2.64
	fd2.ratio	-	2.64	2.64	2.64
	fd.inertia	kg*m^2	0	2+2 (front+rear)	2+2
	fd.efficiency	%	98	99	99
Accessory	accelec.power	W	360	350	350
	accmech.power	W	0	1000	1000
Environment	Air Density	kg/m^3	1.1766	1.1766	1.1766

A typical engine fuel map consists of three columns: engine speed, torque, and fueling rate in grams per second. Essentially, the fueling rate is a function of engine speeds and loads. The map data displayed in Figure V-178 are an example of the fueling rate contour as a function of engine torque and speed for a Class 8 combination tractor with a 455-horsepower rating. In this study, the engine fuel rate information was extracted from GEM Version 1, and the data set was converted to a proper format for the Autonomie model and the initialization data.

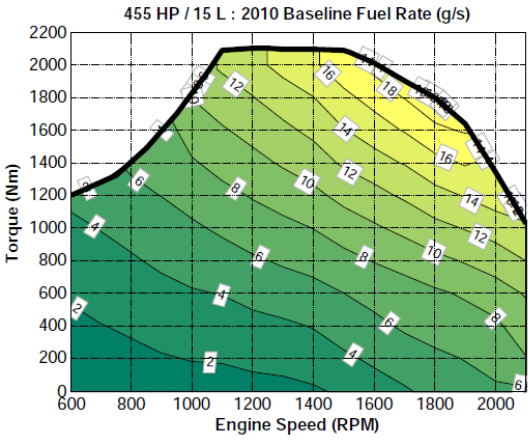

Figure V-178: Fuel Rate as a Function of Engine Torque and Speed for a Class 8 Tractor-Trailer—Source: GEM.

The driving cycles for the calculation of FE are illustrated in Figure V-179. The driving cycles are ARB transient, 55-mph steady speed, and 65-mph steady speed without a gradient on the road. The green-colored section in each driving cycle is the effective driving operation for the FE regulation level.

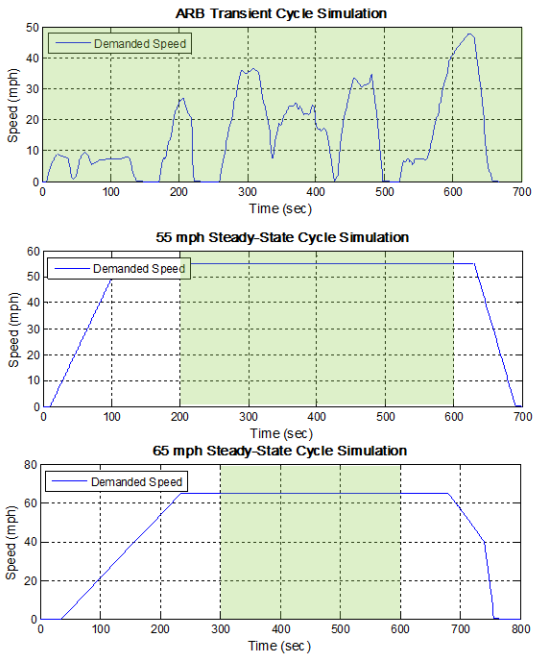

Figure V-179: Required Driving Cycles for GEM and Actual Range (shown in green) for Calculation of the Combined Fuel Economy Level.

Japan: Japan Fuel Consumption Model

For Japan's tool, after considering several testing options based upon multiple criteria (i.e., equipment and labor costs, accuracy, ability to account for non-engine efficiency improvements, and overlaps with emissions test cycles), the Japanese government chose to measure FE under its HD standards through a combination of engine-only fuel consumption testing and simulation modeling of gear shifting and vehicle resistance loads. The procedure is shown in Figure V-180.

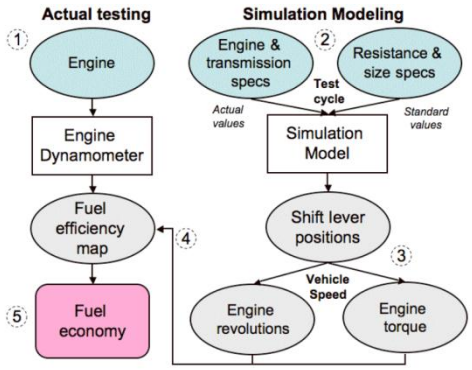

Figure V-180: Scheme for Fuel Economy Determination.

For the JFCM simulation program, the requisite engine specifications include full load torque, idle speed, maximum output speed, and maximum speed with load. The transmission properties used include the number of gears, gear ratios, final reduction gear ratio, and shift lever positions. The actual vehicle curb weight also is a required input, and payload is fixed at 20 tons (half maximum payload for a tractor over 20 tons gross vehicle weight [GVW]). The manufacturer or user also must provide an engine fuel map, which permits the calculation of fuel consumption over the constructed engine cycle and therefore over the vehicle test cycle. The Start window for JFCM is depicted in Figure V-181.

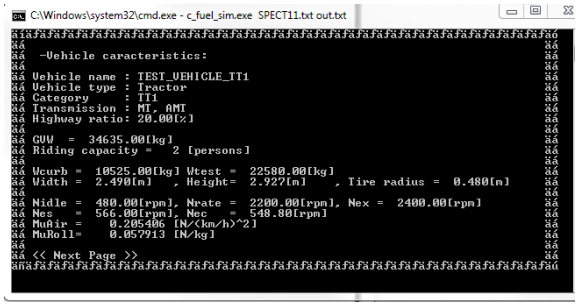

Figure V-181: Main Display for JFCM.

Compliance with the 2015 HD fuel economy standards is measured based upon the aggregated results of two test cycles: a transient test cycle (JE05) meant to represent operation in urban environments, and a steady-state cycle reflecting interurban driving conditions. Fuel economies measured by these tests are weighted according to vehicle application in order to derive an average FE level. Figure V-182 shows the speed profile of the JE05 test cycle and the grade profile used for the steady-speed test cycle, which has been used for HD emissions testing since 2005.

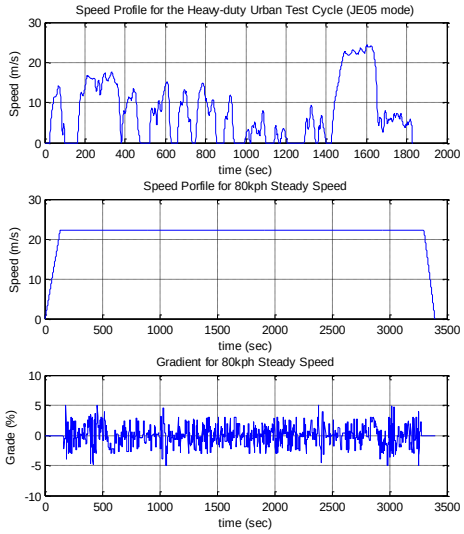

Figure V-182: Speed Profiles and Grade Profile for the 80-kph Steady Speed Used in JFCM.

For the Japan HD vehicle model validation, we used engine data and transmission data identical to those used in the GEM simulation, except for the chassis specifications such as the aero-dynamic coefficient, rolling resistance, frontal area, accessory loss power, and vehicle total mass for simulation. The complete input specifications are summarized in Table V-22.

Table V-22: Specifications for the Target HD Model in Autonomie and JFCM.

			Autonomie		JFCM
			Default	Japan Case version	Default
Simulation	Vehicle name		Conv 10 Speed Manual Trans Class8 Line Haul	Conv_10_Spd_MT_Japan_TT1	TT1
	Driving cycle			JE05, 80km/h SS	JE05, 80km/h SS
	Simulation mass	kg	30000	22580	22580
Engine	Engine max power	kW	321000	339.43	339.43
	Engine displacement	cc	15000	15000	15000
	Engine BSFC map	g/s	eng_plant_ci_15000_324_Caterpillar_C15	eng_plant_ci_15000_339_GEM_Class8	Default Setting Engine Map
	Engine Max torque	Nm	2000	2100	2100
	Engine brake torque	Nm	-500	-500	-500
	Engine idle speed	rad/s	68	640*pi/30	640*pi/30
	Engine rated speed	rad/s	120	1900*pi/30	1900*pi/30
	Engine max speed	rad/s	230	2200*pi/30	2200*pi/30
	Engine inertia	kg*m^2	0.45	4.17	-
Gear box	gb.gear ratio	1	14.78	14.8	14.8
		2	11	10.95	10.95
		3	8.17	8.09	8.09
		4	6	5.97	5.97
		5	4.46	4.46	4.46
		6	3.31	3.32	3.32
		7	2.46	2.45	2.45
		8	1.83	1.81	1.81
		9	1.34	1.35	1.35
		10	1	1	1
	gb.gear efficiency	%	97	0.95 (10: 0.98)	0.95 (10: 0.98)
	gb.inertia	kg*m^2	0.004+0.003(cpl+tr)	0.2+0.5(transfer case)	-
Chassis	chas.body_mass	kg	15000	15000	10525
	chas.cargo_mass	kg	10000	10000	12055 (Half load)
	chas.drag_coeff	-	0.6	0.608	0.608
	chas.frontal_area	m^2	10	7.2882	7.2882
Wheel	# of Axle	-	5	5	5
	Axle inertia	kg*m^2	1 (per whl)	20(per whl)	-
	whl.radius	m^2	0.48925	0.489	0.489
	whl.coeff_roll1		0.006	0.006	
	whl.coeff_roll2	1/(m/s)	0.00012	0	0.00591
	whl.coeff_roll3	1/(m/s)^2	0	0	
	whl.coeff_roll4	1/(m/s)^3	0	0	
Final drive	fd.ratio	-	2.64	2.64	2.64
	fd2.ratio	-	2.64	2.64	2.64
	fd.inertia	kg*m^2	0	2+2 (front + rear)	-
	fd.efficiency	%	98	95	95
Accessory	accelec.power	W	360	0	-
	accmech.power	W	0	0	-
Environment	Air Density	kg/m^3	1.1766	1.202	1.202

European Union: VECTO

While the U.S. test procedure allows users to modify the vehicle parameters with fixed engine and transmissions and the Japan procedure allows users to modify the engine and transmission with fixed vehicle parameters, the European procedure allows eusers to modify any vehicle parameters.

The software tool VECTO was developed for simulation of fuel consumption and CO_2 emissions based on the component test data, as defined by the work in a study funded by the

European Commission ("Reduction and Testing of Greenhouse Gas Emissions from Heavy-Duty Vehicles—Lot 2: Development and testing of a certification procedure for CO_2 emissions and fuel consumption of HDV"). Figure V-183 provides a scheme of VECTO, which fulfils the needs of the verification phase.

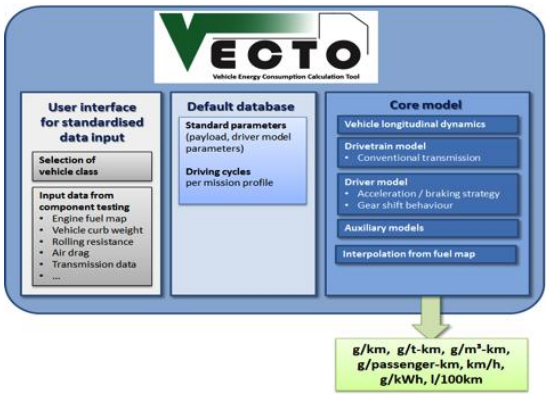

Figure V-183: Schematic Diagram of the Proposed HDV Simulation for the European Union.

The VECTO tool provides output values for CO_2 emissions/fuel consumption for the average of the test cycle and in 1-Hz resolution for the entire test cycle, as well as relevant additional simulation results (i.e., power demand of single auxiliaries, losses in transmission, total driving resistance, share of the single driving resistances, and so forth).

The main window for User Interface of VECTO is depicted in Figure V-184. Users can input the data set of their target vehicle. The data set consists of the engine fuel consumption map, the transmission specification and vehicle exterior, as well as information about the driver model.

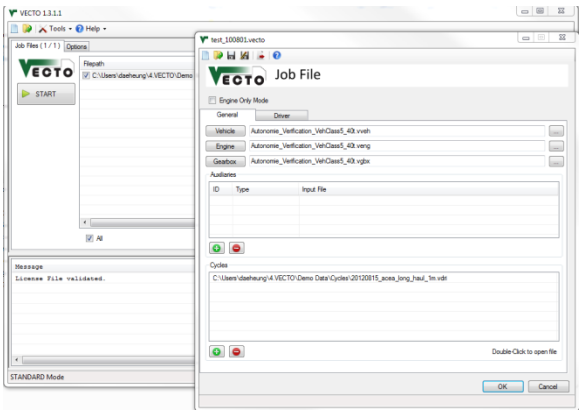

Figure V-184: Main Window of VECTO for Loading the Required Data Files.

The required data set and information for validation with the vehicle model in Autonomie are summarized in Table V-23. For consistency, the engine fuel consumption map and transmission specifications were used as an identical component model to the GEM validation case.

Table V-23: Specifications for the Target HD Model in Autonomie and VECTO.

			Autonomie		VECTO
			Default	VECTO Case version	Default
Simulation	Vehicle name		Conv_10_Spd_MT_Class8_LineHaul		Class5 Truck
	Driving cycle		LongHaul		
	Simulation mass	kg	30000	31300	31300
Engine	Engine max power	W	321	339.43	339.43
	Engine displacement	cc	15000	15000	15000
	Engine BSFC map	g/s	eng_plant_ci_15000_324_Caterpillar_C15	eng_plant_ci_15000_339_GEM_Class8	Default Setting Engine Map
	Engine Max torque	Nm	2000	2100	2100
	Engine brake torque	Nm	-500	-500	-500
	Engine idle speed	rad/s	68	640*pi/30	640*pi/30
	Engine rated speed	rad/s	120	1900*pi/30	1900*pi/30
	Engine max speed	rad/s	230	2200*pi/30	2200*pi/30
	Engine inertia	kg*m^2	0.45	4.17	4.17
Gear box	gb.gear ratio	1	14.78	14.8	14.8
		2	11	10.95	10.95
		3	8.17	8.09	8.09
		4	6	5.97	5.97
		5	4.46	4.46	4.46
		6	3.31	3.32	3.32
		7	2.46	2.45	2.45
		8	1.83	1.81	1.81
		9	1.34	1.35	1.35
		10	1	1	1
	gb.gear efficiency	%	97	0.97(1)/0.96(2-9)/0.98(10)	0.97(1)/0.96(2-9)/0.98(10)
	gb.inertia	kg*m^2	0.004+0.003(cpl+tr)	0	0
Chassis	chas.body_mass	kg	15000	15000	14742
	chas.cargo_mass	kg	10000	10000	17236.8 (Half Load)
	chas.drag_coeff	-	0.6	0.67	0.67
	chas.frontal_area	m^2	10	9.5	9.5
Wheel	# of Axle		5	5	5
	Axle inertia	kg*m^2	1 (per whl)	40 (per whl)	800
	whl.radius	m^2	0.48925	0.4875	0.4875
	whl.coeff_roll1		0.006	0.0054	
	whl.coeff_roll2	1/(m/s)	0.00012	0	0.0054
	whl.coeff_roll3	1/(m/s)^2	0	0	
	whl.coeff_roll4	1/(m/s)^3	0	0	
Final drive	fd.ratio	-	2.64	2.64	2.64
	fd2.ratio	-	2.64	2.64	2.64
	fd.inertia	kg*m^2	0	2+2 (front+rear)	2+2
	fd.efficiency	%	98	97	97
Accessory	accelec.power	W	360	0	0
	accmech.power	W	0	0	0
Environment	Air Density	kg/m^3	1.1766	1.2	1.2

			Autonomie		VECTO
			Default	VECTO Case version	Default
Simulation	Vehicle name		Conv_10_Spd_MT_Class8_LineHaul		Class5 Truck
	Driving cycle		LongHaul		
	Simulation mass	kg	30000	31300	31300
Engine	Max power	W	321	339.43	339.43
	Displacement	cc	15000	15000	15000
	BSFC map	g/s	Caterpillar_C15	GEM_Class8	Default Engine
	Max torque	Nm	2000	2100	2100
	Brake torque	Nm	-500	-500	-500
	Idle speed	rad/s	68	640*pi/30	640*pi/30
	Rated speed	rad/s	120	1900*pi/30	1900*pi/30
	Max speed	rad/s	230	2200*pi/30	2200*pi/30
	Inertia	kg*m^2	0.45	4.17	4.17
Gear box	Ratios	1	14.78	14.8	14.8
		2	11	10.95	10.95
		3	8.17	8.09	8.09
		4	6	5.97	5.97
		5	4.46	4.46	4.46
		6	3.31	3.32	3.32
		7	2.46	2.45	2.45
		8	1.83	1.81	1.81
		9	1.34	1.35	1.35
		10	1	1	1
	Peak Efficiency	%	97	0.97(1)/0.96(2-9)/0.98(10)	0.97(1)/0.96(2-9)/0.98(10)
	Intertia	kg*m^2	0.004+0.003(cpl+tr)	0	0
Chassis	Boby Mass	kg	15000	15000	14742
	Cargo Mass	kg	10000	10000	17236.8 (Half Load)
	Drag Coeff	-	0.6	0.67	0.67
	Frontal area	m^2	10	9.5	9.5
Wheel	# of Axle	-		5	
	Axle inertia	kg*m^2	1 (per whl)	40 (per whl)	800
	redius	m^2	0.48925	0.4875	0.4875
	whl.coeff_roll1		0.006	0.0054	
	whl.coeff_roll2	1/(m/s)	0.00012	0	0.0054
	whl.coeff_roll3	1/(m/s)^2	0	0	
Final drive	Ratios	-		2.64	
	Inertia	kg*m^2	0	2+2 (front+rear)	2+2
	Efficiency	%	98	97	97
Accessory	Elec Power	W	360	0	0
	Mech Power	W	0	0	0
Environment	Air Density	kg/m^3	1.1766	1.2	1.2

Because the target vehicle is a HD class in which the simulation mass is more than 30 tons, we used one driving cycle, '20120815_acea_long_haul' for the target vehicle being classed in the long-haul category (tractor-trailer) in the European Union. The speed and grade profiles are depicted in Figure V-185.

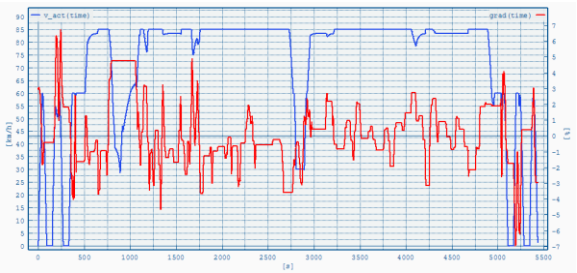

Figure V-185: Speed and Grade Profiles for the Long-Haul Class Simulation in VECTO.

Chinese Simulation Program

Unlike the programs in Japan and the United States, China's proposed program requires chassis dynamometer testing. The manufacturer would test the vehicle over a modified version of the World Transient Vehicle Cycle (WTVC) that consists of 10% rural driving and 90% highway driving. The chassis test results automatically reflect the performance of certain vehicle components and systems, which must be input separately in the simulation-based programs. In particular, engine and transmission properties should be reflected by the chassis test results. However, information related to tractive load, such as drag and rolling resistance coefficients, is still required as inputs to the chassis test in order to arrive at an estimate of on-road fuel efficiency. Furthermore, manufacturers must supply the full array of engine, transmission, and other simulation inputs in China's program, since the fuel consumption of the variants of the basic models tested on the chassis dynamometer is determined through vehicle simulation. That is, for the basic vehicle results, the chassis dynamometer test method could be used to determine fuel consumption. Also, for various types of vehicles, manufacturers can choose to use the simulation method or chassis dynamometer method to determine the fuel consumption. Figure V-186 shows the main window for the China simulation program. Many vehicle manufacturers and information about various vehicle models have already been entered, and users can select the target vehicle and related component data set to run a simulation.

Figure V-186: Main Window of China's Program for the HD Simulation.

The driving cycle used in China's simulation program is shown in Figure V-187. The vehicle models in the program use the cycle for certification, with various weighting factors for specific driving segments such as city mode, interurban mode, and highway mode.

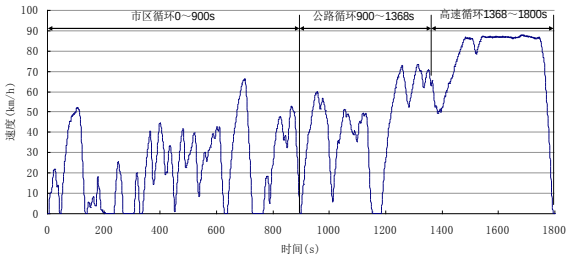

Figure V-187: China Driving Cycle, Including the Urban (0~900 sec), Interurban (900~1,368 sec), and Highway (1,368~1,800 sec) Driving Portions.

The target vehicle for comparing the FE between Autonomie and China's program is the tractor-trailer vehicle model in the HD category. Detailed specifications for the simulation are shown in Table V-24. This program allows users to input their specific component data set for regulatory.

The weighting factors for the calculation of FE are changed according to the vehicle categories and the GVW, as summarized in Table V-25.

Table V-24: Specifications for the Target HD Model in Autonomie and China's Simulation Software.

			Autonomie		China-Sim
			Default	China Model Case	Default
Simulation	Vehicle name		Conv 10 Speed ManualTrans Class8 Line-Haul	Conv_10_Spd_MT_China_Tractor_Trailer	Tractor Trailer
	Driving cycle			WTVC	WTVC
	Simulation mass	kg	30000	30577	30577
Engine	Engine max power	kW	321000	339.43	339.43
	Engine displacement	cc	15000	15000	15000
	Engine BSFC map	g/s	eng_plant_ci_15000_324_Caterpillar_C15	eng_plant_ci_15000_339_GEM_Class8	Default Setting Engine Map
	Engine Max torque	Nm	2000	2100	2100
	Engine brake torque	Nm	-500	-500	-500
	Engine idle speed	rad/s	68	640*pi/30	640*pi/30
	Engine rated speed	rad/s	120	1900*pi/30	1900*pi/30
	Engine max speed	rad/s	230	2200*pi/30	2200*pi/30
	Engine inertia	kg*m^2	0.45	4.17	-
Gear box	gb.gear ratio	1	14.78	14.8	14.8
		2	11	10.95	10.95
		3	8.17	8.09	8.09
		4	6	5.97	5.97
		5	4.46	4.46	4.46
		6	3.31	3.32	3.32
		7	2.46	2.45	2.45
		8	1.83	1.81	1.81
		9	1.34	1.35	1.35
		10	1	1	1
	gb.gear efficiency	%	97	0.95 (10: 0.98)	?
	gb.inertia	kg*m^2	0.004+0.003 (cpl + tr)	0.2+0.5(transfer case)	-
Chassis	chas.body_mass	kg	15000	15000	11900
	chas.cargo_mass	kg	10000	10000	18905
	chas.drag_coeff	-	0.6	0.8	0.8
	chas.frontal_area	m^2	10	7.8	7.8
Wheel	# of Axle	-	5	5	5
	Axle inertia	kg*m^2	1 (per whl)	20(per whl)	-
	whl.radius	m^2	0.48925	0.4649	0.4649
	whl.coeff_roll1		0.006	0.006	-
	whl.coeff_roll2	1/(m/s)	0.00012	0	0.0041+0.0000256*90km/h = 0.0064
	whl.coeff_roll3	1/(m/s)^2	0	0	
	whl.coeff_roll4	1/(m/s)^3	0	0	
Final drive	fd.ratio	-	2.64	2.64	2.64
	fd2.ratio	-	2.64	2.64	2.64
	fd.inertia	kg*m^2	0	2+2(front+rear)	-
	fd.efficiency	%	98	95	?
Accessory	accelec.power	W	360	0	0
	accmech.power	W	0	0	0
Environment	Air Density	kg/m^3	1.1766	1.189	1.189

Table V-25: Weighting Factors for the Fuel Economy Calculation with Respect to the Vehicle Categories.

Vehicle Class	Maximum vehicle mass GCW/GVW kg	Urban	Interurban	Highway
Tractor trailer	9000＜GCW≤25000	0	40%	60%
	GCW >25000	0	10%	90%
Dump Truck	GVW >3500	0	100%	0
Lorry	3500＜GVW≤5500	40%	40%	20%
	5500＜GVW≤12500	10%	60%	30%
	12500＜GVW≤24500	10%	40%	50%
	GVW >24500	10%	30%	60%
Bus	3500＜GVW≤5500	50%	25%	25%
	5500＜GVW≤12500	20%	30%	50%
	GVW >12500	10%	20%	70%
City Bus	GVW >3500	100%	0	0

Results

Comparison with GEM

To compare the FE level between GEM and Autonomie, the HD vehicle models of six cases were simulated under the same conditions. The vehicle classes are as follows:

- Class 8 Sleeper Cab: High Roof
- Class 8 Sleeper Cab: Mid Roof
- Class 8 Sleeper Cab: Low Roof
- Class 8 Day Cab: High Roof
- Class 8 Day Cab: Mid Roof
- Class 8 Day Cab: Low Roof

The specifications of each vehicle simulation case were directly applied according to the standard values in GEM. The FE results are shown in Figure V-188. The combined FE values in the mile-per-gallon unit show a very similar tendency with respect to the vehicle class.

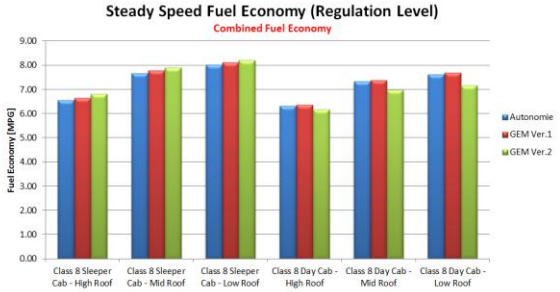

Figure V-188: Fuel Economy Comparison between Autonomie and GEM.

The discrepancy of the combined FE of Autonomie and GEM Version 1 is illustrated in Figure V-189. The discrepancy is within -1.5% in this steady-speed FE. If the fuel consumption on the entire driving is considered, the discrepancy can be reduced to within 1% for the Class 8 Sleeper Cab.

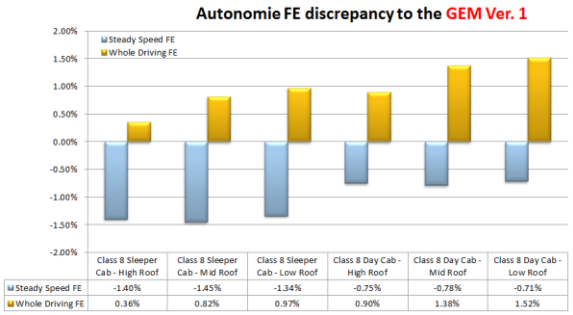

Figure V-189: Discrepancy of the Results between Autonomie and GEM.

The powertrain performance also was compared to determine the difference in operating status, as shown in Figure V-190 and Figure V-191. A noticeable dynamic characteristic of GEM Version 1 is that the vehicle speed is increasing while the engine speed is kept at a constant rotational speed at idle status between 260 and 265 seconds, as depicted in Figure V-190. The second major difference involves the engine fuel-cut-off function when the vehicle is decelerating, as shown in Figure V-191. The vehicle model in GEM consumed more fuel rate during deceleration and gear shifting timing.

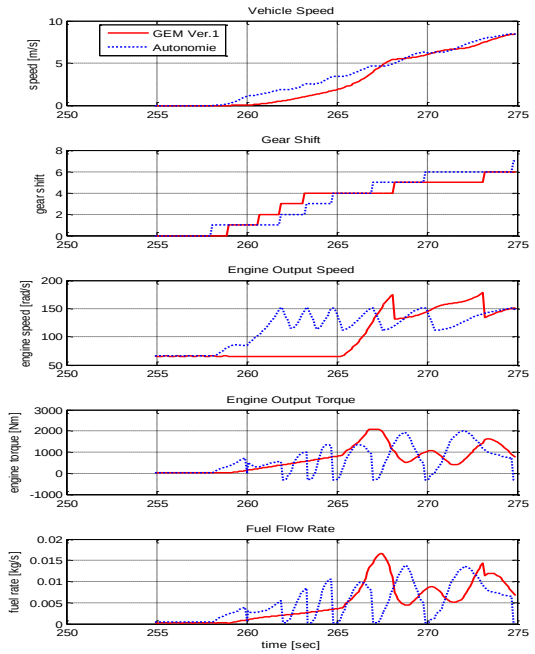

Figure V-190: Comparison of the Dynamic Performance of Two Simulators.

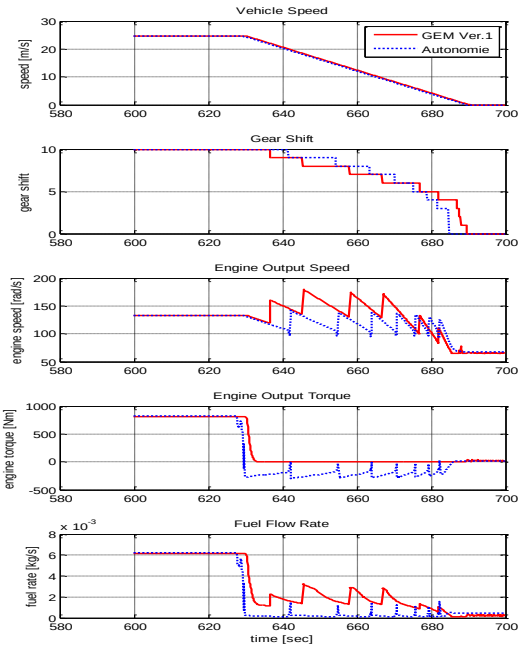

Figure V-191: Dynamic Performance Comparison during Deceleration.

Comparison with JFCM (Japan)

For the Japan model validation, the tractor-trailer vehicle was simulated as the TT1 HD class on the two standard driving cycles in JFCM.

The discrepancy of the combined FE level is almost 2%, and on the 80-kph steady speed with grade the discrepancy results in less than 1%. Therefore, the FE level of the two simulations matches well with each other, although the simulation method is different—FCM is backward-based, and Autonomie is forward-based. Table V-26 shows the FE comparison results between Autonomie and JFCM.

Table V-26: Fuel Economy Comparison Results between Autonomie and JFCM.

			Open Source Program
	Driving Cycle (Weighting Factor)	Autonomie	JFCM
		Fuel Economy [Km/L] (Error % to JFCM)	Fuel Economy [Km/L]
TT1 Tractor	JE05 (80%)	2.496 (-2.28%)	2.554
	80 KPH SS (20%)	4.230 (-0.74%)	4.262
	Combined	2.719 (-2.09%)	2.777

The dynamic analysis results are shown in Figure V-192 and Figure V-193 on the JE05 and 80-kph steady-speed mode, respectively. Similar to the GEM case, the shut off status of the engine output torque during gear shifting and the engine braking torque is different, primarily as shown in Figure V-192.

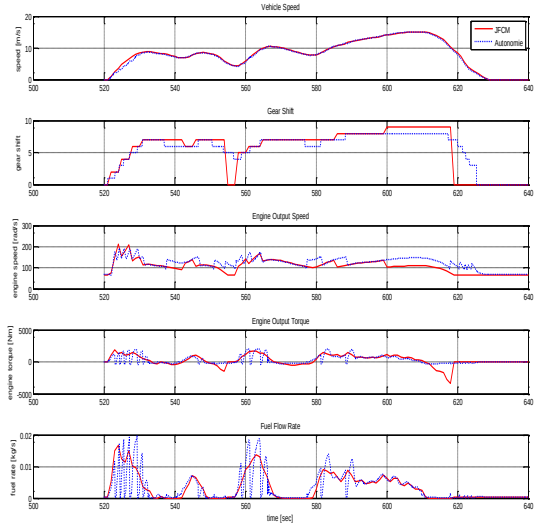

Figure V-192: Dynamic Performance Comparison on the JE05 Mode.

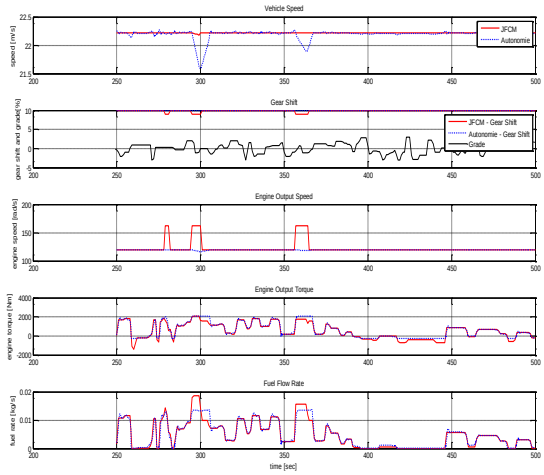

Figure V-193: Dynamic Performance Comparison on the 80-kph Steady-Speed Mode.

Figure V-193 shows the operating status of the powertrain over the constant speed mode of two simulation programs. Most of the compared output signals show similar value, except for the instantaneous gear shifting of JFCM.

Comparison with VECTO (European Union)

The FE calculation for the HD model for the European Union was performed on one driving cycle: long-haul with grade data. The comparison result of the FE between VECTO and Autonomie is shown in Table V-27. The FE from the Autonomie model is almost 3% lower than that of VECTO.

Table V-27: Fuel Economy Comparison Results between Autonomie and VECTO.

			Closed Source Program
	Driving Cycle (with grade)	Autonomie	VECTO
		Fuel Economy [Km/L] (Error % to VECTO)	Fuel Economy [Km/L]
Tractor Trailer	Long Haul	2.92 (-2.99%)	3.01

The fuel flow rate and gear shifting timing are similar during acceleration time, as shown in Figure V-194. However, during deceleration and low steady-speed driving, the gearbox of VECTO uses a higher gear position than that of Autonomie.

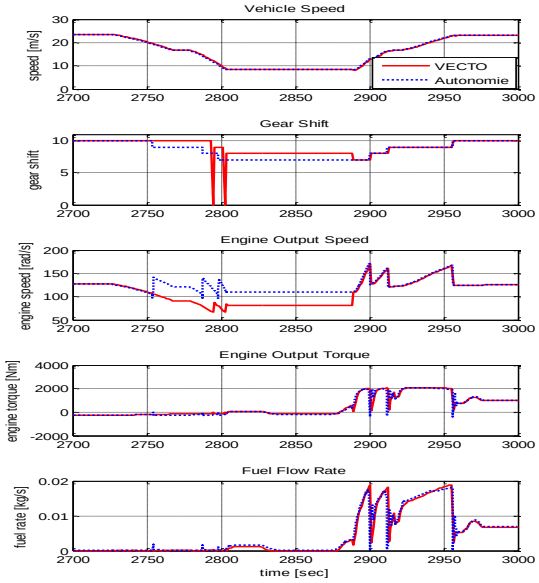

Figure V-194: Output Performance Comparison of the Powertrain on the Long-Haul Cycle for the HD Vehicle—Gear Position.

Generally, the gear box of VECTO uses the third gear when the vehicle is starting and a higher gear position than the gear shifting level of Autonomie, as shown in Figure V-195. The engine braking torque between the compared simulator results is similar in level and tendency, which differs from other simulation results, such as that of the GEM and JFCM cases.

The engine operating points of the two compared results are depicted in Figure V-196. The VECTO model uses maximum torque line more than the operation of Autonomie. However, the overall used operating region is almost similar.

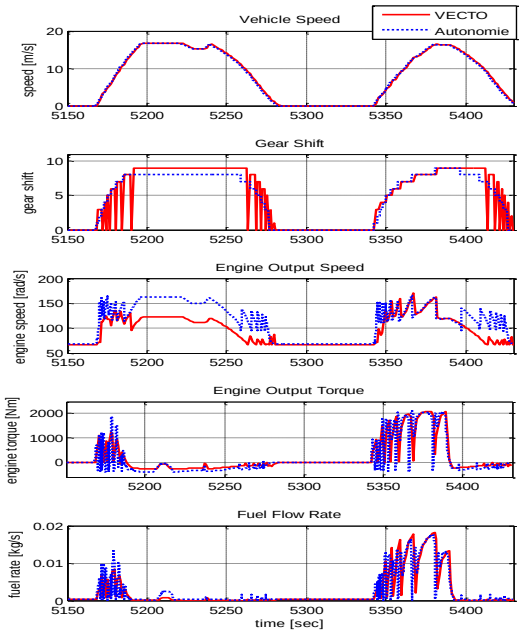

Figure V-195: Output Performance Comparison of the Powertrain on the Long-Haul Cycle for the HD Vehicle—Engine Braking Torque and Gear Position.

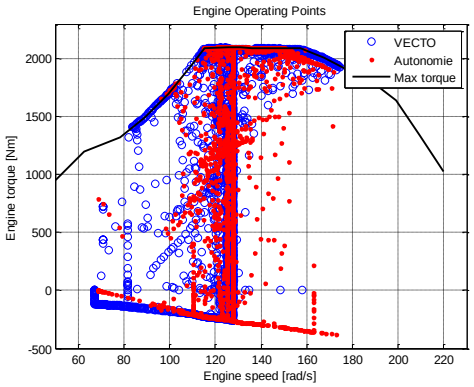

Figure V-196: Engine Operating Points for VECTO Validation.

Comparison with China-Sim (China)

Of all the validation results, the comparison results for the Chinese simulation show the largest difference in FE and the operating status of a powertrain. First of all, the engine operating points of the two simulation programs (illustrated in Figure V-197) certainly differ from the case of VECTO, as shown in Figure V-196. The difference in the engine operating status might come from the gear shifting strategy of each simulator. At this point, we cannot determine the clear reason for the results and the difference in the shifting algorithm, since the Chinese program is not an open source code.

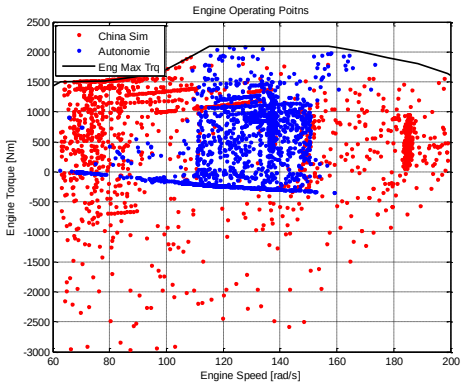

Figure V-197: Engine Operating Points for the Chinese Program Validation.

As shown in Figure V-198, the engine operating speed of the Chinese tool changes drastically depending on the gear shifting pattern, which is a considerably different result than found in the other analysis cases. Also, a higher gear level than that of Autonomie is used on the entire driving region. For the engine braking torque of the Chinese simulation, impractical negative torque occurs (or is calculated) when the vehicle is decelerating, which is analogous to the case of JFCM.

As indicated in Figure V-199, the engine output torque is higher than the torque of Autonomie, since it has a higher level gear position than the Autonomie case. The FE comparison results are summarized in Table V-28. The difference in FE is almost 15% in the combined results.

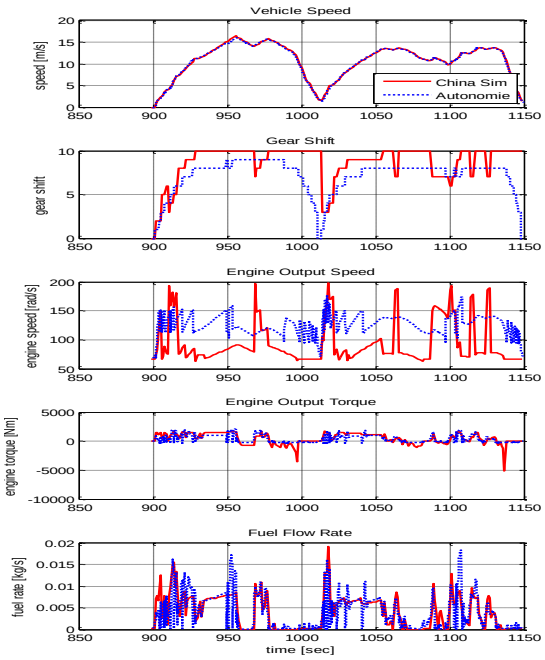

Figure V-198: Operating Performance Comparison between Autonomie and the Chinese Simulator.

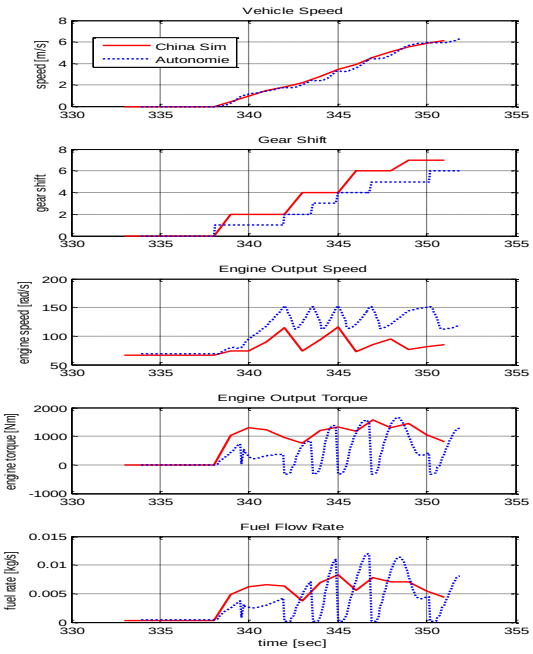

Figure V-199: Operating Performance Comparison between Autonomie and the Chinese Simulator.

Table V-28: Fuel Economy Comparison Results between Autonomie and the Chinese Simulator.

	Driving Cycle (Weighting Factor)		Autonomie	China-Sim
			Fuel Economy [km/L] (Discrepancy % to China-Sim)	Fuel Economy [km/L]
Tractor Trailer (GCW >25000kg)	City (0%)	0 ~ 900sec	1.780 (+16.57%)	1.527
	Interurban (10%)	901 ~ 1368sec	2.260 (+4.44%)	2.164
	Highway (90%)	1369 ~ 1800sec	3.145 (+16.13%)	2.708
	Combined		3.057 (+15.18%)	2.654

Conclusions

This research involved comparing various simulation programs for the MD and HD vehicle regulations with Autonomie. To achieve this, we analyzed the specifications and required data set of each simulator, as well as the internal calculation method in the case of open source code.

For GEM, we could analyze GEM Version 1 as the open source program in detail. The vehicle model configuration of GEM is similar to that of Autonomie when it comes to the component, signal in/out, and definition of parameter. For steady-speed FE, the discrepancy of the FE between GEM and Autonomie is within -1.5%. If the fuel consumption on the entire driving is considered, the discrepancy can be reduced to within 1% for a Class 8 sleeper cab. The main differences between GEM and Autonomie are as follows:

- Fuel consumed when the vehicle is decelerating,
- Fuel consumed during shifting events.

For JFCM, the FE results were similar to Autonomie. Most output signals are comparable except the engine output torque during gear shifting and the engine braking torque during deceleration events.

In the VECTO validation, the FE calculation for the HD model in the European Union was performed on the one driving cycle, and the fuel economy results are within 3%. The fuel flow rate and gear shifting are similar during vehicle acceleration. However, during deceleration and low steady-speed driving, the gearbox from VECTO uses a higher gear position than that of Autonomie. The engine braking torque between the compared simulators has a similar level and tendency, which differ in the other simulation results, as in the case of GEM or JFCM.

In the Chinese tool, the engine operating points between simulation programs differ from each other. The different engine operating status could be the result of the gear shifting strategy of each simulator. The difference in FE is as high as 15% in the combined results.

To summarize the FE comparison, Figure V-200 and Figure V-201 present the compared results of the combined FE and discrepancy between the different simulators.

From this research, we have determined that Autonomie and other simulation tools for supporting regulation programs (except for the Chinese program) show good comparison results for the FE level of the HD vehicle model. We also found some differences in the operating performance of the powertrain and the shifting control methods. Autonomie HD vehicle model is producing results similar to the different regulatory tools currently available.

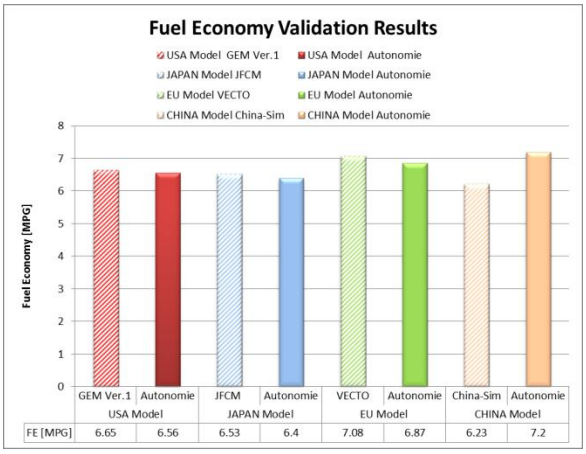

Figure V-200: Fuel Economy Validation Results with Respect to Each Simulation Tool.

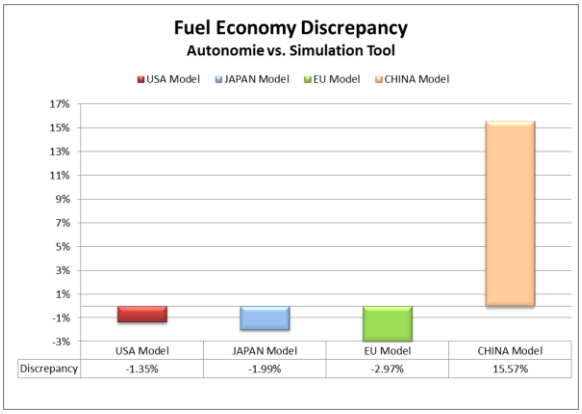

Figure V-201: Fuel Economy Discrepancy between Autonomie and Each Simulation Tool.

V.T.3. Products

Tools and Data

1. Autonomie
2. GEM
3. JFCM
4. Chinese Simulation Program
5. VECTO
6. Matlab/Simulink

References

1. Autonomie, 2012, available at: www.autonomie.net.
2. Langer, T. and S. Khan, "International Alignment of Fuel Efficiency Standards for Heavy-Duty Vehicles," American Council for an Energy-Efficient Economy, report number T131, 2013.
3. International Council on Clean Transportation, "Proposed National Fuel Consumption Standard for Commercial Heavy-Duty Vehicles in China," policy update, 2013.
4. Northeast States Center for a Clean Air Future, International Council on Clean Transportation, and South Research Institute, "Reducing Heavy-Duty Long Haul Combination Truck Fuel Consumption and CO_2 Emissions," 2009.
5. "Fuel Consumption Test Methods for Medium- and Heavy-Duty Commercial Vehicles," China Regulation. [This reference is incomplete.]
6. Kousoulidou, M., et al., "Review and Evaluation of Emission Models and Vehicle Simulation Tools: Version 2," Institute for Energy and Transport, Sustainable Transport Unit, 2013.
7. International Council on Clean Transportation, "Fact Sheet: Japan's 'Top Runner' Fuel Economy Standards for Heavy-Duty Vehicles," 2008.
8. U.S. Environmental Protection Agency, "Greenhouse Gas Emissions Model (GEM) User Guide," EPA-420-B-11-019, 2011.
9. Institute for Internal Combustion Engines and Thermodynamics, "Reduction and Testing of Greenhouse Gas Emissions from Heavy-Duty Vehicles—Lot 2: Development and Testing of a Certification Procedure for CO_2 Emissions and Fuel Consumption of HDV," Graz University of Technology, Graz, Austria, 2012.

V.U. Analysis of Interstate Electrification with Class 8 Trucks

Jeffrey Gonder, Principal Investigator
National Renewable Energy Laboratory
15013 Denver West Parkway, MS 1634
Golden, CO 80401
Phone: (303) 275-4462
E-mail: jeff.gonder@nrel.gov

David Anderson, DOE Program Manager
Phone: (202) 287-5688
E-mail: david.anderson@ee.doe.gov

V.U.1. Abstract

Objectives

- Analyze the potential future opportunity for wireless power transfer (WPT) to commercial vehicles as they drive.
  - Complementary effort to DOE's WPT funding opportunity announcement (FOA) awards, which focus on stationary WPT to light-duty vehicles.

Major Accomplishments

- Demonstrated that WPT technology installation over a relatively small portion of road infrastructure could support electrification (and corresponding operating cost savings) for a considerably larger fraction of vehicle miles travelled.
- Identified particularly strong infrastructure leverage for tractor-trailer (line-/long-haul) vocations, where over three-quarters of operating miles can occur on functional class 1 roads (interstates).
- Conducted vehicle modeling and validation for Class 8 truck applications—complementing similar previous efforts for light-duty vehicles.
- Completed preliminary vehicle-level net present cost analysis suggesting considerable economic opportunity from roadway electrification, particularly for the very operating-cost-sensitive Class 8 tractor-trailer vocation.

Future Achievements

- Extend second-by-second modeling and simulation work to further examine power demand fluctuations and implications for the electric roadway infrastructure and the utility grid.
- Explore additional input parameter sensitivities, and further analyze scenarios where multiple types of vehicles operate simultaneously on the electrified roadway.

✧ ✧ ✧ ✧ ✧

V.U.2. Technical Discussion

Background

Significant advances in wireless power transfer (WPT) technology in recent years has led to the development of many prototype and even some commercial products for stationary charging of plug-in electric vehicles (PEVs). While WPT may increase the convenience of stationary PEV charging in the near to medium term, as the technology continues to advance it has the long-term potential to transform PEV technology through power transfer to driving vehicles. Several technology developers have already been exploring the potential of in-motion power transfer to commercial vehicles, including the Korea Advanced Institute of Science and Technology (KAIST) with inductive power transfer to buses, as well as Siemens and Volvo with conductive power transfer to heavy trucks (using catenary lines and in-roadway conductive tracks, respectively).

Introduction

Due to the large amount of vehicle travel that they support, interstates may be prime locations to introduce these types of in-motion WPT technologies. Similarly, due to their contribution as heavy road users and fuel consumers, Class 8 trucks may prove to be a key vehicle segment for using in-motion power transfer to displace petroleum consumption. While heavy-duty vehicles comprise only about 4% of the vehicles on the road, they account for over 20% of U.S. fuel consumption [1]. This analysis explores the fuel displacement opportunity WPT may offer to Class 8 trucks, as well as the potential economics for various implementation scenarios.

Approach

In approaching this heavy vehicle WPT analysis, the National Renewable Energy Laboratory (NREL) drew from tools and techniques applied toward complimentary light-duty WPT analysis. For the light-duty analysis, NREL analyzed tens of thousands of real-world drive cycles collected using global positioning system (GPS) devices and stored in the Transportation Secure Data Center (TSDC) [2]. Figure V-202 provides the output of an analysis showing the amount of travel overlap from the GPS driving profiles in three metropolitan areas. The graph shows that for these light-duty vehicle samples a relatively small fraction of roads support a large amount of driving miles—e.g., the most heavily traveled 1% of roads supports roughly 20% of all miles traveled. Therefore, in-motion WPT devices installed only on the most heavily traveled roads could potentially support a disproportionately larger fraction of overall travel. Additional analysis shows that the top 1% of most heavily travelled roads

aligns well with the interstate highway system, which if electrified with sufficient WPT coverage and power capability could effectively remove the range limitation for battery electric vehicles [3].

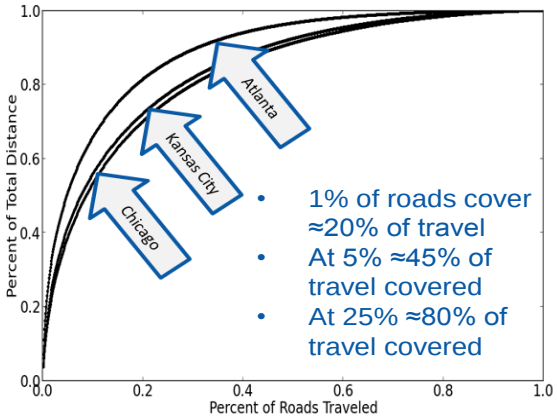

Figure V-202: Analysis of real-world driving data from travel surveys in several U.S. cities shows that a relatively small fraction of roads supports a large percentage of total distance traveled.

Further light-duty WPT analysis indicated that in the absence of continued battery cost reductions, hybrid electric vehicles (HEVs) rather than PEVs may be the preferred powertrain for broad deployment on WPT-enabled infrastructure (because they can displace a similar amount of fuel as a PEV at a lower vehicle cost). Based on this result and the high energy consumption required to propel heavy vehicles, the Class 8 WPT analysis summarized here also assumes HEV powertrains in the vehicles that draw power from equipped road sections.

For the Class 8 truck analysis, NREL considered both straight-truck (regional delivery) and tractor-trailer (line-haul/long-haul) applications, again leveraging real-world travel data (available for these commercial vehicle applications through the FleetDNA database [4]). The GPS driving profiles for both of these Class 8 applications were map-matched to the underlying road network, and each segment of the driving profile was then assigned the corresponding road functional class (FC) value, where FC1 corresponds to high-capacity interstates and FC5 generally corresponds to low-capacity neighborhood streets [5]. Figure V-203 and Figure V-204 show the proportional breakdown of miles traveled by functional class for the two different truck vocations. (NA indicates locations where a road functional class map match was not available, such as in parking lots or truck yards).

The data from the straight-truck sample shown in Figure V-203 came from a regional beverage delivery application in a dense urban area that did not include interstate travel. As a result, the WPT scenario considered for the straight-truck analysis summarized here assumes electrification of the FC2 and FC3 roads in the region. These roads will still support a fairly high fraction of travel, with the vehicle moving at lower speeds (and smaller power demands) relative to FC1 road travel—potentially enabling fewer WPT devices to supply power to the vehicles relative to the FC1 case.

The tractor-trailer sample, originally from an Oak Ridge National Laboratory study [6], includes long-distance travel on predominantly FC1 roads. The analysis results summarized here explore the potential scenarios where these FC1 roads are electrified (i.e., with WPT devices). These draft results rely upon representative fuel consumption rates drawn from the on-road sample (which included instantaneous fuel rate data logging).

As described in the next section, the Class 8 straight-truck analysis included detailed vehicle modeling using NREL's Future Automotive Systems Technology Simulator (FASTSim). Various powertrain configurations were simulated over the real-world driving profiles, and FASTSim was modified to accept electrical power from equipped roadway sections for the evaluated WPT scenarios.

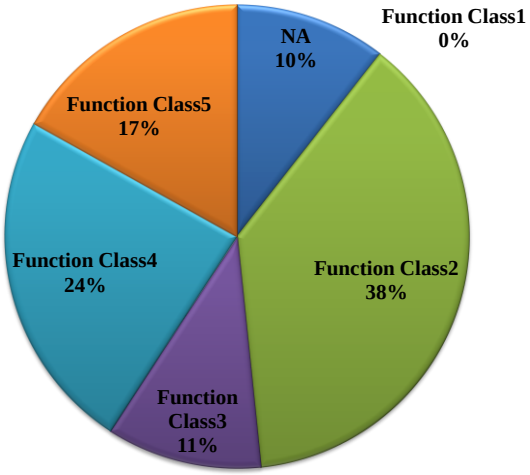

Figure V-203: Proportion of miles traveled by road functional class for the straight-truck data sample.

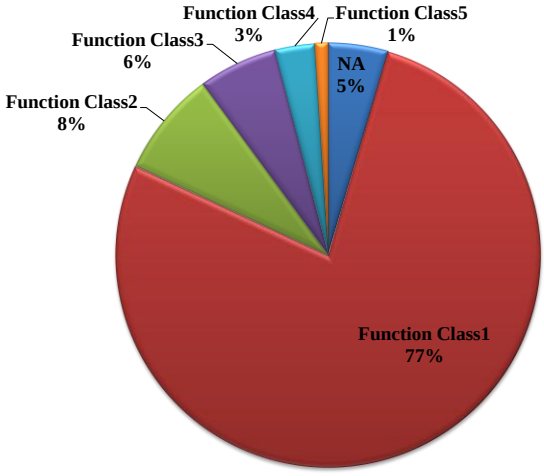

Figure V-204: Proportion of miles traveled by road functional class for the tractor-trailer data sample.

Results

The on-road Class 8 straight-truck dataset included data from both conventional and HEV powertrain variants deployed in the beverage delivery fleet. Both types of vehicles were tested on a chassis dynamometer at NREL's Renewable Fuels and Lubricants (ReFUEL) Laboratory [7]. The ReFUEL Laboratory data helped calibrate the aforementioned conventional and HEV FASTSim models used as baseline vehicles for the WPT analysis. As shown in Figure V-205, for both powertrains, the FASTSim model results closely match those from the ReFUEL testing over multiple standard drive cycles—West Virginia University City (WVU City), Heavy Heavy-Duty Diesel Truck (HHDDT) and Combined International Local and Commuter Cycle (CILCC).

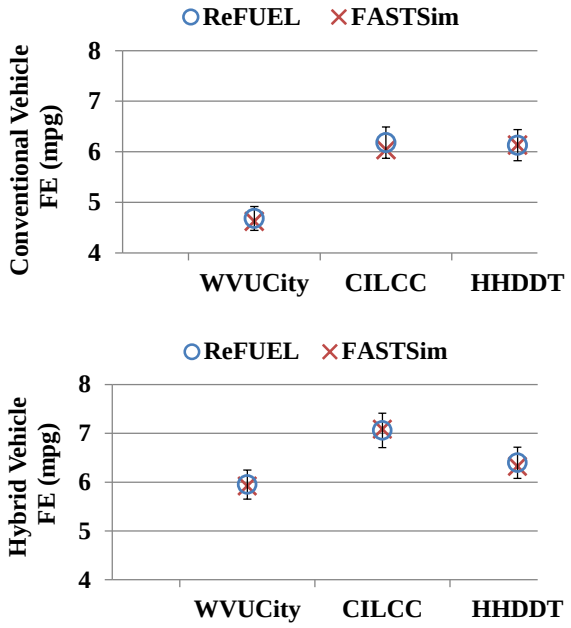

Figure V-205: Validation of conventional vehicle and HEV FASTSim models against ReFUEL Laboratory chassis dynamometer test data.

Building from the validation effort, conventional (CV) and HEV FASTSim models were simulated over the entire real-world data set of 62 regional delivery driving profiles. Several electrified-roadway-capable HEV ("EHEV") variants were also simulated against the full set of drive cycles. Figure V-206 presents a sample set of results showing the reduction in total fuel consumed over all of the simulated drive cycles by moving from a CV to an HEV and then to two EHEV variants (with the indicated average roadway electrification power provided when traveling on FC2 and FC3 roads). For additional reference, the fuel consumption indicated in each column is subdivided by the functional class on which it occurred. Assuming an HEV design that permits engine off at idle, the simulated HEV consumes nearly 20% less fuel than the CV over the regional delivery duty cycles. These savings are spread across all functional class categories, with particularly noticeable benefit occurring on FC4 and FC5 roads where significant stop-and-go driving would be expected. The first EHEV scenario assumes up to 50 kW of roadway power transfer is available on FC2 and FC3 roads. When the vehicle power demand is greater than this amount, the EHEV battery may provide supplemental power (for short time intervals); otherwise the engine makes up the difference. The electrified roadway may also provide less than its maximum power capability for any given moment when the vehicle power demand (including any needed battery charging) is low. The fuel savings achieved for this scenario relative to the CV is over 30%, and for the 100-kW-capable electrified roadway scenario the savings is roughly 45% (the incremental savings relative to the HEV all coming on the electrified FC2 and FC3 sections for both EHEV scenarios).

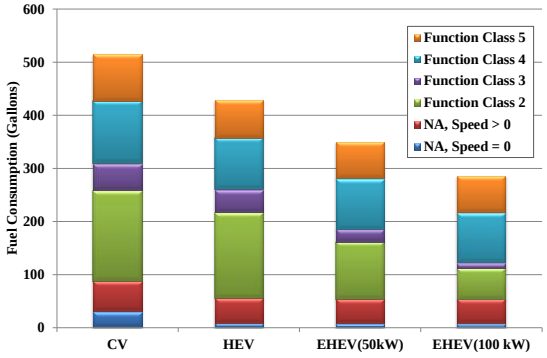

Figure V-206: Fuel consumption (by road functional class) for batch simulations of four powertrain scenarios over nearly 2,700 miles of regional delivery driving cycles.

Table V-29 lists assumptions for annual truck operating miles (tapering over the assumed 19-year life) as well as other inputs used in the following draft cost vs. benefit analysis [8]–[10]. Figure V-207 shows the lifetime fuel use along with net present vehicle and fuel cost calculations for the four straight-truck powertrain scenarios from Figure V-206. Note for these assumptions that while hybridization results in significant petroleum savings (more than 11,000 diesel gallons), this savings is insufficient to overcome the incremental cost of hybridization and results in a 5% higher net present cost. The additional lifetime fuel savings for the FC2 and FC3 EHEV scenarios (another 10,000 gallons for the 50-kW case and another 18,500 gallons beyond the HEV savings for the 100-kW EHEV case) help improve the net present cost, but only slightly.

Table V-29: Assumptions for Draft Class 8 Cost vs. Benefit Analysis.

Inputs	Straight-Truck Assumption	Tractor-Trailer Assumption
Vehicle life (years)	19	19
Beginning of life annual miles	30,000	120,000
End of life annual miles travelled	7,000	30,000
Conventional vehicle cost	$70,000	$110,000
Hybridizing cost increment	$42,900	$61,450
Additional EHEV cost increment	$10,000	$10,000
Diesel cost	$3.98/gal	$3.98/gal
Electricity cost	$0.12/kWh	$0.12/kWh
Discount rate	4.2%	4.2%
Sales tax	7.8%	7.8%

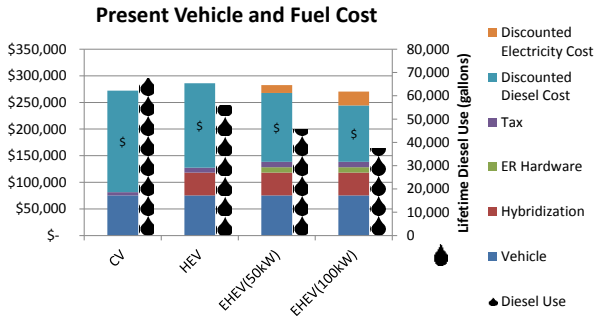

Figure V-207: Net present cost and lifetime fuel savings calculations for the example straight-truck scenarios.

In the tractor-trailer (long-/line-haul) analysis, we extract a representative average CV fuel economy from the on-road data ([4], [6]), and assume a lower hybridization benefit of up to 10% given the predominantly FC1 interstate driving profiles for these vehicles [11]. Factoring in assumptions shown in Table V-29 for much greater lifetime operating miles and a potentially greater hybridization cost increment, along with the fuel cost and other parameters used previously ([1], [8]–[10], [12]) yields the draft net present cost and lifetime fuel savings results shown in Figure V-208.

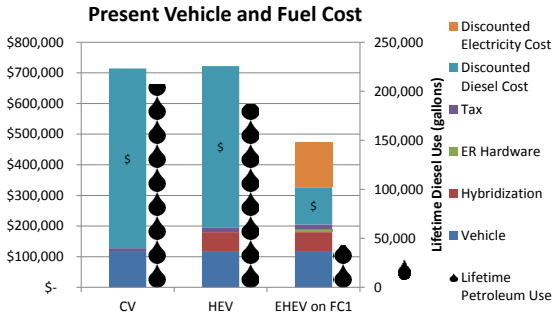

Figure V-208: Net present cost and lifetime fuel savings calculations for the example tractor-trailer scenarios.

Note that due to the much greater operating miles, the lifetime fuel cost for the conventional tractor-trailer is approximately five times the vehicle purchase price. Although the percentage fuel savings from hybridization is less than for the straight-truck application, the savings get applied over this larger fuel use baseline, resulting in a net present vehicle and fuel cost that approaches parity with that for the CV.

The EHEV scenario shown in Figure V-208 assumes all FC1 driving miles are fully electrified, displacing all diesel consumption (during 77% of operating miles as indicated in Figure V-204. The average continuous power requirement for electrified roadway infrastructure to satisfy the FC1 driving demands of a single tractor-trailer is expected to be 100 kW or greater. If such a power demand could be met, it would result in significant reductions in fuel use and net present cost relative to the CV (roughly 80% and 35%, respectively as shown in Figure V-208.

NREL conducted an initial sensitivity sweep on these draft results to evaluate the extent to which various assumptions could be relaxed and still achieve no worse than cost parity between the EHEV and the CV. The findings included that the electricity price could rise (e.g., to help pay back the cost of the road infrastructure installation) from the baseline assumption of $0.12/kWh up to $0.32/kWh. Alternately, the price of diesel could go down from the constant baseline assumption of $3.98/gallon to $1.92/gallon. Finally, with all other assumptions holding constant, the up-front EHEV price increment above the HEV price could rise from the $10,000 baseline assumption for the additional hardware required on the vehicle to as high as $235,000.

Conclusions

NREL's analysis of the potential costs vs. benefits of electrified roadway infrastructure for light-duty as well as Class 8 tractor-trailer and straight-truck operators has included assessments of real-world driving profiles for each vehicle application. The analyses have suggested that WPT technology installation over a relatively small portion of road infrastructure could support electrification (and corresponding operating cost savings) for a considerably larger fraction of vehicle miles traveled. This finding is particularly strong for tractor-trailer (line-/long-haul) vocations where over three-quarters of operating miles can occur on FC1 roads. The preliminary vehicle-level net present cost analysis suggests considerable economic opportunity from roadway electrification in this very operating-cost-sensitive vehicle application.

Next steps for the analysis include extending the FASTSim modeling from the straight-truck analysis to the tractor-trailer application to further examine second-by-second power demand fluctuations and implications for the electric roadway infrastructure. Additional input parameter sensitivities will also need to be explored, as well as further analysis into implications for the utility grid, particularly for scenarios where multiple types of vehicles operate together on the electrified roadway.

References

1. U.S. Department of Energy. "Research and Development Opportunities for Heavy Trucks," June 2009.
2. NREL's Transportation Secure Data Center website, www.nrel.gov/tsdc.
3. Gonder, J., et al. "Analysis of In-Motion Power Transfer for Multiple Vehicle Applications." Proceedings of the DOE Vehicle Technologies Annual Merit Review, May 2013.
4. NREL's Fleet DNA Project website, http://www.nrel.gov/vehiclesandfuels/fleettest/research_fleet_dna.html.
5. NAVTEQ 2011 Q3 NAVSTREETS SDC Data Dictionary.
6. Lascurain, M., et al. "Class-8 Heavy Truck Duty Cycle Project Final Report." Oak Ridge National Laboratory publication TM-2008/122, December 2008.
7. NREL's ReFUEL Laboratory website, http://www.nrel.gov/vehiclesandfuels/refuellab/.

8. Schubert, R., and Kromer, M. "Heavy-Duty Truck Retrofit Technology: Assessment and Regulatory Approach." TIAX Final Report, September 2008. http://www.nrel.gov/vehiclesandfuels/refuellab
9. Windecker, A., and Ruder, A. "MPG, Cost and GHG Results for Alternative Fuel Vehicles in 2011." ACEEE Proceedings, 2012. 1. http://www.aceee.org/files/proceedings/2012/data/papers/0193-000340.pdf.
10. U.S. Energy Information Administration, http://www.eia.gov/.
11. Chambon, P., "Coupling Model-Based Design with Laboratory Experimentation to Enhance Heavy Duty Vehicle Efficiency." Proceedings of the SAE 2012 High Efficiency Heavy Duty Vehicle Symposium, October 2012.
12. California Air Resources Board. "Implementation Manual for the FY2011-12 California Hybrid and Zero-Emission Truck and Bus Voucher Incentive Project." November 2012. http://www.californiahvip.org/docs/HVIP_Year%203_Implementation%20Manual_2012-11-14.pdf.

V.U.3. Products

Publications

1. Gonder, J., Brooker, A., Burton, E., and Markel, A., "Analysis of In-Motion Power Transfer for Multiple Vehicle Applications." DOE Vehicle Technologies Annual Merit Review, May 2013.

Tools and Data

1. ReFUEL Laboratory test data (http://www.nrel.gov/vehiclesandfuels/refuellab/).
2. FASTSim model (www.nrel.gov/fastsim).
3. FleetDNA Project Database (http://www.nrel.gov/vehiclesandfuels/fleettest/research_fleet_dna.html).

VI. COMPONENTS AND SYSTEMS

VI.A. PHEV Advanced Series Gen-Set Development/Demonstration Activity

Paul H. Chambon, Principal Investigator
Oak Ridge National Laboratory
2360 Cherahala Boulevard
Knoxville, TN 37932
Phone: (865) 946-1428
E-mail: chambonph@ornl.gov

David Anderson, DOE Program Manager
Phone: (202) 287-5688
E-mail: david.anderson@ee.doe.gov

VI.A.1. Abstract

Objectives

- The objective of this project is to integrate ORNL advancements in vehicle technologies to properly design, and size a gen-set for various vehicle applications and then simulate multiple advanced series hybrid (HEV/PHEV) vehicles with the genset models.

Major Accomplishments

- Built on first year simulation study to partner with industry and obtain additional data about previously selected technologies
- Industry-supplied experimental data was used to refine component models
- Finalized technology selection based on expanded simulation study

Future Achievements

- Expand simulation study to include larger vehicle platforms

✧ ✧ ✧ ✧ ✧

VI.A.2. Technical Discussion

Background

The cost and weight of a battery limit the range of an electric vehicle. The use of a range extending gen-set (engine-generator set) to convert an EV in a series PHEV (or EREV) can alleviate range anxiety and reduce battery size and cost.

Series HEV and PHEVs present a unique configuration when a gen-set is used to recharge the Energy Storage System (ESS). In a true series architecture, the gen-set is not mechanically coupled to the drivetrain and therefore may be operated at its optimum efficiency point, regardless of driving conditions. As such, gen-sets provide unique opportunities for component sizing optimization, internal combustion engine operating regimes, exhaust after-treatment, cost effective technology components, electric machine and power electronics selection.

Introduction

This project will draw from the extensive experience in power electronics and electric machinery from the Power Electronics and Electrical Power Systems Research Center as well as the broad knowledge in advanced combustion and emissions after-treatment through the Fuels, Engines, and Emissions Research Center. Both centers are parts of the transportation section of ORNL. The emphasis will be placed on technologies currently under development in each respective center. It will attempt to focus on a modular gen-set that could have multiple applications outside of a vehicle, which would reduce cost based on high volume production.

This project will investigate several advanced technologies for each key component considering several aspects in its selection process such as efficiency, cost, strategic benefits (rare earth / non rare earth) and complementarity of the engine and motor technology.

Approach

Based on the simulation study performed during FY12, the project team had selected a technology combination to be further investigated. Partnerships with engine and electric machine manufacturers will help procuring experimental data for such technologies. That data will be converted into new refined models that will be exercised to finalize our technology selection.

Results

The simulation study performed during FY12 had identified alternative fuels such as ethanol and advanced combustion as the most promising engine technologies for increased combustion efficiency, and non-rare earth induction machine as best cost and efficiency balance for electric machine technology.

The focus for FY13 is to find industry partners to collaborate with, in order to further investigate those technologies in the context of a gen-set application.

An NDA was signed with Mahle Powertrain to evaluate their existing gen-set unit as the base for further efficiency improvements. Mahle had designed a 2-cylinder 900cc 4-stroke PFI gasoline engine called REx (for Range Extender) with the intent to be a "low cost unit with a small package volume and good NVH attributes". Mahle is also conducting a separate research study in collaboration with the Department of Energy to "develop a next-generation combined ignition/turbo-charging concept known as 'Turbulent Jet Ignition' ". The effect of that technology on a gen-set application will be quantified.

Figure VI-1: Mahle REx gen-set.

ORNL Power Electronics and Electric Machinery group has a DOE APEEM-funded project involving the development of an inverter for a Remy induction machine machine as well as the optimization of its controls in order to get maximum efficiency over its complete speed and load range. Remy has authorized ORNL to retain that motor after testing and use some of their modeling results to include in our simulation study. Since the prototype machine is more powerful (180kW) than the genset application requires, it will be scaled down for the purpose of the simulation study.

Figure VI-2: Remy Aluminum rotor induction machine.

An Autonomie model of the base (Port Fuel Injected) Mahle REx engine as well as its Turbulent Jet Ignition (TJI) variant were generated based on experimental data provided by Mahle. Also the Remy machine was modeled with Autonomie. Those models were added to the list of technologies tested during FY12.

The PFI REx engine did not perform as well as the original PFI engine used in the preliminary study because that engine used a scaled down version of an Atkinson cycle engine. The TJI variant significantly improves engine efficiency at low load (up to 20%), but its effect is more modest at high load (4%). Because the genset operates the engine at high load and high efficiency points that are independent of road load conditions, TJI does not benefit the genset application as much as expected: it performs better than its PFI variant and is on par with an Atkinson cycle engine (see Figure VI-3).

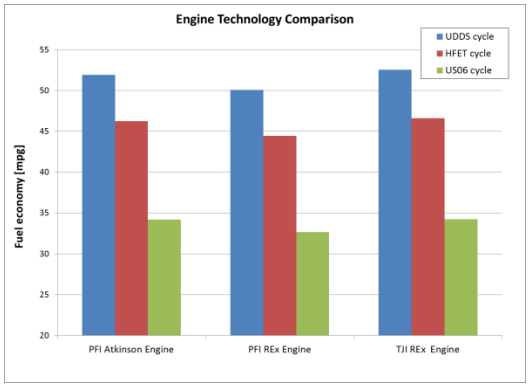

Figure VI-3: Engine technology comparison when combined with an induction machine.

Since the gen-set operates the engine at high loads, as identified previously in this study, ethanol fuel would be beneficial for the REx engine too thanks to its increased knock tolerance at high loads. Therefore an ethanol variant of the REx engine is expected to deliver similar fuel economy at a lower cost than TJI, while not relying on petroleum. Unfortunately, no experimental data is available for that ethanol configuration.

The gasoline PFI REx engine model was then coupled to three different electric machine models: a Remy induction machine, a generic induction machine and a Remy permanent machine. The simulation study showed that the Remy induction machine was on par with the permanent machine thanks to its operation being limited to its most efficient region in a gen-set application.

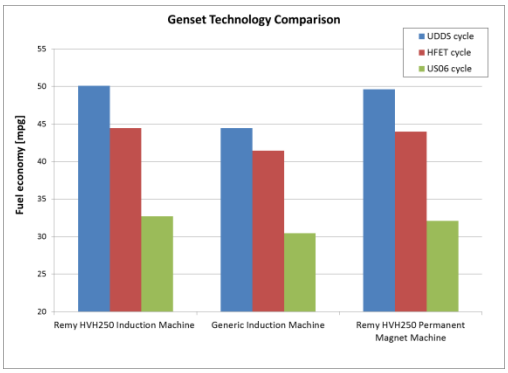

Figure VI-4: Electric machine technology comparison when combined with a PFI engine.

Conclusions

The collaboration with industry partners enabled the upgrade of some of the generic models used so far to some experimental data-based models.The use of such refined models confirmed the findings of the preliminary study conducted during FY12: a 30kW gen-set combining preferably an ethanol PFI engine and induction electric machine offers the best efficiency trade-off for a PHEV passenger car application.

VI.B. Simulation and Controls for Medium and Heavy Duty Dual Mode Hybrid Powertrain

David E. Smith, Principal Investigator
Oak Ridge National Laboratory
National Transportation Research Center
2370 Cherahala Boulevard
Knoxville, TN 37932-6472
Phone: (865) 946-1324
E-mail: smithde@ornl.gov

David Anderson, DOE Program Manager
Phone: (202) 287-5688
E-mail: david.anderson@ee.doe.gov

VI.B.1. Abstract

Objectives

- The purpose of this Cooperative Research and Development Agreement (CRADA) between the Oak Ridge National Laboratory (ORNL) and Meritor,Inc. is to explore the potential of systems optimization through model based design of their Dual Mode Hybrid Powertrain (DMHP) designed for Class 8 long haul trucks. The benefits of this efficiency improvement include reducing petroleum consumption while eliminating the current sacrifice in fuel mileage and corresponding range between vehicle refuel.
- Potential advantages and disadvantages of the DMHP will be explored using a combination of detailed modeling and experiments. The results will then be used to estimate potential improvements in drive-cycle energy efficiency, fuel mileage and emissions.

Major Accomplishments

- Suitable vehicle level models have been created for both a conventional vehicle (reference) and the Meritor DMHP. A baseline supervisory controller has been developed for the Meritor DMHP that allows full functionality of the powertrain. Based upon these simulations, the Meritor DMHP shows potential of up to 12% in real world, line haul applications over the reference vehicle.
- An optimization study has been performed on the Meritor DMHP supervisory controller in order to further the fuel consumption reduction benefits for the system for both series and parallel modes.
- A test engine has been procured, installed, and mapped for performance, fuel use, and emissions at ORNL. The data from this mapping exercvise has been used to develop a more detailed engine model that has been incorporated back into both the reference and DMHP vehicle models.
- Preliminary engine-in-the-loop tests have been performed on the test engine with the complete Meritor DMHP emulated in software.

Future Achievements

- Complete a full suite of engine-in-the-loop testing with the test engine and emulated Meritor DMHP based upon test plan developed by Meritor and ORNL.
- Procure and install the prototype Meritor DMHP Hyrbid Drive Unit at the ORNL Vechile Systems Integration Laboratory.
- Complete a full suite of powertrain-in-the-loop testing with the test engine and prototype Meritor DMHP based upon test plan developed by Meritor and ORNL.

✧ ✧ ✧ ✧ ✧

VI.B.2. Technical Discussion

Background

The purpose of this Cooperative Research and Development Agreement between Oak Ridge National Laboratory and Meritor, Inc. is to develop control strategies and models to optimize the operation of the dual mode hybrid powertrain for Class 8, heavy-duty (HD) trucks. This includes intelligent power and energy apportionment from the engine and the battery pack.

Hybrid powertrains are of considerable interest because of potential reductions in fuel consumption, criteria pollutants and green house gas emissions. Parallel hybrids have been applied to light and medium duty trucks, where urban driving cycles are prevalent, while series hybrids have been successfully used for other applications like transit and school buses. Unfortunately, hybridization of the Class 8, HD powertrain is inherently challenging due the expected long-haul driving requirements and limited opportunities for regenerative braking. Meritor has conceived and demonstrated a transformational Dual Mode Hybrid Powertrain technology developed specifically for the needs and function of Class 8 line haul trucks.

Introduction

The DMHP system enables a new paradigm in powertrain operational efficiency in the Class 8 truck segment. It decouples the connection between the engine operating point and the truck road load demands over a broad operating range through an innovative hybrid design. The DMHP operation choices include running in full series, full parallel and engine-off modes. The DMHP offers the opportunity for an

engine to operate in a narrow range, thus providing a strategy for maximized fuel economy and minimized emissions. Further, it is expected that transient torque and power wheel demands are handled in whole or part by the electric system, thus reducing the frequency and intensity of engine transients and further improving the fuel economy and emissions. Fuel consumption and emissions have been further reduced through the elimination of overnight hoteling and idling at stops. Finally, based on the unique operating profile of an engine integrated into our hybrid powertrain, a transformational HD truck engine design concept next can emerge.

Recent research activities by ORNL have yielded significant data in real-life speed and load profiles of Class 8, long haul trucks. In addition, preliminary simulations of the DMHP carried out by ORNL reveal significant optimization opportunities of the DMHP by applying systematic simulation and controls approaches. An improved understanding of the complex interactions offered by the on-board engine, energy storing system, and electric machines is necessary for the development of control methodologies and practical implementation. We will continue to further this understanding through detailed experimentation and modeling, drawing on and expanding ORNL's core competency in basic engine R&D and advanced controls. This knowledge will be used to develop, implement, and evaluate control strategies on an actual DMHP using the Participant's components and subsystems. Our initial focus will be on optimization of DMHP utilizing a "stock" diesel engine that is commercially available in the market place. A new DMHP-specific engine design concept will be pursued at a later phase of this CRADA.

Meritor will develop the experimental setup, conduct sub-system experiments at their facility, and implement and evaluate potential control strategies resulting from this CRADA partnership. ORNL will develop a real-time simulation model for use in real-time control of the DMHP. The model and potential algorithms will be evaluated on a HD, hybrid powertrain dynamometer facility which will also be developed at ORNL Vheicle System Integration (VSI) facility. Both parties will support each other on all experimental, modeling, and control tasks.

Approach

The successful implementation of DMHP will require a thorough technical understanding of the complex interactions between various energy sources and energy consumption components, for various operating modes of HD, Class 8 on-highway trucks. Further, ORNL has been developing and applying methods for the analysis, interpretation, and control of dynamic engine phenomena in single- and multi-cylinder engines for over fifteen years. Meritor has extensive knowledge and experience in DMHP components and subsystems. A partnership involving these knowledge bases is key to overcoming the critical barriers associated with the realistic implementation of DMHP and enabling a measurable progress in applying hybrid powertrain in the next generation of HD truck transportation systems. ORNL and Meritor have collaborated on a preliminary investigation that warrants much deeper R&D efforts.

Simulation and Virtual Lab

Simulation Model and Control Algorithm Development

ORNL in partnership with Meritor will develop a comprehensive DMHP simulation strategy using the previously conducted analyses as a springboard. A detailed engine model shall be employed evaluating potential control strategies before implementation on an actual DMHP. Synergistic engine strategies will be explored via a low-order, predictive simulation model for integration into the DMHP controller.

- A more detailed model will be developed for integration with the DMHP for understanding the engine interactions within the hybrid powertrain. This model will be the basis for a more computationally efficient model to be used in real-time control of the DMHP.
- Update and further develop a robust DMHP vehicle simulation model for the study and discovery of potential operating scenarios of the total system, major components such as the engine and battery pack, and synergistic interactions under simulated load cycles.

DMHP Optimization Strategy Development

ORNL in partnership with Meritor will develop an optimization strategy, identify optimization parameters, and define the optimization constraints.

- For prescribed duty cycles, various optimization criteria will be developed based on fuel efficiency, freight efficiency, emissions or other relevant influential factors.
- Optimization parameters will be identified for the system, including for the supervisory control strategy. Capacities of engine, E-machines, and energy storage will be studied. Mechanical parameters such as gear ratios, number of transmission gears, and shift points will be included.
- Optimization constraints will include vehicle driveability & performance requirements such as startability, gradeability, and acceleration. Additional constraints such as minimum fuel consumption and emissions will be explored.

DMHP System Optimization Studies

ORNL will carry out an optimization analysis of the DMHP system, using rigorous optimization methods. System variants, optimization criteria, optimization parameters, and constraints shall be considered.

- System variants will include engine types that are of interest.
- The DMHP "5-position sequential shifter" will be analyzed.
- Full independence between various states of the DMHP sub-systems will be studied. This includes configuration (Series vs. Parallel), transmission gear ratio (Lo vs. high), traction motor clutch (engaged vs. disengaged), and possibly a more complex energy storage system (for both energy and burst power.)

Hardware and Experimental Testing

ORNL will utilize expert engine dynamometer testing, the ORNL VSI powertrain laboratory facility and/or mule trucks to validate the virtual (simulation) tasks, provide experimental

data for future simulation and develop methodologies and control strategies for DMHP operation. Testing of SIL, HIL and rapid prototyping of engine systems have been a well-recognized expertise of ORNL. This will be applied and further extended to advanced hybrid powertrains.

DMHP System Development and Baseline

Meritor in partnership with ORNL will construct and baseline a DMHP in support of this activity. The DMHP setup will be located at Meritor's facility.

- Determine appropriate DMHP hardware including motor, generator, battery pack, clutches, sensors, harnesses, etc.
- Build DMHP management system and power electronics.
- Implement latest software set in the controller of the DMHP.
- Build a DMHP for ORNL's experimental setup.
- Develop baseline calibration of DMHP.

Engine Acquisition, Installation, and Mapping

ORNL in coordination with Meritor will acquire a representative HD engine and dynamometer compatible controller and wiring harness. In addition, necessary hardware and software will be identified and developed as necessary to support installation of the engine for dynamometer testing. After installation, a baseline will be performed on the engine to develop a performance/emissions map to support modeling efforts.

DMHP Simulated and Full System Dynamometer Testing

ORNL in coordination with Meritor will develop and test a simulated DMHP on the HD engine acquired in the previous task. This will include the use of a hardware-in-the-loop and advanced control methodologies. The next step will include Meritor delivering a complete DMHP unit and associated components to ORNL. The DMHP system will be installed in the ORNL VSI Laboratory for full system hardware testing.

Results

Simulation and Virtual Lab

Simulation Model and Control Algorithm Development

In order to assess the benefits of the Meritor powertrain, a representative baseline, conventional model was developed in Autonomie. A block diagram of the powertrain for this reference model is shown in Figure VI-5. This model features the same Cummins ISX 15L engine that will be used in conjunction with the Meritor DMHP, as well the same vehicle characteristics. The engine model has been updated with data taken from the actual engine from the preliminary testing conducted during the Hardware and Experimental Phase of the project explained later in this report.

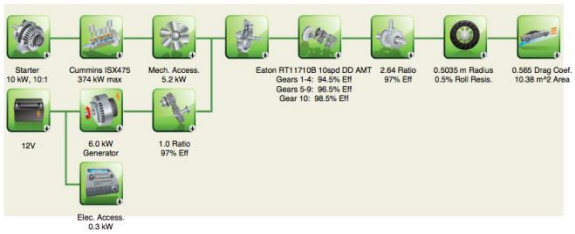

Figure VI-5: Conventional Autonomie reference model.

The Meritor DMHP was also modeled in Autonomie such that a supervisory control strategy could be developed. A block diagram of this powertrain is shown in Figure VI-6, along with high-level assumptions for component sizing and accessory loads. This model was designed to maintain flexibility in assessing the benefits of various gear reductions throughout the powertrain, such as the effects of engine downspeeding.

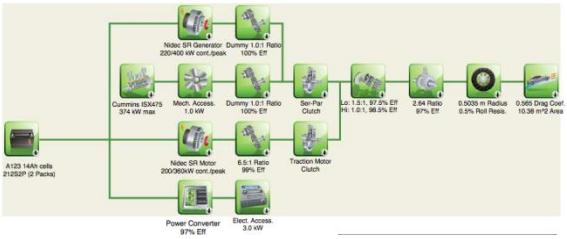

Figure VI-6: Dual Mode Hybrid Powertrain Autonomie model.

A suite of duty cycles was identified to exercise both respective models. Standard cycles were used, such the CSVHR, UDDS Truck, and the HHDDT65. These cycles do not feature a grade element, but provide good insight into basic operational characterisitics of each powertrain, and relative fuel economy comparisons. However, in order to obtain a better understanding of the real benefits of the hybrid system, ORNL developed a couple of "real-world" duty cycles based upon actual vehicle operation in the southeastern United States. These duty cycles were created utilizing actual data for the ORNL Heavy Truck Duty Cycle database, and feature a wealth of information, most notably grade. The first cycle, shown in Figure VI-7, represents a "hilly" long haul cycle. This cycle was based upon a route between Knoxville, TN, and Nashville, TN along interstate I-40W. Figure VI-8 represents a "flat" long haul cycle, based upon a route between Clarksville, TN and Danville, IN.

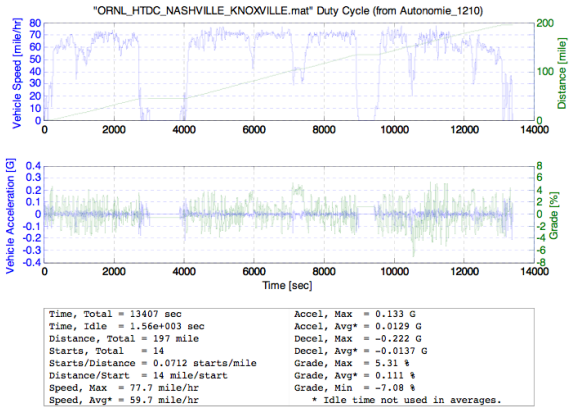

Figure VI-7: "Real world" hilly long haul drive cycle with grade data developed from ORNL Heavy Truck Duty Cycle database.

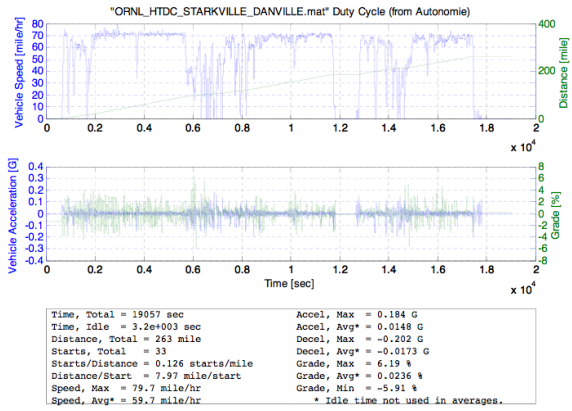

Figure VI-8: "Real world" flat long haul drive cycle with grade data developed from ORNL Heavy Truck Duty Cycle database.

Highlights of some of the results of the modeling effort are shown in Figure VI-9-Figure VI-11. Figure VI-9 represents a comparison of the engine power during series hybrid operation of the Meritor DMHP to that of the conventional vehicle with an automated manual transmission. Power delivery is smooth and constant from the engine, obviously due to lack of transmission shifting.

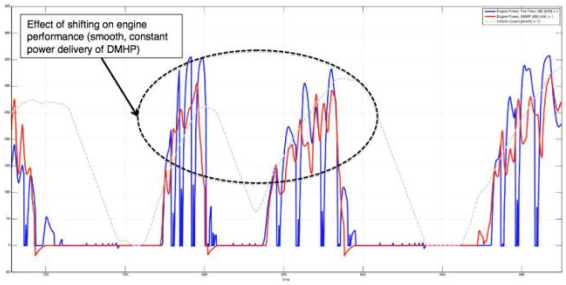

Figure VI-9: Comparison of engine operation for DMHP versus conventional vehicle with manual transmission.

A comparison of the performance of the DMHP versus the convetional baseline is shown in Figure VI-10. Due to the lack of shifts and high torque capability of the traction motor during series operation (at low vehicle speeds), the Meritor DMHP exhibits superior performance compared to the conventional vehicle.

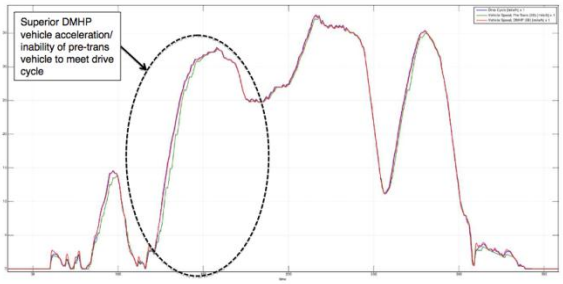

Figure VI-10: Performance comparison of DMHP versus conventional vehicle with manual transmission.

Figure VI-11 representa a high level comparison of the simulated fuel economy improvements found as a result fo the modeling woprk conducted during this study. For the standard cycles, a large improvement was found for the urban cycles (CSHVR, UDDS Truck), and a modest improvement was found for the HHDDT65, which is representative on long haul or highway operation. The real world cycles used as part of the study yielded a slightly higher improvement (4% greater than the standard HHDDT65 case). This is attributed to the inclusion of grade information in the simulation and the regenerative braking implications of the Meritor DMHP.

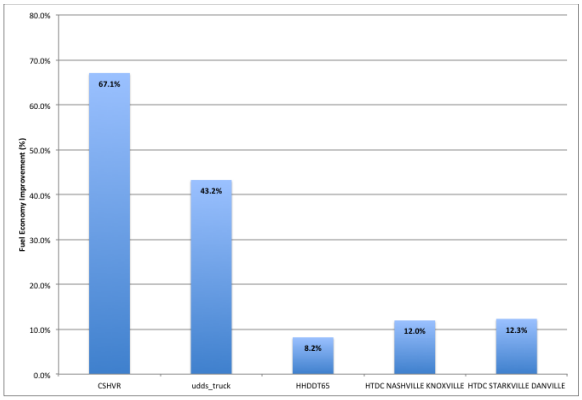

Figure VI-11: Fuel economy improvement for DMHP versus conventional vehicle with manual transmission.

Supervisory Controls Optimization

DMHP—Series Mode

In the approach adapted here, a power management control algorithm is developed that can make series HEVs to continuously operate at their optimal efficiency with respect to fuel economy. The HEV is considered as cooperative multi-agent systems in which the subsystems (i.e., IC engine, motor, generator, and battery) will be treated as autonomous intelligent agents. The agents will attempt through their interaction to jointly maximize overall HEV operation. The problem is formulated as sequential decision-making under uncertainly where the supervisory controller is faced with the task to select those control actions in several time steps to achieve long-term goals efficiently. Sequential decision models are mathematical abstractions representing situations in which decisions must be made in several stages while incurring a certain cost at each stage.

In the series HEV mode of the DMHP, the motor provides all the power demanded by the driver. Thus we can operate the engine at any desired combination of engine torque and

speed. The objective of the centralized controller is to maintain the state-of-charge (SOC) of the battery within a given range while operating the engine efficiently. So the optimal control policy of the controller is a sequence of the optimal engine power at each instant of time corresponding to the engine's current speed. To operate the engine under the condition designated by the centralized controller, a PID controller regulates the engine torque through the generator. The sequence of the engine's optimal power is converted to electrical power through the generator and goes to the battery.

In our problem formulation, engine operation was modeled as a controlled Markov chain with a state space S, and a control space U from which control actions are chosen. The state space S is the entire range of the engine speed and the control space U is the engine power range. Thus the Markov chain is the evolution of the engine speed and the uncertainty is related to the power demanded by the driver through the battery SOC. The evolution of the engine occurs at each of a sequence of stages t = 0, 1, ..., and it is portrayed by the sequence of the random variables X_t and U_t corresponding to the system's state (engine speed) and control action (engine power). At each stage, the controller observes the system's state, and executes an action, from the feasible set of actions at that state. At the next stage t, the system transits to the state $X_{t+1} = j \in S$ imposed by the conditional probability $P(X_{t+1} = j | X_t = i, U_t)$, and a cost $k(X_t = i, U_t) = k(i, U_t)$ is incurred corresponding to fuel consumption. After the transition to the next state has occurred, a new action is selected and the process is repeated. The completed period of time over which the system is observed is called the decision-making horizon and is denoted by T. We are concerned with deriving a stationary optimal control policy (sequence of engine power) to minimize the long-run average cost (average fuel consumption) per unit time.

The first step in designing the centralized controller is to identify the column vector of the cost function that is minimum for each state (engine speed). This can be derived by plotting the minimum brake specific fuel consumption (BSFC) of the engine for each engine speed. From this plot, we can choose the set of admissible state/action pairs. The optimal control policy can be achieved by the centralized controller, if the engine is operated at the speed range ensuring higher probability to the engine speed with lower BSFC values and lower probability to the engine speed with higher BSFC values. However, the centralized controller needs to maintain the battery's SOC close to the target value (70% in this case). To achieve both objectives, we establish a one-on-one correlation between SOC and the optimal engine power range. In particular, the controller is set up to command the engine to provide the power corresponding the minimum allowable value whenever SOC is equal to 70% (target SOC) and gradually increase as SOC drops below 70% all the way down to the minimum allowable value (60% in this case), as illustrated in Figure VI-12.

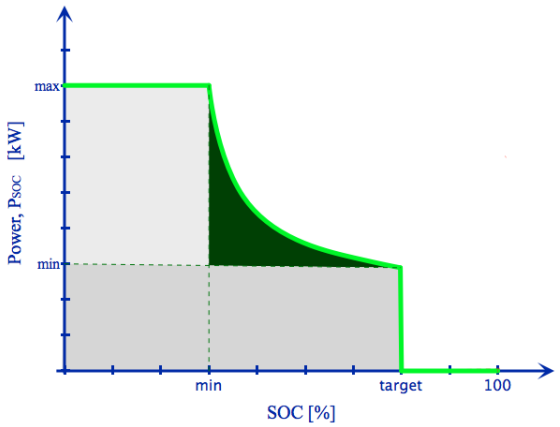

Figure VI-12: Engine power with respect to the state of charge of the battery.

To validate the effectiveness of the equilibrium control policy, we compared it to the baseline controller. Both HEV models, the one having the baseline controller and the one with the optimal controller, were run over the same driving cycle (in this case, the CSHVR) illustrated in Figure VI-13. The inherent algorithm in Autonomie called dichotomy was used to compare the simulation results. The algorithm runs the HEV model over the same driving cycle for multiple times and then provides results corresponding to the same initial and final SOC, as illustrated in Figure VI-14. The optimal control algorithm in the series mode of operation yields a 4.8% fuel consumption improvement as shown in Figure VI-15.

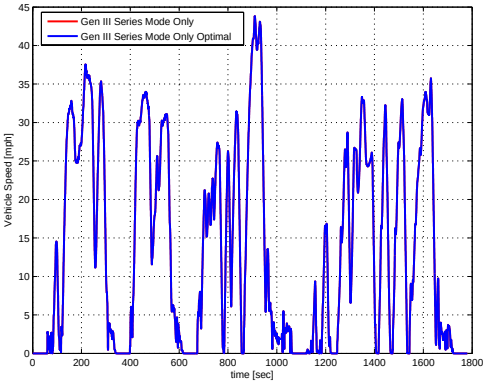

Figure VI-13: Both the Autonomie model with the original controller and the one with the optimal controller were followed precisely the CSHVR driving cycle.

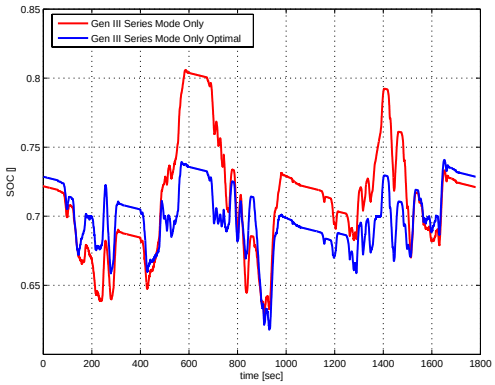

Figure VI-14: SOC variation for both models.

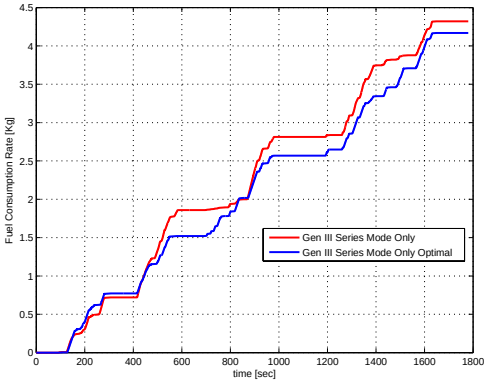

Figure VI-15: Cumulative fuel consumption.

DMHP—Parallel Mode

The power management control problem of the parallel configuration is addressed in a centralized fashion. The objective of the centralized controller is to guarantee the self-sustainability of the electrical path and distribute the power demanded by the driver optimally between the engine and the motor to minimize fuel consumption. The controller observes SOC of the battery as well as the engine and motor speed, and then computes the optimal engine and motor torque, and based on the power demanded by the driver.

In previous research reported in the literature, the SOC of the battery has been used as a component of the state. However, this may lead to a significant large state space with implications to increasing the computational burden associated with solving the problem. In our approach, the SOC is treated as an additional uncertainty by having it correlated to an additional power demand by means of a one-on-one mapping illustrated in Figure VI-12. Namely, depending on the SOC value there is a corresponding amount of power P_{SOC} that needs to be provided to the battery in order to stay at the target SOC. This additional amount is added to the driver's power demanded. The one-on-one mapping aims to provide an increasing power request, P_{SOC}, as the *SOC* drops up to a certain maximum value. If the *SOC* is above the target value, then P_{SOC} is zero.

We seek the theoretical framework and control algorithm that will aim to yield the optimal control policy on-line while the driver drives the vehicle. In our proposed approach, HEVs are considered as cooperative multi agent systems in which the subsystems, i.e., engine, motor, and battery, are treated as autonomous agents. To simplify the problem, the focus in this study is on establishing the equilibrium between the engine and the motor only. However, future research should also consider the battery as an agent and investigate the implications associated with this. To compute the equilibrium operating point we formulate a multi-objective decision making problem consisting of the engine's BSFC, and the motor's efficiency. The objective is to find the optimal torque for the engine and the motor that minimizes HEV fuel consumption for a given speed and torque request.

To validate the effectiveness of the centralized controller using the optimal control policy we employed Autonomie. The DMHP Autonomie model was simulated under the optimal controller and compared with the baseline DMHP controller over the HDDDT65 driving cycle, as shown in Figure VI-16. The optimal control algorithm in the parallel mode of operation yields a 1% fuel consumption improvement, illustrated in Figure VI-17. Higher fuel consumption improvements are expected in non-highway driving cycles. The SOC of the battery for the both cases is shown in Figure VI-18.

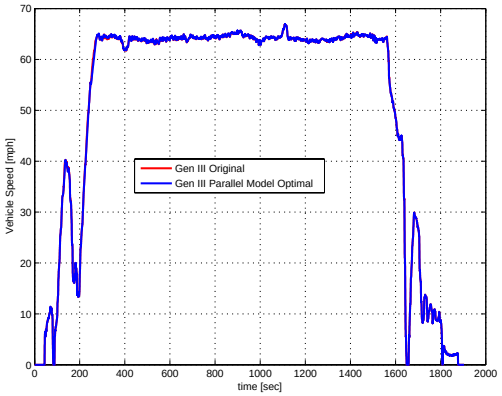

Figure VI-16: Both the Autonomie model with the original controller and the one with the optimal controller were followed precisely the HDDDT65 driving cycle.

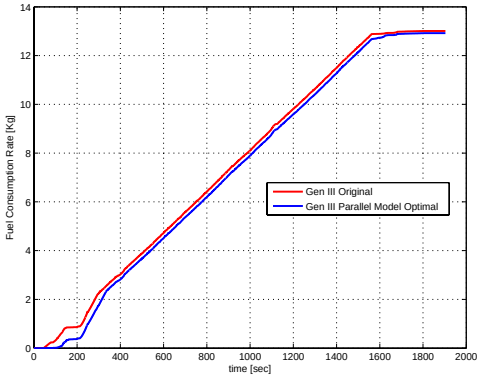

Figure VI-17: Cumulative fuel consumption.

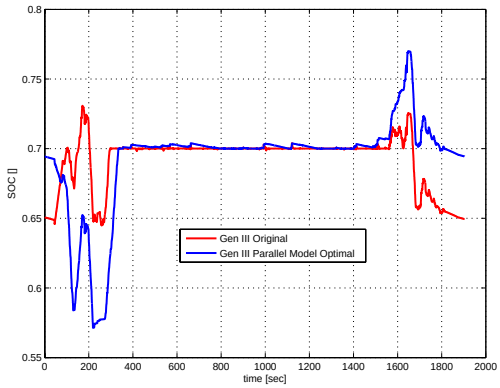

Figure VI-18: SOC variation for both models.

Hardware and Experimental Testing

DMHP System Development and Baseline

Meritor developed and fabricated a DMHP hybrid drive unit (HDU) for the purpose of experimental testing at ORNL's VSI laboratory. The HDU is second-generation prototype consisting of two (2) electric machines, dual inverter, and shift mechanisms. The prototype HDU is shown in Figure VI-19. The HDU has been verified for proper operation at Meritor's facitilies, shipped, and received at ORNL. The HDU is currently awaiting ORNL VSI laboratory commissioning to be completed in order to beign experiemtnal testing in FY2014.

Figure VI-19: Meritor Hybrid Drive Unit (HDU).

Engine Acquisition, Installation, and Mapping

ORNL has acquired a 2010 EPA compliant Cummins ISX 15 liter HD engine and dynamometer compatible controller, wiring harness, and complete emissions aftertreatment system. In addition, necessary hardware and software has been identified and developed to support installation of the engine for dynamometer testing. Figure VI-20 shows the engine and aftertreatment system installed in the ORNL VSI laboratory. A baseline engine mapping was performed on the engine to develop a performance/emissions map to support modeling efforts. Examples of the mapping exercise are shown in Figure VI-21-Figure VI-23.

Figure VI-20: Cummins ISX 15L engine and associated exhaust aftertreatment procured for use during experiemntal phase of Meritor DMHP testing.

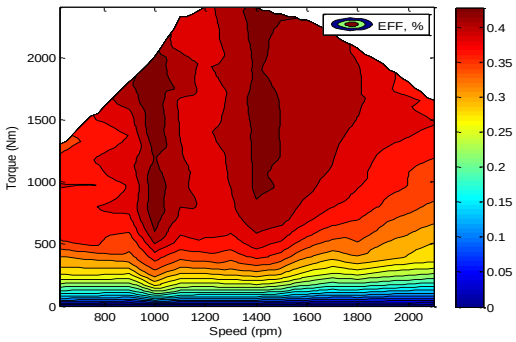

Figure VI-21: Experiemntalley developed efficiency map for Cummins ISX 450hp 15-liter engine.

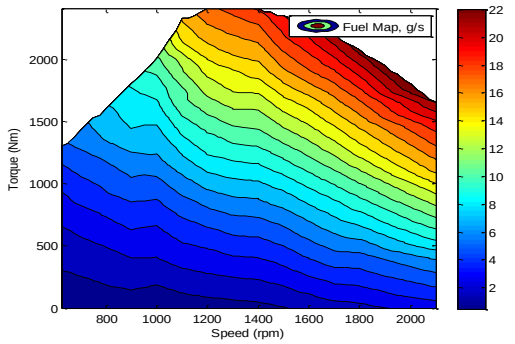

Figure VI-22: Experimentally developed fuel use map for Cummins ISX 450hp 15-liter engine.

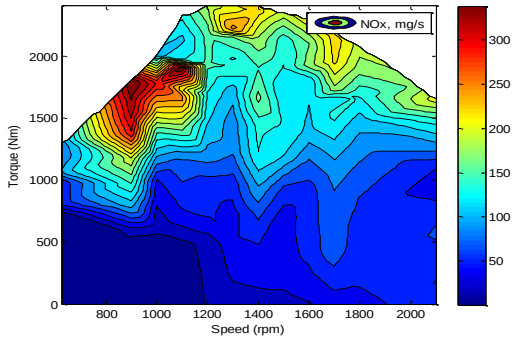

Figure VI-23: Experimentally developed NOx map for Cummins ISX 450hp 15-liter engine.

DMHP Simulated and Full System Dynamometer Testing

The Cummins ISX engine was installed in the ORNL VSI laboratory to begin transient testing, which included the use of hardware-in-the-loop principles and advanced control methodologies. Figure VI-24 shows the engine installed in the engine-in-the-loop configuration.

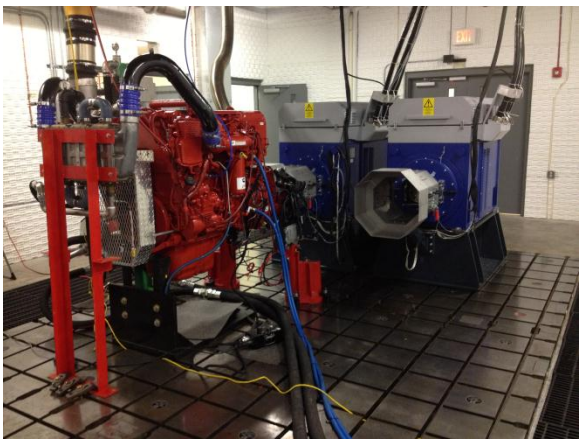

Figure VI-24: Cummins ISX configured for engine-in-the-loop testing.

Preliminary testing was performed with a virtual hybrid Class 8 line haul vehicle consisting of the ISX engine under test in the test cell and a virtual Meritor Dual Mode Hybrid Powertrain emulated on the VSI HIL platform. That configuration cannot be fully tested yet because the dynamometer does not yet have the ability to ramp the engine down to zero speed without flagging a fault that aborts testing. Functionality of the ORNL developed supervisory control system was tested by forcing the virtual hybrid controller to keep the engine on all the time, as shown in Figure VI-25. Here, actual engine torque and speed results are shown with virtual SOC maintenance being achieved.

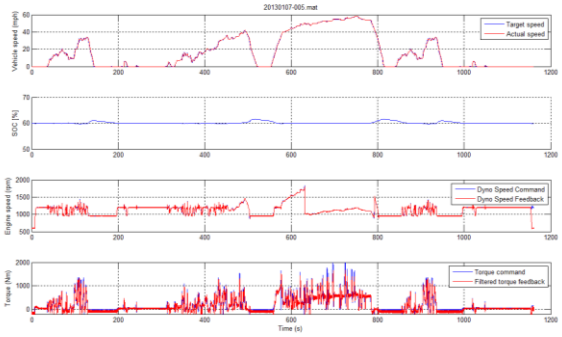

Figure VI-25: Engine-in-the-loop: Meritor DMHP in vehicle driving the UDDS Truck cycle.

The “stop-start” feature was added to the dyno control system so that all hybrid features of the Meritor DMHP transmission could be enabled. Figure VI-26 below shows results of a HD UDDS cycle for the Meritor DMHP. It was discovered that the ISX engine would not allow a torque request during the first engine start for a period of 6-8 seconds. Modifications were made to the DMHP supervisory controller to idle the engine for a fixed period of 8 seconds during the first engine start event, shown below around 60 seconds into the cycle. The same phenomenon was found after an extended period of having the engine off (but keeping the engine control module powered). Additional modifications to the supervisory controller are being made to account for this as well.

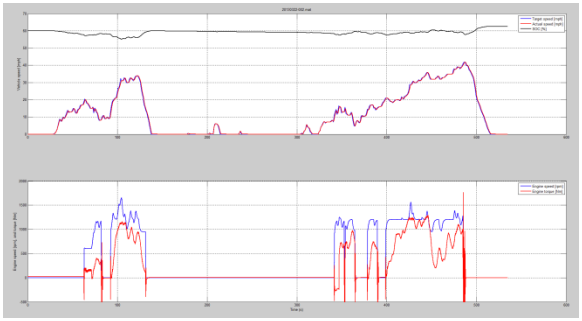

Figure VI-26 Engine-in-the-loop: Meritor DMHP in vehicle driving the UDDS Truck cycle.

Both the conventional and hybrid powertrain models were refined. Heavy-duty truck cycles were run on the engine-in-the-loop test cell (ISX engine under test on dyno with rest of vehicle emulated on HIL platform). Fuel economy was measured for each configuration: conventional manual gearbox and Meritor DMHP over three drive cycles: truck UDDS, HHDDT65, CSHVR. Even though fuel measurements are not validated yet, these tests do highlight the benefits of the Meritor hybrid transmission as shown in Figure VI-27. More rigorous testing of the system will be completed in FY2014.

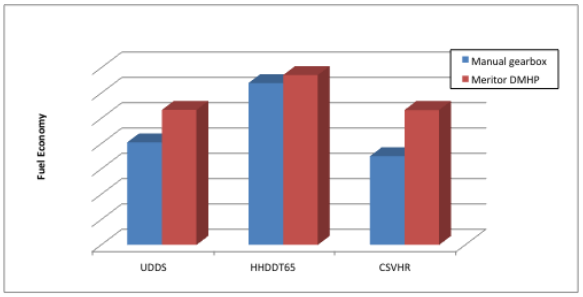

Figure VI-27: Experimental engine-in-the-loop fuel economy results for conventional and hybrid transmission.

Conclusions

The benefits of a full Class 8 hyrbid electric vehicle are being confirmed utilizing model-based desing and hardware-in-the-loop principles. ORNL and Meritor are engaged in cooperative research to understand the merits of the Meritor Dual Mode Hybrid Powertrain operating in “real-world” test conditions, including grade effects. A supervisory controller has been developed, and optimized for both urban and line haul applications.

Advanced hardware-in-the-loop practices are being utilized to get accurate measurements of fuel consumption and emissions reductions in the ORNL Vehicle System Integration Laboratory. Preliminary engine-in-the-loop testing shows promise for the Meritor system. Fully integrated powertrain testing will be conducted during FY2014 to get a clear picture of the merits of the hybrid system for petroleum consumption reduction, and to identify future paths forward for possible commercialization and further system improvements.

VI.C. Direct Evaluation of Oil/Coolant Exhaust Heat Recovery and Pre-conditioning Strategies

Forrest Jehlik, Principal Investigator
Argonne National Laboratory
9700 S. Cass Avenue
Argonne, IL 60439-4815
Phone: (630) 252-6403
E-mail: fjehlik@anl.gov

Lee Slezak, DOE Program Manager
Phone: (202) 586-2335
E-mail: lee.slezak@ee.doe.gov

VI.C.1. Abstract

Objectives

The objectives of this project are to understand the effects of ambient temperature on fuel consumption and to evaluate the potential for minimizing losses through waste heat utilization. A number of technologies are either in-use or under study to address this issue, such as turbo-charging and thermo-electrics. However, the use of engine waste heat currently is limited, and the magnitude of its potential is not well understood.

Major Accomplishments

- Completed thermal cart testing on the Ford Fusion under -7°C ambient conditions
- Obtained a +1.7-kW energy addition to the engine oil over the Urban Dynamometer Driving Schedule (UDDS)/US06 cycles from the start of the cycle.
- Demonstrated +1.7% and 1.0% fuel economy improvements over the UDDS/US06 cycles, respectively, by using heat addition from the thermal cart.
- Completed calculations to determine the quantity of exhaust waste heat available.
- Determined that the exhaust energy availability is much greater than the heat added from the thermal cart, which signifies a greater potential for improvement.

Future Achievements

- Analyze the potential for engineered internal combustion engine solutions through balance of plant (BOP) simulation approaches to retain heat and reduce cold-start fuel use.
- Conduct tests and supply data utilizing the thermal mule for data to collaborate with the National Renewable Energy Laboratory (NREL) study on cold-start testing activity and fuel-penalty model development.
- Determine the effects of inefficiencies of the engine versus transmission over ambient conditions.
- Calculate bookend estimations for thermal management technologies across a broad spectrum of national use by employing real-world trip data and climate histories to understand the distribution of trip distances, dwell times, and thermal response of the engine to ambient conditions.
- Investigate the limits of waste heat utilization and the potential for petroleum displacement.

✧ ✧ ✧ ✧ ✧

VI.C.2. Technical Discussion

Background

Real-world driving conditions coupled with ambient temperature variations result in a significant increase of fuel consumption (independent of drive cycle intensity). Research conducted at the Argonne National Laboratory (Argonne) Advanced Powertrain Research Facility (APRF) has shown variations in the fuel consumption of advanced powertrains on the order of 40%, depending upon the ambient conditions (not including creature comfort effects). Figure VI-28 displays the fuel consumption of a 2011 Ford Fusion, 2.5-L 6-speed sedan, driving four back-to-back UDDS cycles at three different ambient temperatures (-7°C, 15°C, and 22°C). In these results, no additional creature comforts were utilized. The results on this conventional powertrain show a 20+% difference in consumption at -7°C relative to 22°C, at which the powertrain is operating at a more optimal level. Additionally, there is a 9% penalty from the ambient cold start at 22°C relative to the more optimal conditions by the fourth cycle. Under ambient conditions, the NREL analysis of the Argonne APRF data suggests that, on average, there is a ~10% cold-start penalty over the UDDS cycle for a broad spectrum of vehicles between the first 22°C cold start and the last.

To better frame this issue, annual ambient conditions vary greatly depending upon the region where one lives. An example of variations in ambient temperature for three locations is shown in Figure VI-29. By understanding the physical mechanisms of these losses and by researching the potential methods to reduce these losses, significant national fuel efficiency increases might be realized.

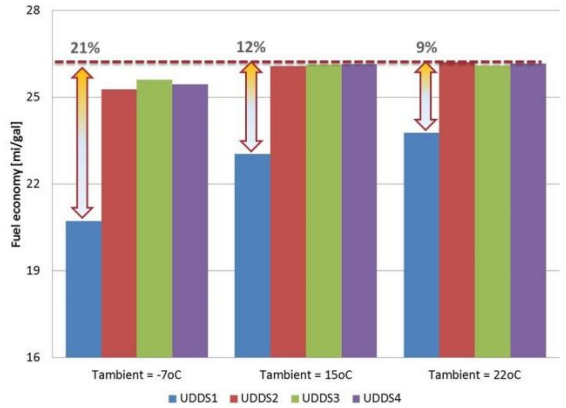

Figure VI-28: Effects of Ambient Temperature on the Fuel Consumption of a 2011 Ford Fusion, 2.5-L 6-Speed Transmission. (The tests are four back-to-back UDDS cycles.)

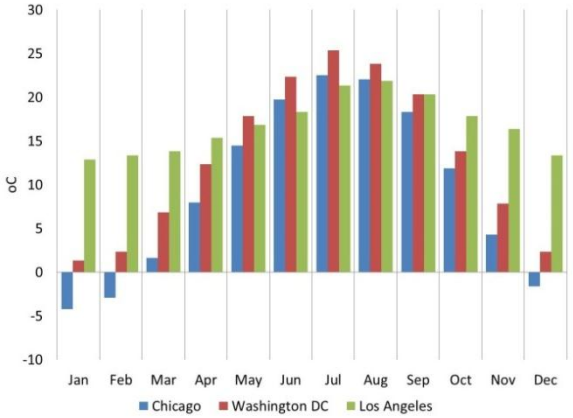

Figure VI-29: National Seasonal Temperature Variations for Select Cities: Chicago, Illinois; Washington DC; and Los Angeles, California.

Introduction

Argonne participates in Advanced Vehicle Testing Activity to advance the successful implementation of advanced vehicle technologies and to promote these energy-efficient technologies in the marketplace. The overall purpose is to reduce the carbon footprint from transportation. The work discussed in this report represents steps taken toward analyzing and addressing waste heat utilization in passenger vehicles across a broad spectrum of operating temperatures and cycles.

Approach

Thermal conditioning was used to apply additional energy to the engine oil over drive cycles of interest. The thermal testing cart contains a 1.7-kW oil heater and a 3-kW coolant heater that run on 440-V AC three-phase power. The cart is shown in Figure VI-30.

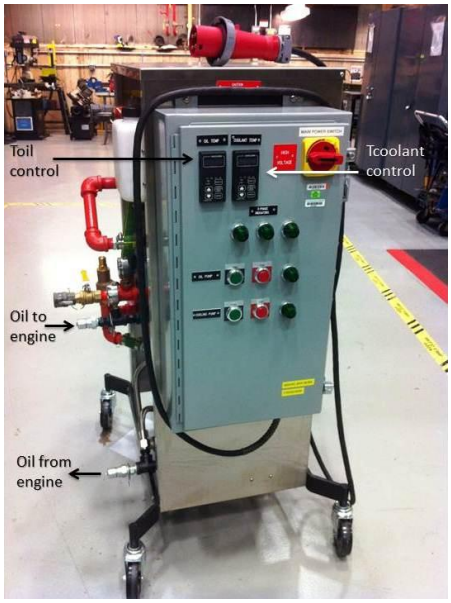

Figure VI-30: Thermal Testing Cart.

The UDDS and US06 cycles were investigated to capture both low and higher intensity driving. Once the vehicle engine was started and the drive cycle began, heat addition from the cart to the oil was added.

The 2011 4-cylinder, 6-speed automatic Ford Fusion that was modified with fluid taps for the engine oil and coolant was utilized for the testing. Figure VI-31 shows the test vehicle on the dynamometer at the Argonne facility.

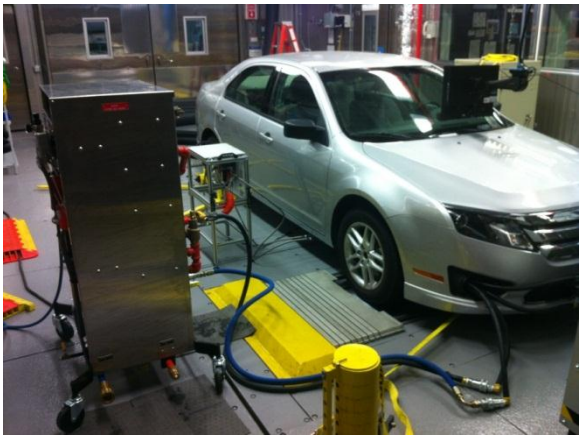

Figure VI-31: 2011 Ford Fusion Thermal Testing Mule. (The thermal testing cart is shown in the lower left-hand corner.)

For FY13, the Fusion thermal mule was further instrumented with a brake torque sensor. This sensor allowed for accurate real time measurement of engine output torque and input power to the transmission. This allows for both engine efficiency and transmission efficiency to be determined as a function of the ambient conditions.

Results

As depicted in Figure VI-32 and Figure VI-33, engine oil temperature was recorded over the UDDS and US06 cycles with and without heat addition to the engine oil during the drive cycle. It should be noted that, in order to account for potential pumping losses, the oil was routed through the thermal cart heater for tests with and without the heater turned on. In the case of the lower intensity UDDS drive cycle, the oil temperature ended approximately 7°C higher, and for the US06 cycle 4°C higher, with the 1.7-kW heat addition than without the heat addition.

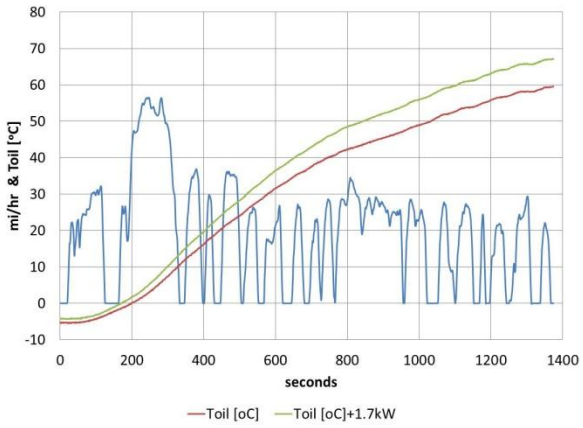

Figure VI-32: UDDS Cycle Engine Oil Temperature Profile with and without +1.7-kW Heat Addition (-7°C ambient temperature).

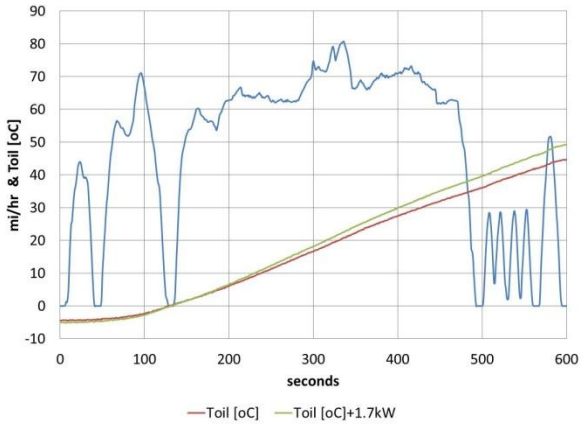

Figure VI-33: US06 Cycle Engine Oil Temperature Profile with and without +1.7-kW Heat Addition (7°C ambient temperature).

Fuel consumption for the drive cycles shown in Figure VI-32 and Figure VI-33 was measured. The results may be viewed in Figure VI-34.

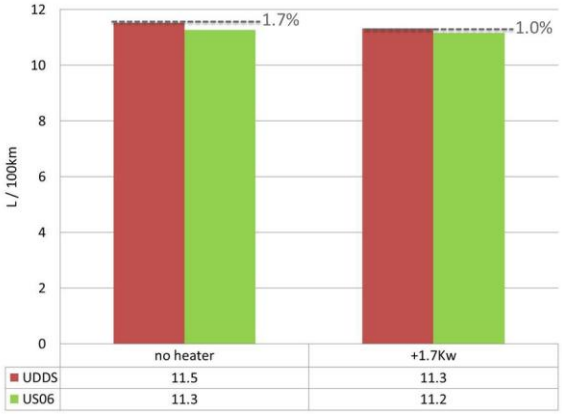

Figure VI-34: UDDS and US06 Drive Cycle Fuel Economy with and without Engine Oil Heat Addition (7°C ambient temperature).

As illustrated in Figure VI-34, the UDDS and US06 drive cycle fuel economy increased 1.7% and 1.0%, respectively, with the thermal cart heat addition. It should be noted that temperature and flow measurements of the oil input and output to the oil heater were not available. Since the oil pan inlet and outlet tubes to the heat exchanger were exposed to both the vehicle fan as well as the cold room temperatures, the power available to heat the oil was reduced. Exact values are not available for this part of the study. However, it may safely be assumed that improved results would be attained by reducing the heat transfer loss between the oil pan and heater.

To ascertain the amount of power available for heating, calculations were done to determine the power in the exhaust heat after the catalytic converter for the UDDS and US06 cycles. These calculations were done after the catalytic converter so that the potential of usable energy for heat addition would be realistic. The results may be viewed in Figure VI-35 and Figure VI-36. It should be noted that the scales are identical for both charts.

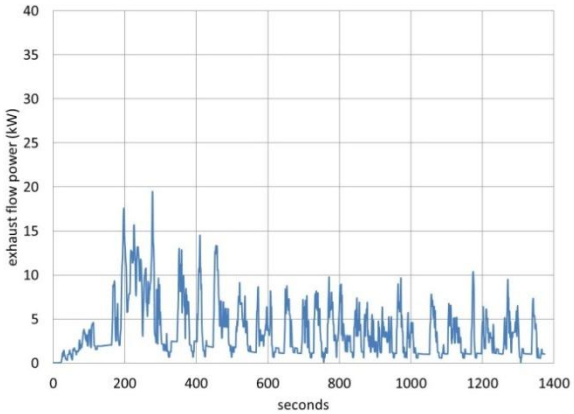

Figure VI-35: Post Catalytic Converter UDDS Cycle Exhaust Power.

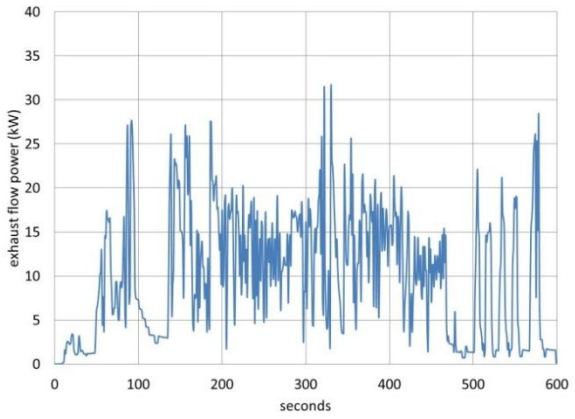

Figure VI-36: Post Catalytic Converter US06 Cycle Exhaust Power.

Figure VI-35 depicts that the peak exhaust power over the UDDS cycle is approximately 20 kW. For the US06 shown in Figure VI-36, it is approximately 32 kW. The average power over the UDDS cycle is almost 4 kW, whereas for the US06 cycle it is 10 kW. Additional calculations were done to establish the amount of energy required to get the oil to a near-optimal viscosity (approximately 95°C) to determine if sufficient energy exists to reduce the viscosity and increase efficiency. The integrated energy out of the exhaust over the UDDS cycle is displayed in Figure VI-37. This figure indicates that, in just over 200 seconds, an amount of energy has passed out of the exhaust that, if it could be totally utilized, would bring the oil to its optimal temperature. However, due to heat transfer and pumping loss issues, this could not be realized. Further analysis must be conducted to determine how effective heating of the engine oil can actually be in reducing efficiency losses. Additionally, no analysis has been conducted that applies this technique to the transmission fluids to determine optimal use of the waste heat.

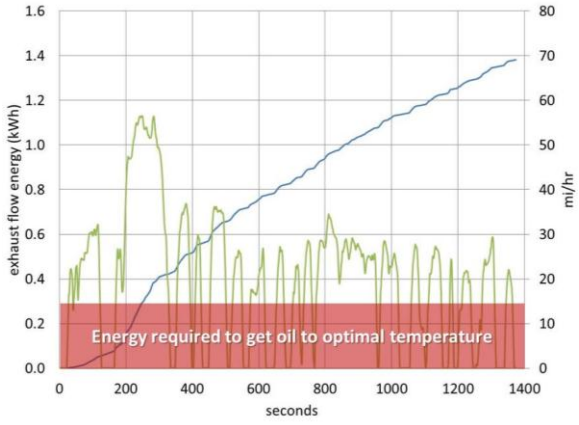

Figure VI-37: Integrated Post Catalytic Converter Exhaust Energy over the UDDS Cycle. (The area in red indicates the amount of energy required to raise the oil to a near-optimal [minimal viscosity] temperature of ~95°C.)

Conclusions

Tests were completed utilizing the 2011 Ford Fusion thermal mule in conjunction with the thermal testing cart to simulate a portion of the exhaust waste heat used to heat engine oil over the UDDS and US06 drive cycles. The ambient temperature was -7°C, and the heater was set to +1.7 kW of power. However, due to the cold ambient temperature and the fan blowing across the inlet and outlet to the heater, the full effects of the heat addition were not realized.

By adding heat to the oil, the end temperatures of the engine oil at the completion of the UDDS and US06 cycles were +7°C and +4°C, respectively. This reduction in viscosity due to the increased temperature resulted in a decreased fuel consumption of 1.7% and 1.0% over the UDDS and US06 cycles. Calculations of exhaust power indicate the availability of significant energy to heat the lubricating oils much further than the outcome that was realized during the test. This finding should result in greater efficiency gains. Testing and analysis have not been completed on the transmission fluids to determine the amount of impact that the heat addition will have on increasing efficiency.

VI.C.3. Products

Publications

1. Shidore, N., F. Jehlik, and E. Rask, "PHEV Energy Management Strategies at Cold Temperatures with Battery Temperature Rise and Engine Efficiency Improvement Considerations," SAE International Journal of Engines, Vol. 4, Detroit, MI, SAE 2011-01-0872, 2011.
2. Jehlik, F. and E. Rask, "Development of Variable Temperature Brake Specific Fuel Consumption Engine Maps," SAE Powertrain Fuels and Lube Conference, San Diego, CA, SAE 2010-01-2181, 2010.
3. Jehlik, F., E. Rask, and M. Christenson, "Simplified Methodology for Modeling Cold Temperature Effects on Engine Efficiency for Hybrid and Plug-in Hybrid Vehicles," SAE Powertrain Fuels and Lube Conference, San Diego, CA, SAE 2010-01-2213, 2010.
4. Jehlik, F., "Methodology and Analysis of Determining Plug-in Hybrid Engine Thermal State and Resulting Efficiency," SAE World Congress, Detroit, MI, SAE 2009-01-1308, 2009.

VI.D. Evaluation of the Fuel Economy Impact of Low Temperature Combustion (LTC) Using Simulation and Engine-in-the-Loop

Neeraj Shidore, Principal Investigator
Argonne National Laboratory
9700 South Cass Avenue
Lemont, IL 60439
Phone: (630) 252-7416
E-mail: nshidore@anl.gov

David Anderson, Gurpreet Singh, DOE Program Managers
Phone: (202) 586-2333; (202) 287-568
E-mail: gurpreet.singh@ee.doe.gov
david.anderson@doe.ee.gov

VI.D.1. Abstract

Objectives

Evaluate the impacts of low temperature combustion (LTC) technology on fuel economy and engine-out emissions by using simulations and engine-in-the-loop:

- Quantify the fuel economy benefits of LTC on standard drive cycles using engine-in-the-loop.
- Evaluate test-to-test variability with LTC compared to diesel.
- Assess the transient behavior of LTC.
- Compare the fuel economy benefits of LTC technology to PFI (Port Fuel Injection) and SIDI (Spark Ignition Direct Injection) technologies by using simulations.
- Use a systems approach to reduce engine-out emissions and improve fuel consumption through shift parameter optimization.

Major Accomplishments

- Completed the simulation study comparing the fuel economy benefits of LTC to those of PFI and SIDI.
- Completed engine-in-the-loop setup.
- Developed a process for systems to optimize shift parameters between engine-out emissions and fuel consumption improvement.
- Engine-in-the-loop testing with diesel fuel is under way.

Future Achievements

- Demonstrate the impact of system optimization on improving fuel consumption and reducing emissions with diesel fuel.
- Quantify fuel consumption and engine-out emissions for LTC technology at a vehicle system level.

VI.D.2. Technical Discussion

Background

Low Temperature Combustion

Low temperature combustion (LTC) technology research is being conducted by the Advanced Combustion Engines research group at the U.S. Department of Energy (DOE) to improve the efficiency of engines for light-duty passenger vehicles. One of the goals of the vehicle systems research at DOE is to rapidly evaluate components and systems through model-based design and component-in-the-loop. This project evaluates DOE-developed strategies for LTC of 87 anti-knock index (AKI) gasoline in a systems context by using transient vehicle drive cycles. A 1.9-L TDI engine, with diesel as the default fuel, is used for the LTC combustion study with 87 AKI gasoline.

Introduction

LTC research performed by the Engine Research Group at Argonne National Laboratory (Argonne) with 87 AKI gasoline has shown lower fuel consumption and NO_x emissions as compared to gasoline SI (spark ignition) engines (Figure VI-38).

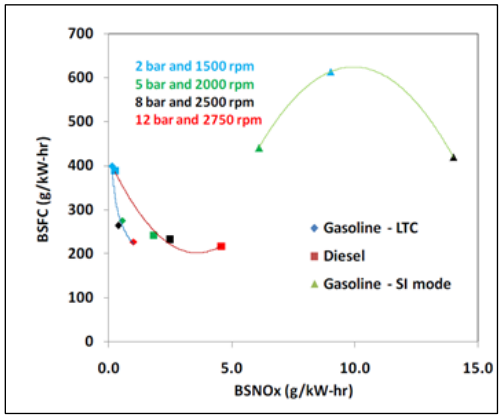

Figure VI-38: Brake Specific Fuel Consumption and Engine-out NO_x for LTC Compared to Gasoline—SI and Diesel.

This project evaluates the fuel consumption and emissions benefits of LTC over transient cycles at a vehicle system level.

Approach

The design of the experiment for the project is shown in Figure VI-39. The PFI and SIDI engine technologies, which act as a baseline to which LTC will be compared, are evaluated in simulation. Fuel consumption and engine-out emissions with LTC of gasoline will be measured from engine-in-the-loop tests. Before the engine-in-the-loop tests with LTC, a simulation study to compare the LTC (in simulation) to SIDI and PFI was conducted, and engine-in-the-loop tests were conducted with diesel fuel to validate the system approach to reduce engine out emissions and improve fuel consumption. For these fuels and combustion technologies, the comparison between fuel consumption and emissions is performed for a midsize sedan (conventional powertrain) over the Urban Dynamometer Drive Cycle (UDDS) and the highway drive cycle (HWFET).

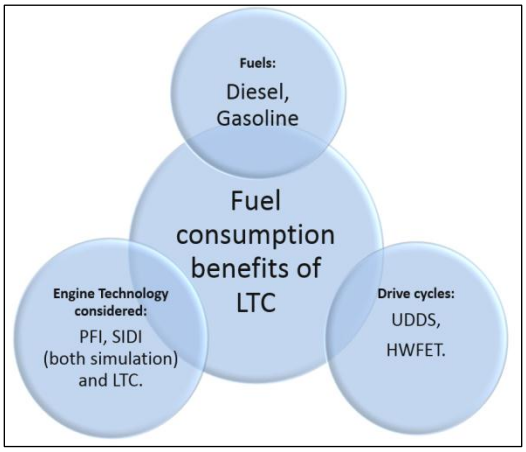

Figure VI-39: Design of Experiment.

In order to compare the LTC combustion technology to PFI and SIDI in simulation, a fuel rate map of LTC gasoline was generated from limited steady-state points available through engine steady-state test data. This was done by creating efficiency lines proportional to available efficiency curves from the steady-state data [1].

The specifications for the conventional vehicle used for the study are listed in Table VI-1. The specifications are those of a MY2007 Cadillac BLS Wagon, which has the same diesel engine as the one used at Argonne for the LTC research.

Table VI-1: Vehicle Specifications.

Vehicle	Cadillac BLS Wagon
Vehicle Mass	1560 kg
Engine	1.9 L TDI, 110 kW, 320 Nm peak torque, I-4
Transmission	Manual, 6 speed

For a fair comparison among SIDI, PFI, and LTC technologies, the SIDI and PFI engines were scaled in power, in order to meet the vehicle technical specifications of the MY2007 Cadillac BLS Wagon. Different transmission ratios and final drives were selected for the PFI, SIDI, and LTC engines, on the basis of each engine's peak torque and maximum speed characteristics. The fuel consumption map for the SIDI engine was generated from a 2.2-L ECOTEC SIDI engine. The fuel consumption map of the PFI engine was generated from a 1.8-L Peugeot engine. The gear ratio and final drive selection for the PFI and the SIDI engines are listed in Table VI-2.

Table VI-2: Transmission and Final Drive Ratios for the Different Engine Technologies.

	PFI, SIDI	LTC
Gear 1	4.16	3.77
Gear 2	2.20	2.04
Gear 3	1.48	1.37
Gear 4	1.15	1.05
Gear 5	0.92	0.85
Gear 6	0.74	0.71
Final drive ratio	4.43	3.55
Comment	GM F40 recommended for the ECOTEC family of engines	Gear ratios and final drive ratio for the BLS Cadillac Wagon

In order to properly evaluate the impact of the LTC engine technology on fuel consumption and emissions, it is important to optimize the vehicle shift parameters for said engine. This is possible in Autonomie, through a model-based design approach, as shown in Figure VI-40.

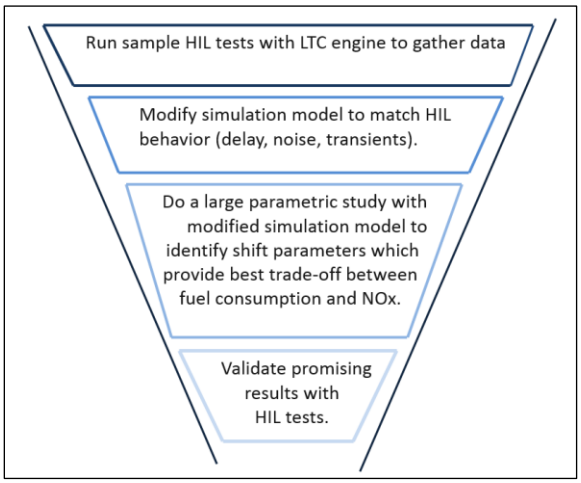

Figure VI-40: Model-Based Design Process for Shift Parameter Optimization.

In the first two steps of the model-based design (MBD) process, the simulation model of the vehicle in Autonomie is modified to match real hardware behavior with such parameters as engine-in-the-loop for transients, noise, signal and delay. Then, in the third step, a large simulation study is performed with the modified simulation. A parameter sweep of three shift parameters, listed inTable VI-3, is performed, and fuel consumption and NO_x (engine out) for all possible combinations are generated. The parameters in bold text are the default parameters. Change in the parameters causes either engine downspeeding or engine upspeeding, both of

which impact fuel consumption and NO_x. The NO_x map used for the simulation was based on steady-state data.

Table VI-3: Shift Parameter Sweep.

Parameter Description	Values for Parameter Sweep
Pedal position for upshift	[0.15, **0.2**, 0.3, 0.4]
Engine upshift speed—1st gear to 2nd gear	[186, **196**, 206] rad/s
Engine upshift speed—5th gear to 6th gear	[221, **241**, 261, 281] rad/s

The fuel consumption and NO_x results generated through the parameter sweep are filtered to remove undesirable results. The following filters are applied:

1. The number of shifts should not be greater than the number of shifts with default parameters by more than 10%.
2. The maximum engine speed for a UDDS cycle should not be higher than 2750 RPM (for a diesel and LTC combustion). The engine speed limit was decided on the basis of data from a midsize diesel vehicle of a similar vehicle class.
3. Engine operation at low speed and high torque is limited to 3% of the drive cycle. This is done to prevent engine noise, vibration, and shaking observed in the low-speed high-torque regions, as well as to prevent turbo-lag. Figure VI-41 shows the actual peak torque limits and the torque limit imposed for drivability conditions.

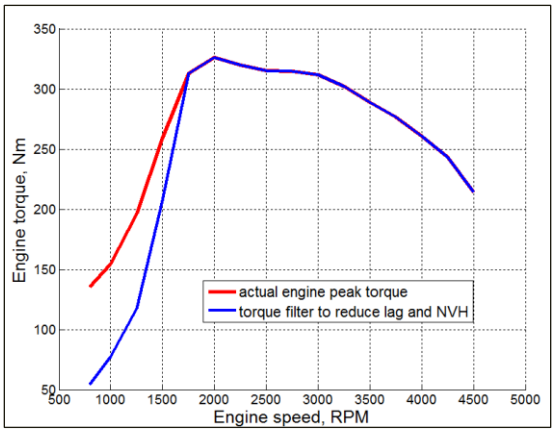

Figure VI-41: Engine Torque Limit for Drivability Conditions.

Results

Simulation Results

As mentioned earlier, the PFI and SIDI engines were scaled in engine power so that the three engine technologies, with corresponding gear and final drive ratios, met the same vehicle technical specifications: initial vehicle movement (IVM) –60 mph of 9 seconds. This resulted in PFI and SIDI engines that had 135 kW and 147 KW of power, respectively. The default engine has 115 kW of power, and the LTC engine has the same peak torque profile as the diesel engine. Table VI-4 shows the fuel economy comparisons among PFI, SIDI, and LTC engine technologies.

Table VI-4: Fuel Economy Benefits of the LTC Combustion over PFI and SIDI (simulation study results).

Fuel Economy [mpg, unadjusted]	PFI	SIDI	LTC
UDDS	26.3	30.4	32
HWFET	33.2	41.5	45.3
Combined[55/45]	29	34.6	37
Improvement over PFI		16%	26%
Improvement over SIDI			7%

As seen in Table VI-4, the LTC technology offers a 26% improvement in fuel economy over the PFI and a 7% improvement over the SIDI for the combined cycle.

Engine-in-the-Loop Implementation

In order to evaluate the fuel consumption and emissions potential of the LTC engine under transient conditions, hardware modifications were made to the engine and dyno test cell of the 1.9-L TDI engine (default diesel fuel), which is used for the LTC. Figure VI-42 shows the various components involved in the engine-in-the-loop setup with the 1.9-L TDI engine.

In addition to modifications to the hardware, the default Autonomie control plant architecture for the engine was changed to the component-in-the-loop configuration. Additional blocks are present in the component-in-the-loop configuration in order to enable low-level control of the engine and the dyno, cycle-independent testing of the hardware components, and low-level control, as well as to ensure emergency stop and other safety actions. The energy management strategy and low-level control are modified to account for noise, response dead time, and feedback delay. As shown in Figure VI-42, the Autonomie simulation (Matlab/Simulink) is embedded in a Labview environment, which forms the interface to the dyno and test cell controller. The Autonomie model, embedded in the Labview environment, sends a speed command to the dynamometer and a pedal position command to the engine control unit. As stated, the same engine is used for both diesel combustion and LTC. With diesel fuel, the stock engine control unit (ECU) is used. With LTC, programmable ECU software/hardware supplied by Drivven is used to define the combustion for each pedal position.

Model-based Design Process

As stated above, in order to provide an accurate estimate of the fuel consumption and engine out emission benefits of LTC, it is important to optimize the shift parameters for a particular engine, by using the model-based design process detailed in the approach section. Figure VI-43 shows a plot of fuel consumption (L/100 km) versus the NO_x (g/mi) for different possible combinations of shift parameters, for a UDDS cycle (Figure VI-43[a]) and a more aggressive LA92 cycle (Figure VI-43[b]), with diesel fuel. The red cross in each figure shows the NO_x and the fuel consumption with default

shift parameters, which are highlighted in Table VI-2 with bold text.

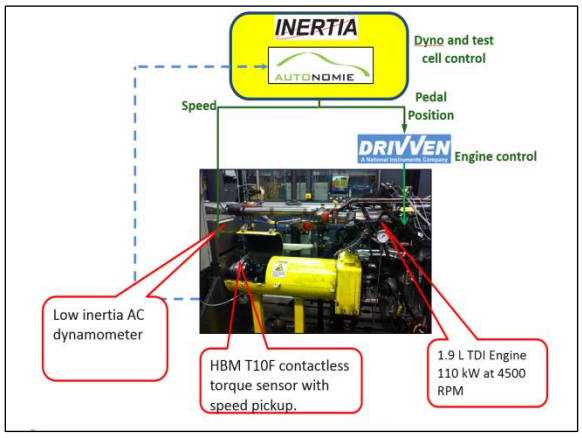

Figure VI-42: Engine-in-the-Loop Setup with the 1.9-L TDI Engine Used for the LTC Combustion.

(a)

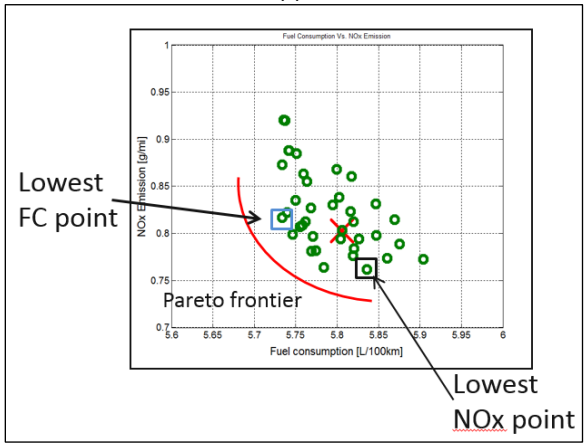

(b)

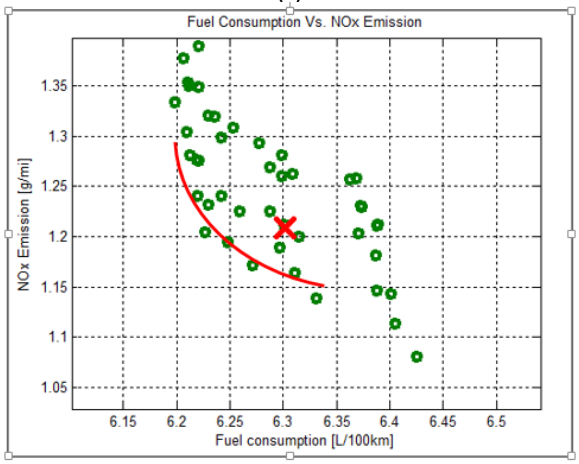

Figure VI-43: (a) Fuel Consumption and NOx for a UDDS Cycle with Different Combinations of Shift Parameters. (b): Fuel Consumption and NOx for a LA92 Cycle with Different Combinations of Shift Parameters.

Table VI-5 shows the improvements in fuel consumption or NO_x made possible by choosing parameters that produce the lowest NO_x or lowest fuel consumption, in comparison to the default values.

Table VI-5: Possible Improvement in Fuel Consumption or NO_x for the UDDS and the LA92.

Cycle	Default FC [L/100 km]	Lowest possible FC	% improvement	Default NOx[g/mi]	Lowest possible NOx	% improvement
UDDS	5.81	5.73	1.4%	0.8	0.74	7.5%
LA92	6.3	6.2	1.6%	1.22	1.07	12.3%

The above results are for all possible combinations of the shift parameters. As stated in the approach section, these results were filtered for drivability, turbo lag, number of shifts, and maximum engine speed. The filtered results for the UDDS cycle are shown in Figure VI-44 as filled green circles. The results that provide the least fuel consumption, or the least NO_x, are still possible without impacting drive quality or experiencing significant turbo lag.

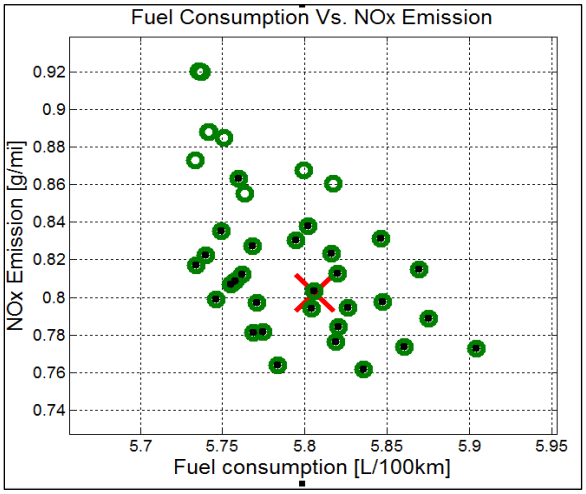

Figure VI-44: Fuel Consumption and NO_x for a UDDS Cycle with Drivability Filter.

Since the validation of the MBD process is being performed with engine-in-the-loop, it is important that the improvement in fuel consumption or NO_x be outside the test-to-test variation observed with engine-in-the-loop evaluation. On the basis of the data generated with the engine-in-the-loop tests on the 1.9-L TDI engine with diesel fuel, a standard deviation of 0.1% of the mean fuel consumption is observed.

Table VI-6 shows a 90% confidence interval (CI) of the default mean fuel consumption (Red cross in Figure VI-43 [a]) and the minimum possible fuel consumption (blue box in Figure VI-43[a]) for a 10-sample and a 5-sample scenario. As seen in the table, the 90% CI for the default shift parameters and the parameters that enable minimum fuel consumption do not overlap for either the 10-sample or the 5-sample case.

Table VI-6: Possible Improvement in Fuel Consumption or NO_x for the UDDS and the LA92.

Shift param	Mean value [L/100 km]	# of tests	90% CI	# tests	90% CI
Default	5.81	10	[5.78 5.83]	5	[5.77 5.84]
Tuned for minimum F.C.	5.73	10	[5.70 5.75]	5	[5.69 5.76]

Therefore, it is possible to validate the improvement in fuel economy and emissions because of shift parameter optimization using engine-in-the-loop.

Conclusions and Future Directions

1. This project evaluates a DOE-developed combustion technology (LTC with pump gasoline) in a systems context through the use of a simulation and engine-in-the-loop. The fuel consumption of a midsize sedan (conventional powertrain) with LTC was compared to the same vehicle with SIDI and PFI engines (SIDI and PFI engines are scaled in power such that the vehicle IVM—60 mph is the same in each case) in simulation. In addition, fuel consumption and engine out emissions for the said technology will be quantified by using engine-in-the-loop. Optimization of shift parameters will be used to minimize the fuel consumption and/or engine out NO_x emissions of the LTC engine.
2. The simulation study has shown that with LTC combustion, a 26% improvement in fuel consumption over a PFI engine and a 7% improvement over SIDI engine technology are possible.
3. Engine-in-the-loop has been implemented on the engine dyno test cell with the 1.9-L TDI engine. The engine-in-the-loop configuration has been implemented in Autonomie to enable, for example, low-level control of dyno, the engine, and DFMEA actions.
4. A model-based design process has been developed to optimize shift parameters to minimize fuel consumption and/or minimize NO_x emissions.
5. After certain hardware upgrades are complete, engine-in-the-loop evaluation for conventional vehicles with diesel fuel will be completed.
6. Optimization of shift parameters will be performed by using fuel rate and NO_x maps for LTC, and the fuel consumption and engine-out emissions for the LTC engine will be quantified.
7. The impact of LTC on the fuel consumption and emissions of an electrified powertrain will be evaluated over different powertrain configurations and drive cycles.

Presentations

1. N. Shidore, S. Ciatti, “Evaluation of the Fuel Economy Impacts of Low Temperature Combustion (LTC) Using Engine in the Loop,” presentation at the 2013 DOE Hydrogen Program and Vehicle Technologies Annual Merit Review, May 15, 2013.
2. N. Shidore, et al., “Evaluation of the fuel economy impacts of Low Temperature Combustion (LTC) Using Engine in the Loop,” presentation to the Department of Energy, June 12, 2013.

References

1. P. Abiven, S. Ciatti, A. Rousseau, “Fuel Consumption Benefit of Low Temperature Combustion Engine for Conventional Vehicle,” presentation to the Department of Energy, September 13, 2012.

VI.E. Lower-Energy Energy Storage System (LEESS) Component Evaluation

Jeffrey Gonder, Principal Investigator
National Renewable Energy Laboratory
15013 Denver West Parkway, MS 1634
Golden, CO 80401
Phone: (303) 275-4462
E-mail: jeff.gonder@nrel.gov

Lee Slezak and David Anderson,
DOE Program Managers
Phone: (202) 586-2335 (Lee)
E-mail: lee.slezak@ee.doe.gov
Phone: (202) 287-5688 (David)
E-mail: david.anderson@ee.doe.gov

VI.E.1. Abstract

Objectives

- Establish a re-usable vehicle test platform for evaluating lower-energy energy storage system (LEESS) devices for power-assist or "full" hybrid electric vehicles (HEVs).
  - HEVs with lower cost or better performing energy storage systems could improve their cost vs. benefit ratio, market penetration and aggregate fuel savings.
- Perform bench testing on one prospective LEESS device and integrate it into the test vehicle.

Major Accomplishments

- Completed bench testing on lithium-ion capacitor (LIC) LEESS devices supplied by JSR Micro.
  - Results indicate sufficient device energy to satisfy standard drive cycle demands and improved efficiency relative to the production battery system.
- Completed conversion of the Ford Fusion Hybrid research vehicle into the re-usable test platform for in-vehicle LEESS device evaluation.
  - Test vehicle retains the ability to switch back and forth between the conversion and the production vehicle configuration.
- Completed integration of the JSR Micro LIC modules into the vehicle test platform, and confirmed successful operation and hybrid system functionality using the LEESS devices (with the production battery disconnected).

Future Achievements

- Complete repeatable back-to-back in-vehicle testing over a variety of driving profiles using the JSR Micro LIC devices compared with the production battery system.
- Remove the JSR Micro LIC devices and repeat the testing with two different LEESS devices.

✧ ✧ ✧ ✧ ✧

VI.E.2. Technical Discussion

Background

Automakers have been mass producing hybrid electric vehicles (HEVs) for well over a decade, and the technology has proven to be very effective at reducing per-vehicle fuel use. However, the incremental cost of HEVs such as the Toyota Prius or Ford Fusion Hybrid remains several thousand dollars higher than the cost of comparable conventional vehicles, which has limited HEV market penetration. The battery energy storage device is typically the component with the greatest contribution toward this cost increment, so significant cost reductions and/or performance improvements to the energy storage system (ESS) can correspondingly improve the vehicle-level cost vs. benefit relationship. Such an improvement would, in turn, lead to larger HEV market penetration and greater aggregate fuel savings.

Introduction

In recognition of these potential benefits, the United States Advanced Battery Consortium (USABC) asked the National Renewable Energy Laboratory (NREL) to collaborate with its Workgroup and analyze the trade-offs between vehicle fuel economy and reducing the decade-old minimum energy requirement for power-assist HEVs. NREL's analysis showed that significant fuel savings could still be delivered from an ESS with much lower energy storage than the previous targets, which prompted USABC to issue a new set of LEESS targets and issue a request for proposals to support their development. In order to validate the fuel savings and performance of an HEV using such a LEESS device, this jointly funded activity (between the U.S. Department of Energy Vehicle Technologies Office Energy Storage and Vehicle Systems Simulation and Testing programs) has designed a test platform in which alternate energy storage devices can be installed and evaluated in an operating vehicle.

Approach

In FY 2012, NREL entered into a Cooperative Research and Development Agreement with Ford Motor Company to support conversion of a Ford Fusion Hybrid into a test platform for evaluating LEESS devices. NREL subsequently acquired a 2012 Fusion Hybrid and began designing the conversion. NREL also established a Non-Disclosure Agreement and a Bailment Agreement with JSR Micro, Inc. to provide (at its expense) lithium-ion capacitor (LIC) modules as the first LEESS device to be evaluated in the vehicle, along with proprietary information about the modules to support their integration and testing. The LICs are asymmetric electrochemical energy storage devices possessing one electrode with battery-type characteristics (lithiated graphite) and one with ultracapacitor-type characteristics (carbon). Additional project steps in FY 2013 included completing the vehicle conversion, conducting bench testing on the LIC replacement pack in comparison to the production nickel metal hydride (NiMH) battery pack from the 2012 Fusion Hybrid, and integrating the LIC modules into the Fusion Hybrid test platform.

Results

Designing the conversion required first understanding the construction of the production high-voltage traction battery (HVTB) and its integration with the rest of the vehicle. Important components of the HVTB include the high-voltage bussed electrical center (BEC), the battery pack sensor module (BPSM), and the battery energy control module (BECM). The BEC acts as an interface between the high-voltage output of the HVTB and the vehicle's electric motor, air conditioning compressor, and DC/DC converter. The BPSM measures the voltage and temperature of the NiMH cells and communicates with the BECM, which manages the charging/discharging of the battery and also communicates with the other vehicle control modules over the high-speed controller area network (CAN) bus. Figure VI-45 shows a schematic of the HVTB, including these components, and a photo of the HVTB in the vehicle, which mounts between the rear seat and the trunk area.

With the conversion strategy established in FY 2012, NREL elected to keep the production HVTB installed in its original position so that direct comparison testing could be conducted by switching back and forth between the production battery and the alternative LEESS under test. Figure VI-46 shows a schematic of this configuration, where parts from a second HVTB acquired by NREL (including the BECM, BEC, BPSM, module sense leads, and various wiring harnesses) were reconfigured to work with the alternative LEESS under test. The dSpace component represented in the schematic is a dSpace MicroAutoBox (MABx), which is used to intercept certain CAN signals pertaining to the BECM's calculations for the production NiMH battery (state of charge, power capability, etc.) and to replace them with corresponding calculations for the alternate LEESS under test. The MABx also records data during the testing.

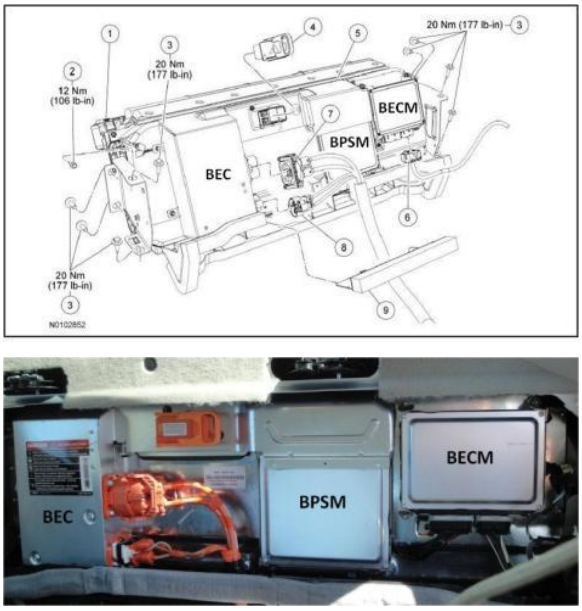

Figure VI-45: Schematic and photo of the Fusion Hybrid's HVTB (Photo credit: John Ireland, NREL).

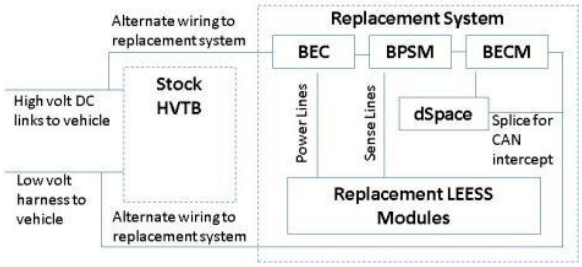

Figure VI-46: Schematic of connections between replacement components and the vehicle.

Figure VI-47 provides the schematic for an additional electronics component established between the voltage sense leads for the alternate LEESS under test and the production BPSM sense leads. This voltage divider circuit divides the full voltage of the alternate LEESS into the 26 evenly divided increments that the BPSM is expecting to measure (corresponding to the 26 NiMH modules that make up the production battery pack). This helps keep the BECM operating as if the production batteries were still connected and leaves actual module-level voltage measurement and safety controls for the LEESS under test to be handled by the MABx.

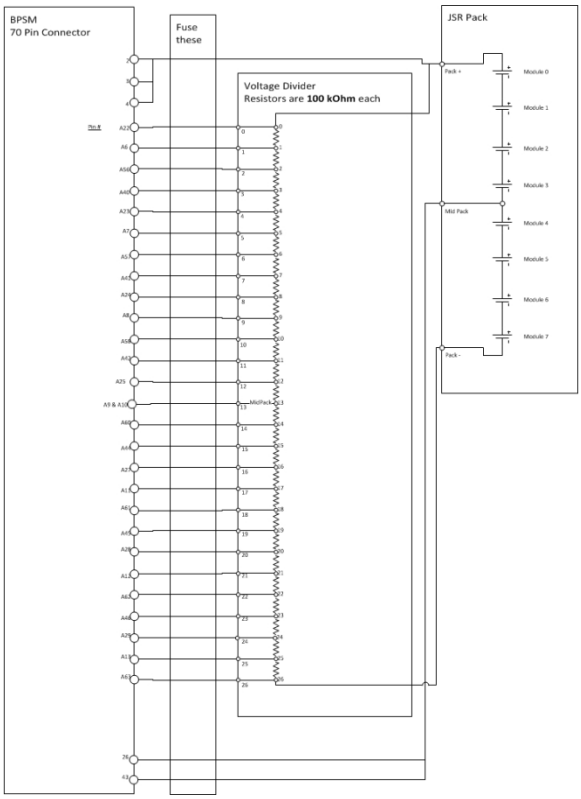

Figure VI-47: Schematic of voltage divider circuit between the replacement BPSM and the LEESS modules.

Prior to actually integrating the JSR LIC modules into the test vehicle, NREL first performed bench testing with the modules mounted in an environmental chamber (see Figure VI-48). The purposes of the bench testing included confirming expected LIC performance, comparing the LIC pack's operation to that of the production battery over a representative driving profile, and generating test data for calibrating the custom state estimator model to implement in the dSpace MABx.

Figure VI-48: JSR LIC modules in an environmental chamber during bench testing, with the production 2012 Fusion Hybrid NiMH modules in the background (Photo credit: John Ireland, NREL).

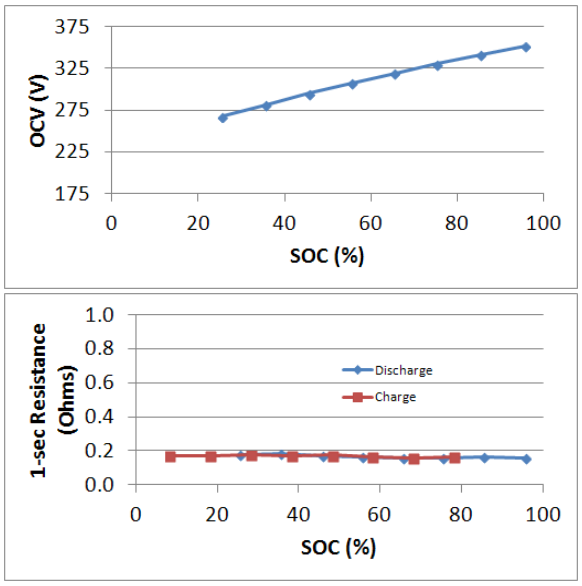

Figure VI-49: LIC pack performance calculations from bench testing.

Figure VI-49 shows the performance results from hybrid pulse power characterization testing on the LIC pack. The results show greater open circuit voltage variation, but also two to three times lower resistance as compared to the production NiMH pack, based on calculations from pack testing performed for the DOE's Advanced Vehicle Testing Activity (AVTA) [1]. In order to evaluate the LIC pack operation during bench testing against a representative in-vehicle load profile, NREL referenced production Fusion Hybrid chassis dynamometer test results available from Argonne National Laboratory. The LIC modules were able to satisfy the exact load profile provided by the production NiMH pack during chassis dynamometer testing over the aggressive US06 drive cycle. Figure VI-50 shows the resulting profile for the internal energy state of the stock NiMH battery (from chassis testing) compared to that of the LIC modules (from bench testing). The results indicate a rise in the internal energy state for both devices, but a roughly 50-Wh larger rise for the LIC pack due to its lower internal resistance. The follow-on in-vehicle testing of the LIC pack will help reveal to what extent the lower energy losses help offset any limitations caused by its lower total energy content as compared to the NiMH pack.

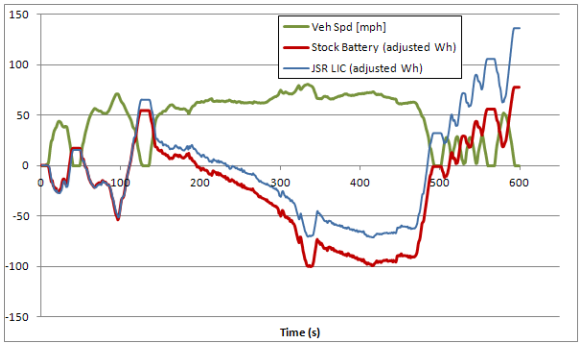

Figure VI-50: ESS energy profile comparison over the aggressive US06 drive profile.

The final FY 2013 result highlighted in this summary report is the integration of the LIC modules into the Fusion Hybrid test platform to enable the in-vehicle comparison testing (which will wrap up in the early part of FY 2014). Figure VI-51 shows a picture of the fully integrated conversion system, including LIC modules, mounted in the trunk of the Fusion Hybrid. The LIC modules along with the replacement BEC are shown in the large box with the clear lid; off to the side the picture shows the MABx mounted on top of an electronics box containing the voltage divider circuit and related components.

Figure VI-51: Fully integrated conversion system mounted in the trunk of the Fusion Hybrid test platform (Photo credit: Jon Cosgrove, NREL).

Along with the physical components shown in Figure VI-51, the custom state estimator code (to estimate the LEESS state of charge and charge/discharge capability at any moment in time) has been validated against the bench test data and incorporated into the MABx, with temperature dependence functionality included. The ability to operate the vehicle while intercepting and re-broadcasting modified signals over the vehicle CAN bus has also been confirmed. Finally, following validation testing of the safety controls implemented in the vehicle, the project team completed NREL's safety readiness verification and received a Safe Work Permit to operate and test the vehicle platform in the conversion configuration from NREL's Environment Health and Safety Office.

Conclusions

Alternate HEV storage systems such as the LIC modules described in this report have the potential for improved life, superior cold temperature performance, and lower long-term cost projections relative to traditional battery storage systems. If such LEESS devices can also be shown to maintain high HEV fuel savings, then future HEVs designed with these devices could have an increased value proposition relative to conventional vehicles, thus resulting in greater HEV market penetration and aggregate fuel savings. The vehicle test platform developed through this project is helping to validate the in-vehicle performance capability of alternative LEESS devices and to identify unforeseen issues.

This report describes successful creation of the Ford Fusion Hybrid test platform for in-vehicle evaluation of such alternative LEESS devices, bench testing of the initial LIC pack provided by JSR Micro, and final integration of the LIC pack into the test vehicle. On-going work into FY 2014 will include completion of in-vehicle comparison testing between the LIC pack and the production NiMH batteries and subsequent testing with LEESS devices from other manufacturers. Non-Disclosure Agreement and Bailment Agreement paperwork have been initiated with Maxwell Technologies to provide ultracapacitor modules as the next system to evaluate for the project. Other possible future work topics include evaluating the potential offered by LEESS devices with more extensive vehicle modification, such as by increasing the motor size to leverage a higher-power capability ESS.

Reference

1. "2010 Ford Fusion-4699 Hybrid BOT Battery Test Results, Hybrid System Specifications." U.S. Department of Energy Office of Energy Efficiency and Renewable Energy. http://www1.eere.energy.gov/vehiclesandfuels/avta/pdfs/hev/batteryfusion4699.pdf.

VI.E.3. Products

Publications

1. Gonder, J., Ireland, J., Cosgrove, J., and Pesaran, A. "Evaluation of a Lower-Energy Energy Storage System for Full-Hybrid Electric Vehicles." SAE 2013 Hybrid and Electric Vehicle Technologies Symposium, February 2013.
2. Cosgrove, J., Gonder, J. and Pesaran, A., "Performance Evaluation of Lower-Energy Energy Storage Alternatives for Full-Hybrid Vehicles." Abstract accepted for presentation at the Supercapacitors USA International Conference and Tradeshow, November 2013.

Tools and Data

1. The converted Ford Fusion Hybrid test vehicle serves as a reusable tool for evaluating multiple alternative LEESS devices.
2. Data collected from bench and in-vehicle LEESS device testing is detailed in the publications listed above.

VI.F. APEEM Components Analysis and Evaluation

Paul H. Chambon, Principal Investigator
Oak Ridge National Laboratory
2360 Cherahala Boulevard
Knoxville, TN 37932
Phone: (865) 946-1428
E-mail: chambonph@ornl.gov

David Anderson, DOE Program Manager
Phone: (202) 287-5688
E-mail: david.anderson@ee.doe.gov

VI.F.1. Abstract

Objectives

- Support the evaluation of current and proposed electric machine and power electronics technologies in a vehicle context to understand the applicability of a particular powertrain technology to a given vehicle and to determine areas/regions for component design improvement based upon system usage patterns
- Enhance the current benchmarking and prototype evaluation capabilities of DOE APEEM programs with the addition of transient-capable testing facilities for power electronics and electric machinery components.

Major Accomplishments

- Supported DOE APEEM group modeling activities, so that electric machine and power electronics designers know how to use a vehicle simulation tool (Autonomie) to evaluate electric powertrain technologies at the vehicle system
- Initiated the procurement of a dynamometer suitable for electrical component characterization and validation through hardware-in-the-loop testing

Future Achievements

- Perform hardware-in-the-loop testing of electric hybrid powertrain components

✧ ✧ ✧ ✧ ✧

VI.F.2. Technical Discussion

Background

Part of the Vehicle System Integration (VSI) Laboratory, Oak Ridge National Laboratory has commissioned a powertrain test cell capable of testing a complete heavy-duty hybrid vehicle powertrain by combining the use of two 500kW dynamometers and a 400kW e-storage unit that can emulate the behavior of a battery. It is also equipped with a hardware-in-the-loop platform to emulate vehicle components not present in the testcell, such that the powertrain behaves as if it were in a real vehicle on real world road conditions; this is referred to as Powertrain-In-the-Loop.

Introduction

Testing electric machine and power electronics technology in the context of a vehicle using a hardware-in-the-loop approach is critical in order to understand transient, application specific, and real world conditions limitations associated with that component. These findings can be used to optimize its design and obtain a better match between the component and the vehicle application in order to achieve improved overall vehicle efficiency.

Approach

This project will provide vehicle engineering support to ORNL's Power Electronics and Electric Machinery (PEEM) group while they conduct simulation studies funded by DOE APEEM (Advanced Power Electronics and Electric Motors) programs.

This project will also specify and procure key components for a testing facility suitable to characterize hybrid traction components in transient operations representative of vehicle conditions thanks to a hardware-in-the-loop set-up. That facility, called component test cell, will be part of ORNL's Vehicle System Integration laboratory.

Results

Vehicle Simulation Support

Training and support was provided to members of the Power Electronics and Electric Machinery group so that they can use the vehicle simulation tool from Argonne National laboratory, Autonomie, to perform vehicle level evaluations of electric powertrain components. Copies of Autonomie were obtained and installed for two members of the PEEM group. Those reseachers were also provided with the model of a Nissan Leaf developed during FY12 for other DOE funded projects. This will be one of the vehicle platforms used to benchmark the vehicle suitability of novel motor concepts developed by APEEM programs.

Testing Facilities Enhancement

A list of requirements was created for the component testcell dynamometer selection:

- About 200kW power level, to be able to handle passenger car engines and traction motors

- High rotational speeds (~14000rpm), to cope with higher speed trend in automotive traction motors.
- Low inertia (<0.5kgm2), to be capable of replicating fast transients (up to 5000rpm/s) experienced by actual components in a vehicle context.
- Remote high speed dyno control interface to integrate dynamometer with external real time platform

The selection team identified the AVL PLP 525/220/12 dynamometer as a suitable trade-off for those requirements:

- 220kW max power
- 12000rpm max speed
- 0.325kgm2 inertia
- High speed CAN interface for remote control

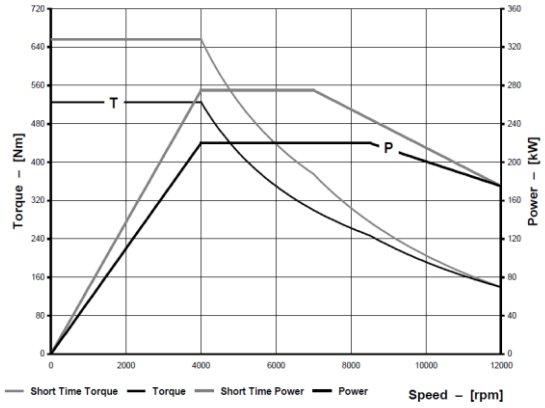

Figure VI-52: Torque and power curve for AVL PLP 525/220/12 AC dynamometer.

The procurement process was initiated and the dynamometer will be commissioned at ORNL in Q2 FY2014 due to the long lead time for that item. The procurement of this dynamometer is also financed by DOE APEEM programs since it will be also supporting their activities once commissioned.

The VSI laboratory is already fitted with an e-storage unit (also known as battery emulator) that is shared with the larger powertrain test cell. The e-storage unit is capable of up to 800V, 600A and 400kW (see Figure VI-53). It can emulate the behavior of most energy storage systems such that the electric machine under test can be subjected to a variety of operating conditions representative of real world operations.

The new high speed dynamometer and existing e-storage unit will be integrated with a real time computer running models of virtual vehicles so that the electric machine will behave as if it were fitted under an actual vehicle driving in real world conditions.

Figure VI-53: AVL e-storage unit installed at ORNL VSI laboratory.

To achieve this, the dynamometer and e-storage unit will operate as slaves to the real time computer. The dynamometer is mechanically coupled to the electric machine; it will apply the reaction torque calculated by the vehicle model on the real time computer. The e-storage unit is electrically connected to the electric machine; it will apply the operating voltage calculated by the vehicle model. This arrangement is known as Hardware-In-the-Loop and is described in Figure VI-54.

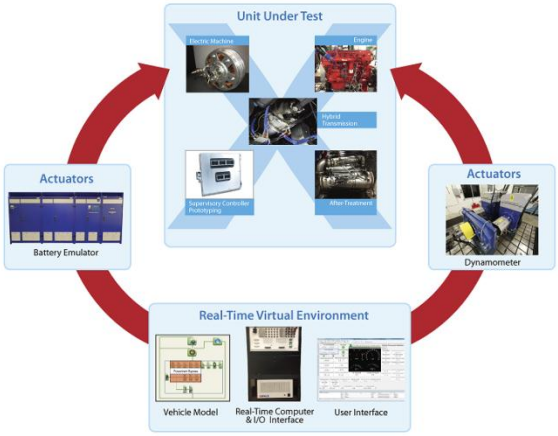

Figure VI-54: Hardware-In-the-Loop diagram.

Conclusions

This project supported vehicle simulation activities within the PEEM group at ORNL so that vehicle considerations are taken into account when designing new advance electric machinery and power electronics components.

Also the specification phase was completed for testing facilities suitable to evaluate those same components on a test cell while still emulating real world conditions, thanks to a high speed transient dynamometer, a battery emulator and a Hardware-In-the-Loop real time platform. The procurement phase was initiated; the commissioning is expected for Q2 of FY14.

VII. CODES & STANDARDS

VII.A. Codes and Standards and Technical Team Activities

James Francfort, Principal Investigator
Idaho National Laboratory
P.O. Box 1625
Idaho Falls, ID 83415-2209
Phone: (208) 526-6787
E-mail: James.francfort@inl.gov

Lee Slezak, DOE Program Manager
Phone: (208) 586-2335
E-mail: Lee.slezak@ee.doe.gov

VII.A.1. Abstract

Objectives

- To contribute vehicle, component, and fueling infrastructure testing knowledge gained by Idaho National Laboratory (INL) staff from 120 million miles of benchmarking to industry and government groups developing and modifying standards, codes, best practices, and regulations.

Major Accomplishments

- Simply being recognized as an industry expert and being a voting member of these industry and government committees is a major accomplishment in itself
- The current committees/organizations that INL staff are contributing to include the following:
  - Society of Automotive Engineers (SAE) J2954 Wireless Charging Task Force
  - SAE J2894 Power Quality Requirements for Plug-in Electric Vehicle Chargers
  - National Institute of Standards and Technology's U.S. National Work Group on Measuring Systems for Electric Vehicle Fueling and Submetering
  - U.S. Drive: Vehicle Systems Analysis Tech Team
  - U.S. Drive: Grid Integration Tech Team
  - Electric Power Research Institute—National Electric Transportation Infrastructure Working Council
  - National Fire Protection Association: Project Technical Panel and Battery Technology Advisory Panel.

Future Achievements

- Continued future participation on various committees and panels, representing U.S. Department of Energy (DOE) interests and providing expertise and testing results from testing of cutting edge advanced technologies.

✧ ✧ ✧ ✧ ✧

VII.A.2. Technical Discussion

Background

DOE's Advanced Vehicle Testing Activity (AVTA) is part of DOE's Vehicle Technologies Office, which is within DOE's Office of Energy Efficiency and Renewable Energy. AVTA is the only DOE activity tasked by DOE to conduct field evaluations of fueling infrastructure vehicle technologies that use advanced technology systems and subsystems in light-duty vehicles to reduce petroleum consumption. A secondary benefit is reduction in exhaust emissions.

Most of the advanced technology vehicles, subsystems, and fueling infrastructure that AVTA tests include the use of electric drive propulsion systems and advanced energy storage systems. However, other vehicle technologies that employ advanced designs, control systems, or other technologies with production potential and significant petroleum reduction potential are also considered viable candidates for testing by ATVA. AVTA and INL's first priority is providing DOE feedback on the performance of advanced technologies that DOE has made funding investments in.

The AVTA light-duty activities are conducted by INL for DOE. INL has responsibility for AVTA's execution, direction, management, and reporting; as well as data collection, analysis, and reporting. INL is supported in this role by various subcontracts for specific tasks when greater value can be achieved for DOE if INL conducts research in partnerships with other organizations.

The AVTA sections of the FY 2012 Annual Program Report jointly cover the testing work performed by INL and any subcontractor conducting work that INL manages. When appropriate, AVTA partners with other governmental, public, and private sector organizations to provide maximum testing and economic value to DOE and the United States' taxpayers via various cost-sharing agreements.

Introduction

DOE's AVTA is evaluating grid-connected plug-in electric drive vehicle (PEV) technology in order to understand the capability of electric grid-recharged electric propulsion technology to significantly reduce petroleum consumption when vehicles are used for transportation. In addition, many companies and groups are proposing, planning, and have started to introduce PEVs into their fleets.

Knowledge that INL staff has gained from 20 years of testing electric drive and other vehicle technologies and

fueling infrastructure for more than 120 million miles is used by INL staff to contribute to various industry and government groups that are primarily interested in developing policies, standards, codes, and regulations that ensure safety and interoperability within technologies sectors.

Approach

As a member of a technical committee or industry group, participation is intended to contribute to the common body of knowledge being applied to develop standards and other industry practices. Participation is also intended to represent DOE interests.

Results

SAE International

SAE J2954 Wireless Charging Task Force: INL supports the SAE J2954 committee as a full voting member and by providing detailed test results from wireless charging systems. The test results detail system efficiency and EM-field strength. Additionally, multiple factors (such as misalignment, coil gap, component temperature, and debris tolerance; all of which impact the system efficiency and EM-field strength) are tested and detailed to the SAE J2954 committee in order to support the safety and test procedures sections of the document.

INL has performed the only independent testing of a wireless power transfer technology and published the testing results. The testing was conducted under a non-disclosure agreement with Evatran; Evatran has graciously allowed INL to publish very detailed testing results. The detailed results are provided elsewhere in this annual report. From the information learned from the Evatran test results, INL has provided numerous revisions to the SAE J2954 document.

SAE J2894 Power Quality Requirements for Plug-in Electric Vehicle Chargers: The SAE J2894 committee is developing requirements and test procedures to ensure that electric vehicle supply equipment (EVSE) do not cause power quality issues and that EVSE can continue to function properly in the presence of power quality issues caused by adjacent loads. Because both conductive and wireless power transfer systems testing are being conducted at INL, INL staff participation as a full voting committee member and INL input is considered as a valuable resource of expertise and hands-on experience for the committee.

The EVSE testing has included fourteen Levels 1 and 2 conductive EVSE, one DC fast charger, and one wireless power transfer system.

National Institute of Standards and Technology

U.S. National Work Group on Measuring Systems for Electric Vehicle Fueling and Submetering: This National Institute of Standards and Technology committee is developing a draft standard of rules and regulations that EVSE must adhere to if the EVSE sells power and they are the point of metering. INL staff participation in this meeting is important, because in the future, EVSE will need to be tested to ensure they are following the standard. By participating in this standard development, INL staff engineers are helping to direct future EVSE testing needs, methods, and procedures.

U.S. Drive (United States Driving Research and Innovation for Vehicle efficiency and Energy Sustainability)

Vehicle Systems Analysis Tech Team: INL is a long-time member of the Vehicle Systems Analysis Tech Team because of the history of the testing INL performs for DOE. INL staff contributes, via presentations and papers, the results of benchmarking advanced automotive powertrain components and subsystems from INL's whole vehicle system testing and component testing. This includes fuel use, efficiencies, auxiliary loads, and energy storage results that are subsequently used by other team members as modeling inputs.

Grid Integration Tech Team: INL is a founding member of the Grid Integration Tech Team by nature of the infrastructure testing INL performs for DOE. This includes wireless power transfer and conductive charging, including DC fast charging and INL's data collection, analysis, and reporting as to how PEV drivers operate 16,000 Level 2 EVSE.

Electric Power Research Institute—National Electric Transportation Infrastructure Working Council

Infrastructure Working Council: INL is a 20-year member of the Infrastructure Working Council, which is sponsored by the Electric Power Research Institute and is a group of individuals whose organizations have a vested interest in the emergence and growth of the electric vehicle and plug-in hybrid and electric vehicle industries, as well as the electrification of truck stops, ports, and other transportation and logistic systems. Infrastructure Working Council members include representatives from electric utilities, vehicle manufacturing industries, component manufacturers, government agencies, related industry associations, and standards organizations. The various committees meet several times a year to address the main areas of electric vehicle, plug-in hybrid electric vehicle, truck stop and port electrification, and infrastructure research and development. INL supports both the Plug-in Hybrid and Electric Vehicle Working Group and the Transportation Electrictrification Committee, as well as serving on the Infrastructure Steering Committee. The results from INL's testing of vehicles and infrastructure, as well as data collection from 24,000 vehicles and charging infrastructure units with data loggers, is of great interest and support to the Infrastructure Working Council's decision processes.

National Fire Protection Association

In an effort to bolster preliminary guidance issued by the National Fire Protection Association for fire emergencies involving electric drive vehicles (EDVs), full-scale fire suppression tests were conducted to collect data and evaluate any differences associated with EDV fires as compared to traditional internal combustion engine vehicle fires. EDVs may pose new, unknown risks and variables to emergency responders. In particular, members of the emergency response community have questions regarding: (1) personal protective equipment (PPE); (2) firefighting suppression tactics; and (3) the best practices for overhaul and post-fire clean-up. Specifically, questions from the emergency

response community regarding these three topics include the following:

1) Appropriate PPE to be used for responding to fires involving EDV batteries:
   a) Is current PPE appropriate with regard to respiratory and dermal exposure to vent gases and combustion products?
   b) Is current PPE appropriate with regard to potential electric shock hazards?
   c) What is the size of the hazard zone where full PPE, including respiratory protection, must be worn?
2) Tactics for suppression of fires involving EDV batteries:
   a) How effective is water as a suppressant for large battery fires?
   b) Are there projectile hazards?
   c) How long must suppression efforts be conducted to place the fire under control and then fully extinguish it?
   d) What level of resources will be needed to support these fire suppression efforts?
   e) Is there a need for extended suppression efforts?
   f) What are the indicators for instances where the fire service should allow a large battery pack to burn rather than attempt suppression?
3) Best practices for tactics and PPE to be used during overhaul and post-fire clean-up operations.

AVTA at INL was tasked by DOE and the U.S. Department of Transportation to develop a first responder program for EDVs and their energy storage systems. This request was partially based on INL staff experience with several EDV thermal events during AVTA testing. Most recently, that experience included gaining significant knowledge over a multi-day event that included fire suppression while maintaining the integrity of a lithium-ion traction battery in order to perform a post-event autopsy and the safe discharging of the battery's energy in a field environment.

INL partnered with the National Fire Protection Association and its research arm, the Fire Protection Research Foundation, to conduct a research program to develop the technical basis for best practices for emergency response procedures for EDV battery incidents, with consideration for certain details, including suppression methods and agents; PPE; and clean-up/overhaul operations. A key component of this project goal was to conduct full-scale testing of large-format Li-ion batteries used in today's EDVs. INL's participation included controlling Federal funding and providing staff to serve on the Project Technical Panel and Battery Technology Advisory Panel.

The other major project sponsor was the Alliance of Automobile Manufacturers. The Technical and Battery Panel participants included staff from many first responder organizations and original equipment manufacturers.

Both laboratory and field tests were conducted on numerous in-vehicle and non-vehicle scenarios. The result is a significant document, *Best Practices for Emergency Response to Incidents Involving Electric Vehicles Battery Hazards: A Report on Full-Scale Testing Results, that* is referenced in the Publications section.

As stated in the foreword of the report:

The overall goal of this project is to conduct a research program to develop the technical basis for best practices for emergency response procedures for electric drive vehicle battery incidents, with consideration for certain details including: suppression methods and agents; personal protective equipment (PPE); and clean-up/overhaul operations. A key component of this project goal is to conduct full-scale testing of large format Li-ion batteries used in these vehicles. This report summarizes these tests, and includes discussion on the key findings relating to best practices for emergency response procedures for electric drive vehicle battery incidents.

At least for now, this document is considered the standard for fire responders when they encounter an EDV with a battery fire.

Conclusions

The intent of the work that is described in this section is to leverage the benchmark testing results and staff knowledge gained as a resource to various industry groups that are either putting in place industry-lead or government-lead codes, standards, requirements, or best practices.

VII.A.3. Products

Publications

The intent of this work decidedly is not to publish results as products of INL, because the outcomes are usually the sole intellectual rights of other organizations. Similarly, there will not be any INL patents or tolls generated by these types of activities. The exception to this is the results from the First Responder Project and that document is listed as follow:

1. Long, R. T., A. F. Blum, T. J. Bress, and B. R. Cotts, 2013, Best Practices for Emergency Response to Incidents Involving Electric Vehicles Battery Hazards: A Report on Full-Scale Testing Results, Fire Protection Research Foundation, Quincy, MA, June 2013.

INL/MIS-13-30556

VII.B. Model Reusability

Chuck Folkerts, Principal Investigator
Argonne National Laboratory
9700 South Cass Avenue
Argonne, IL 60439-4815
Phone: (630) 252-7261
E-mail: cfolkerts@anl.gov

Lee Slezak, DOE Program Manager
Phone: (202) 586-2335
E-mail: Lee.Slezak@ee.doe.gov

VII.B.1. Abstract

Objectives

- Establish dynamical modeling and simulation standards.
- Facilitate dynamical modeling and simulation of automotive systems.
- Make dynamical models universally reusable using plug-and-play technology.

Major Accomplishments

- Submitted the approved SAE Standard Recommended Practice J-2998, called "Model Description Documentation Recommended Practice" (Task 1), to SAE for formatting, final approval, and adoption as a standard.
- Defined, refined, and validated the architectural partitioning for a ground vehicle system model (95% complete).
- Developed a proposal for the interfaces of the subsystems of a ground vehicle system (Task 2), which currently is in the review, verification, validation, and revision process.
- Developed a proposal for the content and structure of the Model Data Dictionary Interface Information file, which will enable and facilitate model reuse and exchange.

Future Achievements

- Finish defining the ground vehicle system model architectural partitioning and interfaces.
- Submit the draft of Model Architecture and Interfaces Standard, SAE J-3049.
- Establish a Model Data Dictionary Interface Information file standard to support automated model integration.
- Establish a Model Portability and Interoperability standard.

✧ ✧ ✧ ✧ ✧

VII.B.2. Technical Discussion

Background

The complexity of automotive systems (as used in passenger cars, heavy-duty trucks, military vehicles, and agricultural, mining, and construction equipment) is increasing at a rapid rate, as are competitive pressures to reduce product development cycle times. Development of these modern automotive systems requires highly coordinated collaboration between the disciplines of engineering and physics within organizations and among a network of original equipment manufacturers (OEMs), suppliers, research laboratories, and universities across the industry and around the globe.

To keep up with technology changes and competitive pressures, these global teams need virtual engineering methods to enable responsive, cost-effective, and efficient collaborative development. To make global enterprise and cross-enterprise virtual engineering methods cost effective, efficient, and robust, automotive-industry-wide standards for virtual engineering of dynamical modeling and simulation are required.

Introduction

Background

Future development of automotive systems will continue to be driven by the same forces and trends that drive it today: continual improvements in fuel efficiency, quality and reliability, emissions performance, and safety and more value to the customer at a lower cost. To minimize costs and time, automotive systems will be developed by global teams collaborating across an industry network using virtual engineering processes and methods with minimal physical builds, which will be required only to confirm designs and performance. Virtual engineering of automotive systems will require dynamical modeling and simulation that integrates models from different companies and disciplines that have varying levels of abstraction (fidelity and complexity). Such models will enable global teams to engineer and develop automotive systems rapidly, efficiently, and effectively and facilitate an integrated development process that seamlessly flows between all processes from research to production.

A committee of experts from industry, academia, and the national laboratories was formed to address these issues and requirements by developing standard recommended practices for dynamical modeling and simulation of a ground vehicle system.

Objective

The objective of the committee is to establish modeling and simulation standards to facilitate dynamic modeling and simulation of automotive systems. These standards will facilitate integrated and multidisciplinary virtual engineering processes for highly coordinated and collaborative engineering work. SAE Standards, Recommended Practices, and Information Reports (standards) will be established and published to facilitate and promote the following:

1) Cost-effective, efficient, and robust model and data sharing and reuse;
2) Seamless modeling, simulation, and analysis workflows;
3) Virtual engineering processes;
4) Interoperability in modeling and simulation tools; and
5) Portability across simulation tools.

Scope

The committee will focus on developing standards for dynamical models and simulations that mathematically describe an automotive system's time-varying response and behavior and the interactions of subsystems and components. These standards will include processes, methods, performance metrics, and analyses related to dynamic modeling and simulation of automotive systems. The goals are to make models reusable and simulation results predictable and repeatable across engineering and physics disciplines, application tools, and the automotive industry.

Benefits

The established standards will improve the overall efficiency of development processes by providing a "common language" and a means for sharing and reusing data and mathematical simulation models of dynamic systems across engineering disciplines within companies and across the industry network. Hence, these standards will facilitate virtual engineering of automotive systems, resulting in optimized performance, improved process efficiency, and reduced development time and costs for the automotive industry and individual companies. Such process enhancements will accelerate the rate of development and adoption of new technologies, thereby providing improvements in fuel economy, efficiency, and displacement.

Approach

The committee developed a charter and a work plan for developing standards to enable and facilitate model reusability. After defining its charter, the committee identified and prioritized four main standards development projects (tasks) to be developed in the following order.

1) Model Description Documentation Project
   - Define the content of documentation necessary to decide whether a model is appropriate for a given task.
   - Define model uses or applications for which the model is appropriate.
   - Define what the model does; what principles, theories, and/or equations it is based upon; and what approximations or assumptions were made.
   - Provide any verification and validation work (i.e., test data and reports).
2) Model Architecture and Interfaces Definition Project
   - Define model organizations for vehicle system and subsystems (i.e., input/output), including the location of model controls in the architecture.
   - Define conventions for naming, data types, units, and so forth.
   - Define how model parameters are set and their impact on interfaces (parameterization).
   - Define MIL, SIL, RCP, and HIL interfaces to controls models.
3) Model Data Dictionary Information Project

   Define the file format for the metadata needed to describe the fundamental information required to support import/export reuse of models between simulation models of ground vehicle systems through plug-and-play for a given simulation tool. The model information metadata include:
   - Model classification type, version, creator, fidelity, accuracy, computational workload, tool version compatibility, and other model classification characteristics; and
   - Model interfaces (inputs, outputs, and buses), variables, and parameters, including names, data types, data ranges, and meanings of interfaces, variables, and parameters.
4) Model Portability and Interoperability between Tools Project

   Define the methods, procedures, and file formats needed to support plug-and-play import/export reuse of models between software applications by means of interoperability (e.g., co-simulation or wrapped-code) or porting of models between tools with repeatable results. The methods and procedures for model portability and interoperability include:
   - Defining model simulation requirements needed to make it function in the simulation of a system with repeatable results;
   - Defining simulation details related to precision of arithmetic, integration interval, integration type (fixed or variable), required sampling interval, and required ordinary differential equation (ODE) solvers;
   - Defining task scheduling for models of control algorithms; and
   - Defining model simulation initialization processes or methods for establishing initial conditions.

The projects are designed to be developed sequentially with some overlap between them. Each project is dependent upon the projects that precede it. Hence, as one project approaches a sufficient level of maturity, the succeeding project can be ramped up. The sequentially interdependent relationship between the projects is shown in Figure VII-1, where the increasing capabilities to enable or facilitate model reusability by each project are summarized.

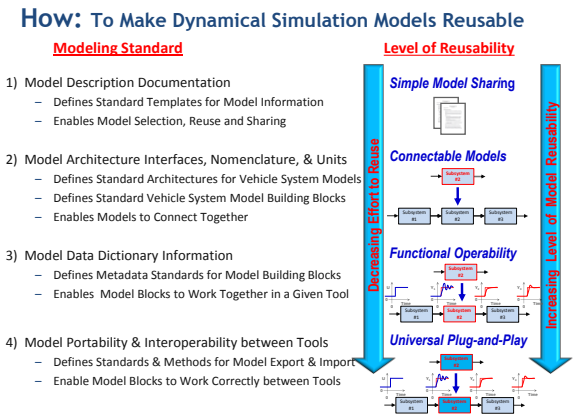

Figure VII-1: Relationship between the Four Major Projects for Enabling and Facilitating Model Reusability.

The Principal Investigator of this project is the chair of the SAE Dynamical Modeling and Simulation Technical Committee (DM&S TC). He develops proposals for each of the projects. These proposals are submitted to the committee for review, comment, revision, and refinement. As they approach maturity, the proposals are submitted to the committee for a vote to ensure that the committee is reaching a consensus. Once the proposals are approved, the materials are used to produce a draft standards document, which is then reviewed and revised by the committee. Next, the draft is submitted to the DM&S TC for an official vote. After approval, the draft is sent to SAE for final formatting before it is submitted to the Motor Vehicle Council for approval and adoption as an official SAE standard.

Results

Model Description Documentation Project

The committee completed development of a draft version of a standard for Model Description Documentation, a task that was started in fiscal year (FY) 2011. The SAE Standard J-2998 is called “Model Description Documentation Recommended Practice for Ground Vehicle System and Subsystem Simulation.” This standard defines information recommended for completely describing and documenting dynamical models of ground vehicle systems, subsystems, and components. It makes models reusable by providing a clear, concise, and complete description of their capabilities, requirements, applications, and assumptions.

Dynamical modeling, as part of enterprise-wide and/or industry-wide engineering processes, requires different types of documentation to support different engineering functions. These functions require both unique and common information about a model. In addition, to protect intellectual property, different levels of documentation are required for engineering collaboration functions internally (i.e., within a company), externally (i.e., between companies), and globally (i.e., for internal and external work across national borders).

The standard defines the information recommended as necessary to document a model for supporting model selection, compatibility, specification, management, application, development, and modification. Seven different use cases for the model description information are defined, and the information needed to support each use case is specified in the form of a template. Each template describes the information that is recommended to provide a user with sufficient data to apply the model for that use case.

Specifically, Model Description Documentation is defined for the following four general categories of work.

1) Model users and simulation analysts from different disciplines apply models for various engineering and analysis tasks. For sharing and reusing existing models, they require a high-level overview description to select an appropriate model with the capabilities, features, and performance required for their specific analysis purposes.
2) Model developers or producers (simulation modelers/developers/providers/suppliers) create new models or maintain, integrate, and modify existing models. To develop new models, they need to receive documentation that specifies the requirements for the model to provide the performance for the intended analyses. They also must create documentation so users can understand and apply the models. In addition, the users need information to maintain, enhance, and continuously improve existing models. They require more detailed information about the physical principles, equations, assumptions, and approximations used to develop the models.
3) Simulation model requestors are model users and simulation analysts who require new or improved models to perform specific engineering tasks or analysis functions for which models do not exist or are inadequate. To request new models or improved models, they must provide documentation that specifies the requirements for model performance.
4) Modeling and simulation process management requires documentation to control the introduction, update, and removal of models from model libraries available for standard engineering analyses. This documentation information ensures that the models are thoroughly tested, documented, and meet required performance measures before they are released for engineering work. To guarantee the quality of simulation results, information about model documentation, performance, verification, validation, change history, and theoretical basis are needed.

The documentation recommended to completely describe a model is captured in the following outline of major categories of information, which define all of the template section headings recommended for supporting all of the use cases:

1. Model Title (provide a name for the model)
2. High-Level Description of Model
3. Purpose/Applications/Usage
4. Features and Capabilities
5. Model Applicability and Limitations
6. External Interface Variables (or inputs and outputs)
7. Internal Variables
8. Parameters and Calibration Procedures
9. Model Architectural Structure
10. Detailed Functional Description
11. Implementation Requirements and Dependencies

12. Performance
13. Operating Instructions
14. Verification and Validation
15. Model Administrative Information

Model Architecture and Interfaces Project

The fundamental objective of this task is to establish modeling standards and conventions for the architectural structure and interfaces of dynamic ground vehicle simulation models. The project goal is to define: (1) a standard vehicle system modeling architecture, (2) standard fundamental model building blocks that can be used to define any ground vehicle system, and (3) standard interfaces for the model building blocks. Another goal is to clarify the interaction among complex systems, subsystems, and components across disciplines to facilitate interdisciplinary understanding and collaboration. This task will (1) establish a basis for model plugability and (2) define the standards required to establish fundamental model building blocks that can be reused and exchanged within and between organizations across the automotive ground vehicle industry.

The purpose and benefits of defining standards for architectural structure, interfaces, and implementation conventions for dynamical models are as follows:

1) Enable and facilitate exchange, reuse, and sharing of models across all disciplines of engineering and physics within organizations for enterprise-wide collaboration and across the industry (among OEMs, suppliers, research laboratories, government agencies, and universities) for inter-organizational collaboration;
2) Reduce or eliminate duplication of modeling work products by defining the boundaries and scope of models for subsystems;
3) Reduce the effort required to integrate models of all of the systems, subsystems, or components needed to create a functional system model for any ground vehicle system;
4) Make models of varying fidelity or abstraction rapidly connectable and functional in an overall system or subsystem model (i.e., make models “pluggable and playable”);
5) Reduce model development time and costs and improve model quality; and
6) Enable and facilitate management of large systems development projects through parallel development paths (i.e., decoupled development).

Ground Vehicle System Model Architectural Structure

The committee has developed a model of the architectural structure for a ground vehicle system. The architecture is a hierarchical structure showing the interconnection of the fundamental subsystem building blocks. The architecture and subsystem partitioning has been validated against all known or proposed alternate vehicle and propulsion configurations for automotive, trucking, military, agricultural, mining, construction, and off-road equipment applications. A ground vehicle system architecture was proposed, modified, and refined through an extensive validation process that included the following propulsion alternatives: combustion engines, electrics (battery and fuel cell), hybrids (parallel and series), hydraulic hybrids (parallel and series), and flywheel hybrids; and the following chassis alternatives: front-wheel drive, rear-wheel drive, all-wheel drive, tractor trailer, and tandem or double-bottom trailers.

The results of this validation process demonstrated that any ground vehicle system can be described by the hierarchical model architecture structure shown in Figure VII-2 through Figure VII-8. The first level of the hierarchy or top-level view of the model for a ground vehicle system consists of three major subsystems, as depicted in Figure VII-2. The three main components of the vehicle subsystem are shown in Figure VII-3. Next, Figure VII-4 and Figure VII-5 present some of the third level in the hierarchy, which defines the internal structure of the three major subsystems. In these figures, the power subsystem and the chassis subsystem models reveal the architecture of their internal subsystems. Figure VII-5 shows an example of a fourth level of the hierarchy, where the internal subsystem architecture of the trailer subsystem (an internal subsystem of the chassis subsystem) is defined. Note that the trailer subsystem also includes a trailer 2 subsystem located on the far right, which would describe a fifth-level subsystem for a tandem trailer application. Finally, an example of a trailer train is displayed in Figure VII-8, where the internal architecture of the i-th trailer in the train is shown.

The internal architecture of the power subsystem architecture is shown in Figure VII-4 as being composed of, at most, eight subsystems. The internal architecture for the chassis subsystem is defined in Figure VII-5 and composed of, at most, eight subsystems. Finally, the trailer subsystem internal architecture is defined in Figure VII-6 as being composed of six subsystems. This layered approach to organizing models in a hierarchy can continue for each of the subsystems to reveal their internal subsystem architecture until the lowest subsystem level is reached; at that level, the internal architecture of each subsystem is composed of components. Each component would be described at the lowest level of the hierarchy by a mathematical model of its dynamic behavior.

This discussion demonstrates that complete definition of a ground vehicle system hierarchical model to the equation level would require several hundred models. Therefore, the scope of the current Model Architecture and Interfaces Project is limited to defining the architecture and interfaces for the top three levels, as described in Figure VII-2 through Figure VII-6, to establish a standard for plugability of ground vehicle subsystems. After the standards for architecture and interfaces for subsystems in the first three levels are defined, the focus of the standards development activity will shift to the development of standards for playability, portability, and interoperability of these models. The development of model architecture and interface standards for other lower-level subsystems and components is beyond the scope of the current effort. The intention of the current project is to lay a foundation for model reusability through standards that establish plugability and playability of dynamic models for ground vehicle systems. This foundational methodology can be extended to lower-level subsystems and components in the future.

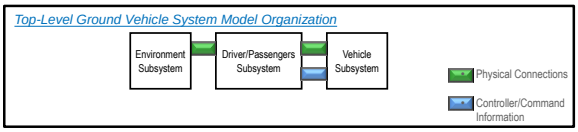

Figure VII-2: Top-Level Ground Vehicle System Model Organization.

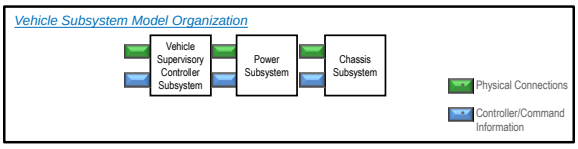

Figure VII-3: Vehicle Subsystem Model Organization.

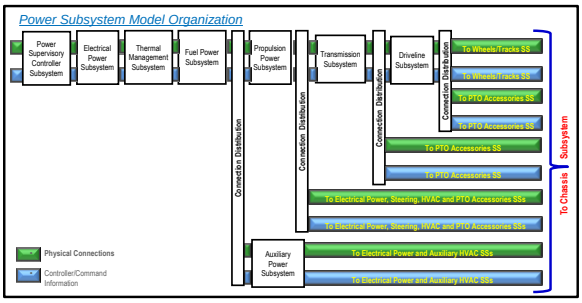

Figure VII-4: Power Subsystem Model Organization.

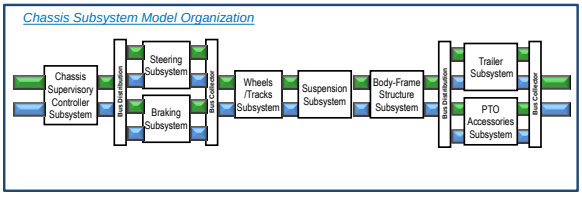

Figure VII-5: Chassis Subsystem Model Organization.

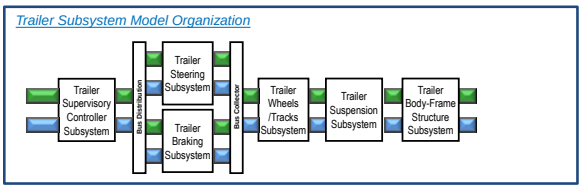

Figure VII-6: Trailer Subsystem Model Organization (for a single trailer).

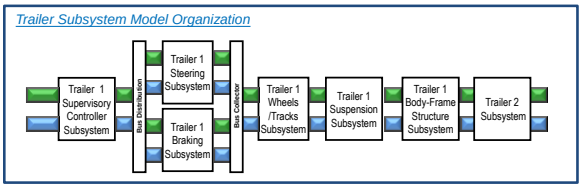

Figure VII-7: Trailer Subsystem Model Organization (for a tandem trailer).

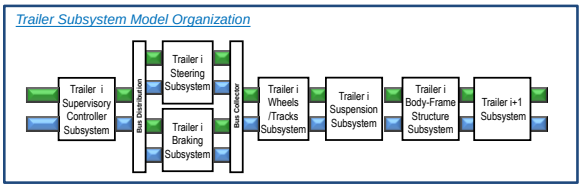

Figure VII-8: Trailer Subsystem Model Organization (for the i-th trailer of a train of trailers).

Ground Vehicle System Model Interfaces

A proposal for the interfaces of the subsystems of a ground vehicle system has been created and is in the process of review, validation, and refinement. The focus has been on identifying the types of energy or power that are transferred between the subsystems. For each subsystem in the top three layers of the ground vehicle system, a summary of its function, power production and consumption, and interfaces (that connect it to other subsystems in the ground vehicle system) has been developed and converted into a single subsystem connection diagram that shows the surrounding architecture and interfaces for each subsystem. Figure VII-9 shows an example of a summary of the function and interfaces. Figure VII-10 depicts a single subsystem connection diagram of the surrounding architecture and interfaces for the propulsion power subsystem. (For a conventional automobile, this would represent an internal combustion engine subsystem.)

A total connectivity diagram for the power, chassis, and trailer subsystems is produced by overlaying the single subsystem connection diagrams for all of their internal subsystems. The result of combining all the internal subsystems for the power subsystem, chassis subsystem, and trailer subsystem are shown, respectively, in Figure VII-11,Figure VII-12, and Figure VII-13.

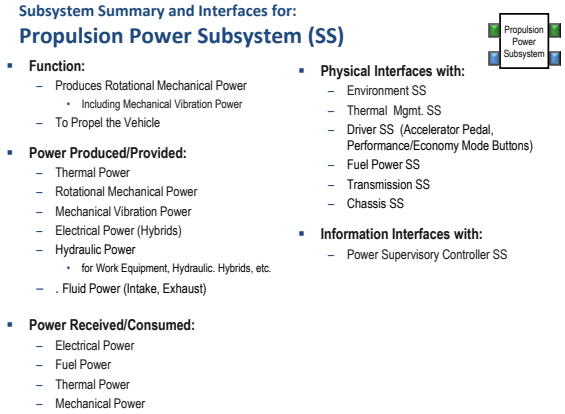

Figure VII-9: Example of a Subsystem Summary and Interface Definition for the Propulsion Power Subsystem.

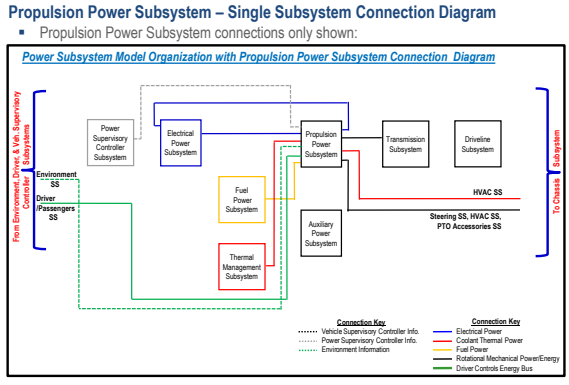

Figure VII-10: Example of a Single Subsystem Connection Diagram for the Propulsion Power Subsystem.

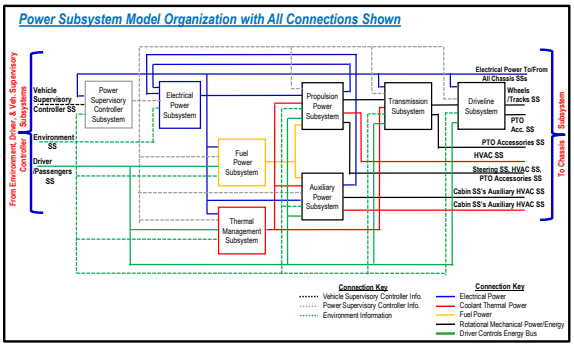

Figure VII-11: Total Connectivity Diagram for the Power Subsystem.

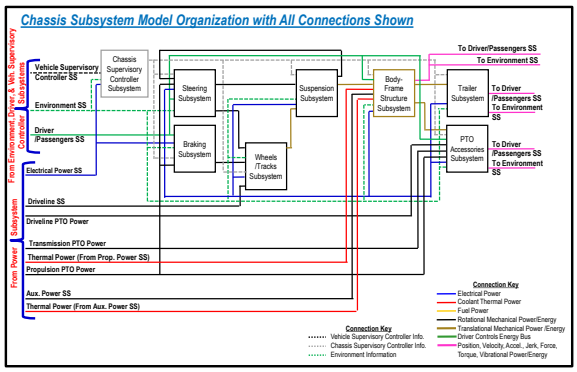

Figure VII-12: Total Connectivity Diagram for the Chassis Subsystem.

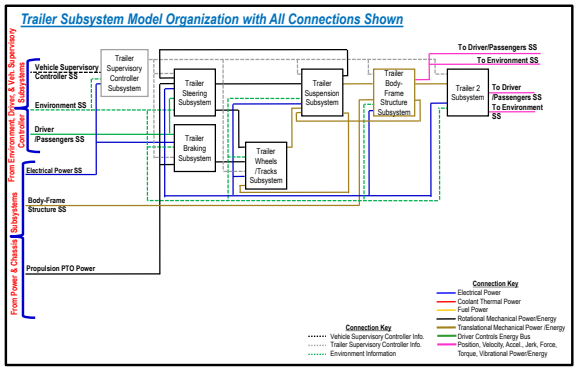

Figure VII-13: Total Connectivity Diagram for the Trailer Subsystem.

Conclusions

During this year, a draft for an SAE Standard (J-2998), called "Model Description Documentation Recommended Practice for Ground Vehicle System and Subsystem Simulation," was approved by the SAE DM&S TC. The standard was submitted to SAE for formatting. After formatting is completed, it will be submitted to the SAE Motor Vehicle Council for review, voting, and approval as an official SAE standard recommended practice.

A second major standards project (J-3049), called "Model Architecture and Interfaces Recommended Practice for Ground Vehicle System and Subsystem Dynamical Simulation," was officially initiated through a vote of the DM&S TC. For this project, the definition of the system architecture structure and model partitioning of a ground vehicle system model into subsystems is maturing and is ~95% complete. Subsystem model interfaces have been discussed, revised, and refined over the last year, but they have not been verified, validated, and finalized. The next steps will be to finish the architecture and the definitions for the interfaces of the subsystems. A draft of the standard is in process and expected to be available for a vote by June 2014.

The definition of model interfaces will lead to the third major standards project to establish a definition for the Model Data Dictionary Interface Information, which will provide playability for models in any single modeling and simulation tool, but not across tools. Initial discussions and proposals for this project have been presented the DM&S TC and are currently in the development, review, and revision process. This project will be complemented by a fourth project to establish standards for model portability and interoperability between modeling and simulation tools.

VII.B.3. Products

Publications

1. SAE J-2998—Model Description Documentation Recommended Practice for Ground Vehicle System and Subsystem Simulation (Submitted to SAE for formatting, final approval, and adoption as a standard).

VII.C. Green Racing Technical Support

P.T. Jones, Principal Investigator
Bob Larsen, Senoir Technical Lead (OboTech)
Oak Ridge National Laboratory
2360 Cherahala Boulevard
Knoxville, TN 37932
Phone: (865) 946-1472
E-mail: Jonespt@ornl.gov

Lee Slezak, DOE Program Manager
Phone: (202) 586-2335
E-mail: Lee.Slezak@ee.doe.gov

VII.C.1. Abstract

Objectives

- Incentivize vehicle manufacturers to develop, validate, and promote advanced technology relevant to production vehicles through motorsport participation.
- Increase the use of renewable fuels and petroleum alternatives in racing, and provide an avenue to introduce new fuels or bio-fuel blends.
- Increase the use of electric drive technologies in racing.
- Use racing as a platform to educate the public:
  - on the potential of renewable fuels and the concept of well-to-wheels fuel life cycle;
  - on the performance and efficiency benefits and capabilities of advanced vehicle technologies.
- Diversify the success of the Green Racing Initiative beyond American Le Mans Series (ALMS) to include other racing series with the final goal of establishing advanced transportation technologies as a foundation for all motorsports.
- Gain automotive industry support in the validation of "green racing" in the United States and internationally.
- Maintain collaborative partnership with the U.S. Environmental Protection Agency (EPA) and SAE International.
- Support Revisions to SAE J2880 Green Racing Protocols

Major Accomplishments

- All of the full season GT class cars racing with the ALMS. The Chrysler SRT Viper, returning in mid 2012, used E85 to capture its first win for the new car in 2013.
- Provided guidance to ACO with regards to regulations for 2014 announced at 2012 Le Mans, which include fuel allocations and Hybridized powertrains for LMP1 category vehicles in 2014.
- HEVs from Audi and Toyota dominated at the 24 Hours of Le Mans in 2013, taking the first five places with Audi HEVs in first, third, and fifth and Toyota HEVs in second and fourth place.
- The Audi R18 diesel HEV won the World Endurance Championship overall and in the LMP1 class.
- The Light weight, downsized engine—Elan DeltaWing raced in 8 races in the ALMS, finishing as high as second place in the LMP1 class. The new coupe version of the car debuted at Mazda Raceway Laguna Seca using a bespoke chassis for the first time. The DeltaWing is being offered to other teams to race in 2014.
- Mazda won the GRAND AM GX category using a race version of their production diesel engine in the Mazda 6. The 100% renewable synthetic diesel fuel was made available through the DOE's Green Racing program technical support.
- Dyson Racing used the Flybrid KERS at several of the longer races in 2013. Began working relationship with FlyBrid Automotive to provide basic Autonomie model of flywheel system.
- The ALMS, over the entire 2012 season on a distance-weighted basis, displaced over 39.9% of the petroleum typically used in racing with renewable fuels. GHG emissions were reduced by over 20%.
- Increased visibility for the "Clean, Fast, Effiicient" Green Challenge tagline was achieved on international television coverage and race teams and media.
- Assembled Green Racing Protocol Committee for SAE J2880 Green Racing Protocol revision and produced a precident-setting approach to encouraging Green Racing activities in the future.
- Initiated discussions with INDYCAR about becoming a Green Challenge race series in 2014; offered to supply 2nd Generation (cellulosic) ethanol in support of the series.
- Monitored development, adoption of the HySpy fuel flow meter as the FIA-approved approach to limit power and implement fuel allocations for the 2014 Forumula 1 and LMP1 category in the World Endurance Championship.
- Transported and displayed the Green Racing Simulator (E85 CORVETTE HEV race car simulator) at three ALMS races and several additional events around the country.

Future Achievements

- Obtain balloted approval of revised SAE J2880, the Green Racing Protocols, to reflect a new emphasis on electric drive technology; update definitions and life cycle analysis approaches to keep it current with evolving technology and the needs of racing.
- Work with new TUDOR United Sports Car Championship (USCC) to incorporate renewable fuels and advanced technology into racing in 2014 and beyond.
- Make advanced renewable fuel sources available to TUDOR USCC and INDYCAR for SI and CI engines.
- Work with INDYCAR as they become a Green Racing series for the first time in 2014 and help them move

towards achieving Green Challenge status and recognition from DOE, EPA, and SAE International.

- Monitor major changes moving Formula 1 and the LMP1 category towards the pinnacle of Green Racing incorporating energy allocations and fuel flow limitations in addition to greatly expanded use of energy recovery and electric drive.
- Support and incentivize the use of energy recovery technology in race cars, and identifying methods available to properly limit and/or record use of technologies to allow for performance balancing.
- Move towards a scoring system based on energy allocation, working with industry partners to develop fuel flow measurement technologies applicable in a racing vehicle.

✧ ✧ ✧ ✧ ✧

VII.C.2. Technical Discussion

Background

The Green Racing Initiative started in 2006 with a working group of industry, government and national lab representatives. The team sought to take advantage of the efforts and opportunities in motorsports to further develop advanced transportation technologies that could be applied to street vehicles. This effort focused on providing a proving ground for petroleum displacement and technology advancements in a competitive setting. Once the working group had built the foundation for GR, a set of protocols was approved through SAE and in 2008 the J2880 'Recommended Green Racing Protocols' were established.

The American Le Mans Series (ALMS) acknowledged these protocols and awarded the first Green Challenge Award in October 2008.

The Green Challenge Award and the Michelin Green X Challenge soon became an integral part of ALMS racing, where Michelin awards the teams and the DOE EPA and SAE recognizes the manufacturers who perform best when evaluated using the Green Racing formula for competition. This formula takes into account measured performance and fuel consumption to determine a total score: Clean, Fast and Efficient terms are calculated in real time for each lap for each vehicle in the Prototype and GT categories.

Introduction

The 2012 racing season ended at the beginning of FY13 and went on record to show that sustainable motorsports activities advance both technology and performance, as the acquired speeds and efficiencies of the vehicles both increased. The 2013 season has been extrememly competitive in the renewable fuel-powered GT class of the ALMS. Teams have applied new technologies and sanctioning bodies have confirmed future rules which incorporate sustainable practices and require advanced technologies for future racing vehicles. The Green Racing Initiative seeks to coordinate the strategies and guide motorsports requirements to optimize efforts within motorsports to highlight advances in transportation technologies.

Approach

Motorsports are the only professional sports that can directly help attain critical national energy and environmental objectives. The rapid developmental cycles in racing, and focused development budget on increasing the use of advanced transportation technologies, and alternative fuels, in the search for more efficienct and capable vehicles ties directly to our national transportation goals. These efforts reduce our dependence on petroleum and lower the carbon footprint of vehicles—and still provide the entertainment and drama that has made racing one of the most followed forms of sports around the world. Racing is one of the best platforms for reaching a large audience with the message that, through advanced vehicle technologies and renewable fuels, we can maintain the personal mobility and performance customers want while moving toward the energy security and sustainable transportation the country needs.

Racing brings out the best in automotive technology and places it in a demanding competitive environment allowing a technology showcase that resonates with the public. Racing also inherently values efficiency as successful teams operate in alignment with sanctioning body rules to optimize fuel use with other racing parameters, like distance between required tire changes. Efficiency and petroleum displacement are attributes that underpin our national energy and environmental objectives. Building on core values in racing and adding renewable fuels and advanced transportation technologies as ways to improve sustainability, we have developed the Green Racing Initiative with our partners.

Results

The 2013 racing season had a number of highlights in advancing transportation technologies through motorsports. Of particular interest was the domination by five hybridized racing vehicles in the world's most important sporting event, the 24 hours of Le Mans. Audi and Toyota each brought hybridized Le Mans Prototype (LMP1) vehicles to the event, with the Audi's diesel HEVs taking the pole and finishing in first, third and fith place.

Figure VII-14: Audi R18 e-tron quattro diesel HEVs won the 24 Hours of Le Mans and the World Endurance Champtionship in 2013 (photo: Audi Sport).

Toytota's ultra-capacitor SI HEVs often matched the pace of the Audis finishing in second and fourth places. The Automobile Club de l'Ouest (ACO) refined their 2014 rule package for the LMP1 premiere category vehicles expanding

the size and type of energy recovery and hybrid technologies by a factor of 4 as well as allowing a limited amount of energy (fuel) per lap depending on the level of hybrid technologies applied to each car. These ACO rules were developed to enhance efficiency and not performance in consultation with the Green Racing Initiative. The rules are remarkably open with regards to technologies allowing the factory teams to be innovative in creating and applying advanced technologies. Porsche acknowledged the importance of this new rule package by announcing they will again compete in the LMP1 category with an all-new hybrid car. This shift of motorsports to using energy allocations, rather than purely speed, as a way to structure future competition represents a substantial change in the perspective of sanctioning bodies, and places a renewed relevance in the sport, as energy efficiency is something the manufacturers deal with in every vehicle they produce.

The Green Racing Initiative has become an integral part of the ALMS which maintains its claim as the global leader in green racing. The 2013 season continued the growth and acceptance of green racing activities in the series. The ALMS continues to search for opportunities to support alternatives to petroleum and renewed its interest in allowing LNG to race during the season.

Figure VII-15: DeltaWing Coupe debuts in 2013 (photo: deltawingracing.com).

The experimental DeltaWing from the 2012 Le Mans race returned in production form in the ALMS in 2013. Initially using the same chassis from Le Mans, the car sported a new engine that was moving towards extensive use of light weight materials. Half way through the season, a completely new chassis made its debut in coupe form to comply with sporting regulations. The DeltaWing led the Orion Energy Systems 245 race and consistently placed third in the LMP1 class in 2013. The coupe, produced by Elan in Georgia, will be offered for sale to other teams in 2014. It retains its ability to race in the USCC despite being orginally designed as a LMP1 car. It remains a fan favorite due to its innovative, light weight design and tiny front wheels.

The 2013 ALMS season continued to offer alternative fuels for use by its competing teams. Every Green Challenge victory in the GT category was won by a car using advanced fuels. The LMP category was dominated by Honda-sourced vehicles using E10, but the FlyBrid KERS-Isobutanol Turbocharged 4 cylinder Mazda raced by Dyson Racing finished second overall in P1 points.

Figure VII-16: Flybrid system employed in #16 Dyson/Mazda (photo by Eric Gilbert Motorsport.com).

"Without being able to race our hybrid systems in motorsport we would be much further behind in the technical development for our road car and bus hybrid systems," said Tobias Knichel FlyBrid Commercial Manager and Racing Engineer. "The ALMS is the leader in green racing and the perfect series to showcase this technology," added Chris Dyson team owner.

In the GT, E85R dominated as the fuel of choice in this ultra-competitive category. All the top three finishers in all the races used E85R fuel. The GT class is based on cars that are on the road today and puts rival teams in door-to-door competition that may be the most competitive class in racing anywhere in the world. All the BMW, Corvette, Ferrari, and Porsche factory and most of the privately entered cars used this renewable fuel with great success. The wholesale movement to E85R was primarily motivated by the performance potential of this excellent fuel, but the message with respects to its upstream impact and its energy security and environmental advantages have provided an excellent outreach opportunity for DOE goals. The Green Challenge scoring system accurately reflects each fuel's characteristics in terms of its greenhouse gas and oil replacement attributes without rewarding a team's selection of bio-fuels over conventional fuels. That makes this switch to renewable fuels at this level of motorsports all the more impressive and significant.

For the entire 2013 season and taking into account the total number of miles raced, 39.9% of the oil that would have been used before the Green Racing Initiative was begun was replaced by renewable and non-petroleum fuels in the ALMS. This noteworthy accomplishment demonstrates that these fuels are capable of outstanding performance, reliability, and capable of widespread use in street vehicles.

This year brought more visibility for DOE's involvement in the ALMS Green Challenge awards through a concerted effort of DOE, ORNL, and EPA staff in cooperation with ALMS media relations representatives. More television and radio time was devoted to Green Challenge scoring and explanations.

Figure VII-17: Green Challenge Awards were given in all ten ALMS races in 2013 (photo: alms.com).

In the final season of the GRAND-AM series, the new GX class for alternative fuels and advanced technology race cars produced a new manufacturer champion—Mazda and their diesel-powered Mazda 6 race car. This remarkable triumph for a production-based diesel engine was highlighted by its use of 100% synthetic renewable diesel fuel made from waste vegitable oil thanks to the Green Racing program. Its high cetane, zero sulfur content allowed impressive power density and virtually no PM emissions. This engine and fuel will play significant roles in the new TUDOR USCC next season.

Figure VII-18: Mazda Skyactiv-Diesel production-based race engine captured GRAND AM GX Championship using 100% renewable synthetic diesel fuel (photo by mazdamotorsports.com).

The close of FY13 brought the final races for the two rival sports car racing series in the U.S. The long-anticipated merger of GRAND-AM and the ALMS in 2014 to form the TUDOR USCC has opened up new opportunities for GR and also presented obsticales as the overlap of cars from the two series will take time to integrate into a common racing series. TUDOR USCC President Scott Atherton is committed to GR and the adoption of the Green Racing Protocols in the new unified series.

Figure VII-19: Fans and professional racing drivers alike try their hand at the GRS. Tommy Milner of Corvette Racing puts the simulated E85/Hybrid Corvette to the test.

Following on the success of the last years Green Racing Simulator (GRS), the mobile outreach simulator was deployed again this season for the Green Racing program. The GRS, developed by Argonne National Laboratory, incorporates a program that calculates the amount of regenerative braking energy captured and fuel used during two laps of simulated racing. This simulator was set up at two ALMS races in 2013, as well as other events. It served as a notable means of disseminating the DOE Green Racing's key message that the use of renewable fuels and hybrids can displace a substantial amount of imported petroleum.

Conclusions

Motorsports in FY 2013 reacted positively from efforts and developments in the Green Racing Initiative. Significant petroleum reduction was recorded by the ALMS in 2013 with nearly 40% displacement of petroleum when compared to a baseline of the 2005 series. All vehicles in GT class are running on E85 racing fuel, and the SRT Viper returned to victory lane in the ALMS GT series running on E85. GRAND-AM, sports car series owned by NASCAR crowned the first GX champion manufacturer that used a diesel engine and all renewable fuel, and the merger of ALMS and GRAND-AM into the USCC is ripe with opportunities to expand the recognition of Green Racing and sustainable transportation developments through motorsports.

Important accomplishments in incorporating energy recovery into world class sports car racing were showcased multiple times during the year. Two of the most significant events being the Audi Diesel HEV victory at the 24 hours of Le Mans with theToyota HEV also on the podium and conversion of the entire field of the ALMS GT class to E85 renewable fuel. Openning the door to Green Racing in the INDYCAR series marks the first serious inroads to adoption of the Green Racing Protocols by another major racing series.

The relationship between DOE and partners at EPA and SAE International is strong and there are many opportunities for building acceptance of Green Racing principles as the working group moves forward with the revisions to the Green Racing Protocol. The Green Racing Initiative continues to impact the future of motorsports in alignment with DOE's transportation goals.

VII.C.3. Products

Tools and Data

Cooperative development of systems and performance information is provided by partners and contacts made through the Green Racing Innitiative.

During FY13, proprietary data and opportunities to be included in test/development were made available to the GRWG representatives. As these are projects in process reports will be generated in FY14.

1. SAE J2880 Green Racing Protocol revision.
2. HySpy fuel flow measuring systems ability to enable enforcement of energy allocation regulations.
3. Mazda SkyActiv-D engine PM data will be utilized for BioDiesel fuel selection for 2014 racing season and beyond.
4. Dyson Racing/Flybrid racing data used to support component model creation.

VII.D. Grid Connectivity Support

Jason Harper, Principal Investigator
Argonne National Laboratory
9700 South Cass Avenue
Argonne, IL 60439
Phone: (630) 252-1032
E-mail: jharper@anl.gov

Lee Slezak, DOE Program Manager
Phone: (202) 586-2335
E-mail: Lee.Slezak@ee.doe.gov

VII.D.1. Abstract

Objectives

- Support the DOE Vehicle Systems Simulation and Testing (VSST) Program as the technical lead for technology and standards development/verification related to grid connectivity with electric and plug-in hybrid electric vehicles (EVs).
- Co-chair the U.S. DRIVE partnership's Grid Interaction Technical Team (GITT).
- Identify gaps in technology and recommend enabling solutions through the creation of proof-of-concept hardware/software and validation of proposed approaches.
- Establish the technical capability to support an international EV-Smart Grid Interoperability Center at Argonne National Laboratory.

Major Accomplishments

- Contributed to the SAE standardization process by providing laboratory test data and analysis to support fact-based deliberations in the SAE committees related to EV-grid communication (SAE J2836, J2847, J2953, and J2931).
- Created hardware/software to construct an interoperability test fixture designed to measure, record, and validate the analog interaction between EVs and AC electric vehicle supply equipment (EVSEs). The validation of this test setup and procedures supports the creation of the SAE J2953/2 interoperability test procedure standard.
- Created new technology to serve as a communications controller platform to fill an identified gap to support the standardization of SAE J2847/2 as applied to DC charging. This Argonne-licensed technology has been named the SmartGrid EV Communication (SpEC) module. The SpEC module has been adopted by one DC EVSE manufacturer and has the interest of two automotive original equipment manufacturers (OEMs).
- Argonne completed the design and fabrication of a prototype 3-axis test fixture for evaluating the performance of wireless EV charging systems. The validation of this test setup and procedures will guide the creation of the SAE J2954 interoperability test procedure standard.
- Demonstrated EV-to-EVSE-to-grid communication (SAE J1772, J2847, J2931, and J2953). A grid demand response scenario was demonstrated with actual EVs and EVSEs for the U.S.-EU participants at the July 18, 2013, launch event of the EV-Smart Grid Interoperability Center.

Future Achievements

- Maintain focus on near-term needs with long-term impact by providing direct support of SAE standards committees and global cooperation/harmonization for the following initiatives:
  - Interoperability: Define laboratory test procedures for AC EVSE interoperability, verify with production-intent vehicles and EVSEs, and provide input for the SAE J2953 standards publication.
  - Interoperability: Define the testing approach and procedures to validate DC charging interoperability. Demonstrate compliance with OEM-provided vehicles and DC EVSE units.
  - Communication: Create the technology to enable DC Level 1 charging and EV-to-EVSE-to-network-to-smart grid communication.
  - Enabling technologies: Fabricate and distribute limited copies of the EV-EVSE DC communication controller hardware (SpEC) to license partners for joint testing/evaluation and harmonization.
  - Wireless EVSE test procedures and interoperability: Utilize the new wireless charging test fixture to evaluate samples of wireless power transfer (WPT) units to support the SAE J2954 committee's deliberations, and write the associated standards and test procedures governing this equipment.
  - Communication: Create the hardware/software technology to enable reverse power flow communication from EV-to-smart grid.

✧ ✧ ✧ ✧ ✧

VII.D.2. Technical Discussion

Background

Meeting the Obama Administration's goal of having one million EVs on the road in the United States by 2015 requires finalizing specifications for components and interfaces as soon as possible, thereby obviating the need for ratified standards. Otherwise, suppliers and OEMs will be assuming the risks of fielding 'nonstandard' products. Hence, a common objective of suppliers, OEMs, DOE, and the national laboratories is to support the Society of Automotive

Engineers (SAE) committees as they define, refine, and verify the standards that are focused on EVs. (Refer to the report on task 1000201.00, "Codes and Standards Support for Vehicle Electrification," for a detailed description of all the EV-related Codes and Standards under SAE development.)

The EV-grid interface has been defined, from a standards perspective, in terms of the charge coupler (the physical connector for power and communication, messaging, and protocols), the EVSE (charging technology and power quality), and interoperability (EV-EVSE compatibility, communication, and security) (Figure VII-20). Steady progress has been made in these standards in FY 2013, with substantial technical support contributions provided by Argonne.

Figure VII-20: Scope of EV-Grid Connectivity from a Standards Perspective.

Introduction

Argonne is the technical lead for technology development and/or standards verification related to EV-grid connectivity and co-chair of the GITT, whose objective is to support a transition scenario to large-scale grid-connected vehicle charging. The scope of the GITT is connectivity between light-duty EVs, the charging infrastructure, and the electric power grid. Argonne's activities are aligned with the GITT, with substantial effort in refining and verifying EV-grid standards in direct support of the SAE committees related to the charge coupler, EVSE, and interoperability.

Refinement and verification of standards requires hardware and software for testing and evaluation. Because components are not readily available for EV-grid connectivity, Argonne utilized its embedded controls/network laboratory and leveraged support contractors to develop components to fill the gaps, thus enabling lab testing and quantitative data to be provided to the SAE committees.

Approach

1. Interoperability Test Equipment Development to Support J2953 Interoperability Test Procedures

Validation of EV and AC EVSE Interoperability

SAE J2953 defines interoperability between a plug-in electric vehicle (PEV) and its EVSE. Interoperability testing is conducted using a specific PEV–EVSE pair. In order to conduct non-evasive testing, SAE J2953 procedures require the use of a breakout fixture capable of monitoring and reporting on all PEV and EVSE circuits. Argonne addressed the need for creating a bench-top test system to validate and support the standardization of AC vehicle charging interoperability for the purpose of standard test procedure development.

Figure VII-21 shows a generic interoperability test setup. With this setup, a test operator can readily measure the status of a charge system's control pilot circuit, proximity circuit, and charge circuit. Since the breakout fixture is designed to connect to existing EVSE and PEV equipment, it does not require any modification to the PEV and EVSE hardware.

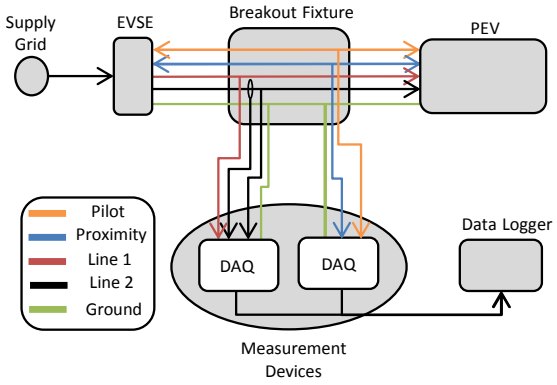

Figure VII-21: SAE J2953/2 Test Procedures for PEV Interoperability with Non-evasive EVSE Test Setup.

Argonne's interoperability test fixture (Figure VII-22) is designed to validate J2953/2 test setup and procedures. The core of the fixture is a pass-through box that is equipped with a J1772 charge inlet and charge connector. The pass-through box contains National Instruments (NI) cRIO-9081 FPGA real-time controller with current and voltage measurement modules; NI 9221 8-channel ± 60-V 12-bit Analog Input module; NI 9225 3-channel 300-Vrms 24-bit Analog Input module; and NI 9227 4-channel ±5A 24-bit Analog Input module. The cRIO FPGA is programmed to collect the data from the modules at 200 MHz and to serve the measurement data to an Ethernet-networked PC running LabView software. A similarly networked Agilent oscilloscope monitors the oscillating control pilot circuit and serves data on frequency, duty cycle, and rise/fall times to the LabView-loaded PC.

The PC contains programmed LabView virtual instrument software that collects, analyzes, and creates reports based on the SAE J2953/2 procedure. The software is networked to the previously mentioned data acquisition devices, and it gathers and stores the data into an easily readable file. During the test session, the software graphs the various data vs. time. Once a test session is completed, the software automatically post-processes all of the data in accordance with J2953/1 circuit and timing requirements. The software creates and saves two separate reports that outline the requirements and pass/fail results of the test session. The design plans of the subject test fixture, built and programmed by Argonne, will be published along with the final test procedure steps in the SAE J2953/2 document when finalized by the standards committee.

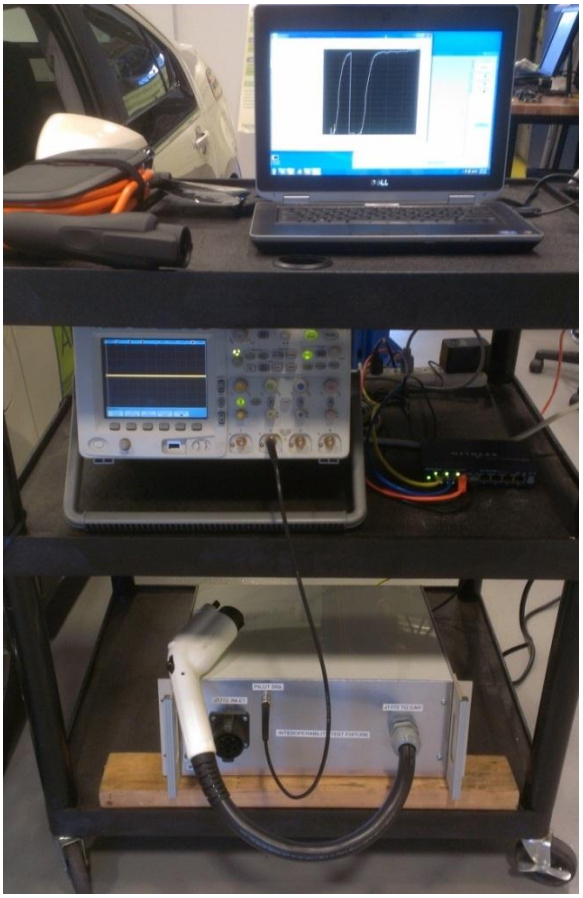

Figure VII-22: Argonne Interoperability Test Fixture (The test fixture is designed to test an EV charging system to the interoperability requirements of SAE J2953/1, in accordance with the test procedures of SAE J2953/2.).

2. SmartGrid EV Communication Module

Through previous FY 2012 funded efforts, Argonne provided invaluable power line communication test results and technical support to the SAE J2931 committee. These results helped to solidify HomePlug Green PHY (HPGP) as the standardized physical layer communication technology for PEV-EVSE communication. Our focus of effort then turned to harmonizing and establishing a standardized DC charging communication protocol. Argonne identified a technology gap that needed to be addressed to validate and support the standardization of SAE DC charging. This need led to the design of a communication controller platform, termed the SpEC module.

Figure VII-23 shows the SpEC module platform. The SpEC module utilizes the Qualcomm Atheros QCA7000 single-chip HPGP implementation to communicate via broadband power line communication (PLC) over the control pilot. An Arm9 Freescale i.MX287 32-bit, 454-MHz microprocessor is utilized as the central processing unit of the SpEC modules. The SpEC modules are designed to be able to communicate with an array of peripheral I/O via Ethernet, USB, RS-232, SPI, and CAN, thus allowing the ability to utilize this hardware platform for other tasks involving PEV to EVSE communication applications.

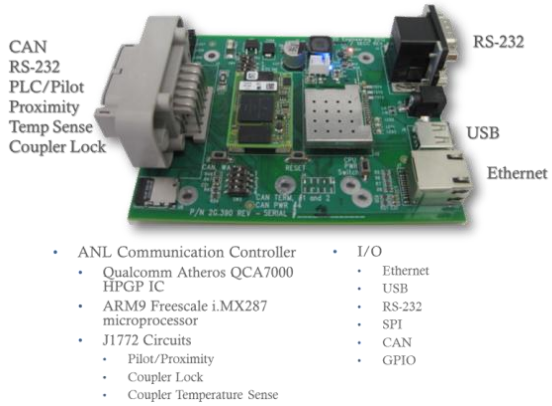

Figure VII-23: SpEC Module Platform (Argonne's technology is integrated into DC chargers or EVs in order to accomplish DC charging. The hardware itself enables PLC over the J1772 control pilot. The software implements the SAE DC charging communication protocols.).

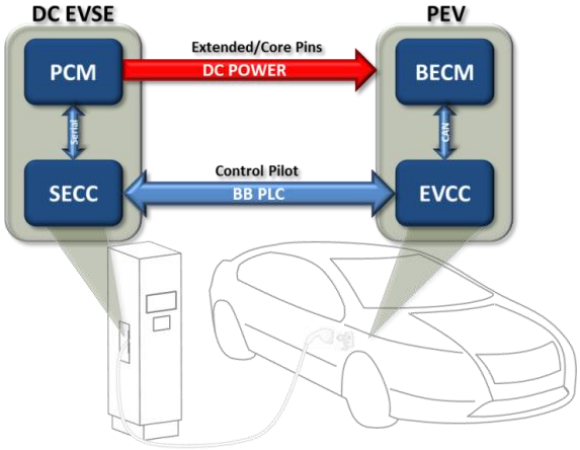

Figure VII-24: SAE DC Charging Block Diagram [1].

A typical SAE DC charging block diagram is shown in Figure VII-24. The SpEC modules were utilized to create a DC charging debug and test platform that uses an AeroVironment ABC-170CE power processing system to emulate the system shown in Figure VII-25 [1]. The ABC-170CE is a 125-kW programmable, bi-directional, dual channel power processing system. One channel of the ABC-170CE was used to emulate an SAE DC off-board charger, and the other channel was used to emulate an SAE DC PEV RESS. Both channels can be monitored/controlled via a CAN bus. This platform, along with the software developed to emulate both a DC charger communication controller and PEV communication controller, will aid in future standards development and interoperability work. In addition to DC charging, the SpEC Module can be utilized to accomplish smart grid communication as well as wireless charging communication. These areas will be explored in FY 2014.

Figure VII-25: SAE DC Charging Test System Utilizing ABC-170.

To facilitate EV communication standards harmonization and to aid OEMs in their development of PLC-based EV/EVSE communication controllers, a set of 31 SpEC modules were manufactured for distribution to collaborative entities. Figure VII-26 shows a photo of the 31 SpEC modules ready to be shipped to partners. Industry feedback about the hardware and software implementation has been encouraging. Through Argonne's Technology Development and Commercialization office, the SpEC module technology has been successfully licensed to Broadband TelCom Power, Inc., to enable SAE DC charging on their 50-kW charging stations.

Figure VII-26: Photo of 31 SpEC Modules Ready for Shipment.

3. Wireless EV Charging System Test Fixture to Support Wireless EVSE Communication Development

Figure VII-27 displays the automated fixture constructed to test wireless charging systems or their components. This aparatus will assist in the development of methods for wireless EVSEs to communicate operational details to the smart grid to address requirements under SAE J2847/6. More detail on the wireless charger test fixture can be found in the annual report no.1000270.00, titled **"Wireless Charging Unit Evaluation & Communications Implementation."**

Figure VII-27: Argonne Wireless Charging System Test Fixture.

Results

Argonne contributed substantially to resolving the technical challenges of EV-grid connectivity this year:

- Contributed to the SAE standardization process by providing laboratory test data and analysis to support fact-based deliberations in the SAE committees related to EV-grid communication (SAE J2836, J2847, J2953, and J2931).
- Provided design and development of proof-of-concept EV-grid communication systems, identified the need for enabling technologies, supported fact-based deliberations in committee deliberations, and provided insight into the scope of assessing interoperability.
- Created new technology to serve as a communications controller platform to fill an identified gap to support the standardization of SAE J2847/2 as applied to DC charging. This Argonne-licensed technology is named the SmartGrid EV Communication (SpEC) module. The SpEC module has been adopted by one DC EVSE manufacturer and has the interest of two automotive OEMs.
- Demonstrated EV-to-EVSE-to-grid communication (SAE J1772, J2847, J2931, and J2953). A grid demand response scenario was demonstrated with actual EVs and EVSEs for the U.S.-EU event participants at the July 18, 2013, launch of the EV-Smart Grid Interoperability Center.
- Created hardware/software to construct an interoperability test fixture designed to measure, record, and validate the analog interaction between EVs and AC EVSEs. The validation of this test setup and procedures supports the creation of the SAE J2953/2 interoperability test procedure standard.
- Defined test requirements for wireless EVSEs and designed and fabricated a prototype test fixture for evaluating the performance of wireless EV charging systems. The validation of this test setup and procedures will guide the creation of the SAE J2954 standard test procedure and facilitate SAE J2847/6: Wireless Charging Communication between Plug-in Electric Vehicles and the Utility Grid.

Conclusions

Argonne's grid connectivity activity directly addresses the technology gaps in the EV-grid interface and provides quantitative evaluations to support the SAE committees. These efforts contributed to a better understanding of the issues associated with EV-grid connectivity and the potential benefits of global harmonization.

Argonne and support contractors successfully demonstrated joint development of rapid prototypes from a commercial perspective (e.g., SpEC communication modules), thereby assuring relevance and mutual benefit to DOE and industry.

Focusing on near-term needs with long-term impact has been an effective approach for the grid connectivity activity. Interoperability between EVs, EVSEs, and the grid is a pressing near-term issue, which necessitates the development and verification of SAE J2953 (interoperability) standards as soon as possible. The EV-Smart Grid Interoperability Center is specifically designed to address the associated issues.

Argonne will continue to provide direct support to the SAE standardization process. This endeavor will include committee participation, development of enabling technologies, system integration, and laboratory testing.

VII.D.3. Products

Publications

1. Dobrzynski, D., "Development and Implementation of SAE J2953 for AC Charging," SAE Technical Paper 14-AE-0125, to be presented at the SAE 2014 World Congress and Exhibition.
2. Harper, J., "Development and Implementation of SAE DC Charging Digital Communication for Plug-in Electric Vehicle DC Charging," SAE Technical Paper 2013-01-1188, 2013, doi:10.4271/2013-01-1188.

Patents

1. SpEC Module Invention Numbers ANL-PB-13-068 and ANL-SF-13-030

References

1. Harper, J., "Development and Implementation of SAE DC Charging Digital Communication for Plug-in Electric Vehicle DC Charging," SAE Technical Paper 2013-01-1188, 2013, doi:10.4271/2013-01-1188.

VII.E. HEV, PHEV, EV Test Standard Development and Validation

Michael Duoba, Principal Investigator
Argonne National Laboratory
9700 South Cass Avenue
Argonne, IL 60439
Phone: (630) 252-6398
E-mail: mduoba@anl.gov

Lee Slezak, DOE Program Manager
Phone: (202) 586-2335
E-mail: Lee.Slezak@ee.doe.gov

VII.E.1. Abstract

Objectives

- Using newly available original equipment manufacturer (OEM) production vehicles, validate the SAE International test procedure standard for advanced vehicles (this includes battery electric vehicles [BEV] and plug-in hybrid electric vehicles [PHEV]).
- Provide data, input, and guidance by serving as a member of three SAE committees:
    1. Hybrid Technical Standards Committee
    2. Light-Duty Vehicle Performance Committee
    3. Economy Measures Committee
- Start new SAE task force entitled, "Hybrid Electric Powertrain Power Test Methods and Definitions."

Major Accomplishments

- Tested new Ford Focus BEV according to expanded SAE J1634 "short-cut" method by measuring consumption and range for the urban dynamometer driving schedule (UDDS), highway fuel economy driving schedule (HFEDS), and Supplemental Federal Test Procedure (SFTP) US06 cycles.
- Tested Chevy Volt, Prius plug-in hybrid vehicle (PHV), and Ford C-max Energi PHEVs according to SAE J1711; validated various aspects of the methodology; and recommended which J1711 options are best for future PHEV testing.
- Conceived of and began a new task force that will develop a standard method for defining total powertrain power for all types of hybrid electric vehicles (HEVs).

Future Achievements

- Finish developing and ballot the HEV powertrain power standard (SAE J2908).
- Support road load determination procedures with new coast-down testing methods for advanced vehicles.

✧ ✧ ✧ ✧ ✧

VII.E.2. Technical Discussion

Background

The SAE has been involved in standards development for almost 100 years. Vehicle technology is undergoing many radical changes. The U.S. Department of Energy (DOE) is investing in many new technologies, with the goal of providing pathways to achieve our current objectives of reducing petroleum usage in the transportation sector. A new technology's capability to increase efficiency and lower environmental impact can only be found by using appropriate laboratory tests. To ensure that these new technologies are properly and accurately evaluated, Argonne National Laboratory has been developing new, robust analytical testing techniques for close to two decades that match the unique characteristics of advanced vehicles (such as HEVs, BEVs, PHEVs, and others). This expertise has provided leadership and guidance for SAE committees that are involved in many vehicle testing areas.

In 2006, Argonne staff was recognized by industry to be the best choice to chair the HEV/PHEV test procedure (SAE J1711). Argonne staff, acting as objective arbiters who are impartial to specific technologies, used state-of-the-art testing facilities to help guide testing practices, especially for new and quickly advancing vehicle technologies.

Introduction

SAE J1711 "*Recommended Practice for Measuring the Exhaust Emissions and Fuel Economy of Hybrid-Electric Vehicles including Plug-in Hybrid Electric Vehicles*" was finished in 2010; however, Argonne was not able to validate the procedure with OEM hardware until the Chevy Volt was available for testing. Since then, Argonne has been able to leverage the Advanced Vehicle Testing and Evaluation (AVTE) program to receive several OEM plug-in vehicles and test them according to the newly developed procedures.

Argonne also serves on several other SAE committees that relate to testing of advanced vehicles. For example, SAE J2951 defines dynamometer driver quality metrics that help explain variations in results. Argonne has developed metrics for J2951, specifically for hybrid vehicles, and supplied openly available data to the committee OEMs and the U.S. Environmental Protection Agency (EPA) are restricted in their abilities to share sensitive test results. Another example of an advanced vehicle testing standard is the new SAE J2908 committee, which will define hybrid powertrain power for any HEV/PHEV without ambiguity or opportunity for OEMs to find ways to "one-up" their competition by creative interpretation of undefined terminology.

Approach

Validating SAE J1711

During the development of SAE J1711 (HEV and PHEV dyno test procedure), the number of sample PHEVs for running through the new testing concepts was very limited. We did not have any production-quality PHEVs to test, and we were not going to have any until procedures were in place and their development was complete. Argonne and others were limited to after-market PHEV conversions and internal prototype test platforms. In 2010/2011, the Chevy Volt was available, and in FY 2012, this vehicle was tested successfully according to J1711 procedures. Now in 2013, there are several production PHEVs available, notably those that do not have full electric capability and must blend the engine and electric motor during high-demand instances while being driven in the charge-depleting mode.

To have confidence that J1711 has been fully validated, the hope is to be able to test vehicles across the PHEV design space (as depicted in Figure VII-28). The Chevy Volt with full electric vehicle capability is at one end of the design space. The PHEV Prius converted by the company Hymotion is shown near the other end. In FY 2013, the design space between these two extremes was explored by testing a production Toyota Prius PHV and a Ford C-max Energi PHEV.

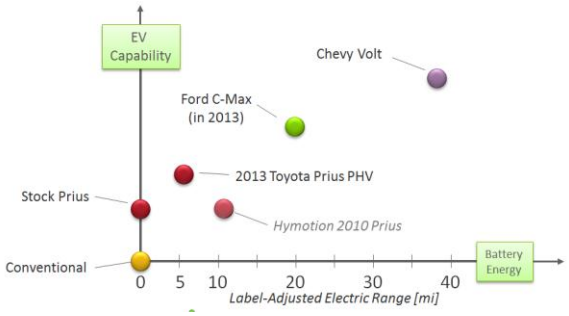

Figure VII-28: Testing J1711 for PHEVs in the Design Space.

Validating and Improving SAE J1634

Leveraging the Level 2 testing of the Ford Focus BEV, further investigations of the J1634 Multi-cycle Test (MCT) were performed. The conventional MCT consists of multiple UDDS (a.k.a. the urban cycle) and HFEDS (a.k.a. highway cycle) cycles across the entire battery state of charge (SOC). It was estimated that the range of this vehicle is sufficient to run a longer MCT that included UDDS, HFEDS, and the US06 cycles.

An important aspect of all dynamometer testing is the critical step of breaking in the vehicle to test it for stable conditions. Current testing protocols dictate conventional vehicles are given 4000 miles to establish stable conditions for fuel consumption and emissions. What about an electric vehicle? There is currently no guidance in J1634 or in the federal register for recommended mileage accumulation. Emissions are not at issue, but battery capacity and consumption need to be at stable conditions for representative and repeatable results. The obvious difficulty with electric vehicle mileage accumulation is the limits to daily mileage accumulation. After every 100 miles of driving, the accumulation must halt for many hours to recharge the batteries. Steps must be taken to find the accumulation distance that is appropriate for an EV. If it is too long, an unnecessary expense must be taken for each test vehicle and if it is too short, there may be issues with data stability.

The Ford Focus BEV test car was purchased with less than 200 miles on the odometer. The approach was to periodically test the vehicle according to J1634 with mileage accumulation in between. For added control of parameters, the mileage accumulation was conducted on the dynamometer in the form of repeated days of about 81 miles of HFEDS cycles that were run back to back. Over several weeks of testing with a robot driver, small changes in efficiency and battery capacity were observed.

Finishing Second Version of J2951

The SAE J-doc J2951 is a list of calculations that are performed to the 10-Hz speed data for any chassis dynamometer test. The desired speed schedule is compared to the driven speeds to find specific aspects of variance. For example, if the total work energy driven per distance of the vehicle (calculated by using test weight and the road load curve) is significantly higher than that of another test with a lower cycle energy, then we would expect this test to consume more fuel. Or, if the number of transient inflections is higher in a test, then this could translate to more engine starts in an HEV and, thus, higher fuel consumption. The task this fiscal year was to update the J-doc with added guidance in the form of statistical limits of the amount of variance that could be expected for each parameter on the basis of many inputs from many labs. Argonne was the only lab to provide all the results without normalization; thus, the values could be examined by everyone without obfuscation.

Founding and Chairing SAE J2908

As the number of HEV models has increased, and manufacturers are now competing in a marketplace of new vehicles with highly complex powertrains. Comparisons among vehicles in terms of power ratings are not always reported according to the same definition. There are currently very strict standards for reporting engine power in conventional vehicles. Certainly, engine power alone cannot be used for HEV comparisons, since electric-assist is an integral function of the HEV powertrain performance.

In many cases, individual component ratings can be very misleading in terms of defining and comparing a vehicle's total powertrain power. Argonne has taken the lead in assembling a new task force to address these concerns and provide the industry standard definitions and test procedures that address these undefined measures. As this is a new effort, the approach this fiscal year was to get a solid start to the project. This included recruiting and assembling a task force and organizing several meetings to define the scope and task force approach. Plans for next year include prototyping and testing dynamometer and on-road power determination methods—as such, no results are available this year.

Results

The Prius PHV was tested according to J1711, and the unique parameters for PHEVs were calculated for various standard test cycles. An internal tool is commonly employed to plot data and calculate J1711 parameters from all the tests that are conducted for a given cycle. The J1711 results for the UDDS cycle are shown in Figure VII-29. The fact that the vehicle exhibits both EV and blended behavior on the UDDS cycles in charge-depleting mode challenged the robustness of the J1711 methods. Our conclusions are that J1711 methods performed flawlessly, as intended. There were no issues with uncertain or ambiguous applications of the test procedures or anomalies in the set of results for any of the vehicles that were tested.

At the very end of FY 2013, the Ford C-max Energi test program started (results shown in Figure VII-30). These preliminary tests are validating J1711, including challenging components like the "End of Test Criterion," for example.

Both the Prius PHV and the Ford C-max Energi PHEVs were adapted from conventional charge-sustaining HEV products. The most notable difference between the vehicles is the larger battery capacity and power level in the C-max Energi. The C-max was able to run 3 full UDDS cycles before the engine was engaged for charge-sustaining operation. The Prius PHV, however, needed the engine to drive on the high-power portion of the 2nd UDDS cycle—before the usable battery was consumed. The Prius PHV exhibits EREV and blended operation in the UDDS full charge test (FCT). Early PHEV test procedure concepts would have had trouble managing the data from such a result. Again, the final J1711 methods and equations worked well in the cases of both of the PHEVs that were tested.

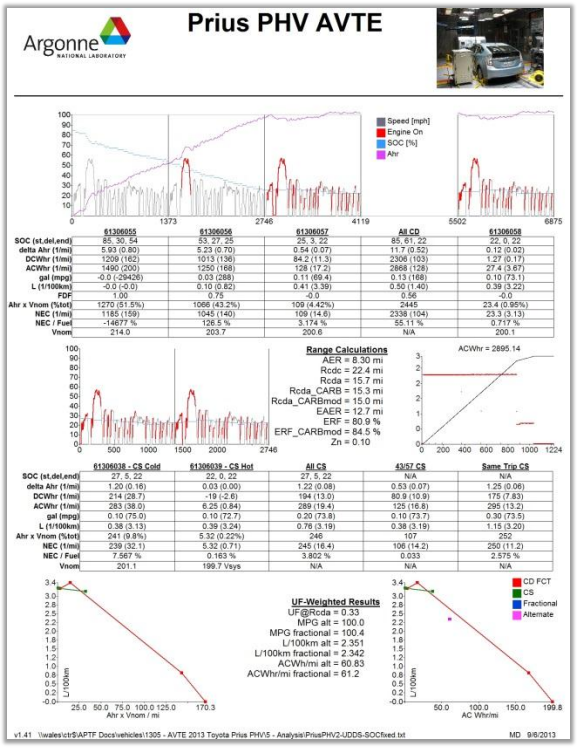

Figure VII-29: J1711 One-Pager Tool Output for Prius PHV.

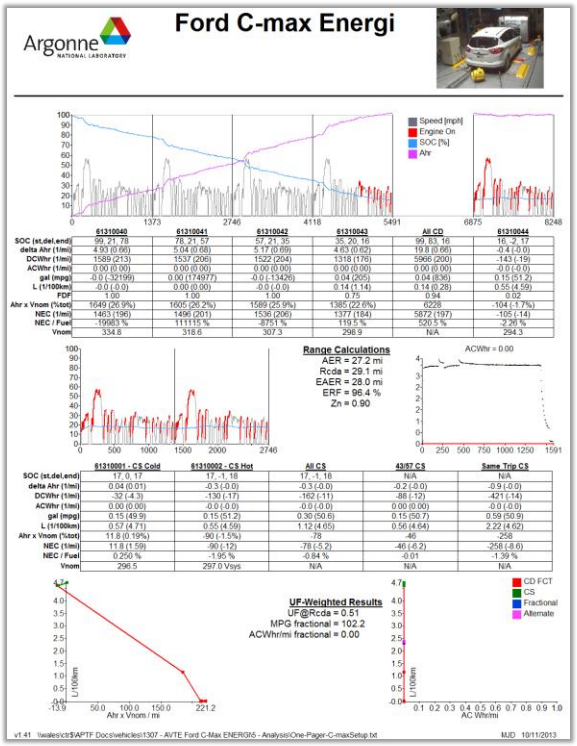

Figure VII-30: Output from a J1711 One-Pager Tool for the UDDS Cycle.

J1634 Testing and Validation Results

Validating the Expanded MCT

The Ford Focus Electric vehicle was tested according to the J1634 optional expanded MCT. The test sequence is shown in Figure VII-31.

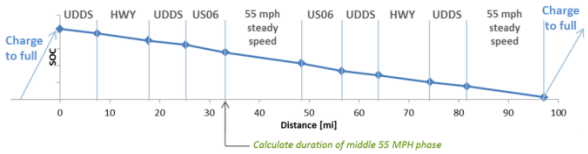

Figure VII-31: J1634 Test Sequence.

The results of the test are shown in Table VII-1. The respective cycle consumption data and the total battery capacity are included.

Table VII-1: Results from J1634 Test.

	Whr	Whr/mi
UDDS	1346.8	180.5
HWY	2092.7	203.5
UDDS	1275.2	171.0
US06	2302.1	286.8
SS55	3241.5	
US06	2268.5	282.8
UDDS	1251.0	167.7
HWY	2044.4	199.0
UDDS	1246.9	167.1
SS55	3245.7	
Test Discharge	**20315**	
AC Recharge	**24048**	

From these data, the consumption and range for each cycle can be determined. Weighting can be applied to the results to better match the old J1634 results (in this case, it was applied to the UDDS cycle data). Figure VII-32 is a worksheet stepping through the J1634 calculations to define electric energy consumption rates and range.

Weighting UDDS for "First Cycle Effect"
K1 = 1346.8 / 20315 = 0.06629
K2 = K3 = K4 = (1 – 0.06629)/3 = 0.31123
DC Wh/mi = K1*UDDS1 Wh/mi + K2...
DC Wh/mi = 169.4

Recharge Allocation Factor
RAF = DC $kWh_{total\ test}$ / AC $kWh_{recharge}$
RAF = 20315 / 24048 = 0.8447

AC Energy Consumption*
UDDS:
AC Wh/mi = 169.4 / 0.8447 = 200.5
HWY:
AC Wh/mi = 238.2
US06:
AC Wh/mi = 337.1

Range Extrapolations*
Usable Battery Energy (UBE)
UBE = 20315 Wh

UDDS
R = 20315 / 169.4 = **119.9 miles**
HWY
R = 20315 / 201.3 = **100.9 miles**
US06
R = 20315 / 284.8 = **71.3 miles**

**Unadjusted for in-use expectations*

Figure VII-32: Worksheet for J1634 Calculations.

J1634 Electric Vehicle Break-in Investigation

For the break-in investigation, Argonne's robot driver was employed to reduce any driver-related influence on the results. The task was to find suitable accumulation distances that would provide stable consumption and range results for an electric test vehicle. Because range is a combination of both consumption rates and usable battery energy, these two results are investigated separately (eliminating any compensating errors).

Usable Battery Energy during Accumulation

As explained in the Approach section, the vehicle was subjected to a J1634 MCT test and then, in the days following, driven in successive HFEDS cycles to advance the break-in miles before another MCT test was performed. This process continued for several weeks.

The J1634 MCT continues until the battery is empty and the vehicle cannot maintain a 55-mph steady cruise. This procedure provides a repeatable condition for the end of the usable battery energy. The tests were analyzed, and a plot of changes in usable battery energy as accumulation distance (odometer reading) progressed is shown in Figure VII-33.

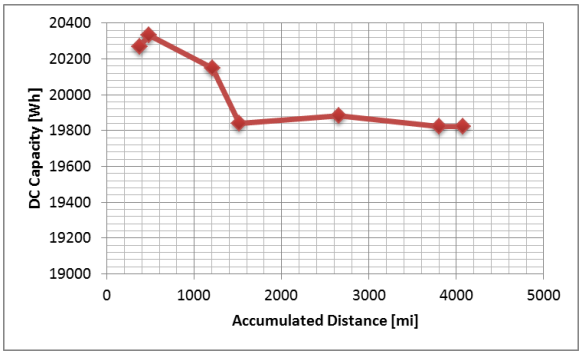

Figure VII-33: Usable Battery Energy as Vehicle Mileage Is Accumulated.

Ideally, researchers like to gather as much data as possible to ensure the highest-quality findings. In our case, the battery energy data are somewhat inadequate for precise conclusions. On one hand, the data do show that by 2000 miles, there may be some evidence of stable usable battery energy. On the other, is it possible that there may be a more general trend toward gradual capacity loss as mileage accumulates? We know all batteries will experience gradual capacity loss as they are cycled, but from 200 to 4000 miles, the maximum variation is on the order of 2.5%—a very small value. A clear choice of when to stop the accumulation does not appear to be found in the battery energy data. Consumption data may provide more information.

Consumption Results during Accumulation

There were many more consumption data points than battery energy data points available. Too many repeated full discharge events would be problematic. Repeated discharge to empty may not be fully representative of normal driving, and it could be forcing faster deterioration of energy capacity than if the test only consisted of mileage accumulation. The consumption data analyzed were taken from the 3rd HFEDS cycle (adequate thermal stability) in each set of mileage accumulations tests. The data in Figure VII-34 show a general trend that supports the testing of the vehicle at an accumulation distance of anywhere from 1000 to 3000 miles. There is a noticeable efficiency drift for the test results starting at roughly 500 miles. Comparable data were not available for less than 500 miles. On the basis of these data, to save considerable expense in the mileage accumulation period,

1000 miles may be an appropriate break-in distance for this test vehicle. This investigation may be revisited in the future, with another vehicle, to provide more insight into the matter.

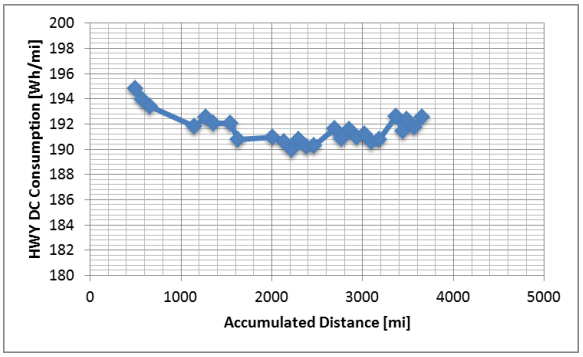

Figure VII-34: Consumption Data, HFEDS, as Vehicle Mileage Is Accumulated.

J2951 Development, Refinement, and Re-issue

Argonne has been one of the principal supporters of J2951 (calculations of quality parameters for dynamometer tests) for both versions of its publication. In this fiscal year, there was an emphasis on the statistics of actual tests. Argonne provided many J2951 results from the Argonne dynamometer tests to be included in the second document issue as aggregate information (along with OEMs' and other government-funded laboratories' data).

Because Argonne's results were not normalized like those of the other test labs, a discussion was possible and insights were presented to the group. An example of the type of data discussed is shown in Figure VII-35. Root mean square (RMS) error is a straightforward metric that tells how closely the driver met the trace throughout the entire cycle. Various methods of driving were investigated, including tests driven by our robot driver. All of the tests shown were valid tests according to EPA rules (no violations outside of the speed tolerances). The plot shows that the highest errors are associated with the lowest consumptions. This statement is true because the objective of the drivers in the lowest-consumption tests was to drive in particular ways to improve fuel efficiency. Driving techniques include attempting smoother accelerations and/or speed changes, rounding corners, and coasting long in braking, as well as using other driver tricks that are known to provide better results—especially for HEVs. The most experienced (pro) drivers were able to get the lowest overall error results, but this came at some expense in extra fuel consumption (compared to other tests). Note that the consumption results of the robot driver are to those of the pro and engineer, the error is higher (engineer drivers are competent, but less experienced than pro drivers). In this case, the robot was not as accurate as the best drivers, but none of this inaccuracy is associated with a desire to achieve lower consumption. The robot was ambivalent to fuel consumption and, thus, was not subject to the fuel consumption and/or accuracy trade-off that was seen with the human drivers.

These results show that experienced drivers can get improved fuel economy results if that is their intention, but these actions will likely be revealed in the J2951 results. This work could lead to less discrepancy between OEM certification data and other testing and/or in-use driver experiences. These efforts bring more accuracy and fidelity to standard testing—especially for new technologies that are the focus of DOE's R&D portfolio.

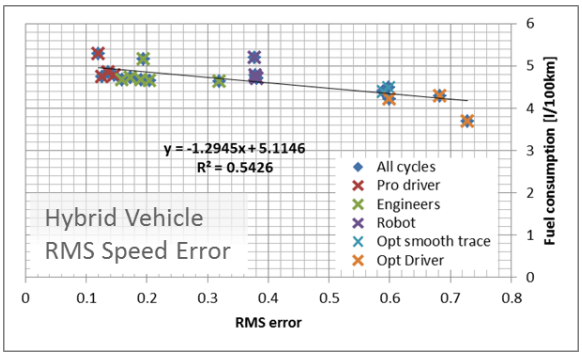

Figure VII-35: Correlation between RMS Speed Error and Fuel Consumption of an HEV.

Conclusions

The critical role of proper test procedures for advanced vehicles cannot be overstated. DOE's goals of reducing petroleum can only be met if the measured achievements made by new technologies are accurate and based on sound science. If a particular measurement approach provides results that are biased, there will be an inappropriate allocation of attention and resources directed at technologies with inflated expectations of achievements.

There are substantial and immediate risks to DOE objectives if inaccurate measurement approaches cause the public to (1) reject some technologies after they find that they do not fulfill expectations or, conversely, (2) ignore others that are capable of more benefit than what was found from inadequate testing methods.

This fiscal year was highlighted by an effort to test new production vehicles according to the existing PHEV and BEV test procedures. It is critical that the procedures are run through their paces for new vehicle designs as they become available. Rapid calculation of J1711 parameters was supported by internal software tools to validate J1711 calculation methods and equations.

Another important achievement was obtaining unique break-in data for a BEV. These important efforts are disseminated to the SAE committee members (EPA included) to make sure that testing is fair and equitable for all current and future advanced vehicles.

VII.E.3. Products

Publications

1. Duoba, M., "Developing a Utility Factor for Battery Electric Vehicles," SAE Int. J. Alt. Power. 2(2):362-368, 2013, doi:10.4271/2013-01-1474.
2. SAE J2951_2013, "Drive Quality Evaluation for Chassis Dynamometer Testing," SAE Light Duty Vehicle Performance and Economy Measure Committee.

Patents

None

Tools and Data

1. "Advanced Powertrain Research Facility—Downloadable Dynamometer Database (D3)." Argonne TTRDC. Argonne National Laboratory, n.d. Web. 10 Oct. 2013.
2. Test data from CAERI-owned (China organization) Prius PHV. Over 100 tests of many standard cycles in normal ambient temperatures, hot and cold.
3. J1711 “1-Pager Calculator and Plotting Tool,” written in LavVIEW™ software.

VII.F. International Smart Grid Cooperation to Support Electrified Vehicles

Keith Hardy, Principal Investigator
Argonne National Laboratory
955 L'Enfant Plaza S.W.
Washington, DC 20024
Phone: (630) 816-7383
E-mail: khardy@anl.gov

Lee Slezak, DOE Program Manager
Phone: (202) 586-2335
E-mail: Lee.Slezak@ee.doe.gov

VII.F.1. Abstract

Objectives

- Facilitate international cooperation to support harmonization of electric vehicle (EV)-grid interface standards and U.S. policy initiatives related to electromobility (e-mobility).

Major Accomplishments

- Established effective programmatic and scientific working relationships between the U.S. Departments of Energy (DOE), State, and Commerce and the European Commission (EC) regarding e-mobility.
- Facilitated the launch of the U.S. EV-Smart Grid Interoperability Center at Argonne National Laboratory (Argonne), fulfilling U.S. commitments made by the Transatlantic Economic Council and DOE.

Future Achievements

- Form an industry working group to ensure awareness of and promote participation in U.S. and EC interoperability center activities.
- Establish a joint testing work group at Argonne and the EC's Joint Research Centre-Institute for Energy and Transport (JRC-IET) to verify compatible test capabilities, procedures and protocols regarding
  - Electric and hybrid vehicles;
  - Battery cells, modules and packs; and
  - Interoperability of EVs, EV supply equipment (EVSE), and EV-grid interfaces.
- Facilitate a joint meeting of the Departments of Energy, State and Commerce to coordinate e-mobility initiatives in Europe and Asia.
- Facilitate joint EV-EVSE compatibility/interoperability testing at Argonne/JRC-IET to evaluate current products and identify opportunities to harmonize standards for future products.
- Facilitate joint assessment of the applicability of EV-grid technology and standards to grid integration, i.e., a holistic approach considering grid connectivity requirements of electric transportation, distributed energy resources, building systems and municipal infrastructure.
- Facilitate a site-specific EV interoperability activity in the EU in cooperation with JRC-IET.
- Facilitate an agreement to establish a cooperative EV interoperability center in China.

✧ ✧ ✧ ✧ ✧

VII.F.2. Technical Discussion

Background

An international cooperation activity was initiated in 2009 to promote the introduction of electric vehicles (EVs) (including battery electric and plug-in hybrid vehicles) in the U.S. by identifying opportunities for cooperation in Europe and Asia that would address common barriers and benefit global automotive manufacturers and suppliers. The objectives are to facilitate harmonization of EV- grid connectivity and communication technology and standards.

Activities of this task are coordinated with diplomatic organizations in the U.S., Europe and China to ensure consistency with U.S. policy, promote awareness of U.S. Department of Energy (DOE) technical initiatives, and provide input/review of the strategic direction of technical cooperation regarding electromobility (e-mobility) and grid integration.

U.S.-EU Cooperation

Initially focused on bilateral technology demonstration projects in individual EU Member States, the activity was elevated to the European Commission (EC) level in FY 2011, culminating in the Transatlantic Economic Council (TEC) *Work Plan to Advance Transatlantic Cooperation on E-Mobility,* which outlined cooperative e-mobility initiatives aimed at minimizing regulatory divergence and harmonizing standards in the interest of mutual economic growth. As a component of the development of the plan, this task ensured that the technical objectives were aligned with DOE and Argonne National Laboratory (Argonne) activities, i.e., joint standardization and research initiatives related to e-mobility.

In addition to adopting the e-mobility work plan, the TEC sponsored an agreement between DOE and the EC, formalized in a Letter of Intent signed in November 2011, to establish EV-Smart Grid Interoperability Centers in the U.S. (at Argonne) and Europe (at the EC's Joint Research Centre-Institute for Energy and Transport [JRC-IET]). The technical objectives of the agreement can be found in the *Codes & Standards, EV-Smart Grid Interoperability Center* report.

U.S. Government Coordination

Technical cooperation with the EU regarding e-mobility is governed by U.S. policy initiatives defined by the TEC and the EU-U.S. Energy Council. Since the TEC is co-chaired by the White House and the EU Energy Commissioner, regular reports on the progress of the initiative are required. Therefore, the TEC coordinators in the DOE and the Departments of State and Commerce, as well as DOE Policy & International Affairs, are regularly briefed on progress toward achieving the elements of the e-mobility work plan. Within DOE, discussions with the EC regarding grid integration are coordinated with the Office of Electricity Delivery and Energy Reliability, which is responsible for smart-grid R&D.

Activities are coordinated with U.S. agencies in Europe through the U.S. Mission to the EU (Brussels) that includes representatives of the Departments of State and Commerce (i.e., Foreign Commercial Service) and their counterparts in the U.S. Embassies in EU Member States such as Germany.

With the aid of the Mission, international activities are coordinated with several EC Directorates-General, including the Joint Research Centre, Enterprise and Industry, Trade, and Energy.

U.S.-China Cooperation

The U.S.-China EV Initiative (EVI), an agreement between Presidents Obama and Hu in FY 2010, established China as the focal point in Asia with respect to EVs. Initially focused on data exchange between EV demonstration programs in the U.S. and China, the vehicle roundtable of the EVI more recently (in August 2012) recommended establishing a cooperative EV interoperability center in China.

Introduction

With working-level relationships established and official agreements in place, the U.S.-European focus has been realization of the EV-Smart Grid Interoperability Centers at Argonne and JRC-IET through coordination with DOE, the U.S. Mission to the EU, the EC, and JRC-IET.

The technical focus for future cooperation with Europe has grown slightly—to EV-grid integration—to be consistent with the strategic direction of DOE and the EC. The emphasis is on the technology and standards that have been developed to connect EVs to the grid; they should be compatible with smart-grid implementation for distributed energy resources, building systems, and municipal infrastructure as well—as basic elements in a smart-city/smart-energy community.

Cooperation with China has been limited to support of EVI coordination activities and maintaining communication with the technical organizations active in standards development (e.g., the China Automotive Technology and Research Center, or CATARC), while the requirements, capabilities and resources of the U.S. and EU interoperability centers were being finalized.

Approach

U.S.-EU Cooperation

The approach to maintaining support for international harmonization of EV-grid interface standards and U.S. policy initiatives related to e-mobility included the following activities during this past year:

- Supporting DOE strategic planning activities regarding U.S.-EU cooperation
  - Concept papers and proposals regarding EVs, grid integration and smart cities; direct participation in U.S. and EU coordination activities
- Promoting industry-government cooperation in the U.S. and EU to harmonize EV-grid technology and standards
  - Technical presentations, joint publication and expert panel participation in the U.S. and EU
- Preparing to launch the U.S. EV-Smart Grid Interoperability Center at Argonne
  - Coordination of U.S. and EU participation, content of launch event and technical seminar
- Developing a joint work plan for the Argonne and JRC-IET interoperability centers

U.S.-China Cooperation

Since the joint recommendation from the EVI meeting in 2012, CATARC has visited the interoperability center at Argonne (in April 2013) and clearly indicated its support for a similar activity in China. The U.S. Embassy in China (Foreign Commercial Service) has become directly involved in determining the appropriate Chinese government agencies and next steps toward an agreement to establish a center. The experience gained in establishing the cooperative U.S.-EU activity should aid the U.S.-China discussions.

Results

The most obvious result of this activity is the fulfillment of commitments made by the TEC and DOE to launch the U.S. EV-Smart Grid Interoperability Center at Argonne. But the establishment of effective programmatic and scientific working relationships between the DOE, Departments of State and Commerce, and the EC is also notable because it will aid in the efforts to involve multinational manufacturers and suppliers and promote global cooperation on e-mobility (e.g., with China).

Conclusions

The programmatic and scientific working relationships established with the EC are effective and were instrumental in fulfilling U.S. and DOE commitments in international agreements related to e-mobility.

The U.S. EV-Smart Grid Interoperability Center at Argonne is fully operational and equipped to aid in the development and verification of proposed international EV standards.

VII.G. Codes and Standards Support for Vehicle Electrification

Theodore Bohn, Principal Investigator
Argonne National Laboratory
9700 South Cass Avenue
Argonne, IL 60439
Phone: (630) 252-6592
E-mail: tbohn@anl.gov

Lee Slezak, DOE Program Manager
Phone: (202) 586-2335
E-mail: Lee.Slezak@ee.doe.gov

VII.G.1. Abstract

Objectives

- Support the U.S. Department of Energy (DOE) Vehicle Systems Simulation and Testing (VSST) Program in the capacity of both chairing technical standards committees in cooperation with Standards Defining Organizations (SDOs) and through active participation in the highly interrelated breadth of committees across the spectrum of SDOs involved with vehicle electrification standards.
- Identify gaps in standards development activities as well as leverage grid connectivity capabilities and research at Argonne to support and validate standards procedures/approaches with proof-of-concept hardware and software on Argonne testing assets.
- Attend and participate in high-level standards gap identification meetings, such as the American National Standards Institute (ANSI) Electric Vehicle Standards Panel (EVSP), to concisely summarize the "state of the standards" within the rapidly evolving and multifaceted EV standards landscape, especially when addressing vehicle-grid interactions.

Major Accomplishments

- After a long period of inactivity, an Argonne technical staff member assumed leadership as the new chair of the Society of Automotive Engineers (SAE) J2953 Plug-in Electric Vehicle-Electric Vehicle Supply Equipment (PEV-EVSE) Interoperability Standard Committee. Via technical community support of industry stakeholders, complemented by multiple Argonne technical staff members at each meeting, the quarterly J2953 meetings increased to a weekly or biweekly pace to facilitate progress on SAE J2953, and publication of two sections of the standard in FY 2013.
- Final publication of *SAE J2953/1 PEV-EVSE Interoperability Requirements* standard (for AC fundamental pilot/proximity communication).
- Preliminary draft publication of *SAE J2953/2 PEV-EVSE Interoperability Procedures* standard (for AC fundamental pilot/proximity communication). This work is validated by and complements the DOE-sponsored Grid Connectivity activities at Argonne (covered in Section 1000190.00 of this report).
- Coordinated professional standards support contractor (ThinkSmarGrid) to restart *SAE J2931/7 Security for Plug-in Electric Vehicle Communications* after a hiatus due to the departure of the previous chairperson in 2012. Contract deliverables include publication of SAE J2931/7, with the input of industry cybersecurity experts on the committee, stakeholders in EV charging equipment, vehicle manufacturers, and charging communications hosts (utilities/EV charging network service providers).
- ANSI EVSP *Standardization Road Map for Electric Vehicles* (version 2.0) was published in May 2013, with significant input from Argonne technical staff.
- Via significant input to the National Working Group on Electric Vehicle Fueling and Submetering (NWGEVF&S), published National Institute of Standards and Technology (NIST) Handbook 130, *Uniform Regulation for the Method of Sale of Commodities,* as part of the 2013 Weights and Measures National Congress. This included a specific rewrite requiring submetering of electricity as a fuel, whether or not it is sold by a bundled service, time of use, or specific energy delivered.
- In parallel with NIST Handbook 130, an updated draft of Handbook 44, Section 3, "Device Code Requirements for Electric Vehicle Fueling and Submetering," was released for comment. An Argonne technical staff member stepped forward as the chair of the Handbook 44, *EVSE Meter Test Procedure and Equipment Drafting,* subcommittee.
- Leveraged other submetering standards activities (above) via the Smart Grid Interoperability Panel (SGIP) to support the initiation of inter-SDO coordination of standards activity for *PAP22: EV Fueling Submetering Requirements*. This is a step beyond liaison activities and may lead to the creation of a reference standard on submetering for EV fueling among SDOs.
- Assisted in committee input and editing of *SAE J2847/3 Communication between Plug-in Vehicles and the Utility Grid for Reverse Power Flow*, which led to publication in 2013.
- Significant input on draft *SAE J2894/2 Power Quality Test Procedures for PEV Chargers* standard that was expected to go to ballot for publication by the end of FY 2013. Validation testing using SAE J2953 leveraged tools and software at Argonne to SAE J2894 procedures explored as well.
- As described in task 1000270.00 of the annual report, the Wireless Charging test fixture in support of the SAE J2954 Wireless Charging standard was specified, designed, fabricated, and tested. Interoperability requirements for combinations of primary and secondary side electronics and electromagnetics for wireless charging (off-vehicle

and on-vehicle) have been initiated but not finalized by the end of FY 2013. The fixture can be used for evaluating performance, efficiency, misalignment effects, safety, and interoperability. Communication protocol evaluation is possible but has yet to be standardized (in FY 2014).

- Facilitated the standardization process by providing laboratory test data and analysis to support fact-based deliberations in the SAE committees related to EV-grid communication (SAE J2836, J2847, J2953, and J2931).
- Created hardware/software to construct an interoperability test fixture designed to measure, record, and validate the analog interaction between EVs and AC EVSEs. The validation of this test set-up and procedures supports the creation of the SAE J2953/2 interoperability test procedure standard.

Future Achievements

- Maintain focus on near-term needs with long-term impact; that is, by providing direct support of SAE standards committees and global cooperation/harmonization for the following initiatives:
  - Interoperability; Define laboratory test procedures for AC EVSE interoperability, verify with production-intent vehicles and EVSE, and provide input for the SAE J2953 standard publication.
  - Interoperability; Define testing approach and procedures to validate DC charging interoperability. Demonstrate compliance with vehicles provided by OEM and with DC EVSE units.
  - Communication; Create the technology to enable DC Level 1 charging and EV-to-EVSE-to-network-to-smart grid communication.
  - Wireless EVSE test procedures and interoperability; utilize the new wireless charging test fixture to evaluate samples of wireless power transfer (WPT) units to support the SAE J2954 committee's deliberations and write the associated standards and test procedures governing this equipment.

✧ ✧ ✧ ✧ ✧

VII.G.2. Technical Discussion

Background

Meeting the Obama Administration's goal of having 1 million EVs on the road in the United States by 2015 requires finalizing specifications for components and interfaces as soon as possible, obviating the need for ratified standards. Otherwise, suppliers and original equipment manufacturers will be assuming the risks of fielding "nonstandard" products. Thus, a common objective of suppliers, original equipment manufacturers, DOE, and the national laboratories is to support the SAE committees as they define, refine, and verify the standards that are focused on EVs. The report on task 1000190.00, Codes and Standards Grid Connectivity Support, provides a detailed description of all the EV-related technology-based project work that supports codes and standards under SAE development.

The EV-grid interface has been defined, from a standards perspective, in terms of the charge coupler (the physical connector for power and communication, messaging, and protocols), the EVSE (charging technology and power quality), and interoperability (EV-EVSE compatibility, communication, and security).

Introduction

Argonne is the technical lead for technology development and/or standards verification related to EV-grid connectivity and co-chair of the Grid Interaction Technical Team (GITT), whose objective is to support a transition scenario to large-scale, grid-connected vehicle charging. The scope of the GITT is connectivity between light-duty EVs, the charging infrastructure, and the electric power grid. Argonne's activities are aligned with the GITT, with substantial effort in refining and verifying EV-grid standards in direct support of the SAE committees related to the charge coupler, EVSE, and interoperability.

Refinement and verification of standards require hardware and software for testing and evaluation. Because components are not readily available for EV-grid connectivity, Argonne utilized its embedded controls/network laboratory and leveraged support contractors to develop components to fill the gaps. The results from these support activities are used in standards development.

Approach

1. End-to-end Definition of Vehicle Electrification Oriented Standards

The end-to-end path of electricity from generation to end use in a vehicle battery passes through many points, both in control and actual flow of energy. The approach is to facilitate a broad reach of interrelated, yet critical path standards to accommodate this energy flow control. These standards and the related infrastructure elements are shown in Figure VII-36.

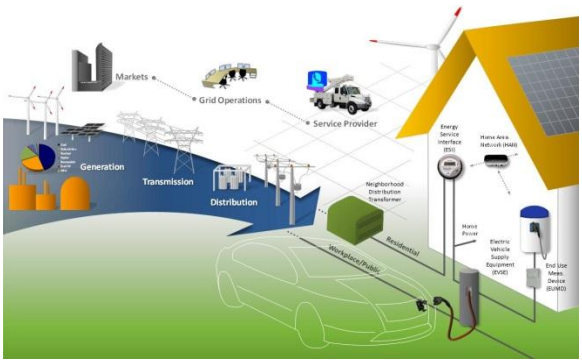

Figure VII-36: Electric vehicle support infrastructure.

Argonne's participation in SAE committees related to PEV charging and vehicle electrification standards. These PEV charging standards are interrelated, as shown in Figure VII-37. Argonne engineers both chair and support all of the standards represented in these groups.

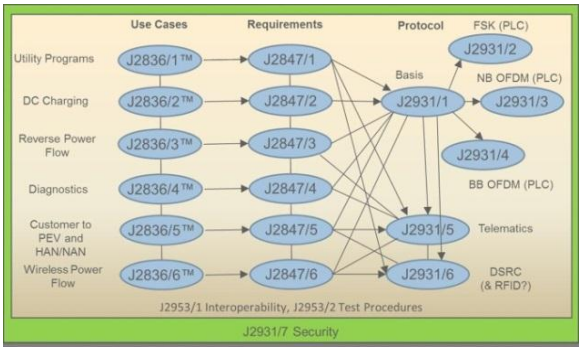

Figure VII-37: Interrelated SAE PEV charging standards related activities. The J2953 interoperability standard blankets all other charging standards and the J2931/7 cybersecurity requirements standard encircles interoperability, etc.

2. Interoperability Standards Test Equipment Development To Support J2953 Interoperability Test Procedures

SAE J2953 defines interoperability between a PEV and its EVSE. Figure VII-38 shows the limits of interoperability for EVs.

Figure VII-38: Scope of EV-grid connectivity from a standards perspective.

Interoperability testing is conducted using a specific PEV –EVSE pair. In order to conduct non-evasive testing, SAE J2953 procedures require the use of a breakout fixture capable of monitoring and reporting on all PEV and EVSE circuits. Figure VII-39 shows the compact self-contained version of a tool that is a test point pass-through of signals without affecting the dynamic performance of the system, while inserted in series with the PEV-EVSE pair being examined. The EVSE under test is on the left, the oscilloscope for taking timing and magnitude test data is on the right of an adjustable height mobile platform, and the test point pass-through device is in the center, with the EVSE connector inserted.

Figure VII-39: Non-invasive interoperability standard (J2953/2) test procedure test point pass-through tool, EVSE, and data collection oscilloscope, ported to a PC via Labview software.

Argonne addressed the need for creating a bench-top test system to validate and support the standardization of vehicle AC charging interoperability for the purpose of standard test procedure development.

Non-invasive, simple to use mechanical interoperability test fixtures and procedures defined in SAE J2953/2 were designed, fabricated, and field trials performed to assess usefulness and repeatability of the procedures/results. Figure VII-40 shows the mechanical insertion force tool operator using this tool and procedure.

Figure VII-40: SAE J2953/2 test procedures for PEV interoperability-mechanical insertion force measurements.

SAE J2954 standard calls for wireless charging systems to be tolerant of misalignment of ±100 mm in the *X* and *Y* direction between the primary and secondary coils, as well as wide variations in the *Z* direction (see Figure VII-41 for orientation). The fixture shown in Figure VII-42, as a component-level configuration (no vehicle or vehicle ground plane effects), is composed of an *X-Y* table with a 1,000-mm *Y* direction closed-loop linear actuator.

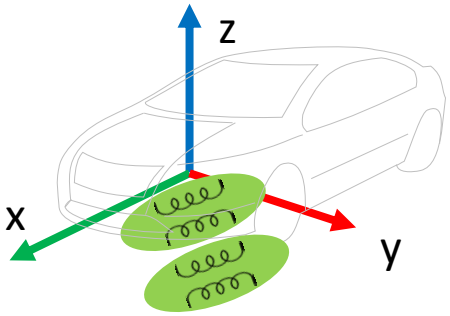

Figure VII-41: Basic wireless vehicle charging orientation of ground-mounted (transmitting) primary side coil and vehicle-mounted (receiving) secondary coil, typical 100-mm gap.

Figure VII-42: Wireless vehicle charging positioning apparatus; 1,000-mm *Y* and *Z* actuators, 1,500-mm *X*-axis actuator.

This apparatus is designed to be reconfigurable and easily transportable between lab spaces, as well as between test facilities. Figure VII-43 shows the vehicle system configuration with the Chevy Volt plug-in hybrid electric vehicle (PHEV) and wireless charging secondary coil apparatus on the *Z*-axis actuator and primary coil on the floor, between the vehicle wheels, on the *X*-*Y* positioning table. The Narda EHP-200 field measurement probe is shown to the left of the vehicle as well.

Figure VII-43: Wireless charging vehicle system-level configuration of positioning apparatus. Grey boxes house *X*, *Y*, and *Z* servo amplifiers/safety stops.

The NIST Handbook 44 subcommittee on drafting a requirements document for traceable field testing of EVSE electrical energy-measuring devices that clearly addresses accurate measurement from the point where the test connection occurs relative to the vehicle connection required a practical validation document for the proposed approach. Figure VII-44 shows a sub-$1,000 compilation of slightly modified off-the-shelf components to perform the equivalent of a "graduated cylinder for electrons." More directly stated, it is a NIST traceable meter with adjustable (field transportable) AC modular load bank and PEV emulator for triggering and measuring the response of the EVSE dispensing "electricity as a fuel."

The brown boxes on the left are 4 kW/240 vac commercial-grade resistance heaters, with semi-custom current regulators. The grey box in the center is a NIST traceable 0.1% meter with an 8000:1 turn down ratio (accurate down to low current readings as well), and the black box on the right is the EVSE under test. The PEV emulator is based on a modified off-the-shelf EV interface/battery charging system controller. The round premise meter (ANSI C.12 form factor) and box beneath is a NIST traceable field meter calibration set capable of 0.025% accuracy measurements.

Figure VII-44: NIST Handbook 44 reference proof-of-concept field verification of electricity as a fuel-dispensing system.

Results

Argonne contributed substantially to resolving the technical challenges of EV-grid connectivity this year:

- Volunteered for and committed to serve as the chair of several standards committees that were previously stalled such as SAE J2953 PEV-EVSE Interoperability and NIST Handbook 44 Measurement System Requirements for Dispensing Electricity as a Fuel.
- Defined test requirements for wireless EVSE and designed and fabricated a prototype test fixture for evaluating the performance of wireless EV charging systems. The validation of this test set-up and procedures guided the creation of the SAE J2954 standard test procedure standard.
- Provided prolific information dissemination on the state of the standards updates to key vehicle electrification and infrastructure deployment stakeholders in the presence of rapidly changing standards developments.
- Contributed to the SAE standardization process by providing laboratory test data and analysis to support fact-based deliberations in the SAE committees related to EV-grid communication (SAE J2836, J2847, J2953, and J2931).

Conclusions

Argonne's standards development support activities directly address technology gaps in the EV-grid interface and provide quantitative evaluations to support SAE committees. These efforts contributed to a better understanding of the issues associated with metrology standards that lead to regulatory policy and unification of state-to-state variability in policies toward distribution of electricity as a fuel. This standards development support also reinforces the pathway to EV-grid connectivity and the potential benefits of global harmonization.

Argonne and support contractors successfully demonstrated joint development of rapid prototypes for proof-of-concept and compilation of related reference datasets for vehicle-EVSE communication and metrology.

Focusing on near-term needs with long-term impact has been an effective approach to standards development support activity. Interoperability among EVs, EVSE, and the grid is a pressing near-term issue, necessitating the development and verification of SAE J2953 (interoperability) standards as soon as possible. The EV-Smart Grid Interoperability Center is specifically designed to address the associated issues.

Argonne will continue to provide direct support to the SAE standardization process, including committee participation, development of enabling technologies, system integration, and laboratory testing.

VII.G.3. Products

Publications

1. Bohn, T.P., Numerous standards status update presentations at Technical Conferences: IEEE ITEC (Dearborn, MI, June 2013), Underwriters Laboratory Annual Users Conference (Willowbrook IL, July 2013), NFPA EV Safety Summit (Detroit, MI, Oct. 2013).
2. Bohn, T.P., Significant contribution to the second edition of the *ANSI Electric Vehicle Standards Panel Roadmap*, published May 2013.

Patents

1. By definition, standards must be open and free of patent intellectual property ownership conflicts. That is, no patents can be associated with open standards.

Tools and Data

1. As referenced in annual report sections 1000190.00 (Grid Connectivity) and 1000270.00 (Wireless Charging), significant amounts of data were collected from vehicle testing, EVSE evaluation, Wireless-EVSE evaluation, and in general, cost/obstacles to infrastructure deployment. Cost assessments, efficiency of components, as well as diversity of minimum and maximum cases in the above topics, have been compiled and are regularly accessed in the process of standards development decision-making.

VII.H. SAE Standards Development Support

***Krishnan Gowri,* Principal Investigator**
Pacific Northwest National Laboratory
P.O. Box 999, MS-BSRC/377
Richland, WA 99354
Phone: (206) 528-3216
E-mail: krishnan.gowri@pnnl.gov

Lee Slezak, Principal Investigator
Phone: (202) 586-2335
E-mail: Lee.Slezak@ee.doe.gov

VII.H.1. Abstract

Objectives

- PNNL will contribute to accelerating the development and harmonization of vehilce to grid communication standards by supporting the SAE, ANSI and NIST/SGIP technical working groups to develop use cases and technical requirements in the development of the following standards:
  - J2847/1—Communication between Plug-in Vehicles and the Utility Grid
  - J2847/3—Reverse energy power flow
  - J2847/5—Customer to vehicle communication
- PNNL will provide leadership to the Smart Grid Interoperability Panel (SGIP) vehicle to grid domain expert working group (V2G DEWG) to identify and address high priority industry needs for standardization.

Major Accomplishments

- PNNL helped the SAE committees develop and performed technical reviews of the following standards. They have completed committee preparation and are approved for publication.
  - J2847/1—Communication between Plug-in Vehicles and the Utility Grid
  - J2847/3—Reverse energy power flow standard development
- PNNL prepared and presented use cases for J2836/5—Customer to Vehicle communications standard.
- PNNL analyzed the impact of communication standards and V2G benefits using EV Project data
- PNNL coordinated with industry stakeholders to develop a new priority action plan (SGIP/PAP-22) for developing submetering requirements for EV fueling.

Future Achievements

- J2836/5 committee is moving forward on use case development for Customer to Vehicle communications and will be completed in FY 2014.
  - J2847/5 message development
- PNNL will continue to provide leadership to the NIST V2G DEWG and plans to add 2 SAE standards to the catalog of standards in FY 2014.
  - PNNL will work with vehicle OEMs, EVSE providers and utility providers to coordinate the development of submetering requirements.

✧ ✧ ✧ ✧ ✧

VII.H.2. Technical Discussion

Background

EV Standards Development

The interoperability between vehicles, charging stations and electric utilities is critical to the success of electric vehicle deployment. SAE, ISO and IEC are leading the U.S. standards development to define the communication architectures, protocols and messages.

To expedite the standards development process DOE / EERE / VSST has been funding national laboratories (PNNL, ANL, ORNL and INL) to provide technical support for the SAE, ANSI, and NIST standards development process.

FY 2013 SAE communications standards development began with a recognition that several standards needed to be updated (i.e., J2847/1 and J2847/2), several needed to be completed (i.e. J2847/3 and J2847/5), and contributing to the gap analysis of standardization efforts.

Introduction

In order to promote the widespread adoption of electric vehicles, interoperable charging infrastructure must be made available. While the majority of electric vehicle charging events currently take place at home using residential AC Level 1 or Level 2 charging equipment, the availability of public and commercial (such as workplace and retail) charging infrastructure may alleviate “range anxiety,” increasing driver confidence and the overall utility of electric vehicles.

Approach

PNNL participated in the monthly committee meeetings and actively contributed to the development and technical review of SAE EV/EVSE communication standards J2847/1 and J2847/3. PNNL prepared and presented use cases to the J2836/5 committee.

PNNL led and contributed to the ANSI Electric Vehicle Standards Panel working groups and NIST SGIP Vehicle to Grid domain working group on smart charging communications and related standards and roadmap development activities.

PNNL conducted an analysis of the economic benefits of intelligent vehicle infrastructure for the consumer and the utility by analyzing the EV project data and considering several different use case scenarios. Vehicle charging patterns, utility programs and peak demand profiles are used to evaluate the impact of using vehicle as grid resources, time-of-use rates, and load balancing strategies.

Results

PNNL participated in the SAE Hybrid committees to review and finalize the J2847/1 and J2847/3 standards. Further, PNNL led the NIST Smart Grid Interoperability Panel (SGIP) vehicle to grid domain expert working group (V2G DEWG) and contributed to the formulation of a priority action plan (PAP-22) for EV fueling submetering requirements. Several new use cases including submetering and vehicle telematics have been developed for includesion in the SAE J2836/5 standard.

In addition to the standard support, PNNL undertook EV Project data analysis to identify potential economic benefits and grid impact of Intelligent Charging including:

- the potential of increased regional peak demand for power in regions without time-of-use (TOU) rates,
- reduced costs of PEV charging by shifting timing to off-peak periods,
- significant ramping of PEV charging load when off-peak TOU rates take effect, leading to potential distribution constraints,
- lost economic benefits from participating in wholesale markets for reserve capacity.

Conclusions

The value of thoughtfully developing electric vehicle communications standards provides five necessary electric vehicle and charging infrastructure capabilities:

- enables EVSE and EV interoperability between vendors.
- provides a basis for U.S. vehicle manufacturers to be competive overseas.
- causes international vehicle and EVSE manufacturers to be compliant to U.S. standards.
- allows the electric vehicle charging process to coexist in harmony with the existing electric power generation, transmission, and distribution systems (i.e. residential transformers)
- provides a basis to enhance utilization of renewable energy resources.
- These communications capabilities provide a very important element in a comprehensive and consistent set of codes and standards addressing the interface between electric vehicles and charging infrastructure that is essential for the market success of these vehicles. There is a need to develop reference design and implementation of communication modules in vehicles and further support their adoption by utilities in order to realize the economic benefits identified from the EV project data analysis.

VII.H.3. Products

Publications

1. Letendre, S., Gowri, K., Kintner-Meyer, M., & Pratt, R., Intelligent Vehicle Charging Benefits Assessment Using EV Project Data, Pacific Northwest National Laboratory, Oct. 2013.
2. RM Pratt and K Gowri. 2013. "Vehicle to Grid Communication Development." Presented by Rick Pratt (Invited Presenter) at DOE Office of Vehicle Technology—Annual Merit Review 2013, Washington, DC on May 13, 2013. PNNL-SA-94337.

VII.I. Vehicle to Grid Communications Field Testing

***Rick Pratt*, Principal Investigator**
Pacific Northwest National Laboratory
P.O. Box 999, MS-K3-07
Richland, WA 99354
Phone: (509) 375-3820
E-mail: rmpratt@pnnl.gov

Lee Slezak, DOE Program Manager
Phone: (202) 586-2335
E-mail: Lee.Slezak@ee.doe.gov

VII.I.1. Abstract

Objectives

- Field testing of SAE EV/EVSE standards will enable performance and implementation evaluations of SAE adopted communication technologies and methods. PNNL will utilize its Lab Homes EVSE infrastructure to perform testing of J2847/1 messages between the EV (PNNL Prius) and EVSE.
  - Obtain and integrate evaluation PLC boards into the EV and Lab Homes infrastructure
  - Test J2847/1 messages between the EV and EVSE.

Major Accomplishments

- Panasonic PLC evaluation boards were integrated into the Lab Home infrastructure and EV in a manner that enabled testing of PLC communications between the Lab Home and the EV (PNNL PRIUS).
  - Digital communications capability was added to existing EVSEs such that three different EVSE manufacturer's products could be tested.
  - Digital communications capability was developed to enable the EV (PNNL PRIUS) to communicate battery status information to the EVSE
  - J2847/1 messages were communicated between the EV and EVSE.
- A method of electricity demand management between the home and one or more EVs was developed. The approach developed uses the vehicle charging capabilities described by the J1772 standard.

Future Achievements

- Automation of EVSE / EV / home demand management using Home Area Network charging control to reduce peak residential loads.
- Integration of residential EV charging requirements with regional electricity availability.
- Customer to Vehicle and EVSE communications implementation and testing capability is available.
  - J2836/5 Use Cases and J2847/5 messages can be integrated into the system for evaluation and testing.
  - Home Area Networks provided with EV charging information could more effectively limit peak residential loads.

✧ ✧ ✧ ✧ ✧

VII.I.2. Technical Discussion

Background

EV Standards (J2847/1) Verification Testing

The primary purpose of J2847/1 standard is grid-optimized energy transfer for plug-in electric vehicles—that is, ensuring that vehicle operators have sufficient energy for driving while enabling the delivery of that energy to vehicles in ways that minimize stress upon the grid. This can be accomplished, for example, by vehicle owners' voluntary participation in a utility controlled-charging program in return for incentives, and the specification therefore supports information flows that enable such mechanisms. SAE J2931/1 standard specifies digital communication requirements to implement the vehicle to grid communication messages specified by J2847/1.

Introduction

Laboratory testing of the J2931/1 standard in FY 2012 demonstrated that HPGP was the preferred communication technology. Vehicle to grid communication testing is needed to validate the messages specified in J2847/1. None of the available vehicles and/or EVSEs currently support digitial communications hence, prototype communication modules need to be developed for field testing.

Approach

A vendor search was conducted to identify a commercial source of PLC communication technology. Two companies were identified—CODICO and Panasonic. The Panasonic evaluation board was chosen primarily because it was the more mature evaluation board product and directly enabled IPv6 communications. At the time, the CODICO product required significant development effort to meet the requirements of this application. After implementing a modification to the Panasonic HDPLC evaluation boards that enabled coupling to the Control Pilot line, HDPLC communication over the Control Pilot was achieved with measured jPerf and ping test results similar to hardwired connections.

Figure VII-45: Panasonic HDPLC Module

The approach chosen leveraged three EVSEs installed at the Lab Homes. Each EVSE was from a different manufacturer—EATON, SPX, and AeroVironment (see Figure VII-45). These EVSEs were modified to obtain the capability for HPGP communications by capacitively coupling a coaxial cable to the EVSE's Control Pilot line. The coaxial cable was routed to an indoor area were the Panasonic HDPLC evaluation board was located. Simple wiring connection changes enabled the Panasonic evaluation board to be used for communication testing of any of the installed EVSEs. In the EV, an identical coupling circuit allowed the Panasonic HDPLC evaluation board to connect to the Control Pilot signal line.

Figure VII-46: Lab Home EVSEs.

The simplest communication system configuration is shown in Figure VII-47 with the HDPLC module acting as a network bridge between the EVSE to the EV. The EVSE could be directly connected to the HAN network and the EV to a network within the vehicle.

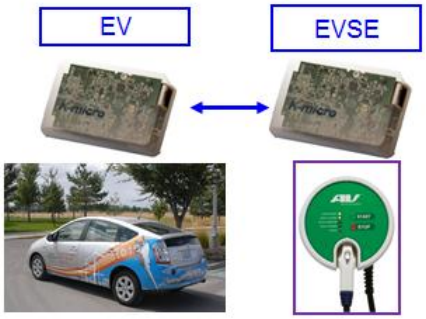

Figure VII-47: Network Bridge Configuration.

Neither the existing HAN network nor the vehicle network is currently advanced enough to implement the bridged configuration. The vehicle needs an interface with the vehicle CAN bus to enable access to State of Charge and other battery information. Both the EV and EVSE sides need either the J2847/1 messages in SEP 2.0 implemented in order to pass the necessary charging information using a standardized protocol. This capability was implemented using a low-cost, network-capable microcontroller. Since SEP 2.0 was not complete, portions of ISO/IEC 15118 were implemented using the open source OpenV2G code as a starting point and J2847/1 message content. This approach allowed the EV microcontroller to directly connect to the CAN bus and translate the required information to the EVSE microcontroller. The EVSE µController provided a translator connection to the HAN / Utility. Figure VII-48 shows the architecture implemented for field communications testing.

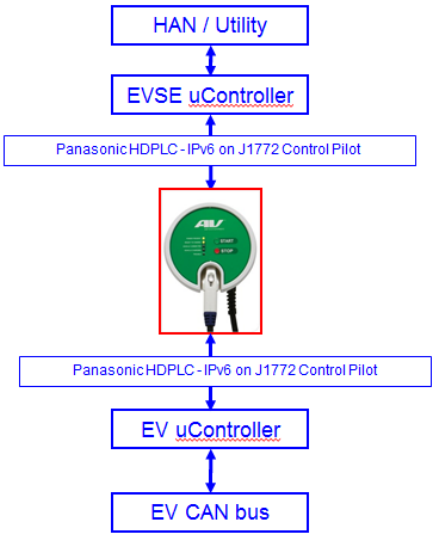

Figure VII-48: System Architecture.

Implementation of the Figure VII-48 system architecture required development of the EVSE / HAN / Utility interface and the EV CAN bus interface. The EV CAN bus interface was developed using a commercial module, PCAN-USB, and the Linux CAN libraries now typically part of the Linux kernel. The Hymotion CAN addresses for the PRIUS's extended range battery pack were obtained through an NDA with A123 and other needed Toyota PRIUS CAN address were found through a web search. The EV µController communicated the battery information to the EVSE µController and adusted the battery charging rate as commanded by the EVSE µController.

The EVSE µController interfaced with the remainder of the HAN / Utility system using an IPv4 interface. The HAN / Utility system uses the JSON-RPC protocol, a simple protocol similar to XML-RPC, and provides access to the regional Pacific Northwest SmartGrid Demonstration project data server.

Results

Initial system testing was performed using the system configuration between the EVSE µController and the EV µController shown in Figure VII-49. The primary areas tested include impacts on the Control Pilot signal by the Panasonic HDPLC, the network latency and throughput performance of HDPLC when its signal amplitude is limited to the same amplitude as HPGP.

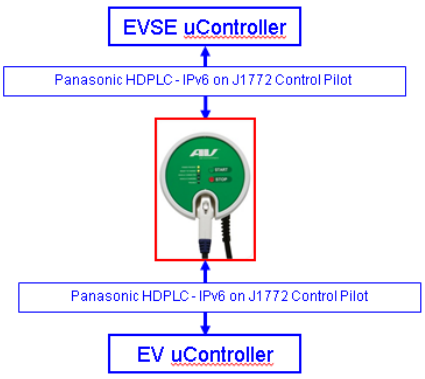

Figure VII-49: System Testing using J2931/1.

The J2931/1 Control Pilot Impairment, Latency and Throughput tests were performed on an EATON Level II EVSE to verify that the Figure VII-49 configuration would meet the specified performance requirements. The Panasonic HDPLC signal amplitude was adjusted using vendor software to be less than $\pm 1V_{pp}$ and oscilloscope measurements verified the Control Pilot PWM signal rise and fall times were unaffected. The round-trip latency was measured using the specified J2931/1 IPv6 ping test. The measured latency was ~5 milliseconds, well within the specified 25 millisecond requirement. The Throughput measured using jPerf was above 500kbps which also exceeds the 100kbps system requirement.

The J2847/1 messages implemented allowed information necessary to control and monitor the charging process from connection to charging completion to be exchanged between the EV and EVSE / HAN. In addition to these basic J2847/1 messages, demand response and tariff messages were implemented. Communication testing is planned for FY 2014.

With over 100,000 electric vehicles currently operating that have no communications capability, the system shown in Figure VII-49 was updated to enable the EVSE µController to send variable PWM signals to the EV µController using the SAE J1772 Control Pilot signal. This configuration was tested while simulataneously charging the PNNL PRIUS and a Nissan Leaf at the Lab Homes. The total power being used in the Lab Home was monitored and changing PWM signals to both vehicles were transmitted to maintain total power being used at the home at a prescribed level. This was demonstrated while the home's heat pump and water heater cycled ON and OFF.

Conclusions

Initial field testing using a Panasonic HDPLC module showed that communication performances similar to those achieved during J2931/1 Lab Communication testing are achievable.

The potential of using only SAE J1772 signals to vary electric vehicle charging rates was demonstrated to reduce peak loading on a residential transformer by delaying when charging occurs or reducing the charging rate. This is one potential solution to reducing residential transformer peak loads. EV Project data validates the potential for his approach since actual vehicle charging is occurring less than 50% of the time the vehicle is connected (EVProject Charging Infrastructure Report, Q2 2013, p.39).

A simple circuit was developed that measured the Control Pilot pulse width to each of the three charging stations and generated appropriately scaled changes to the power meter µController was very important. Providing and coordinating charging sessions of personally-owned EVs with software developer schedules were challenging during the testing process.

VII.I.3. Products

Publications

1. RM Pratt and K Gowri. 2013. "Vehicle to Grid Communication Development." Presented by Rick Pratt (Invited Presenter) at DOE Office of Vehicle Technology—Annual Merit Review 2013, Washington, DC on May 13, 2013. PNNL-SA-94337.

Patents

1. U.S. Patent No. 8,478,452 B2, Grid Regulation Services for Energy Storage Devices based on Grid Frequency, Pratt, RM, Hammerstrom, DH, Kintner-Meyer, MK, and Tuffner, FK., July 2013. (Note: This is a PNNL patent developed from prior year projects funded/cost-shared by Office of Electricity and Vehicle Technologies tasks related to smart charging and communication standards).

Tools and Data

1. PNNL has invested in the capability to perform the field testing using the infrastructure made available by the PNNL Lab Homes and an internal PNNL investment to install 3 charging stations on the Lab Homes. This field testing capability enables the 3 co-located charging stations to perform field interference, crosstalk, shared network, co-existence and association testing measurements.
2. Interfacing HPGP-based EVSE / PEV communications to the Lab Home Home Area Network will enable standards testing beyond the EVSE. This field testing site can be made available to OEMs for their off-site testing.
3. The PNNL PRIUS was retrofitted to add HPGP communication capability with two-way vehicle CAN bus communication that enables live parameters to be transferred during testing.
4. The field testing equipment includes GridTest's Electric Vehicle Charger Test equipment to verify operation of EVSEs that have been updated prior to connecting to personally-owned electric vehicles.

VII.J. Wireless Charging Unit Evaluation and Communications Implementation

Theodore Bohn, Principal Investigator
Argonne National Laboratory
9700 South Cass Avenue
Argonne, IL 60439
Phone: (630) 252-6592
E-mail: tbohn@anl.gov

Lee Slezak, DOE Program Manager
Phone: (202) 586-2335
E-mail: Lee.Slezak@ee.doe.gov

VII.J.1. Abstract

Objectives

- Support the DOE Vehicle Systems Simulation and Testing (VSST) Program as the technical lead for technology and standards development/verification that pertain to wireless plug-in electric vehicle (PEV) charging capabilities.
- Provide validation of procedures and characterization of existing wireless charging apparatus, in parallel with standards document development that includes safety, performance, efficiency, and interoperability aspects of wireless charging standardized systems.
- Identify gaps in technology and recommend enabling solutions through the creation of proof-of-concept hardware/software and validation of proposed approaches, specifically for positioning fixtures and instrumentation.
- Leverage wireless charging evaluation technical capability to support an international EV-Smart Grid Interoperability Center at Argonne National Laboratory.

Major Accomplishments

- Contributed to the Society of Automotive Engineers (SAE) standardization process by providing laboratory test data and analysis to support the SAE, the *Institute of Electrical and Electronics Engineers* (IEEE), and the International Organization for Standardization (ISO)/*International Electrotechnical Commission* (IEC) committees related to wireless PEV charging technology (SAE J2954, UL 2750, SAE J2847/6, SAEJ2931/6, and IEC61980-1).
- Created a 3-axis positioning apparatus under computer control to servo-mechanically coordinate wireless PEV charging system electromagnetic components, including the vehicle itself. Functional testing has been completed, and the formal test procedure is under development.
- Obtained, configured, and verified the test equipment array to measure power flow (power in and power out), magnetic and electric fields, contact and non-contact temperatures, DC external loads on output, and AC programmable sources on input, as well as monitored communication messages between on-board and off-board charging apparatus components.
- Procured two Evatran Plugless Power Wireless charging (pre-production) systems—one evaluated at the subsystem/component level and one at the vehicle level—for installation on an Argonne Chevrolet Volt.

Future Achievements

- Maintain focus on near-term needs with long-term impact by providing direct support of SAE standards committees and global cooperation/harmonization for the following initiatives:
  - *Wireless electric vehicle supply equipment (EVSE) test procedures and interoperability*: Utilize the new wireless charging test fixture to evaluate samples of wireless power transfer (WPT) units to support the SAE J2954 committee's deliberations, and write the associated standards and test procedures governing this equipment.
  - *Collaboration*: Continue collaboration with professional test and certification agencies that will implement the UL2750 wireless charging safety standard and verify SAE J2954 compliance, including Underwriters Laboratory, Intertek, and TUV SUD-America.
  - *Communication*: Create the hardware/software technology for wireless charging that matches the developing standards and protocols (SAE J2931/6, J2947/6).

✧ ✧ ✧ ✧ ✧

VII.J.2. Technical Discussion

Background

Meeting the Obama Administration's goal of having one million EVs on the road in the United States by 2015 requires finalizing specifications for components and interfaces as soon as possible, thereby obviating the need for ratified standards. Otherwise, suppliers and original equipment manufacturers (OEMs) will be assuming the risks of fielding 'nonstandard' products. Hence, a common objective of suppliers, OEMs, DOE, and the national laboratories is to support the SAE committees as they define, refine, and verify the standards that are focused on EVs. (Refer to the report on task **1000201.00, Codes and Standards Support for Vehicle Electrification,** for a detailed description of all the EV-related Codes and Standards under SAE development.)

Wireless charging of EVs via resonant electromagnetic coupling at high efficiency and a wide gap between vehicle and infrastructure is being defined by several Standards Defining Organizations (SDOs) around the world. Harmonization of these international standards is important to allow equipment manufactured in different countries to be acceptable and interoperable in other regions. Interoperability of wireless charging equipment built to the same standard by different manufacturers is also a primary concern with regard to the ability of any vehicle to access various types of public wireless charging infrastructure, and vice versa. Steady progress has been made in these wireless PEV charging standards in FY 2013, with substantial technical support contributions provided by Argonne.

Introduction

Argonne is a leader for technology development with respect to laboratory-level evaluation of PEV wireless charging components at the subsystem and system level. As the international community of SDOs down-selects candidate approaches to various aspects of wireless charging equipment solutions, Argonne will continue to play a role in providing data from real-world components, subsystems, and systems that are used to make decisions in the iterative standards development process.

Refinement and verification of standards requires hardware and software for testing and evaluation. Because components are not readily available for wireless charging evaluation, Argonne has created testing hardware and software to evaluate interoperability, performance, efficiency, safety, alignment indication accuracy, and communication of candidate PEV wireless charging components and systems.

A key benefit of wireless charging of EVs, especially in the context of the now 20-year-old SAE J1773 inductive charging (also wireless) standard, is the greater air gap distance between the primary and secondary coils. Figure VII-50 shows the GM/Hughes MagnaCharge inductive system for the GM EV-1 electric car. The dotted line shows the off-board equipment (electronics and user 'paddle') that is the equivalent of the primary side ground-mounted coil in J2954. The electronics and battery to the right of the dotted line represent the secondary side of the J2954 system. The air gap for J1773 was typically several mm. The air gap between the primary (ground) and secondary (vehicle) coils in J2954 will be <100 mm.

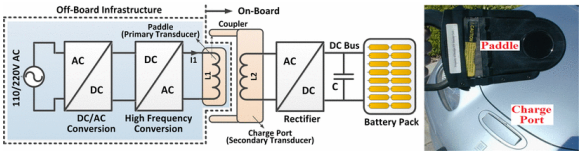

Figure VII-50: MagnaCharge J1773-mm gap wireless charging.

Approach

1. PEV Wireless Charging Component/System Test Equipment Development: J2954 Wireless Charging Standard

3-Axis Wireless Electromagnetic Coil Positioning System

SAE J2954 specifies many attributes and requirements of the primary (ground-mounted) side equipment, and secondary (vehicle-mounted) side equipment. The SAE J2954 standard has not yet been published. Therefore, at the request of the J2954 Committee Chair, only public domain attributes will be quoted in this report to keep draft document details out of public documents until the standard is finalized.

The J2954 standard calls for wireless charging systems to be tolerant of a misalignment of ±100 mm in the X and Y direction between the primary and secondary coils, as well as wide variations in the Z direction (see Figure VII-51 for the orientation conventions referenced here).

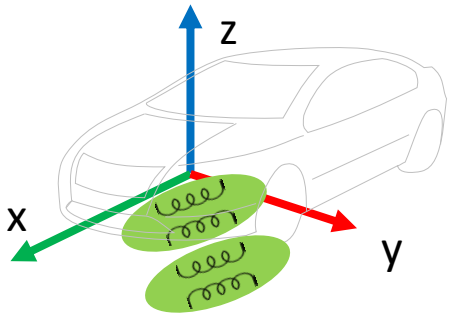

Figure VII-51: Basic wireless vehicle charging orientation of the ground-mounted (transmitting) primary side coil and vehicle-mounted (receiving) secondary coil-typical 100-mm gap.

Figure VII-52: Wireless vehicle charging positioning apparatus (1,000-mm Y and Z actuators; 1,500-mm X-axis actuator).

The fixture without any vehicle mounted shown in Figure VII-52, is comprised of an X-Y table with a 1,000-mm Y-direction closed loop linear actuator. In this configuration, the primary coil is on the ground, and the secondary coil is on the X-Y-Z positioning apparatus. The four red mini-column lifts are ACME screw-based, with a 5,000-lb capacity each. The X-axis table is 1,500 mm.

This apparatus is designed to be reconfigurable and easily transportable between lab spaces, as well as between test facilities. Figure VII-53 shows the vehicle system configuration with the Chevy Volt PHEV (with the wireless charging secondary coil mounted under the rear of the car) on the Z-axis actuator and the primary coil on the floor, between the vehicle wheels, on the X-Y positioning table. The Unistrut frame of the X-Y positioning table can accommodate several types/shapes of wireless charging hardware. The configuration shown here fits between the wheels (Y-axis) of the vehicle under test, since the secondary coil is beneath the trunk of the Chevy Volt in this case.

Figure VII-53: Wireless charging vehicle system-level configuration of the positioning apparatus (X, Y, and Z servo amplifiers/safety stops housed in the grey boxes; RF chamber behind).

The Narda EHP-200 field measurement probe is shown to the left of the vehicle as well. In FY14, this probe will be connected to a cascaded control loop (with X-Y-Z servos) to automate field measurements in and near the vehicle on the same graphical user interface (GUI). The ETS-Lindgren 100-dB attenuation vehicle-sized RF shielding chamber, which houses the vehicle/apparatus as per test plans that require shielding, is shown in the background. The apparatus in storage mode is shown in Figure VII-54.

Figure VII-54: Wireless vehicle charging positioning apparatus in storage/transport mode (stacks compactly; self-contained).

Safety and Reliability of the Positioning Apparatus

Figure VII-55 shows some safety and reliability enhancement features of the positioning apparatus. The Z-axis actuators are based on upgraded commercial column lifts, capable of 2,500 kg each, with CE and other safety certifications. The screw stop locks the pedestal in place during operation. The grey cabinets contain servo amplifiers, which direct power from the AC source to the closed loop, gear-reduced permanent magnet synchronous motor (PMSM) servos.

The Z-axis actuator motor was upgraded from a v-belt connected AC induction motor with on/off control to (5:1) gear-reduced 400-W closed loop PMSM servo motors driven through a cogged belt (shown in Figure VII-55). The gearbox along with the ACME lead screw is fail-safe and cannot be back driven by the mass of the vehicle in the event of a power failure or emergency stop. The system can maintain 1-mm repeatable accuracy over the 1,000-mm lift height.

Power from a single AC source for the servo amplifier is daisy-chained between all five grey enclosures (four z-axis, X-Y axis). Similarly, the serial fiber optic data lines (the orange leads visible in Figure VII-53) for communication and control of the positioning apparatus, are cascaded (send/receive loop) between enclosures back to the host PC/laptop outside the RF isolation chamber.

Figure VII-55: Wireless vehicle charging positioning apparatus safety and reliability features: stop screw, interlocks, limit switches, and upgraded gearbox servo systems (1-mm accuracy).

This setup avoids any electromagnetic interference into the control system from the wireless charging device under test and from the servo system into the device under test. It also avoids ground loops through the chamber pass-through barrier. Interrupting data communication (disconnecting the fiber optic link) or triggering a single unit E-stop halts the entire system in less than 1 second. The Z-axis lift and X-Y axis fiberglass Unistrut frame have redundant limit switches (shown in Figure VII-55) to cease travel at the end of stroke of the actuators in the case of user or software errors to maintain preset position limits.

User Interface Software for the Positioning Apparatus

Figure VII-56 shows the touch screen user interface on a host laptop with fiber optic serial communication to the X-Y-Z positioning apparatus. The Z-axis positioning user functions include coordinated Z-axis motion (all the same) or differential Z (pitch and roll of the vehicle) within preset vehicle angle safety limits. The user interface contains several innovative and time-saving features, such as the ability to 'auto-zero' the

Z-axis lifts to a repeatable point while engaging the lift arms on the deformable vehicle tires. The torque measurement system has a programmable threshold that is used to calculate when the vehicle is about to 'lift off' the ground and set that distance as 'zero' for the Z-Axis in a repeatable fashion. The X-Y axis actuators 'home' themselves to a lower count limit switch and then calculate 'zero' axis reference points from there.

Figure VII-56: J2954 Wireless charging system touch-screen user interface (multiple X-Y-Z inputs, preset locations, matrix of position arrays [script with jog], and direct coordinate entry).

Figure VII-57 shows a 'zero' position at the mechanical center of the vehicle secondary pad. Some SAE J2954 committee members want to make the primary side the zero reference point. However, others want to use the electromagnetic center as the zero point, which usually is not the mechanical center, as shown in the Evatran system primary-secondary alignment in Figure VII-57.

Figure VII-57: Example of the magnetic center of the wireless charging apparatus (not the same as the mechanical center, with respect to setting zero reference on the positioning fixture).

Electromagnetic Safety Monitoring/References

Figure VII-58 shows a summary of magnetic field (B, in µT) strength limits of exposure set by the standards/regulatory agencies, listed on the legend of the figure as a function of frequency. The solid and dashed green lines indicate the limits published by the German-based International Commission on Non-Ionizing Radiation Protection (ICNIRP). For the general frequencies proposed for wireless EV charging (>40 kHz–<150 kHz) standards, the approximate magnetic field exposure limits are 65 µT within 1 m of the edge of the vehicle. The definition and limits with 'zones' of field exposure around the vehicle are still under development within the SAE, IEEE, and IEC wireless vehicle charging standards.

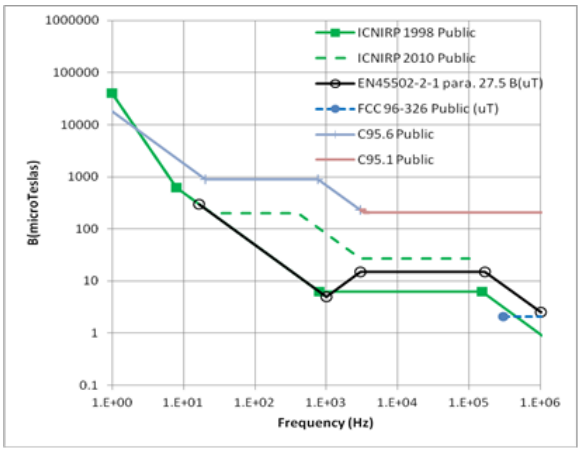

Figure VII-58: Summary of electromagnetic field safety limits, with regard to each SDO's interpretation of safety.

The Argonne wireless charging apparatus uses the industry consensus default electric and magnetic field 100-mm probe-based Narda EHP-200. Figure VII-59 shows the probe connected to the Argonne positioning apparatus control interface, to measure field strength as a function of throughput and misalignment. The data link for this instrument is also fiber optic-based. A safety perimeter is established with this probe. In FY14, this will be an automated process to 'sweep' the volume around and inside the vehicle via the door openings and probe mount. An FLIR E65 thermal imaging device is also tied to the host PC to collect min/max temperatures on the test apparatus.

Figure VII-59: Wireless charging positioning apparatus with Narda EHP-200 field probe (next to cart) and FLIR E60.

Figure VII-60 shows the non-ferrous fiberglass grating material proposed for testing of wireless charging systems over a conductive ground plane (such as in an industry standards RF shielding chamber). Testing of subsystem (component-level) wireless charging systems has the

advantage of being able to raise the combined primary and secondary coil mechanisms above the ground plane.

While testing complete vehicles in a shielded chamber (as opposed in an open space with a marked boundary/safety perimeter), the primary side coil must be separated from the ground plane to avoid interactions that are not present in earth/aggregate-based charging environments (non-conductive foundation, without steel reinforcing bars). The fiberglass grating provides a 'false floor' to raise the primary side coil positioning apparatus. The Z-axis lifts are already in place to raise the vehicle such that only a larger Z-position is required for more spacing above the ground plane to maintain the ~100-mm air gap between the primary/secondary side coils.

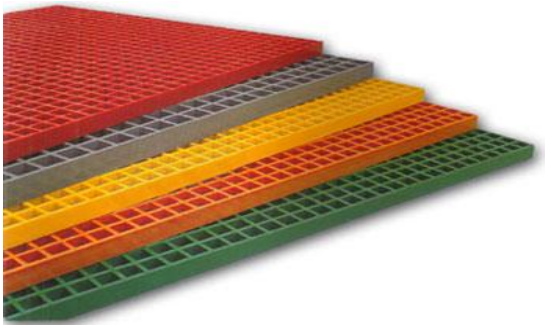

Figure VII-60: Commercial reinforced fiberglass grating to separate the primary coil positioning apparatus above the conductive ground plane while testing in the RF shielding chamber.

2. PEV Wireless Charging Test Equipment: Measurements for Evaluation of Production/Prototype Wireless Charging Hardware in Support of the J2954 Wireless Charging Standard

Inputs, Outputs, and Data Collection Systems

Figure VII-61 shows a section of the 'wall-to-wheels' power conversion sections to be evaluated for performance (throughput) and net energy delivered efficiency. Consistent with SAE J2894/2, the efficiency is Pout/Pin (where marked).

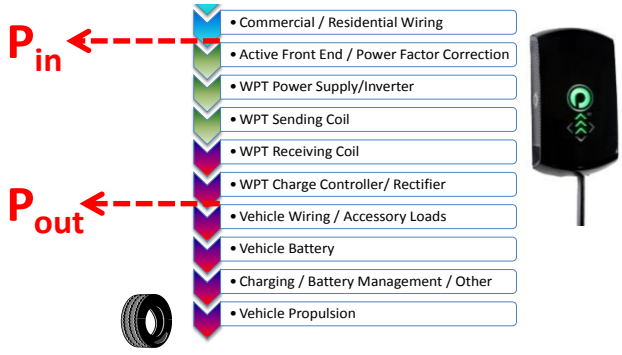

Figure VII-61: J2954 Wireless charging system performance and efficiency definition, consistent with the SAE J2894 EVSE-PEV power quality/efficiency recommended practice standard.

The SAE J2954 Wireless Charging recommended practice includes a section on testing recommended methods. The four areas addressed by testing include:

1. Safety (object detection, alignment guides, etc.)
2. Performance (net output or throughput)
3. Efficiency (net output divided by input)
4. Electromagnetic Field (EMF)—field emissions/leakage

The Argonne test equipment list related to evaluating wireless vehicle charging systems includes the following items:

1. AC programmable source (Ametek 6000LS; 6 kW)
2. DC programmable load (NHR 4760-600V; 6 kW)
3. 4-channel power meter (Hioki 3390)—Pin, Pout, Pcoil-in, and Pcoil-out
4. Electromagnetic field measurement (Narda EHP-200, 100-mm probe fiber optic)
5. RS485 via fiber optic, 8-channel thermocouple reader (Omega DIN-132)
6. Thermal/visible light imaging system (FLIR E60)
7. Communication link between the primary/secondary side (IEEE 802.11p/proprietary; vehicle information)
8. Coil position information (Argonne 3-axis positioning apparatus/GUI)

Wireless Charging Communication Implementation

At the request of the vendor via an executed Non-Disclosure Agreement (NDA), no detailed description of the Evatran wireless charging communication system will be provided in this report. Generally speaking, the Evatran Plugless Power aftermarket wireless charging system for Chevy Volt and Nissan Leaf vehicles is comprised of three sections, as shown in Figure VII-62:

1. Wall-mounted primary side 3.3-kW power electronics and controls (with Bluetooth communication link)
2. Floor-mounted primary side coil (1,100-lb drive over, 2.5"H x 22"W x 18"D)
3. Vehicle-mounted secondary coil and electronics (with Bluetooth communication link) (5"H x 30"W x 18"D)

Figure VII-62: Evatran wireless charging system hardware with Bluetooth communication between stationary and vehicle side electronics (open-loop interaction with the vehicle/CAN).

Communication messages with this evaluation unit are proprietary and cannot be compliant with the upcoming SAE J2931/6 wireless charging physical layer (IEEE 802.11p) implementation of international wireless charging standards for communication between the vehicle and stationary infrastructure.

Figure VII-63 shows the Argonne vehicle-infrastructure communication controller, which is described further in the Annual Report section **1000190.00 Grid Connectivity Support**. This module was constructed to support SAE J2931/4 (powerline communication over pilot wire) for DC

charging communication between the PEV and DC EVSE. It contains an iMX28 'system on module' computer, capable of serving as a proof-of-concept development platform for IEEE 802.11p (wireless) communication for wireless charging, and uses the SAE J2847/2 communication message that may be similar to the upcoming SAE J2847/6 wireless charging messages. These tasks are proposed for FY14, as standards are defined on the way to publication.

Figure VII-63: Argonne PEV-EVSE off-board charging system communication controller (also can accommodate the proposed IEEE 802.11p standard in J2931/6 wireless charging communication physical layer requirements).

3. Interoperability Evaluation Requirements for PEV Wireless Charging Test Equipment

Acquiring Sample Systems and Summarizing Attributes

Figure VII-64 shows another product from Brusa Electronics, a Swiss manufacturer of PEV charging electronics that claims 92% wall-to-battery efficiency at 3,700 W, with all electronics and communication built into the primary and secondary coil packages.

Figure VII-64: Commercial product (Brusa Electronics) self-contained 3.7-kW power electronics and electromagnetics with IEEE 802.11p wireless vehicle-charging communication.

Figure VII-65 shows another approach from Hevo, Inc. (New York) that uses faux manhole cover flush-mount implementation and square secondary side-vehicle-mounted coil/electronics.

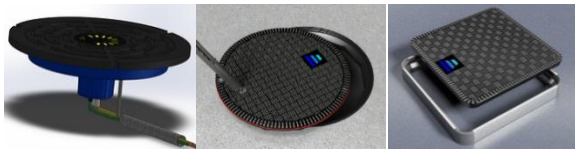

Figure VII-65: J2954 wireless charging system interoperability requirements. Example from Hevo Electronics: faux manhole-cover-shaped, sub-surface mount.

Figure VII-66 shows a very small air gap Qualcomm-Halo IPT wireless charging system implementation, which may not physically clear other manufacturer's surface-mounted primary pad coil (with sufficient air gap to allow for variation of vehicle ride height). Smaller air gap systems tend to have higher efficiency, but they are more selective and require better alignment.

Figure VII-66: Halo IPT wireless charging system interoperability requirement variations in the air gap (flush vs. surface mount).

Results

Argonne has designed, fabricated, and tested a transportable and reconfigurable 3-axis wireless charging positioning system to complement other traditional test equipment. This apparatus has and will continue to assist in collecting information used in development of wireless charging standards, including communication and interoperability:

- Contributed to the SAE standardization process by providing cursory test data from a representative (Evatran) pre-production W-EVSE device to support data-based decisions on EMF and safety aspects for the SAE committees/task groups related to wireless charging, testing, and communication (SAE J2954, J2931/6, J2847/6).
- Provided design and development of the aforementioned positioning fixture and test tools, with emphasis on collaboration with certification and test agencies to transfer knowledge and demonstrated capabilities to those who will provide the ultimate safety, throughput, efficiency, and EMF validation assessment for standardized, interoperable W-EVSE products.

Conclusions

Argonne's wireless charging apparatus and evaluation activity directly addresses the technology gaps in the area of wireless charging technology quantitative evaluations to support the SAE committees. Argonne and support contractors successfully demonstrated joint development of wireless charging positioning equipment and software as well as process development, thereby assuring relevance and mutual benefit to DOE and industry.

Focusing on near-term needs with long-term impact has been an effective approach for wireless charging system positioning apparatus and evaluation methods. These activities, with the collaboration of standards certification and compliance evaluation test agencies, facilitate development and verification of SAE J2954 (wireless charging) standards

as soon as possible. The EV-Smart Grid Interoperability Center is specifically designed to address the associated issues.

Argonne will continue to provide direct support to the SAE standardization process. This endeavor will include committee participation, development of enabling technologies, system integration, and laboratory testing.

VII.J.3. Products

Publications

1. Bohn, T., "Systems of Systems; Interactions of Wireless Charging Safety," presented at Underwriters Laboratory Annual Meeting, Willowbrook, IL, July 2013.

Tools and Data

1. Bohn, T., Python software-based user interface and safety system for 3-axis wireless charging positioning system. (RS485 serial interface control software package to set vehicle position, with optional control of the field measurement probe actuator system.)

VII.K. EV-Smart Grid Interoperability Center

Keith Hardy, Principal Investigator
Argonne National Laboratory
955 L'Enfant Plaza SW
Washington, DC 20024
Phone: (630) 816-7383
E-mail: khardy@anl.gov

Lee Slezak, DOE Program Manager
Phone: (202) 586-2335
E-mail: Lee.Slezak@ee.doe.gov

VII.K.1. Abstract

Objectives

- Establish an EV (Electric Vehicle)-Smart grid Interoperability Center at Argonne National Laboratory (Argonne) to accomplish the activities outlined in the Letter of Intent between the U.S. Department of Energy and the European Commission (EC) Joint Research Centre-Institute for Energy and Transport (JRC-IET)

Major Accomplishments

- Completion of facility modifications and development or installation of test equipment to conduct interoperability testing and verification according to proposed standards; as evidenced by the launch of the U.S. EV-Smart Grid Interoperability Center at Argonne on July 18, 2013.

Future Achievements

- Finalize and implement a joint Argonne/JRC-IET interoperability center work plan.
- Host an industry working group to ensure industry awareness and promote participation in U.S. and EC interoperability center activities.
- Support a joint testing work group at Argonne and JRC-IET to verify compatible capabilities, procedures and protocols.
  - EV performance, fuel and energy consumption, emissions and environmental impact (includes battery electric and plug-in hybrid electric vehicles)
  - Battery cells, modules and packs (performance, efficiency and abuse)
  - Interoperability of EVs, EV supply equipment (EVSE), and grid interfaces (connectivity and communication)
- Perform EV-EVSE compatibility/interoperability testing to identify opportunities to harmonize standards for future products.
- Support a joint study to identify opportunities to harmonize grid integration technologies and standards.
- Support a site-specific, cooperative EV interoperability project in the EU.

✧ ✧ ✧ ✧ ✧

VII.K.2. Technical Discussion

Background

As a result of the Transatlantic Economic Council's *Work Plan to Advance Transatlantic Cooperation on E-Mobility*, the U.S. Department of Energy (DOE) and the European Commission (EC) agreed to establish EV (Electric Vehicle)-Smart Grid Interoperability Centers in the U.S. (at Argonne National Laboratory [Argonne]) and Europe (at the Joint Research Centre-Institute for Energy and Transport [JRC-IET]). The Letter of Intent, signed in November 2011, included the following activities:

- *Establish state-of-the-art facilities* for development and testing of interface technologies encompassing connectivity between EVs, charging equipment, communication networks, electric transmission and distribution grid operators, and electric service providers.
- *Play an active role in standardization* by supporting data-driven standards refinement and development as well as a common approach for U.S. and EU testing of relevant EV and smart-grid equipment, all in an effort to promote cooperative development of and support for global standards.
- *Undertake projects to enhance interoperability* of EVs, recharging systems, and smart grids through, among other approaches, the development of more harmonized standards for connectivity, communication and component compatibility.
- *Participate, with EV-Smart Grid interoperability testing facilities for EVs and EV supply equipment (EVSE), in inter-laboratory comparisons through "round-robin" testing.*

Introduction

Programmatic activities have focused on realization of the Interoperability Center at Argonne through coordination with DOE, the U.S. Mission to the EU, the EC, and JRC-IET.

Technical activities focused on preparation of facilities and equipment to accomplish interoperability testing according to the proposed standards. This task required acquisition and/or development of components and test equipment as well as facility modifications. Descriptions of devices specifically developed for the Interoperability Center are included in the *Codes & Standards, Grid Connectivity R&D* report.

Approach

The three technical areas addressed in the interoperability centers—electric and hybrid vehicles, batteries, and interoperability—share a common objective to harmonize test procedures and protocols between the U.S. and EU. The basic approach is to perform comparable tests, compare and identify procedural and/or data acquisition differences, assess the potential for harmonization, and propose a compatible solution that meets the respective legislated/typical test conditions.

However, preparing the centers in the U.S. and EU to conduct comparable tests requires adequate resources, facilities and equipment. Financial resources for Argonne and JRC-IET are part of the direct research expenditures of DOE's Office of Vehicle Technologies and the EC's Seventh Framework Programme for Research, respectively. The approach to utilizing existing or new facilities/resources to support the Interoperability Center activities is summarized in the following paragraphs.

Vehicle Test Facilities

The well-established vehicle laboratories at JRC-IET and Argonne will conduct and compare system-level electric and hybrid vehicle tests to identify opportunities for harmonization of procedures and protocols employed to assess performance, fuel/energy consumption, efficiency, and emissions under legislated and realistic operating conditions.

JRC-IET's Vehicle Emissions Laboratory (VELA) is capable of measuring the emissions and environmental impacts of a range of vehicles from motorcycles to trucks; the lab determines the pre-certification test procedures for the EC. Since 2011, JRC-IET has been extending its VELA installations to specifically address EVs, and the modifications are expected to be complete by mid-2014.

Argonne's Advanced Powertrain Research Facility (APRF) was designed specifically as a testing laboratory for alternative-fuel vehicles. The APRF staff has extensive experience with electric and hybrid vehicle testing, previously defining the SAE standard fuel economy and emission test procedures for hybrid vehicles, and performs vehicle benchmarking and propulsion system studies for DOE on a regular basis. No modifications or support systems enhancements are required to support Argonne's activities to harmonize test procedures and protocols with JRC-IET.

Battery Test Facilities

Argonne has extensive test capabilities in place to evaluate battery cells, modules and battery packs. Argonne performs cell and module testing in the Center for Electrochemical Energy Storage and integrated battery pack testing at the APRF. No facility modifications or support systems enhancements are required to support Argonne's activities to harmonize test procedures and protocols with JRC-IET.

JRC-IET has been equipping its laboratories at Petten, Netherlands with test stands and X-ray tomography devices to enable battery cell performance testing, material studies, and abuse testing. JRC-IET and Argonne have collaborated on capabilities and equipment; the new laboratory is expected to be fully operational by the end of 2014 or early 2015.

Interoperability Standards

Interoperability standards are in the standards committee review process; hence the requirements for compliance have not been finalized. But Argonne has been active in developing the draft standards, facilities and tools to evaluate interoperability according to the proposed standards and test procedures.

U.S. EV-Smart Grid Interoperability Center

Argonne has equipped an existing high-bay facility with workbenches and installed or developed specialized equipment to perform AC and DC charging communication studies, assess EV-EVSE compatibility/interoperability, and evaluate inductive ("wireless") charging.

A key addition was a vehicle-sized electromagnetic isolation chamber to allow measurement of magnetic fields associated with wireless charging in a controlled environment.

To support the development and evaluation of energy management systems for controlling multiple EVSEs (e.g., workplace charging), a circuit was constructed for hardware-in-the-loop studies with multiple EVs, EVSEs, EV energy meters, and an interactive grid simulation.

Role in Standardization

Argonne technical staff members are very active in SAE standards committees related to grid connectivity and communication and participate in the related IEEE, NIST, ANSI and ISO activities. More specific information regarding committees and contributions is included in the ***Codes & Standards, Support for Vehicle Electrification*** report.

Projects to Enhance Interoperability

Argonne projects have focused on preparing the Interoperability Center to support the development and verification of EV-grid connectivity and communication standards. Several key enablers for interoperability testing were completed this year, including a communication controller platform, interoperability test fixtures, and an inductive "wireless" charging test fixture. These activities are summarized in the Results section below and detailed in the *Codes & Standards, Grid Connectivity R&D* report.

Results

Notable results this year include the launch of the U.S. EV-Smart Grid Interoperability Center at Argonne (with a technology demonstration of EV-EVSE-grid communication using proposed standards and technology) and hardware to enhance the Center's ability to perform interoperability testing.

U.S. EV-Smart Grid Interoperability Center

The EV-Smart Grid Interoperability Center at Argonne was successfully launched in mid-July 2013 with an event that included remarks by DOE and EC officials, a ribbon cutting (see Figure VII-67), and technology demonstrations. The technical session that followed addressed the immediate needs to accomplish interoperability and relevant technical

capabilities at the DOE national labs as well as European and U.S. perspectives from OEMs and standards organizations.

Figure VII-67: Official launch of the EV-Smart Grid Interoperability Center at Argonne.

Projects to Enhance Interoperability

Smartgrid EV Communication module

Argonne designed a communication controller platform, termed the Smartgrid EV Communication (SpEC) module, to support standardization and verification of DC charging communication displayed in Figure VII-68. The module can also be used to accomplish smart-grid communication and inductive "wireless" charging communication (FY 2014 projects). This platform was demonstrated successfully at the launch of the Center with a GM Volt, a BTC smart charger, and a workplace charging network simulation. With the software developed to emulate both a DC charger communication controller and a plug-in electric vehicle (PEV) communication controller, the platform will aid future standards development and interoperability activities.

Figure VII-68: Argonne communication controller platform (SpEC module).

Interoperability test fixture

Verifying interoperability necessitates testing the connectivity and communication between vehicles, charging systems, and the grid interface according to standard requirements and test procedures. Argonne developed a bench-top test system that displays real-time data versus the requirements, automatically post-processes the data, and generates reports that outline the requirements and indicate pass/fail. The inset in Figure VII-69shows the prototype of the next-generation fixture, a breakout tool that fits between the vehicle and standard SAE J1772 connector, resulting in a smaller, more mobile test system.

Figure VII-69: Argonne interoperability test fixtures.

Inductive "wireless" test fixture

Argonne and 2G Engineering designed and constructed an automated, flexible fixture to test "wireless" charging systems or components, with or without vehicles, using SAE standard interoperability requirements and test procedures. This system as pictured in Figure VII-70fits within the electromagnetic isolation chamber and supports a wide range of relative positions of the transmitter and receiver according to the standard. The system will automatically "zero" and gather electromagnetic field data in a predetermined pattern.

Figure VII-70: Argonne non-conductive "wireless" test fixture.

Inter-laboratory comparisons through round-robin testing

To ensure comparable procedures and results for vehicles, batteries and interoperability, tests will be conducted with the same or identical components/systems at Argonne and JRC-IET. Comparative testing will commence in mid-FY 2014.

Conclusions

The U.S. EV-Smart Grid Interoperability Center at Argonne is fully operational, supporting standards activities, and is well-equipped to aid in the development and verification of EV connectivity and communication standards.

Collaboration with JRC-IET is ongoing to ensure compatible capabilities at the interoperability centers in the U.S. and EU. The schedule for facility modifications and equipment enhancements at JRC-IET will allow cooperative projects to commence in FY 2014.

VIII. VEHICLE SYSTEMS OPTIMIZATION

THERMAL CONTROL

VIII.A. Thermal Control through Air-side Evaporative Heat Removal

Dileep Singh, Principal Investigator
Argonne National Laboratory
Address: 9700 S. Cass Avenue
Argonne, IL 60439
Phone: (630) 252-5009
E-mail: dsingh@anl.gov

Lee Slezak, DOE Program Manager
Phone: (202) 586-2335
E-mail: Lee.Slezak@ee.doe.gov

VIII.A.1. Abstract

Objectives

- Explore possibilities of using evaporative cooling for air-side heat removal in heavy-duty truck radiators
- Determine radiator air-side heat removal rate for evaporative cooling
- Determine radiator size reductions for evaporative cooling
- Optimize radiator evaporative fin designs

Major Accomplishments

- Developed theoretical models for analyses of radiator air-side evaporative cooling
- Completed detailed calculations to establish the benefits of the concept
- Conducted numerical simulations for investigations of the air flow effect on water droplets

Future Achievements

- Investigate coating or surface treatment methods and materials to generate proper surface tension
- Experimentally measure the droplet contact angle
- Experimentally investigate droplet evaporation and movement

✧ ✧ ✧ ✧ ✧

VIII.A.2. Technical Discussion

Background

This project is aimed at exploring the possibilities of reducing the cooling system size and, therefore, aerodynamic drag on class 8 heavy-duty trucks by using evaporative cooling under the extreme temperature, load, and road grade conditions that would be encountered in the United States.

Introduction

Aerodynamic drag is a major contributor to fuel consumption in class 8 heavy-duty trucks, especially at highway speeds. Aerodynamic drag, i.e., the resistance to truck movement through the air, consists of two main components, pressure drag and shear drag. The shear drag for trucks usually is small compared to the pressure drag, and the basic shape of a truck imposes the pressure drag on the vehicle. Typically, a high-pressure zone is created in the front of the tractor due to the stagnation effect, and a low-pressure zone is created in the rear of the truck, both resulting in pressure drag. The frontal shape of the tractor is dictated, in large part, by the radiator, resulting in a large stagnation area. The method for reducing aerodynamic drag on trucks proposed in this study is to modify the front of the tractor by using a hybrid radiator-cooling system, a combination of conventional air-side finned surface cooling and active evaporative water cooling.

Approach

Figure VIII-1b shows a hybrid radiator compared to the conventional radiator of Figure VIII-1a. The example hybrid radiator-cooling system is similar to the conventional radiator with vertical coolant channels and fins between them on the air side. However, the channels have been extended beyond the fins on the downstream air side of the radiator. Liquid water flows downward by gravity along the extended surfaces, providing evaporative cooling to the engine coolant. The hybrid radiator also includes a liquid supply and distribution system not shown in Figure VIII-1.

Figure VIII-2 shows a top view of a section of the hybrid radiator. In this schematic, the extended channel surfaces are cooled by evaporating water flowing downward by gravity into the plane of the figure. The combination of the conventional cooling from the finned surfaces and the evaporative cooling from the extended channel surfaces is the total heat transfer

from the radiator to the atmosphere. Under the thermal design condition, both cooling mechanisms would be functioning. However, at most thermal loads (q_{total}) below the design condition, only the conventional air-side finned surface cooling would be required. Thus, the active cooling of the water evaporation would be used only at or very near the thermal design condition.

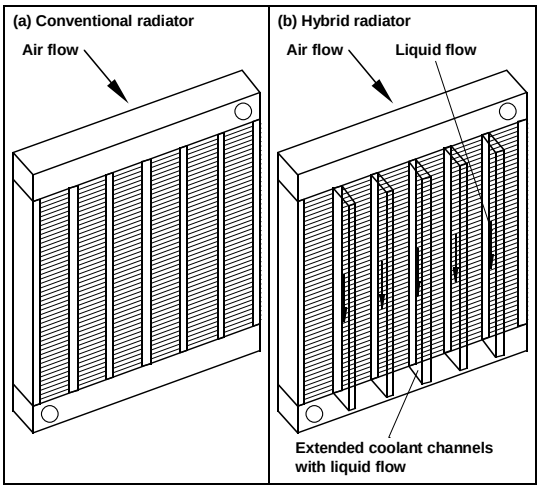

Figure VIII-1: Hybrid Radiator System.

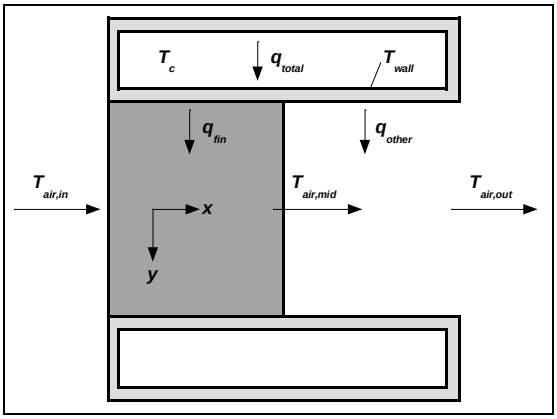

Figure VIII-2: Top View of a Section of the Hybrid Radiator.

This limited use of the active evaporative cooling component of the hybrid radiator cooling system is important because evaporative cooling requires a supply of water. Using evaporative cooling only at or very near the thermal design condition serves to optimize the parameters of reduced radiator size (or increased maximum radiator heat transfer) and minimized water use/transport.

Results

Heat Transfer Increases

Heat removal rates were calculated for the hybrid radiator with a 221.8-kW heat rejection rate and outside air temperature fixed at 47°C. Figure VIII-3 shows the heat removal rate as a function of water consumption rate generated using falling liquid film evaporation. At water consumption rates of 76 L/h (20 gal/h) and 189 L/h (50 gal/h), the total heat removal rate increases by 42 kW and 102 kW, respectively, which are equivalent to the heat removal rate increase of 19% and 46%, respectively. A small part of this increase (~3 kW) is due to the increased surface area associated with the coolant channel extensions of the hybrid radiator design. The rest of the sizable increase in the heat removal rate is due to evaporative cooling. At both of these flow rates, the cooling water would have completely evaporated before reaching the bottom of the radiator.

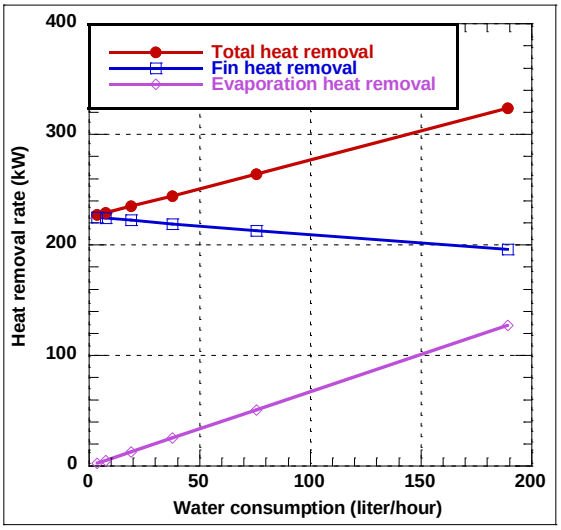

Figure VIII-3: Increased Radiator Heat Transfer.

Radiator Size Reductions

The radiator width as a function of the water consumption rate was calculated for a thin falling film under the conditions of an engine speed of 1700 rpm with a 221.8-kW heat rejection rate and the outside air temperature of 47°C. The original width of the radiator in this study was 988 mm. As shown in Figure VIII-4, at water consumption rates of 76 L/h (20 gal/h) and 189 L/h (50 gal/h), the width could be reduced to 778 mm and 478 mm, respectively, which correspond to radiator frontal area decreases of 21% and 52%, respectively. In each case studied, the film was assumed to completely evaporate before reaching the bottom of the radiator. Using droplets instead of a film will give the same potential for area reduction as long as the droplets completely evaporate. Note that if the frontal area of the tractor were modified to account for the reduced radiator size that can be achieved by the hybrid cooling system, aerodynamic drag would also be reduced, thereby increasing fuel efficiency.

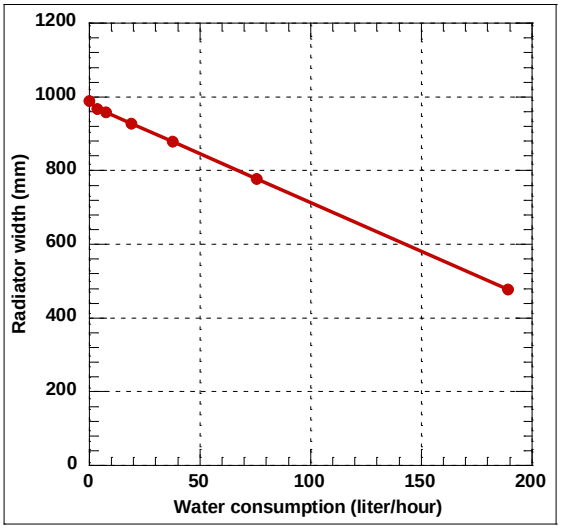

Figure VIII-4: Reduced Radiator Size.

Radiator Design Optimization

The design condition for truck and automobile radiators usually is the most severe condition possible: the highest air temperature and the steepest road grade. Many vehicles may never encounter the extreme conditions found at places such as Baker Grade in California or Union Pass in Arizona in a hot summer afternoon. A good approach to evaporative cooling is to size the finned portion of the radiator for an alternative design condition corresponding to a steep road grade away from the desert hills. Thus, water for evaporative cooling would be needed only when a vehicle travels through the desert hills under extremely hot conditions. An 11-kilometer (7-mile) stretch of land along Interstate Highway 24 near Monteagle, Tennessee, is an example of a steep road grade that could be used for the alternative design condition for the finned portion of the radiator. In a typical meteorological year for Chattanooga, Tennessee, near Monteagle, the highest temperature can reach 37 °C. If the radiator were sized for this location with the same coolant temperatures and heat transfer rates, then the radiator could be 22% smaller in width compared to the Baker Grade design condition. Thus, on the majority of roads in the United States, the smaller radiator would be sufficient. Under conditions of 47 °C and constant full engine power for a long period of time, the water flow rate of approximately 76 L/h (20 gal/h) would be needed to remove the remainder of the heat. Since it takes less than one hour to traverse the 40-kilometer (25-mile) Baker Grade and 48-kilometer (30-mile) Union Pass, the amount of water consumed would be less than 76 liters (20 gallons) for either of them with this design modification.

Effect of Surface Contact Angle

At a 76-L/h (20-gal/h) flow rate, the actual flow rate on each extended surface of the hybrid radiator is only 0.107 mL/s. At this low flow rate, the liquid film across the 20-mm radiator extension surface is only 0.11-mm thick and has a tendency to break up into rivulets or droplets such as streaks. Because of this tendency, an analysis was performed with the evaporating liquid film replaced by evaporating discrete droplets falling along the extended radiator channel surfaces. Such droplets have good potential to be maintained at the required thickness. For 100% evaporation of the droplets as they reach the bottom of the radiator, the amount of additional heat transfer using the droplets is similar to that using the falling film.

The droplet evaporation results showed that the thickness of the droplets from the radiator extension surfaces is the most important parameter governing both the evaporation rate of the droplets and the speed at which the droplets travel along the surfaces. As shown in Figure VIII-5, the droplet moves downward under the influence of gravity. By using this model, we calculated the droplet evaporation percentage as a function of the initial contact angle (a key factor for the thickness of the droplet). As evident in Figure VIII-6, a small droplet contact angle (or equivalent small droplet thickness) is necessary for complete evaporation.

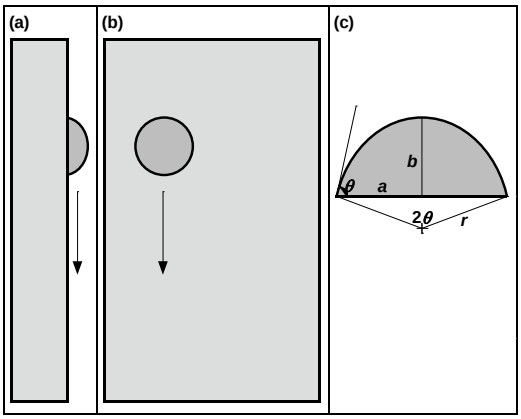

Figure VIII-5: Droplet Movement.

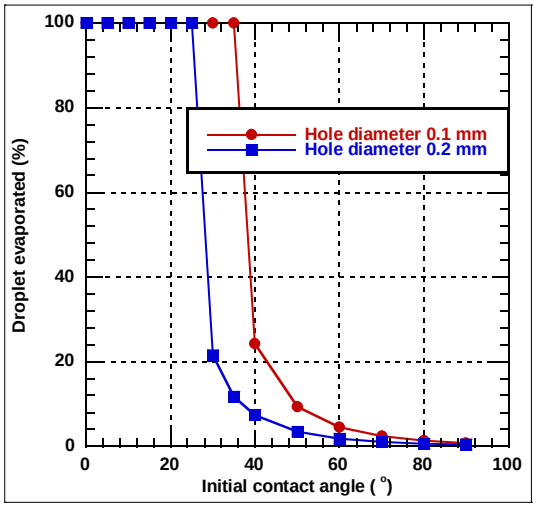

Figure VIII-6: Droplet Evaporation.

Air Flow Effect on Droplet Movement

For a moving vehicle, the droplet is under the influence of the drag force in addition to gravity. As shown in Figure VIII-7, the droplet moves downwards and in the air flow direction during the evaporation process. The droplet movement depends on the force balance among gravity (F_g), air drag force (F_d), and wall shear force (F_s). These forces and the

velocity (u) are related by the following equations for a droplet volume V (Figure VIII-7):

To analyze the air-flow effect on droplet movement, we performed numerical simulations using the commercial software COMSOL for various air flow speed and droplet hole size combinations. Figure VIII-8 shows the evaporation percentage of the droplet as a function of its initial contact angle for an air flow speed of u_{air}=35 mph, an extended surface width of 20 mm, and droplet hole sizes of 0.1 mm and 0.2 mm. As can be seen from Figure VIII-8, droplets with a small initial contact angle were able to stay on the surface until they completely evaporated. Thus, the droplet generation and surface characteristics of the radiator extension surface must produce a small initial drop thickness for the most efficient operation of the hybrid radiator-cooling system. This condition requires a small droplet size and a small surface contact angle.

$$\begin{cases} F_d - F_s \dfrac{\bar{u}_x}{\sqrt{\bar{u}_x^2 + \bar{u}_z^2}} = \rho_w V \dfrac{d\bar{u}_x}{dt} \\ F_g - F_s \dfrac{\bar{u}_z}{\sqrt{\bar{u}_x^2 + \bar{u}_z^2}} = \rho_w V \dfrac{d\bar{u}_z}{dt} \end{cases}$$

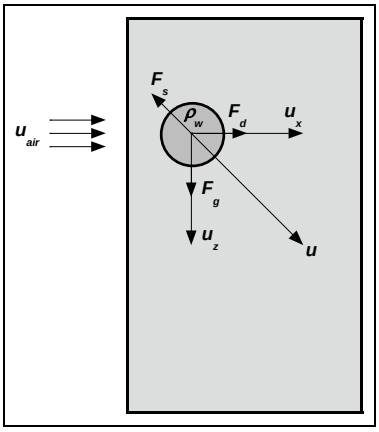

Figure VIII-7: Air Flow Effect.

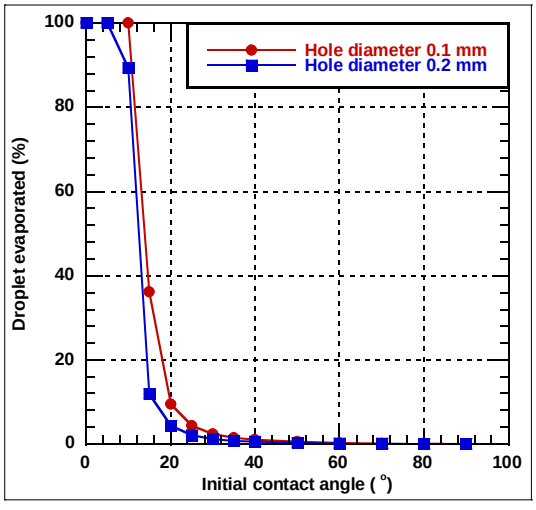

Figure VIII-8: Droplet Evaporation with Air Flow Effect.

There are several approaches to increase the droplet evaporation percentage: (a) larger width of the extended surface, which is usually limited by the available space, (b) frontal extended surface arrangement instead of rear extended surface arrangement, which increases the effective surface width for droplet movement, and (c) smaller surface contact angle, which reduces the air drag force and enhances evaporation. Because the surface contact angle for the common radiator material 3003 aluminum alloy is about 90°, surface treatment or coating will be necessary to reduce the surface contact angle to acceptable levels. Current technologies are able to produce such levels. Therefore, the third approach provides good potential for small thickness of a droplet and effective evaporative cooling for vehicle engines.

Conclusions

Coolant radiators in trucks and automobiles were shown to be amenable to evaporative cooling. Using a hybrid truck radiator, heat transfer increases of 19% and 46% were obtained with water flow rates of 76 L/h (20 gal/h) and 189 L/h (50 gal/h), respectively. These results are dependent on the establishment of water flow with small thickness from the radiator surfaces. We found that such thickness could readily be obtained by using droplet flow with contact angle management.

An alternative to the heat transfer increase from an existing radiator with the addition of evaporative cooling is reduction in radiator size. It was shown that, at the design heat load, the water flow rates of 76 L/h (20 gal/h) and 189 L/h (50 gal/h) yield radiator area reductions of 21% and 52%, respectively.

A good potential utilization of evaporative cooling was considered wherein the finned portion of the radiator was designed to accommodate all driving conditions except for desert hills. In this case, water for evaporative cooling would only be needed when a vehicle travels through desert hills under extremely hot conditions. We found that the radiator area could be reduced by 22% when only 76 L (20 gal) of water is used to traverse an extreme desert hill, such as the Baker Grade.

Numerical simulations using the commercial software COMSOL showed that the key factor for effective use of evaporative cooling is the initial droplet thickness, which depends largely on the droplet size and the surface contact angle. Small droplets and contact angles generate small droplet thicknesses with effective evaporative cooling. Future research will focus on these aspects to realize the evaporative cooling technology.

VIII.A.3. Products

Publications

1. D. M. France, D. S. Smith, and W. Yu, Efficient, *Active Radiator-Cooling System*, to be published in the SAE Journal of Commercial Vehicles.

Patents

1. D. M. France, D. S. Smith, W. Yu, and J. L. Routbort, *Hybrid Radiator Cooling System*, patent pending, U.S. 2013/0233517 A1, September 2013.

VIII.B. Aerodynamics and Underhood Thermal Analysis of Heavy / Medium Vehicles

Tanju Sofu, Principal Investigator
Argonne National Laboratory
9700 S. Cass Avenue
Argonne, Illinois-60439
Phone: (630) 252-4500
E-mail: tsofu@anl.gov

Lee Slezak, DOE Program Manager
Phone: (202) 586-2335
E-mail: Lee.Slezak@ee.doe.gov

VIII.B.1. Abstract

In this work, external aerodrag analysis and underhood cooling simulations are carried out using STAR-CCM+V8® commercial software.

A significant reduced aerodrag is observed with modified roof, trailer box and side extenders and side skirts. The performed analysis shows side deflectors increases the drag by 1.5%. 10% drag reduced with modified roof, which is aligned to the height of the trailer box. 5% reduced drag observed with flat bed and smooth surface trailer box. 10% drag reduced with rounded smooth corners in a trailer box. The overall improved design saves 14% of the fuel as compared to the base case.

The observed temperatures in Charge Air Cooler (CAC) and radiator using the modified side edges drops to value of 2°C as compared to base case. On the other hand, the significant reduction of the temperature predicted with fan blade angles. The highest reduced temperature observed at 45° fan blade angle. Moreover, with lowering the flow resistance across the CAC and radiator also reduces the temperature as compared to the base case.

Objectives

- **Medium Vehicle:** The aim of this project is to develop a methodology to simulate medium vehicle external areodynamics. The main focus of this project is to optimize the external vehicle design by modifying surfaces of the cabin and trailer.
- **Heavy Vehicle:** The aim of this project is to develop a methodology to simulate heavy vehicle underhood and its external areodynamics. The main focus of this project is to optimize the underhood compartment by modifying Charge Air Cooler (CAC) and radiator.

Major Accomplishments

- A significant aerodrag reduction is observed with modified roof, trailer box, side extenders and side skirts
- 10% drag reduced with modified roof, which is aligned to the height of the trailer box
- 5% drag reduced with flat bed and smooth surface trailer box
- 10% drag reduced with rounded smooth corners in trailer box
- The overall improved design saves 14% of the fuel as compared to the base case
- Modified side edges of CAC and radiator performs better thermal efficiency
- Tight clearance, i.e., closed gap, between CAC and radiator improves the thermal efficiency

✧ ✧ ✧ ✧ ✧

VIII.B.2. Technical Discussion

Background

The importance of optimizing the heavy vehicle thermal system is inevitable due to continuous increase in energy demand. The heavy vehicle thermal system consists of underhood compartment which comprises of engine, cooling devices, radiators etc. The available underhood configuration utilizes a fraction of total fuel energy in terms of mechanical power and the rest is lost through the exhaust system and heat rejection. An accurate temperature distribution in and around the engine allows redesign of a heavy vehicle underhood configuration and helps achieve fuel efficiencies through cooling system optimization. The proposed work is strongly recommended to replace experiments to design feasible prototypes of the heavy vehicle. Computational Fluid Dynamics (CFD) will be the main tool in designing, simulating and optimizing the underhood configuration and the external aerodynamics of the heavy vehicle.

Due to stringent environmental regulations, emission control technologies have to meet the new diesel engine emission requirements and the involved challenges for the optimization of unique heavy vehicle underhood thermal control. The optimization of the heavy vehicle performance can be obtained by reducing the size of cooling system or reducing the air inflow.

Technical Barriers

- The imported CAD data from the Cummins Inc. has to be cleaned and generate the mesh in a preprocessing tool
- Identifying the state-of-the-art models from the literature
- Developing the methodology
- Testing the models for generic cases
- Including additional physics in the model, if necessary
- Model validation with prototypes

- Finally, optimizing the external aero drag and underhood configuration

Technical Targets

- CAD surface cleaning, i.e., surface wrapping
- Surface and volume mesh generation
- Physics models (e.g., turbulence)
- Identifying and improving the external vehicle surfaces to reduce the drag
- Identifying the possible thermal efficient underhood configuration design of the vehicles

Introduction

The optimum designing of the new/existing medium/heavy vehicles are invaluable to increase the fuel economy. To meets today's energy demand the improved designs are inevitable in achieving energy efficient vehicles in the transport sector. Several Industries and research institutions are focusing on fuels and fuel efficient vehicles [1]. In this work, aerodynamic and underhood thermal analysis of the medium and heavy vehicles are performed to optimize the design.

The external aerodynamic analysis is carried out using STAR-CCM+ CFD tool by several combinations of modifying the design including the second generation drag reduction devices, i.e., underbody skirts, roof deflectors, avoiding the sharp corners and rough surfaces of the trailer, adjusting the alignment of the trailer and roof deflector and including side extenders.

On the other hand, thermal analysis is performed for underhood design of heavy vehicle using STAR-CCM+ [2]. The external airflow cooling is performed by varying geometry configurations and operating conditions of fan and heat exchangers including modified side edges, fan blade angles and flow resistances across the Charge Air Cooler (CAC) and radiator.

Approach

Aerodrag simulations: 3d isothermal steady state simulations are carried out using segregated solver in STAR-CCM+. The gas-phase turbulence is modeled using k-ε with standard parameters. The operating and feed conditions are seen in Table VIII-1.

Underhood simulations: 3d non-isothermal steady state simulations are carried out using segregated solver in STAR-CCM+. The gas-phase turbulence is modeled using k-ω with standard parameters. For Fan, Moving Reference Frame (MRF) is implemented with fan performance curve table. The operating and feed conditions are seen in Table VIII-2.

Table VIII-1: Medium vehicle operating conditions for aerodrag simulations.

Operating conditions	
Velocity Inlet [m/s]	25
Temperature Inlet [K]	300
Yaw angle [deg]	0–6
Outlet Pressure [atm]	1
Wind tunnel dimensions [m^3] [Length x width x height]	65 x 30 x 16
Number of hexahedral cells [millions]	30
Side walls	Periodic

Table VIII-2: Heavy vehicle operating conditions for underhood simulations.

Operating conditions	
Velocity Inlet [m/s]	8.94
Temperature Inlet [K]	300
CAC heat rate [kW]	48.5
Radiator [kW]	110
Fan rotation speed [RPM]	1400
Yaw angle	0
Outlet Pressure [atm]	1
Wind tunnel dimensions [m^3] [Length x width x height]	41 x 20 x 11
Number of polyhedral cells [millions]	30

Results

As seen in Figure VIII-9, the base case model consists of cabin, side deflectors, mirrors, roof, chassis tires and trailer.

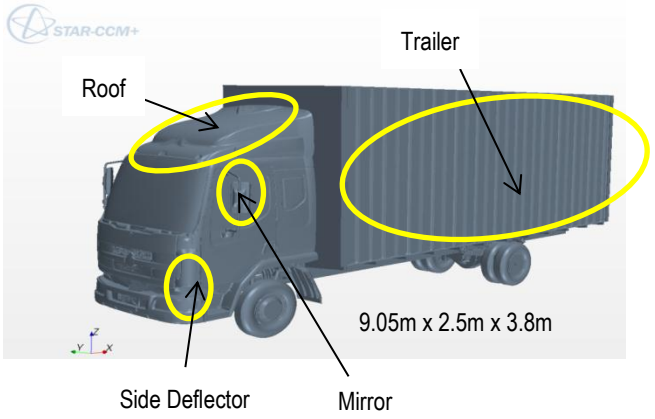

Figure VIII-9: Schematic diagram of medium vehicle.

Cabin Analysis

As seen in Figure VIII-10, the following observations are made:

- 2.2% drag coefficient reduced with M7 mirrors as compared to M3 mirrors (M7&M3 mirrors geometry supplied by Cummins Inc. Columbus, Indiana)
- 1.5% drag coefficient raised with side deflectors as compared to without side deflector

The observed drag reduced with M7 mirrors as compared to M3 mirrors. On the other hand, the side deflectors doesn't improve drag coefficient instead it rises as compared to without the side deflectors.

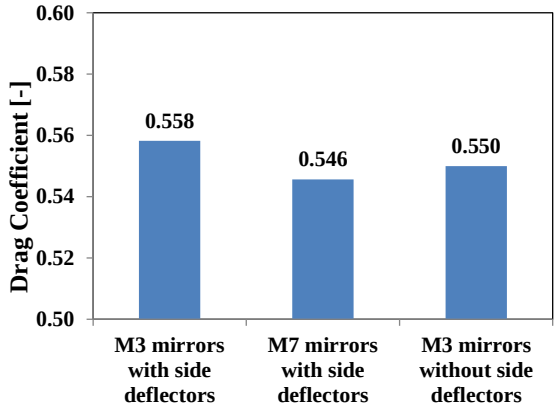

Figure VIII-10: Medium vehicle drag comparison of different mirror configuration.

Cabin+Trailer

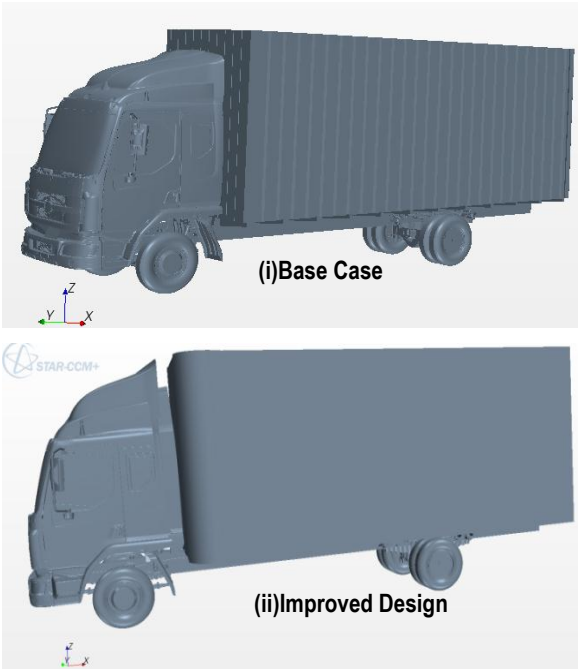

Figure VIII-11: Schematic diagram of (i) Base case (ii) Improved design of medium vehicle.

Table VIII-3: Comparison of Base case Vs. Improved design.

Base Case	Improved Design
Rough surface Bed & Trailer	Smooth surface Bed & Trailer
Base case roof extender	Modified roof extender
No side extenders	Side extenders
Sharp corners trailer box	Rounded corners trailer box

As seen in Table VIII-3, the main improved design changes are including smooth surface bed and trailer with rounded front corners, modified roof extender which is aligned with the height of the trailer box and side extenders.

As seen in Figure VIII-11, the significant drag reduction observed with improved design for all Yaw angles as compared to the base case.

Underhood Simulations

As seen in Figure VIII-12, the highest mass flow rate is observed at fan blade angle of 45° and it consequently reduces the temperatures of the radiator and the CAC (not shown). The fan operating conditions can be seen in Table VIII-2.

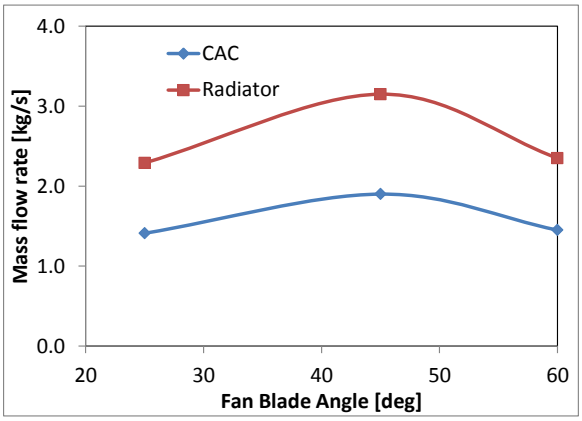

Figure VIII-12: Heavy vehicle mass flow rates Vs. Fan blade angle.

As seen in Figure VIII-13, the following recirculation zones are observed (i) In-front of the CAC, (ii) top of the radiator and shroud, (iii) between fan and engine block and (iv) beyond and top of the engine block. These recirculation zones can be avoided by using modified configuration (e.g., flaps).

As seen in Figure VIII-14, low velocity and high pressure zones are due to partial opening of the front grill in heavy vehicle. Consequently low velcoity zones leads to high temperature regions in CAC. These zones are avoided by using flaps infornt of the CAC inorder to obtain uniform velcoity and temeprature distributions (not shown). The flaps can help to avoid hot spots, i.e., high temperature zones in the heat exchangers or engine components.

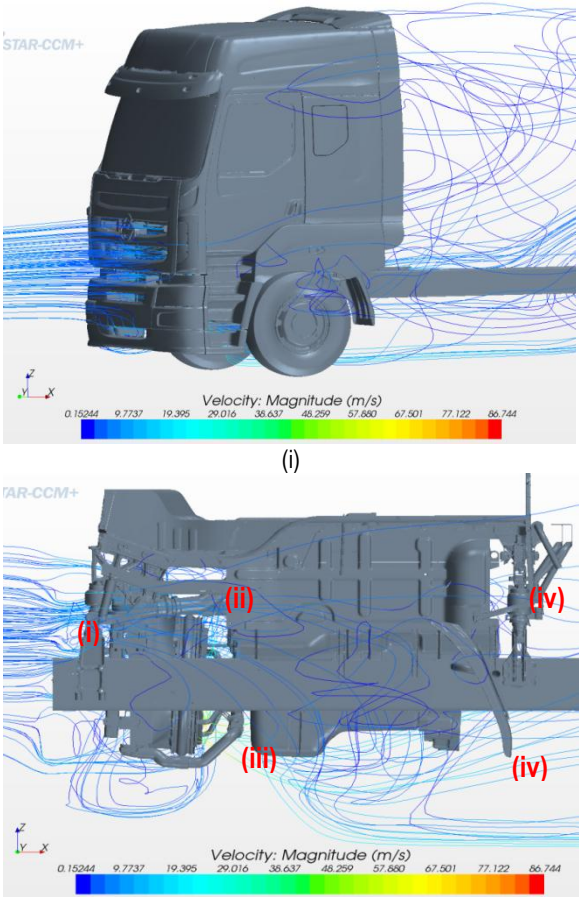

Figure VIII-13: (i&ii) Velocity streamlines of heavy vehicle.

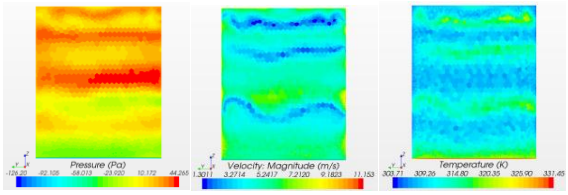

Figure VIII-14: CAC (i) Pressure (ii) Velocity and (iii) Temperature.

As seen in Figure VIII-15, the highest temperature zone is observed in the center of the radiator. This is due to CAC hot stream and it directly enters to the radiator without mixing fresh cold air as compared to the side edges (only part of the radiator is coverd by CAC, see in Figure VIII-16).

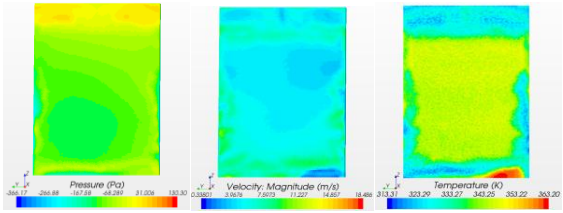

Figure VIII-15: Raditor (i) Pressure (ii) Velocity and (iii) Temeprature.

As seen in Figure VIII-16, at side edges low temperatures are due to fresh cold air from the sides of the CAC (due to difference in size of the CAC and radiator)

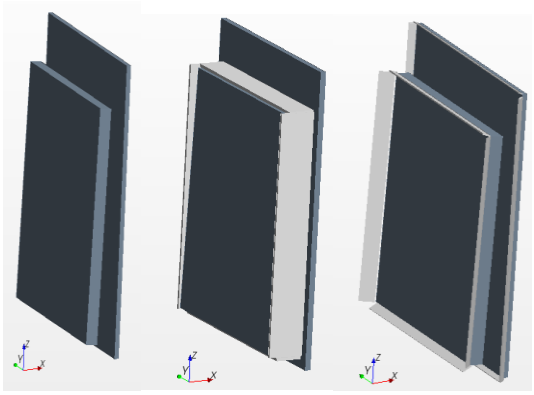

(i) Base Case (ii)Tight Clearance (iii)Side edges

Figure VIII-16: Underhood configuration of CAC and radiator (i) Base case (ii) Tight clearance between CAC and radiator and (iii) Modified side edges.

Table VIII-4: Thermal comparison of different configurations of the CAC and radiator (Figure VIII-16).

Component(s)	Temperature reduction as compared to base case [%] [CAC and Radiator gap closed]	Temperature reduction as compared to base case [%] [Modified side edges]
CAC	14.0	3.50
Radiator	2.10	3.53

As seen in Table VIII-4, the highest temperature reduction in CAC is observed in tight clearance configuration as compared to the base case. This is due to the effective fan suction pressure on CAC. On the other hand, the temperature reduction is same in the both modified geometry as compared to the base case (Figure VIII-16).

Conclusions

A significant reduced aerodrag was observed with modified roof, trailer box, side extenders and side skirts. The performed analysis shows 10% drag reduced with modified roof, which was aligned to the height of the trailer box. 5% reduced drag observed with flat bed and smooth surface trailer box. 10% drag reduced with rounded smooth corners in a trailer box. The overall improved design saves 14% of the fuel as compared to the base case.

The observed temperatures in CAC and radiator using the modified side edges drops to value of 2°c as compared to base case. This was mainly due to the high cross sectional flow surface area in the modified design. On the other hand, the significant differences of the temperature were predicted with various fan blade angles. The highest reduced temperature observed at 45° fan blade angle. This was mainly due to the high pressure drop that leads to high flow rates.

Future Plan

- Minimizing/avoiding underhood air recirculation with modified design (e.g., using flaps). In general recirculation, drops the temperature of CAC and radiator
- Moving shroud and fan to center of the radiator
- Closing the outer ring of the fan with shroud
- Cross validation of the results with Exa PowerFLOW® and STAR-CCM+V8®

References

1. Lee, S. Advanced vehicle technology Analysis and Evaluation Activities and Heavy Vehicle Systems Optimization Program. U.S. DOE APR, 2008.
2. Brotz, F.; Guilbaud, F. BEHR Fan Modeling Approach: Star European Conference, 2011.

VIII.B.3. Products

Publications

1. S.N.P.Vegendla and T. Sofu. External Aerodynamic Analysis for Optimization of Medium/Heavy Vehicles. 2013 PostDoctoral Research and Career Symposium, 10th&11thOct'2013
2. S.N.P.Vegendla and T. Sofu. Underhood Thermal Analysis for Optimization of Heavy Vehicles. 2013 PostDoctoral Research and Career Symposium, 10th&11thOct'2013

Tools and Data

1. STAR-CCM+V8®
2. Pro-Engineer, PTC®

VIII.C. Experimental Investigation of Coolant Boiling in a Half-Heated Circular Tube—CRADA with PACCAR

Dileep Singh/Wenhua Yu,
Principal Investigators
Argonne National Laboratory
9700 S. Cass Avenue
Argonne, IL 60439
Phone: (630) 252-5009
E-mail: dsingh@anl.gov

Lee Slezak, DOE Program Manager
Phone: (202) 586-2335
E-mail: Lee.Slezak@ee.doe.gov

VIII.C.1. Abstract

Objectives

- Understand and quantify heat transfer for subcooled engine coolant boiling in heavy-duty vehicles.
- Experimentally determine subcooled flow boiling heat transfer rates and limits in the cylinder head region of heavy-duty vehicle engines.
- Develop predictive mathematical models for subcooled boiling heat transfer.
- Provide measurements and models for development/ validation of heavy-duty vehicle engine computer codes.

Major Accomplishments

- Completed the conceptual design, the technical design, and the fabrication of the an experimental test facility and support systems.
- Completed the LabVIEW-based data acquisition and test control hardware and software.
- Completed heat loss calibrations of the experimental test facility.
- Completed single-phase convective heat transfer experiments and data reduction with three test fluids.
- Completed subcooled boiling heat transfer experiments and data reduction with three test fluids for various flow rates.

Future Achievements

- Develop predictive mathematical models for subcooled boiling heat transfer based on experimental data.
- Perform subcooled boiling experiments and data analyses for three test fluids at the higher pressures of heavy-duty vehicle engine applications.

✧ ✧ ✧ ✧ ✧

VIII.C.2. Technical Discussion

Background

Started in FY 2010 as a cooperative research and development agreement (CRADA) between Argonne National Laboratory and PACCAR Inc./DAF Trucks N.V. (PACCAR/DAF), this project aims to provide heat transfer and critical heat flux (CHF) measurements and models of subcooled coolant boiling in the cylinder head region of heavy-duty vehicle engines to be used for development and validation of heavy-duty vehicle engine computer codes.

Introduction

Currently, the engine cooling systems in heavy-duty vehicles are designed to use an approximately 50/50 ethylene-glycol/water (EG/W) mixture in the liquid state. Boiling is usually a phenomenon that has been avoided in conventional engine cooling systems in heavy-duty vehicles. However, while the conventional engine cooling systems in heavy-duty vehicles are designed to eliminate coolant saturation boiling, coolant subcooled boiling in the cylinder head regions is unavoidable at high thermal loads due to the high metal temperatures. Because of its order-of-magnitude higher heat transfer rates, there is interest in using controllable nucleate-boiling precision cooling instead of conventional single-phase forced convection cooling in vehicle cooling systems under certain conditions or in certain engine areas to remove ever increasing heat loads, eliminate potential hot spots in engines, or further optimize the parasitic losses of the coolant pump. Theoretical, numerical, and experimental investigations have been conducted on the potential and the practical application of nucleate boiling cooling systems in heavy-duty vehicles. Consequently, there is great interest in the flow boiling heat transfer rates and limitations under these application conditions.

One of the unique characteristics of coolant subcooled boiling in the cylinder head regions of heavy-duty vehicle engines is that boiling generally occurs only on the cooling channel side facing the flame plate because of the one-sided heating condition. Although many investigations have been completed on subcooled flow boiling with one-sided heating, most of this effort was focused on fusion reactor system cooling with water as the coolant. Despite the importance of EG/W mixture boiling in practical applications, theoretical and experimental studies are generally lacking.

PACCAR/DAF is designing engines to take advantage of subcooled boiling heat transfer below the CHF, but the CHF and heat transfer rates have not been determined under realistic conditions. The experiments of this program address this situation using a design specified by DAF. The data will be

used in computational fluid dynamics (CFD) models and designs by PACCAR/DAF, and could result in more efficient engines for heavy-duty vehicles. The objective of this project is to measure heat transfer rates during subcooled boiling of engine coolants in a geometry typical of valve bridge areas in heavy-duty vehicle engines under various operating conditions.

Approach

The general approach for this project is to experimentally investigate subcooled boiling of water and EG/W mixtures for heavy-duty vehicle engine applications.

The experimental apparatus used in this study is shown in Figure VIII-17. It consists of a closed-loop system with main components of a pump, two preheaters, an experimental test section, a heat exchanger (cooler), and a flowmeter. The system was designed and fabricated to study the heat transfer of subcooled flow boiling of water and EG/W mixtures with heat supplied only to the bottom half surface of the experimental test section. As shown in the schematic diagram of the experimental apparatus in Figure VIII-17, the test fluid was pumped through the test loop by a turbine pump (MTH Pumps, Model T31FAB), and the system was open to the atmosphere through the fill port at the flowmeter. The turbine pump was driven by an alternating-current adjustable-frequency driver (Dayton Electric Manufacturing Company, Model 1XC95), which made it possible to fine adjust flow rates through the experimental test section. Exiting the pump, the test fluid flowed through two preheaters arranged in series, in which, for a given test, the fluid temperature was raised to the desired subcooled level and monitored through two in-stream thermocouples. Each preheater was made of AISI type 304 stainless steel tubing (9.779-mm inside diameter, a 15.875-mm outside diameter, and a 3.9624-m resistance-heated length) and was heated by passing current through its wall. A direct-current power supply (Sorensen Company, Model DCR 16-625T) was used for each preheater, the output power of which could be regulated from 0 to 10 kW with a maximum voltage drop of 16 V and a maximum current of 625 A. As a safety precaution for protecting the preheaters from overheating, each preheater was provided with a temperature interlock. At the end of each preheater, the wall temperature was measured and then fed to a high-temperature limit switch (Omega Engineering, Inc., Model CN8500) that would terminate power to the preheater when a preset upper-temperature limit was reached. After passing through the preheaters, the fluid entered the horizontal experimental test section. The experimental test section was heated with a direct-current power supply (Electronic Measurements, Inc., Model EMHP 40-450-D-11111-0933) by passing current through an AISI type 304 stainless steel heating wire (1.6256-mm diameter) attached to the bottom half of the experimental test section surface, as shown schematically in Figure VIII-18. The output power could be regulated from 0 to 18 kW with a maximum voltage drop of 40 V and maximum current of 450 A. The voltage drop across the heating wire was measured directly, and the current through the heating wire was determined from a measurement of the voltage drop across a shunt resistor with known resistance of 0.00001 Ω. The heat input to the experimental test section was calculated by using the product of the voltage drop and the current. Electrical isolation for eliminating ground loops was provided for the preheaters and the experimental test section by short high-pressure hoses, designated ISO in Figure VIII-17. The test fluid out from the experimental test section was cooled in a compact plate-and-frame heat exchanger (Affiliated Steam Equipment Company, Model WP1-14) that used laboratory water as a heat rejection fluid. The volumetric flow rate of the test fluid was measured by an electromagnetic flowmeter (Endress+Hauser, Inc., Model 10H08-A00A1RA0B4AA). A thermocouple probe (Omega Engineering, Inc.) just upstream from the flowmeter provided a means to determine the density of the fluid and, subsequently, its mass flow rate. Flowing out of the flowmeter, the test fluid returned to the pumps to close the test loop.

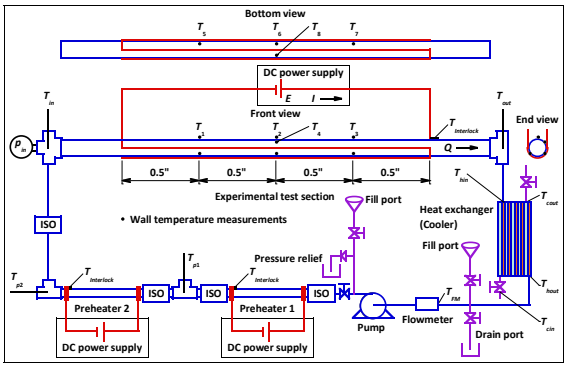

Figure VIII-17: Schematic of Heat Transfer Facility.

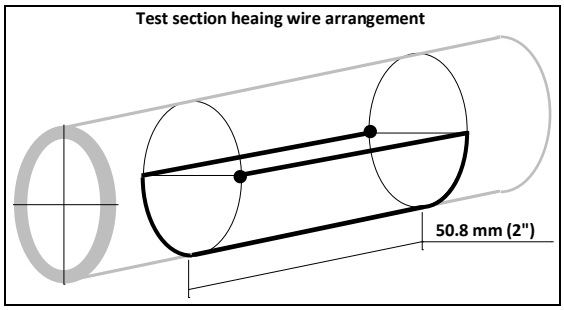

Figure VIII-18: Test Section Heating Wire Arrangement.

The experimental test section, shown schematically in Figure VIII-17, was fabricated from an AISI type 1010 carbon steel tube (10.9-mm inside diameter and 12.7-mm outside diameter with a 50.8-mm heated length). The in-stream bulk fluid temperatures were measured at the inlet and the outlet of the experimental test section with type K thermocouple probes (Omega Engineering, Inc.). As shown schematically in Figure VIII-17, the wall temperatures were measured at eight locations along the experimental test section and around the test section circumference over the heated length with type K thermocouple junctions (Omega Engineering, Inc.) spot welded to the test section surface. The inlet fluid pressure was measured in all tests with a diaphragm pressure transducer (Omega Engineering, Inc., Model PX309–100A5V). These measurements were incorporated in the data reduction to calculate the average in-stream temperatures and the average

wall temperatures. As a safety precaution for protecting the experimental test section from overheating, it was provided with a temperature interlock. At the end of the experimental test section, the wall temperature was measured and then fed to a high-temperature limit switch (Omega Engineering, Inc., Model CN8500) that would terminate power to the experimental test section when a preset upper-temperature limit was reached.

A data acquisition system consisting of a personal computer and a multiplexor (Hewlett-Packard Company, Model HP 75000 Series B) was assembled to record outputs from all sensors. A data acquisition program, including all calibration equations and engineering-unit conversions, was written with the LabVIEW graphical programming software. The data acquisition system functioned in two modes. During experimental test setup, the data acquisition system provided an on-screen display of analog signals from all sensors and graphs of representative temperature measurements as a function of time to facilitate determination of steady-state conditions. When the system reached a steady-state condition at desired parameters, the data acquisition system read all sensor-output voltages of in-stream temperatures, wall temperatures, ambient temperature, inlet pressure, volumetric flow rate, voltage drop across the heating wire, and current through the heating wire. These sensor-output voltages were read 30 times, averaged, and stored as a data set for future data reduction.

An overview of the completely fabricated heat transfer test facility is shown graphically in Figure VIII-19 before it was insulated.

Figure VIII-19: Overview of Heat Transfer Facility.

Results

Heat Loss Calibration

Although the experimental test section is well insulated thermally from the atmosphere to minimize heat loss to the environment, the heat loss was not negligible during flow boiling heat transfer experiments because of the relatively high driving temperatures. Therefore, heat loss experiments were performed for the wall temperatures in the experimental test section up to the boiling heat transfer conditions, and the heat loss was subsequently incorporated into the data reduction procedures for results on single-phase convective and two-phase subcooled boiling heat transfer. The heat loss was characterized through a special series of experiments with no fluid in the experimental test section. Power was applied to the experimental test section to bring its wall temperature to a selected level. The heat loss rate q_{loss}, the input power required for maintaining the wall temperature at the selected value, was calculated by the product of the voltage drop across the heating wire and the current through the heating wire ($q_{loss}=EI$). It is related to the difference between the experimental test section wall temperature T_w and the ambient temperature $T_{ambient}$. Experimental results confirmed a linear dependence on this driving temperature difference. Then, the heat loss rate can be expressed approximately as $q_{loss}=c(T_w-T_{ambient})$, where the proportional constant c, which depends on the heat transfer coefficient and the heat transfer surface area between the experimental test section and ambient temperature for this particular experimental apparatus, was determined from the heat loss experiments. Figure VIII-20 shows the heat loss rate as a function of the driving temperature difference for the experimental test section. The test section heat loss was <3% of the applied input power to the experimental test section in all subsequent heat transfer tests.

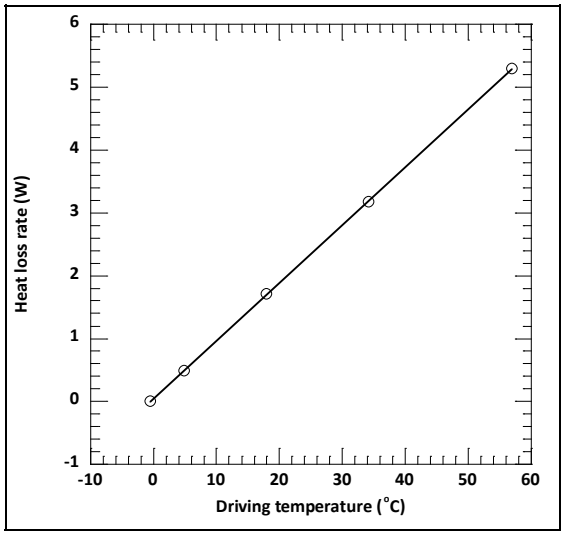

Figure VIII-20: Heat Loss Calibration.

Single-Phase Heat Transfer Experiments

Investigations of heat transfer under the condition of heat supplied only to one half surface of an experimental test section are limited in the engineering literature, and no standard data reduction process exists. Therefore, to validate the test apparatus in this study and to establish a baseline, a series of single-phase heat transfer experiments was carried out prior to the two-phase subcooled flow boiling experiments. For the single-phase heat transfer experiments, the system pressure was kept near atmosphere pressure, similar to the experiments of two-phase subcooled flow boiling. The single-phase heat transfer experiments were performed under a turbulent flow condition mirroring the flow region of the two-phase subcooled flow boiling experiments, and the liquid heat transfer coefficients were correlated as functions of the Reynolds number (Re) and the Prandtl number (Pr) by

modifying the Dittus-Boelter equation (Dittus and Boelter, U. California Pubs., 1930). As shown in Figure VIII-21, the experimental heat transfer coefficients are in good agreement with the predicted values from the above equation, with a mean deviation of <4%. Almost all experimental data are within ±5% of the predictions. The need to modify the Dittus-Boelter equation is not surprising because it is not based on one-sided heating conditions. The need for different equations for each fluid is also not surprising because the Dittus-Boelter equation was not developed for fluid mixtures. These equations were only used in the data reduction of this study to account for the single-phase heat transfer at the top of the experimental test section under subcooled boiling conditions at the bottom.

In addition to the turbulent flow, single-phase heat transfer experiments were performed under the laminar flow condition with ethylene glycol and water mixtures to establish a baseline for the two-phase subcooled laminar flow boiling that occurred at the lowest flow velocity of ethylene glycol and water mixtures. The liquid heat transfer coefficients were correlated as a function of Re and Pr by modifying the Shah equation (Heat & Mass Transfer Conf., 1975). As shown in Figure VIII-22, the experimental heat transfer coefficients are in good agreement with the predicted values from the Shah equation with a mean deviation of <2%. All experimental data are within ±5% of the predictions.

Subcooled Boiling Experiments

A series of subcooled flow boiling heat transfer experiments was conducted for water and 40/60 and 50/50 EG/W mixtures under both the laminar and the turbulent flow conditions at various flow velocities and inlet subcooling temperatures. During the subcooled flow boiling heat transfer experiments, the system was kept close to atmospheric pressure through the open fill port at the flowmeter. For each set of experiments, the heating power of the preheaters was chosen to maintain the test fluid inlet subcooling temperature at a desired level, and the heating power of the test section was increased progressively until the preset upper-temperature limit was reached. During the process of increasing the test section heating power, the test fluid changed gradually from single-phase convection-dominated heat transfer to subcooled flow boiling heat transfer. For each heating power increment, enough time was allowed for the experimental system to reach a steady state, and then all the test-related sensor outputs were averaged and recorded in a data set with appropriate engineering units for future data reduction.

The approach used for analyzing subcooled flow boiling heat transfer was to separate the overall heat transfer into two parts: top heat transfer and bottom heat transfer. It was assumed that the top heat transfer was always single-phase convection, even when subcooled flow boiling occurred at the bottom; this condition was verified by the top wall superheat being below a certain threshold. The results for heat flux and heat transfer coefficients are discussed below.

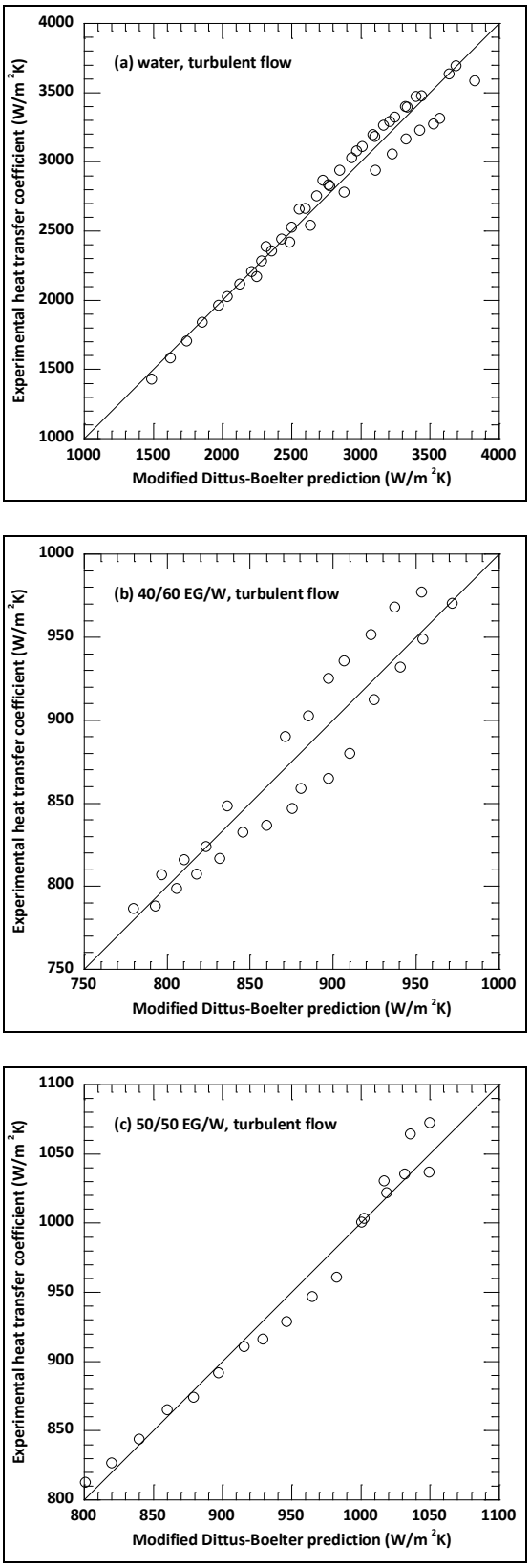

Figure VIII-21: Experimental vs. Predicted Turbulent Heat Transfer Coefficient for Water, 40/60 EG/W, and 50/50 EG/W.

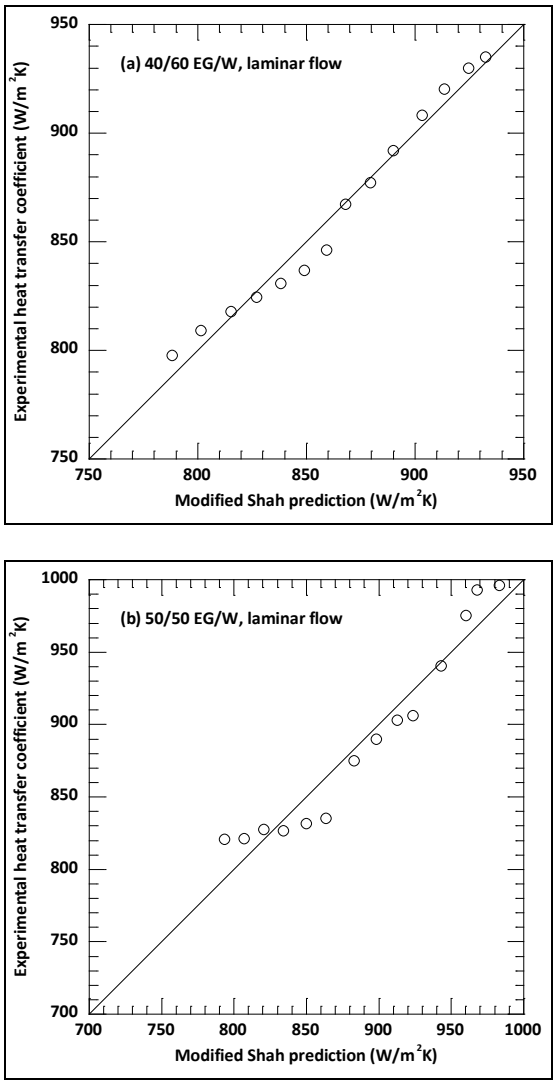

Figure VIII-22: Experimental vs. Predicted Laminar Heat Transfer Coefficient for 40/60 and 50/50 EG/W Mixtures.

Heat Flux

The heat flux curves for subcooled flow boiling of water and 40/60 and 50/50 EG/W mixtures are shown in Figure VIII-23 (laminar flow with flow velocity of 0.125 m/s) and Figure VIII-24 (turbulent flow with flow velocity of 0.25 m/s) for four inlet subcooling temperatures. The inlet temperatures were chosen to obtain the same inlet liquid subcooling for all three test fluids in the range of 10–25°C. The heat transfer curves in Figure VIII-23 and Figure VIII-24 can generally be divided into two regions: single-phase convection dominated and subcooled flow boiling, which is similar to subcooled flow boiling of fluids in test channels with the all-around heating condition. Several other observations were made from Figure VIII-23 and Figure VIII-24: (a) the wall superheats at which heat transfer changes from single phase to two phase are similar for all three test fluids at approximately 10C; (b) for the same heat flux increment, the wall superheat increment of the subcooled flow boiling region is smaller than that of the convection-dominant region; (c) for various inlet liquid subcooling levels, the boiling curves follow a parallel pattern in the convection-dominant region but a gradually merging pattern in the subcooled flow boiling region; (d) due to the gradually merging pattern in the subcooled flow boiling region, the heat transfer curve trend change at approximately 100176°C is sharpest for the highest inlet temperature or the lowest inlet liquid subcooling; and (e) also due to the gradually merging pattern in the subcooled flow boiling region, the influence of the inlet liquid subcooling becomes less significant with the increase of subcooled flow boiling.

Boiling Heat Transfer Coefficients

The heat transfer coefficients of subcooled flow boiling of water and 40/60 and 50/50 EG/W mixtures are shown in Figure VIII-25 as a function of the wall superheat for various inlet temperatures. Several observations were made from Figure VIII-25. First, for the positive wall superheat region, the heat transfer coefficients follow a similar trend to that of the heat flux curves, where the heat transfer coefficients can be divided into two regions at a wall superheat of approximately

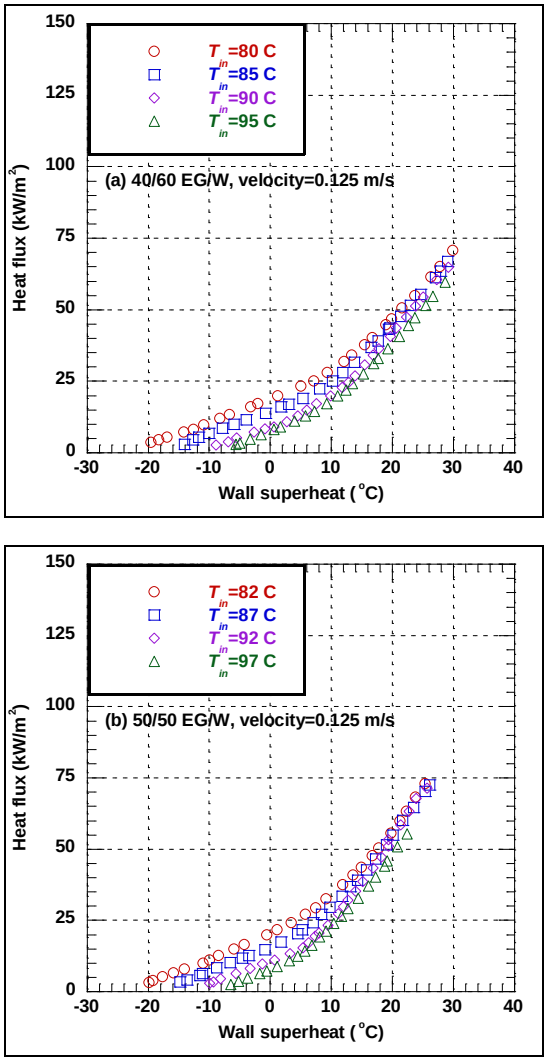

Figure VIII-23: Heat Flux for Laminar Subcooled Boiling with 40/60 and 50/50 EG/W Mixtures.

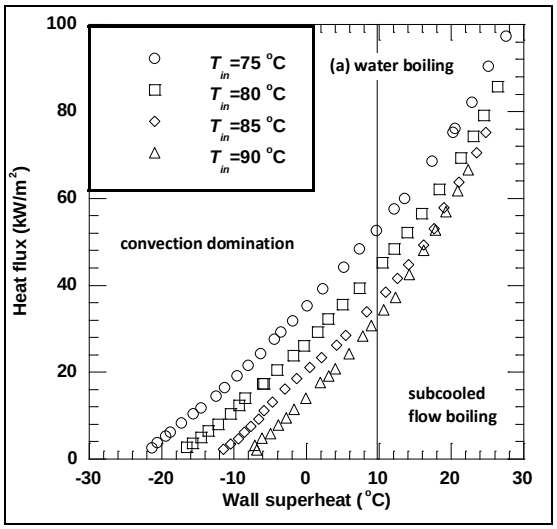

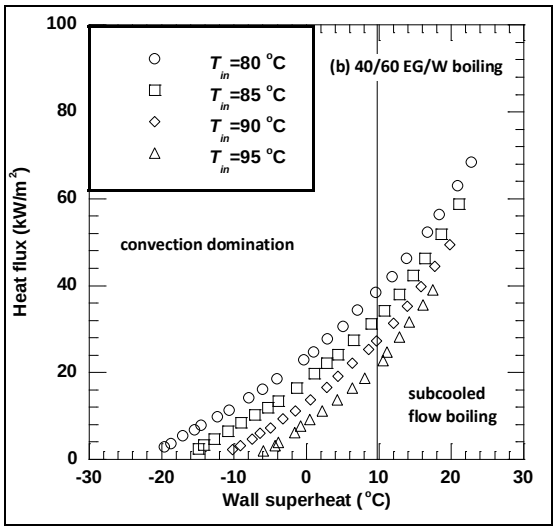

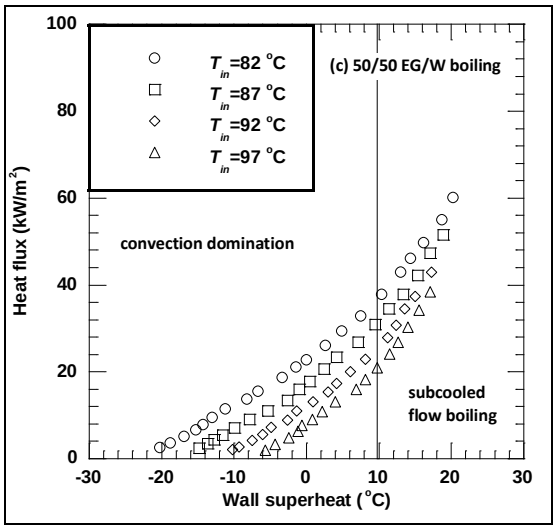

Figure VIII-24: Heat Flux for Turbulent Subcooled Boiling with Water, 40/60 EG/W, and 50/50 EG/W.

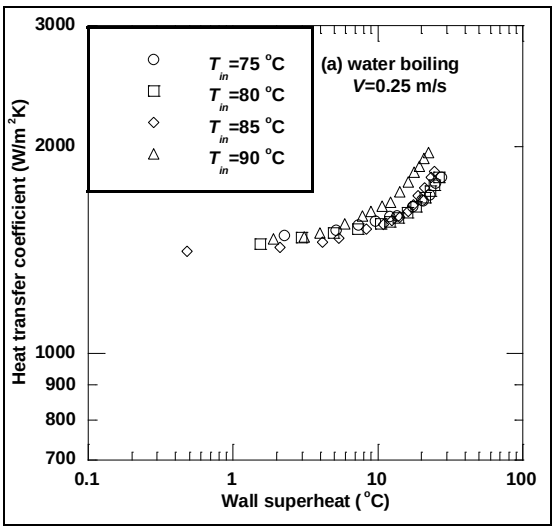

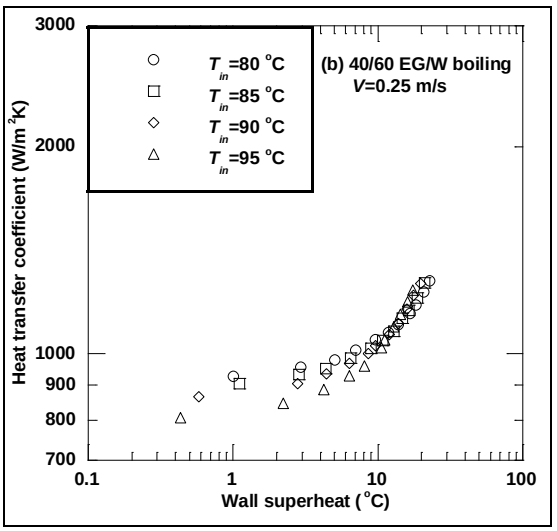

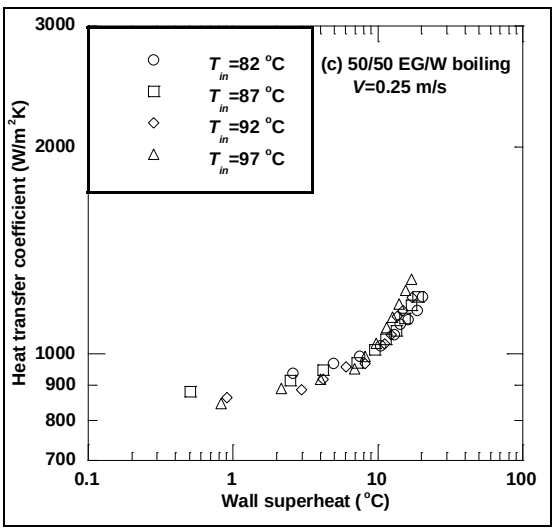

Figure VIII-25: Boiling Heat Transfer Coefficients for Water, 40/60 EG/W, and 50/50 EG/W.

10°C. For the low wall superheat of <10°C, where single-phase convection dominates, the heat transfer coefficients change insignificantly with the wall superheat. For the high wall superheat of >10°C, the heat transfer coefficients increase with the wall superheat, indicating the development of subcooled flow boiling. Second, while there is a clear difference between the heat flux for water and EG/W mixture boiling, the heat flux difference between boiling of the 40/60 50/50 EG/W mixtures is insignificant; this finding may be due to the relatively small difference of the ethylene glycol concentration. Third, the heat transfer coefficients in the subcooled flow boiling region with the wall superheat of >10°C show very weak inlet liquid subcooling effects, which is important in developing correlation equations for the subcooled flow boiling heat transfer coefficients.

Heat Transfer Coefficients

The experimental data for subcooled flow boiling heat transfer coefficient from this study are compared to the predicted values from four existing correlation equations in the engineering literature (McAdams et al., Indus. & Engg. Chem. Res.,1949; Jens & Lottes, Argonne Report ANL-4627, 1951; Shah, ASHRAE Trans., 1977; Kandlikar, J. Heat Transfer, 1998). Note that the correlations were not developed from data for mixture boiling and one-sided heating. Notwithstanding those conditions, it can be seen from Figure VIII-26 that the agreement between measurements and predictions are not unreasonable for subcooled flow boiling of 40/60 and 50/50 EG/W mixtures, and all the predicted values are within ±30% of the experimental data although the data trends are not as well predicted. For subcooled flow boiling of water, the comparisons are comparable when the heat flux range of the water data is considered. Although the overall predictions of the experimental data of this study are not unreasonable considering the data bases of the correlation equations, at this time in the development of correlations for subcooled flow boiling data in the cylinder head regions of heavy duty vehicles, the data themselves are best used for heat transfer coefficient predictions.

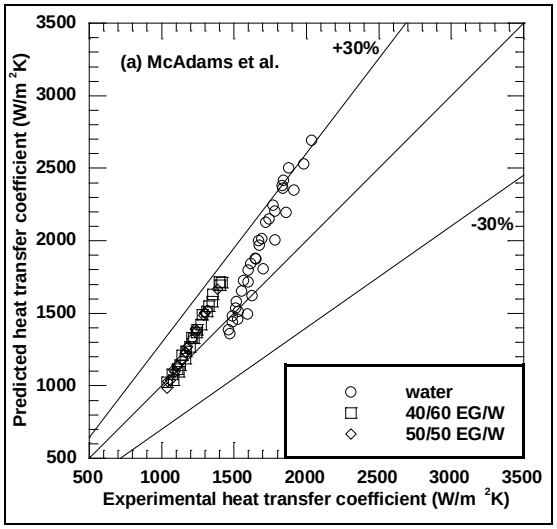

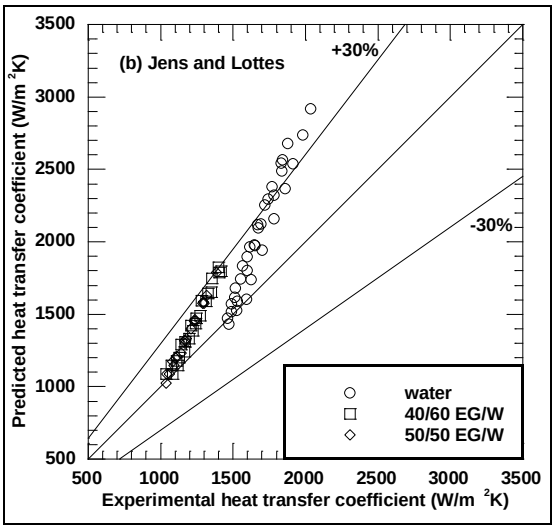

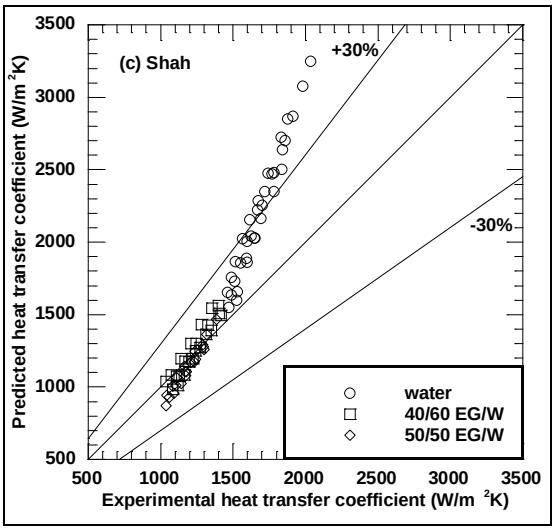

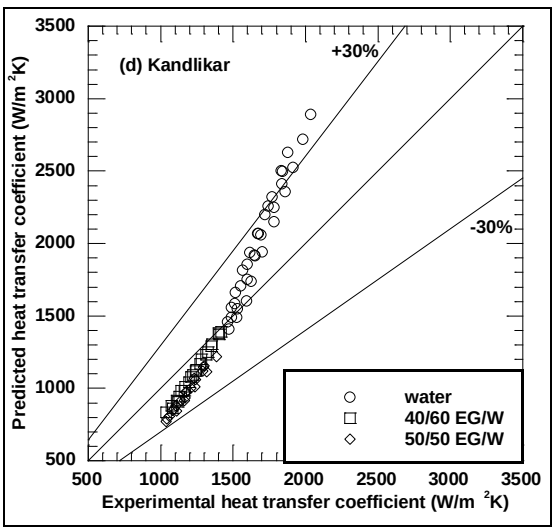

Figure VIII-26: Predicted vs. Experimental Boiling Heat Transfer Coefficient for Water, 40/60 EG/W, and 50/50 EG/W. Predictions used different equations in the literature.

CFD Simulation Results

The experimental data were also compared to computational fluid dynamics (CFD) simulations, where the simple boiling model was based on the Rohsenow expression (Rohsenow & Hartnett, Handbook of Heat Transfer, 1973) for nucleate boiling, the Rohsenow boiling model was based on the Eulerian multiphase model (which works with nucleate and film boiling), and the transition boiling model was based on the Eulerian multiphase model (which works with nucleate and transition boiling) (Zhou, Theory & Numerical Modeling of Turbulent Gas-Particle Flows and Combustion, 1993). Figure VIII-27 shows that, while the CFD model predicts some experimental data reasonably well, the differences between the experimental data and the CFD model predictions are significant. Therefore, predictive equations based on the experimental data are needed to better simulate coolant subcooled boiling in the cylinder head region of heavy-duty vehicle engines.

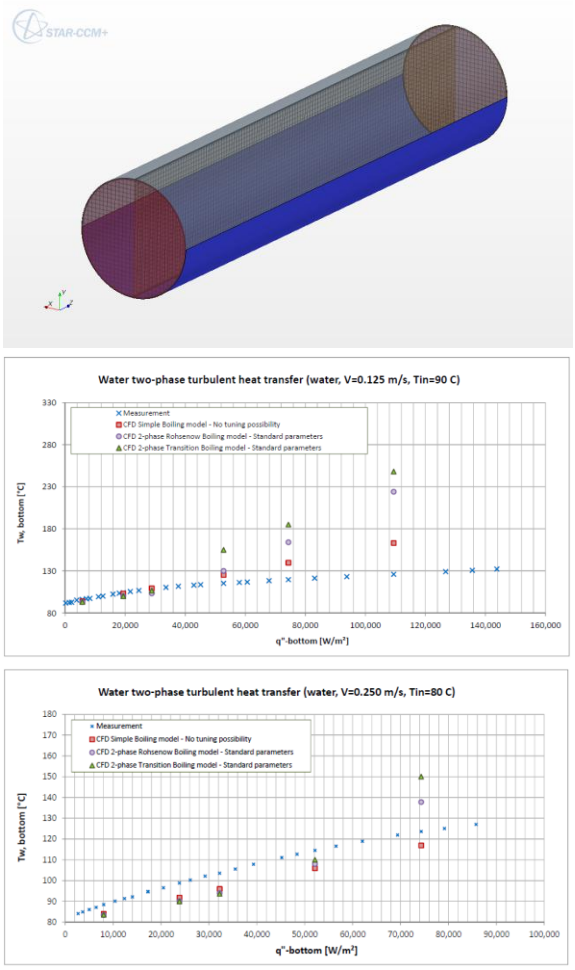

Figure VIII-27: CFD Simulation Results.

Conclusions

In summary, the design and fabrication of the PACCAR heat transfer test facility have been finished; the LabVIEW-based data acquisition and test control hardware and software have been established; the experiments and data reduction for single-phase convective heat transfer with three test fluids have been completed; and experiments for two-phase subcooled boiling with three test fluids have been performed at various flow rates. The project is on schedule, and the future work will be focused on the development of predictive equations for two-phase subcooled boiling with water and EG/W mixtures and on the extension of experiments to higher pressures.

VIII.C.3. Products

Publications

1. Wenhua Yu, David M. France, Dileep Singh, Roger K. Smith, Jason Ritter, Thomas Vijlbrief, and Yves Menger, “Subcooled Flow Boiling of Ethylene Glycol/Water Mixtures in a Bottom-Heated Tube,” submitted to the *International Journal of Heat and Mass Transfer*.

VIII.D. Development of Nanofluids for Cooling Power Electronics for Hybrid Electric Vehicles

Dileep Singh, Principal Investigator
Argonne National Laboratory
9700 S. Cass Avenue
Argonne, IL 60439
Phone: (630) 252-5009
E-mail: dsingh@anl.gov

Lee Slezak, DOE Program Managers
Phone: (202) 586-2335
E-mail: Lee.Slezak@ee.doe.gov

VIII.D.1. Abstract

We investigated the effects of nanoparticle morphology and surface treatment on the thermo-physical properties of nanofluids with graphitic nanomaterials in ethylene glycol (EG)/H_2O base fluid. Using a simple, low cost, and up-scalable surface modification method for graphitic nanoparticles, we were able to formulate a nanofluid coolant that allows >90% improvement in heat transfer coefficient when used in laminar flow and >30% enhancement in heat transfer coefficient when used in turbulent flow. The implementation of this technology in hybrid and all-electric vehicles will result in reducing the size, weight, and number of heat exchangers, further improving vehicle efficiency and fuel economy.

Objectives

- Assess use of nanofluids for cooling of power electronics.
- Develop nanofluid with enhanced properties to fulfill DOE's goals of a single cooling system for the engine and power electronics in hybrid electric vehicles that would allow reducing vehicle weight and improve fuel economy.
- Experimentally evaluate the heat transfer performance of new coolants.

Major Accomplishments

- Thermal analysis of heat exchanger indicated that:
  - nanofluids with thermal conductivity enhancements >50% over base fluid in laminar flow could (a) eliminate one of the heat exchanges, (b) increase the heat load by 50%, or (c) reduce the junction temperature by >10°C.
- Developed carbon-based nanofluid in EG/H_2O that:
  - exceeds the coolant property requirements, providing 75-90% heat transfer improvements in laminar flow and 30-40% in turbulent flow regimes at only 2.25 vol% of solids.

Future Achievements

- Process scale-up and optimization
- Test performance of formulated nanofluid(s) in heat transfer loop

✧ ✧ ✧ ✧ ✧

VIII.D.2. Technical Discussion

Background

Power electronics (PE) provides control and conversion of electric power in hybrid electric vehicles (HEVs). Uninterrupted operation of PE requires liquid cooling systems to enhance heat dissipation, improve energy efficiency, and lengthen device lifetime. In current HEVs, two cooling systems are used: a higher temperature system for cooling the gasoline engine and a lower temperature system for cooling the power electronics.

A DOE goal is to eliminate the lower temperature system and to accomplish all cooling with a single higher temperature system. Heat transfer analysis for a typical heat exchanger has shown that an enhancement in thermal conductivity of between 50% and 100% could, without a significant increase in pumping power, allow either elimination of one radiator in HEVs or an increase of the power loading.

Introduction

Nanofluids are engineered by stably dispersing nanometer-sized solid particles in conventional heat transfer fluids to enhance the thermal conductivity and the heat transfer coefficient.

Previous studies of nanofluids [1] have demonstrated that thermal conductivity can be improved with either addition of metallic or high-aspect-ratio graphitic nanoparticles. Production of metal-containing nanofluids faces some major challenges, such as stability toward agglomeration and surface oxidation, availability, cost of materials, and manufacturing issues. By contrast, carbon nanomaterials are commercially available, with prices dropping each year. Roughly 200-300% increases in thermal conductivity were reported for nanofluids with carbon nanotubes [2-5] and graphene oxides [6, 7]. Such dramatic increases are most likely due to the anisotropic nature of carbon nanomaterials, which allows multiple heat transfer mechanisms in suspensions (effective medium theory, percolation, and plasmon resonances) as depcied in Figure VIII-28.

The drawback of carbonaceous nanofluids with high aspect ratio particles is very high viscosity (up to three orders of magnitude higher than the viscosity of the base fluid). Such viscosity increases result in pumping power penalties that are higher than the benefits in thermal conductivity of the suspensions. Thus, the practical value of previously reported carbonaceous nanofluids was not sufficient for commercialization of the technology.

Approach

This study focuses on assessment, optimization, and experimental evaluation of nanofluids with commercially available carbon nanomaterials in 50/50 ethylene glycol/water (EG/H_2O) base fluid. The selection of carbon nanomaterials for this study was based on our previous work on nanofluid engineering [8, 9] indicating that spherical or nearly spherical particles are more beneficial for heat transfer applications compared to nanomaterials with high aspect ratio. Our recent findings in nanofluid engineering indicate that thermal conductivity enhancements significantly above the effective medium theory can be achieved by engaging alternative heat transfer mechanisms through the nanofluid and nanoparticle morphology. Concentration effects are deemed to be critical for balancing the benefits of increased thermal conductivity and penalties from increased viscosity.

For this study, we selected graphitic nanoplatelets, also marketed as multilayered graphene nanoplatelets (GnP) by XG Sciences, due to variety of sizes and platelet thicknesses and also low cost (current cost $70/lb and projected future cost of less than $20/lb). These features make GnP commercially feasible as a heat transfer fluid additive. The present work covers our investigation of the effects of nanoparticle shape (thickness and diameter) and surface functionalization on thermal conductivity, viscosity, and the resulting heat transfer coefficient of graphitic nanofluids.

We investigated the following factors for three grades of GnP, which are commercially available in large scale at low cost:

- Variations in diameter and thickness **=> shape effects**
- Dispensability in EG/H_2O **=> surface functionalization**

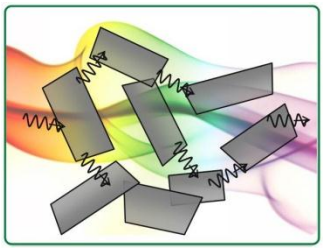

Figure VIII-28: Illustration of the percolation heat transfer mechanism in high-aspect-ratio graphitic nanofluids.

Results

Scanning electron microscopy (SEM) images of as-received GnP powders are presented in Figure VIII-29. The difference in platelet thickness is not obvious from the image resolution, but platelet diameters are clearly different. All GnP nanoparticles have irregular shape with diameters of 0.1-1 micron for A grade, 1-10 microns for B grade, and 3-25 microns for C grade. As-received GnP nanoparticles assemble into compact clusters on a Si wafer surface, especially A grade, indicative of the hydrophobic nature of the nanoplatelets.

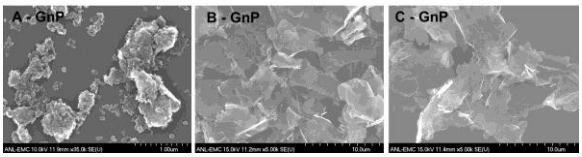

Figure VIII-29: SEM images of three grades of as-received GnP materials.

As-received GnP powders have very poor suspension ability in water and EG/H_2O, especially at low concentrations. The manufacturer suggests using surfactant to improve the dispersion stability of graphitic nanopowders in aqueous solutions. We have conducted a series of tests that investigated the effect of cationic and anionic surfactants on the thermal conductivity and stability of suspensions with A-grade GnP in deionized water. However, the most efficient approach to achieving stable suspensions of GnP in EG/H_2O base fluids was the use of surface functionalization/oxidation of sp2 graphite platelets. Functionalized GnP (f-GnP) after treatment of nanoparticles in 3:1 mixture of concentrated H_2SO_4 and HNO_3 show change of morphology and surface chemistry observed with SEM and Raman spectroscopy.

An alternative way of producing stable dispersions of graphitic nanoparticles is surface modification of carbon surfaces with hydrophilic groups (Figure VIII-30). Surface functionalization increases surface concentration of hydroxyl and carboxylic groups and charges, resulting in electrostatic stabilization. Graphitic core/graphene oxide shell nanoplatelets produce a high stability suspension in water and provide percolation paths for heat conduction.

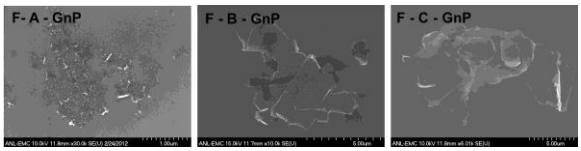

Figure VIII-30: SEM images of corresponding surface functionalized (f-GnP) graphitic materials.

We also used Raman spectroscopy to confirm changes in f-GnP compared to as-received GnP. Because nanoparticle oxidation occurs only at the surface of nanoparticles, f-GnP essentially represents a core-shell structure with graphitic core and oxide shell (Figure VIII-31). The thickness of the platelets and total surface area of nanoparticles will affect a change in Raman spectra with functionalization.

Raman spectroscopy is most sensitive to highly symmetric covalent bonds with little or no natural dipole moment. The carbon-carbon bonds fit this criterion perfectly; as a result, Raman spectroscopy is highly sensitive to changes in chemistry and morphology of carbon nanomaterials and is able to provide a wealth of information about their structure. Graphite has several bands in the Raman spectrum, with the main band at 1582 cm^{-1}, corresponding to sp2-bonded carbon in planar sheets, also

known as the G band. The presence of additional bands in the graphite spectrum indicates some carbon bonds with different bond energies in the sample. The band at ~2700 cm^{-1}, which is known as the 2D or G' band, is much more intense in graphene compared to graphite. Widening and shifts of the peak observed in graphite are a result of interactions among the stacked graphene layers.

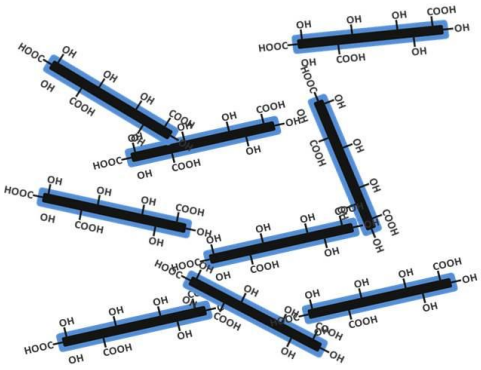

Figure VIII-31: Schematic illustration of f-GnP, resulting in electrostatic stabilization and percolation in suspension.

The band at 1620 cm^{-1} and shoulders on the 1620 cm^{-1} and 1582 cm^{-1} bands are indicative of sp2-bonded carbon that represents surface defect modes.

A prominent band around 1350 cm^{-1}, known as the D band, originates from a hybridized vibrational mode associated with graphene edges. It indicates the presence of some disorder to the graphene structure, and its intensity relative to that of the G band is often used as a measure of the quality of graphitic nanomaterials. The very broad band around 500 cm^{-1} is indicative of some amorphous sp3-bonded carbon.

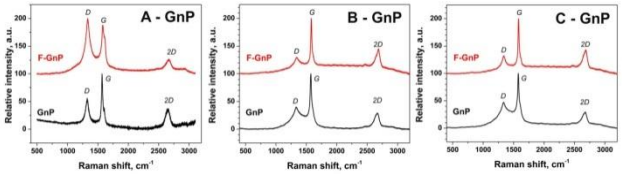

Figure VIII-32: Raman spectra of unmodified GnP (bottom) and f-GnP (top) nanoparticles for three grades of GnP nanoparticles.

Thus, Raman spectroscopy is very sensitive to even slight differences in the molecular morphology of carbon nanomaterials and was used for characterization of GnP nanomaterials before and after surface functionalization. The information obtained in this series of tests is used in correlating the thermal properties of nanofluids that would allow better control of the nanofluid properties in the future.

Figure VIII-32 shows the Raman spectra of the smallest nanoplatelets (A grade). The change with surface functionalization is very well pronounced: increased intensity of D band, lower intensity of G, and shoulder at ~1620 cm^{-1}, indicating a higher degree of disorder and defect concentration in f-GnP. The decreased intensity of the 2D peak also indicates fewer interacting graphite layers in the nanoplatelets.

The larger particles (grades B and C) show less dramatic changes in the Raman spectra because the smaller surface area and thicker graphite layers result in a less significant contribution from the surface.

So far all observations are in agreement with surface oxidation of GnP. The ratio of oxide/ graphite may be critical for efficient thermal conductivity enhancements, i.e., the surface area and morphology of nanoplatelets needs to be optimized for advanced heat transfer performance.

Zeta potential can be related to the stability of suspensions and is defined as the electric potential in the interfacial double layer at the location of the slipping plane versus a point in the bulk fluid away from the interface. The higher the value of the zeta potential, the higher is the electrostatic repulsion between nanoparticles and, therefore, the stability of the dispersion. When the potential is low, attraction among particles exceeds repulsion, resulting in agglomeration and settling of nanoparticles. Although the zeta potential indicates nanoparticle surface chemistry, it changes with ionic composition of the bulk solution. For water-based systems, adjusting solution pH could be used for controlling the stability of suspensions. We have investigated the zeta potential as a function of pH in a diluted suspension of unmodified GnP and f-GnP in EG/H_2O (Figure VIII-33 for B grade). The results clearly demonstrate that f-GnP nanoparticles have 10 mV higher zeta potential than unmodified GnP, which can be attributed to a higher concentration of surface groups resulting in higher stability of the f-GnP suspensions. At pH between 7 and 9, zeta potential values for the f-GnP suspension are below 40 mV, which is considered as a threshold for good stability of suspensions. High zeta potential minimizes agglomeration of nanoparticles and also results in lower viscosity for the same particle concentration [10]. Thus, for optimized heat transfer performance, the nanofluid pH should be maintained between 7 and 9. Further comparisons of nanofluids with different particle shapes were conducted at the same pH.

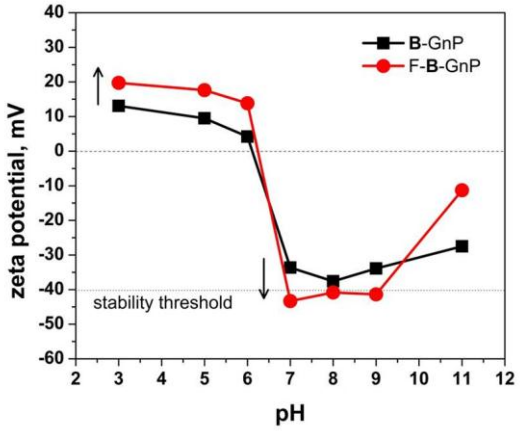

Figure VIII-33: Zeta potential of B grade unmodified GnP (black squares) and f-GnP (red circles) nanoparticles in EG/H_2O as a function of suspension pH.

The effect of GnP surface functionalization on the thermophysical properties of nanofluids was compared for unmodified GnP and f-GnP at 5 wt% loadings. Thermal conductivity enhancements measured in different grades of GnP and f-GnP nanofluids are presented in Figure VIII-34. One can see that the highest increases in thermal conductivity were achieved in C grade, followed by B grade and A grade. The observed enhancements are well beyond the effective medium theory prediction. Surface functionalization of graphitic nanoparticles improves thermal conductivity across all grades by 30-50% compared with the analogous unmodified GnP suspensions. Also, the increases in thermal conductivity are significantly beyond the effective medium prediction for various nanoparticle loadings, reaching 75-85% above the base fluid at ~2.25 vol. %.

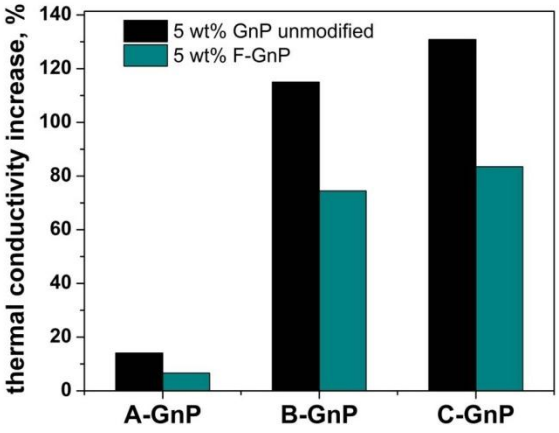

Figure VIII-34: Increase in thermal conductivity of graphitic nanofluids with unmodified GnP and f-GnP nanoparticles at 5 wt. % concentration (measured at room temperature).

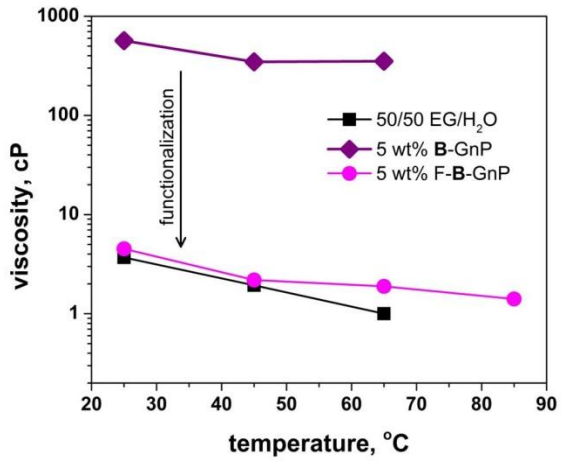

Figure VIII-35: Viscosity of 5 wt/% B grade dispersions with unmodified GnP (purple diamonds) and f-GnP (magenta circles) compared to viscosity of the base fluid (black squares).

The effect of surface modification on the viscosity of nanofluids is demonstrated in Figure VIII-35, which shows the viscosity of unmodified GnP and f-GnP dispersed in EG/H_2O at the same concentration (5 wt%). As shown, the viscosity of f-GnP is nearly two orders of magnitude less than that of the same grade of unmodified GnP. The viscosity of the nanofluid with unmodified particles is still ~30% higher than that of the base fluid, which is very promising for heat transfer considering the significant increase in nanofluid thermal conductivity. It should be mentioned here that B grade had the most dramatic drop in viscosity among all three grades.

The thermal conductivity of nanofluids with various particle morphologies was measured as a function of particle concentration for the f-GnP series (Figure VIII-36). Particles with the smallest diameters and thicknesses (A grade) show the smallest increase in thermal conductivity, closely following the prediction of effective medium theory. This finding indicates that no percolation paths are formed in this nanofluid, or that the high surface area of graphite oxide prevents effective thermal conduction through such percolation networks. The B and C grades provide higher thermal conductivity increases at higher particle concentrations. This behavior agrees with the proposed percolation heat transfer mechanism for anisotropic carbon nanomaterials. Interestingly, the C grade shows slightly lower enhancements than B at lower concentrations and slightly higher enhancements at higher particle concentrations. These results can be interpreted as an effect of the two different particle morphologies. The nanofluid with the thinner B-grade particles has a larger number of particles for the same concentration; thus, the percolation threshold can be achieved at lower concentration than for C grade. However, once the percolation threshold is reached, the thermal conduction is better due to the thicker, larger diameter C-grade particles as compared to the network of smaller diameters and thinner B-grade nanoparticles. The B-grade particles create more interfaces, thereby increasing interfacial thermal resistance and resulting in less efficient thermal pathways.

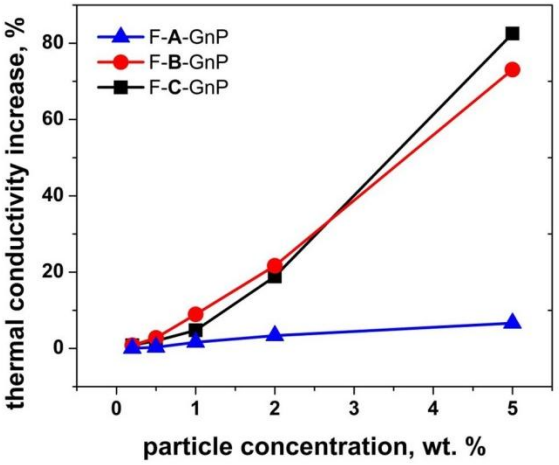

Figure VIII-36: Thermal conductivity increase as a function of particle concentration for three grades of f-GnP.

The changes in thermal conductivity and viscosity were found to be temperature dependent, such that even higher heat transfer enhancements were achieved at elevated temperatures (45-85ºC). Such a thermal effect is expected for disordered materials, where the heat conduction mechanism is the hopping of localized excitations.

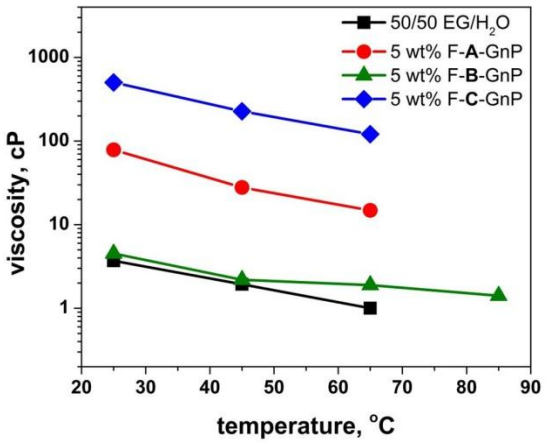

Figure VIII-37: Viscosity as a function of temperature for 5 wt.% f-GnP of all three grades.

Figure VIII-37 shows the viscosity of f-GnP with different morphologies for 5 wt.% f-GnP concentrations. One can see that, despite similar functionalization treatment and pH adjusted to 8.5±0.5, the viscosity of f-GnP nanofluids varies significantly with the particle morphology. The lowest viscosity is observed in nanofluid of B grade, and it is only 20-30% higher than that of the base fluid. In fact, at 65°C the viscosity of this nanofluid is close to the lower limit that can be measured with a rotational spindle viscometer. The viscosity of C grade GnP changed insignificantly from surface functionalization, decreasing from ~600 cP to 500 cP at 25°C. An interesting result was obtained with the A grade material, where f-GnP suspensions actually showed higher viscosity than the same concentration of unmodified GnP in EG/H_2O. At the same time, the stability of the nanoparticle suspension was noticeably improved. This effect is most likely due to the very poor dispersion of unmodified GnP: the granular structure of nanoparticle agglomerates is seen with SEM images, while f-GnP nanoparticles appear as individual platelets. Broken apart grade-A flakes represent a significantly higher area of solid/liquid interface than granules, thus increased effective volume fraction and viscosity of nanoparticles. Since the cooling efficiency of the heat transfer fluids is the main consideration in the current nanofluid development, the ratio of heat transfer coefficients for the suspensions and the base fluid was estimated for fully developed (hydrodynamically and thermally) laminar and turbulent flow regimes using fluid dynamic equations [11, 12]. The ratio of heat transfer coefficients is a convenient measure for comparison of two fluids flowing in the same geometry and at the same flow rates. In a laminar flow regime, the heat transfer coefficients are proportional to the thermal conductivity (within the acceptable range of inlet/outlet temperature difference), but in a turbulent flow regime the heat transfer coefficients depend on a set of thermophysical properties [11]. Introduction of nanoparticles to the fluids changes the density, thermal conductivity, viscosity, and specific heat of the coolant.

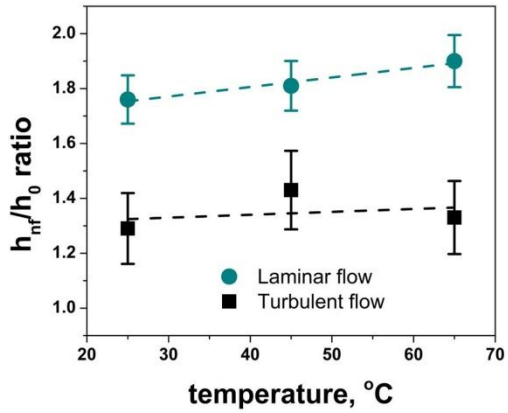

Figure VIII-38: Calculated ratio of heat transfer coefficients for 5 wt.% f-GnP (grade B) in EG/H_2O in laminar and turbulent flow regimes.

Experimental values for thermal conductivity, and viscosity and density and specific heat (determined by rules of mixtures) were used for evaluation of the heat transfer benefits of nanofluid with 5 wt.% of B grade f-GnP (Figure VIII-38). The ratio of heat transfer coefficients (h_{nf}/h_0) for the nanofluid and the base fluid, calculated for different temperatures, shows that the inclusion of graphitic nanoparticles in EG/H_2O coolant can provide significant (75-90%) improvement in heat transfer rates when used in the laminar flow regime, improving with an increase in temperature. Heat transfer coefficients in the turbulent flow regime show 30-40% improvement in heat transfer compared to the base fluid. Uncertainty in the viscosity measurement at higher temperatures doesn't allow us to reach any firm conclusion on the temperature dependence, but it can be established in future experimental heat transfer tests. Previously we observed that the heat transfer coefficient improves with temperature for nanofluids in both water and organic base fluids [10, 13, 14]. These results are very encouraging, since the enhancement levels not only meet the power electronics cooling criteria, but also will be beneficial in medical and military applications.

Conclusions

We investigated the effects of nanoparticle morphology and surface treatment on the thermophysical properties of nanofluids with graphitic nanomaterials in EG/H_2O base fluid. Using a simple, low cost, and up-scalable surface modification method for graphitic nanoparticles, we were able to formulate a nanofluid coolant that allows >75% improvement in heat transfer coefficient when used in laminar flow and >30% enhancement in turbulent flow. The implementation of this technology in hybrid and all-electric vehicles would result in reducing the size, weight, and number of heat exchangers, thus improving vehicle efficiency.

VIII.D.3. Products

Publications

1. Yu, W., D.M. France, E.V. Timofeeva, and D. Singh, *Effective thermal conductivity models for carbon nanotube-based nanofluids*, J. of Nanofluids, 2013, **2**, 69–73.
2. Timofeeva, E.V., D. Singh, W. Yu, and D.M. France, *Engineered nanofluids for heat transfer and novel applications*, Conference Proceedings of TechConnect NanoTech Conference and Expo, May 12-16th, 2013, Washington, DC, USA.
3. Yu, W., D.M. France, E.V. Timofeeva, D. Singh, and J.L. Routbort, *Comparative review of turbulent heat transfer of nanofluids*, Int. J. Heat Mass Transfer, 2012, **55**, 5380-5396.
4. Timofeeva, E.V., W. Yu, D.M. France, D. Singh, and J.L. Routbort, *Nanofluids for heat transfer: An engineering approach*, Nanoscale Res. Lett., 2011,**6**, 182.
5. Routbort, J.L., D. Singh, E.V. Timofeeva, W. Yu, D.M. France, *Pumping power of nanofluids in a flowing system,* J. Nanopart. Res., 2011, **13**, 931-937.
6. Timofeeva, E.V., W. Yu, D.M. France, D. Singh, and J.L. Routbort, *Base fluid and temperature effects on the heat transfer characteristics of SiC in ethylene glycol/H_2O and H_2O nanofluids,* J. Appl. Phys., **109**, 2011, 014914.
7. Yu, W D.M. France, E.V. Timofeeva, D. Singh, and J.L. Routbort, *Thermophysical property-related comparison criteria for nanofluid heat transfer enhancement in turbulent flow*, Appl. Phys. Lett., **96**, 2010, 213109.
8. Timofeeva, E.V., D.S. Smith, W. Yu, D.M. France, D. Singh, and J.L. Routbort, Particle size and interfacial effects on thermo-physical and heat transfer characteristics of water and a-SiC nanofluids, Nanotechnology, 2010, **21**, 215703.
9. Yu, W., D.M. France, D. Singh, E.V. Timofeeva, D. Smith, and J. Routbort, *Mechanisms and models of effective thermal conductivities of nanofluids, J. Nanoscience and Nanotechnology, 2010, **10**, 1-26.*
10. Timofeeva, E.V., J.L. Routbort, and D. Singh, *Particle shape effects on thermo-physical properties of alumina nanofluids*, J. App. Phys., 2009, **106**, 014304.

Patents

1. Nonprovisional Patent Application “Advanced Thermal Properties of a Suspension with Graphene Nano-Platelets (GNPs) and Custom Functionalized F-GNPs”, Inventors: Elena V. Timofeeva; Dileep Singh, filed April 21, 2013.

References

1. Timofeeva, E.V., Nanofluids for heat transfer: Potential and engineering strategies, in Two Phase Flow, Phase Change and Numerical Modeling, A. Ahsan, Editor, 2011, InTech. pp. 435-450.
2. Sastry, N.N.V., et al., *Predicting the effective thermal conductivity of carbon nanotube based nanofluids,* Nanotechnology, 2008. **19**: p. 055704.
3. Choi, S.U.S., et al., *Anomalous thermal conductivity enhancement in nanotube suspensions,* Applied Physics Letters, 2001, **79**(14): pp. 2252-2254.
4. Zhang, X., H. Gu, and M. Fujii, *Effective thermal conductivity and thermal diffusivity of nanofluids containing spherical and cylindrical nanoparticles*, Journal of Applied Physics, 2006, **100**(4).
5. Hwang, Y., et al., *Stability and thermal conductivity characteristics of nanofluids,* Thermochimica Acta, 2007, **455**(1-2): pp. 70-74.
6. Yu, W., H.Q. Xie, and D. Bao, Enhanced thermal conductivities of nanofluids containing graphene oxide nanosheets, Nanotechnology, 2010, **21**(5): p. 055705.
7. Yu, W., et al., *Significant thermal conductivity enhancement for nanofluids containing graphene nanosheets,* Physics Letters A, 2011, **375**(10): pp. 1323-1328.
8. Timofeeva, E.V., J.L. Routbort, and D. Singh, *Particle shape effects on thermophysical properties of alumina nanofluids,* Journal of Applied Physics, 2009, **106**: p. 014304.
9. Timofeeva, E.V., et al., *Nanofluids for heat transfer: An engineering approach,* Nanoscale Research Letters, 2011, **6**: p. 186.
10. Timofeeva, E.V., et al., *The particle size and interfacial effects on thermo-physical and heat transfer characteristics of water based a-SiC nanofluids*, Nanotechnology, 2010, **21**(21): p. 215703-13.
11. Yu, W., et al., *Thermophysical property-related comparison criteria for nanofluid heat transfer enhancement in turbulent flow*, Applied Physics Letters, 2010, **96**: p. 213109-3.
12. Etherington, H., ed., *Nuclear engineering handbook*, 1958, McGraw-Hill Book Company, Inc., New York, USA.
13. Timofeeva, E.V., M.R. Moravek, and D. Singh, *Improving the heat transfer efficiency of synthetic oil with silica nanoparticles,* Journal of Colloid and Interface Science, 2011, **364**(1): pp. 71-79.
14. Timofeeva, E.V., et al., *Base fluid and temperature effects on the heat transfer characteristics of SiC in EG/H_2O and H_2O nanofluids, Journal of Applied Physics*, 2011, **109**: p. 014914.

FRICTION AND WEAR

VIII.E. Development of High Power Density Driveline for Vehicle Efficiency Improvement

Oyelayo Ajayi, Cinta Lorenzo-Martin, Aaron Greco and George Fenske
Argonne National Laboratory
9700 South Cass Avenue
Argonne, IL 60439
Phone: (630) 252-9021
E-mail: ajayi@anl.gov

Lee Slezak, DOE Program Manager
Phone: (202) 586-2335
E-mail: lee.slezak@hq.doe.gov

VIII.E.1. Abstract

Objectives

- Enable significant reduction in transportation vehicle weight and consequent fuel savings through size and weight reduction of driveline systems, such as transmission and axles.
- Develop materials, surface finishes, and lubricants to enable development of durable and reliable high-power-density (HPD) driveline systems that are smaller and lighter than current systems.
  - Increase wear, scuffing, and contact fatigue lives for HPD driveline to facilitate up to 25% size reduction in gears and bearings.

Major Accomplishments

- Completed preliminary analysis of the contact kinematics for specific size reduction in a simple planetary gearbox.
- Assessed the effect of new contact kinematics in terms of Hertzian contact stresses, effect of surface velocities of meshing gear teeth on wear, and scuffing and contact fatigue lives.
- Identified potential synergy between thin-film coatings and lubricant additives resulting in low friction and more than twofold improvement in wear life under the boundary lubrication regime.
- Evaluated scuffing performance attributes of lubricant and surface coatings individually and in combination to achieve greater than fivefold increase in scuffing life.
- Developed a new lubricant additive blend that interacts with many commercially available coatings and steel surfaces for substantial reduction in friction and a significant increase in both wear and scuffing lives under severe contact conditions.

Future Achievements

- Complete contact fatigue evaluation of appropriate lubricant and coating technologies individually and in combination for required increase in fatigue life for HPD driveline systems.
- Integrate materials, lubricant, and surface technologies to produce adequate simultaneous increase in wear, scuffing, and contact fatigue lives to enable at least 25% size reduction in driveline systems.

✧ ✧ ✧ ✧ ✧

VIII.E.2. Technical Discussion

Background

DOE Goal

One of the main goals, perhaps the ultimate goal, of the U.S. Department of Energy's Vehicle Technologies Program (DOE-VTP) is the dramatic reduction of the amount of petroleum oil used in transportation vehicles. This would reduce the nation's dependence on foreign oil, thereby enabling greater energy independence and homeland security. In addition, consumption of less oil in vehicles would reduce environment-degrading emissions, such as greenhouse gases and particulates. Such emissions have been associated with climate change and detrimental effects on human health.

Project Goal

The ultimate objective of this project is the development of technologies that will enable original equipment manufacturers (OEMs) and their suppliers to successfully develop smaller, lighter, and more efficient driveline system for transportation vehicles by increasing the power density without sacrificing reliability and durability. Such a system will result in significant vehicle weight reduction and concomitant increase in fuel savings. Furthermore, an HPD driveline may enable the downsizing of the powertrain system, resulting in further fuel savings.

Introduction

Significant fuel savings can be achieved in all classes of transportation vehicle through weight reduction. Numerous analyses have shown that 2-5% reduction in fuel consumption is possible with a 10% reduction in automobile weight. Table VIII-5 shows such a calculation for three classes

of vehicles based on the New European Drive Cycle (NEDC) for both gasoline- and diesel-fueled internal combustion engines (ICEV-G and ICEV-D, respectively). Consequently, all OEMs are adopting vehicle weight reduction as a prime approach to reduce fuel consumption.

Table VIII-5: Calculated fuel savings for NEDC in different classes of gasoline and diesel automotive vehicles.

	NEDC ICEV-G	NEDC ICEV-D
Compact Class	-2.6 %	-3.5 %
Mid-Size Class	-1.9 %	-2.7 %
SUV	-2.4 %	-2.6 %

Weight reduction must be accomplished without sacrificing safety, reliability, and durability for a vehicle to gain public acceptance and market share. Figure VIII-39 shows the weight distribution for a typical automobile, highlighting the systems and components that present an opportunity for weight reduction. The DOE-VTP currently has programs and projects devoted to weight reduction in vehicle structures and engines (light-weight materials program). The driveline system constitutes about 20% of a vehicle's weight, making it an excellent target for weight reduction. One route to reducing the size and weight of the driveline system without sacrificing performance, or compromising reliability and durability, is by increasing its power density.

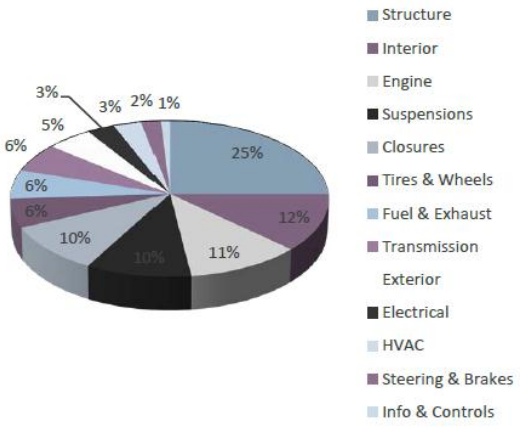

Figure VIII-39: Typical weight distribution of different systems in automotive vehicle.

Approach

Vehicle driveline systems such as transmission and axles consist of planetary gears and bearings to form a gearbox, as exemplified in Figure VIII-40. Development of HPD gears and bearings would enable a size and weight reduction of the gearbox. Size reduction of the gears and bearings would increase the contact severity of the gear teeth and bearings, leading to reduction in wear, scuffing, and contact fatigue lives. To mitigate the tribologically induced reliability and durability issues expected in an HPD gearbox, materials, surface technologies, and lubricants have to be developed and integrated into the system—the focus of the present project.

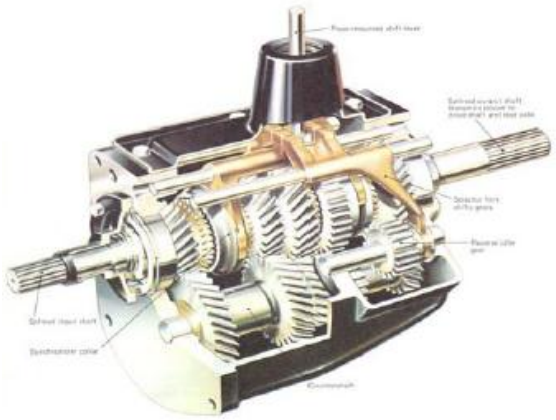

Figure VIII-40: Typical automotive transmission gearbox.

To begin, we are conducting gear contact kinematic analyses for different levels of size reductions to establish material, surface, and lubricant requirements in terms of wear scuffing and contact fatigue lives. Performance evaluation/testing methodologies are being developed to determine wear, scuffing, and contact fatigue life. The test methodologies will be used to evaluate state-of-the-art and newly developed materials, surface finishes, and lubricants for the gearbox. If the project is successful, optimized technologies that can facilitate different levels of size reduction in drive systems will be available to OEMs and their suppliers for implementation and commercialization. The key technical barrier that this project seeks to overcome is the need for the simultaneous increase in wear, scuffing, and contact fatigue lives. Often measures and technology that enhance one of these attributes will result in the degradation of another. For example, measures to increase surface wear resistance are often accompanied by the surface being more susceptible to failure by contact fatigue.

Results

Based on contact kinematic analysis of meshing gear teeth conducted in the early stage of this project, a 25% reduction in size will reduce the scuffing and wear life by one-third and the contact fatigue life as much as two-thirds. The challenge then is to develop materials, surfaces, and lubricant technologies to simultaneously increase wear and scuffing life by at least two times (preferably higher), and contact fatigue life by at least three or four times.

In the previous years, we had assessed the impacts of thin-film surface coatings in combination with lubricant technology on their friction and wear performance. Several commercially available thin-film coatings were evaluated, and their tribological performance was compared with the state-of-art case of carburized 4118 steel gear material. The evaluation was conducted with advanced commercially available lubricants and a new model lubricant formulated at Argonne National Laboratory (ANL). Results of these evaluations showed that wear life can be increased five times

by combination of coatings and the ANL model lubricant. Furthermore, friction was substantially reduced with ANL lubricant and steel as well as some coatings. Thus, wear life requirements for a HPD driveline system capable of 25% size reduction are achievable through combination of coating and innovative lubricant technologies.

The FY 2013 efforts in this project were devoted to the assessment of the effect of surface coatings on transitions in lubrication regimes for concentrated contacts. Efforts were also devoted to the development and evaluation of the contact interface with scuffing resistance adequate for the HPD system. For lubricated concentrated contacts, such as gears and bearings, the friction and surface damage are lowest in the hydrodynamic and elastohydrodynamic regimes. The operating lubrication regime is determined by the lubricant rheological properties, the surface material properties, and surface roughness. The presence of thin-film coatings will affect the surface material properties and perhaps surface roughness.

The impact of about ten commercially available coatings on the transitions in the lubrication regime for concentrated contact was studied by using a ball-on-flat contact configuration in unidirectional sliding. A step speed variation in six different cycles was used as a means of varying the lubricant fluid film thickness and, hence, the lubrication regime. All the tests were conducted at a constant contact pressure of 1 GPa, which is typical for gear teeth contact. The operating lubrication regime can be estimated from the lambda (λ) ratio, which is the ratio of lubricant fluid film thickness to the composite roughness of the contacting surfaces. The lower the λ ratio, the higher the severity of contact and more dominant the boundary regime.

Figure VIII-41 shows the friction coefficient as a function of λ ratio for steel/steel contact, steel/TiN coating contact, and a steel/diamond-like carbon (DLC) coating contact as an illustration of the range of behaviors observed on the impact of coatings on lubrication regime transitions. Some coatings have little or no effect on fluid film lubrication while others are beneficial. For steel/ steel contacts, a clear transition from a near constant friction coefficient of about 0.1 to a significant higher value (as high as 0.25) is seen as the lubrication condition changed from the fluid-film-dominated elastohydrodynamic regime at higher λ ratios to the surface-material-dominated boundary regime at lower values of λ (Figure VIII-41a). Figure VIII-41b shows an example of coatings that did not exhibit much effect on lubricant fluid film lubrication and transition in the lubrication regime. The friction behavior is nearly identical to that of steel on steel. By contrast, other coatings, as exemplified in Figure VIII-41c, clearly show no transition in the lubrication regime, even at extremely low λ ratios. This observation is very significant and warrants further study and elucidation. It suggests that the tribological performance of the lubricant fluid film can be improved when coupled with the appropriate thin film coating. Worth noting is that this observation has implications beyond the scope of the present project, as thin film coatings are increasingly becoming popular in lubricated tribological applications.

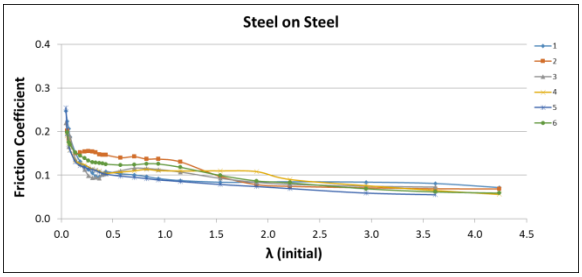

(a)

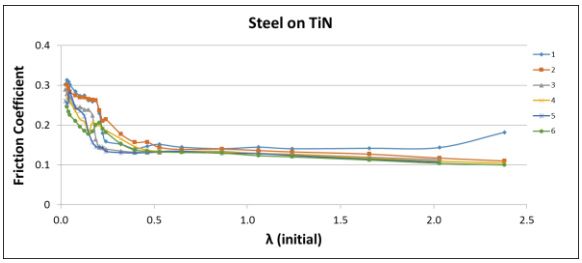

(b)

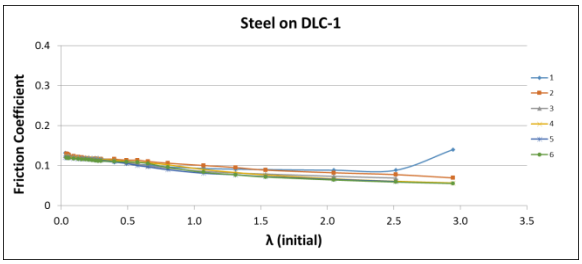

(c)

Figure VIII-41: Friction coefficient vs. λ ratio for steel on steel, TiN, and diamond-like carbon coating.

Another major focus of the FY 2013 effort is the evaluation of coatings and lubricant technologies to enhance scuffing resistance to a level than can enable at least 25% size reduction in driveline gearbox. This will require at least a twofold increase in scuffing life. We evaluated the scuffing life of potential technologies (more specifically coatings and lubricant) with a block-on-ring contact configuration using a commercially available Falex test rig. Tests were conducted at a constant rotating speed of 1000 rpm using a step-load-increase protocol. Each test was started with a normal load of 50 N, followed by an increase of 25 N every minute until scuffing occurs, as indicated by a sudden, rapid, and permanent increase in friction or the test reaching the maximum capacity of the test rig, which is 2800 N. Scuffing is also accompanied by an increase in noise and temperature. Scuffing life is judged by the contact load at which scuffing occurs.

Figure VIII-42 shows the variation of friction with time during the scuffing test of steel on steel contact pairs with three commercially available, fully formulated, state-of-the-art gear oils and ANL's partially formulated oil with synthetic polyalphaolefin (PAO) basestock.

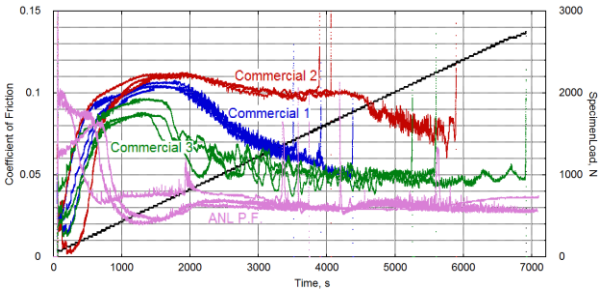

Figure VIII-42: Variation of friction during scuffing test of gear steel with different lubricants (load indicated by black line).

Similar and repeatable tribological behavior was observed in the tests with the three commercial lubricants. Three repeat tests were conducted for each lubricant, and the friction behavior was repeatable for each lubricant. At the start of the tests, at relatively low loads, the lubricant fluid film thickness is high enough to completely separate the surfaces, thereby enabling hydrodynamic lubrication. Hence, the friction coefficient is low. As the load increases, the lubricant fluid film thickness decreases as a result of higher load and increased friction heating and consequent reduction in oil viscosity. The result is an increase in friction coefficient. As the contact moves into the boundary lubrication regime, wherein severe interaction occurs between the surfaces, the friction coefficient reaches a maximum. Formation of tribochemical surface films or the so-called boundary film from the additives in the oil results in a gradual decrease of friction. As shown in Figure VIII-42, the rate of decrease is different for the three commercial lubricants; an indication of differences in their additive content. Scuffing did occur in all the tests with the commercial lubricants. The frictional behavior of the ANL formulated lubricant is significantly different from that of the commercial lubricants. This difference is due, in part, to the lower viscosity and, in part, to the additive composition. Because of the lower viscosity of the oil, the test started in the boundary lubrication regime, even at the low loads. As the load increased, a tribochemical surface film with low friction forms, resulting in very low friction coefficient, even as the load increases. The three tests with the ANL lubricant formulation all run to the maximum load capacity of the test rig (2800 N) with scuffing.

Figure VIII-43 shows the average scuffing load capacity for the different lubricants. The figure also includes the results of tests with basestock PAO fluid. The average scuffing load for the synthetic basestock is about 475 N, while the advanced fully formulated lubricant showed load-carrying capacity ranging from 1500 to 2250 N, with an average of about 1800 N. In spite of it lower viscosity, the ANL formulated lubricant has a load-carrying capacity greater than 2800 N, as none of the three tests with this formulation failed. These results demonstrated that the lubricant formulation (especially Argonne's) provides a pathway to overcome one of the tribological technical barriers (scuffing) to the development of HPD driveline system.

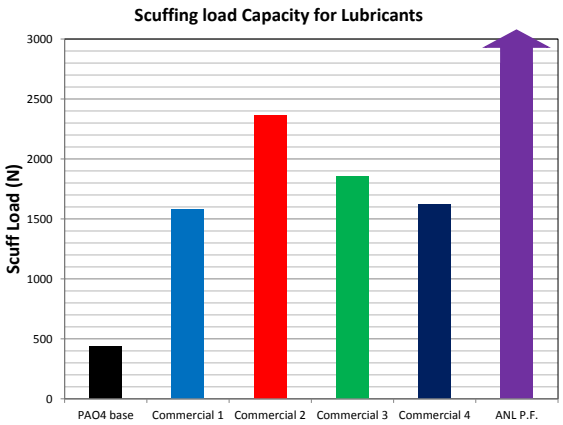

Figure VIII-43: Average scuffing load capacity for different lubricants.

In addition to the lubricant approach to enhancement of scuffing resistance, we also investigated the use of thin film coatings. We determined the scuffing resistance of the commercially available coatings listed in Table VIII-6, all of which had shown adequate wear life in the wear performance evaluation done in the previous year. Table VIII-6 shows the list of the coatings evaluated. Also included in the table are the composition, method of deposition, and some properties of the coatings.

Table VIII-6: Coatings evaluated for scuffing performance improvement.

Name	Group	Composition	Deposition Method	Thickness measured (µm)	Thickness manufacturer (µm)	Hardness manufacturer
C3	Composites	CrN/CrC	PVD	3.83	1-5	2000-2200
C3S	Composites	CrN/CrC/(Mo, W)S_2	PVD	3.29	3-7	2000-2200
C7	Composites	TiAlSiCN	PVD	4.19	2-10	3200-3500
C10	Simple Coatings	DLC (ta-C)	PVD	1.07	0.5-2.5	5000-9000
C11	Simple Coatings	DLC(a-C:H)	PaCVD	2.58	1-4	2000-3000
C12	Simple Coatings	Me-DLC	PVD	6.89	1-5	1000-2000
TiN	Simple Coatings	TiN	PVD	3.35	1-5	2300-2500
Tribologix	Non-vacuum Deposition	complex composite	sprayed	3.45		
NiPTFE	Non-vacuum Deposition	Ni + teflon	electrochemical	8.05		

PVD = physical vapor deposition; CVD = chemical vapor deposition

The scuffing tests were conducted in four different contact combinations; uncoated ring/uncoated block, coated ring/uncoated block, uncoated ring/coated block, and coated ring/coated block. The coating-on-coating contact pair used the same type of coating, e.g., C3 coated ring against C3 coated block. Thus far, tests were conducted with two types of lubricants: the low-viscosity synthetic PAO basestock and the same fluid with the ANL lubricant formulation. Plans are in place to evaluate the scuffing performance of coated surfaces when lubricated with commercially available advanced gear oils.

Figure VIII-44 typifies the variation of friction coefficient with time for the contact pair of uncoated base gear steel (3 tests) and C10 coating (2 tests) when lubricated with the unformulated PAO4 basestock fluid. Very good repeatability was observed in tests with both contact pairs. The friction behavior indicates that the boundary lubrication regime was operational during the entire test, mainly due to the relatively

low viscosity of the test fluids. The friction coefficient of the coated pair was substantially lower (about 50%) than that of the uncoated pair. Similarly, the average scuffing life expressed in terms of scuffing load for the coated pair is about two times that of uncoated steel.

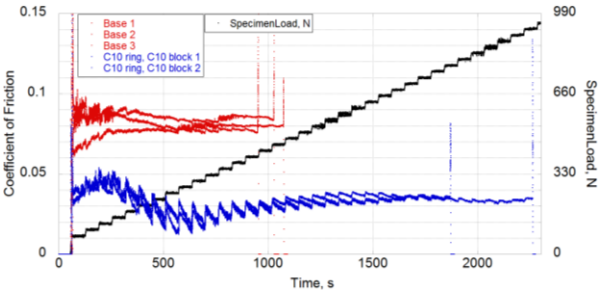

Figure VIII-44: Friction variation during scuffing test with uncoated-steel contact pair and C10-coated contact pair when lubricated with PAO4 basestock oil.

For the C10 coating, when only one surface is coated, as illustrated in Figure VIII-45, the friction coefficient shows only a slight decrease compared to the uncoated surface, and scuffing life increases by only 40%.

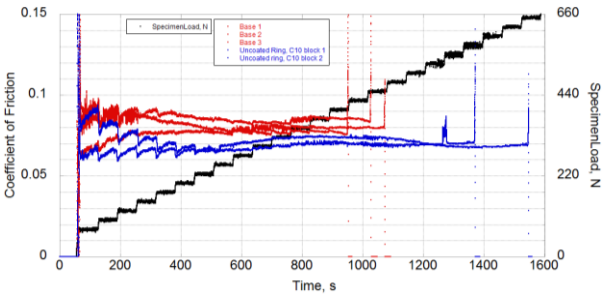

Figure VIII-45: Friction variation during scuffing test with uncoated-steel contact pair and uncoated ring against C10-coated block when lubricated with PAO4 basestock oil.

The effect of various coatings on scuffing life in both basestock and ANL formulated oils when only one of the surfaces is coated is shown in Figure VIII-46, which is for the uncoated steel rings on coated blocks. In the base fluid, many of the coatings significantly increase the scuffing load (as much as four times for TiN and C3), while others have a marginal effect on the scuffing load. In tests with the ANL formulated lubricant as compared with basestock fluid, scuffing life increased significantly with all the coatings. In two coatings (NiPTFE and Tribologix), scuffing did not occur up to the maximum load capacity of the test rig (2800 N). However, excessive or severe wear occurred in the coatings. These two coatings are examples of enhancement of one performance attribute (scuffing life) at the expense of another (wear). Recall that one of the main challenges of this project is to simultaneously increase the scuffing, the wear, and the contact fatigue life of surfaces.

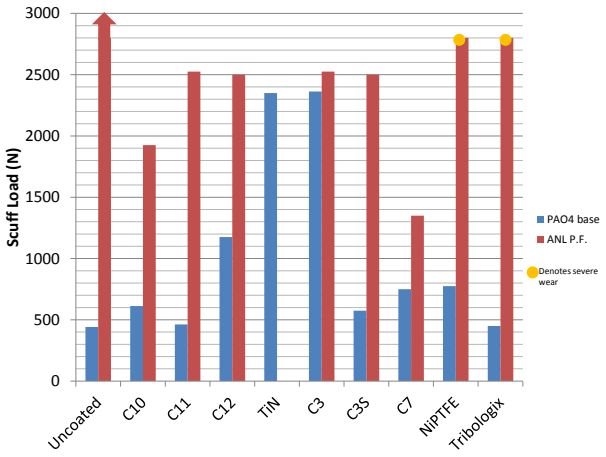

Figure VIII-46: Scuffing load for uncoated ring on coated block when lubricated with PAO4 basestock and ANL formulated lubricant.

When both surfaces in sliding contact are coated, scuffing life significantly improved for most of the coatings in both base fluid and ANL formulated lubricants. Some coatings also showed vastly different behavior. Figure VIII-47 shows the scuffing loads in tests with base fluid and ANL formulated lubricant for coating-on-coating contact pairs. Coating C11, in particular, showed a remarkable scuffing behavior in both fluids tested in that all the tests reached the maximum load capacity of the test rig without scuffing; in addition, wear was minimal in both the ring and the block samples. The use of ANL formulated lubricant also increased the scuffing load of several coatings to the maximum without failure and with minimal wear. These include C10, C11, NiPTFE, and Tribologix coatings. Two other coatings showed very good scuffing resistance, but at the expense of wear.

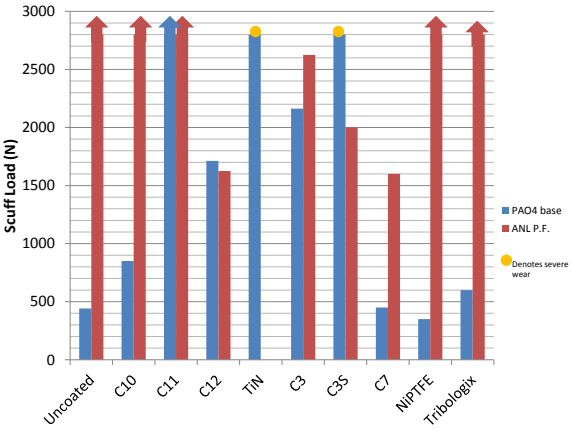

Figure VIII-47: Scuffing load for coated ring on coated block when lubricated with PAO4 basestock and ANL formulated lubricant.

Conclusions

Development of a HPD driveline system that can enable 20-25% size and weight reduction without sacrificing reliability and durability will require, at the very least, doubling the wear and scuffing life as well as tripling the contact fatigue lives of key components in the system. Often, a method or approach to enhance one of these attributes leads to the degradation of another, e.g., scuffing life improves but wear decreases. The challenge of this project is to simultaneously increase the wear, scuffing, and contact fatigue lives of surfaces. Previous efforts in this project identified combinations of coatings and lubricants with significant wear reduction (as much as five times) compared with the current state-of-art driveline component materials and lubricants. In this reporting period, we evaluated coating and lubricant combinations that can provide adequate scuffing resistance for the HPD system. Several coatings were identified that worked synergistically with a new lubricant formulation developed at ANL to simultaneously provide very good scuffing and wear resistance, with friction reduction an additional benefit. Some other coating and lubricant combinations also provided good scuffing resistance but at the expense of wear. Future effort in the project will concentrate on contact fatigue evaluation and enhancement without sacrificing the wear and scuffing life gains. This effort will no doubt require careful integration of materials, coatings, and lubricant technologies.

VIII.E.3. Products

Publications

1. O. O. Ajayi, C. Lorenzo-Martin, R. A. Erck, and G. R. Fenske, “Analytical predictive modeling of scuffing initiation in metallic materials in sliding contact,” *Wear* Vol. 301 (2013), 57-61.
2. C. Lorenzo-Martin, O. O. Ajayi, A. Erdemir, G. R. Fenske, and R. Wei, “Effect of microstructure and thickness on the friction and wear behavior of CrN coatings,” *Wear* Vol. 302 (2013), 963-971.
3. K. E. Pappacena, D. Singh, O. O. Ajayi, J. L. Routbort, O. L. Erilymaz, N. G. Demas, and G. Chen, “Residual stresses, interfacial adhesion and tribological properties of MoN/Cu composite coatings,” *Wear* Vol. 278-279 (2012), 62-70.
4. C. Lorenzo-Martin, O. O. **Ajayi,** S. Torrel, G. R. Fenske, and R. A. Erck, “Experimental investigation of transition in lubrication regime for thin-film coated surfaces,” *Proceeding of ASME/STLE International Joint Tribology Conference (IJTC),* Denver, CO (2012).
5. C. Lorenzo-Martin, O. O. Ajayi, S. Torrel, N. Demas, and G. R. Fenske, “Effect of hard thin film coatings on tribochemical film behavior under lubricated sliding contact,” *Proceeding 36th International Conference on Advanced Ceramics and Composite,* 2012.
6. O. O. Ajayi, C. Lorenzo-Martin, D. Singh, and G. R. Fenske, “Performance evaluation of hard ceramic coatings for tribological applications,” Presented at 36th International Conference and Exposition on Advanced Ceramics and Composites, ICACC, Daytona Beach, FL (2010).
7. C. Lorenzo-Martin, O. O. Ajayi, S. Torrel, N. Demas, and G. R. Fenske, “Tribological behavior of Ti-based thin film coatings under boundary lubrication regime,” Presented at 2012 STLE Annual Meeting, St. Louis, MO, May 6–10, 2012.

Patents

1. O. O. Ajayi, C. Lorenzo-Martin, and G. R. Fenske, “A tribochemical synthesis method for producing low-friction surface film coatings,” Pending.

Tools and Data

None.

VIII.F. DOE/DOD Parasitic Energy Loss Collaboration

George Fenske, Principal Investigator
Argonne National Laboratory
9700S. Cass Avenue
Argonne, IL 60439
Phone: (630) 252-5190
E-mail: gfenske@anl.gov

Co-Investigators:
Aaron Matthews (Aerotek), Nicholaos Demas, Robert Erck

CRADA Contact:
Ricardo, Inc.

Lee Slezak, DOE Program Manager
Phone: (202) 586-2335
E-mail lee.slezak@ee.doe.gov

VIII.F.1. Abstract

Objectives

- Develop a web-based toolkit based on FMEP (friction mean effective pressure) maps to predict the impact of key tribological engine parameters on vehicle fuel economy.
- Identify pathways to reduce parasitic friction losses in engines.
- Develop high-fidelity database on key tribological parameters (boundary friction) for use in a toolkit for identifying low-friction solutions.
- Validate mechanistic models by performing instrumented, fired-engine tests with single-cylinder engines to confirm system approaches to reduce friction and wear of key components.
- Identify common issues associated with commercial and military ground vehicles on the impact of low-friction lubricant technologies to reduce parasitic friction losses and vehicle efficiency.

Major Accomplishments

- Established a cooperative research and development agreement (CRADA) with Ricardo, Inc. to utilize their suite of design codes (PISDYN, RINGPAK, VALDYN, and ENGDYN) to model parasitic friction losses in critical engine components.
- Installed codes on Argonne computer system, completed training on use of software, and demonstrated functionality of codes on Argonne system.
- Established non-disclosure agreements with vehicle original equipment manufacturers (OEMs) to share design models for use in the CRADA.
- Established protocols to utilize laboratory-based test rigs to measure critical input data (asperity friction) for use in Ricardo codes.
- Developed data analysis techniques to extrapolate asperity friction data from friction tests—decouple asperity friction from hydrodynamic friction.

Future Achievements

- Complete parametric study of FMEP for a midsized diesel engine as functions of engine speed, load, lubricant viscosity, asperity friction, and surface finish for mineral and synthetic oils.
- Complete parametric study of asperity friction for commercial and advanced lubricant friction modifiers.
- Evaluate engine friction measurement techniques to validate predictive models and identify site for future engine validations.

✧ ✧ ✧ ✧ ✧

VIII.F.2. Technical Discussion

Background

Multiple approaches are being pursued to improve the fuel economy of vehicles, including the development of advanced tribological systems involving lubricants, materials, coatings, and engineered surfaces to reduce parasitic friction losses in engines (and drivelines). This project focuses on the development of a user friendly, web-based calculator to predict the impact of tribological parameters such as the boundary friction coefficient, lubricant viscosity, temperature, surface finish, speed, load, and visco-piezo properties on the fuel economy of engines typically used for ground transportation vehicles.

Introduction

Friction, wear, and lubrication affect fuel economy, durability, and emissions of engines used in ground transportation vehicles. Total frictional losses in a typical engine may alone account for more than 10% of the total fuel energy (depending on the engine size, driving condition, etc.). The amount of emissions produced by these engines is related to the fuel economy of that engine. In general, the higher the fuel economy, the lower the emissions. Higher fuel economy and lower emissions in future diesel engines may be achieved by the development and widespread use of novel materials, lubricants, and coatings. For example, with

increased use of lower viscosity oils (that also contain lower amounts of sulfur- and phosphorus-bearing additives), the fuel economy and environmental performance of future engine systems can be dramatically improved. Furthermore, with the development and increased use of smart surface engineering and coating technologies, even higher fuel economy and better environmental soundness are feasible.

Integration of advanced lubricant chemistries, textured surfaces (plateau-honed, fine-honed, etc.), and advanced component materials and coatings necessitates pursuing a systems approach. Changes in one system component can readily change the performance of other components. For example, application of a hard coating on a liner to improve its durability may decrease the durability of the mating rings. Also, lowering the viscous drag will cause certain components (e.g., bearings) to operate under boundary lubrication regimes not previously encountered, resulting in accelerated degradation. A systems approach is required to not only identify the critical components that need to be addressed in terms of energy savings, but also to identify potential pitfalls and find solutions.

The main goal of this project is to use advanced models of engine-component friction and contact loading to predict the impact of advanced surface engineering technologies (e.g., laser dimpling, near frictionless carbon, and superhard coatings) and energy-conserving lubricant additives on parasitic energy losses from diesel engine components. The project also aims to develop more realistic databases on the boundary or asperity friction that are used in advanced codes to predict total (asperity and hydrodynamic) friction losses and, in the future, to validate the predictions in tests using fired engines. Such information will help identify critical engine components that can benefit the most from the use of novel surface technologies, especially when low-viscosity engine oils are used to maximize the fuel economy of these engines by reducing churning and/or hydrodynamic losses. The long-term objective of the project is to develop a database that provides a “look-up” capability to predict the impact of lubricant viscosity, asperity friction, and surface finish on FMEP and contact severity at different engine operating modes.

Approach

Under the Argonne/Ricardo CRADA, multiple codes (PISDYN, RINGPAK, VALVDYN, and ENGDYN) will be integrated to calculate from first principles the parasitic friction losses (FMEP) under prescribed engine conditions (load and speed) for a range of tribological parameters (asperity friction, lubricant viscosity, surface finish, and pressure-temperature-viscosity coefficients). The information will be provided in a series of spreadsheets that will enable users to calculate changes in FMEP and fuel consumption scaling factors (FCSFs) to predict changes in fuel consumption for different driving cycles.

For a given engine type (diesel or gas) and size (small, medium, or large), the database will consist of FMEP contributions from the ring pack, piston skirt, engine bearings, and valve train as a function engine mode (load and speed) for different lubricant viscosities, asperity friction, type (mineral or synthetic), and component surface finish. The database users will employ a recommended baseline configuration (viscosity, asperity friction, surface finish, and oil type), or users can specify their own baseline configuration and a new (variant) configuration. The users will also specify the engine modes (speed and load) and weighting factors. The web-based calculator will utilize the FMEP database to calculate differences in the FMEP (relative to the baseline), which will be used to scale the fuel consumption at each specified engine mode (speed and load) and thus predict the change in fuel consumption from the baseline.

Our primary task for this project is to perform FMEP calculations for the following range of parameters: engine type [spark ignition (SI) or compression ignition (CI)], engine size, engine mode (speed and load), lubricant viscosity, asperity friction, surface finish, oil type (mineral or synthetic), and additive (friction modifier), as discussed previously [1]

The codes used to model the FMEP allow detailed calculations of the dynamic forces on the engine components and, in the process, provide information on the severity of the contact loading between moving components (e.g., between the rings and cylinder liner). Such information will also be tracked and used to predict changes in the contact severity for different tribological conditions as well as changes in the minimum oil film thickness. This information can, to a first approximation, be used to estimate the impact of the parameters on component durability (gradual wear) and reliability (sudden catastrophic failure, e.g., scuffing) and the need for improved wear resistance and/or surface finishes to accommodate a given low FMEP strategy.

A second task focuses on developing a high-fidelity database on asperity friction for use in the calculator. Our approach in this effort utilizes laboratory-scale tribometers to simulate engine conditions to measure asperity friction for a range of conventional and experimental material and lubricant combinations.

A third task, not discussed here, focuses on fired-engine validation studies to be performed in the second and third years of the CRADA.

Results

As reported last year [1], previous FMEP results [2-6] typical of a large (9-12 L) diesel engine were analyzed by using FMEP maps to illustrate FMEP as functions of engine speed and load. The FMEP maps serve as the basis to calculate FMEP difference maps for various parameters (engine type, engine size, lubricant viscosity, asperity friction, surface texture/finish, and mineral type). Figure VIII-48 shows an FMEP difference map for the large diesel engine modeled in the previous study.

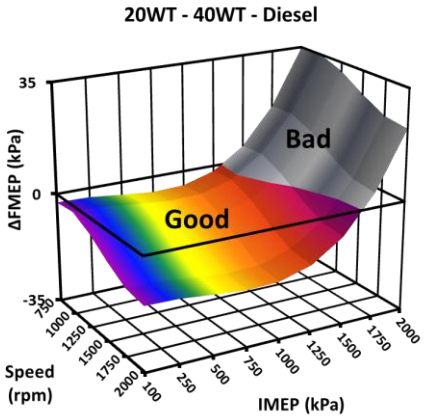

Figure VIII-48: FMEP difference map showing ΔFMEP between 20 WT and 40WT oil as function of speed and load.

The finite difference maps will be used to calculate FCSFs for the different cases from the following equation:

$$FCSF = (IMEP + \Delta FMEP)/IMEP$$

where IMEP is the indicated mean effective pressure. Figure VIII-49 illustrates the reduction in fuel consumption as a function of engine condition (load and speed) for the case illustrated in Figure VIII-48.

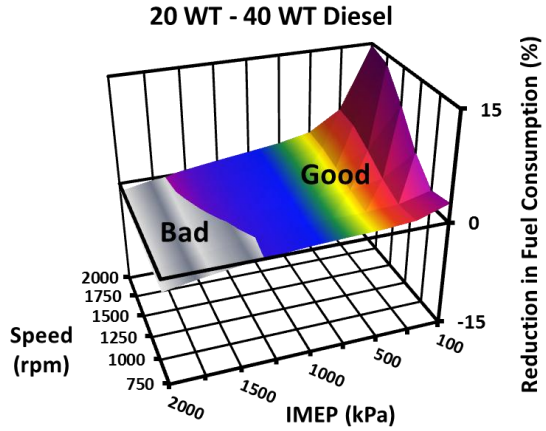

Figure VIII-49: Reduction in fuel consumption as a function of load and speed.

During FY 2013, the latest version (2013.2) of the Ricardo software codes (PISDYN, RINGPAK, VALVDYN, and ENGDYN) was installed on an Argonne computer, and work was initiated to validate their functionality to model FMEP for a small SI single-cylinder research engine (Ricardo Hydra gasoline engine). The results were compared with previous calculations using the same engine model parameters [7]. The results with the 2013.2 version codes were in good agreement with the previous (2006) version results.

Subsequent to demonstrating the functionality of the versions installed at Argonne, a series of parametric studies was initiated using the Hydra engine model, which is representative of a small SI engine with 500 cubic centimeter (CC) displacement per cylinder. Case studies were performed at four speeds and five load conditions for different lubrication grades (5W, 5W/30, 30 WT, and 50 WT) using the RINGPAK and PISDYN codes to determine frictional losses in combustion chamber components (skirt/liner, rings/liner, and wrist pin)—which typically represent 60% to 70% of an engine's frictional losses.

Figure VIII-50 shows an example of the calculated friction of the piston (piston skirt and wrist pin) and ring pack (top compression ring, scraper ring, and a three-piece oil control ring) as a function of crank angle for a "baseline" case (5W/30 oil) at a motor speed of 2000 rpm and an indicated load (IMEP) of 9 bar, corresponding to 7.5 kW indicated horsepower. The dashed lines correspond to crank-angle averages of the absolute values of the friction forces.

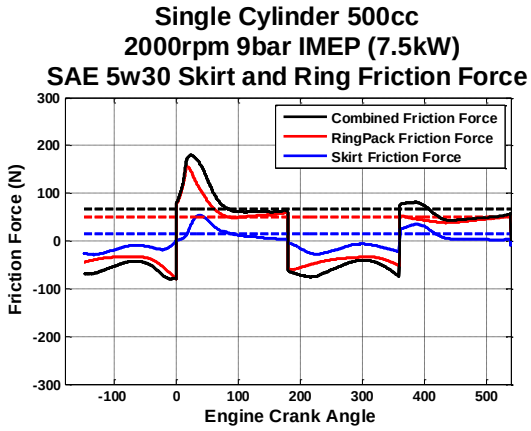

Figure VIII-50: Friction force of piston and ring pack as a function of crank angle for single-cylinder SI engine (500 CC displacement, 2000 rpm, 9 bar IMEP, 5W/30 oil).

Figure VIII-51 shows the friction power losses for the same conditions as those shown in Figure VIII-50. The dashed lines correspond to the crank-angle averaged values of the friction power. A comparison of the averaged data with the indicated power (7.5 kW) is an indicator of the fraction of power lost to friction. In this case approximately 400 W is attributed to friction power in the rings and piston, or roughly 5% of the indicated power. The majority of the power losses due to cylinder friction arises from the piston contributions (piston skirt and wrist pin).

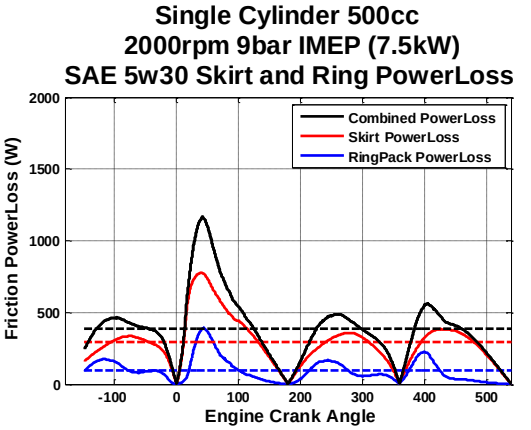

Figure VIII-51: Friction power as a function of crank angle for single-cylinder SI engine (500 CC displacement, 2000 rpm, 9 bar IMEP, 5W/30 oil).

Also examined was the effect of the lubricant viscosity of the combustion chamber friction and friction power loss. Figure VIII-52 shows the total friction power loss (rings and piston) for the baseline case for three lubricant viscosities (a light oil, 5W; a multigrade oil, 5W/30; and a heavy oil, 50WT).

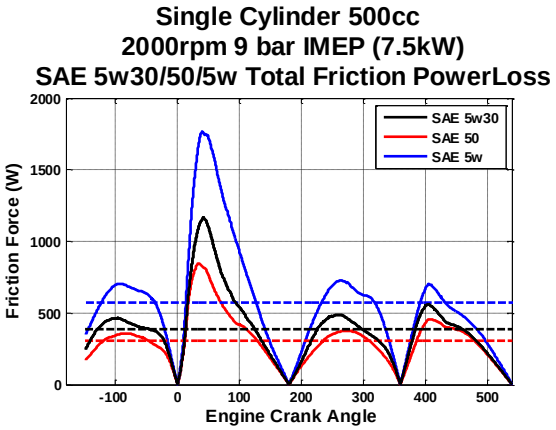

Figure VIII-52: Friction power as a function of crank angle for three oil viscosities for single-cylinder SI engine (500 CC displacement, 2000 rpm, 9 bar IMEP).

As seen in Figure VIII-52, the greatest power loss occurs for the lightest oil (5W), while the lowest losses occur with the heavier oil (50 WT), suggesting that this engine design (and test condition) operates primarily in the boundary/mixed lubrication regime, where increases in viscosity reduce asperity friction and move more into hydrodynamic conditions. At higher speeds, where hydrodynamic lubrication dominates, the 5W/30 oil exhibits the lowest friction losses.

Task 2 of the CRADA addresses developing a high fidelity database on asperity friction for use in the models. As reported last year [1], Argonne has established a number of laboratory-scale test protocols to simulate engine conditions and to quantify asperity friction coefficients for different lubricant packages, temperatures, and surface finishes. The protocols utilize reciprocating ring-on-liner and ball-on-flat configurations as well as a unidirectional (rotating) ball-on-flat configuration to measure friction during 1- to 3-hour long tests. The protocols include speed ramps at the start and end of the tests to obtain speed-dependent data. The friction data were analyzed by using a Stribeck approach wherein the friction is plotted first as a function of speed, then as a function of the Stribeck parameter (ηs/L), where η is the viscosity, s is the speed, and L is the applied load.

An example of the friction data obtained during a reciprocating test is shown in Figure VIII-53 (red curve shows the friction trace). At ring reversal, where the speed is low/zero, the friction is high, representative of asperity friction. Near midstroke, the friction decreases when the condition transitions from asperity to mixed to hydrodynamic friction. The traces are not symmetrical since the rings are non-symmetrical.

Figure VIII-54 shows an example of the friction data plotted as a function of the Stribeck number for tests at 20 and 100°C. In this case data are shown for unformulated synthetic oils and commercial fully formulated oil.

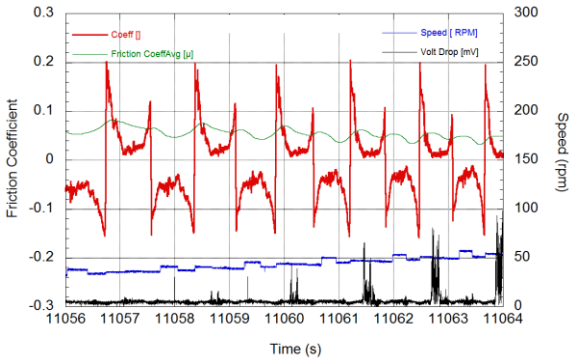

Figure VIII-53: Friction trace obtained during a ring-on-liner laboratory-scale test with a synthetic lubricant at 25°C.

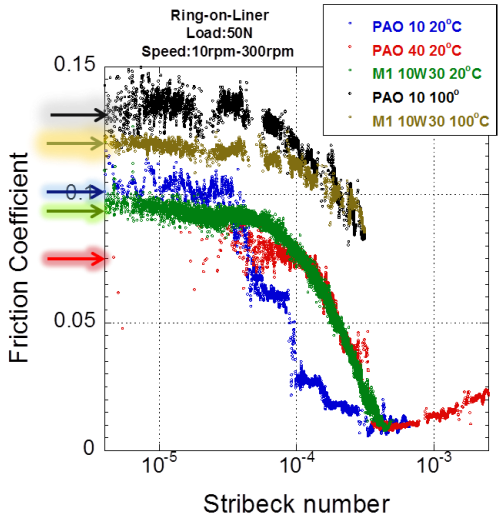

Figure VIII-54: Friction as a function of Stribeck number for unformulated and formulated synthetic engine lubricants at different temperatures.

The friction data, denoted by the multicolored arrows along the friction axis in Figure VIII-54, are not constant, but rather are dependent on the temperature and formulation package. Tests thus far, using different configurations (ring-on-liner, skirt-on-liner, and ball-on-flat) have exhibited asperity friction coefficients that range from 0.04 to 0.15 depending on the temperature, oil formulation, and surface texture.

Conclusions

The Parasitic Energy Loss Reduction project is examining the effects that tribological variables such as viscosity, boundary friction, and surface finish have on the friction losses in an engine and the overall vehicle fuel economy. A CRADA was established with Ricardo Inc. to develop a fuel economy calculator using their commercial codes and experimental asperity friction data to quickly estimate the impact of advanced tribological concepts on fuel economy.

Studies on a high frequency reciprocating rig and pin-on-disk rig indicate that more realistic information on boundary friction coefficients can be achieved as functions of temperature and composition. Several candidate additive

approaches have been identified that show significant improvements in friction.

Future activities will focus on CRADA activities to model parasitic friction losses for a large diesel engine using OEM engine models. Work will continue to "data mine" existing friction data for a range of tribotests performed during the past 5-10 years at Argonne as well as to identify novel friction modifiers under development. Efforts to further define a cohesive collaboration with the U.S. Army Tank Automotive Research, Development and Engineering Center (TARDEC) are in progress under a formal memorandum of understanding developed between the Departments of Energy and Defense to pursue advanced vehicle power technologies.

References

1. G. Fenske, N. Demas, and R. Erck, "DOE/DOD Parasitic Energy Loss Collaboration," FY 2012 Annual Progress Report, DOE/EE-0834.
2. I. Fox, "Numerical Evaluation of the Potential for Fuel Economy Improvement due to Boundary Friction Reduction within Heavy-Duty Diesel Engines," ECI International Conf. on Boundary Layer Lubrication, Copper Mountain, CO, Aug. 2003.
3. George Fenske, "Parasitic Energy Loss Mechanisms," *FY 2006 Progress Report for Heavy Vehicle Systems Optimization* (2006).
4. George Fenske, "Parasitic Energy Loss Mechanisms: Impact on Vehicle System Efficiency," U.S. Department of Energy Heavy Vehicle Systems Review, Argonne National Laboratory, Argonne, IL, April 18-20, 2006.
5. G. Fenske, O. Ajayi, R Erck, C. Lorenzo-Martin, A Masoner, and A. Comfort, "Reliability of Powertrain Components Exposed to Extreme Tribological Environments," Proceedings of the 2010 Ground Vehicle Systems Engineering and Technology Symposium, Dearborn, MI, 2010.
6. George Fenske, Nicholaos Demas, and Robert Erck, "Efficiency Improvements through Parasitic Loss Reduction," *FY2011 Annual Progress Report for Vehicle Systems Optimization* (2011).
7. Phil Carden and David Bell, "Piston Assembly Friction Losses: Comparison of Measured and Predicted Data," SAE 2006-01-0426.

VIII.F.3. Products

Publications

1. Tribological evaluation of piston skirt/cylinder liner contact interfaces under boundary lubrication conditions, N. G. Demas, R. A. Erck, and G. R. Fenske, Lubrication Science, 22:3, 73–87, 2010.
2. Tribological studies of coated pistons against cylinder liners in laboratory test conditions, N. G. Demas, O. O. Ajayi, R. A. Erck, and G. R. Fenske, Lubrication Science, DOI: 10.1002/ls.1175, 2012.
3. Tribological effects of BN and MoS_2 nanoparticles added to polyalphaolefin oil in piston skirt/cylinder liner tests, N. G. Demas, E. Timofeeva, J. L. Routbort, and G. R. Fenske, Tribology Letters, 47:1, 91-102, 2012.
4. Influence of surface texture on micro EHL in boundary regime sliding, R. A. Erck, O. O. Ajayi, C. Lorenzo-Martin, and G. R. Fenske, Extended Abstract, ASME/STLE 2012 International Joint Tribology Conference, October 8-10, 2012.
5. Effect of hard coatings on tribochemical film behavior in lubricated sliding contact, N. G. Demas, A. Navratil, O. O. Ajayi, and G. R. Fenske, 35th International Conference and Exposition on Advanced Ceramics and Composites (ICACC'12), Daytona Beach, FL, January 22-27, 2012.
6. Tribological behavior of Ti-based thin film coatings under boundary lubrication regime, C. Lorenzo-Martin, N. G. Demas, and O. O. Ajayi, STLE Annual Meeting, St. Louis, MO, May 6-10, 2012.
7. Investigation of MoS2 and BN nanolubricants and their effect on the tribological behavior of combustion engine parts, Poster, N. G. Demas, E. Timofeeva, J. L. Routbort, and G. R. Fenske, APS/CNM/EMC Users Meeting, Argonne National Laboratory, 2012
8. Tribological effects of BN and MoS2 nanoparticles added to polyalphaolefin oil in piston skirt/cylinder liner tests, N. G. Demas, E. Timofeeva, J. L. Routbort, and G. R. Fenske, ASME/STLE International Joint Tribology Conference, Denver, CO, October 8-10, 2012.
9. Effect of coating thickness on tribological performance of CrN in dry sliding contact, C. Lorenzo-Martin, O. O. Ajayi, S. Torrel, N. G. Demas, A. Erdemir, and R. Wei, ASME/STLE International Joint Tribology Conference, Denver, CO, October 8-10, 2012.

Tools and Data

Software tools that are provided for use in this project as part of the CRADA with Ricardo, Inc., include: RINGPAK, PISDYN, ENGDYN, and VALDYN.

FAST AND WIRELESS CHARGING

VIII.G. INL Wireless Power Transfer and EVSE Charger Testing

James Francfort, Principal Investigator
Idaho National Laboratory
P.O. Box 1625
Idaho Falls, ID 83415-2209
Phone: (208) 526-6787
E-mail: James.francfort@inl.gov

Lee Slezak, DOE Program Manager
Phone: (208) 586-2335
E-mail: Lee.slezak@ee.doe.gov

VIII.G.1. Abstract

Objectives

- Provide the U.S. Department of Energy (DOE) with independent and unbiased benchmarked testing requests evaluating technologies that DOE and industry have invested in
- Benchmark the efficiencies and safety of wireless power transfer (WPT) systems and conductive electric vehicle supply equipment (EVSE) and DC fast chargers (DCFC)
- Benchmark the cyber security of charging systems
- Benchmark DCFC and Level 2 compatibility with new generations of plug-in electric vehicles (PEVs)
- Continue to provide testing results to other DOE programs and national laboratories, as well as several U.S. Drive technical teams that Idaho National Laboratory (INL) staff are members of.

Major Accomplishments

- Designed and fabricated non-metallic test platform for wireless testing of WPT systems.
- Completed and published testing results for the first WPT system ever to have testing results publicly disseminated. Testing included efficiencies and EMF emissions at 2,600 test positions during lab testing.
- Provided significant support to Society of Automotive Engineers (SAE) J2954 in their development of WPT codes and standards.
- Completed testing of fourteen Level 1 and 2 EVSE, with 9 of the 12 tested during Fiscal Year (FY) 2013.
- Completed testing of one DCFC and published the testing results.
- Completed non-disclosure agreements (NDAs) and held kickoff meeting with four industry companies that are developing smart EVSE funded by the DOE Office of Electricity Delivery and Energy Reliability.
    - Testing will include cyber security and efficiency testing.
- Completed cyber security testing of a smart EVSE.
- Initiated joint SAE, ETEC Labs, and INL charging compatibility testing of approximately 40 DCFC, EVSE, and vehicles.
- Additional NDAs have been signed and are being signed in anticipation of additional testing candidates.

Future Achievements

- Continue identifying WPT, DCFC, and EVSE test partners and obtaining test systems.
- Conduct cyber security testing on four new smart EVSE developed with funding from DOE Office of Electricity Delivery and Energy Reliability.
- Continue close coordination with the SAE J2954 committee.
- Conduct charging compatibility testing of DCFC, EVSE, and vehicles when Argonne National Laboratory has completed developing the delayed test monitoring software.
- Test WPT system that has been installed on a Chevy Volt.
- Determine EMF exposure levels onboard the Volt.

✧ ✧ ✧ ✧ ✧

VIII.G.2. Technical Discussion

Background

DOE's Advanced Vehicle Testing (AVTA) is part of DOE's Vehicle Technologies Office, which is within DOE's Office of Energy Efficiency and Renewable Energy. AVTA is the only DOE activity tasked by DOE to conduct field evaluations of vehicle technologies and fueling infrastructure that use advanced technology systems and subsystems in light-duty vehicles to reduce petroleum consumption. A secondary benefit is reduction in exhaust emissions.

Most of these advanced technologies include the use of electric drive propulsion systems and advanced energy storage systems (ESS). However, other vehicle technologies that employ advanced designs, control systems, or other technologies with production potential and significant petroleum reduction potential are also considered viable candidates for testing by ATVA.

Charging infrastructure for electric drive vehicles is also a study area of focus, because there is no singular successful business model that has been developed for public charging. In addition, there is much discussion within both the vehicle

and charging infrastructure industries as to what the appropriate level of charging (kW) will be in the future and where will that placement occur (e.g., public, workplace, and/or residential?). In support of this uncertainty, INL is testing the efficiencies, standby power, unit power during charging, and non-alignment (for WTP) impacts on efficiency and EMF emissions.

The AVTA light-duty activities are conducted by INL for DOE. INL has responsibility for AVTA's technical execution, direction, management, and reporting, as well as data collection, analysis, and test reporting.

The current AVTA staff has 20+ years of experience testing grid-connected PEVs and PEV charging infrastructure. This experience includes significant use of DCFCs with various battery chemistries since the middle 1990s; that important legacy of experience is still available today. In addition, INL has significant experience performing cyber security testing for various Federal agencies that are also being used for this project. AVTA is currently collecting performance and use data from more than 16,000 Level 2 EVSE from the two largest providers of EVSE, as well as several additional EVSE manufacturers.

Introduction

With the expanding introduction and use of grid-connected PEVs by fleets and individual taxpayers, in parallel, there is continuing development of both private and public PEV charging infrastructure, collectively known as conductive EVSE. EVSE currently takes the form of Level 1 (110 Volt) and Level 2 (240 Volt) levels that safely supply AC electricity to the vehicle and the charger that resides on the vehicle. The third type of EVSE is the DCFC, which provides DC electricity to the vehicle and the power electronics equipment onboard the vehicle. For DCFC, the charger is actually located offboard the vehicle in the DCFC unit itself. Level 1 and 2 EVSE may either be in the form of smart EVSE, with functionalities such as revenue grade electricity meters, bidirectional communication capabilities, and other smart features. The opposite of this is "dumb" EVSE, which only provide electricity with minimal communication and metering capabilities. Regardless if an EVSE is smart or less than optimally smart, its basic function is to safely transfer AC electricity from the consumers' side of the electric utility meter to a PEV, which has an onboard vehicle battery charger and power electronics. By nature of its design, DCFC are also at least somewhat smart units to ensure a minimal amount of communication between the DCFC charger and the vehicle's battery control system.

Normally, the term EVSE will refer to Levels 1 or 2 and DCFC will be referred to by its acronym. It should be noted that most installed EVSE are Level 2 units, which provide significantly shorter charge times than Level 1.

Adding to the complexity of charging infrastructure selection and placement is the introduction of wireless charging systems, which transfer power without having the conductive connector of today's EVSE and DCFCs (thus the term wireless power transfer or WPT). To support the introduction of safe and efficient wireless charging systems, DOE and the AVTA are conducting a series of activities to test and benchmark WPT systems. These activities include grants to support development of smart EVSE and wireless charging, as well as benchmarking the efficiencies of the different charging options and testing for the vehicle-to-charging infrastructure compatibility. The activities discussed here detail the support activities being conducted by INL and some of the benchmarked results.

Approach

INL has created a process to benchmark wireless charging systems developed with DOE technology funding and with other wireless providers. Initial testing has been conducted and the results for the first system tests will be discussed in the next section. Of significant importance is the creation of NDAs in order to support the development of test procedures and sharing of protected proprietary information, while protecting the release of the proprietary information. This is currently ongoing with several NDAs signed to date.

INL has benchmarked the cyber security of the first Level 2 smart EVSE in partnership with the EVSE manufacturer. This is not an area that will receive significant disclosure due to the nature of the subject.

Much discussion has occurred regarding efficiency of emerging wireless systems. For this reason, INL obtained, tested, and provided the first independent test results for a WPT system.

Of concern to industry and DOE is the compatibility of both DCFC and EVSE Level 2 equipment with original equipment manufacturer vehicles. AVTA has already benchmarked some compatibility problems with the new generations of PEVs; therefore, this task has been expanded and a test regime has been designed in conjunction with SAE and Argonne National Laboratory. When the Argonne National Laboratory-designed testing software is finished, approximately 40 vehicles, EVSE, and DCFC will be compatibility tested by AVTA under the supervision of INL engineers.

INL has developed a testing regime for benchmarking Level 1 and 2 conductive EVSE efficiencies and this is being used to document grid-to-vehicle energy transfer efficiencies. This work is being leveraged to support benchmarking of the DOE Office of Electricity Delivery and Energy Reliability-developed smart grid EVSE. The smart EVSE are scheduled for delivery in late Calendar Year 2013 and testing will commence then.

In accordance with AVTA's normal process, fact sheets and reports are used to document benchmarking procedures and results and the quantitative results are published, with the exception of cyber security findings.

Results

EVSE Testing

There have been 14 Level 1 and 2 EVSE that have completed benchmark testing and the results are available at: http://avt.inel.gov/evse.shtml. Note that results for only 12

EVSE are published at the time of this report because the fact sheets for the other two were in the final review process. A single fact sheet is published for each EVSE and the documented results include the following:

- Features
- Specifications
- Model tested
- Test conditions
- Test vehicle used
- Test results, including the following:
  - AC watt energy consumption prior to (Figure VIII-55), during steady-state (Figure VIII-56), and at post charge
  - Steady-state charge efficiency (Figure VIII-57)
  - Charge start (Figure VIII-58) and end profiles (Figure VIII-59).

The amount of EVSE standby energy consumption is directly tied to the "smartness" or features offered by each of the Level 2 EVSE. The more features the units offer, the more energy each EVSE will consume internally. Note that the energy transfer efficiencies range from a low of 97.91% to a high of 99.68% (Figure VIII-57).

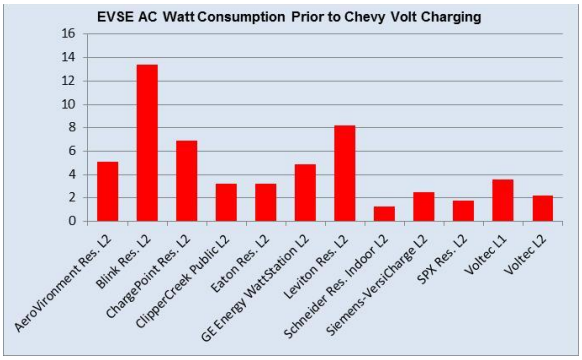

Figure VIII-55: Level 1 and 2 EVSE energy consumption prior to Chevy Volt charge event testing.

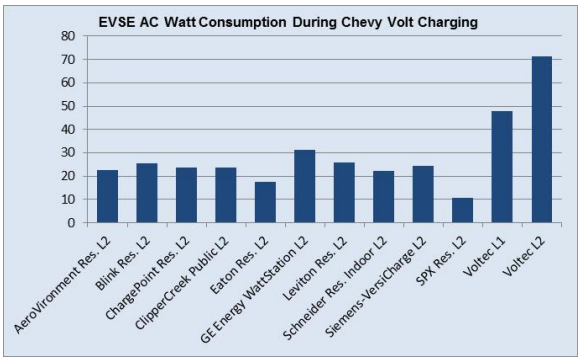

Figure VIII-56: Level 1 and 2 EVSE energy consumption during Chevy Volt charge event testing.

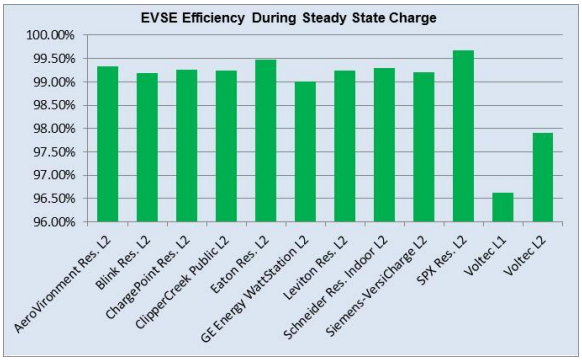

Figure VIII-57: Level 1 and 2 EVSE efficiency during steady-state Chevy Volt charging.

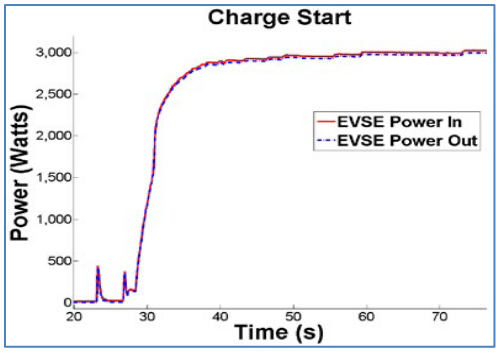

Figure VIII-58: Typical Level 2 EVSE charge profile at start of charging a Chevy Volt.

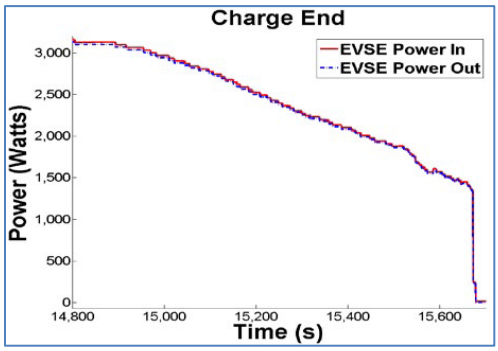

Figure VIII-59: Typical Level 2 EVSE charge profile at the end of a Chevy Volt charge event.

DCFC Testing

To further establish benchmark efficiencies for charging PEVs by different charging technologies, INL conducted a structured test of the Hasetec DCFC (Figure VIII-60). It has an input voltage of 480 VAC, three-phase and maximum input current of 120 amps. A Nissan Leaf was used as the test vehicle for the fast charging via a CHAdeMo connector.

Figure VIII-60: Hasetec DCFC.

A published fact sheet provides the below information:

- Specifications
- Test conditions
- Test vehicle used, including initial Leaf ESS state of charge 9% and final Leaf ESS state of charge 86%
- Test results, including the following:
  - Peak power draw from the grid, 53.1 AC kW
  - Energy from grid, 15.0 AC kWh
  - Peak charge power to Leaf ESS, 47.1 DC kW
  - Energy delivered to Leaf ESS, 13.3 DC kWh
  - Charge time, 31 minutes, 40 seconds
  - Overall charger efficiency (480 Vac to ESS DC) 88.7% (Figure VIII-61)

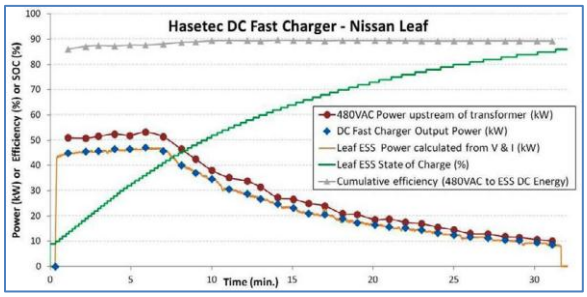

Figure VIII-61: Hasetec DCFC profile for charging a Nissan Leaf.

WPT Charger Testing

INL recently completed the first independent public testing of a wireless charging system. INL performed 2,600 separate tests of the Evatran Group Inc's PLUGLESS Level 2 Charging System (Figure VIII-62) at various distances and off-sets. The INL-produced Evatran testing results are the first wireless power transfer technology to be independently documented and published. The testing results document the efficiency results, magnetic and electric fields, and overall system performance. Evatran supported the testing process with pretesting engineering input.

Figure VIII-62: Evatran WPT system. Note that the cable will be longer in actual use and possibly located subsurface.

The Evatran PLUGLESS system uses WPT technology to charge the PEV traction battery. Instead of the usual physical connection that PEV owners must make when they have to connect the offboard EVSE cable to the vehicle's charge port, WPT systems require the PEV owner to park their vehicle over the top of the charging coil in a designated parking manner for charging to start. In addition to the convenience of avoiding plugging in a vehicle to the EVSE, a guidance system helps guide the PEV driver to park in the best position for efficient charging.

WPT involves charging electric vehicles without the more common wire-to-wire conductive connections used by most of the electric vehicle charging infrastructure currently in use. Static wireless charging provides the potential to greatly increase the number of electric vehicle miles driven by making the recharging of a vehicle's battery pack possible without any driver responsibilities to initiate charging sessions by plugging in. The only driver responsibility is to park the vehicle over the primary wireless charging coil, which can either be lying on the ground or imbedded in the surface. This allows for potentially higher charging participation, which, again, allows for more electric miles.

It should be noted that testing to-date has not made any economic life-cycle cost comparisons between the EVSE, DCFC, and WPT technologies. While EVSE and DCFC product and installation costs have been well benchmarked by INL, WPT technologies are too early in the development stage to attempt to determine their technology costs with a high degree of certainty.

For wireless charging system testing, it is important to define the coordinate system and origin utilized for testing and presentation of results. The origin is defined to be at the geometric center of the secondary coil and at the bottom plane of the enclosure hosing the secondary coil. This geometric center of the secondary coil is not necessarily the center of the housing that encloses the secondary coil because the coil may not necessarily be positioned in the center of the enclosure. From this origin, the positive X direction is toward the front of the vehicle, the positive Y direction is toward the left side (driver's side) of the vehicle, and the positive Z direction is up vertically toward the roof of the vehicle. Figure VIII-63 shows a drawing of the coordinate system with respect to a vehicle.

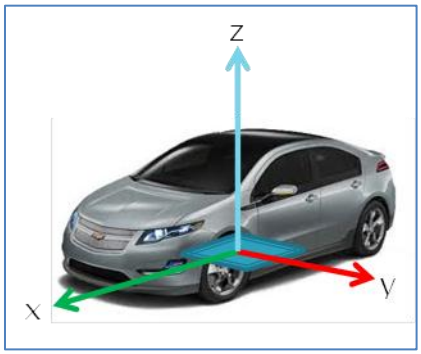

Figure VIII-63: Coordinate system for testing wireless charging (image provided by SAE J2954).

Figure VIII-64 shows the positioning table and the fiberglass support frame for testing the wireless charging systems.

Figure VIII-65 shows a schematic of power flow from electricity generation to the vehicle propulsion system. The green arrows indicate the portion of this flow path that is enabled by the wireless charging system; therefore, it shows the system interaction with the entire well-to-wheels path.

Figure VIII-66 shows the system efficiency of the Evatran system when operating at 3.3-kW output power at a coil–to-coil gap of 100 mm for various coil offset alignments. It should be noted that 2,600 tests are required at various locations within the three axes in order to correctly represent some of the efficiencies seen in Figure VIII-66.

Note that the maximum efficiency for this operation condition of 100-mm gap at 3.3 kW is 88.8% at X = -90 mm and Y = -30 mm. The system efficiency can be seen to be slightly lower when the coils are aligned (i.e., X = 0, Y = 0). Also note that at the outer extent of the operating envelope, where the offset alignment is greater than 90 mm, the system efficiency is also reduced.

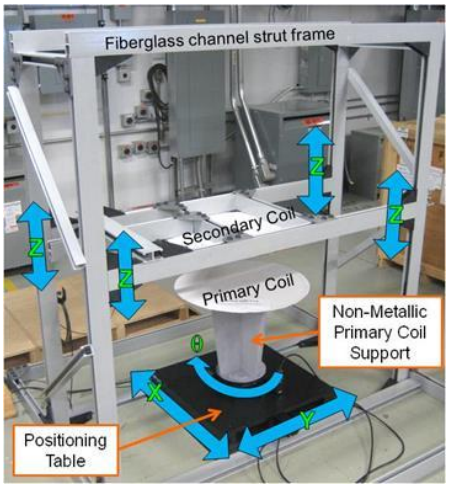

Figure VIII-64: Laboratory test fixture for wireless charger alignment positioning.

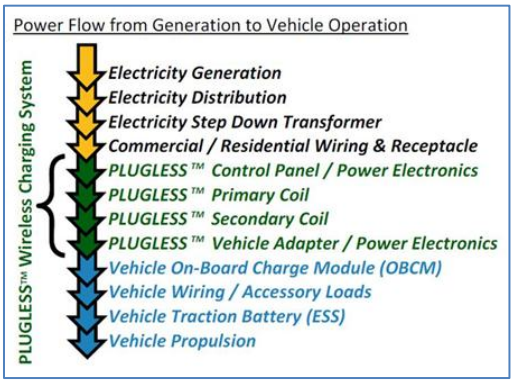

Figure VIII-65: Schematic and definition of system efficiency.

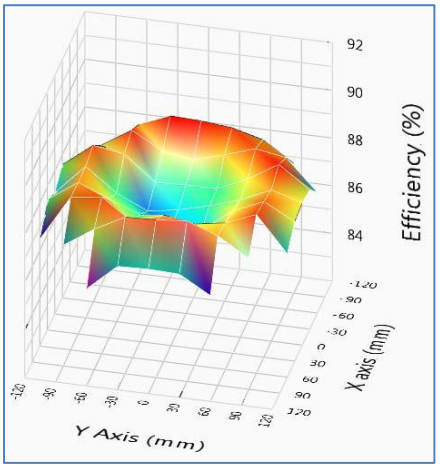

Figure VIII-66: Evatran WPT efficiency for 2,600 tests.

Conclusions

INL will be testing additional wireless charging technologies with industry participation during the next 12 months. Industry, DOE, and INL are also conducting research into dynamic vehicle charging technologies that will use wireless power transfer technologies for possibly charging vehicles while they are driven on roadways.

Most wireless charging companies are working toward a level of 90% or greater efficiency. This efficiency is often compared to Level 2 EVSE efficiency, but an apple-to-apple comparison of EVSE Level 2 and wireless charger efficiencies is not realistic due to the contrast in the power electronics of the competing technologies. Therefore, AVTA is working with industry to develop equitable methods and onboard vehicle locations to benchmark energy efficiencies of different charging technologies.

The development of NDAs in preparation of performing charging performance testing and cyber security testing is a significant accomplishment and, as FY 2013 ended, INL has completed several of these legal processes with respective manufacturers.

VIII.G.3. Products

Publications

1. PLUGLESSTM *Level 2 EV Charging System (3.3 kW) by Evatran Group Inc*, 2013, INL/MIS-13-29807, Idaho National Laboratory, Idaho Falls, ID, August 2013.
2. *Production EVSE Fact Sheet: DC Fast Charger: Hasetec,* 2012, INL/EXT-11-23986, Idaho National Laboratory, Idaho Falls, ID, November 2012.
3. *Energy Storage for DC Fast Chargers Development and Demonstration of Operating Protocols for 20-kWh and 200-kWh Field Sites,* 2013, INL/EXT-13-28684, Idaho National Laboratory, Idaho Falls, ID, March 2013.
4. *Electric Vehicle Supply Equipment (EVSE) Test Report: GE Energy WattStation,* 2012, INL/EXT-11-23986, Idaho National Laboratory, Idaho Falls, ID, November 2012.
5. *Electric Vehicle Supply Equipment (EVSE) Test Report: Schneider Electric,* 2012, INL/EXT-11-23986, Idaho National Laboratory, Idaho Falls, ID, November 2012.
6. *Electric Vehicle Supply Equipment (EVSE) Test Report: Siemens-VersiCharge,* 2012, INL/EXT-11-23986, Idaho National Laboratory, Idaho Falls, ID, November 2012.
7. *Electric Vehicle Supply Equipment (EVSE) Test Report: Voltec 120V*, 2012, INL/EXT-11-23986, Idaho National Laboratory, Idaho Falls, ID, November 2012.

Patents

This is a test program that is not designed to develop patents. The intent is to provide independent testing and feedback to DOE and industry on DOE and other funded technologies and technology improvements.

Tools and Data

The data generated by this testing are used to populate publications in the form of testing fact sheets, reports, and industry-referred papers.

INL/MIS-13-30556

VIII.H. Fast Charging Systems Integration with Renewables and Storage

Tony Markel, Principal Investigator
National Renewable Energy Laboratory
1617 Cole Boulevard
Golden CO, 80401
Phone: (303) 275-4478
E-mail: Tony.Markel@nrel.gov

Lee Slezak, DOE Program Manager
Phone: (202) 586-2335
E-mail: Lee.Slezak@ee.doe.gov

VIII.H.1. Abstract

Objectives

- Develop an economic optimization model that incorporates potential integration of photovoltaics and energy storage with a fast charger to meet real-world demands of drivers.
- Integrate knowledge gleaned from participation in IEA Task 20 Quick Charging international collaboration meetings
- Testing of fast charge systems hardware integration with renewables and energy storage in the NREL Vehicle Testing and Integration Facility

Major Accomplishments

- Developed an optimization model of a fast charger with energy storage and renewables
- Presented model details and goals at Annual Merit Review
- Conducted orientation analysis of solar systems with fast charger demands and electricity pricing structures

Future Achievements

- Apply the models developed and work toward identifying system scenarios and solutions that extend the capabilities and value proposition of fast-charge systems supporting the successful adoption of electric vehicles
- Utilize field data to guide future analyses

✧ ✧ ✧ ✧ ✧

VIII.H.2. Technical Discussion

Background

The cost and performance limitation of today's electric vehicle batteries has led to a need for alternative strategies to enable new plug-in electric vehicles (PEVs) to meet the demands of consumers. Fast charge technology attempts to provide a refueling experience for PEVs similar to that of conventional gasoline vehicles. A typical gasoline vehicle refueling event provides ~300 miles of range in 5 min. Given that PEVs can and will be charged primarily at home, achieving a fully equivalent performance to conventional vehicles may not be necessary. At 50kW, today's fast charger provides ~50 miles in 20 min. Future fast chargers may extend this current capability. Fast charging is likely to offer supplemental range extension supporting day-to-day variability in longitudinal driving patterns. However, the economic viability of fast charger operation is yet to be determined.

Introduction

Fast charging involves recharging an electric drive vehicle battery from a source with greater than 20kW. Today's fast charger systems deliver ~50kW via a direct current (DC) connection with the vehicle battery pack. The installation of the off-board infrastructure necessary to complete this charging operation can be a significant technical and financial challenge.

The work summarized here focused on development of an economic optimization model for analysis of fast charge stations with integrated renewables and energy storage in addition to systems operation modeling and testing at the National Renewable Energy Laboratory's (NREL's) Vehicle Testing and Integration Facility (VTIF). Past work focused on developing the demand for fast charging based on travel patterns and evaluation of real-world fast-charger usage data. This project leveraged our role as the U.S. Department of Energy's representative on the International Energy Agency (IEA) HEV Annex Task 20 Quick Charging activities.

The integration of solar energy production and energy storage has the potential to maximize the value of fast charger infrastructure investment and reduce operating costs. The models developed during this project provide the ability for the U.S. Department of Energy and potential sites to evaluate system installation scenarios toward making educated investments and installation decisions.

Approach

From the perspective of the fast-charge station owner, many economic parameters must be weighed and evaluated. The scenario analysis should take a day-to-day operational viewpoint and compile that information to assemble a long-term financial outlook.

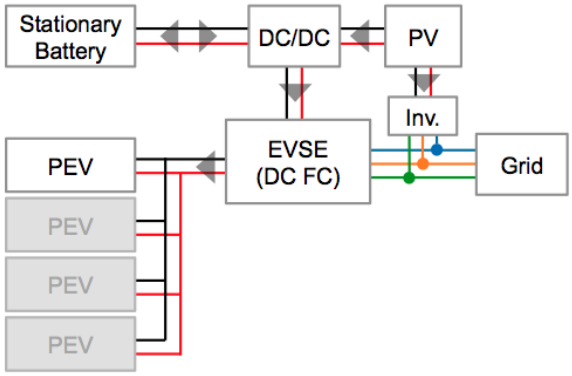

Figure VIII-67: Diagram and depiction of a storage and renewables integrated fast charge system.

The optimization algorithm was allowed to adjust the size of the system components depicted in Figure VIII-67 to meet the demand for fast charging with the goal of creating a financial benefit from the system over a period of time. As described in the Annual Merit Review presentation on this project, (http://www4.eere.energy.gov/vehiclesandfuels/resources/merit-review/sites/default/files/vss114_markel_2013_o.pdf), the following approach was taken:

- Size of the fast charger (# ports), photovoltaic system, and stationary storage were adjusted.
- Dispatch strategy was updated at 15-minute intervals.
- A factor was used to indicate driver preference to initiate fast charge with respect to need.
- Demand charges are accounted for, varying electricity rates in the system operating costs.
- The algorithm is capable of integrating the needs of many vehicles simultaneously.
- The algorithm assumes home charging occurs most often with an occasional "forgetting to plug in" factor driving fast charger demand.

Limited model testing runs were completed this fiscal year with the focus on a "least-cost" implementation approach. The optimization routine converges with the existing structure and inputs.

Results

The results highlight existing challenges to fast-charge system adoption:

- Model tends to build maximum photovoltaic system and sell all electricity to the grid.
- Model tends to not build fast charger or storage but to charge vehicles at home exclusively.
- Forcing the model to build the fast charger (via forget factors or long distance travel requirements) results in minimal fast-charge ports; still no storage.

Given these model results it seems important that significant emphasis be placed on:

- Developing good fast-charge demand models based on vehicle usage patterns
- Incorporating an estimate of cost to operate for systems necessary to meet a defined demand level to complement the least-cost approach results
- Creating a grid application supplemental value stream that is likely necessary to justify the energy storage system inclusion
- Considering the impacts of higher power fast-charge technology on the design and operational attributes.

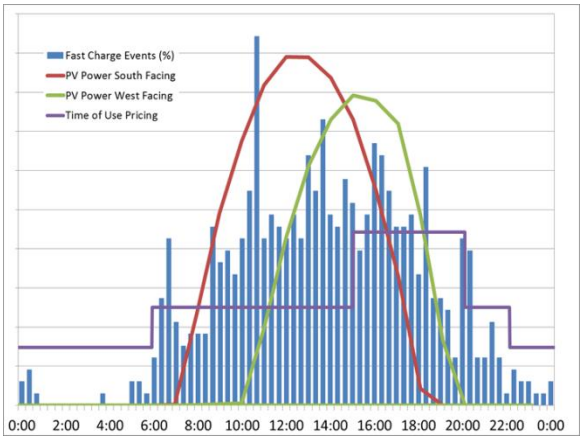

Figure VIII-68: West facing solar array produced 132% more energy during 3-8pm time-of-use electricity pricing period and aligns with fast charger demand.

In Figure VIII-68, we depict the frequency of fast charge events by time of day over the course of several weeks of data from a fast charger installed on Electric Avenue in Portland, Oregon. These data are depicted as the blue bar chart. Overlaid on the fast charger demand is the typical production of solar from arrays facing south (red) and west (green). Finally, the time of use pricing for summer periods in Portland is displayed in purple. Although the south-facing array produces a higher peak power amount and greater overall energy, the west-facing array produces power more aligned with the fast charger demand and electricity rate structure. During the peak time-of-use pricing period from 3 pm–8 pm, the west-facing arrangement produced 132% more energy than the south-facing array. Such orientation impacts and alignment with fast-charge power demand could translate into significant operational cost savings.

Conclusions

It is challenge to justify the business model of fast-charge system installation given the cost of electricity deliver, the potential of increased demand charges and the limited knowledge of demand for fast charging. The work started in this project to address the economic and operational scenarios of fast chargers is important to the introduction of infrastructure that serves a more electrified transportation system. The collaboration and knowledge exchange during IEA Task 20 on Quick Charging also provided international insights. In the coming year, the models developed to date will be run through many more scenarios. Some of these scenarios will leverage data that has been collected on the demand for and use of fast chargers in the field spread across the United States by other DOE VTO projects.

VIII.H.3. Products

Publications

1. "Mitigation of Vehicle Fast Charge Grid Impacts with Renewables and Energy Storage." Vehicle Technologies Annual Merit Review presentation. Tony Markel, May 2013.
2. "DC Fast Charging PEVs Integrated with Renewable Energy." Science Undergraduate Laboratory Internship poster, Joshua Crowley, August 2013.

Tools and Data

1. Fast Charge Integrated Storage and Renewables System Optimization tool (preliminary)

VIII.I. Dynamic Wireless Power Transfer (DWPT) Feasibility

P.T. Jones, Principal Investigator
Oak Ridge National Laboratory
2360 Cherahala Boulevard
Knoxville, TN 37932
Phone: (865) 946-1472
E-mail: Jonespt@ornl.gov

Lee Slezak, DOE Program Manager
Phone: (202) 586-2335
E-mail: Lee.Slezak@ee.doe.gov

VIII.I.1. Abstract

Objectives

- Develop an appropriate scenario for deployment of emerging WPT technologies to provide a hypothetical setting in which the use of dynamic WPT could be evaluated and considerations identified.
- Determine the state of readiness for various technology components and identify additional subsystems which may be required for actual deployment.
- Through the use of analysis tools and evaluation of lab and field data, provide vehicle power requirements for the power transfer rate estimates and total power required by the utility grid for successful utilization of WPT technology.
- Provide a cost estimate and considerations required for optimized power electronics selection.

Major Accomplishments

- Identified deployment scenario considerations and investment estimates for subsystems to enable electrified road sections.
- Determined high level power requirements for grid side support of traffic flow using previously acquired vehicle level lab and field data.
- Performed literature review of current WPT readiness and deployment activities and identified relative all electric range impact with opportunity charging based on typical drive cycles.
- Developed high level construction cost model for electrified roadway that includes roadway construction and power electronics.
- Utilized MA3T studies to validate NREL 'ADOPT' model customer impact projections

Future Achievements

- Project cost for power requirement infrastructure to complete scenario investment total cost for assumed load case.
- Summary and report of completed activity with high level projection for investment cost versus petroleum displacement (and other benefits). Expected early 2014.

✧ ✧ ✧ ✧ ✧

VIII.I.2. Technical Discussion

Background

Wireless Power Transfer (WPT) Technology

Wireless Power Transfer technology has been predicted by many in the automotive industry to become an important technology that will accelerate the adoption of electric vehicles by the general public. This technology allows the recharging of vehicles without the need for the vehicle to plug-in to the electric utility grid to restore the state of charge (SOC) in that vehicle's on board energy storage system (ESS). Even with WPT technology, BEVs still have to overcome the barriers of battery cost, weight and range anxiety to become main stream vehicles.

Dynamic Wireless Power Transfer (DWPT)

Though DWPT or 'in-motion wireless charging' is not a new idea (the literature research portion of this project uncovered patents from 1913.) advancements in technology required for efficient WPT have made DWPT a more realistic transportation energy supply possibility which deserves consideration. If power could be efficiently transferred to a vehicle while the vehicle was in-motion, along common roadways of travel, even properly modified/designed hybrid electric vehicles (HEV) would be able to operate using grid supplied electricity. The effect is an all electric range for vehicles that is only limited by the deployment of the DWPT technology into the road system.

Introduction

Advancing WPT technology into the field of transferring power to vehicles while the vehicle is in motion would further accelerate the adoption of various types of electrified powertrains and would promote the use of electricity for personal transportation. The transfer of grid supplied energy directly to efficient electric motors for propulsion of large numbers of light duty vehicles would provide an opportunity for a significant amount of petroleum displacement. These 'electrified roadways' could be deployed along key routes to effect a higher percentage of properly equipped vehicles and to enable greater range than a typical BEV, or at least reduce the required ESS size (and associated weight and cost).

Approach

Interaction between four of the Department of Energy's National Labs (ONRL, NREL ANL and INL) helped to determine the scope and approach for this study. Using lab testing results from Argonne National Laboratory's (ANL) Advanced Powertrain Research Facility (APRF) Figure VIII-69 and field data from the Idaho National Laboratory's (INL) Advanced Vehicle Testing Activity (AVTA) approximate values were determined to represent the power required for vehicle propulsion.

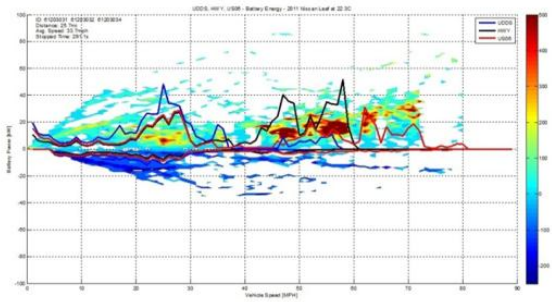

Figure VIII-69: ANL Lab test results for Nissan Leaf EV.

To determine the electrified roadway power requirements for typical traffic volumes and selection of roadways the Georgia DOT and NHTSA traffic data bases were used to select routes, determine approximate traffic volumes and the vehicle category breakdown along the selected routes.

Assessment of roadway construction cost information and maintenance schedules to determine the basic required investment for an electrified roadway deployment for a defined scenario of deployment was accomplished using DOT and construction industry input.

Current ORNL research and development information for the power electronics required to meet the traffic power was used to determine an effective way to distribute energy to vehicles which utilize the electrified road system.

Results

The Atlanta Metro area was selected as the scenario of interest for the hypothetical deployment of this technology due to several factors. The accessibility of traffic information from the Georgia DOT and NHTSA data bases was sufficient to provide traffic volume information which is crucial in developing appropriate power requirements.

Route selection to allow for minimum roadway deployment affecting the greatest percentage of vehicles on a total miles traveled basis was assumed based on vehicle traffic data.

Determination of component cost and placement has been generated based on vehicle power required projections Figure VIII-70. However, the assumptions used to determine the placement and cost assumptions require associated technology and power transfer rate assumptions. For instance at a 25 kW power transfer rate and utilizing a WPT similar to the ORNL non-polarized coupled coil technology (with currently priced supporting power electronics) the cost projection for implementation for a single lane of traffic is roughly $2.8M/mile. This projection does not include bringing the required electricity to the points of connection required for the electrified roadway from the utility perspective.

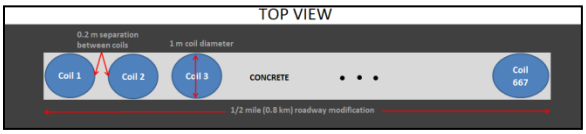

Figure VIII-70: Power transfer rate and # coils/miles drives cost.

Coil and roadway cost is relatively fixed given the assumptions, the real opportunity to reduce costs resides in the ability to reduce the power electronics cost upstream of the coils (PFC, Inverters, HF transformer, etc.).

Conclusions

The main purpose of this study is to identify deployment scenarios, barriers and opportunities and to provide cost guidelines regarding Dynamic Wireless Power Transfer, also called roadway electrification.

Though this study has not yet been completed, many of the subtasks (with appropriate assumptions) have been completed and assembly of the final report is in process. Still required to predict a system implementation cost is the grid side power supply to the points of connection for the DWPT technology. Progress is expected in this area in Q2 of FY2014.

The final report will highlight cost component and deployment characteristics.

VIII.I.3. Products

Publications

1. Future presentation at SAE HEV symposium Feb 2014

Tools and Data

1. Market Acceptance of Advanced Automotive Technologies Model (MA3T)
2. Idaho National Lab AVTA field data
3. Argonne National Laboratory APRF test data

DRAG REDUCTION

VIII.J. DOE's Effort to Improve the Fuel Economy of Heavy Trucks through the Use of Aerodynamics

Kambiz Salari, Project Principal Investigator
Lawrence Livermore National Laboratory
P.O. Box 808,
Livermore, CA 94551-0808
Phone: (925) 424-4635
E-mail: salari1@llnl.gov

Co-Investigators:
Jason Ortega, Katie Lundguist, and Vera Bulaevskaya

Contractor: Lawrence Livermore National Laboratory
Contract No.: W-7405-ENG-48, W-31-109-ENG-38, DE-AI01-99EE50559

VIII.J.1. Abstract

Objective

There are roughly 2.2 million combination trucks on the road today, each traveling an average of 65,000 miles/year and consuming 12,800 gallons of fuel/year for a total of 36 billion gallons of fuel/year. These trucks consume roughly 12-13% of the total United States petroleum usage. At highway speeds, a class 8 tractor-trailer uses over 50% of the usable energy produced by the vehicle engine to overcome aerodynamic drag. To improve the fuel economy of these vehicles Lawrence Livermore National Laboratory has been conducting research on enhanced aerodynamics through the use of add-on devices and new tractor-trailer shape designs. The specific goals of this project include:

- Provide guidance to industry to improve the fuel economy of class 8 tractor-trailer through the use of aerodynamics
- Develop innovative aerodynamic concepts for heavy vehicles that are operationally and economically sound
- Demonstrate the potential of new drag-reduction concepts
- Design the next generation of an integrated highly aerodynamic tractor-trailers
- Establish a database of experimental, computational, and conceptual design information

Approach

- Simulate and analyze the flow field around heavy vehicles using advanced computational fluid dynamics (CFD) tools
- Using various wind tunnel experiments at different scales generate a database for code validation and for understanding the drag producing flow structures around heavy vehicles
- Provide industry with aerodynamic design guidance and insight into the flow physics around heavy vehicles
- Investigate aerodynamic drag reduction concepts and devices (e.g., base flaps, tractor-trailer gap stabilizers, underbody skirts, wedges and fairings, and blowing and acoustic devices, etc.)
- Demonstrate the economic potential of these devices
- Using the available experimental and computational results design the next generation of an integrated highly aerodynamic tractor-trailer

Accomplishments

For the fiscal year (FY) 2013, the DOE Project on Heavy Vehicle Aerodynamic Drag achieved four major accomplishments.

1. Fleet Evaluation of Selected Aerodynamic devices

The first is the collection and post-processing of on-the-road data from class 8 heavy vehicles of two commercial fleets, Frito Lay (76 tractors and 32 trailers tracked, 1.4×10^6 miles of fuel economy data) and Spirit Truck Lines (9 tractor-trailers tracked, 690,000 miles of fuel economy data). These vehicles were outfitted (Figure VIII-71) with various combinations of tractor-trailer gap fairings (Freight Wing), trailer skirts (Freight Wing), trailer boattails (24" Freight Wing and 48" ATDynamics), and wide base tires (Michelin). Aside from the prototype Freight Wing boattail, all devices and tires functioned as expected. Unlike the ATDynamics boattail, which requires manual deployment and retraction, the Freight Wing boattail retracts as the trailer backs against the loading dock. When the trailer pulls away, the boattail automatically deploys. Partway through the test, the top plate of several of these Freight Wing boattails began to sag due to wear and tear on the supporting flexible members (see Figure VIII-72). As a result, the optimum boattail angle was not maintained on the top plate. The failing flexible members were soon replaced and the test proceeded as planned. For the Freight Wing skirts and ATDynamics boattails, we received very positive feedback from the Spirit drivers, who observed better vehicle handling and ride quality for the vehicles outfitted with the devices.

Figure VIII-71: A Spirit trailer outfitted with Freight Wing skirts and an ATDynamics (ATD) four-sided boattail.

Figure VIII-72: Freight Wing 3-sided boattail and a Frito Lay trailer outfitted with a Freight Wing gap fairing.

For the heavy vehicles monitored within the Frito Lay fleet, the data collection and analysis presented several challenges and unique opportunities. We quickly learned that Frito Lay stores more detailed information for each tractor and trailer on any given day (Table VIII-11). Mining meaningful fuel economy data for the 2011 and 2012 calendar years required several months of back and forth iterations with the technical staff at Frito Lay. We finally settled upon a group of sorting parameters (including a consistent latitude and longitude of the vehicle routes, average vehicle speed, and minimum miles driven per route), which made it possible to compare on-the-road fuel economy data of baseline and control vehicles outfitted with aerodynamic drag reduction devices. The results of this comparison are shown in Figure VIII-73 over the course of a 12 month period. The rise and fall of the average fuel economy throughout the year is from seasonal variations due to climate change. We found a substantial level of noise in this dataset that made it particularly difficult to draw out any additional trends from that shown inFigure VIII-73. This was, in part, due to variability in the route, vehicle driver, and fuel consumption uncertainty. For some drivers or vehicles, the drag reduction devices produced a higher mpg, but there were as many drivers or vehicles, for which the devices produced a lower mpg. So on average, there was no observable difference. More formal analyses of the data, which accounted for the effect of the driver and vehicle showed no difference either.

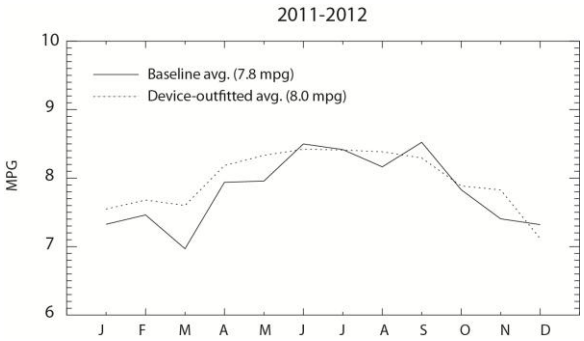

Figure VIII-73: Average monthly fuel usage for the baseline vehicles and vehicles outfitted with aerodynamic drag reduction devices.

To mitigate these shortcomings in the Frito Lay data set, we suggest that future studies incorporate vehicles that have on-board data loggers, which will provide direct engine fuel economy measurements when the vehicle is traveling at highway speeds instead of an averaged value over the entire route. Additionally, we suggest controlling for the effects of the vehicle and driver by having the same driver and vehicle combination with each device, with a good number of

replicates for each such combination. Appendix B presents a detailed statistical analysis that was conducted at the beginning of the Frito Lay evaluation to determine the sample sizes for the study.

On the other hand, data collection and post-processing of the Spirit Truck Lines dataset was very straightforward as this fleet had previously established data monitoring software (PeopleNet) to track their fuel consumption and driver behavior. The data output produced by this software were readily conducive to our analyses. Our team typically received updates on their fuel economy data on a monthly basis through a secure website portal. The resulting data sets extended from September 2011 to March 2012. Example information provided for each tractor-trailer configuration is shown in Table VIII-7–Table VIII-8. It should be noted that since the Kenworth T600 has under-cab fuel tanks, it had a larger tractor-trailer gap by approximately 8". The Spirit vehicles utilized the Michelin XOne XTEs, which are Michelin's high mileage wide base single tire. Spirit stated that their drivers strongly prefer their XOnes to traditional duals because of improved traction. Spirit also uses soft top speed limiters to control their driver's speed and encourage good driving habits. The speed limiter is set to 65 mph, and assuming the driver exhibits good behavior during the run, they are able to run up to 67 mph for a certain period of time. Spirit also has limited their vehicles to operate only up to 60 miles without cruise control engaged. As a result of the speed limiters and Michelin XOnes, the baseline trucks used for the fleet test had an average fuel economy of approximately 7 mpg across their fleet. They currently have 300 trailers with Utility skirts. Spirit believes the Utility skirt improves their fuel economy approximately 0.3 mpg. They were also involved in an evaluation of the Transtex skirt. Spirit has been running these skirts for over three years, and they are pleased their performance and condition.

A basic analysis of variance (ANOVA) with miles per gallon as a response and the device as a predictor was performed on datasets that were separated either by vehicle, combined together across all vehicles, or filtered according to the average trip speed. The average fuel economy for each of the vehicle is shown inTable VIII-9 (see Appendix B for the complete analysis). From this analysis, we determined that the fuel savings of the Freight Wing or ATDynamics boattails combined with the Freight Wing gap fairing and skirts and Michelin XOnes were on average 0.394 mpg (0.306 to 0.482 mpg as a 95% confidence interval) or 0.562 mpg (0.481 to 0.642 mpg as a 95% confidence interval), respectively, compared to the baseline vehicles with only the Michelin XOnes. The corresponding average percent increases in the average fuel economy relative to the baseline vehicle are 5.47% and 7.79%, respectively (Table VIII-10). These results are consistent with our fuel economy savings estimates previously made from CFD simulations and small- and full-scale wind tunnel tests.

For fleets with the desire to understand the fuel economy benefits of aerodynamic add-on devices, we recommend series of controls on the driver, on-the-road vehicle performance, data collection, and data presentation in a manner similar to that of Spirit Truck Lines.

Table VIII-7: Sample fuel economy data from the Spirit fleet (ATD—ATDynamics, FW—Freightwing).

Date_start	Time_start	Date_end	Time_end	Fuel (gal)	Miles	MPG	MPH	Gal/Miles	Device
9/1/2011	0:00	9/1/2011	6:00	17.375	106.5	6.13	62.9	0.163	none
9/1/2011	6:00	9/1/2011	12:00	48.125	344	7.15	62.8	0.14	none
9/24/2011	6:00	9/24/2011	12:00	0.5	0.8	1.6	6.8	0.625	ATD
9/24/2011	18:00	9/25/2011	0:00	33.75	254.8	7.55	58	0.132	ATD
9/25/2011	0:00	9/25/2011	6:00	4.125	30.3	7.35	63.9	0.136	ATD
10/24/2011	6:00	10/24/2011	12:00	29.375	232.3	7.91	61.7	0.126	FW
10/24/2011	12:00	10/24/2011	18:00	35.625	307.5	8.63	60.1	0.116	FW
10/25/2011	0:00	10/25/2011	6:00	1.625	7.6	4.68	19.2	0.214	FW
10/25/2011	6:00	10/25/2011	12:00	24	211.1	8.8	53.8	0.114	FW

Table VIII-8: Vehicle information collected by Frito Lay for each tractor-trailer configuration. Note that all trailers are 2009 Utility 53' dry van trailers.

Truck Number	Truck Type	Driver	Runs
2318	Kenworth T660	Jaime Gonzalez	Nebraska/Iowa/Montana
2337	Kenworth T660	Rey Garza	Alabama/Florida/Mississippi
2317	Kenworth T660	Emilio Sosa	California/Oregon/Washington
2330	Kenworth T660	Erasmo Lopez	Canada/Minnesota
2276	Kenworth T660	Frank Martinez	New Mexico/California/Washington
2327	Kenworth T660	Jesus Reyna	California/Oregon/Washington
2273	Kenworth T660	Eugene Garcia	Alabama/Texas
2255	Kenworth T600	Arnoldo Nunez	Kansas/Missouri/Illinois/Wisconsin/New Mexico/California/Arizona
2304	Kenworth T660	Preston Angell	Canada
2423	Peterbilt 387	Roland Hughes	Canada

Table VIII-9: Change in fuel economy (mpg) for the six Spirit trailers outfitted with Freight Wing (FW) skirts and gap fairing, Michelin XOnes XTE tires, and either the Freight Wing or ATDynamics (ATD) boattails. Note that the baseline case also had Michelin XOnes XTE tires. CI: confidence interval.

Vehicle	FW – Baseline		ATD - Baseline	
	Mean	95% CI	Mean	95% CI
2255	0.457	(0.253, 0.661)	0.46	(0.294, 0.626)
2273	0.5	(0.256, 0.735)	0.269	(0.037, 0.5)
2276	0.35	(0.174, 0.525)	0.404	(0.194, 0.614)
2317	0.237	(0.005, 0.468)	0.372	(0.153, 0.59)
2327	0.509	(0.242, 0.776)	0.988	(0.764, 1.211)
2337	0.439	(0.266, 0.611)	0.638	(0.492, 0.784)
Overall	0.394	(0.306, 0.482)	0.562	(0.481, 0.642)

Table VIII-10: Percent increase in fuel economy for the six Spirit trailers outfitted with Freight Wing (FW) skirts and gap fairing, Michelin XOnes XTE tires, and either the Freight Wing or ATDynamics (ATD) boattails. Note that the baseline case also had Michelin XOnes XTE tires. CI: confidence interval.

Vehicle	(FW – Baseline)/Baseline		(ATD – Baseline)/Baseline	
	Mean	95% CI	Mean	95% CI
2255	6.32	(3.47, 9.22)	6.37	(4.02, 8.75)
2273	7	(3.58, 10.45)	3.79	(0.52, 7.11)
2276	5.27	(2.59, 7.99)	6.09	(2.89, 9.33)
2317	3.44	(0.07, 6.86)	5.41	(2.21, 8.67)
2327	7.13	(3.33, 11.01)	13.81	(10.51, 17.22)
2337	5.79	(3.48, 8.13)	8.43	(6.43, 10.48)
Overall	5.47	(4.24, 6.7)	7.79	(6.67, 8.92)

Table VIII-11: Vehicle information collected by Frito Lay for each tractor-trailer configuration.

Min Session Driving Time Stamp	MinTime	Make
Months	Trip	Axles
Days	DriverName	GEAR
Years	Vehicle	ENGINE
MinSessionTime	Miles	H.P.
MinSessionTimeString	Fuel	EGR/DPF
Hour	MPG	TRANSM
Min	MPH	Trailer
AMPM	Faring	Type
MaxTimeStamp	Trailer	Fairing Description
MaxTime	Baseline	Trip Avg Miles
Min Time Stamp	Trailer	Trip Avg. MPH

2. Improve Tanker-Trailer Aerodynamics for Better Fuel-Economy

The second major accomplishment for this fiscal year is the design and evaluation of aerodynamic drag reduction devices for tanker-trailers (Figure VIII-74). On average, these heavy vehicles operate at a rather low fuel economy of approximately 5 mpg.[1] Although these vehicles comprise a rather small portion of the United States heavy vehicle fleet, we estimate that a 1% fuel economy improvement would yield approximately 31×10^6 gallons of fuel saved per year. High-resolution computational fluid dynamics (CFD) simulations of a baseline tanker trailer demonstrated that these vehicles have an aerodynamic drag coefficient of ≈1 (compared to ≈0.65 for a long-sleeper tractor and straight-frame trailer) at highway speeds (Figure VIII-75). The major contributors to this drag are the blunt nose of the day-cab tractor, windshield, tractor-tanker gap, tanker bogie, and tanker base.

Figure VIII-74: Velocity streamlines about a standard tanker-trailer.

Continuing our effort from last fiscal year in which we assessed the drag reduction of a tractor-tanker gap fairing (Figure VIII-76) and boattail (26% and 4% reductions in aerodynamic drag, respectively), we evaluated an assortment of tanker add-on devices this fiscal year. Two of these devices were tanker side and centerline skirts (Figure VIII-77). Both of these skirts provide a very aggressive underbody treatment with a ground clearance of 6". The simulations were conducted using STARCCM+ for a tanker-trailer traveling at 65 mph in a 7 mph crosswind. The results demonstrated that the centerline and side skirts yielded 1.5% and 10% reductions in drag, respectively, relative to the configuration with only a tractor-tanker gap fairing. Analysis of the underbody velocity magnitude field (Figure VIII-78) showed that although the centerline skirt provides some stabilization and redirection of the trailer underbody flow, the centerline skirt is insufficient at shielding the trailer bogie from the high-speed, freestream flow and, hence, yields a rather small reduction in aerodynamic drag.

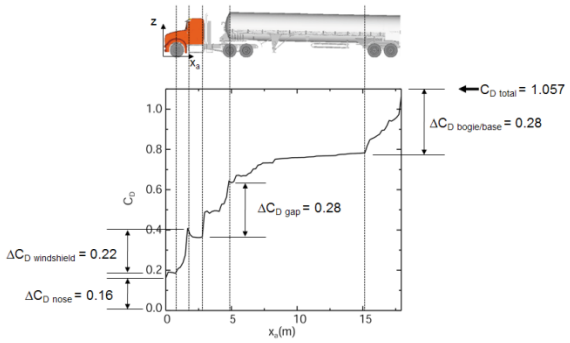

Figure VIII-75: Drag coefficient as a function of length along of a baseline tanker trailer. The total drag coefficient of the vehicle is 1.057. The major drag sources are shown to be the nose of the day-cab tractor, windshield, tractor-tanker gap, tanker bogie, and tanker base.

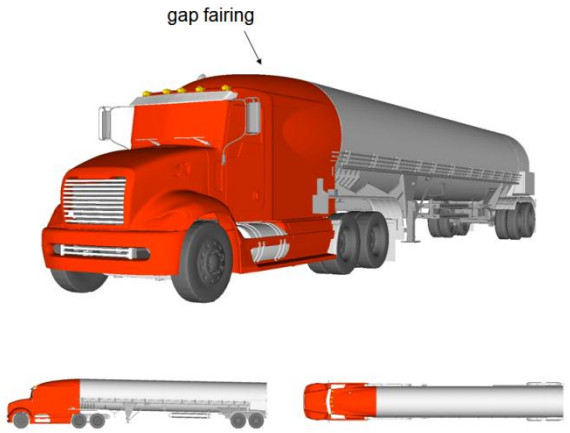

Figure VIII-76: Baseline tanker-trailer vehicle outfitted with a gap fairing.

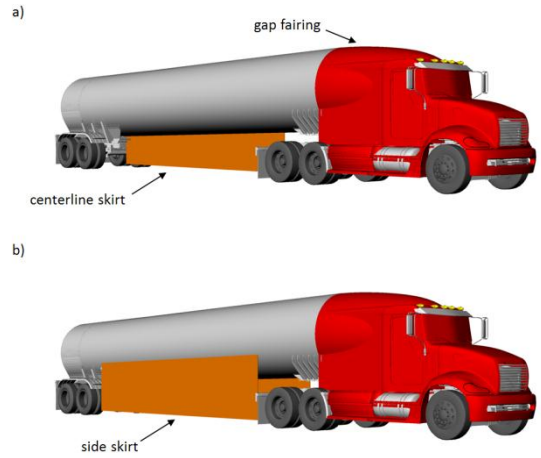

Figure VIII-77: Tanker trailer with a a) centerline skirt and b) side skirts.

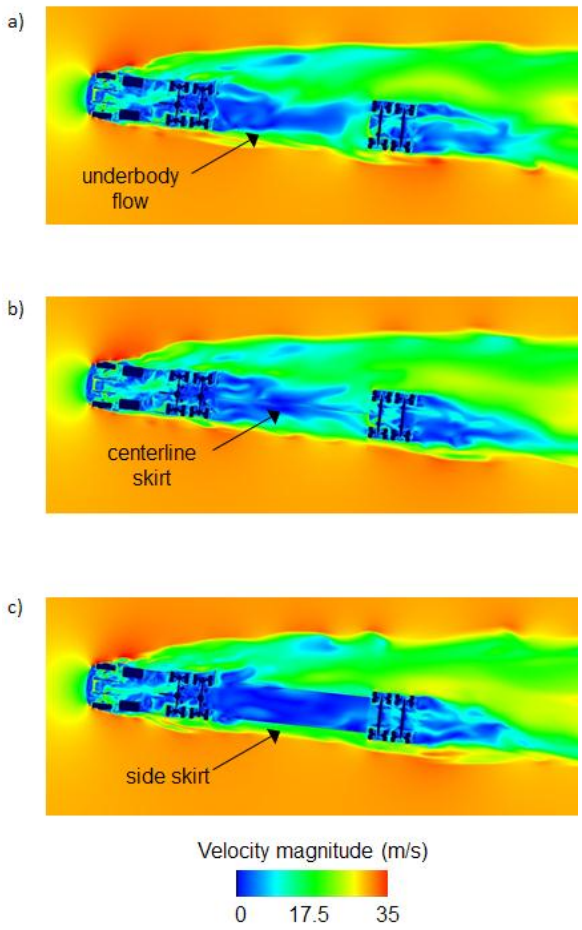

Figure VIII-78: Velocity magnitude field at the mid-axle height for the a) baseline tanker trailer, b) tanker with a centerline skirt, and c) tanker with side skirts.

In addition to skirts, we investigated the impact of tanker fins on the aerodynamic drag of the tanker-trailer (Figure VIII-79). These fins run the entire length of the tanker and extend 14" perpendicularly to the tanker surface. The purpose of the fins is to produce control vortices that alter the flow behavior on the windward and leeward sides of the tanker, as well as in the tanker wake. Two fin configurations (2- and 4-fin) were evaluated. The results of the simulations indicated that the 2- and 4-fin configurations decrease the drag coefficient by 3% and 1.4%, respectively. Iso-surfaces of Q (an indicator of vortex strength) highlight the formation of control vortices from the fins (Figure VIII-80). Future work on this concept can involve optimizing the fin location, angle of attack, number, and size.

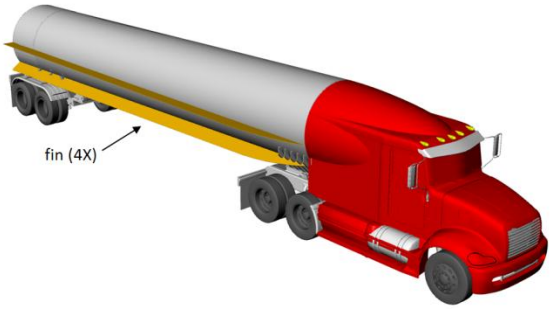

Figure VIII-79: Tanker-trailer with aerodynamic fins. Note that the fins are on both sides of the tanker.

3. Design and test a new curved tail device using an idealized tractor-trailer geometries

The third major accomplishment for this fiscal year is a new design of a curved tail device with the performance comparison to the standard straight tail. To minimize the influence of upstream flow quality on the performance of tail devices and idealized tractor-trailer geometries were devised.

It is well known that tail devices (shown in Figure VIII-81) are an effective means of reducing drag force on tractor-trailer geometries; however, the optimal shape of the device is still a subject of research. The ideal angle, length, and curvature of the boat tail have been studied, with inconclusive results. Researchers have reported various optimal parameters indifferent wind tunnel and road tests, with results rarely in agreement. One possible explanation for this disagreement is differences in the impinging flow quality among tests, which is uniform in the wind tunnel, but highly variable and gusty in a road test. Additionally, the trailer interacts with the boat tail so

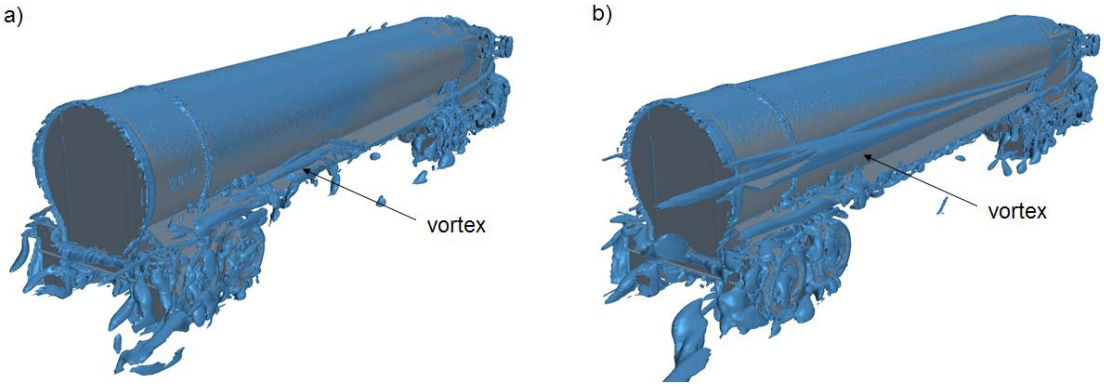

Figure VIII-80: Iso-Q surfaces for the a) 2- and b) 4-fin drag reduction devices.

that changes in the design of the trailer can affect performance of the boat tail. For example, researchers have reported that tapering the trailer or rounding the long horizontal edges reduces drag, but the effect of these changes on the tail performance has not been quantified. The goal of this work is to use numerical simulations to study the effect of a boat tail on reducing drag with inlet flows of various qualities, and to examine the optimal boat tail configuration under these various flow conditions. Additionally, sensitivity of tail performance to upstream flow quality is examined using low-turbulence uniform inlet flow conditions, similar to the flow achieved in a wind tunnel, and an inlet flow conditions with large coherent structures, resembling the atmospheric boundary layer turbulence present on the road.

Figure VIII-81: Trailer with boat tail [http://www.atdynamics.com/trailertail.htm].

Design of Idealized Tractor-Trailer Geometries

Two idealized tractor-trailer geometries are used to isolate the effects of the boat tail geometry, and its interaction with the trailer. Both idealized geometries are streamlined bodies, one with a circular cross section, and one with a rectangular cross section (Figure VIII-82). These idealized bodies are chosen to achieve a clean, attached boundary layer flow along the bluff body. This allows the effects of the inlet flow quality to be studied at the boat tail location, independent of separation or other flow quality issues which may be attributed to a non-idealized geometry, such as a real tractor creating separation upstream of the boat tail. The round bullet-like shape is introduced as a fully idealized geometry for studying boat tail performance, and the rectangular shape more closely mimics a real trailer. The idealized tractor-trailer geometry is a 1/8th scale in size. The free stream velocity is set at 95 m/s. Simulations presented here are based on steady RANS, with the K-Omega turbulence model, and the ideal gas approximation. After completion of a grid refinement study, a base mesh was constructed with approximately 10 million grid cells.

Boat tails were added to the idealized geometries, which have a linear or straight profile along the length of the boat tail. With the round idealized geometry, the boat tail swept 360 degrees, while a 4-sided boat tail was added to the idealized rectangular tractor-trailer. The round geometry with a tail and different tail profiles are shown in Figure VIII-83. A set of simulations was performed with both the round and rectangular geometries, sweeping the tail angle through 13 to 25 degrees, as measured from horizontal.

Drag force as a function of tail angle is reported in Figure VIII-84 for both geometries. In these simulations, the round body has no yaw angle, while the rectangular body has a yaw angle of 6.1 degrees. In cases with yaw, drag force is calculated on a rotated coordinate system, and is reported as the force in-line with the vehicle centerline. Performance and behavior of the boat tail on the two geometries is nearly identical. Drag force decreases rapidly with the addition of a boat tail at angles ranging from 13 to 19 degrees. In both cases, the benefit of the boat tail peaks at an angle of 19 degrees, with a 49 to 50% reduction in drag force. At angles greater than 19 degrees, drag increases due to flow separation on the exterior side of the boat tail. Nearly identical boat tail performance, in terms of percentage of drag reduction, is observed between the two geometries. *Therefore, both geometries create a clean flow upstream of the boat tail, and either geometry can be used to study boat tail performance, and the effects of upstream flow quality.*

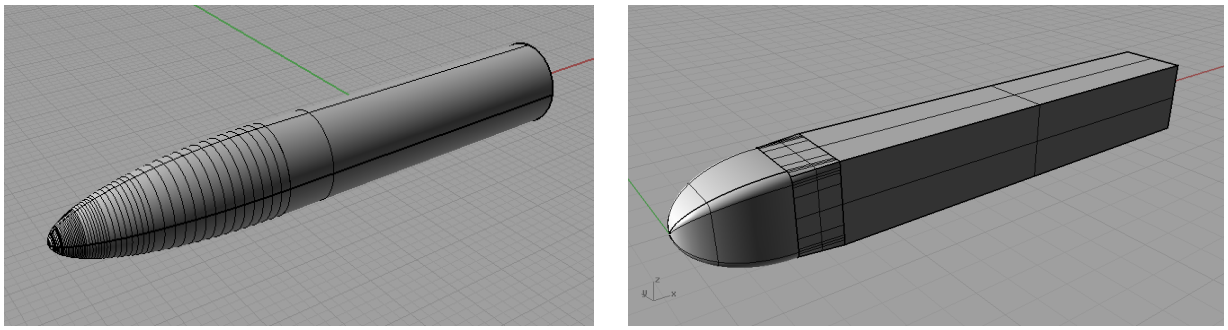

Figure VIII-82: Perspective view of idealized tractor-trailer geometries used for this study. A geometry with a circular cross section is used (left), as well as a geometry with a rectangular cross section (right).

Aerodynamic Performance of Tails

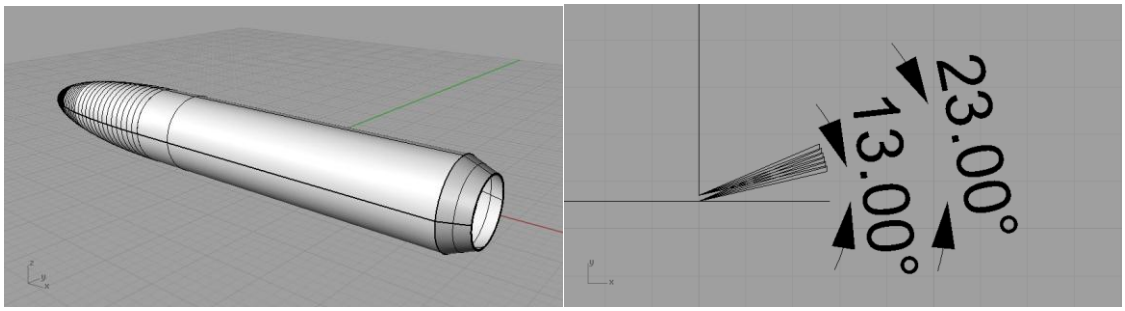

Figure VIII-83: Idealized round geometry with a straight boat tail (left). Profiles of six straight boat tails, ranging in angle from 13 to 23 degrees (right).

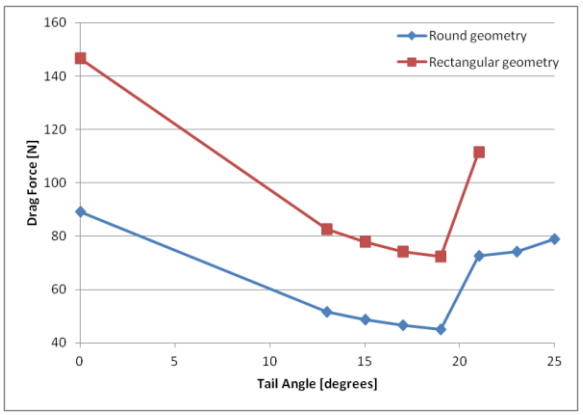

Figure VIII-84: Drag force as a function of tail angle for the round and rectangular idealized trailer geometries with straight boat tails at various angles. The case without a boat tail is reported as a "0" angle.

Additionally, the idealized tractor-trailer geometries were modified by tapering the rear half of the geometry. As an example of tapering, the rectangular geometry tapered on 3 sides, and with the addition of a boat tail is shown in Figure VIII-85. Flow around the tapered bodies was first simulated around the round tapered body at zero degrees yaw with boat tail angles ranging from 8 to 23 degrees, and these results are plotted in Figure VIII-86. At the base of the geometry an 8 degree boat tail was added tangent to the taper angle. For the round geometry, it was observed that tapering alone (i.e. without a boat tail) produced a 34% reduction in drag force. With a tapered body, the boat tail still performed well, but produces a less dramatic drop in drag. For example, the 19 degree boat tail produced a 49% reduction in drag for the geometry with straight sides, and a 35% reduction in drag for the case with tapered sides. *An important finding is that in the tapered case the tail continued to perform at higher angles, so that in the tapered case the drag continued to decrease for tail angles of 21 and 23 degrees*. Additionally, tapering makes performance of the boat tail less sensitive to the boat tail angle, which could have implications for real cases where it is harder to optimize boat tail angle due to variability in flow conditions during operation of heavy vehicles.

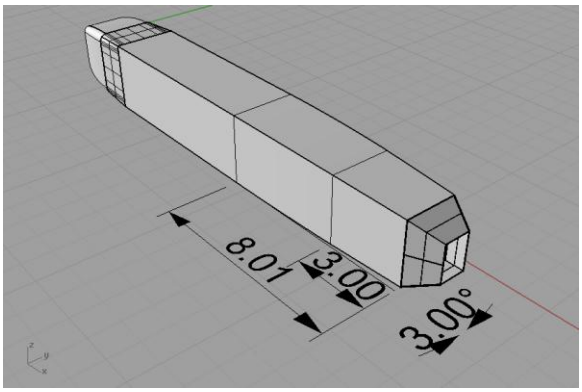

Figure VIII-85: An idealized tractor-trailer geometry with tapering of 3 sides, and a 4-sided boat tail.

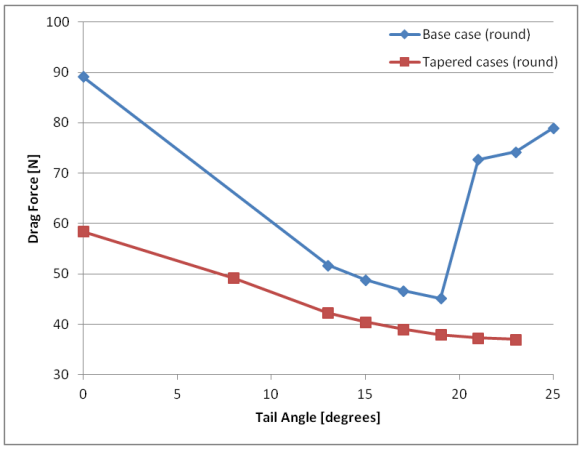

Figure VIII-86: Drag force as a function of boat tail angle for the round idealized trailer geometry with straight and tapered sides. The case without a boat tail is reported as a "0" angle.

In the tapered case for the rectangular geometry, the last 3 m of the trailer is tapered linearly at either a 3 or 8 degree angle (shown previously in Figure VIII-85). Again, flow around this tapered body was simulated at a 6.1 degree yaw with boat tail angles ranging from 13 to 25 degrees. The drag and side forces are included in Table VIII-12 for the straight and tapered cases, and drag force is plotted in Figure VIII-87. For the idealized geometry with straight sides, drag force decreases rapidly with the addition of the boat tail. The

optimum tail angle is 19 degrees, after which point the drag force increases. The optimum 19 degree tail angle is consistent with results from a round "bullet" shaped idealized geometry with no yaw, which also had an optimum angle of 19 degrees. In the tapered case, drag is reduced as compared to the case with straight sides, with or without a boat tail. We tapered 1, 2, 3, and 4 sides, corresponding with tapering of the top only, sides only, top and sides, and all four sides. Drag force decreased with tapering of each additional side. Additionally, drag decreases with increasing taper angle. In the tapered cases, the benefit of the boat tail is less, but the boat tail also continues to perform at higher angles. The boat tail in both the 3 and 8 degree taper cases performed well at 21 degree tail angle. These results indicate that when a boat tail is paired with a streamlined trailer, the boat tail shows less sensitivity to angle. Furthermore, sensitivity continues to decrease with increasing taper angle.

Table VIII-12: Drag and side force are reported in a rotated coordinate system, which aligns with the centerline of the body.

idealized trailer	tail angle	yaw angle	Drag Force (N)	Side Force (N)
base	0	6.1	146.62	273.2
base, 4 sided tail	13	6.1	82.49	240.19
base, 4 sided tail	15	6.1	77.93	236.54
base, 4 sided tail	17	6.1	74.31	232.3
base, 4 sided tail	19	6.1	72.41	229.9
base, 4 sided tail	21	6.1	111.44	114.51
tapered, 3 deg	0	6.1	109.79	247.44
tapered, 3 deg, 4 sided tail	13	6.1	68.31	225.46
tapered, 3 deg, 4 sided tail	21	6.1	60.86	217.66
tapered, 3 deg, 4 sided tail	25	6.1	107.99	262.78
tapered, 8 deg	0	6.1	74.34	222.62
tapered, 8 deg, 4 sided tail	13	6.1	56.3	215.13
tapered, 8 deg, 4 sided tail	21	6.1	54.43	212.96
tapered, 8 deg, 4 sided tail	25	6.1	65.69	248.38

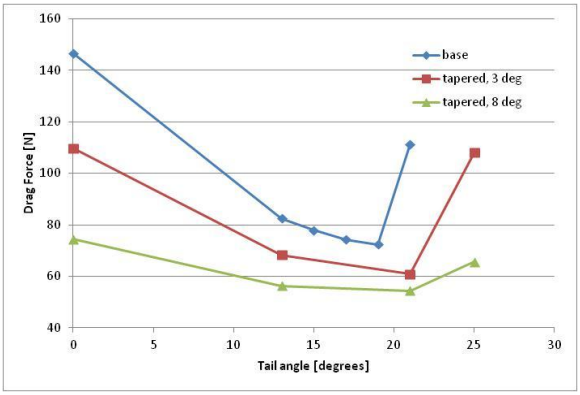

Figure VIII-87: Drag force as a function of tail angle for the idealized trailer geometry with straight sides and 3 tapered sides. The case without a boat tail is reported as a "0" angle.

The effects of tail length and rounded edges on the trailer were additionally investigated. We performed simulations of the idealized tractor-trailer geometry at a 6.1 yaw angle, and using a boat tail with a 15 degree angle and varied the length.

The full-scale tail length was varied between 32 and 60 inches. Drag force was consistently reduced with increasing tail length, and the improvement in this range was tapered on slightly as the tail length increased. Results are plotted in Figure VIII-88. The horizontal edges of the trailer and boat tail were rounded with a 1 inch (full-scale) radius. Rounded of the trailer edges resulted in approximately a 1% reduction in drag force.

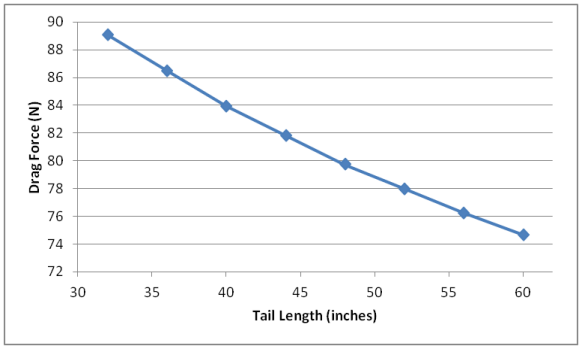

Figure VIII-88: Drag force plotted as a function of tail length for a 4 sided tail on a rectangular idealized tractor-trailer geometry. The trailer is simulated at 6.1 degrees yaw, and the tail angle is held constant at 15 degrees from horizontal.

Curved Tail Design and Performance

A series of curved boat tails with a constant radius of curvature were constructed. An effective tail angle is defined for the curved boat tails as the angle of a straight line connecting the tail base to the tail end. Profiles of 2 curved tails with effective angles of 13 and 21 degrees are shown in Figure VIII-89, along with the corresponding straight tails. Flows around these geometries were tested at a 6.1 degree yaw angle with curved boat tails ranging from 13 to 21 degrees. Flow separated from all of the constant radius tails, resulting in increased drag when compared to a straight tail for all but the 13 degree tail case, where the curved tail resulted in lower drag. With the constant radius tails, the angle at the end of the tail is twice the average (or effective) angle of the tail. Therefore, a curved tail matching a 13 degree straight tail would have an angle of 0 degrees at the base, a 13 degree average angle, and a 26 degree angle at the end of the tail. Flow was unable to remain attached at the higher angles towards the end of the tail, resulting in separation and higher drag forces. The separation point was investigated, and the instantaneous tail angle at the point of separation was approximately 19 to 21 degrees (with slight variations in the 5 cases). Importantly, this finding is consistent with the findings presented in section 3, that 19 degrees is the optimal tail angle for this set-up.

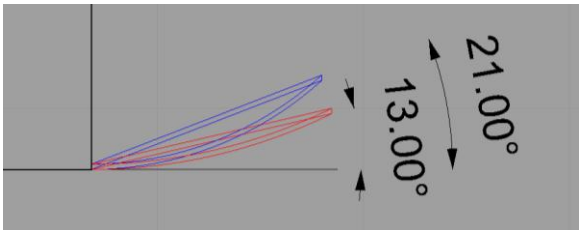

Figure VIII-89: Profiles of 2 curved and straight boat tails with angles of 13 (red) and 21 (blue) degrees. The straight tail is used to illustrate how the "effective angle" of the curved boat tail is defined.

A set of modified curved boat tails was developed, which are curved at the base with a constant radius and then

transition to a straight line segment. Transition to a straight segment occurs before the 19 degree angle, keeping the instantaneous tail angle less than 19 degrees at any point. Flow around geometries with modified curved boat tails were simulated for the idealized tractor-trailer at 6.1 and 15 degrees yaw, as well as the round bullet shape at 0 degrees yaw. In all cases, it was found that drag could be reduced with a modified curved boat tail, in comparison to a straight tail with an equivalent effective angle. Figure VIII-90 shows results for the bullet case with no yaw, and includes lines for straight sides with a straight tail, straight sides with a modified curved tail, and tapered sides with a straight tail. Modified curved tails were additionally developed and tested for tapered geometries; however, drag reductions were small when compared to the tapered geometry with a straight tail.

We are currently developing inlet conditions which will allow us to investigate the upstream flow quality on the performance of boat tails. The options under consideration result in the formation of large coherent structures upstream of e idealized tractor-trailer geometry. Results from these simulations should give further insight into the performance of boat tails.

4. LLNL Aerodynamically-Integrated Tractor-Trailer Design

The fourth major accomplishment for this fiscal year is the preliminary design of a next-generation class 8 heavy vehicle. From our previous CFD simulations and full-scale wind tunnel study, we determined that a complete installation of add-on drag reduction devices (sealed tractor-trailer gap, full trailer skirts, and optimized trailer boattail) yields a reduction in the drag coefficient of about 0.15. While further reductions can be achieved with additional add-on devices, their benefit is likely to be incremental at best. Therefore, a more fundamental approach must be taken if we want to reduce the drag coefficient even further. As a result, we are designing the next-generation class 8 heavy vehicle that has integrated aerodynamic features, such as completely enclosed wheel wells, a rounded tractor nose and A-pillars, a closed tractor-trailer gap, full trailer skirting, a trailer boattail, and a teardrop tractor-trailer shape. For the coming fiscal year, we will continue to evaluate and optimize this vehicle shape with both CFD simulations and a 1/8th scale test at the NASA Ames 7×10 wind tunnel. An overview of these results will be presented in the FY 2014 Annual Report.

Acknowledgments

This work was performed under the auspices of the U.S. Department of Energy by University of California, Lawrence Livermore National Laboratory under Contract W-7405-Eng-48.

References

1. U.S. Department of Transportation, Transportation Energy Data Book, Edition 26, 2007.

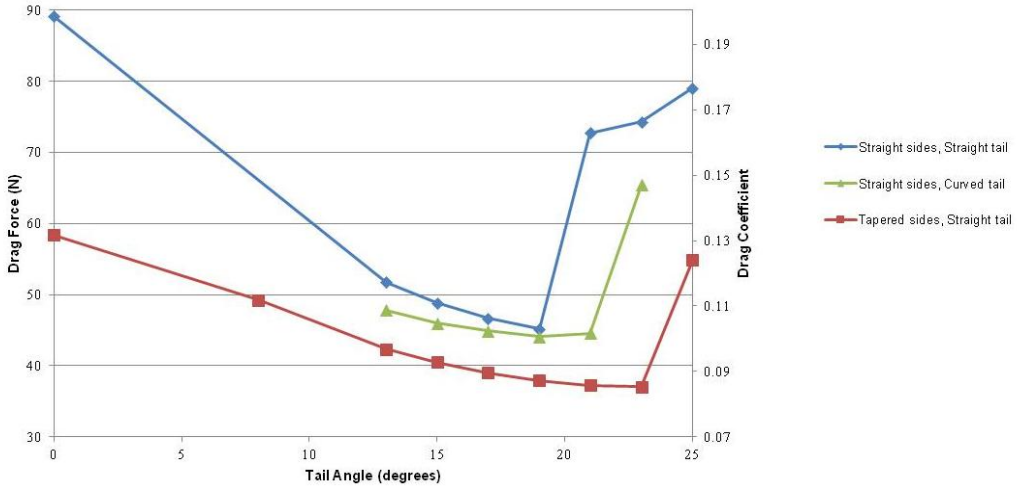

Figure VIII-90: Drag force for idealized bullet shapes with straight and tapered sides and straight and curved boat tails.

Appendix A: Preliminary Sample Size Calculations Based on Frito-Lay Baseline Fuel Consumption Data

Preliminary Sample Size Calculations Based on Frito-Lay Baseline Fuel Consumption Data

Vera Bulaevskaya

1 Problem Statement

The goal is to compare the fuel consumption for the baseline (i.e., no devices) and for a particular configuration of devices to determine whether the latter increases fuel efficiency. If we assume that the distribution of fuel consumption for each group is approximately Gaussian or if the sample size for each group is large enough (at least 40 according to the most commonly used rule of thumb), the easiest way to do this is to collect a sample of baseline and a sample of device fuel consumptions and compare their sample means using the following test statistic T [1]:

$$T = \frac{\bar{x}_d - \bar{x}_b}{\sqrt{\frac{\sigma_b^2}{n_b} + \frac{\sigma_d^2}{n_d}}} \tag{1}$$

where

$\bar{x}_b$ and $\bar{x}_d$ are baseline and device sample fuel consumption averages, respectively,

σ_b and σ_d are baseline and device population fuel consumption standard deviations, respectively, and

n_b and n_d are baseline and device sample sizes, respectively.

If the statistic T in (1) falls below a user-specified threshold (more on the choice of threshold value below), the device configuration is declared to be significantly lower than the baseline in terms of its fuel consumption.

We want to be able to detect a significant difference between the baseline and device fuel consumption whenever there is a difference of at least $(100 \cdot p)\%$ between the population means of the two groups, μ_b and μ_d, i.e.,

$$p = \frac{\mu_b - \mu_d}{\mu_b} \tag{2}$$

(note that as defined above, $p > 0$ since the assumption is that $\mu_b \geq \mu_d$). Before the samples are collected, the question that needs to be answered is: how large should the baseline and device sample sizes be in order to detect such a difference? The determine the sample size required for each group, one needs to specify the following quantities:

- the probability β with which one wishes to detect this difference when it exists (also known as "statistical power") and
- the probability α of a false positive (i.e., detecting a difference when there is not one in reality) that one is willing to tolerate (also known as "statistical significance").

The value of α determines the threshold for the statistic T below which we declare the device fuel consumption to be significantly lower than that of the baseline (the lower the α, the greater the burden of proof to declare a significant difference). Clearly, it is desirable to have a high β and a low α (typical values specified for these are 95% and 5%, respectively), but everything else being equal, higher β and lower α come at the price of a larger sample size needed to detect the desired difference.

2 Data

Frito-Lay has provided five baseline datasets of fuel consumption (in miles per gallon, MPG), each consisting of different trips made by different drivers originating from the same location (Beloit, DBS, Denver, Fayetteville and Frankford). These five locations represent different sets of conditions, such as terrain, wind patterns, weather, etc., and should thus be considered separately in any sample size determination. Furthermore, if any one of these particular locations is of interest, then only the sample size n_d for the device sample needs to be determined, unless the baseline dataset for the particular location proves to be insufficient in light of the calculations discussed in Section 3. If, on the other hand, the fuel consumption comparison is to be carried out at a completely new location, for which there are no baseline data, both the baseline and the device sample sizes n_b and n_d need to be determined. Both of these situations are covered in Section 3.

The five datasets were examined to assess the validity of the Gaussian assumption. The distributions of fuel consumption values in all five datasets

were reasonably close to the Gaussian distribution. Table 1 shows the sample mean $\bar{x}_b$, standard deviation s_b and size n_b of each dataset.

Table 1: The fuel consumption sample mean $\bar{x}_b$ and standard deviation s_b, in MPG, and sample size n_b of each of the five datasets.

	$\bar{x}_b$	s_b	n_b
Beloit	6.53	0.71	1137
DBS	6.73	0.64	950
Denver	6.82	0.99	856
Fayetteville	7	0.53	639
Frankford	6.84	0.59	1730

3 Sample Size Formulas

As discussed above, we consider two cases:

1. We want to perform the fuel consumption comparison between baseline and a particular device configuration at one of the five locations for which we already have the baseline data from Frito-Lay. We will assume that these data are representative of baseline conditions for the location in question in terms of the drivers, trips, weather or any other source of variability, so no additional baseline data would need to be collected unless these datasets are found to be insufficient in light of the sample calculations described below. Consequently, we only need to determine the device sample size n_d.

2. We want to perform the fuel consumption comparison between baseline and a particular device configuration at a new location. Thus, both baseline and the device data need to be collected, so both n_b and n_d need to be determined. Furthermore, it is assumed that a new location in question is comparable to one of the five locations we have the baseline data for, in terms of driver types, trip types, weather, terrain and other important source of variability influencing fuel consumption. Thus, the characteristics of one of the Frito-Lay datasets can be used to inform the calculations of the sample size required for the baseline and device groups at the new location.

In each of these two cases, the equation in (1) can be put together with user-specified values of α and β (defined in Section 1) to obtain the formula for the sample size required to detect a difference of $(100 \cdot p)\%$ in average fuel consumption from the baseline.

3.1 Case 1: Only Device Sample Size Needs to be Determined

As shown in the Appendix, given the baseline sample of size n_b from a population with the standard deviation σ_b and assuming that

$$\frac{\sigma_b^2}{n_b} \leq \left(\frac{p\mu_b}{\Phi^{-1}(\beta) + \Phi^{-1}(1-\alpha)} \right)^2, \tag{3}$$

the required sample size required to detect a decrease of at least $(100 \cdot p)\%$ from the average baseline mean consumption μ_b to that of the device is given by

$$n_d = \text{ceiling}\left(\frac{\sigma_d^2}{\left(\frac{p \cdot \mu_b}{\Phi^{-1}(\beta)+\Phi^{-1}(1-\alpha)} \right)^2 - \frac{\sigma_b^2}{n_b}} \right) \tag{4}$$

where σ_b, σ_d, α and β are as defined in Section 1 and $\Phi^{-1}(x)$ is the quantile of the standard normal distribution, that is, it is the value z such that $\Phi(z) = x$, or the value of the standard normal random variable such that the area to the left of z under the standard normal density curve is equal to x (these quantiles are easily obtained in standard software packages that contain statistical functions, such as Matlab, R, and even Excel). Note that if (3) does not hold, regardless of the device group sample size, one cannot satisfy the specified requirements for α, β and p, so these must be modified (increased, reduced and reduced, respectively) until (3) holds (see the Appendix for details).

As stated above, the assumption we make to obtain the formula in (4) for the sample size is that either the distribution of fuel consumption is Gaussian or that the sample size in each group is large enough. Of course, until one calculates the device sample size, one does not know whether it is large enough. However, the baseline sample sizes provided by Frito-Lay are all large, ranging from 639 to 1730 across the five datasets, as shown in Table 1.

3.2 Case 2: Both Baseline and Device Sample Sizes Need to be Determined

In this case, we assume that both the baseline and device sample sizes need to be calculated. Furthermore, as a starting point, we will assume that the two groups have equal population standard deviations $\sigma_b = \sigma_d = \sigma$,[1] which implies equal sample sizes required for the baseline and the device samples, i.e., $n_b = n_d = n$. As shown in the Appendix, the sample size required for each of the two samples in order to detect a difference of at least $(100 \cdot p)\%$ between the baseline fuel consumption μ_b and that of the device is given by

$$n_b = n_d = \text{ceiling}\left(2 \cdot \left(\Phi^{-1}(\beta) + \Phi^{-1}(1-\alpha)\right)^2 \left(\frac{\sigma}{p\mu_b}\right)^2\right) \tag{5}$$

As in case 1, the assumption that the fuel consumption values have a Gaussian distribution or that the sample sizes n_b and n_d are large is required for the formula in (5) to be valid.

3.3 Results

The calculations in both cases require specifying α, β, p and μ_b. In case 1, we also need to specify n_b, σ_b, and σ_d, while case 2 requires the value of $\sigma = \sigma_b = \sigma_d$. The values of α, β and p are specified according to the user's needs. As stated in Section 1, the most common values for α and β are 0.05 and 0.95, respectively. In addition to these values, we also considered the values of 0.1 and 0.9 for α and β, respectively. The difference we wish to detect is 3%, 4% or 5%, so we considered $p = 0.03, 0.04$ and 0.05. Thus, we have

- $\alpha = 0.05, 0.1$
- $\beta = 0.95, 0.9$
- $p = 0.03, 0.04, 0.05$.

The value of n_b is the value of the baseline sample size for each location and is specified in Table 1. We do not know the population values σ_b, σ_d

[1] This assumption may prove to be invalid once some preliminary datasets of fuel consumption with devices become available, but until then we make the simplifying assumption above.

and μ_b. The baseline sample mean $\bar{x}_b$ and standard deviation s_b of each location (see Table 1) provide us with the best estimates for that location's μ_b and σ_b, respectively. Furthermore, as in case 2, we will assume in case 1 that $\sigma_d = \sigma_b = \sigma$ unless evidence to the contrary emerges in the subsequent analyses and, therefore, use s_b as the estimate for σ in both cases.

When $\bar{x}_b$ and s_b are used as plug-ins for μ_b and σ_b, respectively, the condition in (3) is satisfied for all five samples. Table 2 shows the sample sizes for the device group required for each of the five locations in case 1, calculated using (4) under the assumptions made above. Table 3 shows the required sample sizes for each of the baseline and the device groups for a location similar to one of the five locations in the Frito-Lay datasets, calculated using (5) under the assumptions made above.

Table 2: The **device group** sample size required in **case 1** for each location to detect a difference in fuel consumption (in MPG) of $(100 \cdot p)\%$ from the baseline for a given value of α and β. The three values in each cell correspond to the sample sizes required for $p = 0.03, 0.04$, and 0.05, i.e., a difference of 3%, 4% and 5%, respectively.

	$\alpha = 0.05, \beta = 0.95$	$\alpha = 0.05, \beta = 0.9$ $\alpha = 0.1, \beta = 0.95$	$\alpha = 0.1, \beta = 0.9$
Beloit	163 86 54	125 67 42	94 51 32^2
DBS	121 65 41	94 51 32^2	70 39^2 25^2
Denver	361 172 103	262 130 79	188 97 60
Fayetteville	79 43 27^2	61 33^2 21^2	46 25^2 16^2
Frankford	93 52 33^2	73 41 26^2	56 31^2 20^2

As can be seen from Tables 2 and 3, of the three variables, the probability of false positives (α), the probability of detection (β), and the percent change one wants to detect (p), it is the latter that has the biggest impact on the sample size. Thus, if some of the recommended sample sizes are too large to be practical, the first question one needs to answer is whether one is willing to increase the minimum percent change one wants to detect. Of

[2]These sample sizes are below the rule-of-thumb threshold of 40 of what is considered a large sample. This means that unless the distribution of fuel consumption is approximately Gaussian, these sample sizes may not provide the statistical power to detect the percent change at the significance level indicated in the table. Thus, it is recommended that a sample size of at least 40 is used in all cases unless there is strong evidence that the fuel consumption is Gaussian.

Table 3: The sample size of **each of baseline and device groups in case 2** required to detect a difference in fuel consumption (in MPG) of $(100 \cdot p)\%$ from the baseline for a similar location type, for a given value of α and β. The three values in each cell correspond to the sample sizes required for $p = 0.03, 0.04$, and 0.05, i.e., a difference of 3%, 4% and 5%, respectively.

	$\alpha = 0.05, \beta = 0.95$	$\alpha = 0.05, \beta = 0.9$ $\alpha = 0.1, \beta = 0.95$	$\alpha = 0.1, \beta = 0.9$
Beloit	285 160 103	225 127 81	173 98 63
DBS	215 121 78	170 96 62	131 74 47
Denver	507 286 183	402 226 145	308 174 111
Fayetteville	141 79 51	111 63 40	86 48 31^2
Frankford	177 100 64	140 79 51	107 61 39^2

course, increasing the probability of false positives one is willing to tolerate or decreasing the probability of detection one desires will also help decrease the required sample size.

The sample sizes for case 2 are larger than for case 1, with the difference between the two approaching a factor of 2 for some combinations of α, β and p. This is because the sample sizes for the baseline datasets are quite large, so the required number for the device group in case 1 is smaller than in case 2, in which both baseline and device samples need to be collected (although the total number of required baseline and device data points is much smaller in case 2 than the sum of actual number of baseline and required device data points). Finally, as explained in the footnote, although some of the values in the table are below 40, it is recommended that at least 40 data points are obtained.

4 Future Work

Several assumptions were made in order to produce the recommended sample sizes in this document. As more data for both baseline and device fuel consumption become available and analyzed, the validity of these assumptions can be further examined and modifications to the calculations described here can be made accordingly.

5 Appendix: Sample Size Formula Derivations

The statistical test for comparing baseline and device fuel consumption is based on the statistic T introduced in (1). For convenience, we will denote the denominator of T by $g(n_b, n_d)$, i.e.,

$$g(n_b, n_d) \stackrel{def}{=} \sqrt{\frac{\sigma_b^2}{n_b} + \frac{\sigma_d^2}{n_d}} \tag{6}$$

Once α is specified, we will declare the device fuel consumption to be significantly below that of the baseline if

$$T = \frac{\bar{x}_d - \bar{x}_b}{g(n_b, n_d)} \leq z_\alpha \tag{7}$$

where z_α is the value such that $\Phi(z_\alpha) = \alpha$, where Φ denotes the standard normal cumulative distribution function (e.g., for $\alpha = 0.05, z_\alpha = -1.645$, while for $\alpha = 0.1, z_\alpha = -1.282$). Furthermore, we want to declare such a difference if

$$p = \frac{\mu_b - \mu_d}{\mu_b}, \tag{8}$$

or, equivalently, $\mu_b - \mu_d = p\mu_b$, and we want to do so with probability β.

If (8) is true, and the baseline and device fuel consumptions are both Gaussian or the sample sizes n_b and n_d are large, $\bar{x}_d - \bar{x}_b$ is Gaussian with mean $\mu_d - \mu_b = -p\mu_b$ and standard deviation equal to $g(n_b, n_d)$. Then the quantity

$$Z = \frac{\bar{x}_d - \bar{x}_b + p\mu_b}{g(n_b, n_d)} \tag{9}$$

has a standard normal distribution with the cumulative distribution function Φ. Hence, we have

$$\begin{aligned} \beta \equiv P(T \leq z_\alpha) &= P\left(\frac{\bar{x}_d - \bar{x}_b}{g(n_b, n_d)} \leq z_\alpha\right) \\ &= P\left(\bar{x}_d - \bar{x}_b + p\mu_b \leq z_\alpha \cdot g(n_b, n_d) + p\mu_b\right) \\ &= P\left(Z \leq z_\alpha + \frac{p\mu_b}{g(n_b, n_d)}\right), \end{aligned}$$

so

$$\Phi^{-1}(\beta) = z_\alpha + \frac{p\mu_b}{g(n_b, n_d)}, \tag{10}$$

implying

$$\Phi^{-1}(\beta) - z_\alpha = \frac{p\mu_b}{g(n_b, n_d)}. \tag{11}$$

Since $-z_\alpha = \Phi^{-1}(1-\alpha)$ due to the symmetry of the standard normal density about 0, from (11), we have

$$\Phi^{-1}(\beta) + \Phi^{-1}(1-\alpha) = \frac{p\mu_b}{g(n_b, n_d)}, \tag{12}$$

leading to

$$g(n_b, n_d) = \frac{p\mu_b}{\Phi^{-1}(\beta) + \Phi^{-1}(1-\alpha)}, \tag{13}$$

or

$$\sqrt{\frac{\sigma_b^2}{n_b} + \frac{\sigma_d^2}{n_d}} = \frac{p\mu_b}{\Phi^{-1}(\beta) + \Phi^{-1}(1-\alpha)}, \tag{14}$$

We solve (14) for n_d in case 1 and $n_b = n_d = n$ in case 2.

5.1 Case 1: Only Device Sample Size Needs to be Determined

Note that

$$\lim_{n_d \to \infty} g(n_b, n_d) = \frac{\sigma_b}{\sqrt{n_b}}, \tag{15}$$

so $g(n_b, n_d)$ is bounded below by the right-hand side of (15). As a result, the solution to (14) may not exist. Specifically, this will occur if

$$\frac{\sigma_b}{\sqrt{n_b}} > \frac{p\mu_b}{\Phi^{-1}(\beta) + \Phi^{-1}(1-\alpha)}, \tag{16}$$

or, equivalently,

$$\frac{\sigma_b^2}{n_b} > \left(\frac{p\mu_b}{\Phi^{-1}(\beta) + \Phi^{-1}(1-\alpha)} \right)^2. \tag{17}$$

Put another way, the solution will not exist if either the baseline standard deviation is too large, specifically, if

$$\sigma_b > \frac{p\mu_b}{\Phi^{-1}(\beta) + \Phi^{-1}(1-\alpha)} \cdot \sqrt{n_b}, \tag{18}$$

or if the baseline sample size is too small, i.e., if

$$n_b < \left((\Phi^{-1}(\beta) + \Phi^{-1}(1-\alpha)) \cdot \frac{\sigma_b}{p\mu_b} \right)^2 . \tag{19}$$

Assuming that (17) or any of the equivalent conditions outlined above are not true, we can solve (14) for n_d to obtain

$$n_d = \frac{\sigma_d^2}{\left(\frac{p \cdot \mu_b}{\Phi^{-1}(\beta)+\Phi^{-1}(1-\alpha)} \right)^2 - \frac{\sigma_b^2}{n_b}} \tag{20}$$

Since a sample size must be an integer, we round up the right-hand side of (20) to obtain the solution in (4) (we always round up since rounding down will not meet the requirements of significance level, power and percent change detection imposed by the user).

5.2 Case 2: Both Baseline and Device Sample Sizes Need to be Determined

Setting $\sigma_b = \sigma_d = \sigma$ and $n_b = n_d = n$ in (14) gives

$$\sqrt{\frac{2\sigma^2}{n}} = \frac{p\mu_b}{\Phi^{-1}(\beta) + \Phi^{-1}(1-\alpha)}, \tag{21}$$

which yields

$$n_b = n_d = 2 \cdot \left(\Phi^{-1}(\beta) + \Phi^{-1}(1-\alpha) \right)^2 \left(\frac{\sigma}{p\mu_b} \right)^2 . \tag{22}$$

For the same reason as in Section 5.1, we round up the right-hand side of (22) to obtain the formula in (5).

References

[1] J. Devore and R. Peck. *Statistics: The Exploration and Analysis of Data.* Duxbury Press, Pacific Grove, California, 1996.

Appendix B: Statistical Analysis of the Spirit Truck Lines Fuel Economy Data

Lawrence Livermore National Laboratory

Analysis of Fuel Efficiency Data

Vera Bulaevskaya
June 27, 2012

Approach

- Analyzed 6 out of 9 vehicles in the dataset
  - 3 out of 9 did not have a sufficient number of data points for each device (i.e., at least 30 per device) to perform a meaningful comparison
- Studied MPG rather than GPM as a measure of fuel efficiency since MPG has a much more Gaussian-like distribution than GPM, which is much more suitable for basic analyses
- Performed a basic analysis of variance (ANOVA) with MPG as a response and device as a predictor
  - Separately by vehicle
  - Together across all vehicles (but accounting for individual vehicle effects)
  - Also considered average trip speed as a factor, but it proved to be not a significant predictor of fuel efficiency and was therefore dropped from further analysis

Lawrence Livermore National Laboratory  2

MPG vs. Device by Vehicle

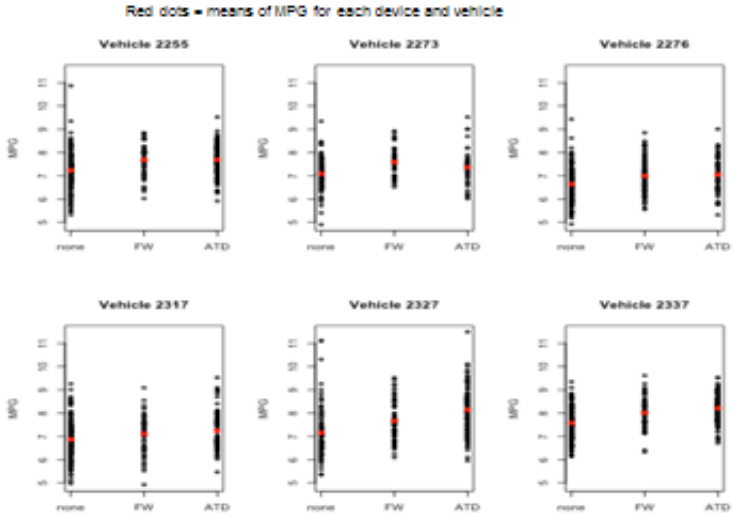

- In terms of absolute MPG, there is some variation from one vehicle to another
- For all vehicles, both devices yield slightly higher MPG than no device
- The two devices tend to yield very similar MPG

Lawrence Livermore National Laboratory

MPG Means by Device and Vehicle

Vehicle/Device	None	FW	ATD
2255	7.23	7.69	7.69
2273	7.09	7.59	7.36
2276	6.64	6.99	7.05
2317	6.87	7.11	7.24
2327	7.15	7.66	8.14
2337	7.58	8.01	8.21

Lawrence Livermore National Laboratory

Means and 95% Confidence Intervals for the Difference Between Each of the Devices and No Device

Vehicle	FW – Baseline		ATD - Baseline	
	Mean	95% CI	Mean	95% CI
2255	0.457	(0.253, 0.661)	0.46	(0.294, 0.626)
2273	0.5	(0.256, 0.735)	0.269	(0.037, 0.5)
2276	0.35	(0.174, 0.525)	0.404	(0.194, 0.614)
2317	0.237	(0.005, 0.468)	0.372	(0.153, 0.59)
2327	0.509	(0.242, 0.776)	0.988	(0.764, 1.211)
2337	0.439	(0.266, 0.611)	0.638	(0.492, 0.784)
Overall	0.394	(0.306, 0.482)	0.562	(0.481, 0.642)

These results confirm the conclusions from the plots

Lawrence Livermore National Laboratory

95% Confidence Intervals for the Difference Between Each of the Devices and No Device

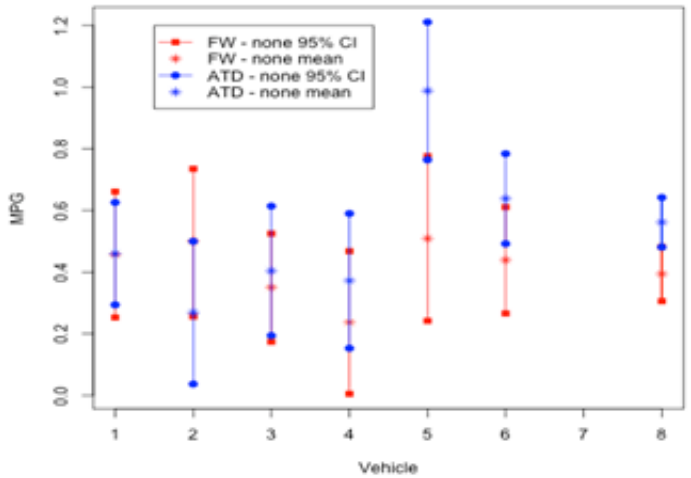

Vehicles are numbered in the order they are listed on the previous slide (i.e., 1 = 2255, 6 = 2337) , 8 = overall

Lawrence Livermore National Laboratory

Means and 95% Confidence Intervals for the % Change for Each of the Devices Relative to Baseline

Vehicle	(FW – Baseline)/Baseline		(ATD – Baseline)/Baseline	
	Mean	95% CI	Mean	95% CI
2255	6.32	(3.47, 9.22)	6.37	(4.02, 8.75)
2273	7	(3.58, 10.45)	3.79	(0.52, 7.11)
2276	5.27	(2.59, 7.99)	6.09	(2.89, 9.33)
2317	3.44	(0.07, 6.86)	5.41	(2.21, 8.67)
2327	7.13	(3.33, 11.01)	13.81	(10.51, 17.22)
2337	5.79	(3.48, 8.13)	8.43	(6.43, 10.48)
Overall	5.47	(4.24, 6.7)	7.79	(6.67, 8.92)

Lawrence Livermore National Laboratory 7

95% Confidence Intervals for Percent Change of Each of the Devices Relative to Baseline

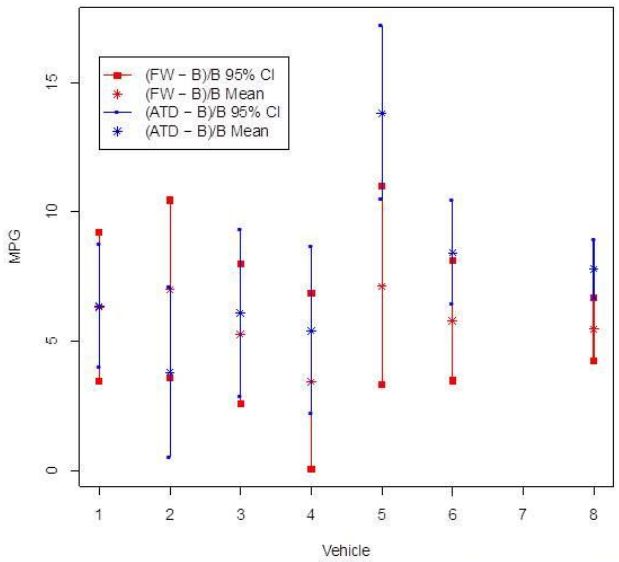

Vehicles are numbered in the order they are listed on the previous slide (i.e., 1 = 2255, 6 = 2337) , 8 = overall

Lawrence Livermore National Laboratory 8

Last Page of VSST 2013 Annual Product

DOE/EE-1023 February 2014
Printed with a renewable-source ink on paper containing
at least 50% wastepaper, including 10% post consumer waste.

U.S. DEPARTMENT OF ENERGY | Energy Efficiency & Renewable Energy

For more information
eere.energy.gov